Files are in Adobe format.
Download the newest version from Adobe.

26th International Symposium on BALLISTICS

Miami, FL

12 – 16 September 2011

Agenda

Tuesday, September 13, 2011

Keynote Address:

- *An Overview of Analyzing Firearm, Tool Mark and Impression Evidence at the Miami-Dade Police Department,* Mr. Gabriel A. Hernandez, Criminalist Supervisor, Miami-Dade Police Department

GENERAL SESSION CHAIRED BY ZHONGYUAN WANG & GORDON JOHNSON

- 11826 - Analyzing Lubrication's Contribution to Cartridge Case Failure, Mr. Mark Minisi, USA
- 11946 - Reinforced Dense High-Explosive Fills for Gun Launch, Mr. Michael Minnicino, USA
- 11892 - Modeling of Fabric Impact with High-Speed Imaging and Nickel-Chromium Wires Validation, Dr. Sidney Chocron, USA; Mr. Trenton Kirchdoerfer, Ms. Nikki King, Dr. Christopher Freitas
- 11981 - Pressure Effects in an Enclosed Volume Due to EFP Impact, Mr. Jo Hagness Kiran, Norway

EXTERIOR BALLISTICS - ASHE AUDITORIUM CHAIRED BY MARC GIRAUD & ED SCHMIDT

- 11803 - Preliminary Testing of a 2-Fin Flechette, Mr. Ilmars Celmins, USA; Mr. Gregory S. Oberlin
- 11835 - Numerical Investigation of Lateral Jet Interaction on a Fin-Stabilized Projectile, Dr. James DeSpirito, USA
- 11894 - Predicting the Dynamic Stability of Small-Caliber Ammunition, Dr. Sidra I. Silton, USA; Mr. Bradley E. Howell
- 11957 - An Automated Visual Scoring Algorithm for Assessing Gunfire Accuracy, Dr. Chris Weiland, USA; Mr. John F. Busic, Dr. Jon J. Yagla
- 11996 - Free-Flight Motion Analysis Based on Shock-Tunnel Experiments, Mr. Pierre Wey, France; Dr. Friedrich Seiler, Dr. Julio Srulijes, Mrs. Myriam Bastide, Mr. Bastien Martinez
- 12015 - Extended Range of 155mm Projectile Using an Improvised Base Bleed Unit: Simulations and Evaluation, Dr. Ing Nils Kubberud, Norway; Dr. Ing Ivar Øye

TERMINAL BALLISTICS & IMPACT PHYSICS - ASHE AUDITORIUM CHAIRED BY MATHIAS WICKERT & CHARLIE ANDERSON

- 11487 - Development of a Novel Ceramic Armor System: Analysis and Test, Dr. David L. Hunn, USA; Dr. Sang J. Lee
- 12030 - Visualization and Analysis of Impact Damage in Sapphire, Mr. Elmar Strassburger, Germany; Dr. James W. McCauley, Dr. Parimal Patel

Wednesday, September 14, 2011

EXPLOSION MECHANICS - ASHE AUDITORIUM CHAIRED BY ANDREAS HELTE & DAVID LAMBERT

- 11755 - Perforator with Energetic Liner, Mr. David Davison, USA; Mr. Dan Pratt
- 11778 - Is Higher Detonation Velocity Needed for Shaped-Charges?, Dr. Meir Mayseless, Israel; Eitan Hirsch, Bill W. Harvey, J.E. Backofen
- 12056 - Glass as a Shaped Charge Liner Material, Dr. Ernest Baker, USA; Mr. Arthur Daniels, Mr. Tan Vuong, Mr. James Pham, S. DeFisher
- 12019 - A Novel Technology for Switchable Modes Warheads, Dr. Werner A. Arnold, Germany, M. Graswald, E.

Rottenkolber
- 11897 - The Potential of FOX-7 in Insensitive Munition Design, Dr. Ian G. Cullis, UK; Mr. Richard Townsley

TERMINAL BALLISTICS & IMPACT PHYSICS - ASHE AUDITORIUM CHAIRED BY DANNY YAZIV & WILLIAM GOOCH

- 11917 - Effects of EFP Solidity in Terminal Ballistics, Mr. Ho Soo Kim, South Korea; Dr. Werner Arnold, Dr. Thomas Hartmann, Mr. Ernst Rottenkolber, Dr. Andreas Klavzar
- 12025 - An Experimental and Numerical Study of Ballistic Impacts on a Turbine Casing Material at Varying Temperatures, Dr. Francisco Gálvez, Spain; Mr. Borja Erice, Dr. David Cendón, Dr. Vicente Sánchez-Gálvez, Dr. Tore Borvik
- 12048 - The Penetration Process of Jets and Long Rods in Water, Dr. Dan Yaziv, Israel; Meir Mayseless, Zvi Cooper, Yehiel Reifen, Eitan Hirsch

INTERIOR BALLISTICS - ASHE AUDITORIUM CHAIRED BY CLIVE WOODLEY & JONATHAN JABLONSKI

- 11495 - Modeling the Internal Ballistics of Lightweight Plastic Driving Band Projectiles, Mr. Clive R. Woodley, UK
- 11782 - Burning Behavior of Gun Propellants Under the Influence of Pressure Oscillations – Theoretical Background and Simulation, Mr. Klaus-Achim Kratzsch, Germany
- 11940 - Multidimensional Interior Ballistics Modeling with Extensions to Igniter Design and Operation, Dr. Michael Nusca, USA

Thursday, September 15, 2011

EXPLOSION MECHANICS CHAIRED BY MARKUS GRASWALD & WILLIAM WALTERS

- 11770 - The Trouble with TNT Equivalence, Mr. Paul M. Locking, UK
- 11926 - Effect of Set Up Parameters of Landmine Blast Over Transferred Energy to a Rigid Body: Experimental and Computational Study, Dr. Juan P. Casas Rodriguez, Colombia; Jose A. Hoyos Uribe, Victor H. Bastidas Poveda
- 12006 - Experimental Studies of Scalable Effects Warhead Technologies, Dr. Markus Graswald, Germany; Dr. Werner Arnold
- 11948 - Results and Analysis from Mine Impulse Experiments Using Stereo-Digital Image Correlation, Mr. Craig Barker, USA; Douglas Howle, Terry Holdren, Jeffrey Koch, Raquel Ciappi
- 12036 - An Investigation of Aerosolization and Associated Phenomena Resulting from the Detonation of Explosives, Mr. Luke S. Lebel, Canada; Mr. Patrick Brousseau, Dr. Lorne Erhardt, Dr. William S. Andrews

LAUNCH DYNAMICS - ASHE AUDITORIUMCHAIRED BY NICHOLAS BRUNO & DON CARLUCCI

- 11764 - Inclusion of Rifling and Variable Centerline in Gun Tubes for Enhanced Modeling of Launch Dynamics, Mr. Charles Eichhorst, USA; Dr. William H. Drysdale, Mr. Michael Minnicino, Mr. David A. Hopkins
- 11937 - 5.56mm M855 Accuracy and Jump Measurements, Mr. Ilmars Celmins, USA
- 12029 - Modeling of the Dynamics of a 40 mm Gun and Ammunition System During Firing, Mr. Nicolas Eches, France; Mr. Didier Cosson, Mr. Quentin Lambert, Mr. André Langlet
- 12062 - Characterization of a Potting Material for Gun Launch, Dr. Aisha Haynes, USA; Dr. Jennifer Cordes
- 12063 - Gun Launch Dynamics of Pyrotechnic Materials, Dr. Aisha Haynes, USA; Mr. Justin John, Mr. Anthony Sherwood

INTERIOR BALLISTICS - ASHE AUDITORIUM CHAIRED BY PAUL LOCKING & MICHAEL NUSCA

- 11956 - Detailed Ballistic Performance Characterization of 120-mm Mortar System with Different Flash Tube Configurations, Dr. Kenneth Kuo, USA; Dr. Eric Boyer, Mr. Heath T. Martin
- 11441 - The Numerical Optimization of the Novel Kinetic Energy Penetrator for Tank Guns, Dr. Mariusz Magier, Poland
- 12024 - A Numerical Tool for Evaluating Solid Propellants Ignition Models, Mr. Christophe Boulnois, France; Dr. Camille Strozzi, Dr. Amar Bouchama, Pr. Philippe Gillard
- 11494 - Modeling the Effects of Non-Gaseous Igniter Combustion Products on the Ignition of Gun Propellants, Mr. Clive R. Woodley, UK
- 11945 - Modeling Explosive Cladding of Metallic Liners to Gun Tubes, Mr. Jack M. Pincay, USA; Dr. Ernest L. Baker, Mr. David G. Pfau
- 12080 - Finite Element Modeling of Primer Impact to Understand the Dynamics of Misfires, Mr. Mark D. Lee, USA

VULNERABILITY - ASHE AUDITORIUM CHAIRED BY PHILIP CUNNIFF & HO SOO KIM

- 11794 - Survivability Evaluation of Blast Mitigation Seats for Armored Vehicles, Dr. Ming Cheng, Canada; Mr. Doug Bueley, Dr. Jean-Philippe Dionne, Dr. Aris Makris
- 11991 - Attenuation of a Blast Wave Through Cranial Bone, Dr. Amy C. Courtney, USA; Dr. Michael W. Courtney
- 12040 - DESCENT Modeling in Rotorcraft Vulnerability Assessment, Mr. Andrew W. Drysdale, USA; Dr. Matthew Floros
- 12065 - Ammunition and Weapon Effects in Confined Operational Urban Theatre in the Vicinity of Own Troops, Mr. Theo Verhagen, The Netherlands; Mr. Martin v.d. Voorde

Thursday, September 15, 2011

TERMINAL BALLISTICS & IMPACT PHYSICS - ASHE AUDITORIUM CHAIRED BY JAMES WALKER & PIERRE CHANTERET

- 11776 - Penetration of Rigid Rods into Sand, Dr. Stephan Bless, USA; W. Cooper, K. Wantawabi
- 11997 - Blast Response Analysis of Reinforced Concrete Slabs: Experimental Procedure and Numerical Simulation, Mr. Gustavo Morales-Alonso, Spain; Dr. David A. Cendón, Dr. Francisco Gálvez, Mr. Borja Erice, Prof. Dr. Vicente Sánchez-Gálvez
- 12035 - Effect of Frictions on the Ballistic Performance of a 3D Warp Interlock Fabric: Numerical Analysis, Mr. Cuong Ha-Minh, France; Dr. François Boussu, Dr. Toufik Kanit, Dr. David Crépin, Prof. Abdellatif Imad
- 12055 - Why Impacted Yarns Break at Lower Speed than Classical Theory Predicts, Dr. James D. Walker, USA; Dr. Sidney Chocron
- 12067 - Unusual Transverse Compression Response of Non-Woven Ballistic Laminates, Dr. Brian R. Scott, USA
- 12108 - Protection of Light Armours Against Shaped Charge Projectiles, Prof. Adam Wisniewski, Poland

GENERAL SESSION CHAIRED BY KLAUS THOMA & JACK PINCAY

- 12095 - AMRDEC Lethality Modeling and Simulation Methodologies for Aerial Targets, Mrs. Dedra C. Moore, USA; Mr. Dustin Clark, Mr. Brent Deerman
- 11730 - Development of Blast Enhanced Explosive for an Anti-Structure Warhead, Mr. Hendrik Lips, Germany
- 11865 - Measurement of Blast Reflected Overpressure at Small Charge Standoff with Tourmaline-Based Piezoelectric Transducers, Dr. Roger L. Veldman, USA; Dr. Mark W. Nansteel, Dr. Charles Chen

Dr. Manfred Held Memorial Presentation

Presentation of Awards

Presentation of the 27th International Symposium on Ballistics Freiburg, Germany

Hypervelocity Impact Symposium 2012

NDIA
National Defense Industrial Association

PROMOTING NATIONAL SECURITY SINCE 1919

IBS

26th International Symposium on BALLISTICS

Sponsored by the International Ballistics Society in association with the Ballistics Division of the National Defense Industrial Association

SEPTEMBER 12-16, 2011
WWW.NDIA.ORG/MEETINGS/1210

HYATT REGENCY MIAMI ▸ MIAMI, FLORIDA

EVENT #1210

26th INTERNATIONAL SYMPOSIUM ON BALLISTICS

SEPTEMBER 12-16, 2011 ▸ MIAMI, FLORIDA, USA

The International Symposium on Ballistics is an opportunity for ballistics scientists, engineers, and others to report, share, and discuss current research and advances in ballistics and visions of the future. The International Symposium on Ballistics is jointly organized and supported by the International Ballistics Society (IBS), in conjunction with the National Defense Industrial Association (NDIA), Arlington, Virginia, USA.

PAPER SELECTION COMMITTEE

Mr. Richard Ames, USA
Mr. Joseph Backofen, USA
Dr. Dennis Baum, USA
Dr. Stephan Bless, USA
Dr. Ronald Brown, USA
Dr. Donald Carlucci, USA
Dr. James Cazamias, USA
Mr. Pierre Chanteret, France
Dr. Sidney Chocron, USA
Dr. Ian Cullis, UK
Dr. William Flis, USA
Dr. Francisco Galvez, Spain
Dr. Marc Girard, France
Dr. Markus Graswald, Germany
Dr. Manfred Held, Germany
Dr. Eitan Hirsch, Isreal
Ms. Melissa Hobbs, USA
Dr. Bo Janzon, Sweden
Dr. Kenneth Kuo, USA
Dr. Eva Liden, Sweden
Dr. Paul Locking, UK
Dr. Mier Mayseless, Isreal
Dr. Michael Murphy, USA
Dr. Brad Pedersen, USA
Mr. Jack Riegel, USA
Dr. Tony Russell, USA
Dr. AdamWisniewski, Poland
Dr. Clive Woodley, UK

INTERNATIONAL BALLISTICS SOCIETY BOARD OF DIRECTORS

Mr. John (Jack) P. Riegel, III, USA
President
Dr. Sidney Chocron, USA
Secretary
Dr. Dennis Baum, USA
Treasurer
Dr. Bo Janzon, Sweden
Dr. Ian Cullis, UK
Prof. Zhongyuan Wang, China
Dr. Meir Mayseless, Israel
Dr. Michael Murphy, USA

SYMPOSIUM LEADERSHIP

Symposium Chairmen
Dr. Ernest Baker, U.S. Army ARDEC
Dr. Doug Templeton, U.S. Army TARDEC

NDIA Ballistics Division Chairman
Dr. Richard Ames, Raytheon Missile Systems

NDIA Symposium Planning Team
Mr. Sam Campagna, Assistant Vice President, Operations
Ms. Kari King, CMP, Associate Director
Ms. Kelly Seymour, Exhibits Manager

PREVIOUS INTERNATIONAL SYMPOSIA ON BALLISTICS

- Orlando, Florida, USA 1974
- Daytona, Florida, USA 1976
- Karlsruhe, Germany 1977
- Monterey, California, USA 1978
- Toulouse, France 1980
- Orlando, Florida, USA 1981
- The Hague, The Netherlands 1983
- Orlando, Florida, USA 1984
- Shrivenham, UK 1986
- San Diego, California, USA 1987
- Brussels, Belgium 1989
- San Antonio, Texas, USA 1990
- Stockholm, Sweden 1992
- Quebec City, Canada 1993
- Jerusalem, Israel 1995
- San Francisco, California, USA 1996
- Midrand, South Africa 1998
- San Antonio, Texas, USA 1999
- Interlaken, Switzerland 2001
- Orlando, Florida, USA 2002
- Adelaide, South Australia 2004
- Vancouver, BC, Canada 2005
- Tarragona, Spain 2007
- New Orleans, Louisiana, USA 2008
- Beijing, China 2010

FUTURE INTERNATIONAL SYMPOSIA ON BALLISTICS

- Freiburg, Germany 2013
- Atlanta, Georgia, USA 2014

AUTHORS & PRESENTERS FROM 30 COUNTRIES

- Australia
- Belgium
- Canada
- China
- Colombia
- Czech Republic
- Egypt
- Finland
- France
- Germany
- Greece
- India
- Israel
- Italy
- Japan
- Malaysia
- Mexico
- The Netherlands
- Norway
- Poland
- Russia
- South Africa
- South Korea
- Spain
- Sweden
- Thailand
- Turkey
- Ukraine
- United Kingdom
- USA

MONDAY, SEPTEMBER 12, 2011

8:00 AM - 7:00 PM — Registration Open - Lobby Level

9:00 AM - 4:30 PM — Tutorial Sessions - Brickell Room
*Additional Registration Fees Apply

AM Tutorial Session

9:00 AM: Warhead Mechanism
- 1.1 Blast Charges
- 1.2 Shaped Charges
- 1.3 Flat Cone Charges

10:45 AM: Coffee Break in Foyer

11:00 AM: Warhead Mechanism Continued
- 1.4 EFP Charges
- 1.5 Fragment Charges (Anti-AC/Anti-TBM)

12: 15 PM: Lunch for AM & PM Tutorial Attendees

PM Tutorial Session

1:30 PM: Overview on Armour for MBTs and APCs
- 2.1 RHA
- 2.2 Ceramics
- 2.3 Glass

3:00 PM: Coffee Break in Foyer

3:15 PM: Overview on Armour for MBTs and APCs Continued
- 2.4 Composites
- 2.5 ERA
- 2.6 NERA or Bulging
- 2.7 Active Defence Concepts

10:00 AM - 4:00 PM — Exhibitor Move-In & Poster Set-Up - Riverfront Hall

5:00 PM — Exhibit Hall Open - Riverfront Hall

5:00 PM - 7:00 PM — Opening Reception in Exhibit Hall - Riverfront Hall

TUESDAY, SEPTEMBER 13, 2011

7:00 AM - 5:20 PM	Registration Open - Lobby Level
7:00 AM - 8:00 AM	Continental Breakfast - Ashe Auditorium Foyer
8:00 AM - 8:10 AM	Welcome & Administrative Remarks - Ashe Auditorium
8:10 AM - 8:45 AM	Update on the International Ballistics Society *Mr. Jack Riegel, President, International Ballistics Society; President, R3 Technology, Inc.*
8:45 AM - 9:30 AM	Keynote Address: An Overview of Analyzing Firearm, Tool Mark and Impression Evidence at the Miami-Dade Police Department *Mr. Gabriel A. Hernandez, Criminalist Supervisor, Miami-Dade Police Department*
9:30 AM - 9:50 AM	Invited Presentation: Effectiveness of Explosive Reactive Armour *Dr. Meir Mayseless, Israel*
9:50 AM - 5:20 PM	Exhibit Hall Open - Riverfront Hall
9:50 AM - 10:10 AM	Break in Exhibit Hall - Riverfront Hall
10:10 AM - 11:50 AM	General Session *Chaired by Zhongyuan Wang & Gordon Johnson*
10:10 AM - 10:30 AM	11826 - Analyzing Lubrication's Contribution to Cartridge Case Failure *Mr. Mark Minisi, USA*
10:30 AM - 10:50 AM	11946 - Reinforced Dense High-Explosive Fills for Gun Launch *Mr. Michael Minnicino, USA*
10:50 AM - 11:10 AM	11892 - Modeling of Fabric Impact with High-Speed Imaging and Nickel-Chromium Wires Validation *Dr. Sidney Chocron, USA; Mr. Trenton Kirchdoerfer, Ms. Nikki King, Dr. Christopher Freitas*
11:10 AM - 11:30 AM	11981 - Pressure Effects in an Enclosed Volume Due to EFP Impact *Mr. Jo Hagness Kiran, Norway*
11:30 AM - 11:50 AM	11993 - Numerical Analysis of the Initiation of High Explosives by Interacting Shock Waves Due to Multiple Fragment Impact *Dr. Andreas Heine, Germany; Mr. Martin Lueck, Dr. Matthias Wickert*
11:50 AM - 1:20 PM	Lunch - Regency Ballroom
1:20 PM - 3:20 PM	Terminal Ballistics & Impact Physics Poster Session - Riverfront Hall - See pg. 10 *Chaired by Tim Holmquist & Pieter Nel*
1:20 PM - 3:20 PM	Exterior Ballistics - Ashe Auditorium *Chaired by Marc Giraud & Ed Schmidt*
1:20 PM - 1:40 PM	11803 - Preliminary Testing of a 2-Fin Flechette *Mr. Ilmars Celmins, USA; Mr. Gregory S. Oberlin*
1:40 PM - 2:00 PM	11835 - Numerical Investigation of Lateral Jet Interaction on a Fin-Stabilized Projectile *Dr. James DeSpirito, USA*
2:00 PM - 2:20 PM	11894 - Predicting the Dynamic Stability of Small-Caliber Ammunition *Dr. Sidra I. Silton, USA; Mr. Bradley E. Howell*

2:20 PM - 2:40 PM	11957 - An Automated Visual Scoring Algorithm for Assessing Gunfire Accuracy *Dr. Chris Weiland, USA; Mr. John F. Busic, Dr. Jon J. Yagla*
2:40 PM - 3:00 PM	11996 - Free-Flight Motion Analysis Based on Shock-Tunnel Experiments *Mr. Pierre Wey, France; Dr. Friedrich Seiler, Dr. Julio Srulijes, Mrs. Myriam Bastide, Mr. Bastien Martinez*
3:00 PM - 3:20 PM	12015 - Extended Range of 155mm Projectile Using an Improvised Base Bleed Unit: Simulations and Evaluation *Dr. Ing Nils Kubberud, Norway; Dr. Ing Ivar Øye*
3:20 PM - 3:40 PM	Break in Exhibit Hall - Riverfront Hall
3:40 PM - 5:20 PM	Exterior Ballistics Poster Session - Riverfront Hall - See pg. 11 *Chaired by Stephan Bless & Paul Weinacht*
3:40 PM - 5:20 PM	Terminal Ballistics & Impact Physics - Ashe Auditorium *Chaired by Mathias Wickert & Charlie Anderson*
3:40 PM - 4:00 PM	11487 - Development of a Novel Ceramic Armor System: Analysis and Test *Dr. David L. Hunn, USA; Dr. Sang J. Lee*
4:00 PM - 4:20 PM	11921 - Penetration Resistance of Porous (Damaged) Glass in Impact Velocities Interval From 300 m/s up to 1000 m/s *Mr. Valeriy V. Kartuzov, Ukraine; Boris A. Galanov, Sergei M. Ivanov, Yegor V. Kartuzov, Douglas W. Templeton, Stephan Bless*
4:20 PM - 4:40 PM	11925 - Scaled Impact Experiments into Borosilicate Glass *Dr. Charles E. Anderson, Jr., USA; Mr. Carl E. Weiss, Dr. Sidney Chocron*
4:40 PM - 5:00 PM	12012 - Interface Defeat of Long Rods Impacting Oblique Silicon Carbide *Mr. Thilo Behner, Germany; Dr. Charles Anderson, Mr. Timothy Holmquist, Dr. Matthias Wickert, Dr. Doug Templeton*
5:00 PM - 5:20 PM	12030 - Visualization and Analysis of Impact Damage in Sapphire *Mr. Elmar Strassburger, Germany; Dr. James W. McCauley, Dr. Parimal Patel*

WEDNESDAY, SEPTEMBER 14, 2011

7:00 AM - 2:10 PM	Registration Open - Lobby Level
7:00 AM - 8:00 AM	Continental Breakfast - Ashe Auditorium Foyer
8:00 AM - 2:10 PM	Exhibit Hall Open - Riverfront Hall
8:00 AM - 8:10 AM	Administrative Remarks - Ashe Auditorium
8:10 AM - 9:50 AM	Interior Ballistics Poster Session - Riverfront Hall - See pg. 11 *Chaired by Carlton Adam & Thelma Manning*
8:10 AM - 9:50 AM	Explosion Mechanics - Ashe Auditorium *Chaired by Andreas Helte & David Lambert*
8:10 AM - 8:30 AM	11755 - Perforator with Energetic Liner *Mr. David Davison, USA; Mr. Dan Pratt*
8:30 AM - 8:50 AM	11778 - Is Higher Detonation Velocity Needed for Shaped-Charges? *Dr. Meir Mayseless, Israel; Eitan Hirsch, Bill W. Harvey, J.E. Backofen*

8:50 AM - 9:10 AM	12056 - Glass as a Shaped Charge Liner Material *Dr. Ernest Baker, USA; Mr. Arthur Daniels, Mr. Tan Vuong, Mr. James Pham, S. DeFisher*
9:10 AM - 9:30 AM	12019 - A Novel Technology for Switchable Modes Warheads *Dr. Werner A. Arnold, Germany, M. Graswald, E. Rottenkolber*
9:30 AM - 9:50 AM	11897 - The Potential of FOX-7 in Insensitive Munition Design *Dr. Ian G. Cullis, UK; Mr. Richard Townsley*
9:50 AM - 10:10 AM	Break in Exhibit Hall - Riverfront Hall
10:10 AM - 11:50 AM	Launch Dynamics Poster Session - Riverfront Hall - See pg. 12 *Chaired by Nicholas Payne & Francisco Galvez*
10:10 AM - 11:50 AM	Terminal Ballistics & Impact Physics - Ashe Auditorium *Chaired by Danny Yaziv & William Gooch*
10:10 AM - 10:30 AM	11887 - The Erosion Threshold for High Velocity Geo-Penetrators *Dr. Norbert Heider, Germany; Mr. Manfred Salk*
10:30 AM - 10:50 AM	11917 - Effects of EFP Solidity in Terminal Ballistics *Mr. Ho Soo Kim, South Korea; Dr. Werner Arnold, Dr. Thomas Hartmann, Mr. Ernst Rottenkolber, Dr. Andreas Klavzar*
10:50 AM - 11:10 AM	12008 - Effects of Lateral Edges Toward Penetration Depths *Mr. Andreas Heine, Germany; Mr. Richard Cunrath, Mr. Hideaki Kobayashi, Mr. Matthias Wickert*
11:10 AM - 11:30 AM	12025 - An Experimental and Numerical Study of Ballistic Impacts on a Turbine Casing Material at Varying Temperatures *Dr. Francisco Gálvez, Spain; Mr. Borja Erice, Dr. David Cendón, Dr. Vicente Sánchez-Gálvez, Dr. Tore Borvik*
11:30 AM - 11:50 AM	12048 - The Penetration Process of Jets and Long Rods in Water *Dr. Dan Yaziv, Israel; Meir Mayseless, Zvi Cooper, Yehiel Reifen, Eitan Hirsch*
11:50 AM - 1:10 PM	Lunch - Regency Ballroom
1:10 PM - 2:10 PM	Vulnerability Poster Session - Riverfront Hall - See pg. 12 *Chaired by Gilles Pageau & Maurice Grudza*
1:10 PM - 2:10 PM	Interior Ballistics - Ashe Auditorium *Chaired by Clive Woodley & Jonathan Jablonski*
1:10 PM - 1:30 PM	11495 - Modeling the Internal Ballistics of Lightweight Plastic Driving Band Projectiles *Mr. Clive R. Woodley, UK*
1:30 PM - 1:50 PM	11782 - Burning Behavior of Gun Propellants Under the Influence of Pressure Oscillations – Theoretical Background and Simulation *Mr. Klaus-Achim Kratzsch, Germany*
1:50 PM - 2:10 PM	11940 - Multidimensional Interior Ballistics Modeling with Extensions to Igniter Design and Operation *Dr. Michael Nusca, USA*
2:30 PM - 7:00 PM	Miami Intercoastal Waterway Cruise & Reception *Aboard the Lady Windridge Yacht; Resort casual attire suggested* **Yacht will depart from the Hyatt dock at 3 pm; please board at 2:30 pm**

THURSDAY, SEPTEMBER 15, 2011

7:00 AM - 5:20 PM	Registration Open - Lobby Level
7:00 AM - 8:00 AM	Continental Breakfast - Ashe Auditorium Foyer
8:00 AM - 8:10 AM	Administrative Remarks - Ashe Auditorium
8:10 AM - 9:50 AM	Explosion Mechanics *Chaired by Markus Graswald & William Walters*
8:10 AM - 8:30 AM	11770 - The Trouble with TNT Equivalence *Mr. Paul M. Locking, UK*
8:30 AM - 8:50 AM	11926 - Effect of Set Up Parameters of Landmine Blast Over Transferred Energy to a Rigid Body: Experimental and Computational Study *Dr. Juan P. Casas Rodriguez, Colombia; Jose A. Hoyos Uribe, Victor H. Bastidas Poveda*
8:50 AM - 9:10 AM	12006 - Experimental Studies of Scalable Effects Warhead Technologies *Dr. Markus Graswald, Germany; Dr. Werner Arnold*
9:10 AM - 9:30 AM	11948 - Results and Analysis from Mine Impulse Experiments Using Stereo-Digital Image Correlation *Mr. Craig Barker, USA; Douglas Howle, Terry Holdren, Jeffrey Koch, Raquel Ciappi*
9:30 AM - 9:50 AM	12036 - An Investigation of Aerosolization and Associated Phenomena Resulting from the Detonation of Explosives *Mr. Luke S. Lebel, Canada; Mr. Patrick Brousseau, Dr. Lorne Erhardt, Dr. William S. Andrews*
9:50 AM - 3:40 PM	Exhibit Hall Open - Riverfront Hall
9:50 AM - 10:10 AM	Break in Exhibit Hall - Riverfront Hall
10:10 AM - 11:50 AM	Terminal Ballistics & Impact Physics Poster Session - Riverfront Hall - See pg. 13 *Chaired by Ewa Lidén & Dennis Nandlall*
10:10 AM - 11:50 AM	Launch Dynamics - Ashe Auditorium *Chaired by Nicholas Bruno & Don Carlucci*
10:10 AM - 10:30 AM	11764 - Inclusion of Rifling and Variable Centerline in Gun Tubes for Enhanced Modeling of Launch Dynamics *Mr. Charles Eichhorst, USA; Dr. William H. Drysdale, Mr. Michael Minnicino, Mr. David A. Hopkins*
10:30 AM - 10:50 AM	11937 - 5.56mm M855 Accuracy and Jump Measurements *Mr. Ilmars Celmins, USA*
10:50 AM - 11:10 AM	12029 - Modeling of the Dynamics of a 40 mm Gun and Ammunition System During Firing *Mr. Nicolas Eches, France; Mr. Didier Cosson, Mr. Quentin Lambert, Mr. André Langlet*
11:10 AM - 11:30 AM	12062 - Characterization of a Potting Material for Gun Launch *Dr. Aisha Haynes, USA; Dr. Jennifer Cordes*
11:30 AM - 11:50 AM	12063 - Gun Launch Dynamics of Pyrotechnic Materials *Dr. Aisha Haynes, USA; Mr. Justin John, Mr. Anthony Sherwood*
11:50 AM - 1:20 PM	Lunch - Regency Ballroom

1:20 PM - 3:20 PM	Explosion Mechanics Poster Session - Riverfront Hall *Chaired by Frederik Mostert & Stan DeFisher*
1:20 PM - 3:20 PM	Interior Ballistics - Ashe Auditorium *Chaired by Paul Locking & Michael Nusca*
1:20 PM - 1:40 PM	11956 - Detailed Ballistic Performance Characterization of 120-mm Mortar System with Different Flash Tube Configurations *Dr. Kenneth Kuo, USA; Dr. Eric Boyer, Mr. Heath T. Martin*
1:40 PM - 2:00 PM	11441 - The Numerical Optimization of the Novel Kinetic Energy Penetrator for Tank Guns *Dr. Mariusz Magier, Poland*
2:00 PM - 2:20 PM	12024 - A Numerical Tool for Evaluating Solid Propellants Ignition Models *Mr. Christophe Boulnois, France; Dr. Camille Strozzi, Dr. Amar Bouchama, Pr. Philippe Gillard*
2:20 PM - 2:40 PM	11494 - Modeling the Effects of Non-Gaseous Igniter Combustion Products on the Ignition of Gun Propellants *Mr. Clive R. Woodley, UK*
2:40 PM - 3:00 PM	11945 - Modeling Explosive Cladding of Metallic Liners to Gun Tubes *Mr. Jack M. Pincay, USA; Dr. Ernest L. Baker, Mr. David G. Pfau*
3:00 PM - 3:20 PM	12080 - Finite Element Modeling of Primer Impact to Understand the Dynamics of Misfires *Mr. Mark D. Lee, USA*
3:20 PM - 3:40 PM	Break in Exhibit Hall - Riverfront Hall
3:40 PM - 6:30 PM	Exhibit Hall Closed; Exhibitor Move-Out & Poster Dismantle
3:40 PM - 5:20 PM	Vulnerability - Ashe Auditorium *Chaired by Philip Cunniff & Ho Soo Kim*
3:40 PM - 4:00 PM	11886 - Experimental Methodology Using Digital Image Correlation to Assess Ballistic Helmet Blunt Trauma *Mr. James C. Gurganus, USA; Dr. Dixie Hisley, Mr. Andrew Drysdale*
4:00 PM - 4:20 PM	11794 - Survivability Evaluation of Blast Mitigation Seats for Armored Vehicles *Dr. Ming Cheng, Canada; Mr. Doug Bueley, Dr. Jean-Philippe Dionne, Dr. Aris Makris*
4:20 PM - 4:40 PM	11991 - Attenuation of a Blast Wave Through Cranial Bone *Dr. Amy C. Courtney, USA; Dr. Michael W. Courtney*
4:40 PM - 5:00 PM	12040 - DESCENT Modeling in Rotorcraft Vulnerability Assessment *Mr. Andrew W. Drysdale, USA; Dr. Matthew Floros*
5:00 PM - 5:20 PM	12065 - Ammunition and Weapon Effects in Confined Operational Urban Theatre in the Vicinity of Own Troops *Mr. Theo Verhagen, The Netherlands; Mr. Martin v.d. Voorde*
6:30 PM - 10:00 PM	Symposium Banquet - Hyatt Riverwalk *Dinner and dancing under the Florida night sky; Business/cocktail attire suggested*

FRIDAY, SEPTEMBER 16, 2011

7:00 AM - 12:15 PM	Registration Open - Lobby Level
7:00 AM - 8:00 AM	Continental Breakfast - Ashe Auditorium Foyer
8:00 AM - 10:00 AM	Terminal Ballistics & Impact Physics - Ashe Auditorium *Chaired by James Walker & Pierre Chanteret*
8:00 AM - 8:20 AM	11776 - Penetration of Rigid Rods into Sand *Dr. Stephan Bless, USA; W. Cooper, K. Wantawabi*
8:20 AM - 8:40 AM	11997 - Blast Response Analysis of Reinforced Concrete Slabs: Experimental Procedure and Numerical Simulation *Mr. Gustavo Morales-Alonso, Spain; Dr. David A. Cendón, Dr. Francisco Gálvez, Mr. Borja Erice, Prof. Dr. Vicente Sánchez-Gálvez*
8:40 AM - 9:00 AM	12035 - Effect of Frictions on the Ballistic Performance of a 3D Warp Interlock Fabric: Numerical Analysis *Mr. Cuong Ha-Minh, France; Dr. François Boussu, Dr. Toufik Kanit, Dr. David Crépin, Prof. Abdellatif Imad*
9:00 AM - 9:20 AM	12055 - Why Impacted Yarns Break at Lower Speed than Classical Theory Predicts *Dr. James D. Walker, USA; Dr. Sidney Chocron*
9:20 AM - 9:40 AM	12067 - Unusual Transverse Compression Response of Non-Woven Ballistic Laminates *Dr. Brian R. Scott, USA*
9:40 AM - 10:00 AM	12108 - Protection of Light Armours Against Shaped Charge Projectiles *Prof. Adam Wisniewski, Poland*
10:00 AM - 10:10 AM	Break - Ashe Auditorium Foyer
10:10 AM - 11:30 AM	General Session *Chaired by Klaus Thoma & Jack Pincay*
10:10 AM - 10:30 AM	12095 - AMRDEC Lethality Modeling and Simulation Methodologies for Aerial Targets *Mrs. Dedra C. Moore, USA; Mr. Dustin Clark, Mr. Brent Deerman*
10:30 AM - 10:50 AM	11730 - Development of Blast Enhanced Explosive for an Anti-Structure Warhead *Mr. Hendrik Lips, Germany*
10:50 AM - 11:10 AM	11865 - Measurement of Blast Reflected Overpressure at Small Charge Standoff with Tourmaline-Based Piezoelectric Transducers *Dr. Roger L. Veldman, USA; Dr. Mark W. Nansteel, Dr. Charles Chen*
11:10 AM - 11:30 AM	Dr. Manfred Held Memorial Presentation
11:30 AM - 12:00 PM	Presentation of Awards
12:00 PM - 12:15 PM	Presentation of the 27th International Symposium on Ballistics *Freiburg, Germany*
12:15 PM	Symposium Adjourned

POSTER SESSIONS & EXHIBITS

TERMINAL BALLISTICS & IMPACT PHYSICS POSTER SESSION
TUESDAY 1:20 PM - 3:20 PM

11441 - The Numerical Optimization of the Novel Kinetic Energy Penetrator for Tank Guns

Dr. Mariusz Magier, Poland

11444 - Estimation of Yield Stress in Tungsten Rods at High Strain-Rates by Taylor's Impact Technique

Dr. Mariusz Magier, Poland; Mr. Rafal Bazela, Mr. Edward Wlodarczyk, Mr. Jacek Janiszewski, Mr. Wojciech Koperski

11480 - Ballistic Analysis of New Military Grade Magnesium Alloys for Armor Applications

Mr. Tyrone L. Jones, USA; Dr. Katsuyoshi Kondoh

11484 - Study on Penetration Resistance of Tubular Spaced Armor by Jet

Mr. HeQuan Cao, China; XiaoNing Zhao, XianFeng Zhang, JianBo Wang, SuJie Sun

11490 - A Computational Constitutive Model for Glass Subjected to Large Strains, High Strain Rates, and High Pressures

Mr. Timothy J. Holmquist, USA; Dr. Gordon R. Johnson

11527 - A Model of Compressible Jet Penetration

Dr. William J. Flis, USA

11585 - Sensitivity of Johnson-Cook Constitutive Model Parameters in Modeling Penetration of Rolled Homogeneous Armor Steel Targets by Tungsten Rods

Mr. Stephen Schraml, USA

11669 - Mass-Flux Model for Non Metallic Reactive Armor

Dr. Meir Mayseless, Israel; Stefano Bianchi, Zachi Katzir, Sergi Chanukaev

11706 - Experimental and Theoretical Study of Interaction Process Between Projectiles Containing Fluoropolymer and Titanium and Aluminum-Based Targets

D.Sc. Eugene A. Khmelnikov, Russia; Alexey V. Styrov, D.Sc. Valery L. Rudenko, Vladimir I. Falaleev, Artyom V. Klimenko

11727 - PELE at Hypervelocity

Dr. Stephan J. Bless, USA; Mr. Bradley A. Pedersen

11728 - Effectiveness of Whipple Shields with Backplate Compared to Homogeneous Mild Steel Alone Against EFP Threats

Dr. Amer Hameed, UK; Mr. Ghulam Hussain, Dr. A.Q. Malik, Peter Barton

11750 - Lethality Analysis Based on a Fragmentation Model for Naturally Fragmenting Shells

Dr. Adam T. Zagorecki, UK; Dr. Amer Hameed, Mr. Anoop Shukla

11753 - Development of Brick and Mortar Material Parameters for Numerical Simulations Using the Holmquist-Johnson-Cook Constitutive Model for Concrete

Mr. Christopher S. Meyer, USA

11754 - Theoretical Analysis on the Interface Defeat of a Conical-Nosed Long Rod Penetration

Mr. Jicheng Li, China; Xiaowei Chen, F. Ning

11768 - Deceleration Analysis on Penetration Projectile Considering Mass Loss

Prof. Xiaowei Chen, China; L.L. He

11817 - Experimental and Computational Study on High Velocity Fragment Impacts

Mr. Fabien Rondot, France; Mr. Julien Nussbaum

11843 - Numerical Study on Kinetic Energy Projectile Penetrating Multilayer Medium Target

Mr. Jian Feng Lou, China; Mr. Zheng Wang, Mr. Fengguo Zhang, Mr. Longhe Liang

11850 - Supersonic Penetration by Jet into Concrete: Research of Shaped Charge for Creating Large Cavity Diameter

Mr. Xiao Qiangqiang, China; Huang Zhengxiang, Zu Xudong, Han Dong-mei

11857 - Time Resolved Engineering Metal Penetration Models

Mr. Geert Roebroeks, The Netherlands; Mrs. Elena Abadjieva, Mr. Erik Carton

11864 - Ballistic Performance and Failure Mode of High Performance 2139-T8 and 7449-T6 Aluminium Alloys

Dr. Cedric Gasqueres, France; Dr. Julien Nussbaum

11866 - Transverse Impact Response of a Linear Elastic Ballistic Fiber Yarn

Mr. Bo Song, USA; Mr. Hwun Park, Mr. Wei-Yang Lu, Mr. Weinong Chen

11873 - Properties of Cross-Plied Unidirectional Aramid Fiber Laminates for a New Detailed Military Specification: MIL-DTL-32378

Dr. James Singletary, USA; Dr. Brian Scott, Mr. Richard Squillacioti, Dr. Karl Chang

11874 - The Dynamic Response of Kevlar and Float Glass Panels to Blast Loading

Mr. Izak Marius Snyman, South Africa; Mr. Frederik Mostert

11876 - Fiber Interfacial Surface Energetics for Controlled Adhesion

Dr. Jeffrey A. Chambers, USA; Ms. Rachel L. McSwain

11879 - The Role of the Wave Impedance of the Sandwich Material in the Composite Armor Against Shaped Charge Jet

Mr. Xu-Dong Zu, China; Zheng-xiang Huang, Qiang-qiang Xiao, Xin Jia

11880 - An Experimental Technique to Characterise the Dynamic Response of Materials, or Material Combinations, to Explosive Blast

Mr. Frederik Mostert, South Africa; Izak Snyman, Marius Olivier

11888 - The Mechanisms of Damage In Ballistic Fibers

Mr. Walter G. McDonough, USA; Dr. Gale A. Holmes, Mr. Kirk Rice, Ms. Amanda Forster, Dr. Haruki Kobayashi, Jae Hyun Kim

11889 - Ballistic Evaluation of Aluminum 7085-T7E01 and T7E02

Mr. Denver B. Gallardy, USA

11891 - Sporicidal Effects of Iodine-Oxide Thermite Reaction Products

Dr. Stephan Bless, USA; Mr. Rod Russell, Ms. Alexandra Blinkova, Ms. Tiffany Chen, M. Pantoya

11898 - 3D Flexible Hybrid Textile Structures Against High Velocity Impact

Dr. François Boussu, France; Jerome Vilfayeau, Julien Nussbaum

11905 - Experimental and Numerical Study of Aluminum 6061-T6 Fragmentation Process at Very High Strain Rates

Dr. Vitaly Leus, Israel; Mr. Yair Neumann, Dr. Eliahu Racah

11908 - Armoured Vehicle Response to the Roadside Mine Threat

Mr. Stanislav Rolc, Czech Republic; Mr. Jaroslav Buchar, Mr. Josef Kratky, Mr. Jan Krestan

11910 - Penetration Behaviour Simulation of Shaped Charge Jets in Water Filled Targets

Mr. Dev Raj Saroha, India; Mr. Davinder Kumar, Mr. Yashpal Singh

11915 - A Model for Behind Armor Debris from EFP Impact

Mr. Ho Soo Kim, South Korea; Dr. Werner Arnold, Dr. Thomas Hartmann, Mr. Ernst Rottenkolber, Dr. Andreas Klavzar

11920 - Modeling and Simulating the Performance of Transparent Spinel and the Effect of Defects on Dynamic Response

Dr. Costas G. Fountzoulas, USA; Dr. James M. Sands

11924 - Eulerian vs. Lagrangian Methods in the Finite Element Analysis of Small Caliber Thick Plate Penetration Events

Mr. Raymond Chaplin, USA

EXTERIOR BALLISTICS POSTER SESSION
TUESDAY 3:40 PM - 5:20 PM

11672 - A Computational Approach to the Determination of Tank Munitions Safety Zones

Aron Pila, Israel; Vadim Kogan, David Touati, S. Peles

11757 - The Effect of a Variable Crosswind on Flat-Fire Trajectories – A Unique Measuring Technique and Compensation Methodology

Mr. Yoav Gur, Israel; Mr. Eugene Adamovski, Mr. Michael Gringauz

11783 - Multi-Core Computing Cluster for Monte-Carlo Analysis of GN&C Systems for Projectiles

Dr. Mark D. Ilg, USA

11845 - GPS-Based High Dynamic Projectile Flight Ballistic Real-Time Measurement Techniques

Dr. Yanning Gui, China; Prof. Yan Yang, Huang Zheng, Cheng Hongtao

11855 - Despin and Roll Attitude Control of a 2D Guided Fuze Kit

Mr. Roelof du Plessis, South Africa; Dr. Gerrit Viljoen

11858 - Magnus Effect: Physical Origins and Numerical Prediction

Dr. Roxan Cayzac, France; Eric Carette, Pascal Denis, Philippe Guillen

11881 - In-Bore Yaw Effects on Lateral Throwoff and Aerodynamic Jump Behavior for Small Caliber Projectiles Firing Sidewise From Air Vehicles

Dr. Elias E. Panagiotopoulos, Greece; Dr. Dimitrios N. Gkritzapis

11885 - Recent Improvements in Ballistic Data Reduction: Data Fusion

Mr. John R. Burnett, Jr., USA; Mr. John Whyte, Mr. Wayne H. Hathaway, Mr. Alan Hathaway, Mr. Mark Steinhoff

11929 - Comparison of Prediction Methods for Ricochet of a 30mm Projectile

Mr. Stephen S. Recchia, USA; Mr. Ernesto Vazquez

11967 - Hypersonic Aerothermal External Flow Field Depicted from Immersed Boundary Technique

Dr. Frederic Plourde, France; Dr. Christophe Grignon, Dr. Chi Cong Nguyen, Van Thuan Luu

11970 - Effects of Aerodynamic Coefficient Uncertainties on Trajectory Simulation of a Short-range Solid Propellant Free Rocket

Mr. Weerawut Charubhan, Thailand; Mr. Pawat Chusilp; Mr. Navapan Nutkumhang

11984 - Adjoint Analysis of Guided Projectile Terminal Phase

Mr. Timo Sailaranta, Finland; Mr. Ari Siltavuori

12021 - Inverse Aerodynamic Coefficients Identification of a Kinetic Energy Projectile from Flight Data

Miss Hélène Demailly, France; Mr. Franck Delvare, Mrs. Settie Heddadj, Mr. Christophe Grignon, Mr. Patrice Bailly

12027 - A Method of Self-Adaptive Container Opening Control for Rocket Assisted Cargo Mortar Projectile

Mr. Li Dong-Guang, China; Mr. Yang Rui-Wei, Mr. Yang Deng-Hong, Ms. Cui Xue-Jun

12032 - A Study on the Aerodynamic Characteristics for a Spin-Stabilized Projectile with PGK

Dr. SangEon Je, South Korea; Mr. Hyunsung Jung, Mr. Minsu Park, Prof. Taehwan Cho

12054 - Numerical Simulation and Experimental Study of Flowfield Around a Bullet with a Partial Core

Mr. Usiel Silva, Mexico; Dr. Juan M. Sandoval, Dr. Luis A. Flores, Dr. Narcizo Muñoz, Víctor Hernández

12077 - The Establishment of Threshold Criteria for Automated Acceptance Test Equipment Based on Battlefield Use of Tracer Ammunition

Ms. Stefana Reilly, USA; Mr. Rob Allen

INTERIOR BALLISTICS POSTER SESSION
WEDNESDAY 8:10 AM - 9:50 AM

11633 - Quasi-Dimensional Interior Ballistic Model and Numerical Simulation of Combustion Light Gas Gun

Mr. Ning Liu, China; Mr. Xiang-yan Zhang

11748 - Experimental and Numerical Investigations on Traveling Charge Gun Using Liquid Fuels

Mr. Xin Lu, China; Mr. Yanhuang Zhou, Mr. Yonggang Yu

11795 - Study of Bulk-Loaded Liquid Propellant Combustion Propulsion Processes with Stepped-wall Combustion Chamber

Prof. Yong-gang Yu, China; Miss Xue-xia Chang, Miss Na Zhao, Miss Shan-shan Mang, Yanhuang ZHOU

11798 - Improved One-Dimensional Unsteady Modeling of Thermally Choked Ram Accelerator in Sub-Detonative Velocity Regime

Dr. Yufeng Yao, UK; Dr. Tarek Bengherbia, Prof. Pascal Bauer, Dr. Marc Giraud, Dr. Carl Knowlen

11806 - Ballistic Diagnostic Methodologies for Gun Propulsion: An Overview

Dr. Lang M. Chang, USA

11812 - Ram Accelerator – State of the Art

Prof. Pascal A. Bauer, France; Dr. Carl Knowlen, Dr. Marc Giraud, Dr. Yufeng Yao, Dr. Tarek Bengherbia

11853 - Research on Burning Characteristics of Microfoam Propellants

Prof. Fu-ming Xu, China; San-Jiu Ying, Xi-ru Chen

11868 - Primer Force and Chamber Pressure Measurements at 5.56 mm Caliber

Dr. Richard A. Beyer, USA; Mr. Joseph W. Colburn

11878 - Reduced Vulnerability $BKNO_3$ Based Igniters for Gun Systems

Mr. Eugene Rozumov, USA; Dr. Thelma G. Manning, Dr. Joseph M. Laquidara, Duncan Park, Kimberly Chung, John O'Reilly, Jeffrey Wyckoff, David Thompson, Elbert Caravaca, Carlton P. Adam, Viral Patel

11890 - The Influence of Propellant Grain Shape, Size and Composition on Solid Phase Motion and Heat Transfer to the Gun Tube

Mr. Albert W. Horst, USA

11902 - Performance Analysis of Interior Ballistics According to Solid Propellant Positions in Chamber

Mr. Jinsung Jang, South Korea; Mr. Hyunggun Sung, Prof. Taeseong Roh, Prof. Dongwhan Choi

11904 - Laboratory Stand for Scale Test of Rocket Propelled Grenades Firing

Mr. Przemyslaw Kupidura, Poland; Mr. Zbigniew Leciejewski, Mr. Zbigniew Surma, Mr. Radoslaw Trlbliski

11907 - On Similarity of Combustion Conditions During Comparative Closed Vessel Tests

Mr. Zbigniew Leciejewski, Poland; Mr. Zbigniew Surma

11939 - Asymmetrical Muzzle Wear – A Historical Perspective

Dr. Elaine M. Humiston, USA; Jeanne C. Brooks

11955 - Initial Temperature Effect on M1020 Ignition Cartridge Behavior

Mr. Heath T. Martin, USA; Ryan W. Houim, Dr. Eric Boyer, Prof. Kenneth K. Kuo

11961 - Explicit Finite Element Model for Determining Influence of Cartridge Case Material Properties on Small Caliber Weapon Function

Mr. Daniel R. Gubernat, USA; C. Fischer

11974 - Simulation of Contamination Prevention for Optical Window in Laser Ignition Systems of Large-Caliber Guns

Dr. Xiaobing Zhang, China; Changjun Ma

11975 - Research for a Projectile Positioning Structure for Stacked Projectile Weapons

Dr. Xiaobing Zhang, China; Qiao Luo

11989 - Multi-Dimensional Two-Phase Flow Modelling Applied to Interior Ballistics

Dr. Julien Nussbaum, France; Philippe Helluy, Dr. Jean-Marc Hérard, Dr. Barbara Baschung

11995 - Benefits of Two Dimensional Internal Ballistics Modelling for Small Calibre Cased Telescoped Ammunition

Dr. Iain Robertson, UK; Dr. Martin P. Pocock, Mr. Clive Woodley, Mr. Simon Georgi, Miss Rebecca Threlfall, Mr. Chris Guyott

12031 - Investigation on Ignition and Combustion Process in Granular Solid Propellant Chamber

Dr. Hiroaki Miura, Japan; Prof. Akiko Matsuo, Dr. Yuichi Nakamura

12039 - Internal Ballistics Simulation of a NAWC Tactical SRM

Dr. Enrico Cavallini, Italy; Prof. Bernardo Favini, Prof. Maurizio Di Giacinto, Dr. Ferruccio Serraglia

12043 - Analyses of Fatigue Life Estimate for a Pressure Tap in a 40mm Gun Breech

Ms. Caitlin M. Weaver, USA; Dr. Jennifer A. Cordes, Mr. Lyonel Reinhardt, Dr. Aisha S. Haynes, Paulo A. Rigg

12072 - Deterred Propellant Optimization for Gun Systems

Mr. Carlton Adam, USA; Dr. Eugene Rozumov

12079 - Ballistic Performance of Steels and Aluminums in FE Firing Simulations

Dr. Justin Mach, USA; Mr. Mark Lee

12084 - Interior Ballistics of Co-Layered Gun Propellant

Dr. Thelma G. Manning, USA; Duncan Park, Kenneth Klingaman, Michael Leadore, Dr. Barrie Homan, Dr. Edmund Liu, Dr. James A. Luoma

LAUNCH DYNAMICS POSTER SESSION
WEDNESDAY 10:10 AM - 11:50 AM

11469 - Stress Relaxation of Composite Gun Barrels with High Tensioned Overwrap – Modeling

Dr. Jerome T. Tzeng, USA; Ryan Emerson

11481 - Measurement Principle of Moment of Inertia for Turret

Mr. Baoyuan Wang, China; Xiao-jun Shao, Hui-min Wu, Gang Heng, Fa-ming Zhou, Hua-sa Yu

11671 - Analysis of 120mm Tank Gun Failure Due to Bore Obstruction

Dr. David Touati, Israel; Irene Gelfeld, Ilan Azulay, Felix Shub

11673 - Launch Dynamics of the APAM-MP Round

Dr. David Touati, Israel; Ilan Azulay, Yoav Gur, Boris Manilov

11827 - Simulation and Instrumentation Used to Develop a Super-Caliber Fin Set for a Precision Mortar

Mr. John A. Condon, USA; Brad Davis, Peter Muller, Ben Topper

11941 - Failure Analysis of .50 Caliber M20 API-T Bullet Burst

Mr. David W. Stubler, USA; Mr. Timothy A. Spears

11947 - Influence of Material Properties on Sabot Performance

Mr. Michael Minnicino, USA

11972 - The Effect of Threaded Joints on the Transmission of Vibrations During Gun Launch

Mr. Lyonel Reinhardt, USA; Dr. Jennifer Cordes, R. Terhune

12088 - Gun Launch Dynamics – Benchmarking State of the Art

Dr. Donald E. Carlucci, USA; Dr. James F. Newill, Mr. Rollie H. Dohrn, Jr.

VULNERABILITY POSTER SESSION
WEDNESDAY 1:10 PM - 2:10 PM

11485 - Blast Mitigation Seats for Armored Platforms – Development and Evaluation Methodology

Dr. Moshe Ravid, Israel; Nimi Shapira, Dr. Zvi Assaf, Dr. Felix Aizik, Dmitry Narodizky, Mr. Hadar Raz, Mr. Doobie Avraham

11675 - A Methodology to Predict Personnel Injury from Reflective Spall

Mrs. Rebecca VanAmburg, USA

11724 - Ballistic Gelatine Behaviour Under Quasi-Static and Dynamic Loadings

Mr. L. Koene, The Netherlands; Mr. J.L. Barou, Mr. P. Viot

11751 - Fragment Analysis for the Joint Trauma Analysis and Prevention of Injury in Combat (JTAPIC) Program

Ms. Karen Pizzolat, USA

11836 - Vulnerability Model Validation for Commercial Aircraft

Dr. Mark A. Fry, USA

11871 - An Automated Methodology for Calculating Optimized Preset Fuze Time Delay Function in Conjunction with the AVAL Code

Dr. Gideon J.F. Smit, South Africa; Dr. Cornelis J. Terblanche

11882 - Analysis of Existing Injury Criteria in Order to Evaluate the Severity of Thoracic Impact Injury

Mr. Nicolas Eches, France; Mr. André Langlet, Mr. Julien Pavier, Mr. Jean-François Jacquet, Mr. Roxan Cayzac

11899 - The Impact of High Accuracy Target Geometry in Modeling and Simulation to Support Live Fire Test and Evaluation

Mr. Scott N. Hornung, USA

11906 - A Comprehensive Approach to Characterizing the Hazards of Explosive Countermeasures with Respect to Dismounted Troops

Ms. Patricia S. Frounfelker, USA; Mr. Stephen P. Swann, Mr. Gregory K. Dietrich

11919 - MUVES 3 - Vulnerability/ Lethality Analysis Tool of the Future

Mrs. Elaine M. Hunt, USA; Mr. Mark Burdeshaw

11935 - Overview of MUVES 3 and the MUVES 3 V/L Service

Mr. Ronald A. Bowers, USA

11952 - Utilizing Vehicle Response Data from Under-Body Blast Tests

Mr. Brian Benesch, USA

11960 - WeaponFX Vulnerability and Optimization Code for Fragmenting Warheads

Mr. John Tartis, USA; Mr. Partick D. Buckley

11962 - Ballistic Vulnerability Analysis of Ground Combat Vehicles, Understanding the Process and Impact

Ms. April Siano, USA

11979 - Standardization of Skin Penetration Assessment for Non-Lethal Impact Projectiles

Dr. Alexandre Papy, Belgium; Mr. Cyril Robbe, Mr. Nestor Nsiampa

11985 - Impact Measurements of Different 40mm Non-Lethal Sponge Grenades

Mr. Cyril Robbe, Belgium; Mr. Nestor Nsiampa, Dr. Alexandre Papy

11987 - Numerical Simulation of Kinetic Energy Non-Lethal Projectiles on Human Thorax

Mr. Nestor Nsiampa, Belgium; Mr. Cyril Robbe, Dr. Alexandre Papy

12018 - Rapid Assessment of the Vulnerability of a Structure to Blast Effects

Dr. Victoria E. Ingamells, UK; Dr. Ian G. Cullis, Mr. Michael Hamblin, Mr. Paul Morrissy

12037 - Numerical Modeling of Rocket Warhead Detonation and Fragmentation

Dr. Joseph D. Baum, USA; Dr. Daniel G. Williams, Dr. Orlando A. Soto, Dr. Fumiya Togashi, Prof. Rainald Lohner

12075 - Capability Improvements for Modeling Fragment Impact in ALE3D

Dr. Lara D. Leininger, USA; Sarah Minkoff, Dr. Robert Dorgan, Stanley DeFisher, Dr. Rose McCallen, H. K. Springer

TERMINAL BALLISTICS & IMPACT PHYSICS POSTER SESSION

THURSDAY 10:10 AM - 11:50 AM

11928 - Shock Impact Failure of Polycrystalline Microstructures: Modeling and Simulation

Dr. Martin O. Steinhauser, Germany

11930 - Rigid-body Concrete Penetration and the Sectional Momentum Effect

Mr. Garet Itz, USA; Mr. Darrel Barnette

11934 - Polymers as Potential Shaped Charge Liner Materials

Dr. Michael R. Edwards, UK; Mr. Romello Arulanandam, Mr. Stefan M. Hille

11943 - A Comparison of Penetration Algorithms: Predictions vs. Test Data for Kinetic Energy Rods

Mr. John R. Auten, USA

11950 - Investigation of Projectile Trajectory in Multi-hit Scenarios and the Influence of Damage Characteristics in Glass-Ceramic Transparent Armor

Mr. Timothy G. Talladay, USA; Ms. Katherine T. Leighton, Mr. John J. Carberry, Mr. Carsten Weinhold, Dr. Douglas W. Templeton

11951 - Innovative Transparent Armor Concepts

Mr. Erik Carton, The Netherlands; Mr. Hans Broos

11953 - Detrimental Effects of Flexible Linear Shaped Charge (FLSC) to Nearby Plates Due to Varying Backspace Distance

Mr. Cagin G. Bingol, Turkey; Dr. Raif O. Yildirim

11954 - Soft Recovery of Medium-Caliber Projectiles

Dr. Stephen Ray, USA; Mr. Michael Hermanson

11963 - Experimental Investigation on Dynamic Crack Propagating Perpendicularly Through Interface in Glass

Mr. Hwun Park, USA; Dr. Weinong W. Chen

11966 - Light Metal-Ceramic Passive Armour for Special Application

Mr. Bartlomiej Plonka, Poland; Dr. Juliusz Senderski, Dr. Adam Wisniewski

11973 - Discontinuity in the Energy Absorbed During Ballistic Impact in Aluminum Targets

Mr. Eldad Shemer, Israel; A. Armon, Z. Bar

11976 - New Generation Maraging Steel and High-Carbon Bainitic Steel for Armours

Mr. Jaroslaw Marcisz, Poland; Mr. Wojciech Burian, Bogdan Garbarz, Mariusz Adamczyk, Adam Wisniewski

11978 - Numerical Investigation of Formation of Steel Linered Shaped Charge Jets

Mr. M. Sarper Yavuz, Turkey; Dr. R. Orhan Yildirim

11980 - A Concrete Tension Failure Model Under Impact Loading

Dr. Wang Zheng, China; Dr. Lou Jianfeng, Dr. Liang Longhe, Dr. Zhang Fengguo

11982 - The Effect of Temperature on AEP 55 Vol. 2 Level 1 DM-31 Surrogate Performance

Dr. Moshe Ravid, Israel; Mr. Nimi Shapira, Dr. Stanislav Rolc, Mr. Ofer Medem, Dr. Felix Aizik, Dr. Josef Kratky, Dr. Jan Krestan

11983 - Improving the Design Capability for Fragment Protection

Dr. Nicholas J. Lynch, UK; Leslie Nyogeri, Philip Church

11986 - Experimental-Numerical Study of Inclined Impact in Al7075-T7351 Targets by 0.3 AP Projectiles

Dr. Zvi Anosh Asaf, Israel; Mr. Vadim Favorsky, Mr. Asaf Borenstein, Mr. Amit Vizel, Dr. Felix Aizik, Dr. Moshe Ravid, Mr. Nimi Shapira

11990 - Influence of Impacting Explosive Formed Projectiles on Long Rod Projectiles

Mr. Stanislav Rolc, Czech Republic; Mr. Jaroslav Buchar, Mr. Zbynek Akstein

11992 - Impact Test of Organic Radical Secondary Battery

Dr. Motoyoshi Ozaki, Japan; Mr. Yusuke Aizawa, Mr. Kensaku Tomura, Dr. Kaichiro Nakano, Dr. Shigeyuki Iwasa

11994 - Experimental Investigation of the Penetration and Perforation of Building Materials by Projectiles

Mr. Andreas Heine, Germany; Mr. Karl E. Weber, Mr. Matthias Wickert

12000 - Optimum Design of Magnesium-Based Multi-Layered Hybrid Armor

Mr. Wonseok Tae, South Korea; Mr. Gunin Kim, Mr. Jonggu Lee, Mr. Maenghyo Cho

12001 - The Effect of Surface Conditions on Dynamic Crack Propagation Through an Interface in Glass

Mr. Hwun Park, USA; Dr. Weinong W. Chen

12010 - Critical Impact Velocity of a Cemented Carbide Projectile Penetrating a Water Target

Mr. Olof Andersson, Sweden; Dr. Patrik Lundberg, Dr. Andreas Helte, Dr. Pernilla Magnusson

12011 - A Modified Johnson-Cook Failure Model for Tungsten Carbide

Dr. John F. Moxnes, Norway; Mr. Jan Arild Teland, Mr. Stian Skriudalen, Mr. Svein Morten Bergsrud

12013 - Fracture Mechanics of Long Rod Projectiles Subjected to Oblique Moving Plates

Dr. Ewa Lidén, Sweden; Dr. Andreas Helte

12016 - Volume Transfer Functions for Aluminium Lined Shaped Charge Penetration into Concrete

Dr. Cornelis Jean Terblanche, South Africa; Dr. Milton Maritz

12028 - Modeling Kinetic Energy Projectile Failure During Strucured Armour Perforation

Mr. Nicolas Eches, France; Mr. Herve Couque

12033 - Deflecting and Rotating Rigid Projectile Hitting Plate Edge

Dr. Meir Mayseless, Israel; Mr. Zvi Cooper, Mr. Yechiel Reifen, Dr. Dan Yaziv

12050 - Damage Mechanisms in Dynamically Loaded AISI 4130 Steel

Dr. Thomas A. Mason, USA; Jessica Stanfield, Dr. Jamie B. Neidert

12051 - Non-Orthogonal Kevlar® Fabric Architectures for Body Armor Applications

Dr. Ronald G. Egres, USA; Dr. Leopoldo A. Carbajal, Clifford. K. Deakyne

12052 - Evaluation of the Response of Friction Stir Processed Panels Under Ballistic Loading

Mr. Timothy Johnson, USA; Mr. Brandon Hinz, Dr. Michael West, Dr. Marius Ellingsen, Dr. Christian Widener, Bharat K. Jasthi, Karim H. Muci-Küchler

12053 - Simulation of Small Ammunitions in Aviation Applications

Mr. Daniel John, Germany; Mr. Robert Bailey, Mr. David Smyth, Mr. Frank Weidermann, Mr. Udo Berthold, Christian Radtke

12086 - Balancing Ballistic and Back-Face Deformation in Helmets: The Role of Alternative Resins, Fibers, and Fiber Architecture in Mass-Efficient Head Protection

Dr. Lionel Vargas-Gonzales, USA; Dr. Shawn M. Walsh, Dr. Brian R. Scott

12087 - Application of a Ductile Damage Model to Ballistic Impact Analyses

Mr. John Ryan, USA; Mr. Shawn Rhodes, Mr. Steven Stawarz

12142 - Consequence of Selecting Deep Drawing as a Performing Technique in the Production of Combat Helmets

Mr. Philip M. Cunniff, USA

12144 - Ballistic Testing of Nanocrystalline Hybrid Plates

Dr. Francisco Galvez, Spain; Jaime Frontán Vicente, Antoine Jérusalem, Yuming Zhang, Ming Dao, Jian Lu

12148 - Computational Hydrocode Study of Target Damage Due to Fragment-Blast Impact

Mr. Thomas J. Hatch-Aguilar, USA; Dr. Fady M. Najjar, Dr. Edwin W. Szymanski

EXPLOSION MECHANICS POSTER SESSION

THURSDAY 1:20 PM - 3:20 PM

11183 - Material Models for Tantalum – A Validation Study for EFP Applications

Dr. Magnus Bergh, Sweden; Dr. Andreas Helte, Jonas Lundgren

11462 - IM Testing and Initiation Trials of the IMX-101 Explosive in the M795 Projectile

Mr. Anthony Di Stasio, USA; Charlie Patel, Ductri Nquyen, Erik Wrobel

11491 - A Probe into the Applicability of Shock Similarity Laws for Underwater Explosion of Aluminiferous Explosive

Mr. Ji-bo Zhao, China; Mr. Duo-wang Tan, Mr. Yuan-ping Zhang

11492 - The Effect of High Impact Environment on the Fire Set of In-line Fuze

Zhu Hong-zhi, China; Yang Yong Hui, Ruan Zhaoyang

11767 - Research on the Deformation Process of a Thin-Walled Metal Tube Subjected to a Pulsed Magnetic Dynamic Load

Mr. Ming Xia, China; Mr. Zhengxiang Huang, Mr. Xiaohui Gu, Mr. Yezhong Wang, Mr. Xin Jia

11796 - The Analogue Simulation Research About the Cloud Detonation Wave's Propagation Process of FAE Warhead

Mr. Ri-sheng Hou, China; Mr. Shao-bo Cheng, Mr. Hui Xie, Mr. Tie-min Xue

11901 - Correction of Gurney Equation for Asymmetric Sandwich in Relation to Linear EFP

Dr. Zbynek Akstein, Czech Republic; Mr. Ladislav Riha, Assoc.Prof. Stanislav Rolc

11936 - Evaluation of Steel Reinforced Fiber Cases for Army Applications

Dr. Thuvan Piehler, USA; Mr. Richard Benjamin

11938 - Characterization of Explosively Formed Steel Fragments Using High Speed Imaging

Mr. Richard Benjamin, USA; Dr. Thuvan Piehler, Dr. Matthew Biss

11959 - Detailed Investigation into the Scaling of Mine Blast Loading to Armors and Vehicles

Mr. Scott A. Mullin, USA; Erick Sagebiel, James Mathis, Joseph Bradley, Carl Weiss, P.A. Cox

11964 - An Experimental Study on an Enhanced Focused Fragmentation Warhead

Mr. Sun Chuanjie, China; Hu Yanhui, Lu Yonggang, Feng Gaopeng, Yang Qi

11969 - Fragmentation of 155mm Artillery Grenade, Simulations and Experiment

Ms. Anne Kathrine Prytz, Norway; Gard Ødegårdstuen

12003 - Application of a Soil Model in the Numerical Analysis of Landmine Interaction with Protective Structures

Mr. Michael Saleh, Australia; Prof. Lyndon Edwards

12004 - Lethality Assessment of High Explosive (HE) Warhead with Preformed Fragments

Dr. Ganchai Tanapornraweekit, Thailand; Weerachart Kulsirikasem

12006 - Experimental Studies of Scalable Effects Warhead Technologies

Dr. Markus Graswald, Germany; Dr. Werner Arnold

12022 - Non-Initiating Precursor Charge Technology Against ERA

Dr. Andreas Helte, Sweden; Mr. Jonas Lundgren

12023 - Development of a Subsonic Anti-Structure-Penetrator

Mr. Hendrik Lips, Germany; Mr. Rolf Rittel

12060 - Investigation of Acceleration Behavior of Shaped Charge Liners

Mr. Eser Gürel, Turkey; Mr. Burak Tarkan

12085 - Parallel Detonation Shock Dynamics Algorithm for Insensitive Munitions Using ALE3D

Mr. David Pfau, USA; Dr. Fady Najjar, Dr. Jin Yao, Dr. Brian McCandless, Dr. Albert Nichols III

12106 - A Small Scale Unitary Demolition Charge

Mr. Daniel Boeka, USA; Arthur S. Daniels, Neal Ouye, Dan Suarez, Steve Hancock

12150 - Axisymmetic Finite Element Simulation of Shape Charges

Mr. Devon Downes, Canada; Dr. Manouchehr Ensan, Dr. Amal Bouamoul, Dr. Yves Baillargeon

EXHIBITORS

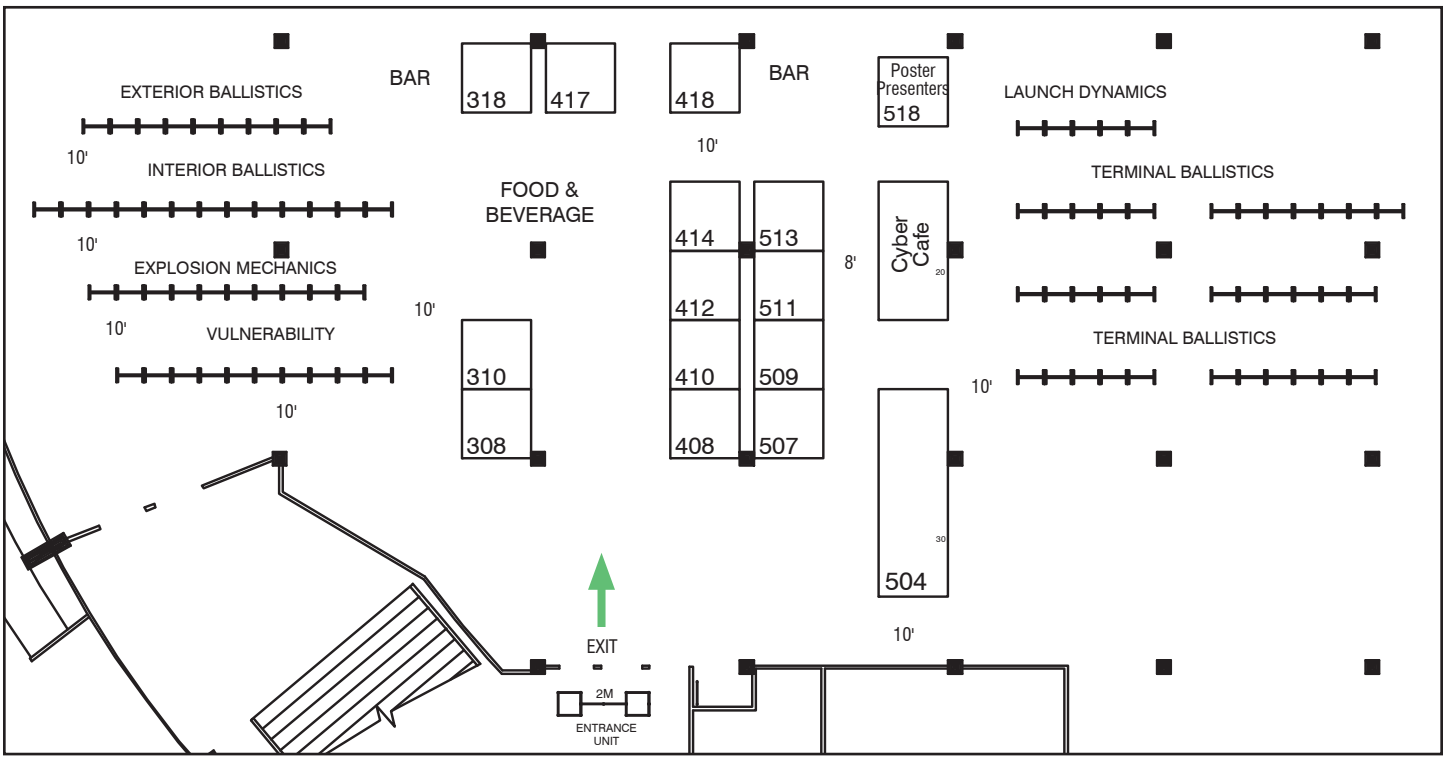

AWARD INFORMATION

THE ROSALIND AND PEI CHI CHOU AWARD FOR YOUNG AUTHORS

The young author of the paper must be 35 years of age or younger at the time of the symposium. The paper may have multiple authors, however, the young author must have made a major contribution to the paper. The young author must be registered at the symposium and must give the oral presentation or the poster presentation to be eligible for the Award.

THE LOUIS & EDITH ZERNOW AWARD

This award is given by Louis and Edith Zernow to the author of the paper with the most significant contribution to the advancement of "fundamental understanding" in the fields of ballistic science.

All papers, both oral and poster, will be considered eligible and reviewed for this award. No application is required. The selection is based solely on technical content of the published paper.

THE NEILL GRIFFITHS MEMORIAL AWARD

The Griffiths Award is presented to the author(s) of the paper judged to have made the most significant contribution to shaped charge technology at the International Symposium on Ballistics.

All papers, both oral and poster, will be considered eligible and reviewed for this award. No application is required. The selection is based solely on technical content of the published paper.

THE SOUTH AFRICAN BALLISTICS ORGANISATION (SABO) AWARD

The SABO Award is presented to the author(s) of the best poster as displayed and presented to appointed adjudicators. The presence of the author at the poster during the session is of paramount importance.

The objective of this award is to inspire poster presenters to present their work in creative, legible and professional fashion thus enhancing the poster sessions as a quality medium for the exchange of information during the symposium.

A maximum of three posters from each poster session will be nominated for the award by the poster chairmen. All nominations will be evaluated on equal footing by the adjudication committee for visual quality, creative skill and layout, and a winner will be selected from the nominations.

THANK YOU TO OUR SPONSOR!

QinetiQ North America

QinetiQ North America, Inc. is a world leader in the development and production of defense and security technology solutions, providing a wide range of products, solutions and services to the defense, civilian government and commercial markets. Headquartered in McLean, Virginia, QinetiQ North America Inc., is a subsidiary of QinetiQ Group PLC. For more information, visit www.QinetiQ-NA.com.

The company's Land Systems division provides a comprehensive suite of survivability solutions to protect the Warfighter in any environment, including ground vehicle and aircraft armor, RPG defeat solutions, blast mitigating seating solutions, precision air drop systems, integrated Warfighter systems, egress lighting and gunfire detection technology to name a few.

QNA is the world's largest add-on armor manufacturer for fixed wing aircraft. The company has delivered armor upgrades on every C-5 and C-17 in the US fleet, and the majority of C-130 aircraft in the US fleet and those of 16 other countries. QNA's LAST® Armor vehicle protection products and flexible ballistic spall liners protect Warfighters in a broad range of ground vehicles.

The Q-Net™ lightweight RPG protection system is best in class for protecting vehicles against the prolific RPG threat. Q-Net is sixty percent lighter than conventional RPG defeat systems, and offers 360 degree protection and multi-hit capability. This combat-proven solution is deployed on more than 8,000 vehicles and has the highest defeat rate of any passive solution.

QinetiQ North America is currently supplying Individual Gunshot Detection Systems (IGDS) to the US Army. These low profile, shoulder worn acoustic targeting systems (SWATS™) detect incoming small arms fire and report the threat's range and bearing in both audible and visual formats in less than one second. The US Army and US Marine Corps have selected SWATS as their technology solution of choice for individual gunfire detection systems.

QinetiQ North America delivers world-class technology, responsive services and innovative solutions for global markets, focusing on government and commercial customers. Its engineers, scientists and other professionals deliver high quality products and services that leverage detailed mission knowledge and proven, reliable tools and methodologies to meet the rapidly changing demands of national defense, homeland security and information assurance customers.

NOTES

THANK YOU TO OUR SPONSOR!

QinetiQ

North America

11487

DEVELOPMENT OF A NOVEL CERAMIC ARMOR SYSTEM: ANALYSIS AND TEST

David L. Hunn, Ph.D. and Sang J. Lee, Ph.D.

Lockheed Martin Missiles and Fire Control
Dallas, Texas 75265

972.603.1842 david.hunn@lmco.com

LOCKHEED MARTIN

•Optimization of new armor systems must be underpinned by a fundamental understanding of high strain rate dynamic events and subsequent material response and failure mechanisms during the impact and penetration event.

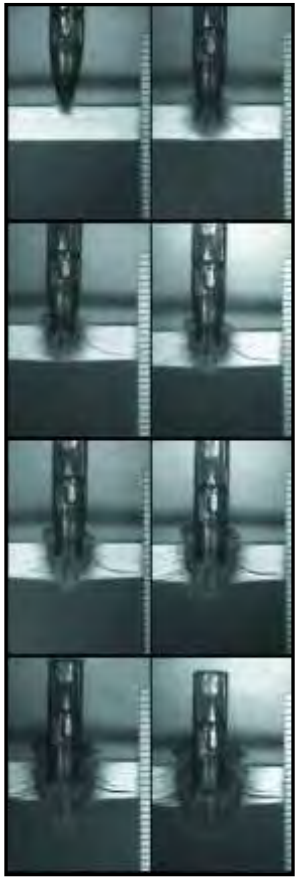

•Development of hybrid armor systems frequently feature combinations of hard ceramics, composites, and metallics in tailored configurations seeking to optimize ballistic performance, weight, volume, and cost.

•The complexity of the physics during the ballistic event makes isolation of armor system key performance parameters difficult, involving mechanisms such as penetrator fracture or blunting, penetrator erosion, loading of armor elements, fracture of armor elements, loading of (and erosion due to) the resulting rubble bed, momentum transfer, ejection of debris, shock and stress wave propagation and interaction, and residual kinetic energy absorption.

• Armor system design must consider each of these mechanisms for increased efficiency.

•Our approach focused on use of discrete embedded ceramic elements (threat defeat, multi-hit and crack arresting improvements), of specific shape and size (shock wave control, rubble bed confinement, threat defeat), separated by low impedance polymers (shock wave and crack control) with suitable cover plates and back-up plates (rubble confinement, dwell increase, momentum transfer).

•Development was guided by and relied heavily on judicious use of analytical predictions correlated with ballistic testing and post-test failure morphology investigations.

•Our approach started with single element studies, followed by multi-component modeling, which were then followed by full armor system modeling. The bulk of our analysis used phenomenological modeling approaches (finite element, particle dynamics and mixed finite element-particle formulations).

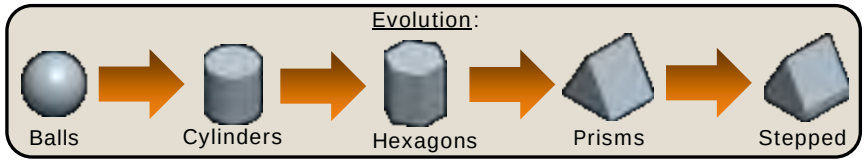

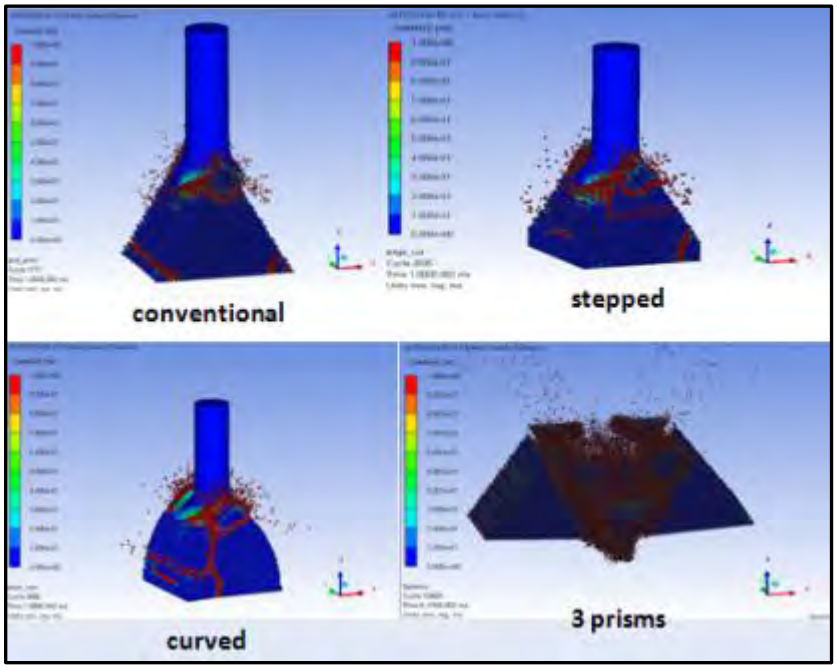

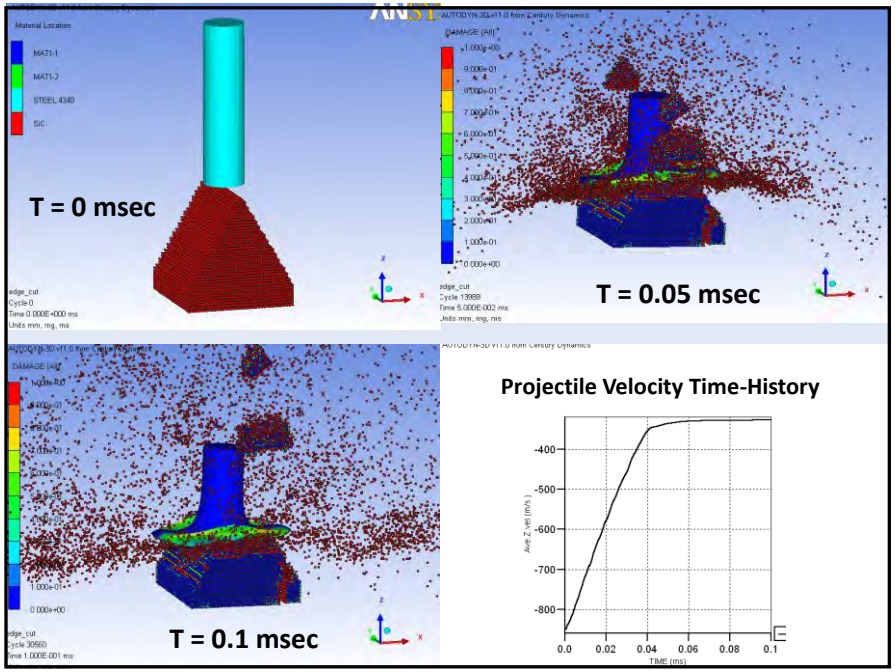

•Single element studies guided ceramic element shape optimization.

•Crack development was studied under representative penetrator impacts

•Ceramic prism is modeled with smooth particle hydrodynamics (SPH); both JH-1 and JH-2 were used. JH-1 showed significantly better correlation with test results, and was used in remaining studies.

•Projectile modeled with regular finite elements, with Johnson-Cook strength and fracture format.

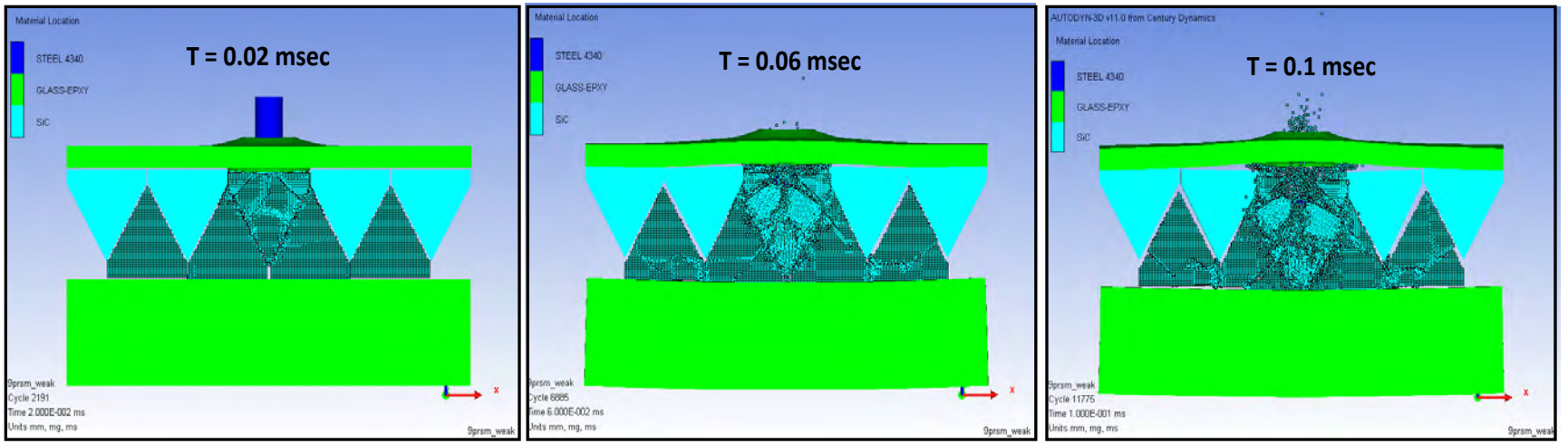

•Modeling complexity progressed to multi-component models to predict interaction of various numbers of stacked prisms coupled with strike and back plates.

•SPH technique is well suited for capturing crack propagation, but is computation intensive for accurate solutions. Our approach combined SPH with finite elements; the prisms which undergo minimum damage are modeled with finite elements; and the prisms which undergo extensive damage are modeled with SPH particles

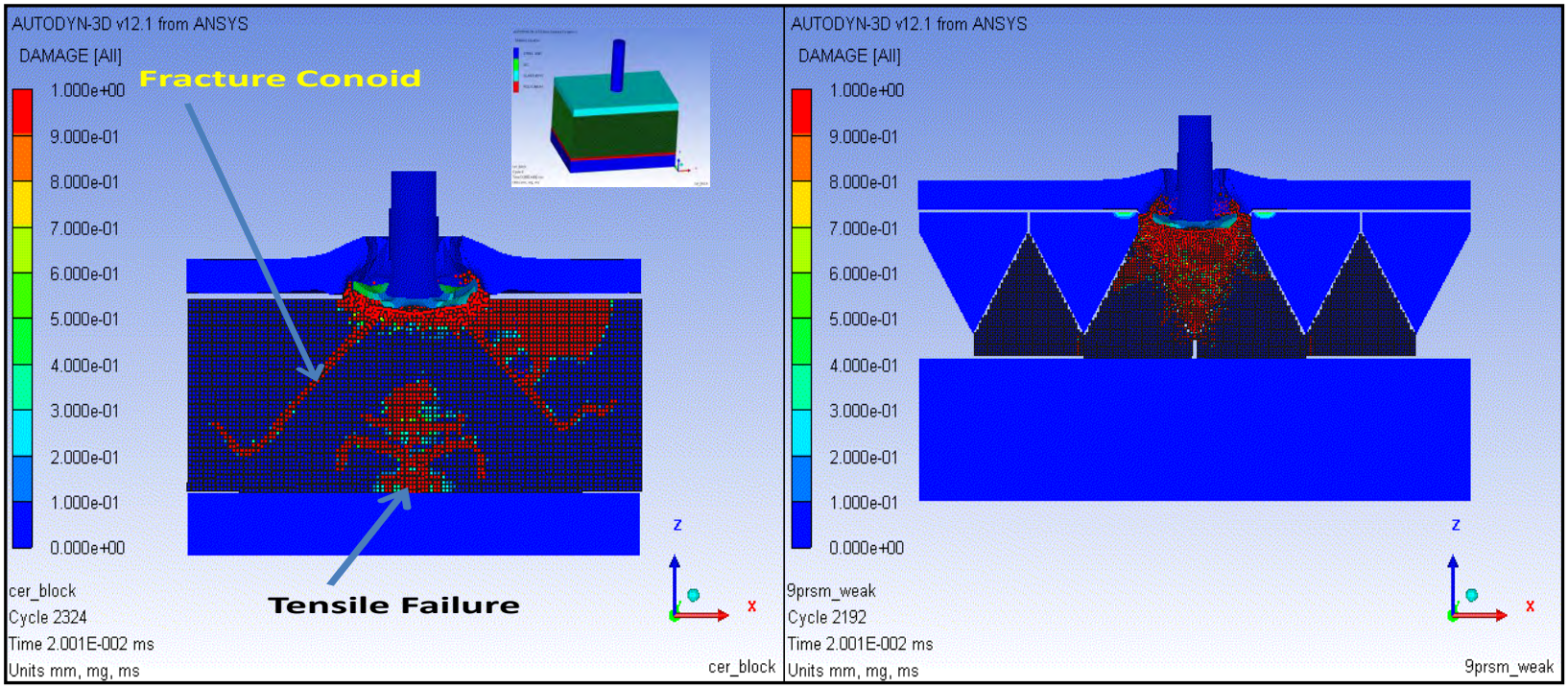

•Comparison of the damaged zone in a monolithic ceramic tile to that of the prism configuration

•Analysis of the velocity time-history of the projectile as it penetrates these prismatic architectures shows multi-stage behaviors, which can be attributed to different mechanisms, including physical confinement of the pulverized rubble bed by neighboring prisms leading to increased erosion of the penetrator as it progresses through the laminate.

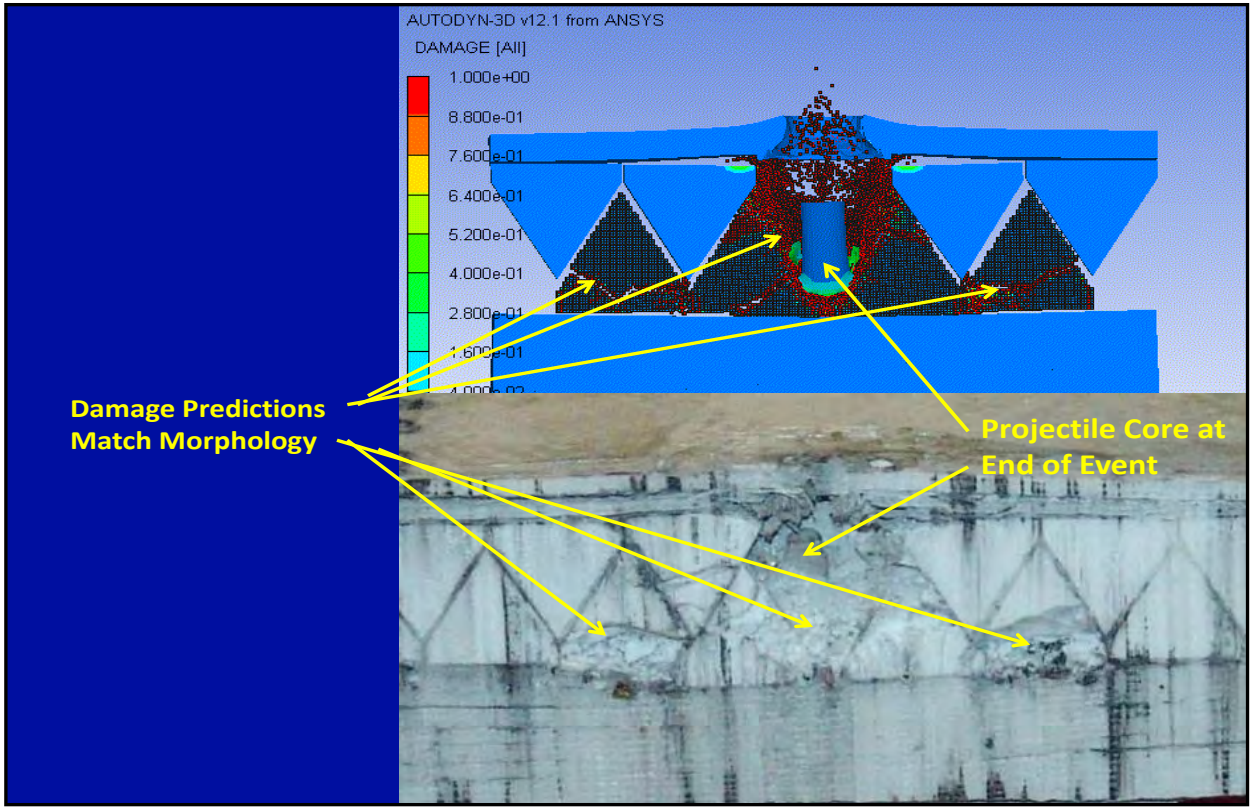

•Ballistic Test Correlation: Damage prediction correlates well with dissected test panels with respect to the pattern and extent of the damage. The containment of the projectile core is also well predicted

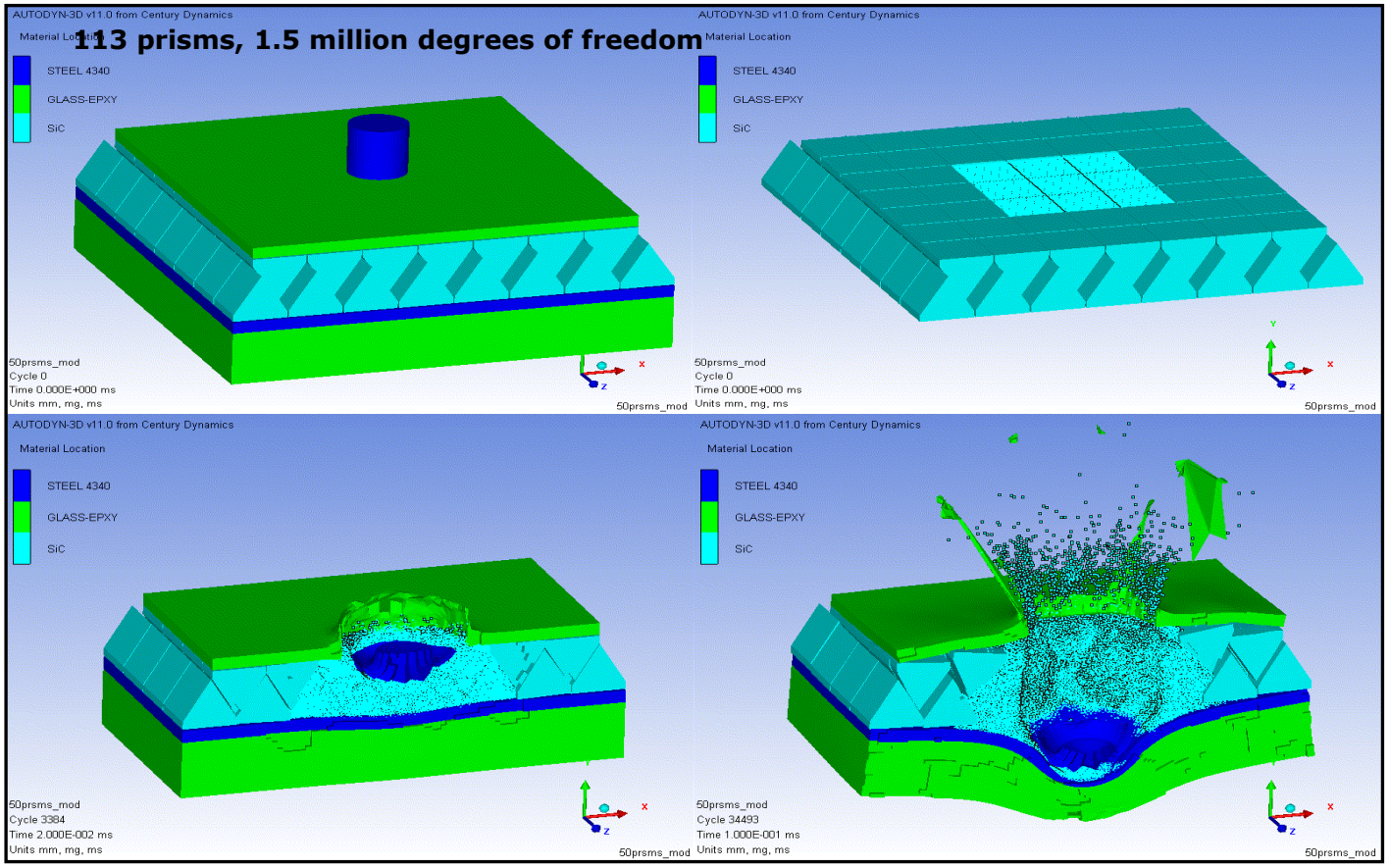

•From the multi-component model, "full armor" models were developed for further increases in simulation fidelity which are closely representative to tactically relevant armor architectures. These full models are used to examine global armor responses to different threats, including larger bullet threats and high speed fragment impacts

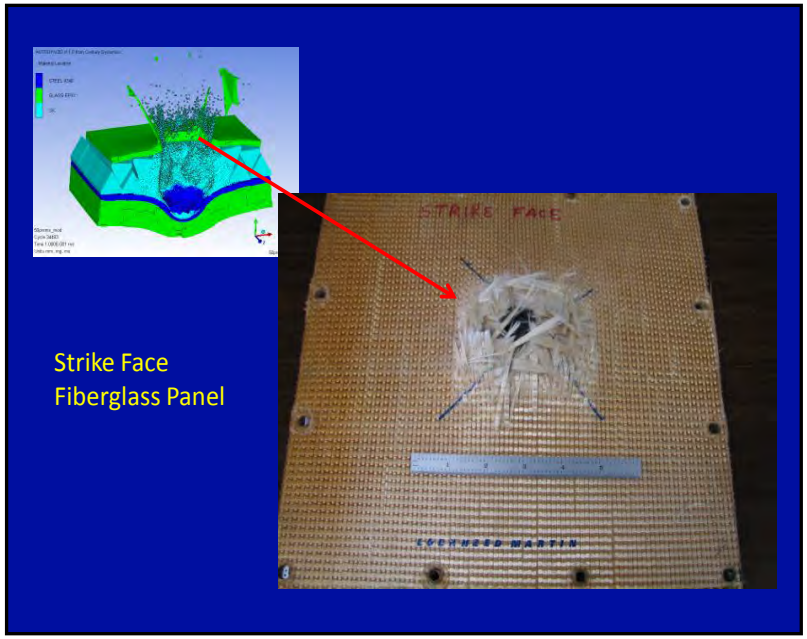

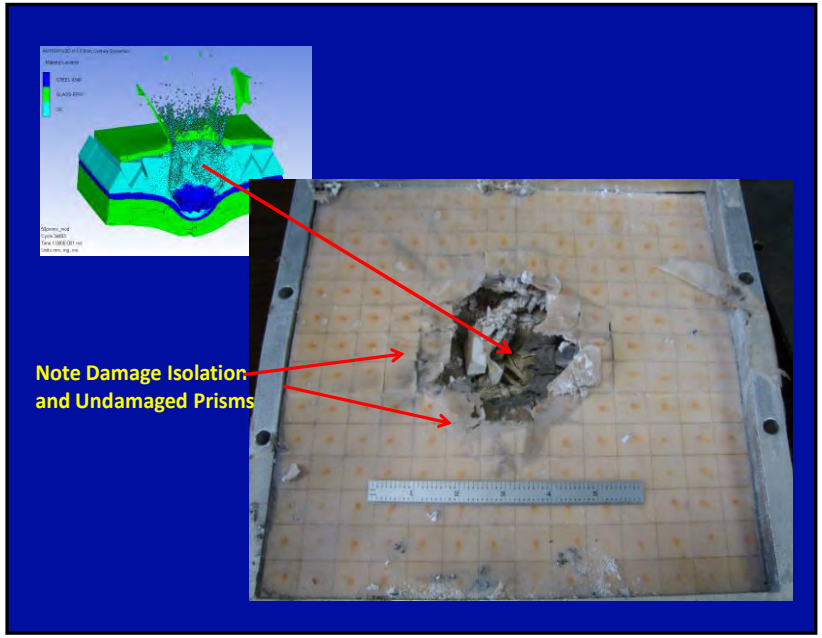

•Panels were built and ballistically tested to examine the failure morphology and ballistic predictions. The numerical predictions correlate well with the damage pattern.

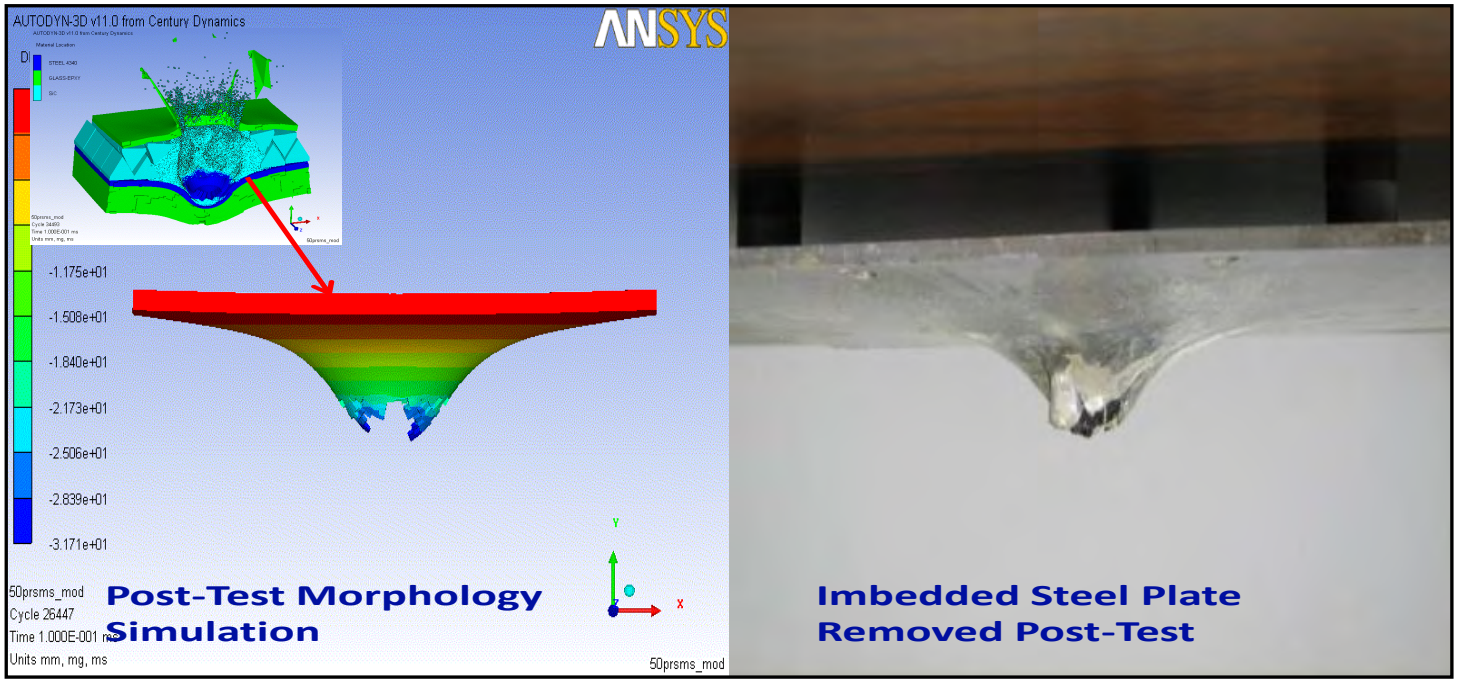

- Numerical simulation of damage to embedded steel plate compares well with the post-test plate morphology

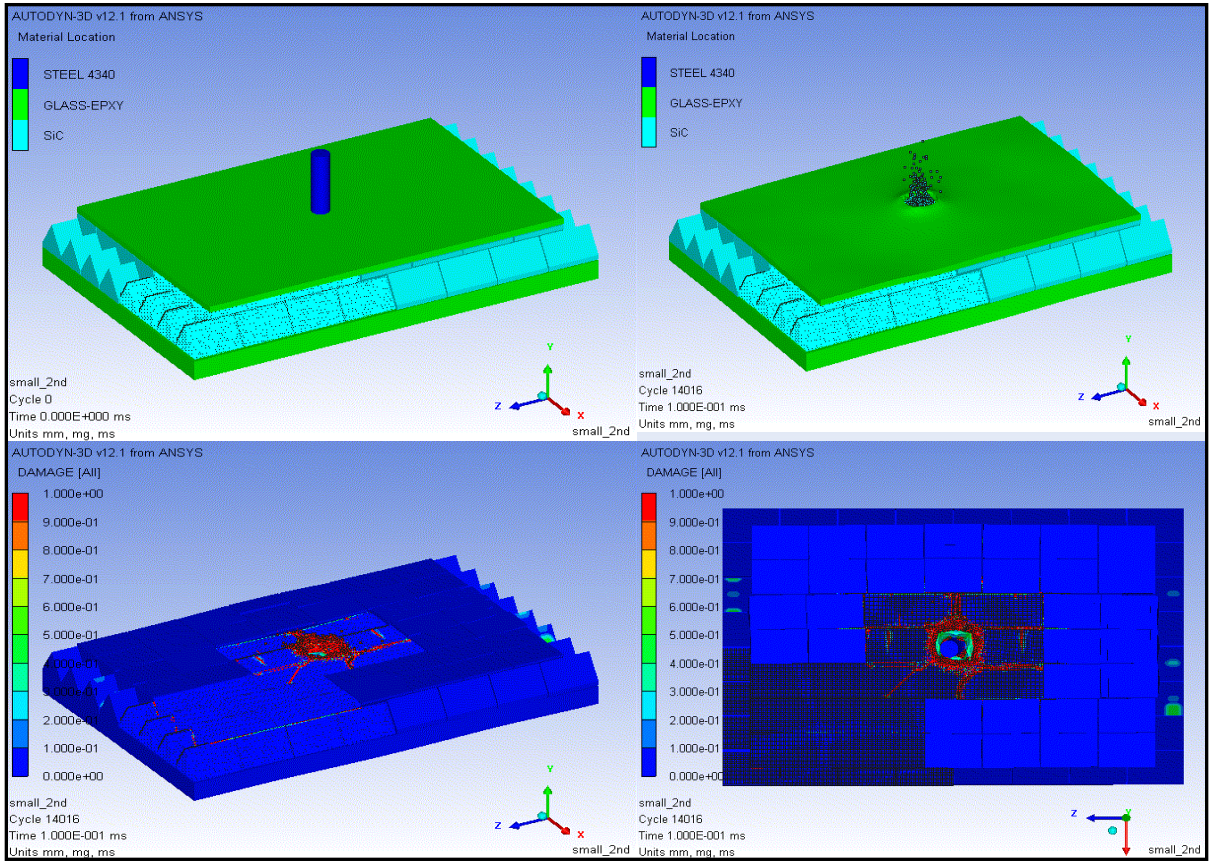

•Multi-strike modeling in work: Numerical simulation of ceramic armor impacted by 1st projectile and damage sustained on ceramic array after the event

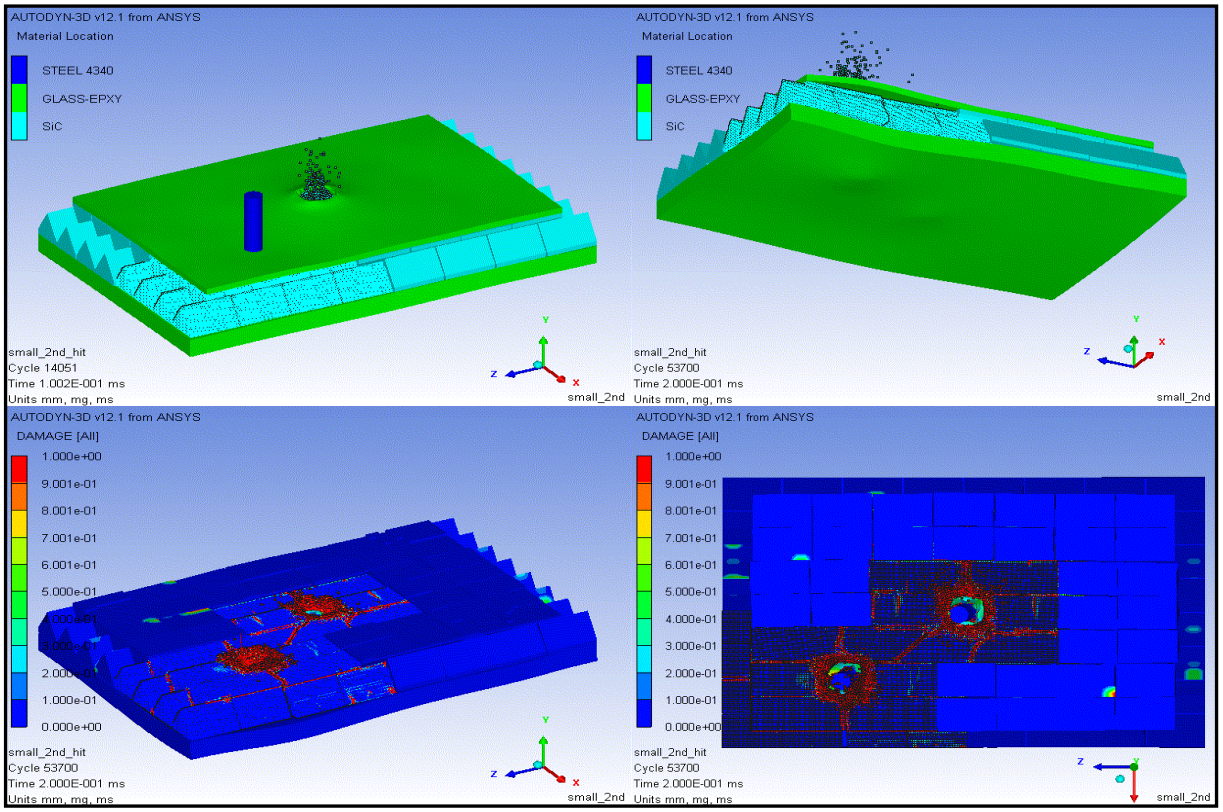

•Numerical simulation of 2nd projectile impact on ceramic armor and damage sustained on ceramic array after the event. Multi-strike capability prediction confirmed by ballistic tests.

Summary and Conclusions

•Fundamental work has been performed developing novel armor topologies that consider shock, dwell, erosion, and subsequent penetration time history to guide armor architecture configurations.

•Results are presented for an advanced ceramic armor system consisting of three dimensional arrays of nested ceramic prisms exhibiting high ballistic performance and multi-strike capability.

•Development was guided by and relied heavily on judicious use of analytical predictions correlated with ballistic testing and post-test failure morphology investigations.

•Test results substantially confirmed the numerical predictions for the projectile containment, the damage propagation through the array of prisms and the extent of the damaged zone in the armor system.

•The effective use of these simulation approaches is limited by the ability to obtain deformation results independent of discretization and very high strain rate material characteristics. For these reasons we are currently extending our work to incorporate microphysical/physics based models as they mature.

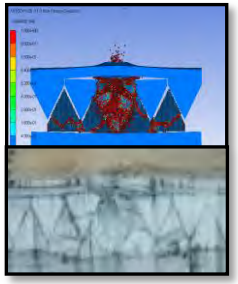

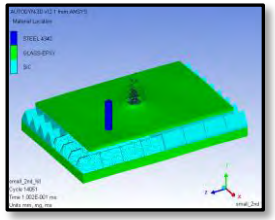

U.S. Army Research, Development and Engineering Command

Preliminary Testing of a 2-Fin Flechette

TECHNOLOGY DRIVEN. WARFIGHTER FOCUSED.

Ilmars Celmins & Greg Oberlin
U.S. Army Research Laboratory, Flight Sciences Branch

26th International Symposium on Ballistics – September 2011

Outline

- Background
  - V-Tail Flight Dynamics
  - Flechettes
- Testing
  - Spark Range Tests
  - Radar Tests
- Summary/Conclusions

V-Tail Concept

- 2-Fin V-Tail projectiles are being investigated for guided munition applications
- Exploring feasibility of a roll-stable flight configuration (paper airplane concept)

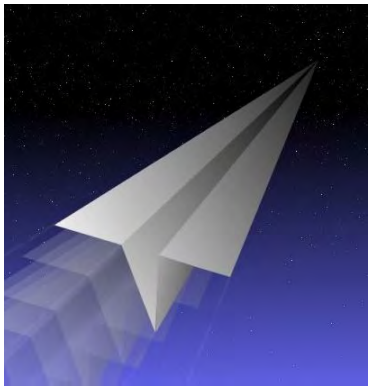

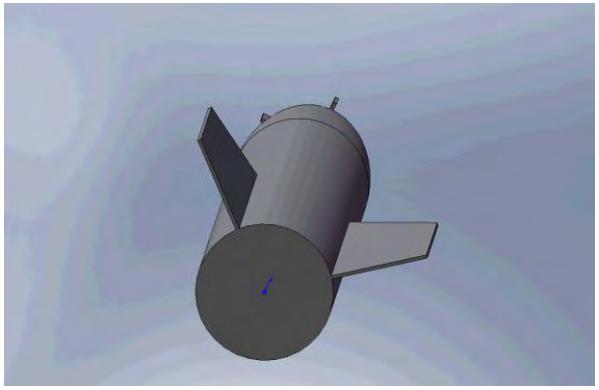

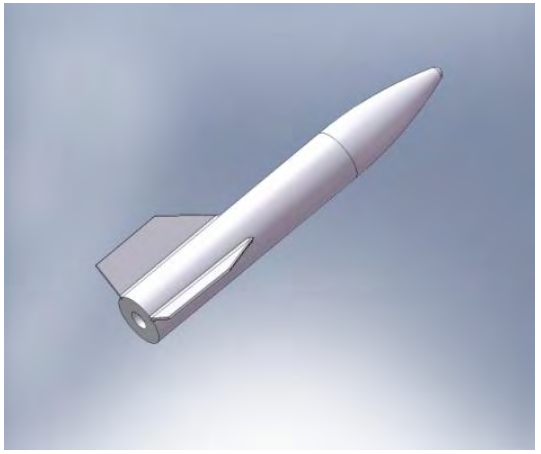

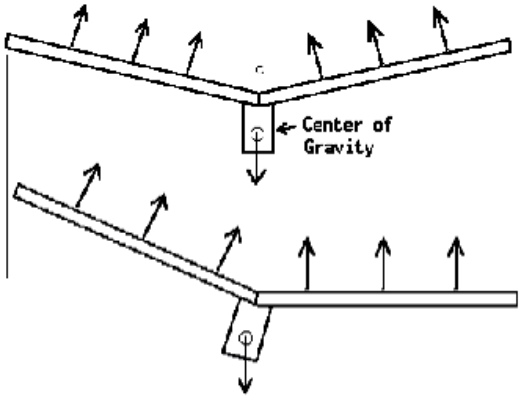

V-Tail Flight Dynamics

- Preliminary research showed a tendency to settle into a stable coning motion
- Did not meet program objectives but potentially useful for other applications

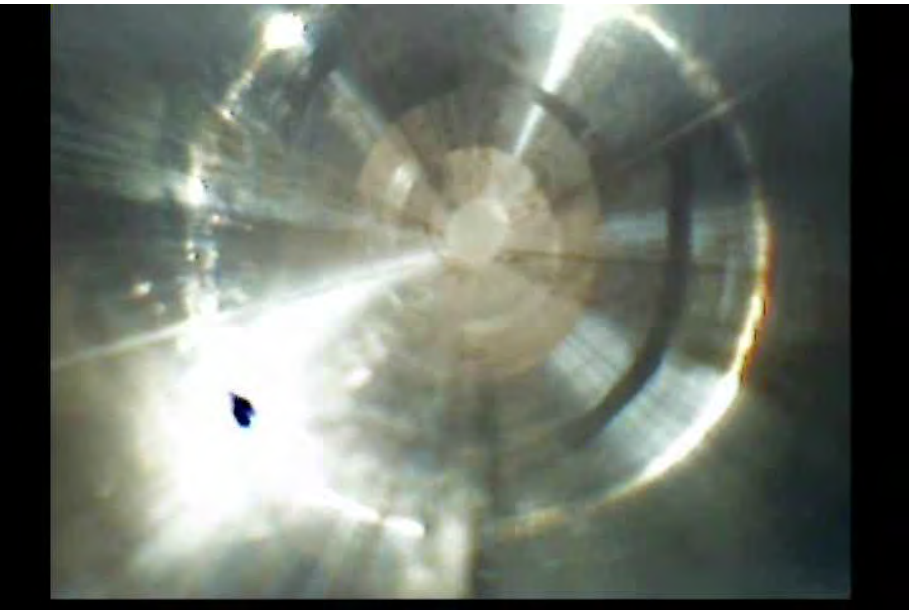

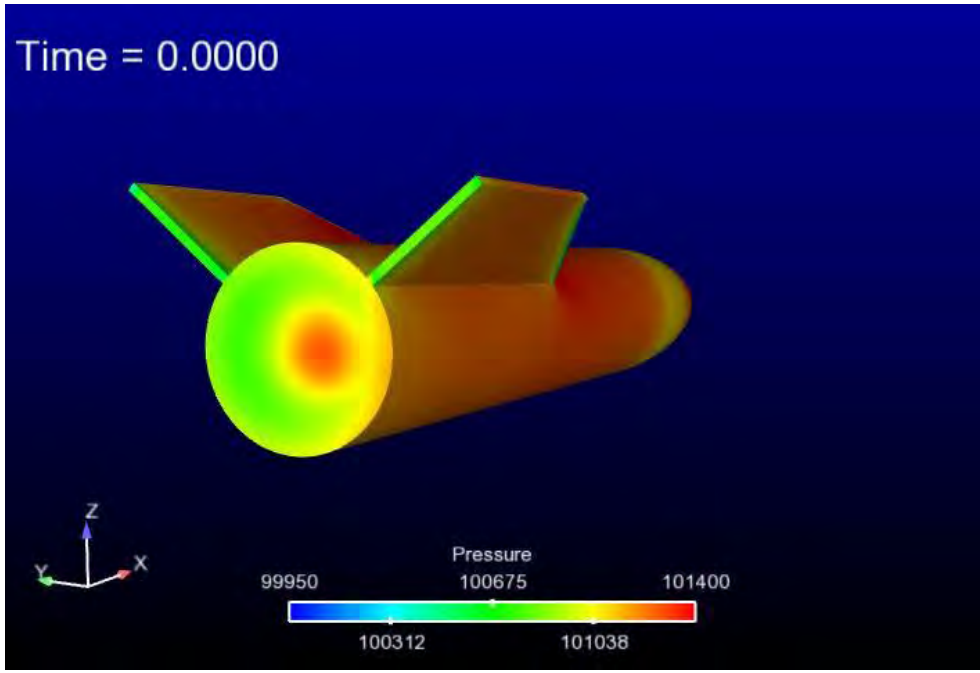

Flechettes

- Typically dispensed in large quantities from a cargo round
- Cloud of flechettes expected to disperse over target area
- Each flechette is a fin-stabilized long rod penetrator capable of penetrating light armor

http://twistedscottishbastard.blogspot.com

<u>Flechette requirements</u>

- Aeroballistic requirements:
  - Fly in a nose first orientation
  - Minimal drag
  - Relatively low yaw at impact
  - No accuracy requirement for individual flechettes
- Other requirements:
  - Producibility
  - Dense packing

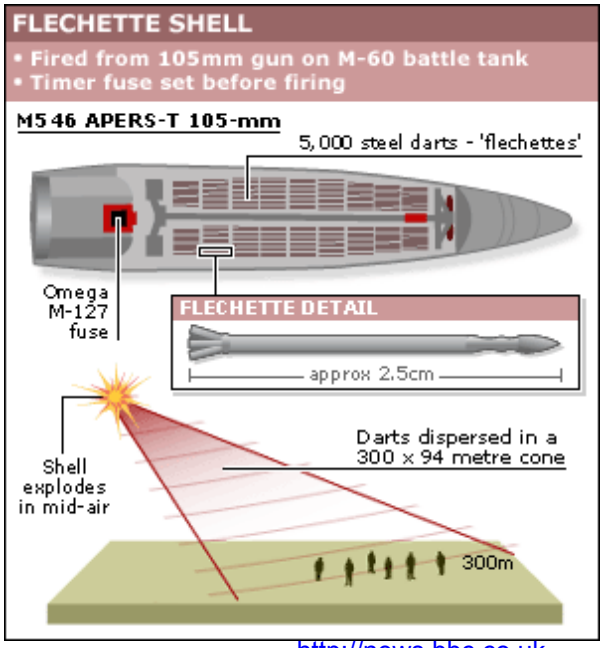

http://news.bbc.co.uk

Flechette Fabrication

- Producibility is very important
- Typically fabricated on automatic nail making machine modified to form fins instead of the nail head
- Produced in large quantities with loose tolerances

http://www.wvguns.com/products_surplus.htm

http://www.auctionarms.com

Flechette Packing

- Standard 4-Fin flechette configuration is a hindrance to dense packing due to fin interference

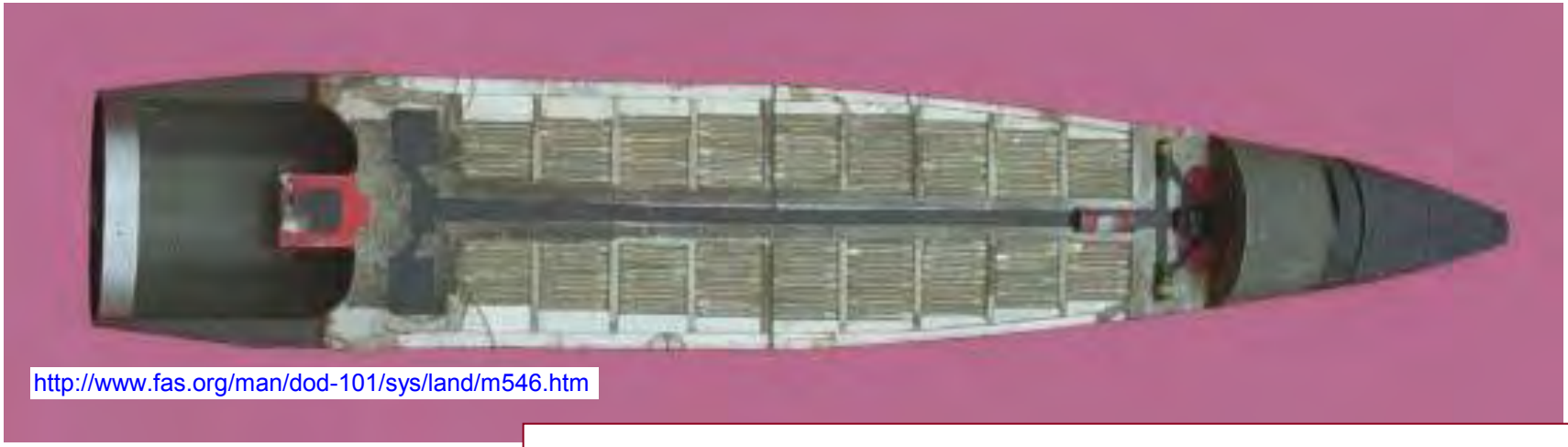

http://www.fas.org/man/dod-101/sys/land/m546.htm

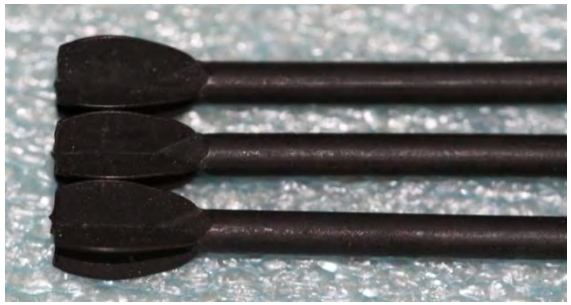

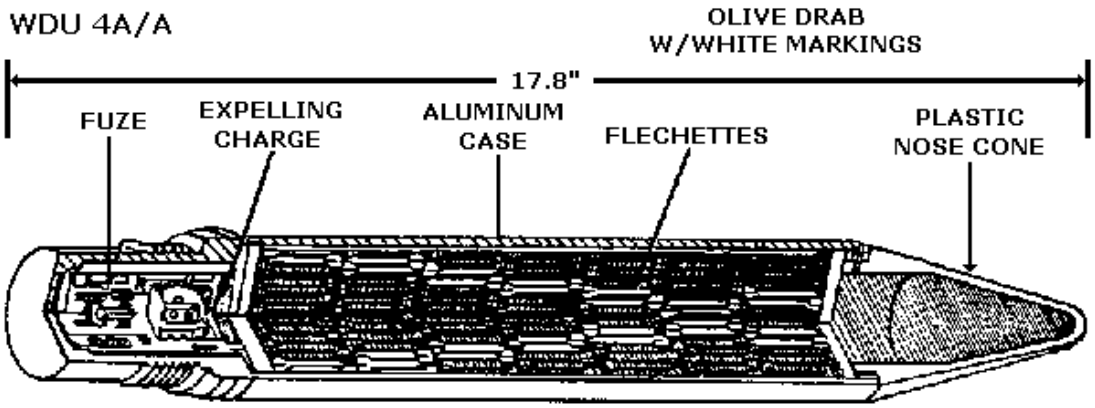

http://www.aircav.com/hydra70.html

V-Tail Flechette

Flechette requirements

- Aeroballistic requirements:
  - Fly in a nose first orientation
  - Minimal drag
  - Relatively low yaw at impact
- Other requirements:
  - Producibility
  - Dense packing

2-Fin V-Tail flechette configuration

- Improved packing (can stack projectiles without fin interference)
- Producibility similar to 4-Fin
- Aeroballistic performance unknown

Spark Range Testing

- Preliminary testing of 2-fin flechette was conducted in the ARL Aerodyamics Experimental Facility (AEF)
- Shots were added to a 4-Fin flechette test program
- 2-Fin flechettes were made by grinding off two adjacent fins from the baseline 4-Fin flechette, leaving a V-tail configuration
- Goal was to have a direct aeroballistic comparison of 2-Fin vs. 4-Fin

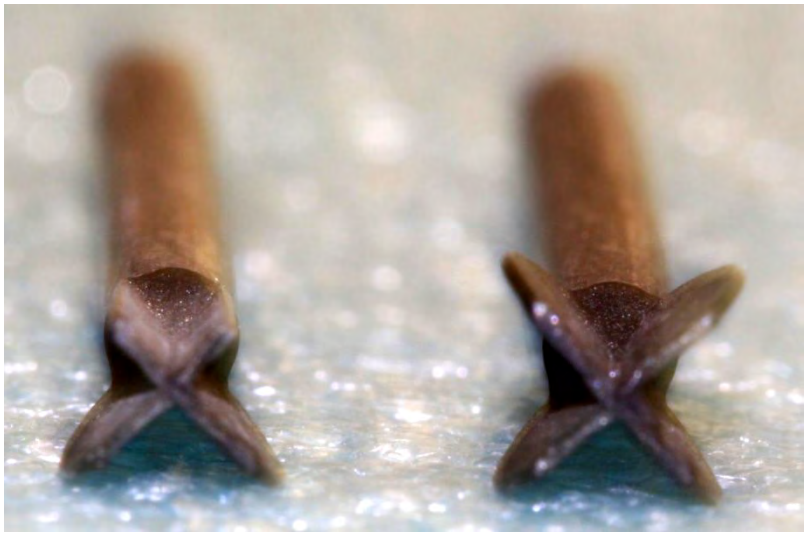

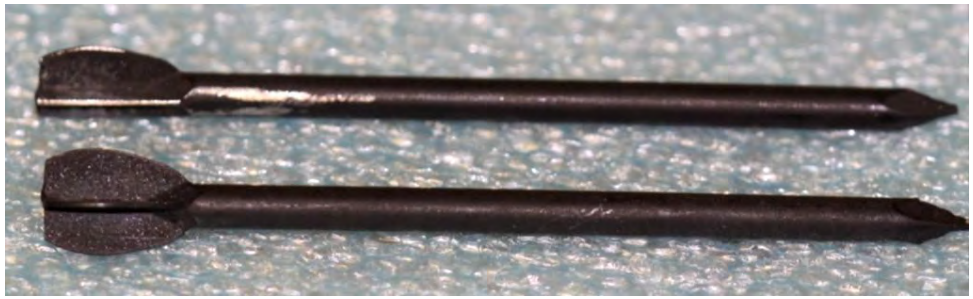

The ARL Aerodynamic Experimental Facility generates aeroballistic data

39 direct image orthogonal shadowgraph stations in 5 groups

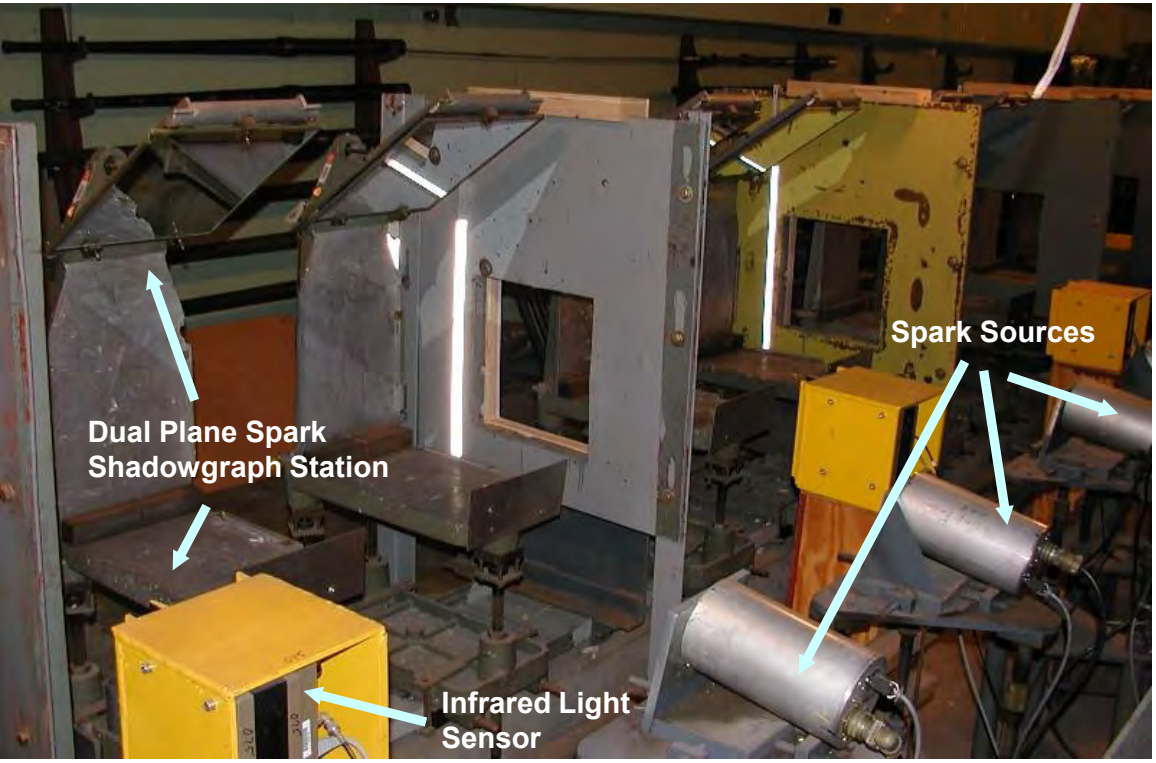

Image window is less than 14 inches across

Spark source triggered at a recorded time after infrared sensor detects passing projectile

Each station surveyed into a fiducial system that is simultaneously imaged on the film with the projectile

The spark shadowgraphs are used to obtain the projectile position and angle

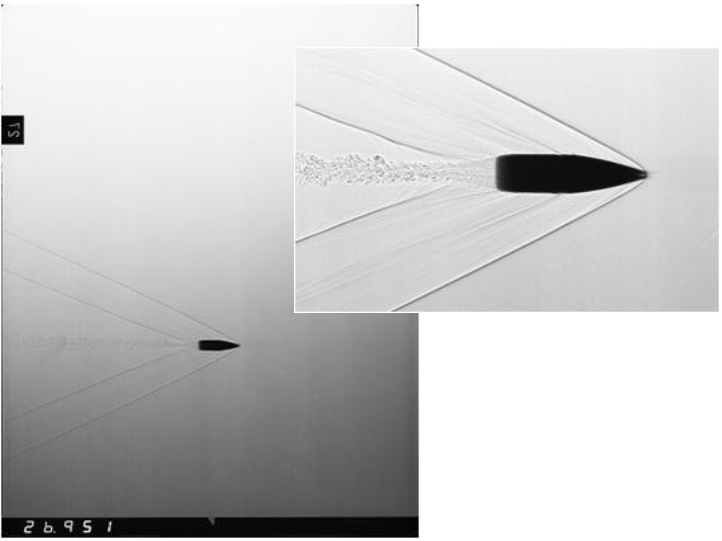

Film is read using a precision light table to determine spatial coordinates and angular orientation of the projectile

Aero Range Facility Data Analysis Software – ArrowTech Associates

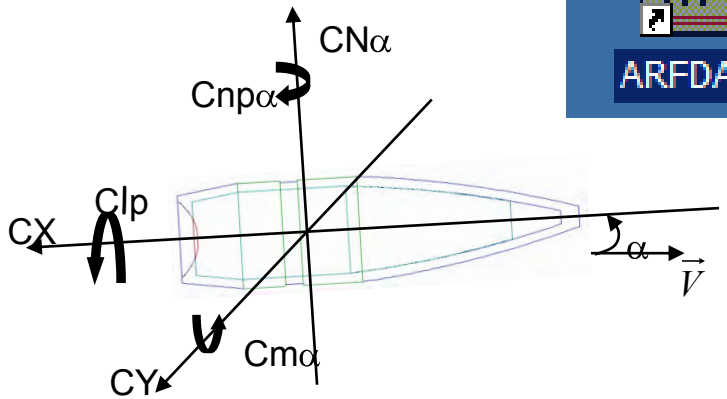

Data is reduced for a 6-DOF fit in order to obtain an aerodynamic model and motion fit

Preliminary Test of 2-Fin Flechette (AEF Shot 32541)


15V


20V


25V

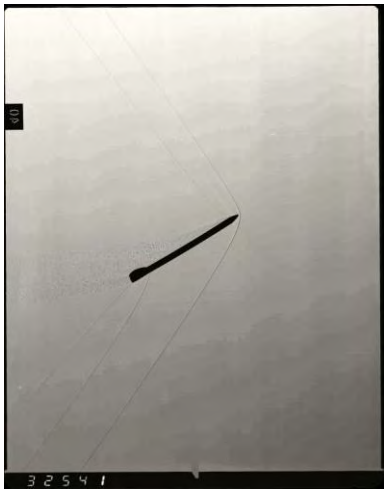
40V


45V

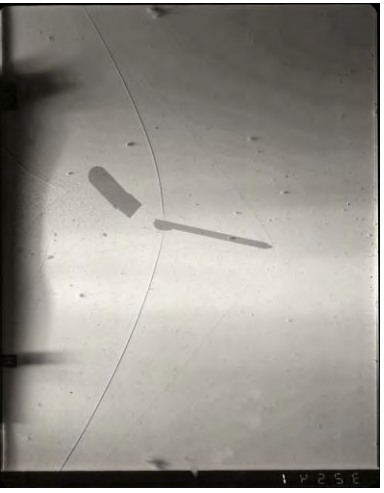
15H


20H


25H

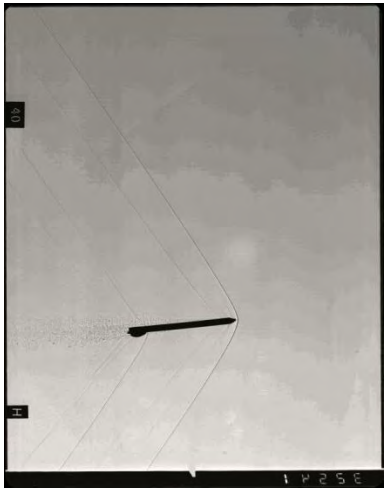
40H

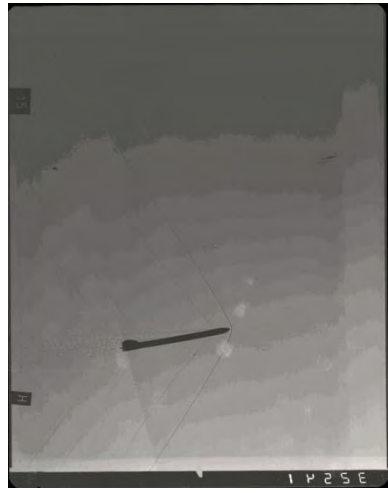
45H

4-Fin Flechette
AEF 32451, M=1.29

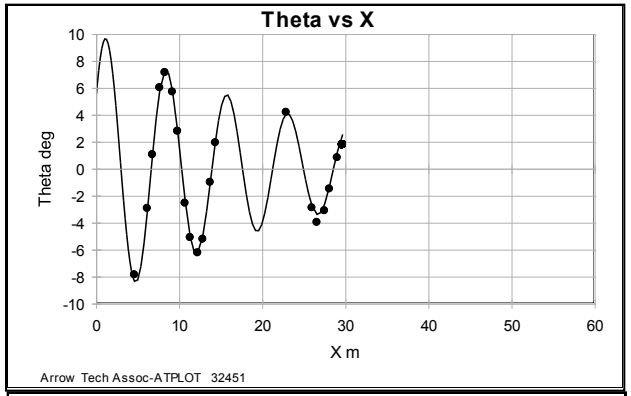

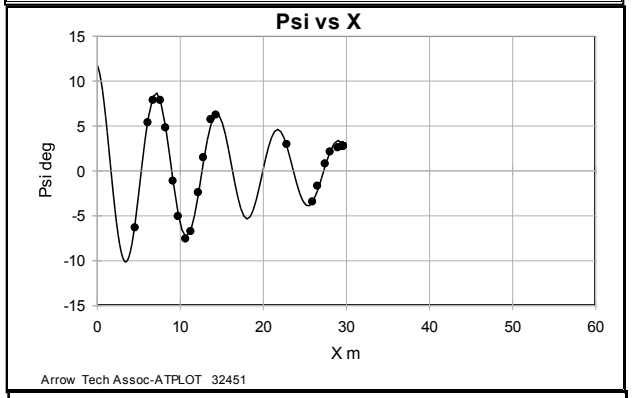

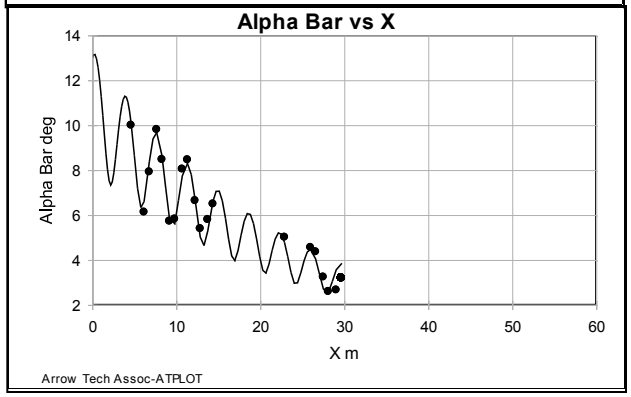

Some rounds were well behaved

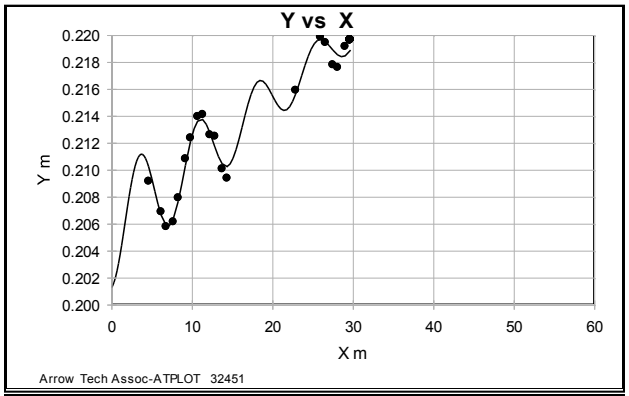

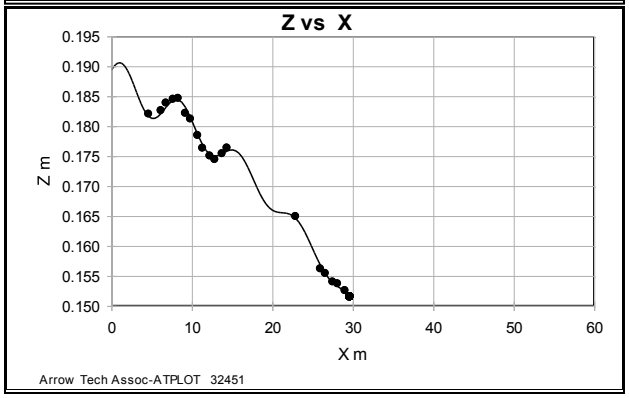

4-Fin Flechette
AEF 32450, M=1.24

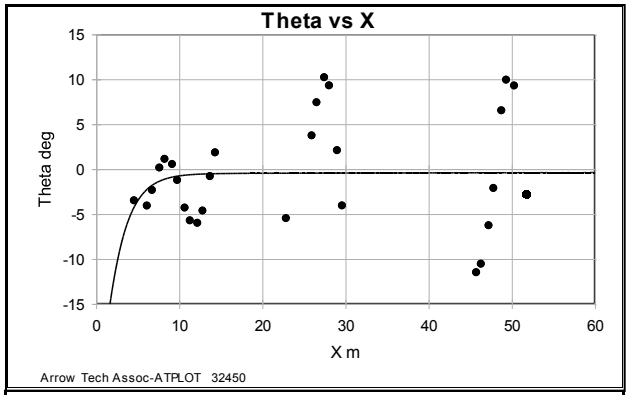

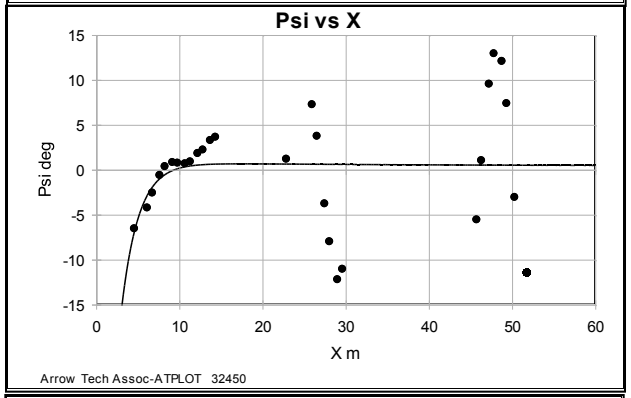

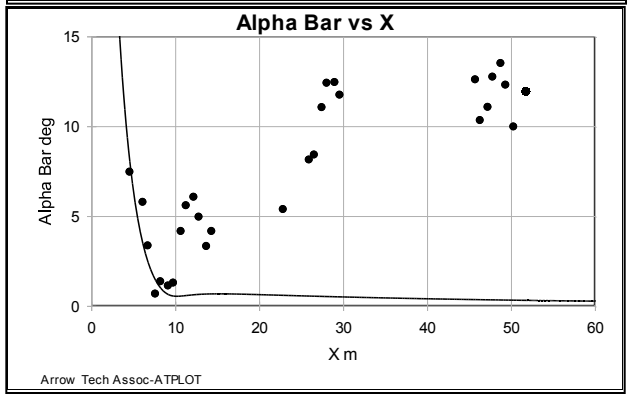

Some rounds behaved strangely

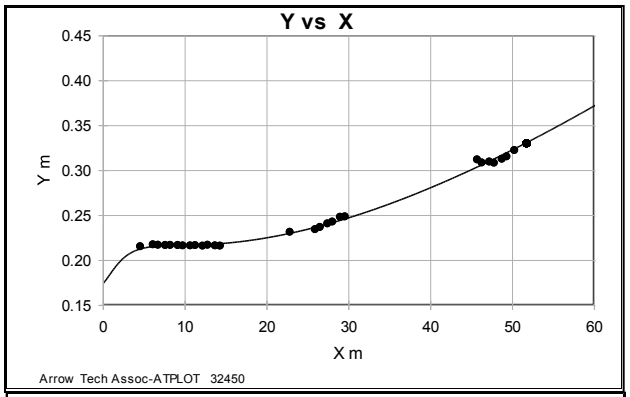

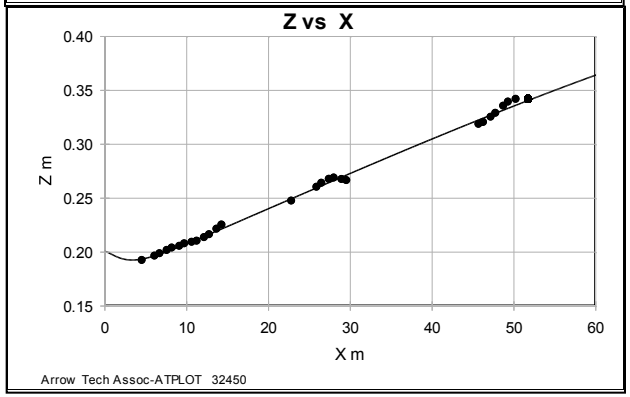

2-Fin Flechettes

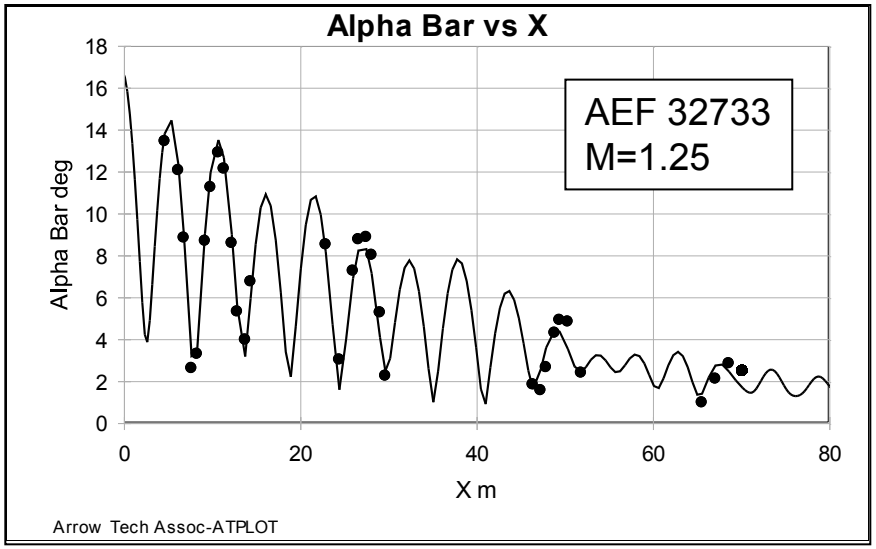

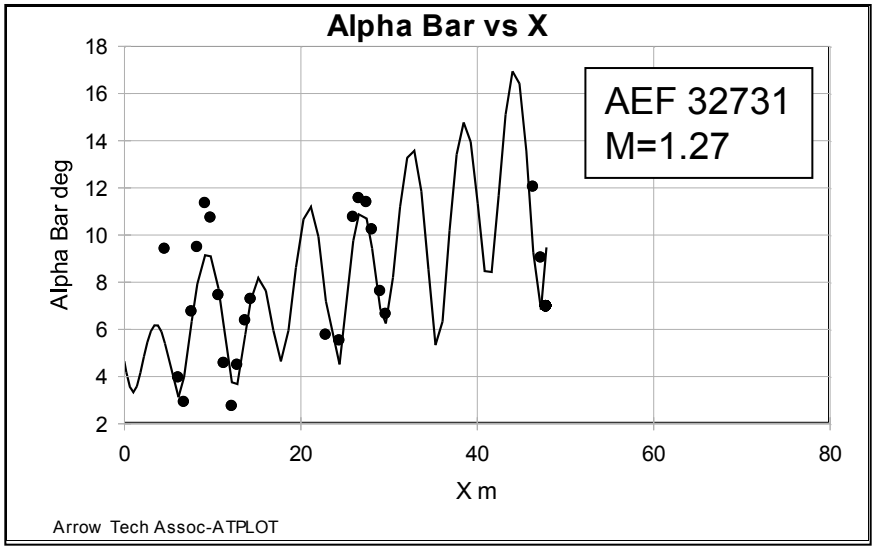

- 2-Fin V-Tail flechettes exhibited similarly inconsistent behavior
- Did not have enough “good” shots to perform standard data analysis
- Desire was to obtain drag comparison
- Difficult due to large yaw variation along trajectory
- A non-traditional approach was used to compare performance

Spark Range Data Analysis

- Evaluated correlation of velocity loss with total yaw
- Velocity loss is fairly independent of velocity

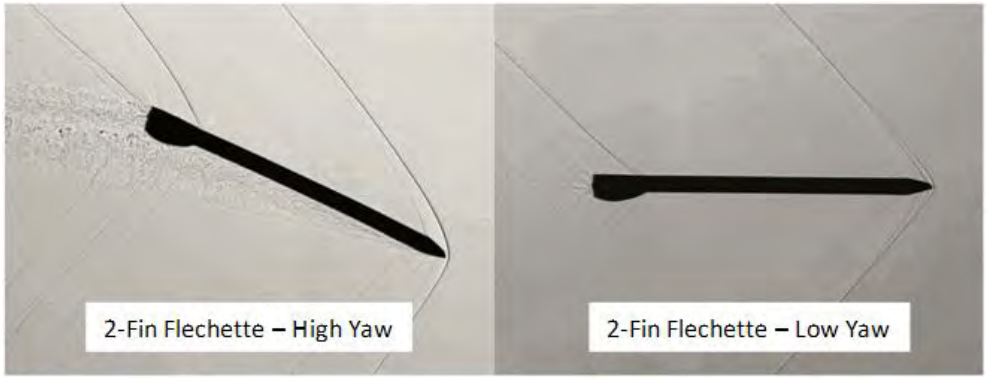

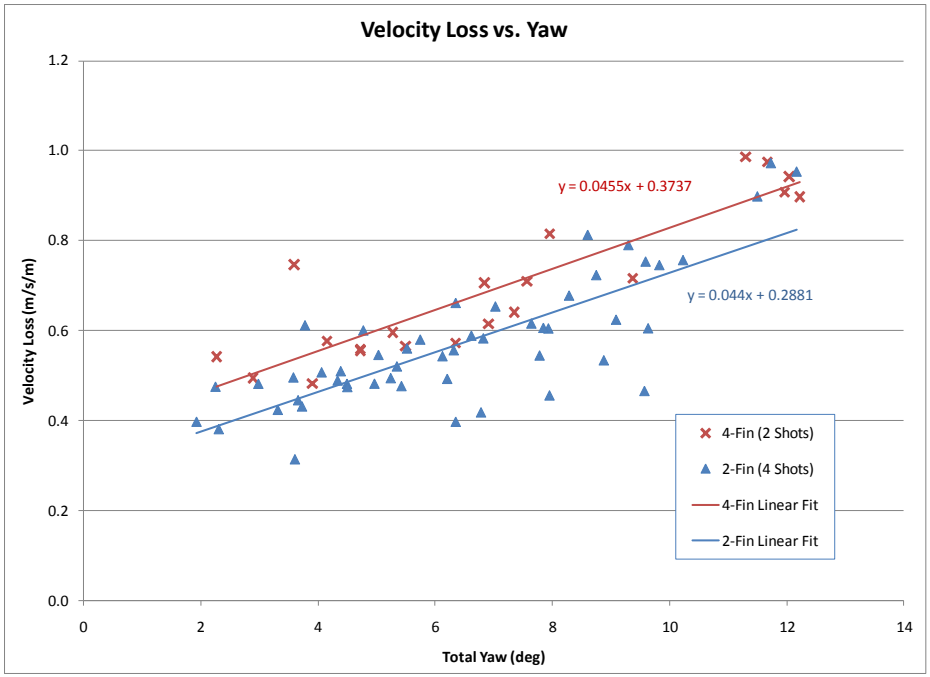

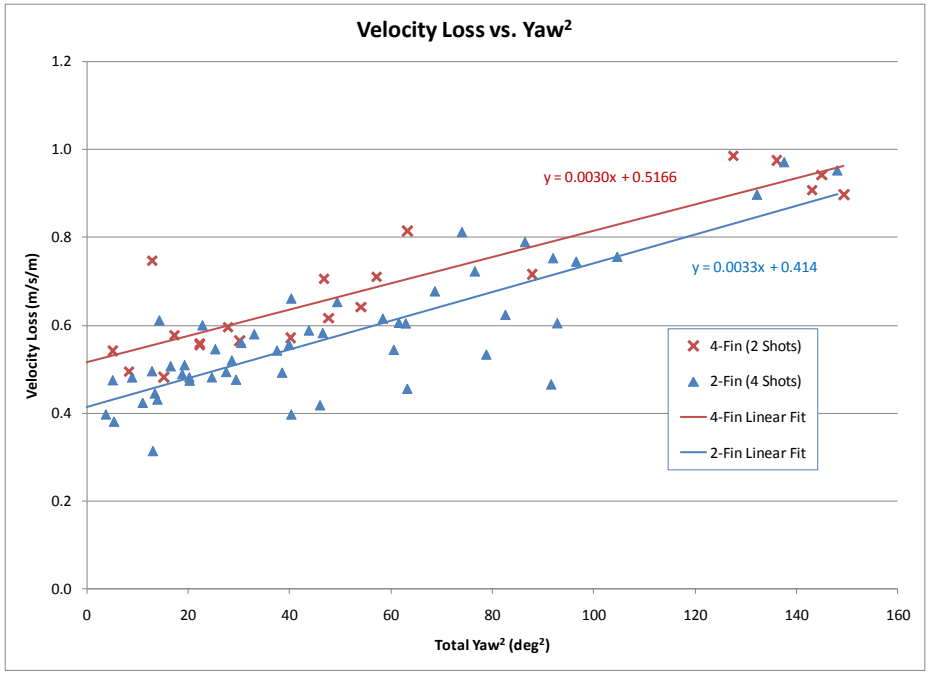

Spark Range Data Analysis

- Data quality leaves much to be desired, but does show trends
- Still need to know downrange yaw levels
- 2-Fin has lower drag if yaw not more than 2 deg. larger than 4-Fin yaw

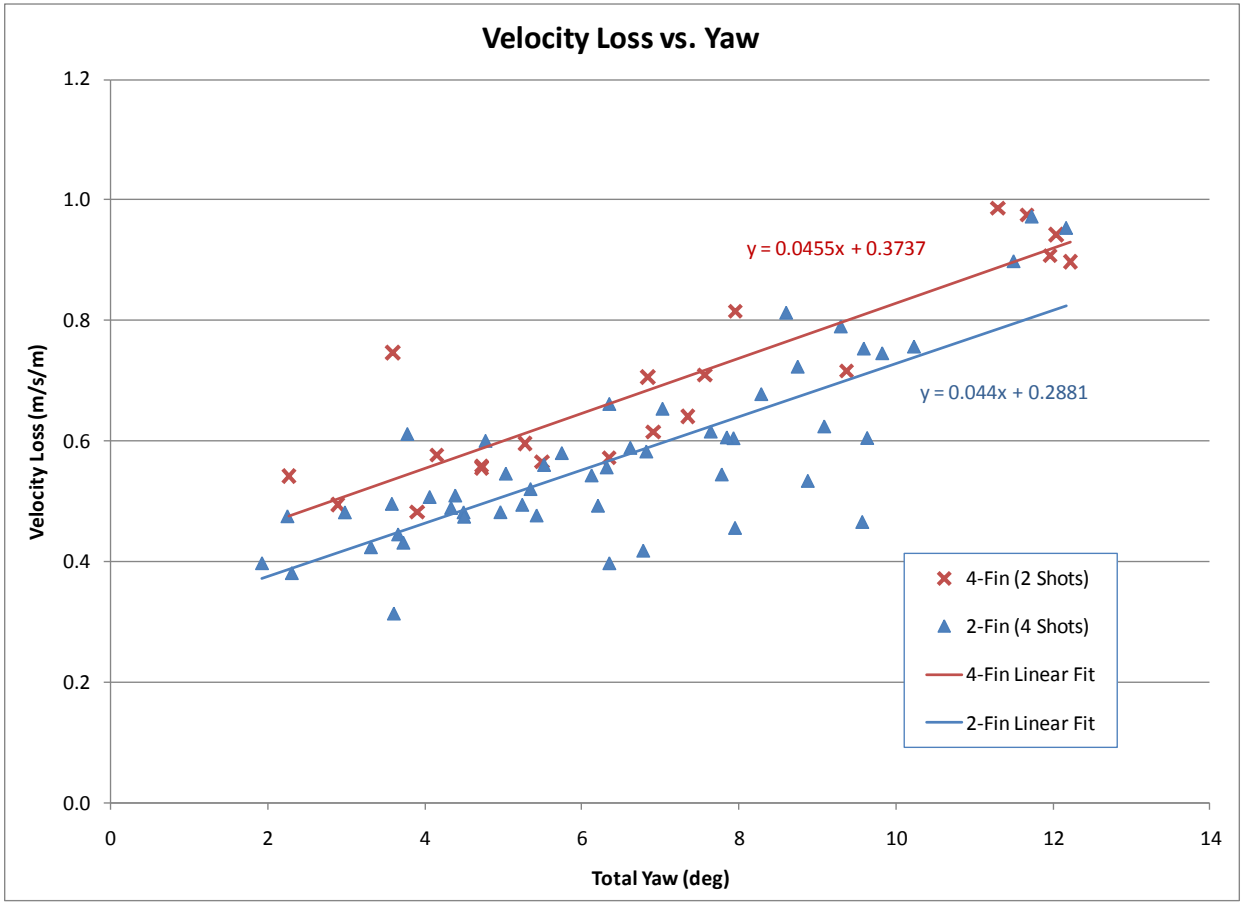

Radar Testing

- Radar testing was conducted of both configurations
  - (4) 4-Fin baseline
  - (5) 2-Fin V-Tail
- Gun elevation = 10 degrees
- Muzzle velocity = ~550 m/s
- Sabot launched from .50 caliber smoothbore test barrel

- Goal was to determine performance after rounds had “settled down”

Radar Test Results

- Radar test results showed very inconsistent velocity loss for both configurations
- Rounds did not “settle down” as expected
- Spin-yaw resonance is one potential explanation

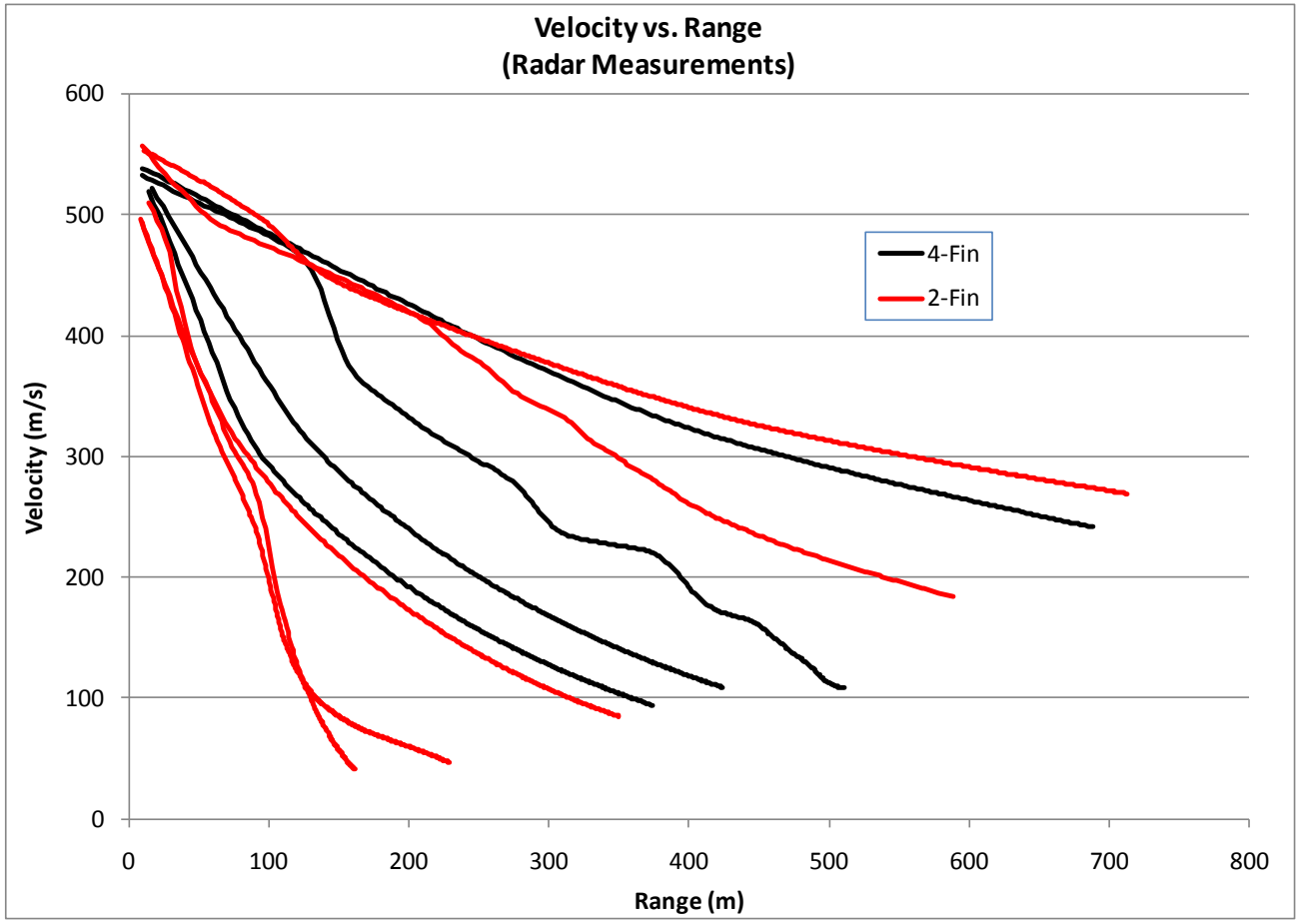

Selected Radar Results

- Velocity above 350 m/s
- 4 “well behaved” rounds
  - 2 of each configuration
- Comparison of velocity loss indicates both configurations have nominal yaw of ~5 degrees

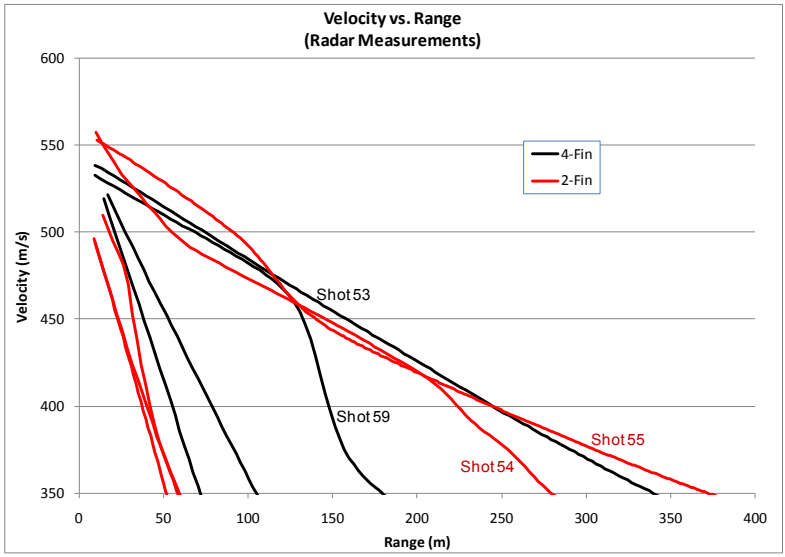

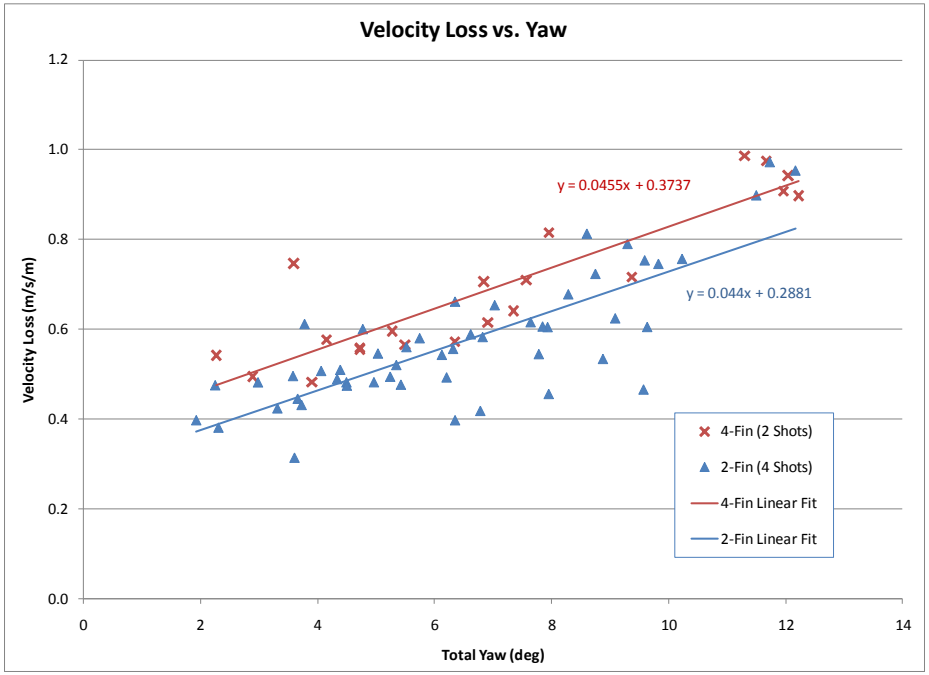

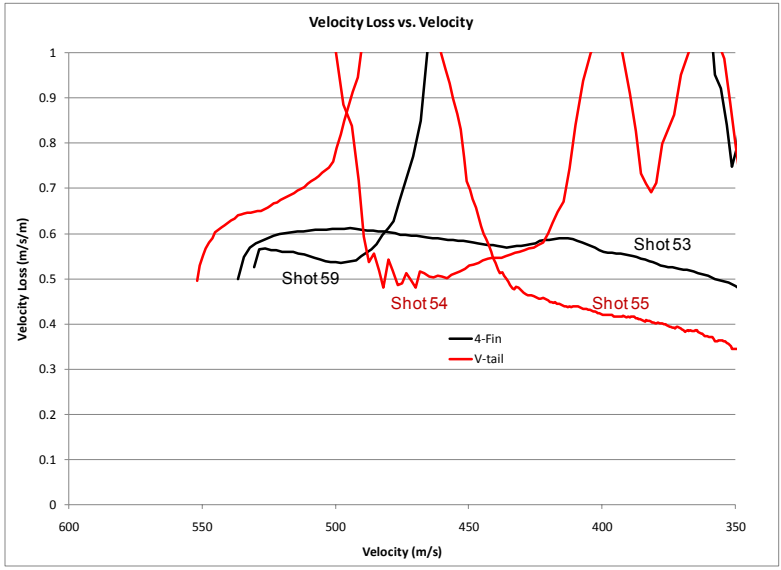

TECHNOLOGY DRIVEN. WARFIGHTER FOCUSED.

Summary/Conclusions

- There are flight stability issues with the baseline 4-Fin configuration
- Ballistic performance of 2-Fin V-tail is similar to 4-Fin baseline
- Comparison of “well behaved” rounds shows lower drag for 2-fin design
- 2-Fin V-tail appears to be a viable alternative for flechettes
- Further research is needed
  - Must address stability issues
  - Evaluate 2-Fin performance for stable baseline

Contact Info

Ilmars Celmins
U.S. Army Research Laboratory
ATTN: RDRL-WML-E
Aberdeen Proving Ground, MD 21005-5066
410-306-0781 Fax: 410-306-0666
Email: ilmars.celmins.civ@mail.mil

TECHNOLOGY DRIVEN. WARFIGHTER FOCUSED.

Malcolm Baldrige National Quality Award 2007 Award Recipient

Lubrication's Contribution to Cartridge Case Failure

ARMAMENT RESEARCH, DEVELOPMENT AND ENGINEERING CENTER PICATINNY ARSENAL, NJ

Presented to: ***NDIA, International Ballistics Symposium***
Presented by: ***Mark Minisi, RDAR-MEM-I, Picatinny Arsenal NJ***
Presented at: ***Miami, Fl.***
Date: ***SEP 2011***

Case Failure

During a U.S. Army test, 5.56mm NATO case ruptures were experienced when firing the M249 in the hot, 160 deg F (conditioned) environment.

Key points from early in the failure investigation

- M249 normally creates more case deformation than M16/M4
- Hot, 160 degree (Higher Pressures, different mechanical fits than at ambient temperatures)
- Low round count barrels
- Weapon was recently cleaned and lubricated
- Failures always occurred within the first 10 rounds of the ammunition belts
- Case bulging frequently observed in rounds preceding ruptured rounds on the belt
- Noticeably shorter cartridge shoulder neck length in ruptured cases
- Failures of this type are not occurring when firing the same ammunition from the M16/M4
- Material analysis of case suggests no significant variations from the norm

Investigation Path

Exploratory testing at multiple agencies (ARL, LCAAP, ARDEC)

- Comparative testing of various ammunition and weapons relevant to failure
- Evaluation of pressure
- Evaluation of temperature
- Evaluation of Lubrication
- Analysis and Identification of failure mechanism(s)

Modeling, Simulation and Engineering Analysis (ARDEC)

- Baseline the brass cartridge case using test data
- Apply loads/constraints to replicate failure
- Enhance knowledge of failure mechanisms by studying what can be shown in testing
- Identify/Quantify failure mechanism(s), verify with testing
- Provide thorough understanding of mechanism(s) to support corrective action

This Brief is focused on the simulation and analysis conducted at Picatinny Arsenal used to support the overall investigation

Initial Models

2D Axis-symmetric FEA Models

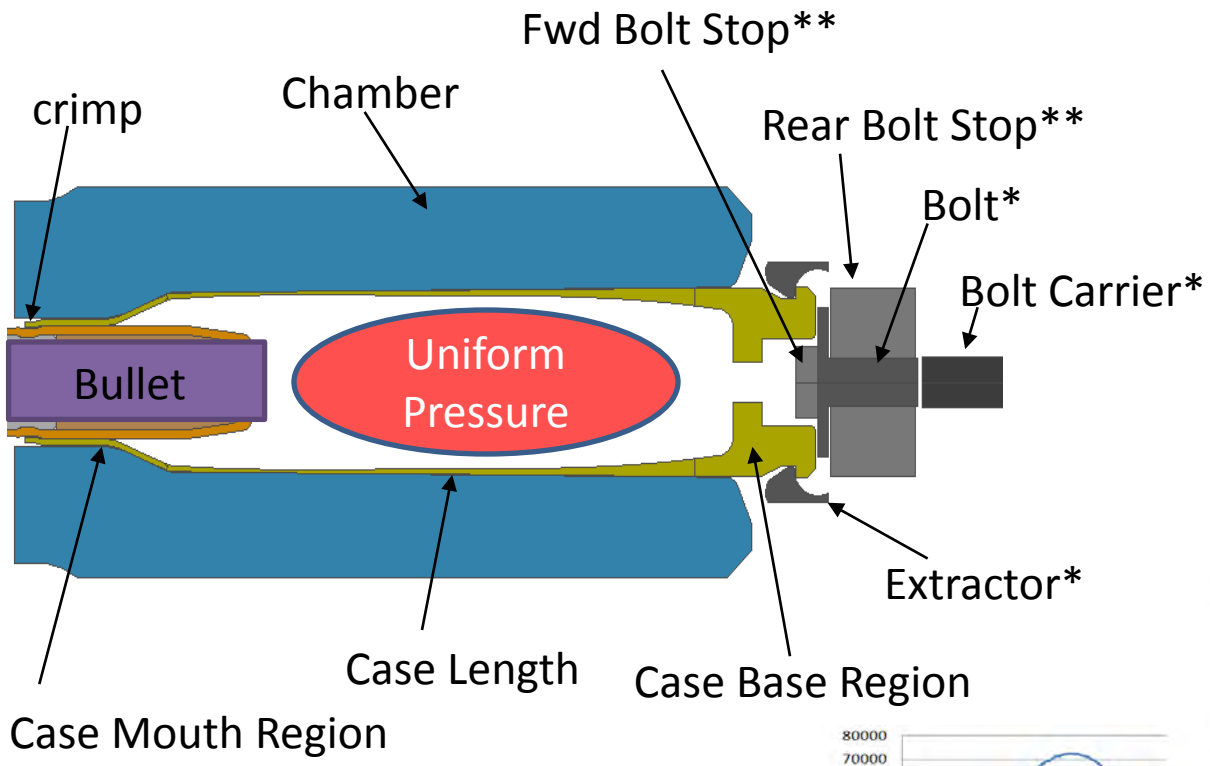

Analyses:

1. Pressure variation
2. Bullet drag on case
3. Head space variation and cartridge location
4. Extraction loads
5. Potential Case defect
6. Friction variation along case length
7. Bolt Face variation

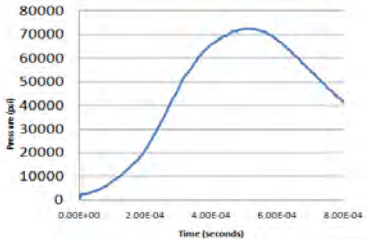

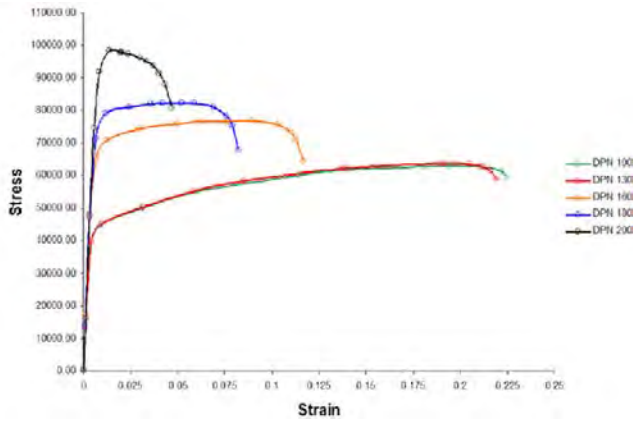

**Simplified for Axis-symmetric model*
*** This geometry sets the head space*

M249

Dynamic rigid body models used to capture timing and loads

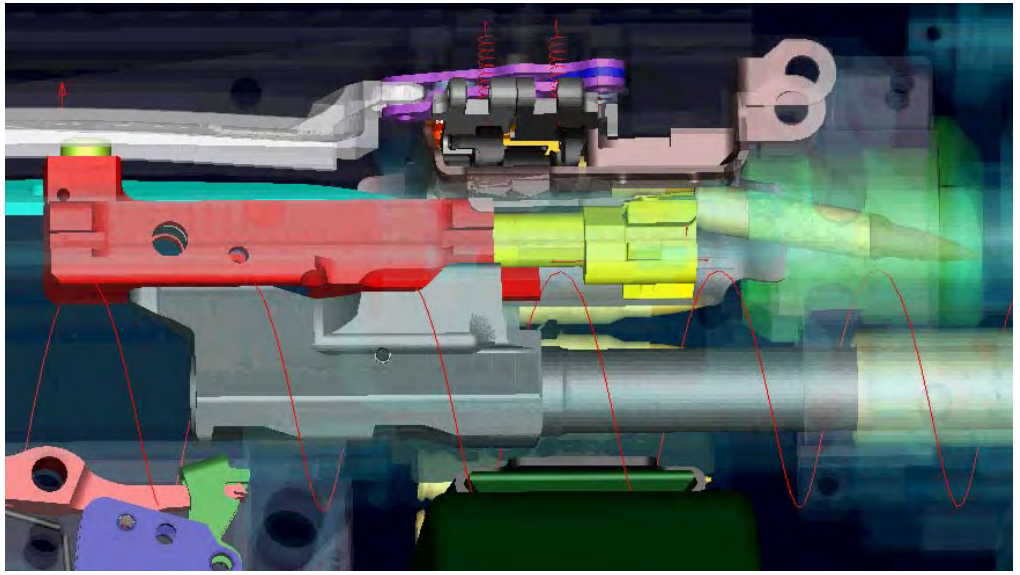

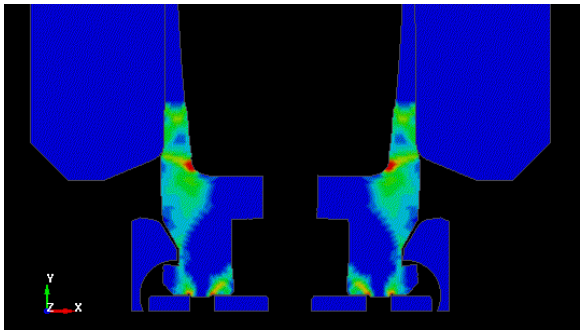

Case bulge from forceful feed of case with out-of-spec length

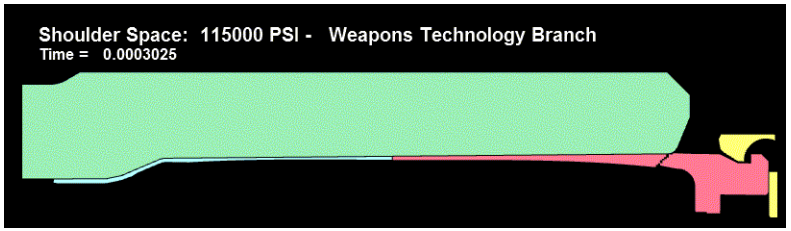

Typical fracture from too much head space: *no bulge*

Close, but backwards

Too much head space typically results in material separation due to exceeding the plastic strain material limits of brass . The failures experienced were not of this nature.

Initial simulations closely replicated case deformation by preventing case to seat properly, or by having a case length that was out of spec. However, M249 operating group was shown (simulation and testing) to be unable to lock and fire if cartridge case prevented from seating in this manner. These simulations created this case deformation by FORCING the bolt closed.

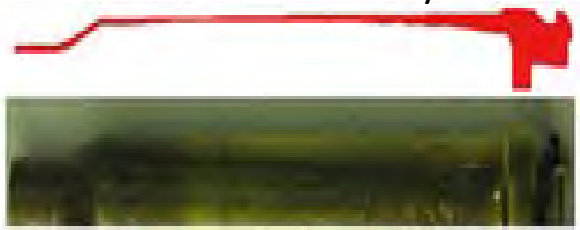

True: Case deformation comes from excessive force at the contact surface of the case and bolt face. However, the increase in force is not caused by head space, and not by pressure alone.

To generate enough bolt face force from a pressure increase alone, the 2D simulations suggested peak pressures well over 90,000 psi would be required, if all else is nominal.

Mechanics of Case loading

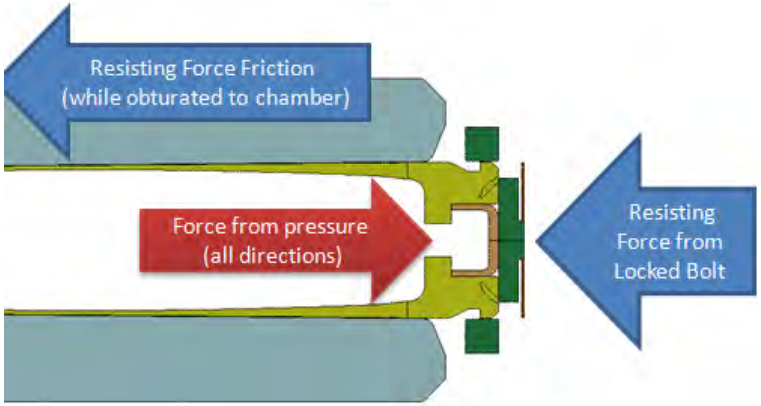

Inside area of cartridge case near base: $A_{case} := 0.068in^2$

Outer diameter of case length: $OD_{case} := 0.375in$

Length of obturating case: $L_{case} := 1.230in$

Peak pressure of P/T curve: $P := 72000psi$

Force against bolt face from Pressure: $F_{press} := P \cdot A_{case}$ $F_{press} = 4896lbf$

Pressure at contact surface between case and chamber: $P_{wall} := 12000psi$

Coefficient of Friction between case and chamber: $\mu := 0.25$ ← Highly Variable

Resistance force from obturation friction: $F_{\mu} := P_{wall} \cdot (\pi \cdot OD_{case} \cdot L_{case}) \cdot \mu$

$F_{\mu} = 4347lbf$

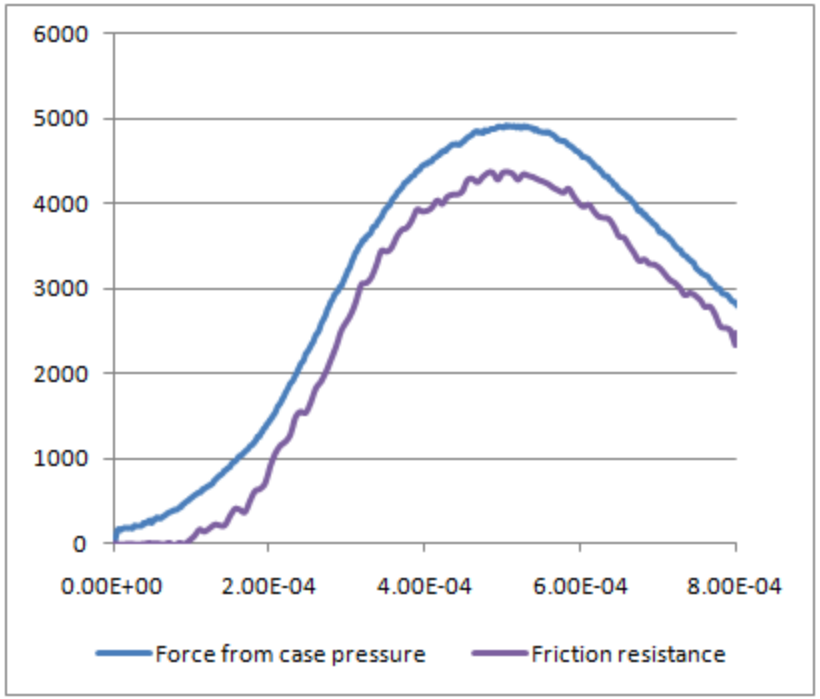

3D Models

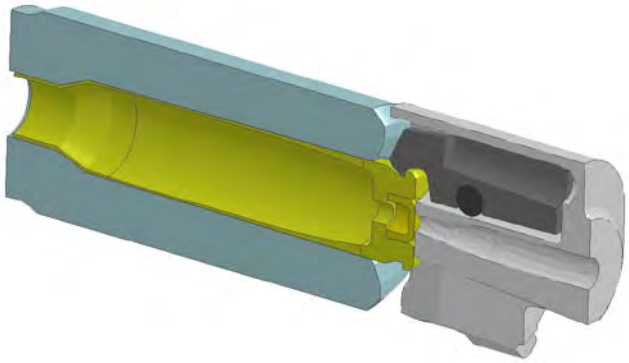

Modeling info

- ½ symmetry (along bolt geometry)
- 500,000 nodes, 2hr run on 32 cpu
- Tet-mesh bolt and extractor
- Hex meshed case and chamber
- Extractor Spring simplified to force
- Uniform pressure assumed

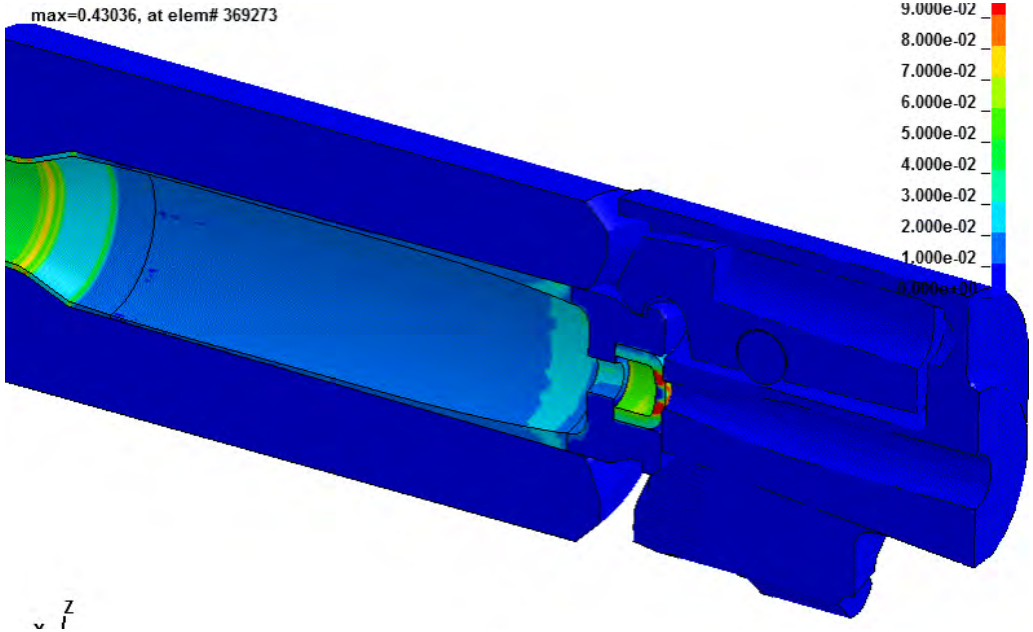

Baseline model

- 72ksi peak pressure
- Friction 0.3s/0.15d
- Red= Plastic strains exceeding 10%

Bolt Face Forces…from Pressure

50 ksi

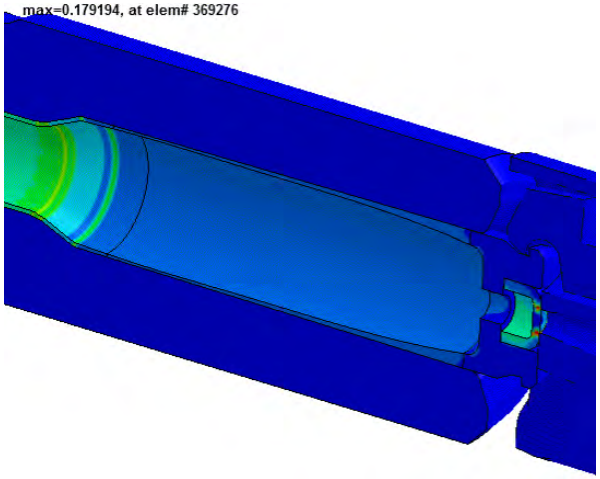

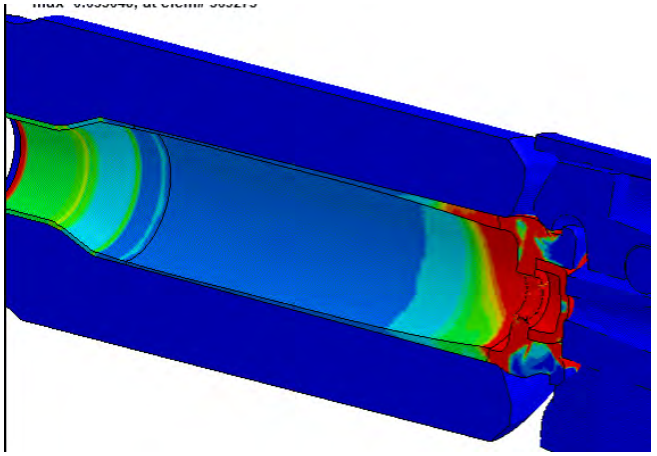

90 ksi

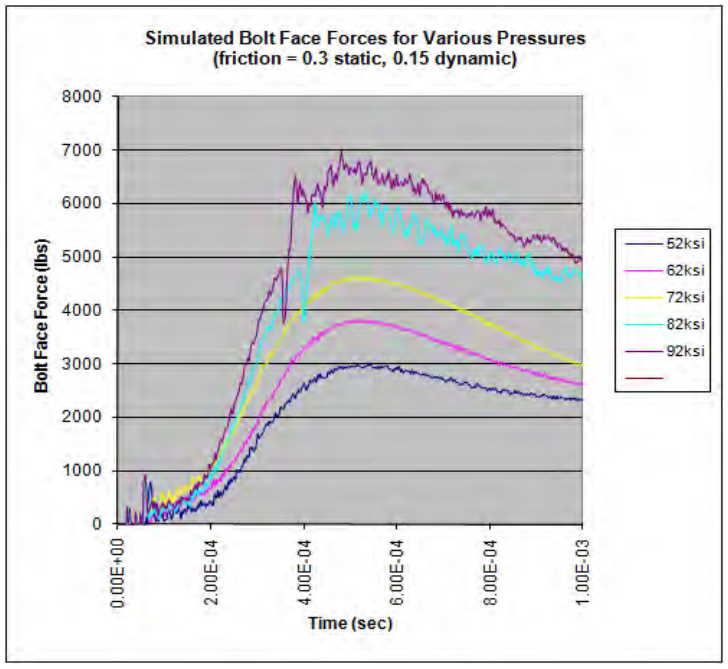

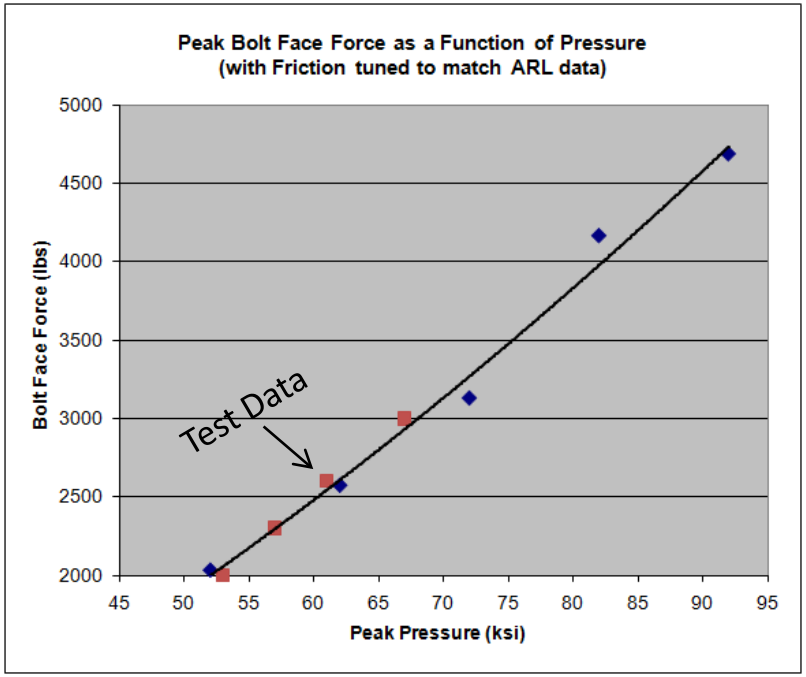

Bolt Face Forces…from Temperature

Pressure variation as a function of temperature.

(Test data generated by ARL (Brosseau/South) showing pressure increase with temperature increase for M855)

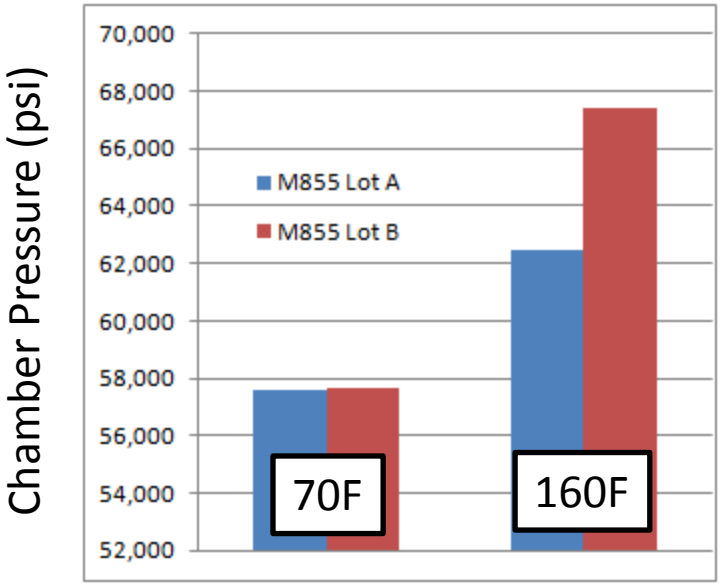

Stress Strain response to temperature increase, for a given hardness

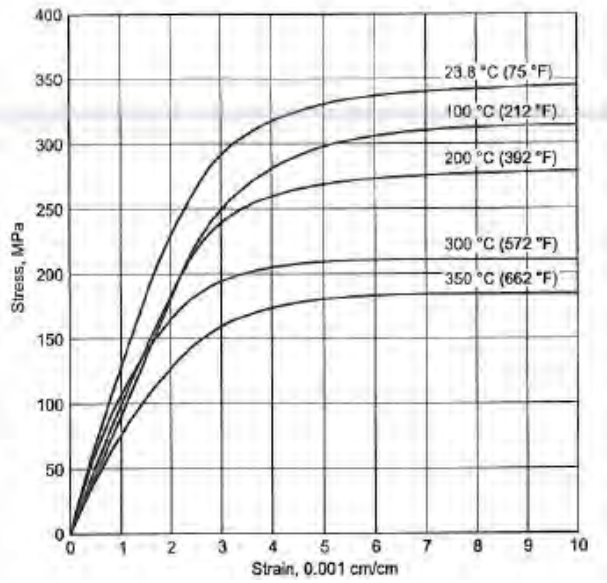

Pressure variations from lot-to-lot, and test-to-test broaden the scope of the analysis. Evaluate concepts, not individual products.

Yield Strengths and flow stress are reduced at higher temps. However, only slightly (~10%) in the temp range of interest.

Bolt Face Forces…from Lubrication

Testing shows NO increase in pressure from lubrication

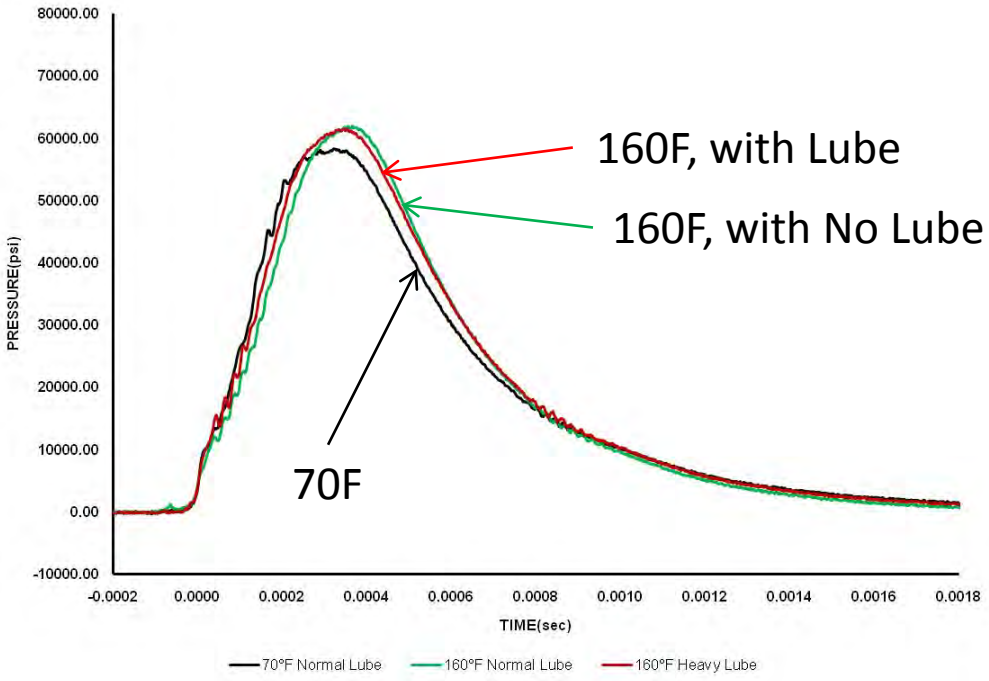

M855 Test data generated by ARL (Brosseau/South)

Friction in Chamber

Typical Static-Dry Coef. Frictions

Steel	Brass	0,35
Steel	Steel	0,78

Lubricated steel-brass can drop to $\mu = 0.05$ or lower

Dynamic (sliding) Frictions are typically 25-75% of static

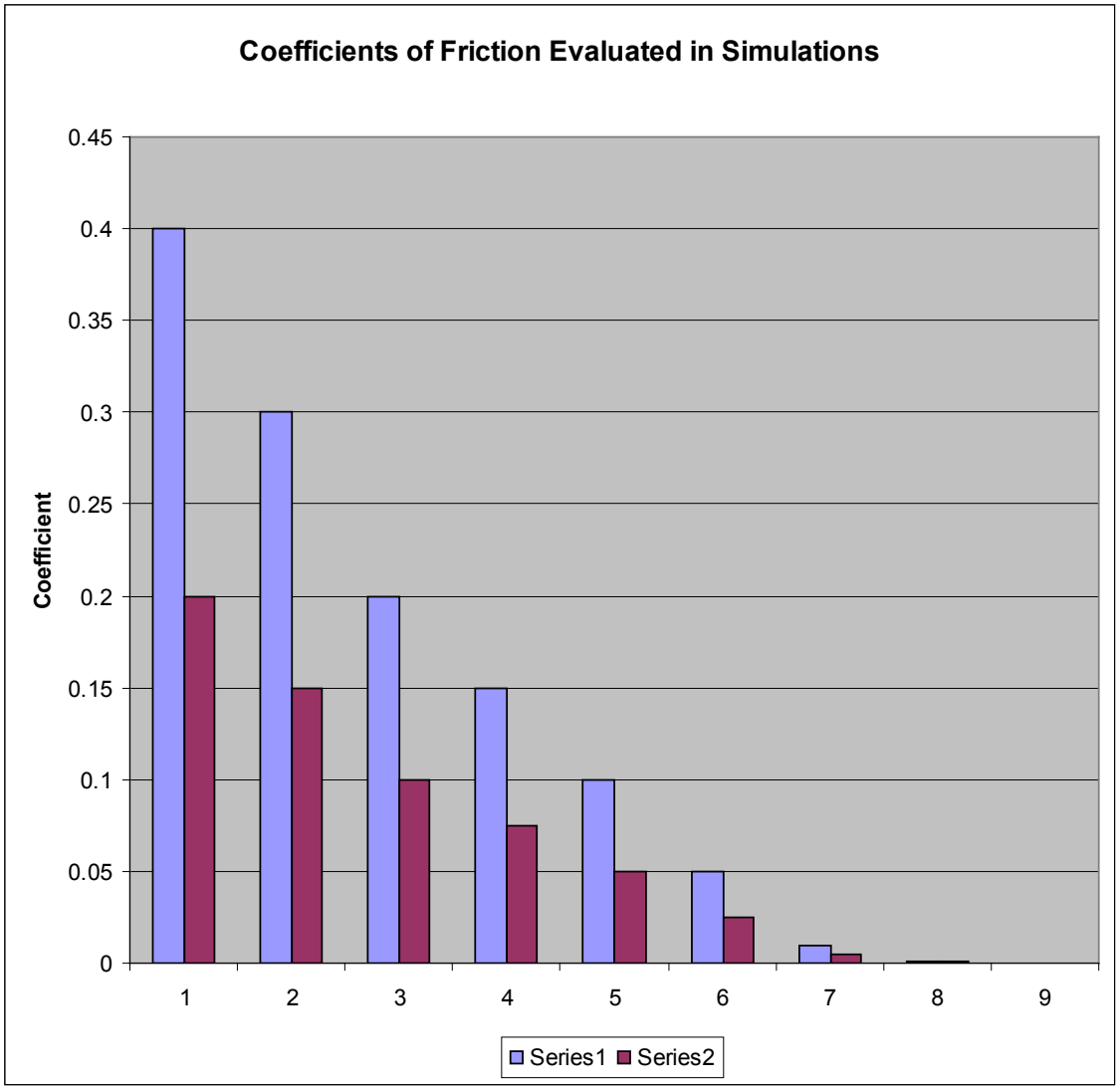

Bolt Face Forces…from Lubrication

S = Static coefficient of friction (μ)
D = Dynamic coefficient of friction

All sims done at 72ksi

Data gathered by Brosseau/South agrees with data generated by Minisi

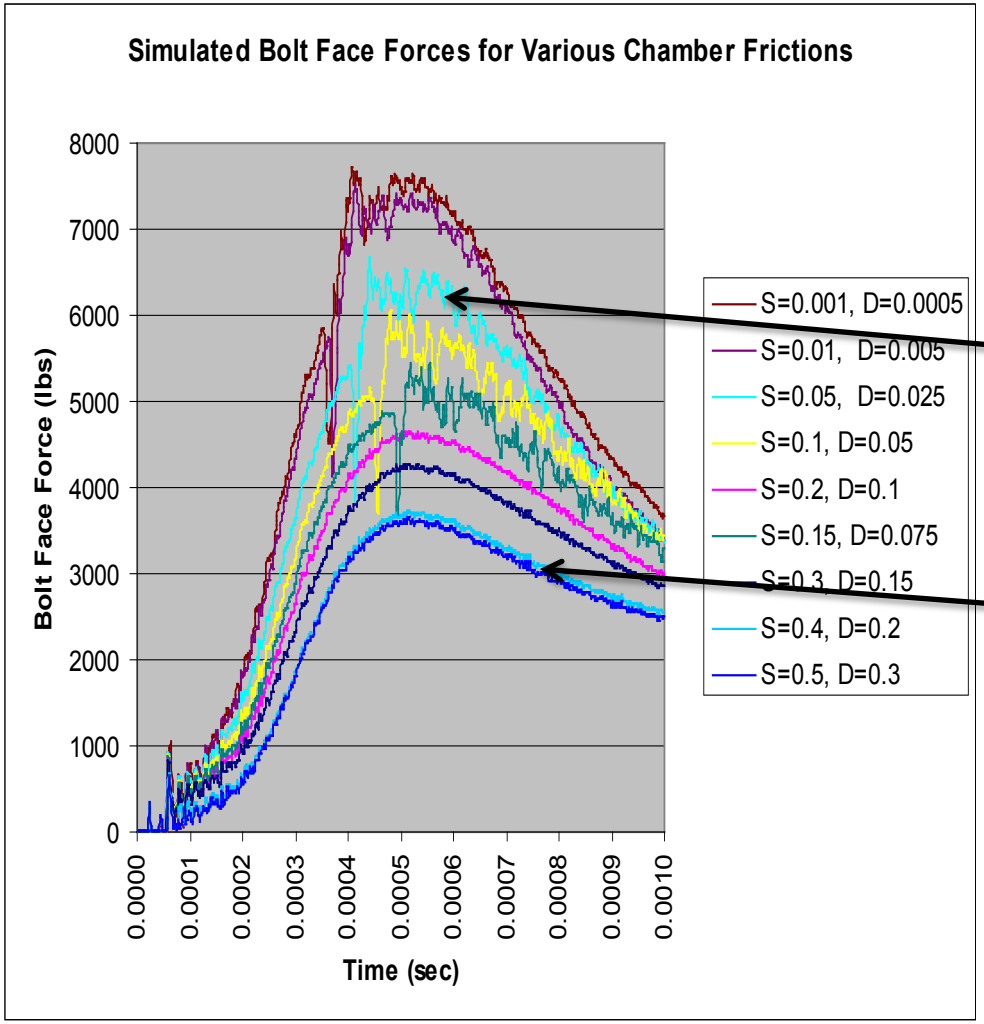

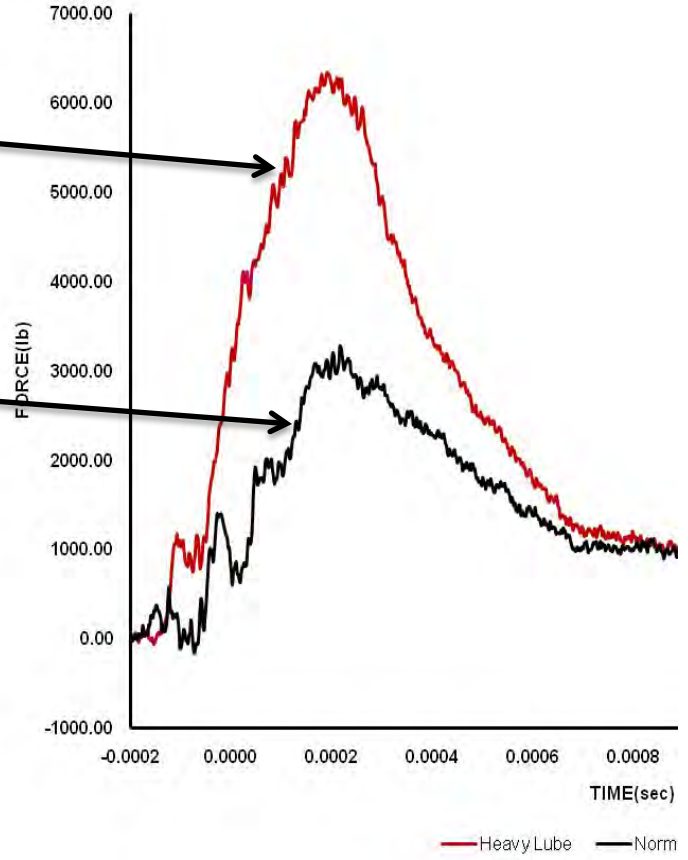

Bolt Face Forces…from Lubrication

All sims at 72ksi peak pressure

S=0.3, D=.15

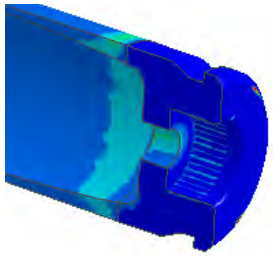

S=0.15, D=.075

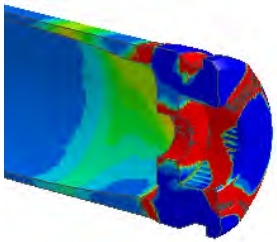

S=0.05, D=.025

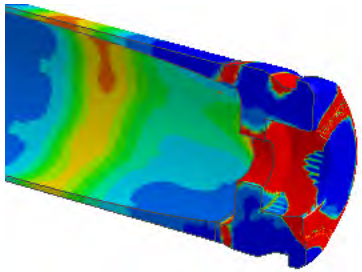

S=0.001, D=.0005

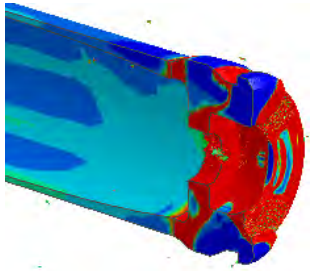

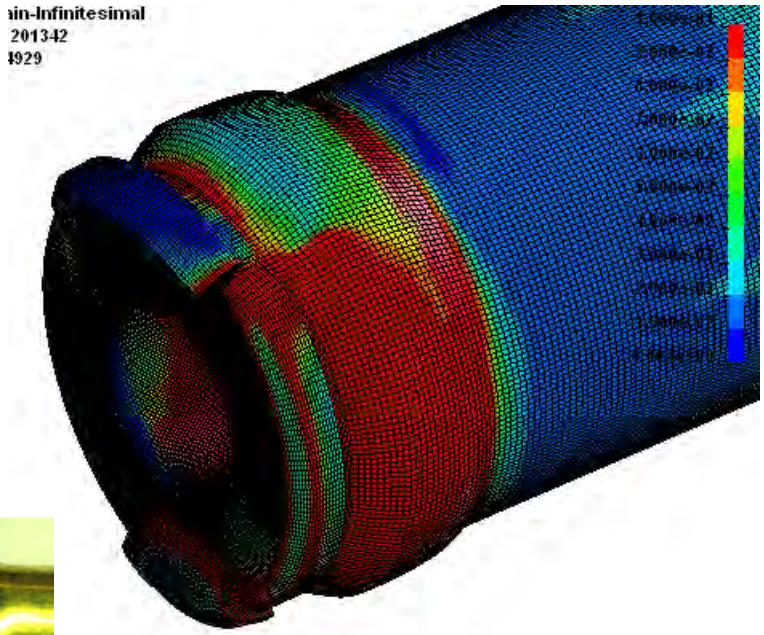

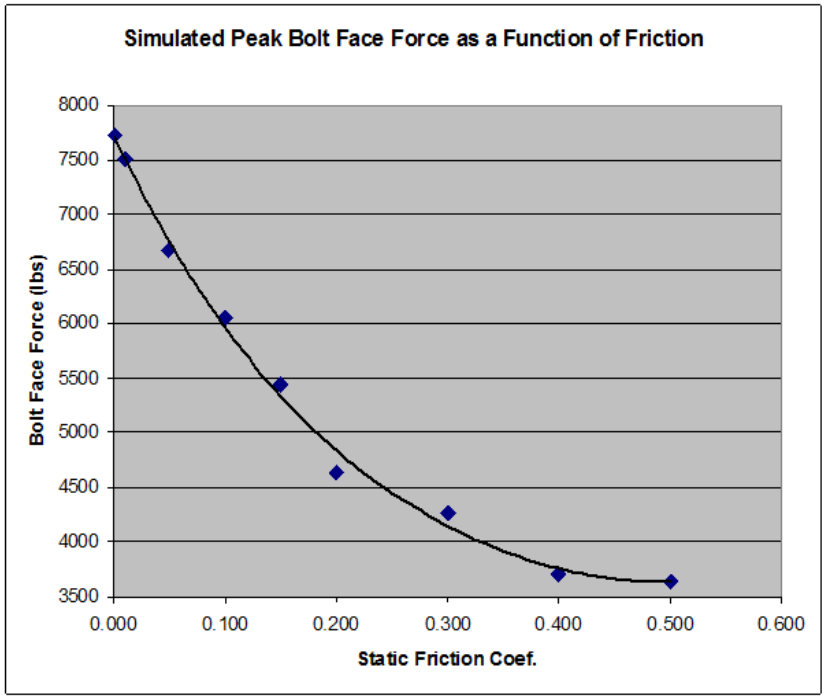

Bolt Face Geometry

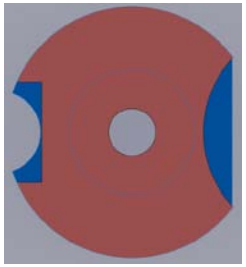

Pictures courtesy of ARL-TR-5377
(Brosseau/South/Michlin)

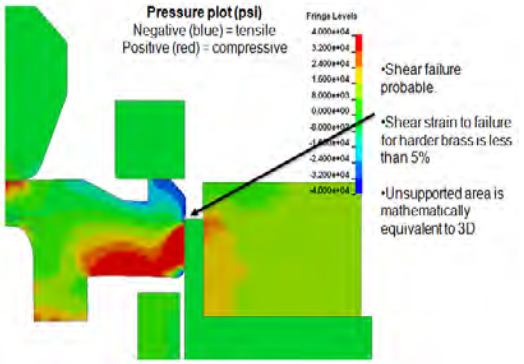

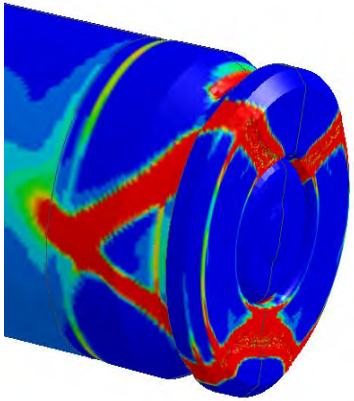

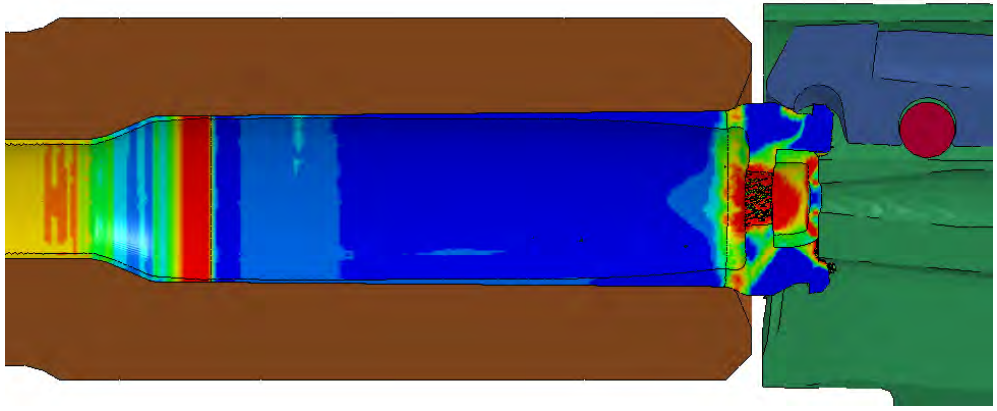

Recall:
Failures occurred on M249, not M4/M16

Supported Bolt Face

Rigid-body disc supports bolt face AXIALLY in this simulation

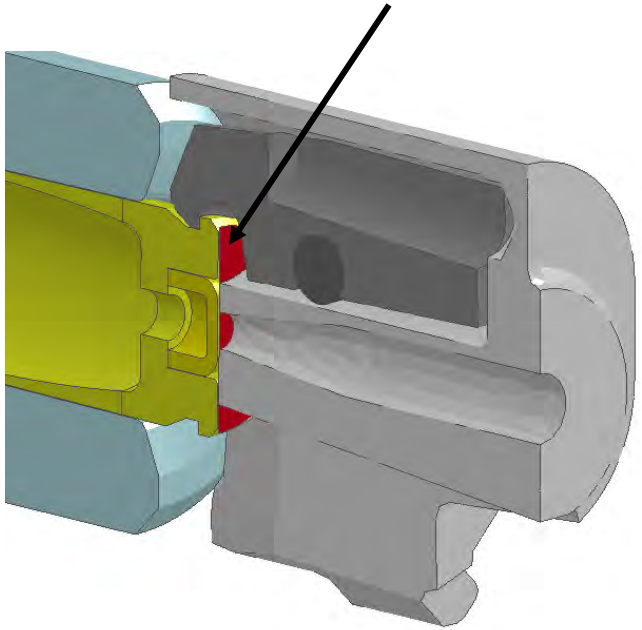

Simulations at 72 ksi

Radial flow not constrained

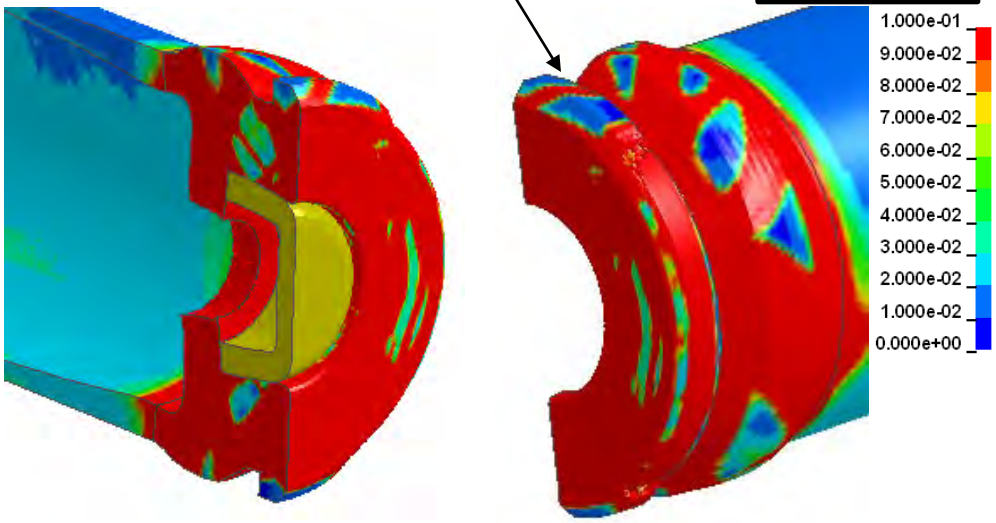

Radial flow contained, bulging in unsupported region is prevented

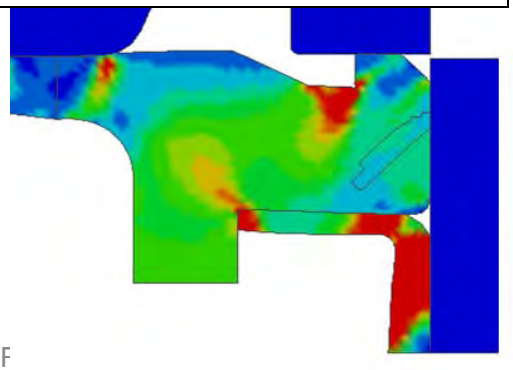

Prevention of axial flow ***alone*** is not enough to stop case bulge at 0-friction

Staking and other “defects”

72ksi with nominal friction

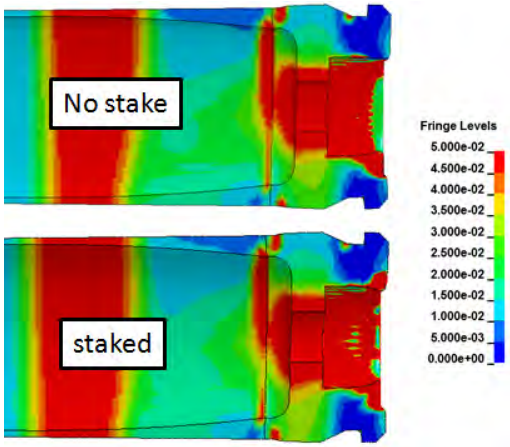

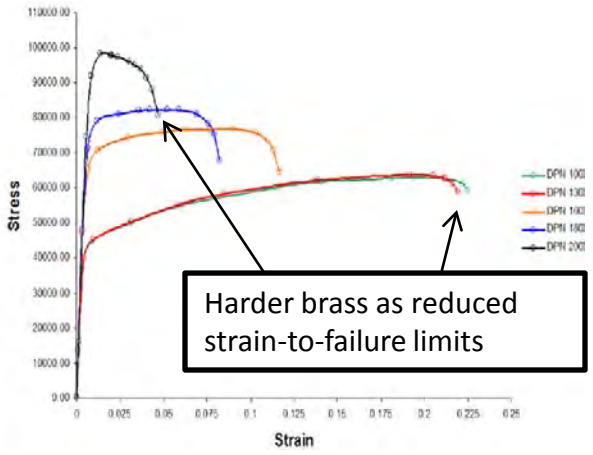

Proposed “roller defect”

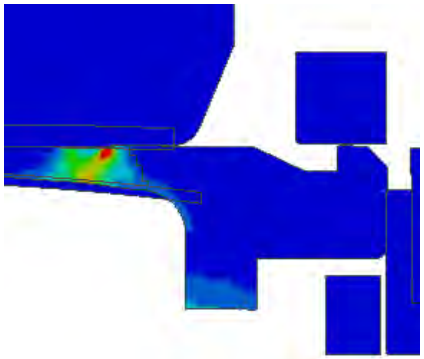

- Stress/strains put into case from observed defects are overcome by the much larger stress/strains caused by material flow into bolt face
- Minor defects create stress concentration points
- Potential for crack propagation should increase wherever stress concentration point is placed in “hard” brass.

Combined loads

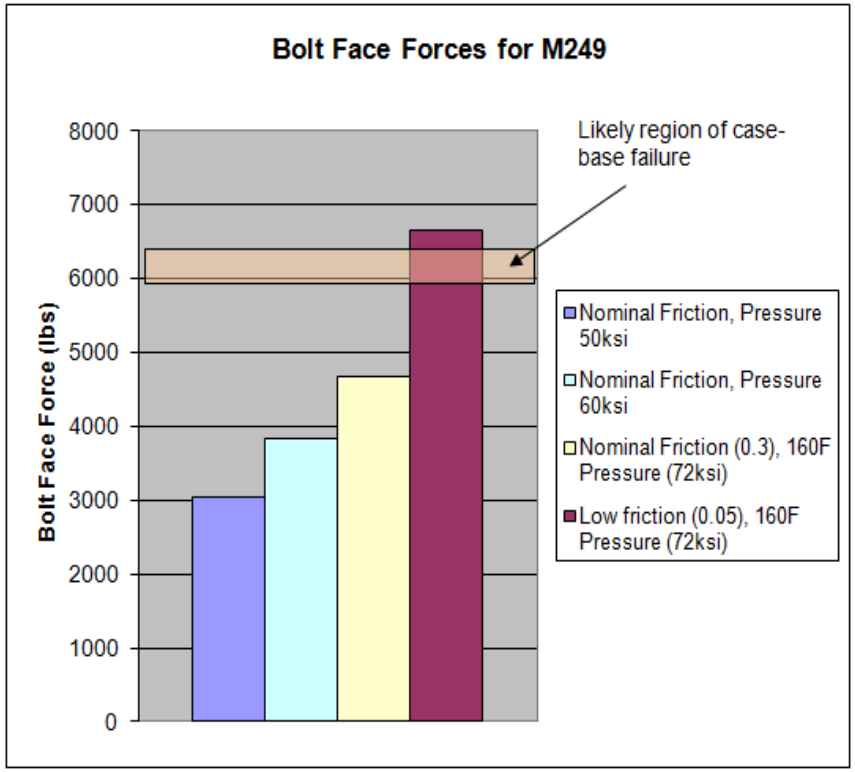

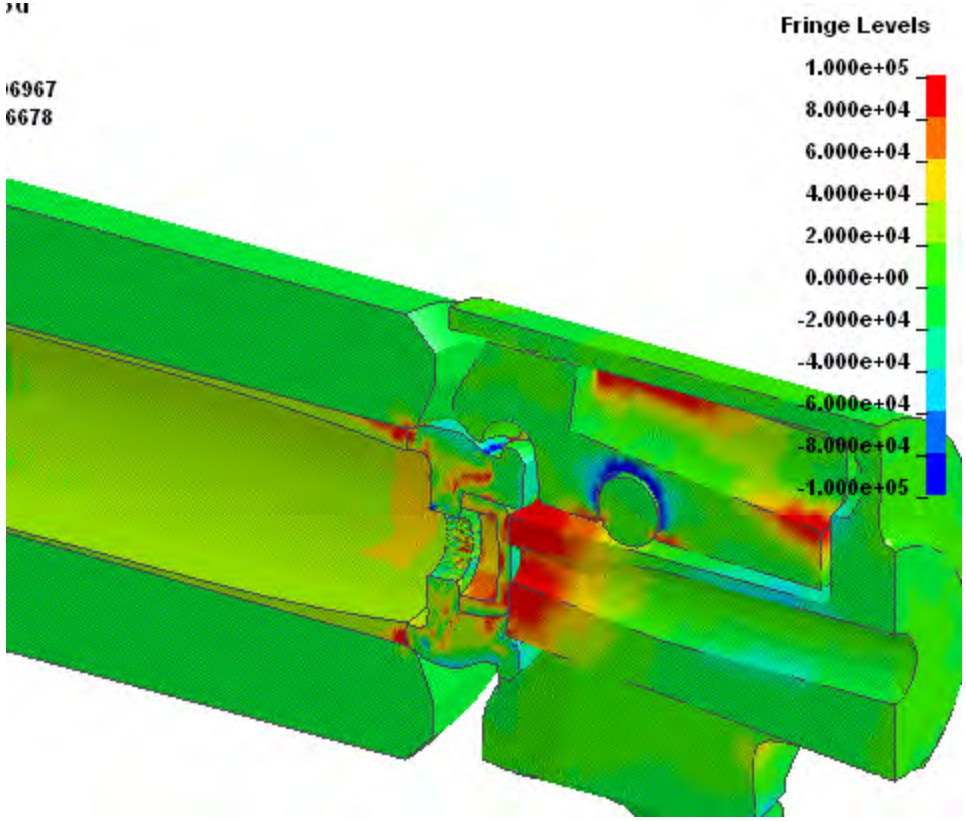

- 1000 lb jump in load for 10,000 psi pressure increase
- 2000 lb jump for reduction in obturation friction (μ= 0.05)

Summary

1. Nominal bolt face forces in ambient conditions (temp/friction) are around 3000 lb

2. Case extrusion and resulting failure occurs around 6000 lbs of bolt face force, in M249

3. **Pressure** increase of ~10,000psi can increase bolt face load an *additional* 1000 lbs

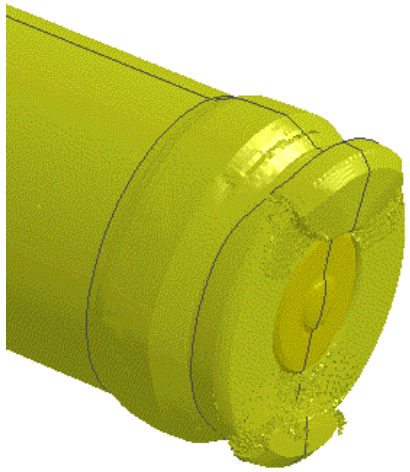

4. **Lubrication** in Chamber can increase bolt face load an *additional* 2000 lbs (μ=0.05), 3000 lbs (μ near zero)

5. Failure less likely to occur on M16/M4 bolt face due to better **case support**

6. These failures should occur regardless of staking or other defects presence/absence

DO NOT ALLOW LUBRICATION TO COME BETWEEN CARTIDGE CASE AND CHAMBER

Numerical Investigation of Lateral Jet Interaction on a Fin-Stabilized Projectile

Jim DeSpirito, Ph. D
U.S. Army Research Laboratory

TECHNOLOGY DRIVEN. WARFIGHTER FOCUSED.

26th International Symposium on Ballistics
Miami, Florida
13 September 2011

Basic Features of Jet Interaction (JI) Flow (2)

M ≤ Jet Issuing From Body of Revolution into *M* > 1 Crossflow

From **Graham** and Weinacht, 2000

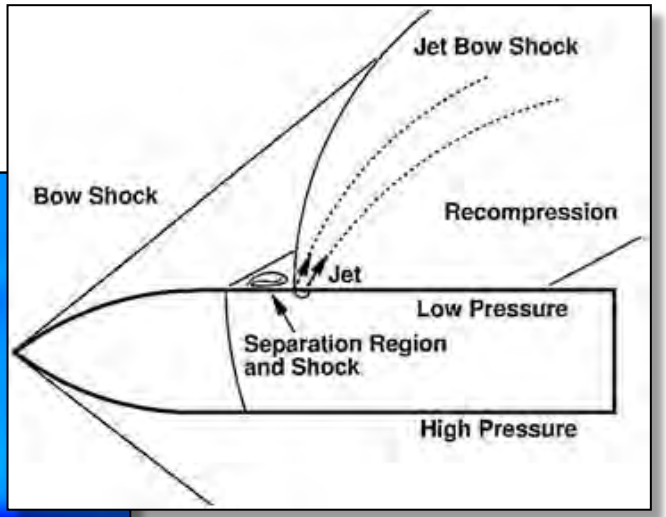

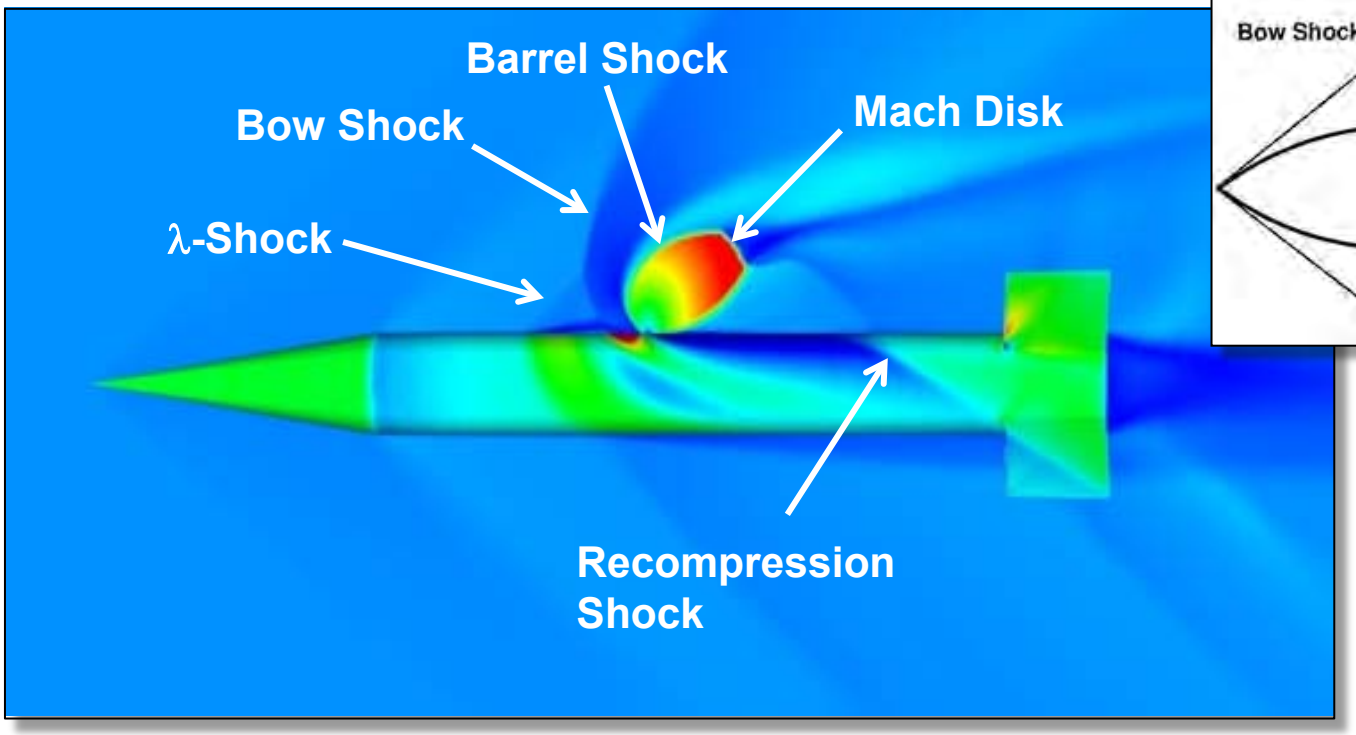

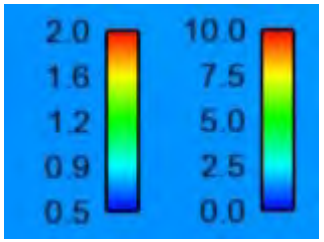

- Sonic Jet
- PR=340
- Mach 1.5 Crossflow

Objective and Approach

- Use computational fluid dynamics (CFD) to investigate the effect of lateral reaction jet control (RJC) nozzle location and resulting jet interaction (JI) effects on control forces and moments on a generic, fin-stabilized projectile.
- Parameters fixed:
  - Jet total pressure to freestream static pressure ratio (PR), p_{0j}/p_{∞} = 340
  - Sonic nozzle, 2.54 mm diameter
- Parameters varied:
  - Jet location along projectile axis
  - Mach number (M = 1.5, 2.5)

Numerical Approach

- CFD++ (v10.1), from Metacomp Technologies, Inc.
  - Finite-volume, point implicit formulation
  - Second-order, upwind HLLC Riemann solver
  - TVD flux limiter
  - Multigrid W-cycle method (4 cycles, 20 grid levels)
- Menter's Shear Stress Transport (SST) turbulence model, based on 2-equation, k-ω model was used.
- High performance computer systems used:
  - SGI Altix ICE 8200 Supercomputer (HAROLD) and Linux Networx Advanced Technology Cluster (MJM) at Army Research Laboratory DoD Supercomputing Resource Center (DSRC), Aberdeen proving Ground, MD.
  - Cray XE6 (RAPTOR) at Air Force Research Laboratory DSRC at Wright-Patterson Air Force Base, OH.

Model Geometry
Army-Navy Finner

- Army-Navy Finner (ANF) missile—a reference configuration reported extensively in the archival literature.
  - 2.84 cal. conical nose
  - 10 cal. total length
  - 1-cal., square planform fins mounted flush with base
  - Center of gravity (c.g.) located 5.5 cal. from nose
- 7 jet locations on top surface, as indicated in figure.
- No lateral reaction jet validation data.

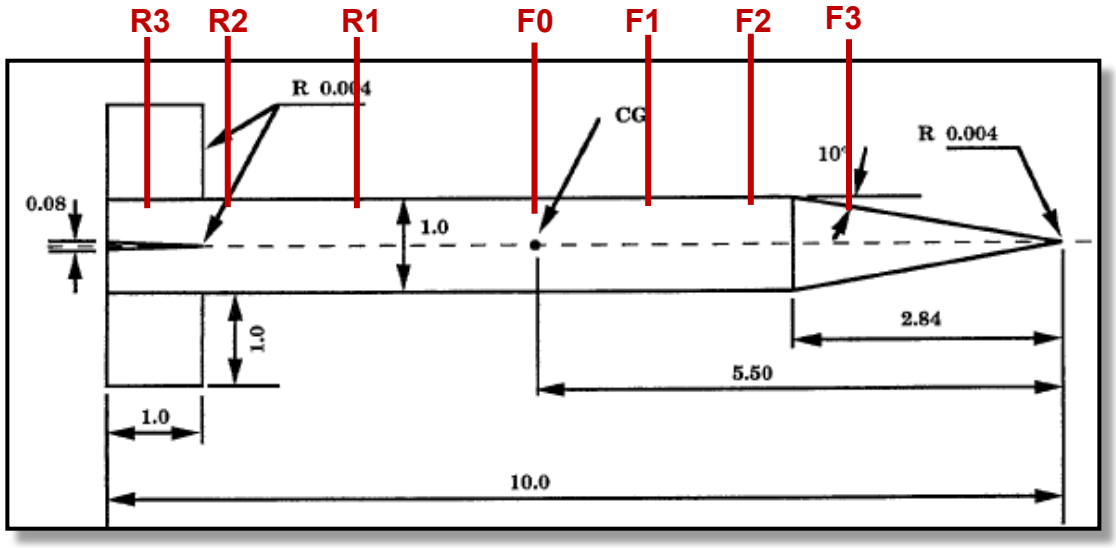

Label	Location from nose (mm)	Location from nose (cal.)	Location from c.g. (mm)	Location from c.g. (cal.)	Description
F3	65.0	2.17	-100.0	-3.33	On conical nose
F2	90.0	3.00	-75.0	-2.50	Just rearward of cone
F1	127.5	4.25	-37.5	-1.25	Between cone and c.g.
F0	165.0	5.50	0.0	0.00	At c.g.
R1	215.0	7.17	50.0	1.67	Between c.g. and tail fins
R2	265.0	8.83	100.0	3.33	Just ahead of tail fins
R3	290.0	9.67	125.0	4.17	Between tail fins

Army-Navy Finner Meshes

- MIME, from Metacomp Technologies, Inc.
  - 8.8 to 10.2 M cells
  - Prism layers on solid boundaries
  - Half domain modeled
- Computational domain
  - 5 cal. forward, 20 cal. behind
  - 14.5 cal. radially from body
- Adiabatic walls, y+ ≤ 1.0
- Freestream M = 1.5, 2.5 at p_∞ = 101.3 kPa and T = 288 K
- Stagnation conditions (p_0, T_0) at nozzle plenum inlet

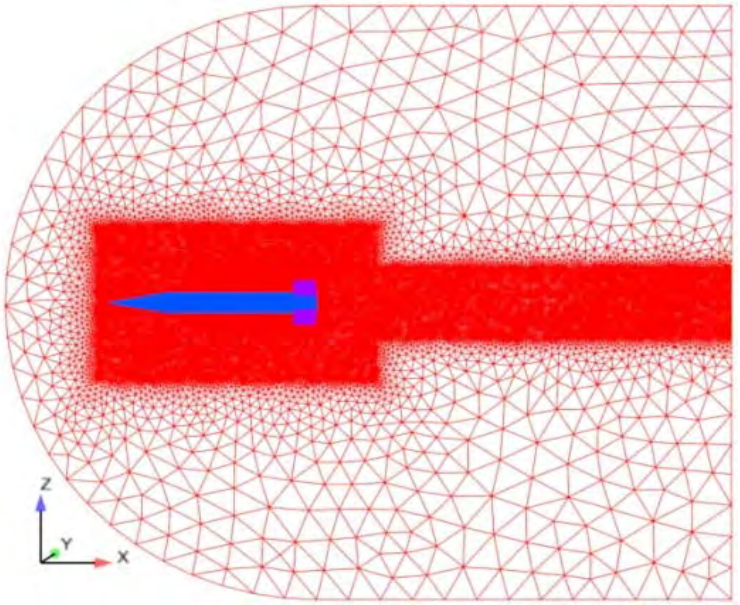

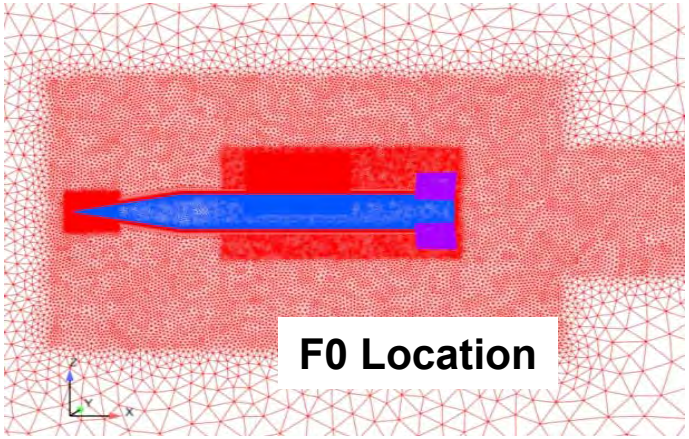

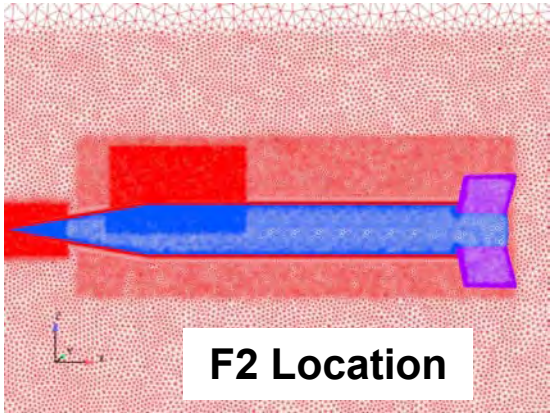

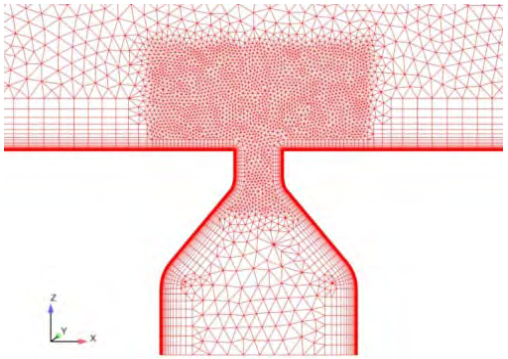

Example Flowfield
Army-Navy Finner (PR=340)

Numerical Schlieren

Mach 2.5

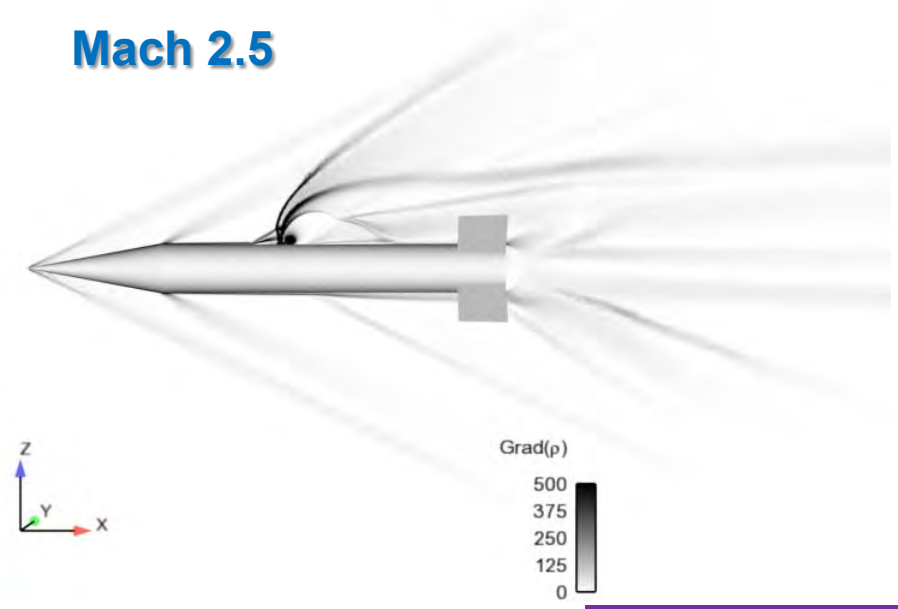

Mach 1.5

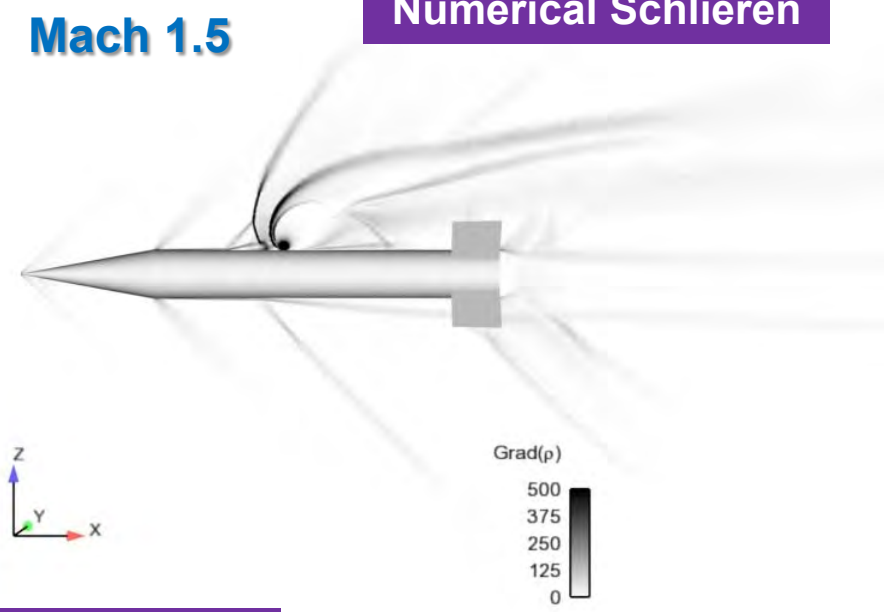

Normalized surface pressure (p/p_∞) and Mach contours

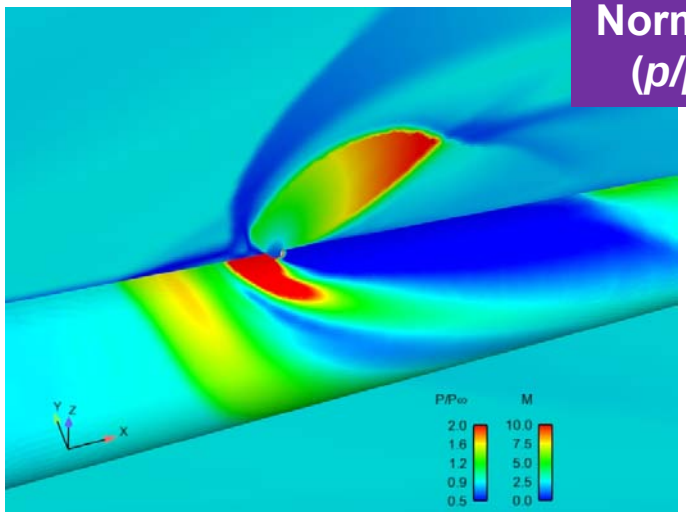

F0 Location

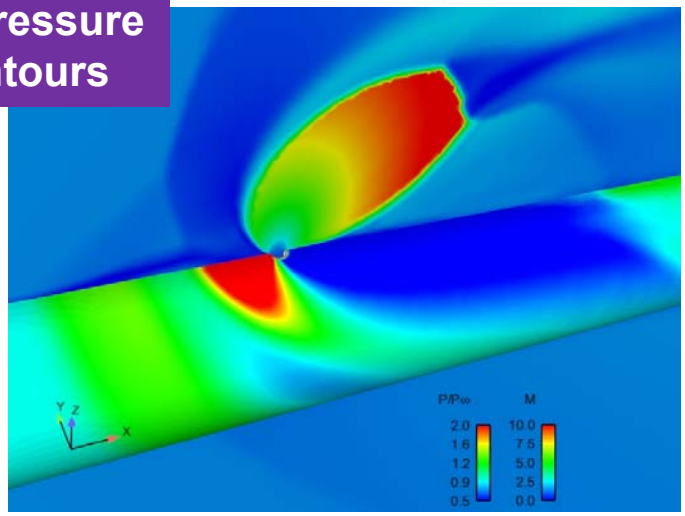

Mach 1.5 Flowfield

p/p_∞ contours on projectile and Mach contours on symmetry plane (PR=340)

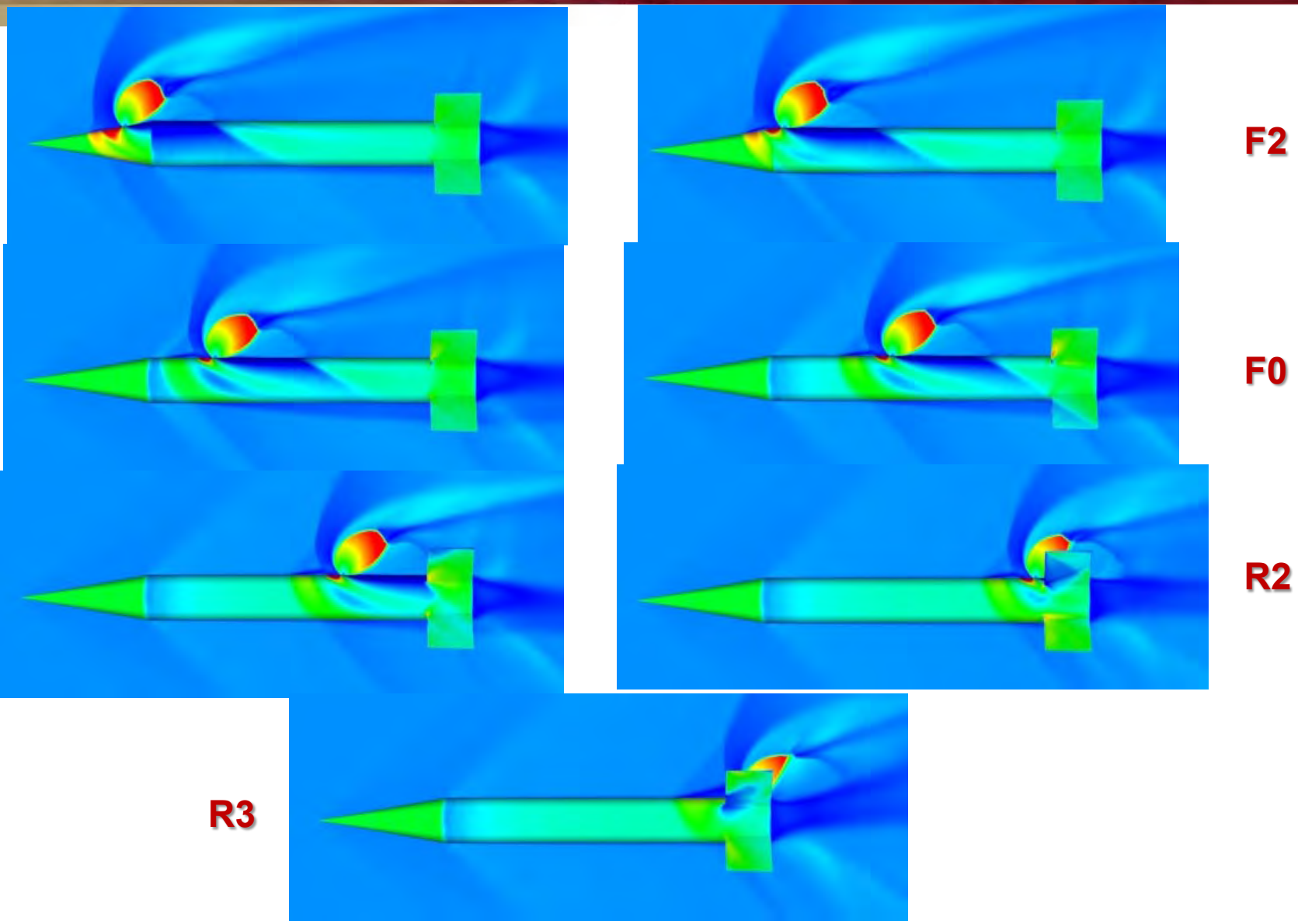

Mach 2.5 Flowfield

p/p_∞ contours on projectile and Mach contours on symmetry plane (PR=340)

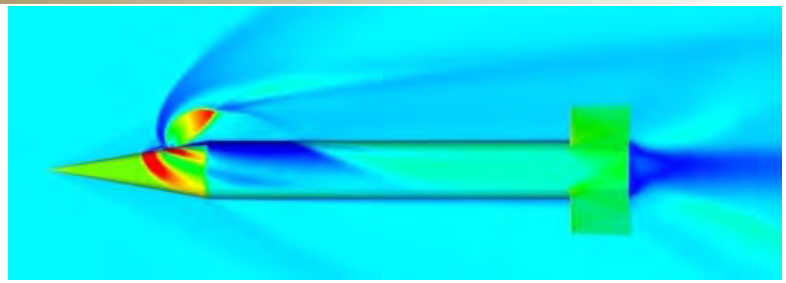

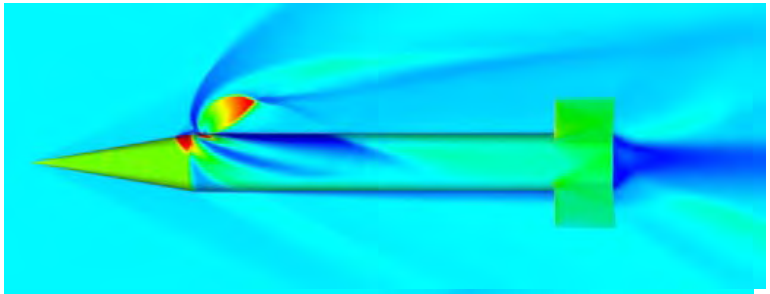

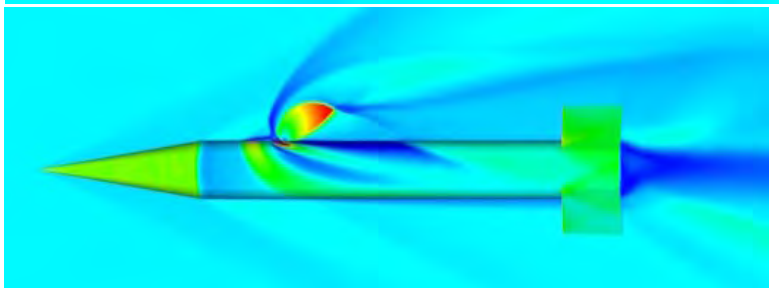

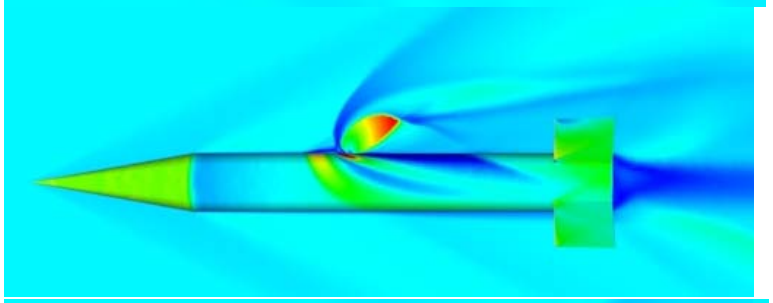

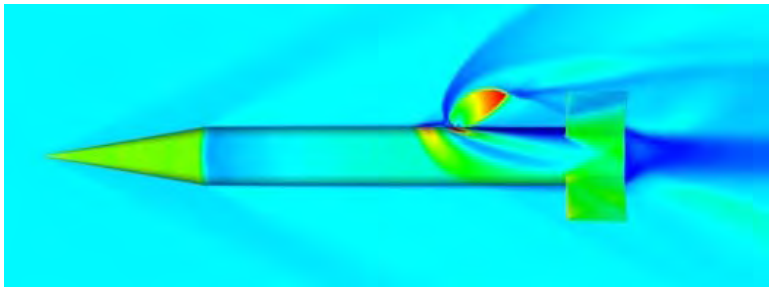

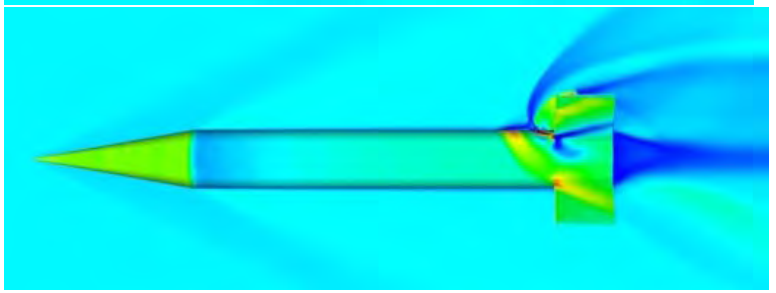

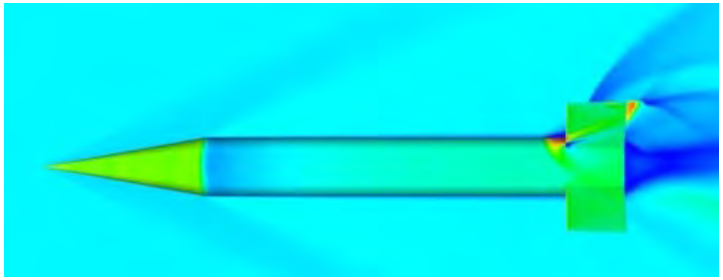

Jet Amplification Factors
PR=340

$$K_f = \frac{C_{N_j} + C_{N_{ji}}}{C_{N_j}} \qquad K_m = \frac{C_{m_j} + C_{m_{ji}}}{C_{m_j}}$$

- Measure of JI effect.
  - > 1 → amplification
  - < 1 → attenuation
  - < 0 → effect opposite jet thrust

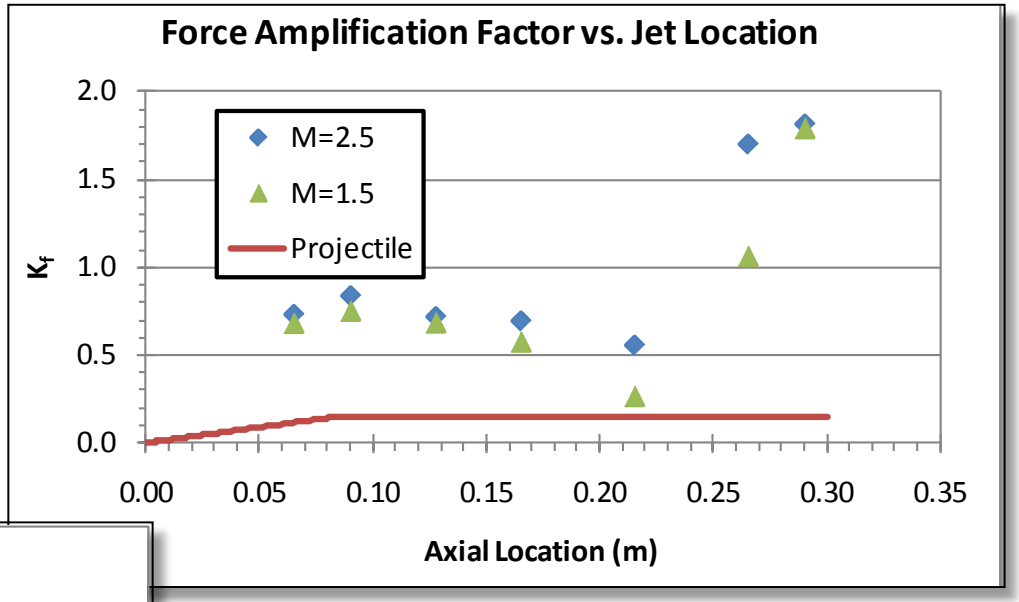

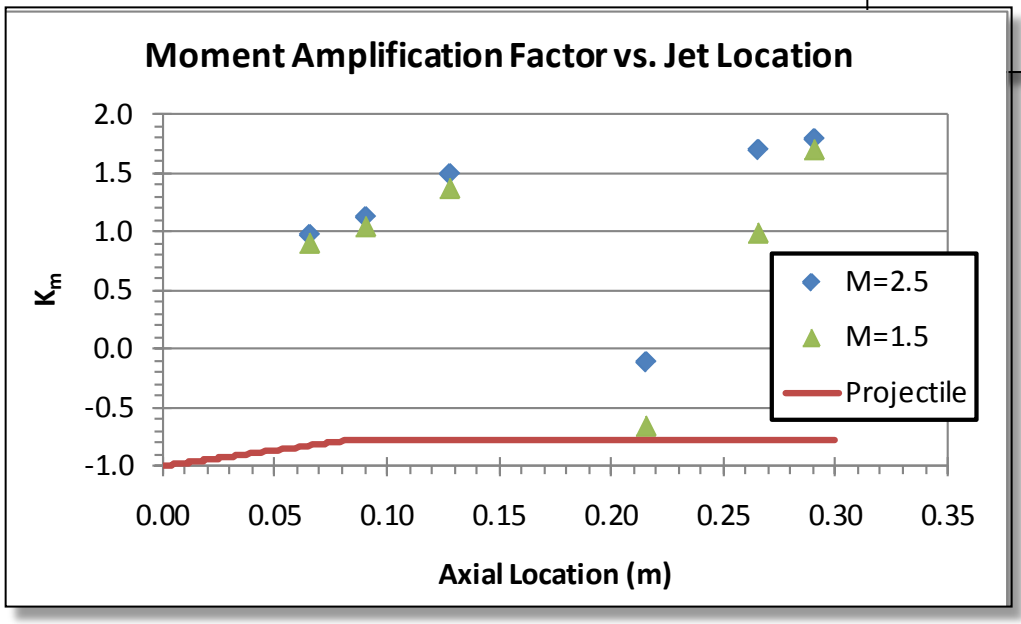

- Jet force attenuated at forward five locations.
- Jet force amplified at rear two locations.
- Moment due to jet thrust amplified at most locations.
- K_m < 0 at the R1 location.

Force & Moment Coefficients
PR=340

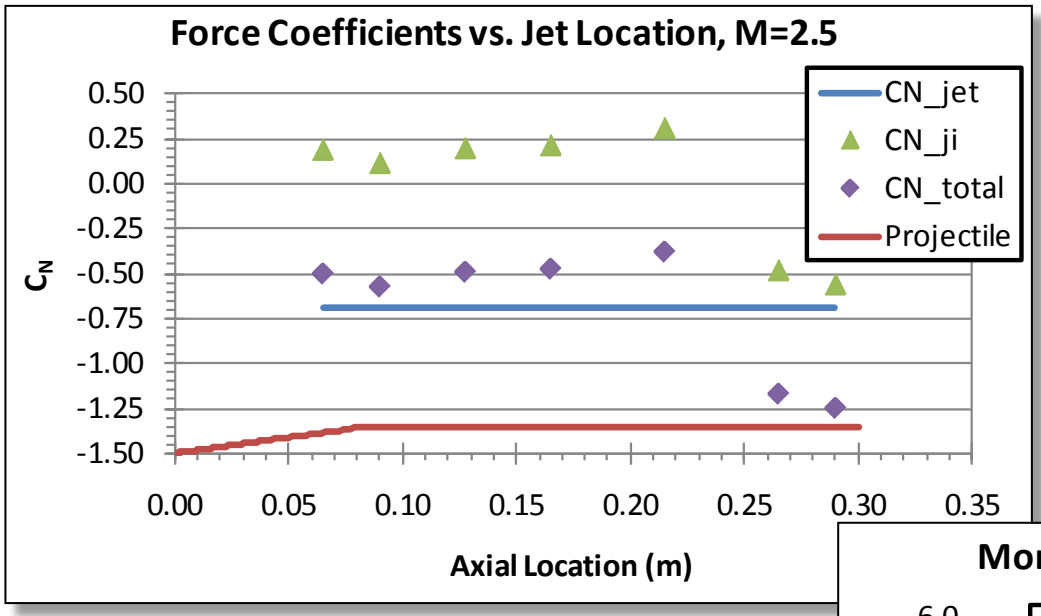

- Jet force constant
- JI force > 0 opposes jet thrust
- "Total" force
  - Magnitude < jet force indicates attenuation
  - Magnitude > jet force indicates amplification

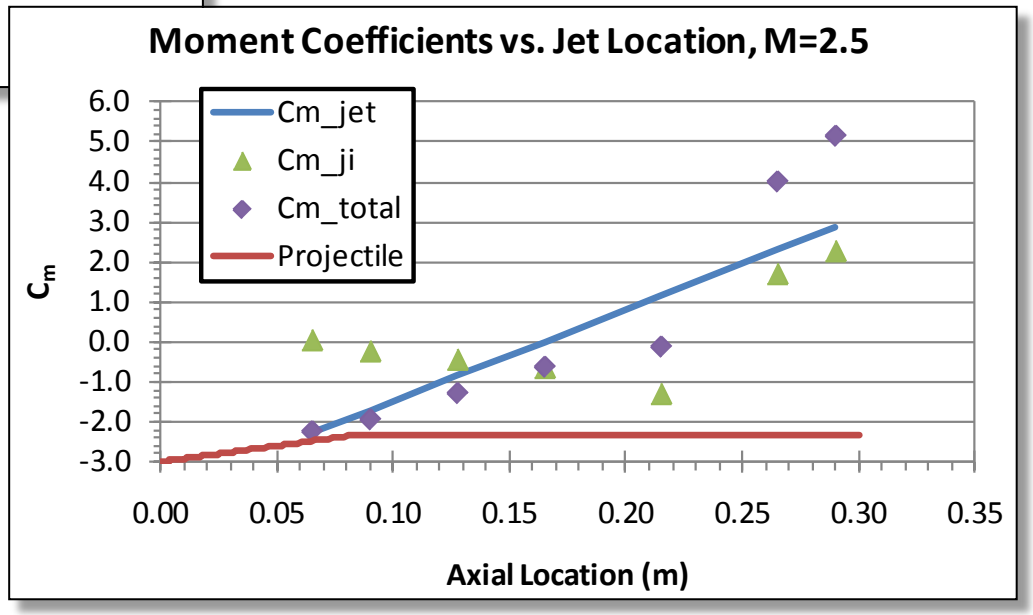

- Moment varies linearly with jet location.
- "Total" moment approaches moment due to jet thrust as location moves toward nose
  - JI moment goes to zero
  - K_m goes to zero
- "Total" moment at R1 opposite that due to jet thrust

Force Centers of Pressure
PR=340

$$x_{cp} = -\frac{C_{m_k}}{C_{N_k}}$$

- Resultant force center of pressure (RFCP, “total”) varies nearly linearly with jet location from c.g. and forward.
- At R1, RFCP is well forward at Mach 1.5.
  - 125 mm forward
  - Interaction with tail fins
  - Negative K_m at R1
- Neither C_{m_total}, nor RFCP, are zero when jet located at c.g.

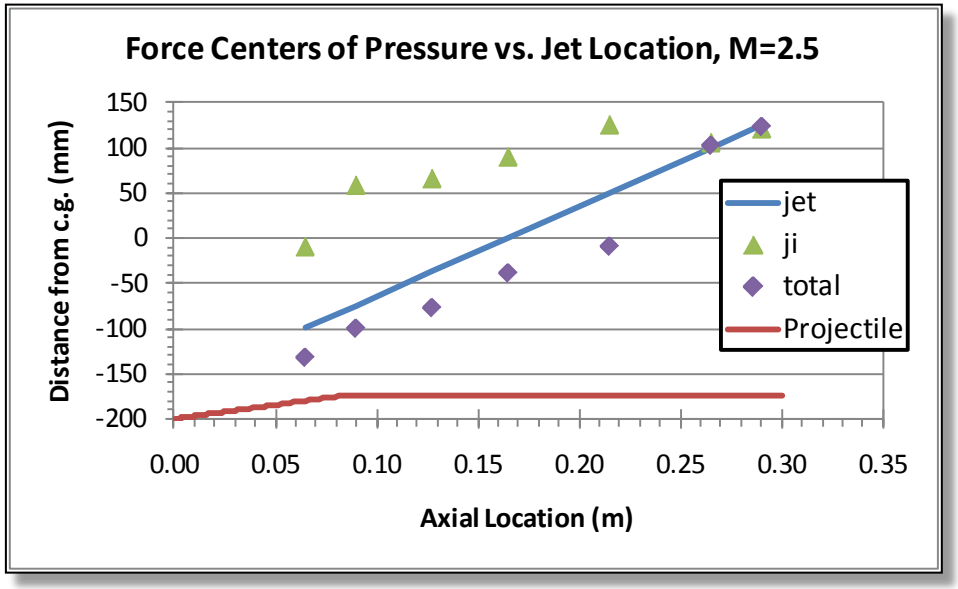

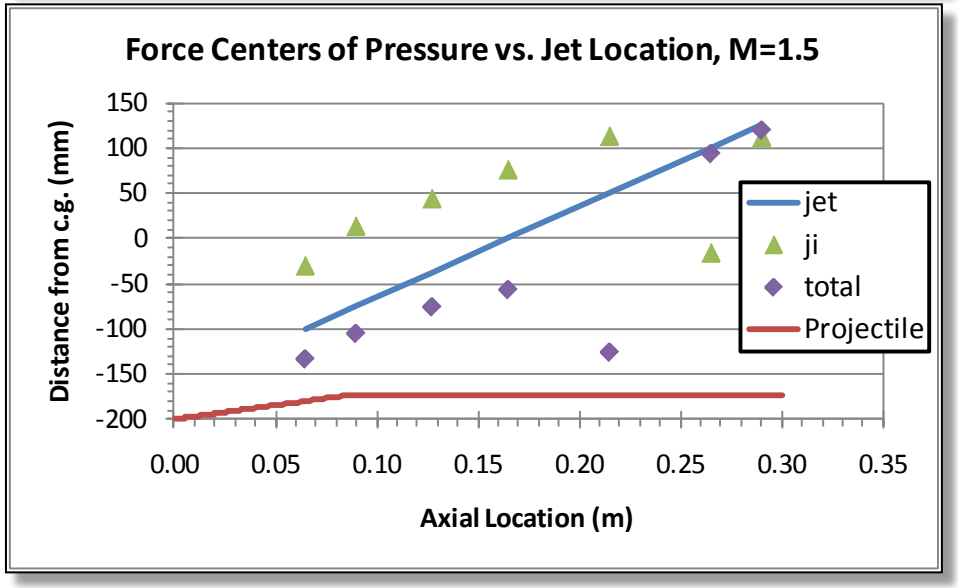

Summary and Conclusions

- Effects of lateral reaction jet location on the forces and moments imparted to basic fin-stabilized projectile were investigated.
- Features of JI flowfield compared well with those presented in archival literature.
- Jet thrust was attenuated at forward five locations
  - 15-45% at Mach 2.5
  - 25-75% at Mach 1.5
- Jet thrust amplified up to 80% when located just forward or between tail fins.
- Locating jet near the tail of projectile can minimize the traditional JI effects that are due to interactions in the jet wake.
- However, the near-jet flowfield interaction between jet and fins must be taken into account.

Future Work

- These results and additional flat plat investigation results presented at the 29th AIAA Applied Aerodynamics Conference, Honolulu, HI, June 2011.
  - DeSpirito, J., "Factors Affecting Reaction Jet Interaction Effects on Projectiles," AIAA-2011-3031, June 2011.
- Plan to extend study to include
  - Higher Mach number
  - Effects of variation of projectile angle of attack
  - Effects of transient jet pulse
  - Effects of projectile rotation
- Also plan investigations in subsonic crossflow.

Acknowledgments

This work was supported in part by grants of high-performance computing time from the U.S. Department of Defense (DOD) High Performance Computing Modernization program at the Army Research Laboratory DOD Supercomputing Resource Center (DSRC), Aberdeen Proving Ground, MD, and the Air Force Research Laboratory DSRC, Wright-Patterson Air Force Base, OH.

Modeling of Fabric Impact with High-Speed Imaging and Nickel-Chromium Wires Validation

Sidney Chocron,

Trenton Kirchdoerfer, Nikki King, Christopher Freitas

Outline

- Tests set-up and diagnostics:
  - Imacon Camera.
  - Phantom Camera.
- Computations with LS-DYNA and multi-pronged validation (single yarn, single layer, multi-layer and V50).
- Principles, main results and validation of Nickel-Chromium wire technique.

Test set-up: fabric with NiCr Wire

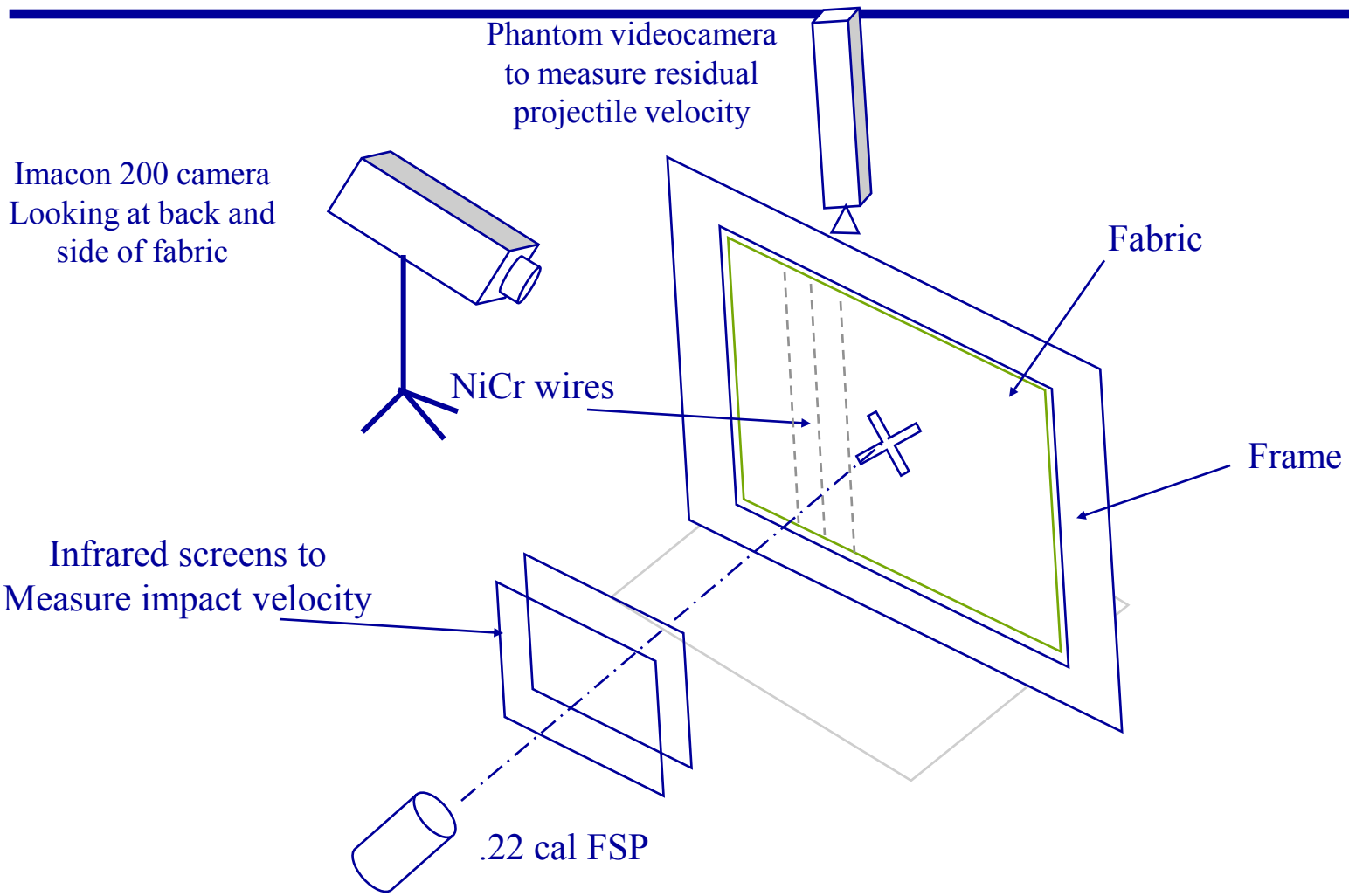

Test set-up

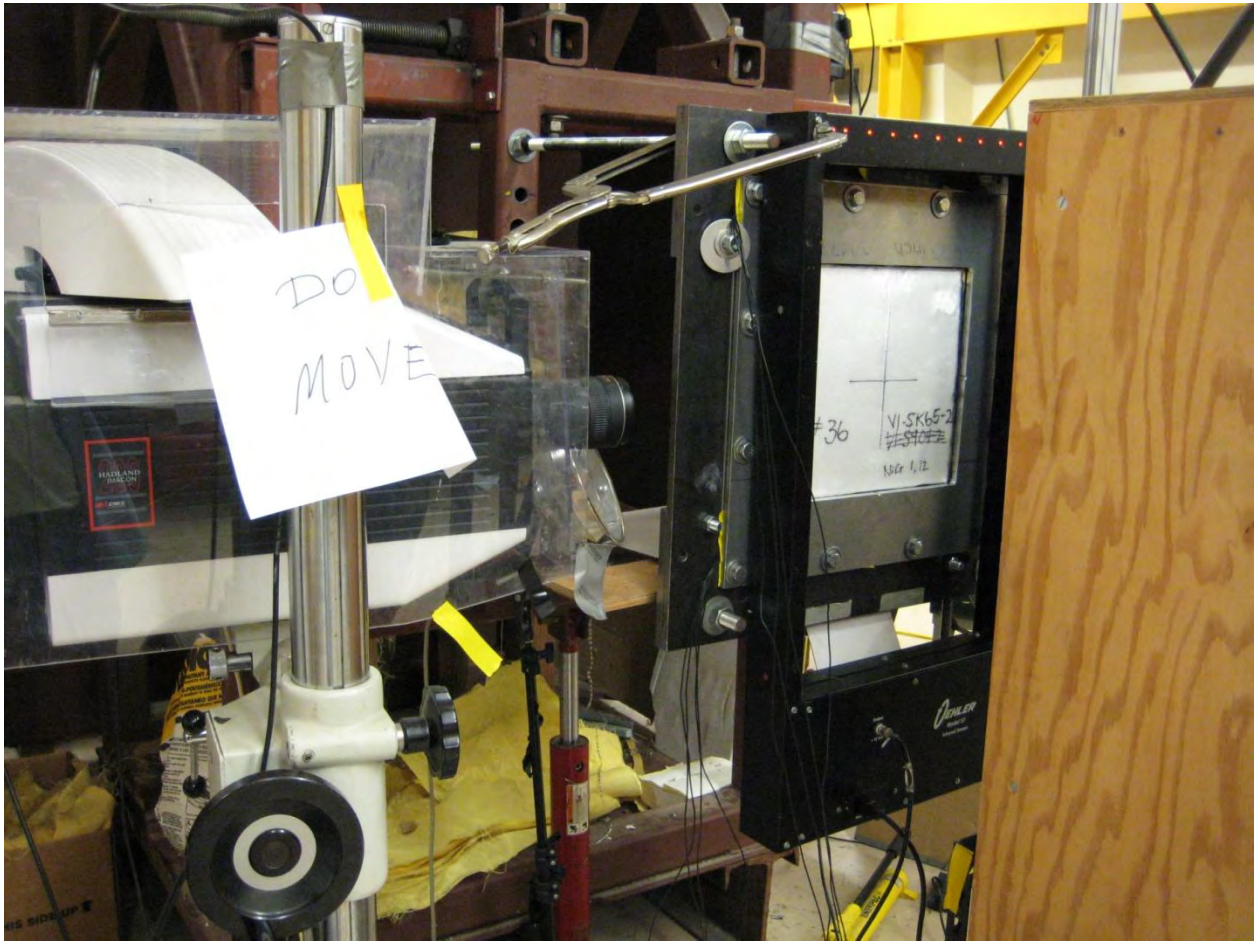

Test set-up

Diagnostics

- Imacon 200
  - 16 frames at a maximum rate of one every five nanoseconds. The resolution is 1200 980 pixels.
  - Used to watch the back of the target (sideways) during the first 50-80 μs at a rate of one frame every 5 μs. Exposure was 800 ns. The area seen was around 6 6 cm^2 (2.4 2.4 in^2) .
  - Provides early time position (and speed) of the transverse wave and the apex of the pyramid, time of penetration of last layer.
- Phantom V7
  - Provides hundreds of images of back of target, used at one frame every 100 μs. Resolution 800 240.
  - Gives residual velocity (and shape) of projectile, late time deflection of target, late time base of pyramid.

Materials

Fabric	Denier	Yarns per inch	Areal Density of one layer (kg/m^2)
Kev KM2 S5705	850	31	0.252
Kev KM2 S5706	600	34	0.186
Dyneema SK-65	792	w: 20, f: 15	0.126
PBO	500	24	0.113

The projectiles used were the .30 in. cal FSP (44 grain) and the .22 in. cal FSP (17 grain).

Numerical validation

- Numerical validation was performed in various ways, providing great confidence on the model:
  - Single yarn impact.
  - Single layer impact.
  - Multi-layer tests.
  - Ballistic limit comparison.
  - NiCr wire comparison.

Single Yarn Impact Validation

Smith theory on transverse impact on single yarns

$$V = c\sqrt{\varepsilon(2\sqrt{\varepsilon(1+\varepsilon)} - \varepsilon)}$$

$$U = c\sqrt{\varepsilon(1+\varepsilon)} - \varepsilon$$

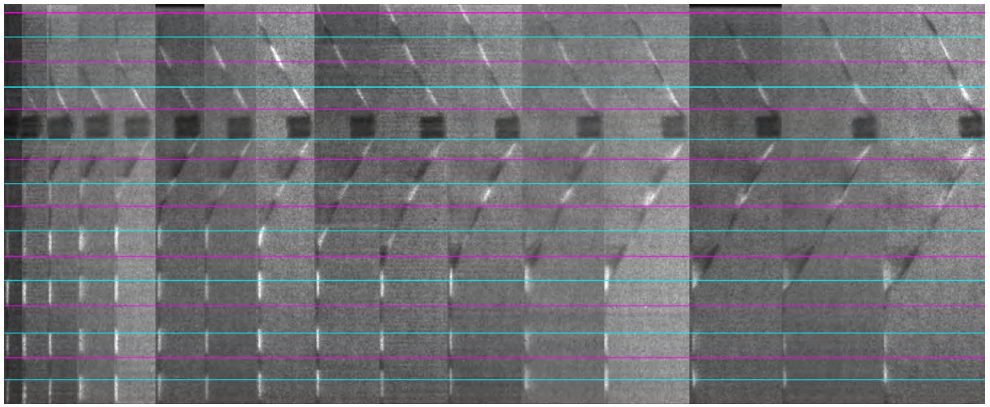

Yarn Material	Density (g/cc)	Sound Speed (km/s)	Strength (GPa)	Theor. Critical Velocity (m/s)
KM2 S5705	1.44	7.45	3.4	945
Dyneema SK-65	0.97	9.89	3.42	1110
PBO	1.56	10.7	5.8	1108

Single Yarn Impact Validation

Validation performed on theoretical transverse wave velocity and not on theoretical critical velocity

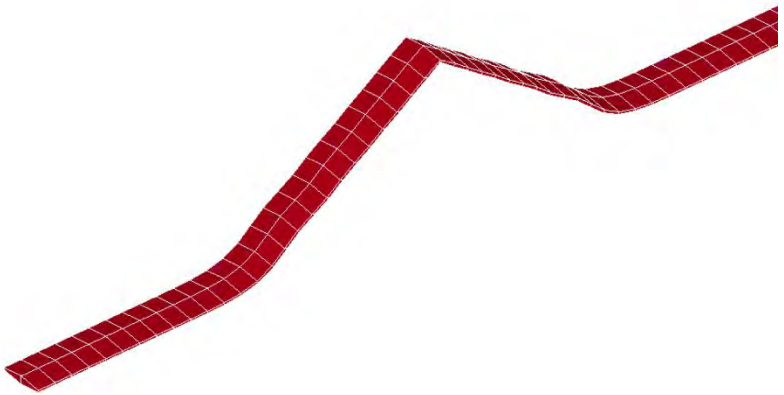

Yarn Material	Impact vel. (m/s)	Theor.Transv. wave vel. (m/s)	Exp. Transv. wave vel. (m/s)	LS-DYNA Transv. wave vel. (m/s)
KM2 S5705	480	851	880	880
Dyneema SK-65	480	954	900	950
PBO	520	1033	1040	1060

Material	Density (g/cm^3)	E_a (GPa)	E_b (GPa)	E_c (GPa)	ν	G (GPa)	σ_u (GPa)
KM2 S5705	1.44	80	8.0	8.0	0	0.8	3.4
Dyneema SK-65	0.97	95	9.5	9.5	0	0.95	3.42
PBO	1.56	180	18	18	0	1.8	5.8

Yarn 03 – Dyneema – 477m/s
5 us per frame

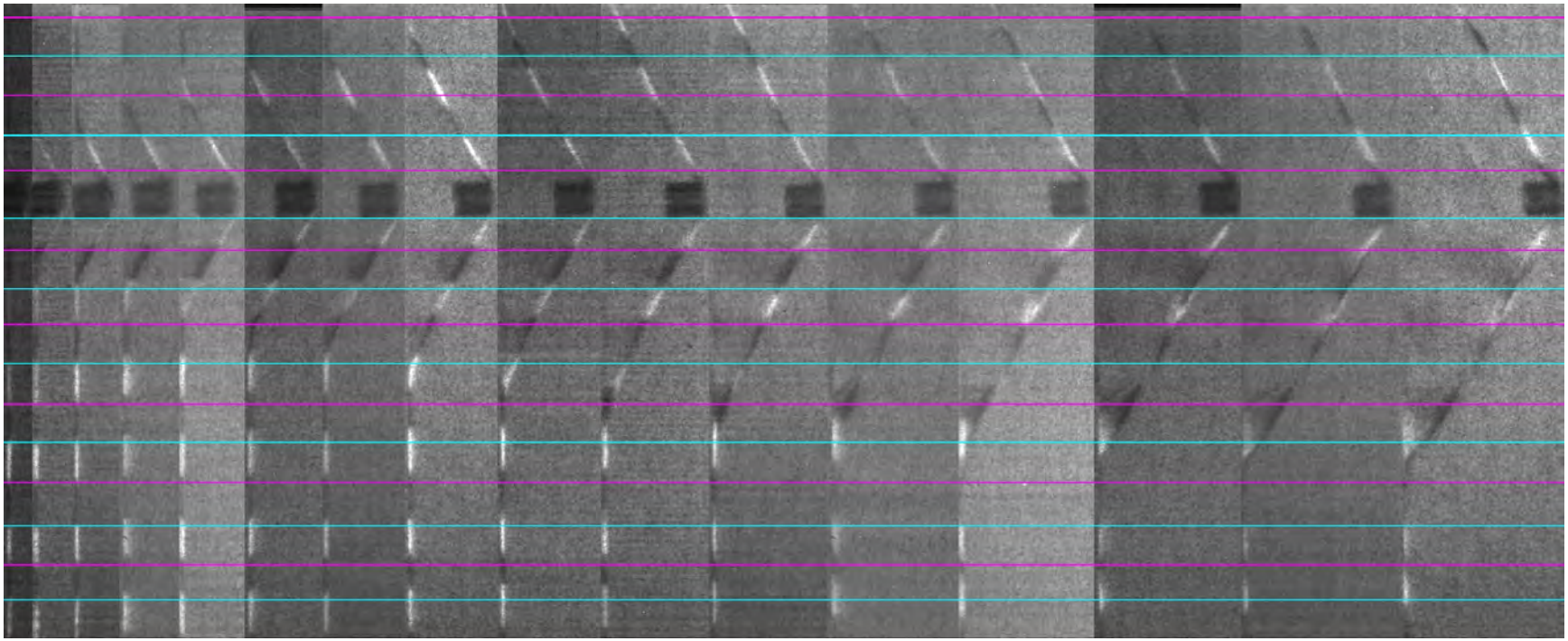

No failure

Yarn 06 – Dyneema – 474m/s
4 us per frame

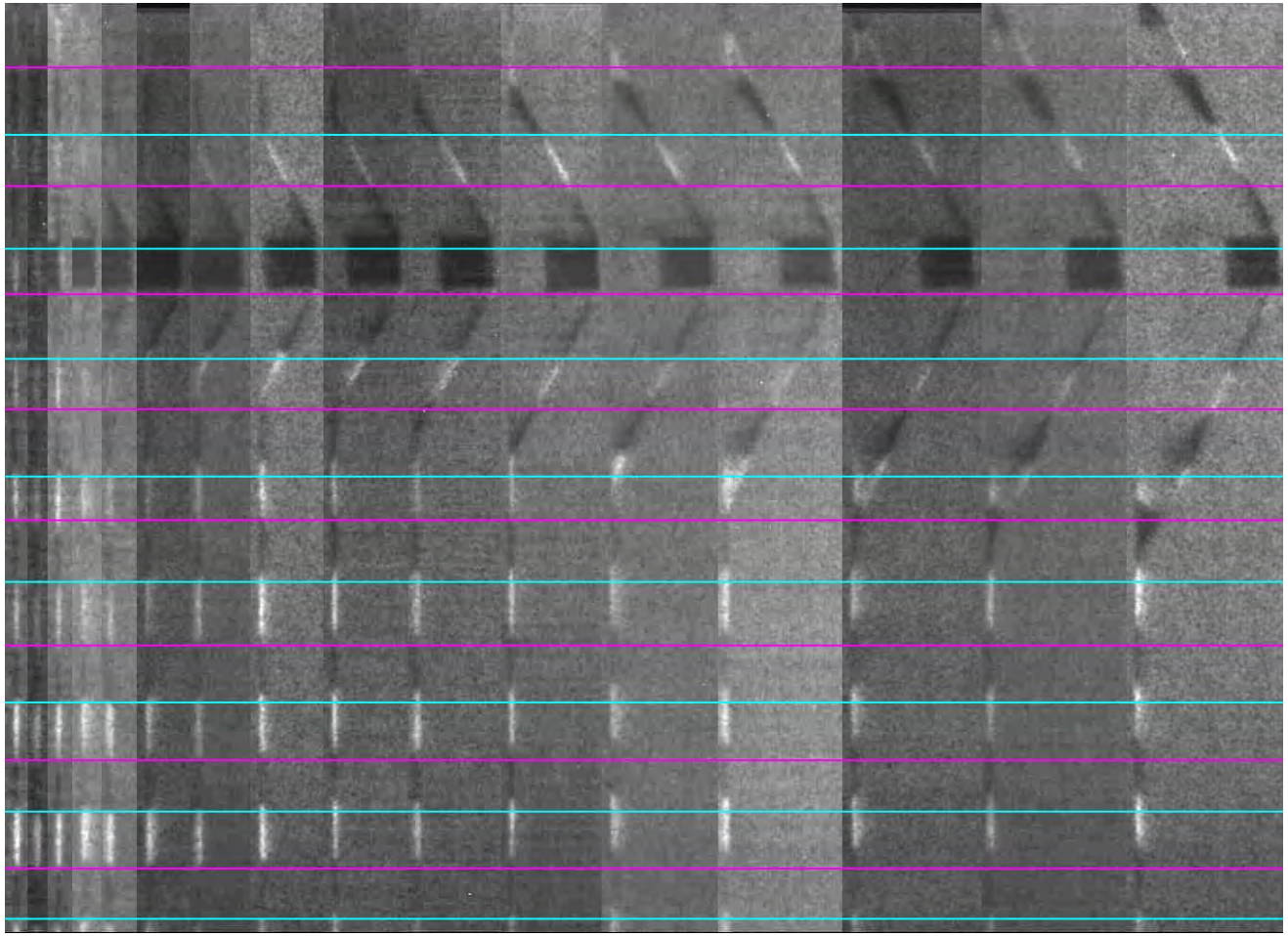

No failure

Yarn 12 – Dyneema – 517m/s
4 us per frame

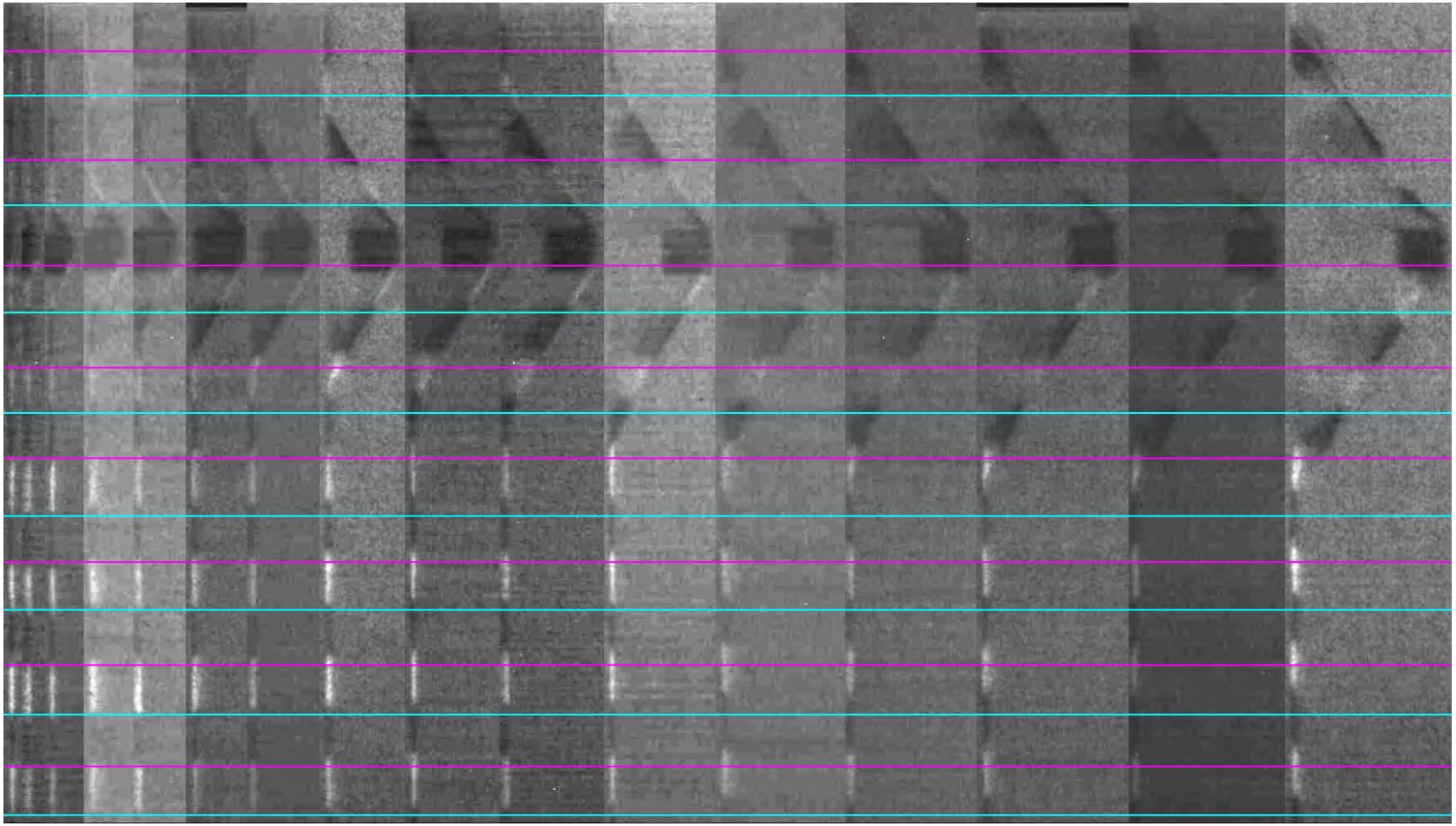

No failure

Yarn 11 – Dyneema – 583m/s
4 us per frame

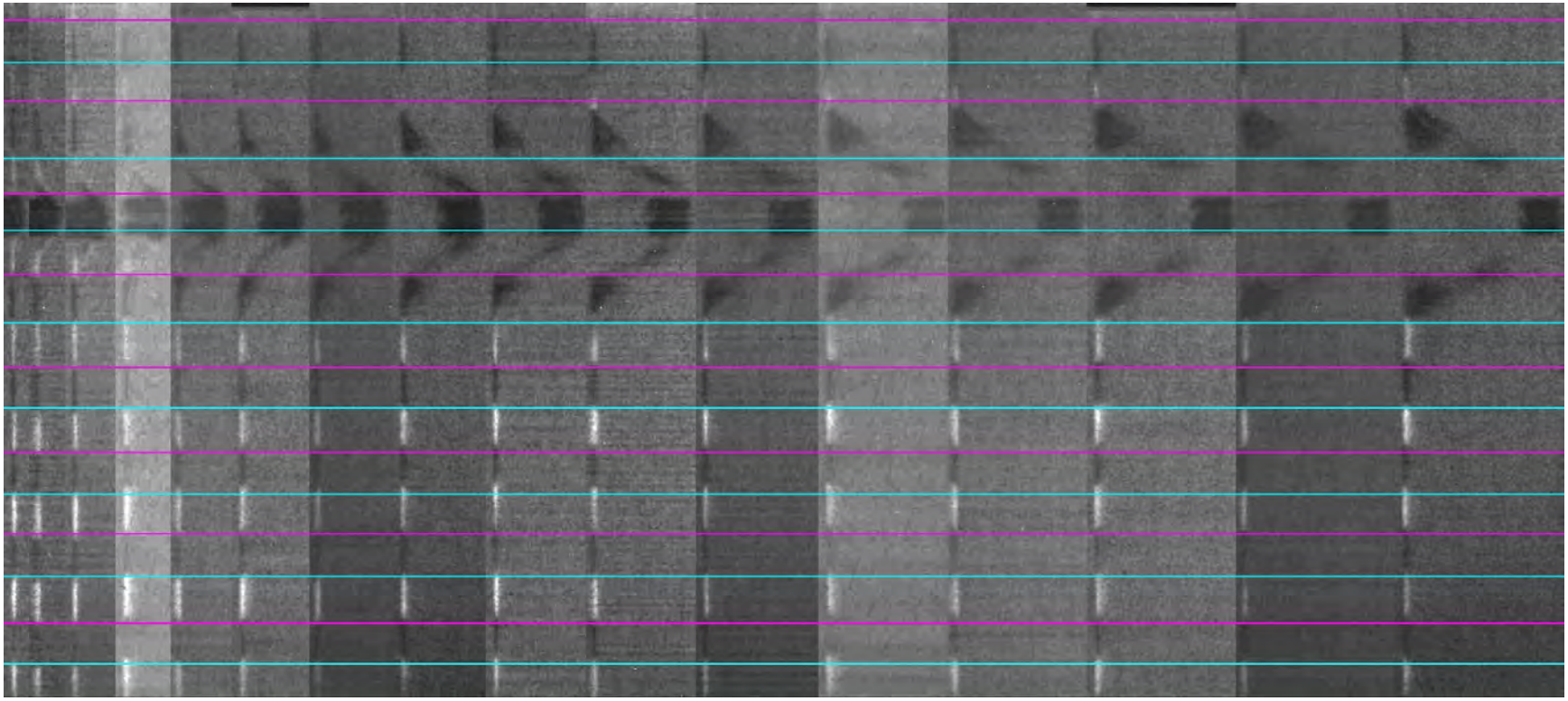

Immediate failure

Yarn 09 – Dyneema – 672m/s
4 us per frame

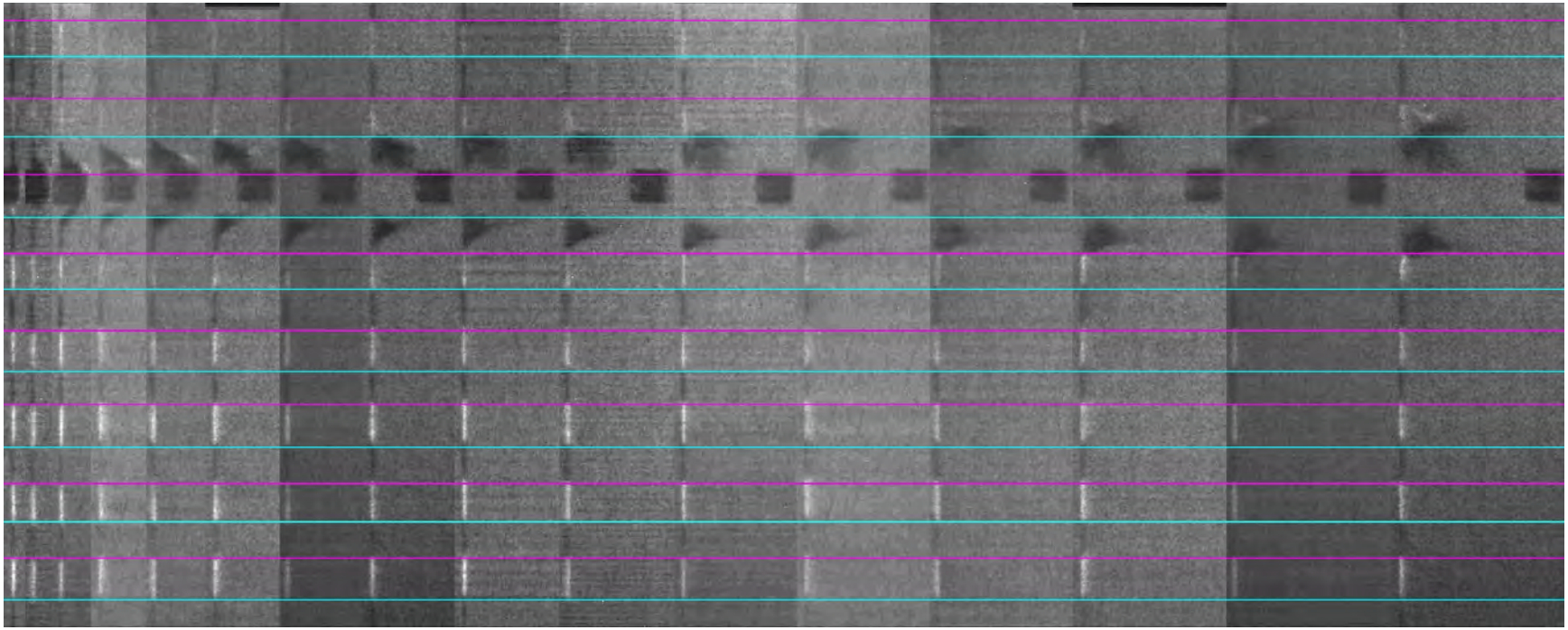

Immediate failure

Yarn 13 – PBO – 523m/s
4 us per frame

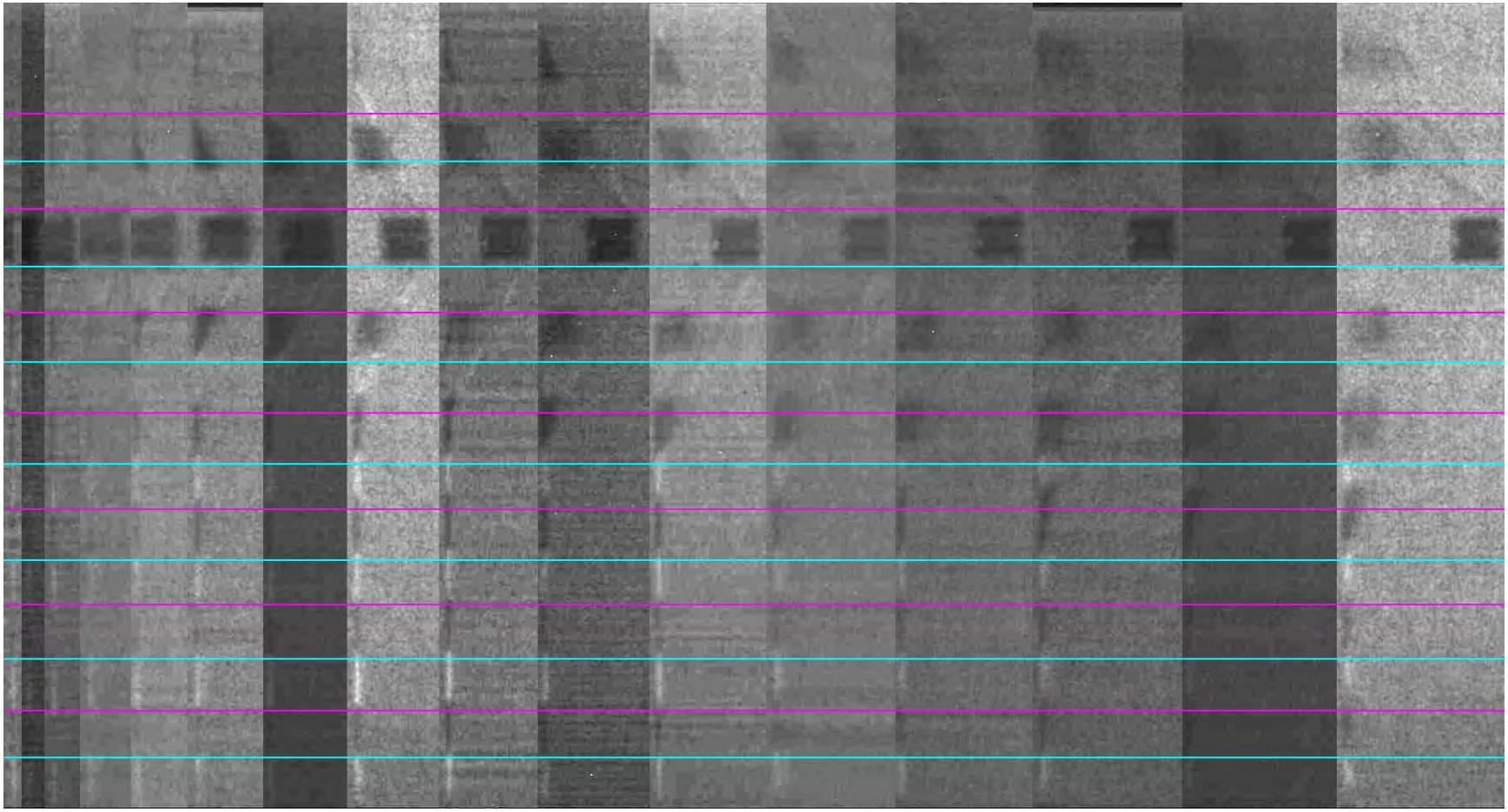

No failure

Yarn 18 – PBO – 610m/s
4 us per frame

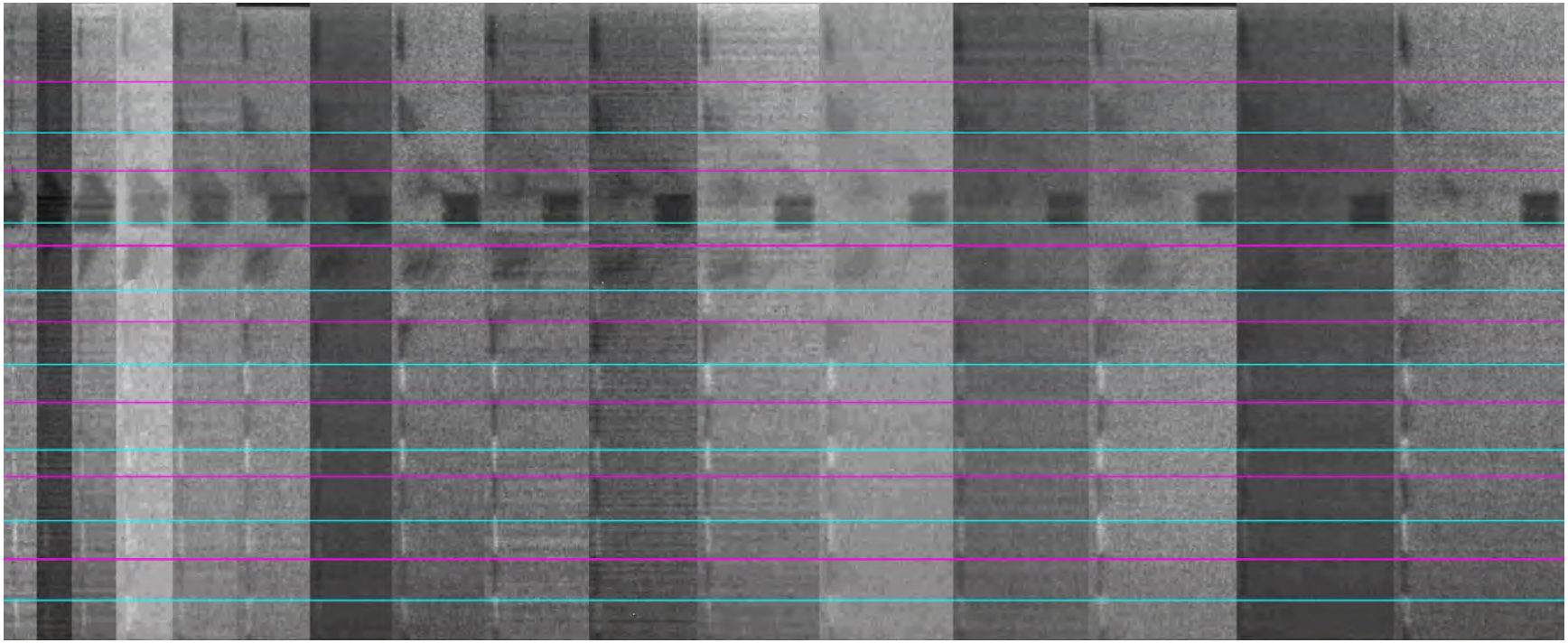

Immediate failure

Yarn 23 – 5705 – 476m/s
4 us per frame

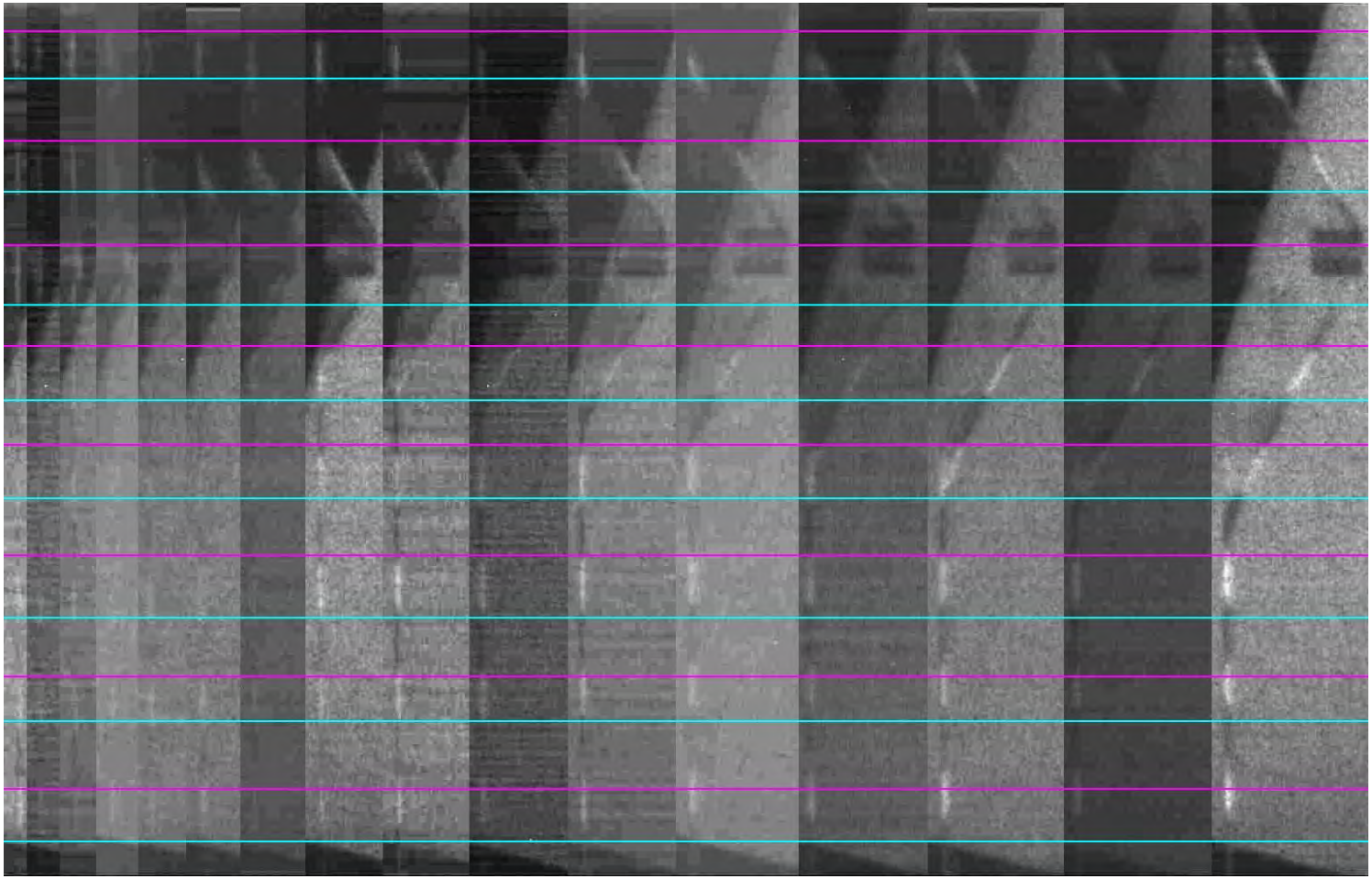

No failure

Yarn 30 – 5705 – 621m/s
4 us per frame

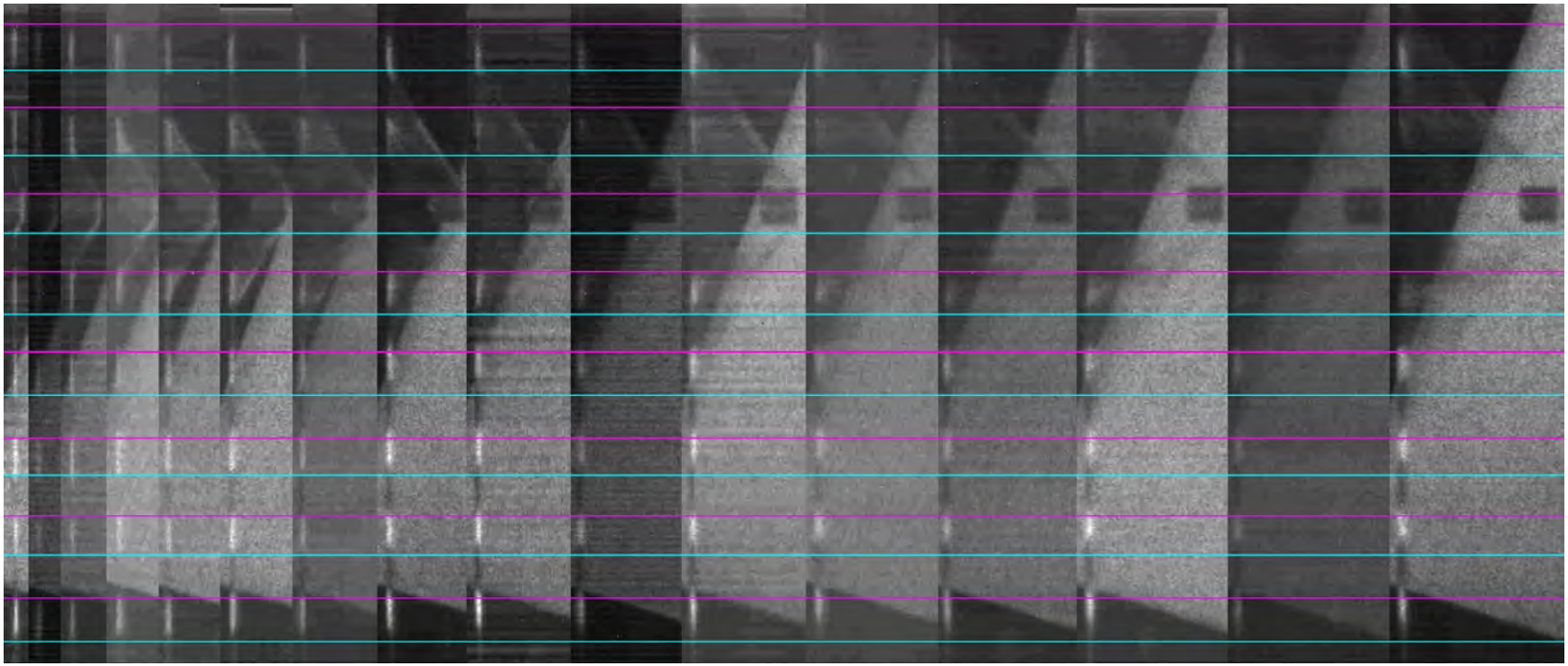

No failure

Yarn 29 – 5705 – 634m/s
4 us per frame

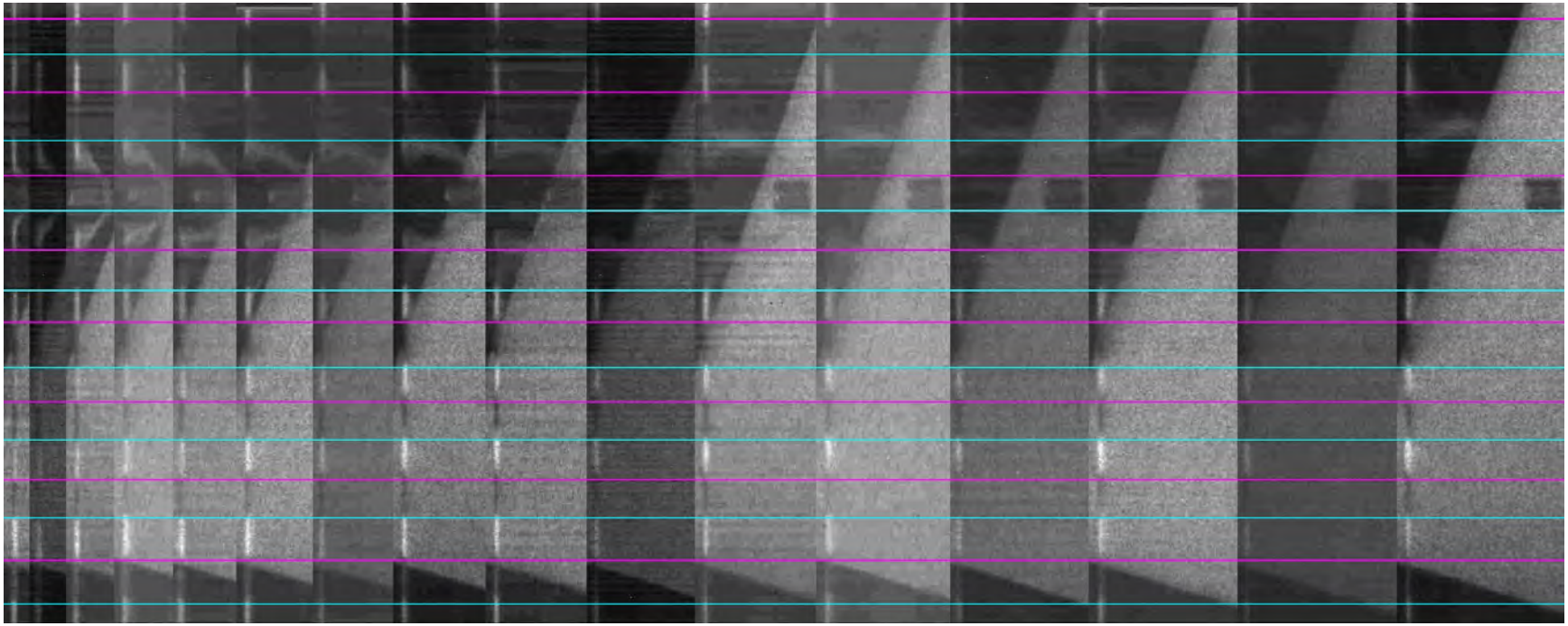

Immediate failure

Single Layer Validation

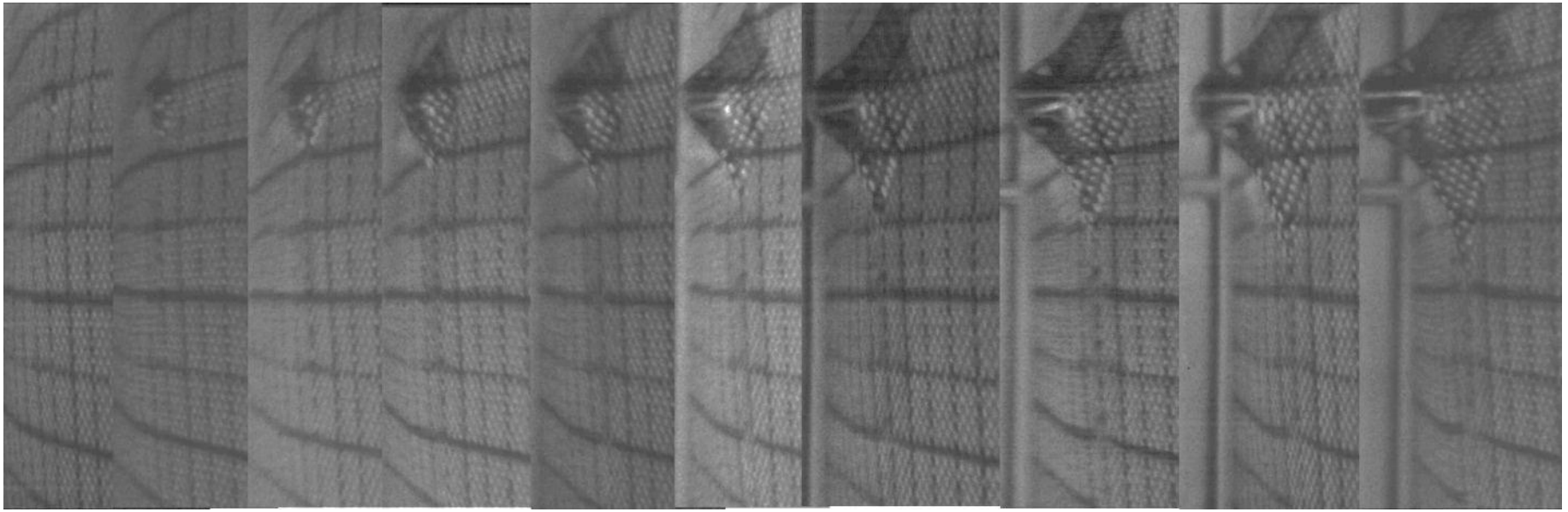

Single layer of Dyneema impacted by a .30 cal FSP at 348 m/s.
The square grid drawn on the fabric has a size of 1 cm × 1 cm.
The rightmost image shows the pyramid 45 μs after impact.

Dyneema SK-65: Single Layer Validation

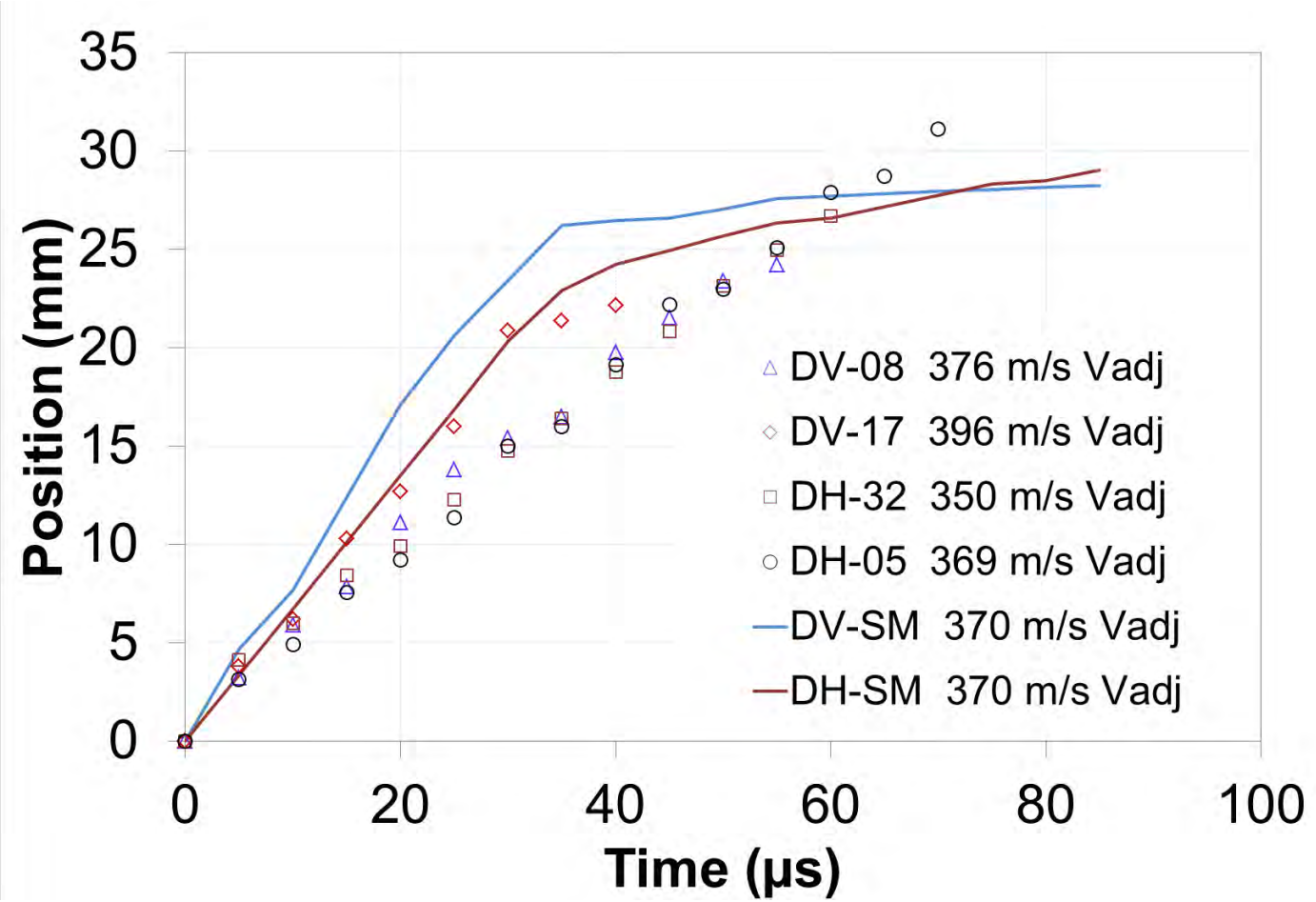

DV: Warp Direction, DH: Fill Direction

Single Layer

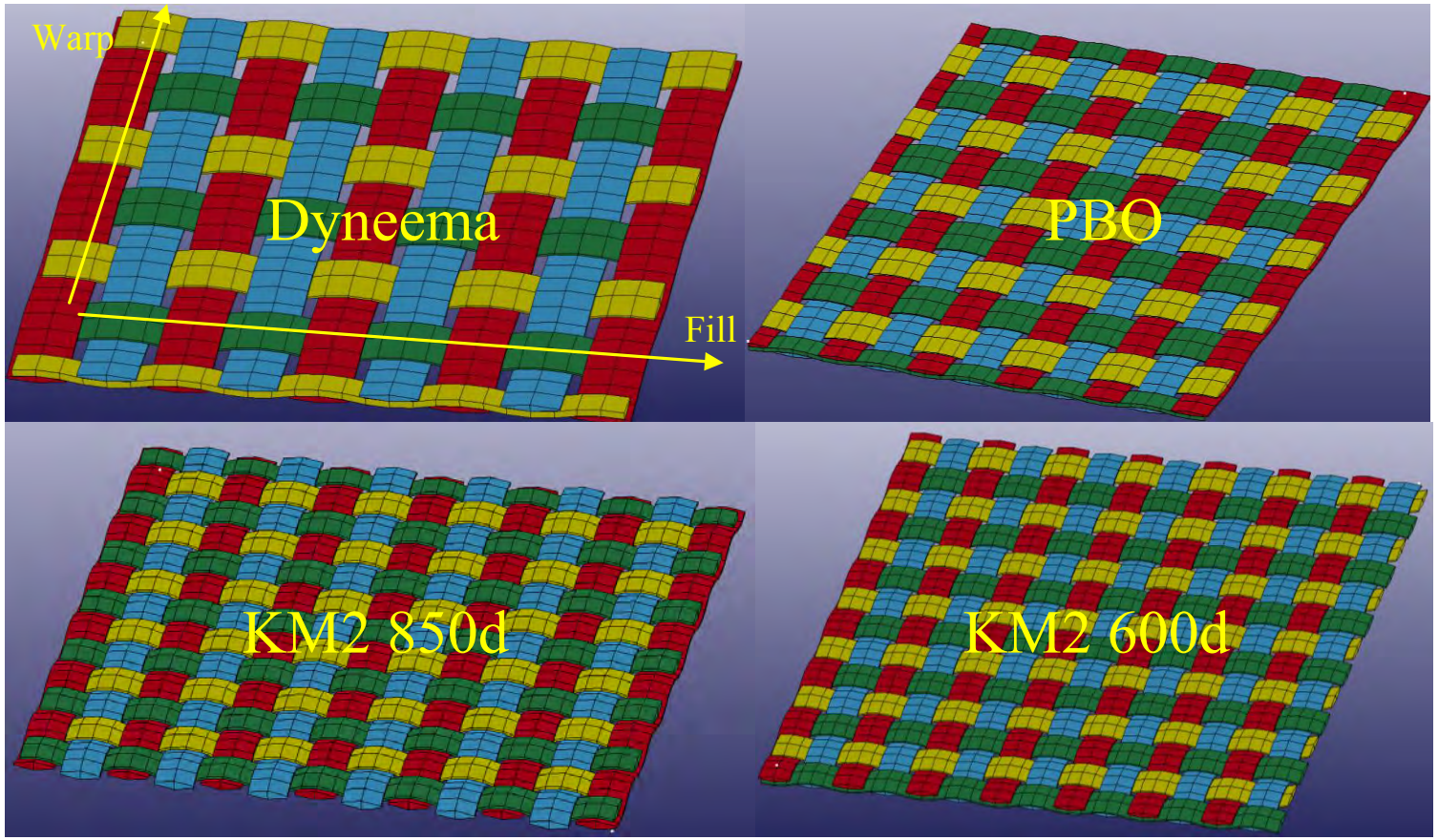

Figure 1: Squares (1 cm × 1 cm) of the fabric models developed: (upper left) Dyneema, (upper right) PBO, (lower left) KM2 850 denier and (lower right) KM2 600 denier.

Squares (1 cm × 1 cm)

Single Layer Transverse Wave

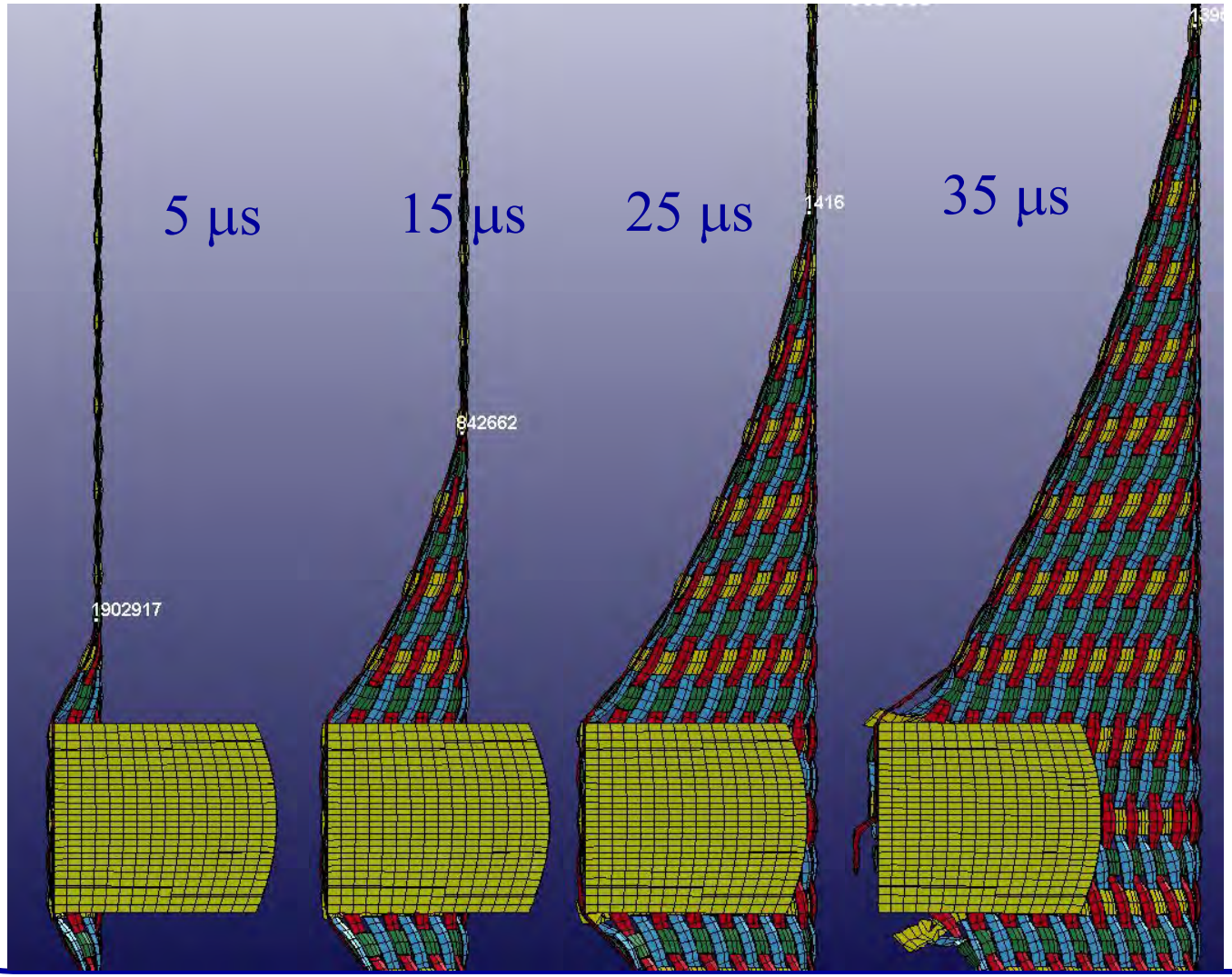

Figure 1: Pyramid development for the .30 cal FSP impacting Dyneema fabric. The pyramid

Dyneema Single Layer

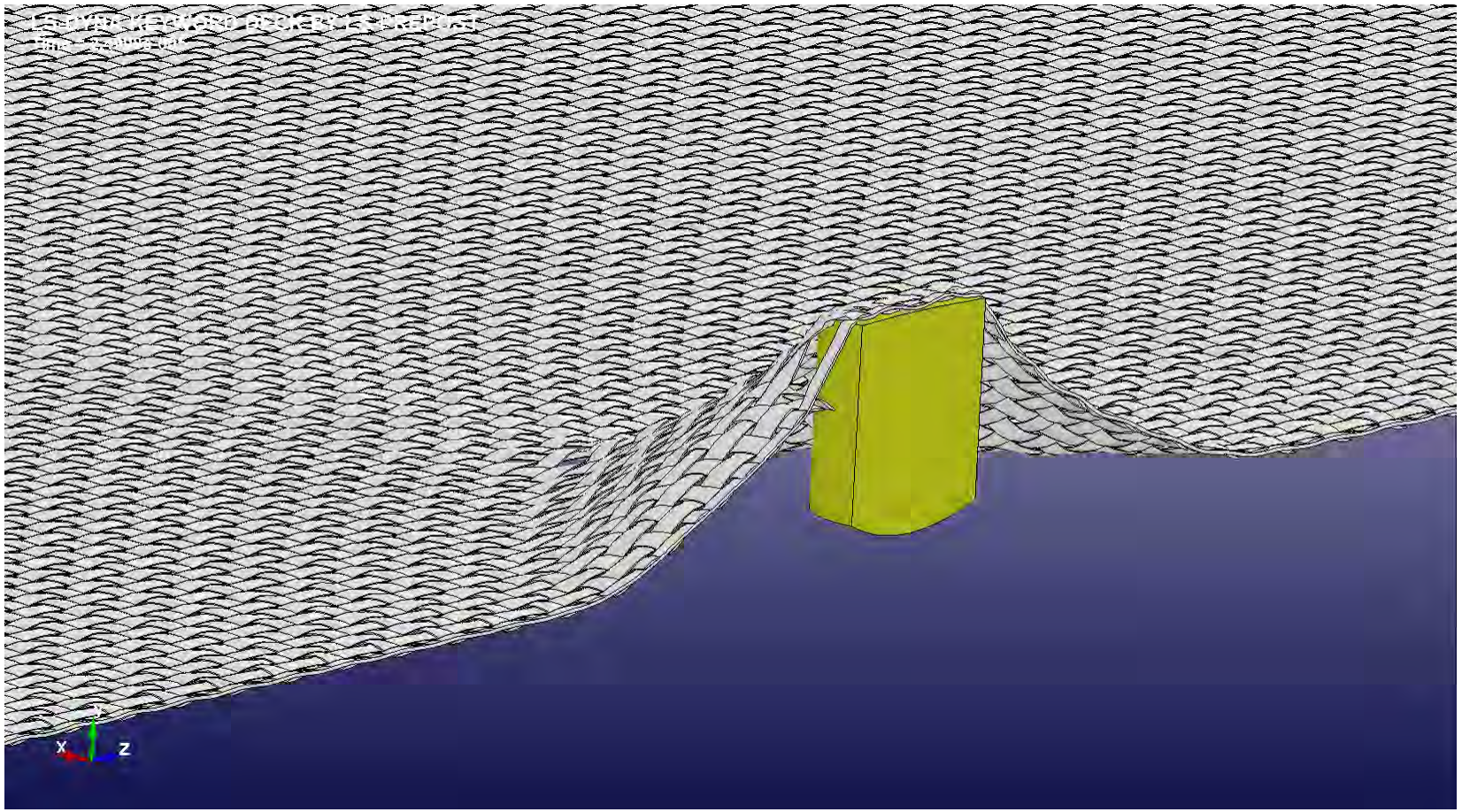

Kevlar KM2: Single Layer Validation

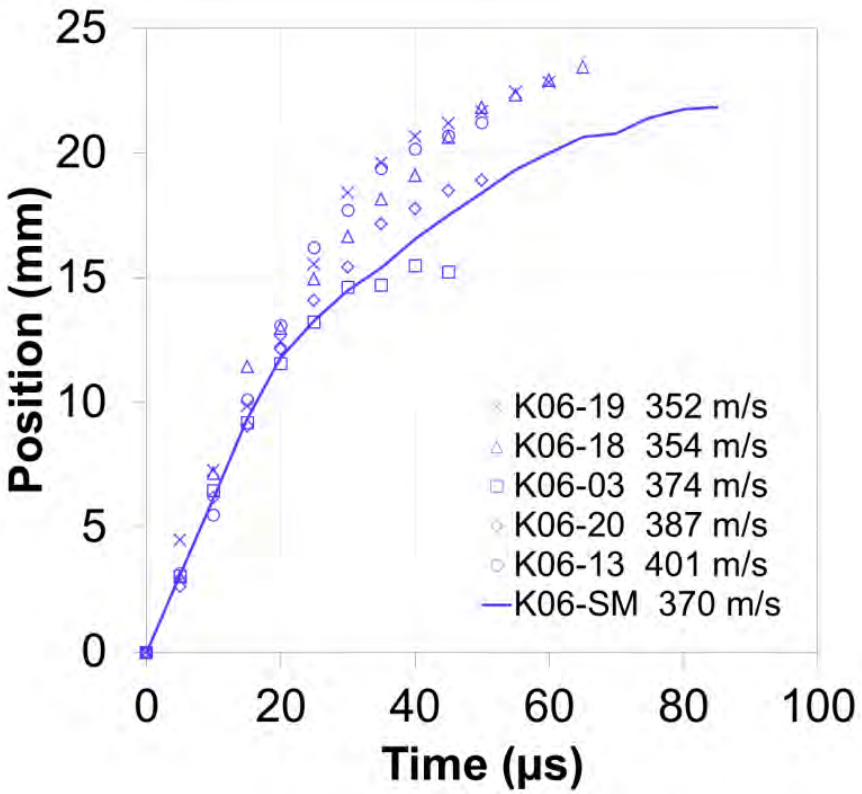

KM2 600d

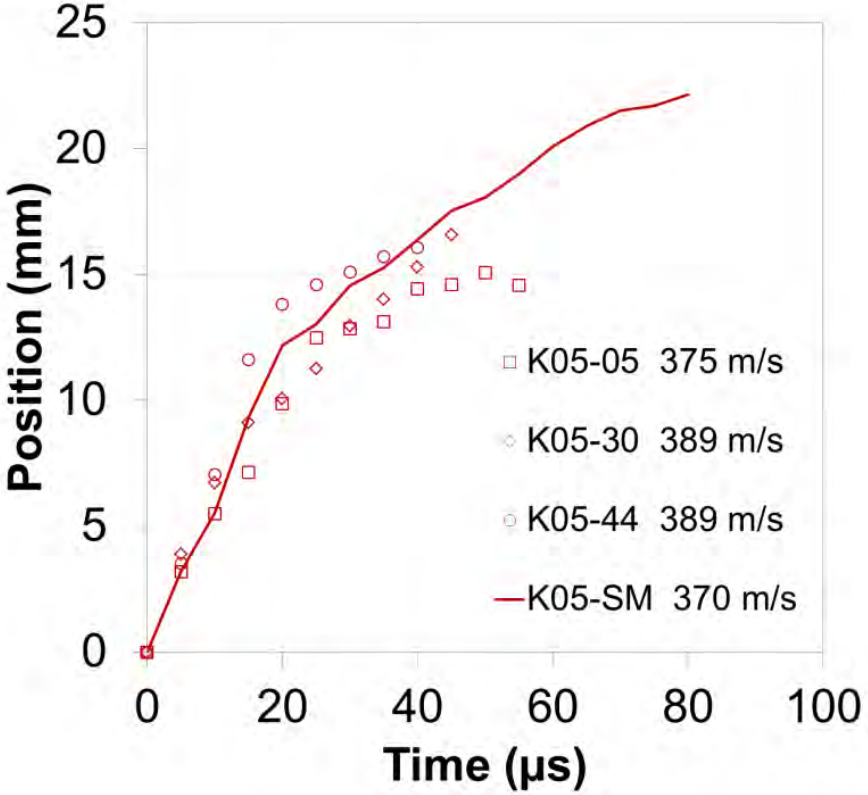

KM2 850d

PBO 500 denier, Single Layer Validation

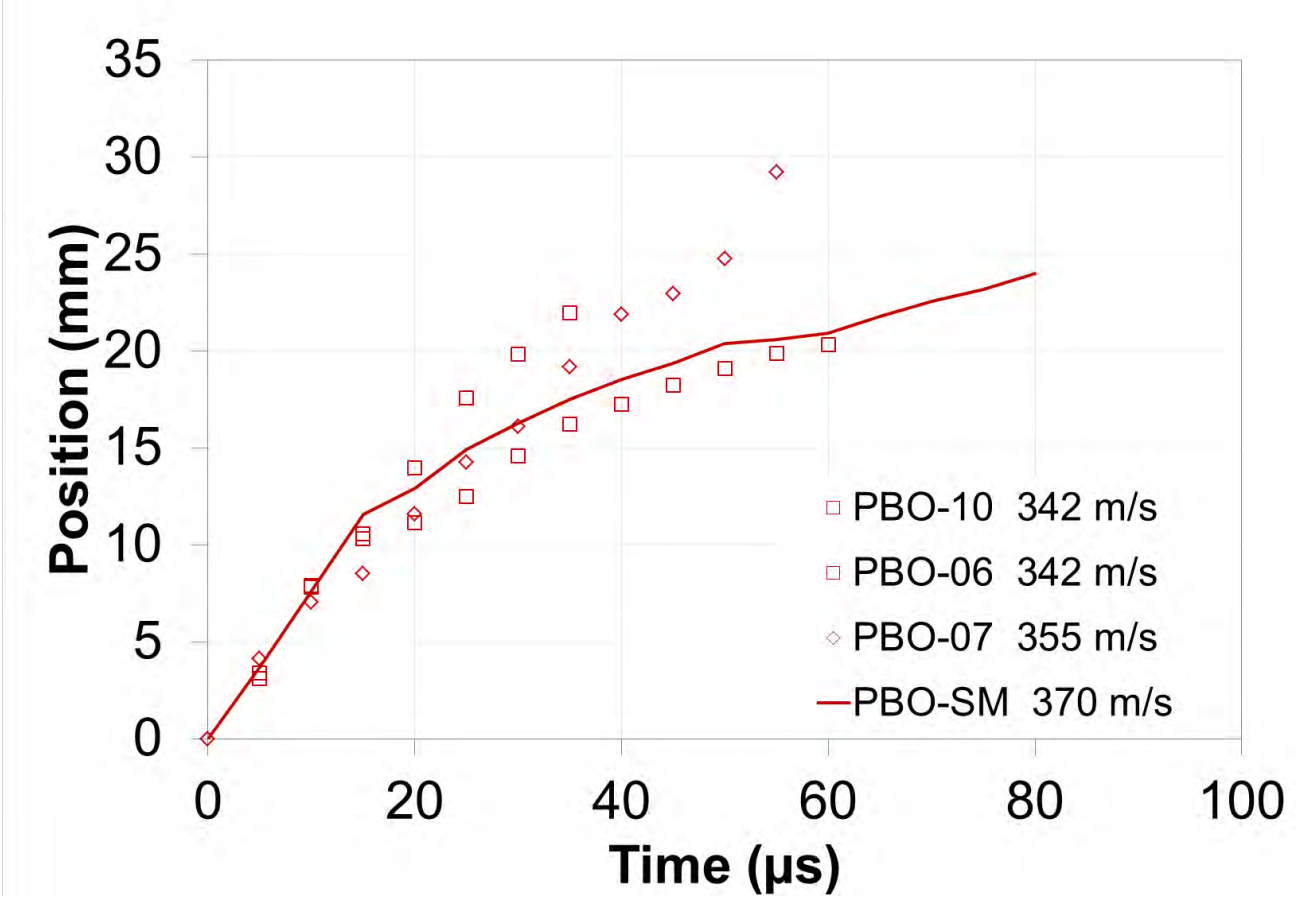

Multi-layer

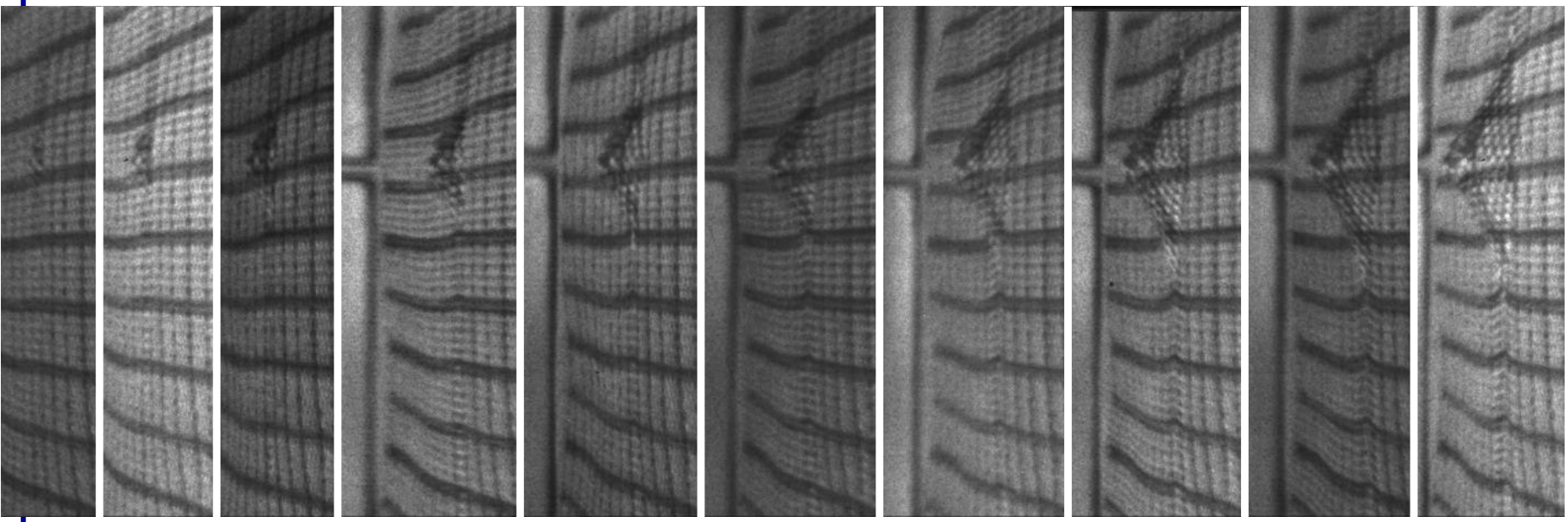

5 μs intervals

Figure 1: Images recorded at 5 s intervals with the Imacon camera for test# 38: 0.22 cal FSP vs. 10 layers of Dyneema at 309 m/s. The projectile was stopped by the target in this test.

0.22 cal FSP vs. 10 layers of Dyneema at 309 m/s.

Impact on 10 Layers of Dyneema

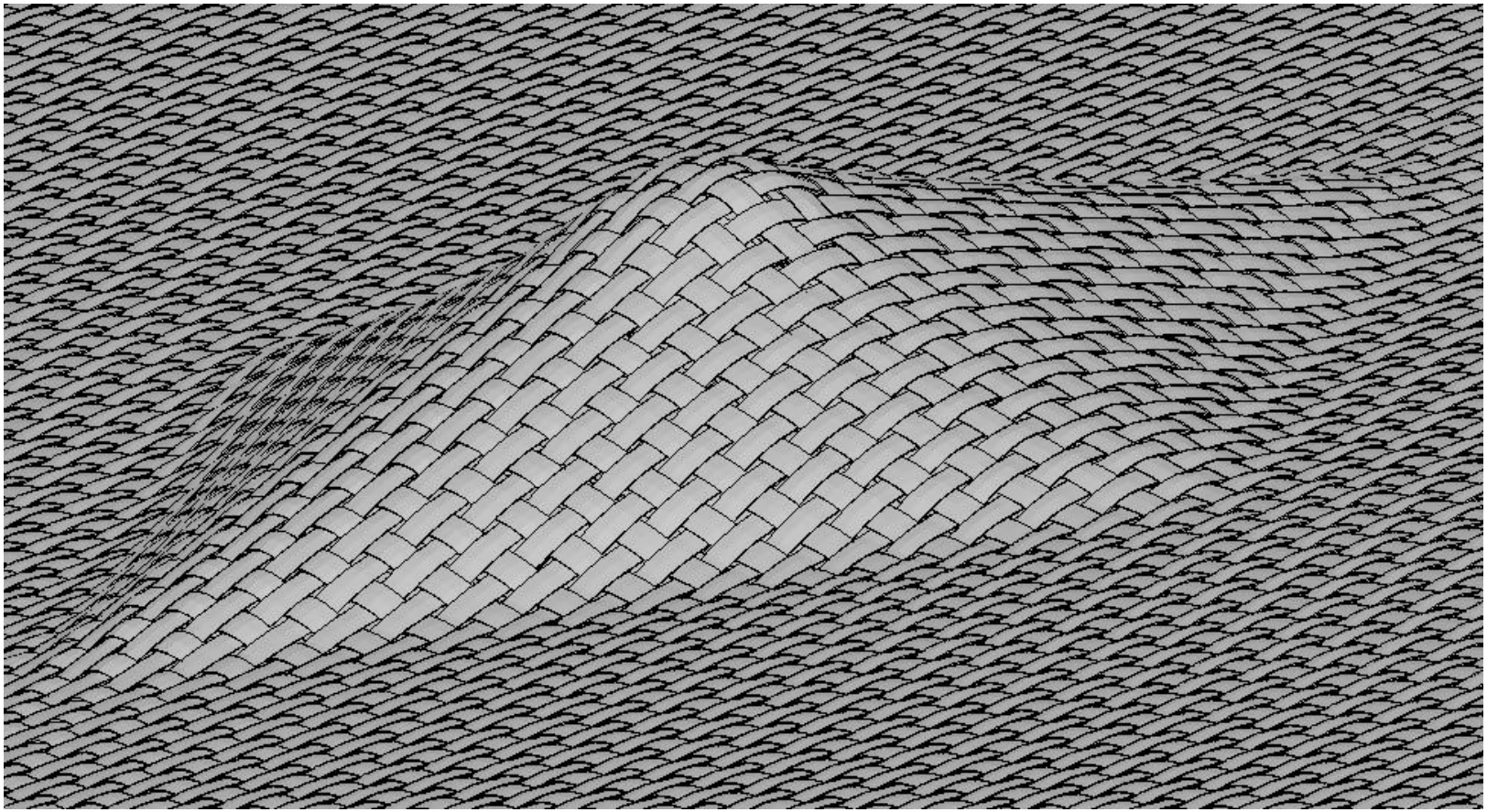

35 μs

Dyneema 10 Layers

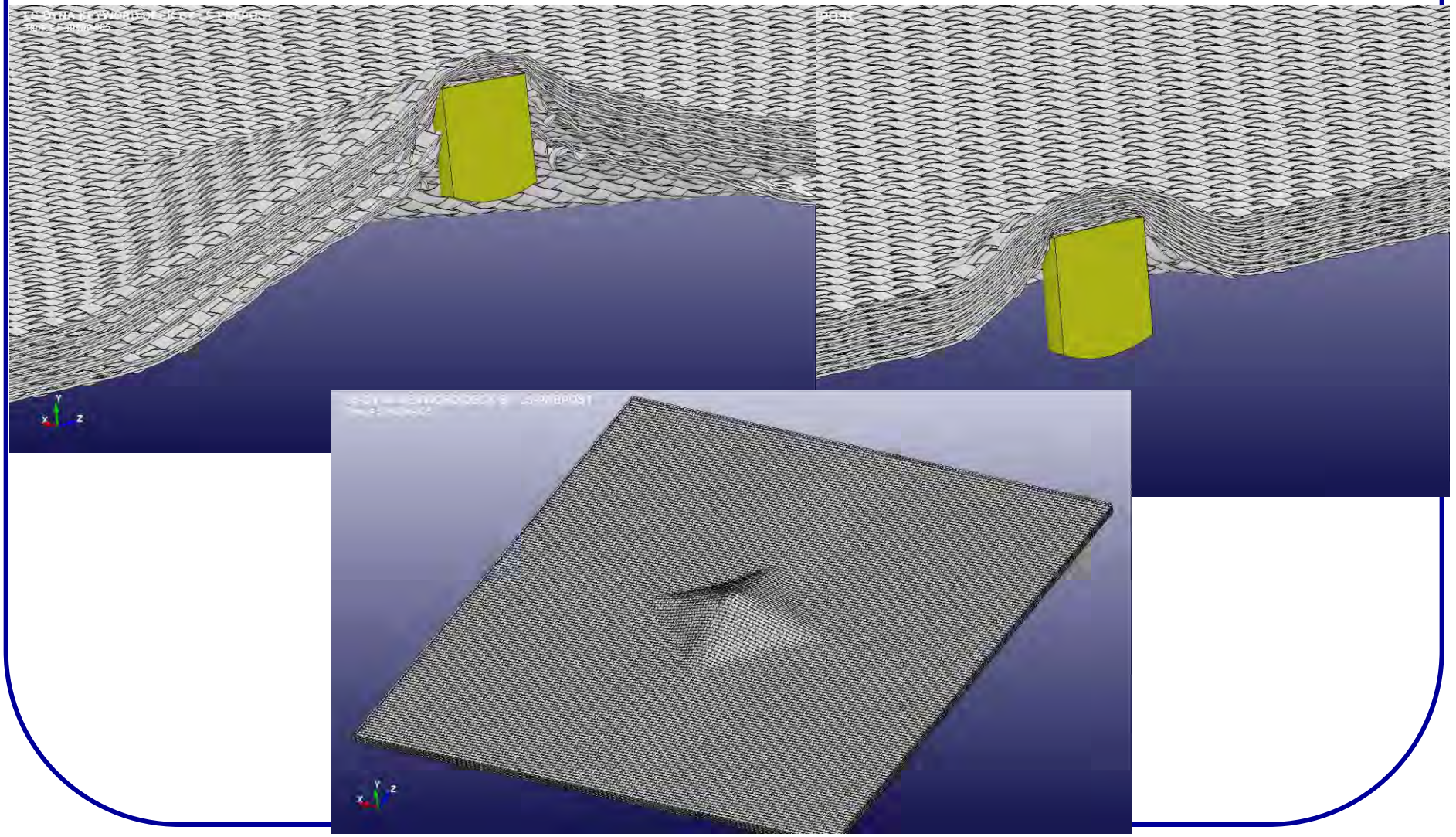

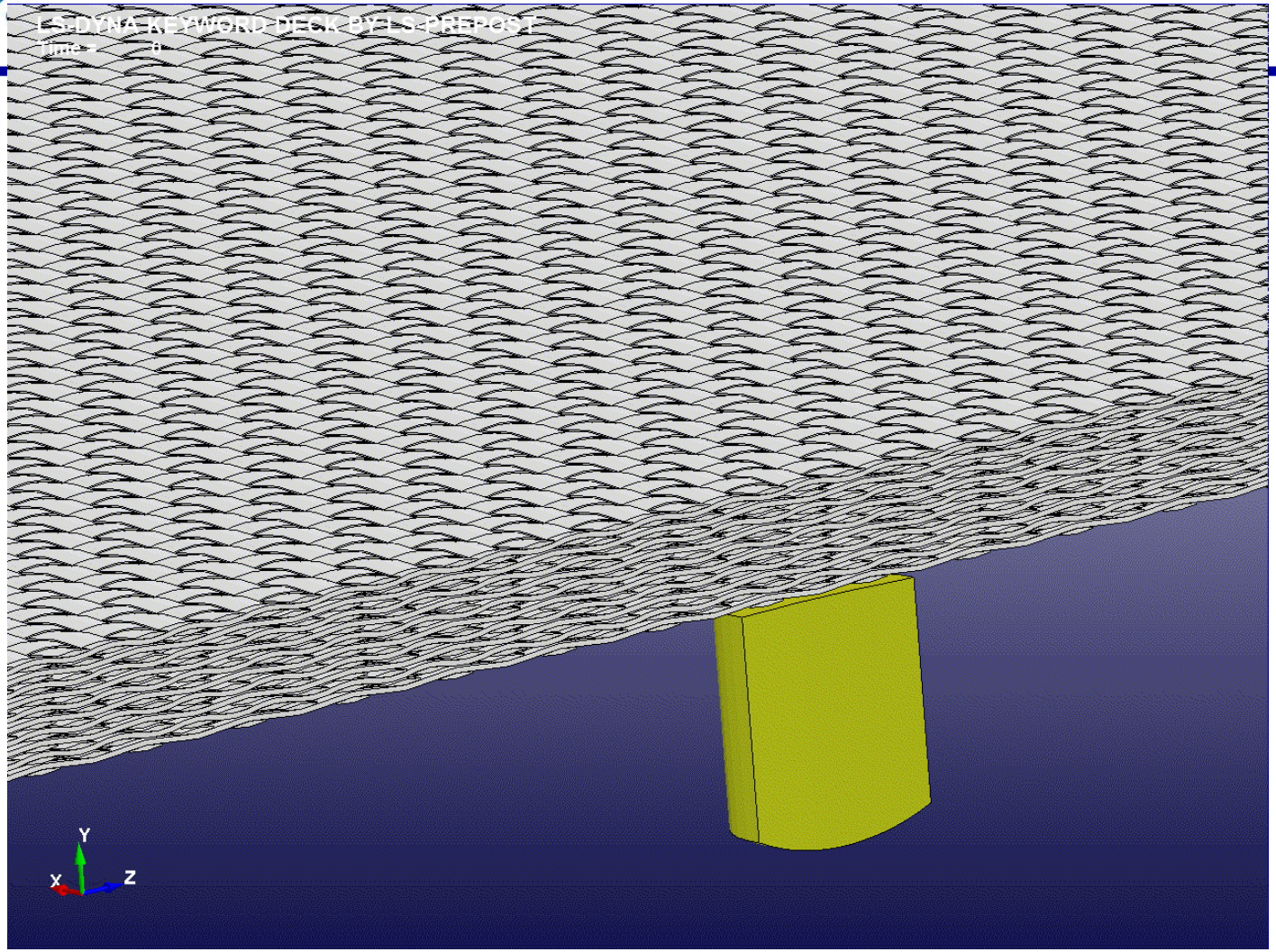
LS-DYNA KEYWORD DECK BY LS-PREPOST
Time = 0
Y
X
Z

Movies

- 10 layer Dyneema and KM2 on Imacon
- 10 layer Dyneema and KM2 on Phantom
- 39 layer PBO on Imacon and Phantom

Dyneema SK-65, Multilayer Validation

Apex Position

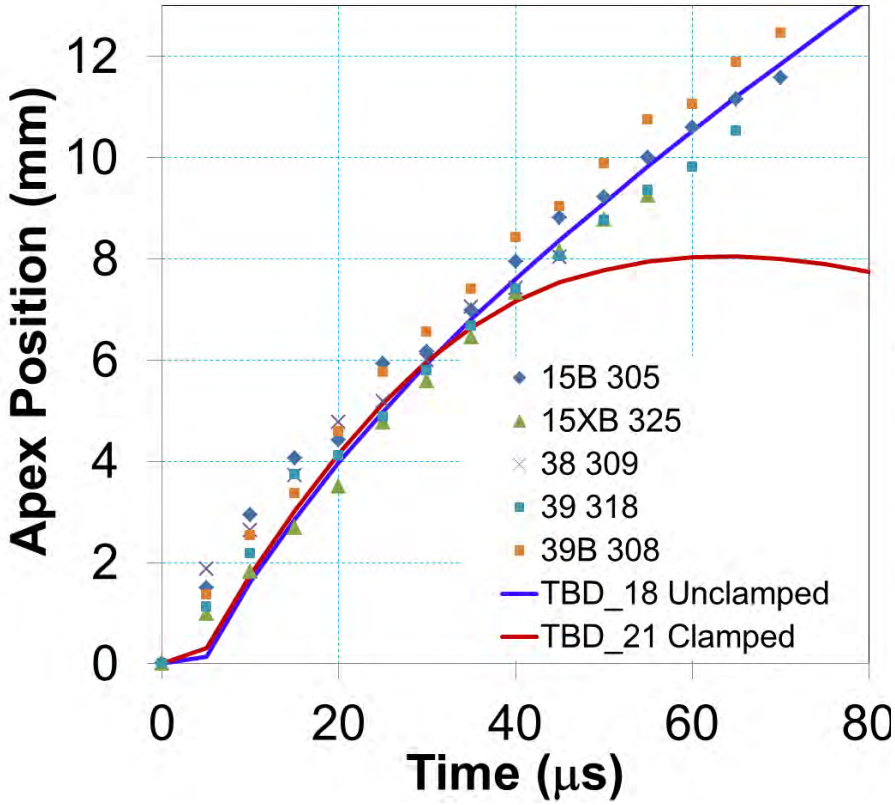

Diagonal Extent

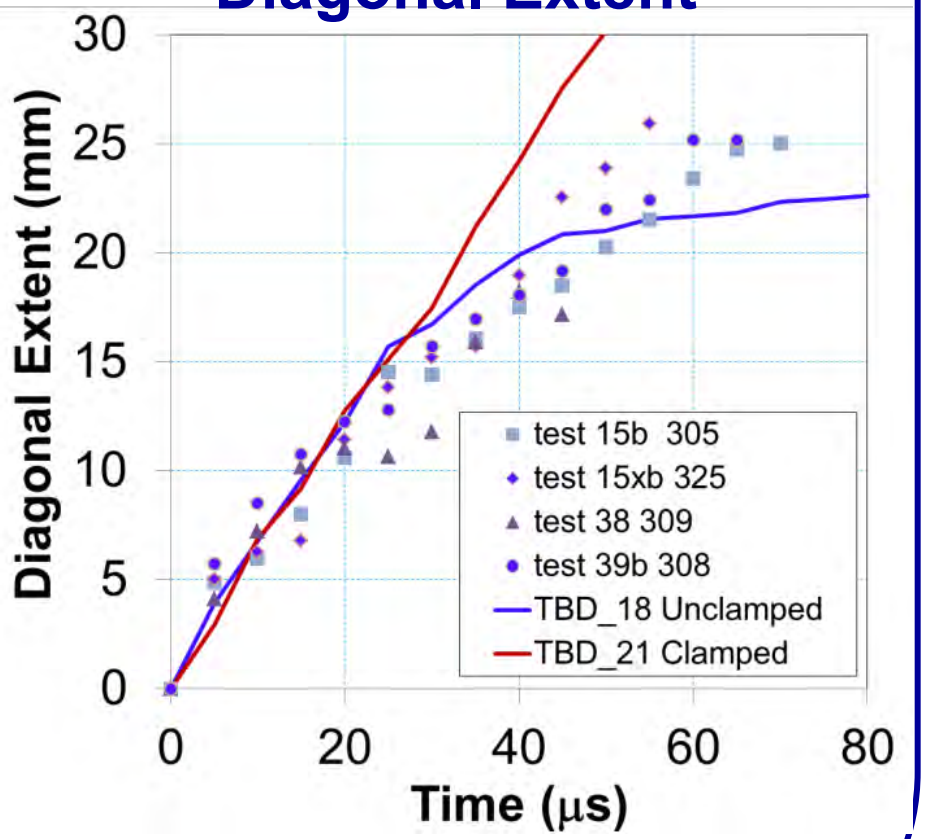

10 layers

PBO 500d, Multilayer Validation

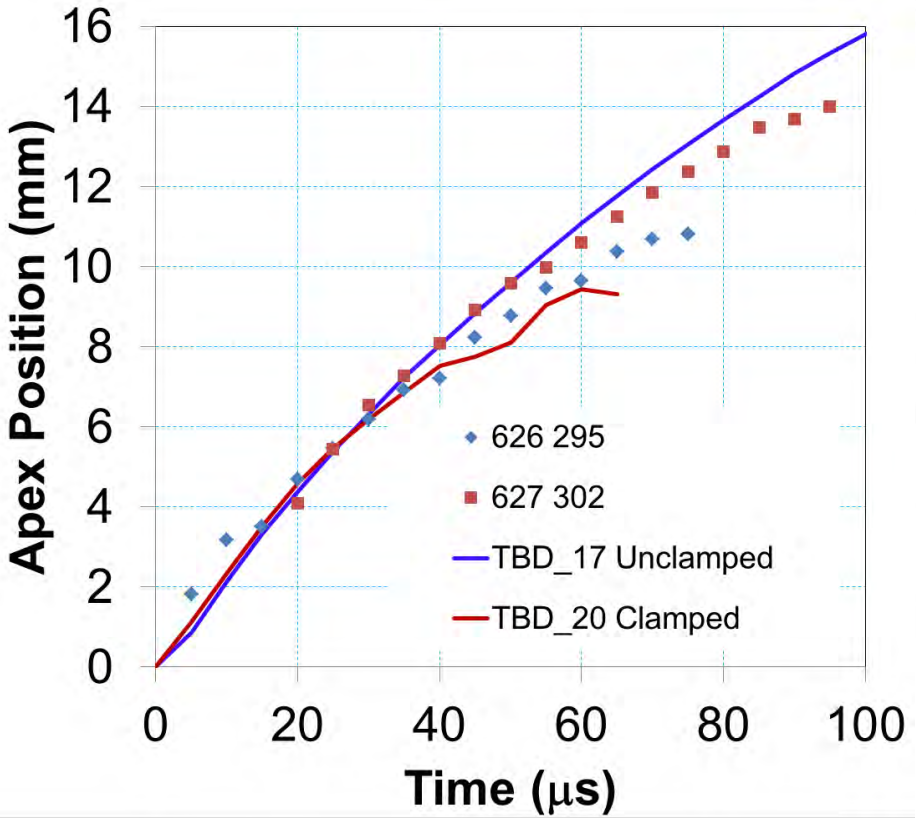

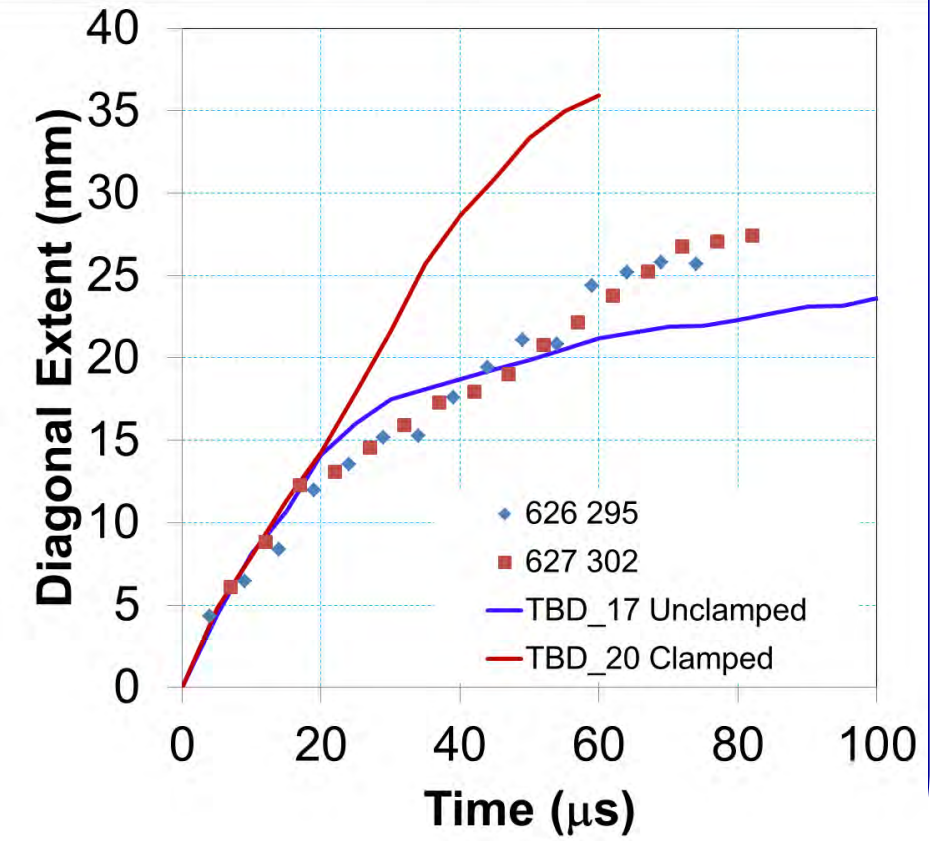

10 layers

KM2 850d, Multilayer Validation

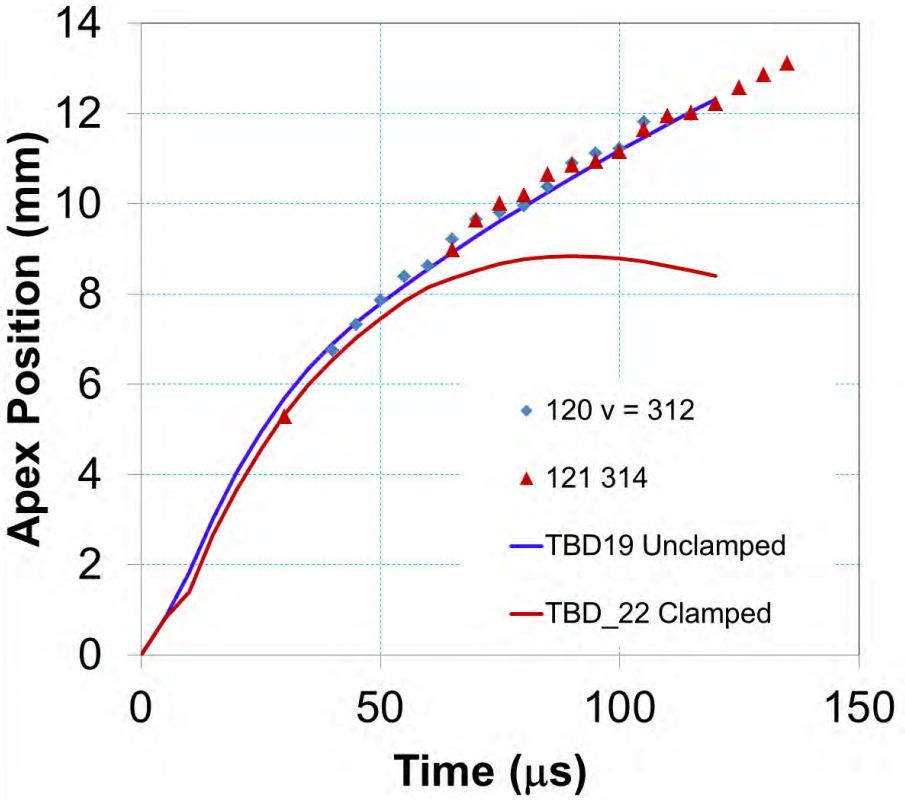

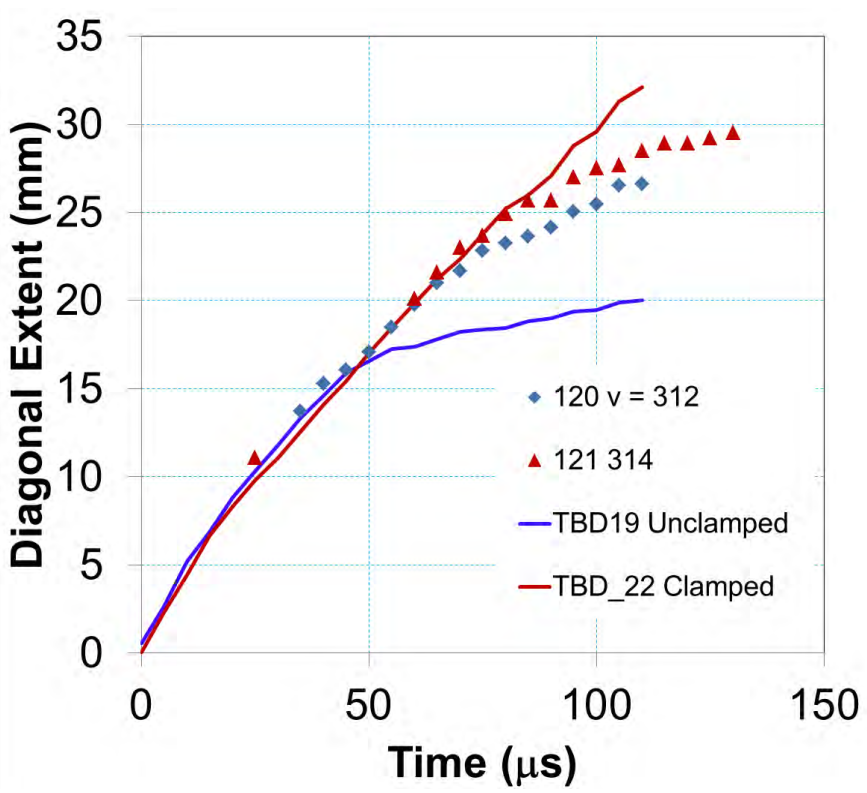

10 layers

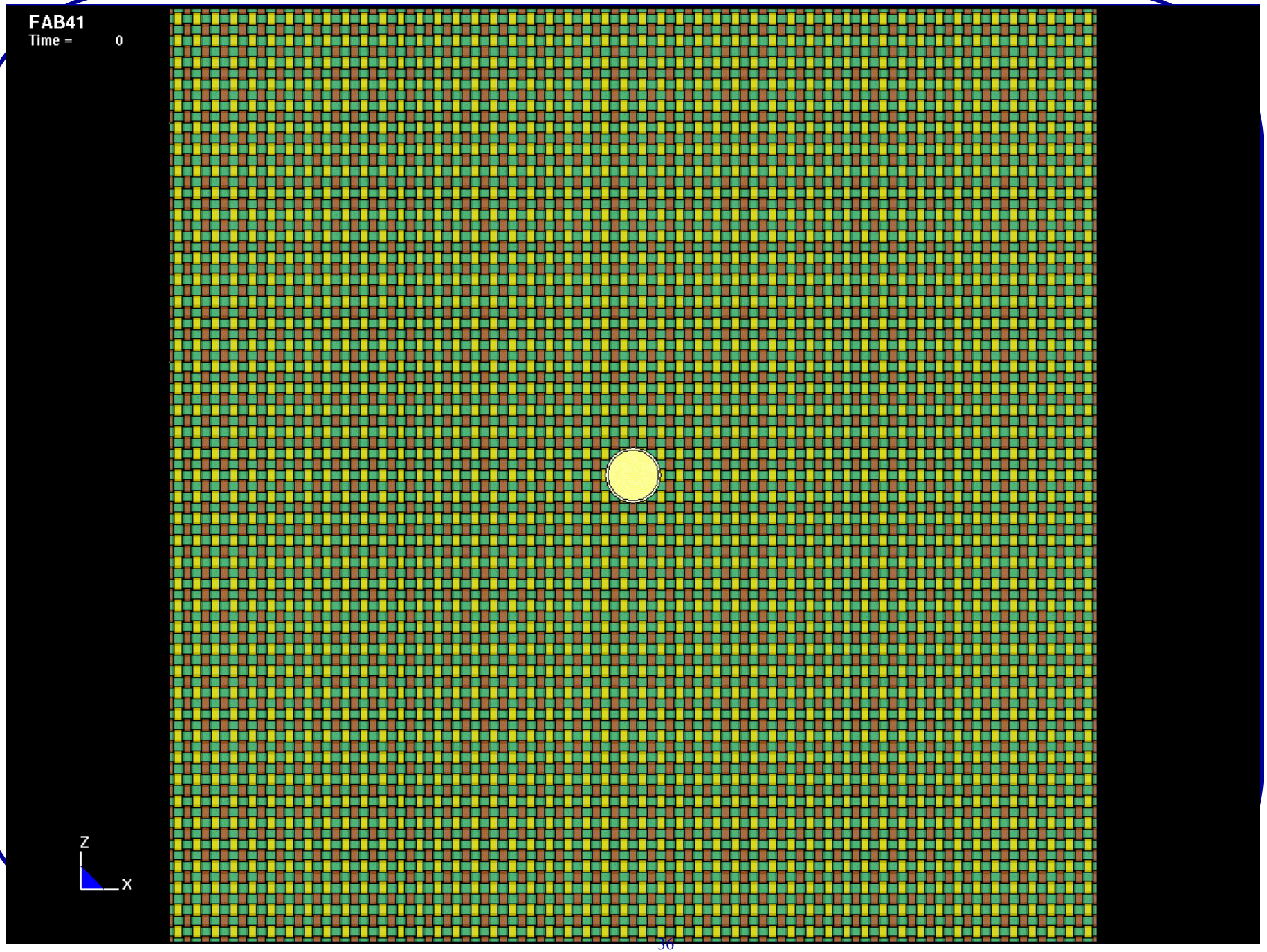
FAB41
Time = 0
Z
X

Ballistic Limits

Material	FSP Projectile	Denier	Layers	Areal Density (kg/m^2)	4-shot Exp. V50/Spread (m/s)	DYNA V50 (m/s)
KM2	.30 cal	850	9	2.27	370/64	325
Dyneema	.22 cal	792	10	1.26	354/23	375
PBO	.22 cal	500	10	1.13	360/56	300

Nickel-Chromium wire technique

Test set-up: fabric with NiCr Wire

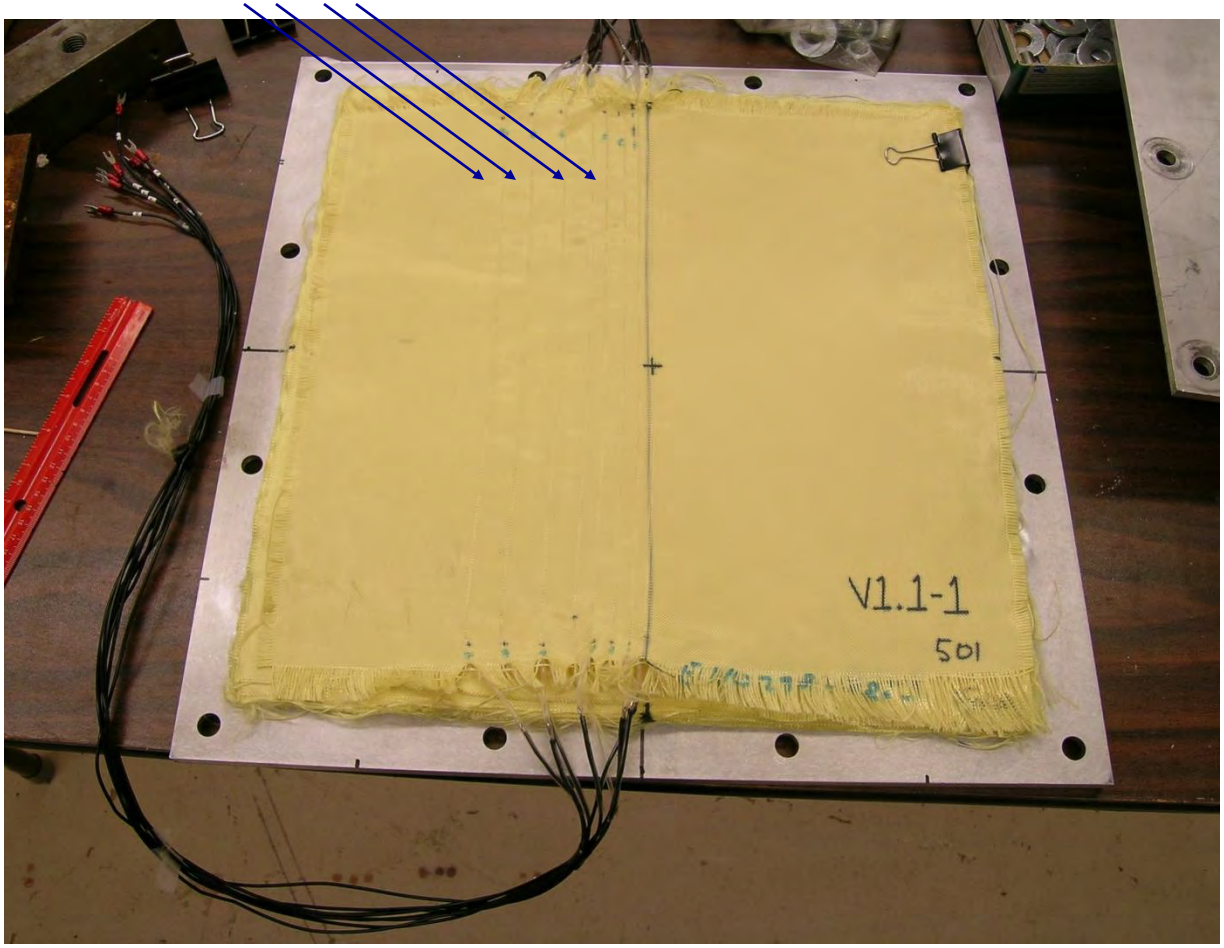

Detail of NiCr wires connections

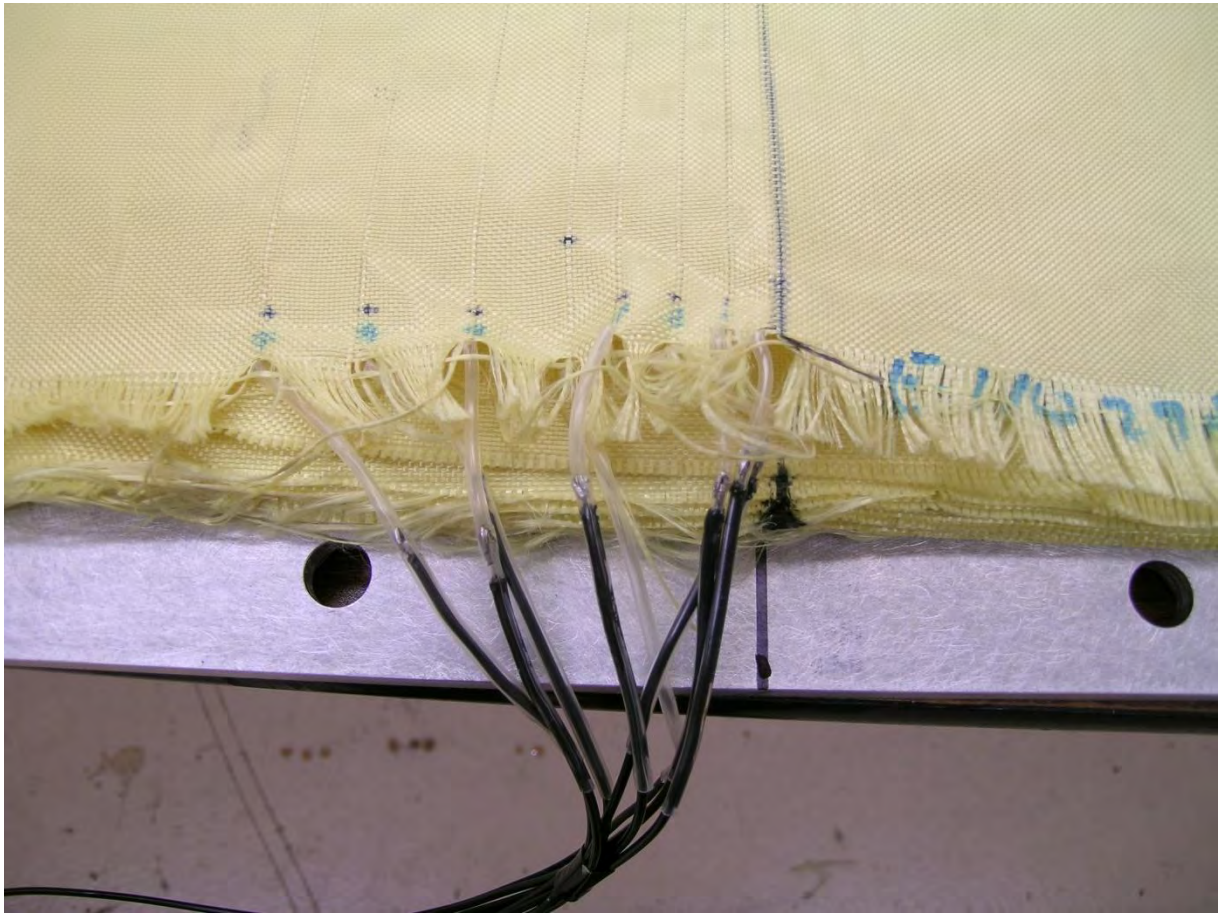

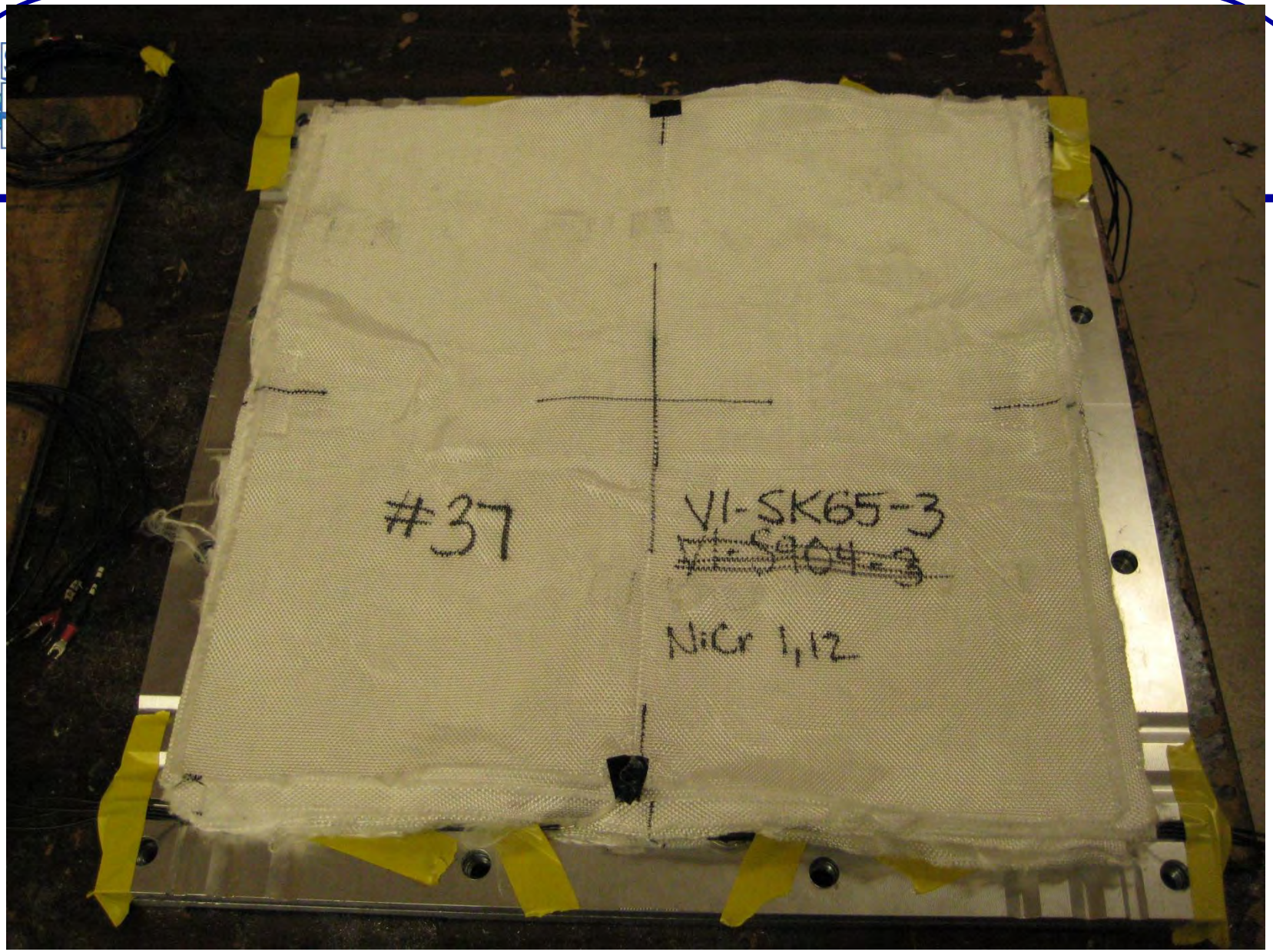
#37
VI-SK65-3
NiCr 1,12

Diagnostics - NiCr wire Acquisition System

- The NiCr wires constitute one of the arms of a Wheatstone bridge (120 Ohm). The other three arms are inside the amplifiers.
- NiCr wires were calibrated in the initial phase of the project. Each NiCr wire is shunted with a 5kΩ calibration resistance to find and fine tune its calibration constant.
- The data acquisition system has a maximum of 8 channels operating at 10 MHz.

Typical Signal on KM2

- The signal is very rich
  - Longitudinal wave
  - Transverse wave
  - Failure of layer
  - Initial strain

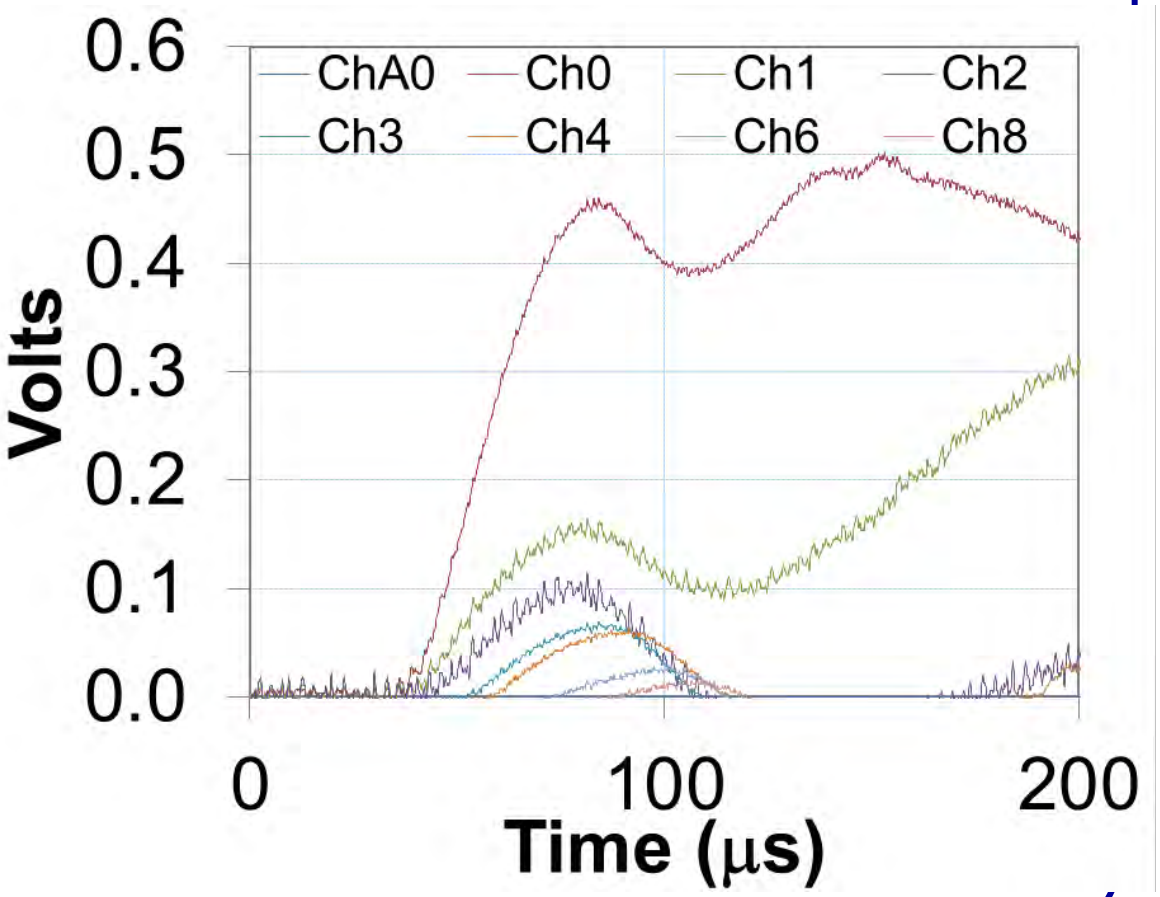

NiCr Validation – Dyneema, 10 layers

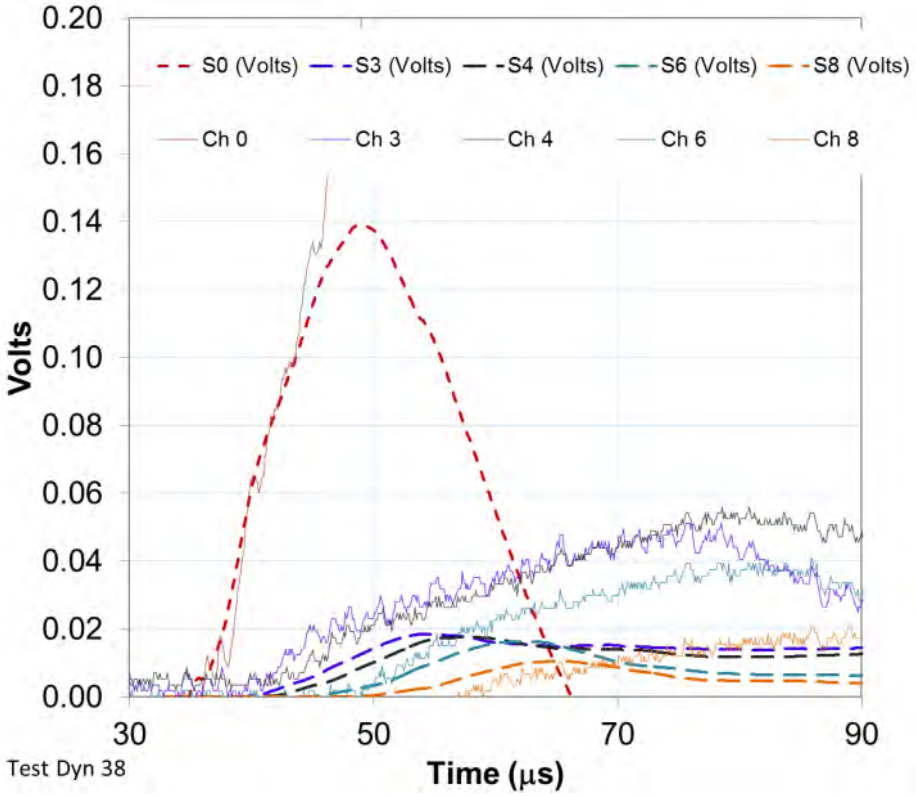

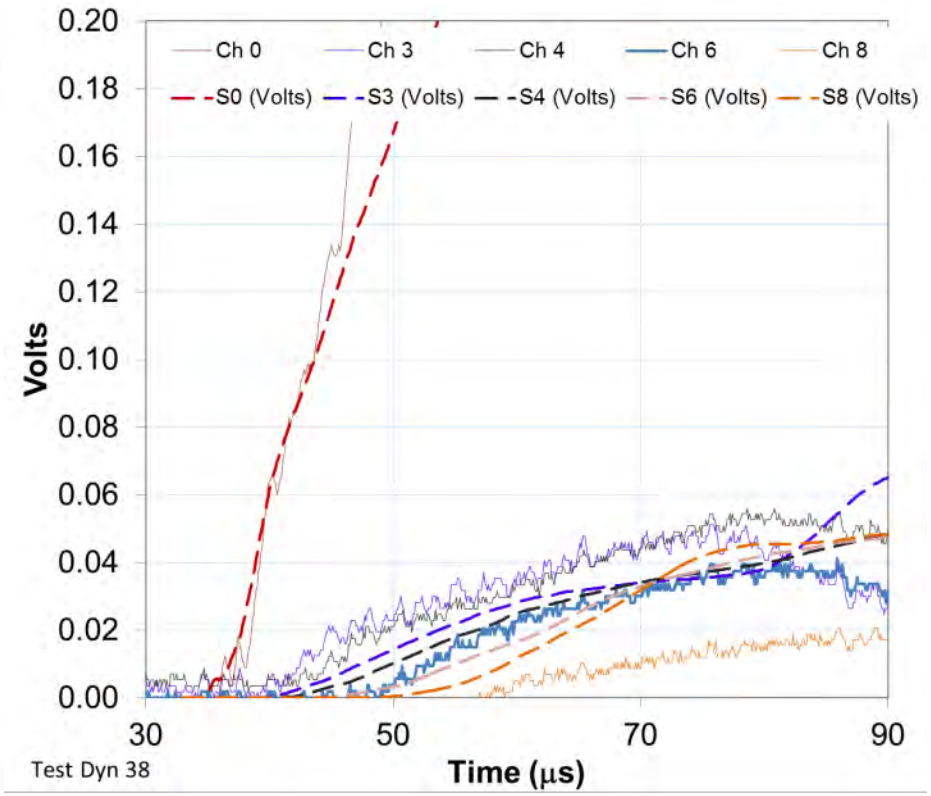

Unclamped in simulations **Clamped**

The dashed lines are the simulations, the thin lines are the waves recorded on the tests

NiCr Validation – PBO, 10 layers

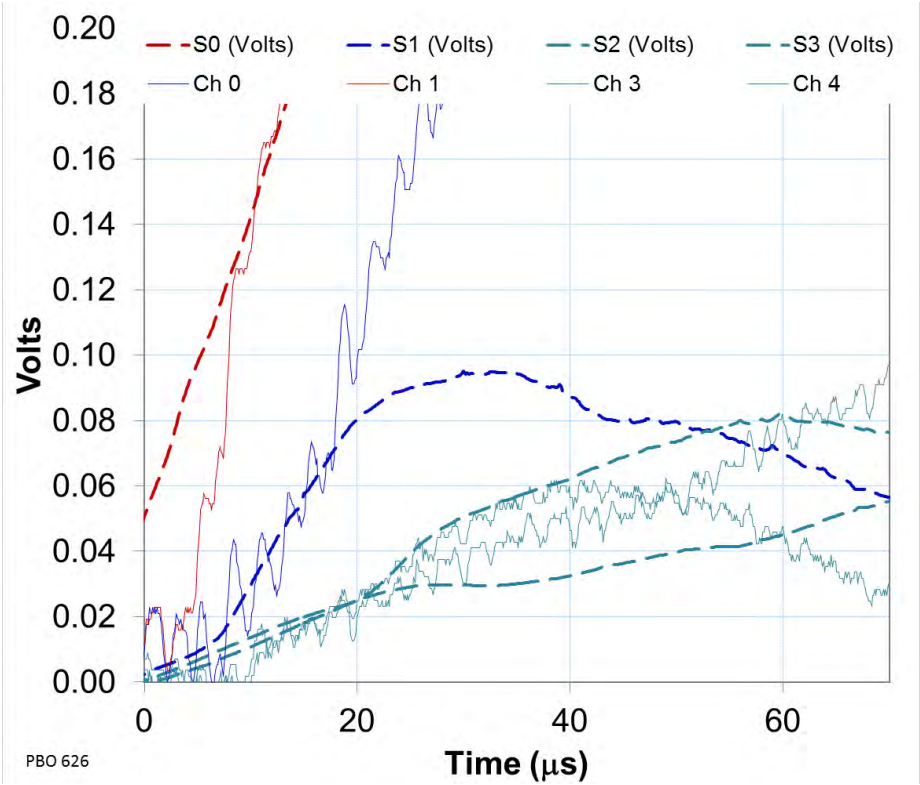

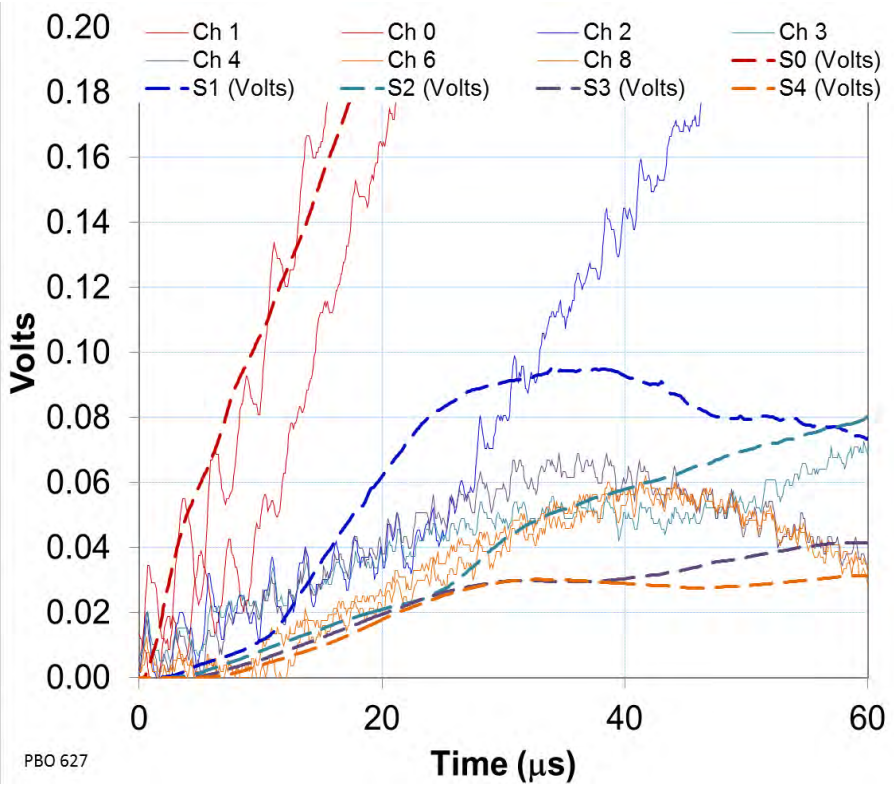

Unclamped in simulations **Clamped**

The dashed lines are the simulations, the thin lines are the waves recorded on the tests

NiCr Validation – KM2 850d, 10 layers

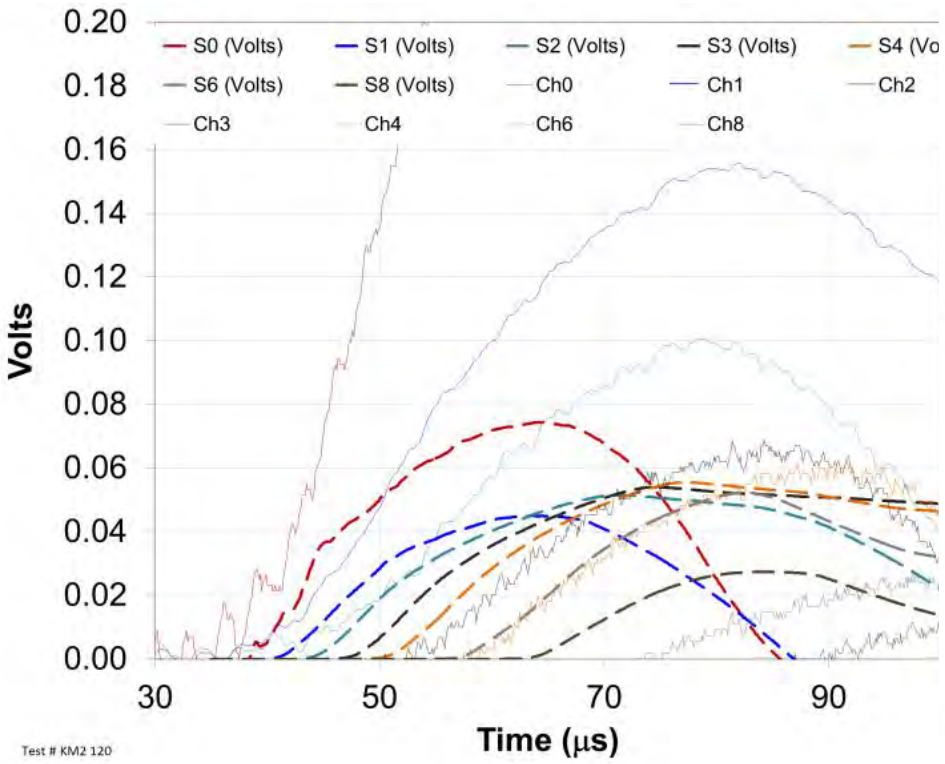

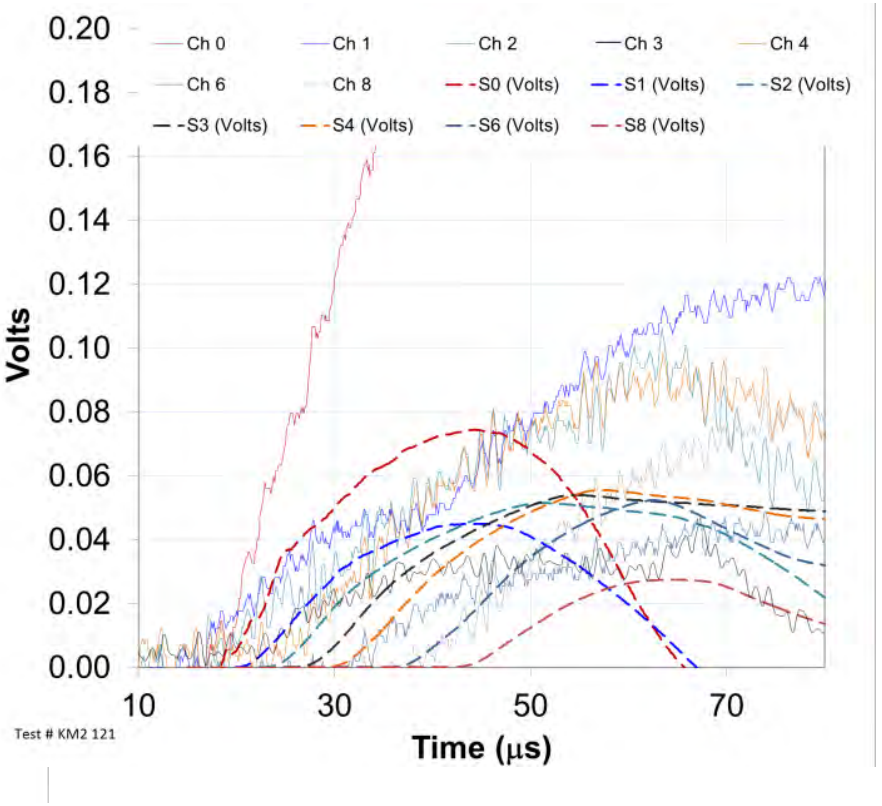

Unclamped in simulations

Clamped

The dashed lines are the simulations, the thin lines are the waves recorded on the tests

Conclusions

- Use of multiple diagnostic techniques during a test increases confidence on the interpretation of the results.
- Numerical validation was performed in various ways, providing confidence on the model:
  - Single yarn impact.
  - Single layer impact.
  - Multi-layer tests.
  - Ballistic limit comparison.
  - NiCr wire waves comparison.
- Is this model perfect? NO
  - Compression of yarn in longitudinal direction has same modulus and strength.

Acknowledgments

- To James Walker for his insights in the physics of the problem.
- To Harm Van der Werff from DSM for pointing out the discrepancy between theoretical and experimental critical velocities on impact on yarns.
- The authors wish to acknowledge funding for this effort provided by the Office of Naval Research through a subcontract from Johns Hopkins University Applied Physics Laboratory.
- In particular the authors wish to thank Lee Mastroianni (ONR), Jim MacKiewicz (Navy Health Research Center), and Andrew Merkle (JHU-APL).

Backup Slides

Wave propagation in yarns (Smith, 1958)

- Yarn wave propagation well known:
  - Longitudinal wave travels at speed of sound c
  - Transverse wave travels slow at a speed U
- Wave reflects on boundary and impact point increasing by Δε at each reflection until yarn breaks.

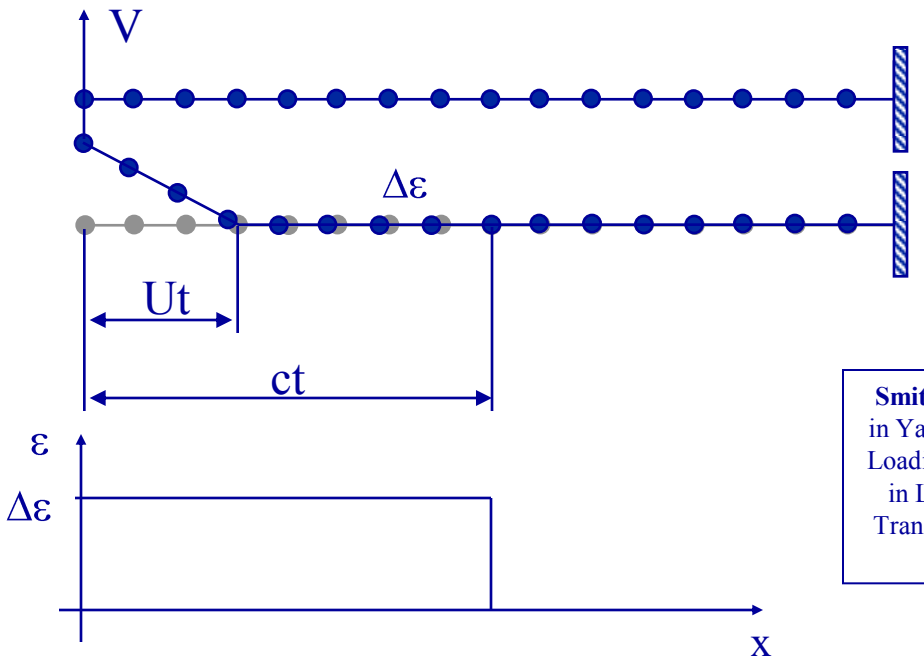

Smith, Stress-Strain Relationships in Yarns Subjected to Rapid Impact Loading: Part V: Wave Propagation in Long Textile Yarns Impacted Transversely, Textile Res. Journal, 1958; 28; 288

Wave propagation in yarns (Smith, 1958)

- Given impact velocity and sound speed in the yarn it is straightforward to determine strain and transverse wave velocity:

$$V = c\sqrt{\varepsilon\left(2\sqrt{\varepsilon(1+\varepsilon)} - \varepsilon\right)}$$

$$U = c\left(\sqrt{\varepsilon(1+\varepsilon)} - \varepsilon\right)$$

Smith, Stress-Strain Relationships in Yarns Subjected to Rapid Impact Loading: Part V: Wave Propagation in Long Textile Yarns Impacted Transversely, Textile Res. Journal, 1958; 28; 288

Local vs. global strain

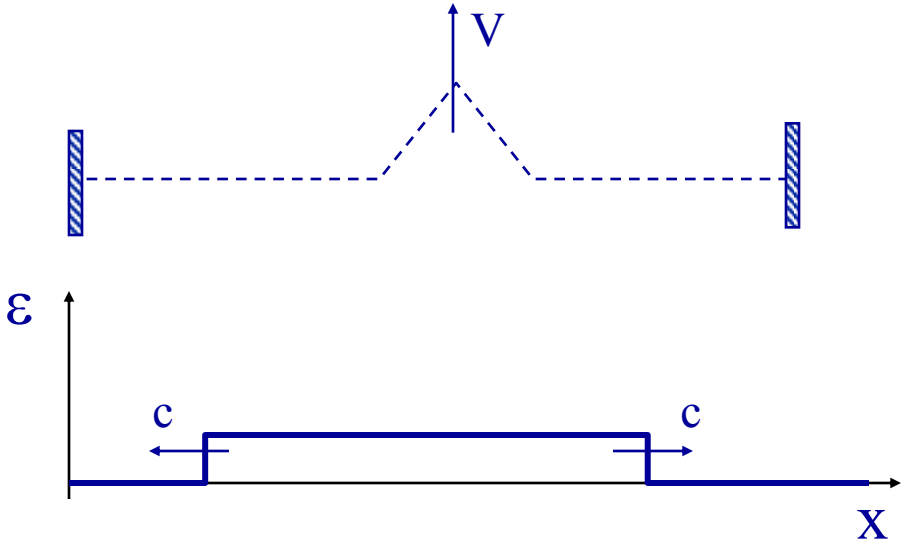

Early time ($t \sim t_c$)
Local response
NiCr does not directly give the strain
Need a model to interpret V(t)

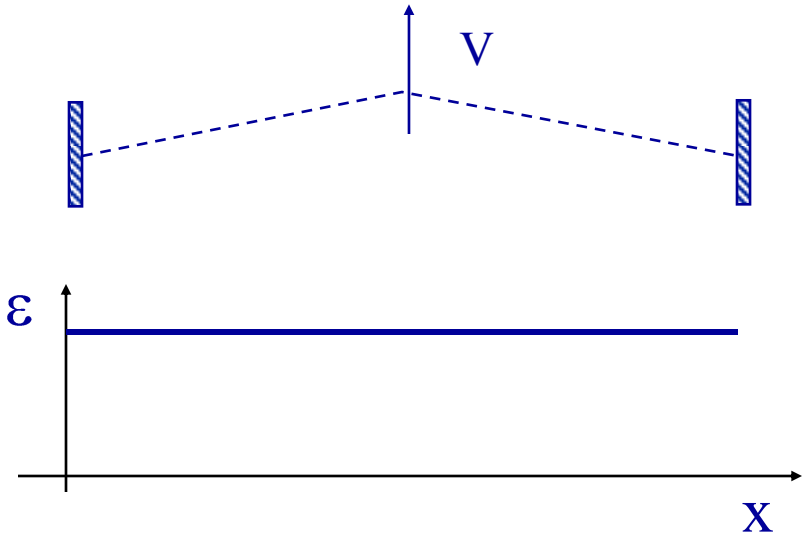

Late time ($t >> t_c$)
Global or structural response.
NiCr "directly" gives strain with $\varepsilon = k \times V$

Characteristic time: $t_c \equiv .5\ L/c$
For our tests: $t_c \sim 40\ \mu s$

"Local" strain - Model for the longitudinal wave

Given the above assumption and the fact that the voltage drop depends on the strain as:

$$V(x,t) = \frac{1}{k_w}\int_0^x \varepsilon(x,t)dx$$

Then

$$V(t) = 2\frac{\varepsilon_0 c_{fab} t}{k_w}$$

Where ε_0 is the strain that is propagating through the yarn. V is then linear with time for the first few microseconds. The *local* strain in the NiCr yarn for the first few microseconds is:

$$\varepsilon_0 = \frac{k_w V(t)}{2c_{fab} t}$$

and, since V is proportional to the time (αt) for the first few microseconds:

$$\varepsilon_0 = \frac{k_w \alpha}{2c_{fab}}$$

Sources of error when evaluating strain

- Local strain:
  - The propagation of the longitudinal wave is in fact much more complex. At each crossover part of the wave is reflected and part transmitted.
  - The wave probably damps at some point and does not seem to be reflected at the boundary since that would mean doubling the slope of V(t), which does not happen in the experiments
- Global strain:
  - Confidence is higher when measuring global strain because the NiCr wire is used as a long strain gage.
  - Nevertheless some error is introduced by not taking into account the slippage of fabric at the boundaries.
  - Maximum slippage is around 3 inches (adding both top and bottom boundaries)
  - This increases the gage length of the wire and, systematically, gives us a strain higher than the real one (if, when converting voltage to strain we keep the gage length constant)
  - If we assume that max. slippage happens at max. strain (conservative assumption) then the max. error is ~0.5% strain (so a 20% relative error for a 2.5% strain measurement). A typical error is ~0.3% strain (12% relative error).
  - Again, the error is not random but systematically we estimate more strain than the real strain.
  - At high velocities or for the Vamac® targets this error is very small (<0.1% strain)

Strain in the Impacted Yarn (LS-DYNA)

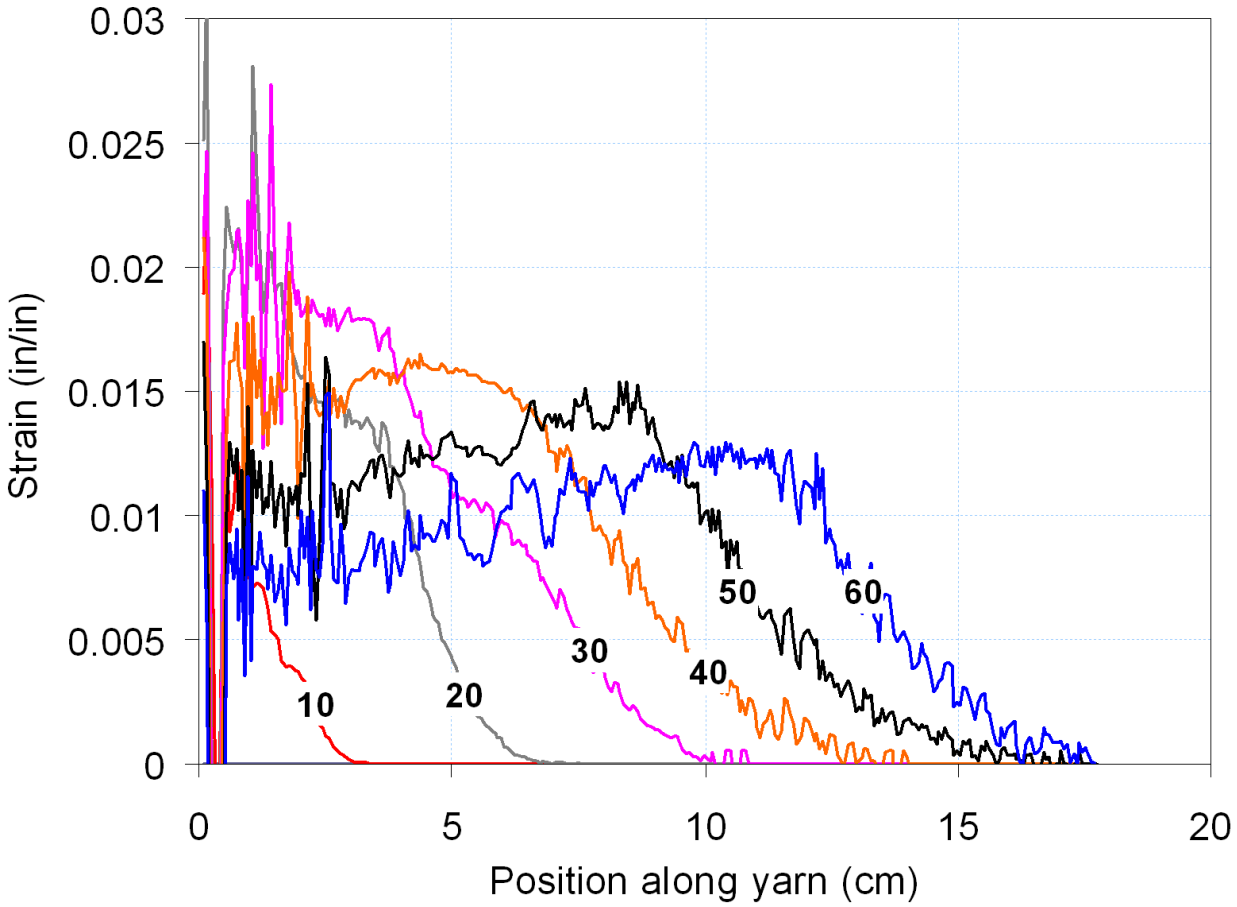

Description of the waves seen in the NiCr wire

- The principles, main assumptions and limitations of the NiCr wire technique are discussed in a paper published in the Int. J. of Impact Engng. in 2010.
- We assume the waves are divided in four parts:
  - Initial pull: First 10 or 15 μs, which, we assume, correspond to a longitudinal wave traveling up the yarn/wire. Linear part.
  - Failure and/or transverse wave (if it happens): following 30 – 50 μs. The transverse wave shows up as a linear segment. Failure shows up as a bump
  - Mixed region: complex wave interaction, region difficult to interpret ~ 500 or 1000 μs
  - Global response: late time (quasi-steady) that can be interpreted as in a static tensile test: ~ 1000 μs or more

V3.1-1

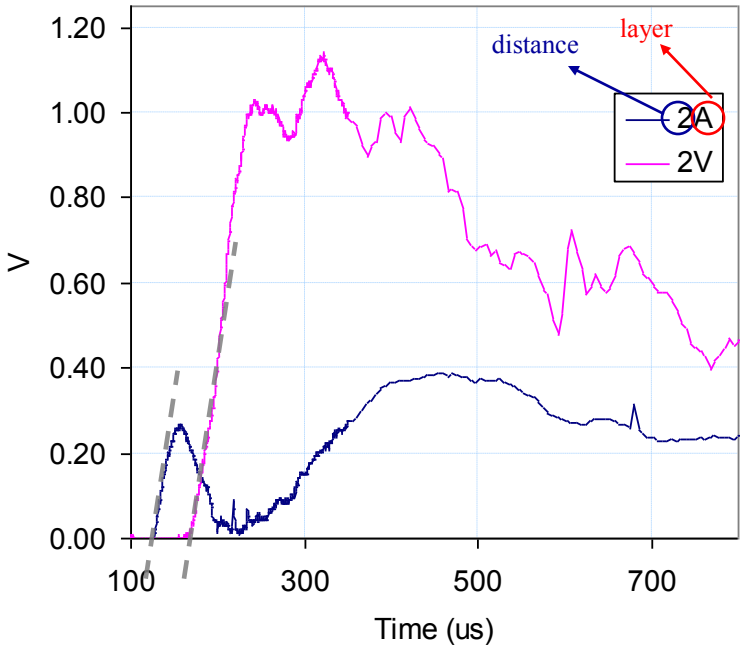

This particular test had a NiCr wire in the first and last layer. The first layer was perforated during the test. The last layer was not perforated

Model for the longitudinal wave

- Assumption: The first slope in V=V(t) is due to a longitudinal wave traveling through the secondary yarn (the one that has the NiCr wire) at a speed c_{fab}.
- This longitudinal wave gives rise to a constant strain that travels along the yarn. This assumption is only good for the first few microseconds, until failure or transverse wave arrival.
- Purpose: Allow to calculate the *local* strain in the secondary yarn. **The strain is proportional to the initial slope**.

$$\varepsilon_0 = \frac{k_w \alpha}{2 c_{fab}}$$

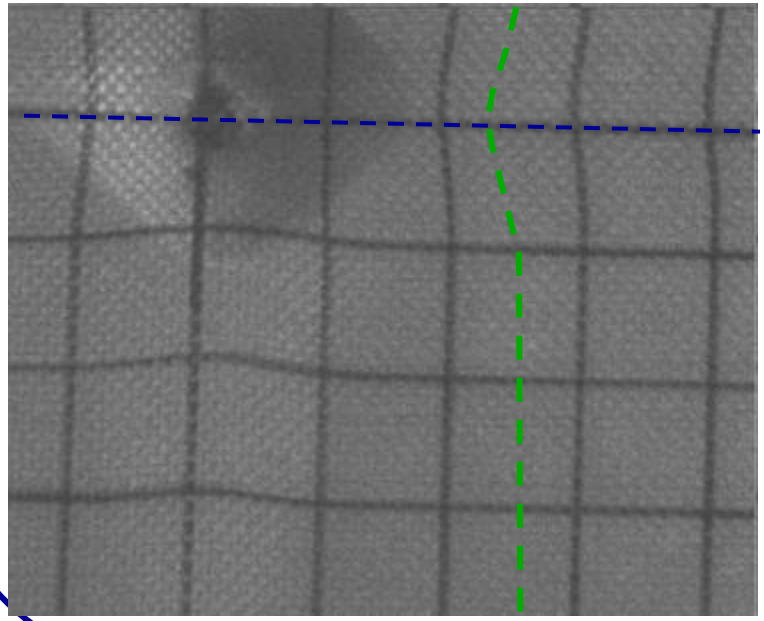

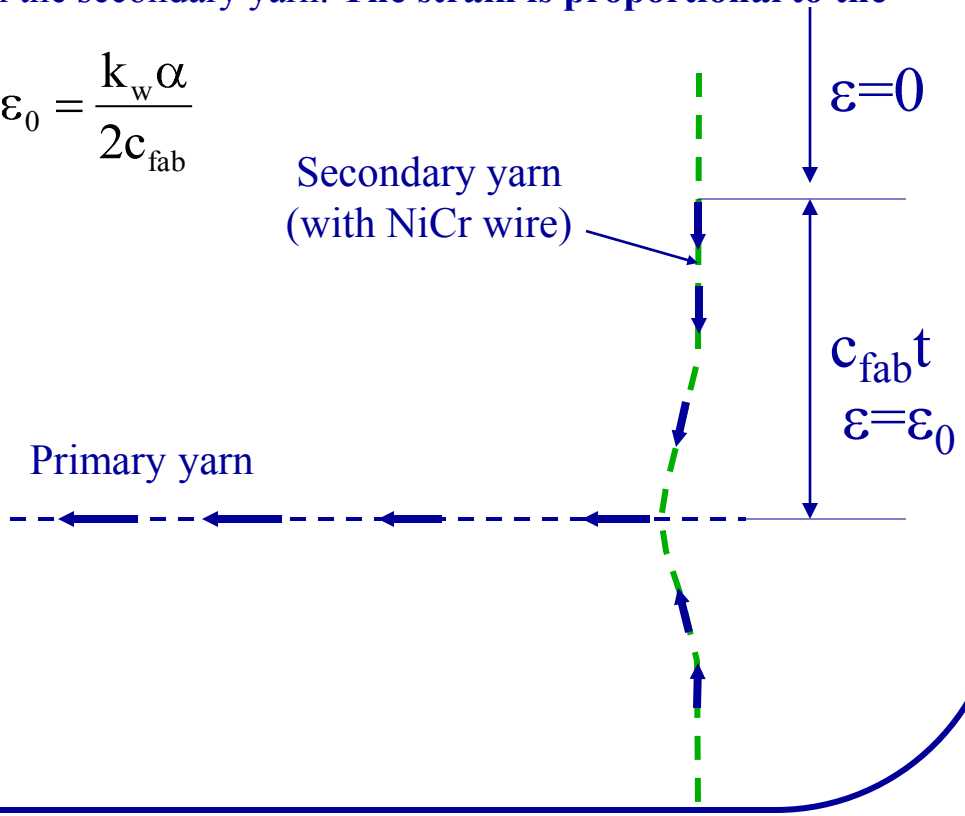

V3.1-1

- It takes ~ 35 μs for the transverse wave to reach the NiCr wire

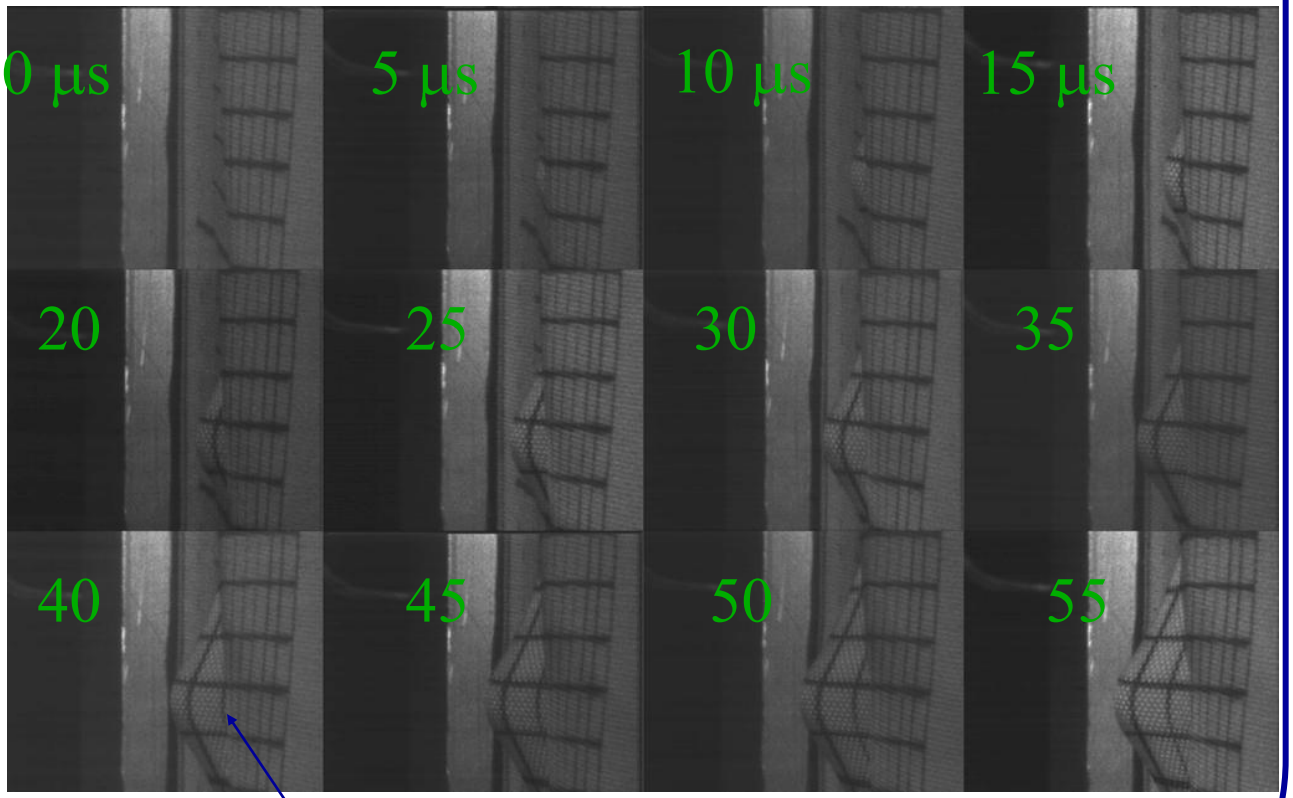

V1.10-2

NiCr on layers 1 and 15; 2 first layers penetrated

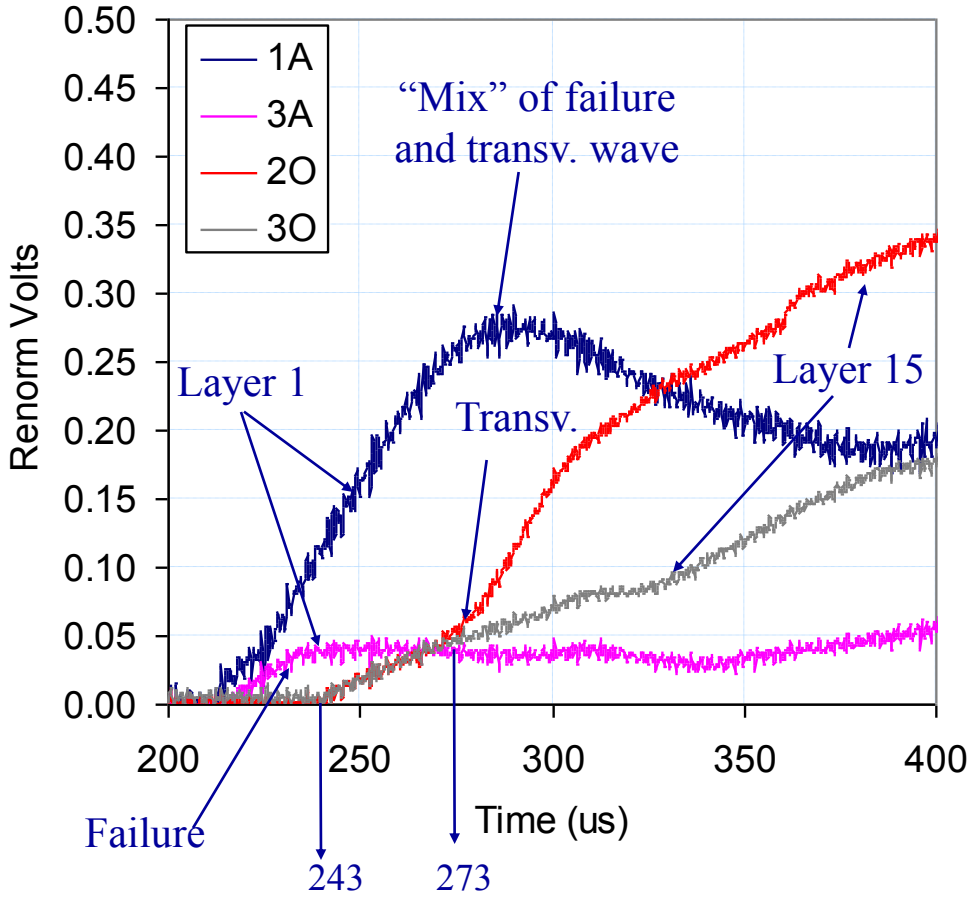

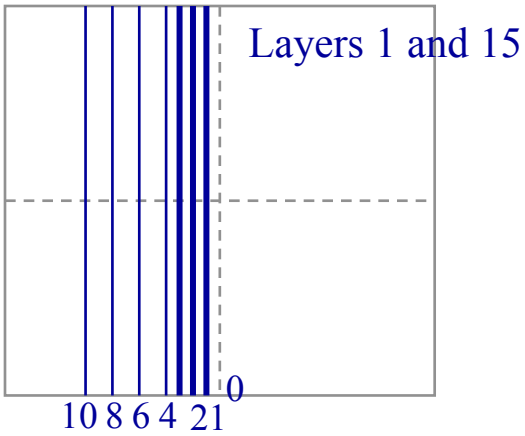

Comparison of signals from tests vs. signals from simulations

DYNA vs. NiCr wire

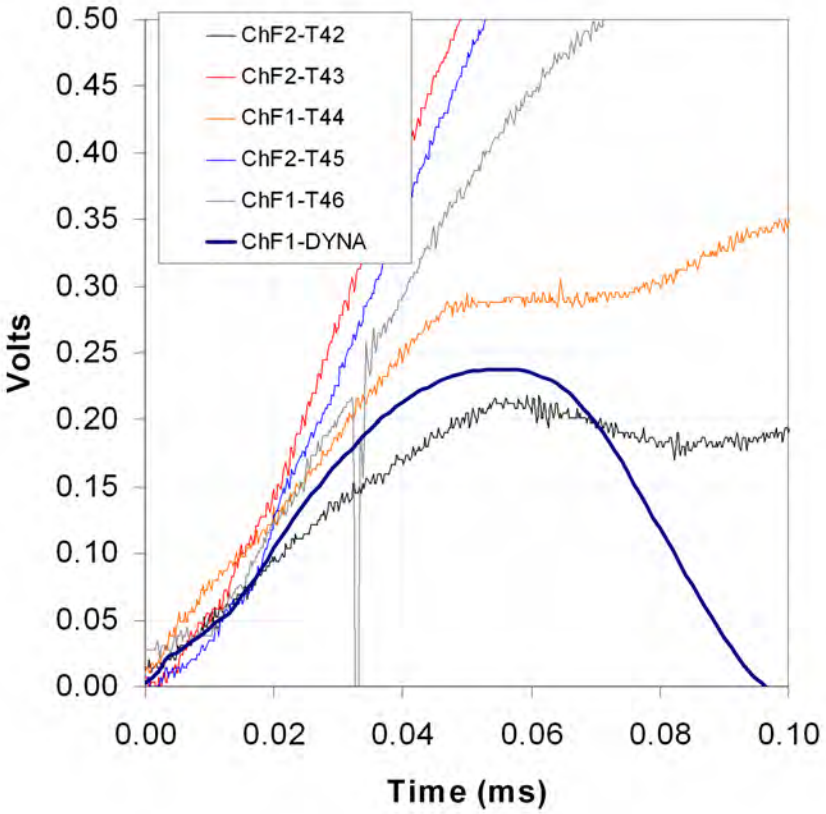

1 cm from impact point

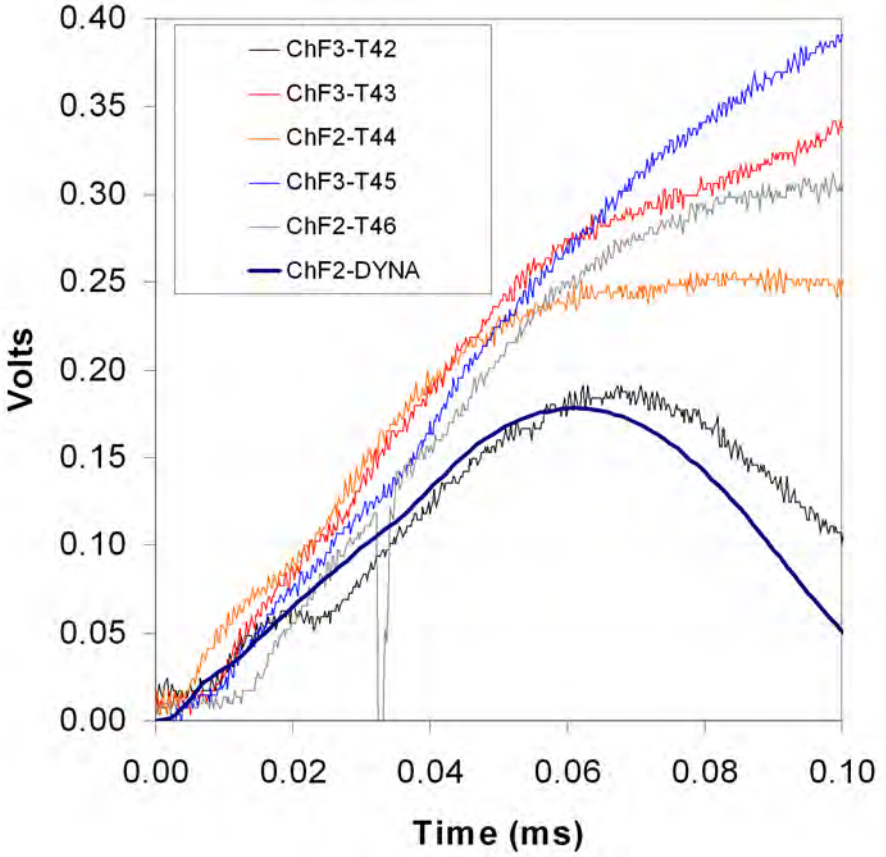

2 cm from impact point

DYNA vs. NiCr wire

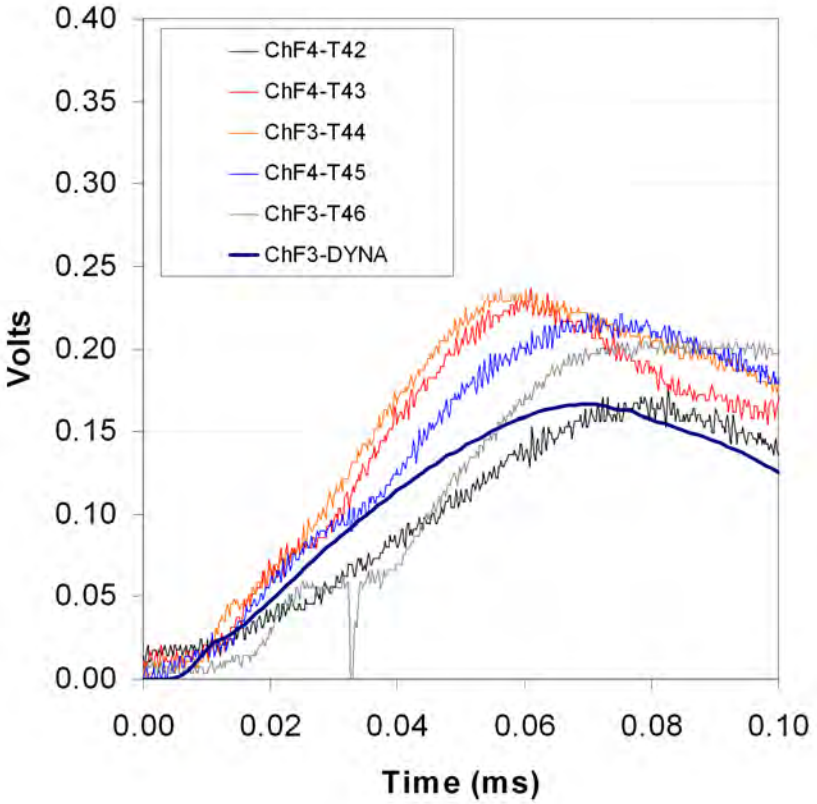

3 cm from impact point

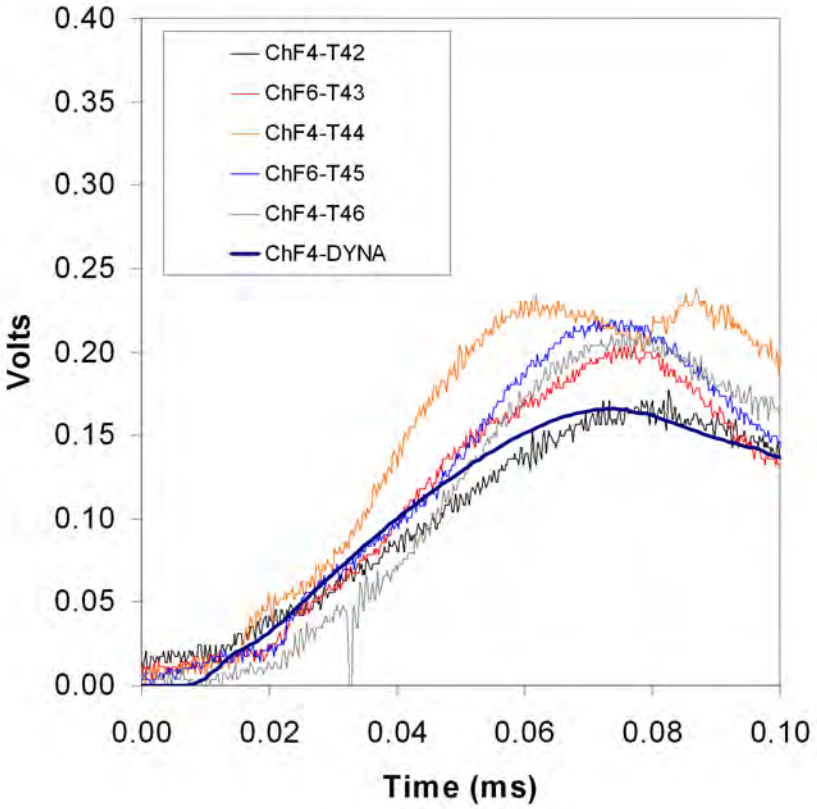

4 cm from impact point

DYNA vs. NiCr wire

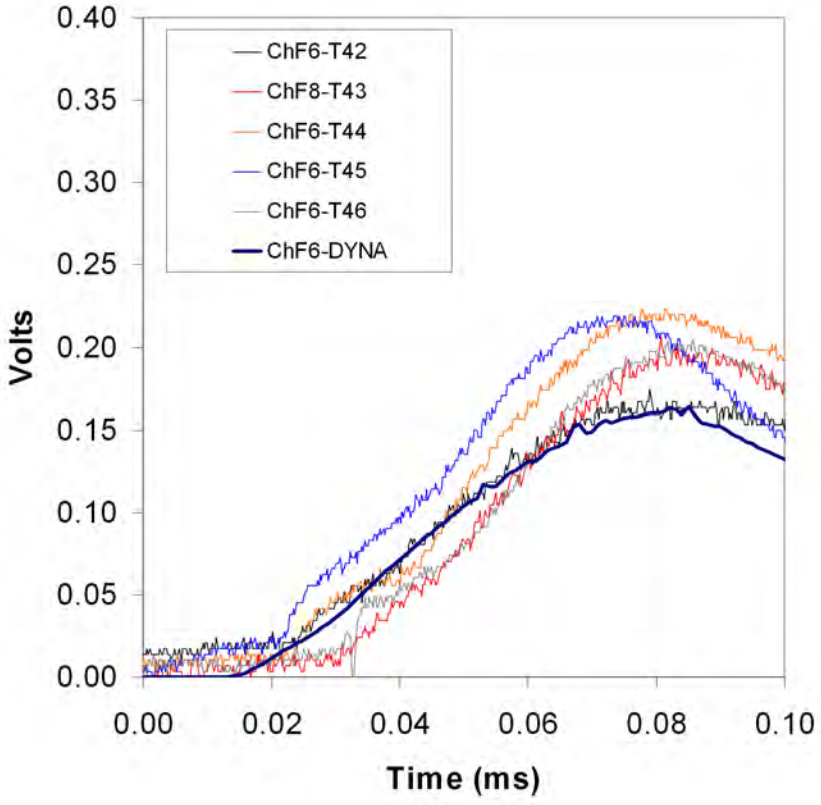

6 cm from impact point

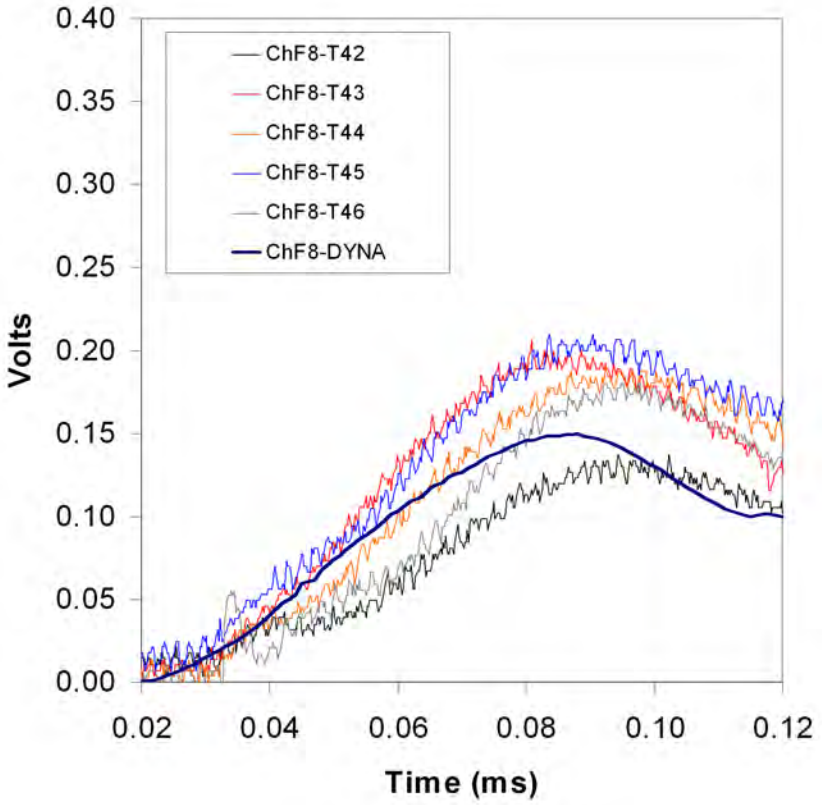

8 cm from impact point

DYNA vs. NiCr wire

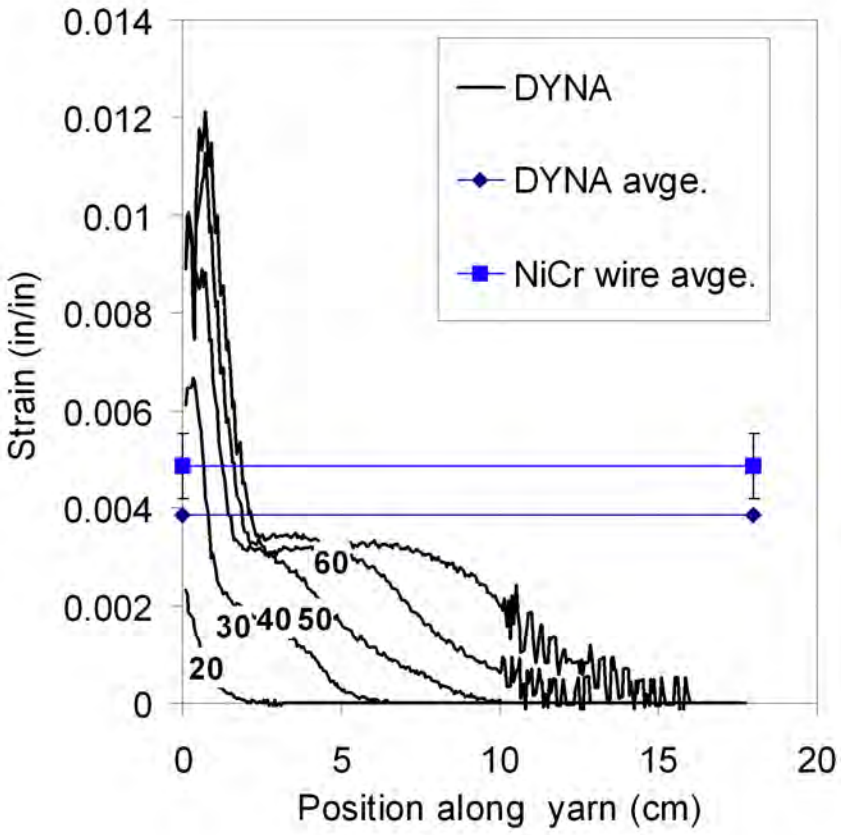

2 cm from impact point

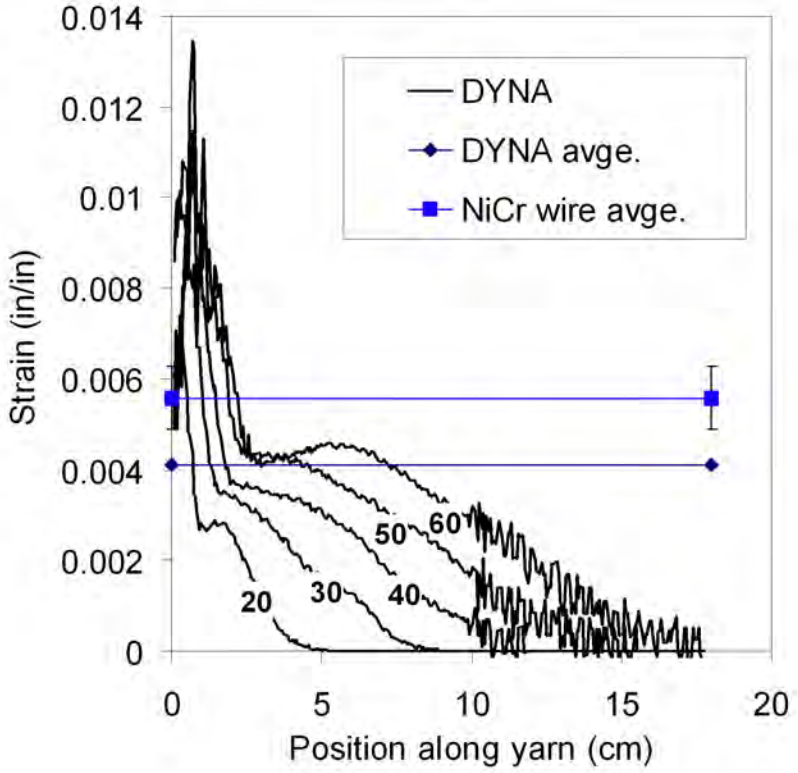

4 cm from impact point

DYNA vs. NiCr wire

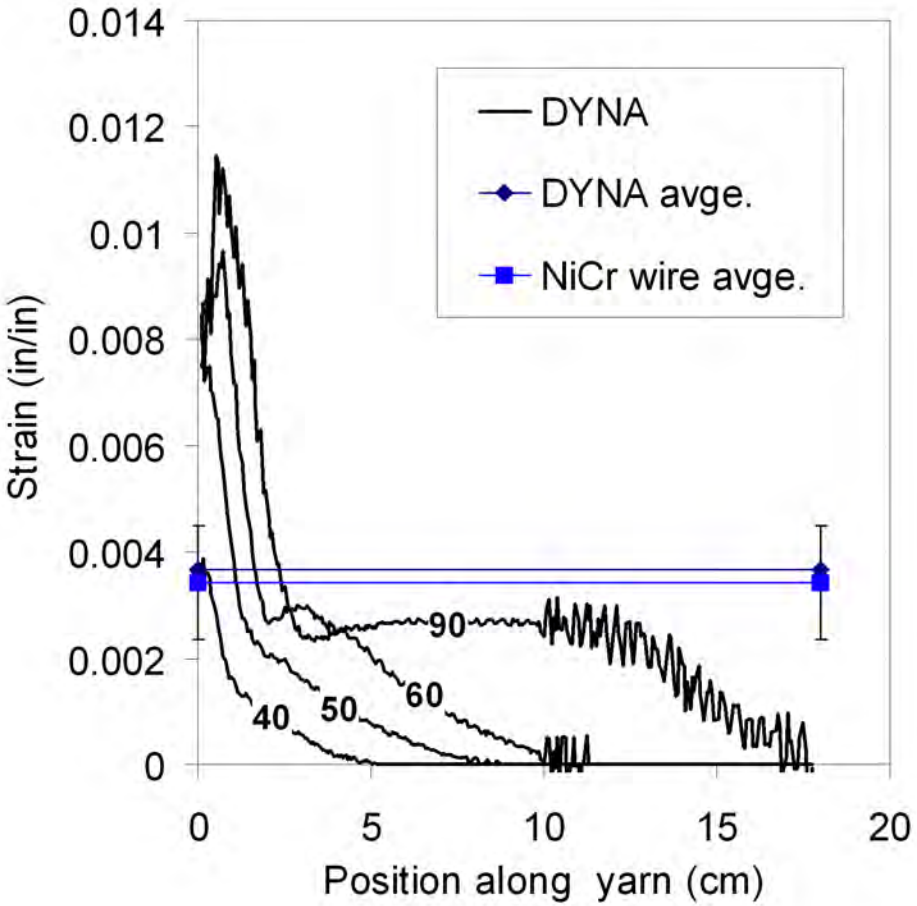

6 cm from impact point

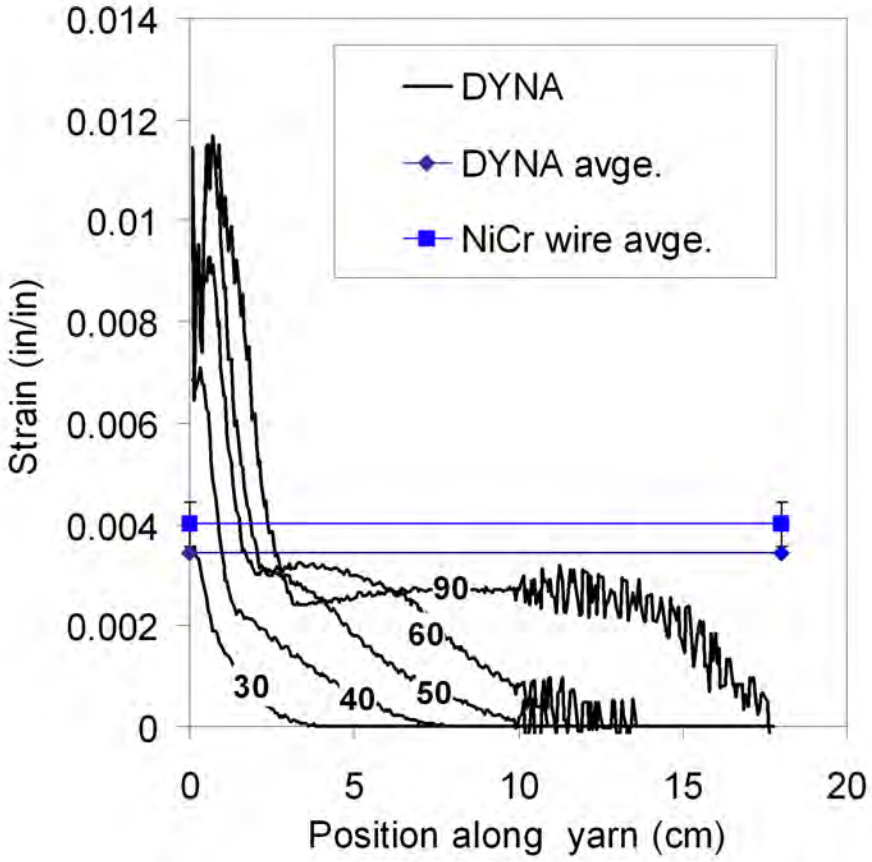

8 cm from impact point

How Strain is Distributed along Fabric NiCr wire and DYNA

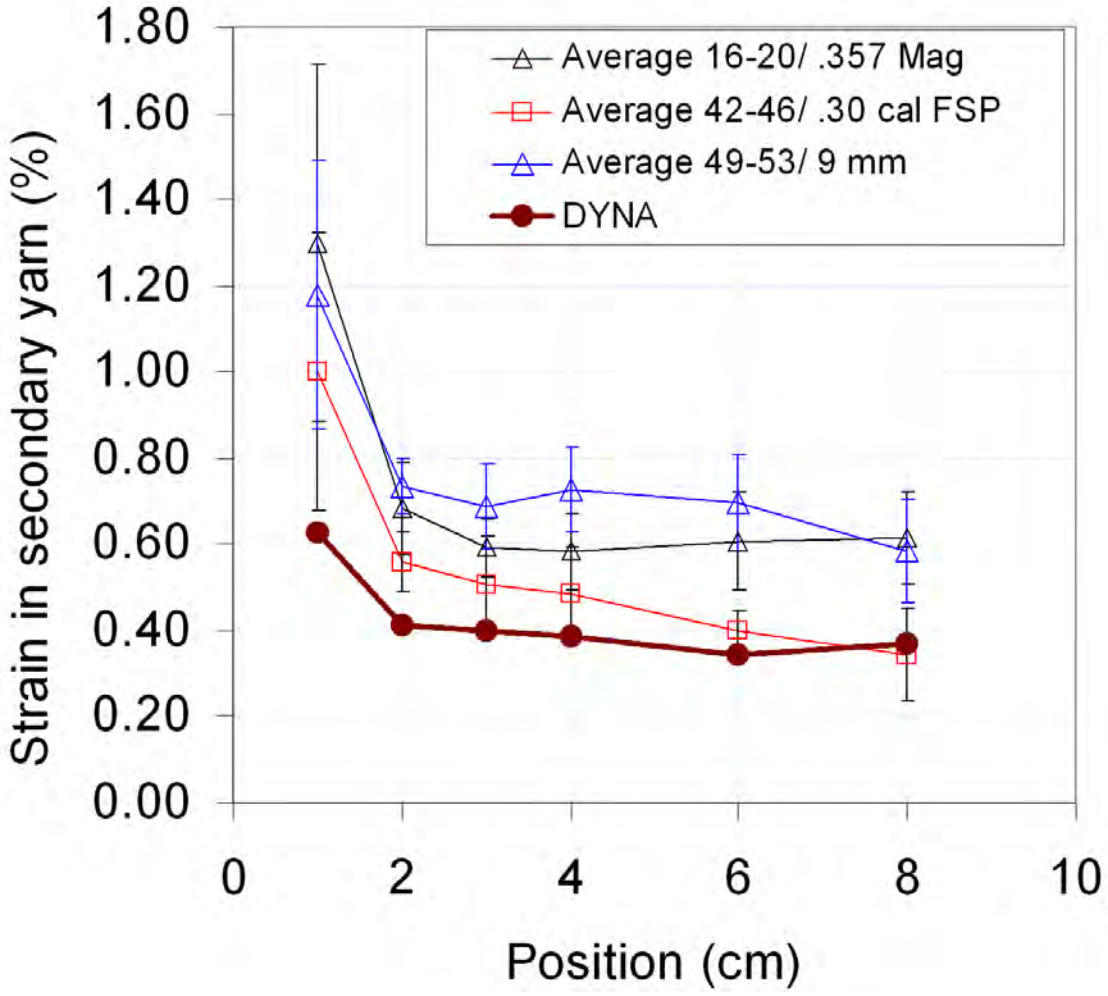

How Strain is Distributed along Fabric NiCr wire

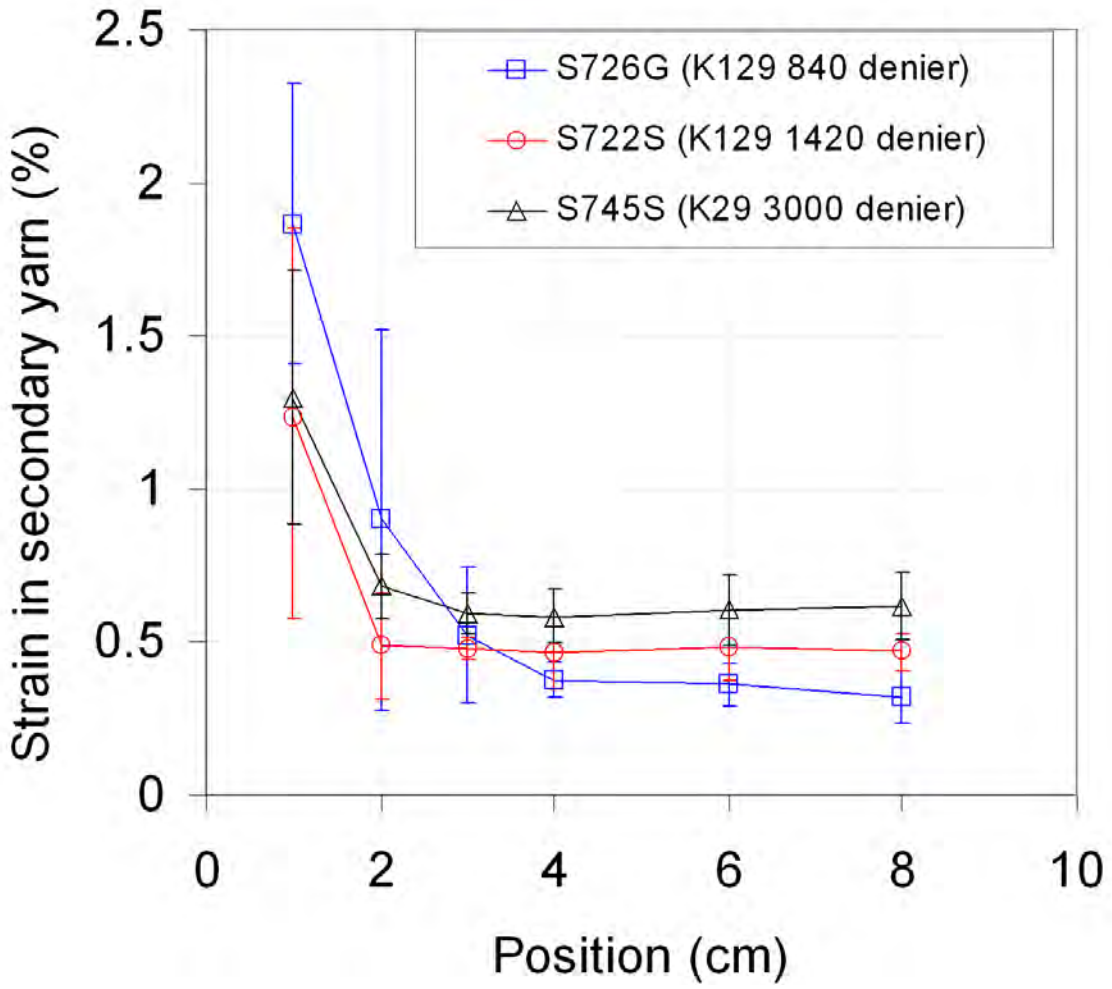

How Strain Distributes from Layer to Layer NiCr wire results

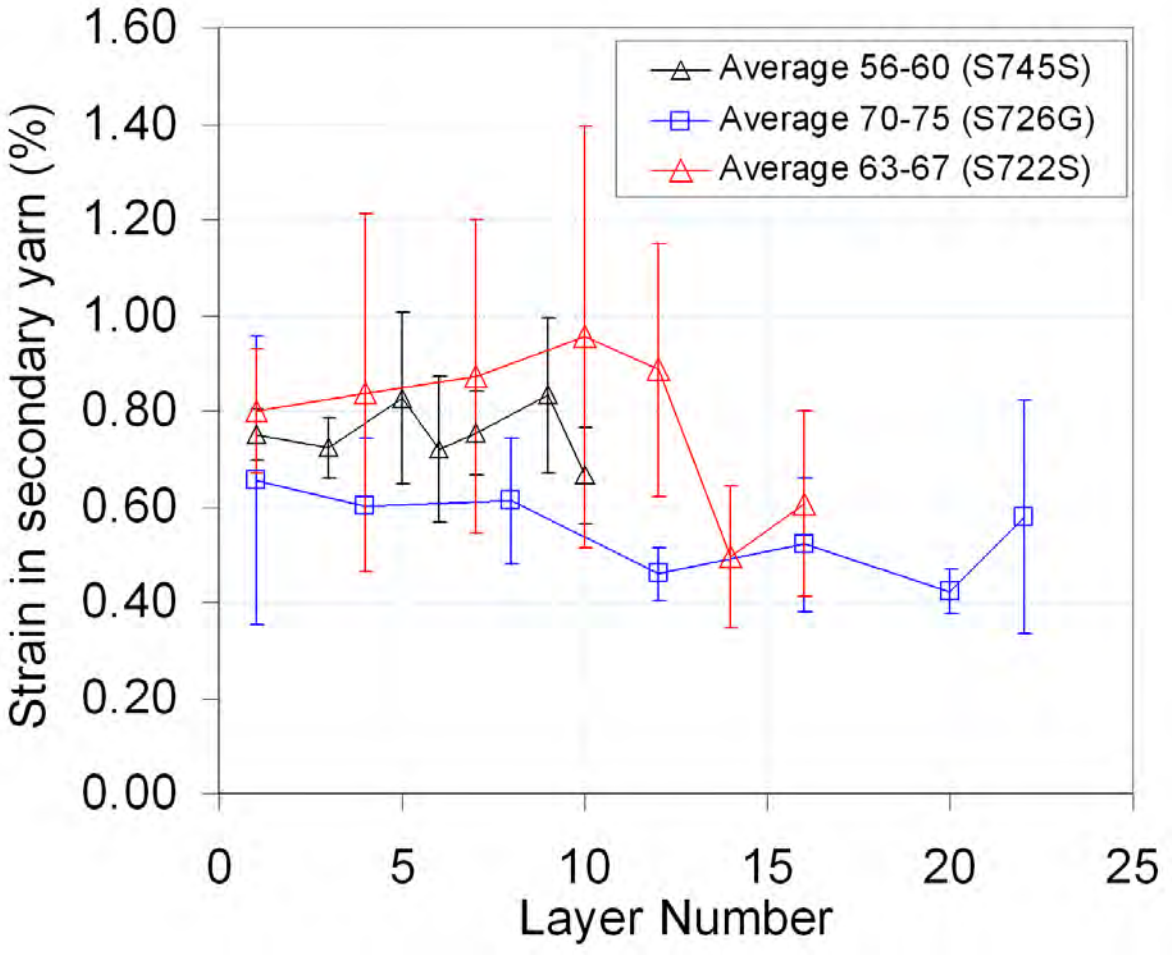

Predicting the dynamic Stability of Small-Caliber Ammunition

26th International Symposium on Ballistics

Miami, FL. Sept. 12-16 2011

TECHNOLOGY DRIVEN. WARFIGHTER FOCUSED.

S. Silton, PhD

Flight Sciences Branch

US Army Research Laboratory

Aberdeen Proving Ground, MD

sidra.i.silton.civ@mail.mil

B. Howell

Formerly of Data Matrix Solutions, Inc.

Possible Improvement of Prediction Methods for Dynamic Stability

Standard tests fire rounds at muzzle twist rates at downrange velocities.

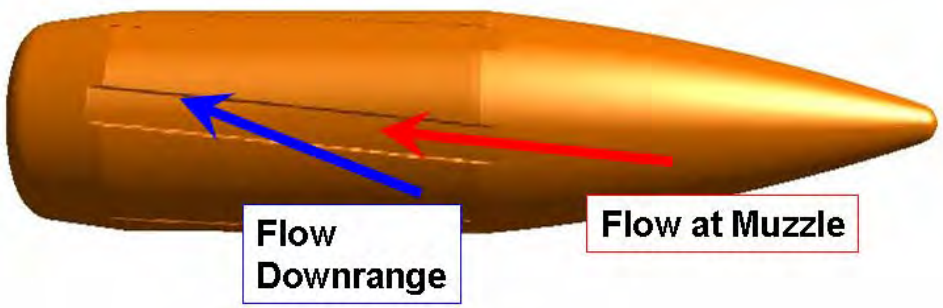

Muzzle twist rates do not accurately resemble spin conditions downrange.

A comprehensive study and comparison of the stability characteristics of two 5.56 mm projectiles at different downrange spin conditions will determine the most accurate method in obtaining the stability characteristics in future tests.

Experiments were carried out in the ARL Aerodynamic Experimental Facility

The 100-m long Aerodynamic Experimental Facility is operated by the Aerodynamics Branch at ARL

39 direct image orthogonal shadowgraph stations in 5 groups

Image window is less than 14 inches across

Spark source triggered at a recorded time after infrared sensor detects passing projectile

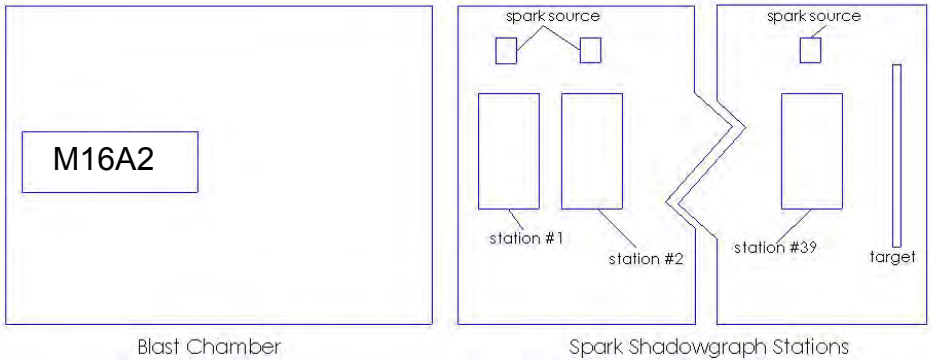

Gun muzzle is located 1.8 meters from 1st station for this test

Spark Facility Layout

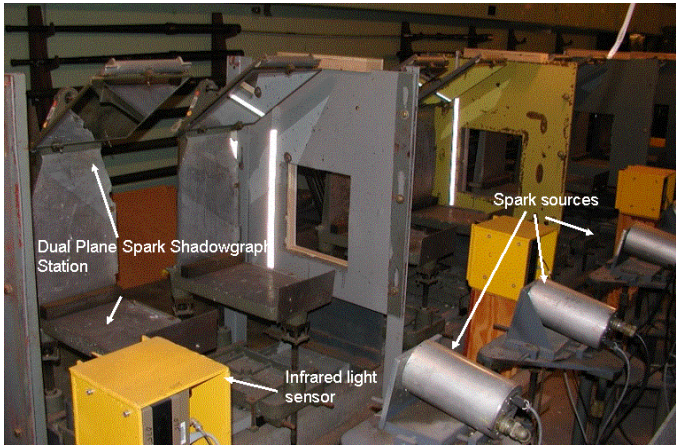

Dual Plane Spark Stations

The dual plane spark shadowgraphs are used to obtain projectile position as a function of time

Shot 26598 – M16A2, muzzle velocity

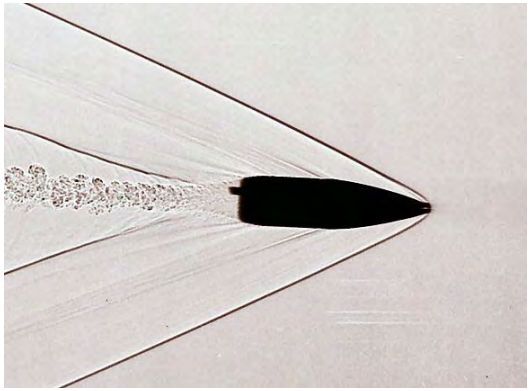

45 vertical

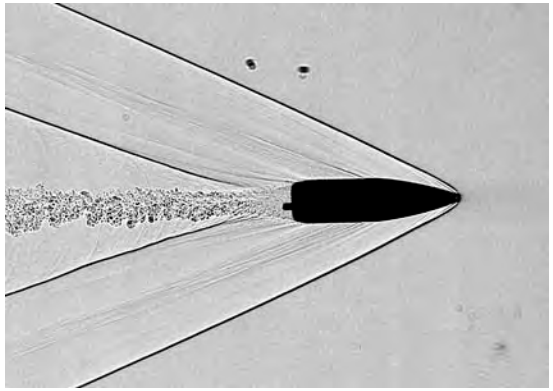

45 horizontal

Film read using a precision light table to determine spatial coordinates and angular orientation of the projectile including roll

Data relative to earth fixed range coordinate system

Data is reduced for a 6-DOF fit in order to obtain an aerodynamic model and motion fit

Aero Range Facility Data Analysis Software – ArrowTech Associates

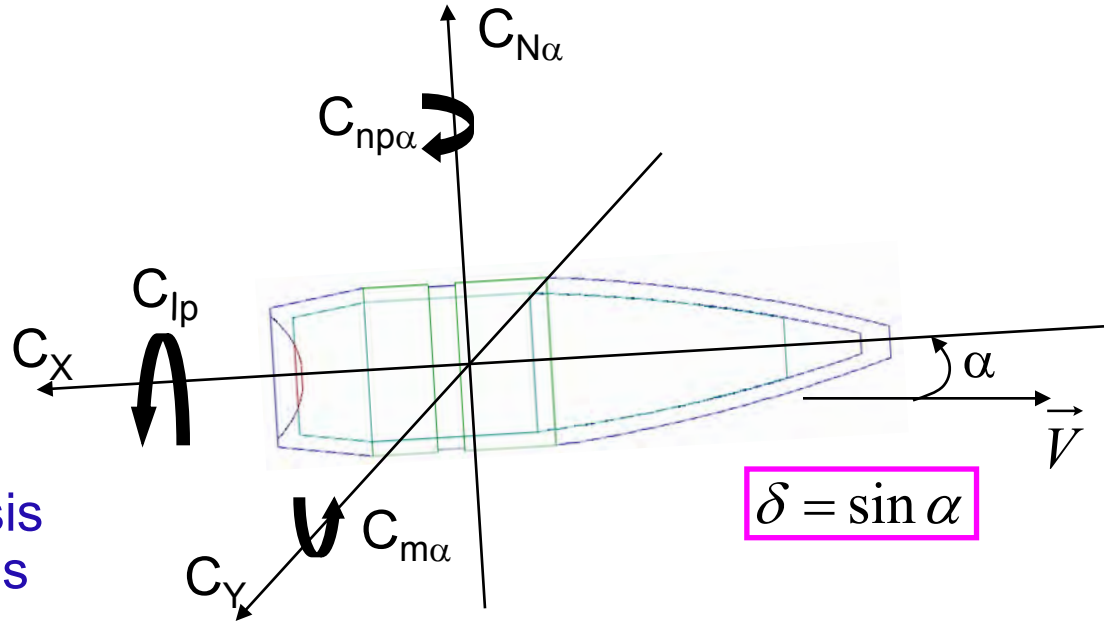

$$\delta = \sin\alpha$$

$$C_X = C_{X_0} + C_{X_2}\delta^2$$

$$C_{m_\alpha} = C_{m_{\alpha 0}} + C_{m_{\alpha 3}}\delta^2$$

$$C_{N_\alpha} = C_{N_{\alpha 0}} + C_{N_{\alpha 3}}\delta^2$$

$$C_{n_{p\alpha}} = C_{n_{p\alpha 0}} + C_{n_{p\alpha 3}}\delta^2$$

$$C_{m_q} = C_{m_q} + C_{m_{\dot{\alpha}}}$$ ← Not shown

Results of the M855 Aerodynamics Test were used to determine its stability characteristics

- M855 projectiles were fired at velocities simulating ranges of 0, 200, 400, 500 and 600-m.
- Fired at muzzle twist rate (1rev in 7 in) from M4 and M16A2 barrels.
- Yaw inducers used as needed.

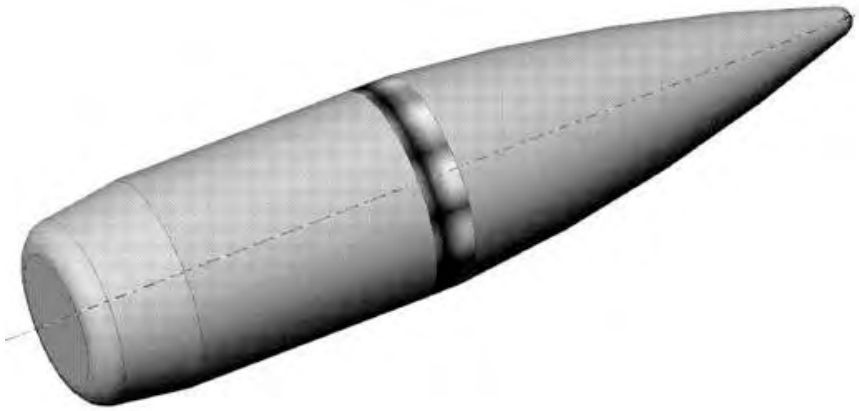

- Stability characterization at muzzle spin and downrange spin rates.
- Yaw limit cycle analysis at muzzle spin and downrange (adjusted) spin rates.

Pitch Damping Exponents can be determined from linear theory

Pitch damping exponents: $$\lambda_{F,S} = -\frac{1}{2}\left[H \pm \frac{P(2T-H)}{\sqrt{P^2-4M}}\right]$$

In which

$$P = \frac{I_x}{I_y}\left(\frac{pd}{V}\right) \qquad M = \frac{C^*_{m_\alpha}}{k_y^2}$$

$$H = C^*_{L_\alpha} - C^*_D - \frac{\left(C_{m_q} + C_{m_{\dot{\alpha}}}\right)^*}{2k_y^2}$$

$$T = C^*_{L_\alpha} - \frac{C^*_{n_{p\alpha}}}{2k_x^2}$$

$$k_x^{\,2} = \frac{I_x}{md^2} \qquad k_y^{\,2} = \frac{I_y}{md^2} \qquad * = \frac{\rho S d}{2m}$$

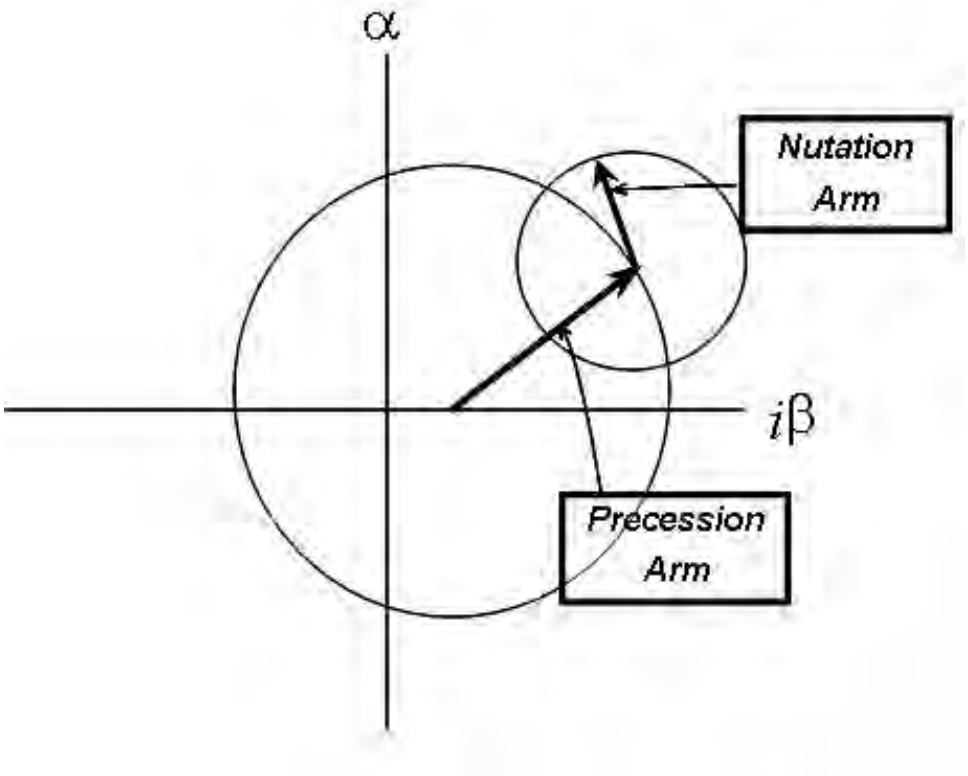

Note: $C_{L_\alpha} = C_{N_\alpha}\cos\alpha - C_X$

$$C_D = C_{N_\alpha}\sin^2\alpha + C_X\cos\alpha$$

Pitch Damping Exponents are recalculated at downrange (adjusted) spin rates

Axial force and roll damping coefficients from 6-DOF fits input into PRODAS to determine downrange spin rates.

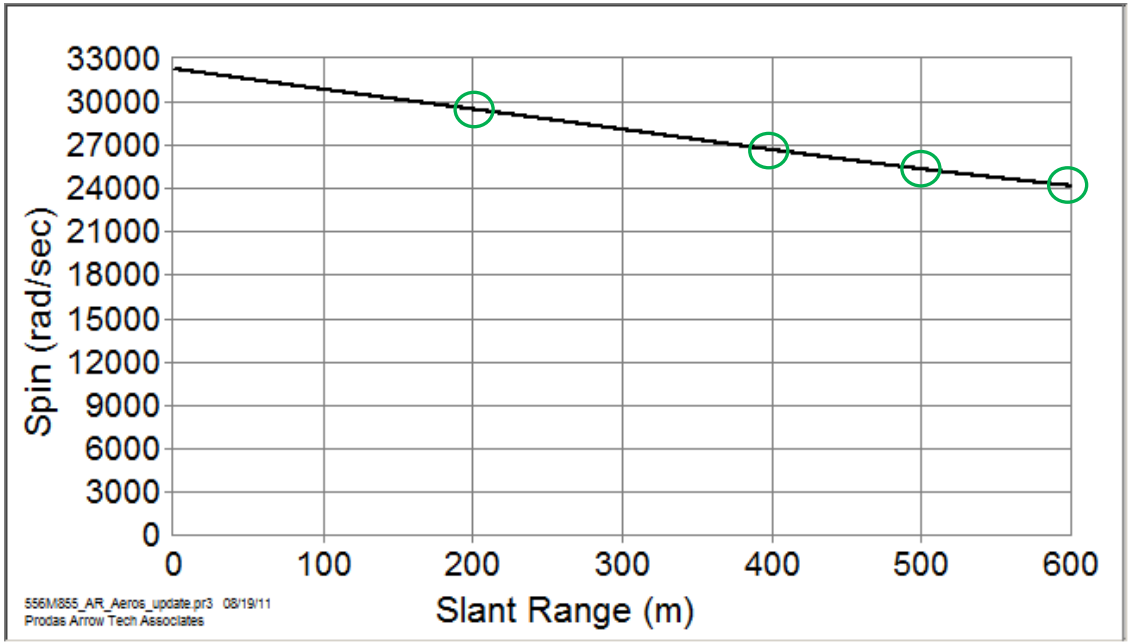

New spin rates are input and used to update the damping exponents

$$\lambda_{F,S} = -\frac{1}{2}\left[H \pm \frac{P(2T-H)}{\sqrt{P^2 - 4M}} \right]$$

Only “P” changes

Slow mode instability appears by Mach 1.7 for M855 using either experimental or adjusted spin

Experimental Spin

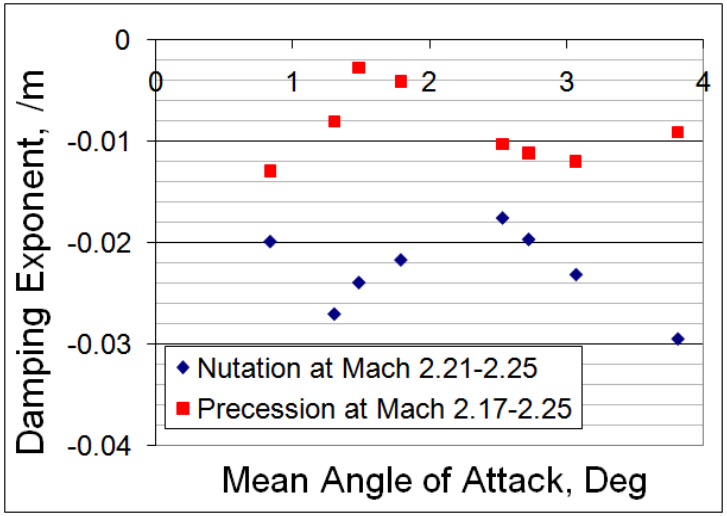

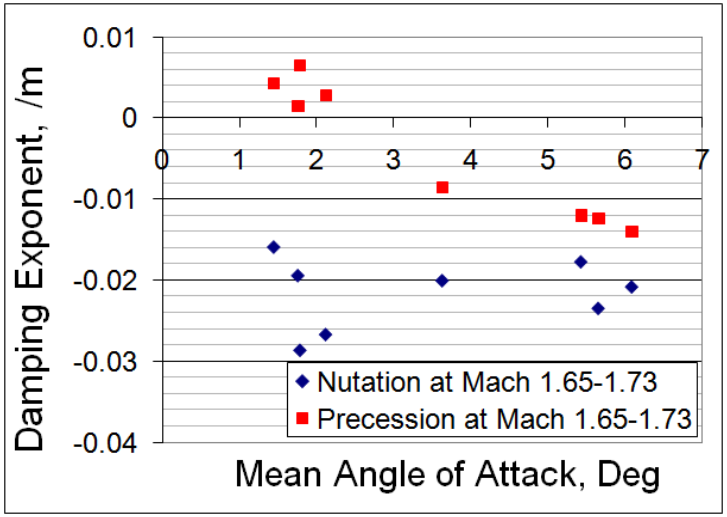

Round Stable at Mach 2.2

Slow mode instability appears at Mach 1.7

Simulated spin decreases magnitude of instability

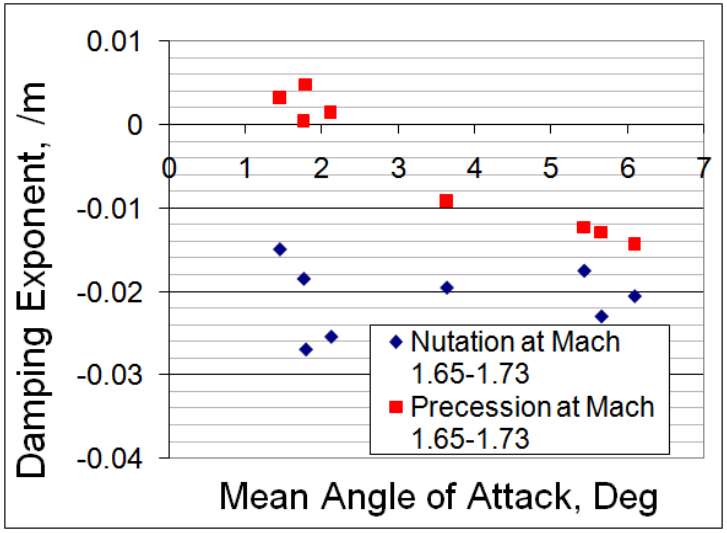

Simulated Spin

Using adjusted spin values decreases the damping exponents as compared to experimental values

Experimental Spin

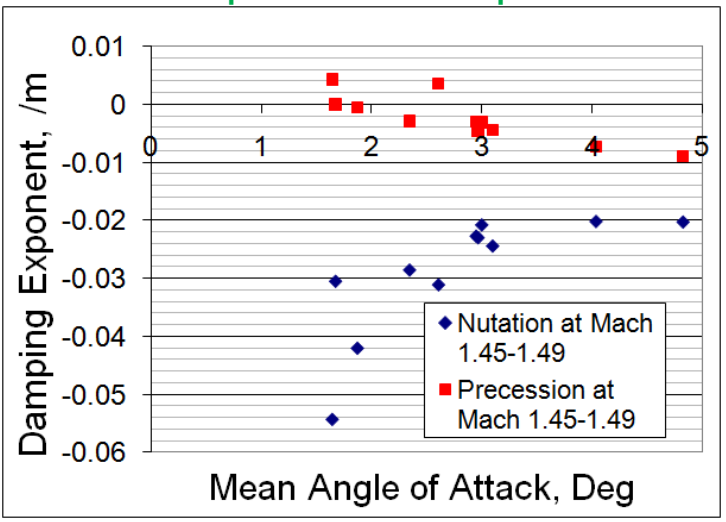

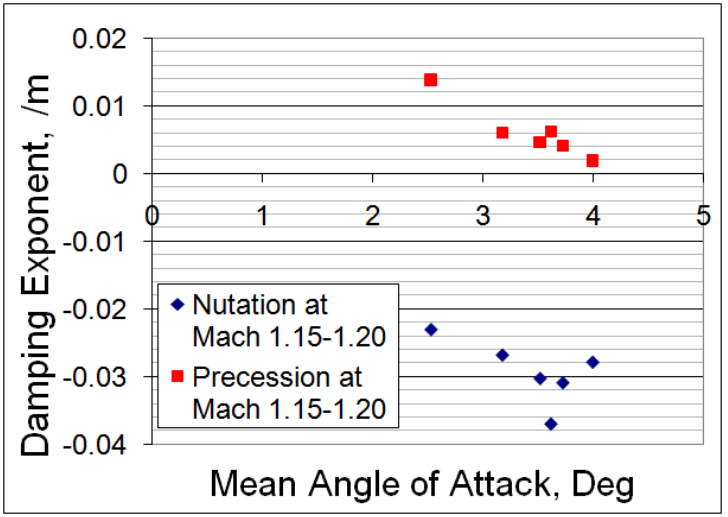

Precession and Nutation arm damping exponents are decreased.

Yaw limit cycle still exists, but is reduced by ~0.5°

Simulated Spin

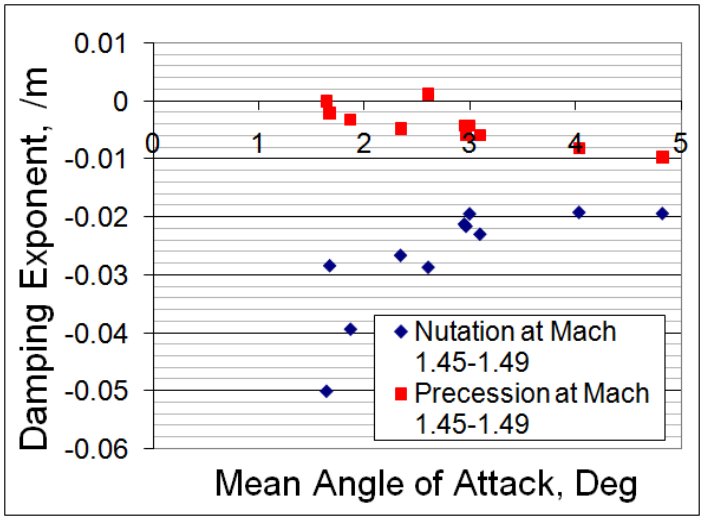

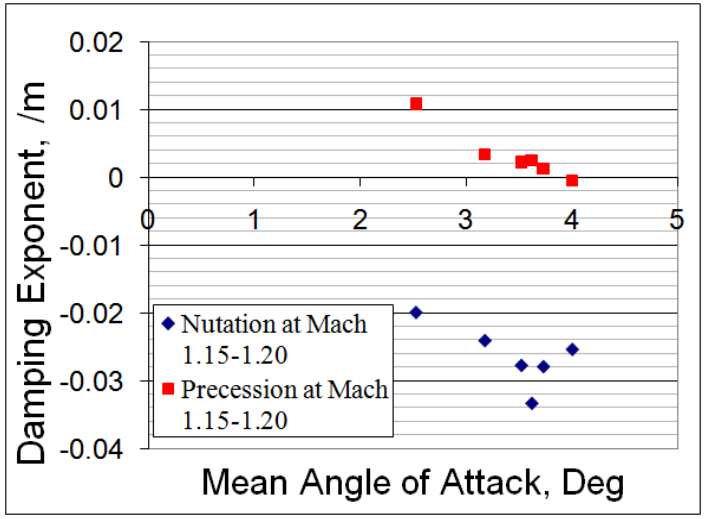

Total Yaw of M855 increases with decrease in velocity under simulated conditions as well as in flight

Average yaw observed 100-m from the muzzle in the spark range (ARFDAS fit)

McCoy data rounds measured at actual downrange locations

Modal damping exponents show expected max yaw for the given velocity

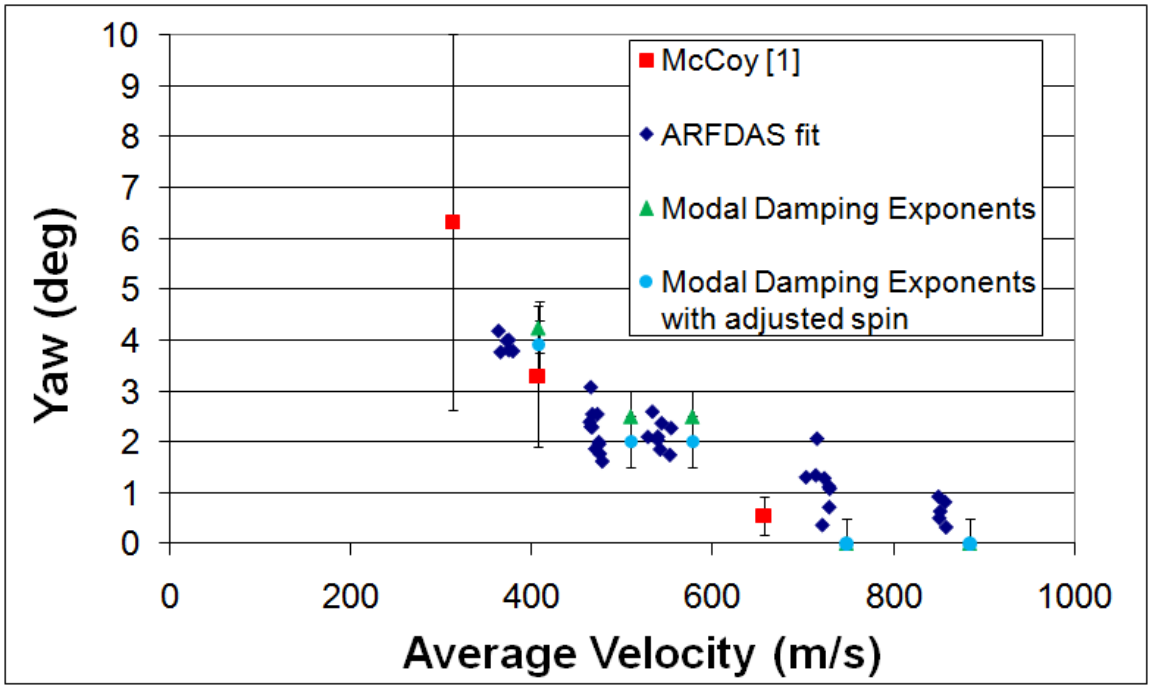

Yaw growth begins to occur at velocities around 600 m/s.

Yaw limit cycles may be as large as 6°(McCoy) but would require additional testing at lower velocities to verify.

Simulation of projectile flight failed to produce expected yaw growth

PRODAS simulation using aerodynamic coefficients generated from range tests.

Minimal yaw growth observed – less than one degree at 600-m

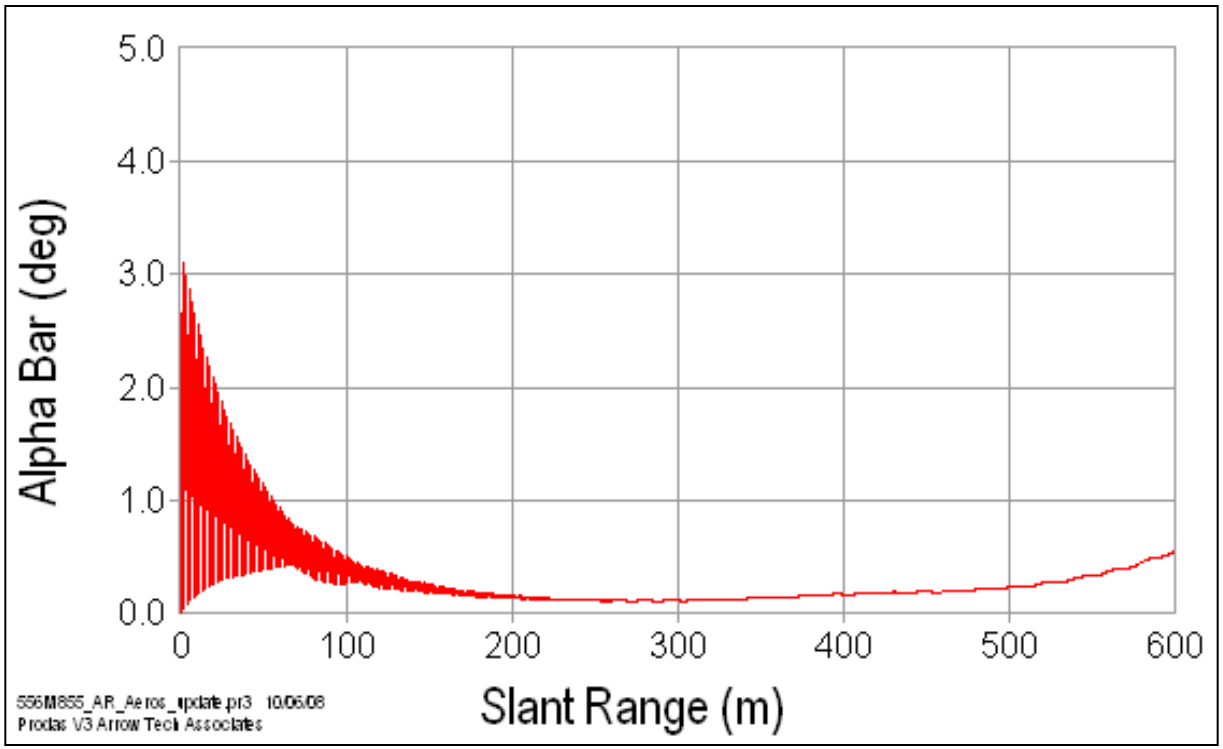

Two possible explanations:

- a small mass asymmetry exists
- spin rate must be matched in the experiment

Results of M193 Aerodynamics Test were reanalyzed to determine effect of matched spin on stability

- M193 projectiles were fired at velocities simulating ranges of 0, 200, 400 and 600-m.
- Fired using two methods
  - Standard firing with muzzle twist from M16A2 barrel
  - Fired from Mann barrels to match down range spin rates
- Yaw inducers used as needed.
- Rounds fired from Mann Barrels required the use of sabots.

- Previous analysis of aerodynamic coefficients showed differences in methodologies likely insignificant
- Stability characterization at muzzle spin rate, adjusted downrange spin rate, and matched spin rate.

Stability can be characterized by examining the Gyroscopic and Dynamic Stability Factors

Gyroscopic stability factor must be greater than one to be stable.

$$S_g = \frac{P^2}{4M}$$

Dynamic stability factor can be defined as: $S_d = \frac{2T}{H}$

Stable rounds must remain within the dynamic stability bound defined as : $\frac{1}{S_g} < S_d\left(2 - S_d\right)$

Reminder: $P = \frac{I_x}{I_y}\left(\frac{pd}{V}\right)$ $M = \frac{C_{m_\alpha}^*}{k_y^2}$ $H = C_{L_\alpha}^* - C_D^* - \frac{\left(C_{m_q} + C_{m_{\dot{\alpha}}}\right)^*}{2k_y^2}$ $T = C_{L_\alpha}^* - \frac{C_{n_{p\alpha}}^*}{2k_x^2}$

Gyroscopic and Dynamic Stability of the M193 depends on firing methodology

Initial yaw levels vary from 1.5-8 degrees.

Rounds with adjusted spin display improved dynamic stability.

Yaw limit cycle evident at Mach 1.1 for standard firing and adjusted spin analysis.

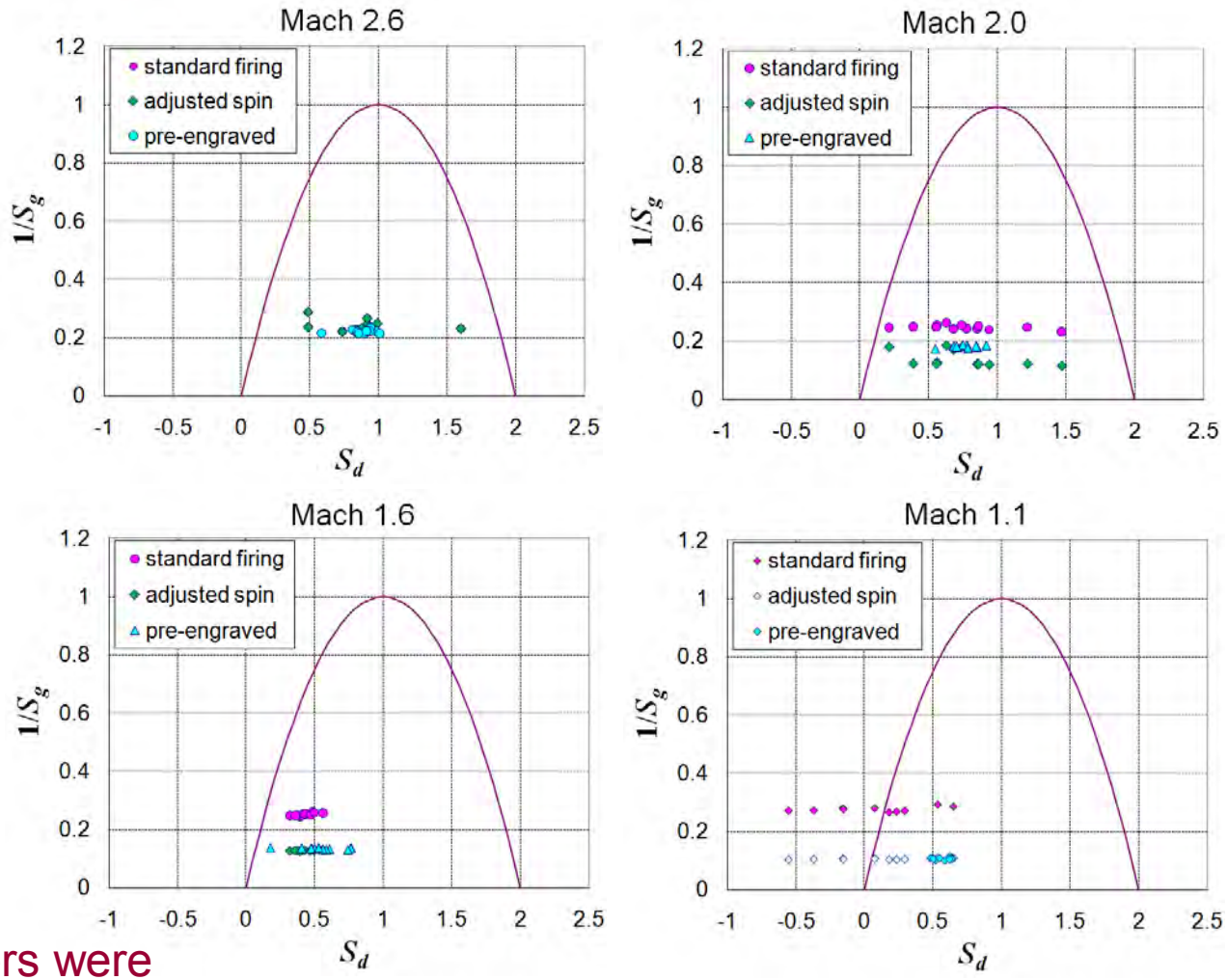

Rounds at all Mach numbers were both dynamically and gyroscopically stable for the matched spin (pre-engraved) firings.

Additional shots with lower yaw levels would be needed to confirm lack of yaw limit cycle for M193 projectile.

Summary

- Standard M855 tests shows yaw growth beginning at 400-m, ultimately growing to 4.5 degrees at 600-m.
- Stability analysis with simulated spin rates can reduce the yaw limit cycle of the M855 by approximately 0.5 degrees.
- Previous full range shots for M855 do not show evidence of a yaw limit cycle until 600-m.
- PRODAS simulations of the M855 do not show evidence of a trim angle at 600-m.
- Gyroscopic and dynamic stability analysis of the M193 show yaw limit cycle is present at 600-m for muzzle spin and adjusted spin cases.
- Matched spin experiment for the M193 is gyroscopically and dynamically stable at all Mach numbers tested

Conclusions

- Level of dynamic instability will be predicted at a higher level than in actuality when muzzle spin rates are used.
- Adjusting spin rates of rounds initially analyzed with muzzle spin does improve the results, yet still predicts yaw growth at earlier ranges than what can be expected at real range.
- Use of in-flight spin rate is necessary to determine the stability of the round at downrange velocities.
- Lower velocities must be investigated if an accurate yaw limit cycle is to be determined

Questions?

Reinforced HE Fills for Gun Launch

Michael Minnicino
U.S. ARL

26th International Symposium on Ballistics
Miami, Florida
13 September 2011

Motivation

Reinforced HE fills may be required if one or more of the following is true:

- Setback acceleration is extreme(1)
- Fill material density is high
- Fill material strength is weak
- Fill material bonds poorly to sidewall
- A minimum mass of HE is required necessitating a reduction in warhead sidewall thickness
- Warhead sidewall burst strength is low

Reinforced HE fills may be required if the warhead sidewall is unable to support the HE fill during gun launch

(1) Burns, B. P., "Positive Approaches for reducing the in-bore axial launch stress in projectile high explosive fills," ARBRL-MR-03055, Aug 1980.

Initial Design Problem

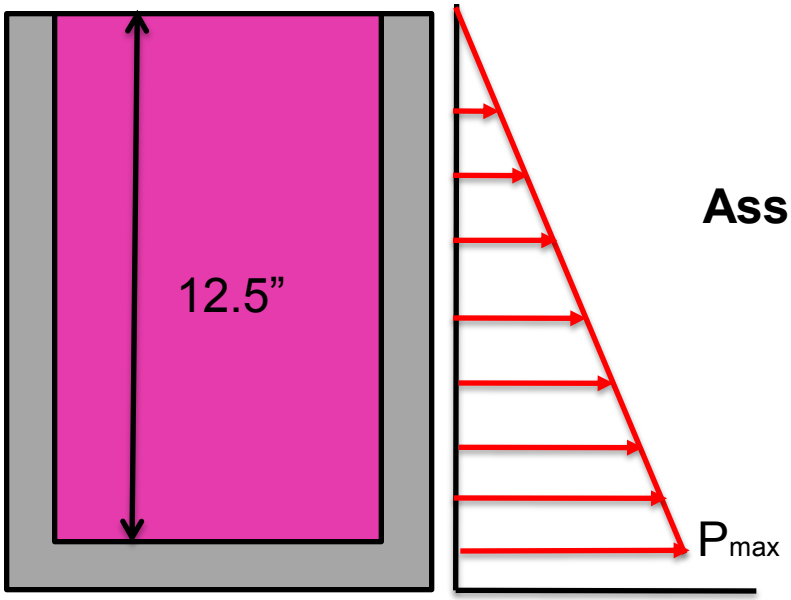

HE fill is a dense, weak, and soft material

Assume HE is a fluid to approximate pressure loading on the sidewall

For assumed max density of 0.234 lb/in^3 (6.5 g/cc) the resulting max pressure is 38 ksi under 13 kG setback

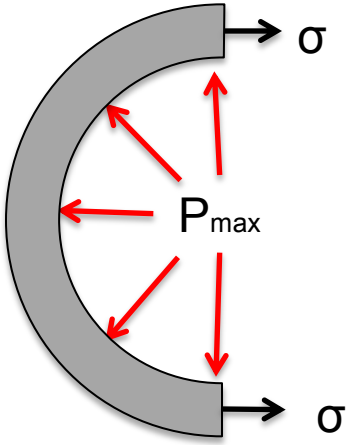

This pressure loads the sidewall and results in the hoop stress σ, the critical design parameter.

A considerable amount of hoop-strength and/or thickness is needed to resist this large internal pressure

Lame Analysis

105 mm Munition
r_i = 1.75 in.
r_o= 2.00 in.
P_i = 38 ksi
P_o= 0 ksi

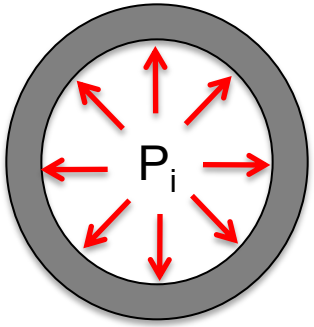

Lame's Equations simplify to (P_o= 0)

$$\sigma_r = \frac{-r_i^2 r_o^2}{(r_o^2 - r_i^2)} \frac{P_i}{r^2} + \frac{r_i^2}{(r_o^2 - r_i^2)} P_i$$

$$\sigma_h = \frac{r_i^2 r_o^2}{(r_o^2 - r_i^2)} \frac{P_i}{r^2} + \frac{r_i^2}{(r_o^2 - r_i^2)} P_i$$

Hoop stress is a order of magnitude greater than radial stress

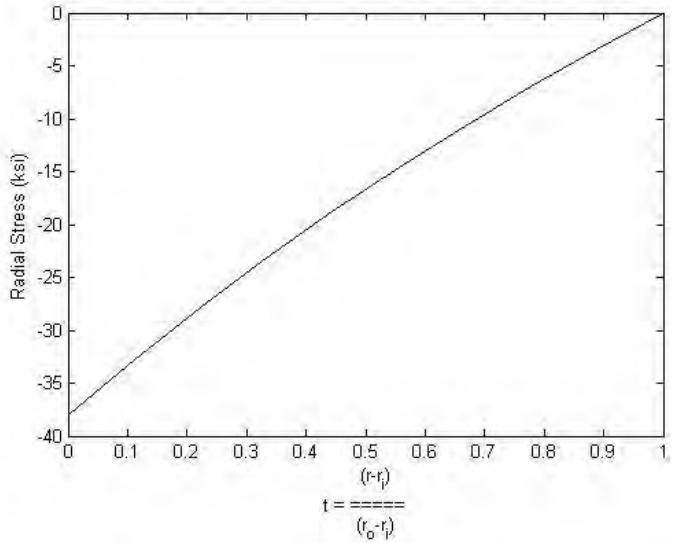

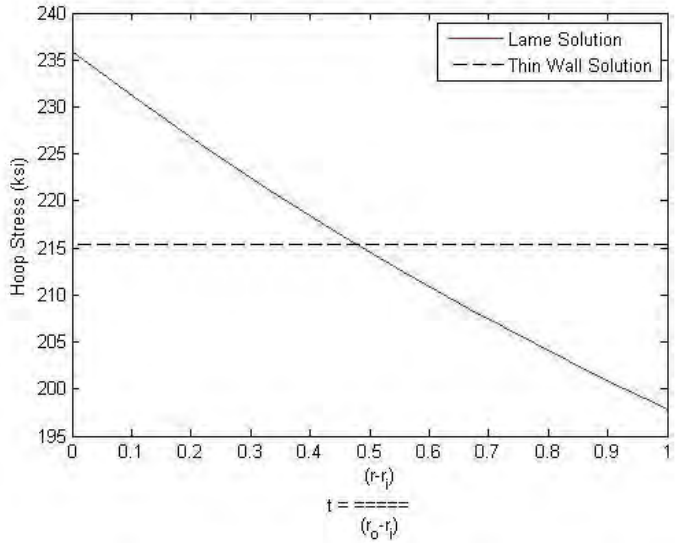

FEA Verification

HE fill properties for elastic-perfectly plastic material model

- density ρ = 0.234 lb/in^3 (6.5 g/cc)
- elastic modulus E = 1.4 Msi
- yield strength σ = 4000 psi

2 Boundary Conditions Considered

- Perfectly bonded - HE fill is permanently bonded to sidewall
- Sliding contact – HE fill is permitted to slide relative to sidewall

FE results indicate that the maximum produced pressure under 13 kG is more severe for the sliding contact boundary configuration than the tied contact boundary configuration.

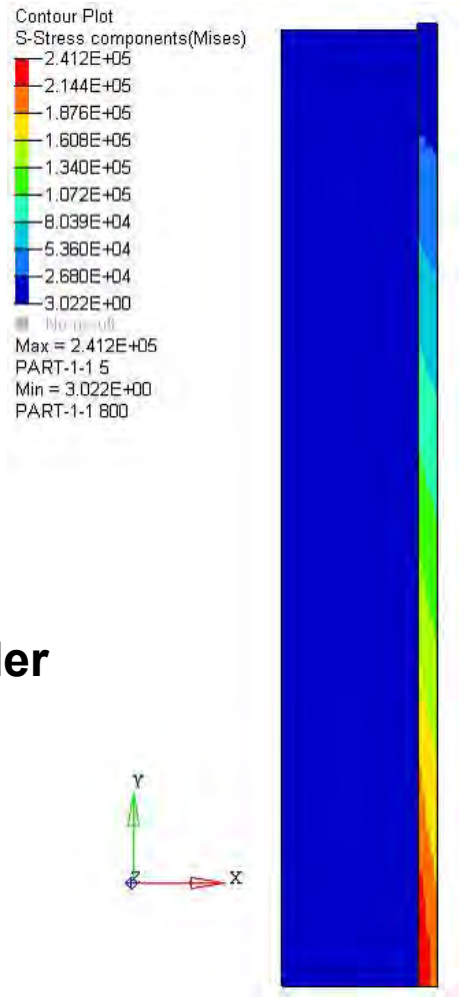

HE Density Study (Elastic-Plastic)

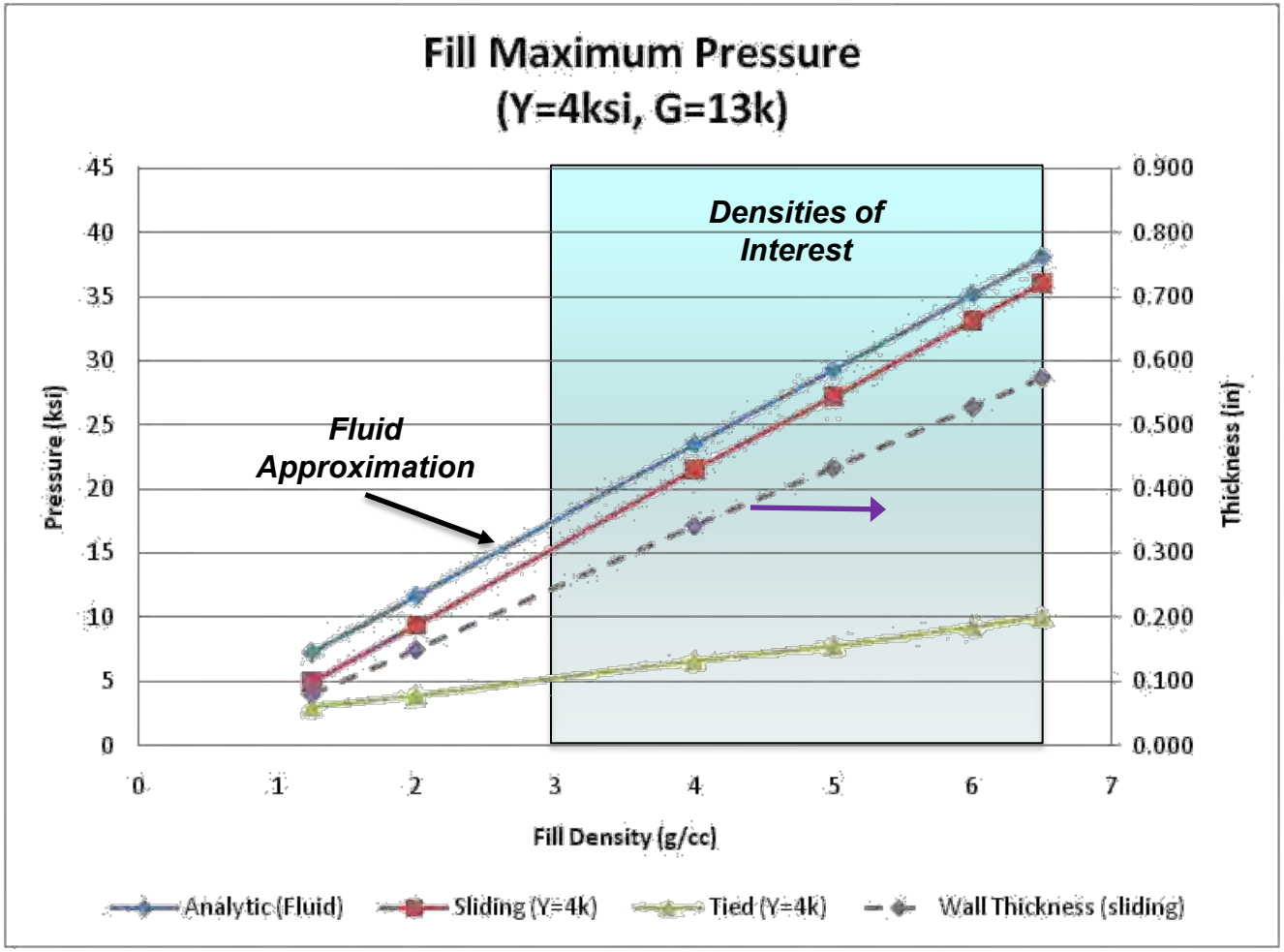

Load on sidewall depends more on boundary condition and less on yield strength of HE material

Thin wall stress approximation uses σ_c=175 ksi in required wall thickness calculation

Honeycomb Reinforcement

CONCEPT: use a honeycomb structure to support/confine dense HE fill thereby limiting the load on the warhead sidewall.

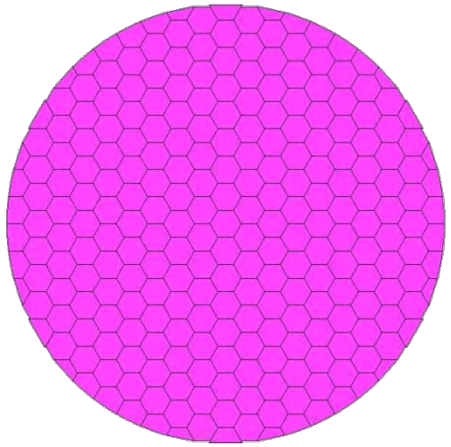

Advantages
- Simple design and fabrication
- Honeycomb fragments are expected to be low collateral

Disadvantages
- Detonation wave propagation may be an issue
- Honeycomb (marginally) reduces payload volume
- Void formation in the HE will have to be managed

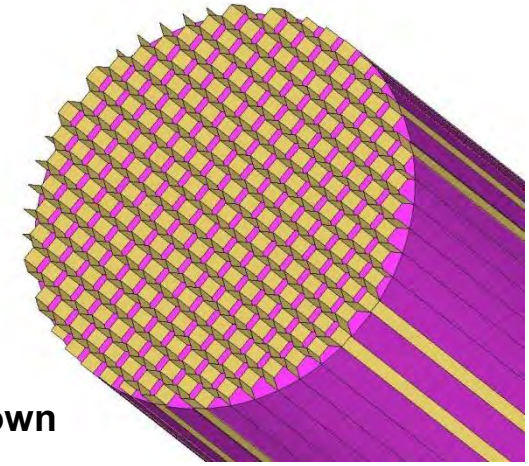

Warhead sidewall not shown

3D FE Model

Quasistatic FE Model

- 10 kG setback is prescribed
- The HE fill mesh is tied to the reinforcement mesh
- Cylindrical coordinate system is defined
- Symmetry is prescribed

  $u(r, {}^{+}/_{-}\,\theta_s, z) \cdot n_s = 0$
- Nodes located on warhead rear face are fixed

  $u(r,\theta,0) = (0,0,0)$
- Steel warhead material is linear elastic
- Aluminum reinforcement material is linear elastic and constitutive thickness is 1/32”
- Fill material is a dense, incompressible hyperelastic HE fill

Two Configurations

- Tied – HE material is perfectly bonded to the warhead
- Sliding – slip is allowed between the HE material and the warhead

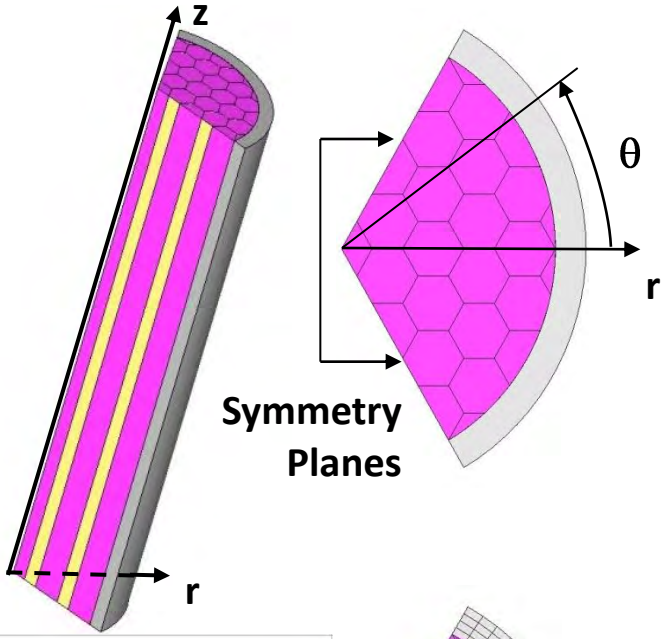

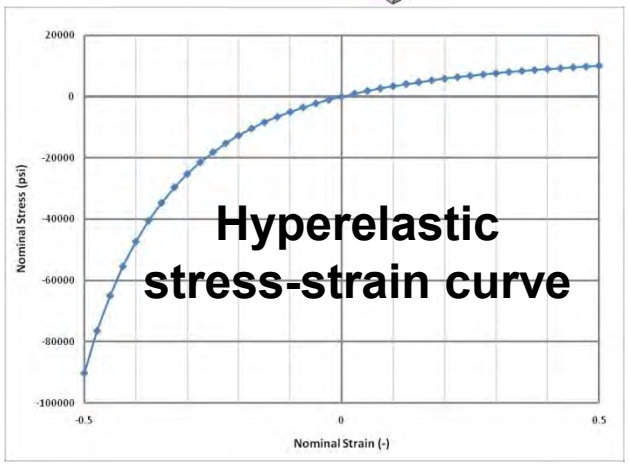

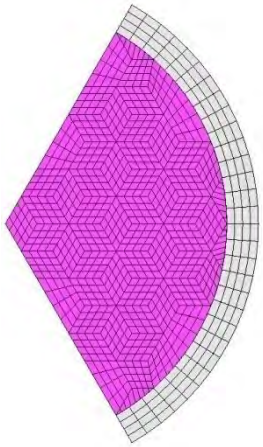

Tied FEM Hoop Stress Results

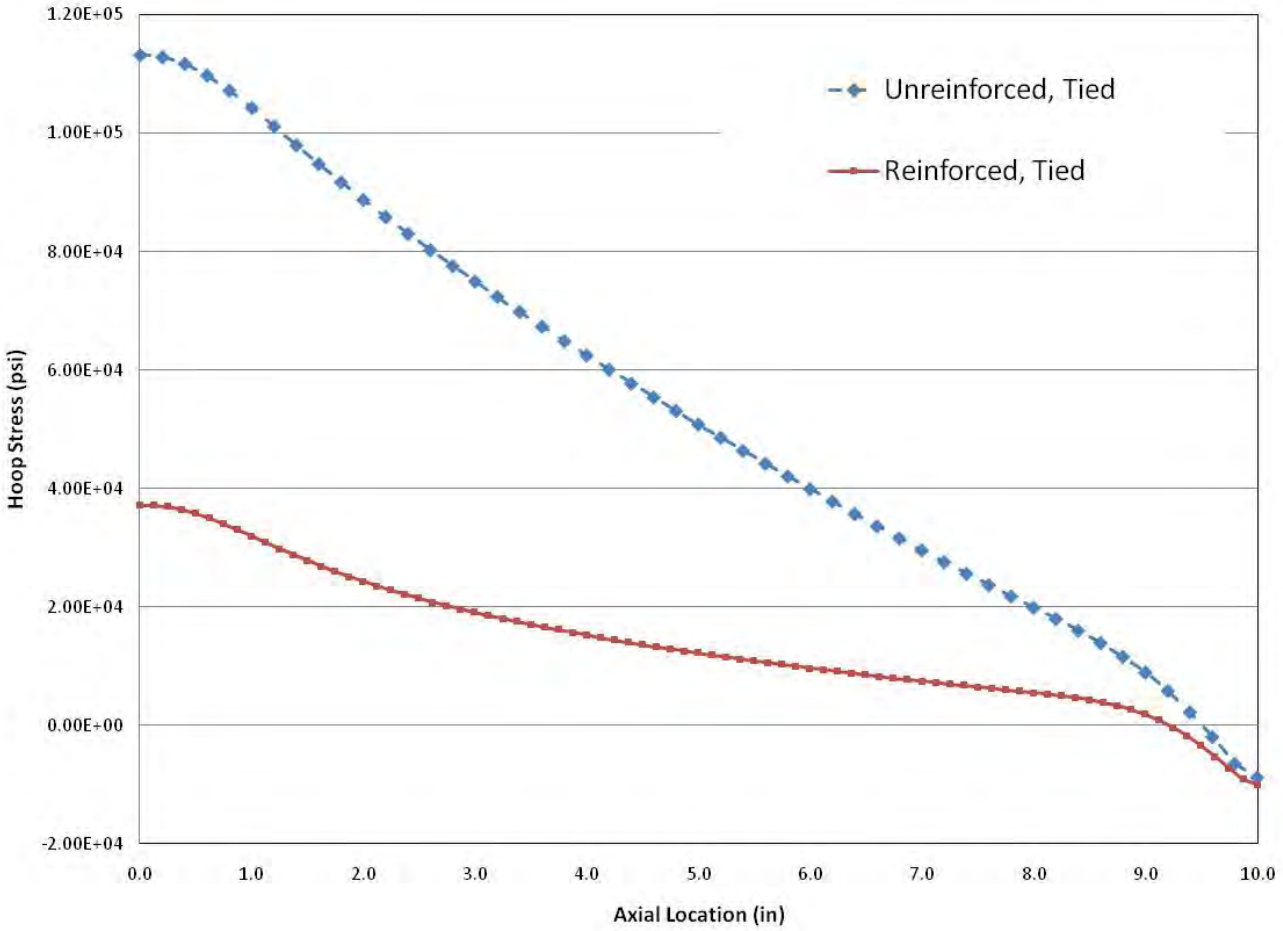

Reinforcement reduces maximum hoop stress by ~65%

Sliding FEM Hoop Stress Results

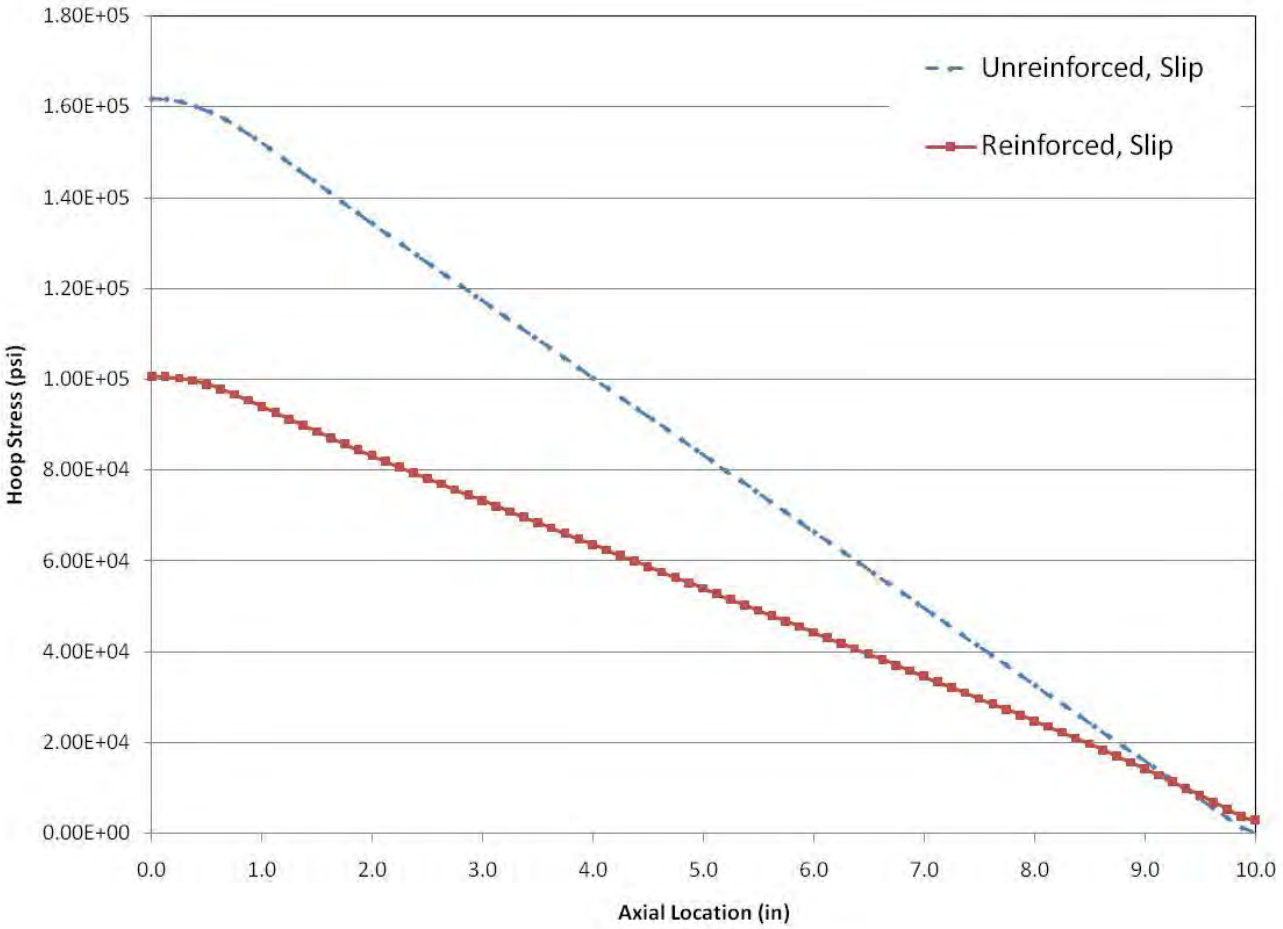

Reinforcement reduces maximum hoop stress by ~38%

Reinforcement Structure von Mises Stress

HE Tied to Sidewall

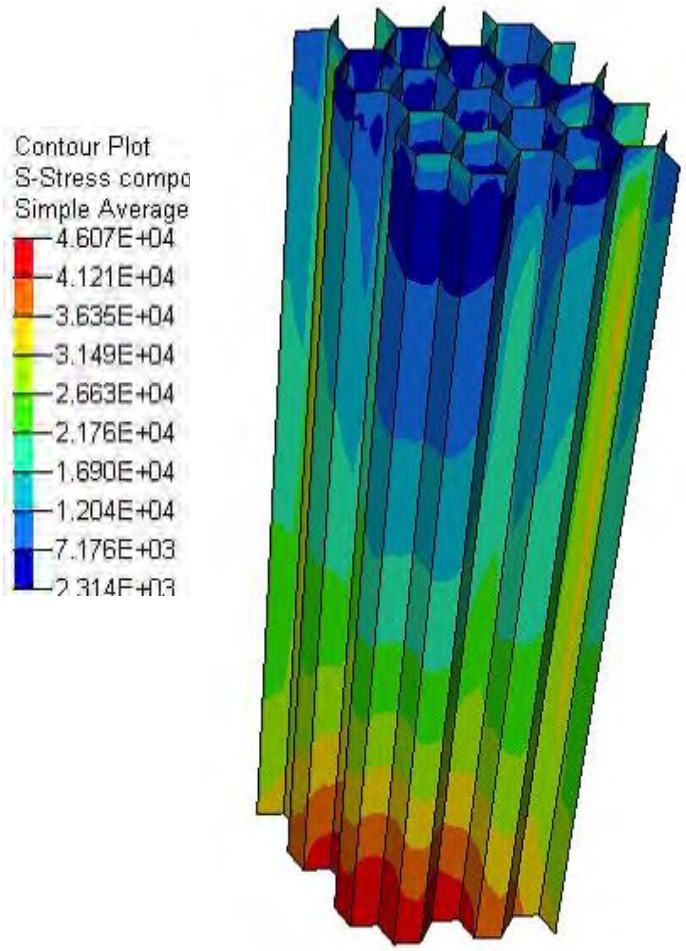

von Mises stress is less than aluminum yield stress

HE Slides Relative to Sidewall

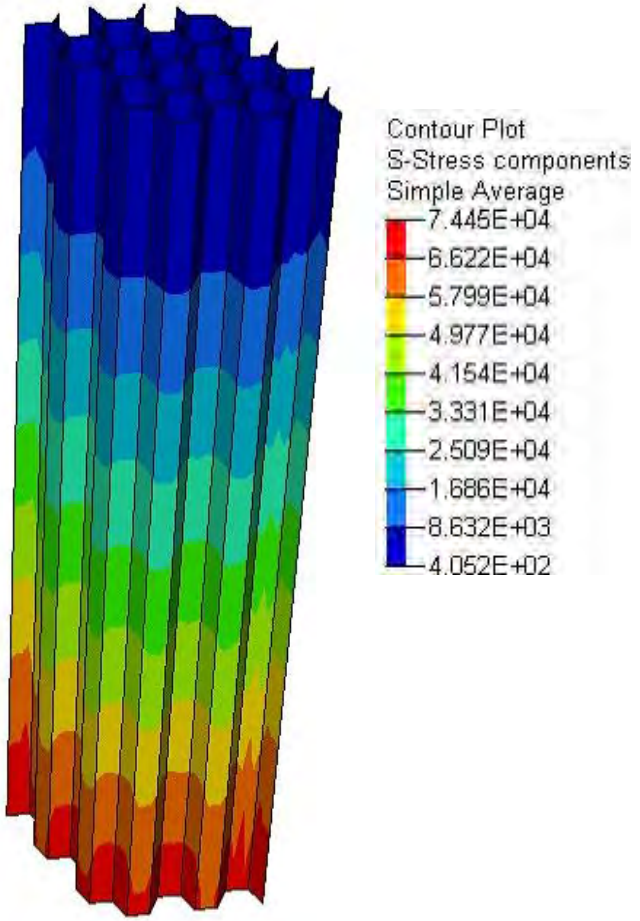

von Mises stress is approximately equal to the aluminum yield stress

HE is always tied to reinforcement structure

FEA Summary

Steel Sidewall Maximum Stress Values

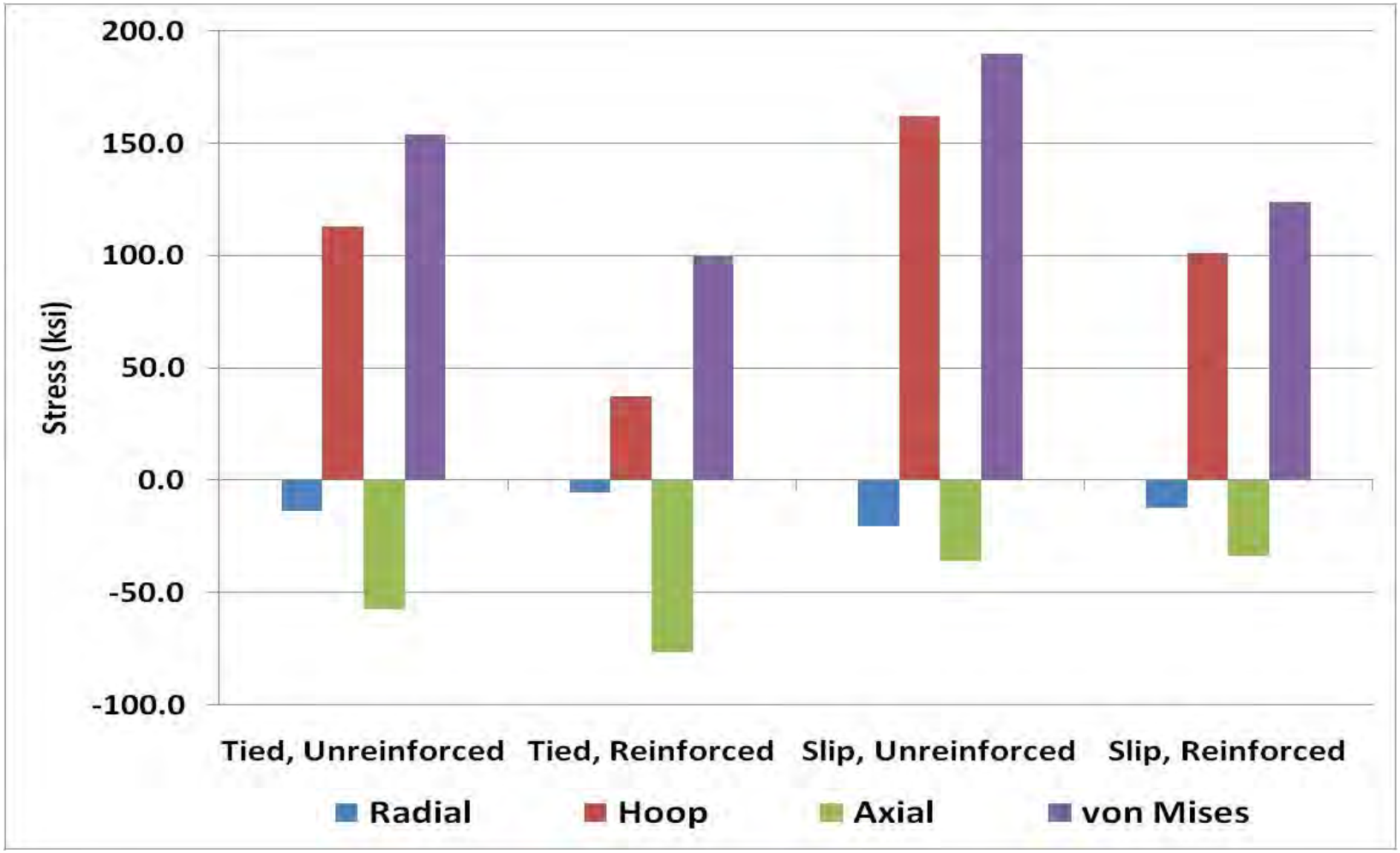

Summary

The reinforcement analyses indicate that honeycomb is effective in reducing the loading on the warhead sidewall for both tied and sliding configurations

Cursory analyses investigating the effect of honeycomb material and cell wall thickness predict further reduction in the sidewall loading and increased structural integrity of the reinforcement

The design path forward exists and the loading resulting from the dense HE fill during gun launch can be managed.

Thank you.

Questions?

Michael Minnicino
U.S. Army Research Laboratory
Aberdeen Proving Ground, MD 21005
michael.a.minnicino@us.army.mil
410-306-1919

NAVSEA
WARFARE CENTERS
DAHLGREN

ENGAGEMENT SYSTEMS

- Chris Weiland
- 540.250.1267
- Naval Surface Warfare Center Dahlgren Division
- christopher.weiland1@navy.mil

NAVSEA
WARFARE CENTERS
DAHLGREN

An Automated Visual Scoring Algorithm for Assessing Gunfire Accuracy

ENGAGEMENT SYSTEMS

ENGAGEMENT SYSTEMS DEPARTMENT

Chris Weiland, PhD
John Busic, PE
Jon Yagla, PhD

Naval Surface Warfare Center
Dahlgren Division
Code G65
christopher.weiland1@navy.mil

Scoring Gunfire on the Potomac River Test Range

- One of the major tests NSWCDD does is to test and score naval gunnery
- The term scoring refers to quantitative measurement of fall of shot (FOS) location relative to the desired/intended target

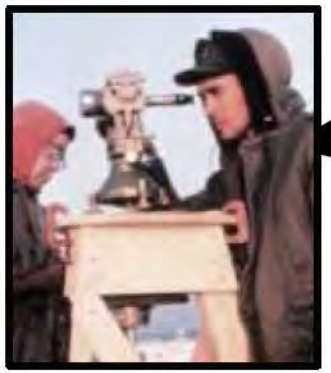

"Surveying Equipment"

A Visual Automated Scoring System

- **This presentation focuses on a computer algorithm to autonomously compute the FOS from digital images**
  - Line of sight
  - Non-line of sight

LINE OF SIGHT (LOS)

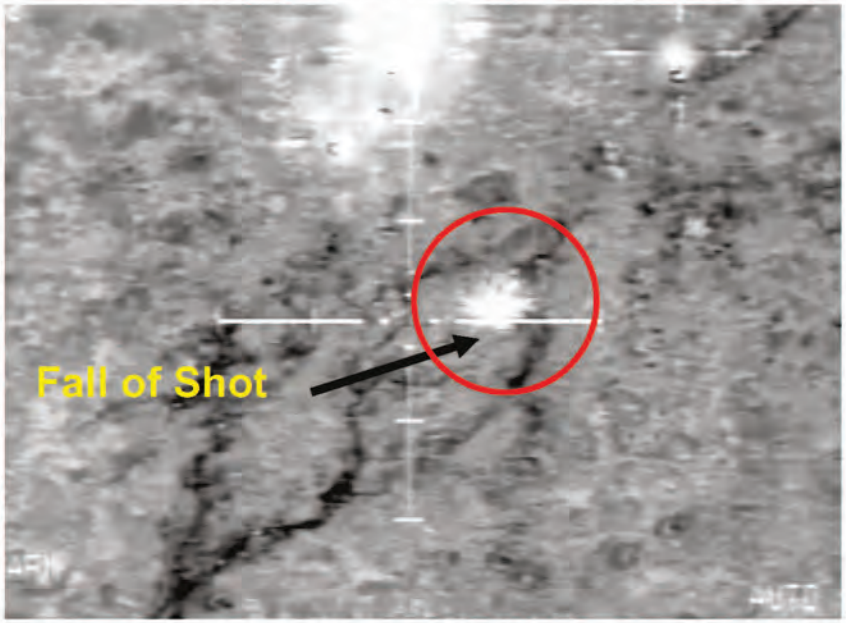

NON-LINE OF SIGHT (NLOS)

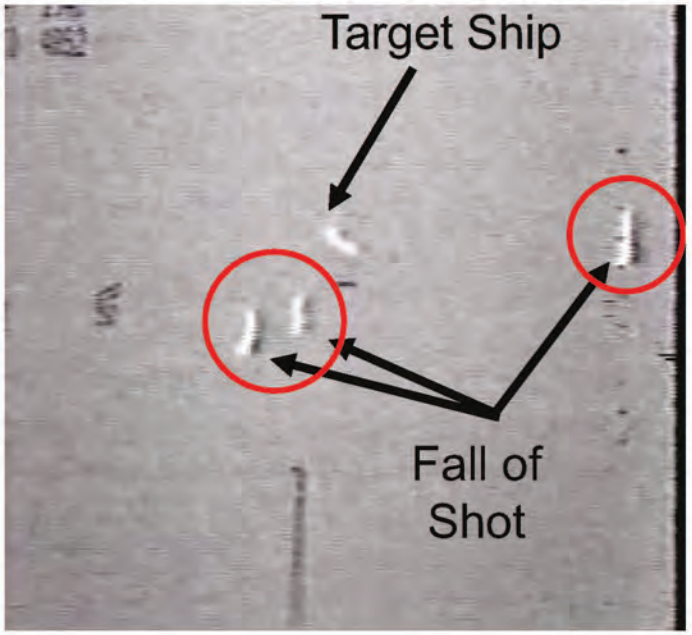

Scoring Non-Line-of-Sight Gunfire Systems

Video Images of Target From UAV Perspective

Data Scored by Computer Algorithm

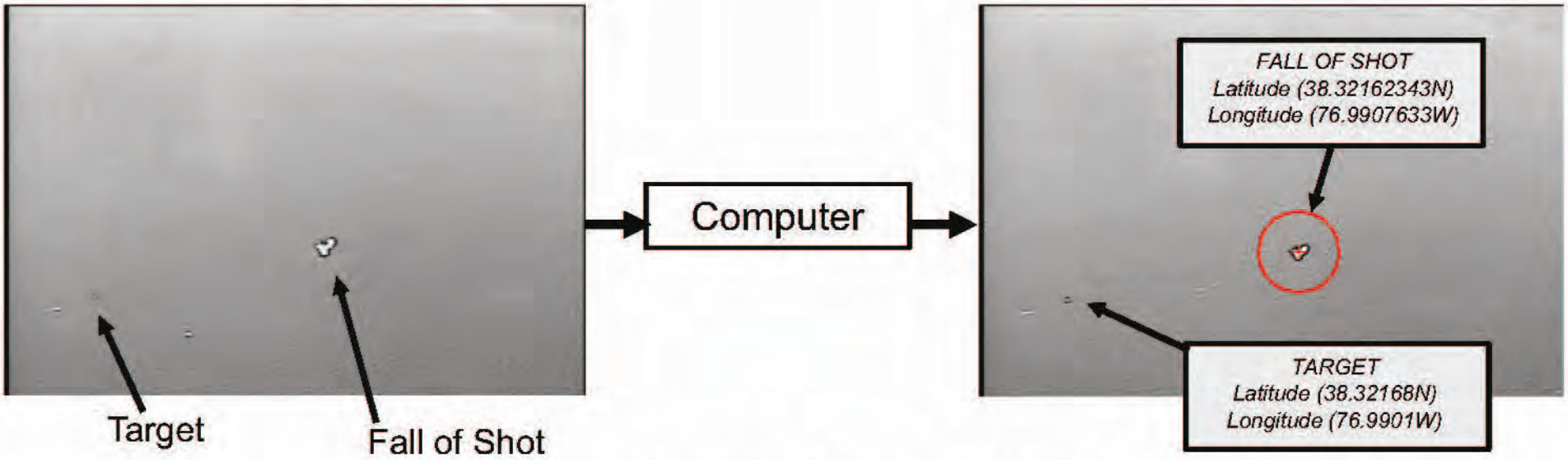

Historical Perspective: 16” Gunfire from USS IOWA

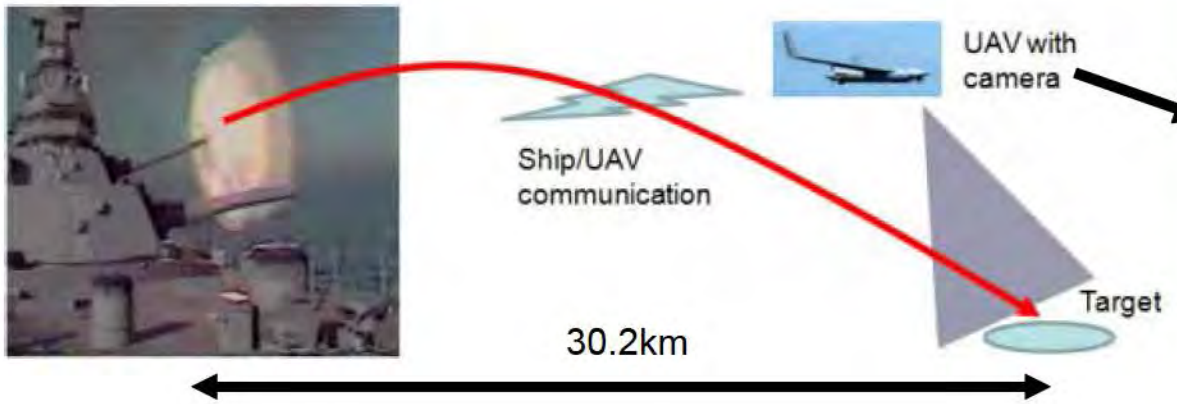

- Dr. Jon Yagla of NSWCDD conducted trials on the USS IOWA in July 1987
- UAV was flying near the target ship collecting video data
- Tests conducted on the open ocean

- Round splashes were observed and FOS were plotted manually (by a human)
- Advances in computer processing allows for near-real time analysis of fall of shot

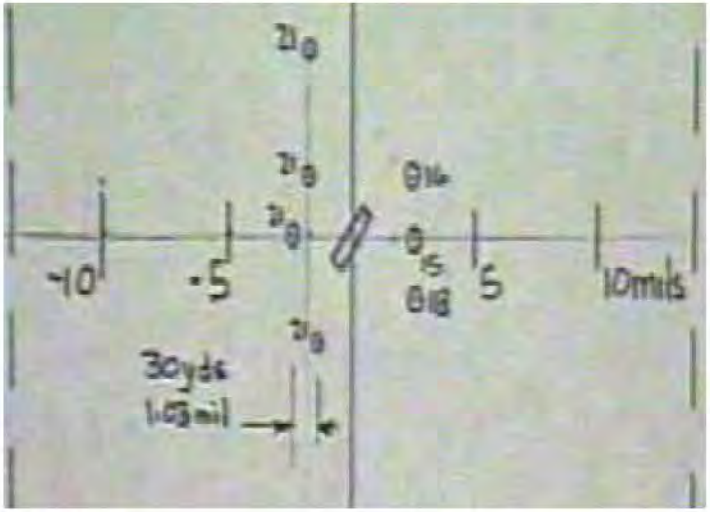

NAVSEA WARFARE CENTERS DAHLGREN

Quantitative Shot Spotting Using Video Data

ENGAGEMENT SYSTEMS

- **How can we score FOS using video data using a computer algorithm?**
- **Tests on PRTR to confirm algorithms**
- **Two algorithms required:**
  - #1 Autonomous shot detection
  - #2 Computation of ground coordinates from aerial photography & miss distance calculation (geolocation)

Autonomous Shot Detection Algorithm

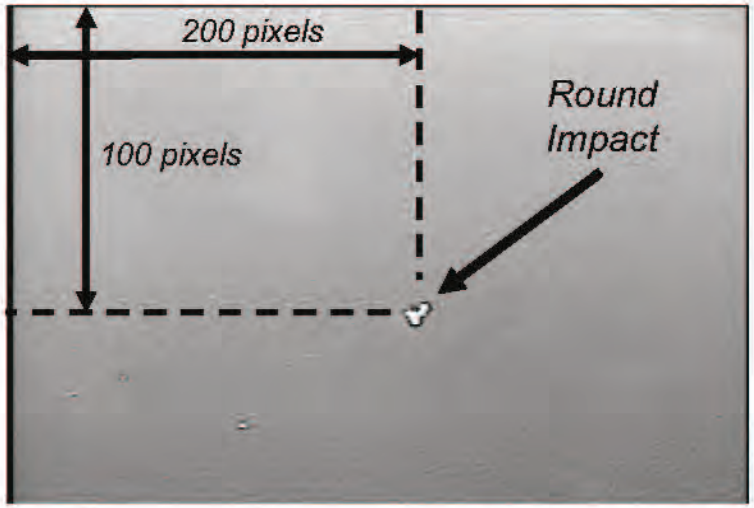

Geolocation Algorithm

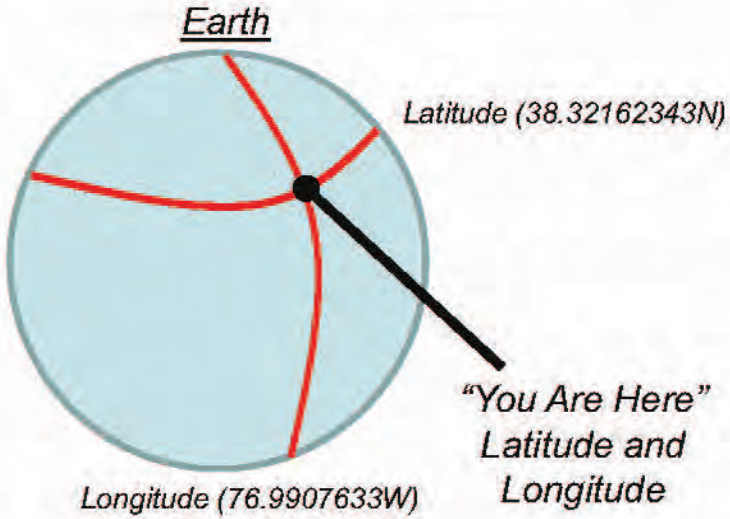

Shot Detection Algorithm

LOW-PASS FILTER OPERATION

INPUT IMAGE

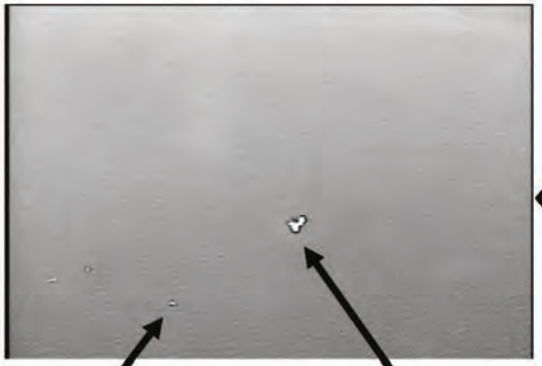

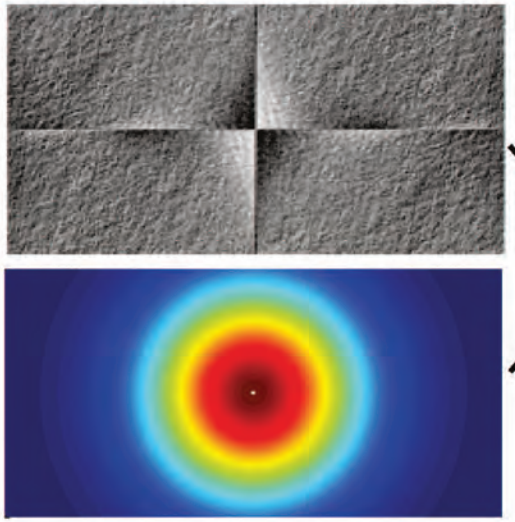

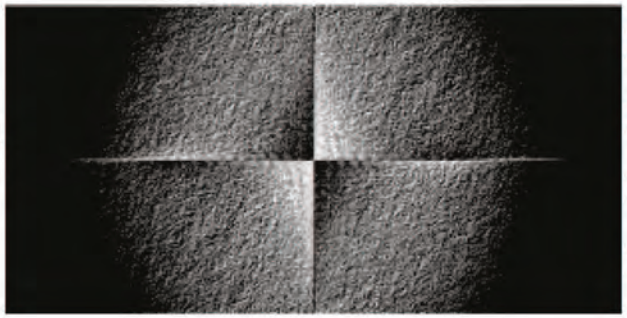

IDENTIFY FOS

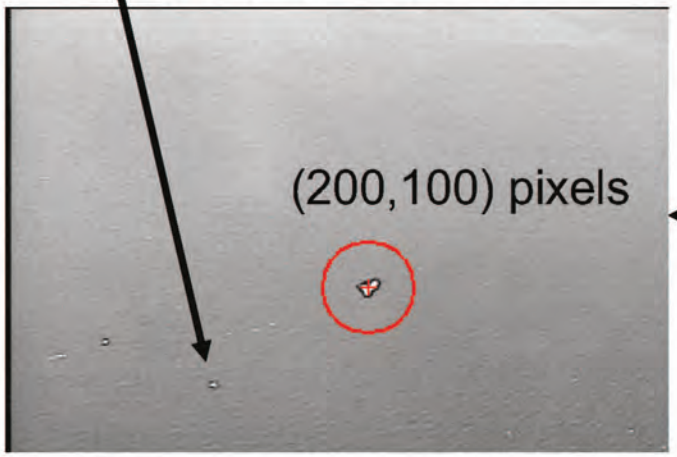

CHANGE POINT ANALYSIS

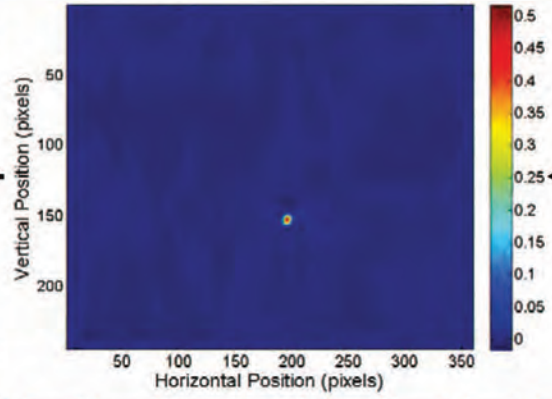

NAVSEA WARFARE CENTERS DAHLGREN

Geolocation Algorithm

ENGAGEMENT SYSTEMS

- **Ground position calculation is handled internally in UAV software, but can be improved**
  - UAV was never intended for precise geolocation
  - Instruments could be improved

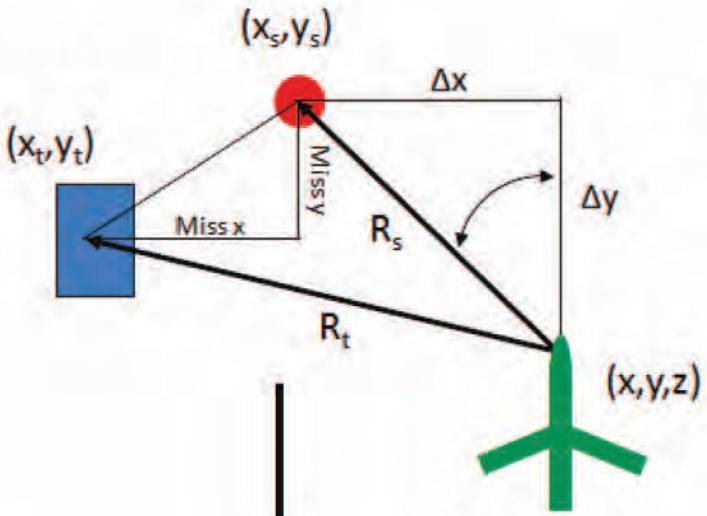

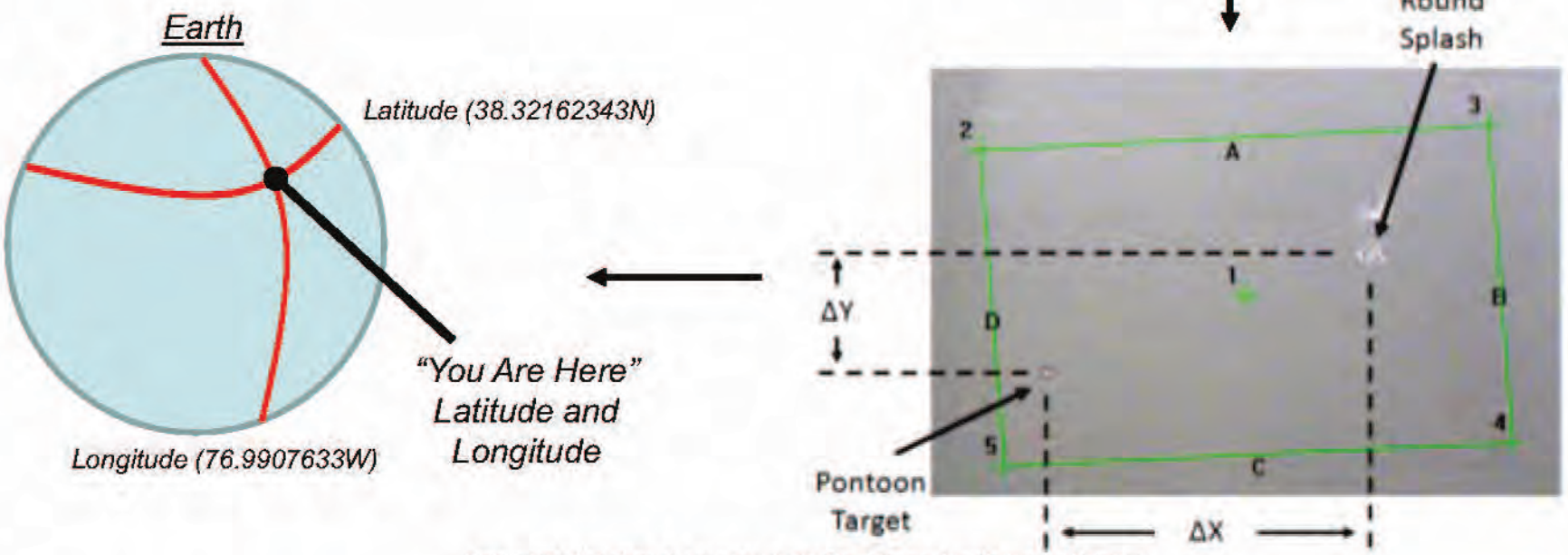

Scoring Line-of-Sight Gunfire Systems

Line of Sight Example: Gun on Aircraft

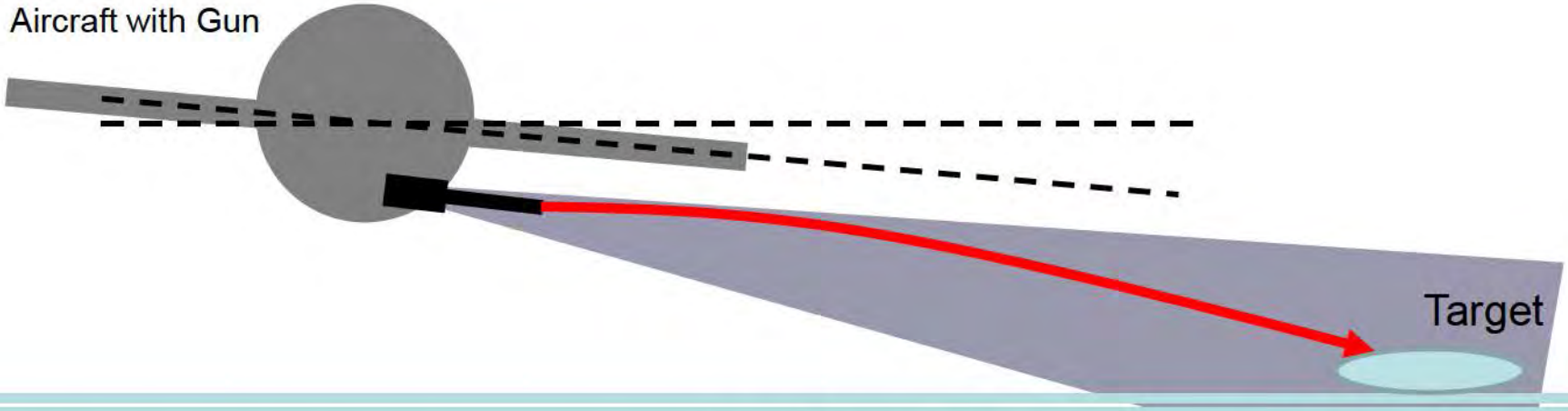

- **Aircraft orbiting target while shooting**
- **How do you score these tests?**
  - Typically 3-4 seconds round time of flight
  - Ground is moving/aim point changing

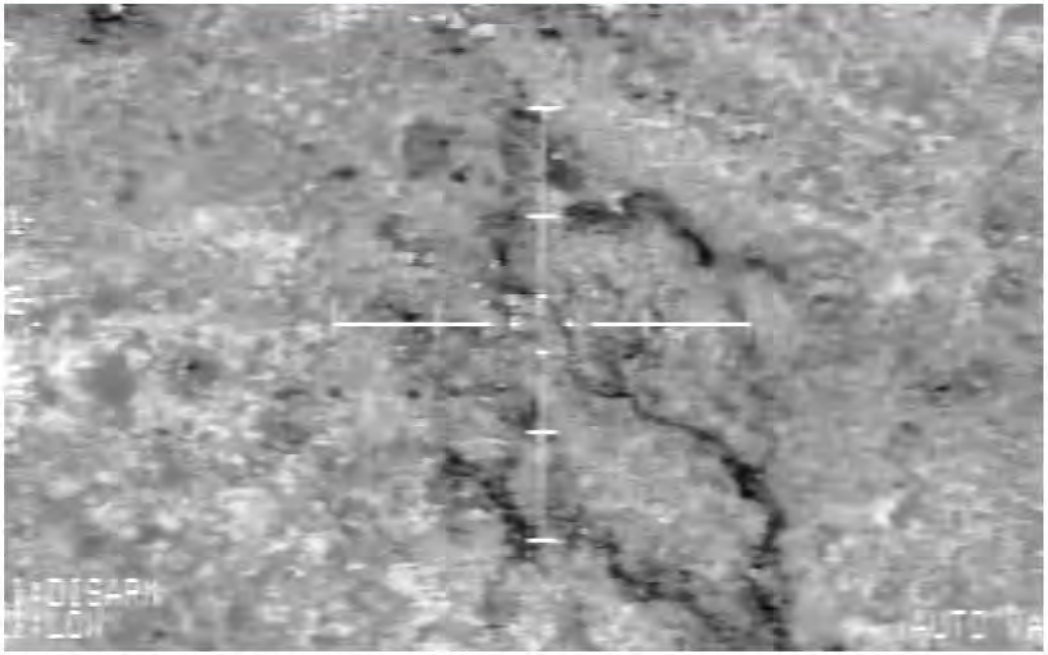

Scoring LOS Gunfire – Different from NLOS

- **When the trigger is pulled, there is a bullet flight time depending on altitude, bullet speed, etc…**
  - Put crosshairs on target in Image 1 and pull the trigger
  - Bullet impact occurs several seconds later in Image 100
- **We must account for this later translation/rotation to score the bullet impact relative to the <u>original aim point</u>**

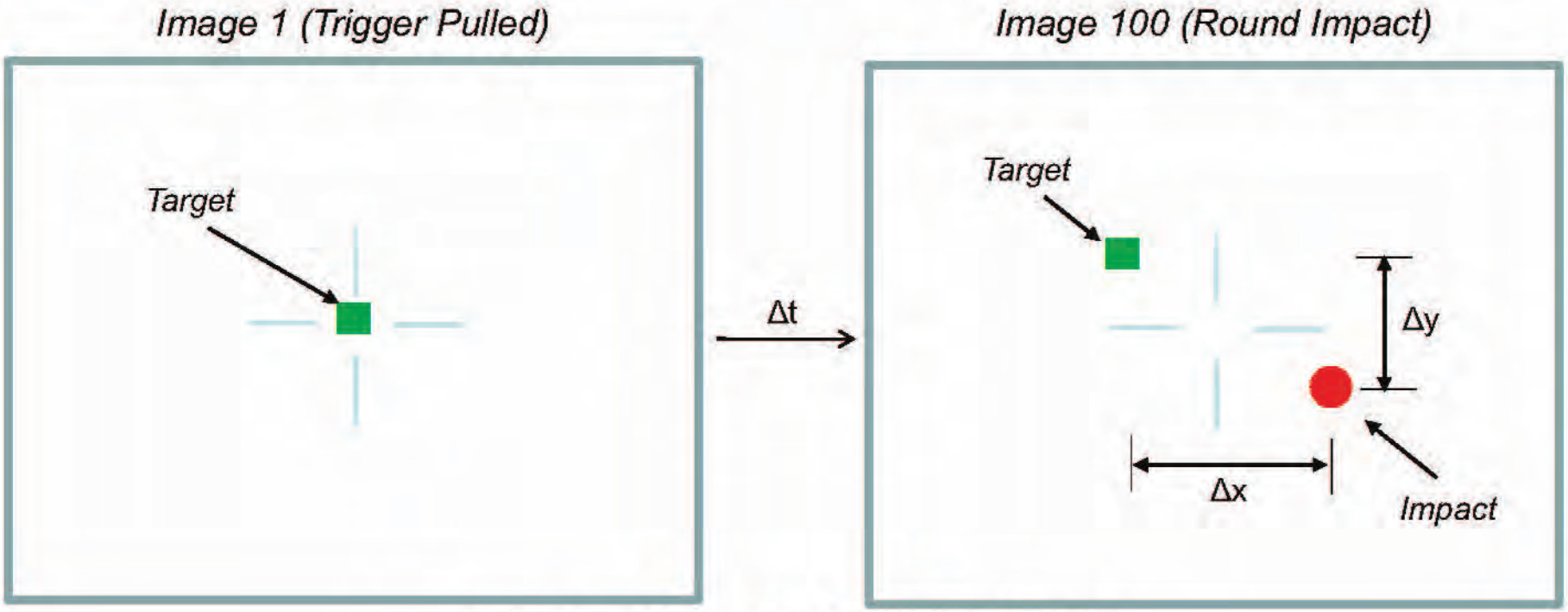

Quantitative Shot Spotting Using Video Data: LOS Algorithm

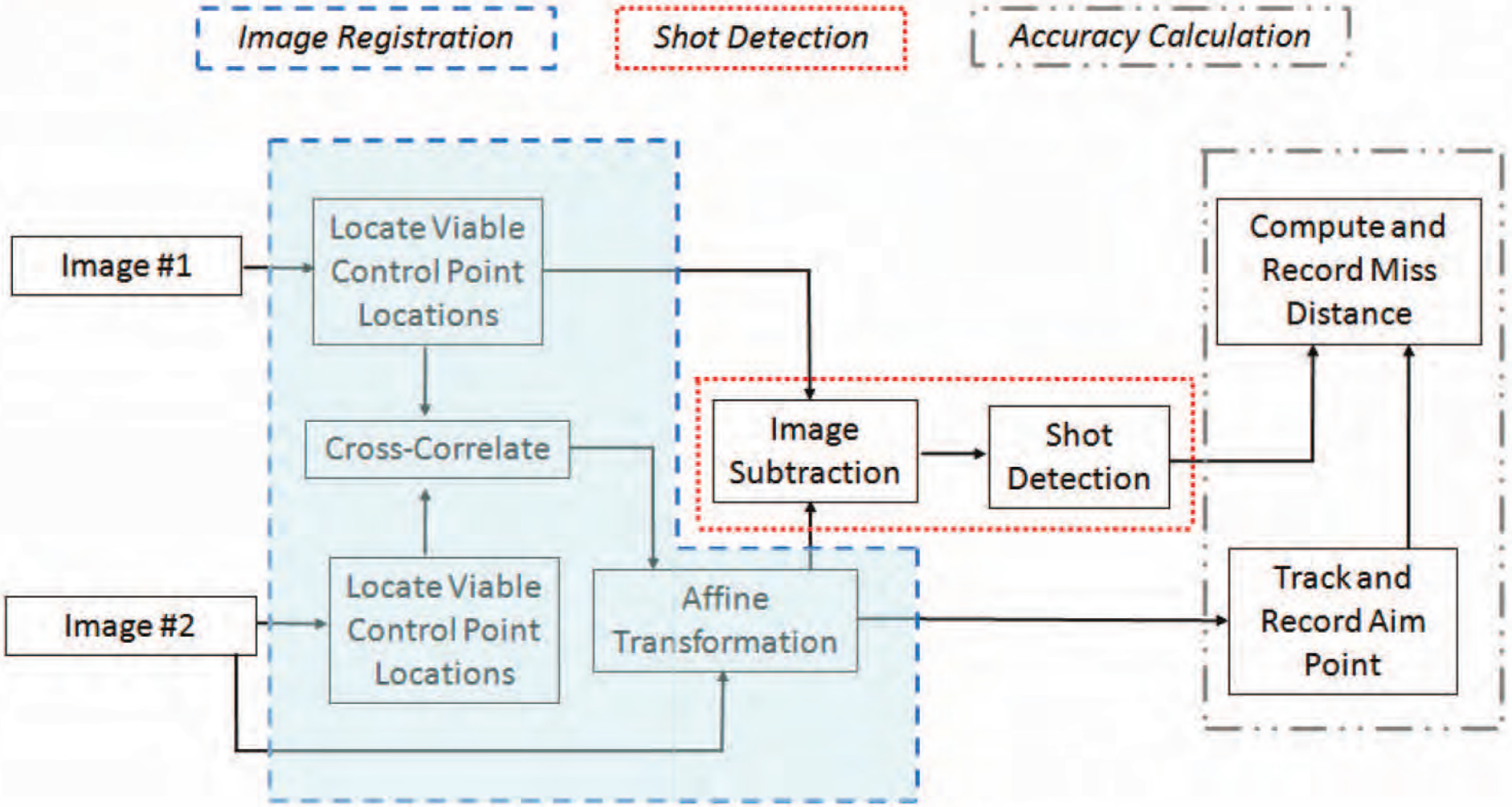

NAVSEA
WARFARE CENTERS
DAHLGREN

Quantitative Shot Spotting Using Video Data: LOS Algorithm

ENGAGEMENT SYSTEMS

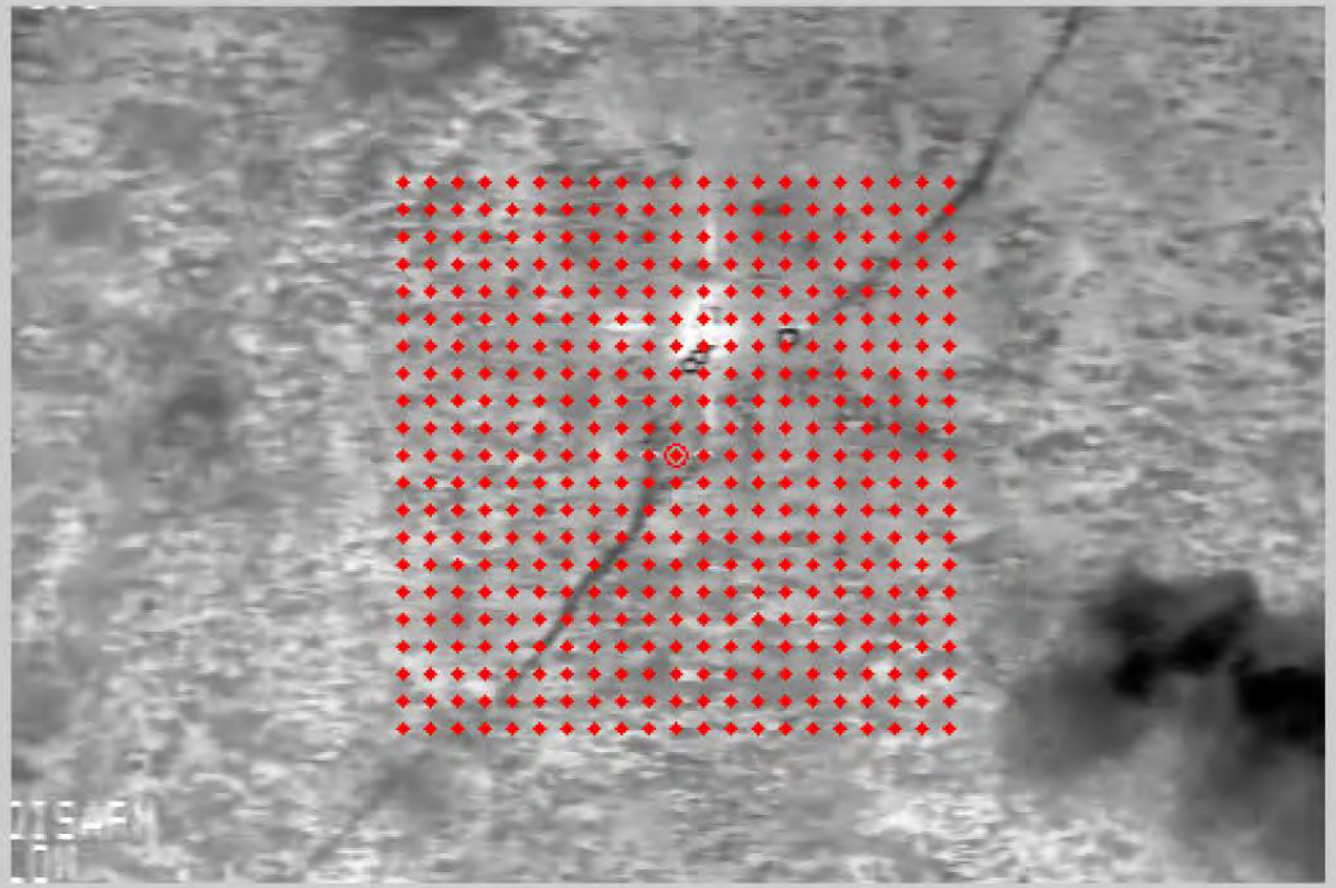

VASS In Operation – LOS

- What type of information do we gather?
  - Miss distance (miss in x & y coordinates)
  - Time of flight (if shot time is known)
  - Location of FOS
  - Kill/injure distances (for a given target)
  - Etc…

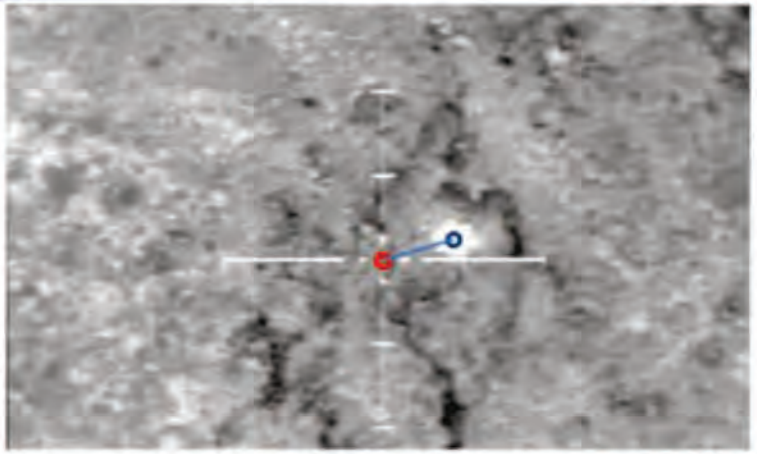

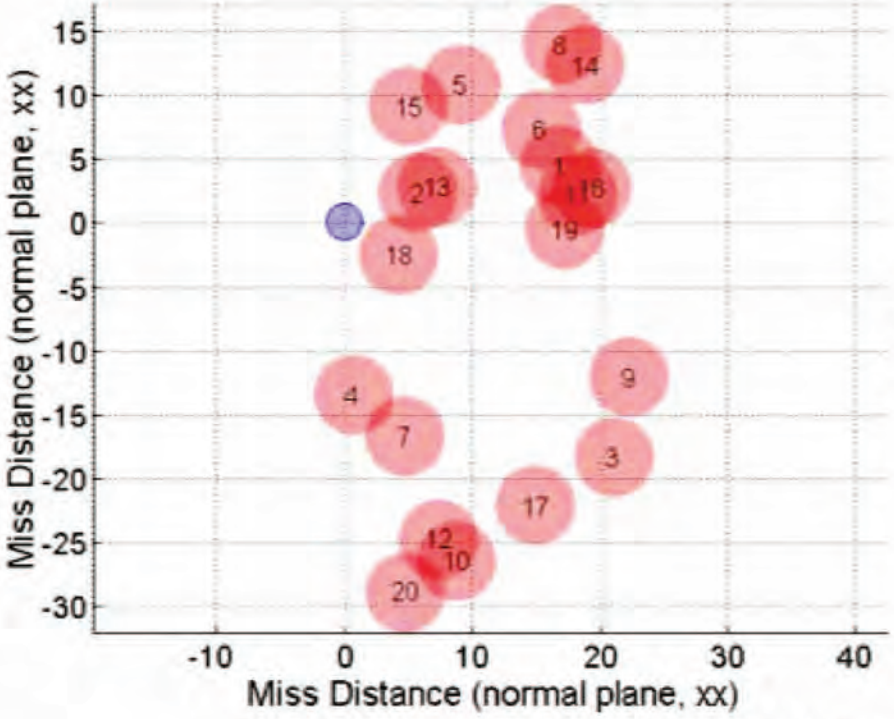

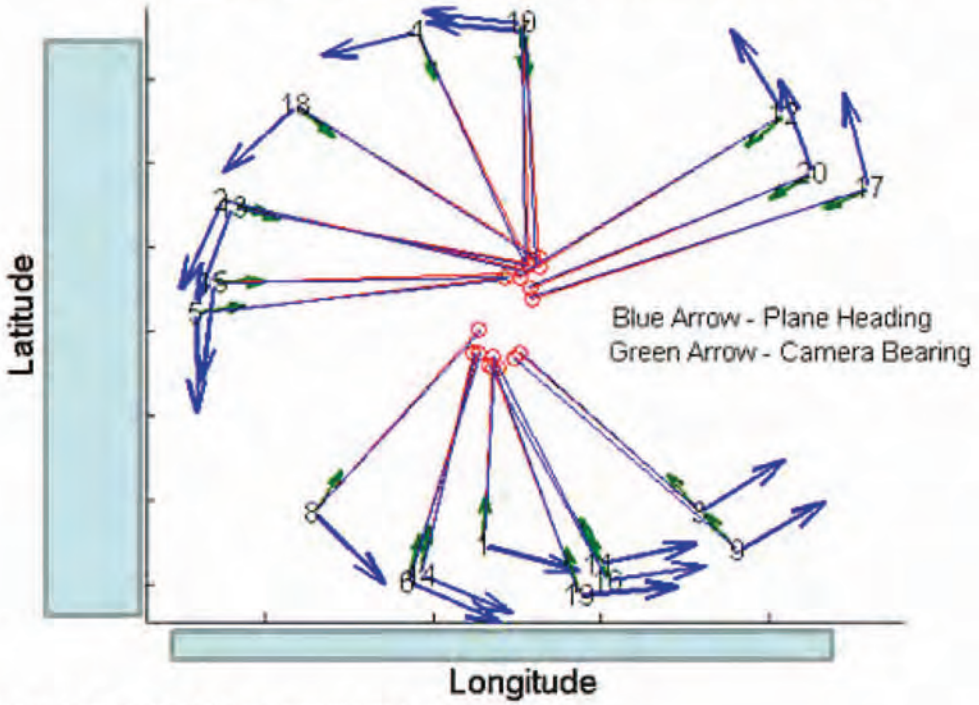

NAVSEA
WARFARE CENTERS
DAHLGREN

Summary: Using VASS to Score Weapon Systems

ENGAGEMENT SYSTEMS

- **An algorithm was developed to autonomously score gunfire from video data**
- **VASS was demonstrated through live-fire tests on the PRTR**
  - Algorithm for auto-detection of FOS worked well
  - Algorithm for conversion of pixels to world coordinate system algorithm needs improvement
- **VASS also works for line of sight weapon systems**
- **Code is getting faster, potentially allowing for real-time adjustments to fire control**

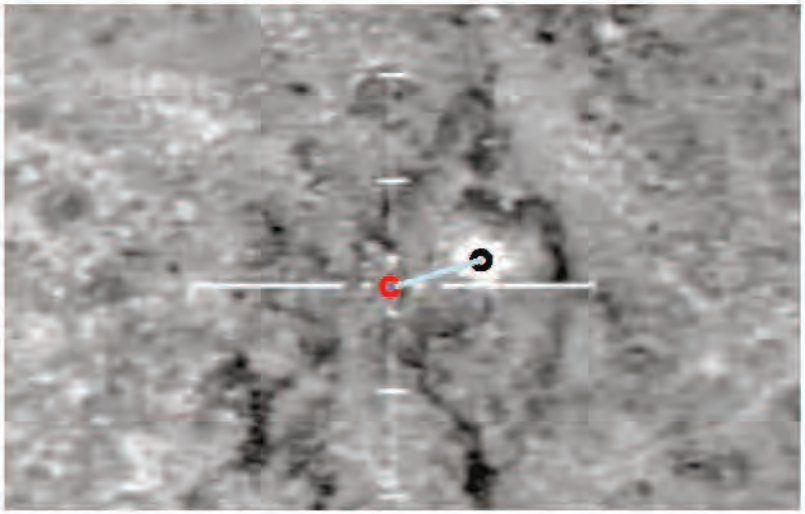

Questions?

Acknowledgements:

This work was sponsored by the NSWCDD Independent Applied Research Program. Several individuals provided key contributions to the PRTR scoring test: Barry Mohle, Patrick Boyd, Lorenz Eber, Cyrus Roohi, and Steve Klopp. The authors gratefully acknowledge their support.

FFI Forsvarets forskningsinstitutt

Pressure effects in an enclosed volume due to EFP impact

Jo Hagness Kiran
Norwegian Defence Research Establishment (FFI)

Jo-Hagness.Kiran@ffi.no
+47 63 80 75 41

Problem

- Is it possible for a build up of dangerous/lethal high-pressure regions inside a vehicle hit by an EFP?

Problem definition

- If complete perforation is assumed, three mechanisms studied:
  - Shock from penetrator.
  - Shock from detonation.
  - Pressure induced by plate vibrations.
- Effects such as chemical reactions, ref. *Heine & Wickert, ESW 2008*, is not considered
- Purely numerical study

Setup

- A generic EFP was modeled in ANSYS AUTODYN

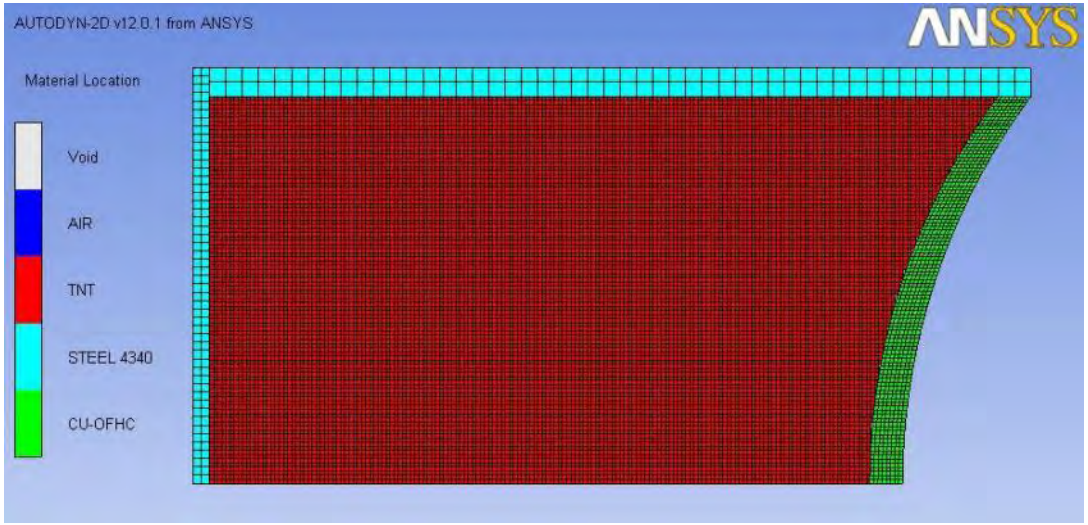

- Charge mass 1 kg TNT
- Liner mass 250 g Cu

Slug

- V ~ 1300 m/s
- Reaches stable configuration after ~ 0,75 ms.

Target

- To simplify the problem, a stand-in target for a vehicle was chosen.

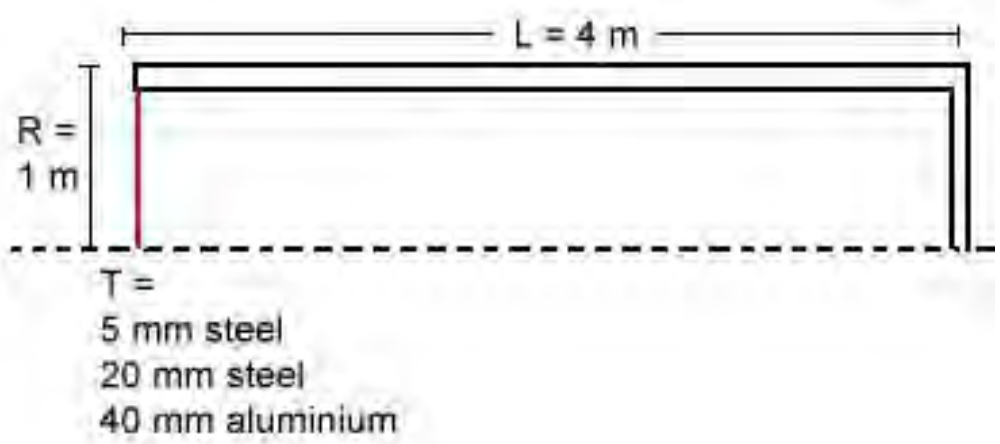

- Slug perforated all target thicknesses.
- Worst case scenario, 5 mm steel, was studied in more detail

Injury Criterion

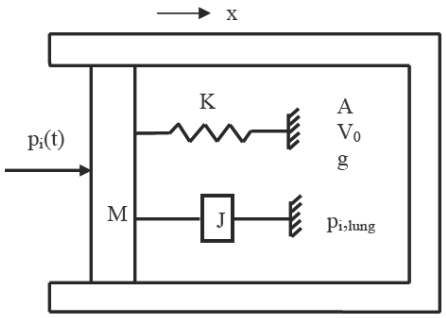

Name	Explanation
A	Effective area
M	Effective mass
V_0	Lung gas volume at x=0
J	Damping factor
K	Spring constant
p_0	Ambient pressure
$p_i(t)$	External (blast) loading pressure
$p_{i,lung}(t)$	Lung pressure
g	Polytropic exponent for gas in lungs
x	Chest wall displacement

- Axelsson

$$m\frac{d^2x}{dt^2} + C\frac{dx}{dt} + Kx = A\left(p(t) + P_0 - \left(\frac{V}{V - Ax}\right)^{\gamma} P_0\right)$$

$$ASII = (0{,}124 + 0{,}117V_{MAX})^{2{,}63}$$

Table 3.4: Injury Levels with Corresponding ASII and CWVP, and Estimated AIS Levels

Injury Level	ASII (-)	V (m/s)	AIS Range
Negative (no injury)	0.0 – 0.2	0.0 – 3.6	0
Trace to slight	0.2 – 1.0	3.6 – 7.5	1 to 4
Slight to moderate	0.3 – 1.9	4.3 – 9.8	2 to 4
Moderate to extensive	1.0 – 7.1	7.5 – 16.9	3 to 5
> 50% lethality	> 3.6	> 12.8	Up to 6

- Single point approximation used

Penetrator Shock

- Impact of the target was simulated using Lagrange parts, slug then remapped to Euler grid to speed up simulation
- After penetration, slug velocity was about 1100 m/s.
- Slug travelled the length of the volume, while pressure was logged at various gauge points.

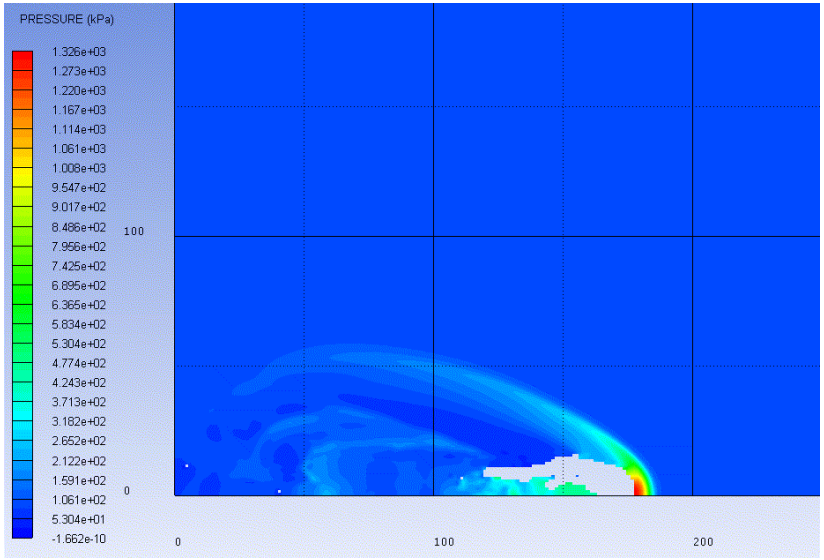

Pressure and Chest Wall Velocity

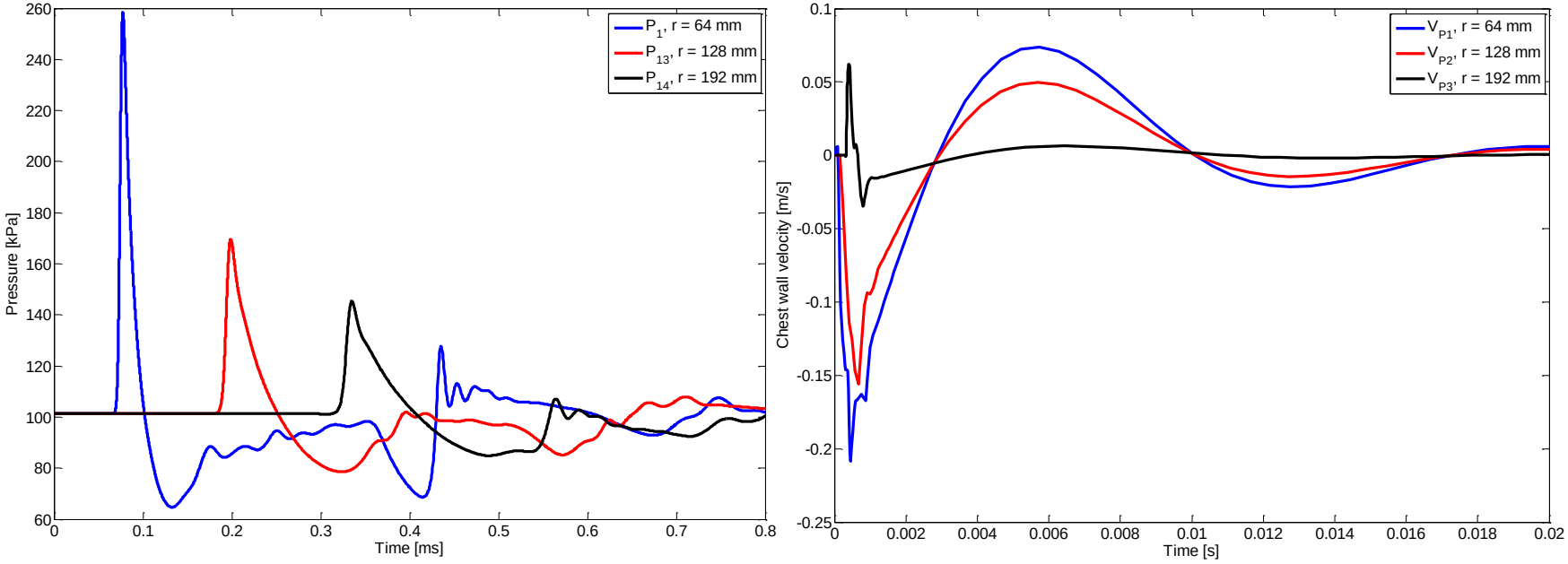

- Three pressure profiles, very close to trajectory of the slug.
- High peak pressure, low duration.
- Solving Axelsson yields a very low chest wall velocity, $ASII_{MAX}$ = 0,0066
  - Trace to slight injury = 0,2 – 1,0 ASII

Detonation Pressure

- Typical stand-off distance of 3 m chosen.
- 1D simulation of 1 kg TNT, remapped to 2D after 1,6 ms.
- Euler grid:
  - 10 mm x 10 mm grid size, 1 mm x 1 mm near symmetry axis
  - Cylinder walls reflect perfectly
  - 20 mm hole from penetration
- Axelsson subroutine for AUTODYN

Pressure Propagation

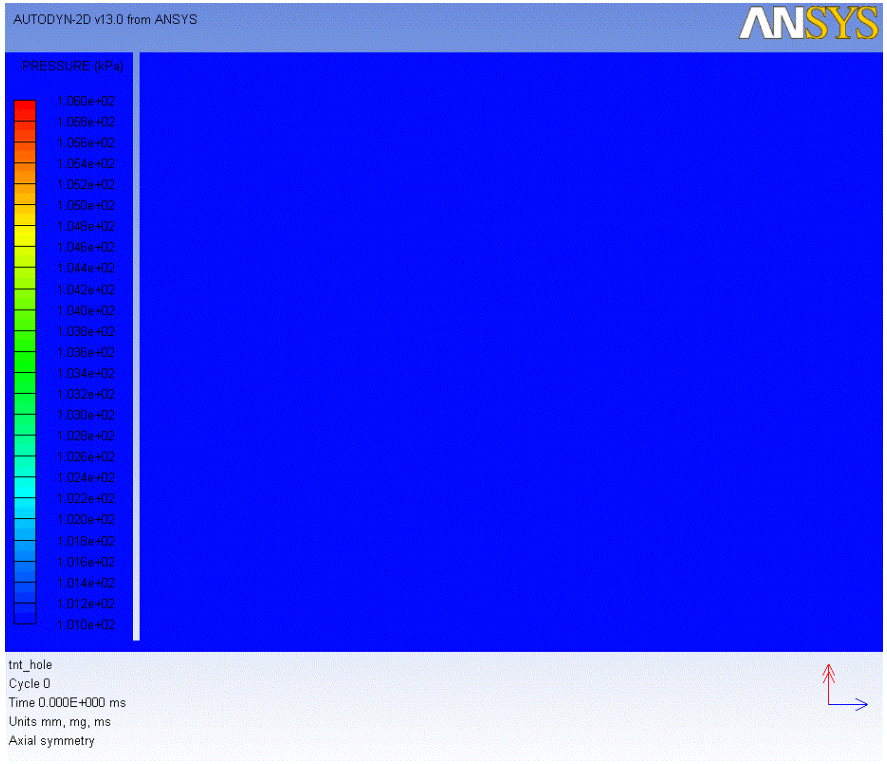

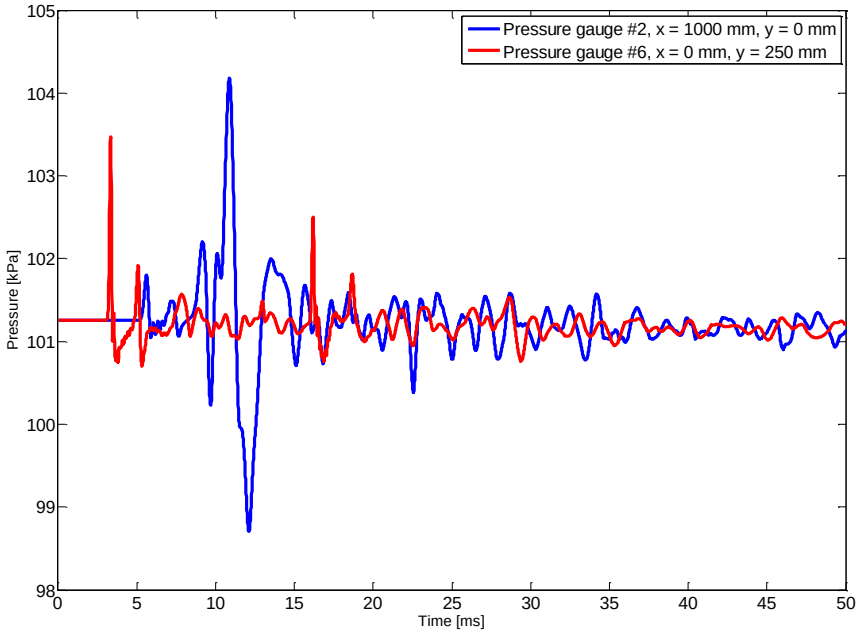

- Peak pressure at hole = 170,5 kPa

ASII Levels

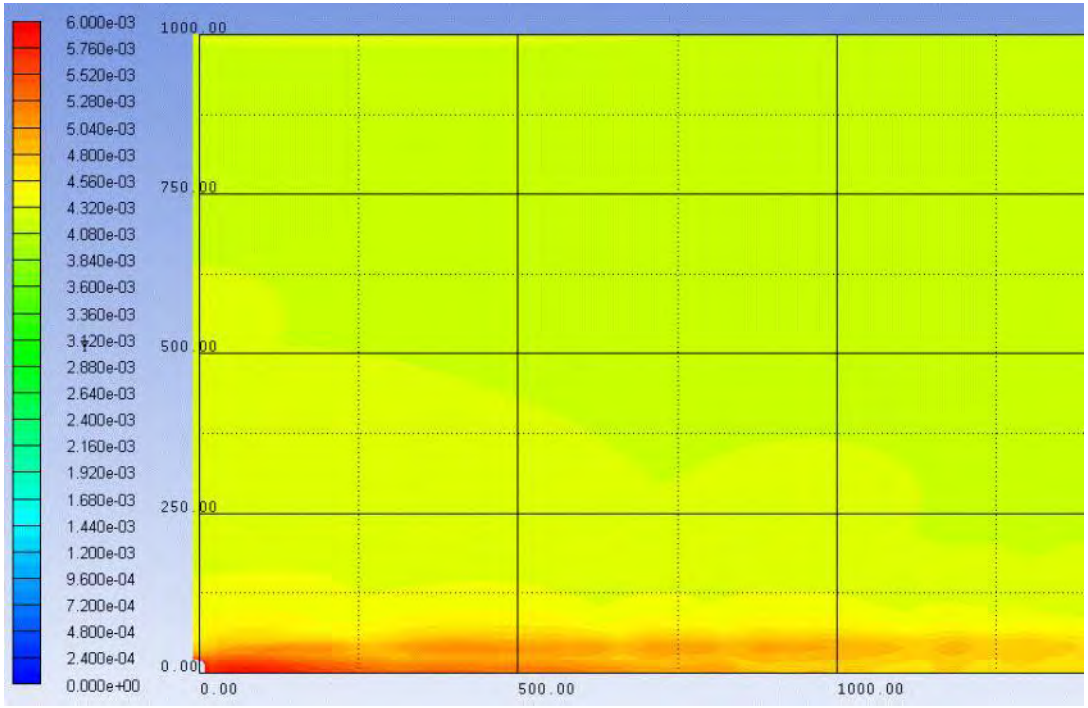

- Highest value along symmetry axis, LOS from point of penetration.
- Max ASII = 0,0096 at opening
  - No injury
- Trace to slight injury = 0,2 – 1,0 ASII
  - Far from lowest injury level

Plate Vibrations

- The impact of the slug on the target incites vibrations and movements in the plate.
- The 5 mm steel plate exhibits the strongest vibrations.
- Acts as a piston the air inside the volume.

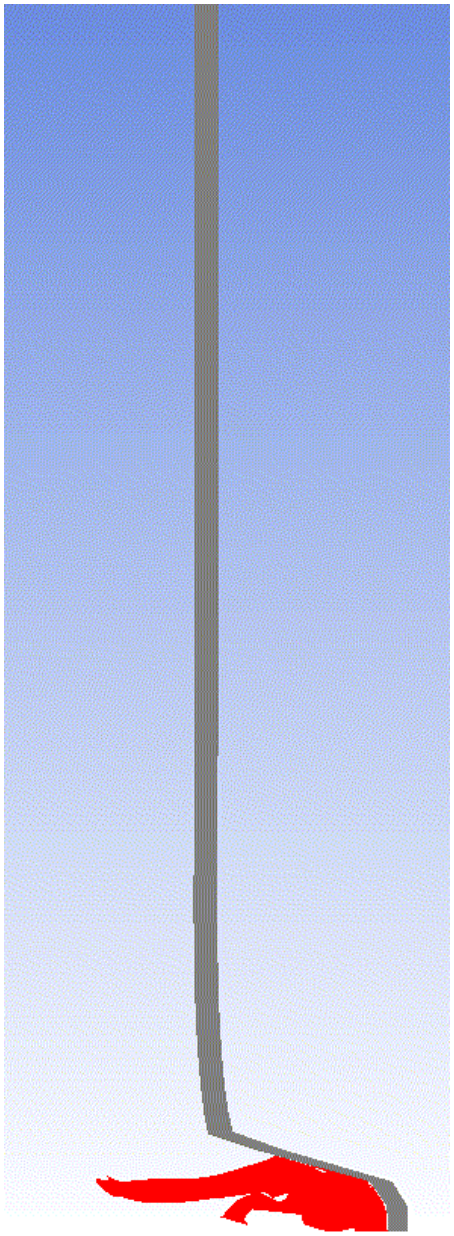

Plate Vibrations - Theory

- From acoustic theory, a circular piston oscillating at

$$U(t) = U_0 e^{i\omega t}$$

sets up a pressure *p* at a distance *r*:

$$p(r,\theta,t) = i\rho_0 c \frac{U_0}{\lambda} e^{i\omega t} \int_S \frac{1}{r'} e^{i(\omega t - kr')} dS$$

- Along the symmetry axis this is solved to give:

$$p(r,0,t) = \rho_0 c U_0 \left(1 - e^{-ik(\sqrt{r^2+a^2}-r)}\right) e^{i(\omega t - kr)}$$

where *a* is the radius of the piston.

Plate Vibrations - Complications

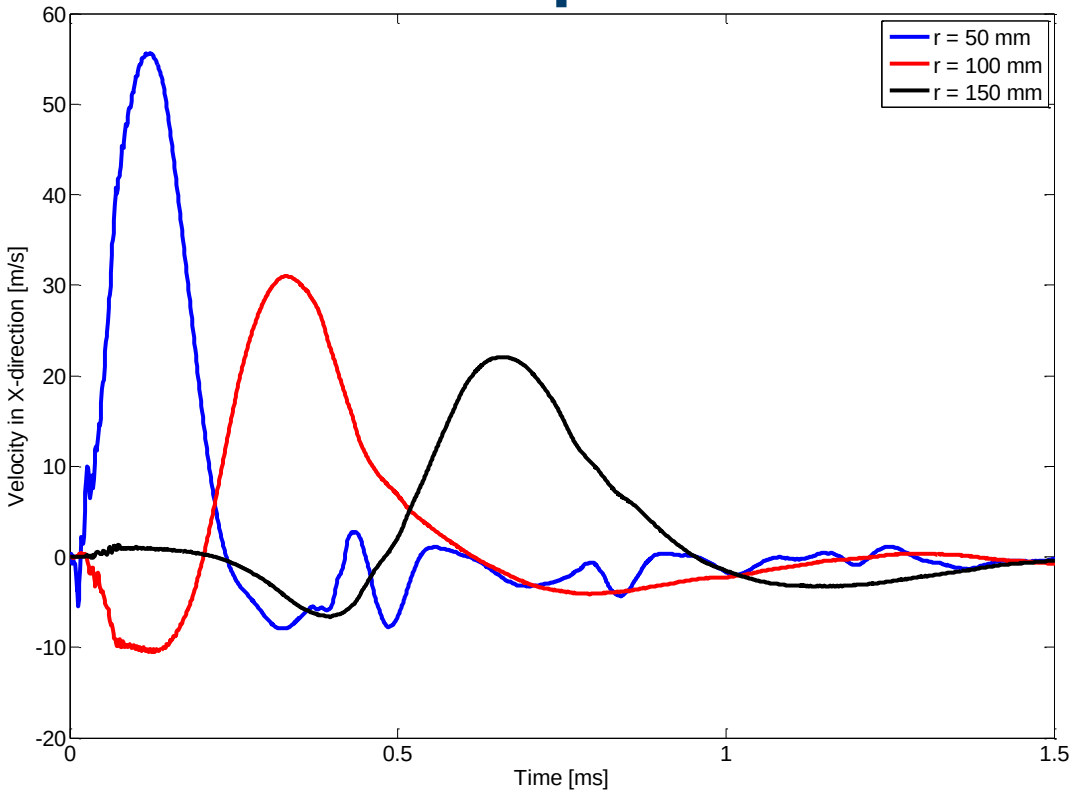

- The perforated plate does not oscillate harmonically.
- Not uniform oscillation along radius of the plate.

Plate Vibrations - Approximation

- Assume piston velocity term can be factored out:

$$p(r,0,t) = \rho_0 c \left(1 - e^{-ik(\sqrt{r^2+a^2}-r)}\right) e^{-ikr}\, V(t)$$

  in which case we can use the velocity profiles.

- The wave number *k* is still unknown
  - Approximation by curve fit, ex. the velocity profile at r = 100 mm gives *k* ≈ 3/m.
- Assume this profile is valid over the entire plate
  - Conservative estimate

Plate Vibrations – Calculated Pressure

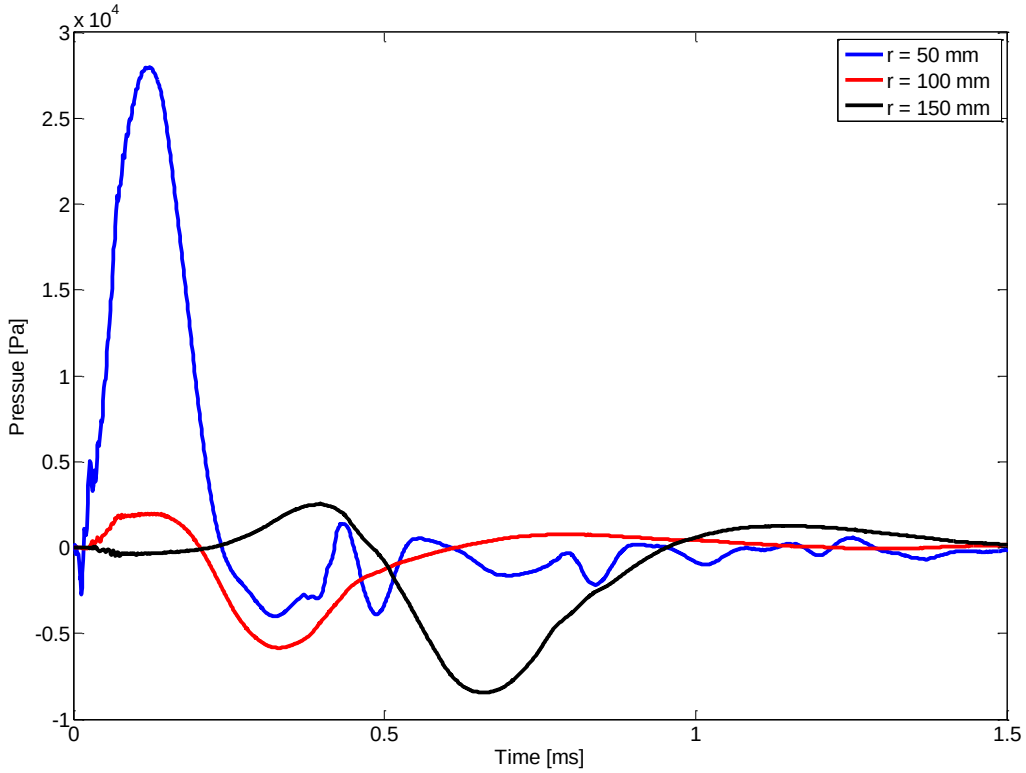

- Overpressure calculated 1 m from plate for three velocity profiles
- Fairly high peak overpressure, but short duration
- ASII = 0,0057 << 0,2 (Trace to slight injury)

Conclusion

- Penetrator shock:
  - P_{MAX} = 160 kPa (Overpressure)
  - $ASII_{MAX}$ = 0,0066
- Detonation shock:
  - P_{MAX} = 70 kPa (Overpressure)
  - $ASII_{MAX}$ = 0,0096
- Plate vibrations
  - P_{MAX} = 28 kPa (Overpressure)
  - $ASII_{MAX}$ = 0,0057

- Very far from lowest ASII injury level
  - Trace to slight injury: ASII = 0,2 – 1,0

Conclusion

- Possible sources of error:
  - Short duration → Questionable validity of Axelsson
  - Single Point Approximation
  - Numerical artifacts

- Combination and interaction of the effects have not been considered

THANK YOU!

Free-Flight Motion Analysis Based on Shock-Tunnel Experiments

Pierre Wey, Friedrich Seiler

Julio Srulijes, Myriam Bastide, Bastien Martinez

French-German Research Institute of Saint-Louis (ISL)
5 rue du Général Cassagnou
68301 Saint-Louis, France
Contact: pierre.wey@isl.eu

Outline of the Study

Objective

To prove the relevance of aerodynamic coefficients extraction based on ultra-short trajectories (10 to 20 cm) observed in shock-tunnels.

Means and Techniques

- Reference model (EFP)
- Shock-tunnel facility (supersonic regime)
- Flow measurement (velocity, pressure)
- Optical set-up (motion visualization and recording)
- Image processing (trajectory tracking)
- Data extraction (model-based fit process)

Free-flight Force Measuring (FFM) Technique

Reference Model

- 12.8 mm caliber Explosively Formed Projectile (EFP)
- Stable in supersonic regime, small size of full scale model, simplicity of manufacturing
- Full aerodynamic data from Mach 3.2 to Mach 5.5 defined using free-flight analyses, wind-tunnel measurements and CFD results (references: ARL 1998, ISL 1999)
- Three models: 1- steel, 2- steel body + tungsten nose, 3- Dural

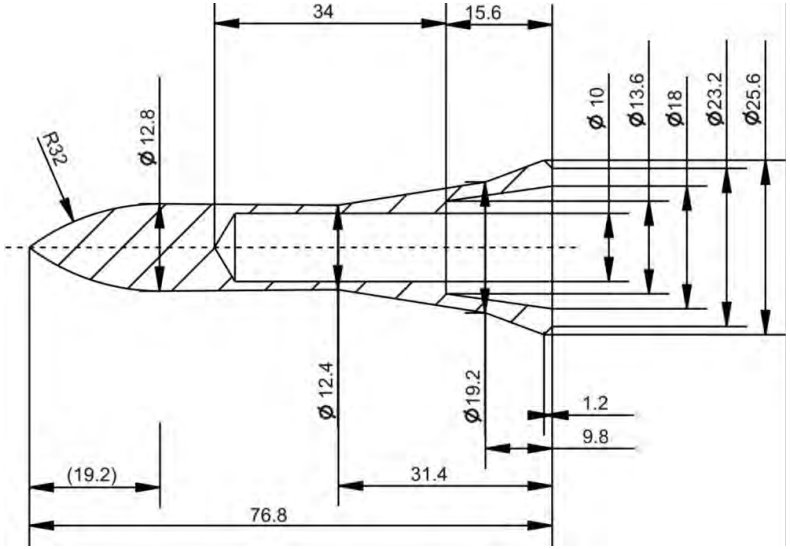

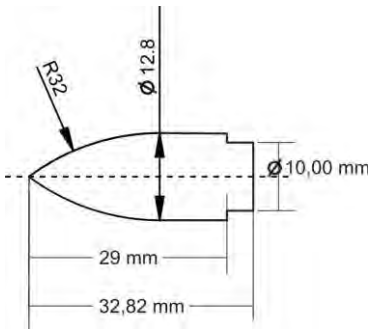

ISL Shock-Tunnel Facility

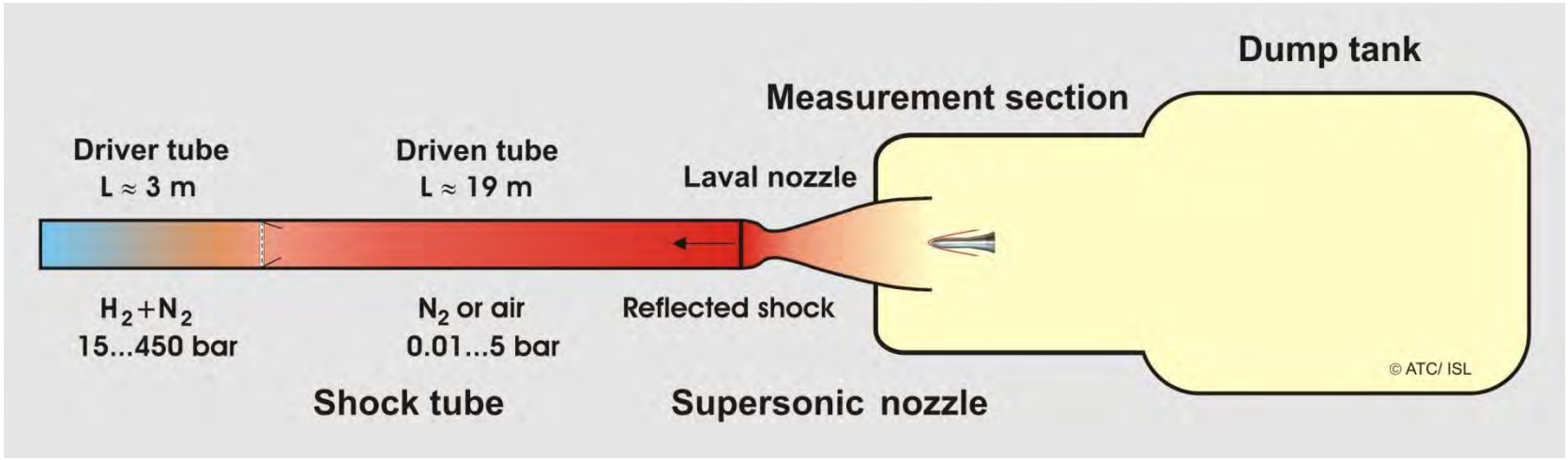

- STA and STB shock tunnels
- Nozzle Mach numbers: 3 to 14
- Nozzle exit diameters: 130 to 400 mm
- Stationary flow conditions: 2 to 4 ms
- Constant Mach number: 15 ms

Measuring the Flow Conditions

- The flow Mach number is constant during 15 ms until the gas driver arrives to nozzle

  → the aerodynamic coefficients are fixed during the testing time

- The flow velocity and pressure are to be recorded because the flow conditions are not stationary

  → time history of the dynamic pressure: $\frac{1}{2}\rho(t)\,u^2(t)$

ISL Laser Doppler Velocimeter

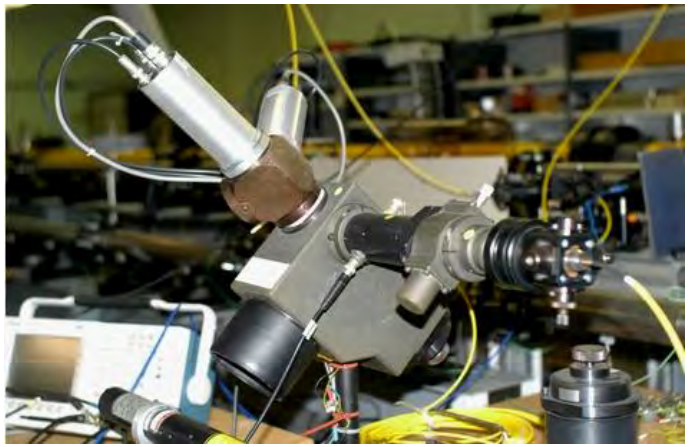

Wall pressure gauge

Flow Measurements at Mach 3

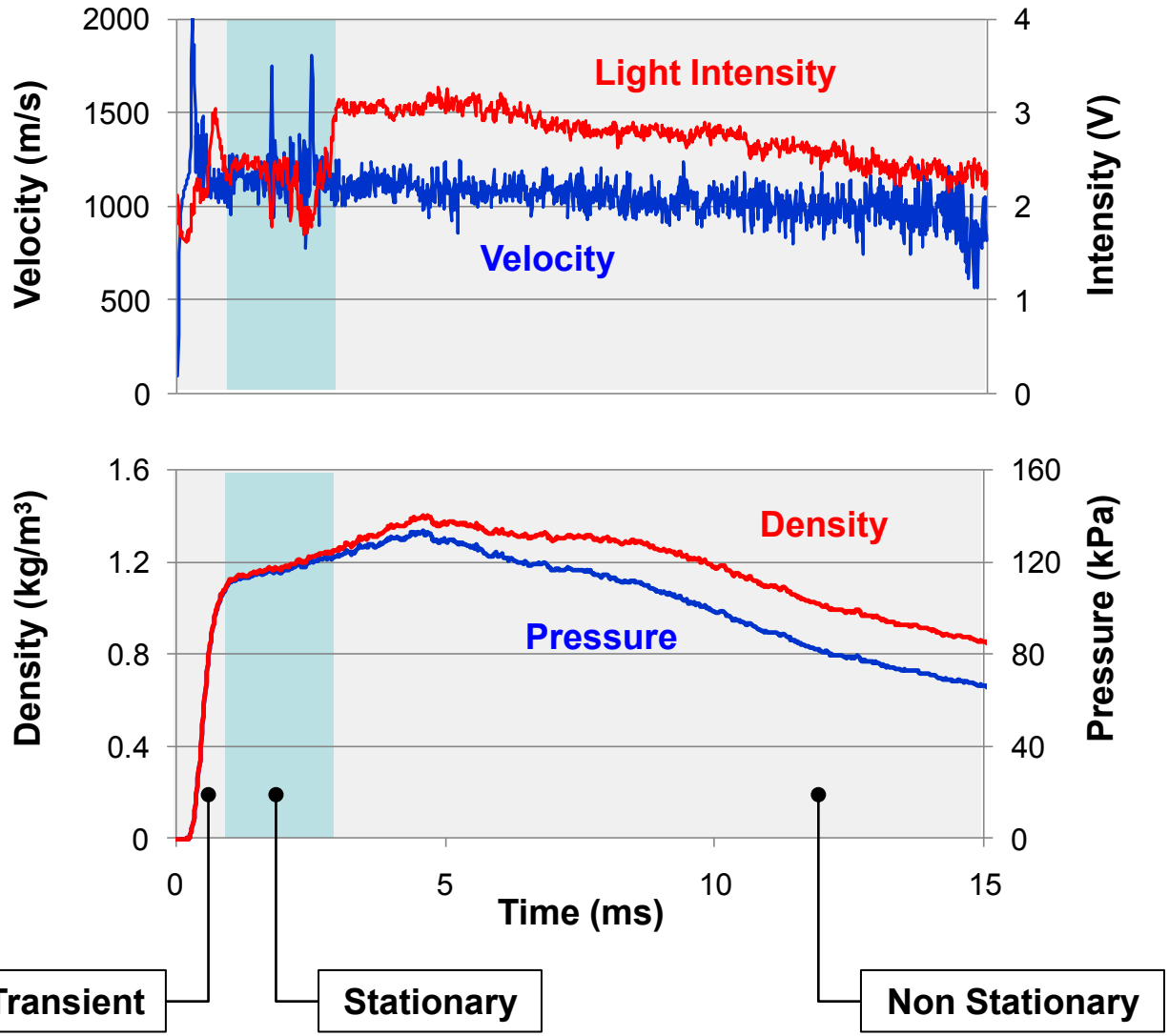

Optical Set-up

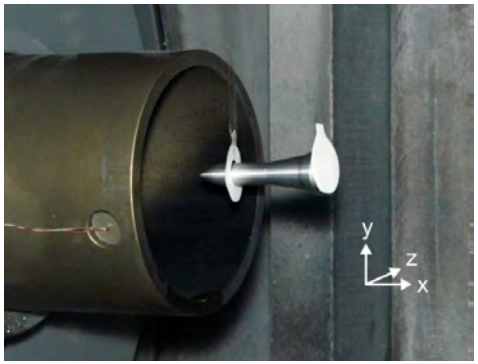

Two cameras are used to visualize the motion of the model in the horizontal and vertical planes.

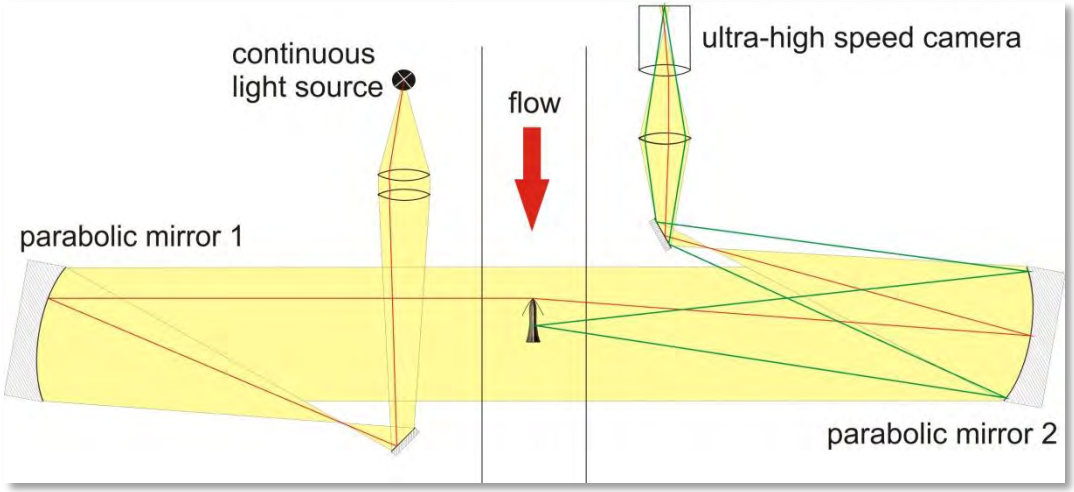

Compared to a standard shadowgraph set-up, the image of the object is sharply focused onto the camera using parabolic mirrors to improve the motion visualization.

Observation Sequences

Videos and pictures are taken with two ultra-high speed Photron cameras to observe the model displacements in the vertical and horizontal planes.

- 12500 frames per second: time interval 80 µs
- Time exposure: 1 µs (no motion blur)

EFP Model #1 at Mach 3, Vertical plane, AOA = 0°

Duration = 10. 72 ms, Displacement = 13.60 cm

Testing Section Limit

The testing section is limited by the Mach cone generated by the Laval nozzle. The section size increases with the nozzle exit size and the Mach number.

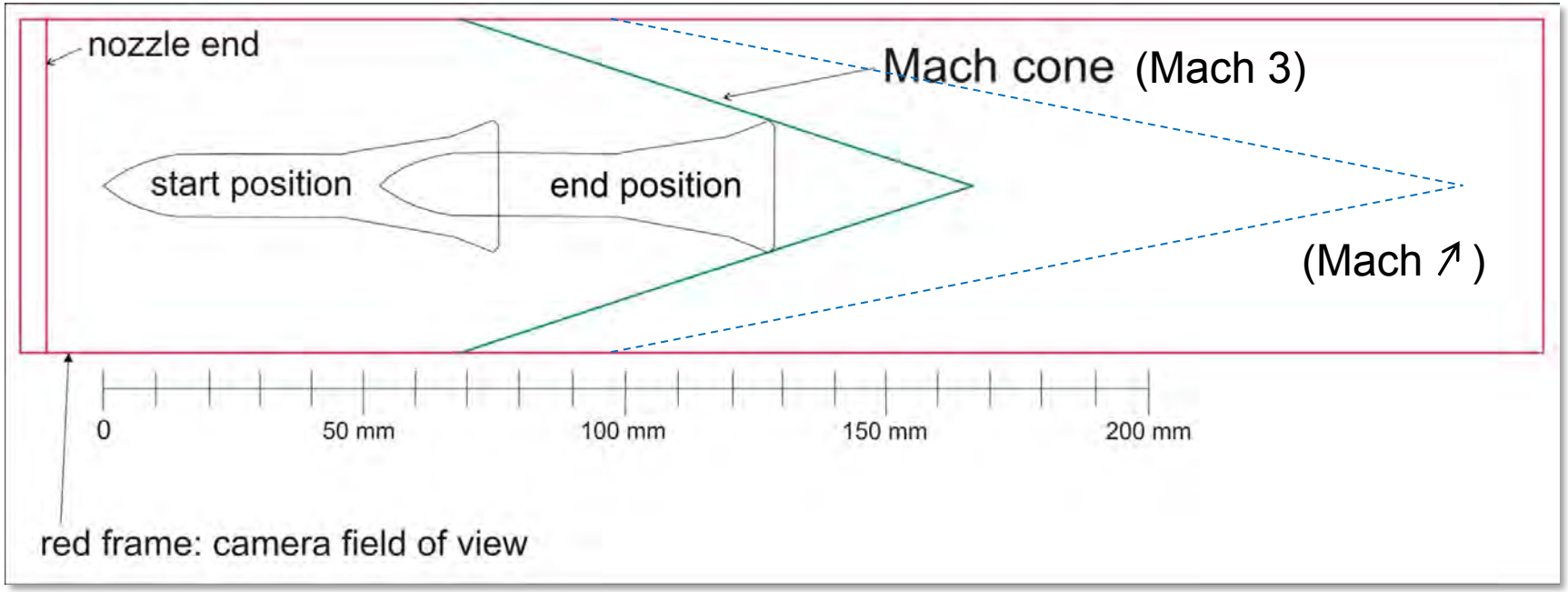

Image Processing

Tracking of three reference points:

→ Trajectory of centre of mass

→ Angular motion

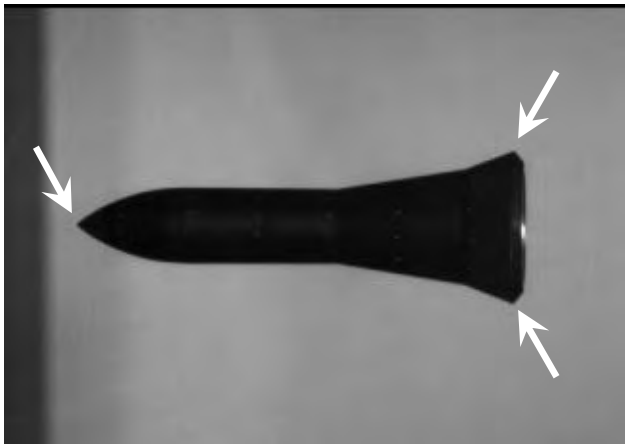

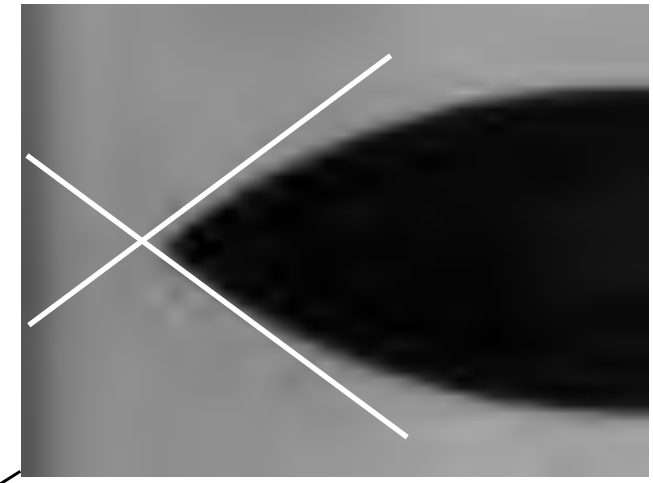

Harris method based on local contrast detection:

→ Specific pattern detection with proper directions (Eigen value analysis)

→ Path of analysis windows is predicted to prevent loss of reference point

Motion Tracking Example

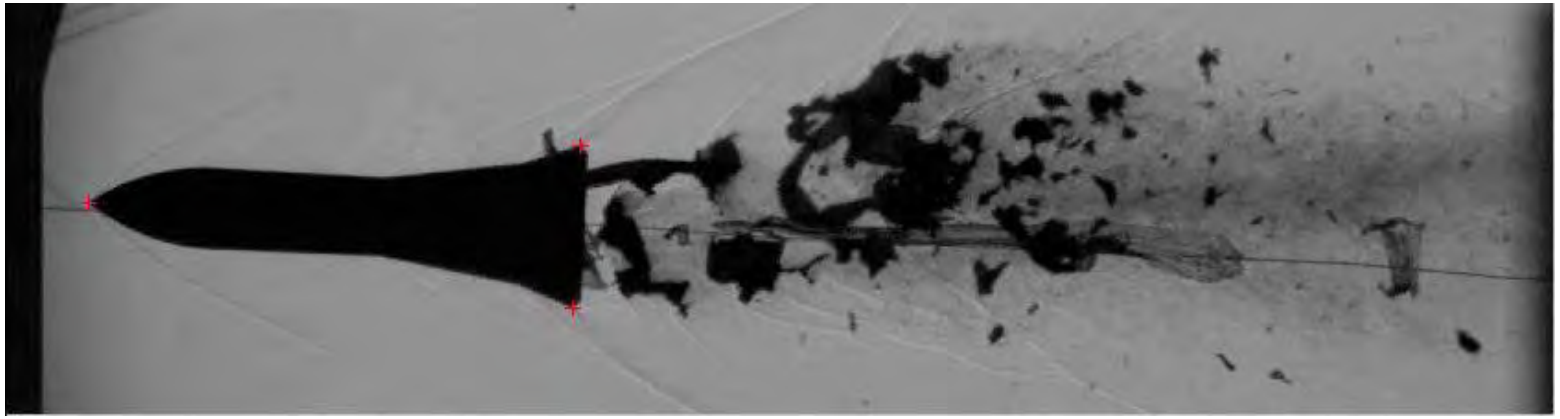

EFP Model #1 at Mach 3, Horizontal plane, AOS = 3°

Duration = 10. 72 ms, Displacement = 13.60 cm

Data Extraction Methodology (1/2)

Basic methodology

The theoretical motion of the model is computed by means of a simple 2nd order Runge-Kutta integration using the time varying flow conditions.

Aerodynamics coefficients are estimated by comparing theoretical and observed motions using a least-square fit process.

Drag force coefficient

Theoretical x-axis acceleration (C_D = 1): $\dot{v} = \frac{1}{2}\rho u^2 \frac{S}{m}$

Initial conditions: $v_0 = 0,\ x_0 = 0$

Quasi-linear fit between the observed and computed x values:

$$x_{obs} = C_D(1 - e^{-bx^c})x + d$$

- d → Origin shift
- C_D → Non-linear fit at the beginning of the trajectory due to transient flow phase and support removal

Drag Coefficient (1/2)

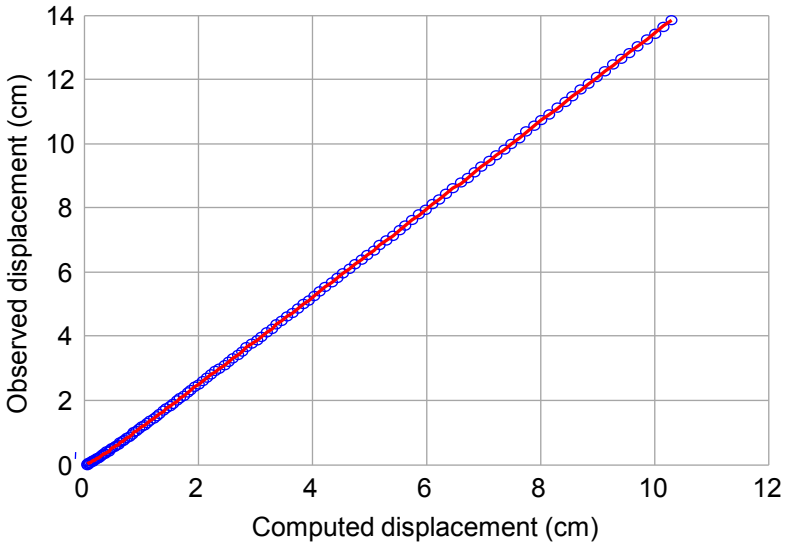

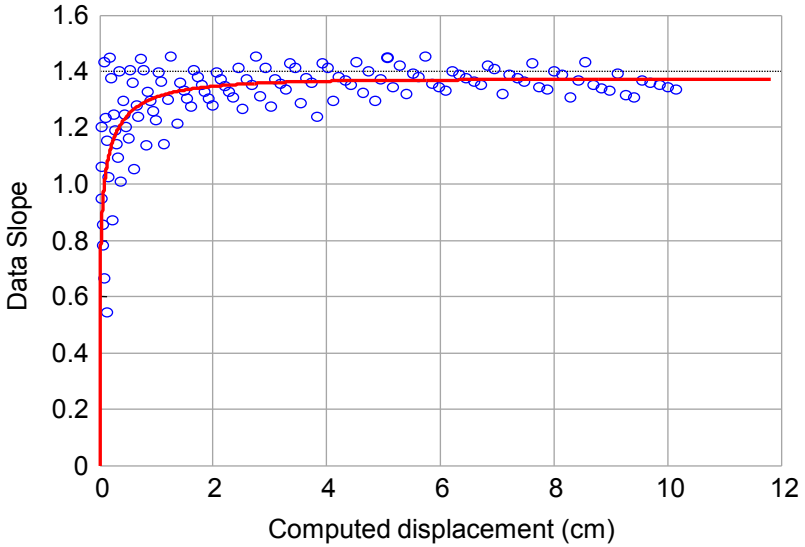

EFP Model #1 at Mach 3

Observation time	10. 88 ms
Observed displacement	13.83 cm
Extracted drag	1.36
Reference drag	1.35

Drag Coefficient (2/2)

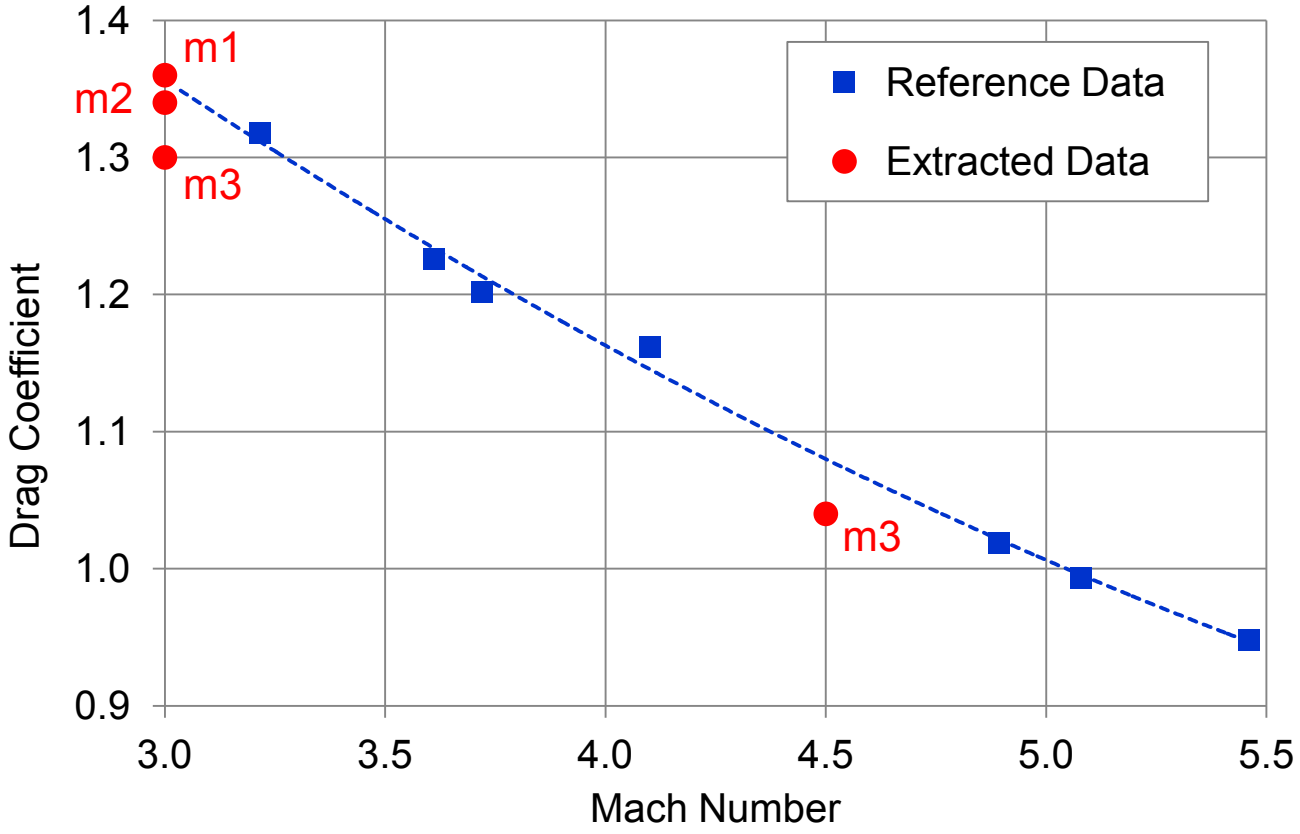

“Heavy” models 1 & 2 compares extremely well with the reference data

Data Extraction Methodology (2/2)

Pitching moment and pitch damping coefficients

Theoretical angular acceleration: $\dot{\omega} = \frac{1}{2}\rho u^2 \frac{S d}{I_t}\left(C_{M\alpha}\sin\alpha + \frac{\omega d}{u} C_{Mq}\right)\delta(t_0)$

Initial conditions: $\omega_0 = 0,\ \alpha_0$

The time-shift $\delta(t_0)$ at the beginning of the trajectory takes into account the transient flow phase and the influence of the support removal.

Cycle through the fit parameters to minimize the sum of square errors.

Static margin and normal force coefficient

These coefficients can be analytically computed using the pitch moment coefficients that are extracted from two models with different center-of-mass positions.

Pitching Motion Coefficients

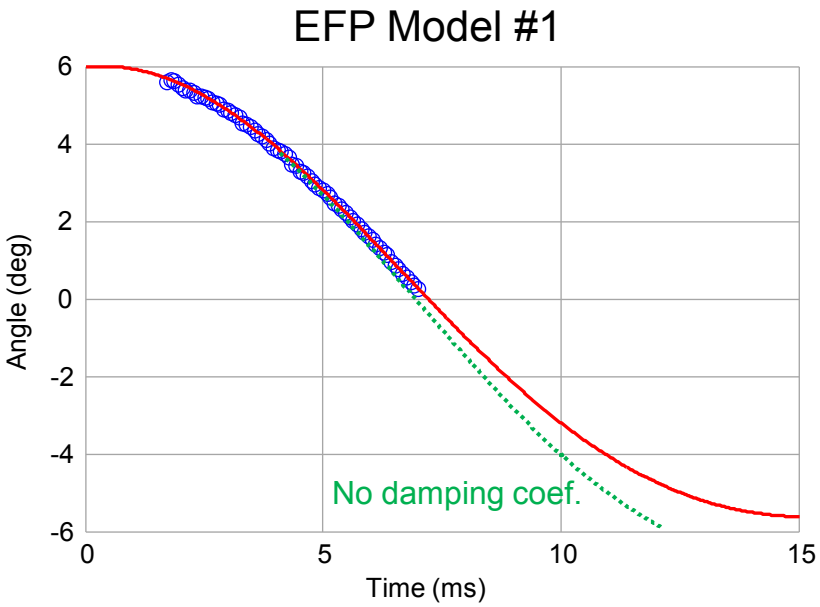

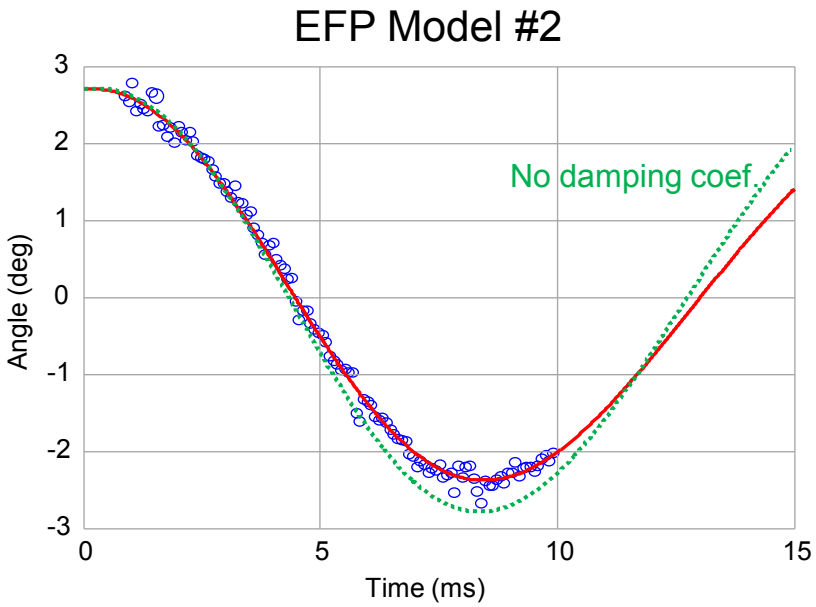

Model	t_0 (ms)	α_0 (deg)	$C_{M\alpha}$	Ref. $C_{M\alpha}$	C_{Mq}	Ref. C_{Mq}
1	0.4	6.0	-1.4	-1.0	-80	-100
2	0.4	2.7	-5.7	-7.1	-90	-100

Pitching Moment Coefficient Slope

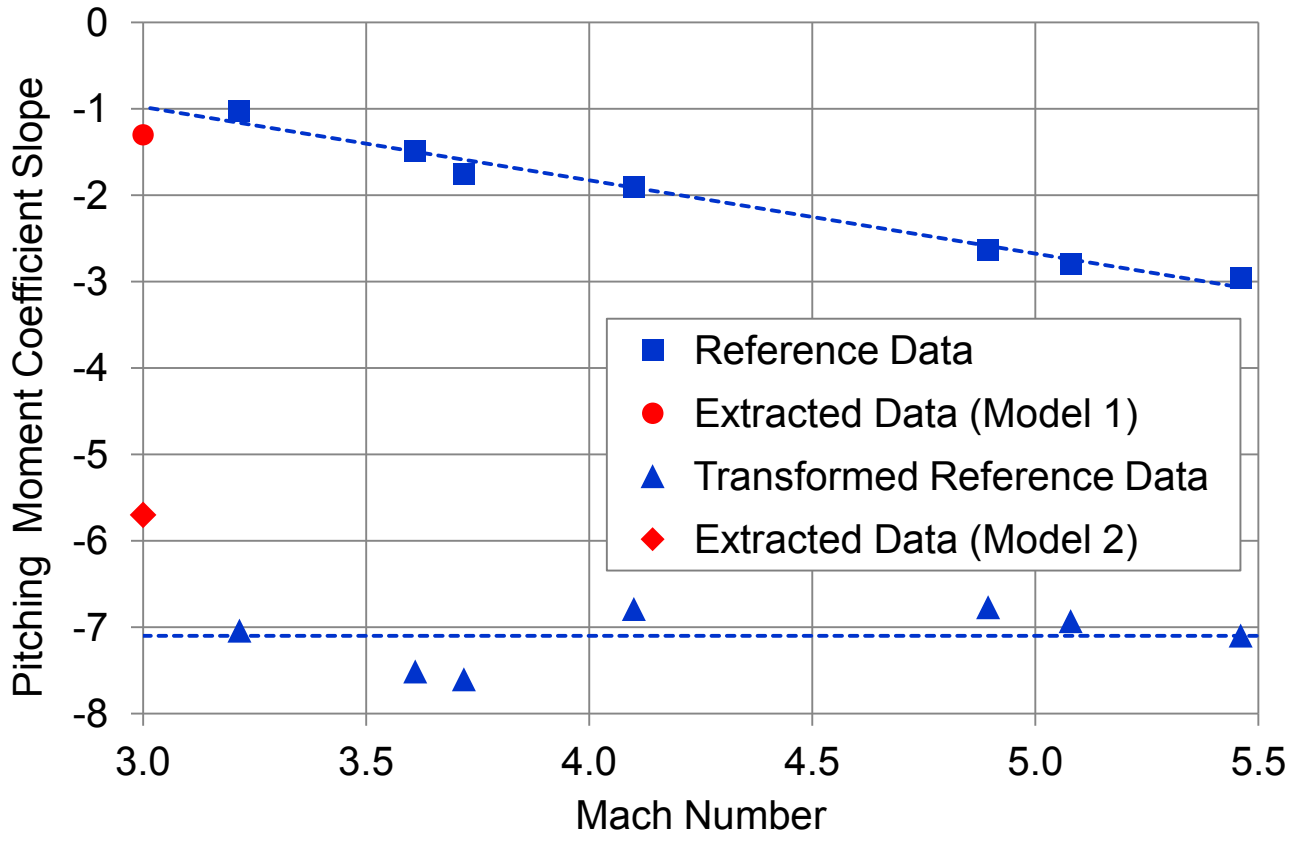

Experiments to be conducted at Mach 4.5 to increase model stability

Summary and Outlook

- The innovative Free-flight Force Measuring (FFM) technique covers a wide range of skills: shock-tunnel facility, flow condition measurement, high-speed video observation, image processing and aerodynamic data reduction.
- The FFM technique was successfully tested against three reference EFP models at Mach 3.
- The extracted drag coefficients compare extremely well with the reference data. The pitching moment and pitch damping coefficients compares fairly well.
- Further experiments will be conducted at Mach 4.5 very shortly.
- The mid-term goal is to provide a low cost facility to extract the aerodynamic coefficients of projectiles or air vehicles operated in the supersonic and hypersonic regimes.

Extended range of 155mm projectile using an improved Base Bleed unit. Simulations and Evaluation

26th International Symposium on Ballistics
September 12-16, 2011
Miami, Florida, USA

Dr. Ing. Nils Kubberud, +47 926 51177, nils.kubberud@nammo.com
Nammo Raufoss AS
Dr. Ing. Ivar J. Øye, +47 480 42948, ivar.oye@computit.no
ComputIT AS

Contents

- Introduction
- CFD modeling
- CFD results
  - Effect of Base Bleed
  - Validation of Results
- Optimization of Base Bleed
  - Effect of Base Cavity
  - Effect of Gas Vent Layout
- Conclusions

PRECISION PEOPLE TECHNOLOGY

Introduction

- The ballistics of artillery shells is, among other factors, dependent on the aerodynamic drag
- Aerodynamic drag is again dependent on the shape of the projectile and the flight conditions, i.e. the two well-known aerodynamic parameters Mach number and Reynolds number
- The shape of a modern projectile is a compromise between aerodynamics and structural concerns, especially during the initial blast
- Usually the drag, C_{D0} of a blunt body is divided into forebody drag, C_{Dpv} and base drag, C_{Db0}

$$C_{D0} = C_{Dpv} + C_{Db0}$$

  - Forebody drag – skin friction and pressure drag
  - Base drag – pressure in base area lower than ambient pressure
  - The base drag is approximately 50% of the total drag.

Base drag reduction

- Base drag reduction achieved by
  - Afterbody boat tailing
  - Base bleed
  - Vortex supression devices
  - Combination of above devices
- Active or passive flow control techniques basically manipulate or alter the near-wake flowfield for an increase in base pressure and consequently reduce base drag

Base Bleed

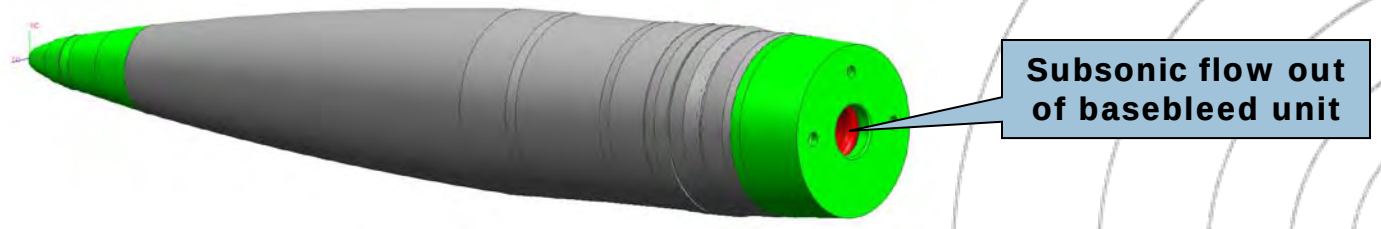

- Base bleed is a gas generator producing hot gas in the aft end of the projectile
- The aim of the base bleed is to fill up the wake zone behind the projectile and thus increase the base pressure. Increased base pressure reduces the base drag and gives increased shooting distance for the projectile
- For projectiles in service, the shooting distance can be increased by 20-30% due to reduced base drag
- Flow out of base bleed unit is subsonic
  - Internal ballistics coupled to external base pressure
  - Base pressure controls base drag
  - Coupling between base drag and internal ballistics often given through empirical expressions due to a lack of understanding of viscous-inviscid flow interactions between a near-wake flow and a freestream

Physical modeling

- Established a physical model for the coupling between base drag and base bleed internal ballistics
  - CFD computations using various turbulence models in the wake zone have been performed
- The first objective was to use computational fluid dynamics (CFD) to establish a numerical model capable of accurately predicting the drag in the supersonic range for the inert shell and yield a proper response to the increasing base bleed flow rates
  - For the verification of the CFD model, radar measurements were available for the 155 mm Heer Mk 2 artillery shell
- The second objective was to investigate the combined effect of afterbody shape and gas vent design on the net drag
  - The nozzle area, the length and diameter of the projectile were kept constant
  - Shape and location of the gas vents were modified

Heer Mk2 projectile

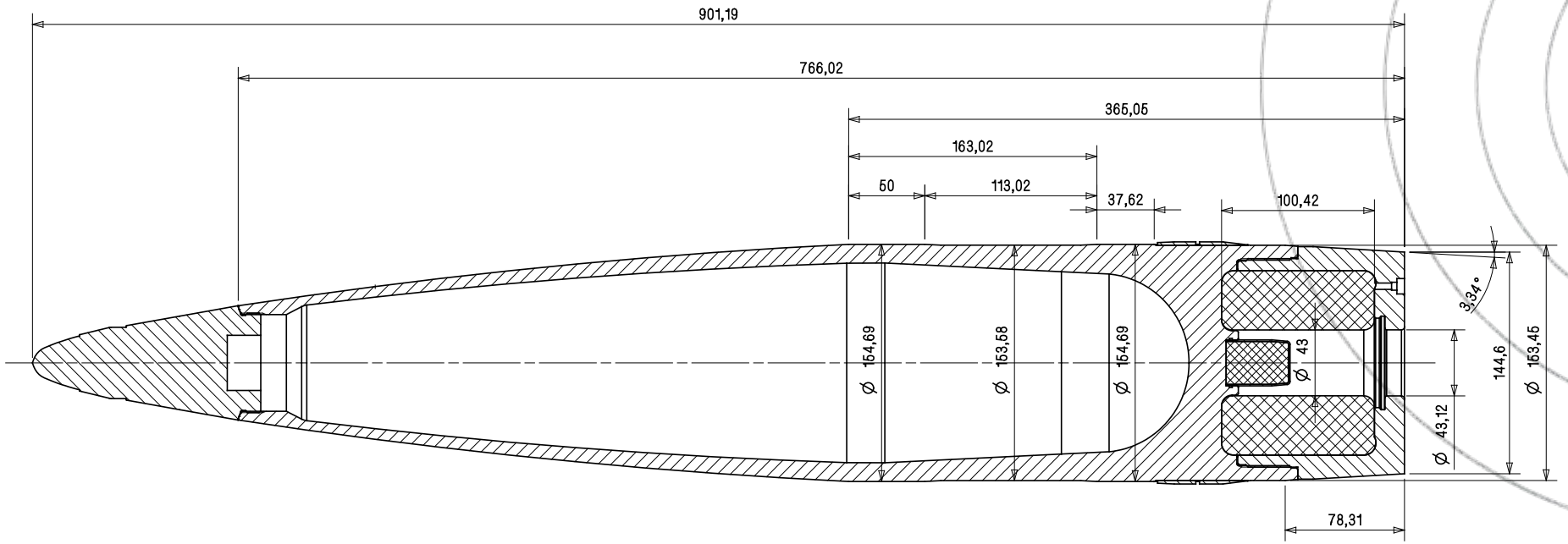

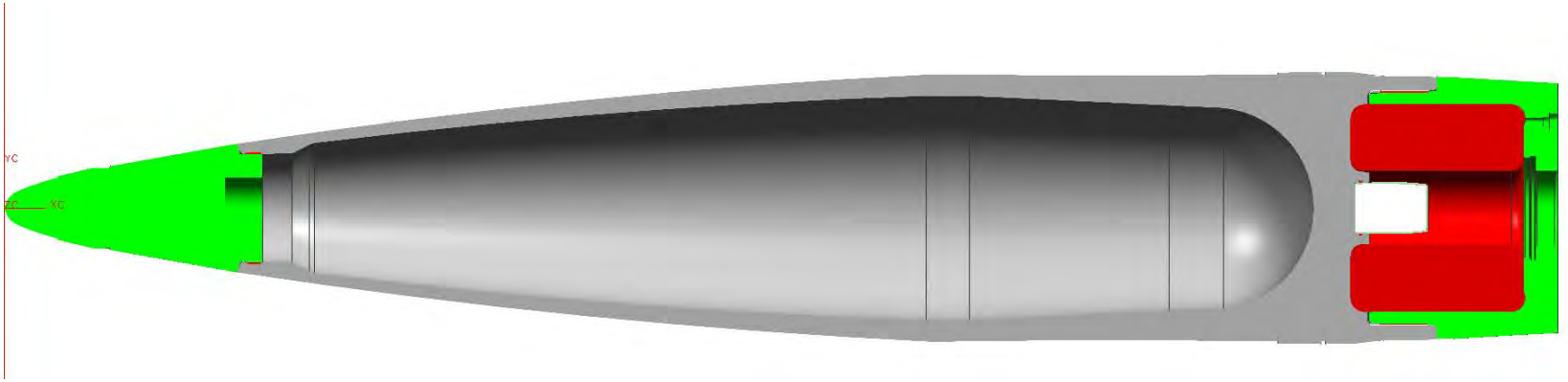

PRECISION PEOPLE TECHNOLOGY

CFD modeling

- The analyses were carried out with two CFD codes
  - Commercial available STAR-CCM+
  - In-house developed code CFDnFlow for compressible flows on structured, multi-block, body-fitted grids
  - Both codes have the option of using the Reynolds Averaged Navier-Stokes (RANS) or the detached eddy formulation (DES)
- Various turbulence models were applied to the base flow problem, from k-epsilon to Reynolds stress models based on the Reynolds-Averaged Navier-Stokes (RANS) equations to the instantaneous Navier-Stokes equations with DES

Grid - model

- To obtain grid- independent results, several grids of different size and resolution were used during the project

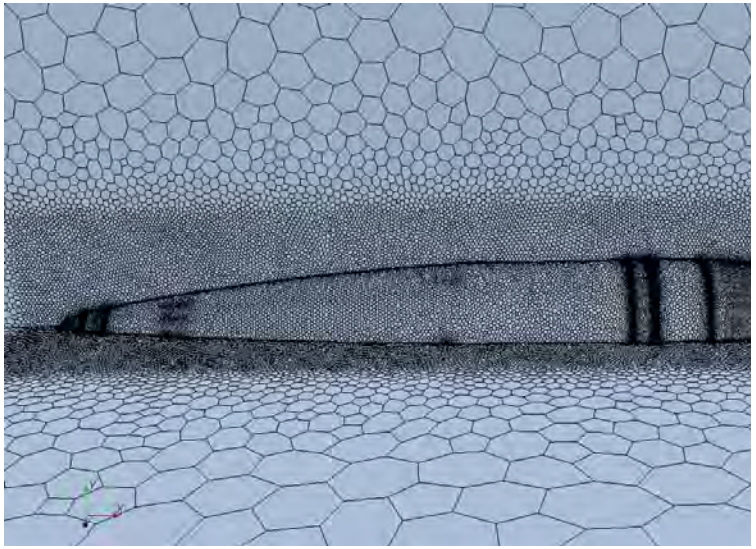

polyhedral volume grid from STAR-CCM+

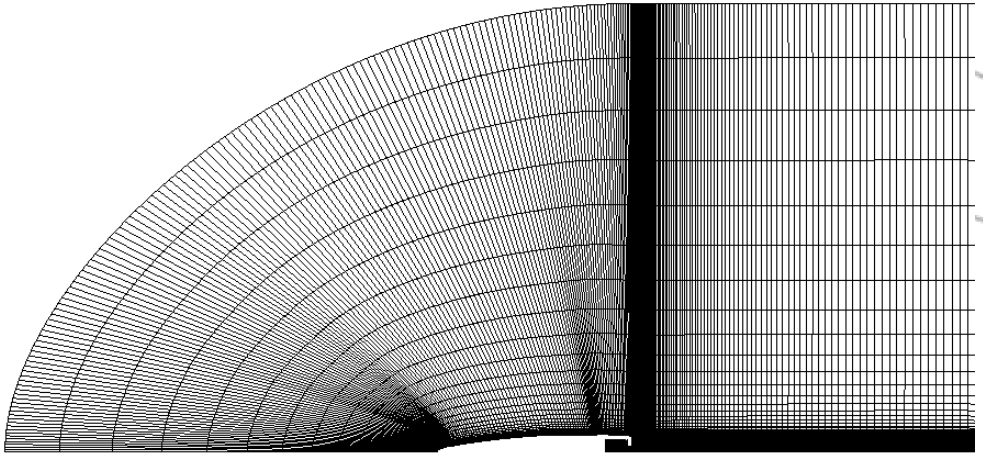

CFDnFlow axisymmetric grid

PRECISION PEOPLE TECHNOLOGY

CFD analysis of projectile without base bleed

The aim of the base bleed is to fill up the wake zone behind the projectile and thus increase the base pressure

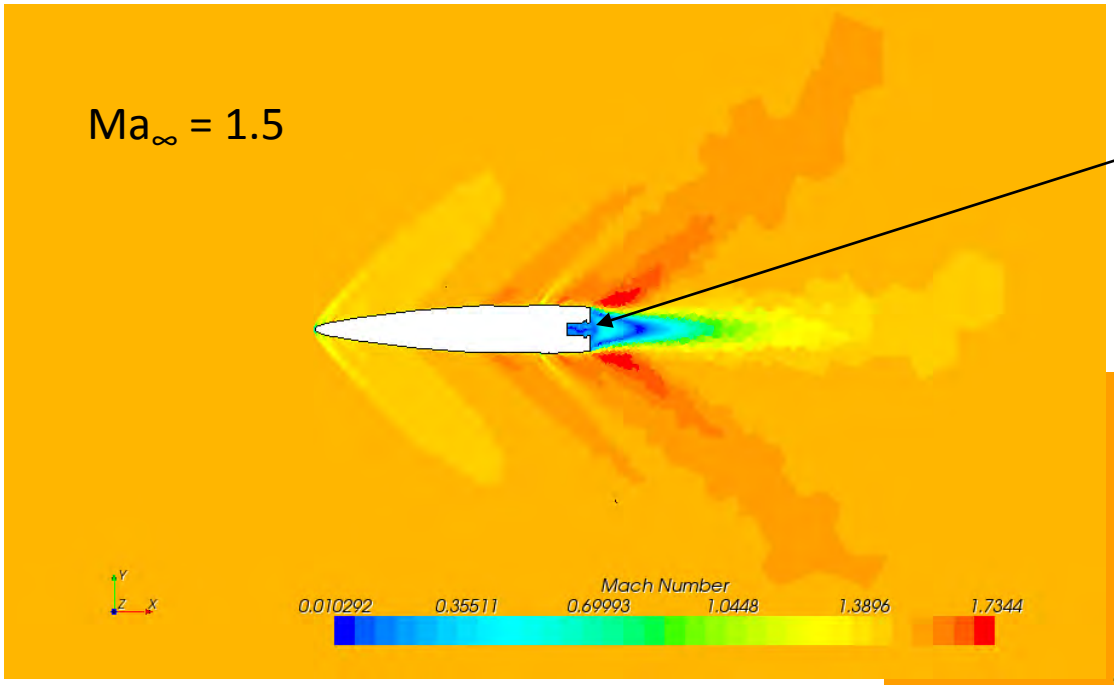

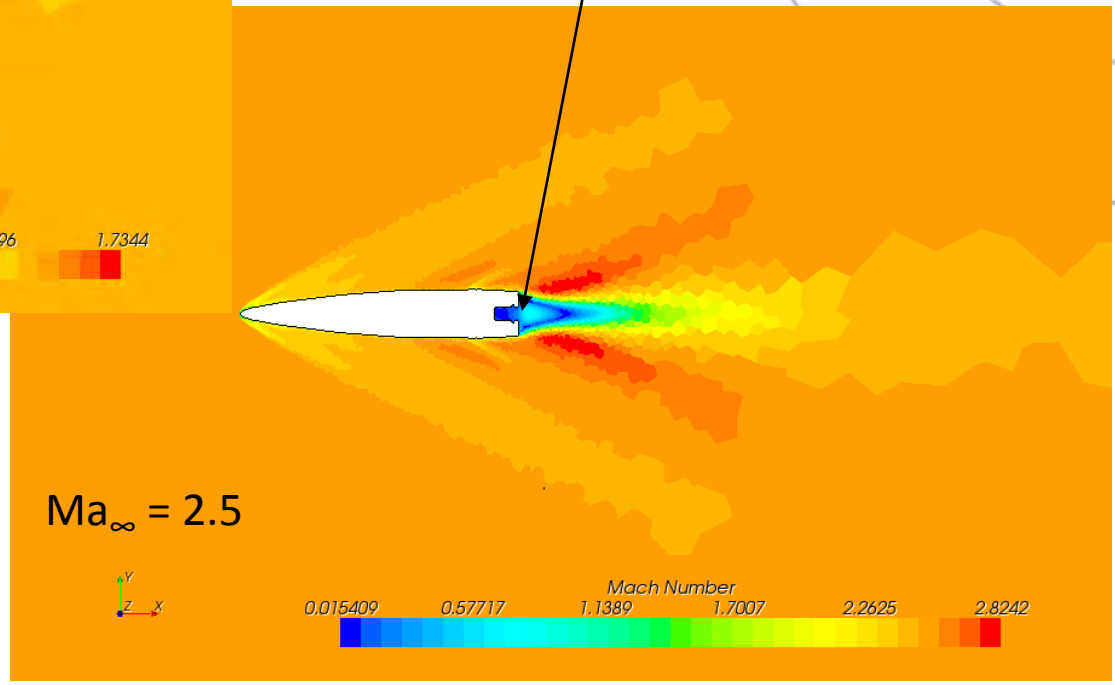

Results – inert base bleed

- The initial axisymmetric computations served the purpose of evaluating turbulence models for the comparison of computed drag coefficient with those from radar-doppler measurements (black curve)

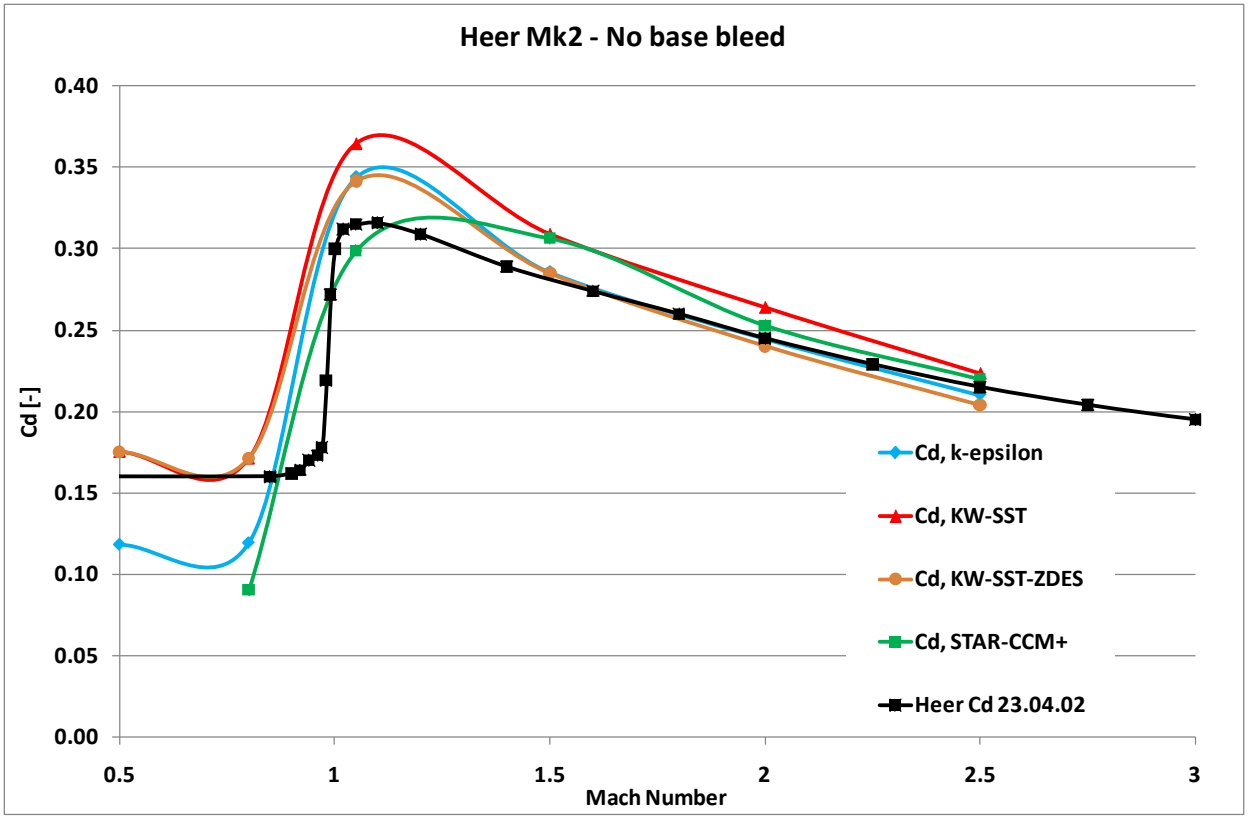

Results – inert base bleed – turbulent mixing

- From experience we suspected that the turbulent mixing in the wake might be too high, so we decided to pursue the use of detached eddy simulations (DES) in the wake
  - High level of turbulent mixing for the k-ω-SST and for the k-ε model
  - Results produced by the DES version of the k-ω-SST model showed much less turbulent mixing and more detailed resolution of the flow structures in the wake
  - DES modelling was used in the base bleed studies

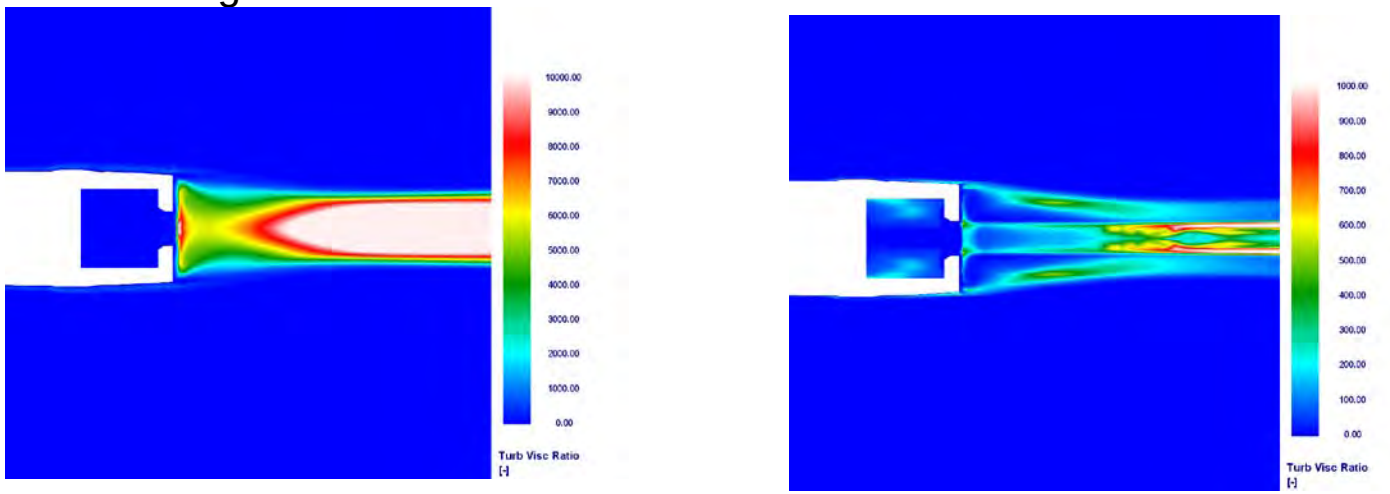

Computed turbulent viscosity ratio at Mach 2.5 with the k-ω-SST model (left), and the k-ω-SST-DES model (right), without mass injection

Effect of base bleed

- The base bleed was simulated with mass injection of hot gas in the cavity at the base of the projectile
  - The mass flow injection is characterized through the injection parameter
  - The injection parameter *I* is defined as the ratio of the injected mass flow rate and the “free stream” mass flow passing through the base area of the projectile
  - Injection parameter *I*, range *I* = 0-0.01

$$I = \frac{\dot{m}_b}{\rho_\infty V_\infty A_b}$$

- Drag reduction factor, C_{red}
  - Subscript «b» denotes active base bleed
  - Subscript «b0» denotes inert base bleed

$$C_{red} = f_{dr} = 1 - \frac{C_{Db}}{C_{Db0}} = \frac{\frac{p_b}{p_\infty} - \frac{p_{b0}}{p_\infty}}{1 - \frac{p_{b0}}{p_\infty}}$$

Drag reduction factor using DES turbulence modeling

- Comparison of STAR CCM+ and the CFDnFlow results showed common trends but also some variation
  - The maximum drag reduction coefficient was found to be roughly 0.4-0.6 for base bleed rates of I=0.006-0.008

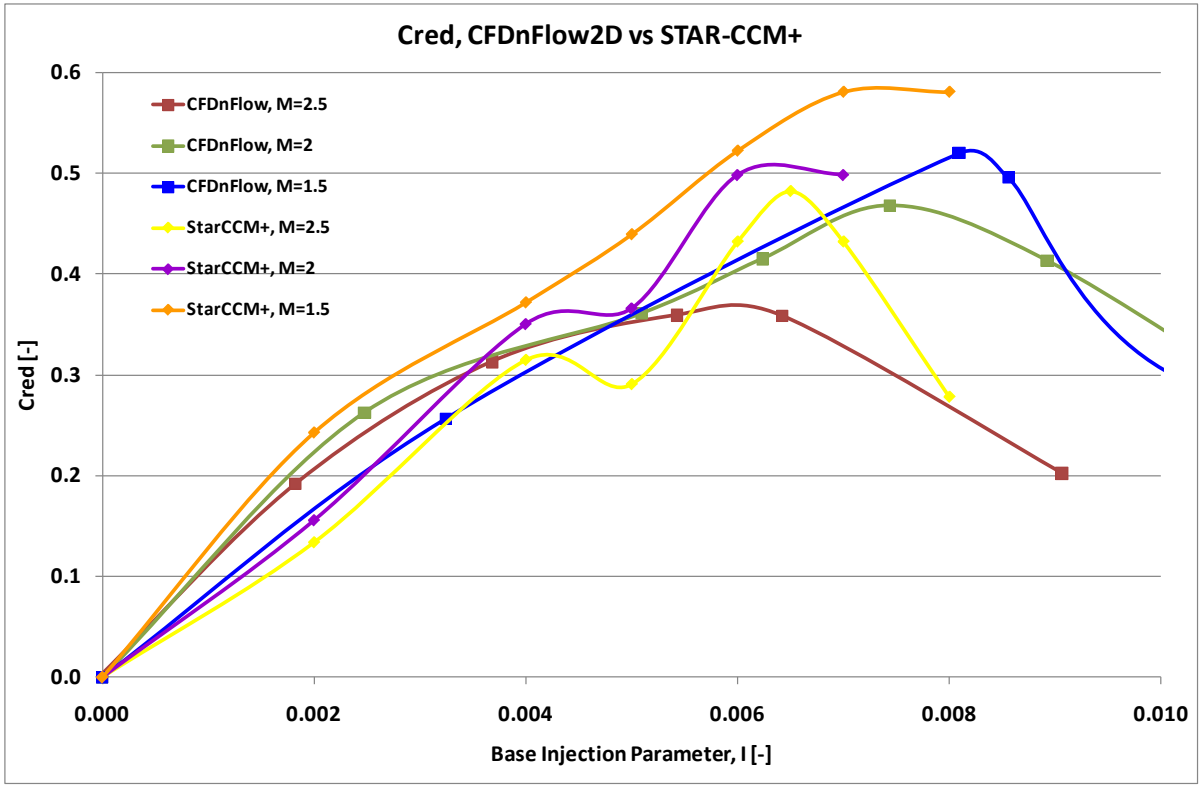

Validation of results

- The computed drag reduction factor, f_{dr} versus injection parameter and flight Mach number were introduced into an in-house developed trajectory model where the effect of the base bleed was included
  - The model uses the inert aerodynamic properties (drag versus flight Mach number) of the projectile as input
  - Once the inert aerodynamic properties have been determined, the base-bleed model which computes the gas generator influence on aerodynamics is invoked
    - This model computes the mass flow, base pressure and gas generator chamber pressure, using iteration, starting with an initial estimate of the base pressure
- Results from trajectory analyses using drag reduction factors from CFD analyses are compared with firing results at 27° and 61° elevations

Comparison firing results and trajectory analyses

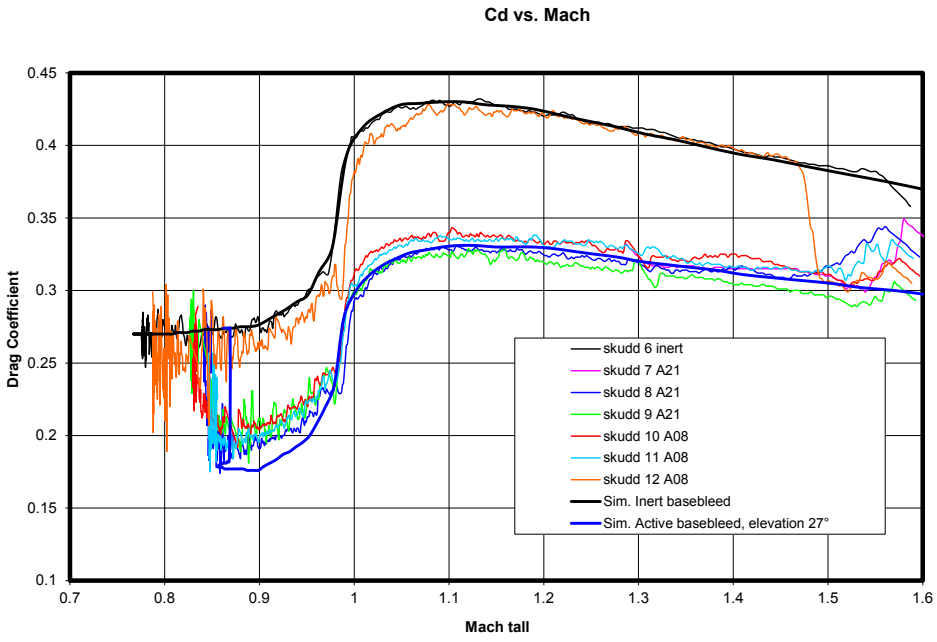

27° elevation

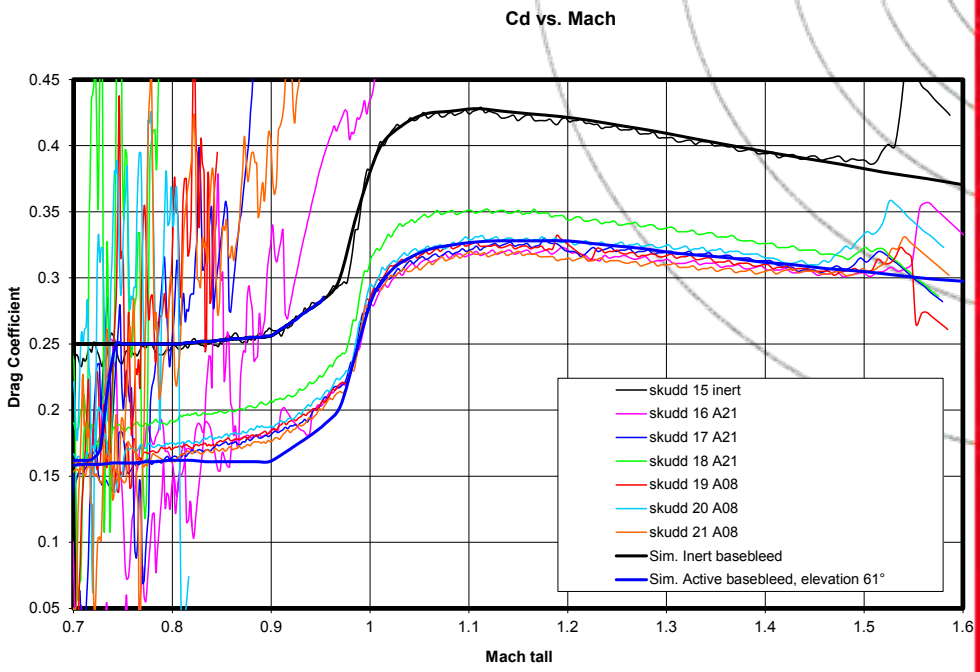

61° elevation

PRECISION PEOPLE TECHNOLOGY

Optimization of base bleed

- Due to the high local velocity in the vortex giving rise to suction in the base, it was decided to try slowing the vortex to recover some of the dynamic pressure and, hence, reduce the base drag

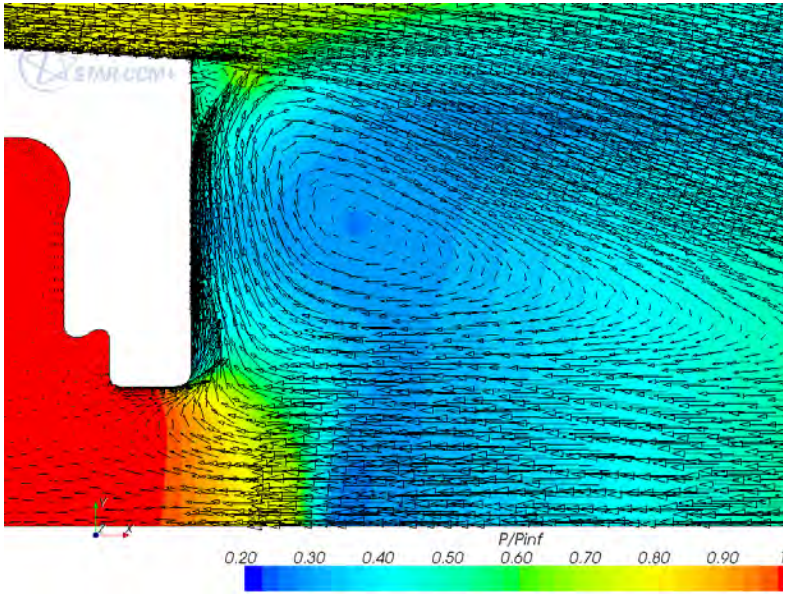

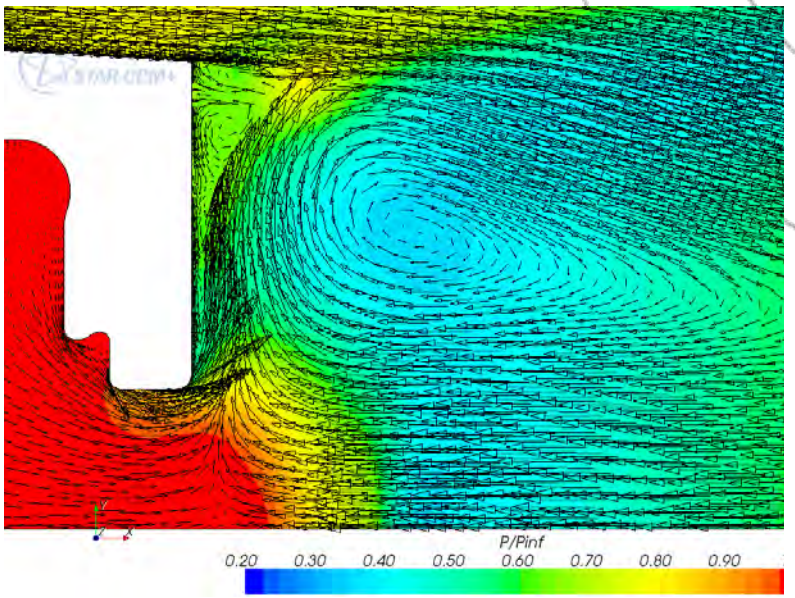

$$I = \frac{\dot{m}_b}{\rho_\infty V_\infty A_b}$$

Mach=2.5, I=0, no injection

Mach=2.5, I=0.004, with injection

Effect of base cavity

- Most efficient with Rc=60mm

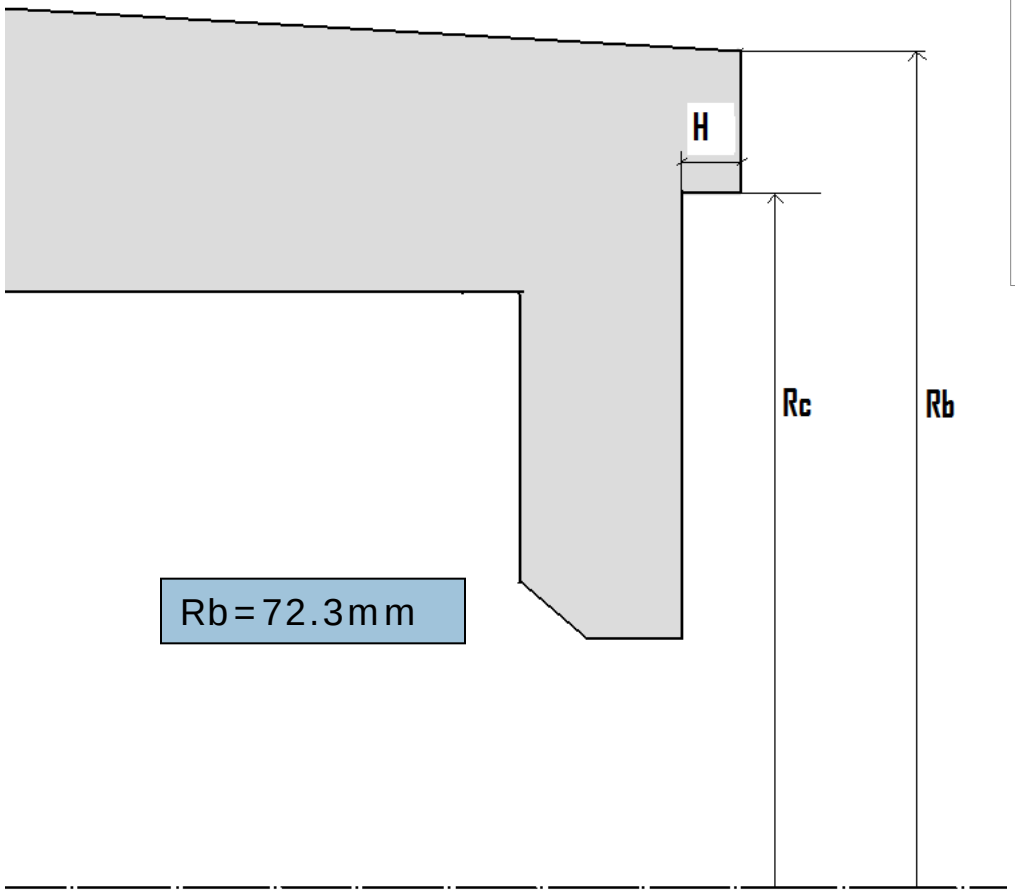

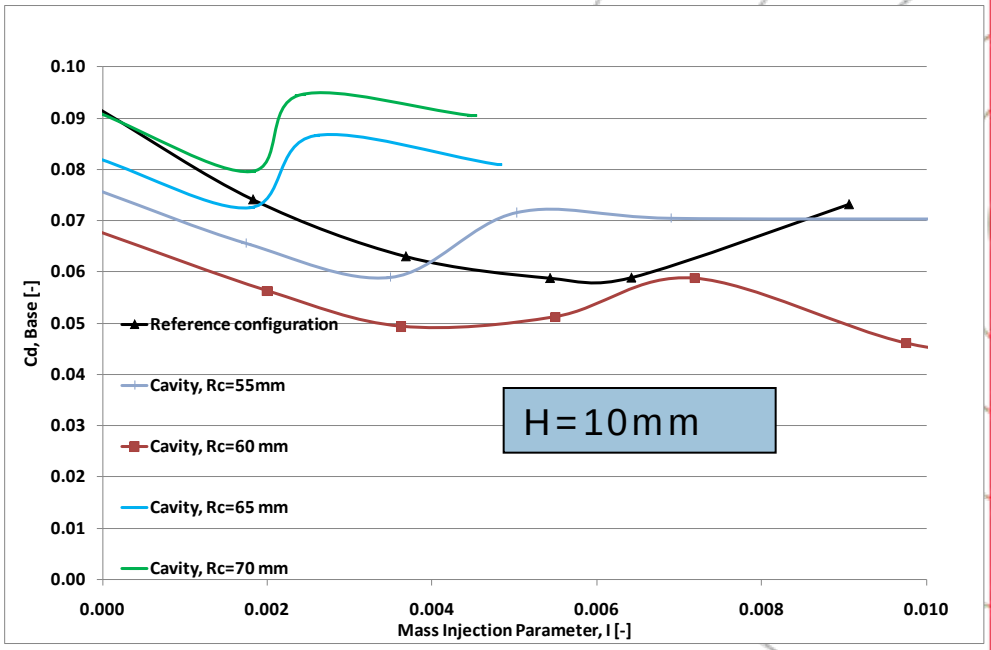

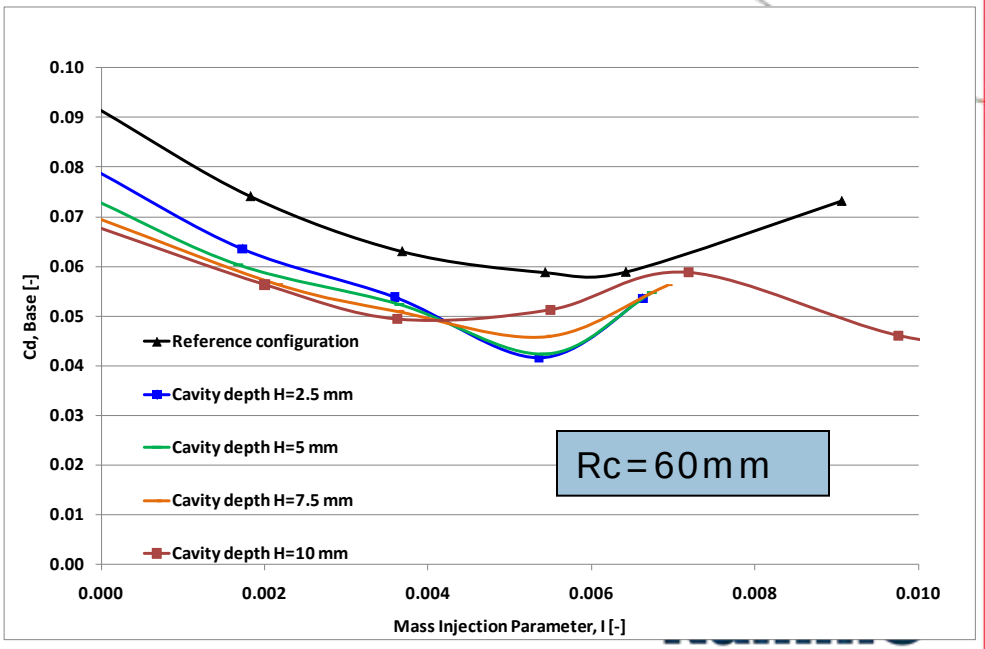

Effect of gas vent layout

- Most efficient with a hollow base having a thin rim protruding

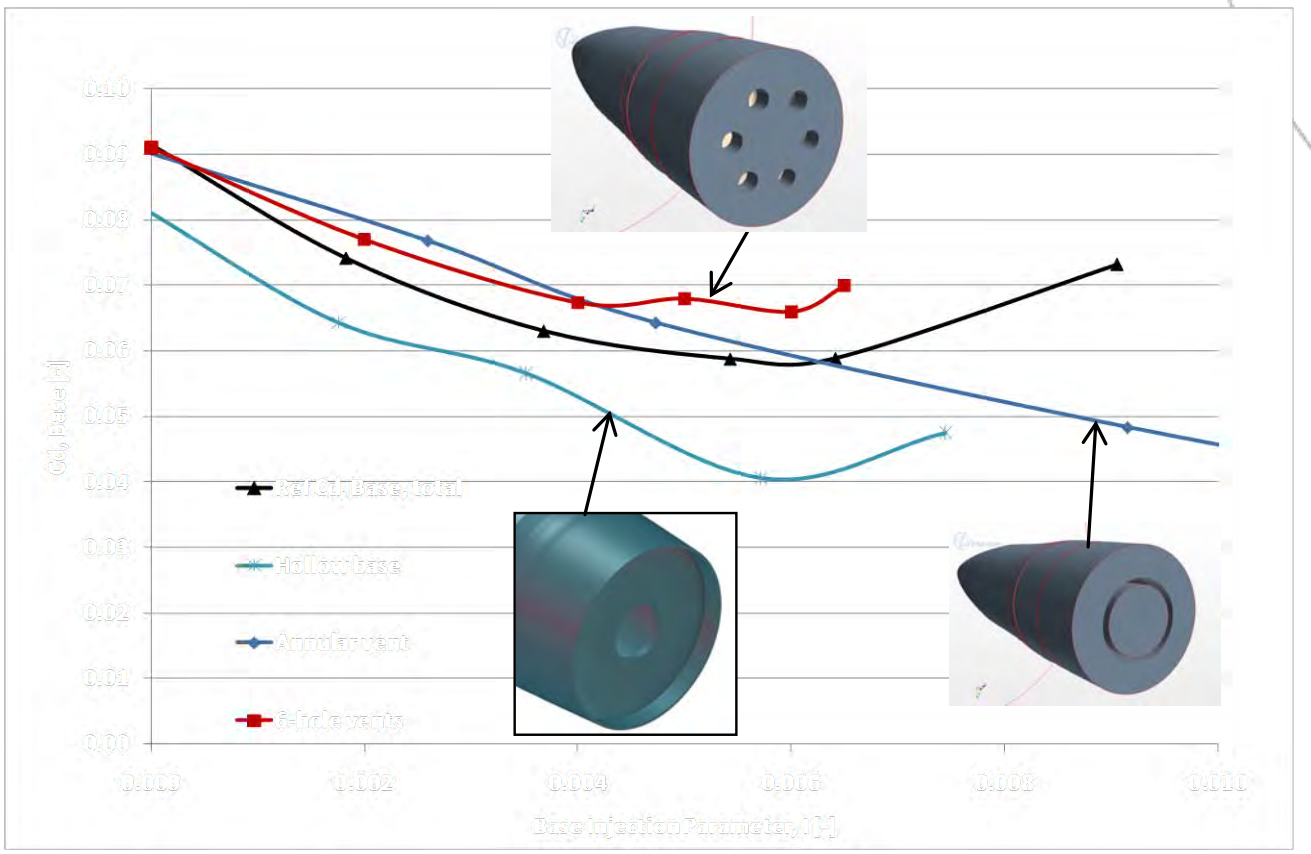

Conclusions

- Numerical tools was applied to the prediction of the 155mm Heer artillery shell performance, both in terms of projectile drag without base-bleed and the drag reduction with such a device
  - Two CFD codes for compressible flows were engaged, the in-house developed CFDnFlow code and the commercial available STAR-CCM+
  - Comparison of drag with available firing data showed good agreement for all supersonic speed
  - DES modelling approach improved the predictions of the effectiveness of the base-bleed device on base drag reduction
- By computing the drag reduction coefficient empirical expressions for base drag was derived enabling complete trajectory simulations
  - The computed trajectories for two elevations compared well with available firing data
- Using the CFD tools, the shape of the base was modified to achieve better pressure recovery, thus reduced base drag
  - Among the analyzed configurations, the one with a hollow base having a thin rim protruding was most efficient

26th International Symposium on Ballistics

Visualization and Analysis of Impact Damage in Sapphire

Elmar Straßburger ,
Parimal Patel and James W. McCauley (U.S. ARL)

Miami, September 13 2011

Fraunhofer EMI

Introduction

- Significant weight reductions when transparent ceramic is used as strike face on a glass-polymer laminate

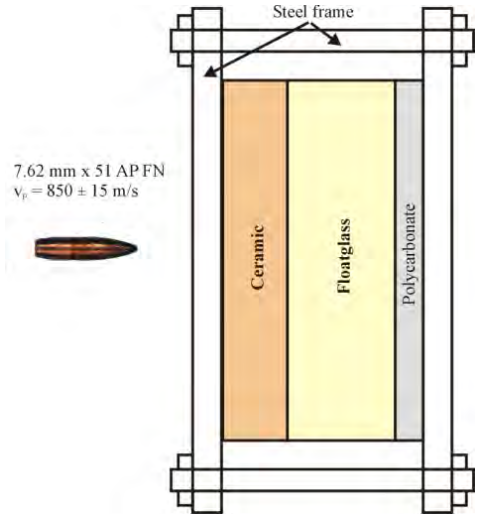

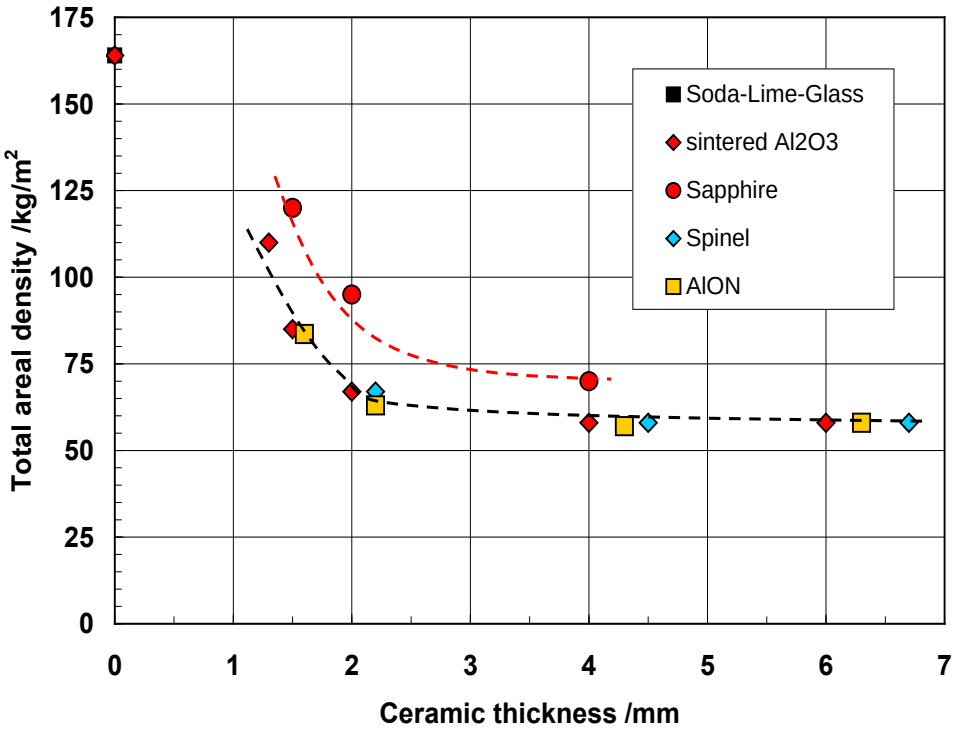

Fraunhofer EMI

Introduction

- High ballistic resistance is related to projectile deformation and erosion
- Ability to deform and erode the projectile depends on damage and failure mechanisms in target material
- Fragmentation of ceramic and glass layers plays a key role

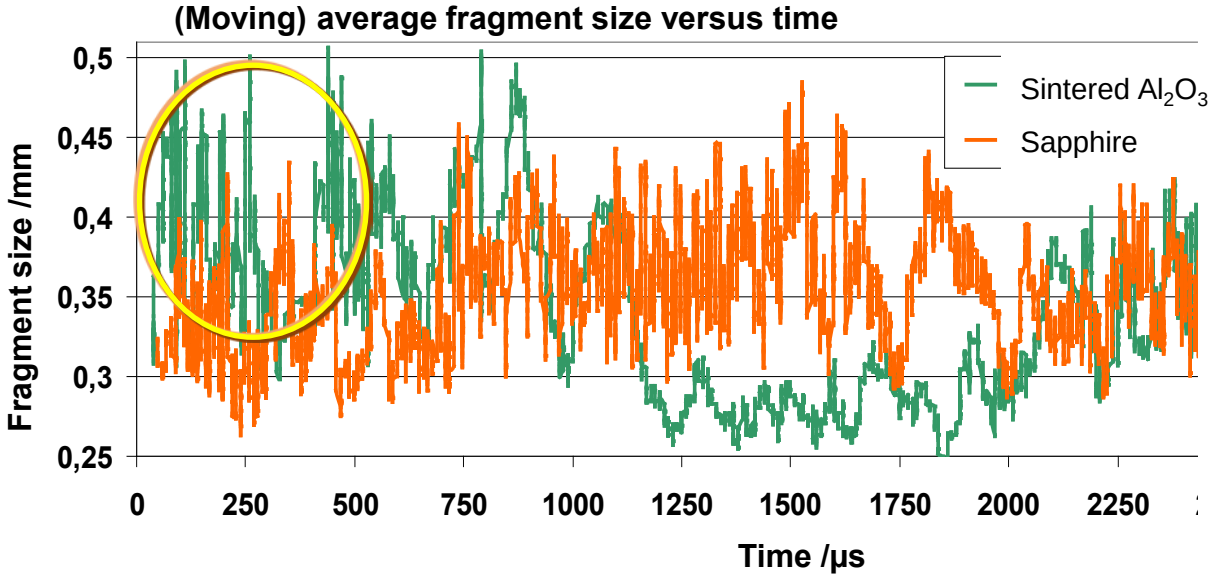

Fraunhofer EMI

Edge-On Impact Test Configuration

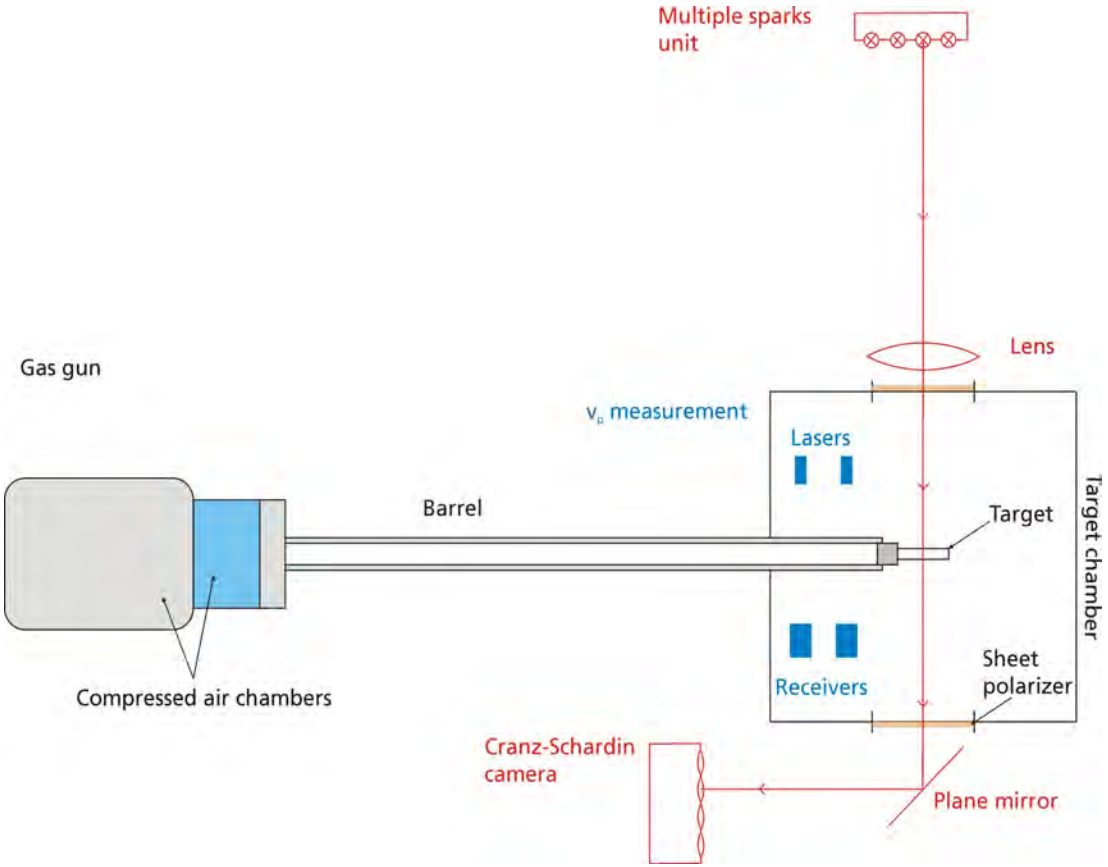

Close-up view of test sample set-up

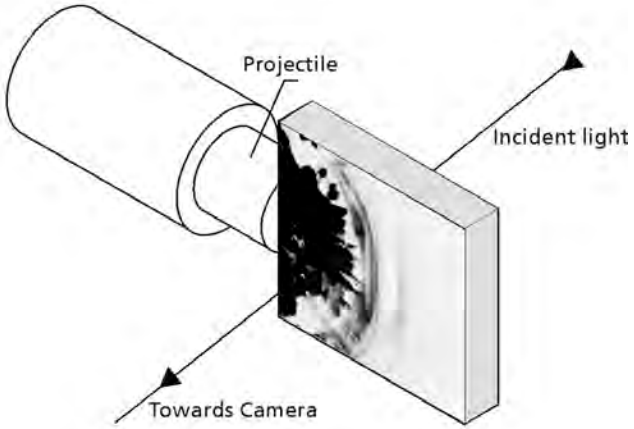

Fraunhofer EMI

Test Matrix

Sapphire crystal geometry and nomenclature

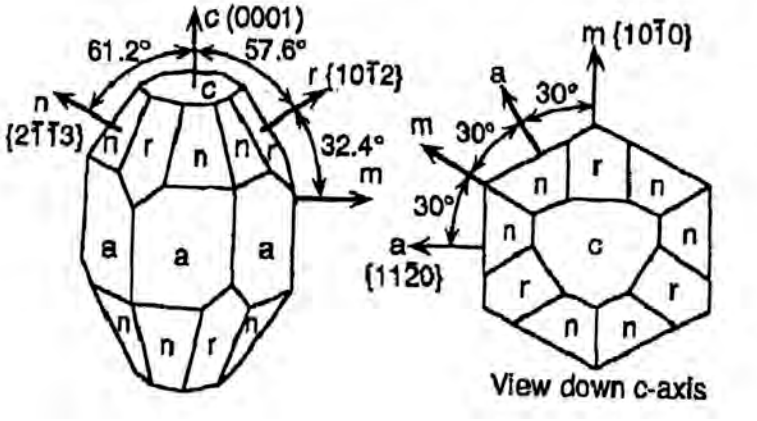

Schmidt and Harris, 1998; J. Am. Ceram. Soc. 81(4)

Config.	Impact Direction	Large Surface	Projectile	EMI Test #
1	a-axis (parallel)	c-plane	sphere	17074
			cylinder	17071
2	a-axis (parallel)	r-plane	sphere	17075
			cylinder	17069
3	c-axis (parallel)	a-plane	sphere	17076
			cylinder	17070
4	c-axis (perpendicular)	a-plane	sphere	17077
5		Edge surface r-plane	sphere	17359

Fraunhofer EMI

Sphere Impact

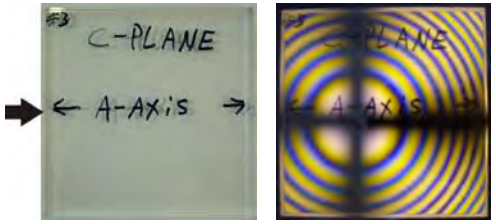

Impact velocity: 453 m/s

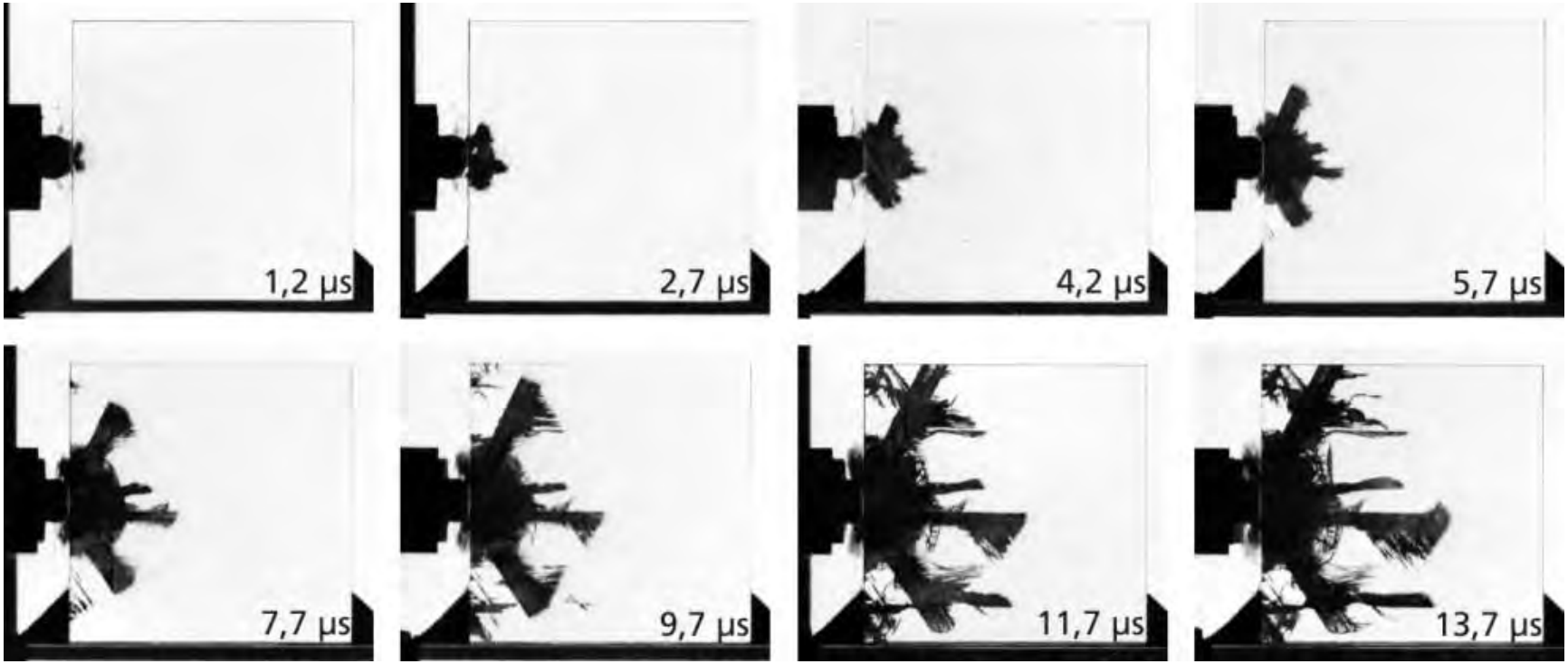

Path-time history of fracture propagation

Sphere impact parallel to a-axis; large surface c-plane

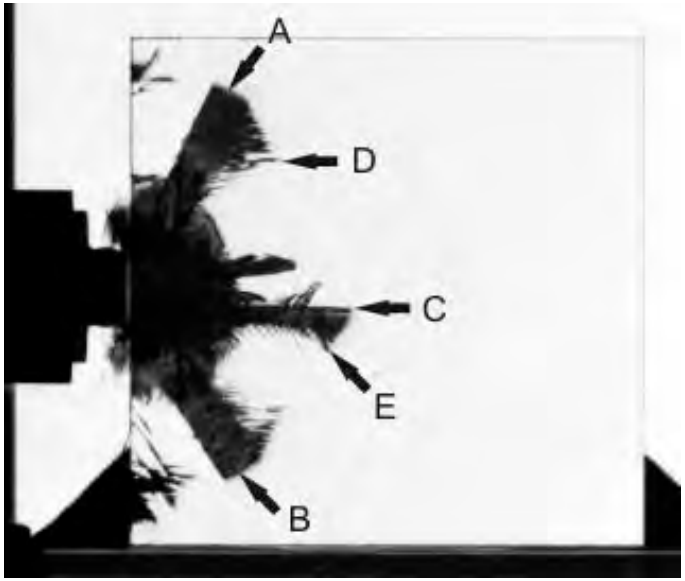

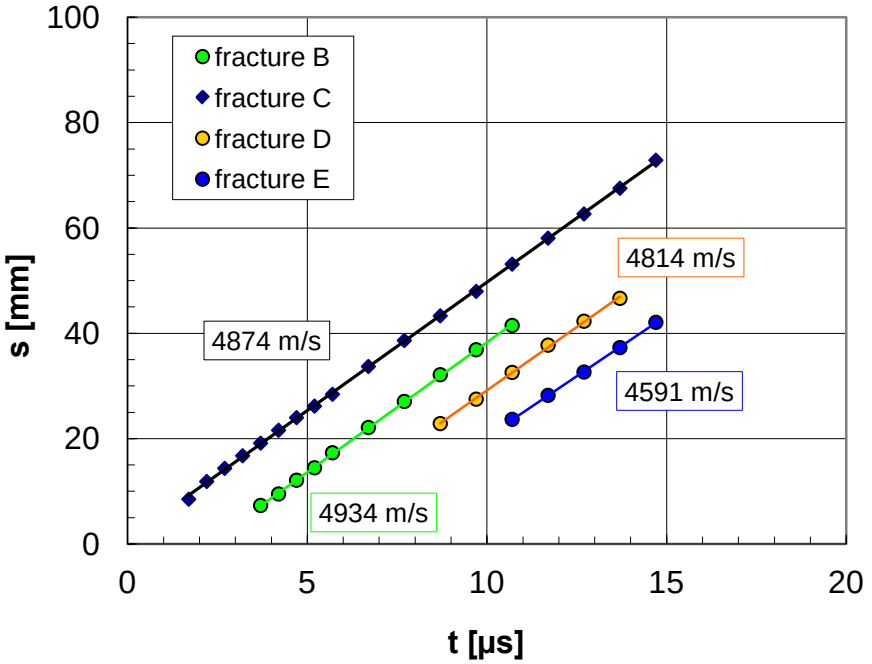

Fraunhofer EMI

Cylinder Impact

parallel to a-axis; large surface c-plane; v_P = 393 m/s

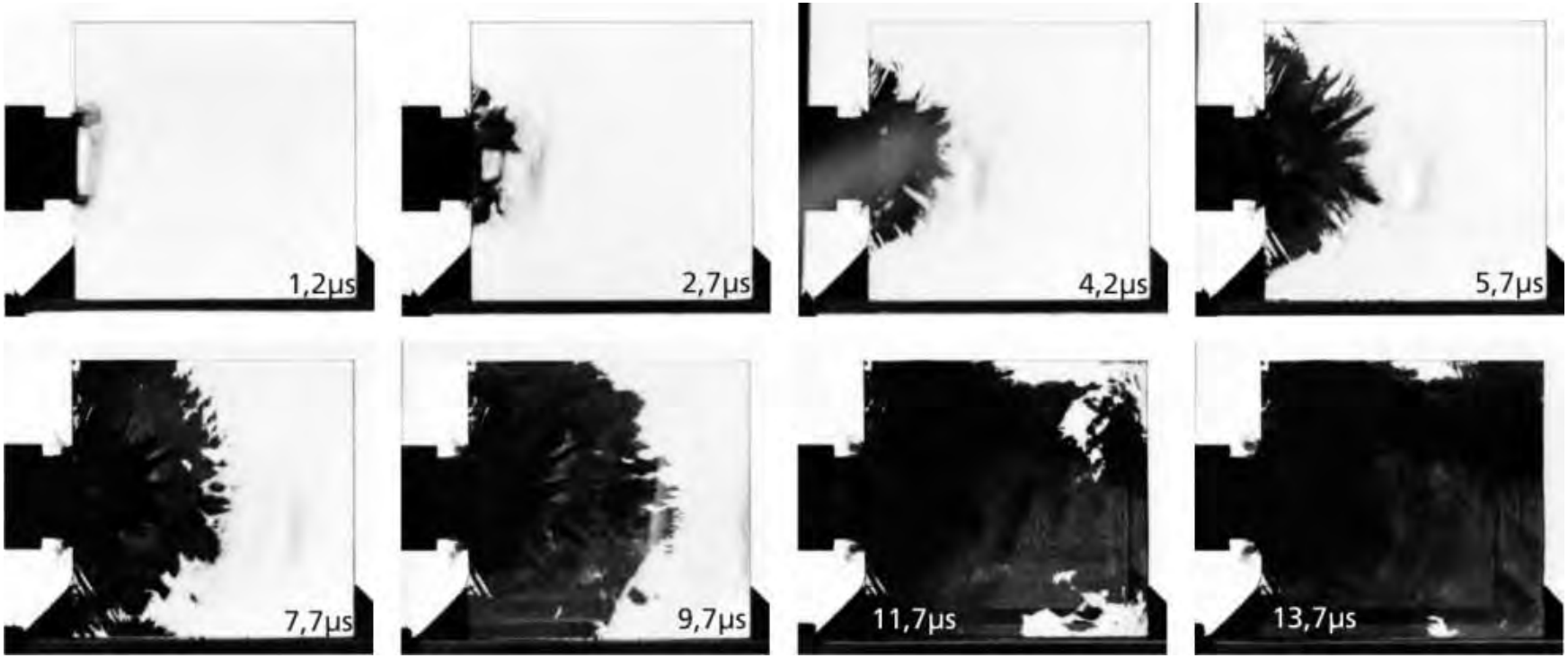

Fraunhofer EMI

Path-time histories of fracture and wave propagation

Cylinder impact parallel to a-axis; large surface c-plane

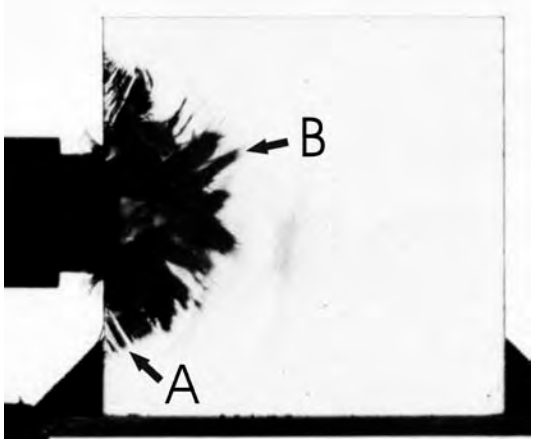

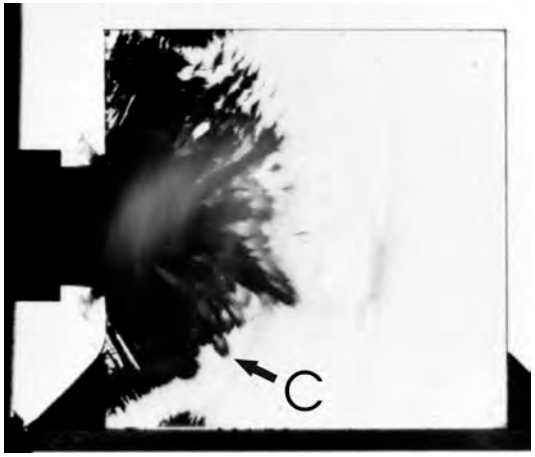

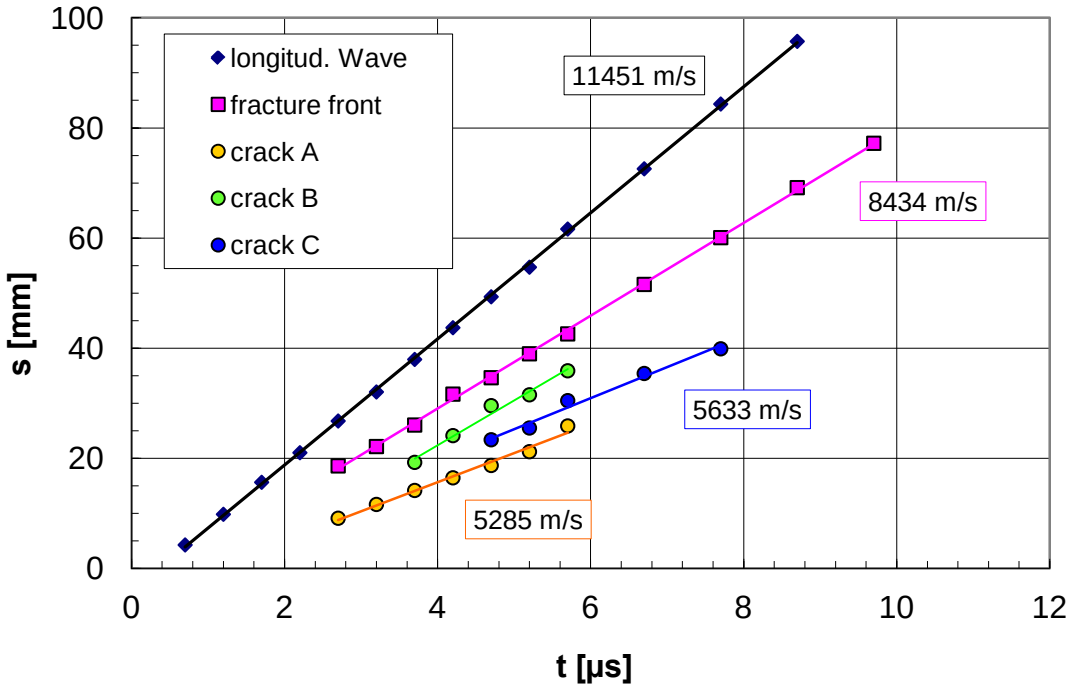

Fraunhofer EMI

Comparison of Damage and Cleavage Controlled Crack Propagation

Sphere impact

Parallel to a-axis

Large surface r-plane

v_S = 457 m/s

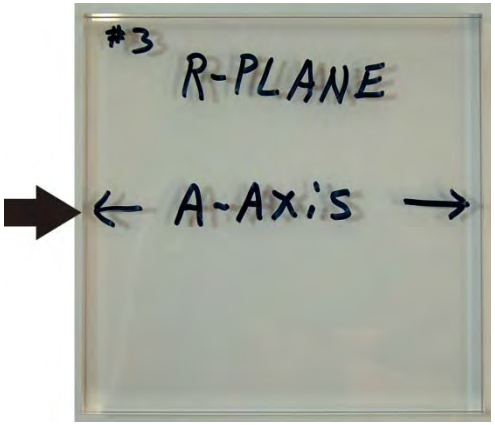

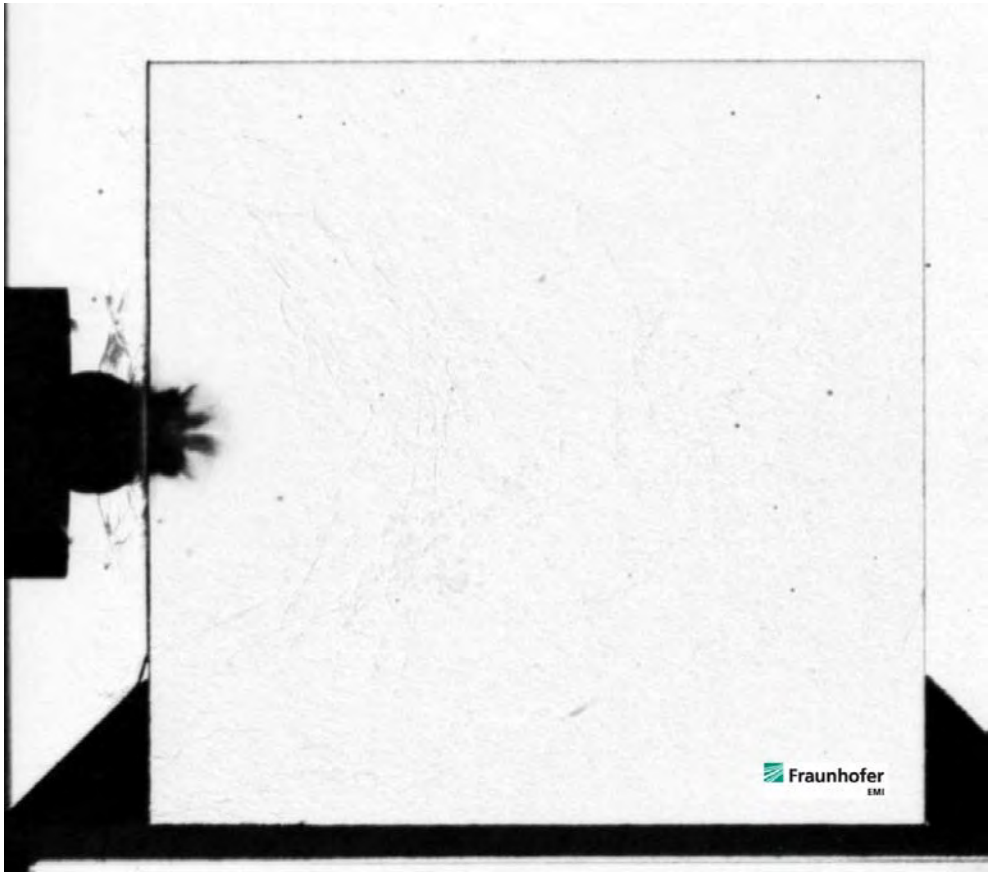

Comparison of Damage and Cleavage Controlled Crack Propagation

Sphere Impact, v_S = 450 m/s

Parallel to a-axis; Large surface r-plane

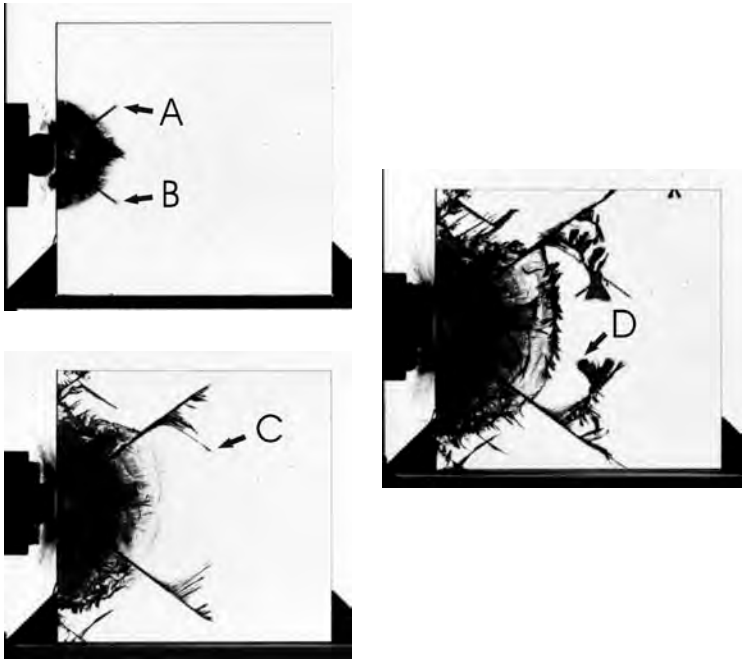

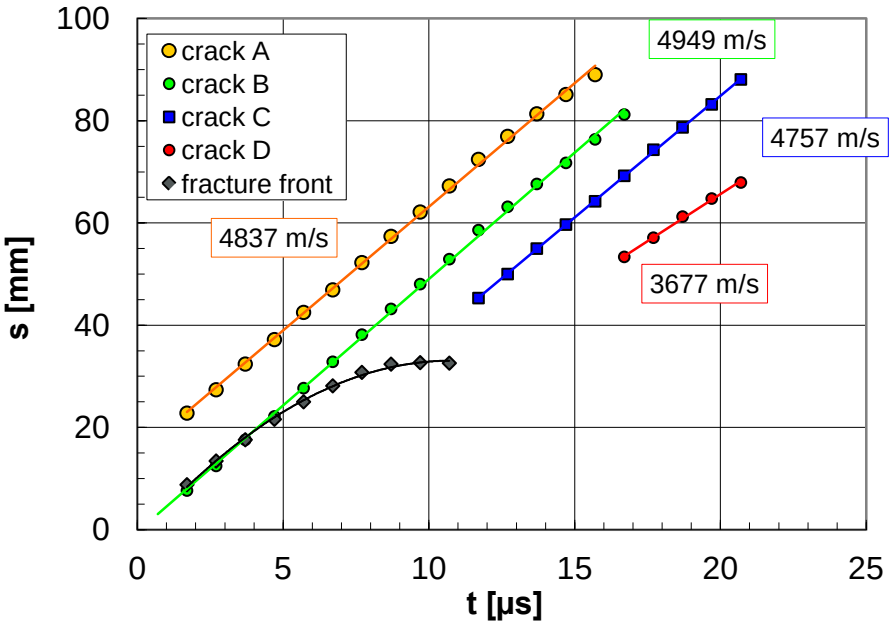

Fraunhofer EMI

Evidence of cleavage controlled crack propagation

Sphere impact, v_S = 450 m/s

Parallel to c-axis; Large surface a-plane

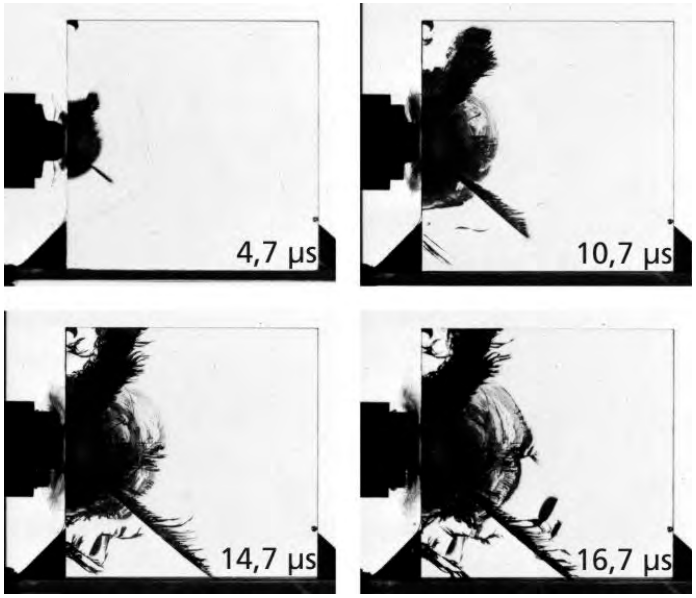

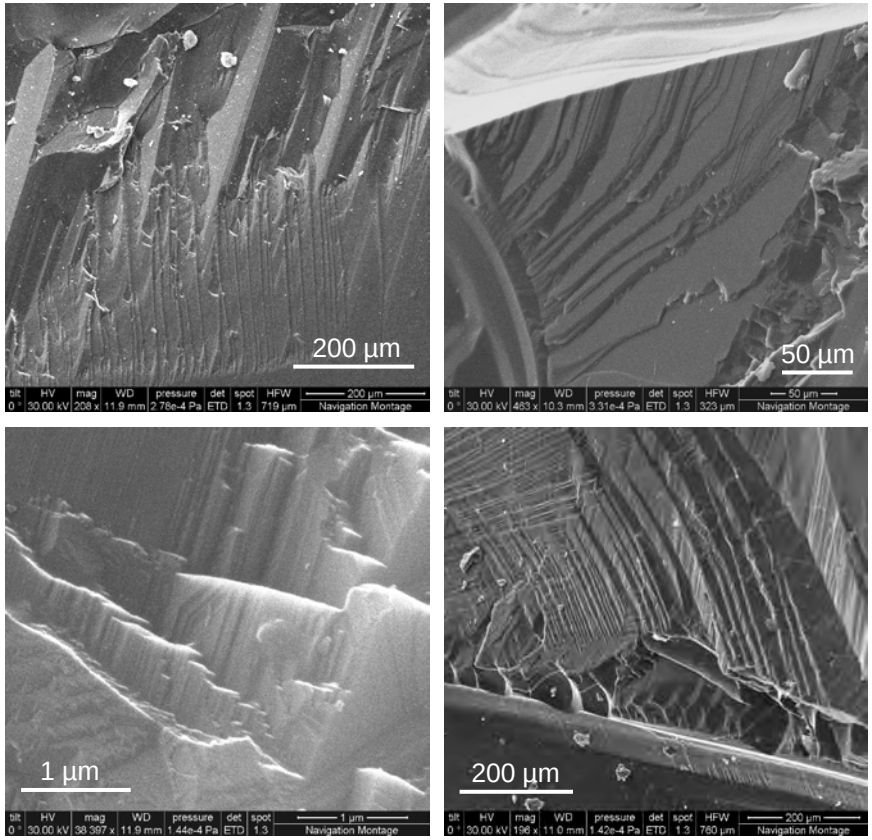

Cleavage energies

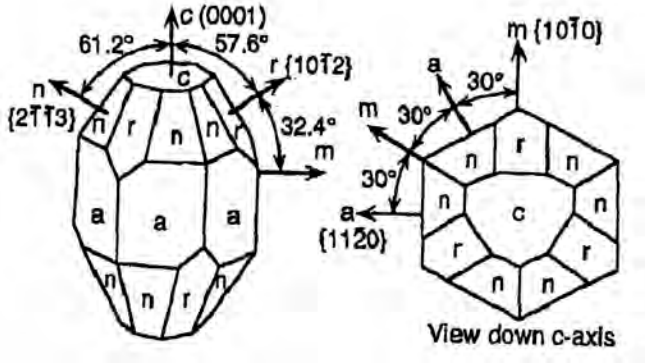

Cleavage plane			Theoret. Cleavage surface energy [J/m²]	Experimental cleavage energy [J/m²]	Fracture toughness K_{IC} MPa·m$^{1/2}$
c-plane	(0001)	basal plane	~6.5	21.54	4.54
r-plane	(10$\bar{1}$1)	rhombohedral plane		6.45	2.38
m-plane	(10$\bar{1}$0)	prismatic plane		11.43	3.14

From R. Bradt: “Cleavage of Ceramic and Mineral Single Crystals“, George R. Irwin Symposium, 1997

Fracture propagation in sapphire under ballistic impact

$(11\bar{2}0)$

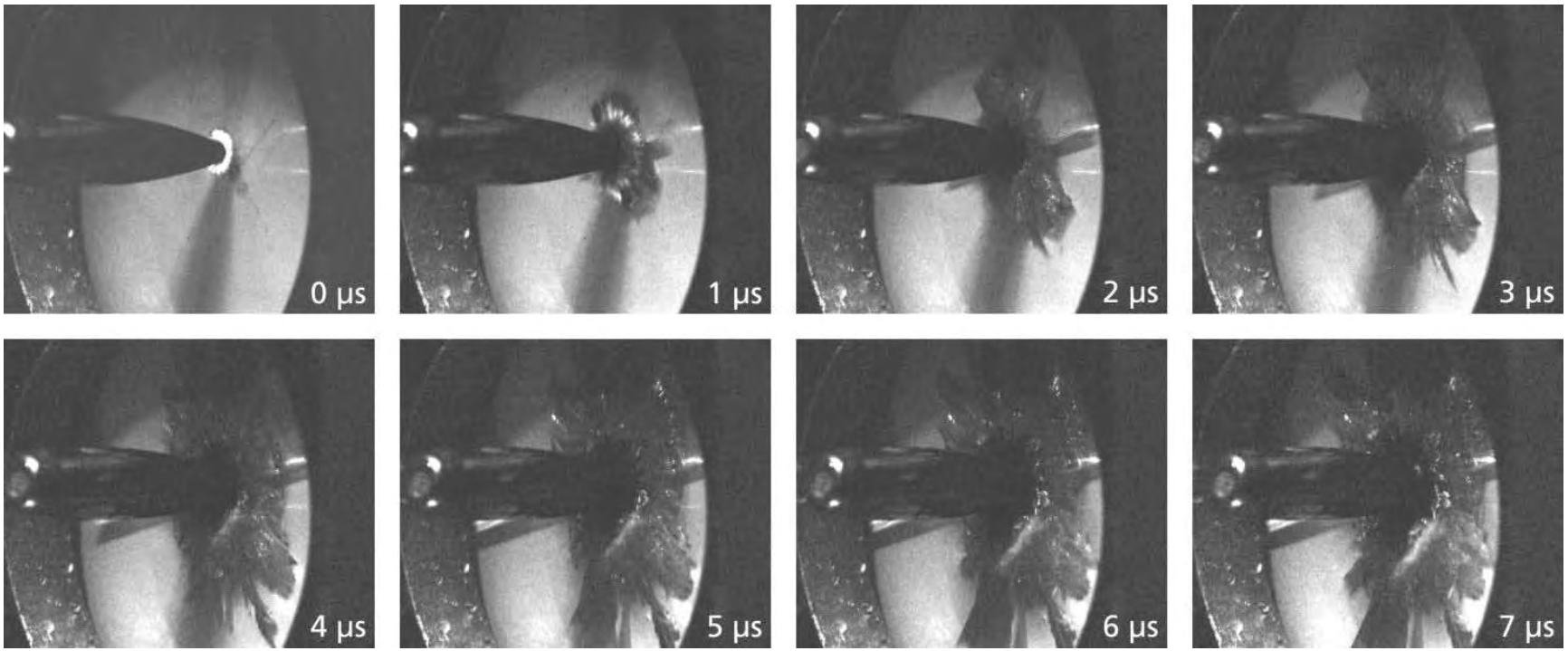

Fraunhofer EMI

Conclusion

- Edge-on impact tests have been conducted in order to generate a set of baseline data for fracture and wave propagation in Sapphire of different crystal orientation.
- At impact of steel cylinders fracture patterns were observed, similar to those in polycrystalline materials.
- In case of impact of spherical steel projectiles, fracture mainly followed cleavage planes of the crystal.
- Crack velocities were determined:
  - Maximum average crack velocity: 5438 m/s
  - Minimum average crack velocity: 3700 m/s

Overview of Analyzing Firearm, Tool Mark and Impression Evidence at the Miami-Dade Police Department

Gabriel A. Hernandez, M.S.

Miami-Dade Police Department

Introduction and Fundamental Principles
(Part 1 of 8)

Firearm and Tool Mark Identification vs. *Forensic Ballistics*

- *Ballistics* deals with the motion of a projectile and the forces which cause and affect this motion.
- *Firearm and Tool Mark Identification* is not concerned with this, but rather the marks imparted from the gun to the bullet and/or casing.
- “Forensic Ballistics” is therefore an improper term that is used, although incorrectly, to describe this discipline of Forensic Science.
- Practitioners prefer the title of “Firearm and Tool Mark Identification” instead of “Forensic Ballistics.”

Evidentiary Value

- **A component of ammunition (casing and/or projectile) from the crime scene can be identified to the firearm that fired it to a reasonable degree of scientific certainty.**

- **A firearm leaves it's unique "fingerprint" on components of ammunition fired in that firearm. This "fingerprint" is in the form of unique impressions or striations also known as a tool marks.**

- **Casing or projectile evidence from a crime scene identified to a firearm in the possession of a potential suspect would represent strong evidence against that suspect.**

Components of Ammunition (anatomy of a cartridge)

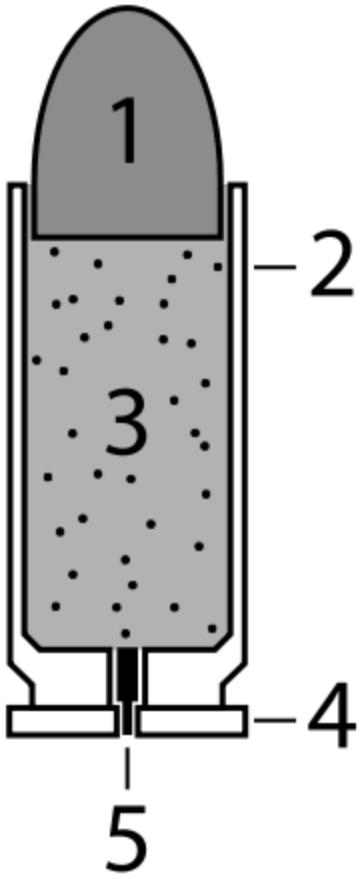

- 1. bullet/projectile
- 2. casing
- 3. gunpowder
- 4. head of casing
- 5. primer

- After firing, one cartridge becomes two pieces of evidence (a projectile and a casing)

Connection to Interior Ballistics

- Firearm and tool mark examiners are concerned with what happens inside the chamber and bore during the firing sequence.

- While the ballistics industry is interested in optimizing the performance of a load by studying breech pressures and primer efficiency. FA-TM examiners are interested in the impressed or striated markings left on the ammunition components from the interior (breech, chamber, barrel) of the gun.

- These marks are transferred to the surface of ammunition components as a result of the pressures involved with setting off a unit of ammunition.

Search for fired evidence

- It is important that the crime scene investigator is thorough in his/her search for fired evidence.
- Ejected casings:
  - Behind, under, and on top of furniture (inside)
  - In grass, under parked cars (outside)
  - If firearm fired in car…between cushions, under seats, down dash board

Search of fired evidence (cont.)

- Projectiles can be found in walls, tree bark, the ground, within a body (medical examiner), within car cushions or furniture cushions, etc., etc.
- Spent projectiles will have land/groove markings.
- Fired casings will have breech face marks, firing pin impressions, extractor marks, ejector marks, chamber marks.

Fundamentals of Firearm & Toolmark Identification

- Definitions
- Fundamental Propositions (1 & 2)
- Examination Method
- Range of Conclusions

Definition:
Firearm & Toolmark Identification

An empirical comparative analysis that can determine if a striated or impressed mark was produced by a particular tool.

Definition: *Tool*

The harder of two objects that comes into forceful contact with one another, resulting in the softer object being marked.

Definition: *Toolmark*

Features imparted on an object by the contact and force exerted from a tool.

- *Two Types:*
  - Impressed Toolmarks
  - Striated Toolmarks

Definition: *Impressed Toolmark*

Features produced when a tool contacts an object with enough compressive force that it leaves an impression.

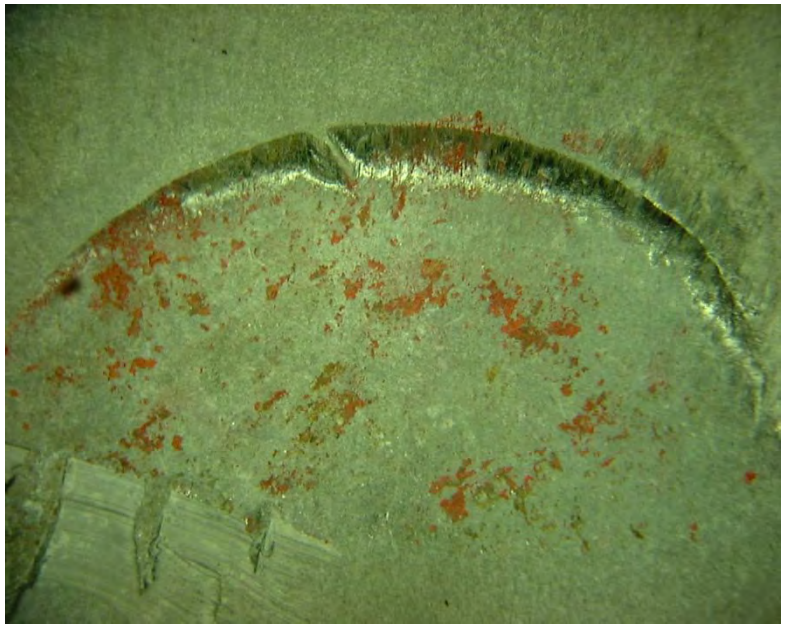

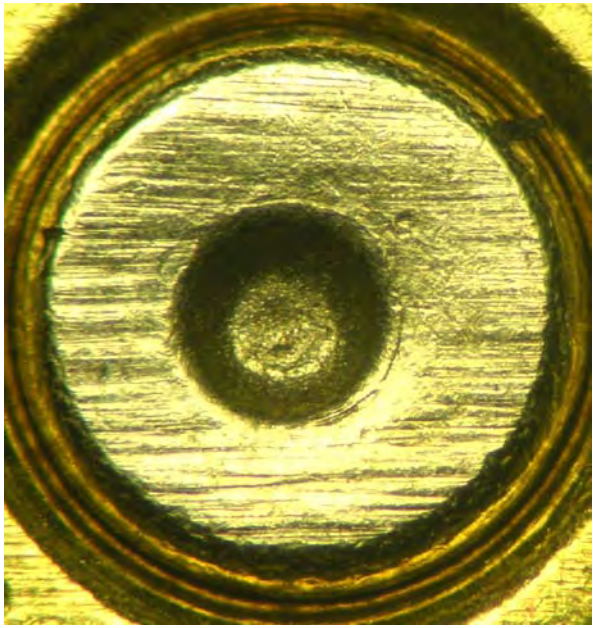

Definition: *Striated Toolmark*

Features produced when a tool contacts an object with lateral force and motion.

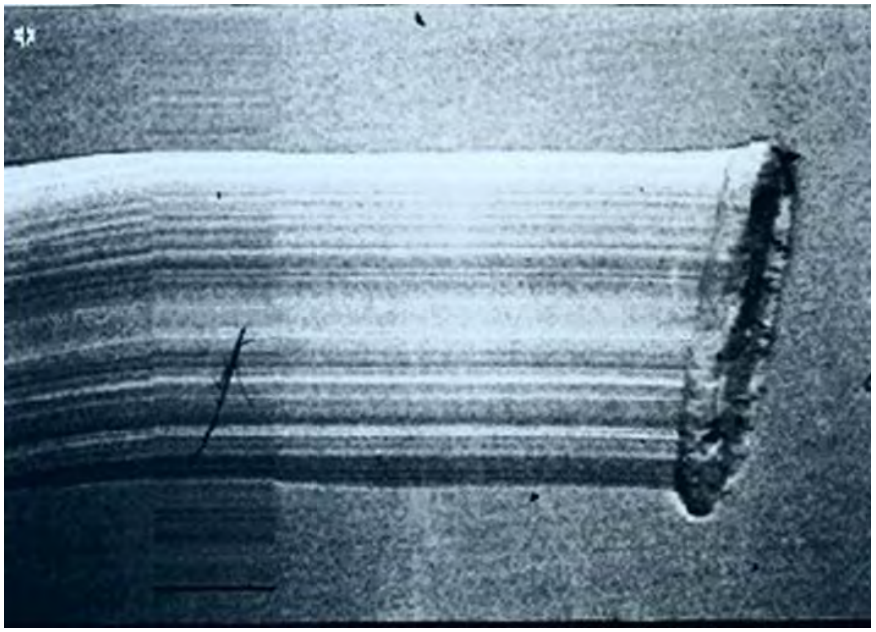

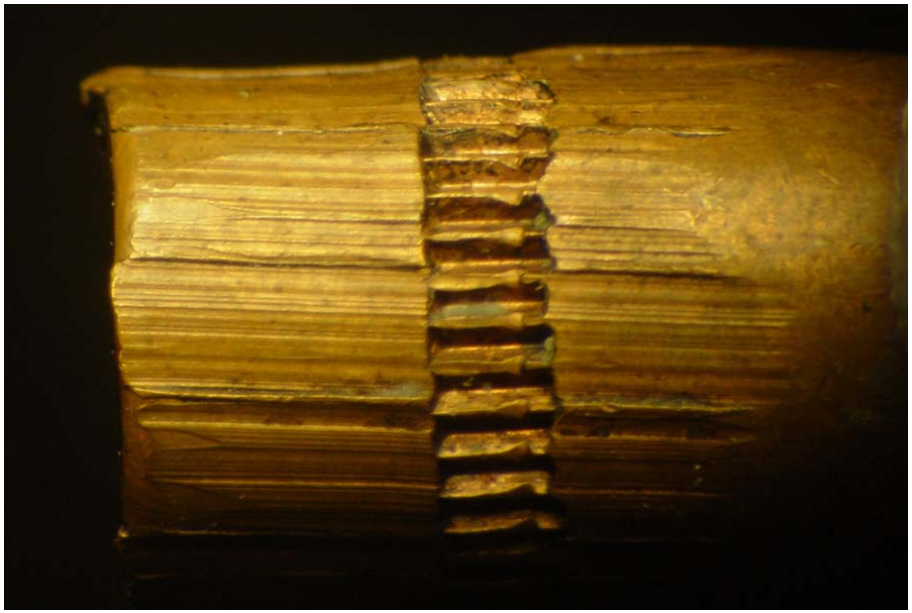

The Science of Firearm & Toolmark Identification is based on two fundamental propositions:

Proposition #1

Toolmarks imparted to objects by different tools will rarely if ever display agreement sufficient to lead a qualified examiner to conclude the objects were marked by the same tool. That is, a qualified examiner will rarely if ever commit a false positive error (misidentification).

Pattern Matching

- FA-TM examiners use pattern matching.
- Pattern matching: A visual comparative examination of the topographical features of two different toolmarks.
  - The relative height or depth, width, curvature, and spatial relationship of the features are defined for one toolmark and are then compared to the corresponding topographical features in the other toolmark.

Proposition #2

Most manufacturing processes involve the transfer of rapidly changing or random marks onto work pieces such as barrel bores, breech faces, firing pins, screwdriver blades, and the working surfaces of other common tools. This is caused principally by the phenomena of chip formation and tool wear, or by electrical/chemical erosion. Microscopic marks on tools may then continue to change from further wear, corrosion, or abuse.

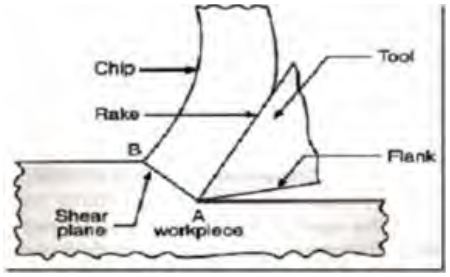

- Manufacturing operations create microscopic random imperfections on/in work pieces that give rise to the individual characteristics on bullets and cartridge casings.
- This is even true with firearm components manufactured in consecutively.

Definition: *Class Characteristics*

General and/or measurable features of a specimen which indicate a restricted group source. They result from design factors, and are therefore determined prior to manufacture.

Examples of Class Characteristics

Known Source:
Rifling

Questioned Item:
Bullet

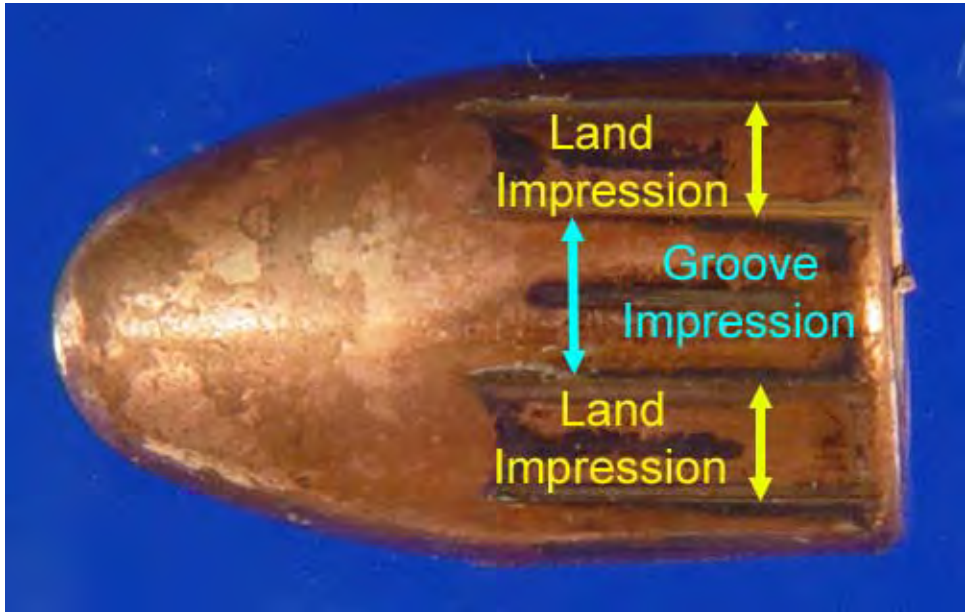

Examples of Class Characteristics

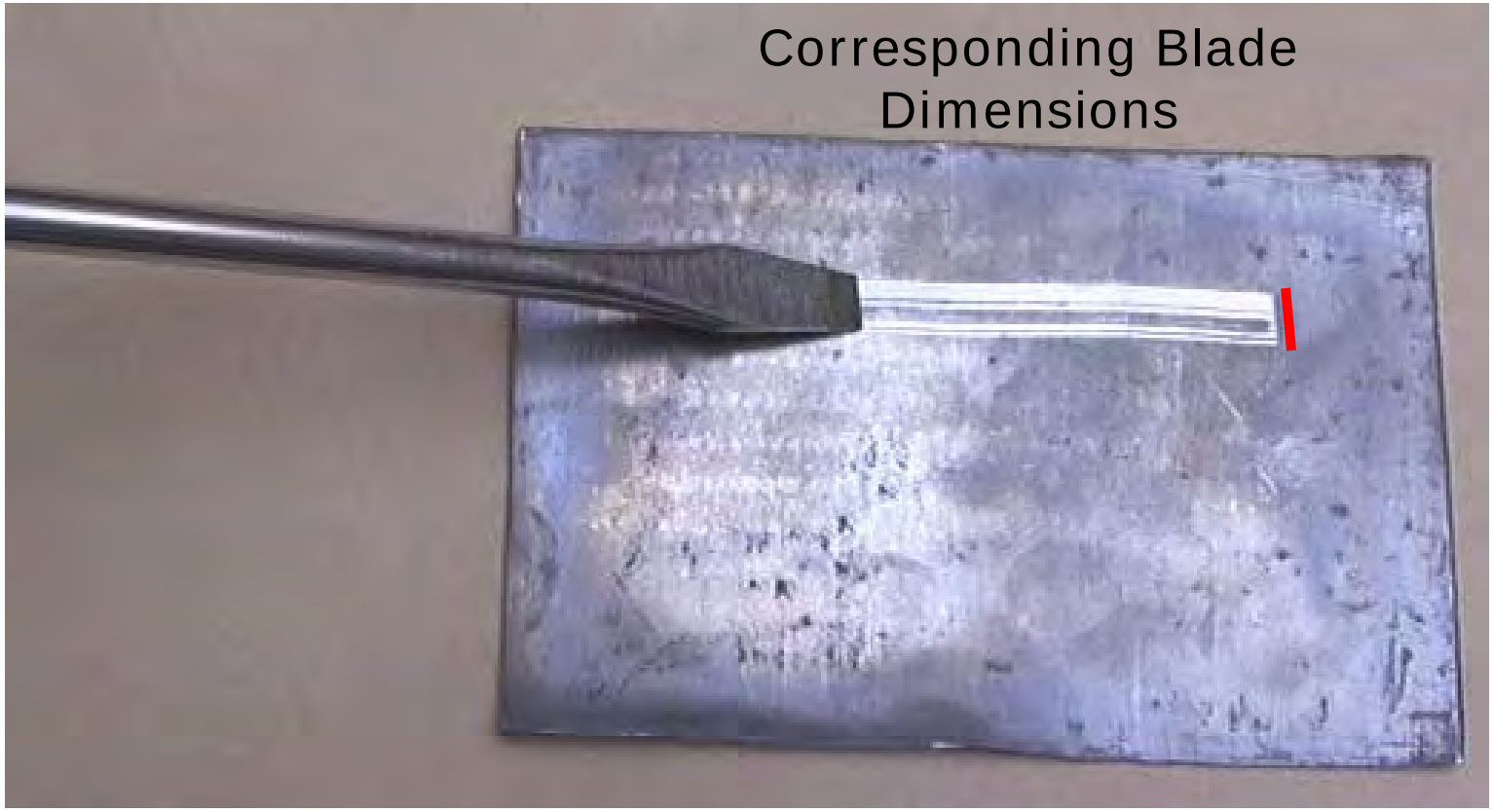

Definition: *Subclass Characteristics*

Features that may be produced during manufacture that are consistent among some items fabricated by the same tool. These are not determined prior to manufacture and are more restrictive than class characteristics.

Example of Subclass

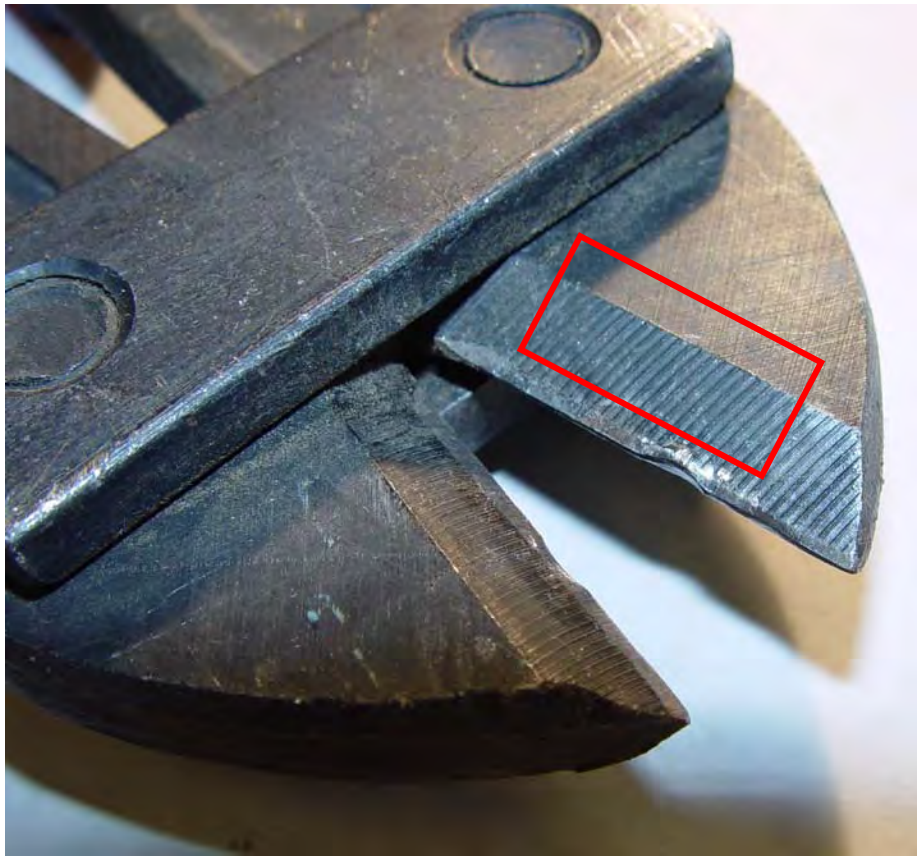

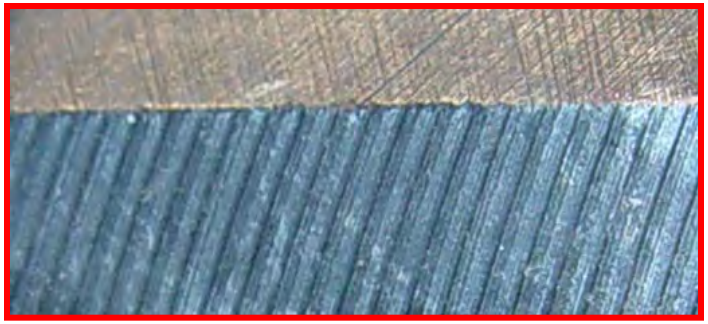

How are individual characteristics produced?

These random imperfections or irregularities can be produced by:

- Manufacture
- Wear from Use
- Wear from Abuse

Example of Individual Characteristics from Manufacture

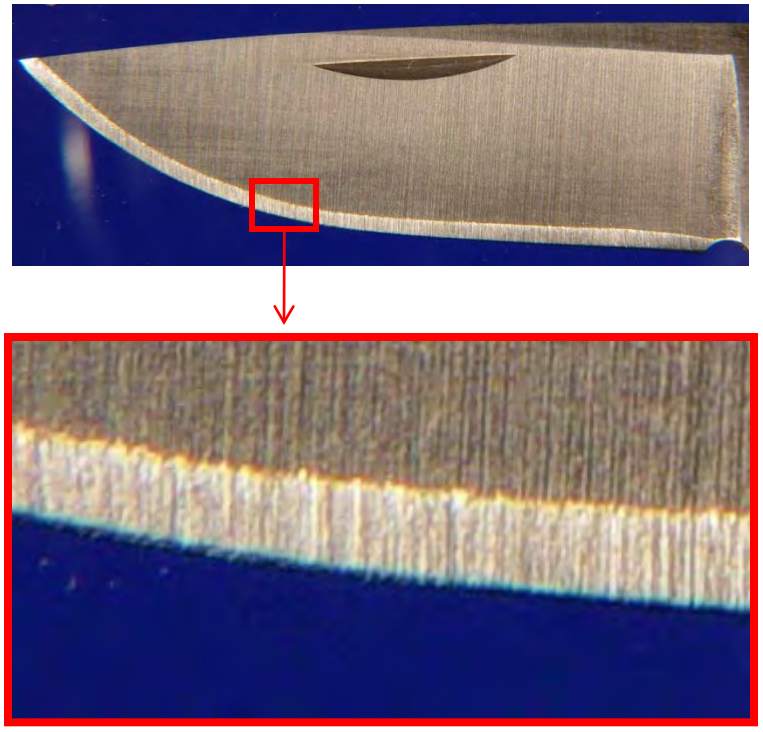

Example of Individual Characteristics from Wear

Use

Abuse

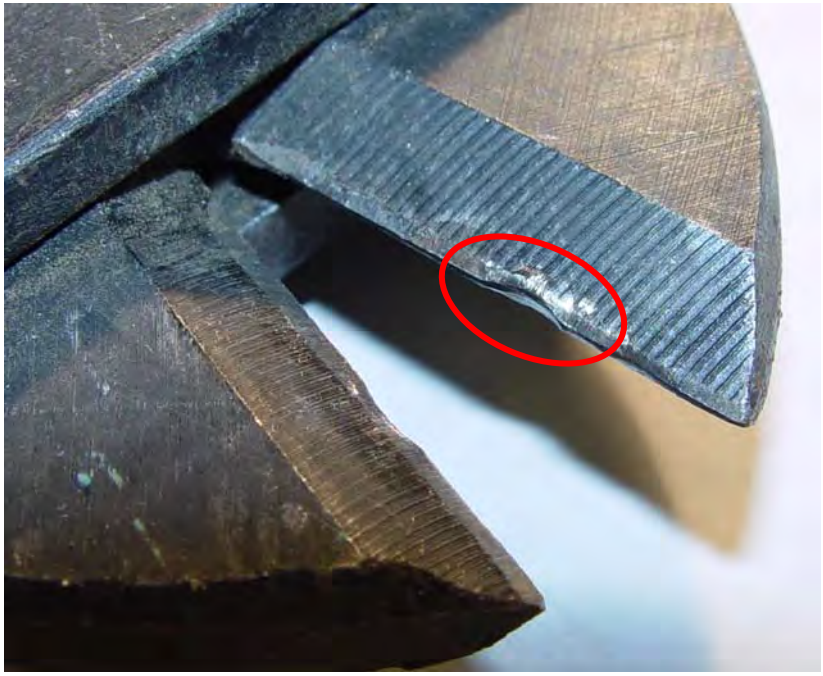

Examination Process

Level 1 analysis - *Class Characteristics*

- Elimination, but not individualization, can occur here

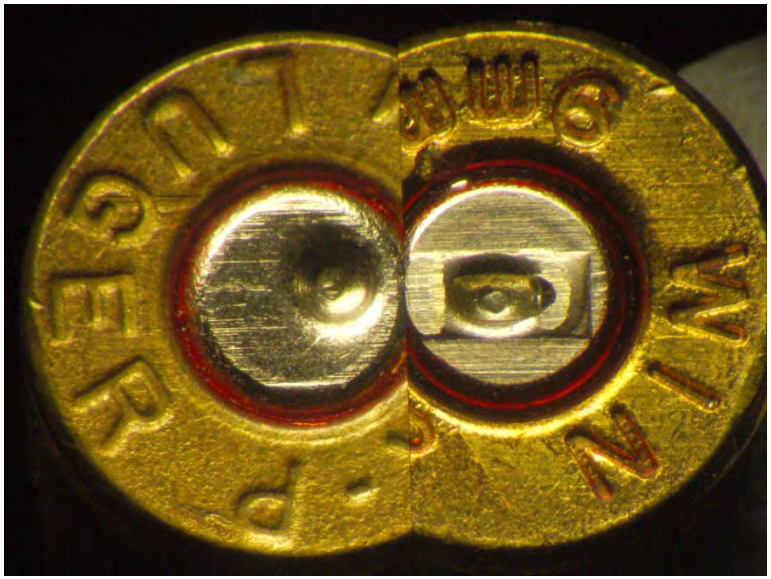

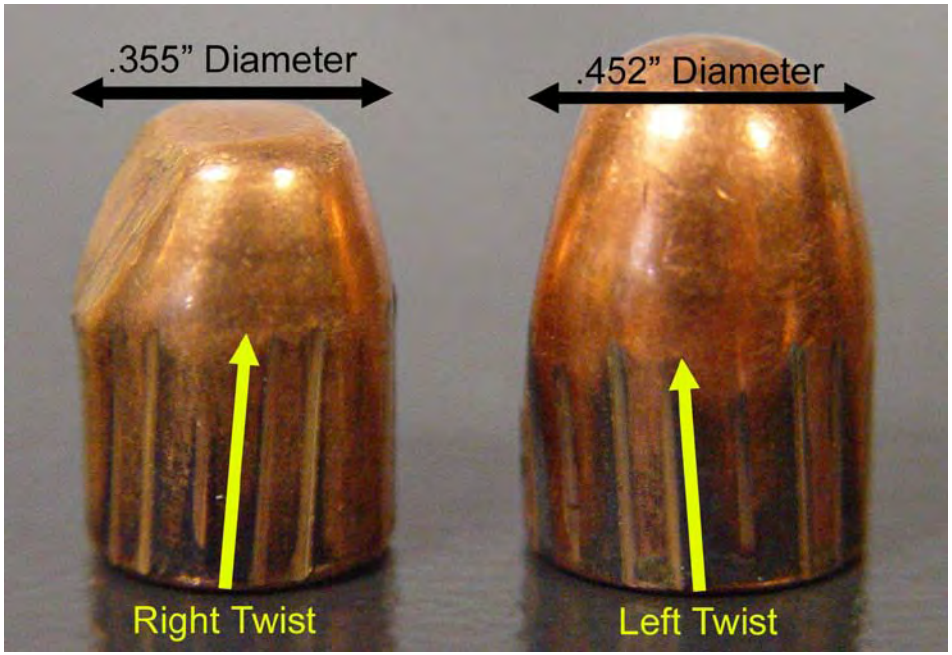

Examination Process

Level 2 analysis - *Comparison Microscopy*

- Individualization occurs only here

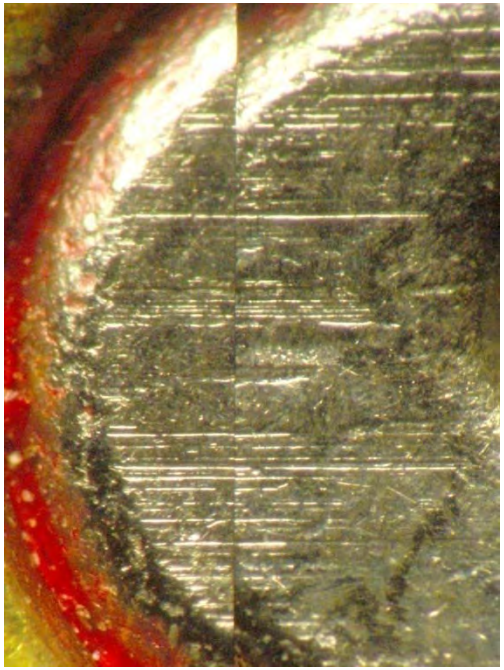

The Comparison Microscope

- The comparison microscope serves as the single most important tool to a firearms examiner.
- Two bullets or two casings can be observed and compared simultaneously within the same field of view.
- The longitudinal striations between two bullets must coincide for there to be a match.
- The breech face impressions and/or firing pin impressions must coincide for there to be a match between two casings.

Range of Conclusions

- Identification
- Inconclusive
- Elimination

Identification with unique marks.

- Unique variations and irregularities caused by scratches, nicks, breaks, and wear may permit the forensic scientist to relate:
  - A spent projectile to a firearm (striations), a fired casing to a firearm (impressions)
  - A scratch or abrasion mark to a single tool (striated and impressed)
  - A tire track to a particular automobile, a shoe print to a particular shoe (both impressed)

Bullet Comparisons (Part 2 of 8)

Firearm Barrel Markings

- The inner surface of the barrel of a gun leaves its markings on a bullet passing through it.
- These markings are peculiar to each gun.
- The gun barrel is produced from a solid bar of steel that has been hollowed out by drilling, then reaming.
- The microscopic reaming marks left on the barrel's inner surface are randomly irregular and serve to impart a uniqueness to e

Firearm Barrel Markings

- The manufacture of a barrel also requires impressing its inner surface with spiral grooves, a step known as rifling.
- The surfaces of the original bore remaining between the grooves are called ***lands.***
- The grooves serve to guide a fired bullet through the barrel, imparting a rapid spin to insure accuracy.

Firearm Barrel Markings

- The diameter of the firearm barrel, measured between opposite lands, is known as **caliber**.
- Once a manufacturer chooses a rifling process, the class characteristics of the weapon's barrel will remain consistent, each will have the same number of lands and grooves, with the same approximate width and direction of twist.

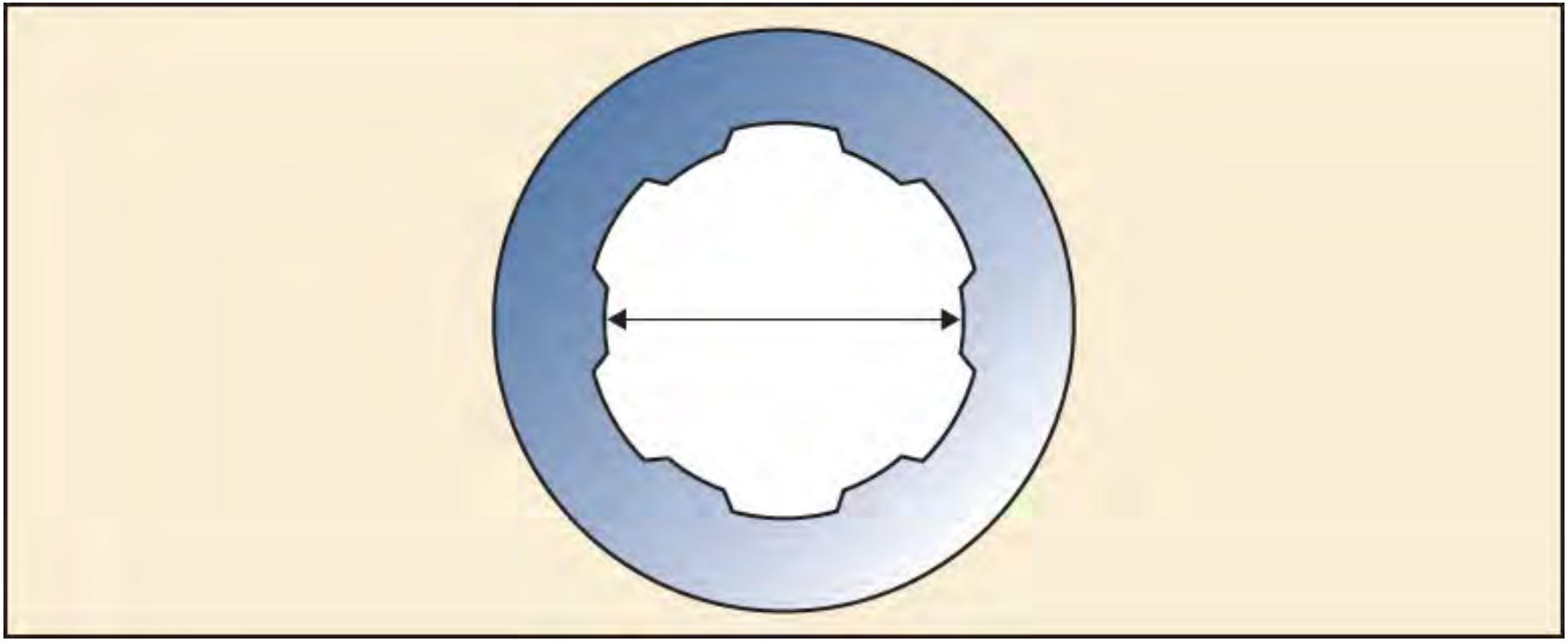

Cross-section of a barrel with six grooves. The diameter of the bore is the caliber.

- Lands and grooves give a spin to a projectile allowing it to stay true on its trajectory.
- Lands and grooves are made during the manufacturing process.

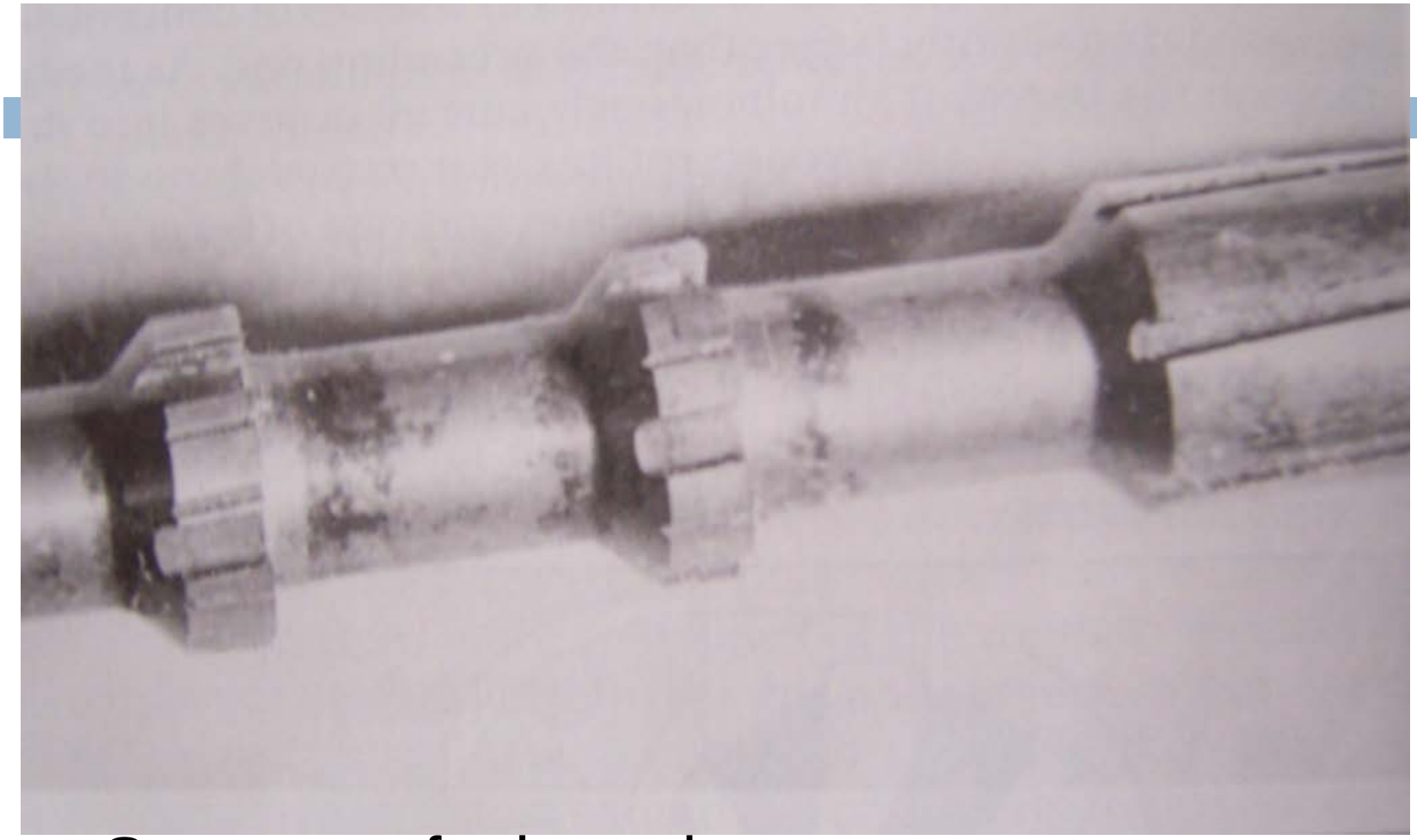

- Segment of a broach cutter

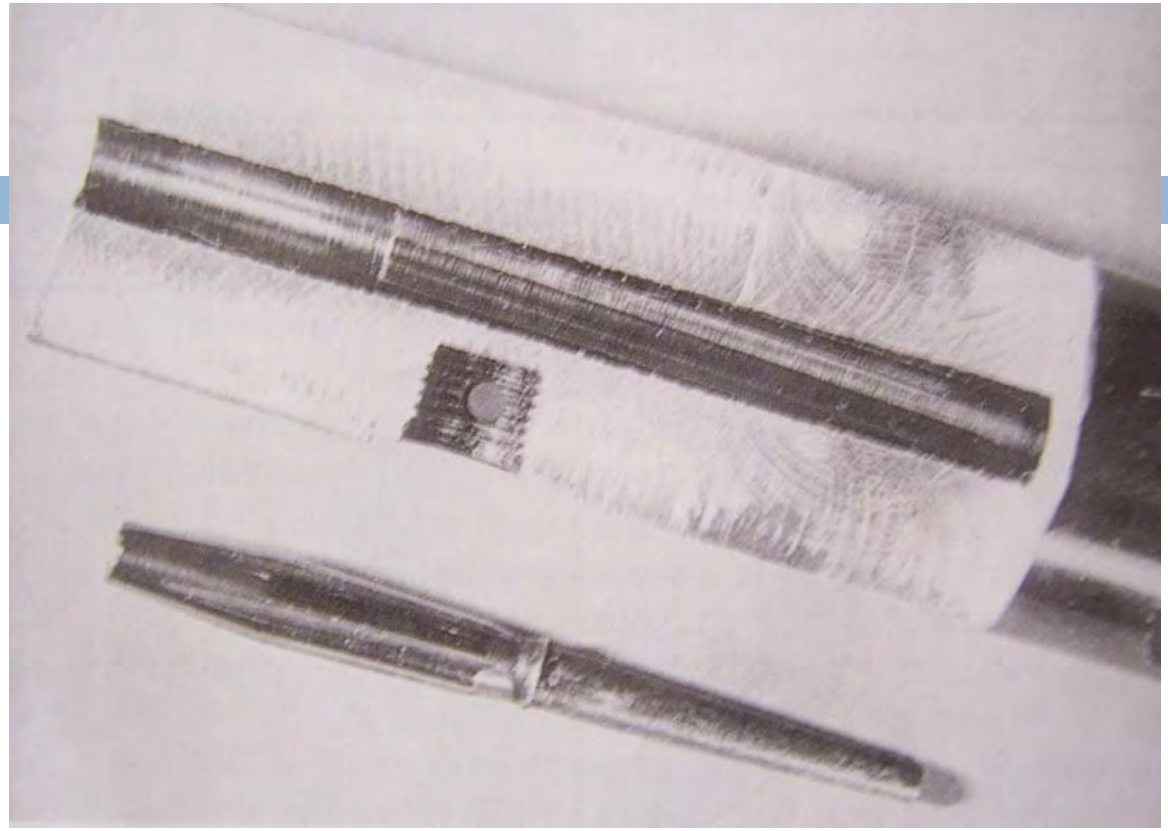

- (Top) Cross section of a .22-caliber rifled barrel.
- (Bottom) Button used to produce the lands and grooves in the barrel

Evidence bullets (different levels received condition)

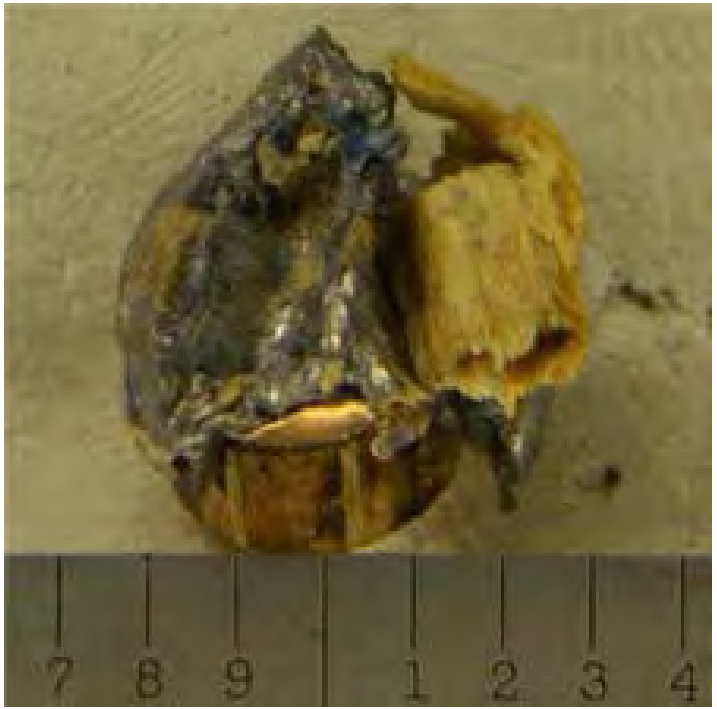

- Pristine value → Damaged → No comparison

Making Standards

- A suspect firearm is test fired into a water filled tank.
- The spent projectile is recovered from the bottom of the tank.
- The fired casings are collected off the floor of the room containing the tank.
- These known standards are used to compare to unknown evidence.

“Pristine” projectile from water tank, great for comparison.

- A bullet is impressed with the rifling markings of the barrel when it emerges from the weapon.

Class Characteristics (Bullets)

- Twist direction (right or left)
- Number of lands and grooves (# lands = # grooves)
- Caliber (9mm, .40 S&W, .357 Magnum, .380 Auto, .45 Auto)
- Land width, Groove width

Striations

- **Striations**, which are fine lines found in the interior of the barrel, are impressed into the metal as the negatives of minute imperfections found on the rifling cutter's surface, or they are produced by minute chips of steel pushed against the barrel's inner surface by a moving broach cutter.

- These striations form the individual characteristics of the barrel.

- It is the inner surface of the barrel of a firearm that leaves its striation markings on a bullet passing through it.

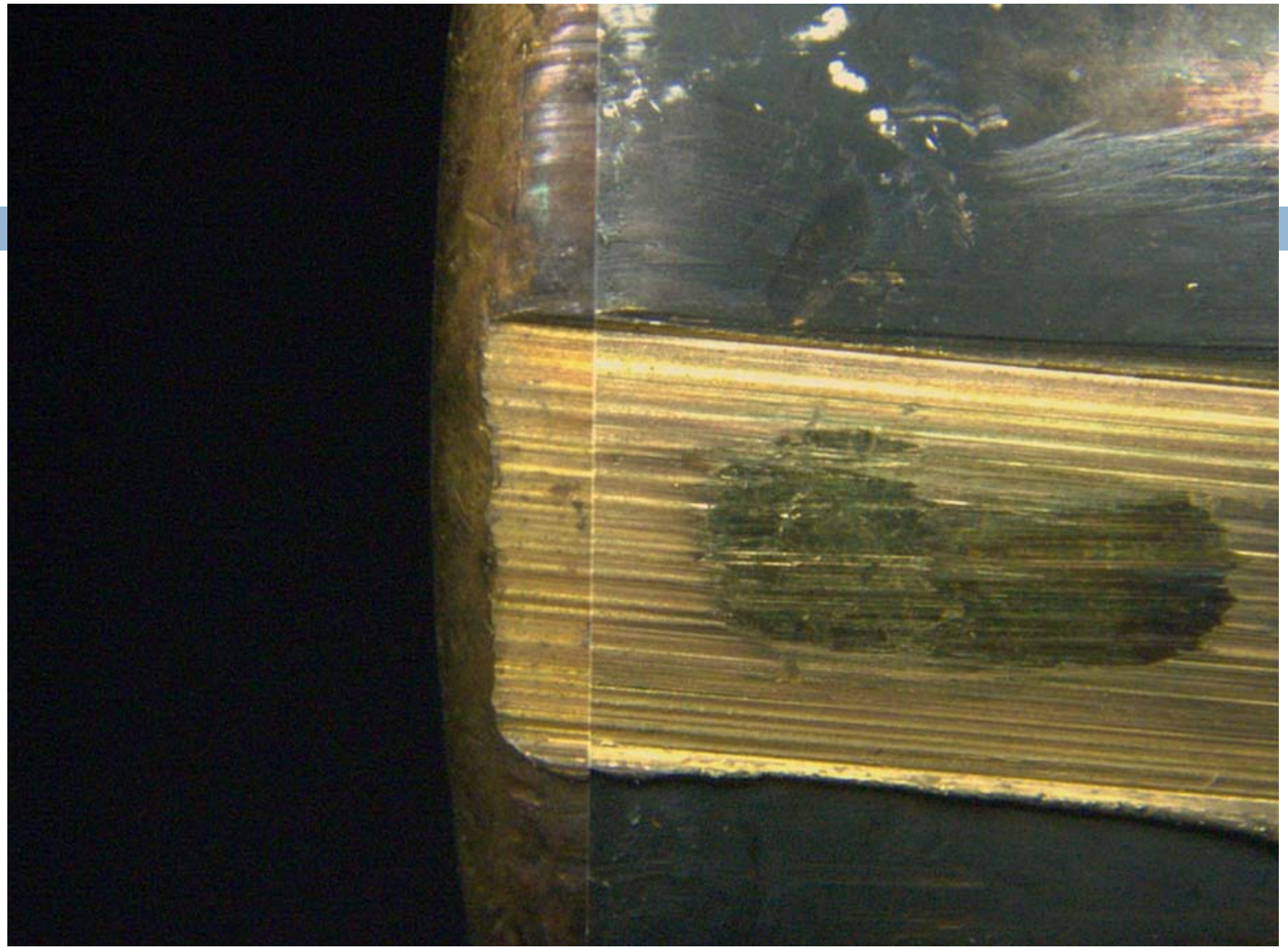

- Photomicrograph of two bullets that match as viewed through a comparison microscope. The test bullet is on the right; the questioned is on the left.

Casing Comparisons (Part 3 of 8)

Fired Casings

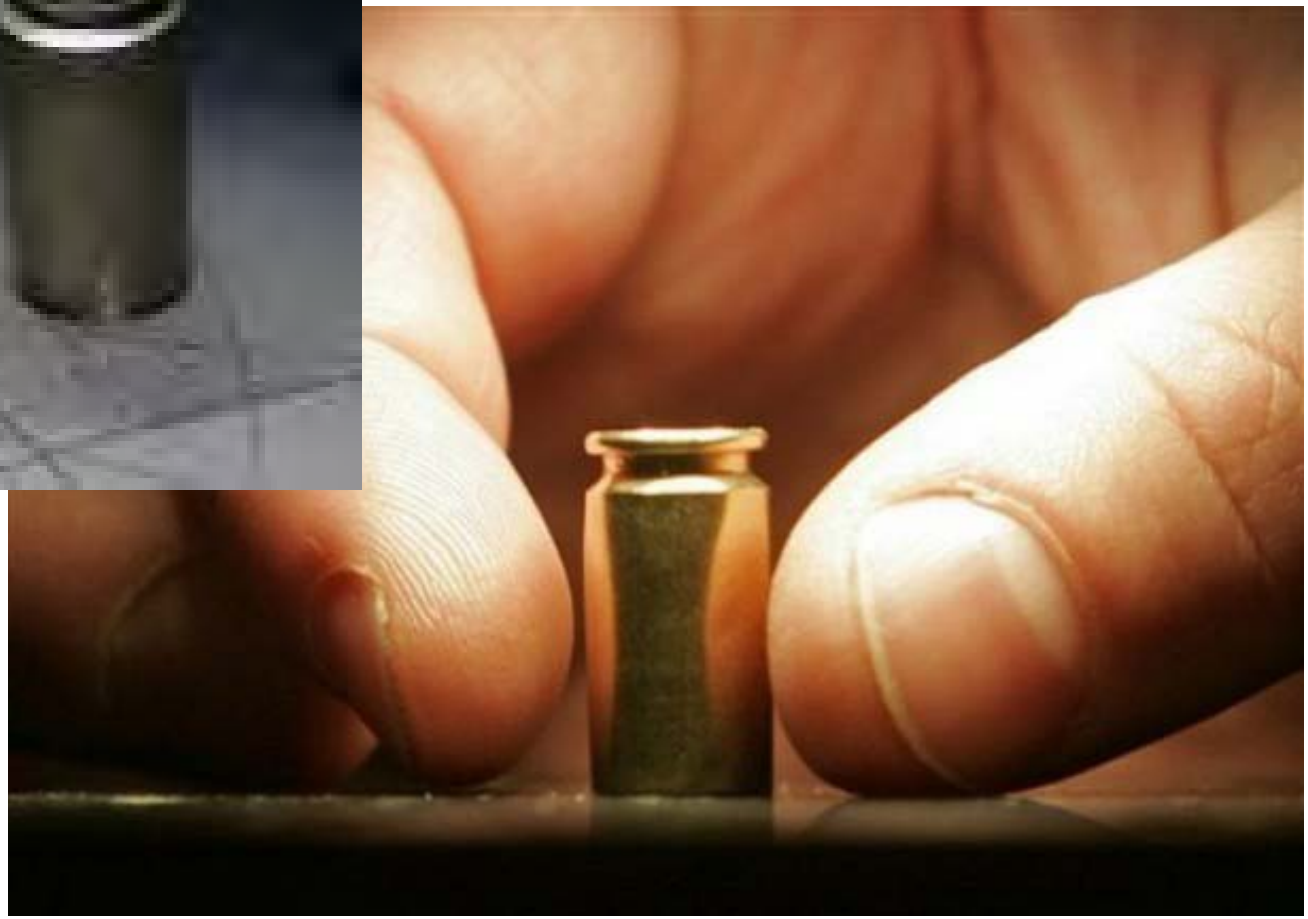

Unfired casing head/primer view vs. fired primer

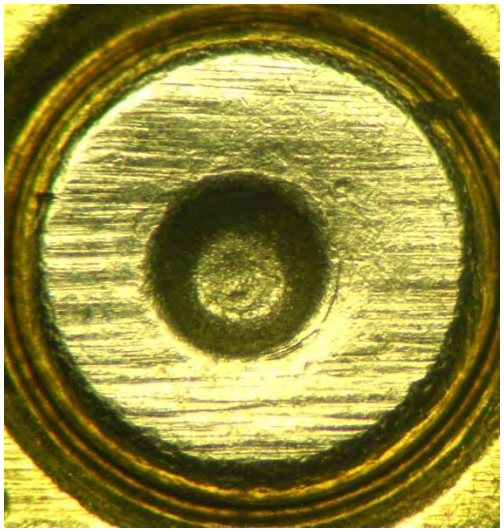

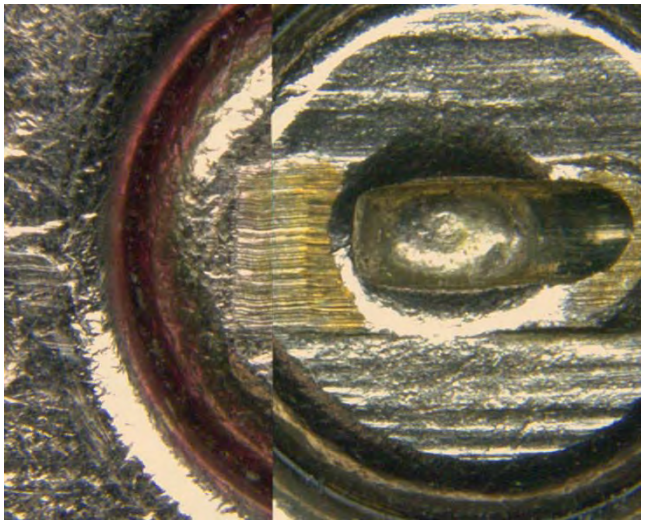

- Breech face, extractor, and firing pin aperture (window for firing pin protrusion).
- These parts are all products of a manufacturing process.

Firing a Weapon

- The act of pulling the trigger serves to release the weapon's firing pin, causing it to strike the primer, which in turn ignites the powder.
- The expanding gases generated by the burning gunpowder propel the bullet forward through the barrel, simultaneously pushing the spent cartridge case or shell back with equal force against the breechblock.
- The shell is impressed with markings by its contact with the metal surfaces of the weapon's firing and loading mechanisms.

Cartridge Case Comparison

- *The firing pin, breechblock, ejector and extractor mechanism also offer a highly distinctive signature for individualization of cartridge cases*.
- The shape of the *firing pin* will be impressed into the relatively soft metal of the primer on the cartridge case.
- The cartridge case, in its rearward thrust, is impressed with the surface markings of the *breechblock*.

Impression marks

- The negative of one surface being imparted onto a second, softer surface.
- A mark, indentation, figure, etc., produced by pressure.

Examples include BFMs, FPIs, Ejector marks.

Cartridge Case Comparison

- Other distinctive markings that may appear on the shell as a result of metal to metal contact are caused by the:
  - *Ejector*, the mechanism in a firearm that throws the cartridge or fired case from the firearm.
  - *Extractor*, the mechanism in a firearm by which a cartridge of a fired case is withdrawn from the firing chamber.
  - *Magazine* or clip, the part of a firearm that holds the bullets.

Class characteristics (Cartridge Casings)

- Firing pin impression (Hemispherical, Elliptical, etc.)
- Breech face marks (cross-hatched, parallel, arcs, etc.)
- Ejector Marks (wedge shaped, circular, etc.)

Class characteristics

- Arched BFMs
- Hemispherical FPI
- FPI is of the concentric circle class

Examples of an Elimination based on differences in Class Characteristics

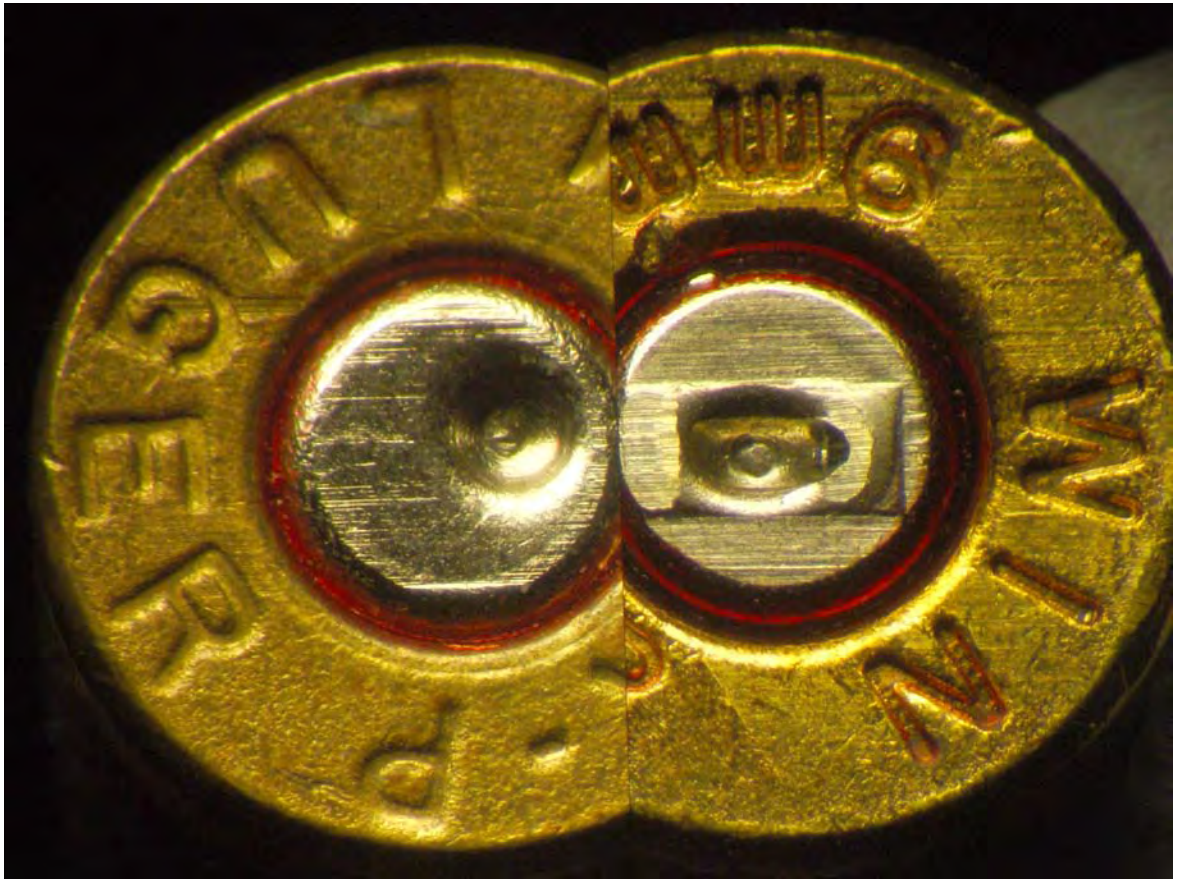

Shotguns

- Unlike rifled firearms, *a shotgun has a smooth barrel.*
- Shotguns generally fire small *lead balls or pellets that are not impressed with any characteristic markings that can be related back to the weapon*.
- Shotgun shells can be compared for firing pin and breech face marking.
- The diameter of the shotgun barrel is expressed by the term *gauge*.
- The higher the gauge number, the smaller the barrel's diameter. (a 12ga. has a larger barrel diameter than a 20ga.)

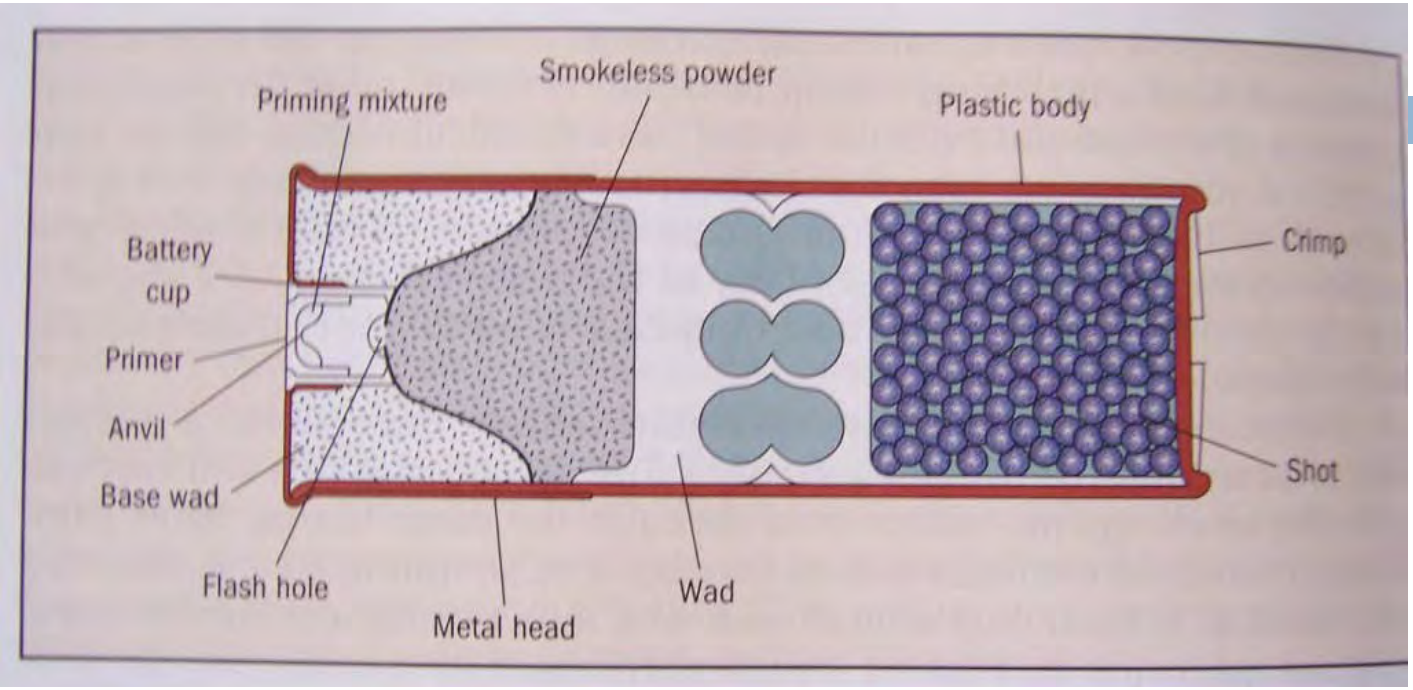

- Cross section of a loaded shotgun shell

Comparison

- The test fired casings and projectiles are then compared to the casings and projectiles from the crime scene.
- This is done with a comparison microscope.

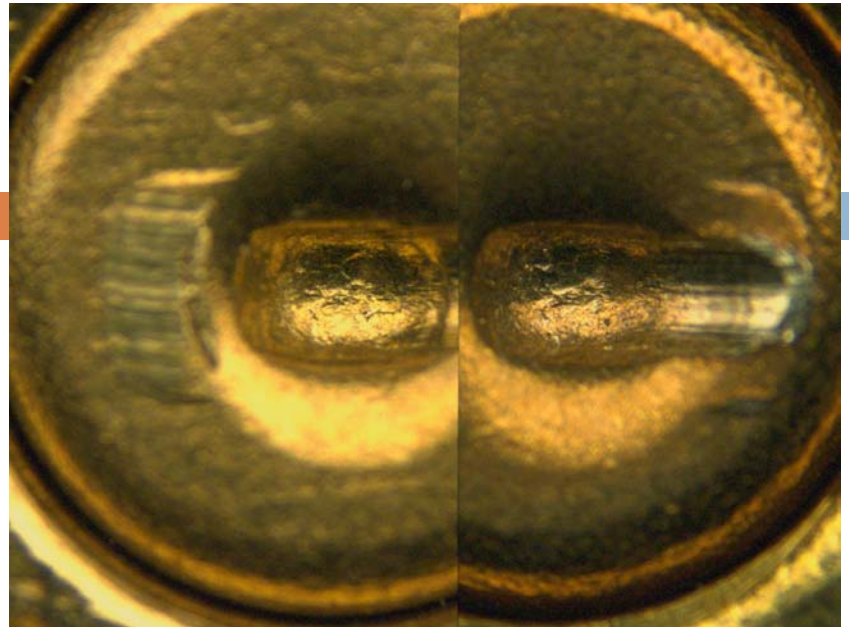

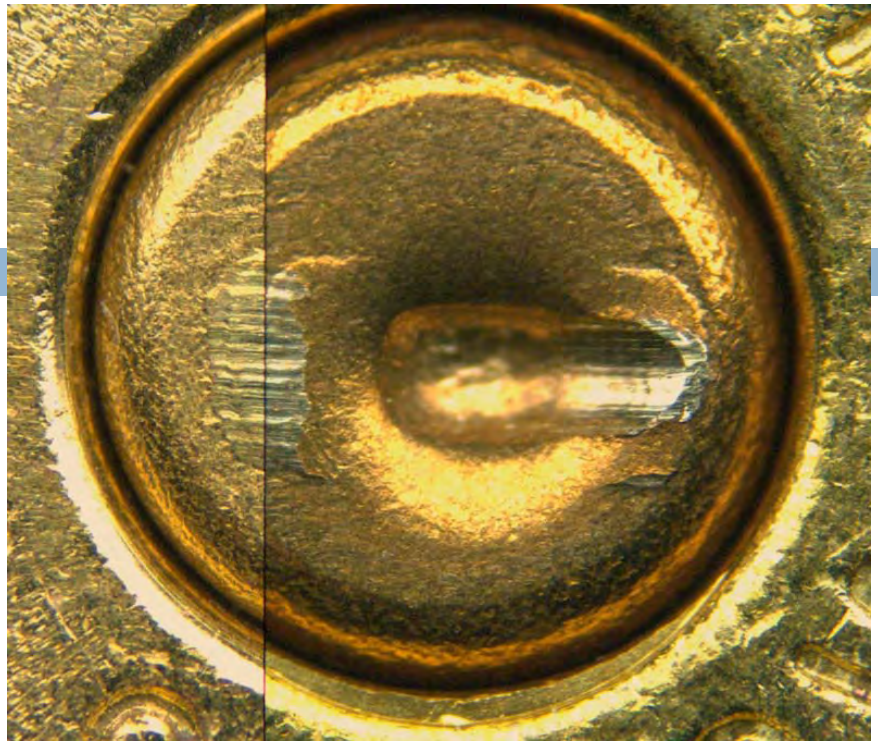

- (Left) Identification between firing pin impressions on two different casings fired from one firearm.
- (Right) Identification between breech face markings on two different casings fired from one firearm.
- Elliptical FPI shown above.

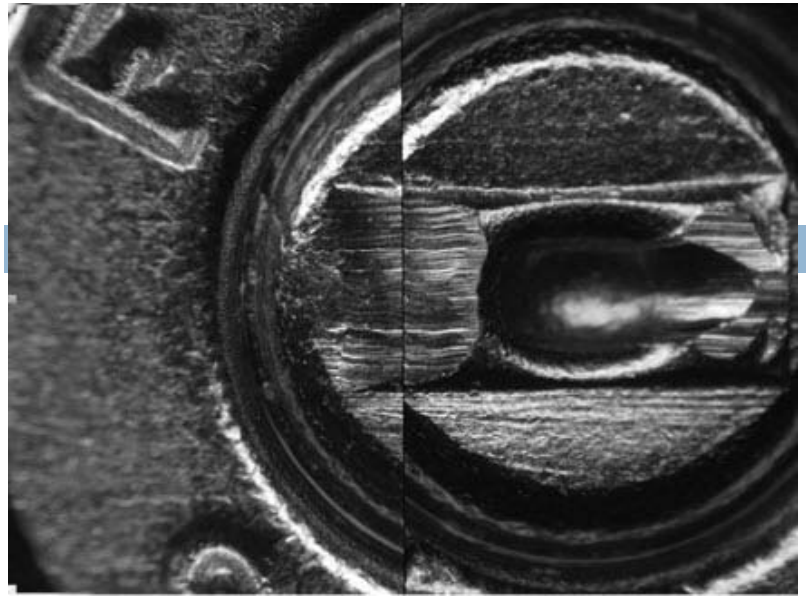

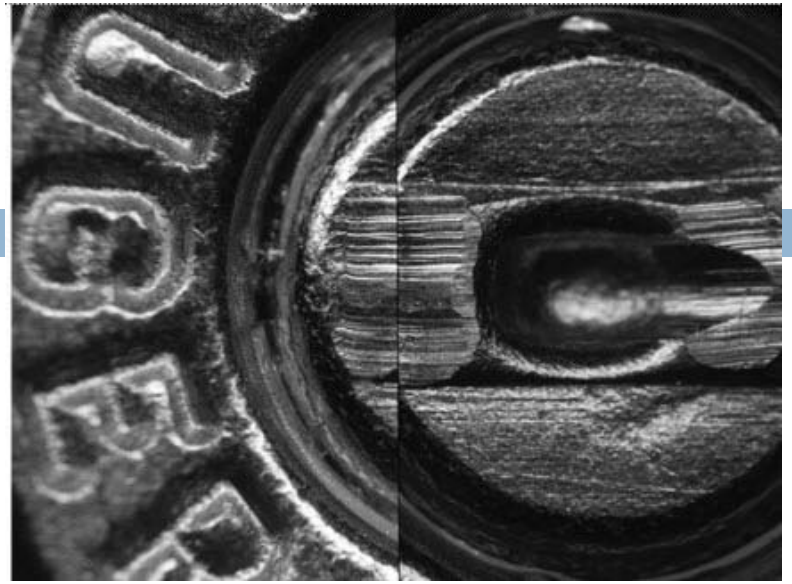

- Sufficient Agreement

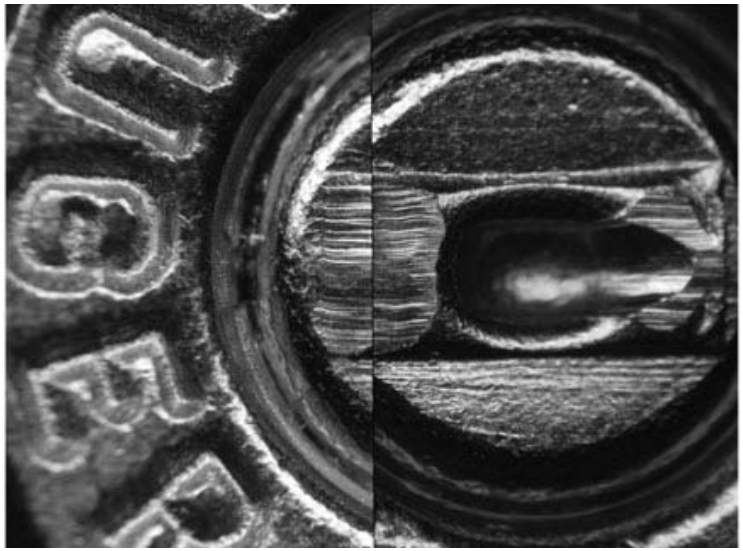

- Lack of sufficient agreement

Individual Characteristics

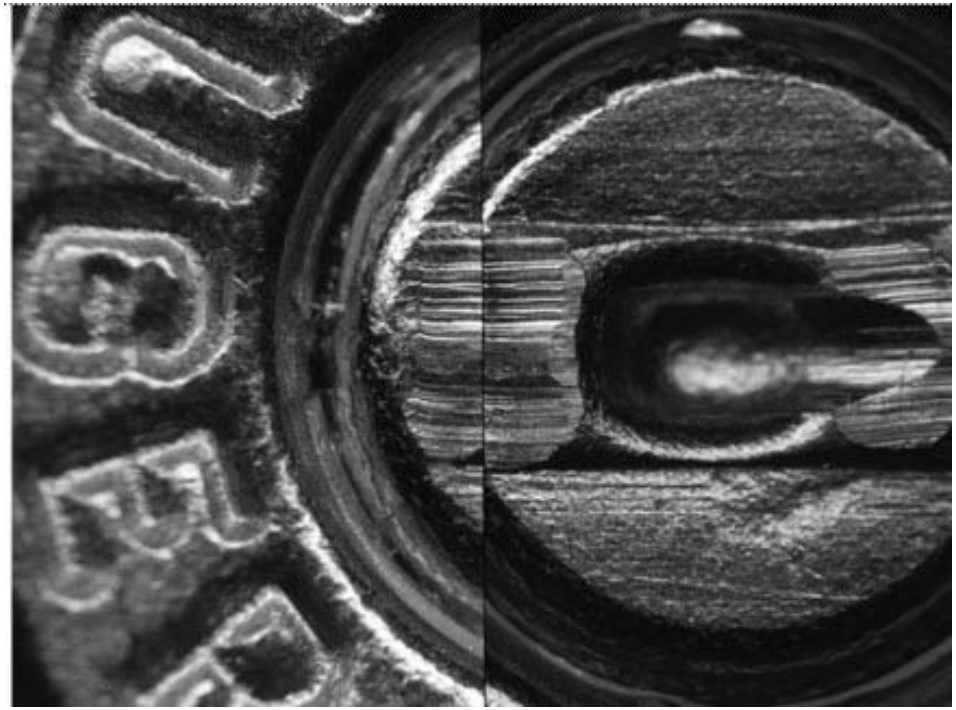

- Example of Identification between Firing Pin Aperature shearing on two casings.
- The length, width, depth, and spatial relationship between the parallel marks make up what are considered the Individual marks.

N.I.B.I.N. (The National Integrated Ballistic Information Network)

(Part 4 of 8)

Computerized Imaging

- The advent of computerized imaging technology has made possible the storage of cartridge case surface characteristics in a manner analogous to automated fingerprint files.
- The National Integrated Ballistic Information Network (NIBIN) produces database files from cartridge cases or projectiles retrieved from crime scenes or test fires from retrieved firearms, often linking a specific weapon to multiple crimes.
- It is important to remember, however, that the ultimate decision for making a final comparison will be determined by the forensic examiner through traditional microscopic methods.


IBIS BRASSTRAX

Collect

IBIS BRASSTRAX-3D

IBIS BULLETTRAX-3D

Store & Compare

IBIS Data Concentrator

IBIS Correlation Server

Analyze & Report

IBIS MATCHPOINT+

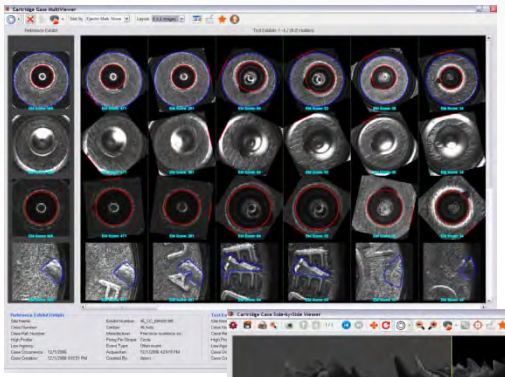

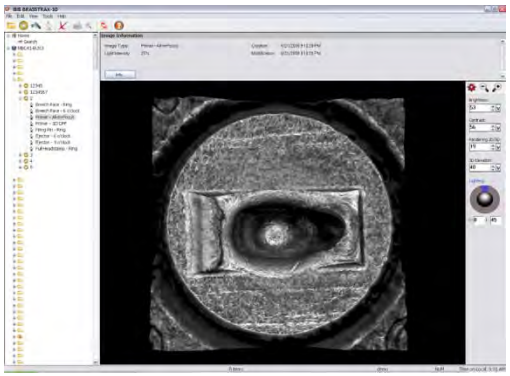

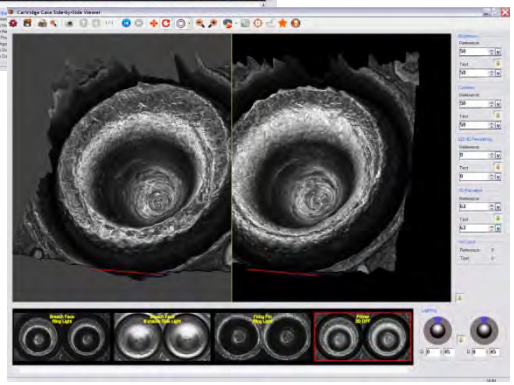

Muzzle to Target Distance Determination

(Part 5 of 8)

Gunpowder Residue

- When a firearm is discharged, unburned and partially burned particles of gunpowder in addition to smoke are propelled out of the barrel along with the bullet toward the target.

- If the muzzle of the weapon is sufficiently close, these products will be deposited onto the target.

- *The distribution of gunpowder particles and other discharge residues around a bullet hole permits an assessment of the distance from which a handgun or rifle was fired.*

Gunpowder Residue

- The distance from which a handgun or rifle has been fired must be determined by means of a careful *comparison* of the powder-residue pattern located on the victim's clothing against test patterns made using the suspect weapon at varying distances.
- By comparing the test and evidence patterns, the examiner may find enough similarity in pattern diameter upon which to base an opinion as to the distance from which the shot was fired.

Gunpowder Residue

- Star-shaped (stellate) tear pattern
- Halo of vaporous lead (smoke)
- Scattered specks of unburned and partially burned powder
- Bullet wipe

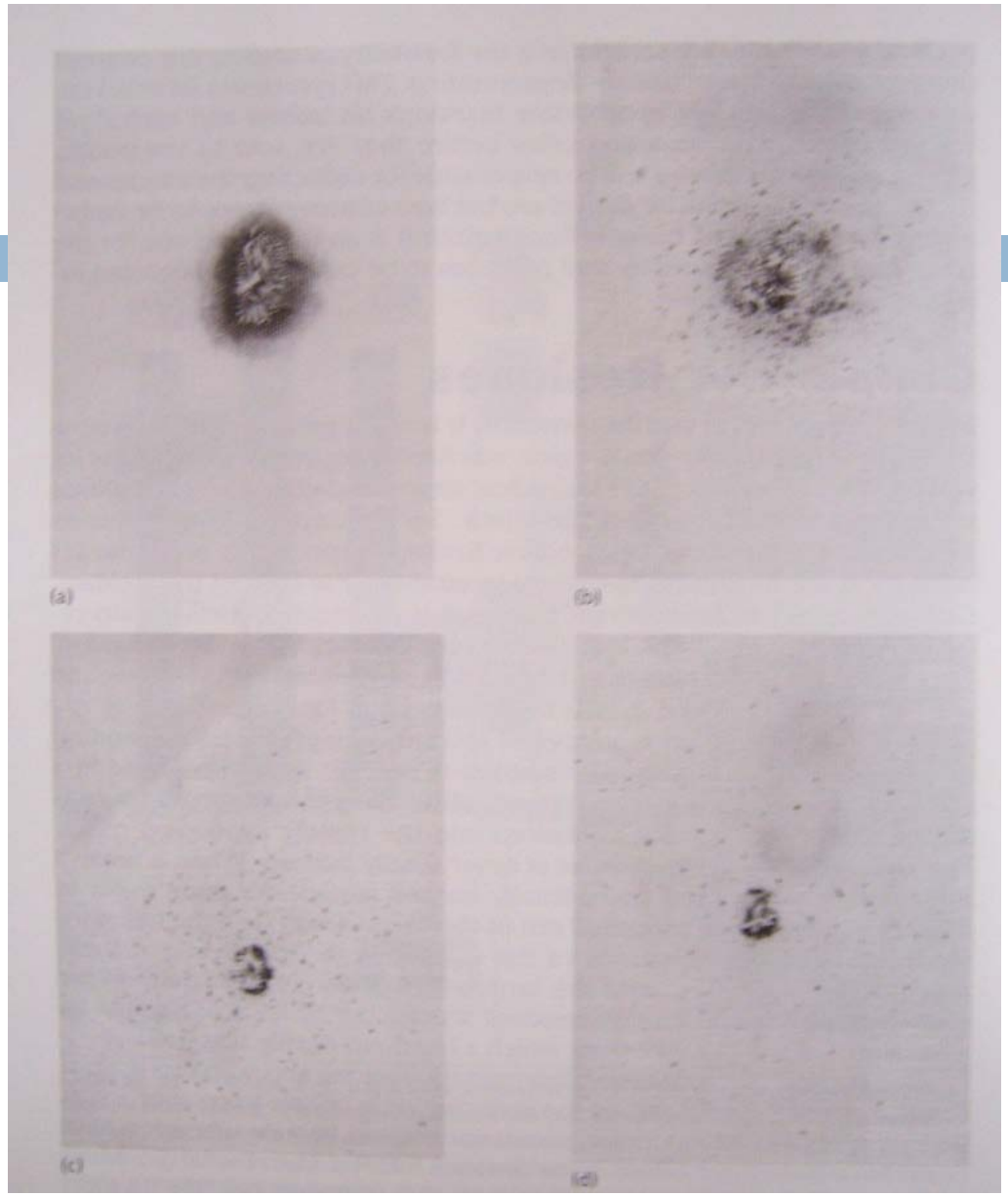

- Test powder paterns made with a .38 Special S&W revolver fired at (a) contact, (b) 6 inches, (c) 12 inches, and (d) 18 inches

- A contact shot (AKA stellate pattern)

Gunpowder Residue

- When garments or other evidence relevant to a shooting are received in the crime laboratory, the surfaces of all items are first examined microscopically for the presence of gunpowder residue.
- Chemical tests, such as the *Modified Greiss test*, may be needed to detect gunpowder residues that are not visible. (positive reaction for *burned* gunpowder…nitrites)
- The firing distances involving shotguns must be related to test firing and the muzzle to target distances can be established by measuring the spread of the discharged shot.

Unknown

- Modified Greiss test comparison of questioned (above) to tests (below)

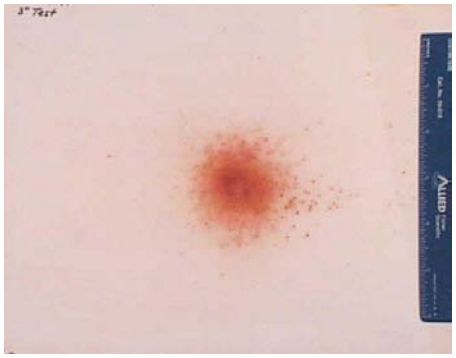

3in

12in

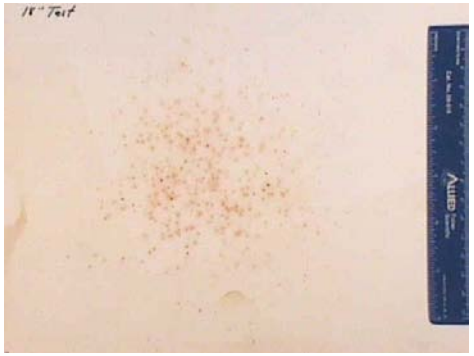

18in

- For the previous example, the muzzle-to-garment distance would then be reported as *greater than 3 inches but less than 18 inches*

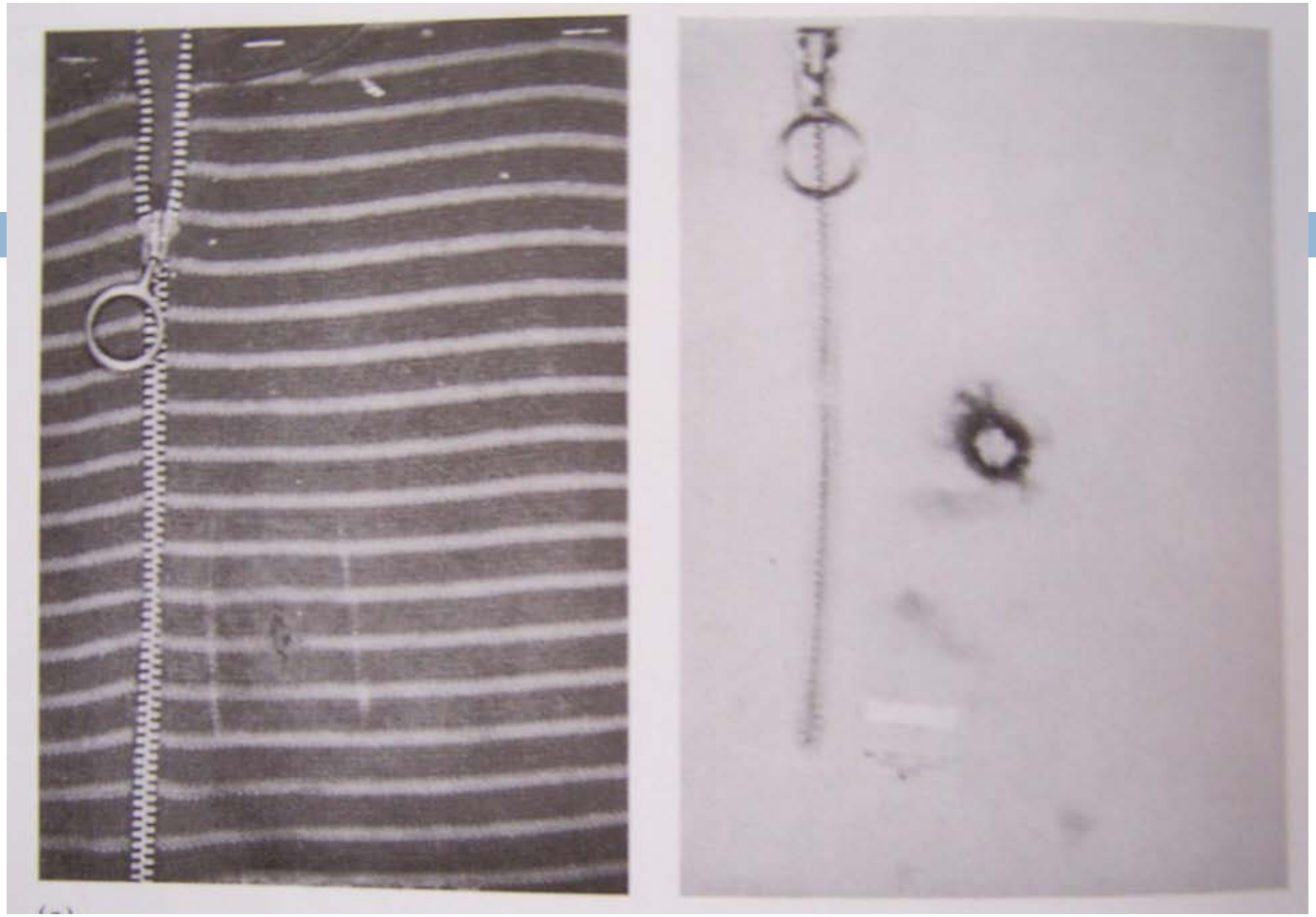

- (left) A shirt bearing a powder stain under normal light, (right) Infrared imaging of the same shirt

Serial Number Restoration
(Part 6 of 8)

Serial Numbers

- Increasingly, the examiner is requested to restore a serial number when it has been removed or obliterated by grinding, rifling, or punching.
- *Restoration of serial numbers* is possible through chemical etching because the metal crystals in the stamped zone are placed under a permanent strain that extends a short distance beneath the original numbers.

Tool Marks
(Part 7 of 8)

Tool Marks

- A *tool mark* is considered to be any impression, cut, gouge, or abrasion caused by a tool coming into contact with another object.
- A careful examination of the impression can reveal important class characteristics, such as the size and shape of the tool.
- The presence of any minute imperfections on a tool imparts individuality to that tool.
- The shape and pattern of such imperfections are further modified by damage and wear during the life of the tool.

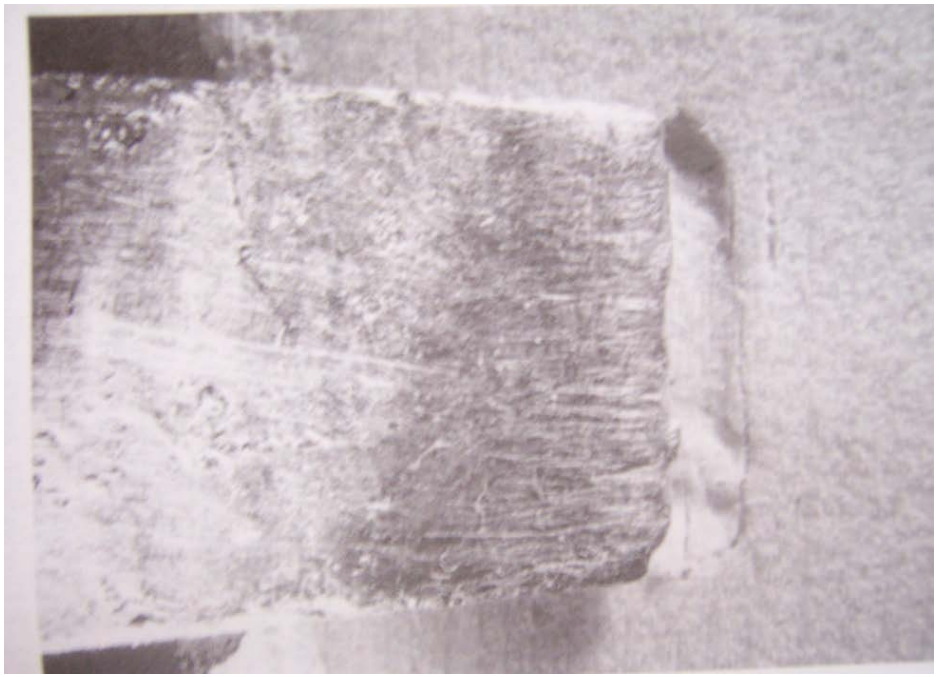

- A comparison of a tool with a suspect screw driver. Note how the presence of nicks and breaks on the tool's edge helps to individualize the tool to the mark.

Tool Marks

- The comparison microscope is used to compare crime-scene toolmarks with test impressions made with the suspect tool.
- When practical, the entire object or the part of the object bearing the tool mark should be submitted to the crime laboratory for examination.
- *Under no circumstances must the crime scene investigator attempt to fit the suspect tool into the tool mark.*
  - *Any contact between the tool and the marked surface may alter the mark and will, at the least, raise serious questions about*

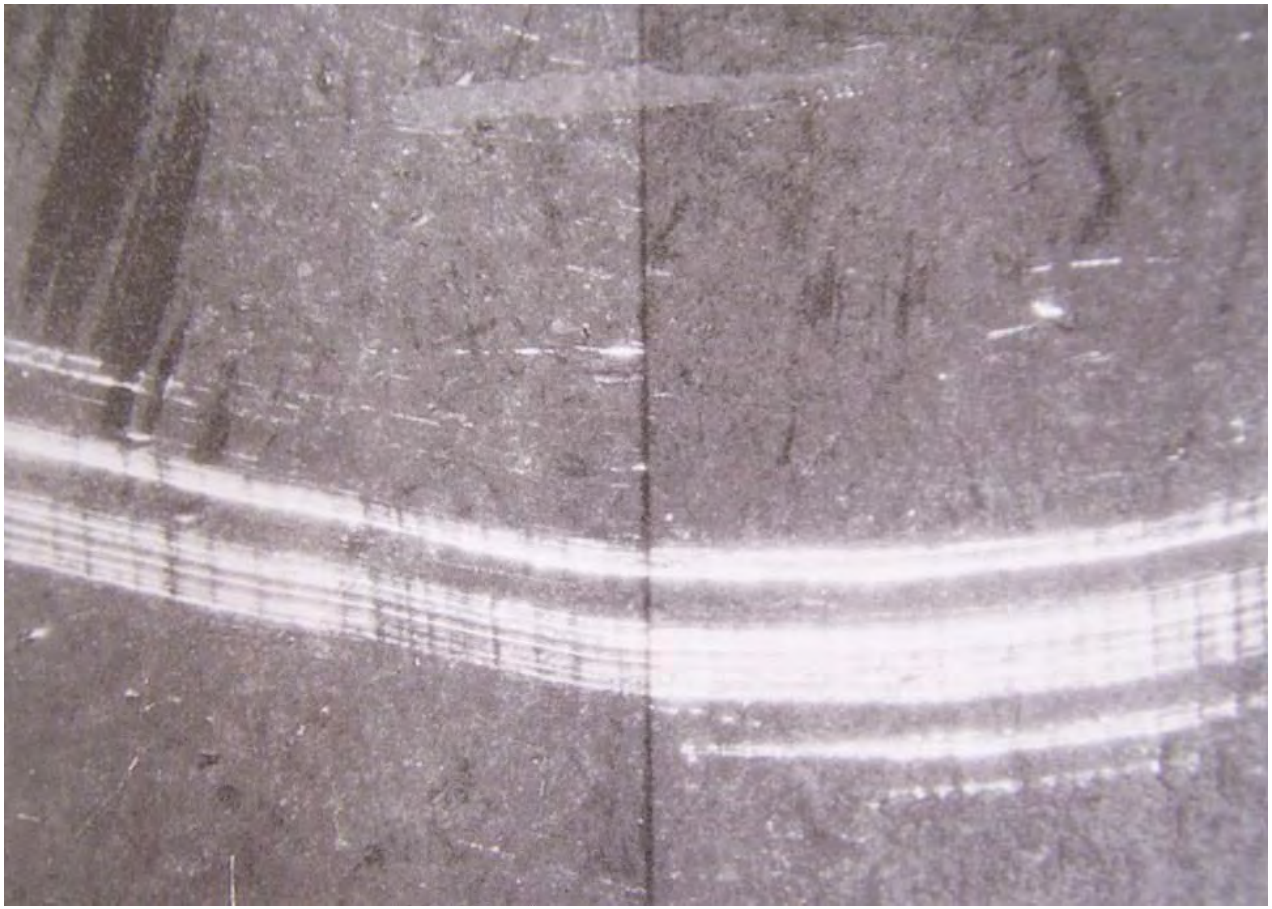

- A photograph of a tool mark comparison seen under a comparison microscope.

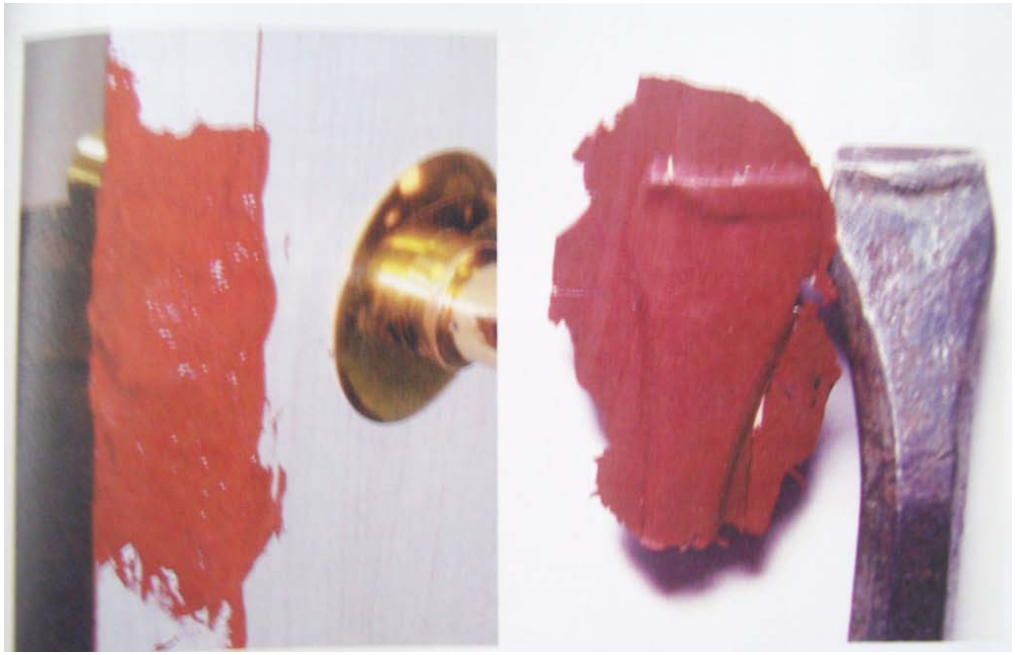

- (left) casting a toolmark impression with a silicone-based putty, (right) impression alongside suspect tool

Footwear impressions
(Part 8 of 8)

- From left to right: Shoe impression in mud, Cast of shoe impression, Shoe suspected of leaving impression in mud

Comparison of Shoe/tire Evidence

- Individual identifying characteristics are those that randomly occur on the shoe outsole from use. Each of these characteristics were not planned or intentionally manufactured and their combined position, orientation, size and features are unlikely to re-occur in another shoe/tire.
- Comparison of such points will support a finding that both the questioned and test impressions originated from one source.
- According to William Bodziak (2000), “If both the questioned impression and a shoe contain sufficient individual identifying characteristics in common, it can be concluded that the shoe positively make that impression.”
- New computer software and web sites may be able to assist in making shoe print and tire impression comparisons.

Bodziak, William J. Footwear Impression Evidence: Detection, Recovery, and Examination 2nd

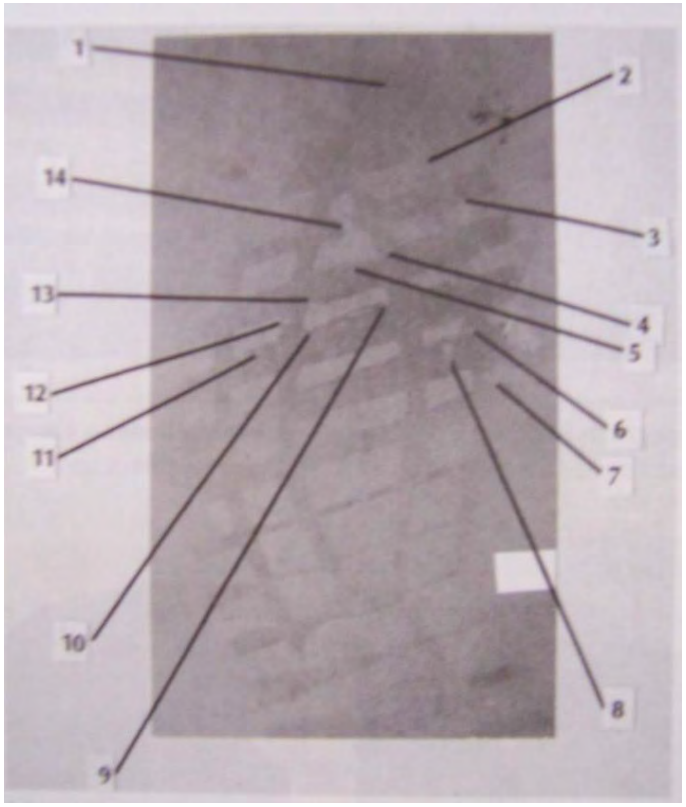

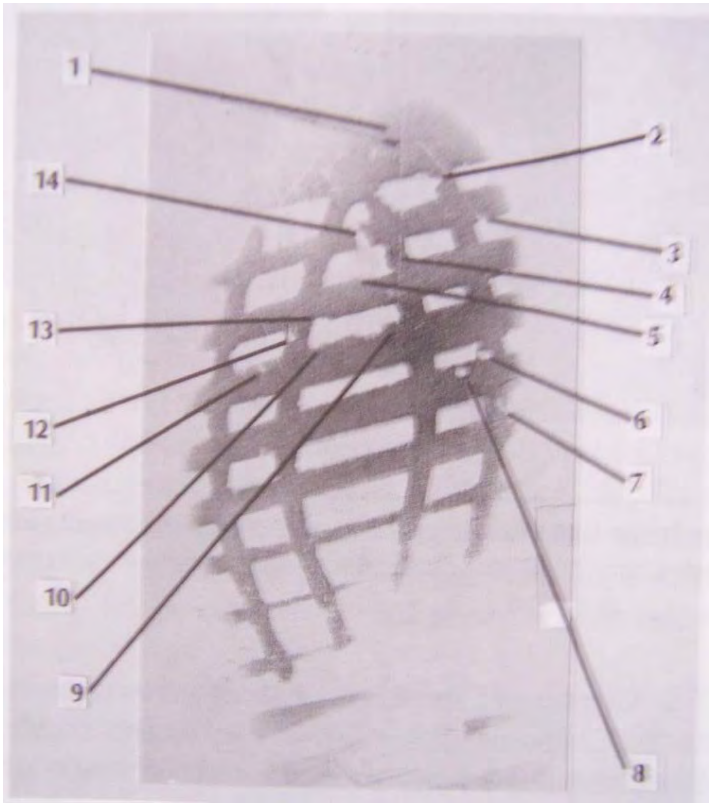

- (Left) Impression of shoe found at a crime scene, (Right) Test impression made with suspect shoe.

The END

Thank You!

Modelling the Internal Ballistics of Lightweight Plastic Driving Band Projectiles

Clive Woodley

A presentation to: 26th International Symposium on Ballistics

September 2011

QinetiQ

Contents

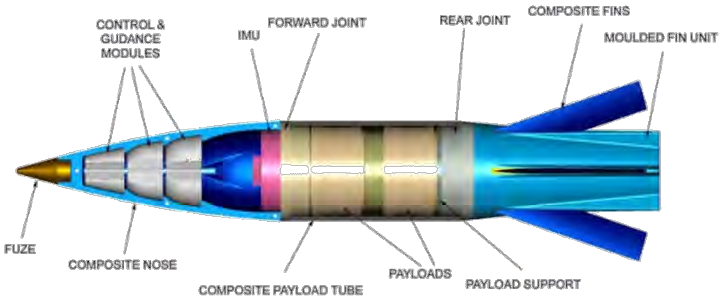

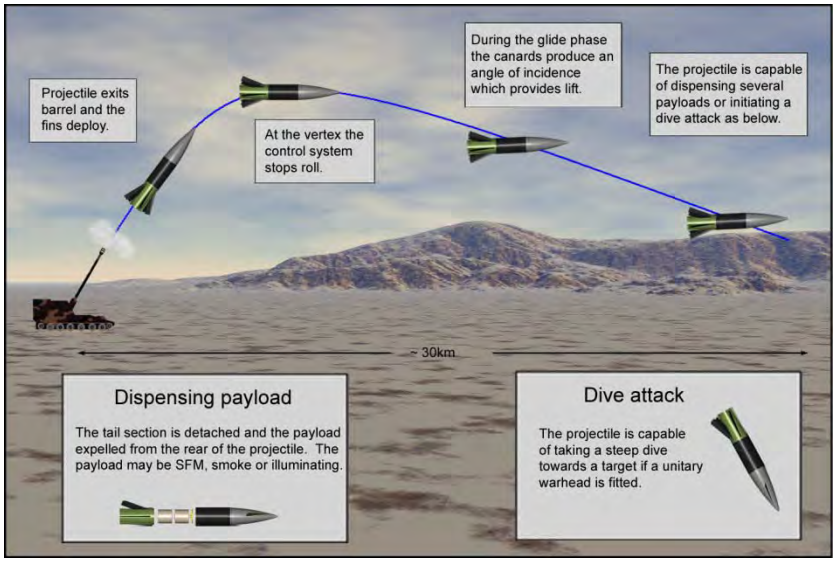

1 Background

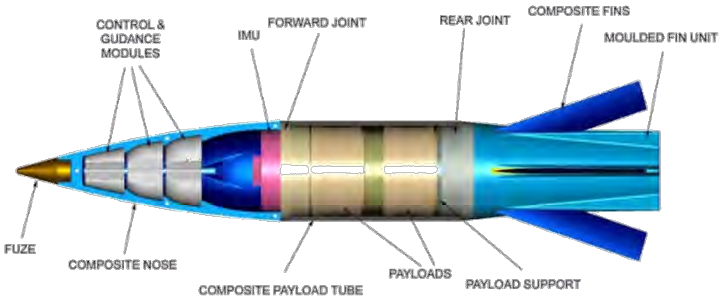

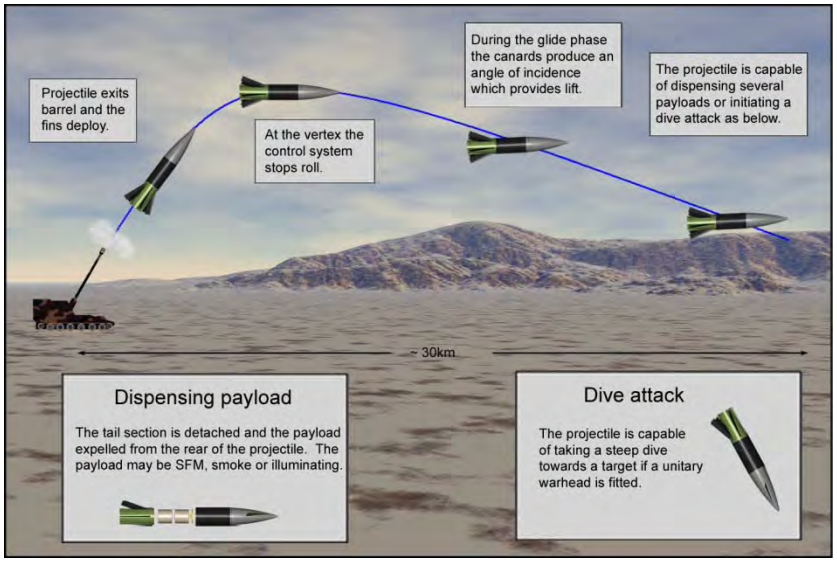

1 Background

History

- Firings of mature charge systems with experimental guided munitions gave lower than predicted maximum pressures and muzzle velocities
- Ballistics were consistent so the phenomenon was not investigated further
- More recently, work commenced on a lightweight guided munition
  - 30 kg mass
  - Reduced recoil
- Firings with well understood charge system resulted in lower than predicted maximum pressure of 40MPa and muzzle velocity of 50m/s
- Ram brake and fin case protection based on previous project

1 Background

Internal ballistics models used in investigation

- Proteus – 0D
- QIBS (**Q**inetiQ **I**nternal **B**allistics **S**oftware) – 1D
- QIMIBS (**Qi**netiQ **M**odular **I**nternal **B**allistics **S**oftware) – 2D

2
Lurch phenomenon

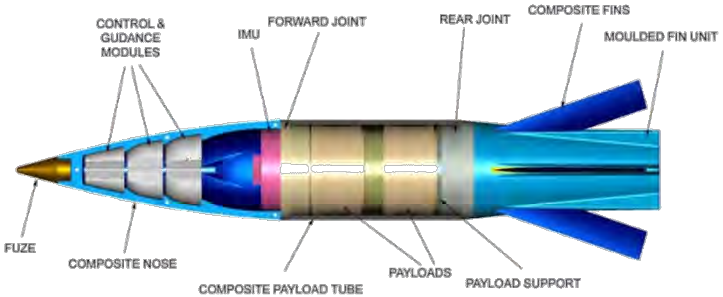

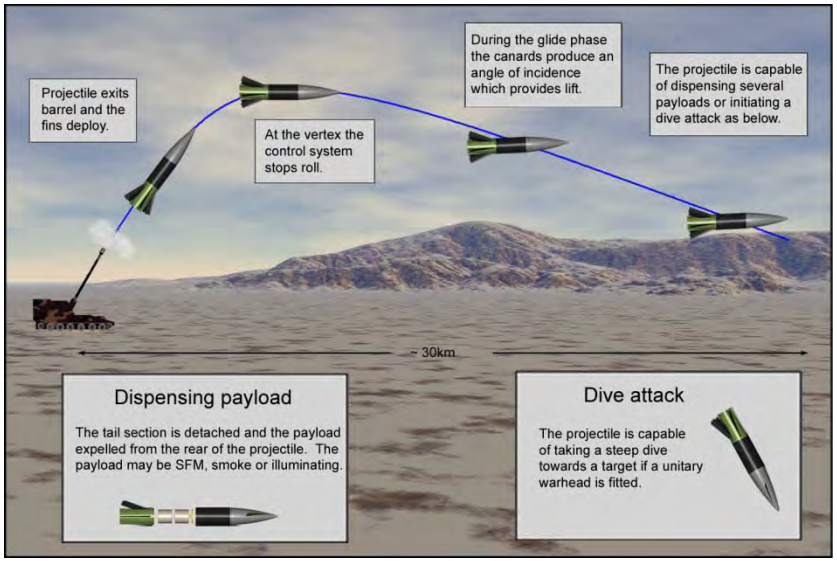

2 Lurch phenomenon

Initial and improved comparisons

- Possible to match pressures by assuming larger than expected chamber volume

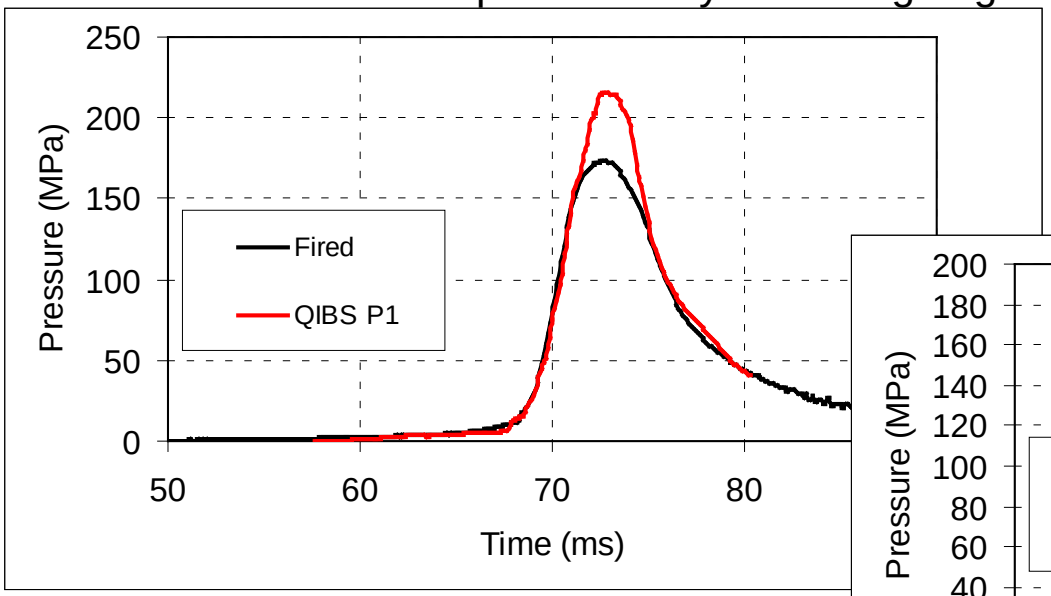

Lurch Phenomenon!

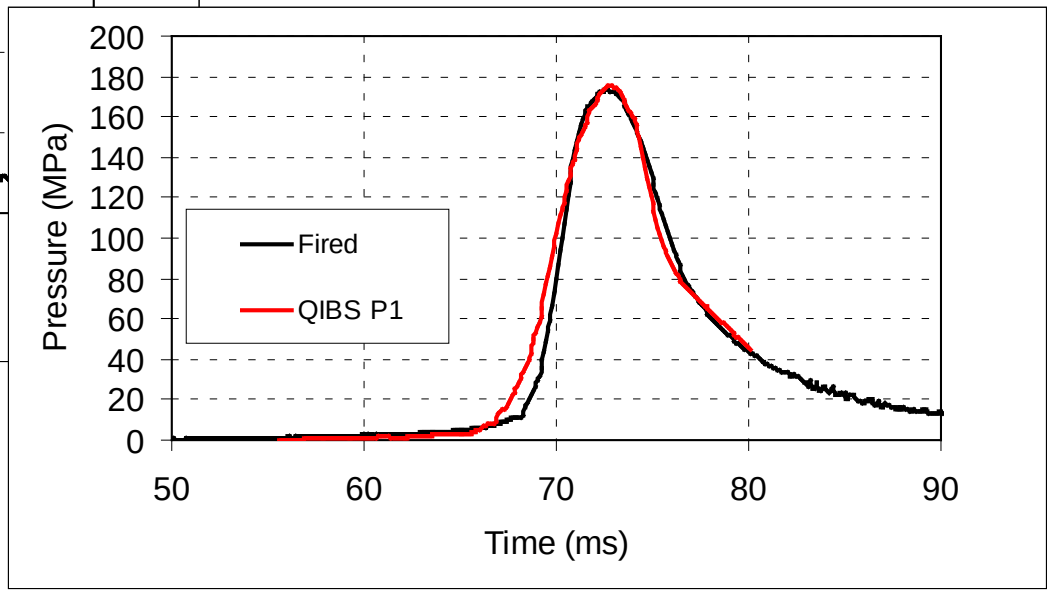

2 Lurch phenomenon

Detailed investigation undertaken to determine cause(s)

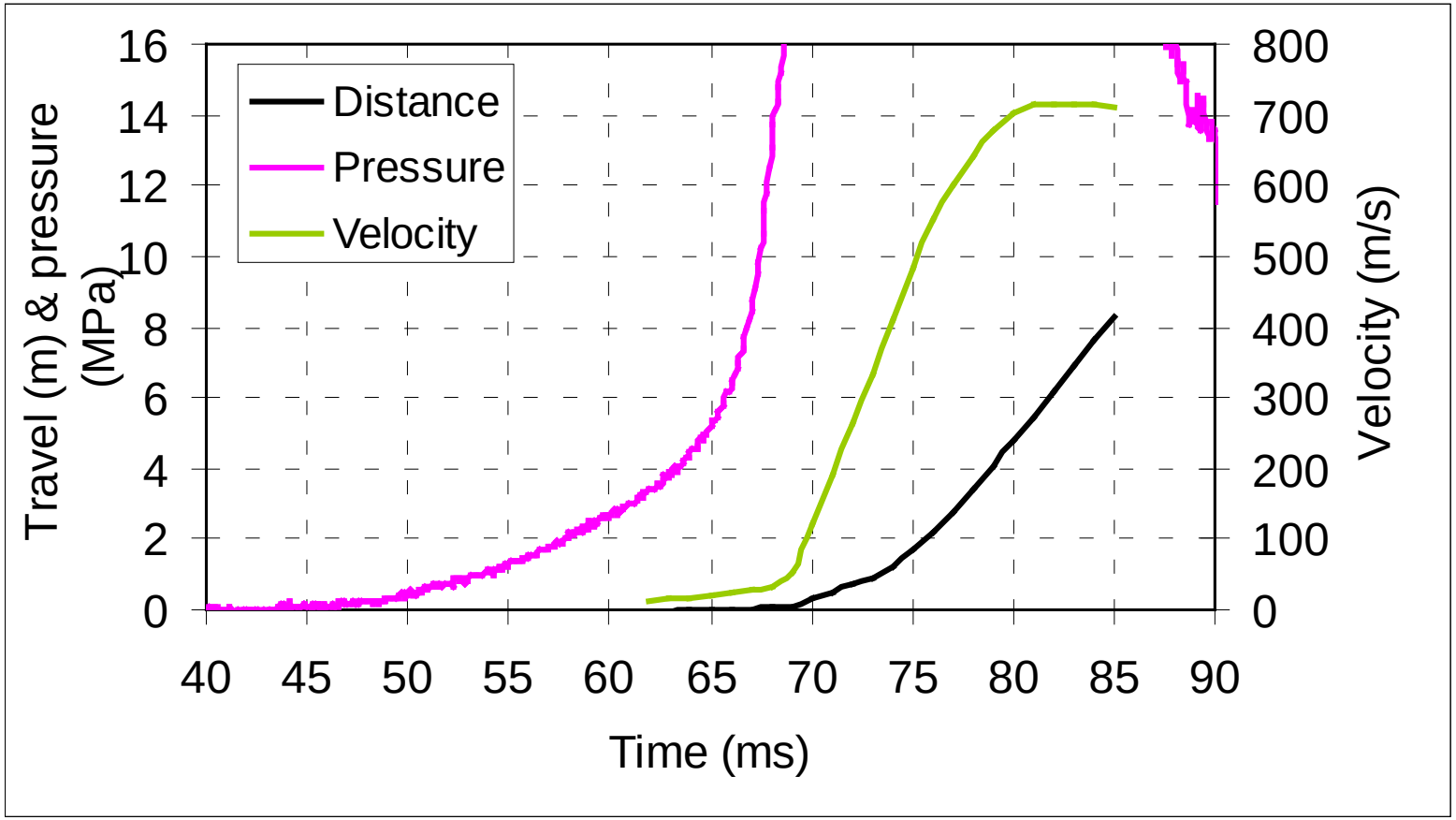

2 Lurch phenomenon

Combustion behaviour of combustible cartridge case significantly different

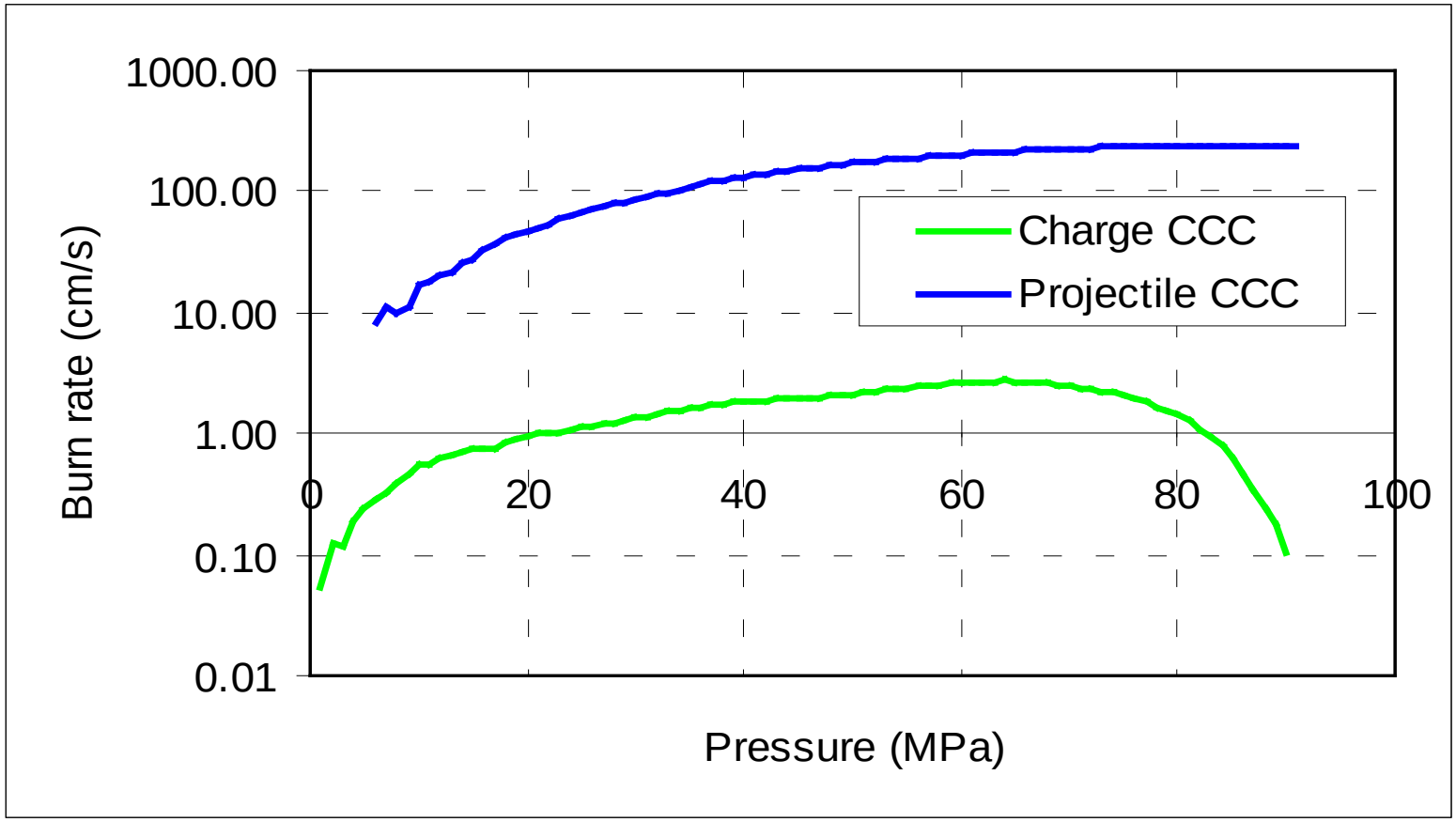

2 Lurch phenomenon

Effect of projectile initially 10cm further forward

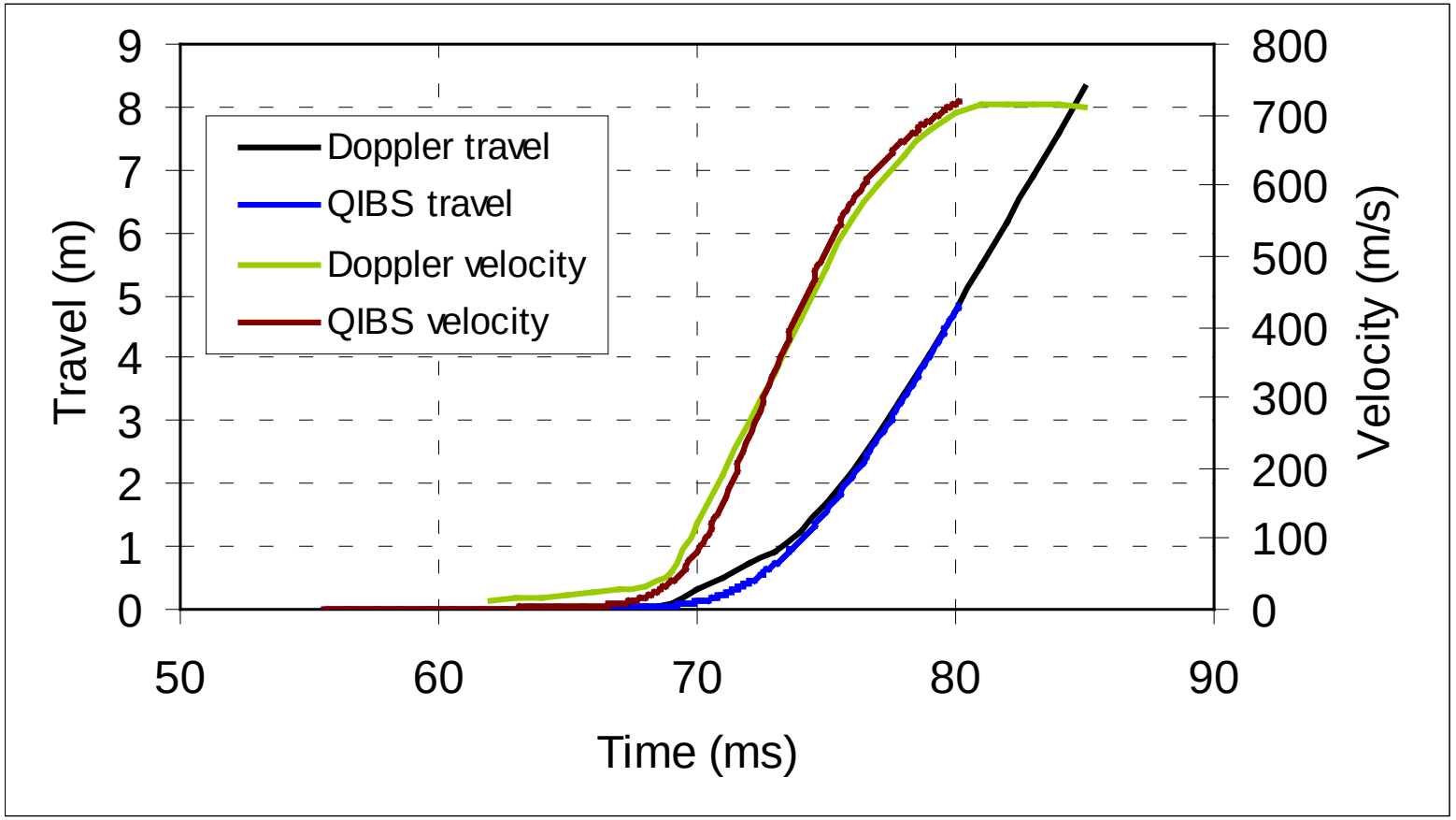

2 Lurch phenomenon

Effect of ignition delay of 19ms (equivalent to stand-off of 12cm)

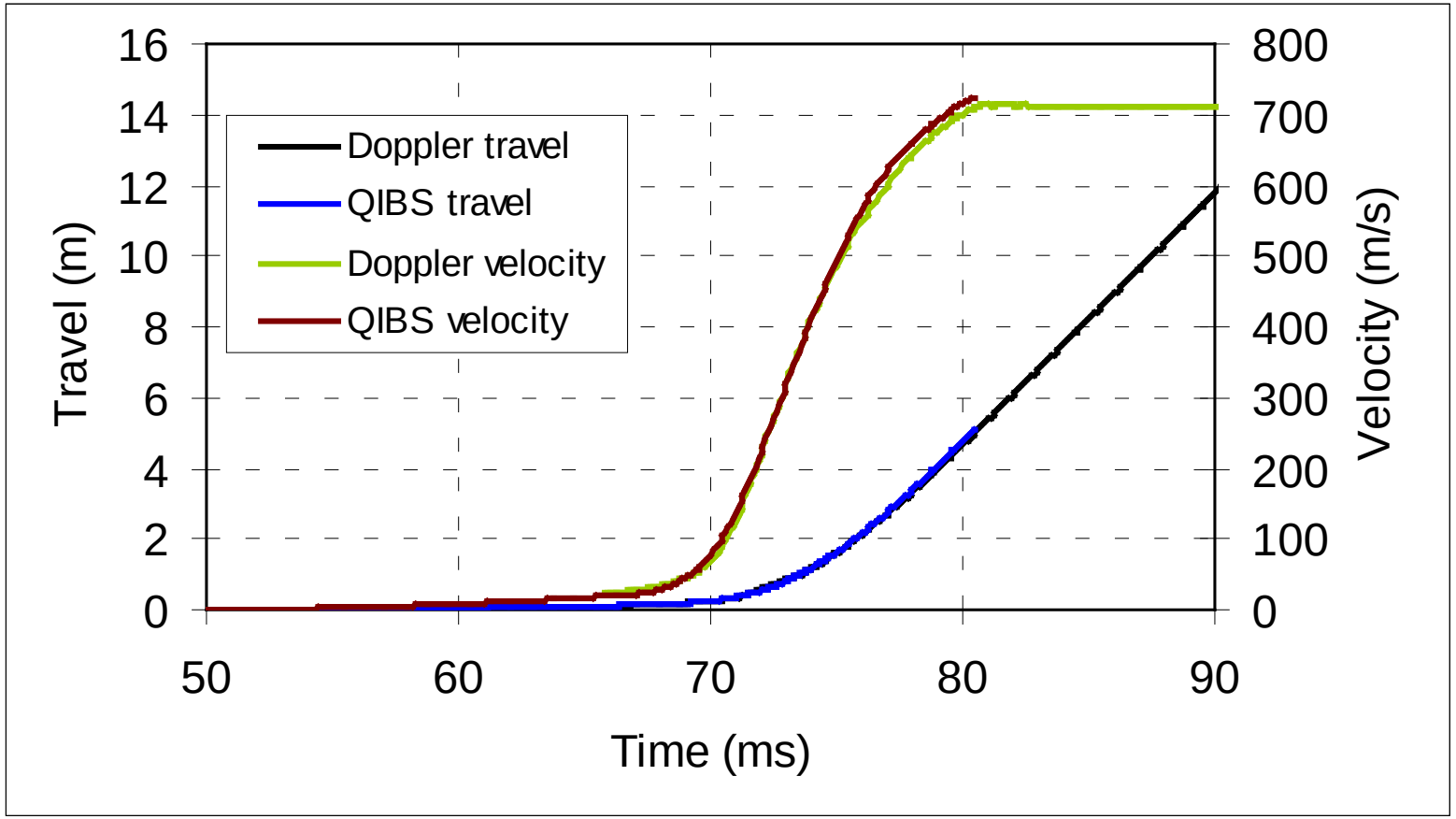

2 Lurch phenomenon

Effect of ignition delay of 19ms (equivalent to stand-off of 12cm)

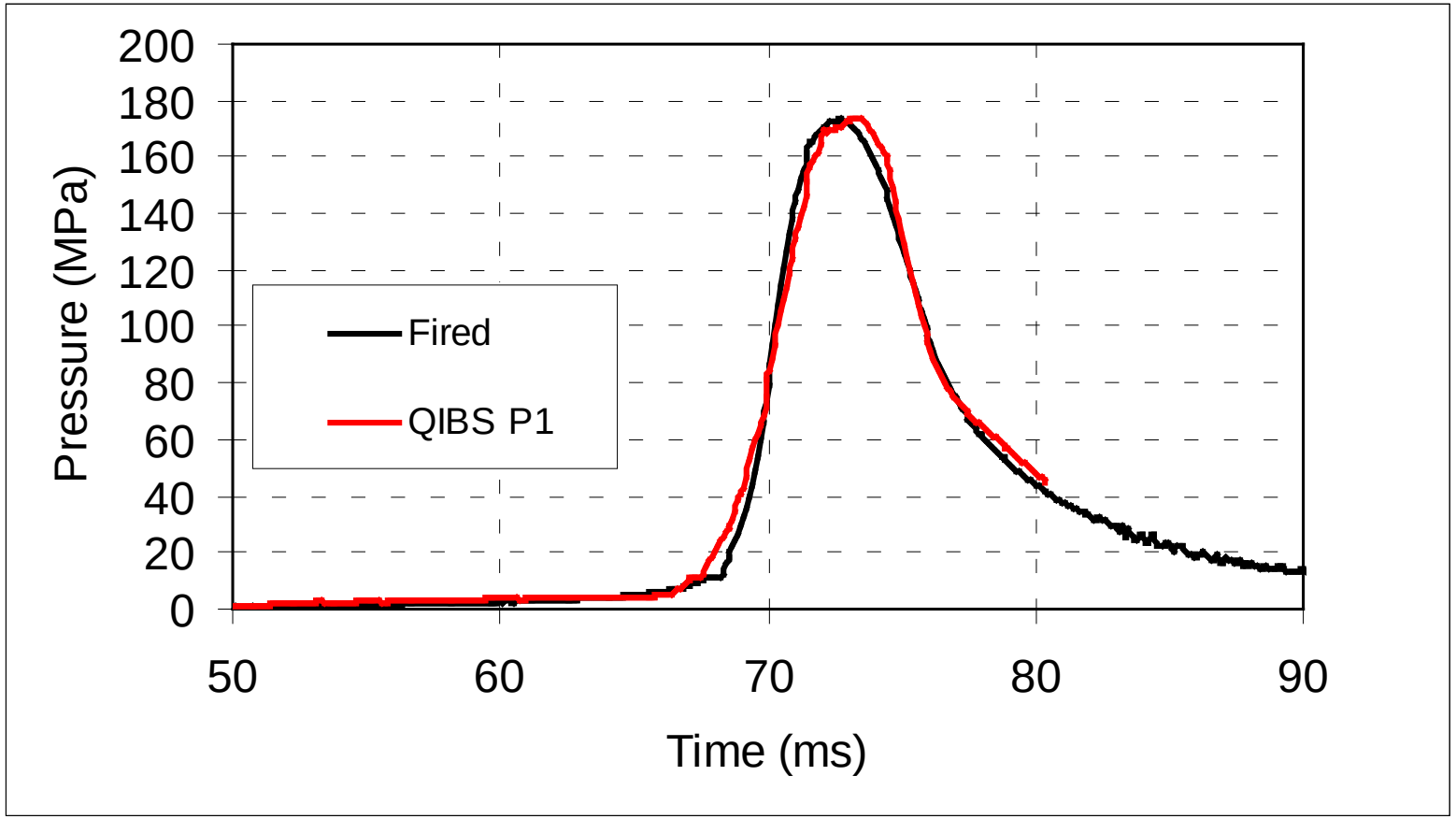

2 Lurch phenomenon

Good agreement for three further rounds fired at similar conditions

- Fitted ignition delays of 20ms, 22ms and 21ms

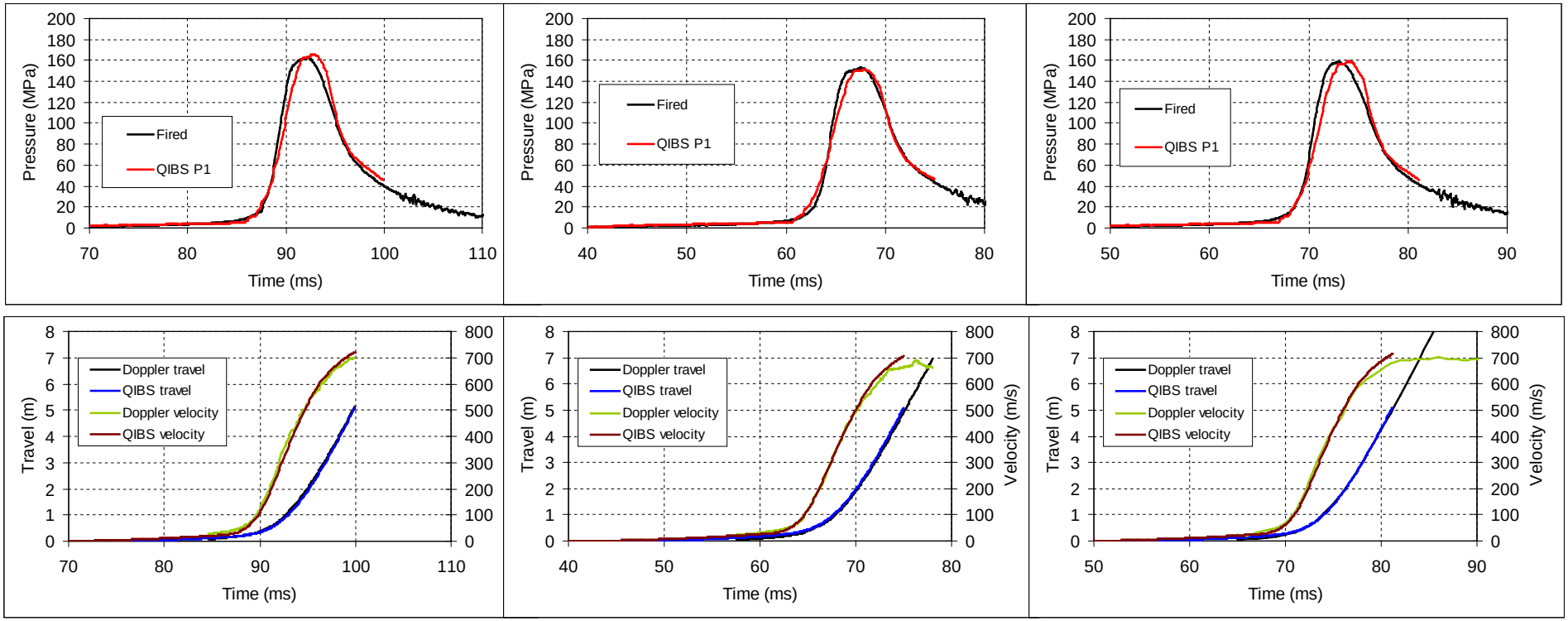

2 Lurch phenomenon

Good agreement for two further rounds with increased charge mass or heavier projectile

- Fitted ignition delays of 23ms and 19ms

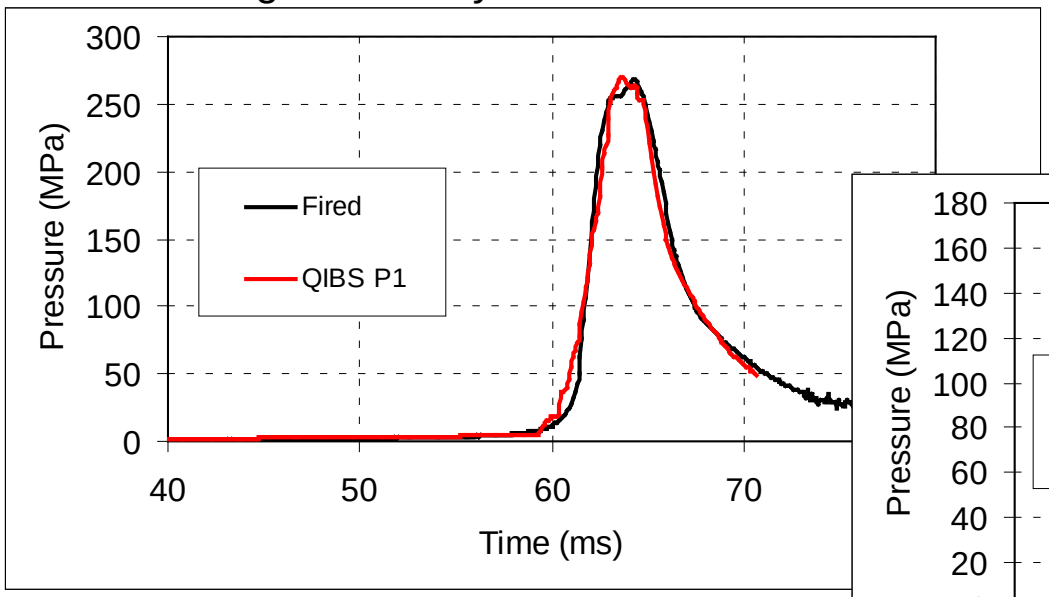

OK but not predictive!

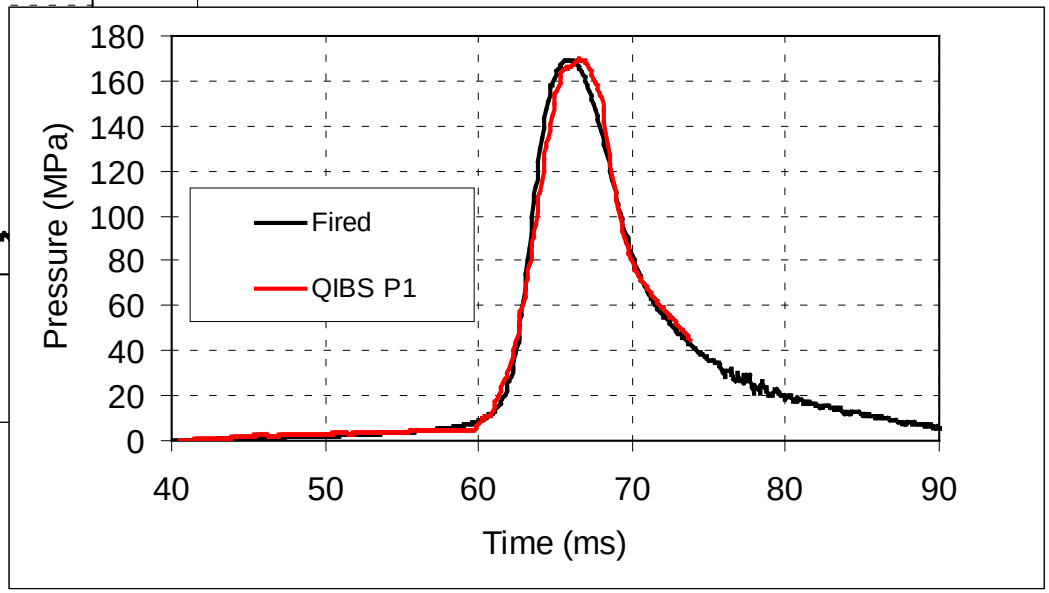

3
Application of QIMIBS

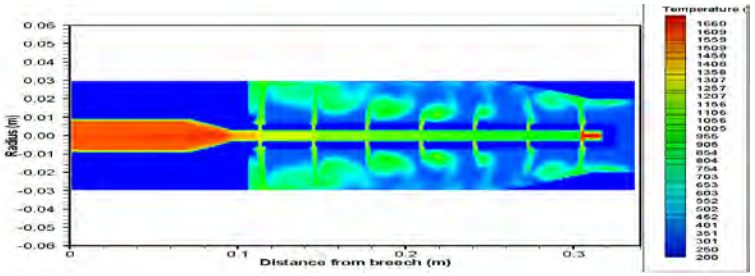

3 Application of QIMIBS

2D internal ballistics code developed to investigate ignition phenomenon

- Predicted the ignition delay for the charge used for the lightweight projectile

3 Application of QIMIBS

First simulation: ignition model not used

- Time base adjusted to align predicted and measured shot motion

3 Application of QIMIBS

Second simulation: ignition model used

- **No adjustment of time base required!!**

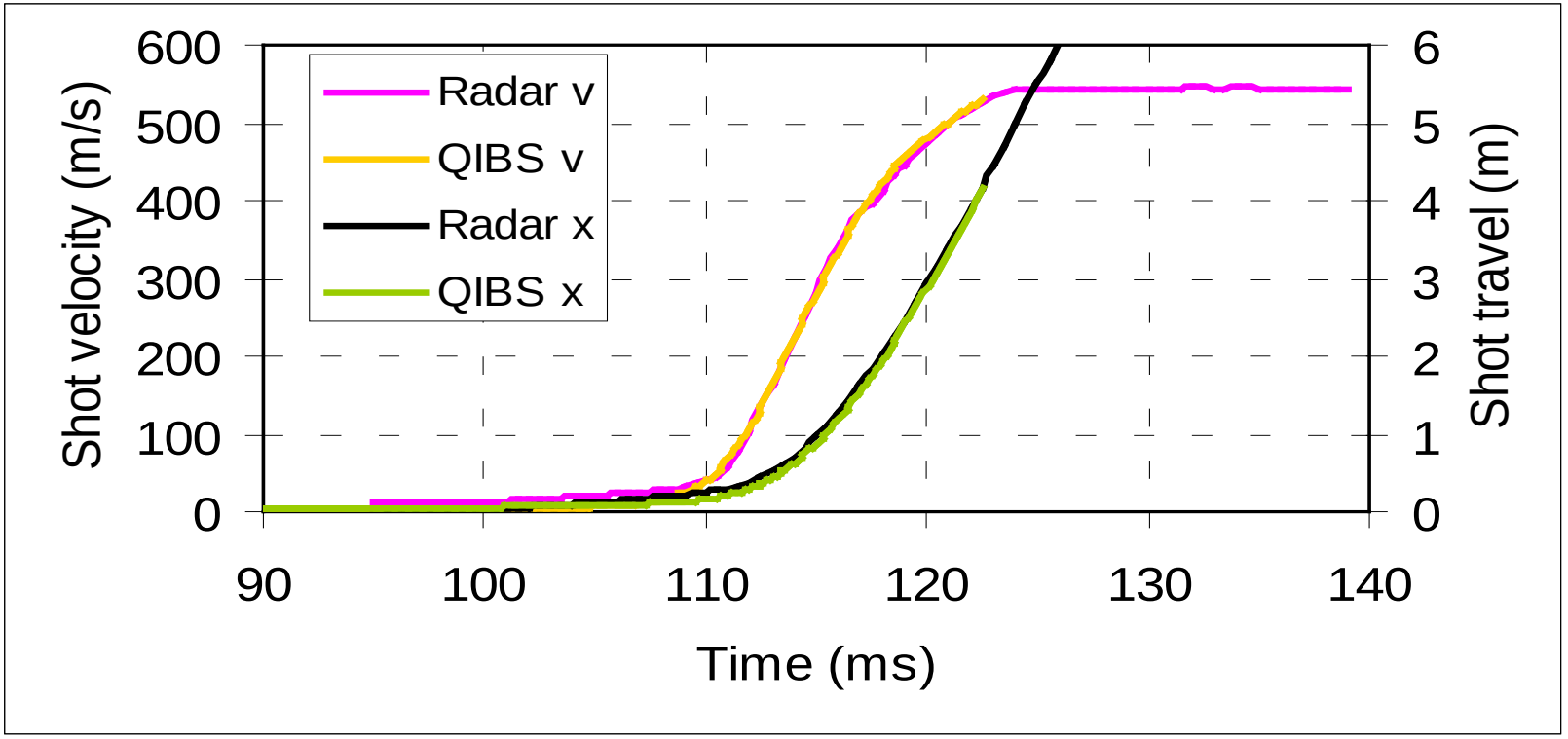

4 Conclusions

- Lurch effect likely to have been caused by a low shot start pressure (i.e. engraving resistance) together with a fast burning CCC material having a low ignition threshold
- Possible to simulate by using an ignition delay in 0D and 1D internal ballistics models
- QIMIBS was able to predict the ignition delay very well and also the maximum pressures for the lightweight projectile
- The advanced ignition models embodied in QIMIBS are able to provide the predictive capability needed for modelling the internal ballistics of the lightweight projectiles

www.QinetiQ.com

Perforator with Energetic Liner

David Davison
Shock Transients, Inc., PO Box 5357, Hopkins, MN 55343 USA
(952) 944-3539, X2 voice/(952) 944-8170 fax — dkd1@shocktrans.com

Dan Pratt
Owen Oil Tools, PO Box 568, Godley, TX 76044 USA
(817) 551-0540, X1074 voice/(817) 551-1674 fax — Dan.Pratt@CoreLab.com

— International Ballistics Symposium, September 2011 —

Summary

- Jet formation process
- MPXI™ insensitivity
- Expansion of copper bands around concrete targets
- Test arrangements
- Holes in steel targets
- Framing camera images of band expansion
- Dual chamber test fixture
- Conclusions

Perforator and Liner Collapse Process

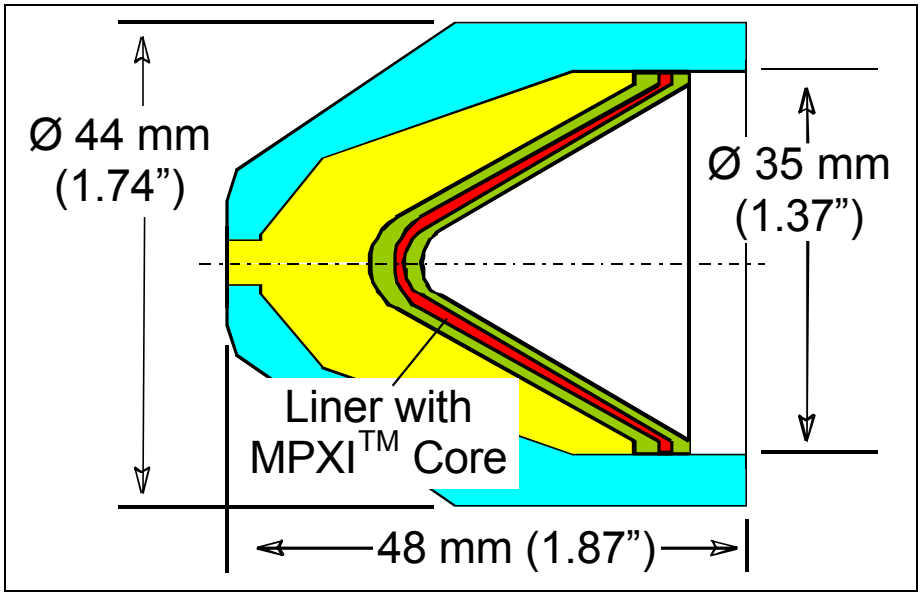

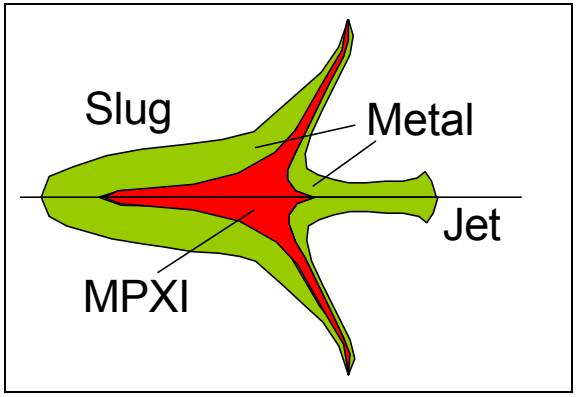

The the MPXI™ material experiences not only the compression from the detonation front and the squeezing during liner collapse but also the distortion that occurs in the jetting process .

Insensitivity of MPXI™ Material

A test of an MPXI™ puck perforated by a shaped charge jet shows insensitivity to extreme impact. The material was also insensitive when “cooked” over a fire for 30 minutes.

Copper Bands around Concrete Targets

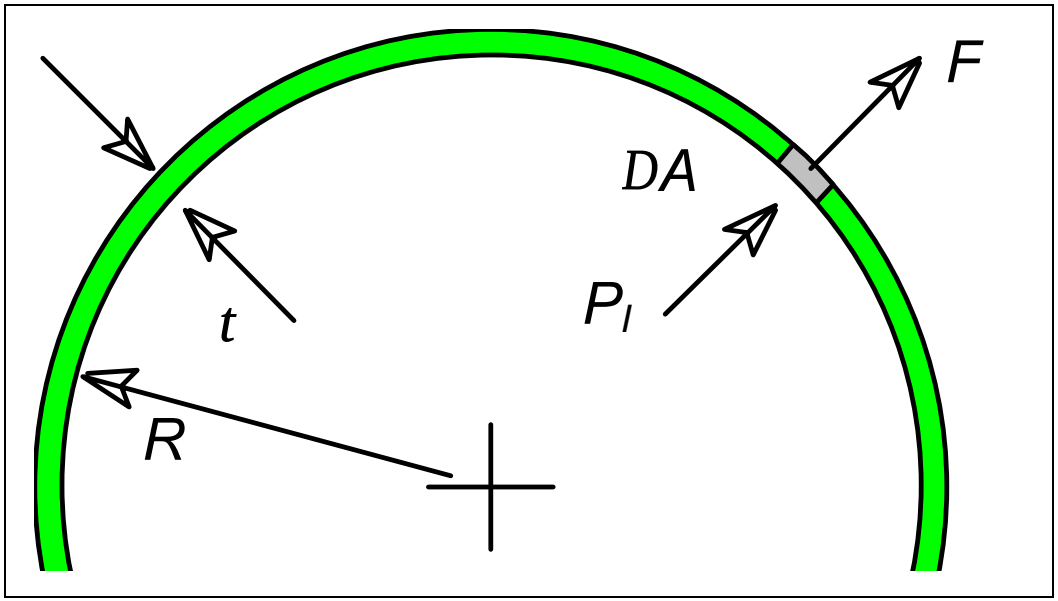

Impulse analysis (Y = 1.0 kbar, r = 8.9 gm/cm³, & $r(t) = R(t)/t(t)$):

Force	$F = (P_I - Y/r)\cdot DA = a\cdot Dm = a\cdot r\cdot t\cdot DA$, where
Acceleration	$a(t) = [P_I(t) - Y/r(t)]/r\cdot t(t)$, and
Impulse/Area	$I/A = \int P_I\cdot dt$.

Impulse/Area for Constant Pressure

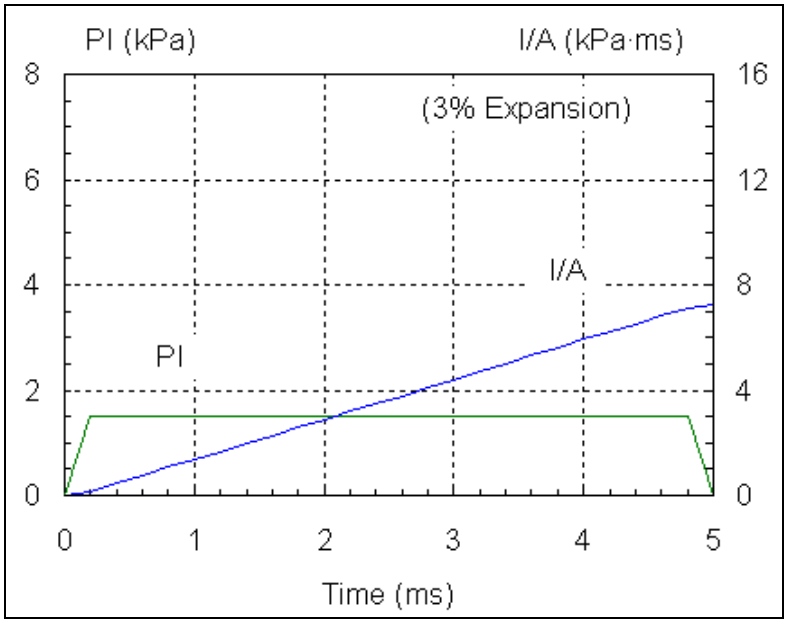

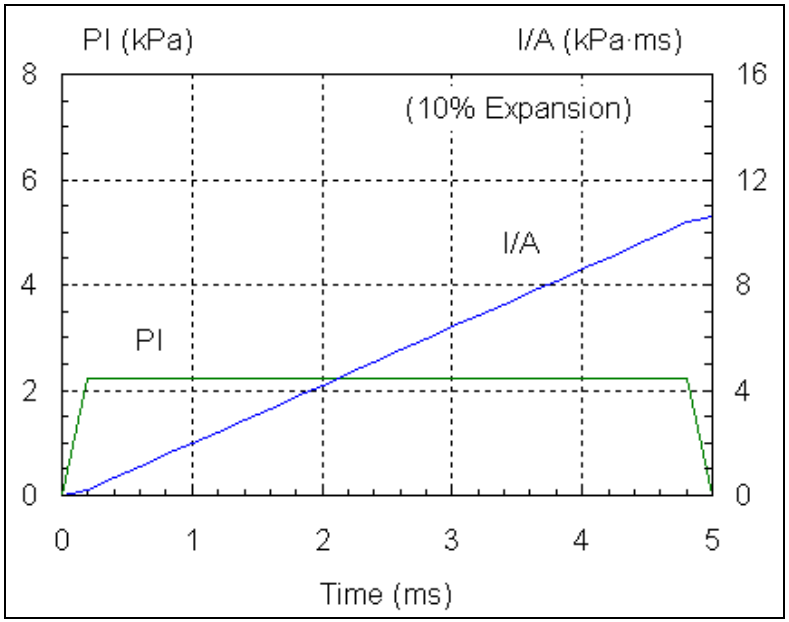

Band expansions were ≈3% for ordinary liners and ≈10% for sandwiched MPXI™ liners of equal mass. Computed impulses per unit area were 7.38 and 10.59 kPa·ms, respectively, indicating a 45% increase in impulse/area for the greater expansion and suggesting a 45% increase in blast effect for sandwiched MPXI™ liners in place of ordinary ones.

Impulse/Area for Constant Expansion

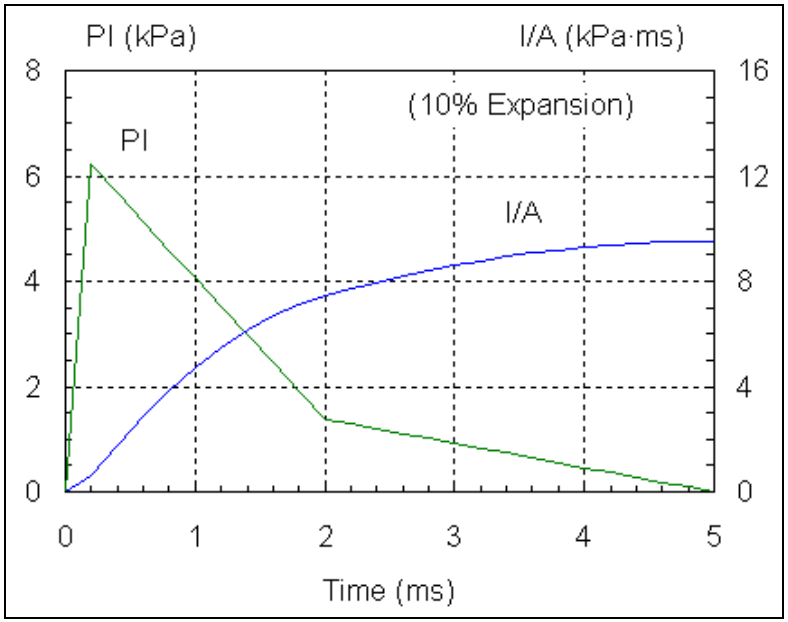

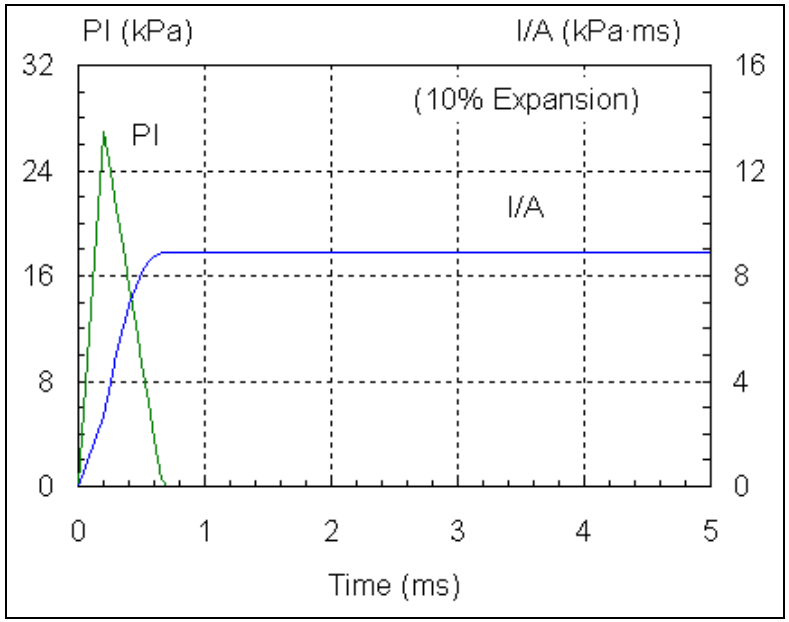

For a 10% expansion, computed impulses per unit area were 10.59 kPa·ms (prior chart) for constant pressure, and 9.52 and 8.89 kPa·ms (above) for progressively sharper pressure spikes, i.e., the shape of the pressure pulse affected the computed impulse/area, so dynamic measurements of expansion are needed to refine the evaluation of MPXI™ benefit.

Test Arrangements

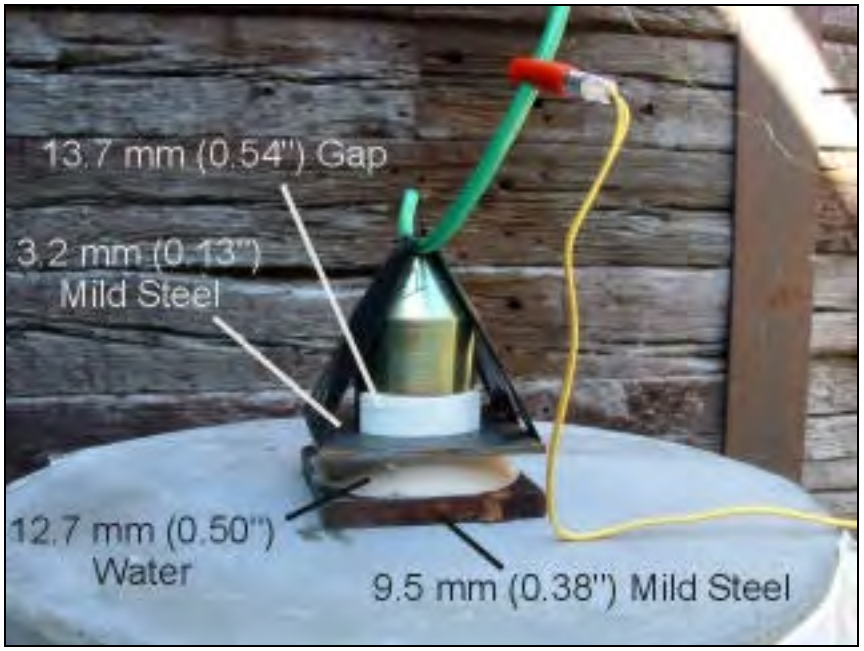

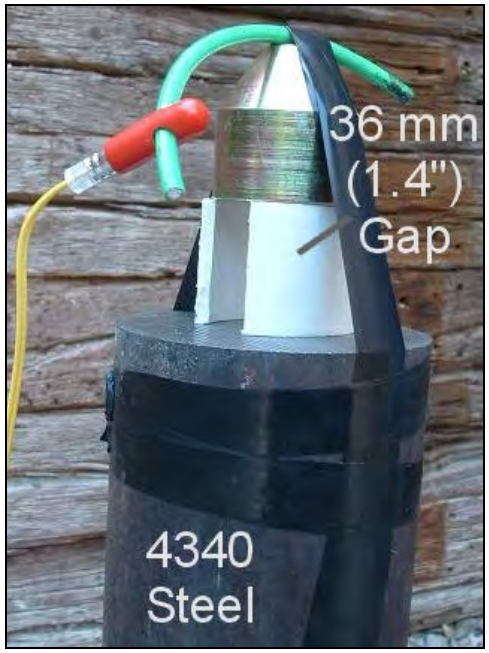

The top arrays for the Ø 305 mm x 610 mm (Ø 12” x 24”) concrete targets were oilfield quality control arrays. The concrete targets were cured for 7 days or more. Short lengths of detonator cord initiated the perforators. The steel targets were Ø 95 mm x 305 mm (Ø 3.75” x 12”), 4340 alloy, hardness 40 on the Rockwell C scale.

Holes in Steel Targets

Holes in 4340 steel targets penetrations for baseline perforators (LS-28) were equivalent to those for MPXI™-boosted perforators (LS-29).

Framing Camera Images of Band Expansion

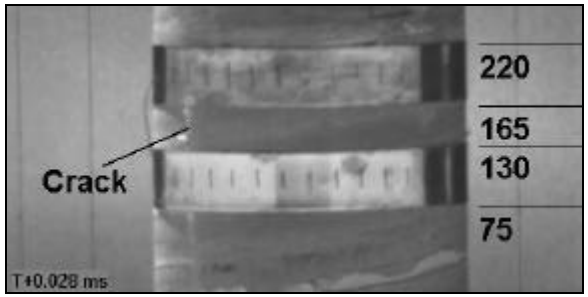

Frame 1 0.000 ms

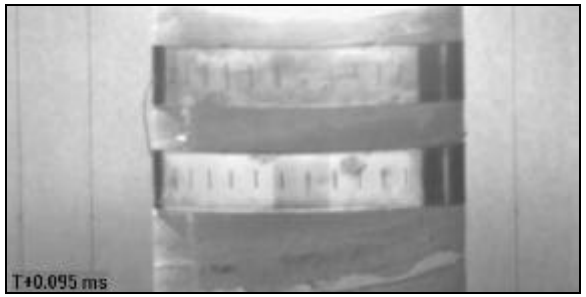

Frame 2 0.067 ms

Frame 9 0.532 ms

Frame 16 0.998 ms

Frame 31 1.995 ms

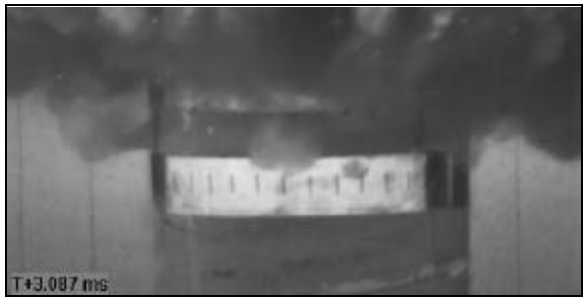

Frame 46 2.993 ms

Scans across Image 1

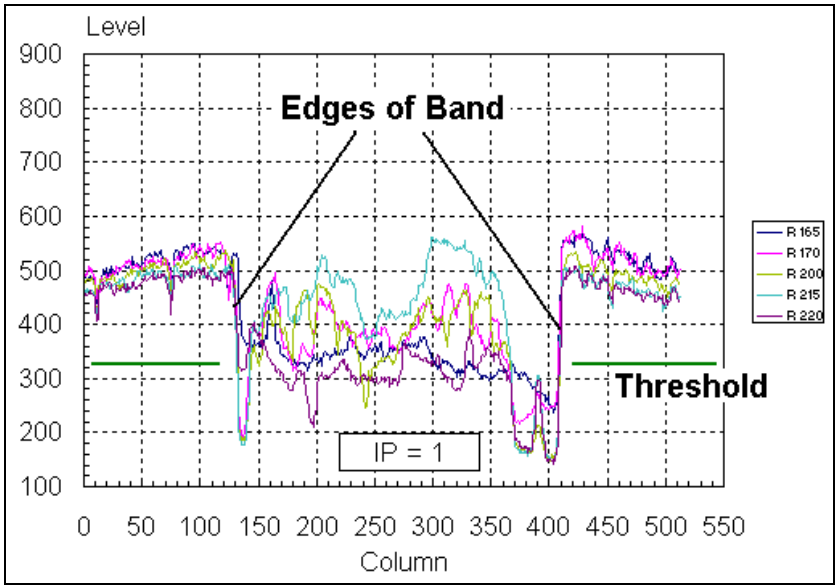

Upper Band

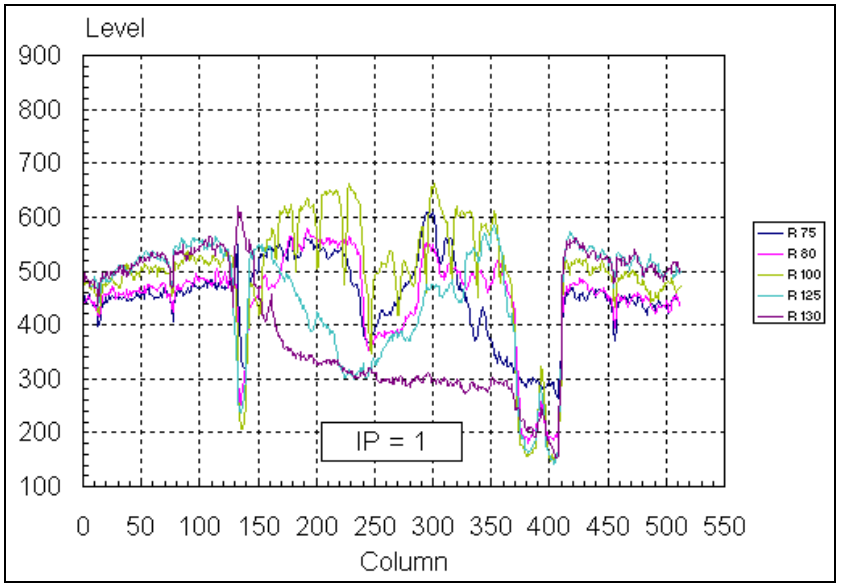

Lower Band

We extracted gray levels for the upper band between pixel rows 170 and 215 and the lower band between pixel rows 80 and 125. The threshold was a third of the way between the minimum and maximum gray levels for the rows of interest.

Band Expansions

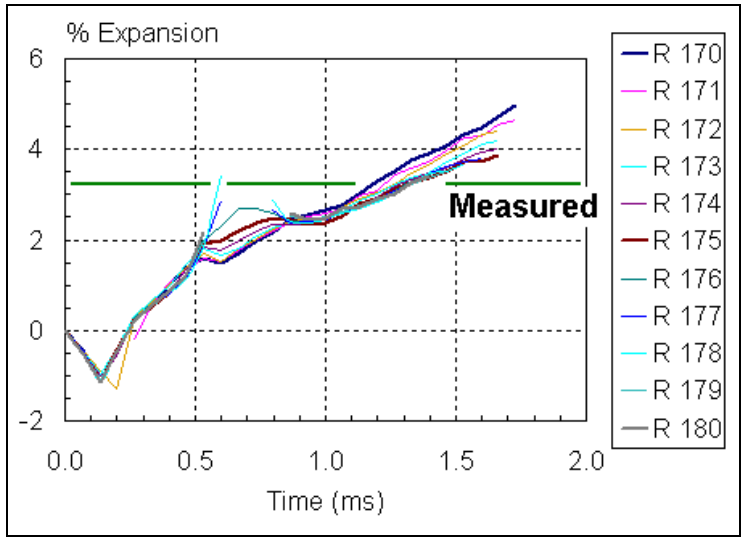

Upper Band

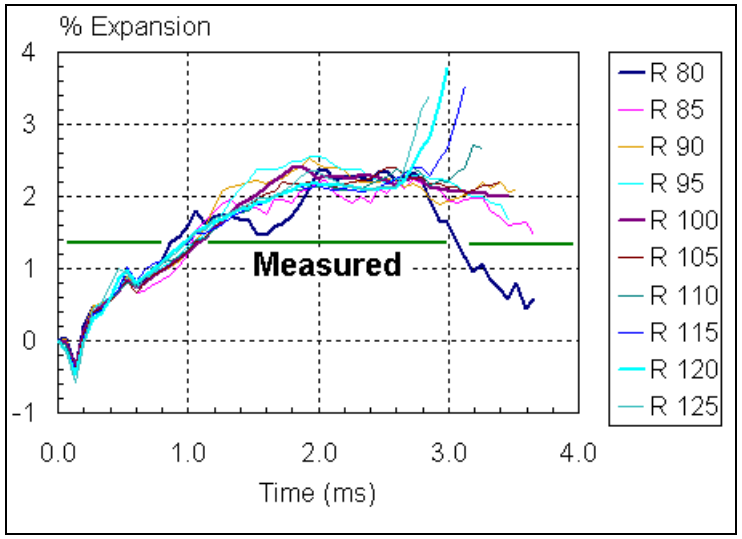

Lower Band

Measured expansions were 3.3% for the upper band and 1.7% for the lower band. Plotted percentages are relative to the band width in frame 1. Rebound to the initial shock loading caused the dips at early time. Smoke covering the upper bands gave breaks in the curves. Elastic response of the copper band caused the late-time rebound.

Dual Chamber Test Fixture

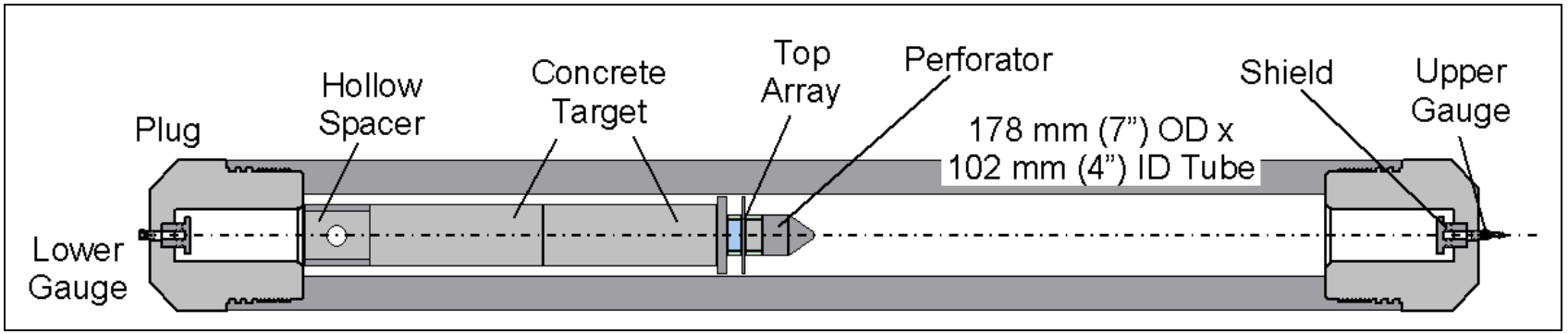

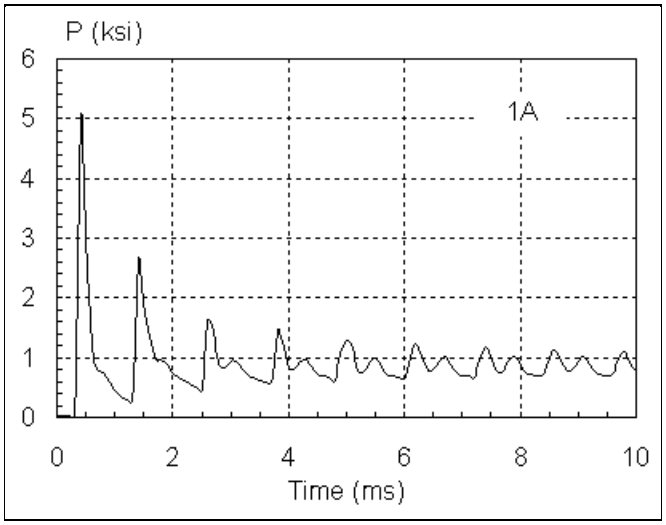

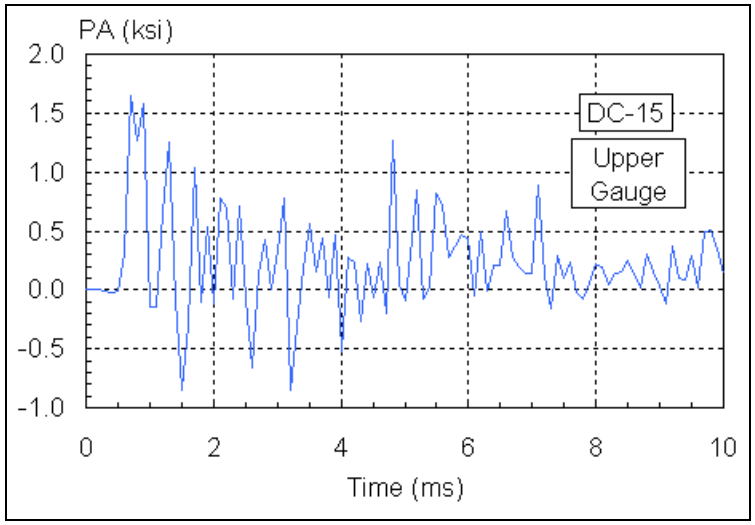

Analysis (1A) gave an initial 5 ksi peak followed by lower peaks and a steady pressure. *Tests* gave erratic data (DC-15 typical) with piezo gauges.

Conclusions

- MPXI™ is safe until activated by extreme impact.
- Steel penetrations for baseline perforators were equivalent to those for MPXI™-boosted perforators.
- Band expansions for baseline perforators were ≈3%; for MPXI™-boosted perforators expansion were ≈10%.
- Piezo gauges may be unsuitable for dual chamber pressure measurements.

IS HIGHER DETONATION VELOCITY *NEEDED* FOR SHAPED-CHARGES *?*

M. Mayseless [1], E. Hirsch [2], W.B. Harvey [3], J.E. Backofen [4]

[1] Ben-Gurion University of the Negev, Israel
[2] 6 Tachkemony St., Netanya, Israel
[3] Baker Hughes Inc., Ballistics Department, USA.
[4] BRIGS Co., USA.

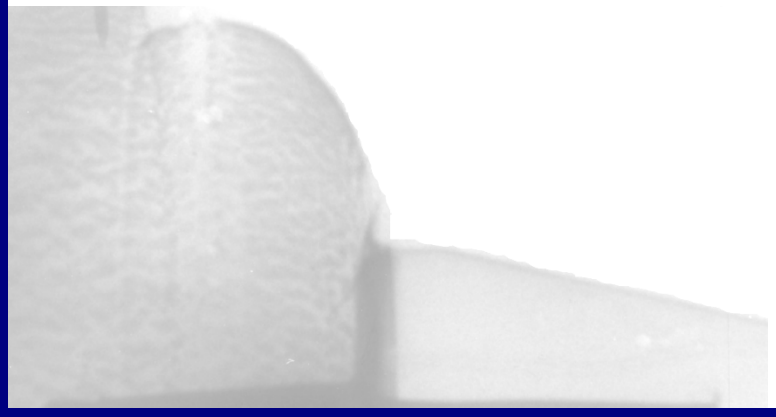

אוניברסיטת בן-גוריון בנגב
Ben-Gurion University of the Negev

BAKER HUGHES

Dedicated to:

Prof. Dr. Manfred Held

who asked many questions and had a direct interest in this topic since at least the late-1970s.

Also presented to honor others
who also worked with us since those times
on modeling, experiments and applications:

- **Mr. Don Butz**
- **Dr. Bob Eichelberger**
- **Mr. Don Kennedy**
- **Dr. Bob Sedgwick**
- **Dr. Lou Zernow**

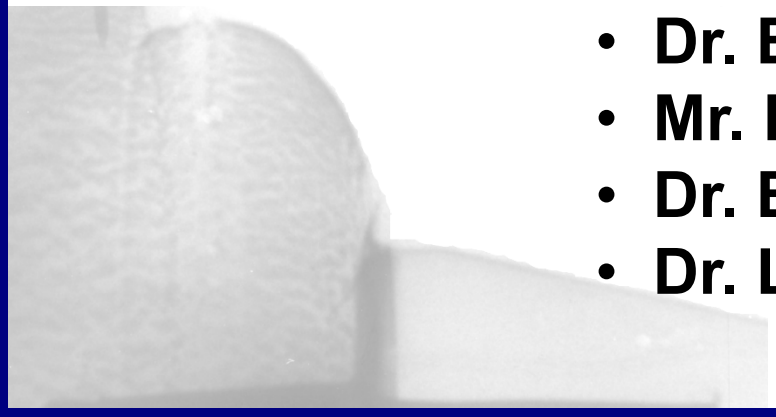

Approach

"*Partial Differential*" look into a multi-parameter, multi-process explosive application … :

- **Effects of explosive performance are envisioned and modeled consistently,**
- ***Two* different modeling methods were validated and extrapolated:**
  - **SCAN analytical model code**
  - **Baker Hughes 2-D 2nd Order Eulerian Grid Code**

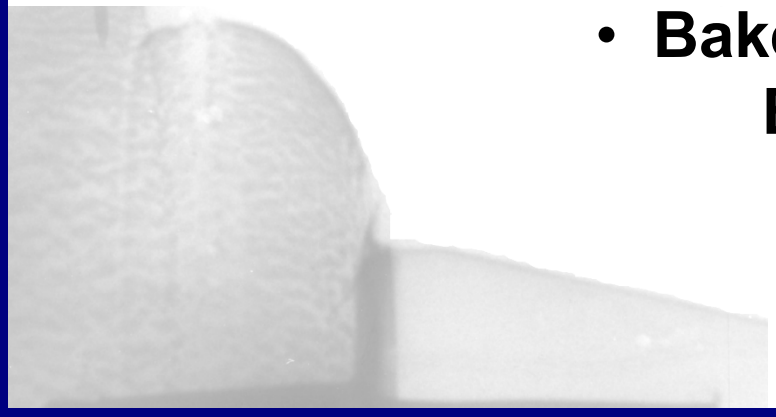

Earlier work using BRIGS is not presented in the paper or presentation.

Detonation Velocity -- *Key* Characteristic of Explosive *Mass* & *Energy Densities*

For an individual energetic material $D = A + B\,\rho_o$

describes performance versus pressed or cast density at less than crystal density

Urtiew & Hayes **provided formula for D from 34 energetic materials and binders.**

Using gas expansion to define propulsion

$\gamma_{\text{average}} = 2.77$ *

$\gamma = -\,d \ln P / d \ln V$

for constant γ **expansion**

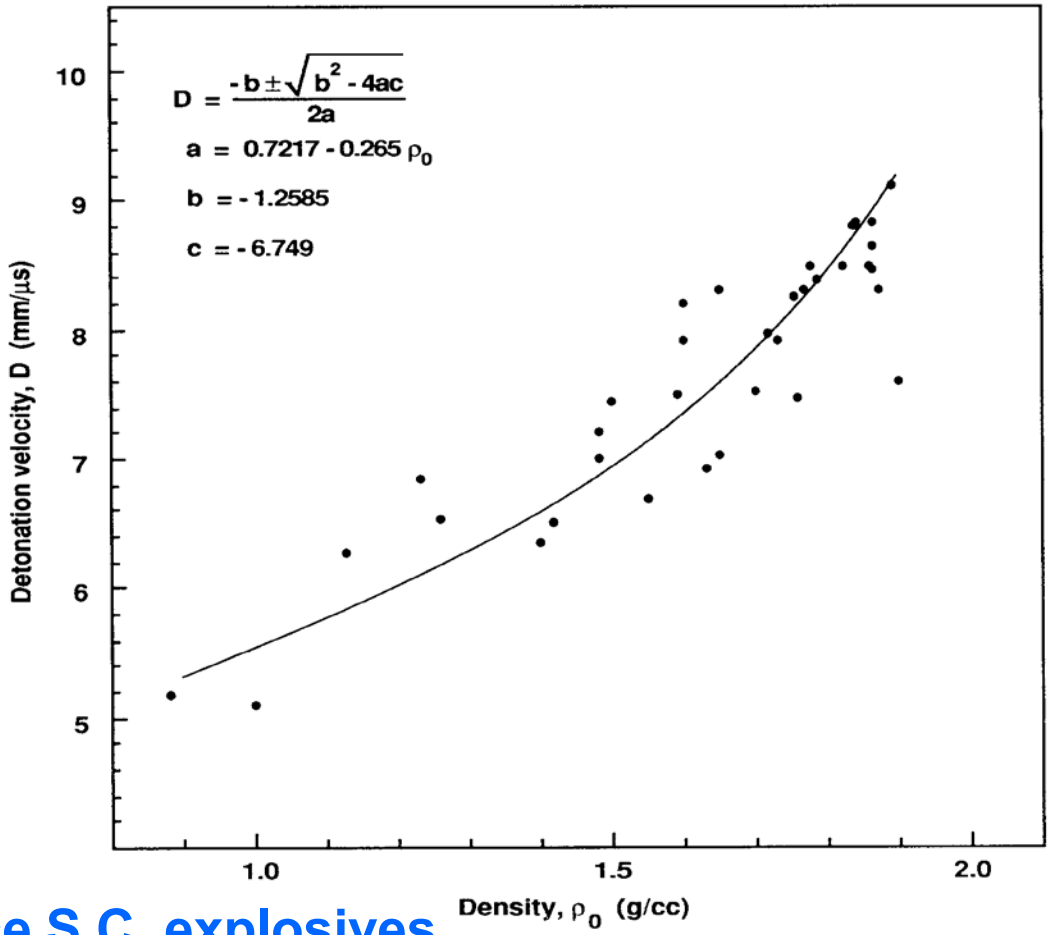

* 2.8+ for high performance S.C. explosives

Different Explosives in Shaped-Charges

SCAN used to reverse-engineer performance of 10 explosives in BRL 81-mm S-C using Gurney formulas where

$$(2E)^{1/2} = D\left((2/\gamma^2 - 1)(\gamma/\gamma+1)^{\gamma} \right)^{1/2}$$

and

$$D = 8.8\,(\rho_o/1.856)^{(\gamma-1)/2}$$

$\gamma = 2.9$

fit to published jet tip velocities

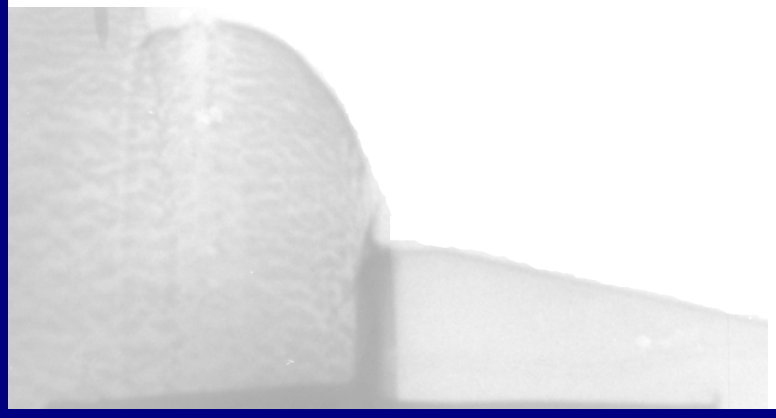

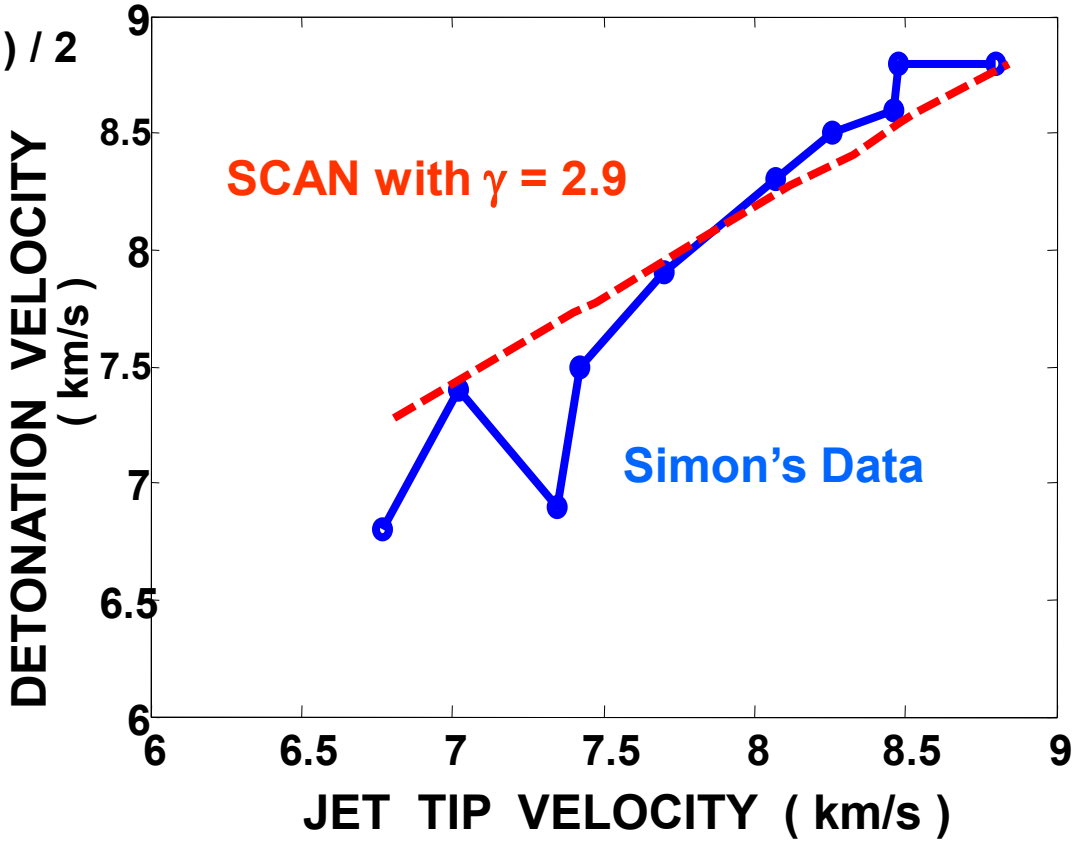

Extrapolating Explosive Performance using a JWL Equation of State

Assumptions:

- expansion isentrope does not change
- initial position for pressure / density changes
- PBX 9404 baseline

  D = 8.8 km/s

  ρ_o = 1.84 g/cm^3

  γ = 2.85

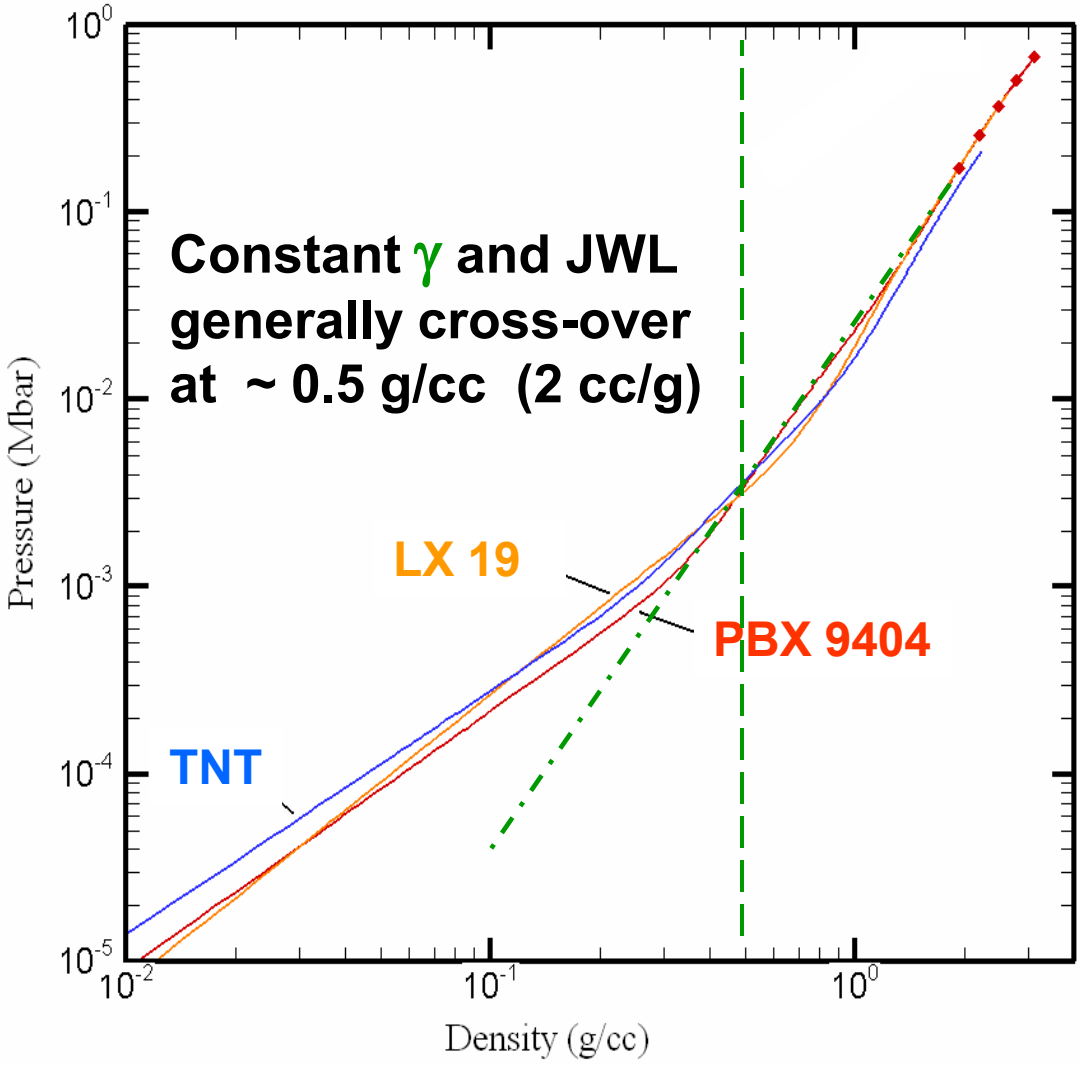

Detonation Velocity *versus* Explosive Density --- JWL & SCAN Models

Comparable **over the range of simulations**

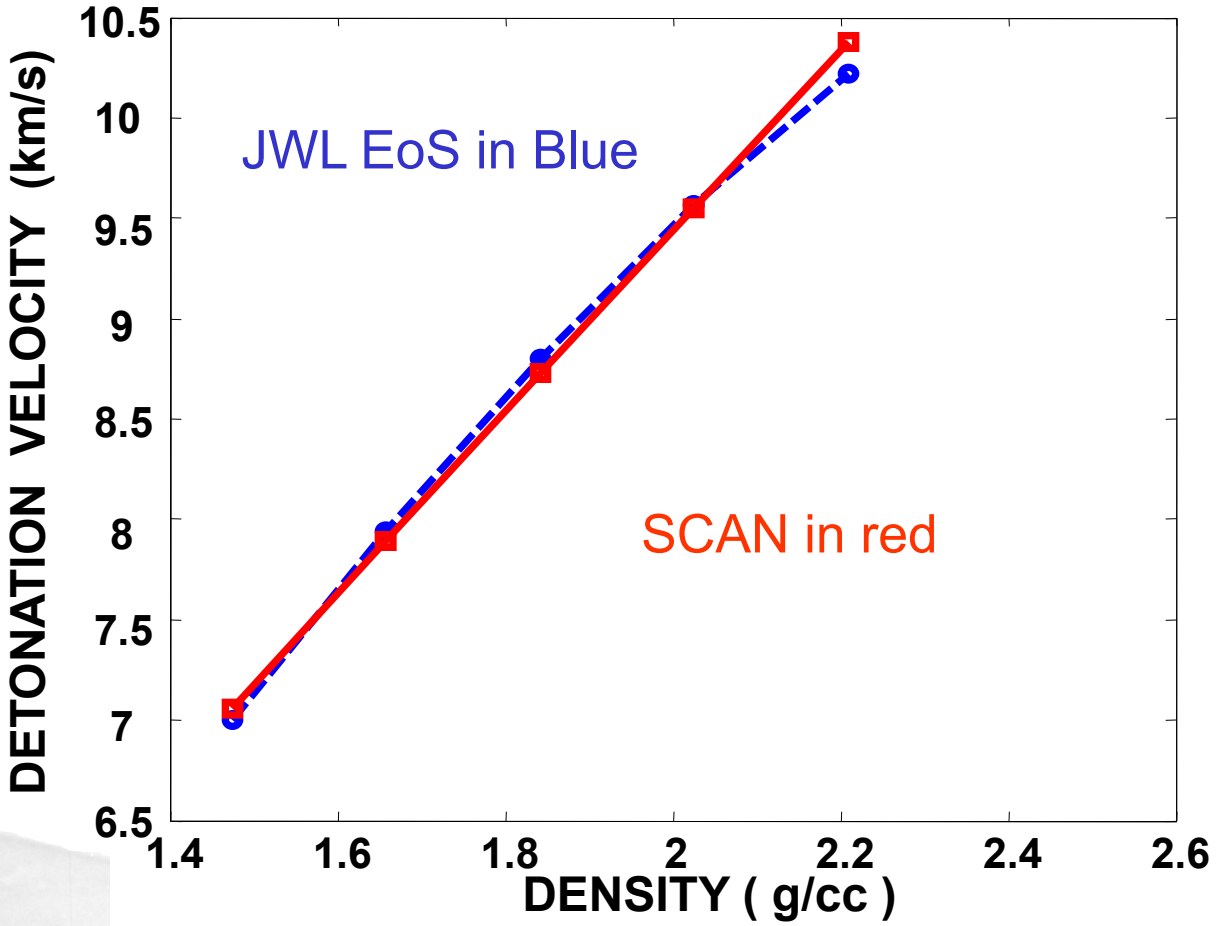

SCAN Modeling using BRL 81mm Configuration

Jet Tip Velocity *increases* until jet formation process reaches *supersonic limitation* at

~ 10.12 km/s at explosive density ~ 2.15 g/cc

then *Jet Tip* disperses as non-coherent expanding tube

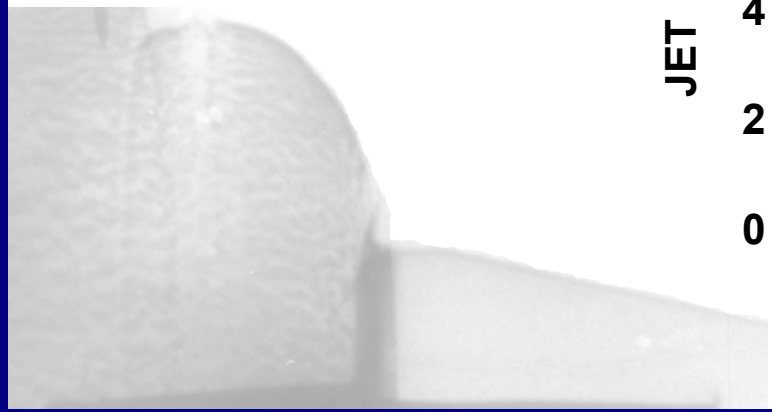

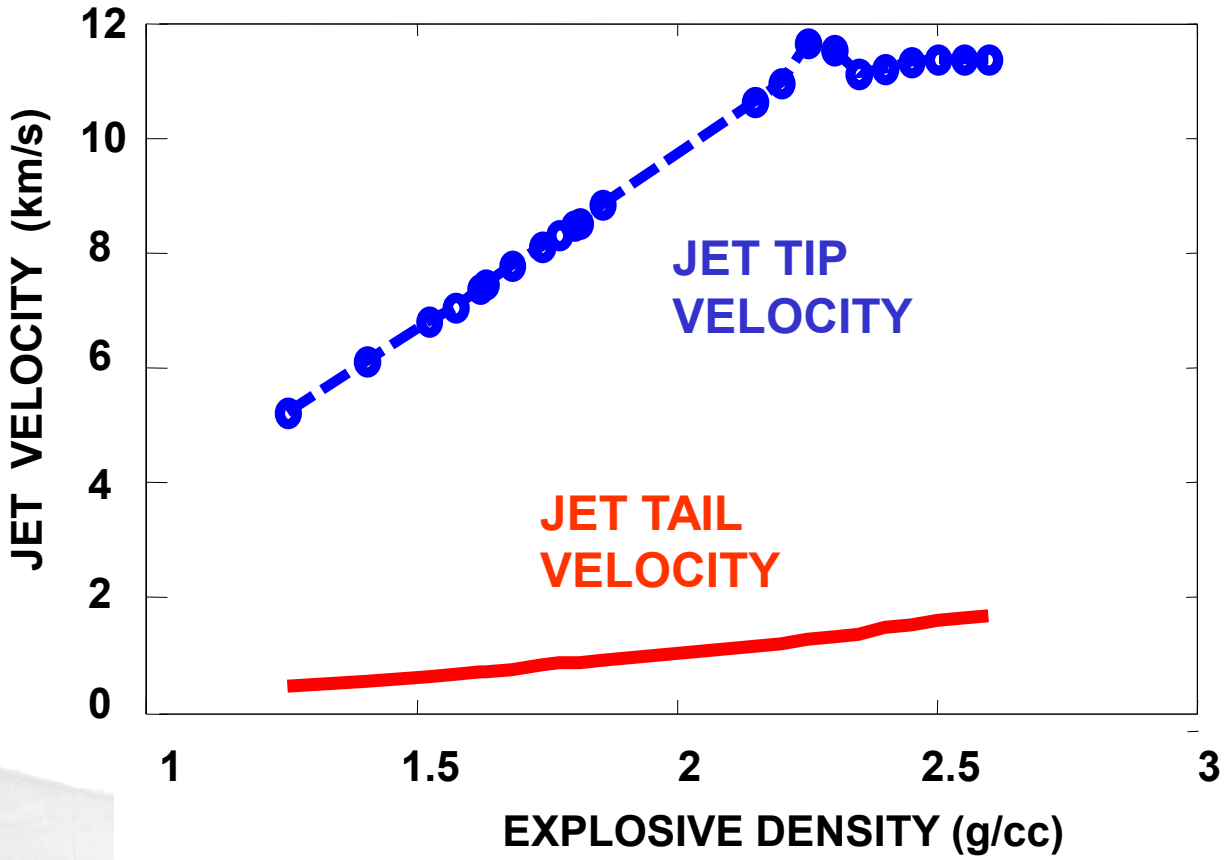

SCAN Modeling using BRL 81mm Configuration

Supersonic collapse *limits* Jet Length, Velocity Gradient and Target Penetration

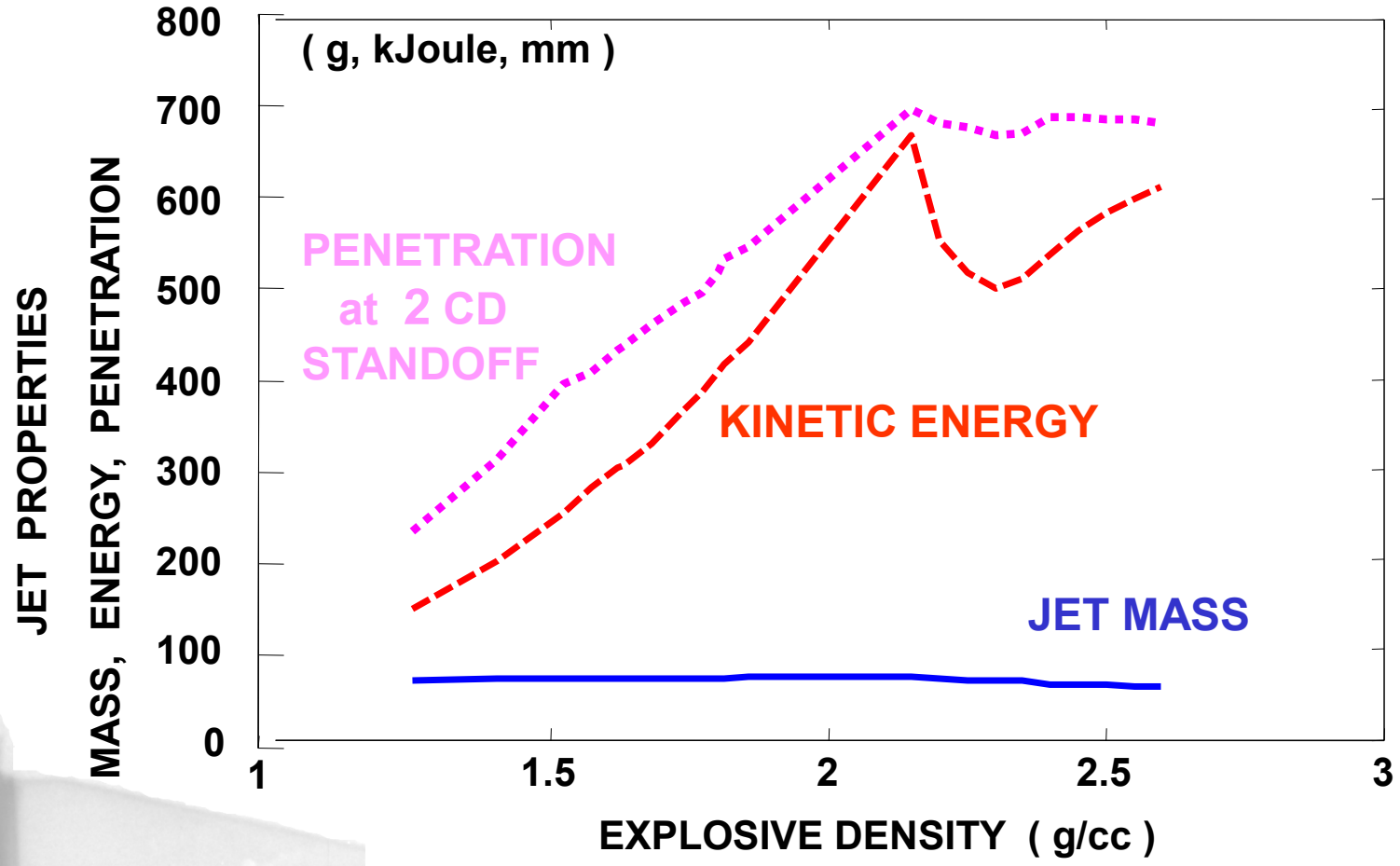

SCAN Modeling using BRL 81mm Geometry

Supersonic jet formation *criterion* applied to combinations of cone angle and explosive density

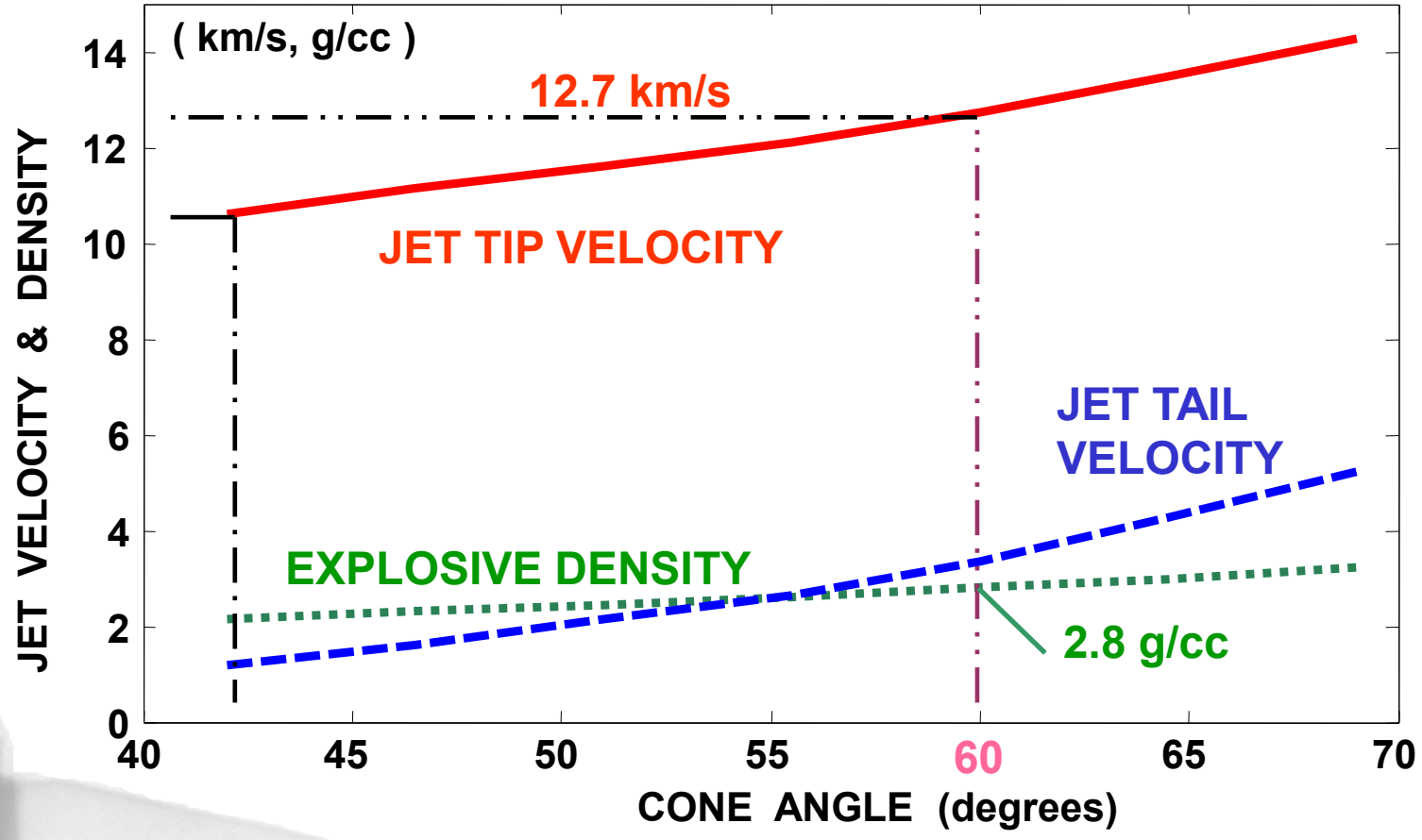

Baker Hughes 2-D 2nd Order Eulerian Code Simulations

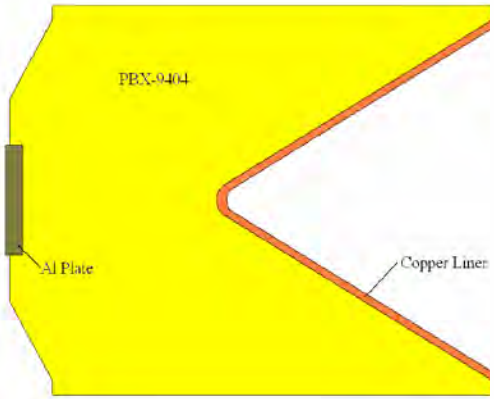

60^0 Cu, t_{liner} 1.65 mm point initiated

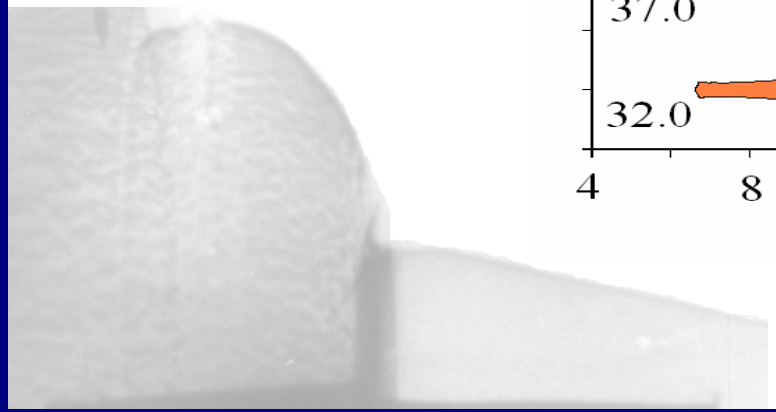

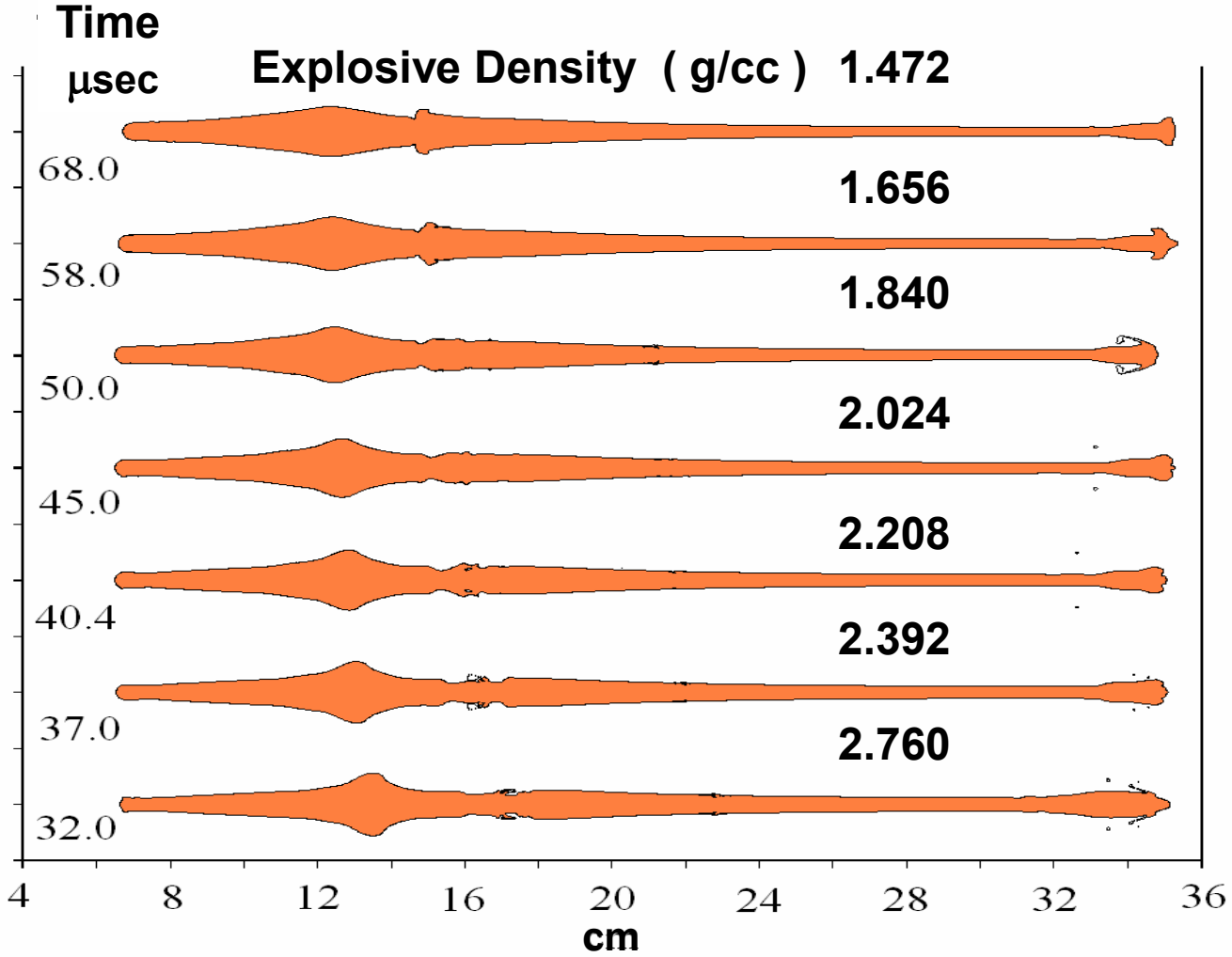

Simulations were stopped when jet tip reached ~ 24 cm from charge face

Baker Hughes 2-D 2nd Order Eulerian Code Simulations:

Increased Density and Detonation Velocity lead to:

- increased Jet:
  - velocities,
  - gradients, and
  - kinetic energy
- *dramatically* increased Slug velocity

From 600 to 700 m/s to ~ 1500 m/s

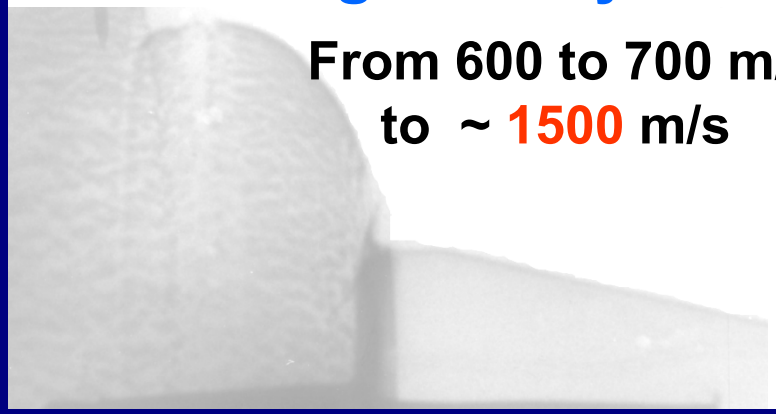

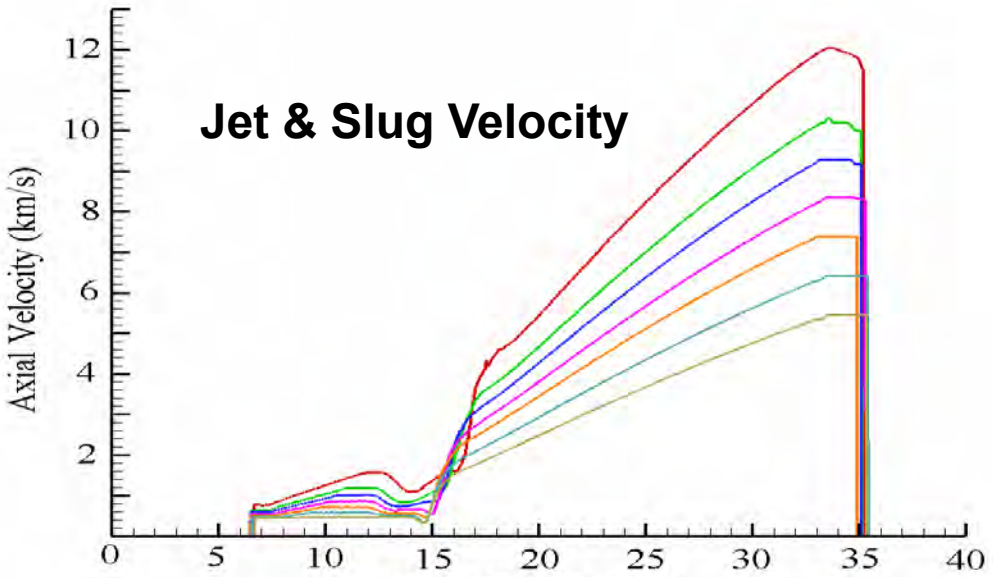

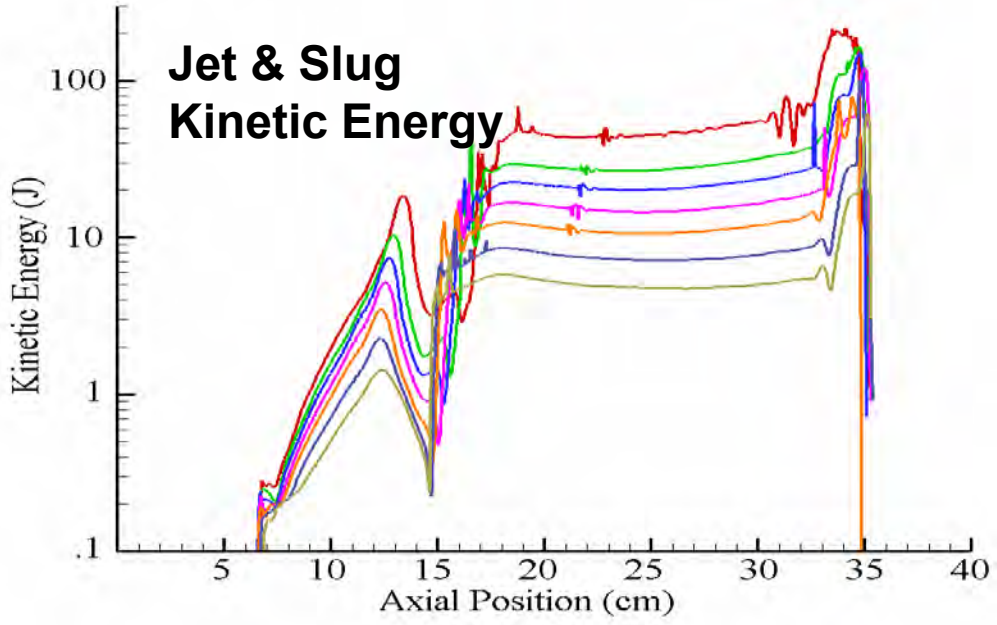

SCAN Modeling of Cone-Shaped Detonation

Detonation wave half angle Θ is determined by the ratio of outer to inner detonation velocities

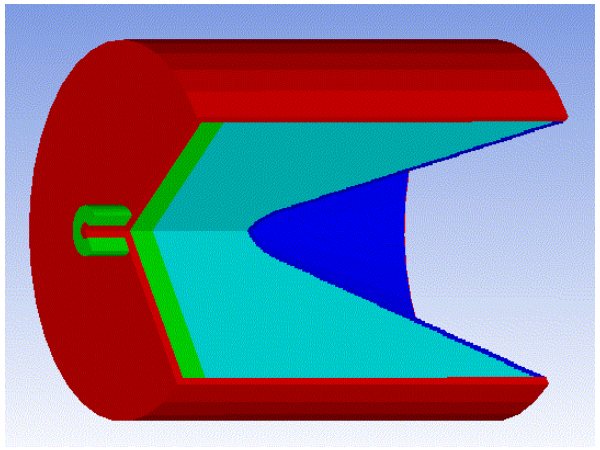

81.3 mm diameter

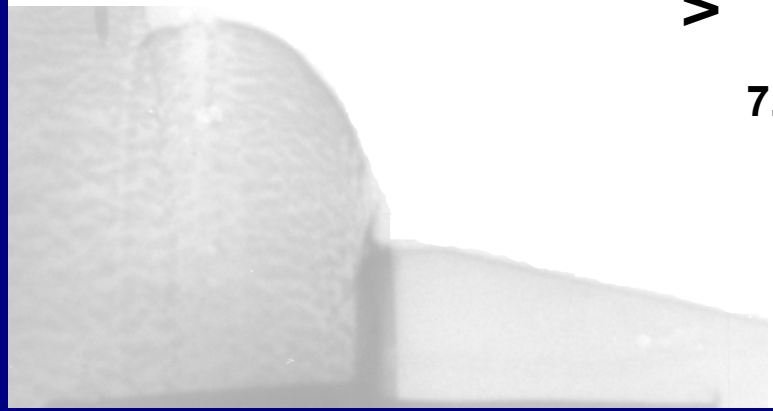

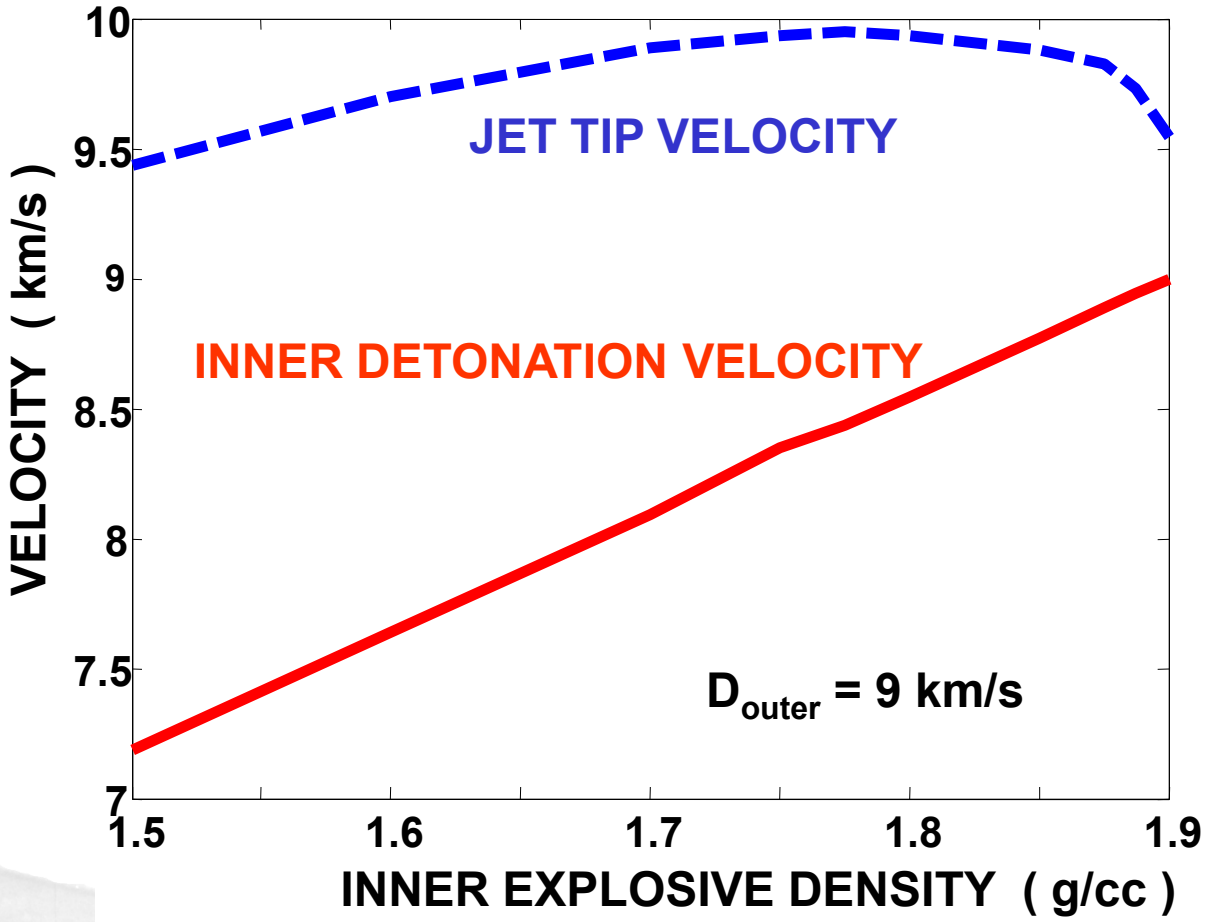

SCAN Modeling of Cone-Shaped Detonation in a BRL 81 mm Shaped Charge

Optimum jet formation (*supersonic criterion*) using lower performance explosive for majority of charge

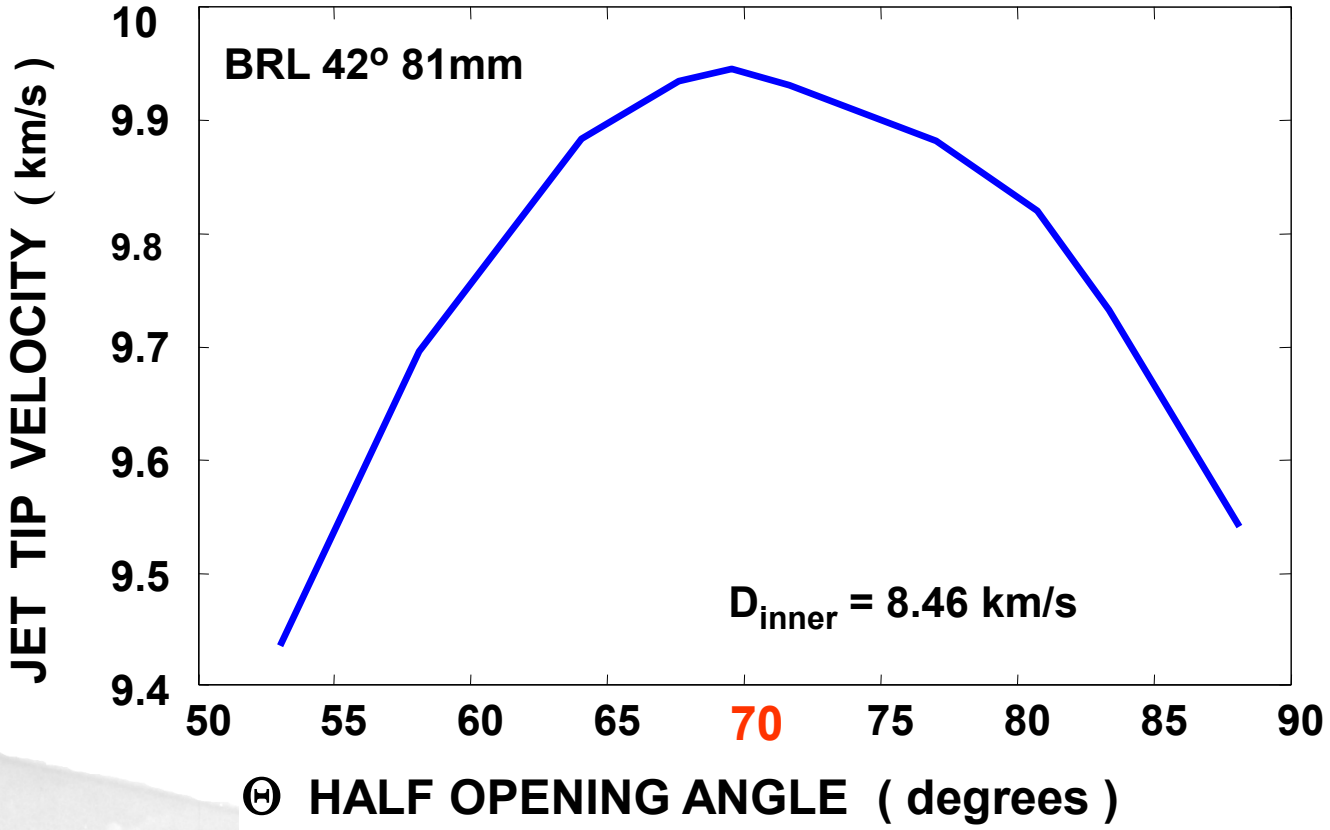

LIFT Charge

(1980)

[Cone-Shaped-Wave Shaped Charge]

Explosive

Water-Based or *Organic* Material

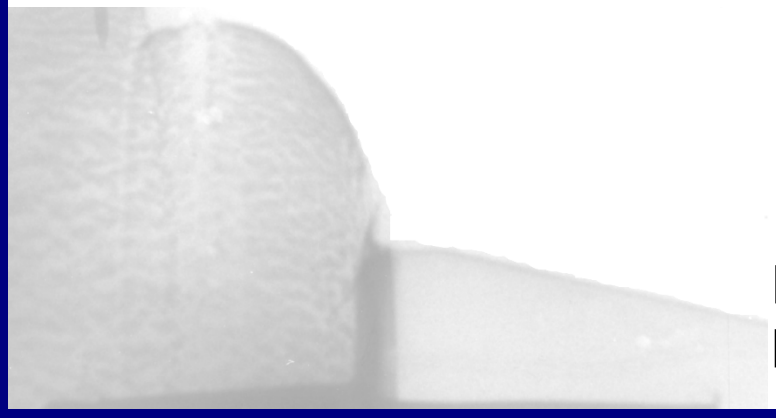

United States Patent [19]

Petrousky et al.

[11] **Patent Number: 4,955,939**

[45] **Date of Patent: Sep. 11, 1990**

[54] **SHAPED CHARGE WITH EXPLOSIVELY DRIVEN LIQUID FOLLOW THROUGH**

[75] Inventors: **James A. Petrousky**, Port Tobacco, Md.; **Joseph E. Backofen**; **Donald J. Butz**, both of Columbus, Ohio

[73] Assignee: **The United States of America as represented by the Secretary of the Navy**, Washington, D.C.

[21] Appl. No.: **471,381**

[22] Filed: **Mar. 2, 1983**

[51] **Int. Cl.**[5] **F42B 12/10**

[52] **U.S. Cl.** **102/476**; 102/306; 102/307; 102/308; 102/309; 102/310

[58] **Field of Search** ..... 102/306–310, 102/476; 86/1 B, 1.1; 89/1 A, 1.11

[56] **References Cited**

U.S. PATENT DOCUMENTS

1,913,015	6/1933	Vadoz .	
3,103,882	9/1963	Gilliland .	
3,117,518	1/1964	Porter et al.	102/307
3,162,121	12/1964	Crawford	102/306
3,188,955	6/1965	Brown	102/306
3,190,219	6/1965	Venghiattis	102/306
3,561,361	2/1971	Kessenich	102/307
4,065,005	9/1977	McDanolds et al.	86/1 B
4,109,575	8/1978	Hashimoto .	
4,169,403	10/1979	Hanson	86/1 B
4,170,940	10/1979	Precoul	102/476

Primary Examiner—Charles T. Jordan
Assistant Examiner—Richard W. Wendtland
Attorney, Agent, or Firm—Kenneth E. Walden; Donald J. Breh

[57] **ABSTRACT**

Disclosed is a non-fragmenting explosive device for perforating a target and injecting a material through the perforation to disrupt structure behind the target. The device is particularly adapted to safely disarm unexploded explosive devices such as bombs without detonation of the bomb. The device includes an outer covering of explosive material for explosively confining the disruptive material to a well defined shape for total injection into the target.

1 Claim, 2 Drawing Sheets

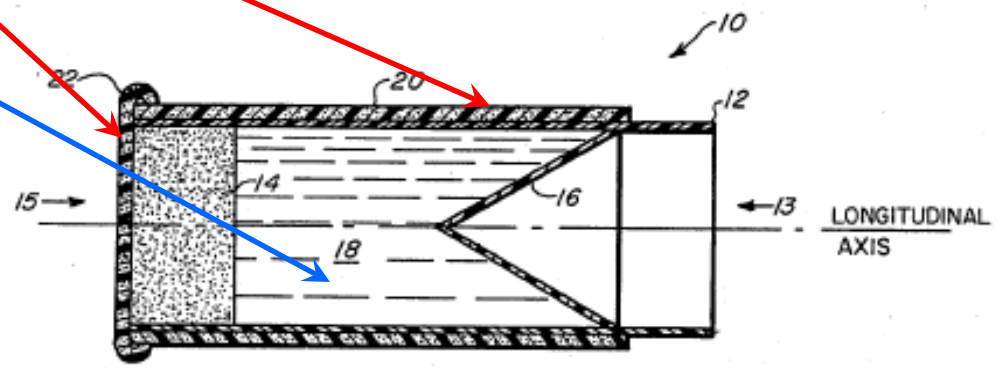

Drs. L. Zernow, M. Held, R. Brown and others have designed and built “over-wrap” devices

Summary and Conclusions

Higher Detonation Velocity Explosives
***can still provide more* shaped charge performance**

Jet & Slug *Velocities* and *Kinetic Energy increased*

as a result, Jet & Slug can be tailored for *increased* target penetration and effect

Higher Detonation Velocity Explosive
can be used as an "*outer-wrap*" to provide:

- **Conical detonation wave**
- **Optimization**
- **Insensitive explosive charge designs**

IS HIGHER DETONATION VELOCITY *NEEDED* FOR SHAPED-CHARGES *?*

NO …. but, it can be very beneficial

[1] Ben-Gurion University of the Negev, Israel
[2] 6 Tachkemony St., Netanya, Israel
[3] Baker Hughes Inc., Ballistics Department, USA.
[4] BRIGS Co., USA.

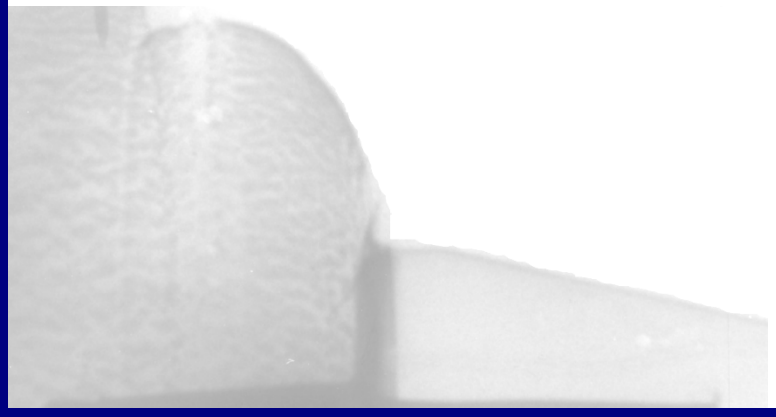

אוניברסיטת בן-גוריון בנגב
Ben-Gurion University of the Negev

BAKER HUGHES

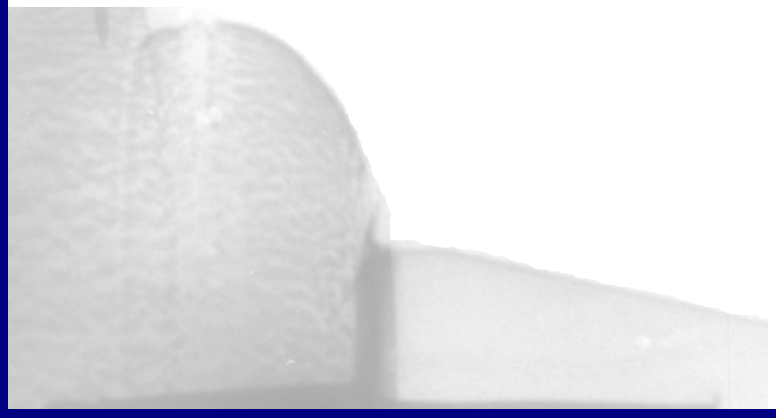

Gurney Velocity / Detonation Rate relationships:

$Vg / D \cong 0.337$ (P.W. Cooper)

$Vg / D \cong (0.605 / [\Gamma - 1])$ (J. Roth per J.E. Kennedy)

where Γ = the adiabatic exponent for the gaseous products

$Vg / D \cong (0.60\ \phi^{-1/2} + 0.648\ \rho_o{}^{1/2}) / (1.01 + 1.313\ \rho_o)$

where $\phi = N\ M^{1/2}\ Q^{1/2}$; N = moles of gaseous detonation products
M = average weight of gases, and Q = chemical energy of detonation
(Hardesty & Kennedy / Kamlet & Hurwitz)

Copper Cylinders

Vg / D	Exp. (Licht)	Cooper	Roth	HK/ KH
TNT	0.346	0.346	0.350	0.351
Comp B	0.345	0.343	0.355	0.385
Octol	0.335	0.330	0.331	0.328
LX-14	-----	0.326	0.348	-----
PETN	0.359	0.355	0.369	0.331

at $\gamma = 2.9$, SCAN formula ==> $Vg / D \cong 0.338$

Joe Backofen
540-297-2640
BRIGS Co.
jebackofen@earthlink.net

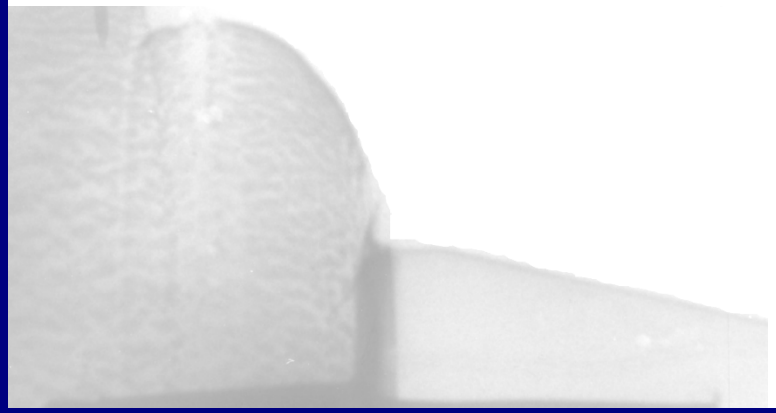

RHEINMETALL DEFENCE

Burning Behavior of Gun Propellants under the Influence of Pressure Oscillations Theoretical Background and Simulation

26th International Symposium on BALLISTICS
Miami, September 12-16, 2011

Dr. Klaus-Achim Kratzsch

Outline

- **Introduction**
- **Experimental Results**
- **Theoretical Approach**
  - Modeling of standing pressure waves in the perfs of gun propellant grains
  - Impact of the standing pressure waves on the burning behavior in the perfs
  - Alternative approach to explain the anomalous burning behavior in the perfs
- **Simulation of Closed Vessel Tests with Pressure Oscillations**
- **Summary and Outlook**

Introduction

During the last 15 years a lot of experimental and some theoretical work has been done in Germany to investigate pressure oscillations which can be seen when single or multi perf propellants are tested in closed vessels.

From the experimental work there is strong evidence that these pressure oscillations are correlated to standing density waves in the perfs arising from a wide spectrum of initial perturbations which occur when the flame ingresses into the perfs of the propellant grains.

Experimental Results

Experimental Results

Closed Vessel Test of a 19 perf Gun Propellant

Dimensions: L ≈ 18.7 mm
D ≈ 13.3 mm
d ≈ 0.26 mm

Recipe:

NC	≈ 68.4 %
NGL	≈ 29.0 %
Plasticizer	≈ 1.3 %
Stabilizer	≈ 1.3 %

CV 200 ml, Loading Density ≈ 0.2 g/cm³, T_c = -40 °C

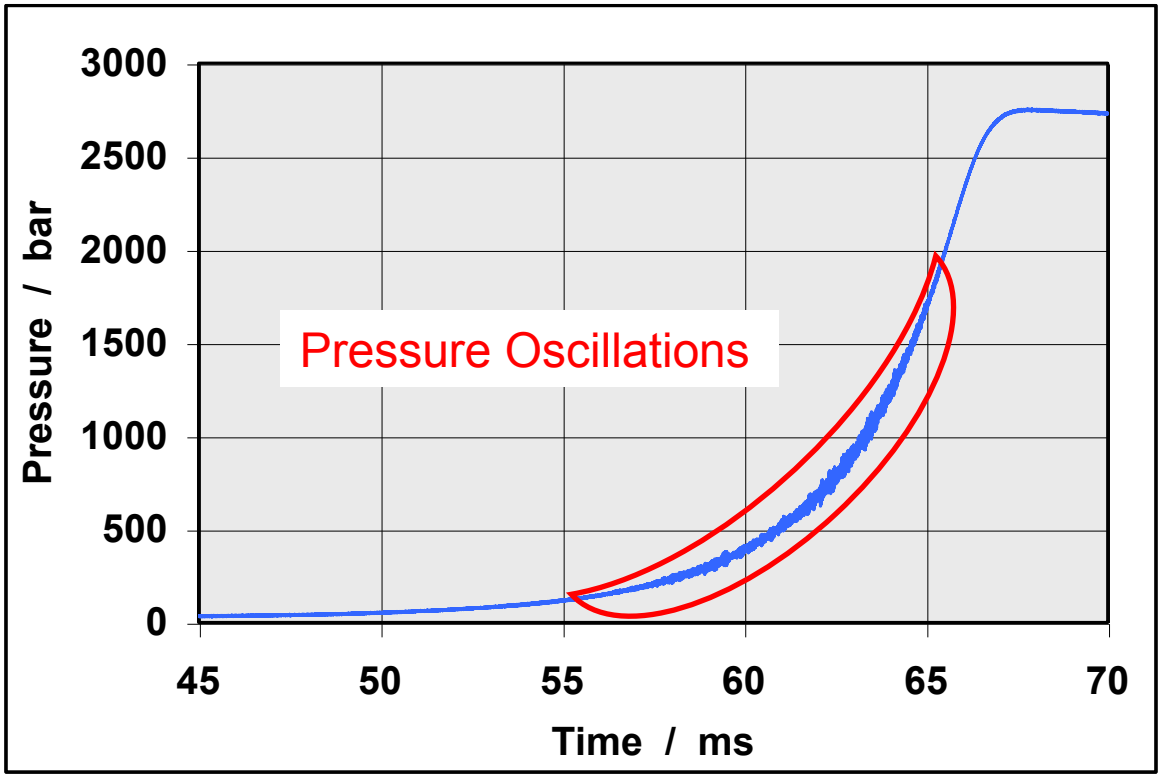

Experimental Results

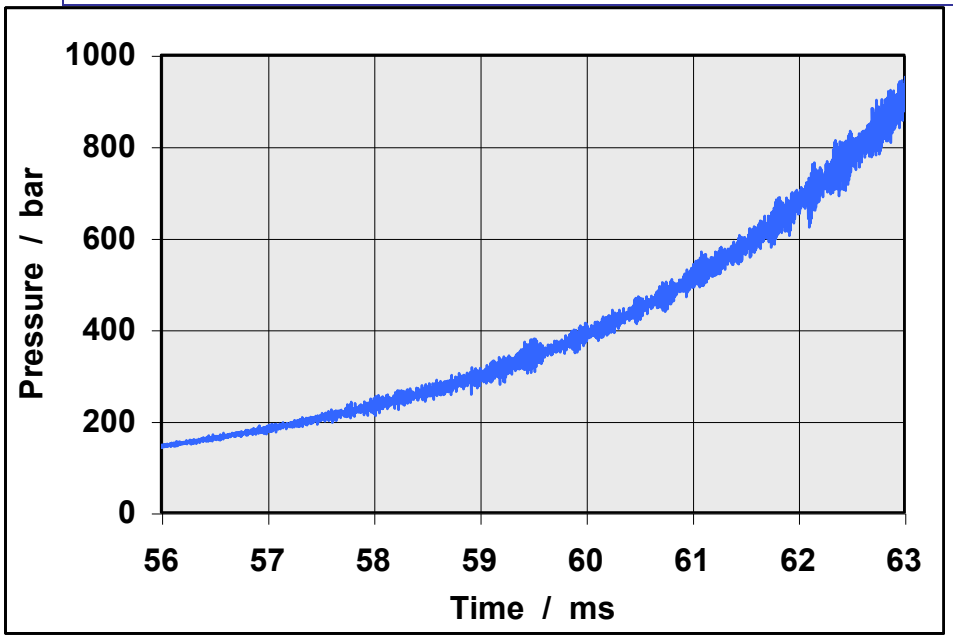

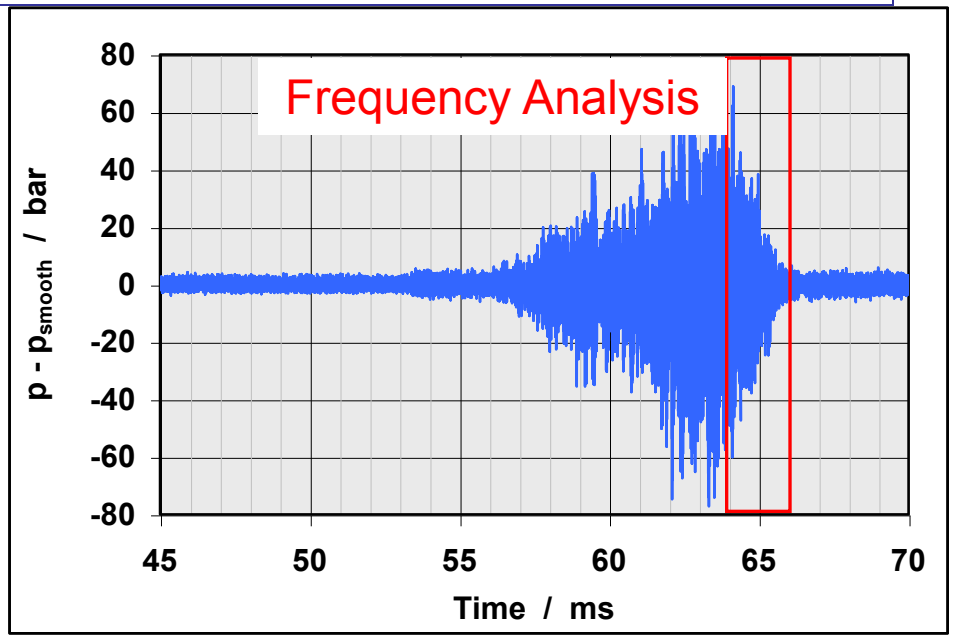

Experimental Results

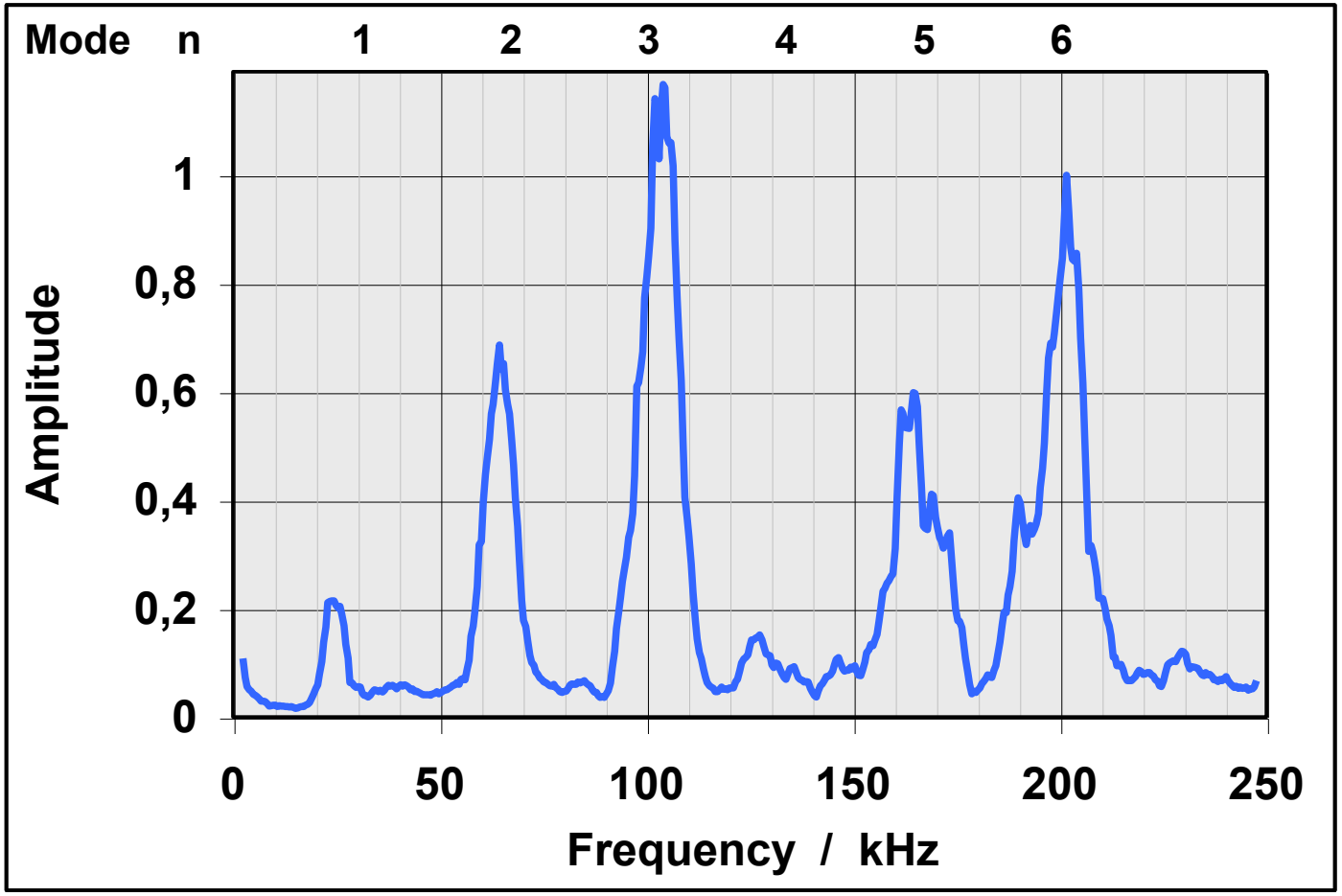

High amplitudes occur at frequencies f which correlate with the velocity of sound c_s and the length L of the grain: $f \approx n \bullet c_s / 2L$

Experimental Results

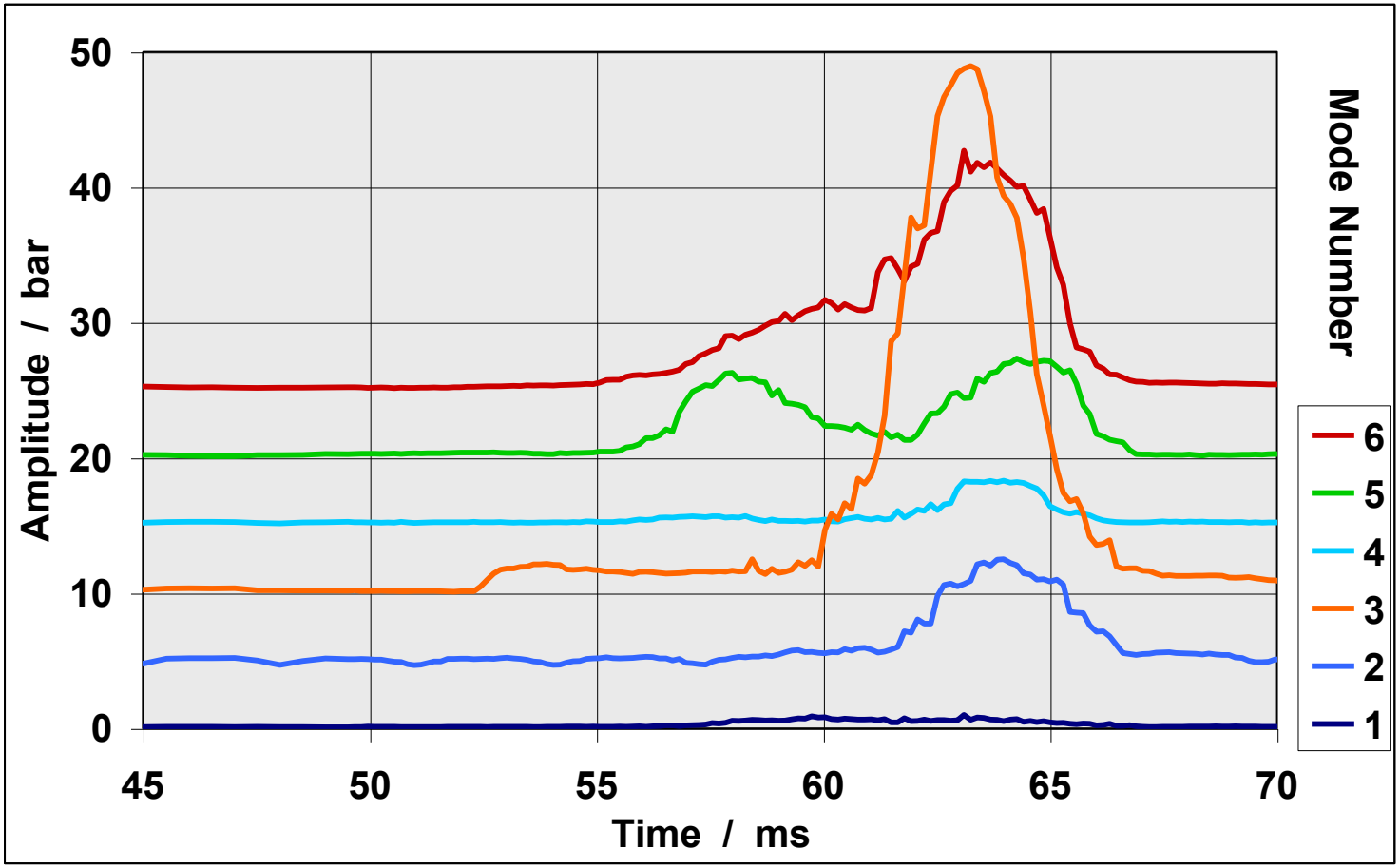

Time dependence of the amplitudes of different modes.
In the given example mode 3 is the dominant mode.

(n-1)•5 bars are added to the amplitudes of each mode to make the figure more readable.

Experimental Results

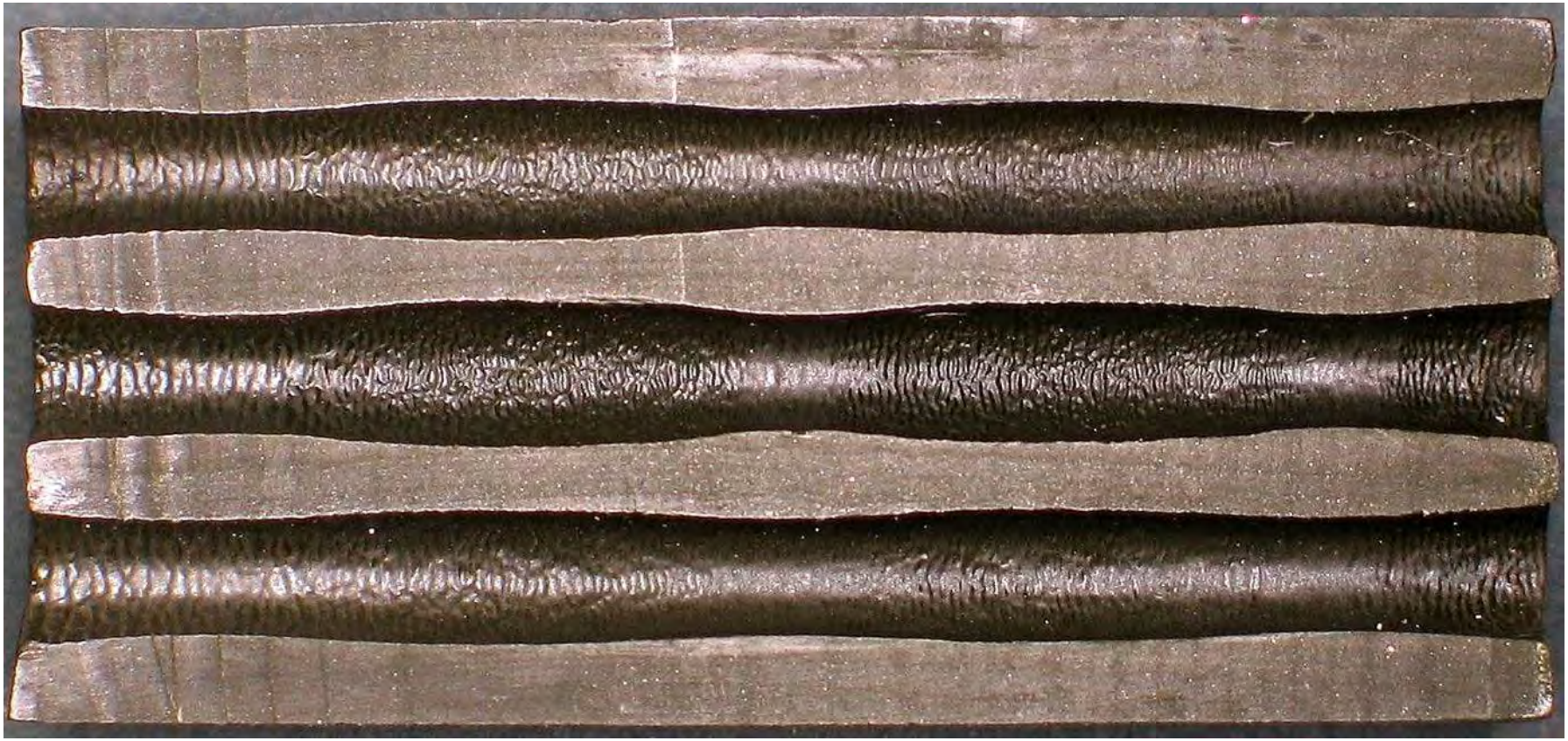

Cross sectional view of a propellant grain after burning interruption test with typical anomalous wavelike perf geometry indicating regions of increased gas production rates correlated to a dominant mode 3.

Theoretical Approach

Modeling of standing pressure waves in the perfs of gun propellant grains

Basis are the standard gasdynamic equations for solid and gas phase which are simplified for closed vessel application.

The goal was to get an analytic solution which describes standing waves in the perfs of gun propellant grains.

Therefore we assume that the solution can be written as series expansion with respect to a formal parameter ε, e. g. $\rho(\underline{r},t) = \rho_0(\underline{r},t) + \varepsilon^1 \rho_1(\underline{r},t) + \varepsilon^2 \rho_2(\underline{r},t) + \ldots$

and get a hierarchy of equations with respect to powers of ε.

Using suitable approximations and linearization we get solutions for the lowest order perturbation quantities

ρ_1 (density perturbation)

$v_{1,y}$ (velocity perturbation in axial direction)

Modeling of standing pressure waves in the perfs of gun propellant grains

$$\rho_{1,n}(y,t) \approx \rho_0^* \begin{Bmatrix} \cos(k_n y) \\ \sin(k_n y) \end{Bmatrix} \cos(\Omega_n t)\, e^{\frac{1}{2}\mu t} \qquad \begin{matrix} n \text{ odd} \\ n \text{ even} \end{matrix}$$

$$v_{1,y,n}(y,t) \approx c_s \begin{Bmatrix} \sin(k_n y) \\ -\cos(k_n y) \end{Bmatrix} \sin(\Omega_n t)\, e^{-\frac{1}{2}\mu t} \qquad \begin{matrix} n \text{ odd} \\ n \text{ even} \end{matrix}$$

$\Omega_n = \pi n c_s / L_{„}$

$k_n = 2\pi/\lambda_n$, $\lambda_n = 2L_{„}/n$

$L_{„} = L + \frac{1}{4}\,\pi\, d_{perf}$ (accoustic length)

Two time scales:

Slow time ~ $1/\mu$

Fast Time ~ $\frac{1}{2}L_{„}/c_s$

Within the framework of the used approximations the perturbation solution of the pressure p_1 is simply given as

$$p_1 = c_s^2\, \rho_1$$

Impact of standing pressure waves on the burning behavior in the perfs

The first idea was that the pressure oscillations directly cause a locally increased burning velocity according to the modified pressure which yields

$$de/dt = (de/dt)_o + (de/dt)_1 = \dot{e}(p_{Ref}) \; (p_o + \varepsilon \, p_1) / p_{Ref}$$

But averaging p_1 over one time period yields a quantity proportional to ½μ/Ω • (…) which is close to zero.
So, no significant change of the burning velocity results.

The general momentum balance equation allows the determination of an approximate nonlinear solution $p_{1,nl}$ (known as acoustic radiation pressure) which yields a significant net effect after averaging over one time period

$$p_{1,nl} = ¼ \; \varepsilon^2 \, c_s^{\,2} \, \rho_o^* \begin{cases} \cos^2(k_n y) & \text{n odd} \\ \sin^2(k_n y) & \text{n even} \end{cases}$$

Impact of standing pressure waves on the burning behavior in the perfs

But this solution as well as the linear one show a wrong phasing, i. e. they have pressure nodes which means no enhanced burning at the end of the perfs whereas the experimental results always show antinodes at these locations.

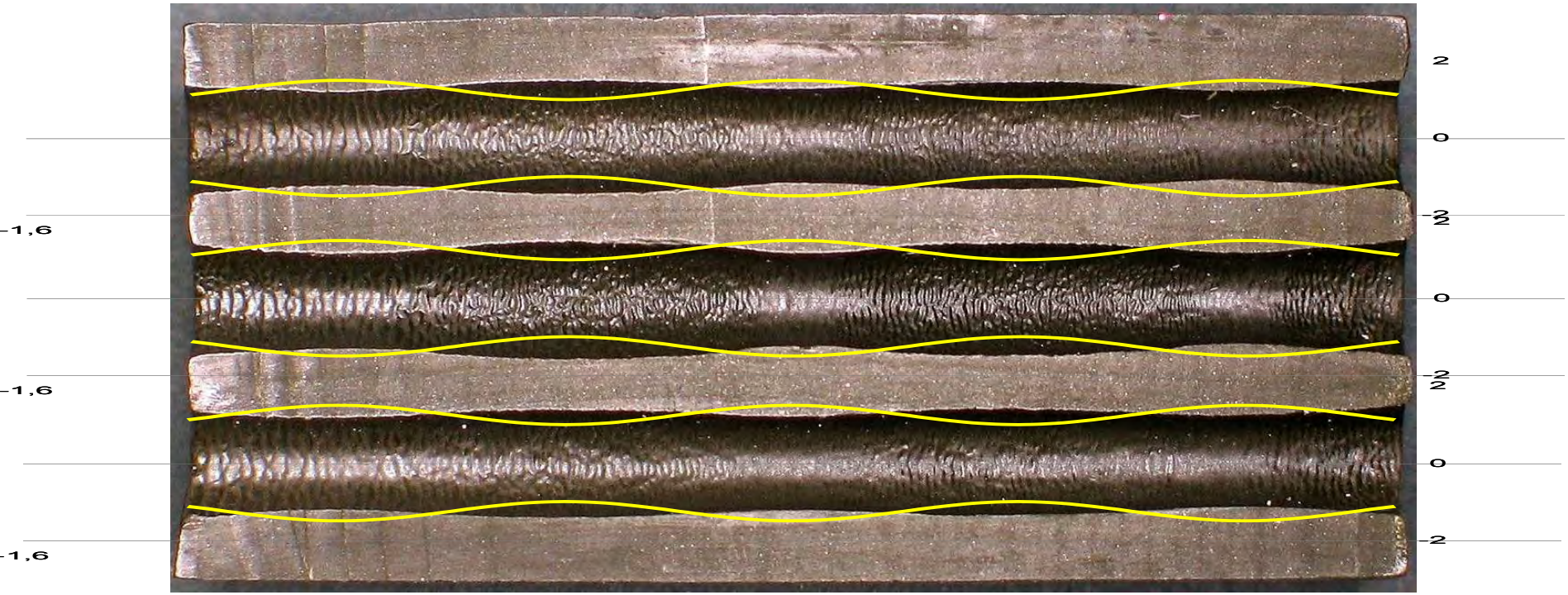

So, the experimentally observed anomalous wavelike perf structure can not be explained as a direct impact even of the accoustic radiation pressure.

Alternative model to explain the anomalous burning behavior in the perfs

We propose that the anomalous burning behavior in the perfs of single or multi perf gun propellant grains is caused by the impact of the ultra sound velocity field $v_{1,y}$ on the thermally isolating foam zone which separates the solid phase of the propellant and the combustion gas phase. The very intensive ultra sound field locally reduces the thickness of this foam zone for instance by cavitation processes and therefore causes an increased heat flow into the unreacted cold propellant. Consequently, an increased gas production rate should occur at positions with high amplitudes of the ultra sound field.

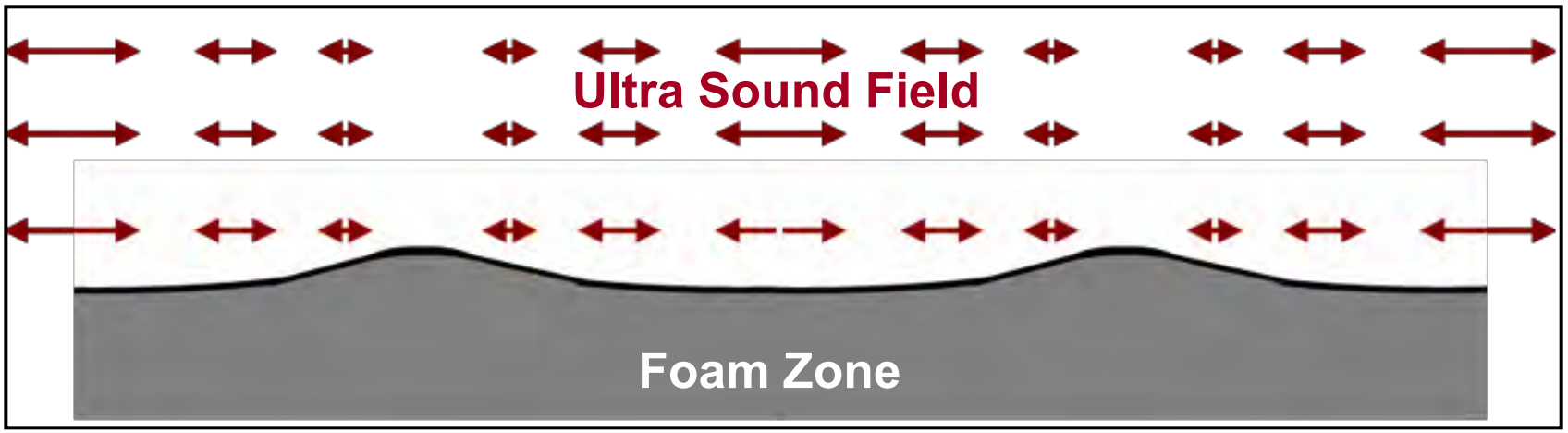

Alternative model to explain the anomalous burning behavior in the perfs

The influence of thickness of the foam zone on the burning velocity can be derived from a simple heat balance. To heat up the small propellant element S•de from T_P to $T_{S,P}$ the heat power

$$dQ/dt = dm/dt\ c_p\ (\ T_{S,F} - T_P\ )$$

is necessary ($dm/dt = \rho_P\ S\ de/dt$, S burning surface area, c_p specific heat of the propellant). This heat power must be generated by the heat flow from the foam surface to the propellant element S•de

$$dQ/dt = \lambda_F\ S\ (\ T_{S,F} - T_P\ )\ /\ D_F$$

(λ_F heat conductivity, D_F thickness of the foam zone). Equating the two expressions yields an equation for the burning velocity de/dt as function of the foam zone thickness:

$$de/dt = \lambda_F\ /\ [\ \rho_p\ c_p\ D_F\ ]$$

Alternative model to explain the anomalous burning behavior in the perfs

Without impact of ultra sound field (regular case) the thickness of the foam zone should be $D_{F,Ref}$ at reference pressure to get the usual burning law. This implies:

$$D_F = D_{F,Ref} / (p/p_{Ref})^{\alpha}$$

At presence of an ultra sound field with an acoustic energy density

$$E_S = ½ \rho_o \varepsilon^2 v_{1,y}^2$$

the last relation must be modified in such a way that we get:

$$D_F = D_{F,Ref} / [(p/p_{Ref})^{\alpha} + K \mathrm{E}_S]$$

with a suitable constant K and E_S denoting the time average of E_S over one period.

Alternative model to explain the anomalous burning behavior in the perfs

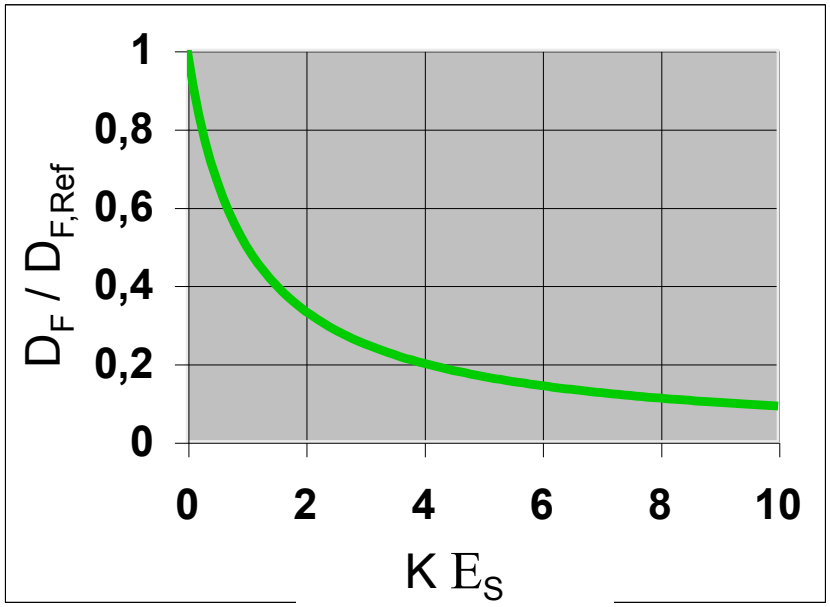

Combining the last equation and the equation for de/dt yields a quite simple expression for the changes of the burning velocity $\Delta(de/dt)$ caused by the presence of the ultra sound field characterized by its time averaged acoustic energy density:

$$\Delta(de/dt) = \dot{e}(p_{Ref}) \; K \; E_S$$

$$= \dot{e}(p_{Ref}) \; K \; 1/T \int E_S \, dt''$$

Alternative model to explain the anomalous burning behavior in the perfs

$$E_S = \varepsilon^2 \tfrac{1}{2} \rho_o v_{1,y}^2 \approx \varepsilon^2 \tfrac{1}{2} \rho_o^* c^2 \left\{ \begin{matrix} \sin^2(k_n y) \\ \cos^2(k_n y) \end{matrix} \right\} \sin^2(\Omega t) \qquad \begin{matrix} n \text{ odd} \\ n \text{ even} \end{matrix}$$

The acoustic energy density does not depend on the „slow time“ anymore which is clearly a consequence of the used approximations.

More important, it shows (as well as the burning velocity change) a phasing which is compliant with the perf shapes experimentally observed.

So, the proposed model which takes into account the impact of the standing ultra sound waves on the thickness of the foam zone is able to explain all experimental observations related to the anomalous burning behavior in the perfs of gun propellants.

Simulation of Closed Vessel Tests with Pressure Oscillations

Simulation of Closed Vessel Tests with Pressure Oscillations

Implementation of the modified burning velocity given before into our closed vessel simulation tool “SimDB” was the easy part of the necessary work.

A little bit more sophisticated was the derivation of information on the growth and absolute values of the amplitudes of the ultra sound field. This was done by treating the gasdynamic equations with a minimum of approximations but nevertheless additional assumptions were necessary with respect to the fade away of the oscillations which is not an outcome even of the more detailed treatment.

However, our simulations correspond very well with experimental results as will be shown in the next slides.

Simulation of Closed Vessel Tests with Pressure Oscillations

As example we take a cylindrical 19 perf gun propellant (length = 12.2 mm, outer diameter = 12.6 mm, perf diameter = 0.19 mm) with conventional L1 recipe which was fired at -40 °C in a 700 cm^3 closed vessel at a loading density of 0.2 g/cm^3. 2 grams of black power were used as ignition charge.

Due to the acoustic hardness of the propellant at cold pronounced pressure oscillations were measured and an anomalous vivacity derived.

Parallel conducted burning interruption test shows a wavelike shape of the perfs with axial mode n = 2 as dominant mode.

Simulation of Closed Vessel Tests with Pressure Oscillations

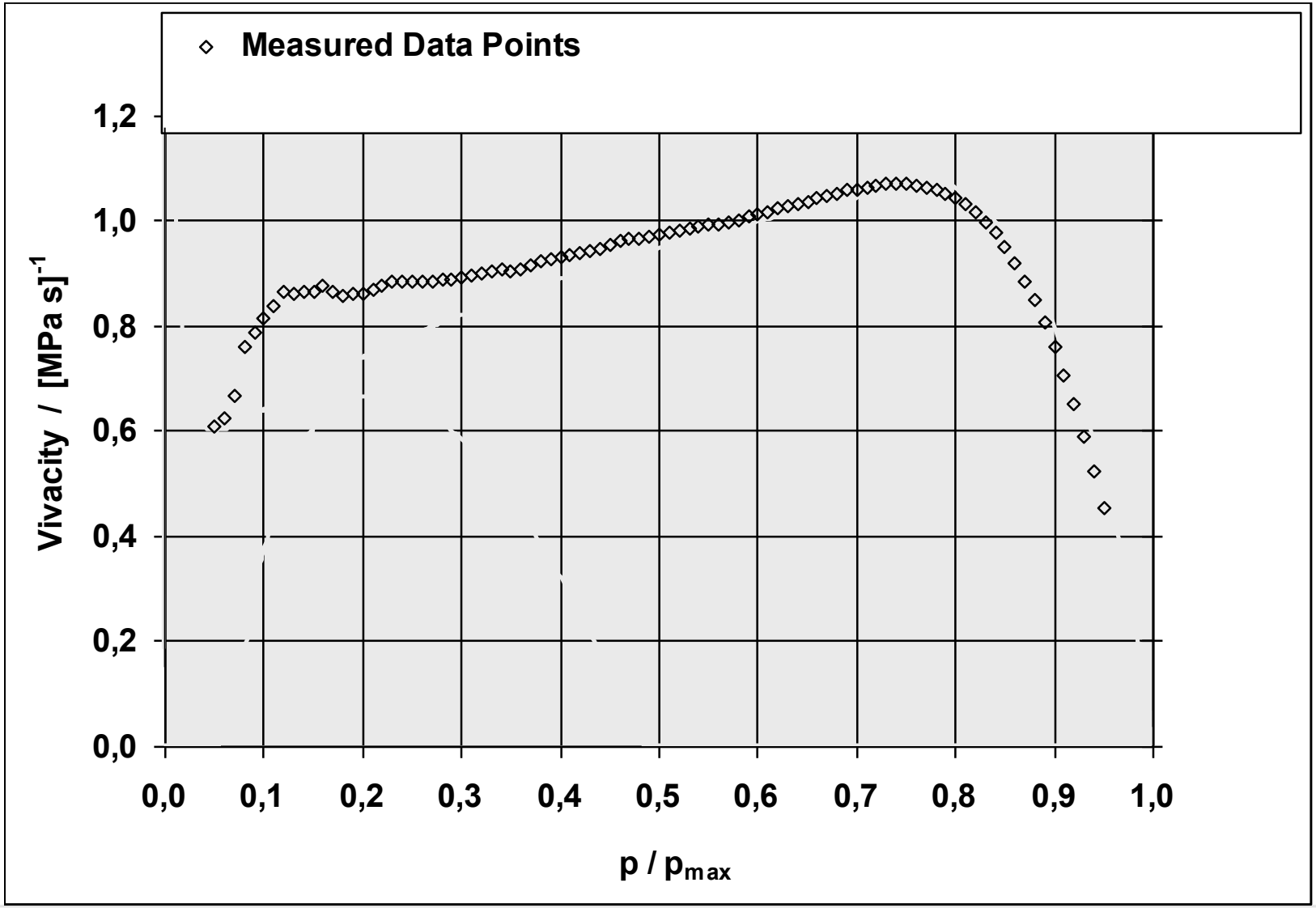

Simulation of Closed Vessel Tests with Pressure Oscillations

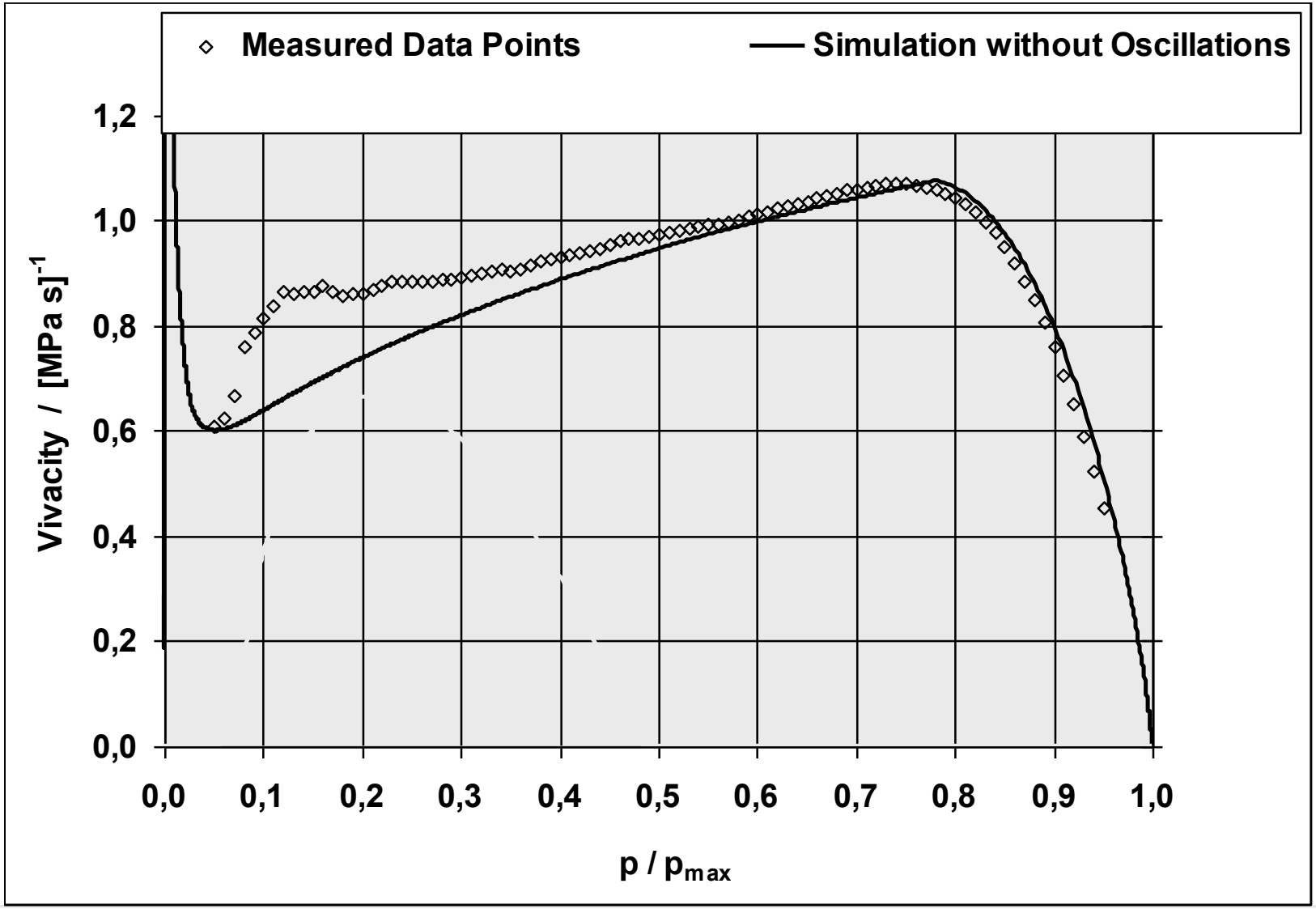

Simulation of Closed Vessel Tests with Pressure Oscillations

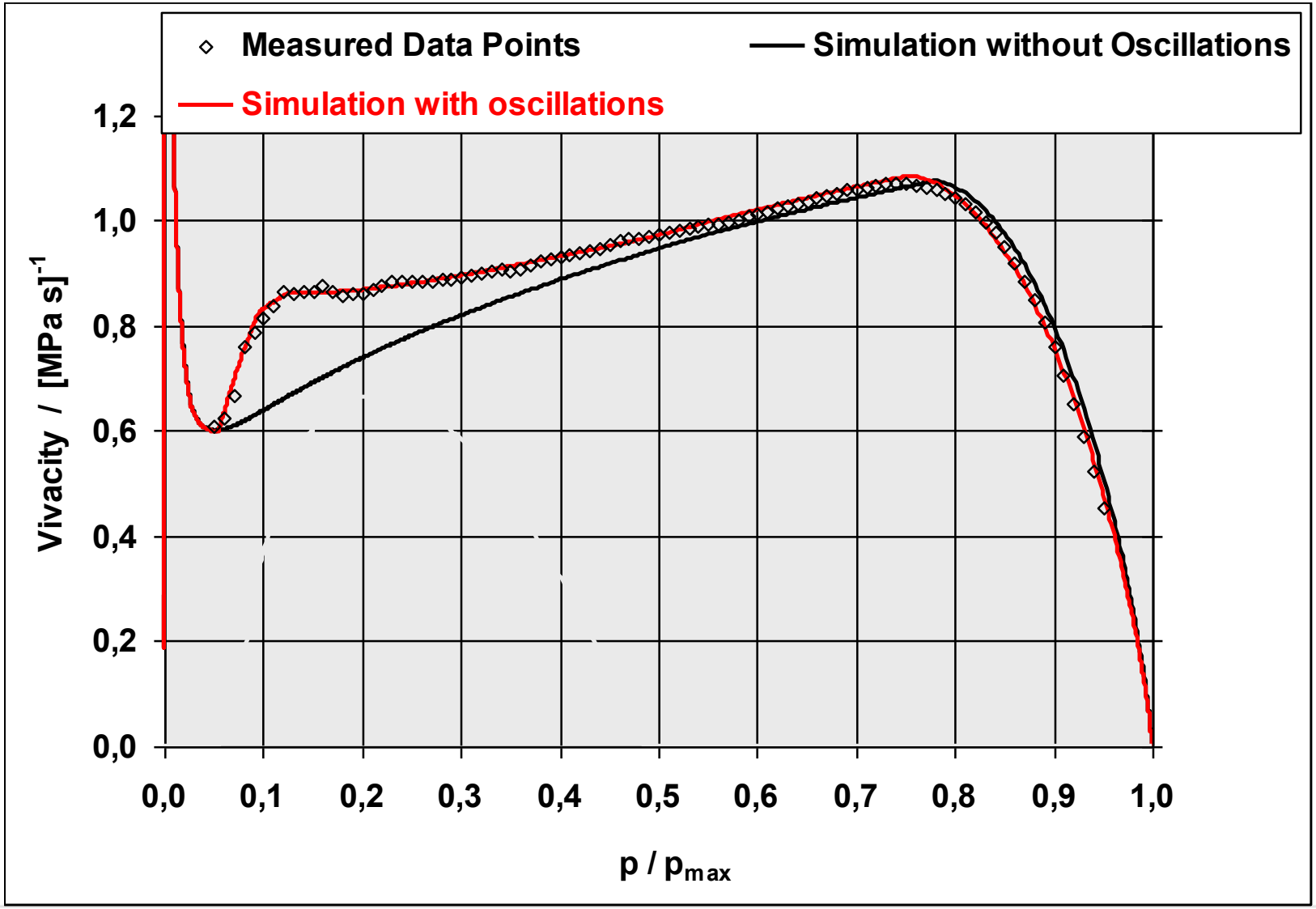

Simulation of Closed Vessel Tests with Pressure Oscillations

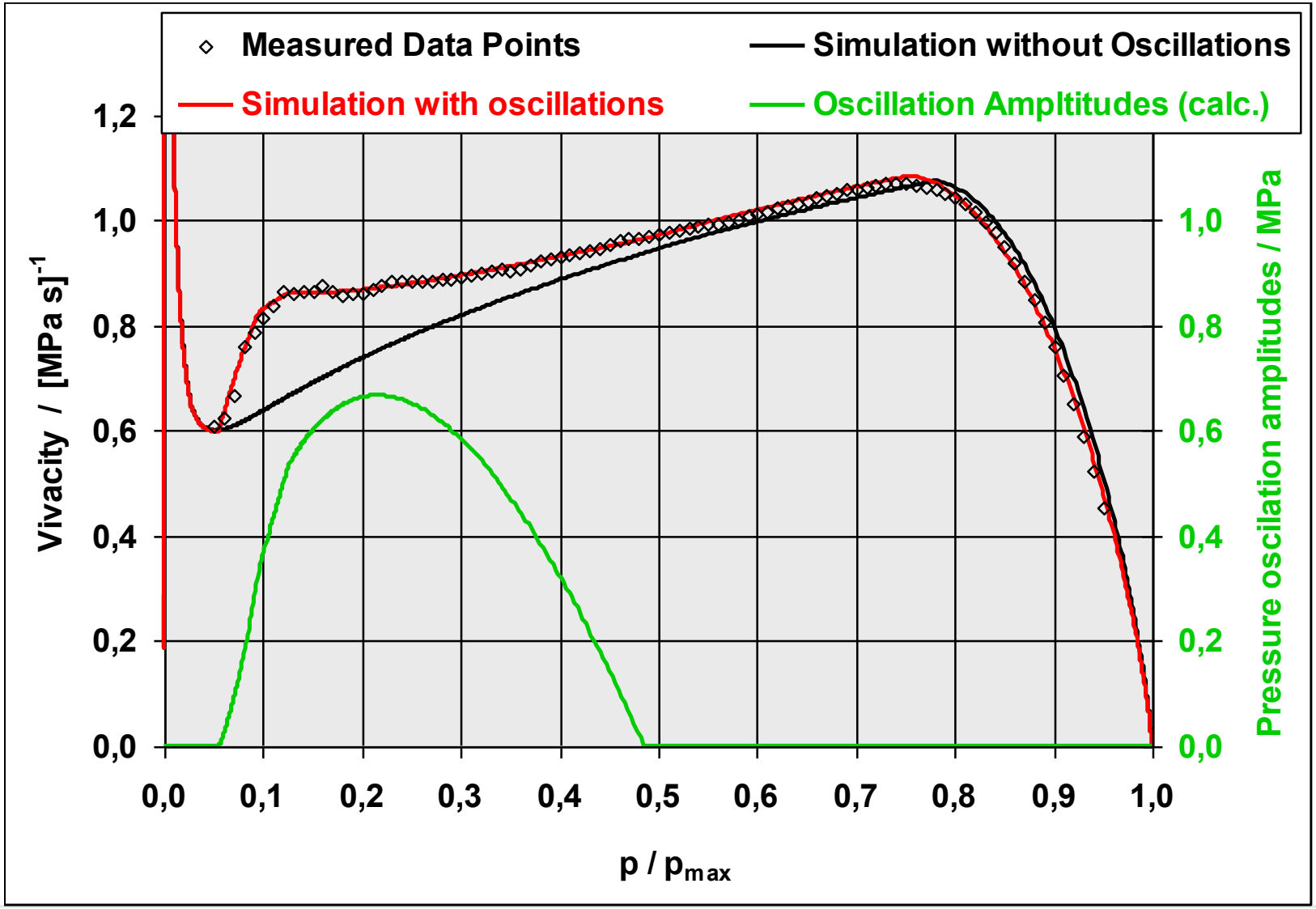

Simulation of Closed Vessel Tests with Pressure Oscillations

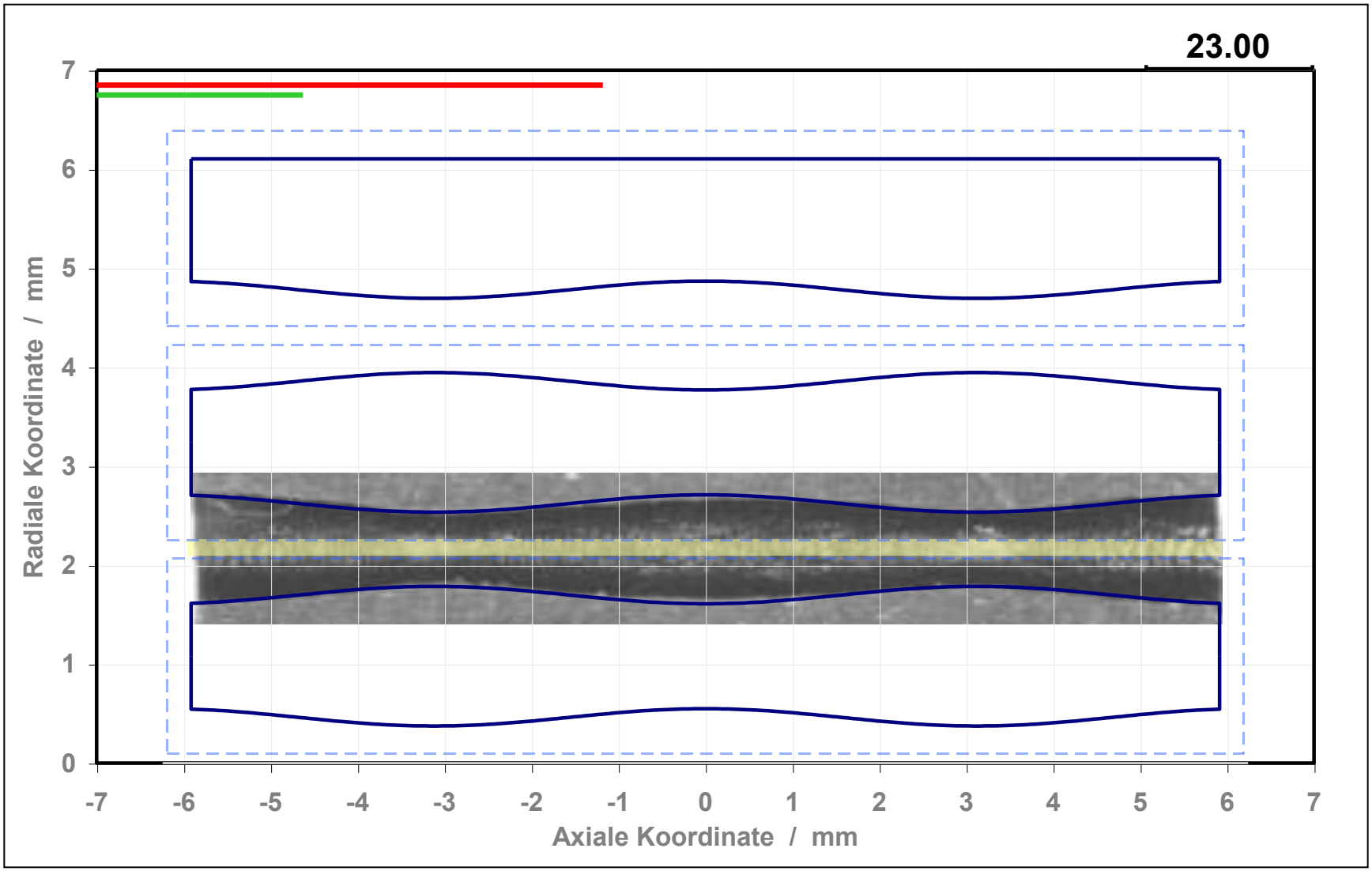

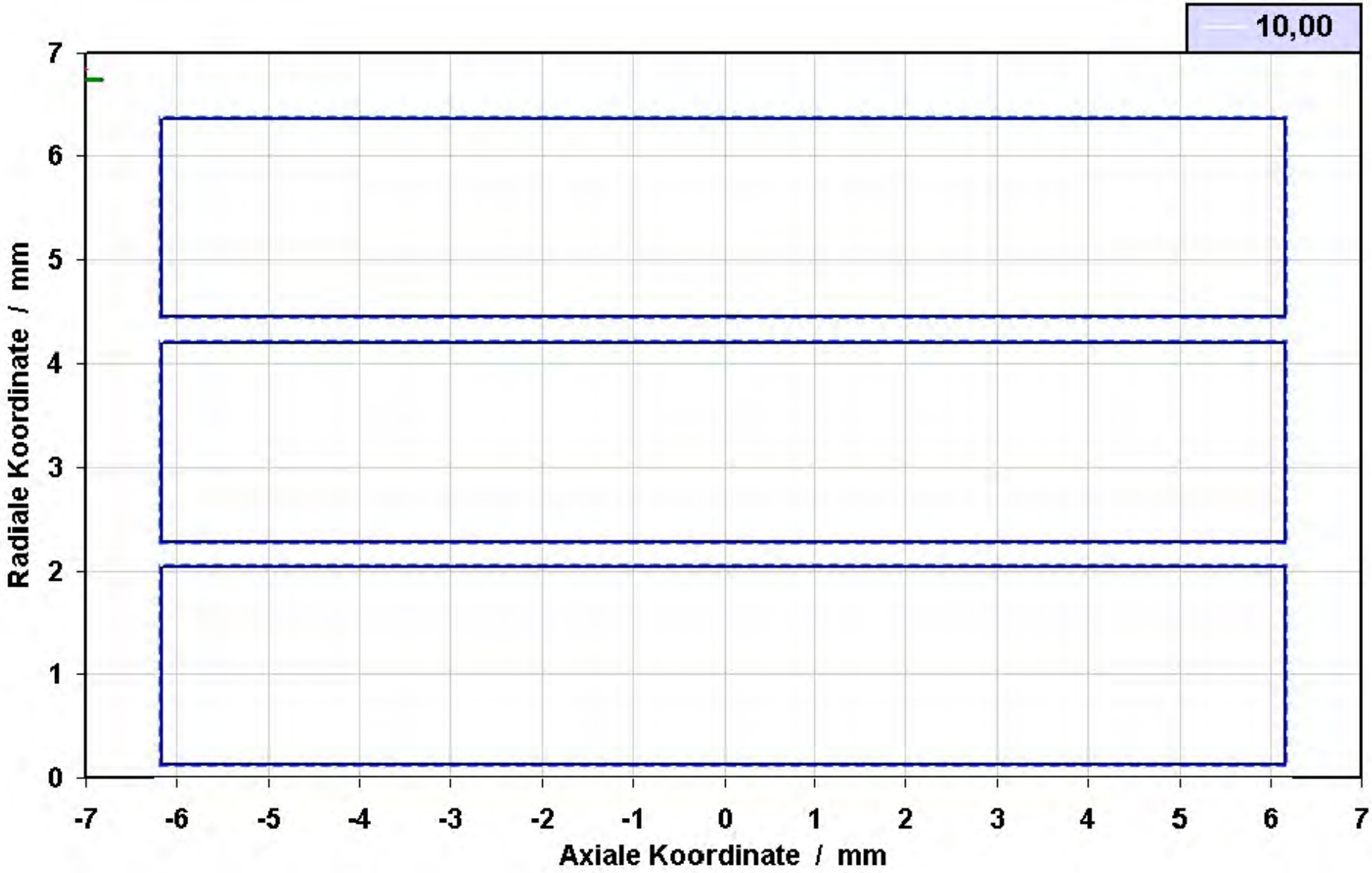

Summary and Outlook

We have proposed a new approach to explain the impact of density / pressure oscillations on the burning behavior of gun propellants when fired in closed vessels.

The hypothesis is that the ultra sound field related to the standing waves in the perfs causes a reduction of the thickness of the isolating foam zone. As consequence the burning velocity of the propellant is locally increased due to an enhanced heat transfer into the unreacted propellant.

Implementation of this model into our closed vessel simulation tool yields results which are in excellent agreement with experimental observations with respect to vivacity changes as well as the wavelike perf geometries.

Currently we try to extend the model to explain the fine structure which can be seen in the perfs. Feed back of stationary vortices induced by the velocity perturbation on these perturbations seems to be a promising approach.

Thank you

for your

attention !

THE POTENTIAL OF FOX-7 EXPLOSIVE IN INSENSITIVE MUNITION DESIGN

Ian Cullis, Richard Townsley

A presentation to: 26th International Symposium on Ballistics

12th – 16th September 2011

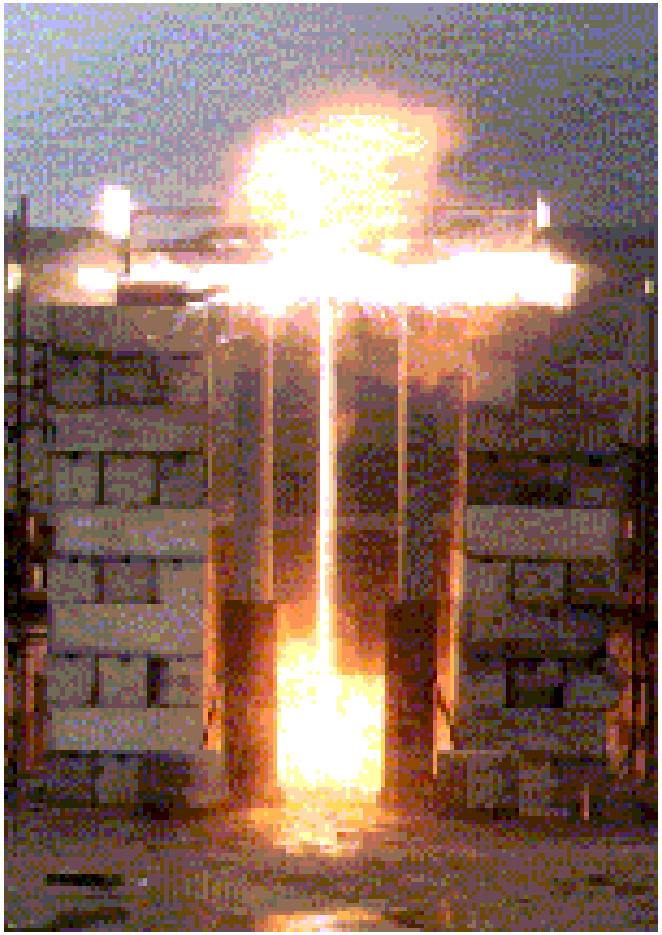

QinetiQ

Contents

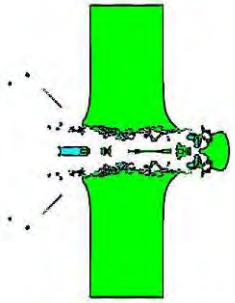

1 Introduction

The UK commitment to effects based planning and operations requires precision weapons to ensure the desired military effects are achieved.

Identifies UK needs:

- Increased flexibility from future weapon systems to ensure that a wide range of targets can be effectively neutralized within increasingly stringent rules of engagement.
- Minimum collateral damage.
- IM compliant.
- To understand the role that explosives and explosives design have in delivering a range of effects from lethal to sub-lethal.

Recent research has sought to develop such an understanding of explosives and explosives design.

1 Introduction

Technical Approach

Integrated modelling – experiment, material characterisation methodology

- Detonation product model for QRX080 (95%FOX-7).
- Identify candidate shaped charge & fragmenting warhead designs.
- Model performance using Eulerian hydrocode GRIM and SPLIT-X® .
- Experimental Firings:
  - Cylinder Tests: QRX080
  - Slow Stretching Jet (SSJ) charges: QRX250, PBXN-110, LX14, EDC1S filled

1 Introduction

Explosives

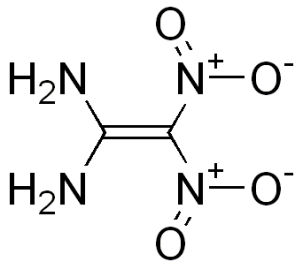

- FOX-7.
  - 1,1-diamino 2,2-dinitro ethylene
  - Developed by FOI, Sweden
  - Improved hazard response with comparable performance of cast cured RDX formulations.
- QRX080 (95% FOX-7 and 5% binder, particle size 56μm/78μm)
- QRX250, used in CE warheads, reduced particle size 36 μm.
- PBXN-110 (88% HMX/12% HTPB/isodecylpelargonate).
- EDC1S (70.25% HMX/4% RDX/24.75% TNT/1% Wax)

2 Explosive Products Model

Cylinder Test Experiment.

- Test to measure the transfer of explosive energy to a metal.
- Hollow metal cylinder, usually constructed of ductile copper, filled with the explosive of interest.
- Two sizes, namely a 2.54 cm inner diameter and a 10.16 cm inner diameter.
- L/D = 12
- Jones-Wilkins-Lee (JWL) Equation of State for detonation products fitted to tube radial expansion and measurement of the detonation velocity.
  - Analytic iteration of JWL parameters to provide best fit to the data.
  - Thermo-chemistry code (e.g. CHEETAH) to provide starting point fit. ☑

2 Explosive Products Model

Cylinder Test Experiment.

$$f_{ICT}(\alpha,\beta,T,A,B) = \alpha\left[t - \frac{e^{-\beta T}}{\beta}\left(1 - e^{-\beta t}\right)\right] + A\left[t - \frac{e^{-BT}}{B}\left(1 - e^{-Bt}\right)\right]$$

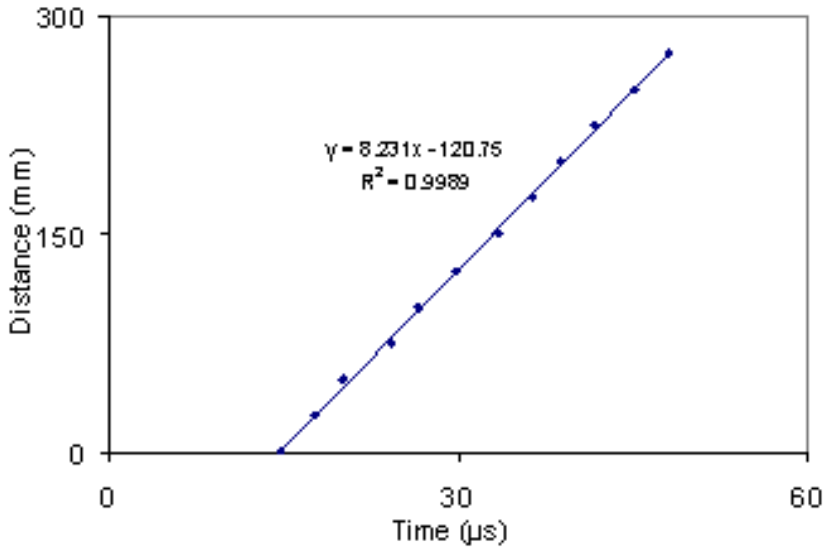

Detonation Velocity Measurement
(8.23 km/s, 8.22 km/s and 8.39 km/s)

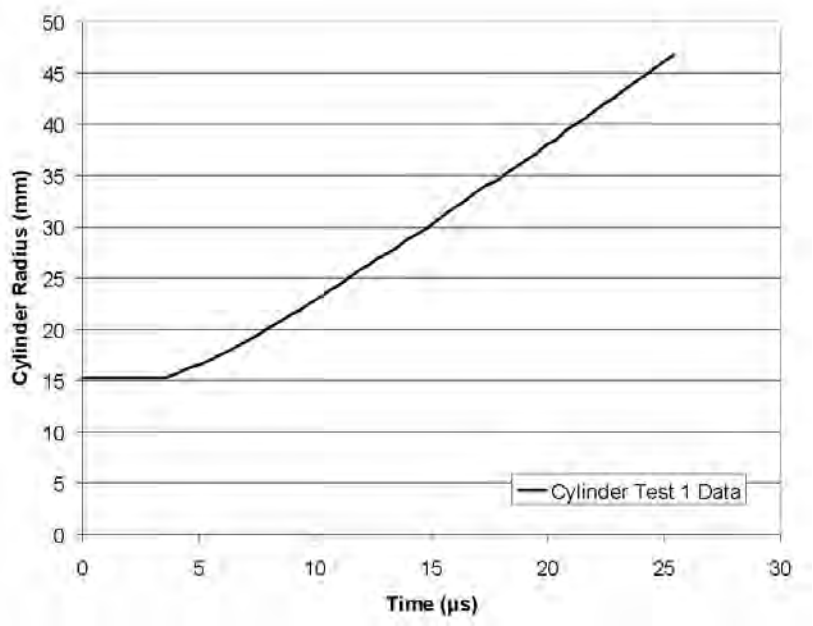

Cylinder Wall Expansion History

2 Explosive Products Model

JWL.

JWL Adiabat

$$P_S = Ae^{-R_1\frac{V}{V_0}} + Be^{-R_2\frac{V}{V_0}} + C\left(\frac{V}{V_0}\right)^{-(\omega+1)}$$

EoS (JWL)

$$P = A\left(1-\frac{\omega}{R_1}\frac{V_0}{V}\right)e^{-R_1\frac{V}{V_0}} + B\left(1-\frac{\omega}{R_2}\frac{V_0}{V}\right)e^{-R_2\frac{V}{V_0}} + \omega\left(\frac{E}{V}\right)$$

JWLB (Baker et. Al.)

$$P = \sum_{i=1}^{5} A_i e^{-R_i\left(\frac{V}{V_0}\right)} + C\left(\frac{V}{V_0}\right)^{-(\omega+1)}$$

2 Explosive Products Model

Cylinder Test Fitting

JWL Parameter	*QRX080 (95% FOX-7, 5% binder)*	*Trzcinski (100% FOX-7)*	*Karlsson (98.5% FOX-7, 1.5% wax)*
A (GPa)	545.35	1414.339	998.578
B (GPa)	5.97	21.6637	8.778
C (GPa)	1.08	1.23412	Not given
R_1	4.09	5.54	4.928
R_2	1.06	1.51	1.119
ω	0.3143	0.32	0.401
Density ($g.cm^{-3}$)	1.76	1.78	1.756
Detonation Energy ($kJ.cm^{-3}$)	8.665	8.9	8.663

2 Explosive Products Model

Cylinder Test –JWL Fitting.

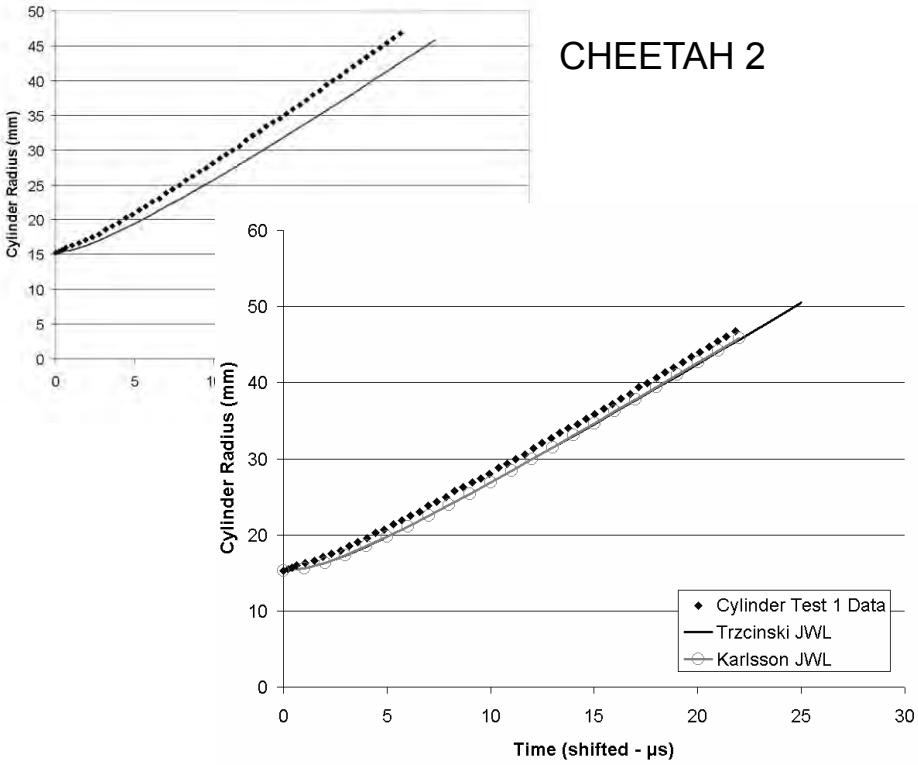

Radius – time fits

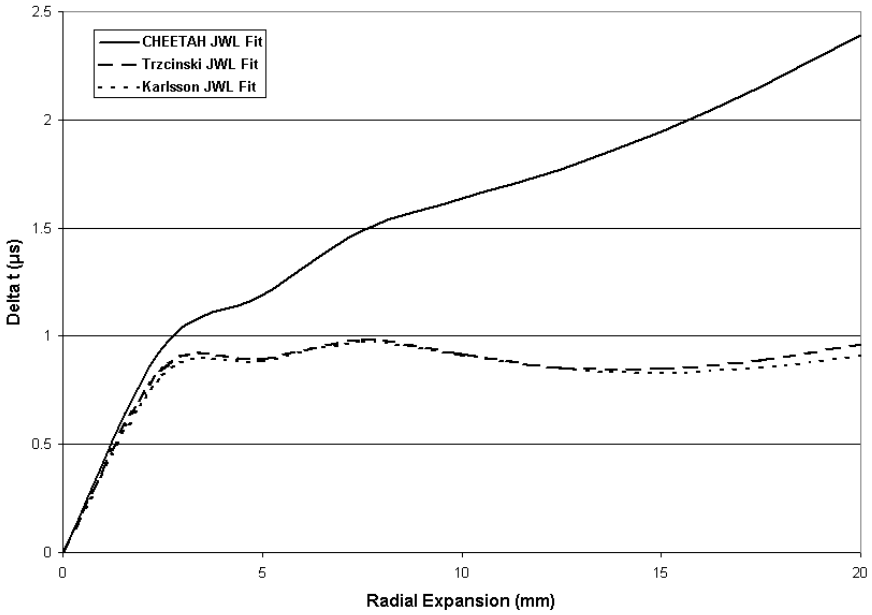

Radial fit time error

2 Explosive Products Model

Conclusions.

- Radial wall motion of the cylinder represents an integration of the products' behaviour, implying the parameter set fitted to the motion is not therefore unique.
- By considering cylinder expansion prior to failure, reasonable JWL fits to the experimental data can be achieved.
- To improve the JWL fit further requires:
  - Further iterative hydrocode modelling
  - Additional cylinder tests capturing early motion data using a VISAR and simultaneous measurements of Detonation Velocity and density.

3 Fragmentation

The warhead design process often needs to accommodate a number of conflicting performance requirements, including blast, fragmentation and penetration within associated mass and volume constraints.

Fragmentation

- Use SPLIT-X® to assess potential fragmentation potential of explosive.
- Needs the Gurney energy, E
- Gurney velocity (V) is then:

$$\frac{V}{\sqrt{2E}} = \left[\frac{M}{C} + \frac{1}{2}\right]^{-\frac{1}{2}}$$

M/C FOX-7 = 3.1; PBXN-110 = 3.3
M=case mass, C=explosive mass

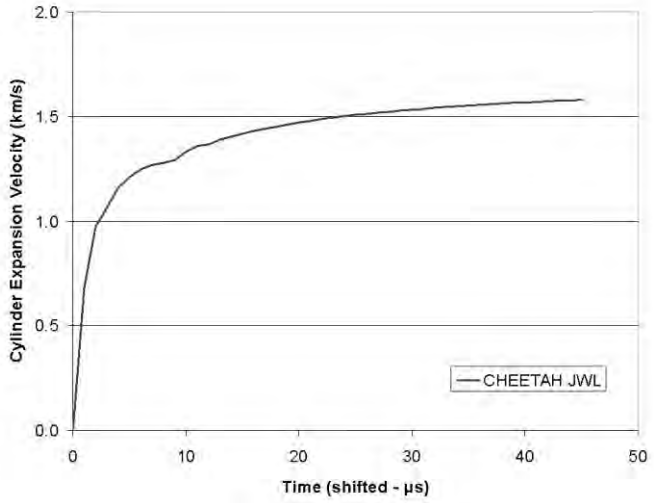

3 Fragmentation

Fragmentation.

- Simple charge

QRX080

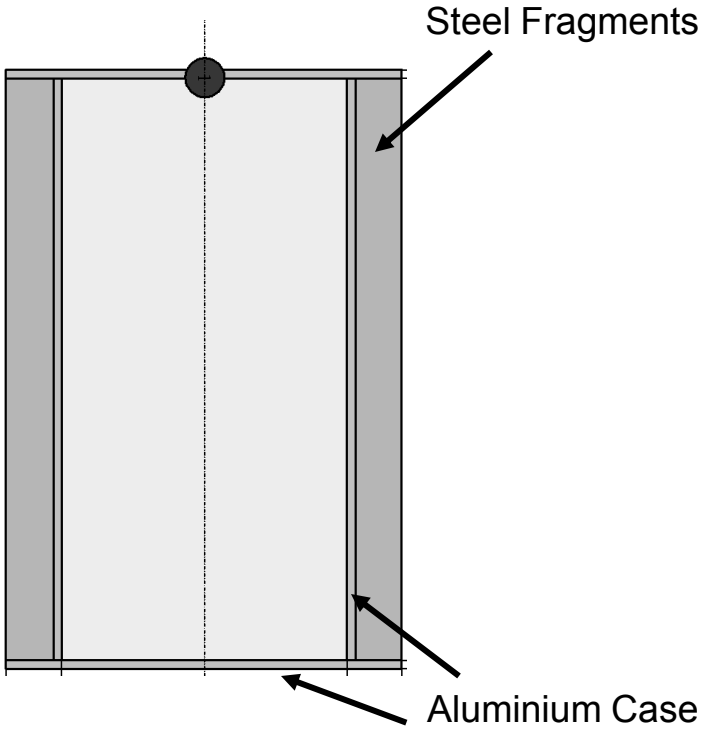

Cylinder Test	*Gurney Velocity (m/s)*	*Gurney Energy (J/g)*
1	2659	3536
2	2668	3559
3	2604	3392

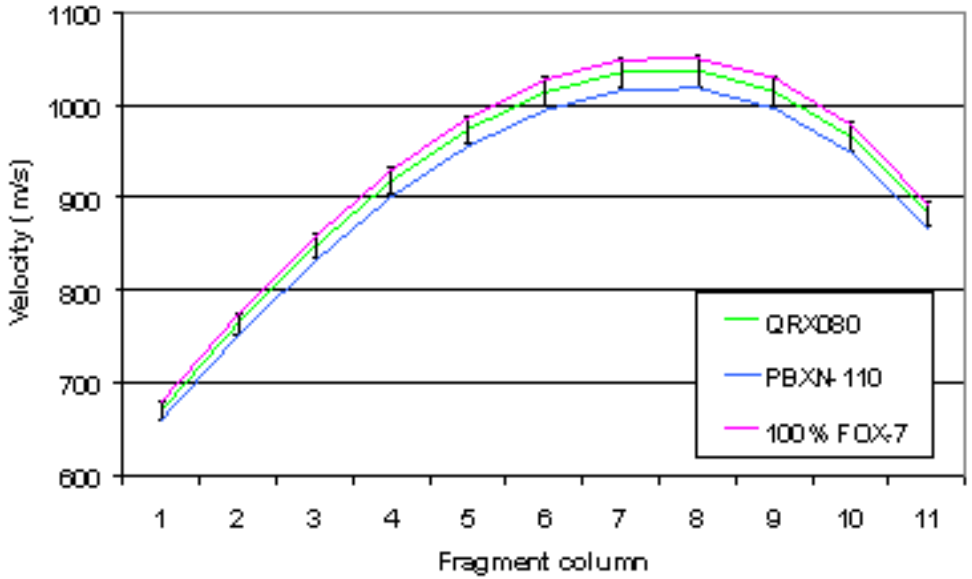

4 Chemical Energy Warheads

Shaped Charges.

- Helte et al.* demonstrated potential of FOX-7 in a conical shaped charge, with jet characteristics superior to Composition B.
- This work explored performance potential of FOX-7 in Slow-Stretching Jet (SSJ) systems.
- Compared performance with PBXN-110, EDC1 and LX14
- Modelling and experimental study.
- Simple charge design.
  - Tulip copper liner
  - 75mm diameter
  - Aluminium body

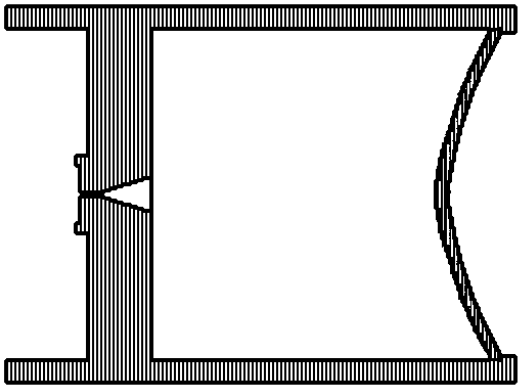

*Helte A. et al., 'Performance of FOX-7 in Shaped Charges', *Proc. 23rd International Symposium on Ballistics*.

4 Chemical Energy Warheads

Experiments

- Heavily instrumented trials arena to visualise the jet and record RHA penetration

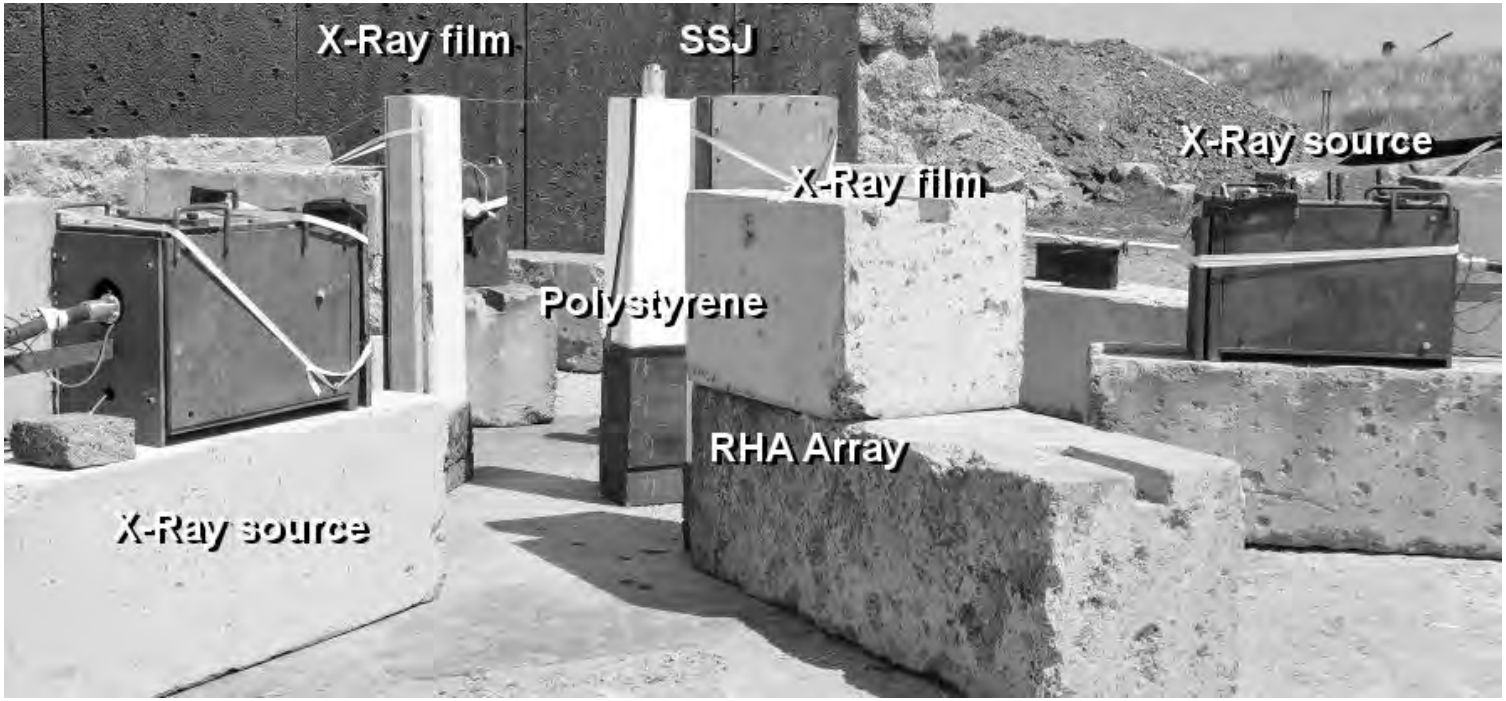

Stand-off = 12 CD (~895mm)

4 Chemical Energy Warheads

Modelling

- GRIM used to predict SSJ characteristics and break-up.

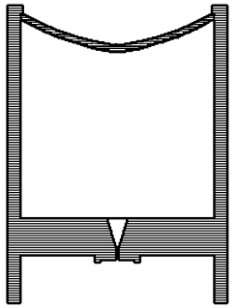

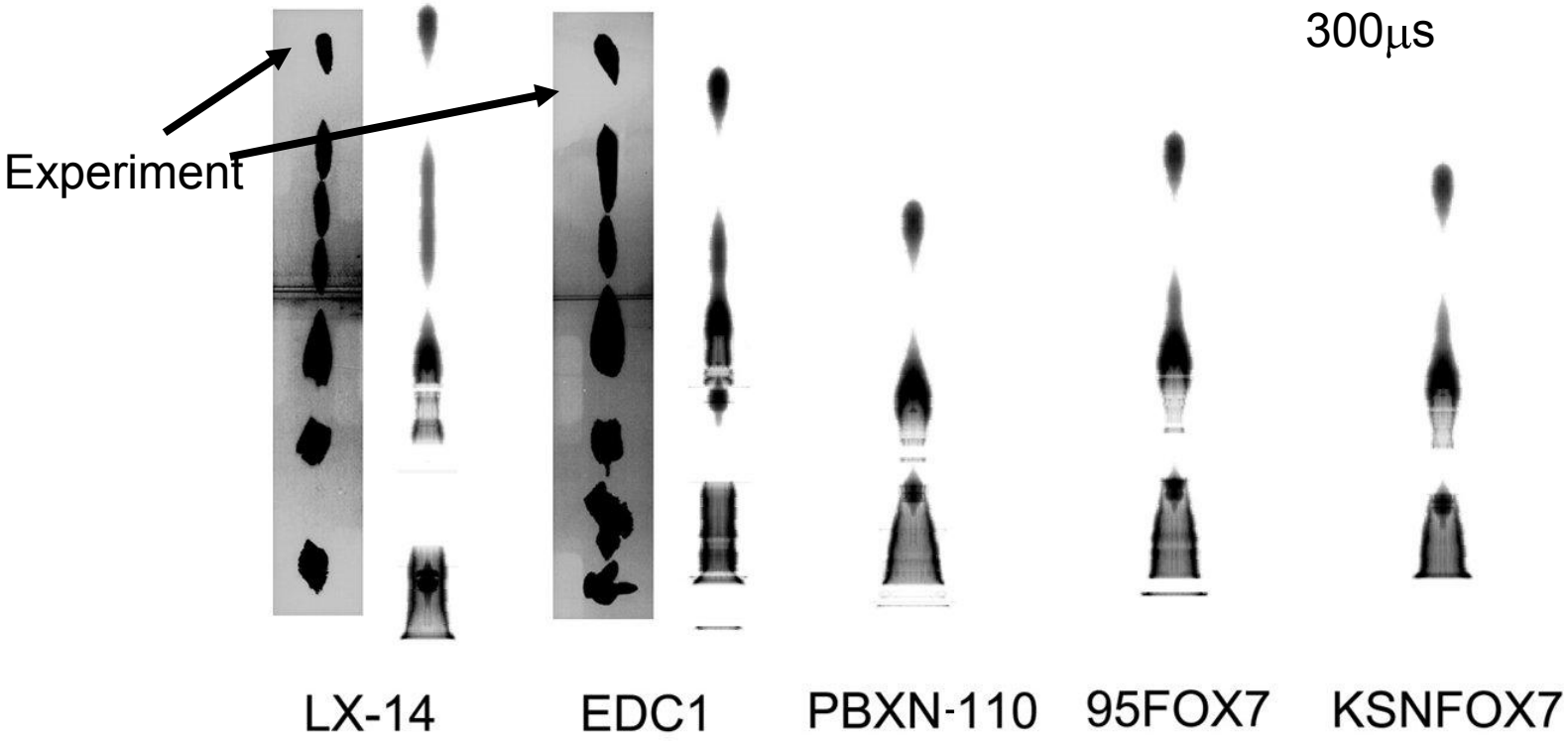

4 Chemical Energy Warheads

Modelling-experiment

- Predicted and experimental tip velocities in good agreement.
- Some subtle differences:
  - PBXN-110 produces a more elongated SSJ, typically composed of up to four ellipsoidal sections.
  - QRX250 SSJ comprised three sections, travelling more slowly.
  - Predicted jet characteristics for QRX250 sensitive to booster pellet size – much smaller booster used in modelling than utilised in trials.

Explosive	***Jet Tip Speed (km/s)***	
	Simulation	Experiment
LX-14	3.02	2.88
EDC1S	2.7	2.7
QRX250	2.58	2.63
PBXN-110	2.44	2.64

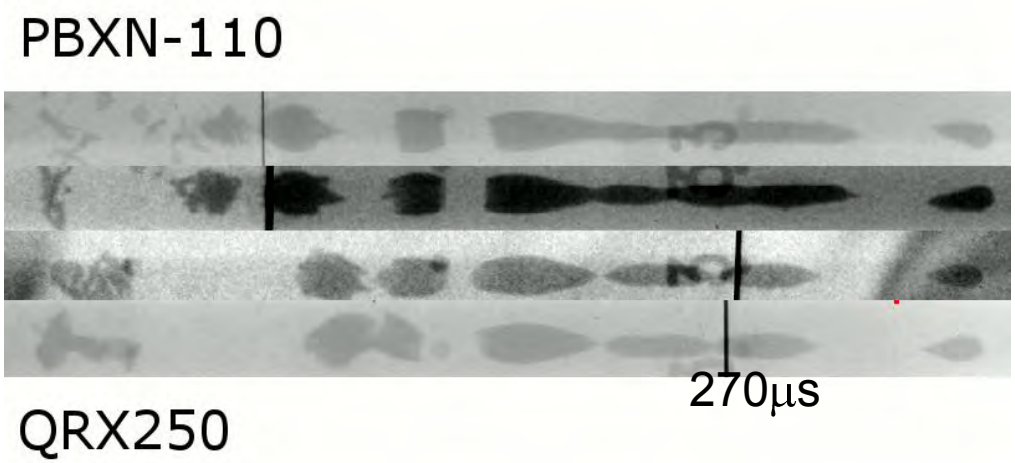

5 Conclusions

Research to compare and contrast the performance of FOX-7 compositions with high performance explosives in a SSJ shaped charge has allowed the following conclusions:

- QRX250 (95%FOX-7 5%binder) formulation offers similar performance in a SSJ charge to but not as good as more energetic and sensitive fillings such as LX14 and EDC1S that are not IM.
- Published FOX-7 cylinder test experimental data fit the QRX080 early time data reasonably well.
- The JWL fit produced by CHEETAH 2 does not fit the data as well as the published models.
- Split-X predicts higher fragment velocities for the FOX-7 compared to PBXN-110.
- SSJ performance for PBXN-110 and FOX-7:
  - Very similar jet velocity and RHA penetration.
  - Subtly different physical jet characteristics.

6 Acknowledgments

We would like to acknowledge:

- Colleagues at Fort Halstead in the manufacture and filling of the charges.
- The trials team at Pendine in helping execute the experimental programme.
- Our sponsor: UK MOD, Defence Science and Technology Laboratory (Dstl) Programme Office

QinetiQ

www.QinetiQ.com

26th International Symposium on BALLISTICS
SEPTEMBER 12-16, 2011
HYATT REGENCY MIAMI
MIAMI, FLORIDA

Effects of EFP Solidity in Terminal Ballistics

Ho Soo Kim
Dr. Werner Arnold
Dr. Thomas Hartmann, Ernst Rottenkolber
Dr. Andreas Klavzar

국방과학연구소
AGENCY FOR DEFENSE DEVELOPMENT
MBDA MISSILE SYSTEMS
NUMERICS
ISL

Outline

- Motivation & Introduction
- Experimental Tests: Setup & Results
- Numerical Simulations
- Modeling Approach
- Summary

Outline

- **Motivation & Introduction**
- Experimental Tests: Setup & Results
- Numerical Simulations
- Modeling Approach
- Summary

Motivation: EFP-Code Development

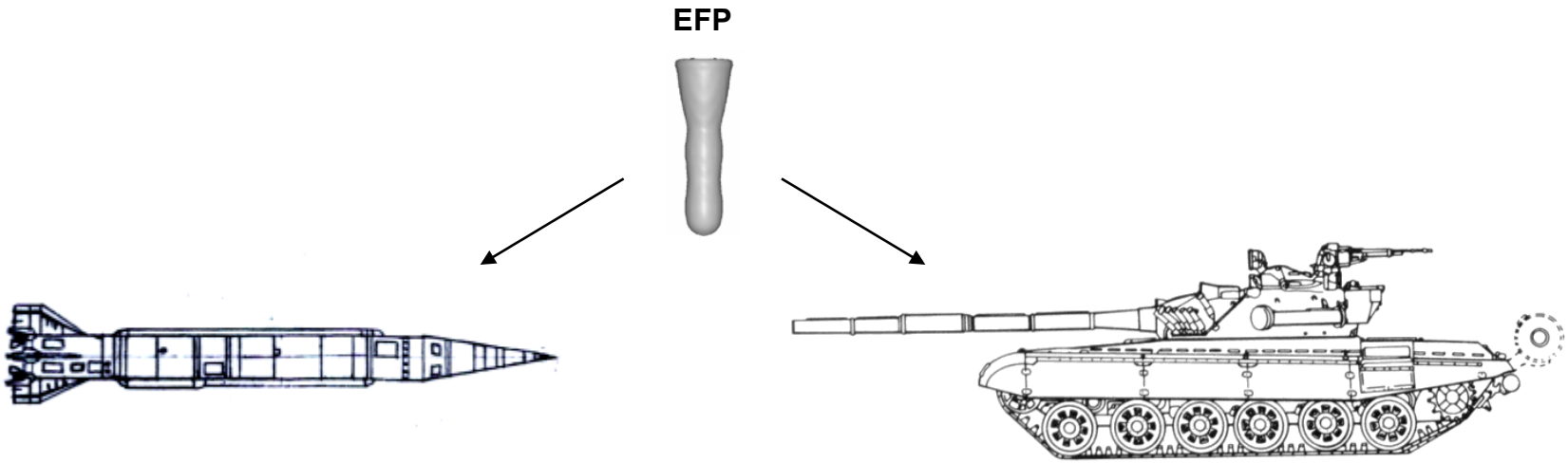

EFP Simulants: Cross Section Sketch and machined Projectiles

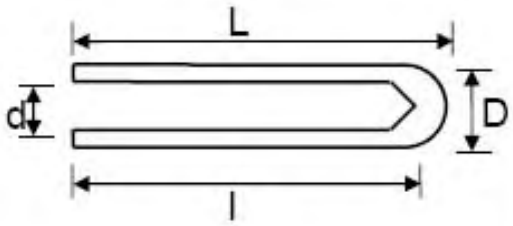

Dimensions of EFP simulants

Solidity	L [mm]	D [mm]	l [mm]	d [mm]
100 %	30	10	0	0
80 %	30	10	26.6	4.3
60 %	30	10	28	6.3

Outline

- Motivation & Introduction
- **Experimental Tests: Setup & Results**
- Numerical Simulations
- Modeling Approach
- Summary

Test Setup for DoP Tests

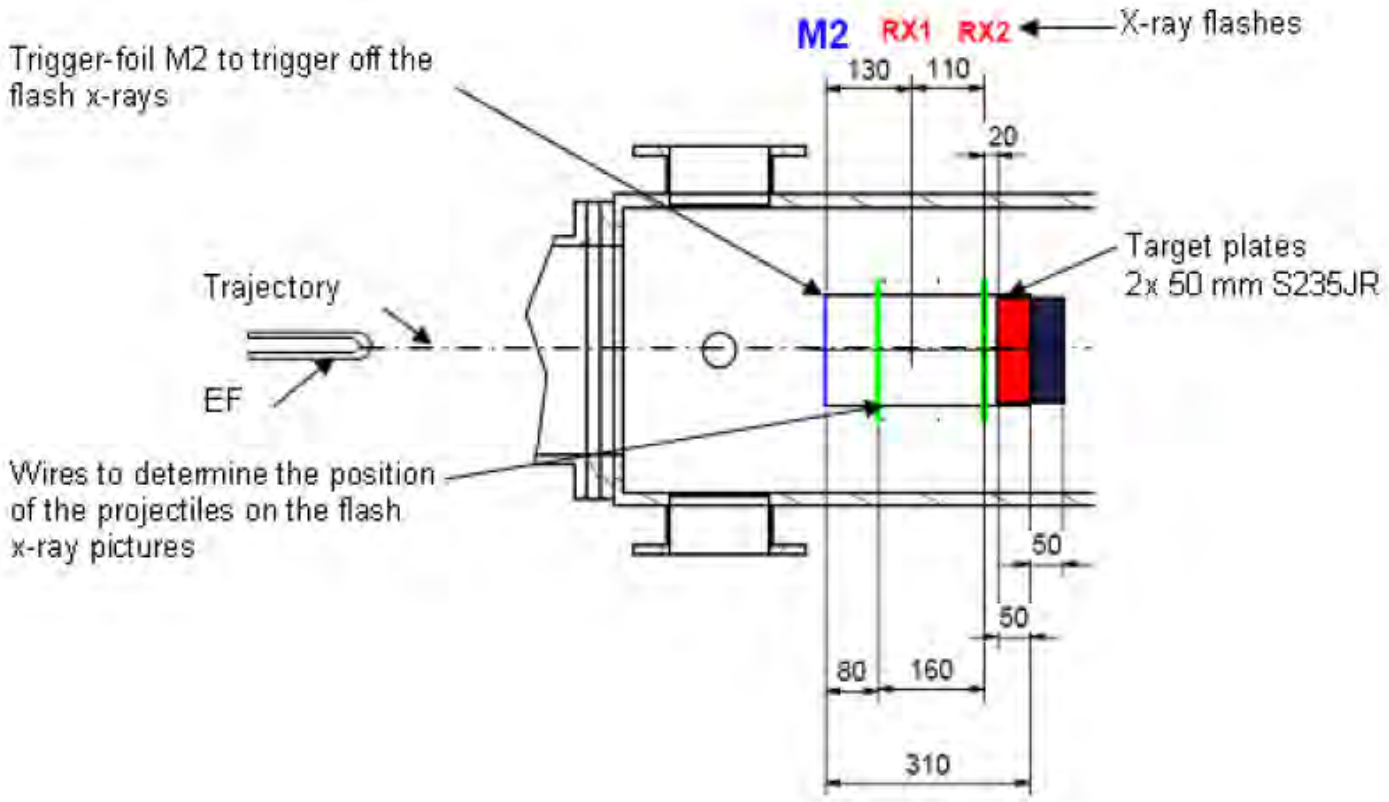

국방과학연구소 AGENCY FOR DEFENSE DEVELOPMENT
MBDA MISSILE SYSTEMS
NUMERICS
ISL

Velocity Evaluation Procedure from FXR Captures

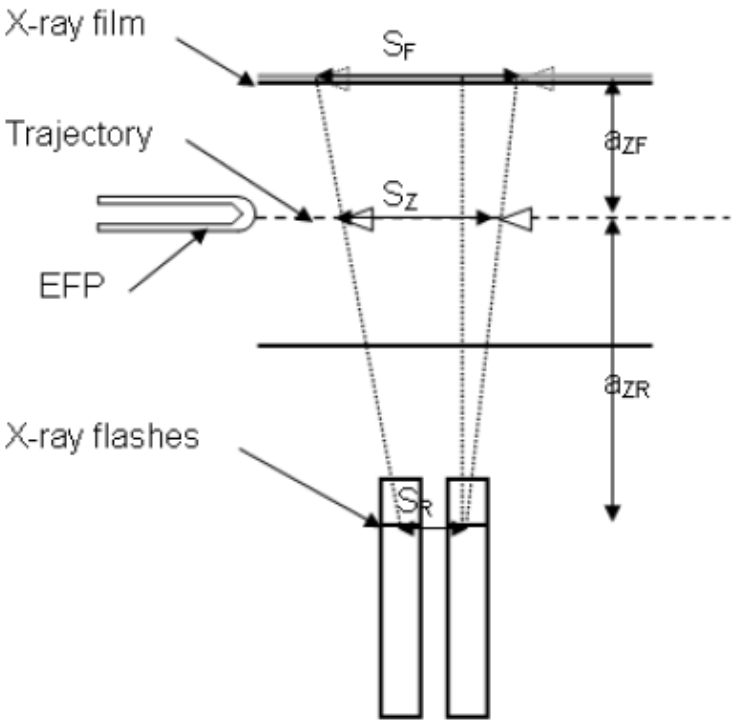

$$S_Z = \frac{S_F \cdot a_{ZR} + S_R \cdot a_{ZF}}{a_{ZR} + a_{ZF}}$$

Evaluation of Impact Depth and Crater Diameter

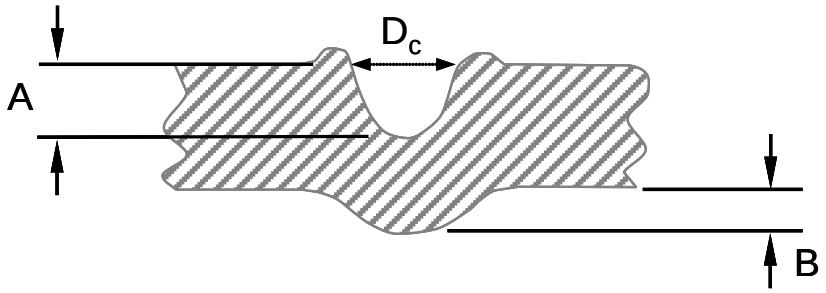

DEPTH OF PENETRATION =
A (HOLE DEPTH) - B

Evaluation of Crater Diameters and DoPs

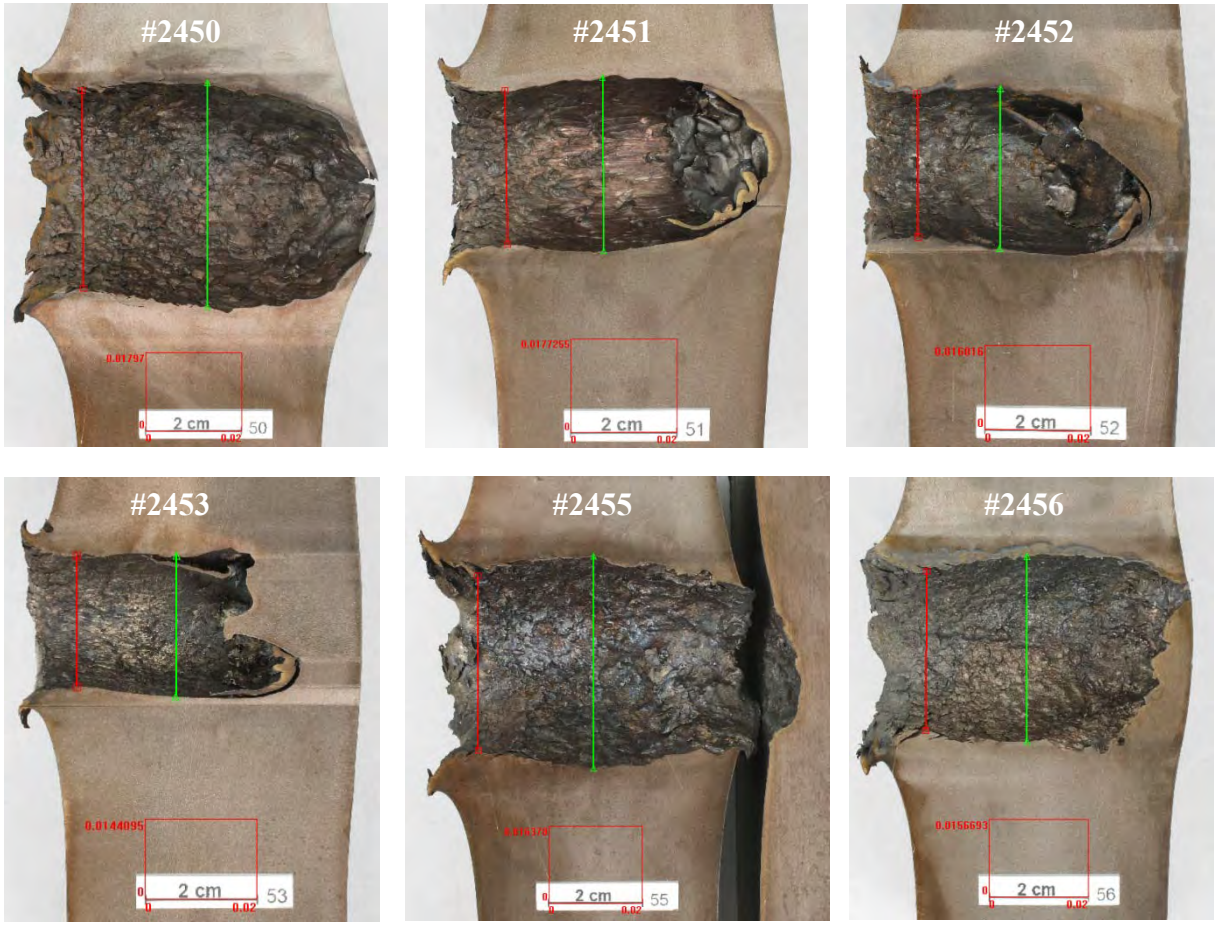

Results of Crater Diameters and DoPs with different Solidity Ta-EFP Simulants

Test #	Solidity	V [m/s]	Crater diameter [mm]	DoP [mm]
2450	100%	2914	39.0	60.4
2451	100%	2075	28.6	53.0
2455	80%	2936	38.5	60.0
2452	80%	2087	26.6	42.4
2456	60%	3129	32.3	53.7
2453	60%	2041	22.7	39.1

Results of Crater Diameters with Different Solidity Ta-EFP Simulants

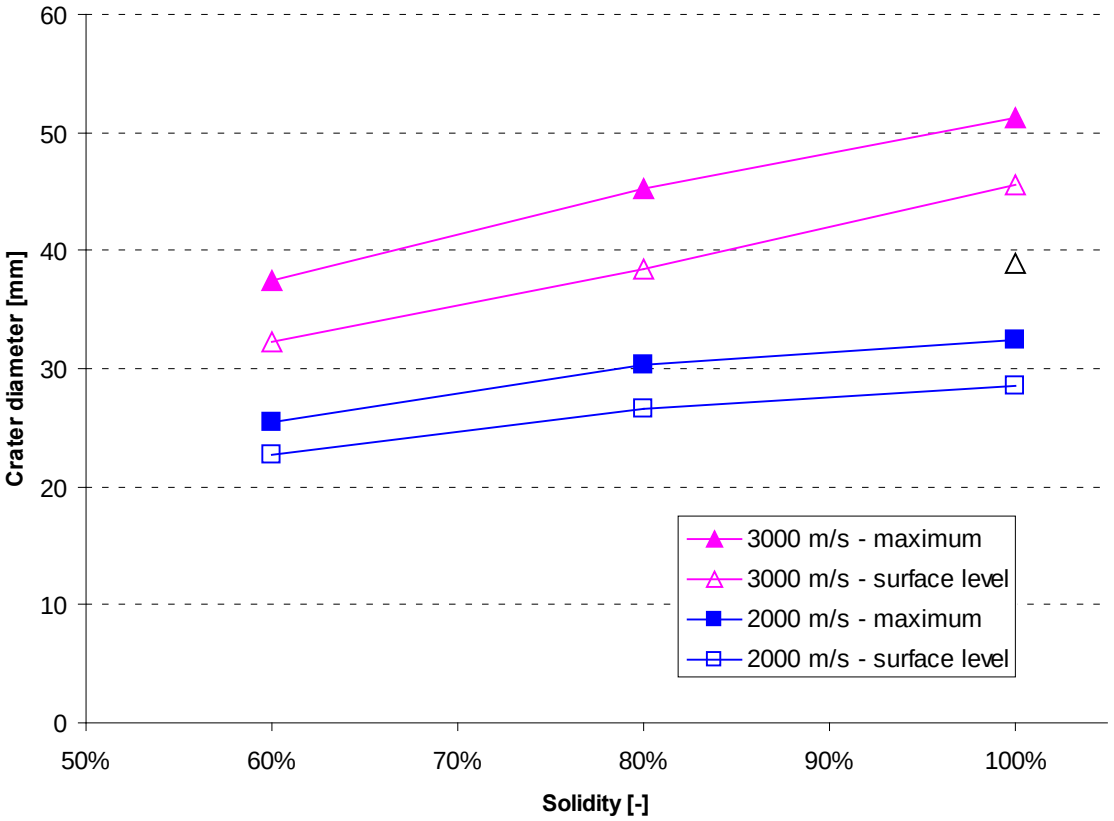

Outline

- Motivation & Introduction
- Experimental Tests: Setup & Results
- **Numerical Simulations**
- Modeling Approach
- Summary

Investigated Constant Dimensions EFPs of Different Solidity

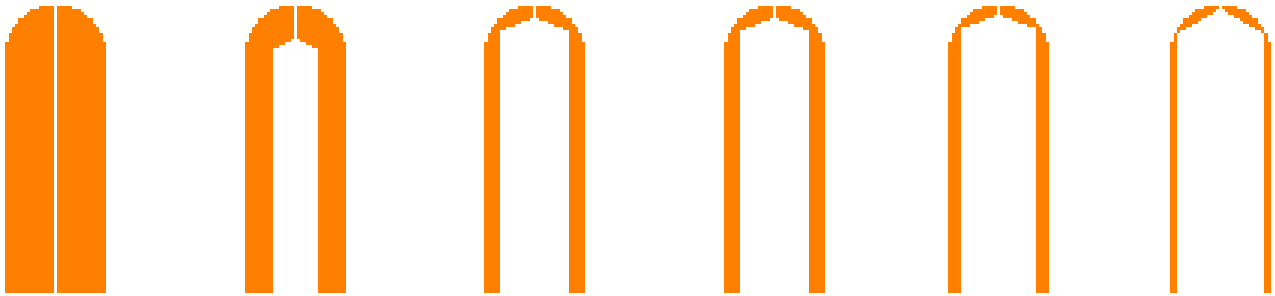

Solidity	100%	80%	60%	50%	40%	20%
Bore diameter d [mm]	0.0	4.3	6.3	7.2	7.8	8.9
Bore length l [mm]	0.0	26.6	28.0	28.6	29.9	29.5

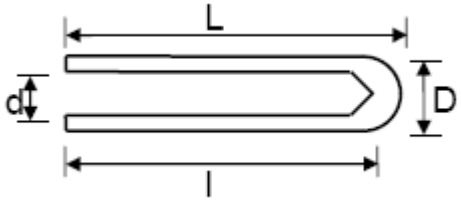

Numerical and Experimental DoP of different Solidity Ta-EFPs

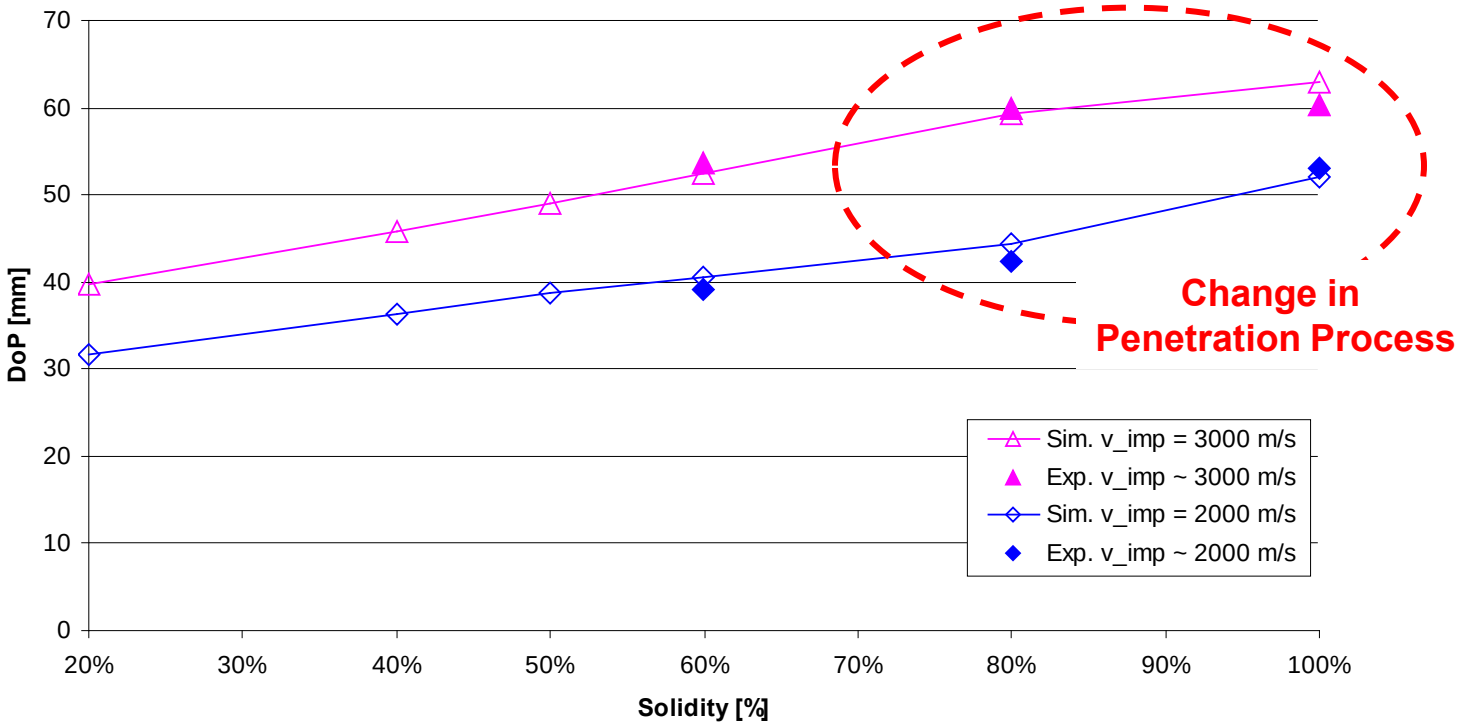

Change in Erosion Pattern from Solid to Hollow Projectiles

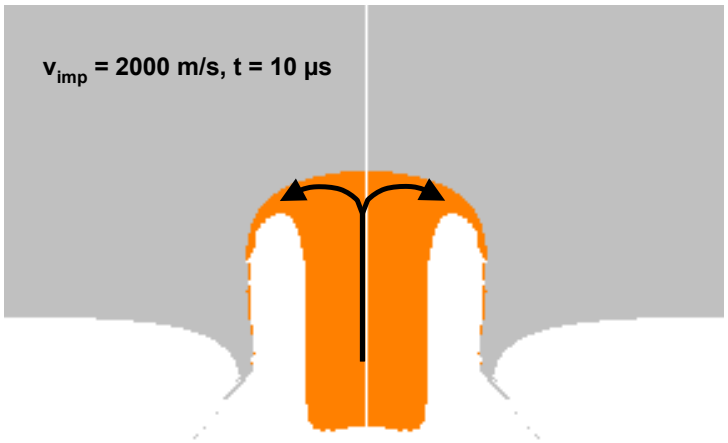

Solid EFP

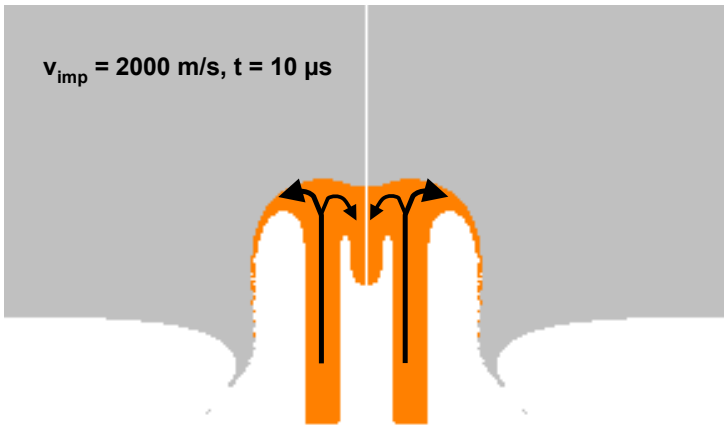

80% Solidity EFP

Numerical Penetration Depths of Different Solidity Cu-EFPs

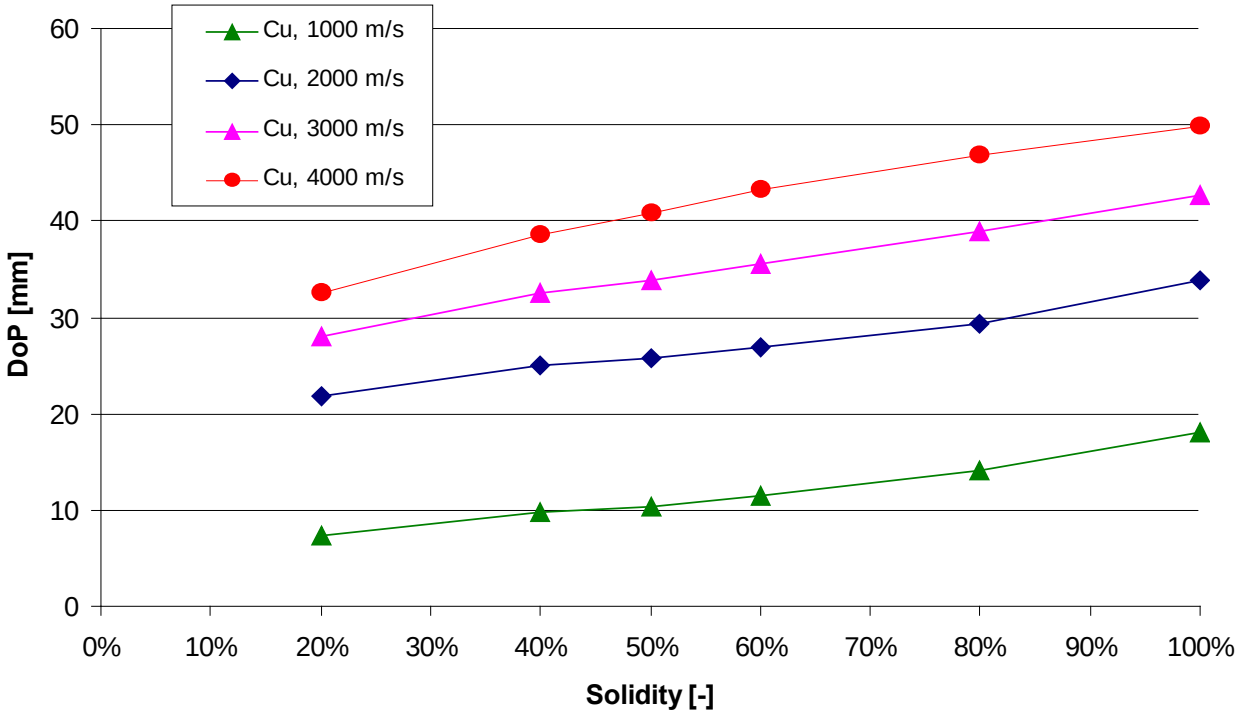

DoP / Mass Unit vs. Solidity of Cu-EFPs for Different Impact Velocities

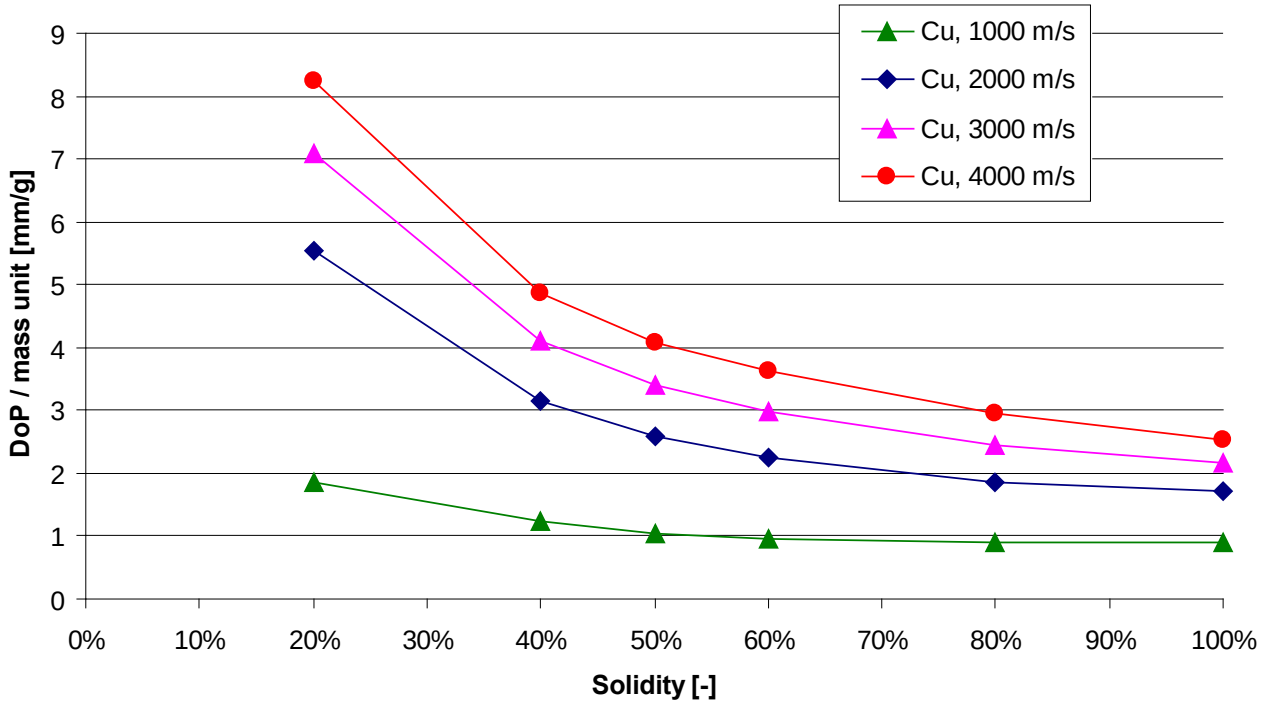

Outline

- Motivation & Introduction
- Experimental Tests: Setup & Results
- Numerical Simulations
- **Modeling Approach**
- Summary

Possible Displacements on Infinitesimal Element of Hollow EFP (simplified)

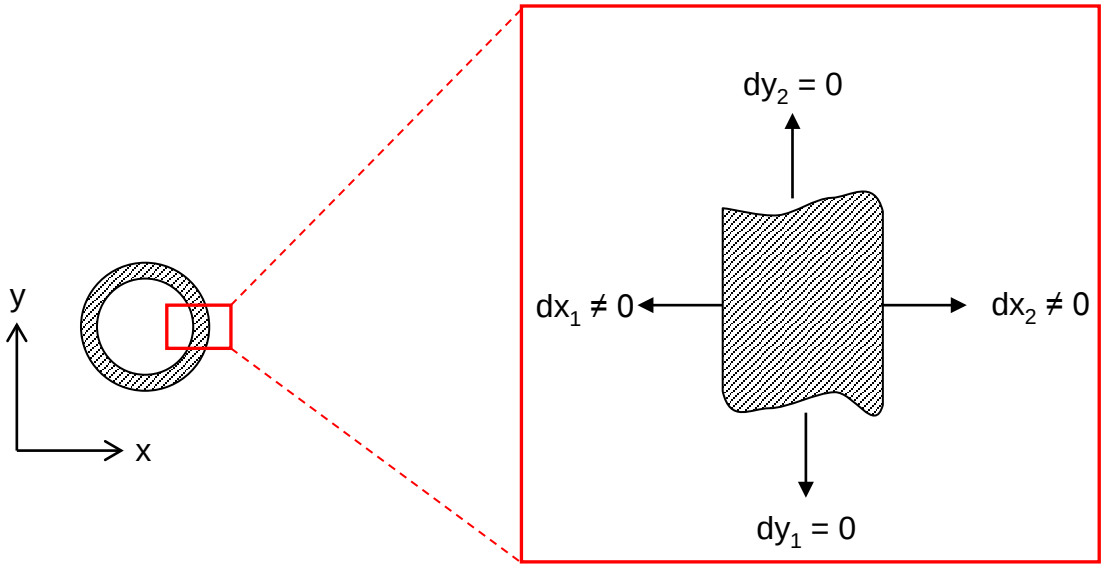

Definition of Effective Length for Planar Simplification

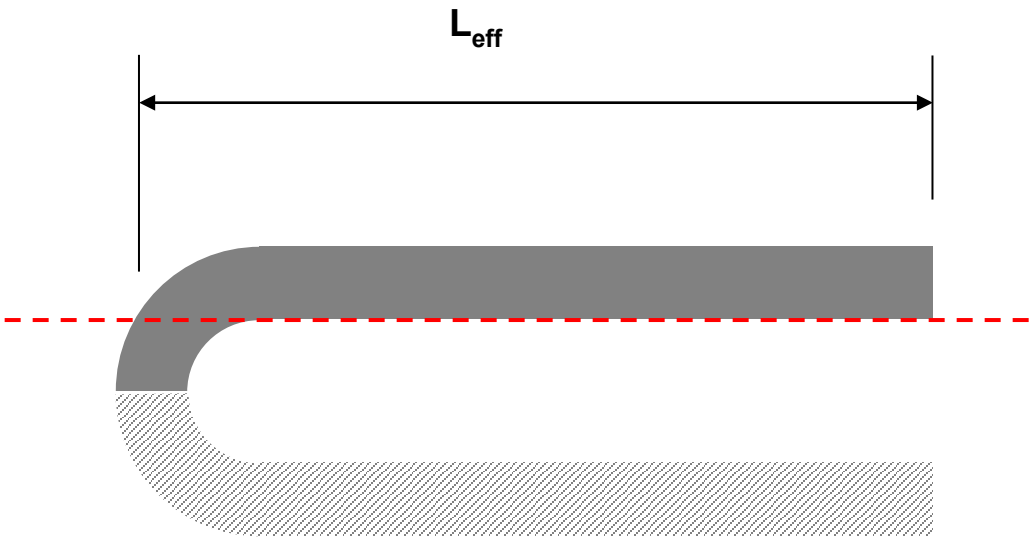

Comparison of EFP and Equivalent Shell Impact @ v_{imp} = 2000 m/s

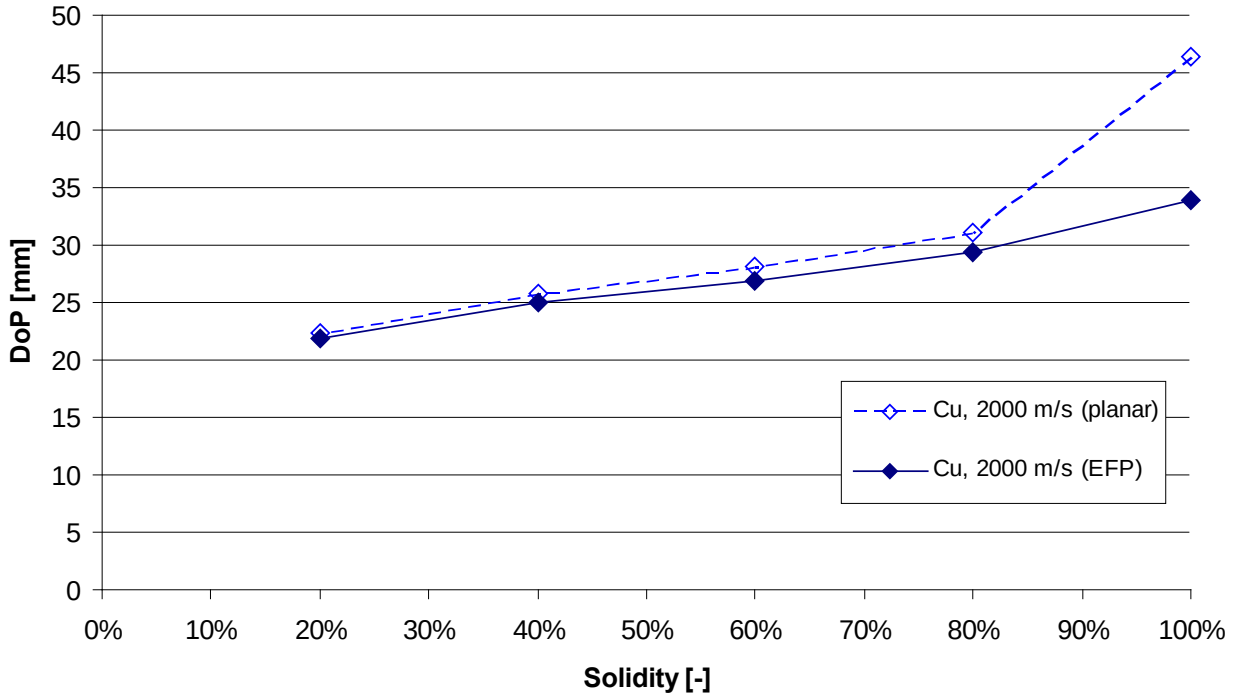

Outline

- Motivation & Introduction
- Experimental Tests: Setup & Results
- Numerical Simulations
- Modeling Approach
- **Summary**

Summary

- Investigation of the Influence of EFP Solidity on Penetration Performance
- Experimental DoP Tests with Ta-EFPs with different Solidities were performed
- Numerical Simulations with Cu- EFPs and Ta-EFPs of different Solidities
- Change in DoP Process from Solid to Hollow EFP

  required Extension of existing Penetration Model
- Good Agreement with Experimental Results

Thank you !

Any Questions ?

E-mail: hoskim@add.re.kr

26th International Symposium on BALLISTICS
SEPTEMBER 12-16, 2011
HYATT REGENCY MIAMI
MIAMI, FLORIDA

A Novel Technology for Switchable Modes Warheads

Werner Arnold
Markus Graswald
Ernst Rottenkolber (*)

MBDA MISSILE SYSTEMS

(*) NUMERICS

Outline

- **Motivation / MPI Objective**
- **Novel MPI - Technology**
- **HEP - Method: Proof of Principle**
- **Warhead Applications**
- **Switchable Warheads**
- **Summary**

Outline

- **Motivation / MPI Objective**
- Novel MPI - Technology
- HEP - Method: Proof of Principle
- Warhead Applications
- Switchable Warheads
- Summary

New Challenges: Asymmetry & Collateral Damage











Example: Axially Switchable Warhead (LOCAAS)

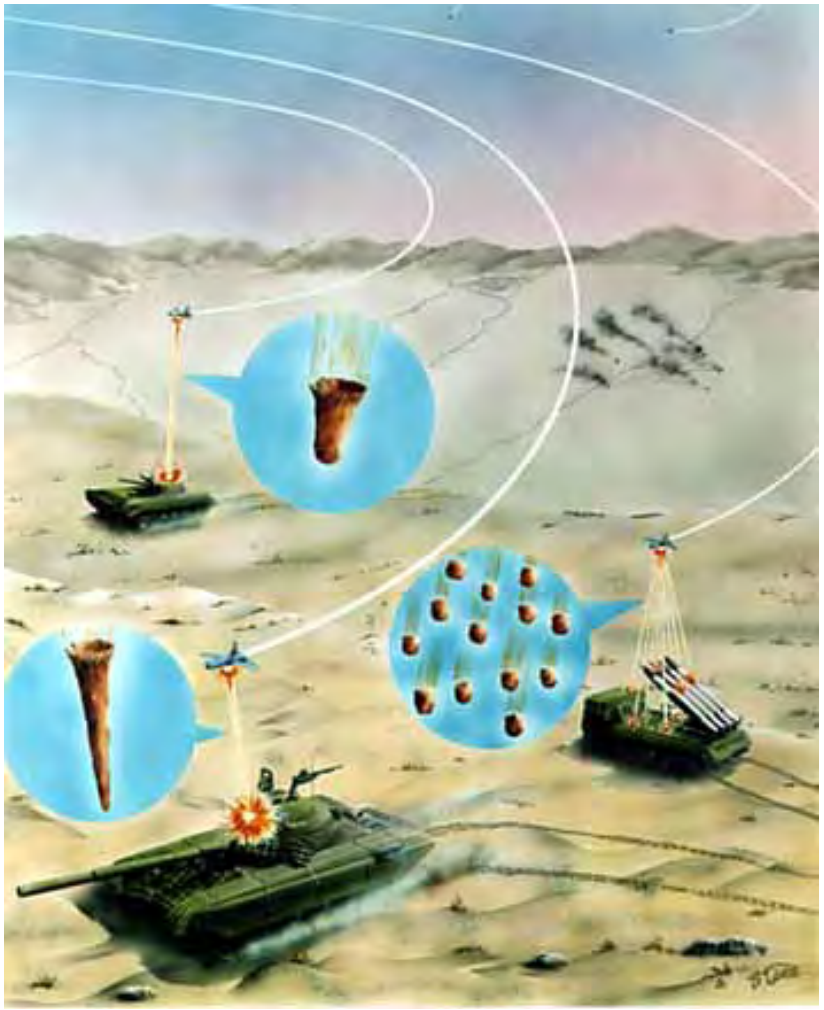

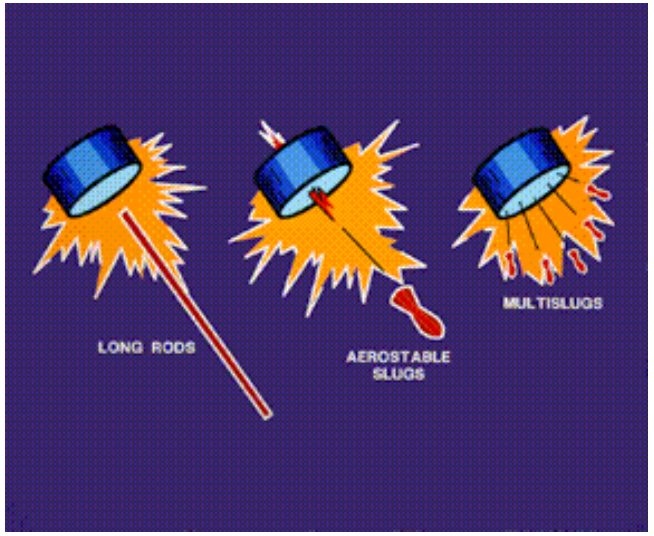

Outline

- Motivation / MPI Objective
- **Novel MPI - Technology**
- HEP - Method: Proof of Principle
- Warhead Applications
- Switchable Warheads
- Summary

Charge with Implemented MPI System (9-fold)

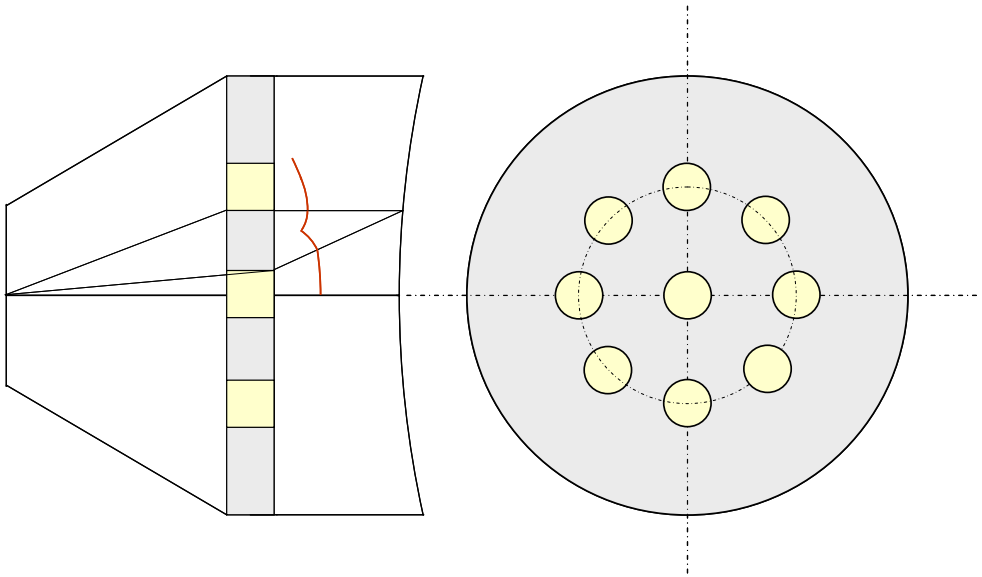

Charge with 9-fold HEP Disc & DotMask Simulation

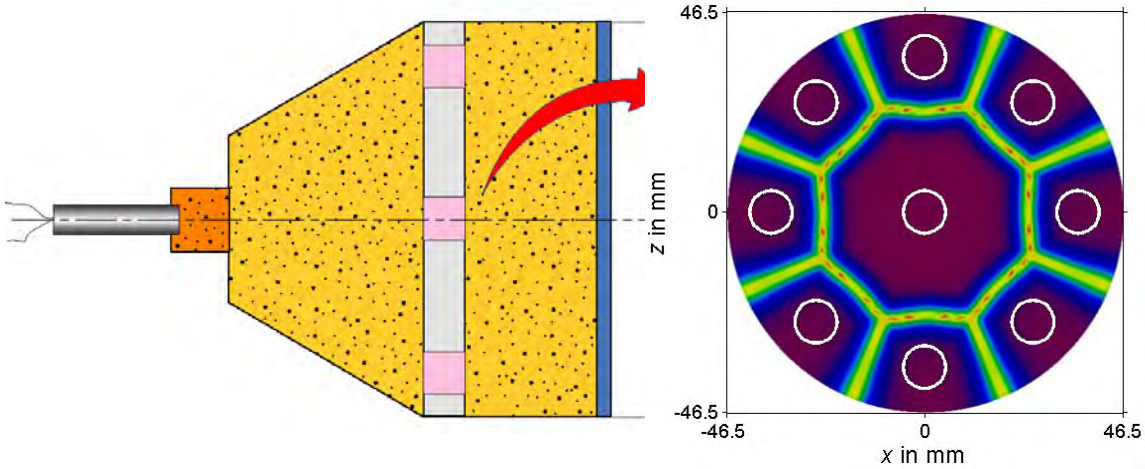

DotMask Simulation

Outline

- Motivation / MPI Objective
- Novel MPI - Technology
- **HEP - Method: Proof of Principle**
- Warhead Applications
- Switchable Warheads
- Summary

Proof of Principle: Static Trials with Witness Block

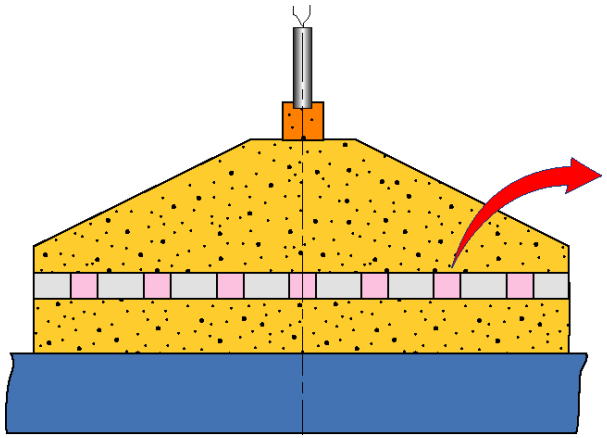

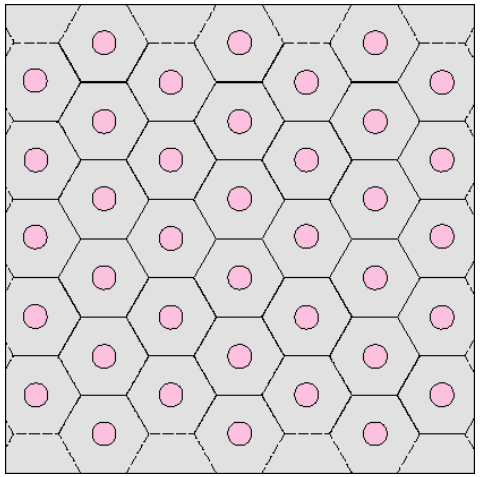

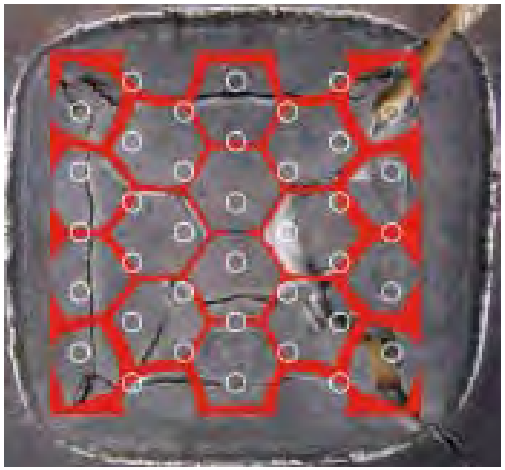

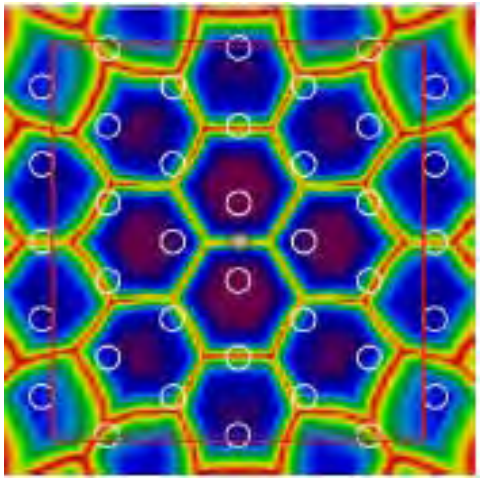

Proof of Principle: Test Setup Dynamic Trials

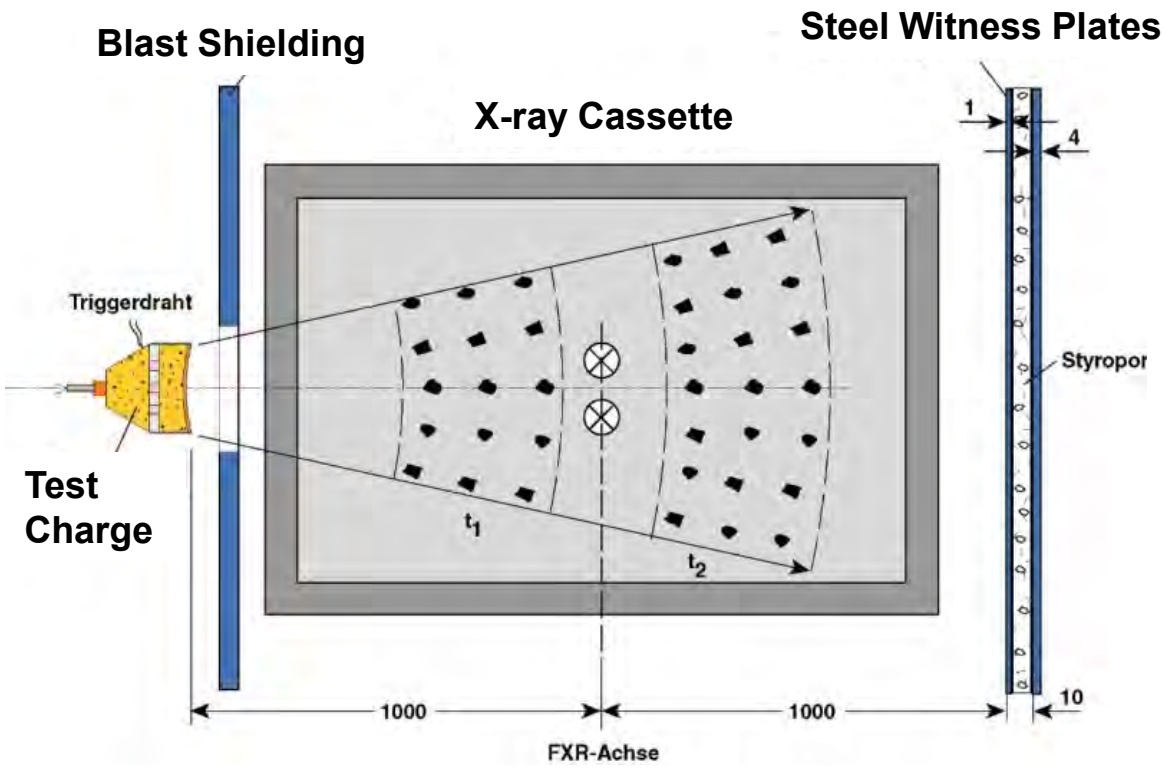

Proof of Principle: Dynamic Trials with Witness Plate

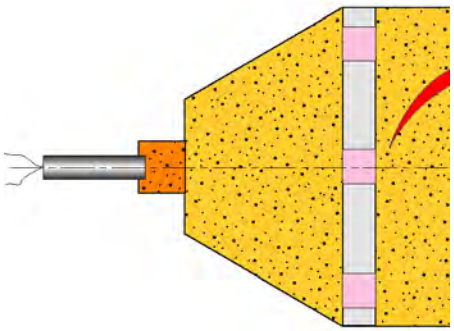

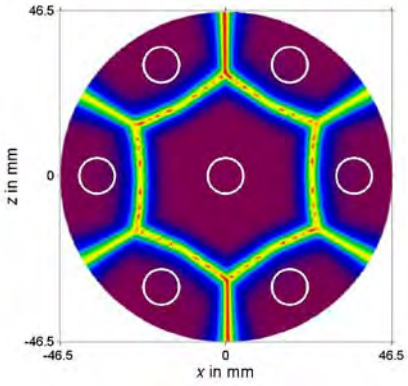

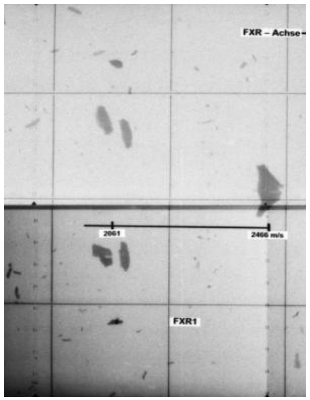

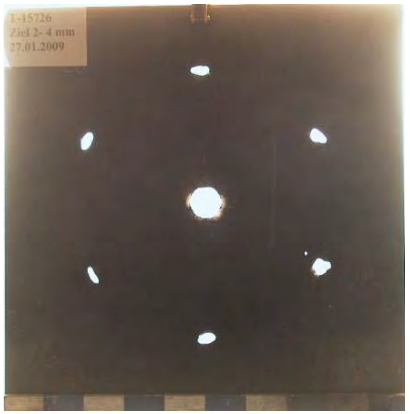

New Spallation Modell

Outline

- Motivation / MPI Objective
- Novel MPI - Technology
- HEP - Method: Proof of Principle
- **Warhead Applications**
- Switchable Warheads
- Summary

Application of HEP - Method on Blast / Frag Warhead

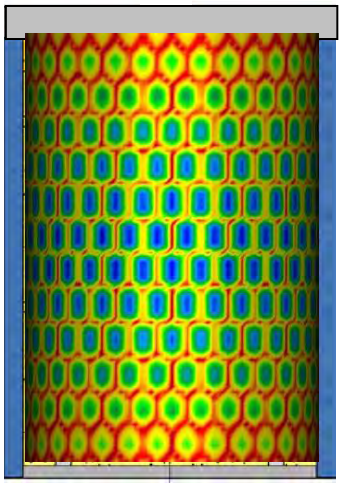

DotMask Simulation

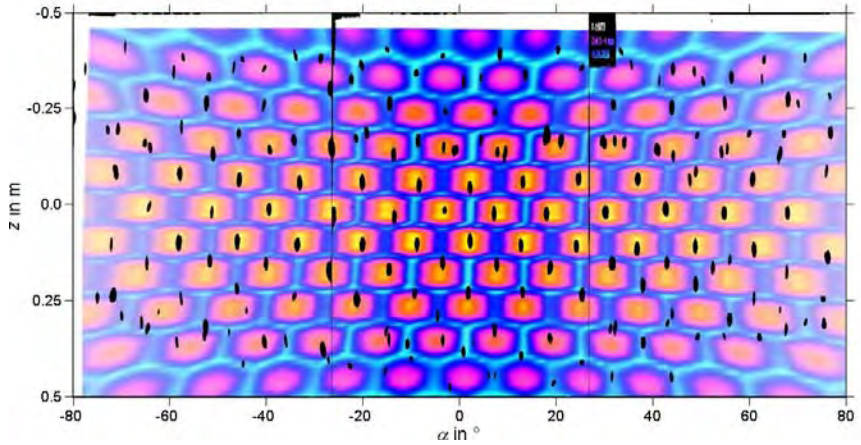

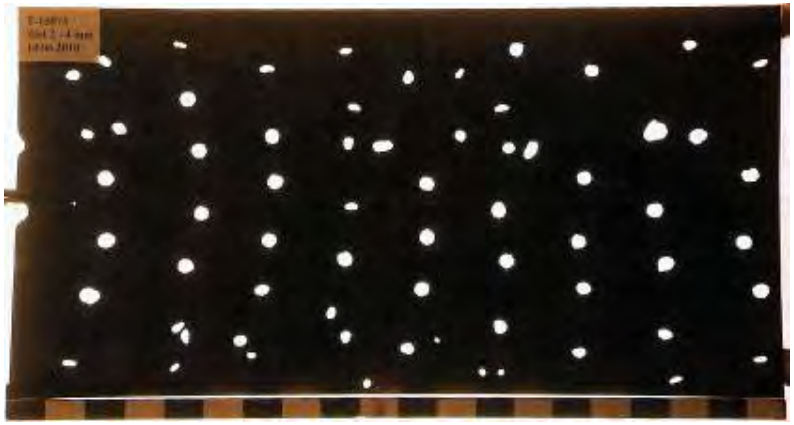

Outline

- Motivation / MPI Objective
- Novel MPI - Technology
- HEP - Method: Proof of Principle
- Warhead Applications
- **Switchable Warheads**
- Summary

Axially Switchable Charge: Fragments vs. EFP

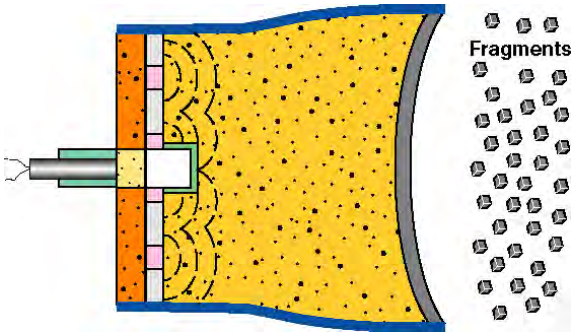

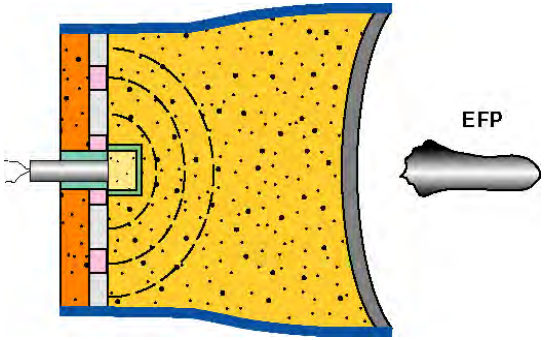

Radially Switchable Charge: Two Initiation Trains

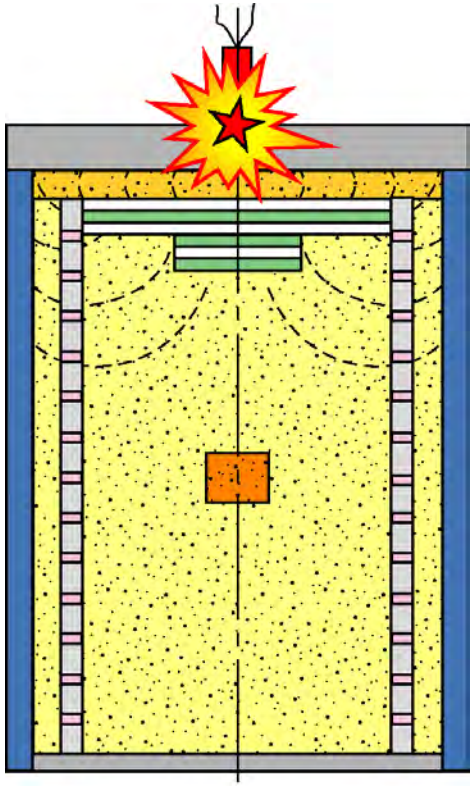

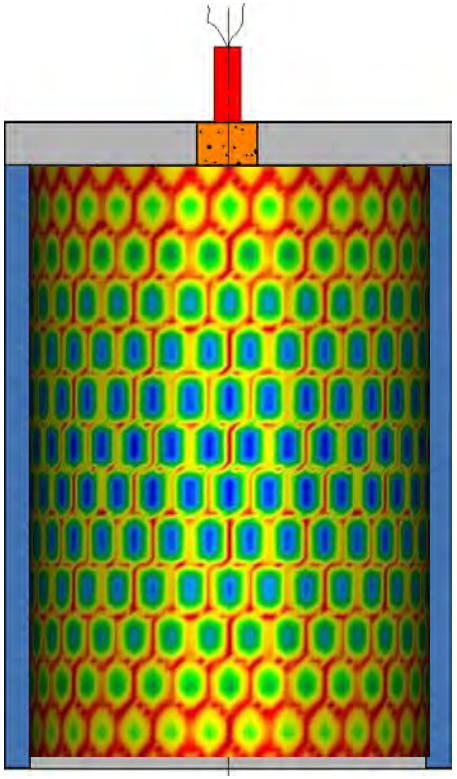

Radially Switchable Charge: Test Setup

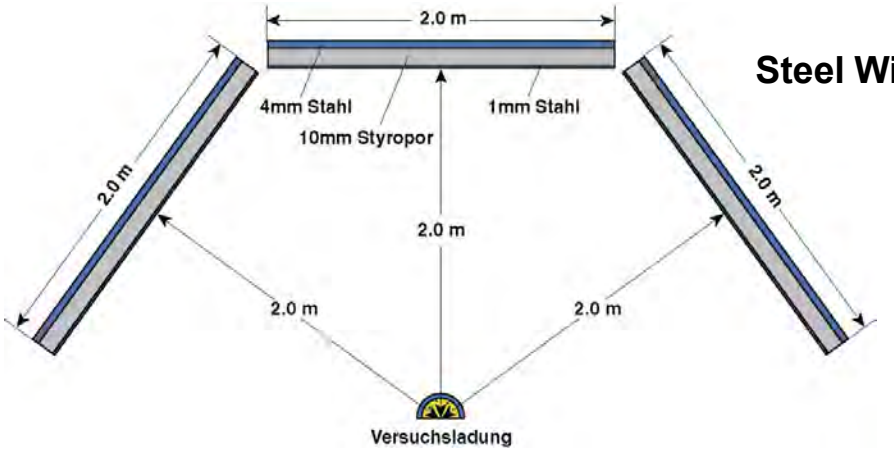

Steel Witness Plates

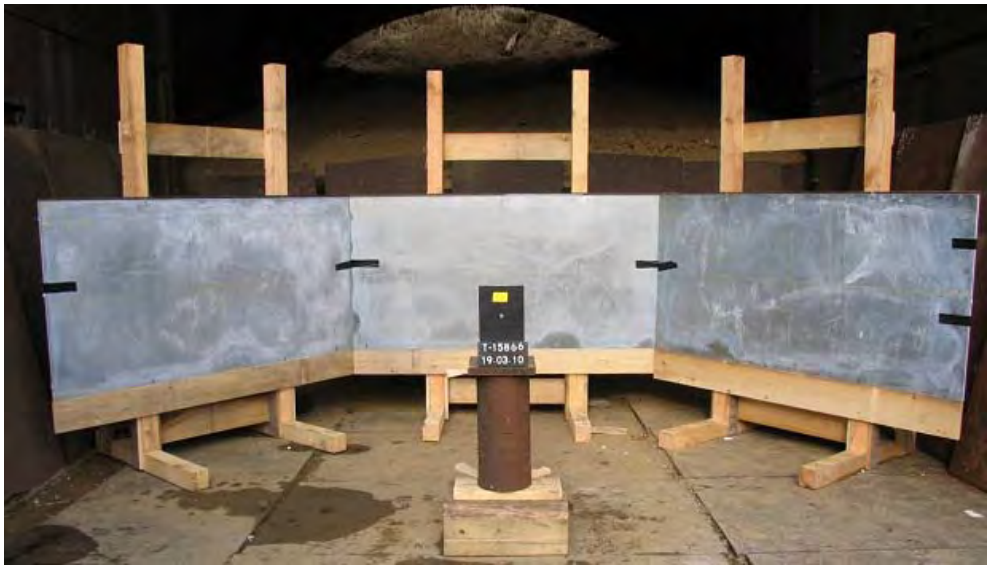

Radially Switchable Charge: Natural Fragments

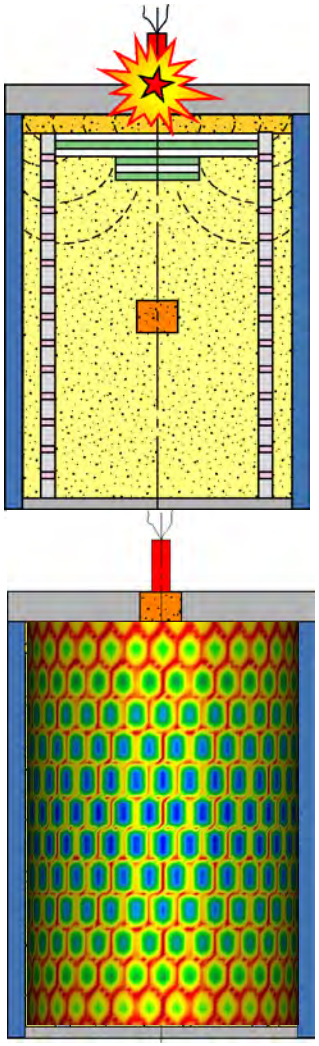

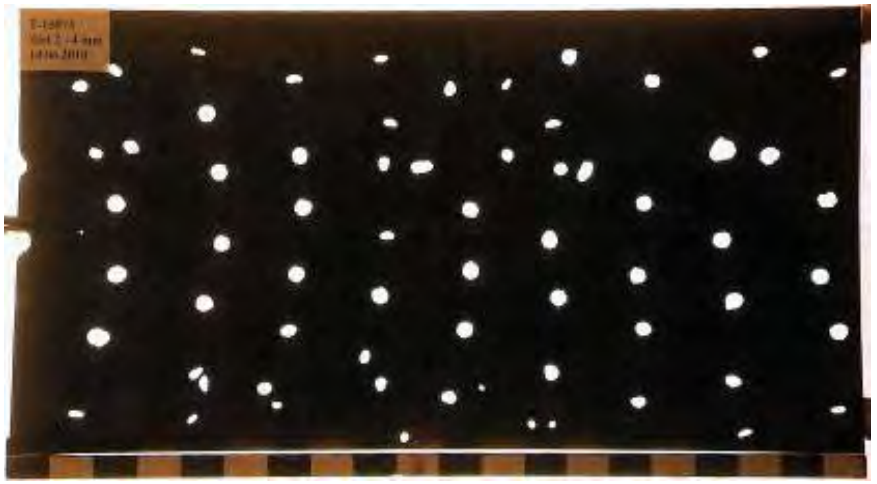

Standard Mode
Natural Frags

Fragmentation Mode
Controlled Frags

Radially Switchable Charge: Pre-Formed Fragments

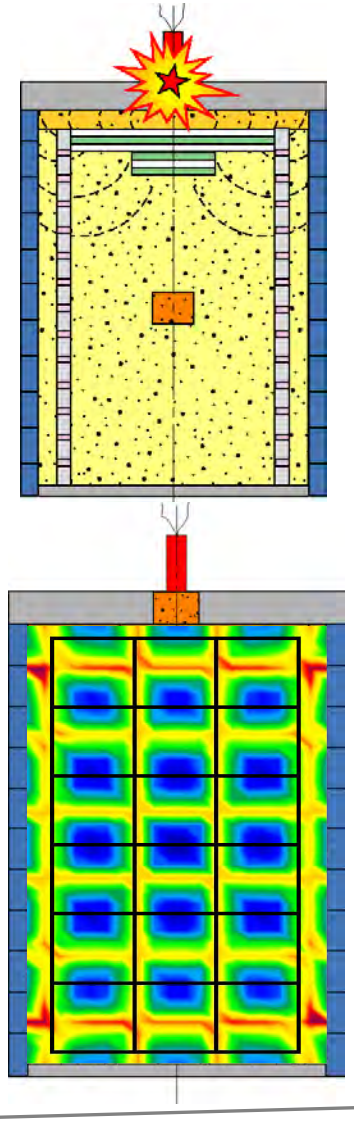

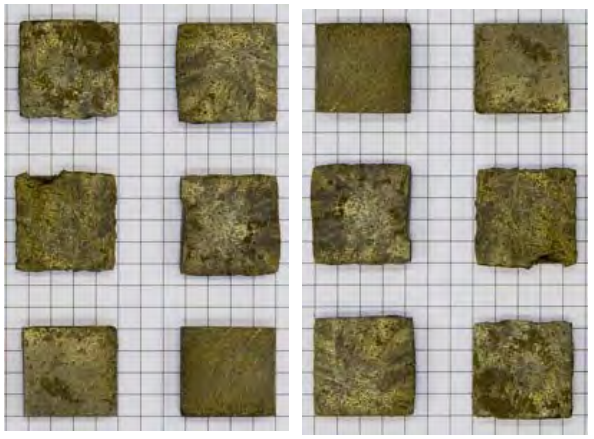

Standard Mode
Pre-Formed Frags

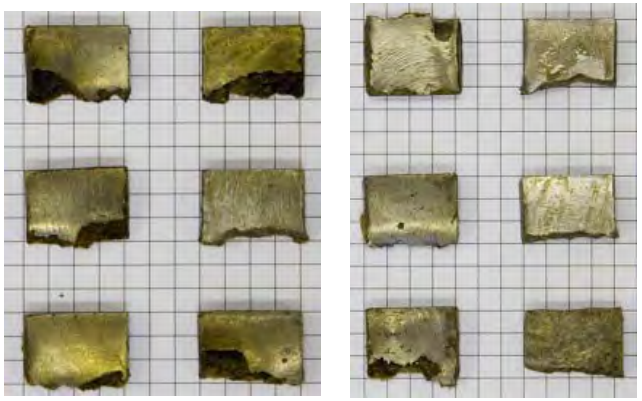

Fragmentation Mode
Cut PF-Frags

Outline

- Motivation / MPI Objective
- Novel MPI - Technology
- HEP - Method: Proof of Principle
- Warhead Applications
- Switchable Warheads
- **Summary**

Summary

- **Novel Multi-Point Initiation (MPI) Method with HE-Pellets**
- **Proof of Principle with static & dynamic Tests was demonstrated**
- **Application for Warheads (axially & radially) was shown**
- **Switchable Warheads:**
  - **Natural Fragments vs. Controlled Fragments**
  - **Pre-Formed Fragments vs. Cut PF-Fragments**

Acknowledgement

Acknowledge the WTD91 GF410 in Meppen for funding

Thank You for Your Attention !

Any Questions ?

Your Contact:
Dr. Werner Arnold
Phone: +49 8252 99 6267
Email: werner.arnold@mbda-systems.de

26th International Symposium on Ballistics

An experimental and numerical study of ballistic impacts on a turbine casing material at varying temperatures

Borja Erice [a,b]
Francisco Gálvez [a,b]
David A. Cendón [a,b]
Vicente Sánchez-Gálvez [a,b]
Tore Børvik [c]

a) **Dept. of Materials Science** Technical University of Madrid

b) **Research Centre on Safety and Durability of Structures and Materials UPM-CSIC**

c) **NTNU – Trondheim** Norwegian University of Science and Technology

Contents

Motivation and objectives

- **Blade-off containment**
- If a turbine blade fails the case must contain all the fragments

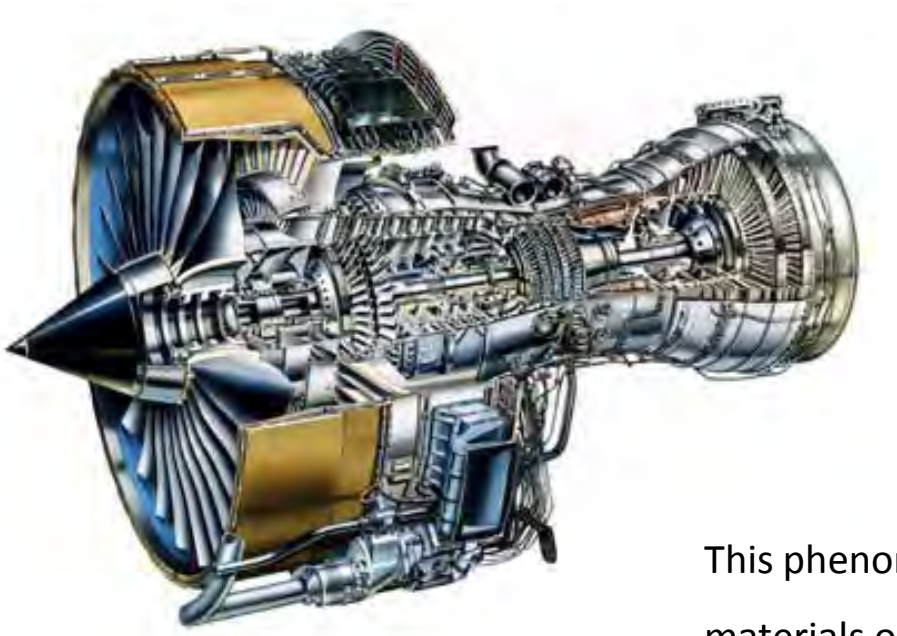

Rotational velocity: 9,000 to 12,000 rpm

Diameter: Fan 2,5m Turbine: 1,2m

Temperature: 800ºC (blade) 500ºC (case)

This phenomenon is a High speed impact of materials operating at high temperature

Motivation and objectives

- Blade-off containment
- Mechanical behavior of FV535 steel

  at high temperature and high strain rate.

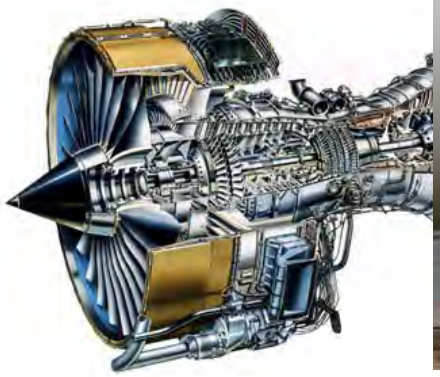

Departamento de Ciencia de Materiales
Universidad Politécnica de Madrid
POLITÉCNICA

Motivation and objectives

- Blade-off containment
- Mechanical behavior of FV535 steel

  at high temperature and high strain rate.

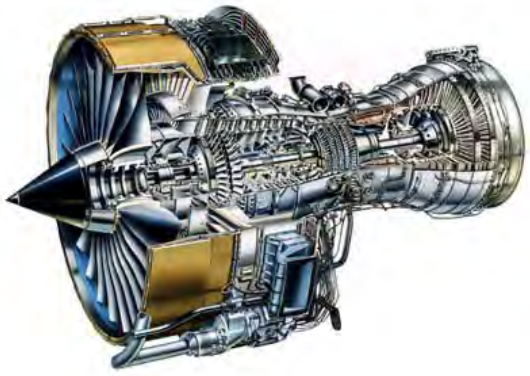

Motivation and objectives

- Blade-off containment
- Mechanical behavior case material at high temperature and high strain rate.
  - Case material: FV535, martensitic stainless steel 0.1%C 11%Cr
- Material modeling.
  - Static and dynamic tests to obtain material data at its operating conditions
  - Material model calibration.
    - Ballistics tests
    - Numerical simulations
- Numerical simulation of a blade-off event

Contents

Johnson-Cook (JC) and Modified Johnson-Cook (MJC)

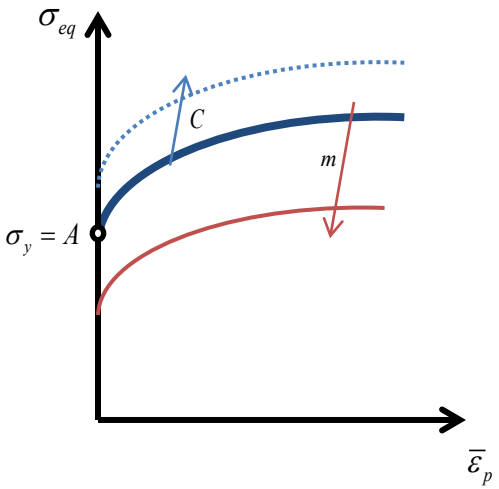

$$\sigma_{eq}^{JC} = \left[A + B\bar{\varepsilon}_p^{n}\right]\left[1 + C\ln\dot{\bar{\varepsilon}}_p^{*}\right]\left[1 - T^{*m}\right] \qquad \dot{\bar{\varepsilon}}_p^{*} = \frac{\dot{\bar{\varepsilon}}_p}{\dot{\varepsilon}_0}$$

$$\sigma_{eq}^{MJC} = \left[A + B\bar{\varepsilon}_p^{n}\right]\left[1 + \dot{\bar{\varepsilon}}_p^{*}\right]^{C}\left[1 - T^{*m}\right] \qquad T^{*} = \frac{T - T_r}{T_m - T_r}$$

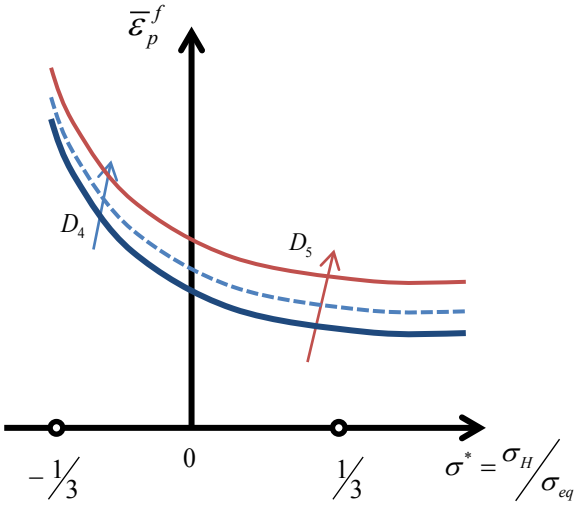

$$\bar{\varepsilon}_p^{f\,JC} = \left[D_1 + D_2\exp\left(D_3\sigma^{*}\right)\right]\left[1 + D_4\ln\dot{\bar{\varepsilon}}_p^{*}\right]\left[1 + D_5T^{*}\right]$$

$$\bar{\varepsilon}_p^{f\,MJC} = \left[D_1 + D_2\exp\left(D_3\sigma^{*}\right)\right]\left[1 + \bar{\varepsilon}_p^{*}\right]^{D_4}\left[1 + D_5T^{*}\right]$$

$$\dot{D} = \frac{1}{\bar{\varepsilon}_p^{f}}\dot{\bar{\varepsilon}}_p$$

Material testing

Low strain rate tests at 10^{-4} s^{-1} from T=24C to T=850C
Even up to 1200C

Hopkinson bar tests at 10^{3} s^{-1} from T=24C to T=850C

Material model

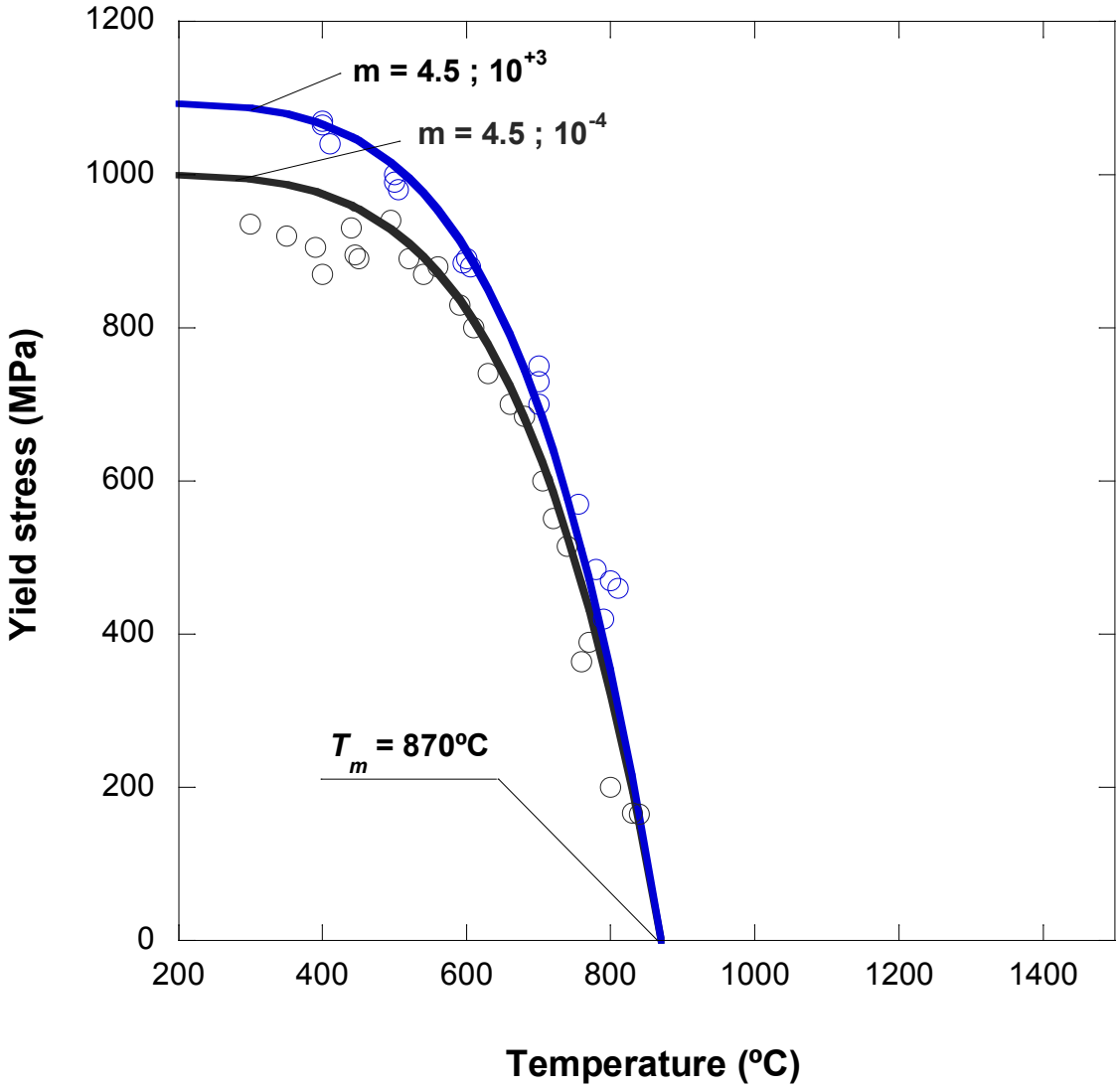

Thermal softening

$$\sigma_{eq}^{JC} = A\left[1-\left(\frac{T-T_r}{T_m-T_r}\right)^m\right]$$

$$T_m = 870^{\circ}C$$

$$m = 4.5$$

Contents

Ballistic tests at high temperature

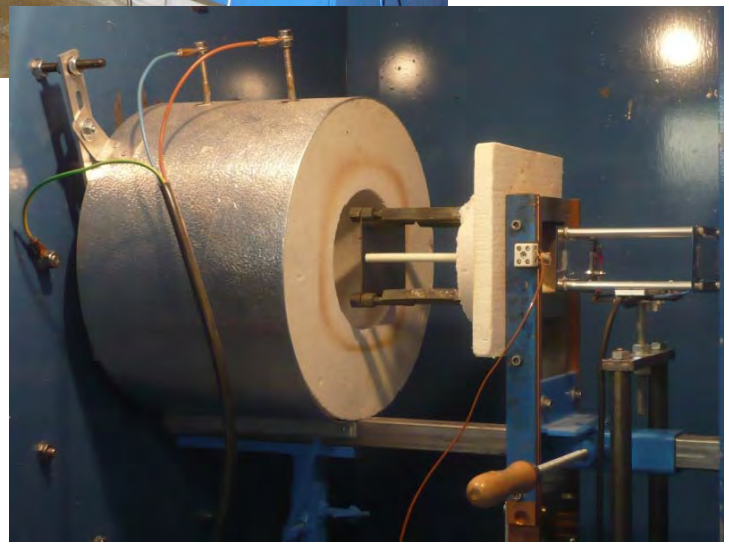

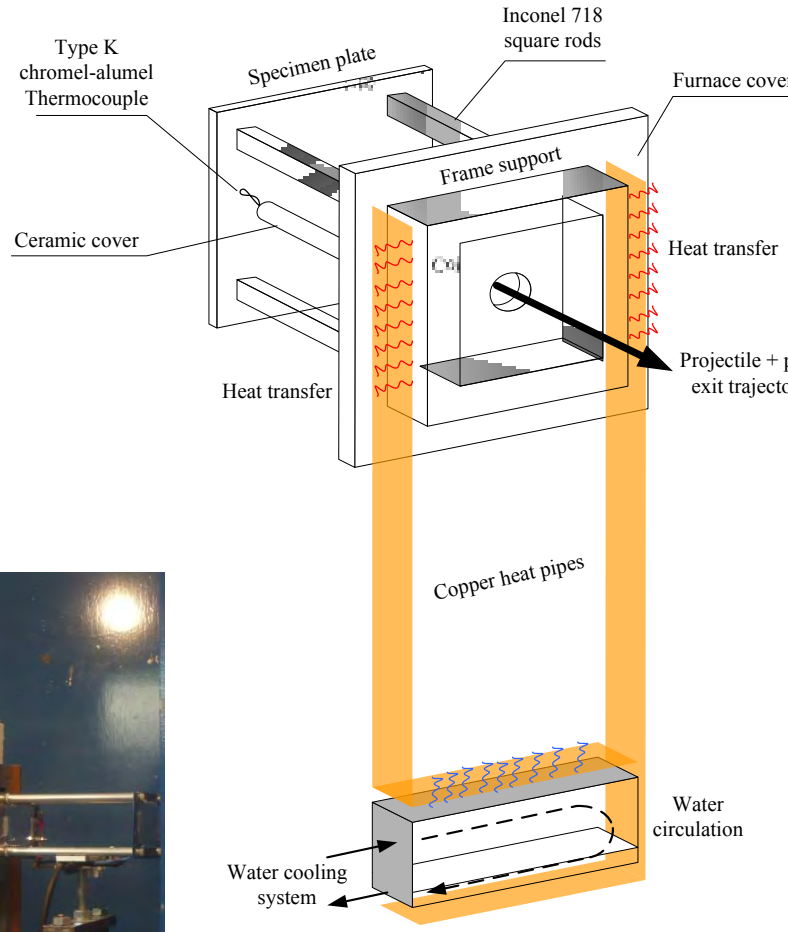

Samples:
Plates 100x100x1.6mm
400ºC and 700ºC

5.5mm ball

Ballistic tests at high temperature. Results

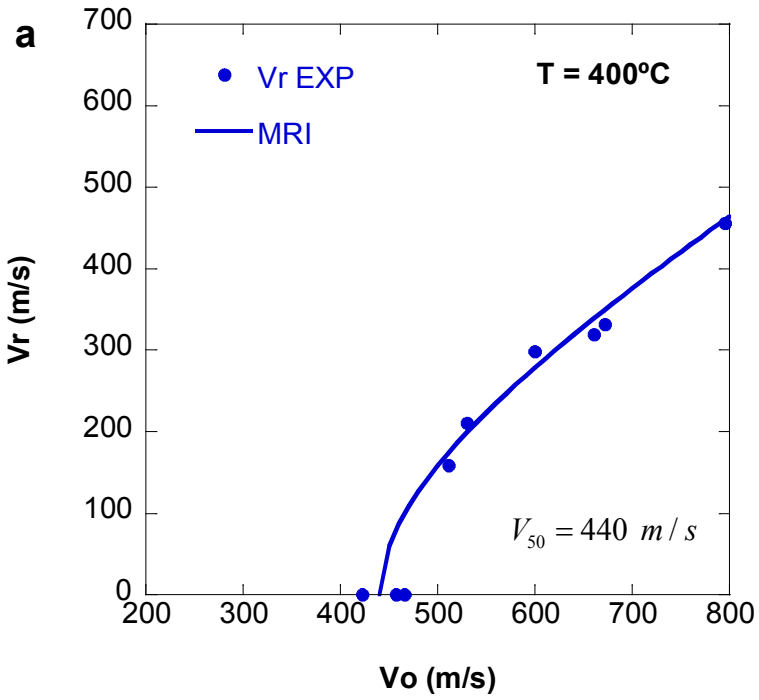

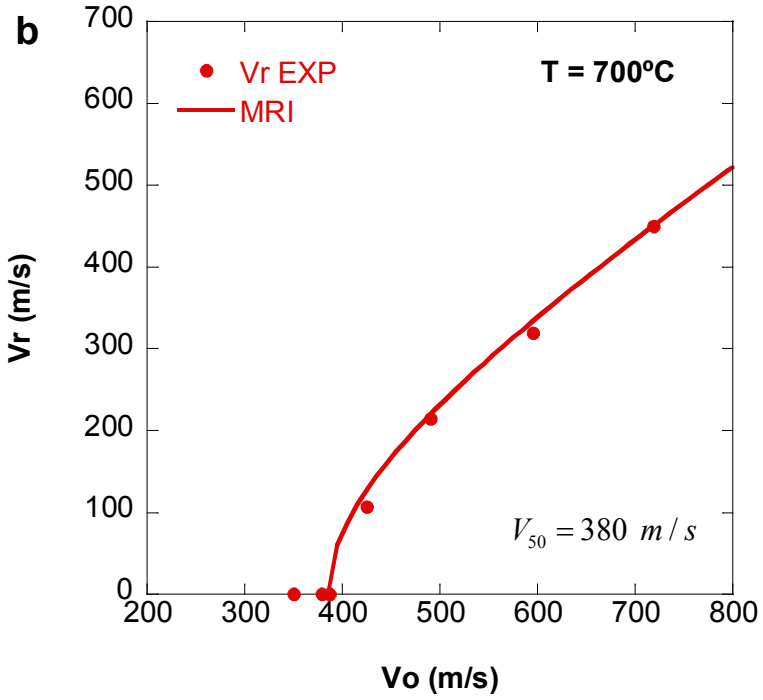

MRI (Modified Recht-Ipson)

$$v_r = \frac{k_1\left(v_0^{k_2} - v_{bl}^{k_2}\right)^{1/k_2}}{1 + m_p/M}$$

Contents

Numerical Simulations

- LS-DYNA, axilsimetric 2D.

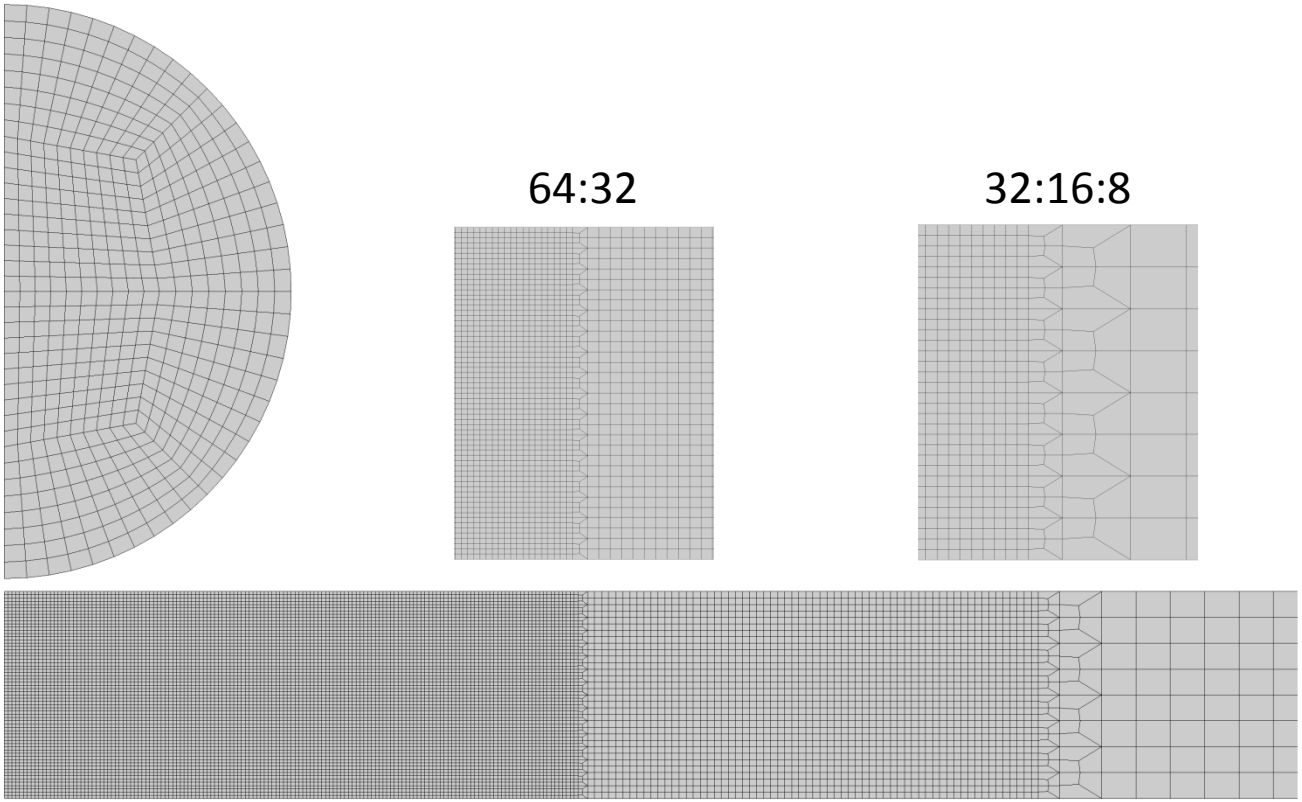

Numerical Simulations: Results using JC model

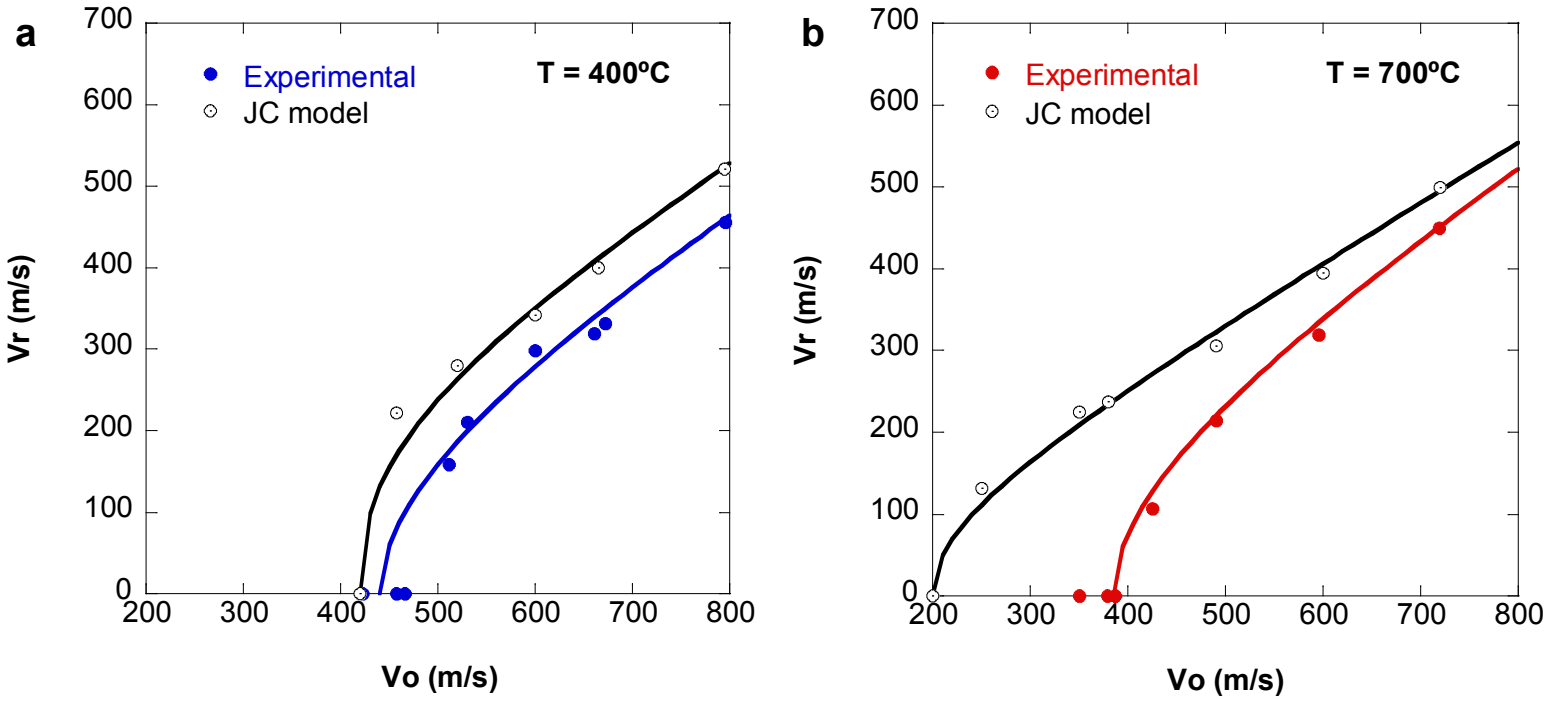

Numerical Simulations: Results using JC model

Temperature 400ºC

Temperature 700ºC

$v_0 = 520\,m/s$

$v_0 = 490\,m/s$

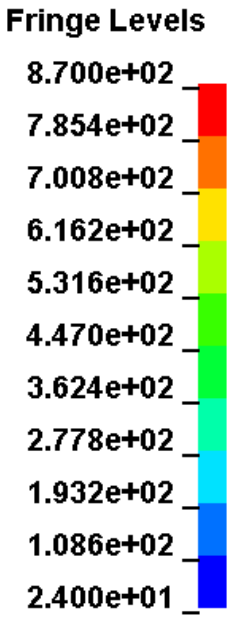

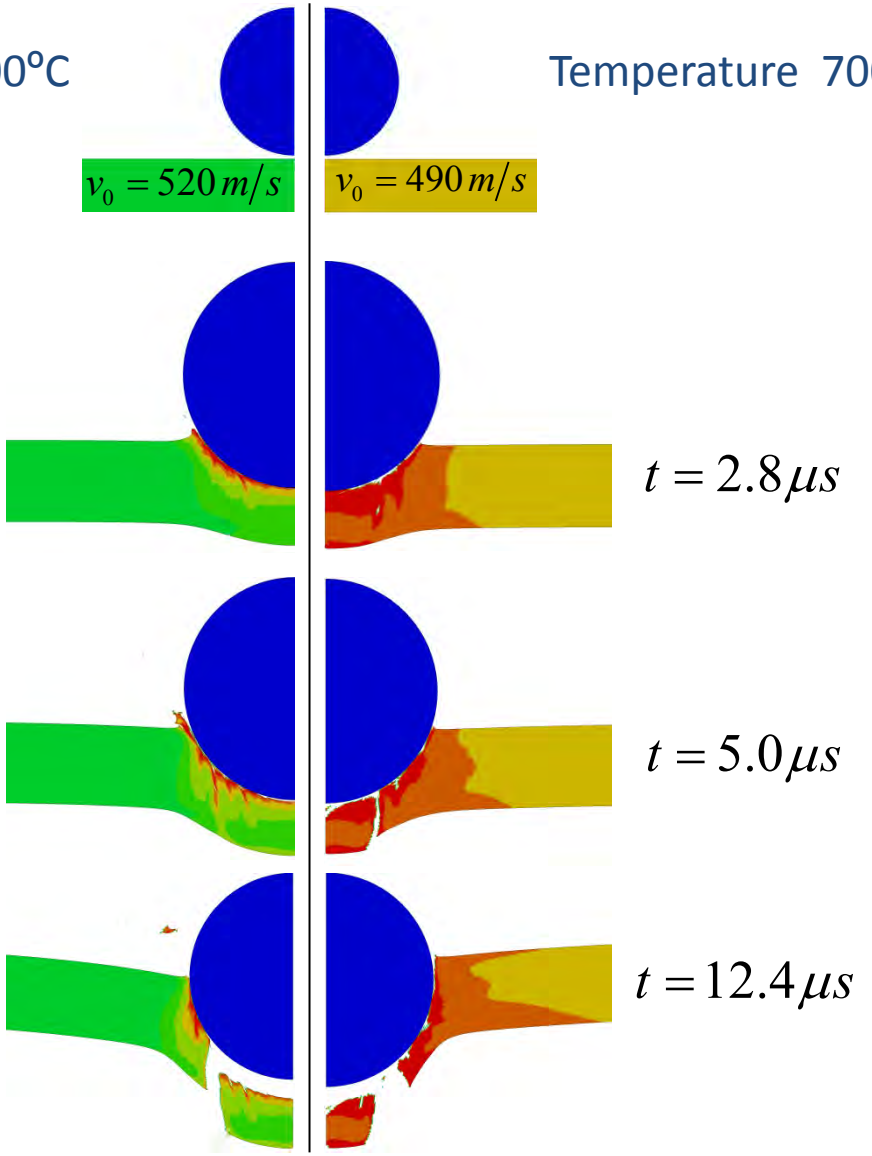

$t = 2.8\mu s$

$t = 5.0\mu s$

$t = 12.4\mu s$

Contents

Modification of JC model: Melt extended temperature (JCT)

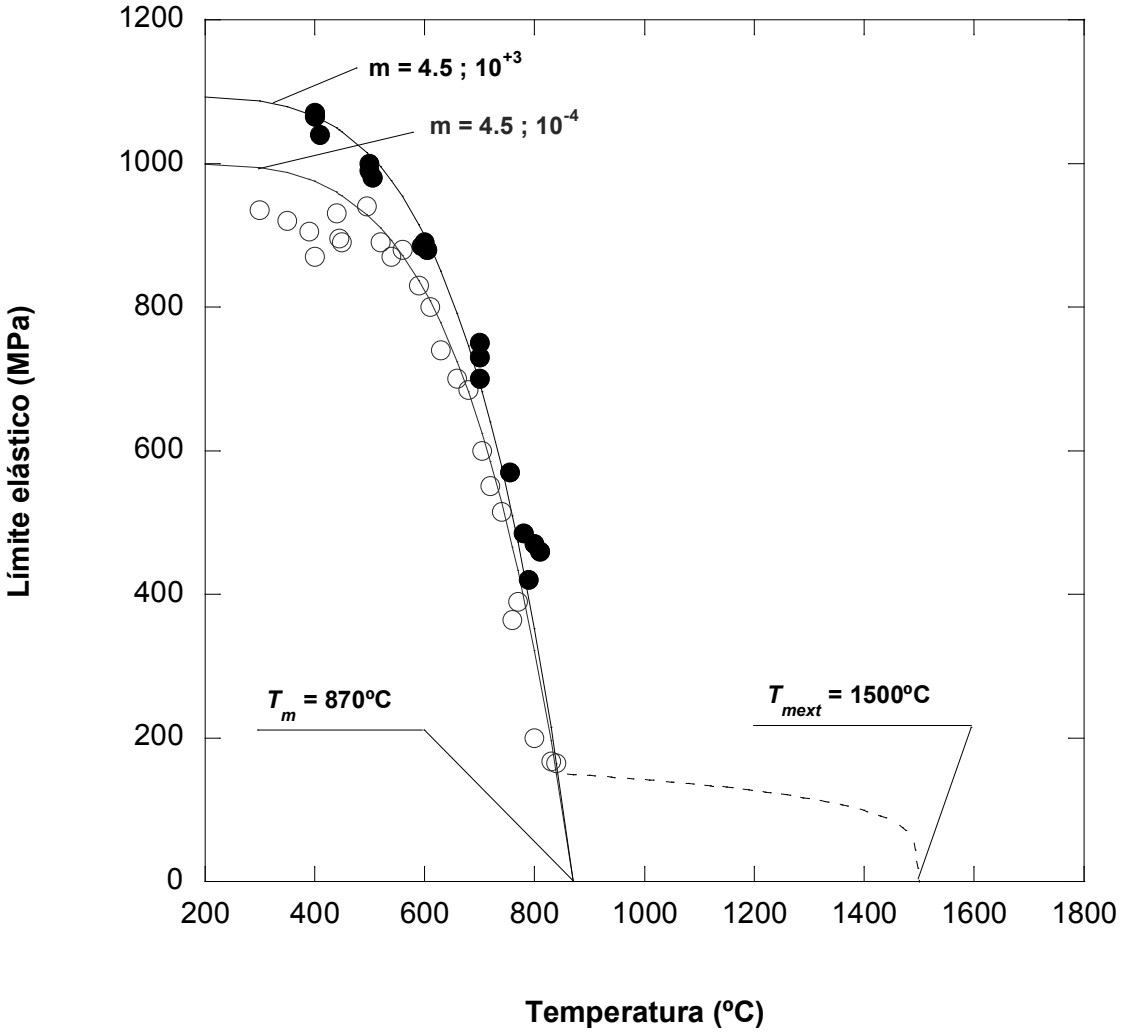

Modification of JC model: Melt extended temperature (JCT)

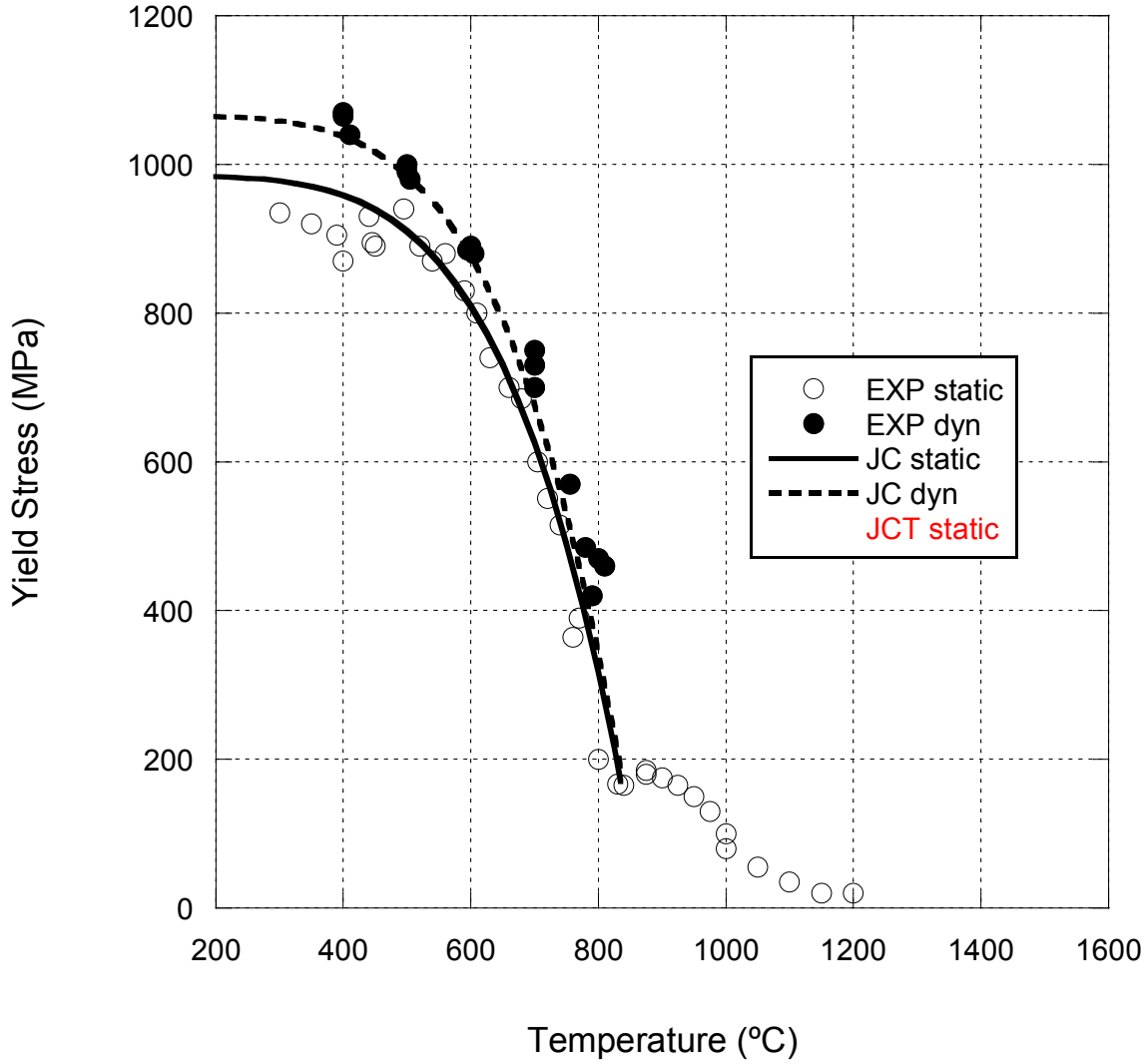

Modification of JC model: Melt extended temperature (JCT)

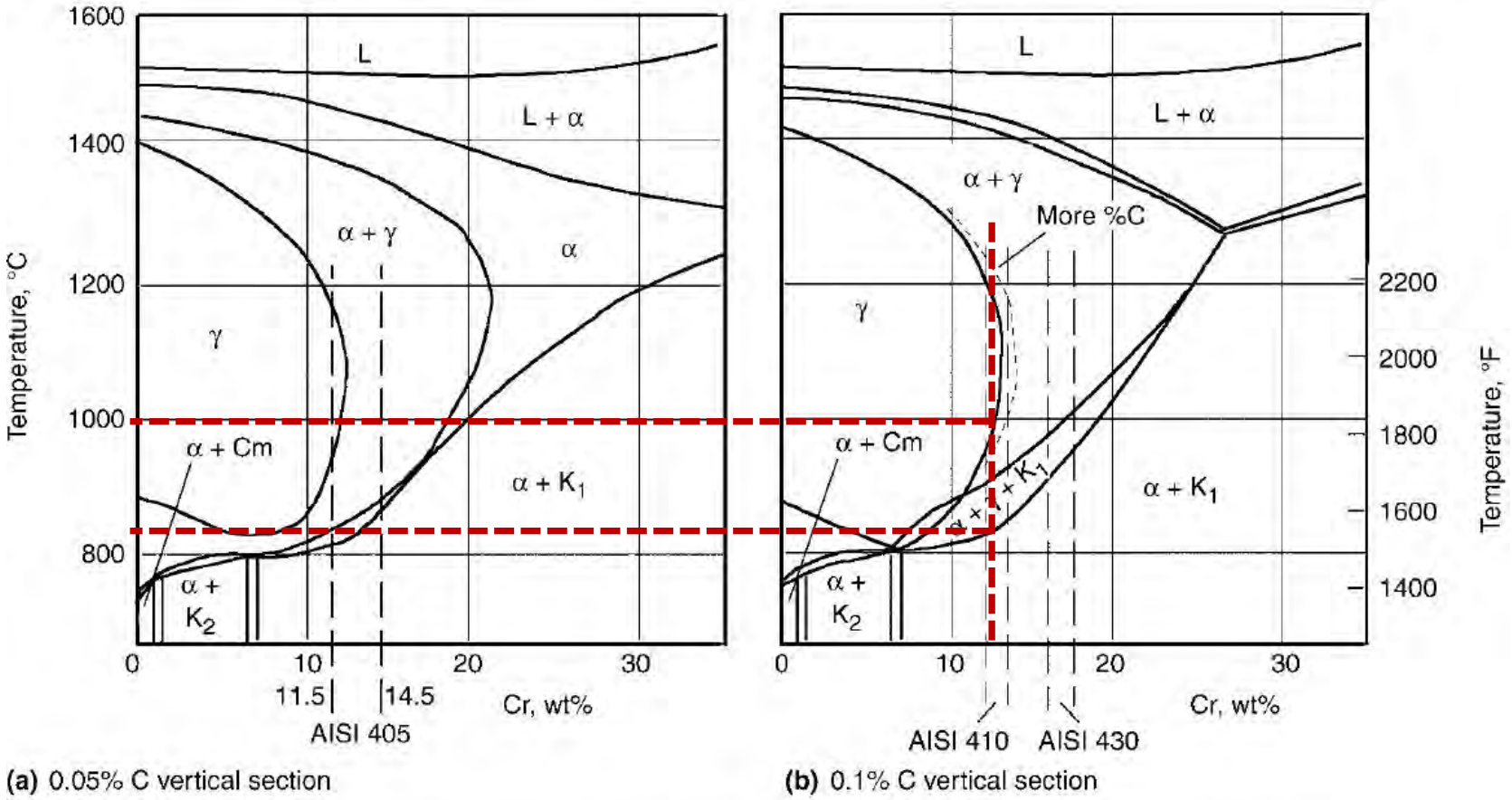

Fig. 13.4 Chromium-iron vertical sections of Cr-Fe-C ternary phase diagram at wt%C values of (a) 0.05 and (b) 0.1. Source: Ref 13.5, p 9-6. Copyright: 1958 Verlag Stahleisen GmbH, Düsseldorf, Germany

Modification of JC model: Melt extended temperature (JCT)

- Se propone la reformulación de la relación constitutiva:

$$\sigma_{eq}^{JC} = \left[A + B\bar{\varepsilon}_p^{n} \right]\left[1 + C \ln \dot{\bar{\varepsilon}}_p^{*} \right]\left[1 - T^{*m} \right]$$

$$\sigma_{eq}^{JCT} = \begin{cases} \sigma_{eq}^{JC} & T_0 \le T < T_{ext} \\ \sigma_{eq\ (T=T_{ext})}^{JC} \cdot T_{ext}^{*} & T_{ext} \le T \le T_{mext} \end{cases} \qquad T_{ext}^{*} = \left(1 - \frac{T - T_{ext}}{T_{mext} - T_{ext}} \right)^{m_{ext}}$$

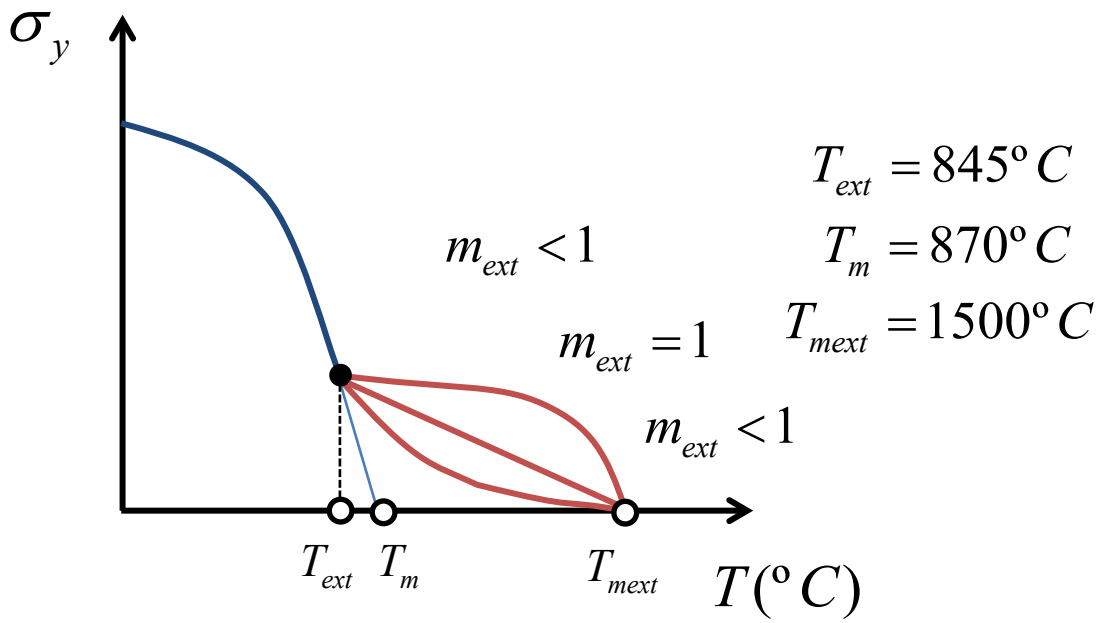

Contents

Numerical Simulations: Results using JCT model

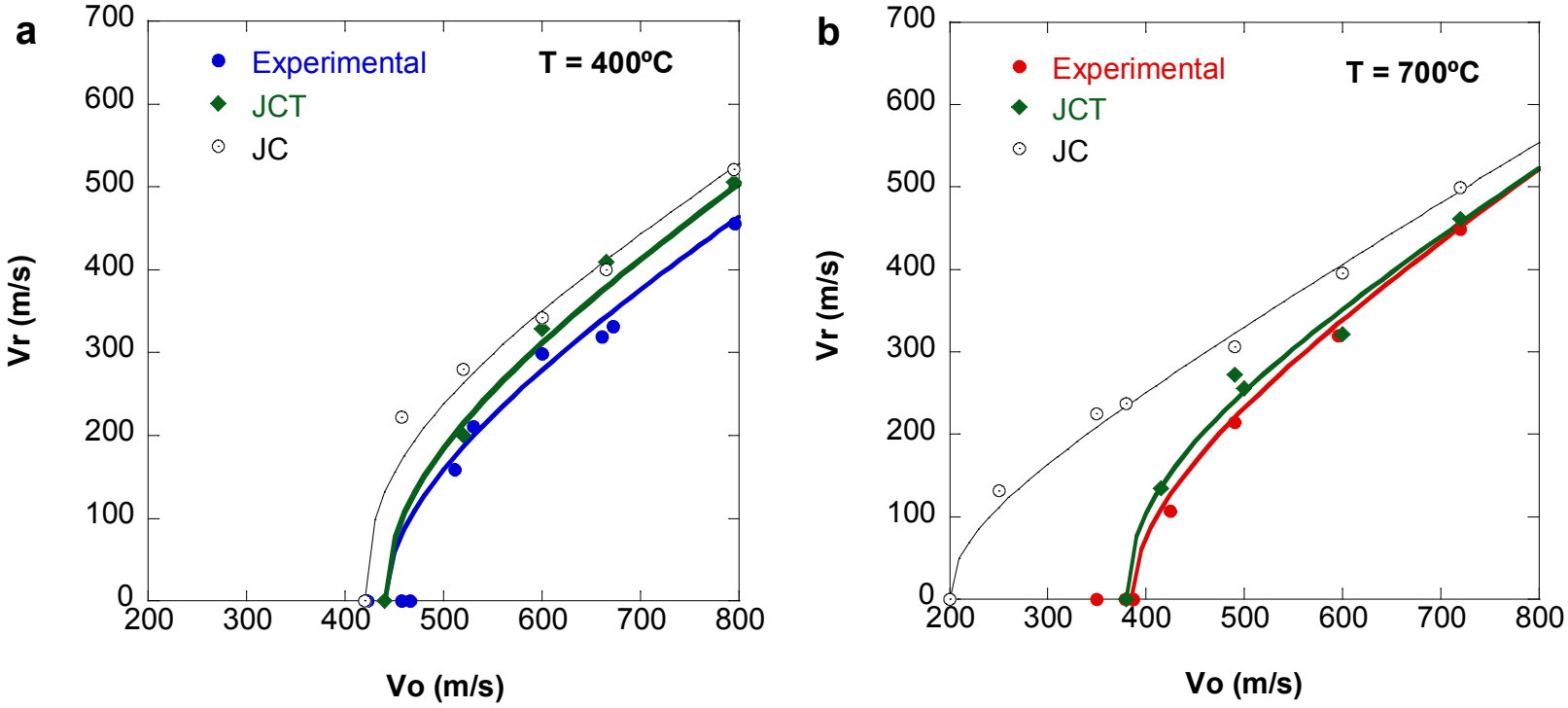

Numerical Simulations: Results using JCT model

Temperature 400ºC

Temperature 700ºC

$v_0 = 600\,m/s$

$v_0 = 600\,m/s$

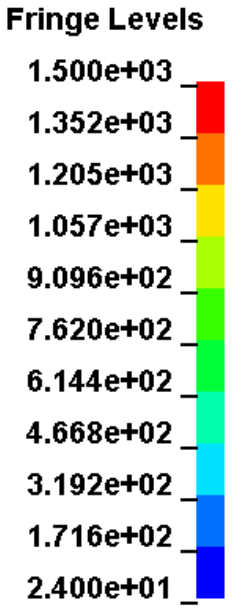

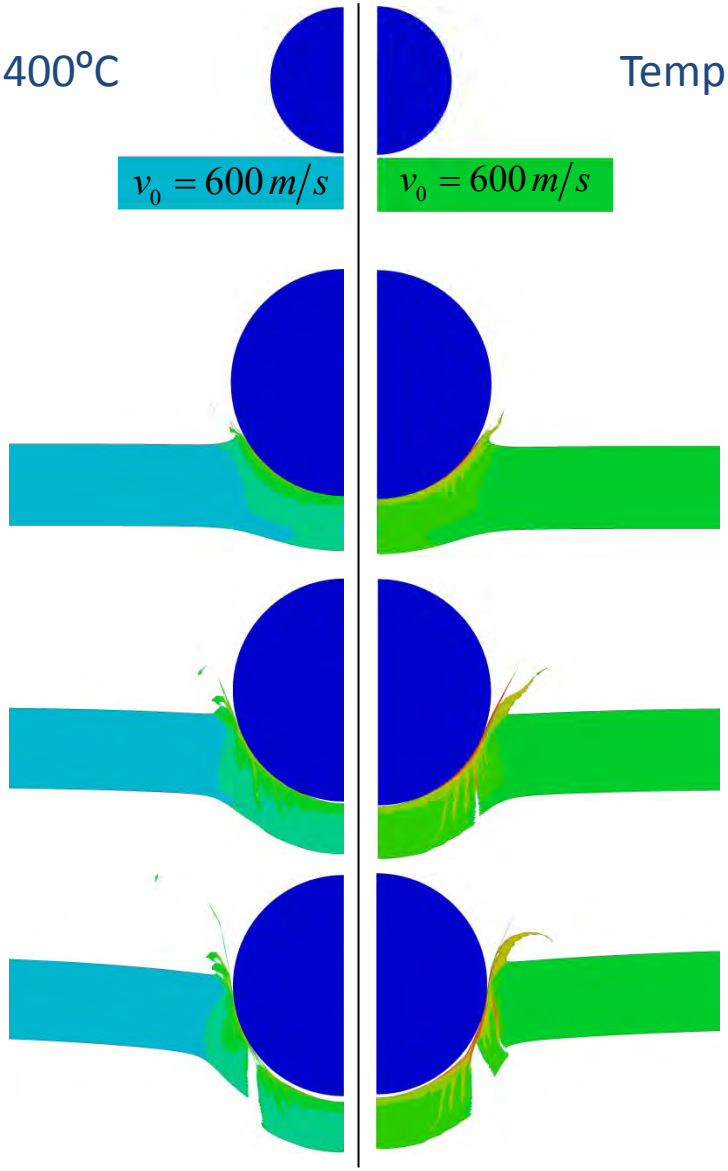

$t = 2.4\,\mu s$

$t = 5.2\,\mu s$

$t = 9.0\,\mu s$

Numerical Simulations: Results using JCT model

700ºC
600m/s

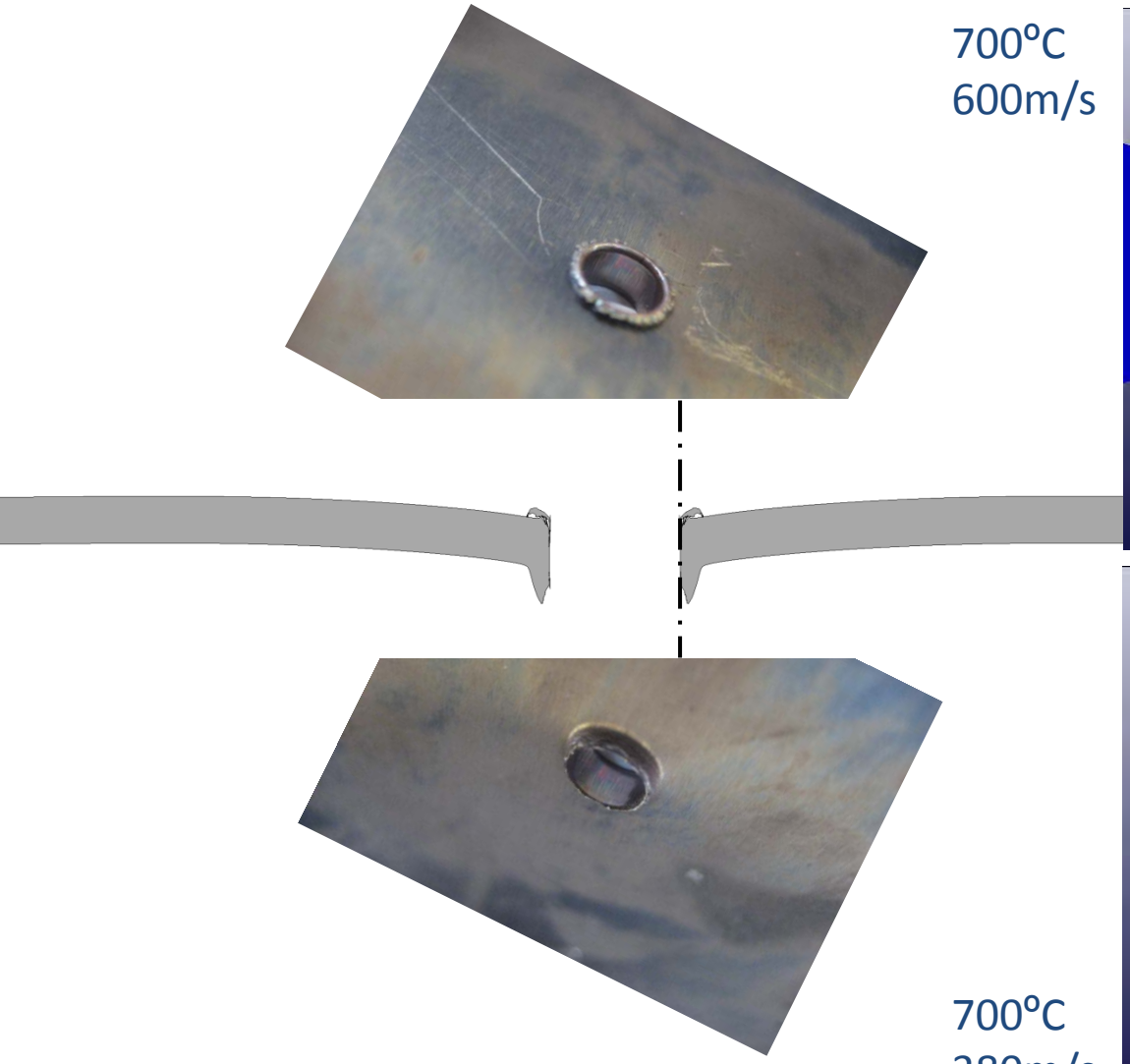

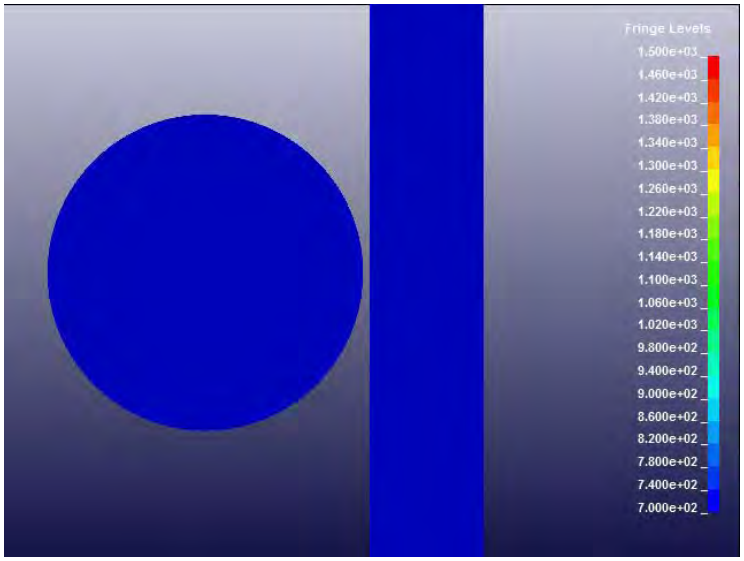

700ºC
380m/s

Contents

Conclusions

- The JC softening model is not capable to reproduce the experimental results of ballistic tests when plates are at high temperature for this material.
- A new model, as a modification of the JC model, is proposed using a melt extended temperature. JCT.
- The model has been implemented in LS-DYNA code.
- The simulations show that the proposed model JCT is able to reproduce the ballistic behavior of the material studied.
- Current work of turbine engine containment is now possible using this model, and it is currently under investigation.

The authors would like to acknowledge ITP for its financial support.

Containment test

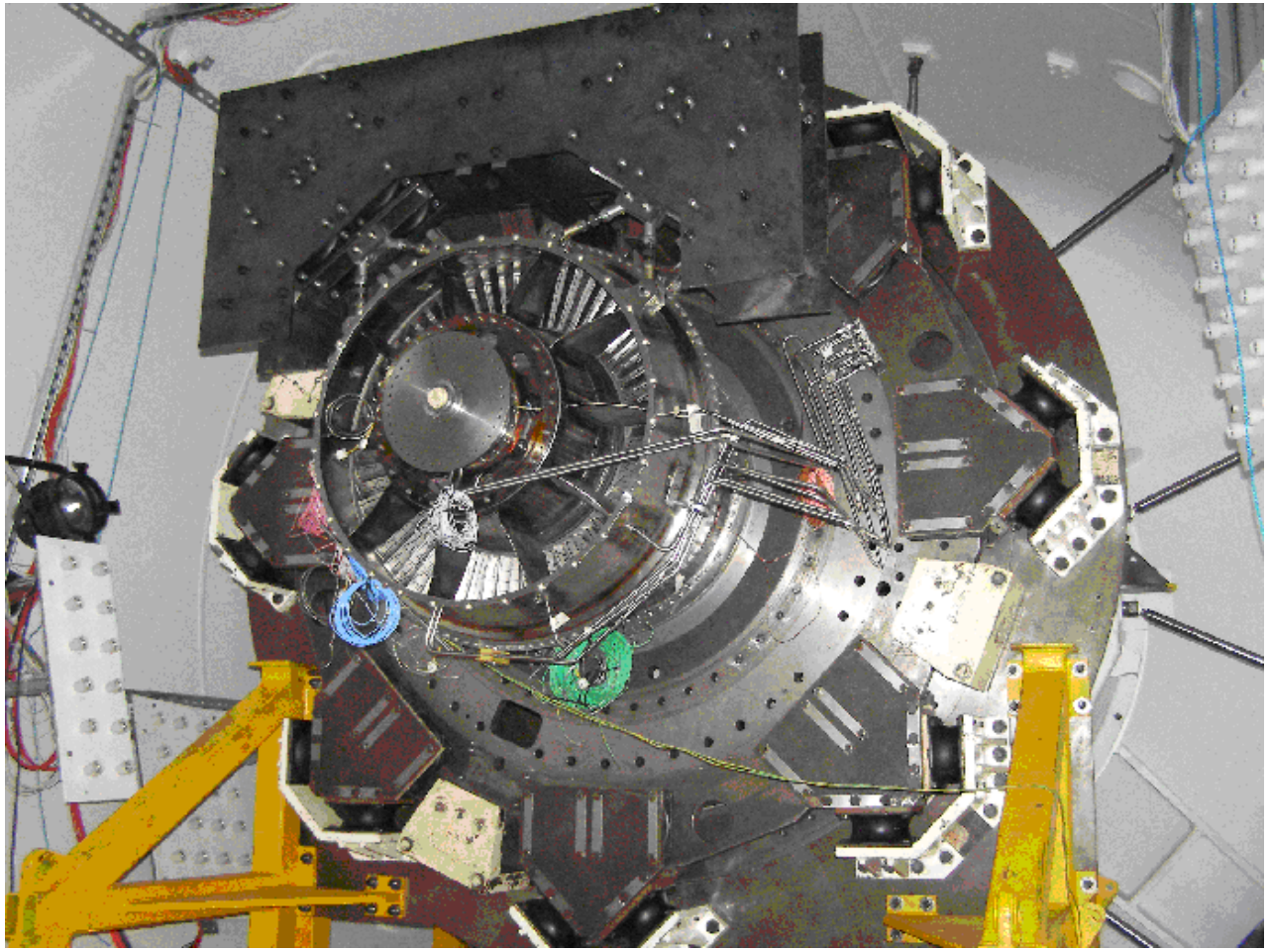

Containment test

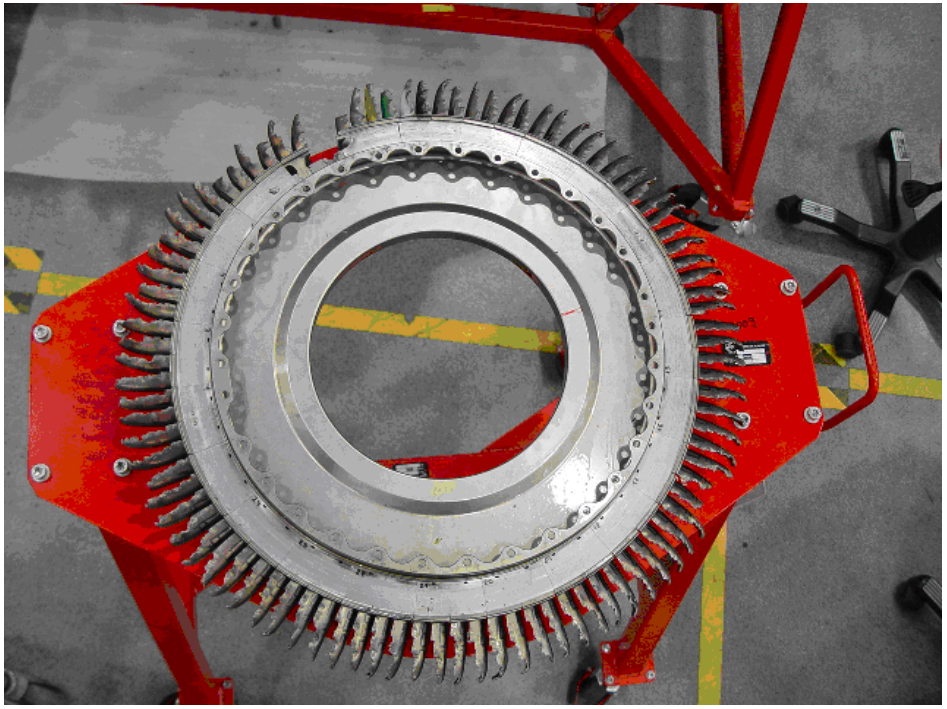

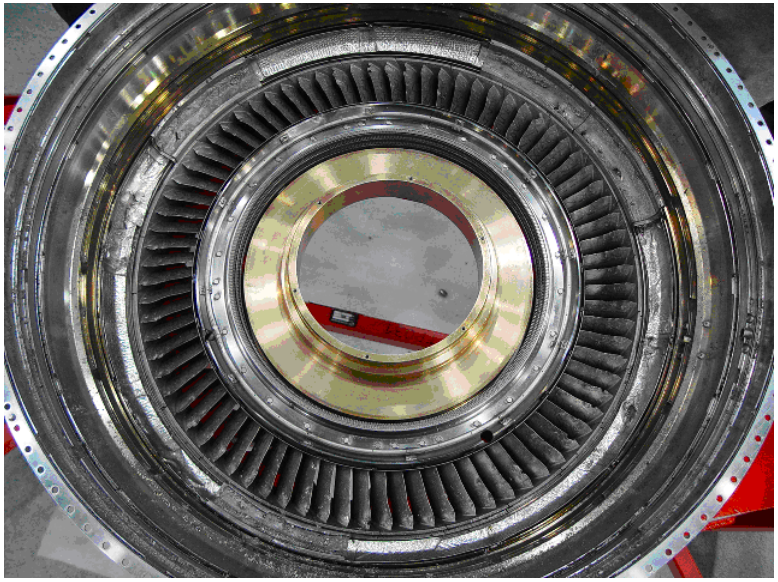

Containment test

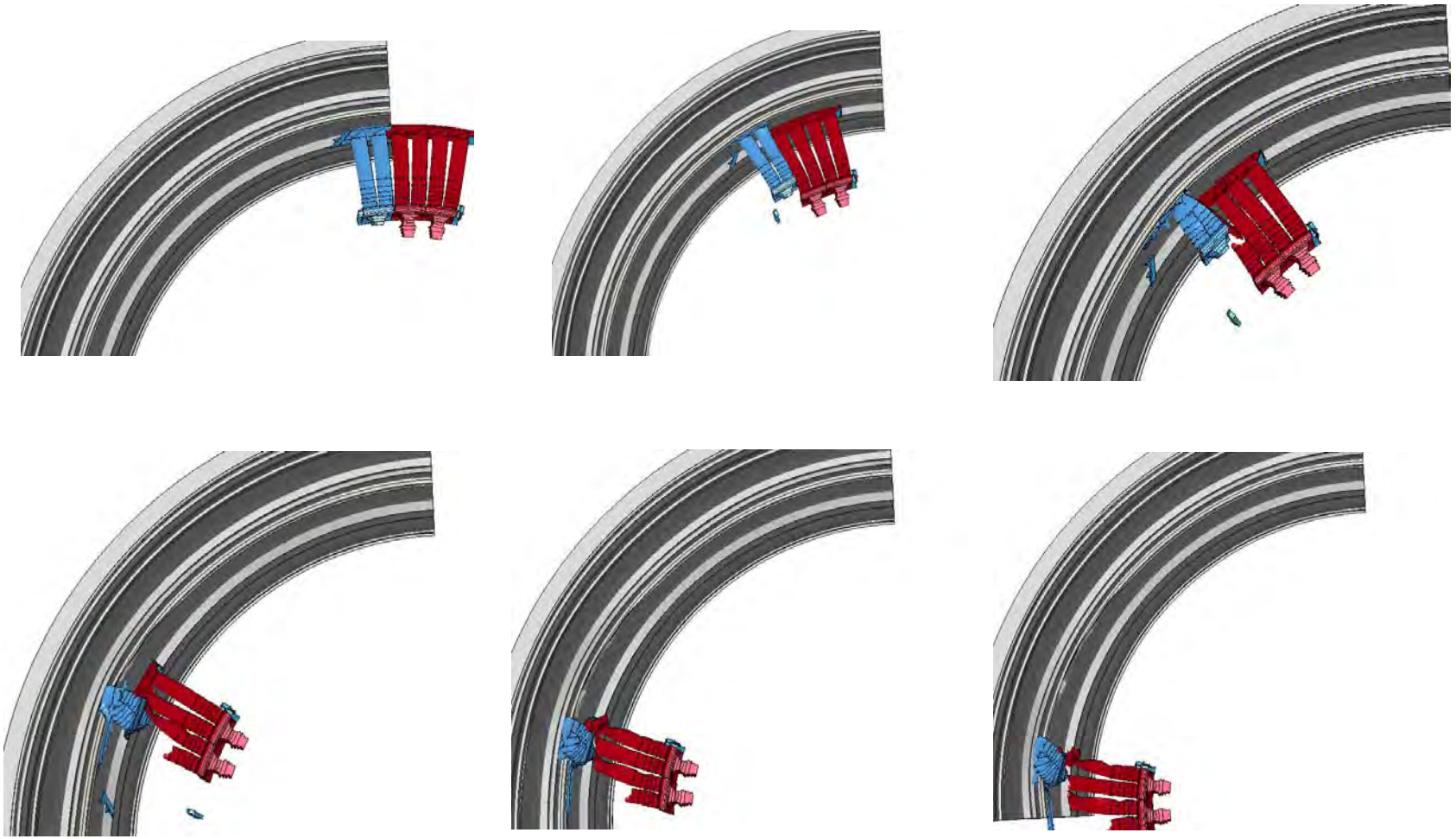

Containment test

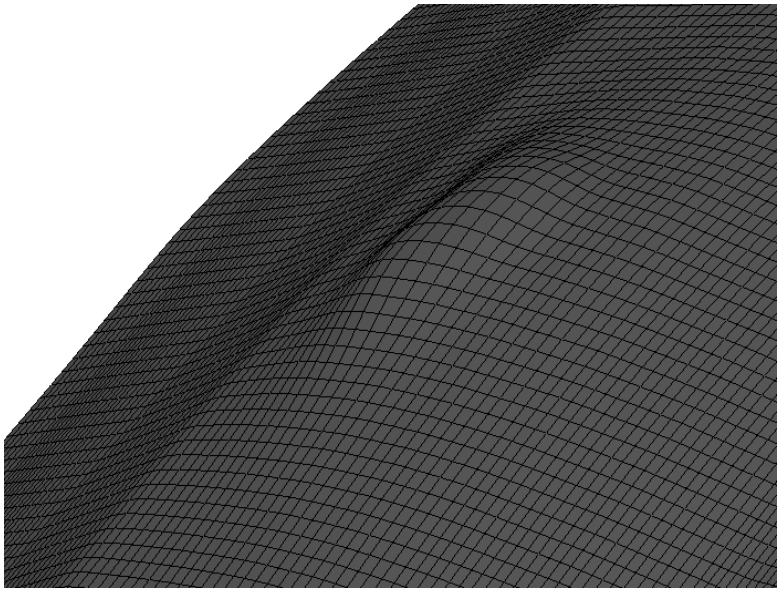

The 26th International Symposium on Ballistics
Miami, FL, 12-16 September, 2011

The Penetration Process of Jets And Long Rods in Water

D. Yaziv, M. Mayseless, Z. Cooper, Y. Reifen, E. Hirsch

1. Penetration of Jets in Water

Shaped Charge Type “R”

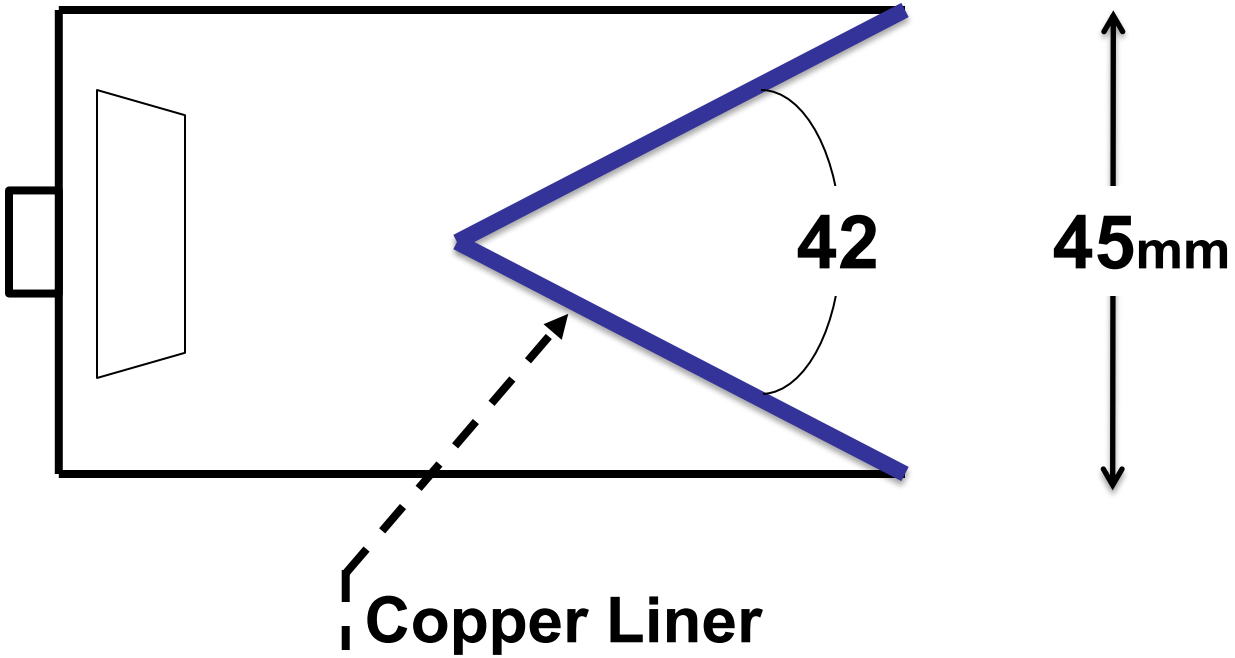

Liner Cone Angle: **42**
Diameter (D): **45 mm**
Standard Standoff: **1.5 D**

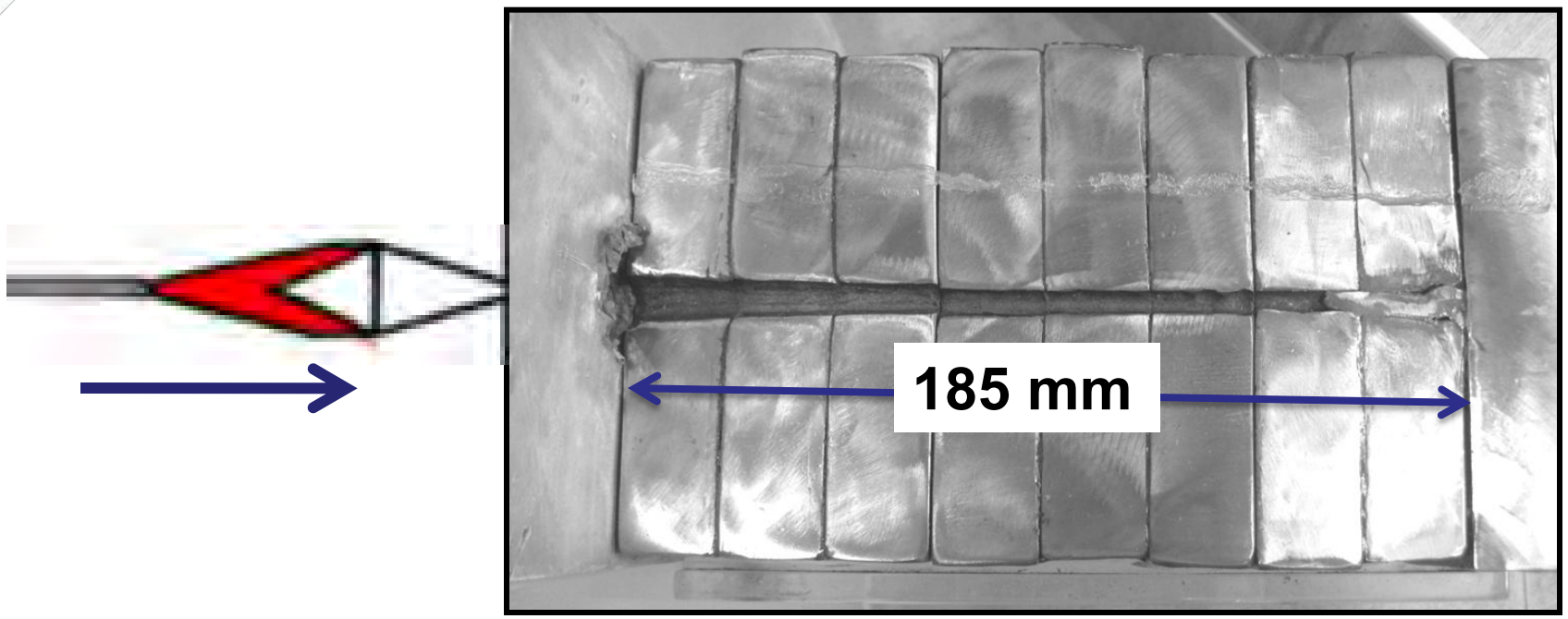

Baseline penetration in RHA : **185 mm**

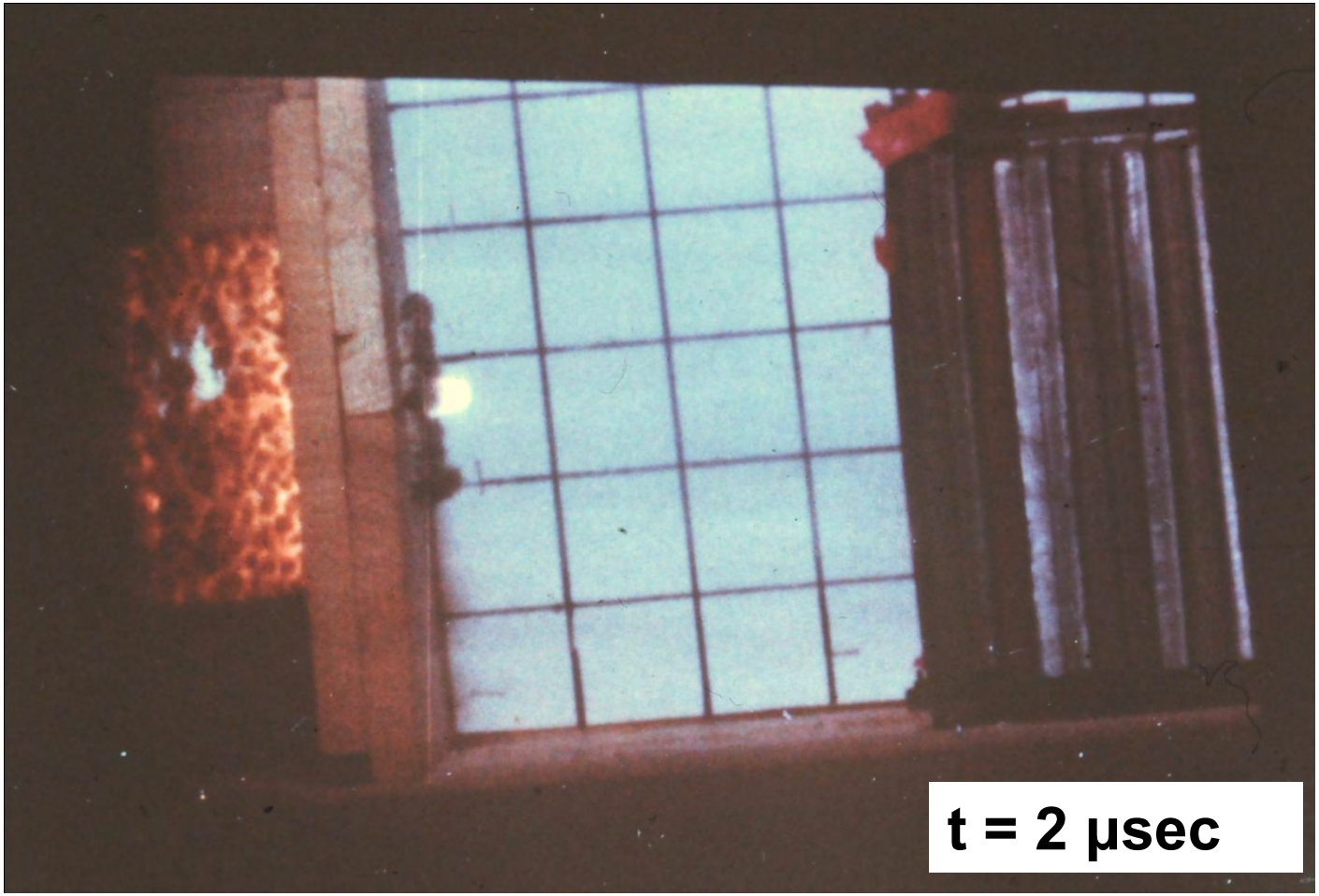
t = 2 µsec

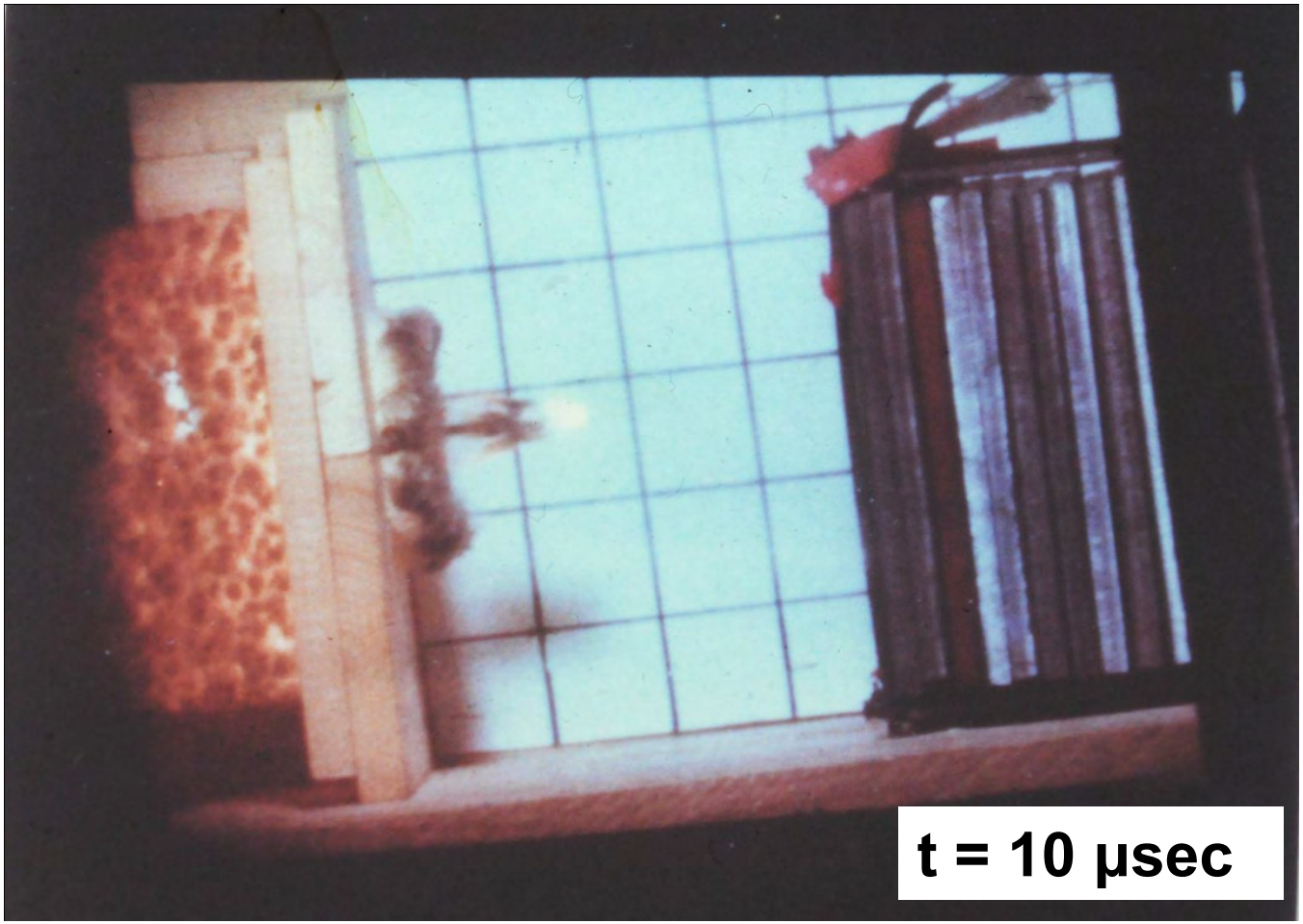
t = 10 µsec

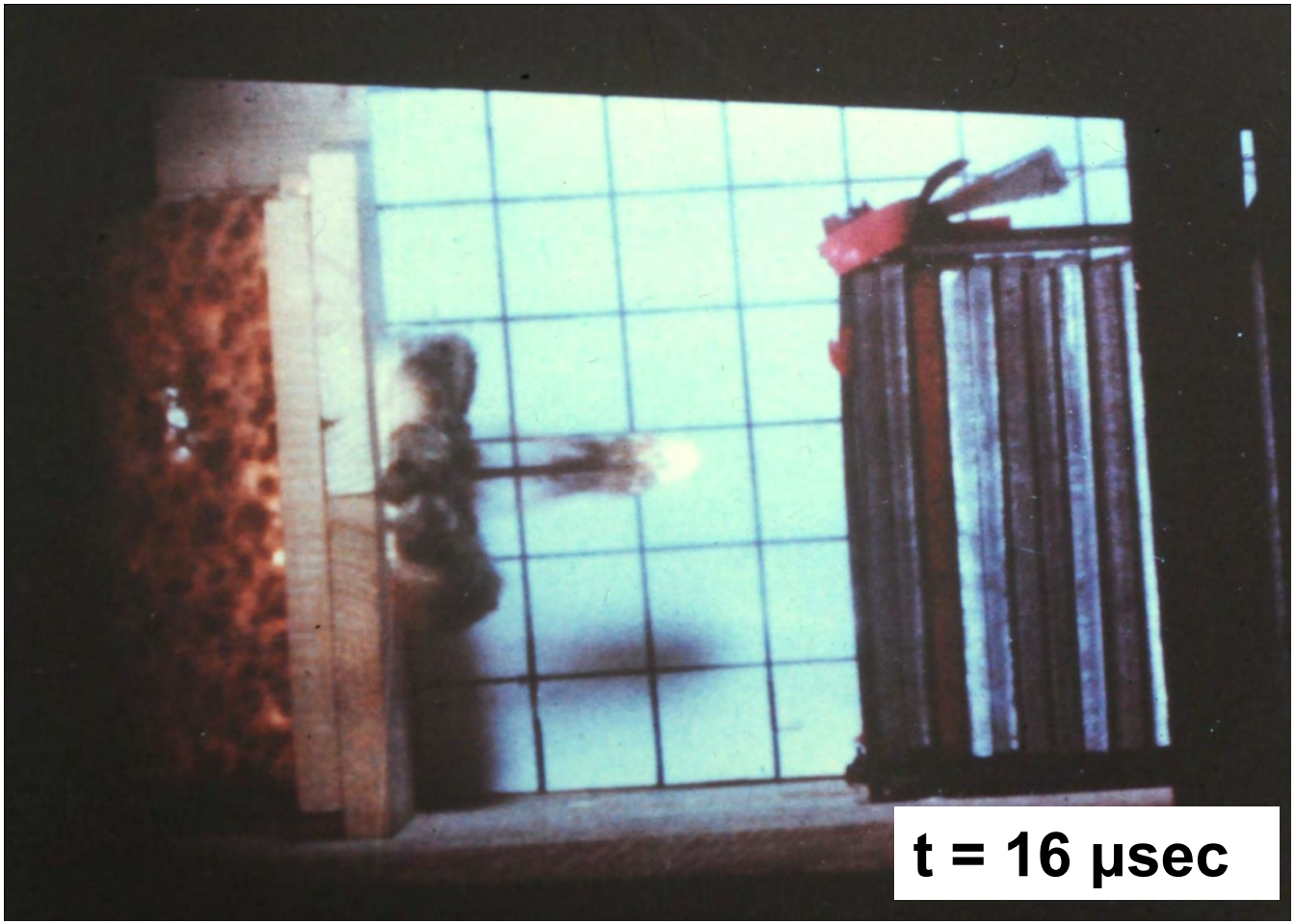
t = 16 µsec

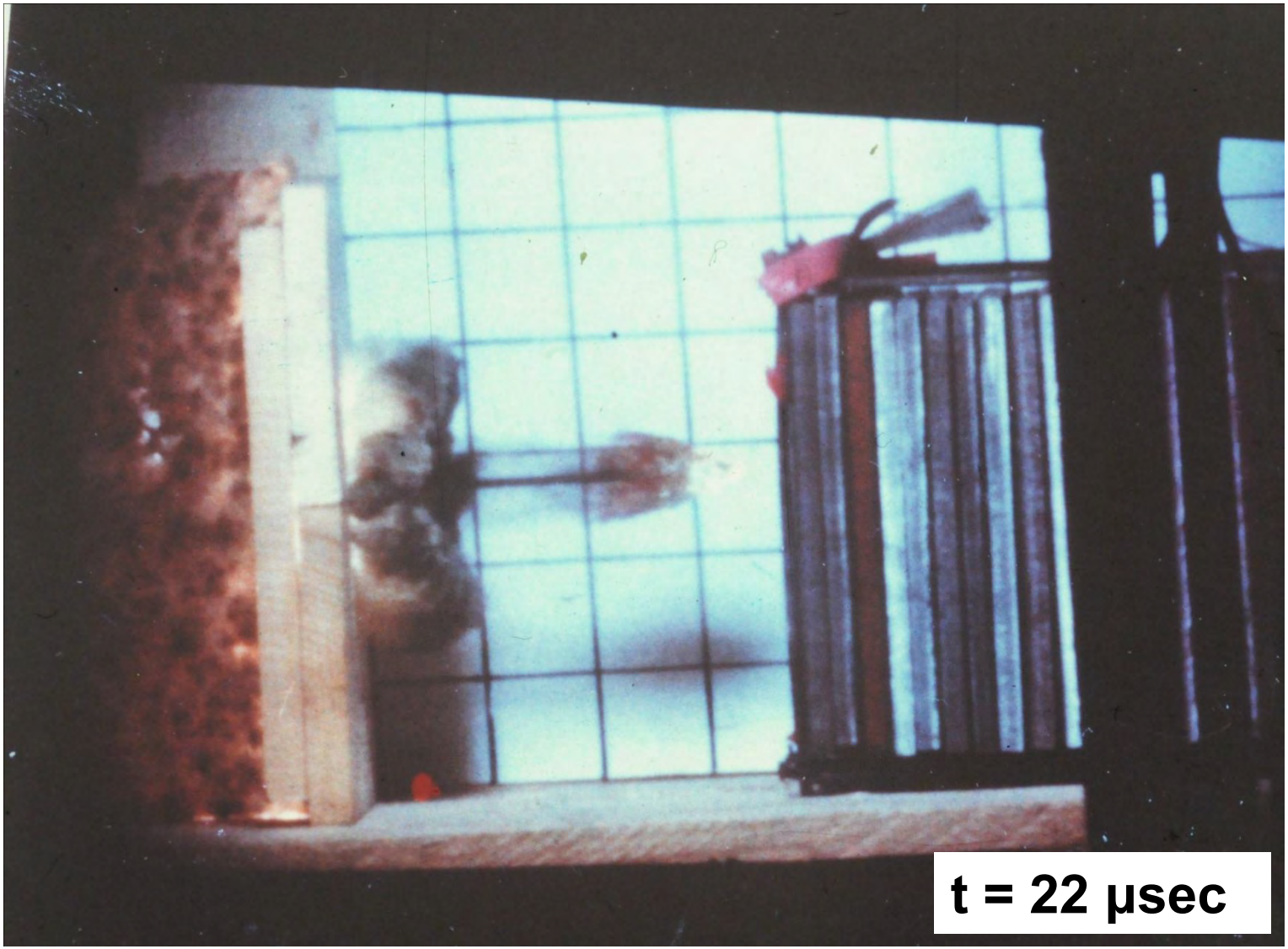
t = 22 µsec

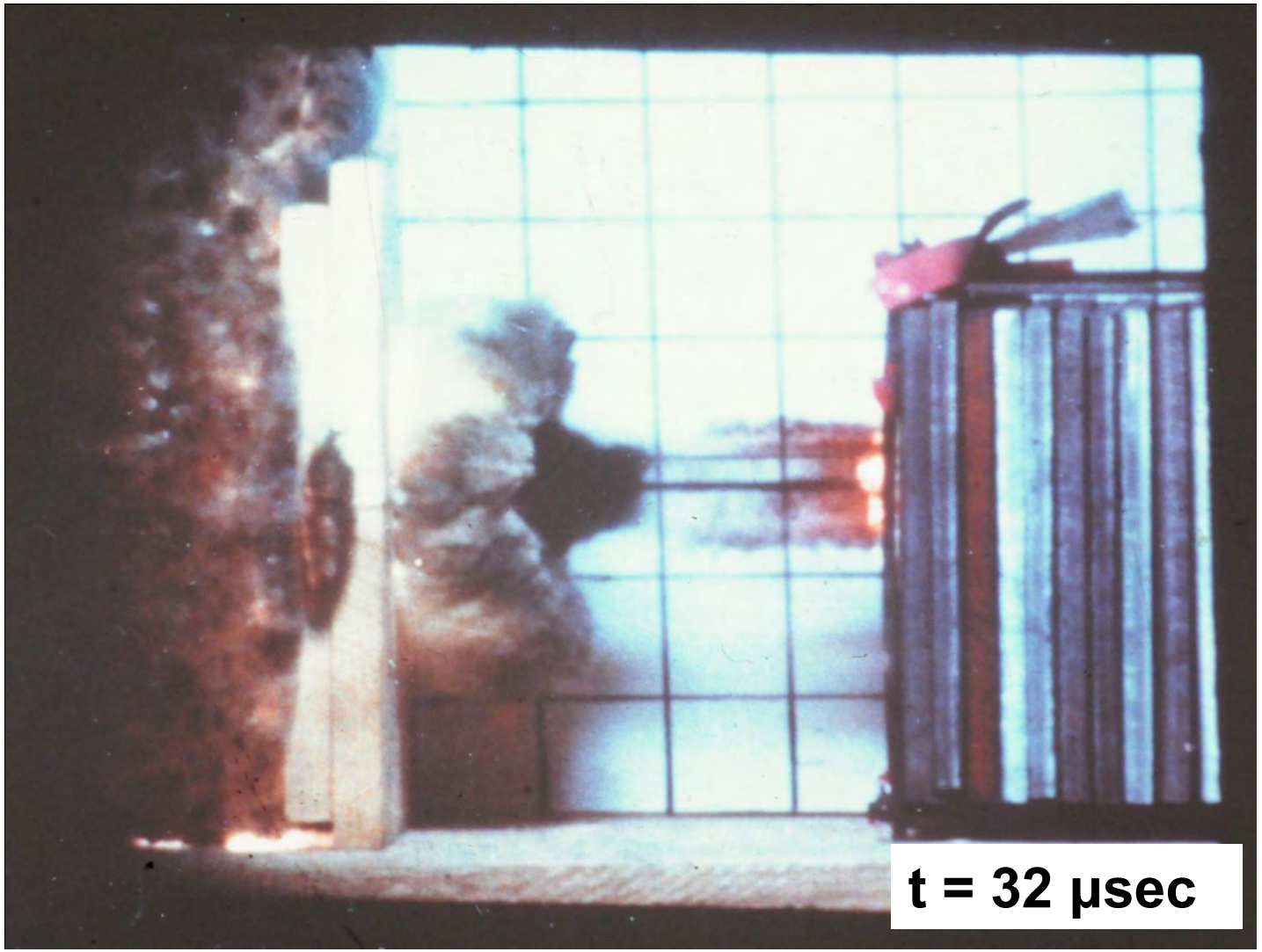
t = 32 µsec




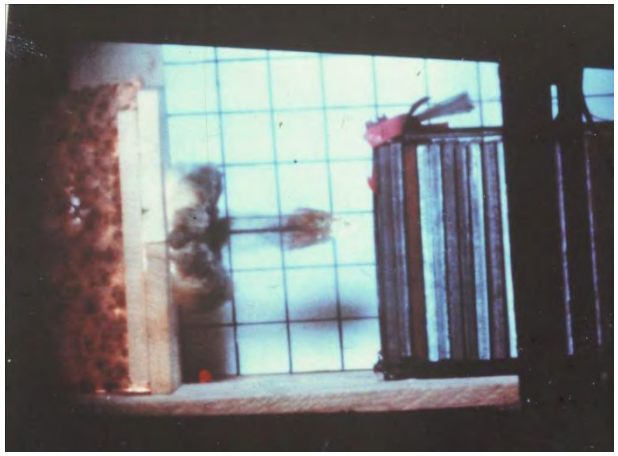


Jet tip velocity = **7,250 m/sec**

Diameter = **1.5 mm**

Experimental Set-up

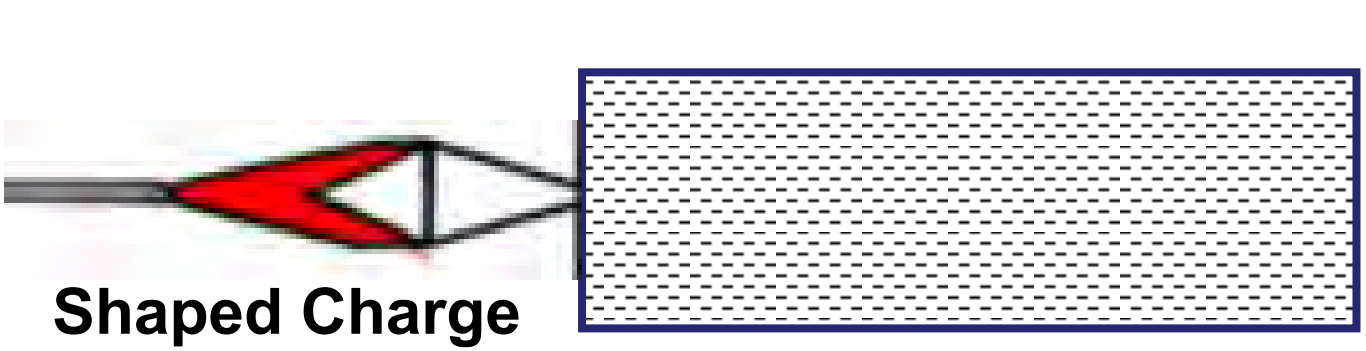

Experimental Set-up

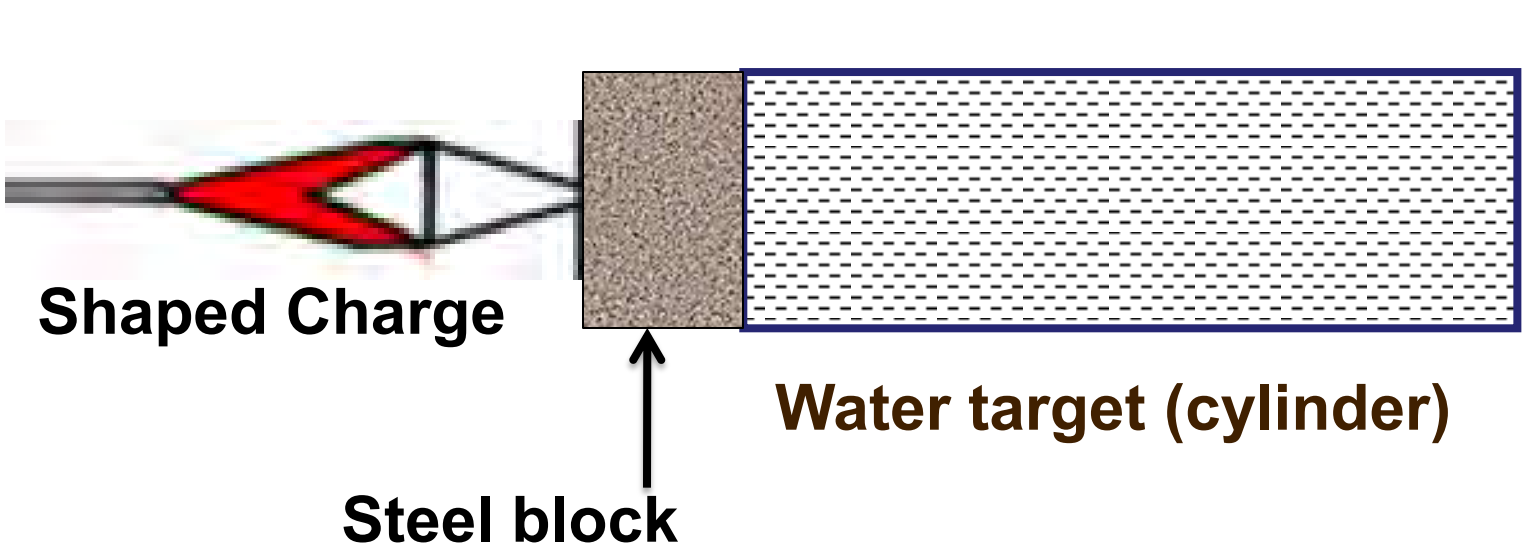

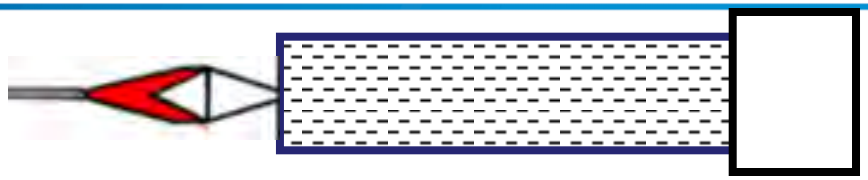

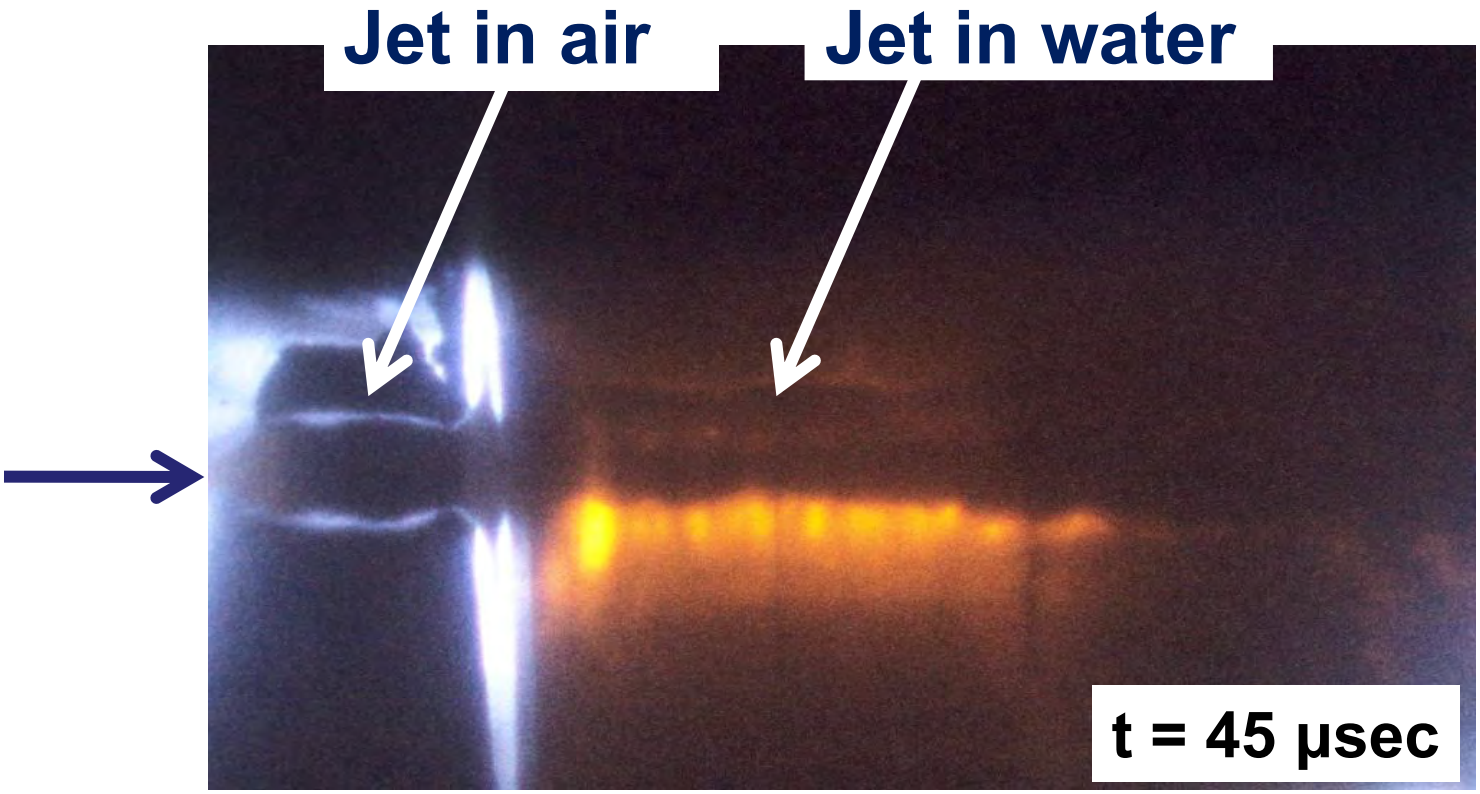

Jet tip velocity

In air=**7,250**m/sec; In water$_{\text{at 250mm}}$ **5,500**m/sec

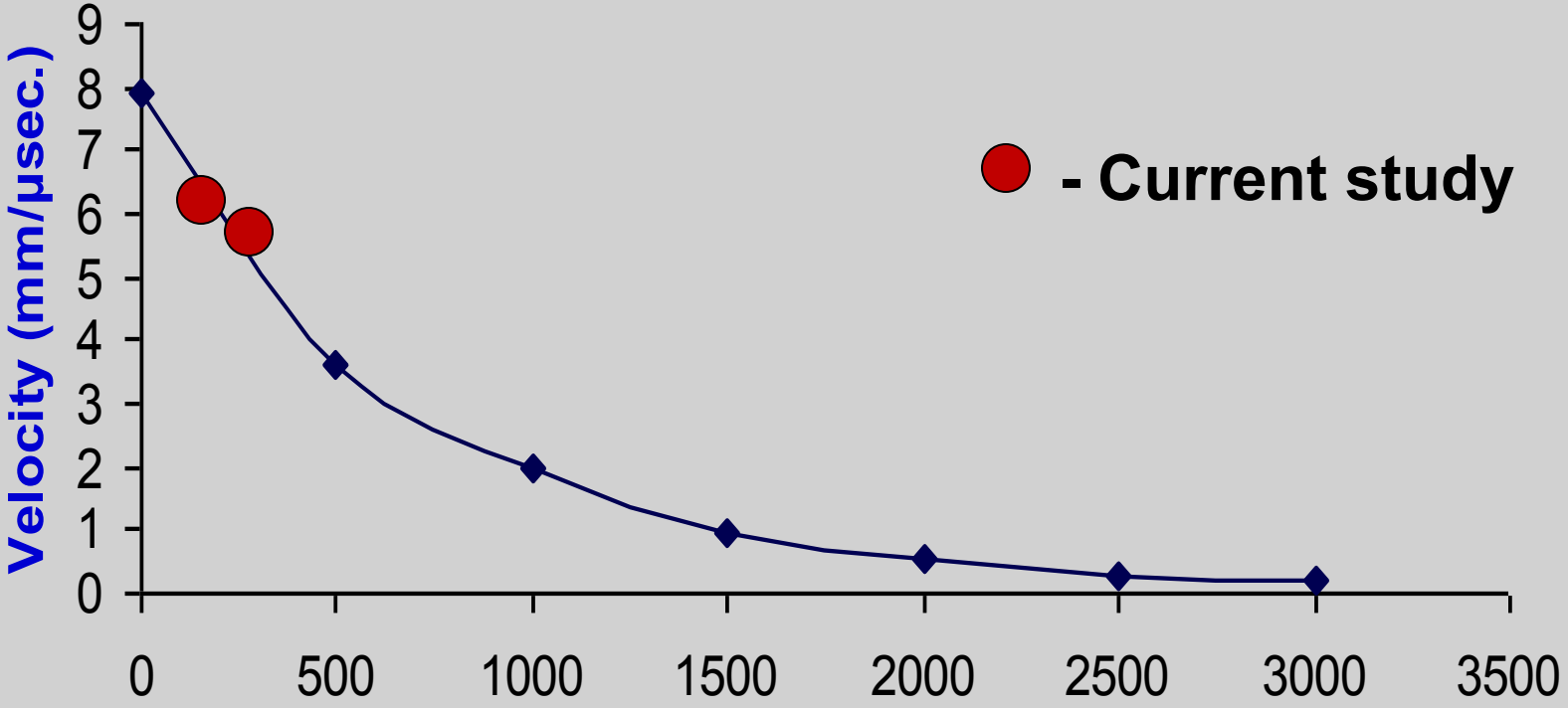

D.R. Saroha et al, 24th Int. Sym. on Ballistics (2008)

Shaped Charge

Steel block

Steel cylinder filled with Water

Steel plates

Penetration Capability in water

Measured

P_{RHA} = 185mm

P_{water} = 680mm

} = P_{water}/P_{RHA} = 3.6

Hydrodynamic penetration

$P_1/P_2 = \sqrt{(\rho_2/\rho_1)}$

$P_{Water}/P_{RHA} = \sqrt{(\rho_{RHA}/\rho_{Water})} = 2.8$

P_{Water} = 520 mm

2. Penetration of Long Rods in Water

Experimental Set-up

Long rod

Tungsten Alloy
L = 100 mm
L/D = 10
V = 1,430 – 1,475 m/sec

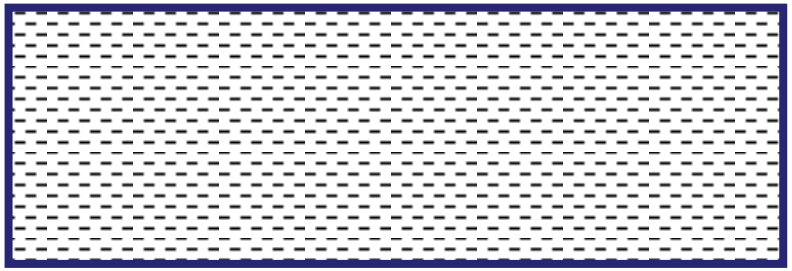

Water target (cylinder)

DOP

Plates

Long rod

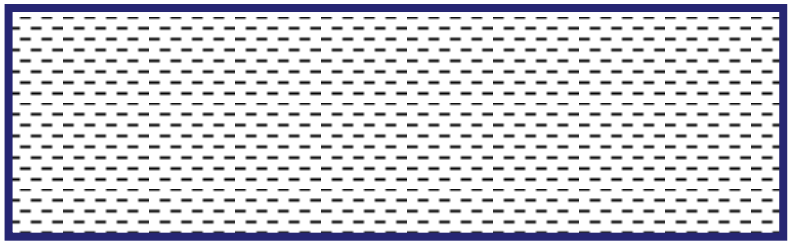

DOP

Plates

Water target (cylinder)

Obliquity = 90 , 60 , 45

C. E.J Anderson, J. S. Wilbeck, et al., *Long-Rod Penetration into Highly Oblique, Water-Filled Targets* Int. J. Impact Eng. (1998)

Shot DM3

Exit Yaw: 4.5

Shot DM6

Exit Yaw: 6.5

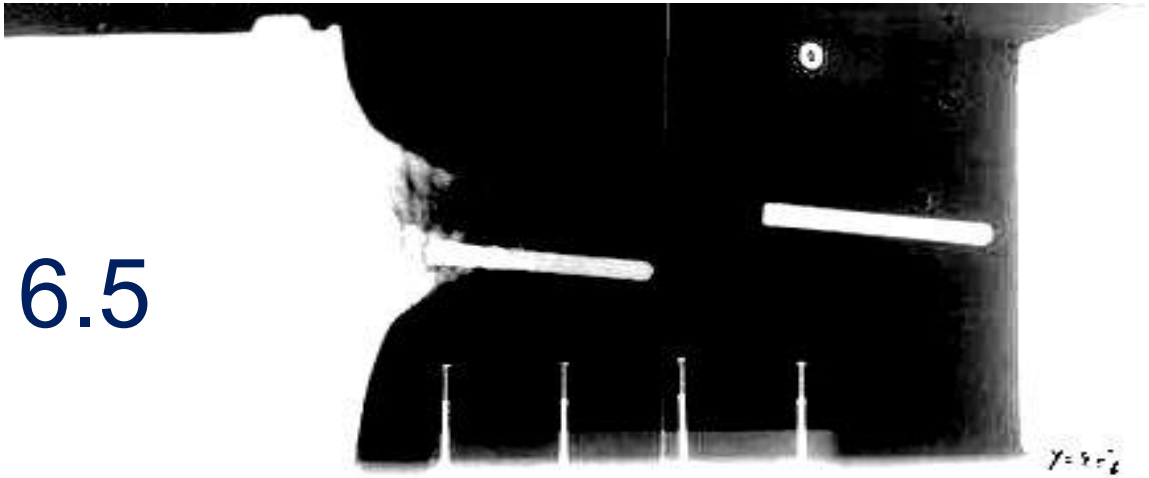

3. Calculations and Analysis

The penetration process in water

can be divided into two phases:

1st Phase:

The classical hydrodynamic penetration

2nd phase:

The inertia of the water influence on the final penetration

.....

C.P. Woidneck "*Rod Penetration in Liquids*", 9th Int. Sym. Ball.

The SCAN Model

Based on the classical hydrodynamic jet penetration theory with Tate's correction

.....

E. Hirsch, D. Goodlin, T.R. Sharon, **SCAN**, "*Shaped Charge Analyzer Model. Computer Program User Manual"*

No steel, 50 mm and 100 mm steel in front of the water

RAFAEL

Ben-Gurion University of the Negev

SCAN predictions

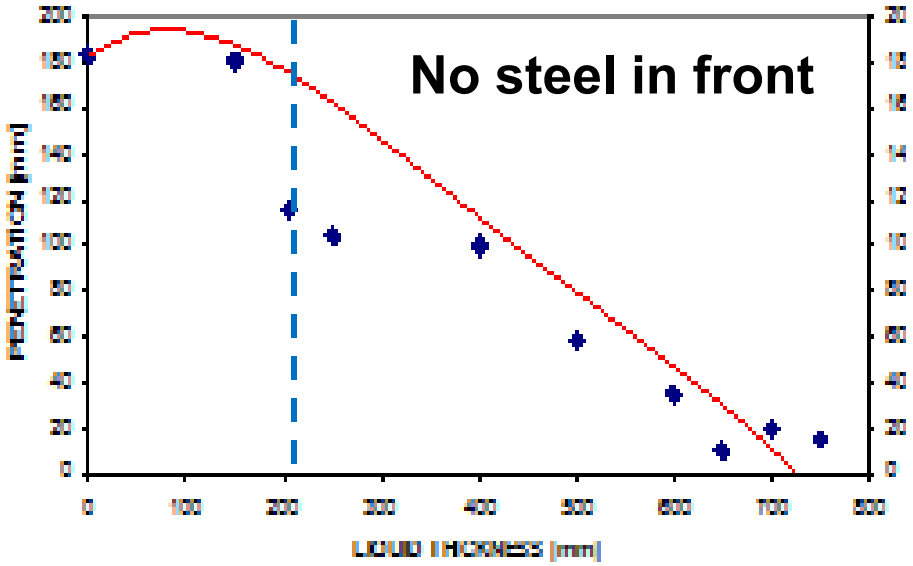

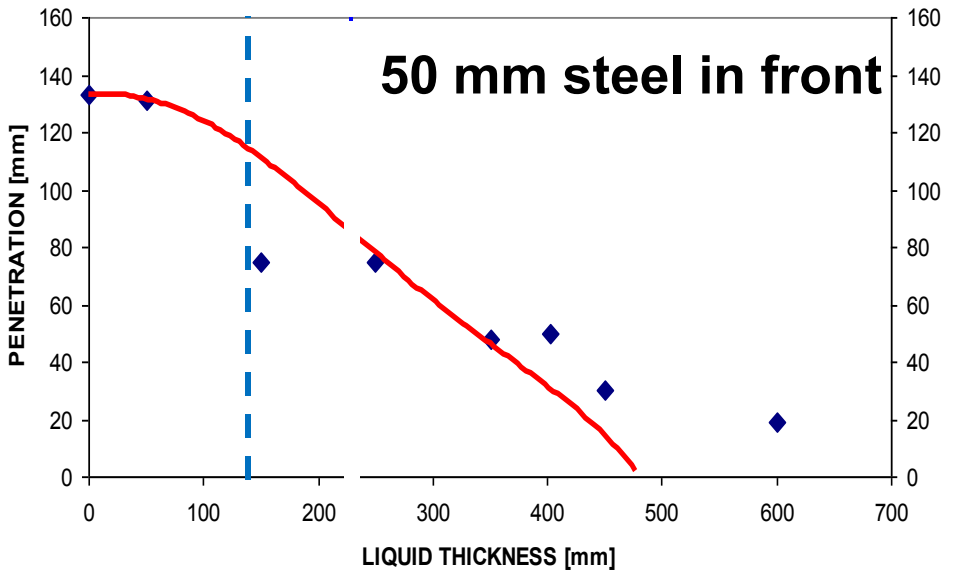

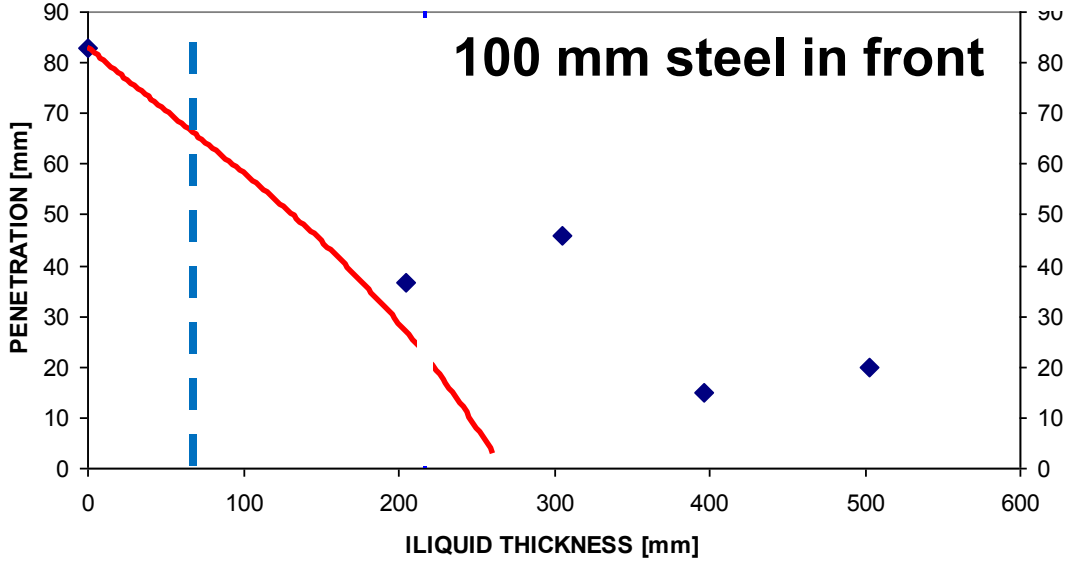

2nd Phase

The Autodyne 2D hydrocode was employed

ASSUMPTIONS:

- The jet was simulated by a rod at a speed of 4,000 m/sec, representing the central part of the jet after particulation
- The rod is eroded during the penetration similarly to the jet
- The water has no strength
- The diameter of the water cylinder is wide enough

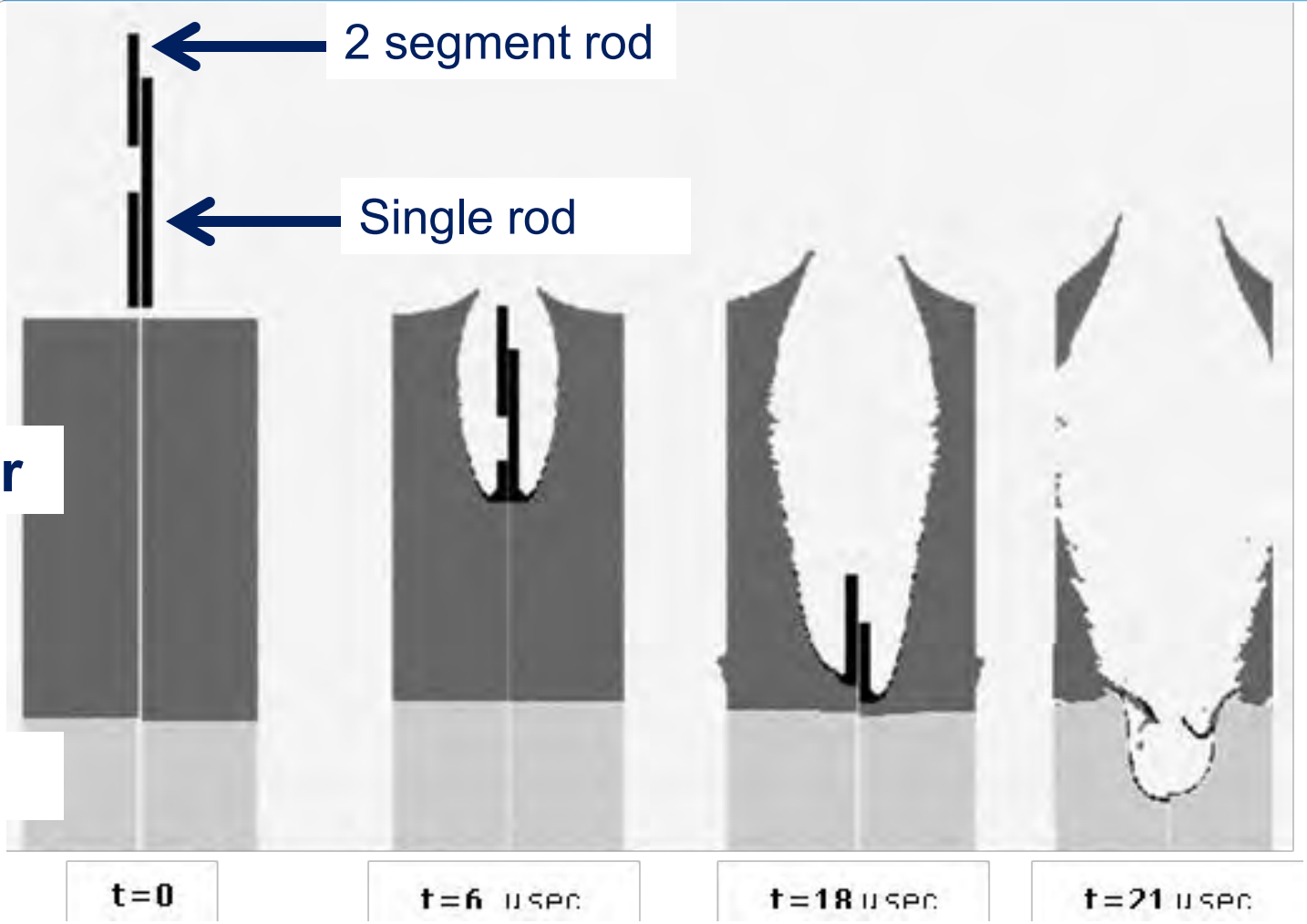

Jet - 2nd Phase

Rod: Cupper; L = 20 mm; V = 4,000 m/sec

DOP = 8 mm (single); 10 mm (segmented)

CONCLUSIONS:

1. The total penetration capability of a jet is larger when the jet is particulated
2. The residual DOPs in steel are greater than predicted by the ideal hydrodynamic theory by approximately 25%

2. Penetration of Long Rods in Water - Analytical Model

The yaw angles at the exit of the water targets were predicted using an analytical model

ASSUMPTIONS:

1. Rigid projectile
2. Incompressible fluid with shear strength
3. The path of the projectile is integrated numerically

Z. Cooper, M. Mayseless, Y. Reifen, D. Yaziv, "Deflecting and Rotating Rigid Projectiles Hitting Plate Edge" – **Poster Session 12033**

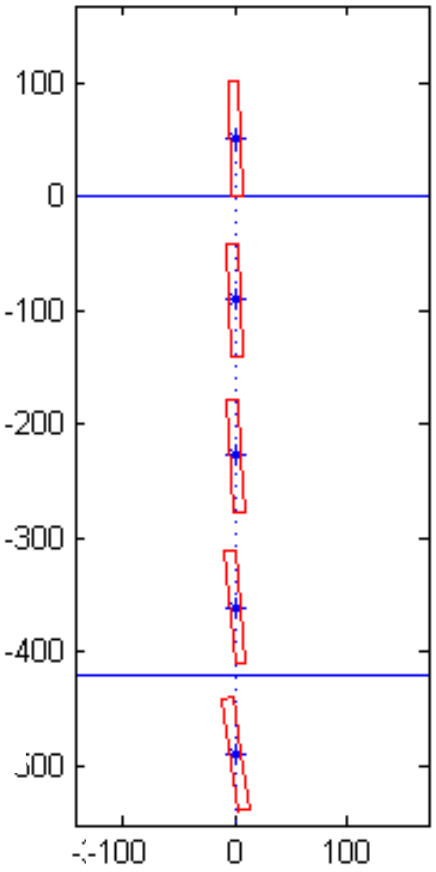

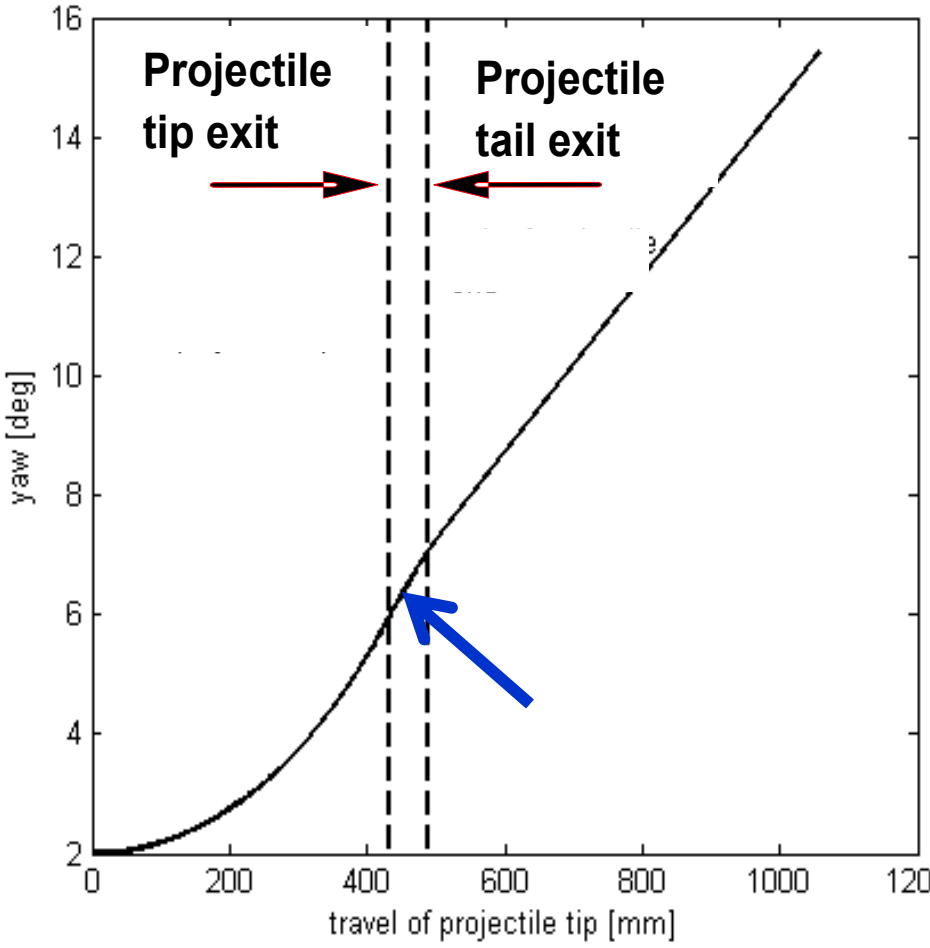

Rod: Tungsten Alloy; L = 100 mm; V = 1,475m/sec;
Water length: 420 mm

Roecker – Ricchiazzi (R & R) Model

$$yaw\ \ s\ \ = yaw\big|_{s=0} \exp\left(\frac{b}{R}s\right)$$

R - *Radius*

s - *Distance (normalized by R)*

b - *Constant related to the turning moment acting on the projectile.*

E.T. Roecker and A.J. Ricchiazzi, "Stability of Penetrators in Dense Fluids", Int. J. Engng. Sci, Vol 16

Rigid Projectile penetrating into water

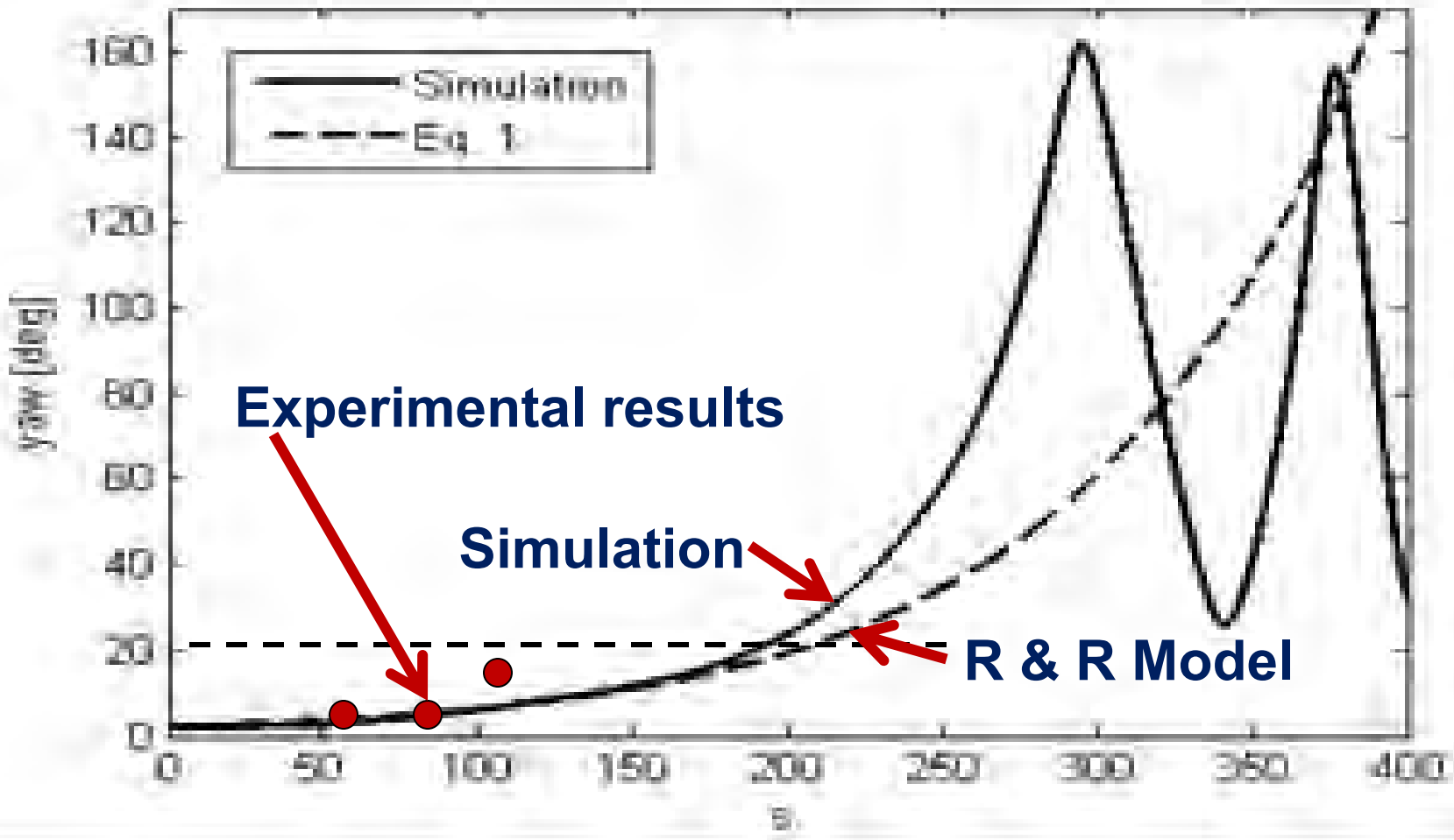

Conclusions

Jet Penetration in Water

- Two major phases: a hydrodynamic phase followed by an inertial phase
- The penetration capability of a jet in water is larger than predicted by the ideal hydrodynamic theory
- The total penetration capability of a jet is larger when the jet is particulated

Long Rods Penetration in Water.

- The Yaw angle is affected mainly by the DOP in water, the velocity and by the initial yaw
- The impact obliquity has an insignificant effect on the penetration, orientation and yaw of the rod in water

Both

- The differential weight efficiency of water is 0.70 to 0.75 (relative to RHA).

Glass as a Shaped Charge Liner Material

TECHNOLOGY DRIVEN. WARFIGHTER FOCUSED.

Dr. Ernest L. Baker
S. DeFisher, A. Daniels, T. Vuong and J. Pham
14 SEP 2011

Outline

- Introduction
- Improvised Shaped Charges
- Standard Demolition Shaped Charges
- Highly Ductile Glass Jets
- High Density Glass Investigations
- Observed Glass Jet Characteristics
- Conclusions

Introduction

- Glass: non-crystalline (amorphous) solid material typically known to be brittle under ambient conditions and often optically transparent
- Soda-lime glass: ~75% silica (SiO2), is the most common type of glass used for bottles and windows with a density of ~2.5 gm/cc
- Lead glass: lead replaces the calcium in the glass formulation, typically 18–40% weight lead oxide (PbO), with final densities between 3.1 and 7.2 gm/cc
- Glass as a shaped charge liner material is an old subject
  - Explosively loaded champagne bottles and other conical based bottles for demolition and special applications is very well known and commonly taught for military use. It is believed that such practice dated to a period of improvised munitions used early in World War II.
  - Glass liners have been used in a variety of shaped charge applications, including demolition munitions and as oil well perforators.

Introduction

- Bulk metallic glass has also been investigated as a shaped charge liner material
  - W.P. Walters, L.J. Kecskes and J.E. Pritchett, “Investigation of a Bulk Metallic Glass as a Shaped Charge Liner Material”, ARL-TR-3864, August 2006.
- The use of higher density glasses for jet studies has been more recently reported
  - K. Cowan and B. Bourne, “Oxide Glasses as Shaped Charge Liners”, Proceedings of the 21st International Symposium on Ballistics, Adelide, South Australia, 2004.
- The US Army ARDEC has undertaken considerable studies of glass shaped charge jet behavior

Improvised Shaped Charges

- Hand packing of bottles using moldable plastic explosives to form shaped charges is commonly taught
- Normally the bottle neck would be cut off to reduce the amount of high explosive required and to ease the hand packing operation
- 750 ml wine bottles were hand packed with Composition C-4 explosive
- Flash x-rays were taken of the jets
  - Extremely curved jets
  - Extreme particulate nature
- Steel penetration testing
  - 3.4 CDs (260mm) at a 5.5 CD (460mm) standoff

Improvised Shaped Charges

Jet Flash x-rays

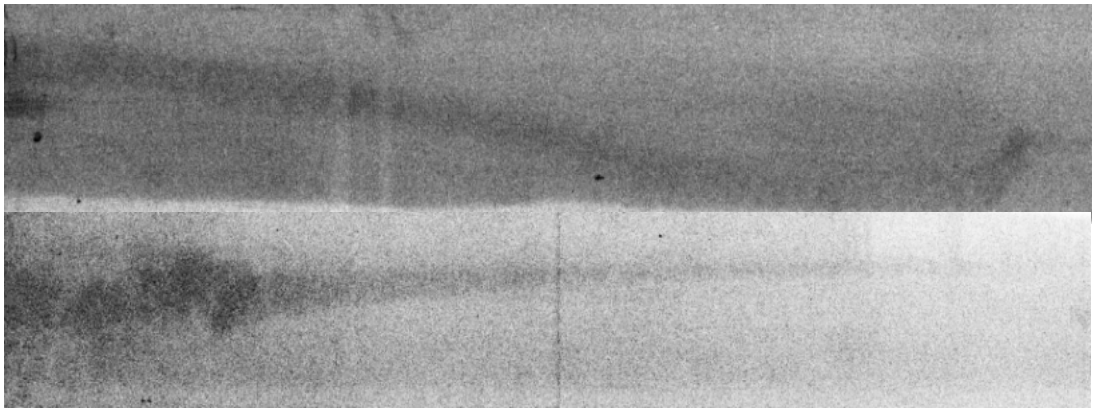

Extremely curved jets, extreme particulate nature

Steel penetration testing

3.4 CDs (260mm) at a 5.5 CD (460mm) standoff

Improvised Shaped Charges

- Beer bottles: 375ml Timmermans Lambic with conical bases
  - Octol 70/30 to a final density of about 1.80 gm/cc
  - Small PBXN-5 booster pellet with an RP87 detonator
  - 150 KV flash x-rays with soft x-ray tubes
  - Jet tip velocity of about 5 km/s with a fairly straight jet
  - Extremely particulated behavior, some repeatable structure
  - Penetration studies against mild steel witness plates
    - 2.6 CD (130mm) of steel at a 6 CD (305mm) standoff
    - 2.25 CDs (114mm) at a 3 CD (152mm) standoff.
- Sparkling wine bottles: 750ml Korbel Extra Dry with conical bases
  - Octol 70/30 to a final density of about 1.80 gm/cc
  - Small PBXN-5 booster pellet with an RP87 detonator
  - 150 KV flash x-rays with soft x-ray tubes
  - Jet tip velocity of about 7 km/s with a fairly straight jet
  - Repeated experiment showed some variation in the jet tip shape and velocity
  - Extremely particulated behavior, some repeatable structure
  - Penetration studies against mild steel witness plates
    - 3.4 CDs (280mm) at a 5.5 CD (460mm) standoff
    - repeated, producing a nearly identical penetration depth.

Improvised Shaped Charges

Beer Bottle

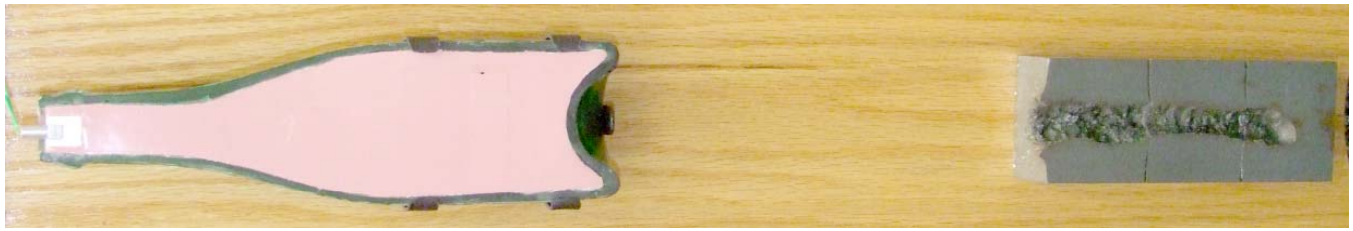

Sparkling Wine Bottle

Test Stand

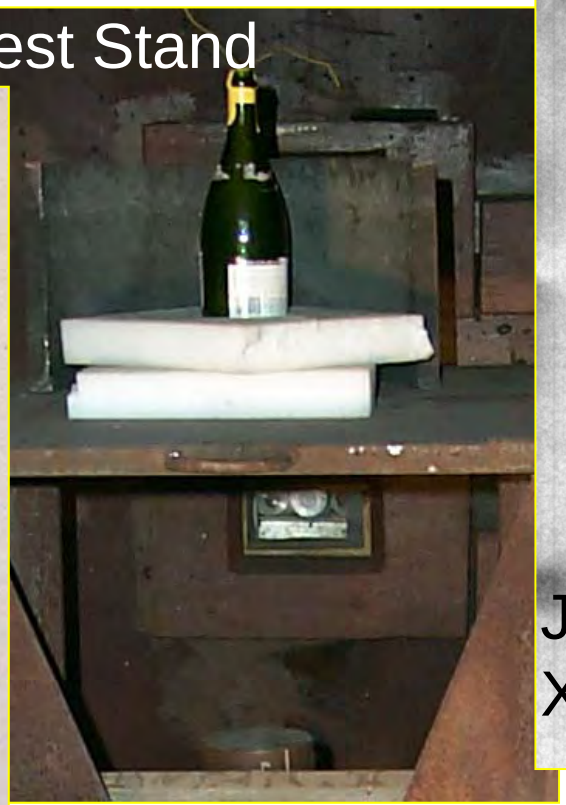

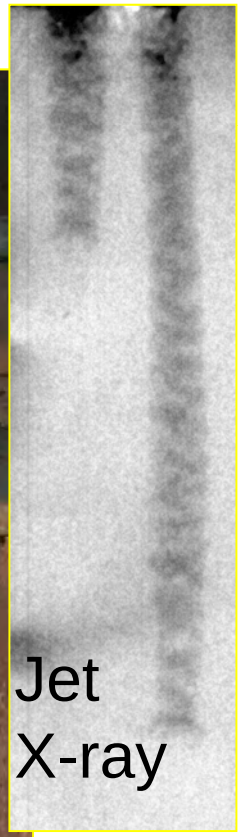

Jet
X-ray

Penetration

Standard Demolition Charge

M2A3/M2A4 Demolition Charges

- *Originally produced at Picatinny!*
- *Developed in early 1940s!*

~9-1/2 pounds Comp-B main charge
~2 pounds 50-50 pentolite booster

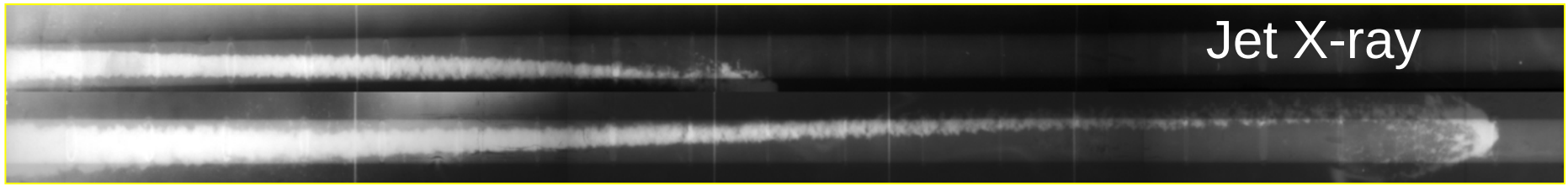

~6.4Km/s Jet Tip Velocity

84” Penetration in soil

Ductile Glass Jets

20 CD flash x-ray comparisons

Tungsten Jet

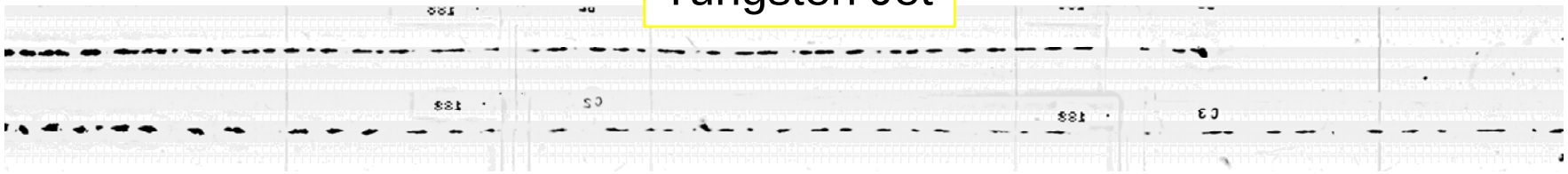

Copper Jet

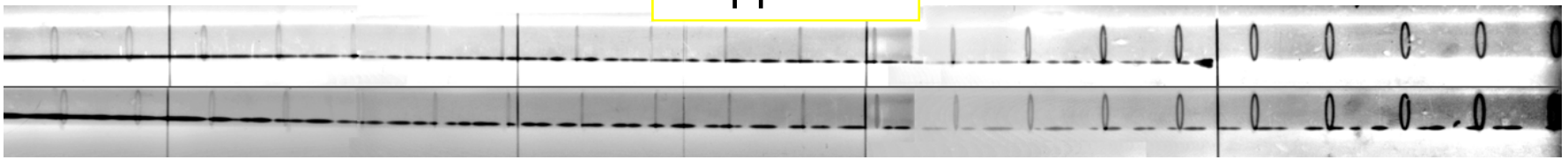

Ductile Glass Jet

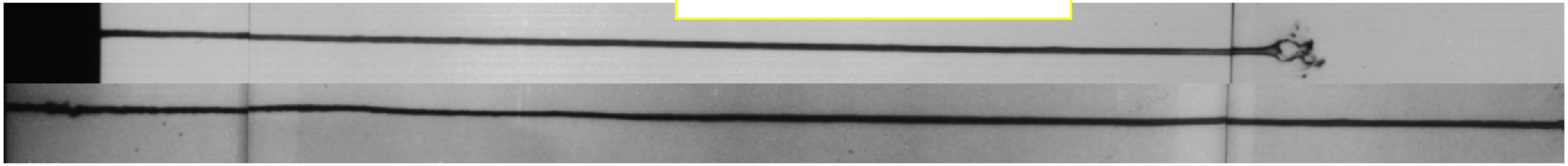

Glass can produce the most ductile shaped charge jets known to date

High Density Glass Investigation

- 70mm shaped charge configuration
- Cast (Octol 70/30, EDC1G) and pressed (LX-14) explosives
- Variety of increased density glasses
  - –up to 5.5 gm/cc glass were identified that were able to produce jets that did not particulate
  - –above this density either could not make the glass or did not form coherent jets

70mm shaped charge

High Density Glass Investigation

Observed Jet Characteristics

- Lower jet velocity shaped charges\tended to produce extreme particulate jet behavior
- May be related to the brittle nature of glasses observed at lower temperatures and pressures
- Similar to jets produced from improvised bottle shaped charges and fielded demolition shaped charges
- Similar jets have been observed from bulk metallic glass lined shaped charge jets

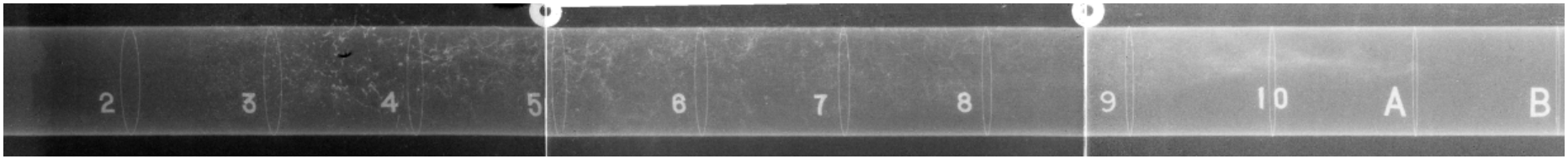

Extremely particulated glass jet

Observed Jet Characteristics

•Extremely ductile jet behavior appears to be associated with higher pressure and resulting glass jet temperatures
•Believed to be a result of traditional glass softening at elevated temperatures

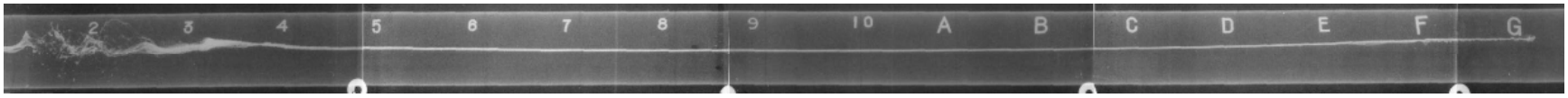

•Very late time jet instability: “wobblization”
•Spiraled into a helical pattern
•Onset of this wobblization: between 40 and 57 CD standoff.

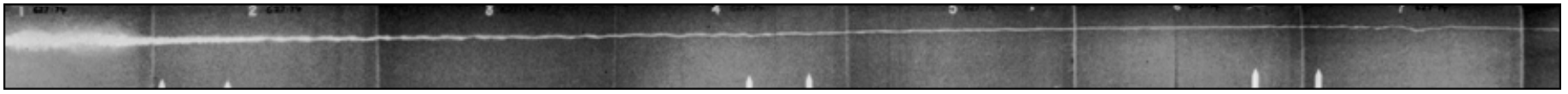

Flash x-ray of a glass jet at 57 charge diameters

Observed Jet Characteristics

- Jet overdriving was often clearly evident
- Many jet tips looking \like traditional highly overdriven metal jet tips
- Radially dispersed jet mass sprayed in front of the coherent jet
- Long portions of hollow jet tip
- Coherent jet was often noted at a velocity of about 6.5 km/s.

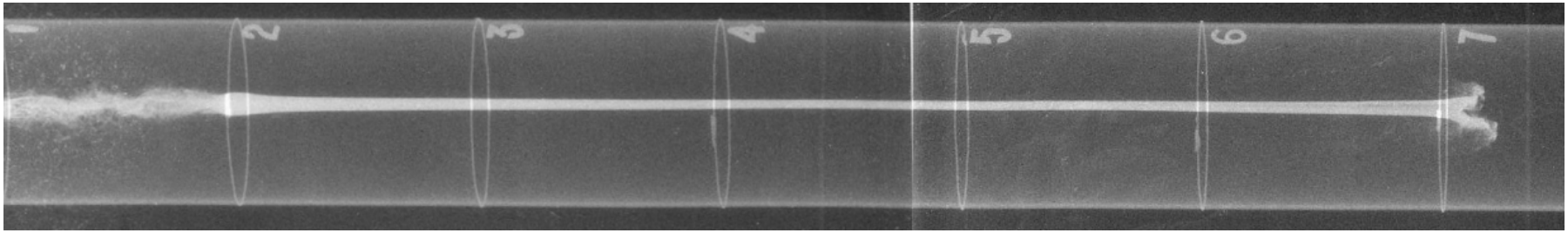

Shaped charge with a hollow section and overdriven jet tip

Observed Jet Characteristics

•Radially dispersed jet tip behavior appears to be associated with the classical observed behavior resulting from supersonic flow conditions in the jet formation region
•The degree of radial dispersion was found to vary from slight hollowing of the jet to complete hollowing of the entire jet that became known as “bubble jets”

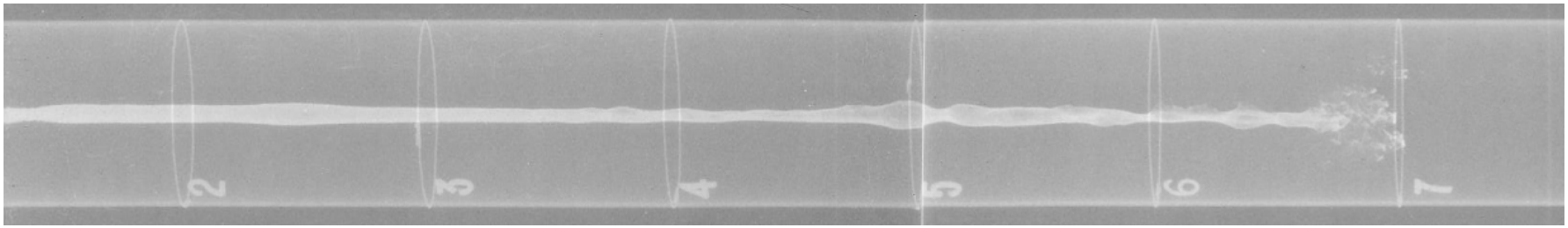

A glass bubble jet

Observed Jet Characteristics

•Some design and glass combinations appears to push the jet beyond standard overdriven and bubble jet conditions
•Entire jet appeared as a series of fluid sections that became known as a “droplet jet

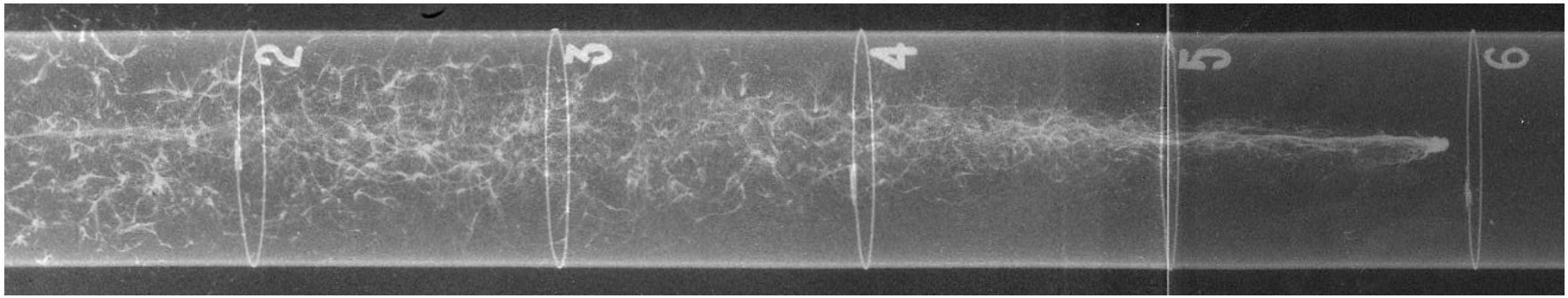

A glass droplet jet

Conclusions

- A variety of traditional silica based glasses, including higher density lead glasses, have been used as shaped charge liner materials
  - Explosively packed bottles have long been used as improvised shaped charges
  - Standard demolition shaped charges use glass liners for geologic materials penetrations.
  - Shaped charge jet radiography reveals the extreme particulate nature of these jets.
- A series of progressively higher density glasses have also been explored.
  - Jet radiography results from these tests show distinct regions of resulting jet behavior with extreme particulate, ductile or radially dispersed behaviors.
  - The resulting jet behavior appears to be both material and design dependent.

Acknowledgements

- Lockheed-Martin UK (N. Hebron) for their support on glass material and design investigations, as well as shaped charge fabrication, loading and testing.
- American Ordnance for their support on shaped charge fabrication, loading and testing.
- Brian Fuchs, Tim Madsen and W. Poulos for ARDEC testing support.

Military Institute of Armament Technology
POLAND

The numerical optimization of the novel kinetic energy penetrator for tank guns

Lt. Col. Mariusz MAGIER PhD

26 ISB - MIAMI 2011

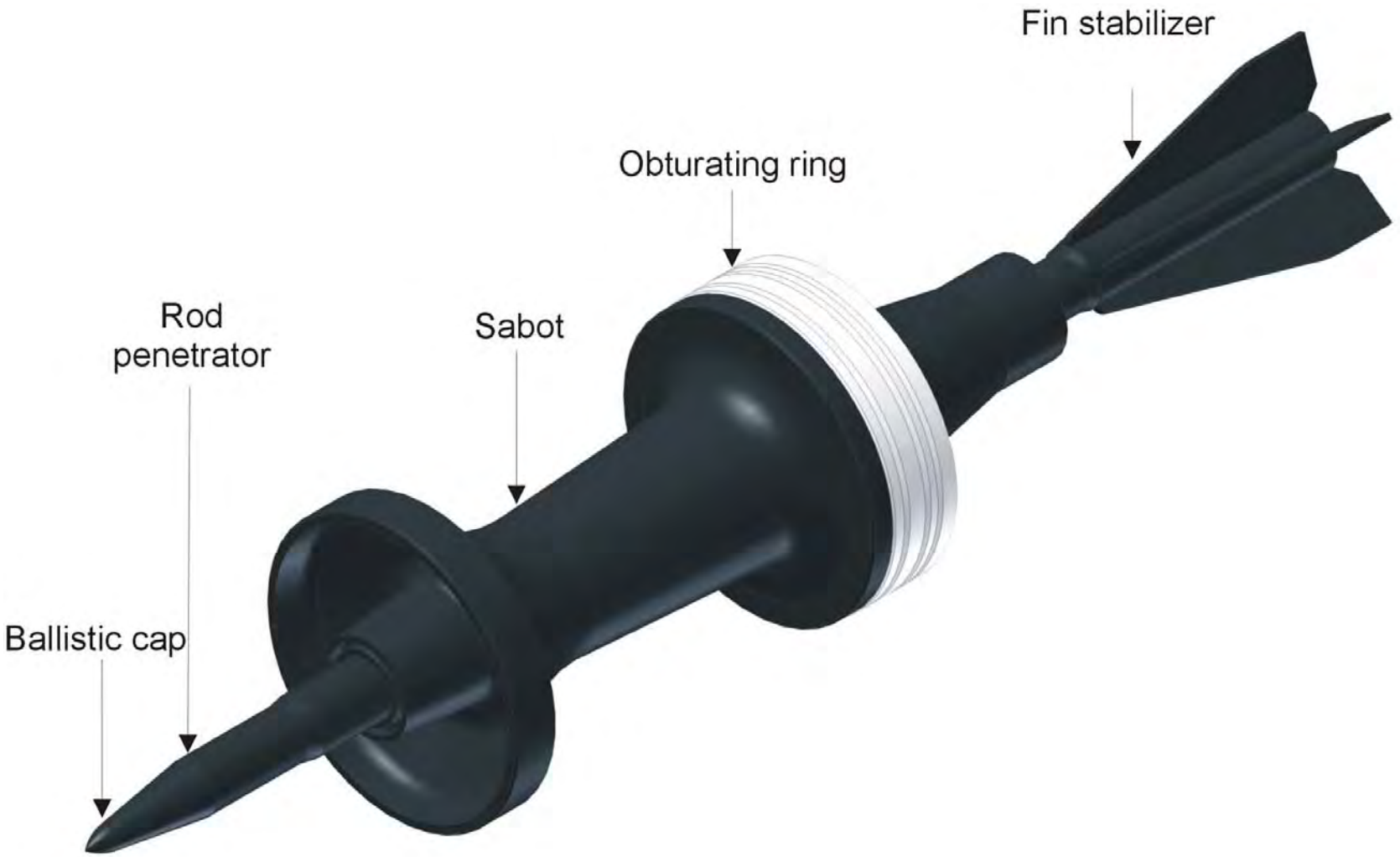

Component parts of the APFSDS projectile.

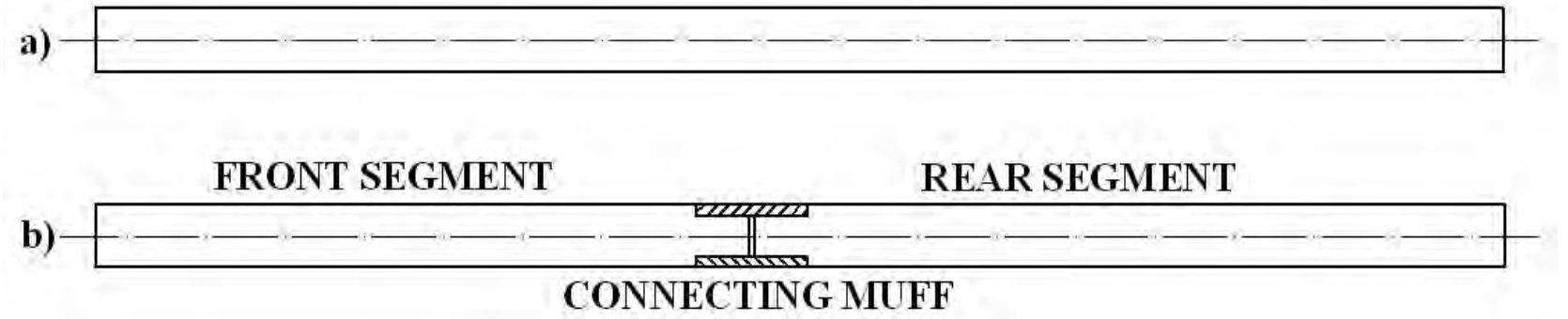

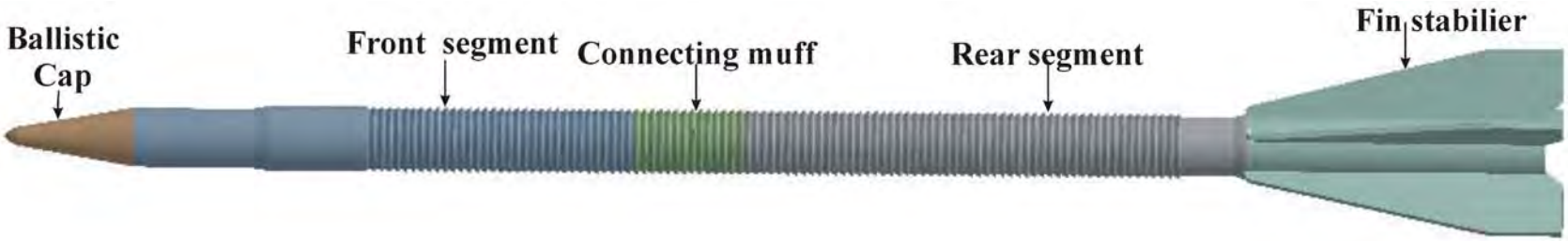

Subcalibre projectile with segmented penetrator (MIAT-Poland)

During 25th ISB in China was present the poster with conception of the of the segmented kinetic energy penetrators for tank guns. The penetrator is composed of two tungsten alloy pieces connected by screwed steel muff. The axial deformation of the connecting muff during penetration process results in decreasing of the distance between tungsten segments. For this reason the rear segment can hit the front segment to give it some additional kinetic energy enhancing penetration depth. During simulations process it was established that for one of the developing variants the penetration depth increases by 10% in comparison with penetration depth of the real penetrator with the same weight and dimension. In the new concept called "*forced segmented penetration*", thanks to application of the 5 cm length connection muff, the penetration depth increased by 10% in comparison with penetrations depth of the monolithic penetrator with the same weight and diameter. This kind of segmented penetration phenomena wasn't presented before.

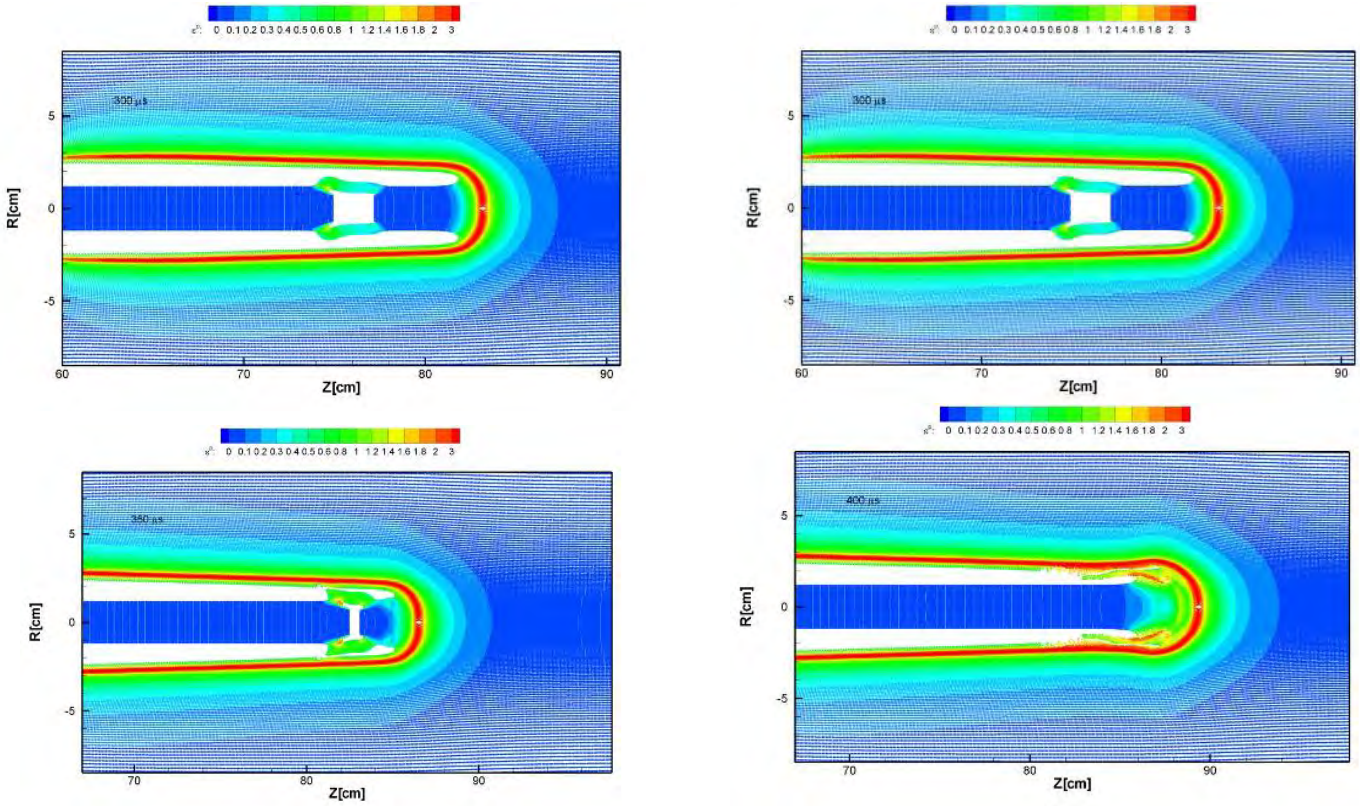

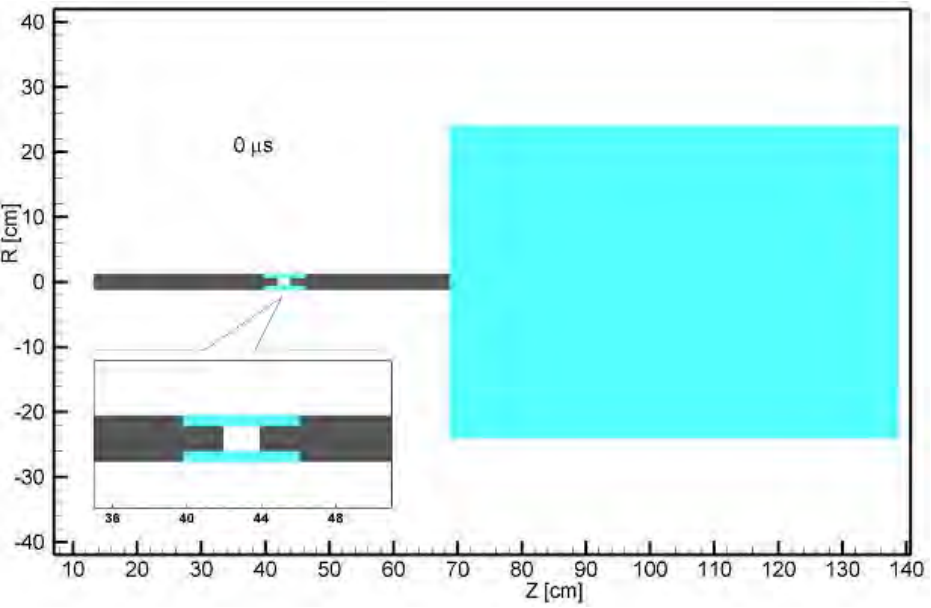

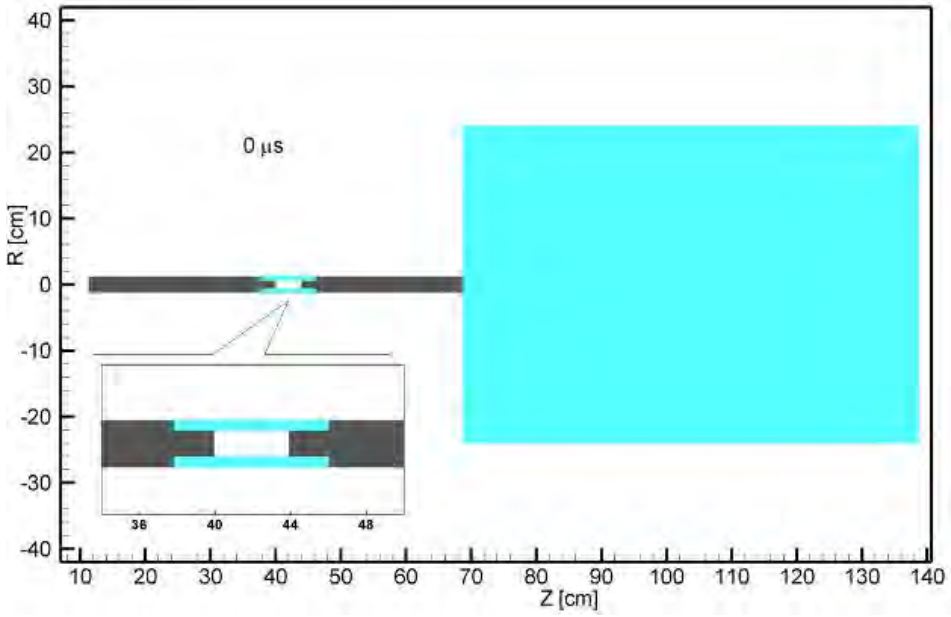

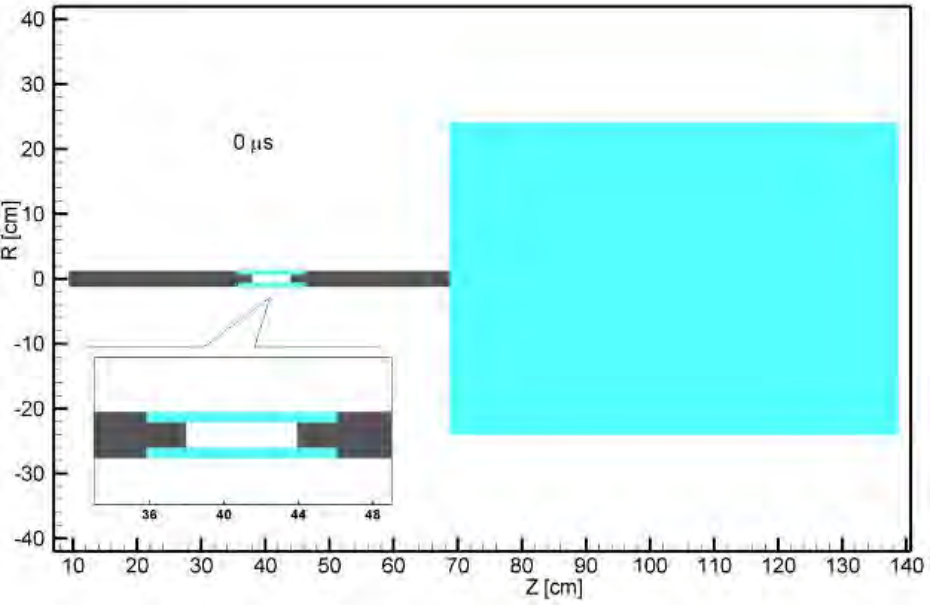

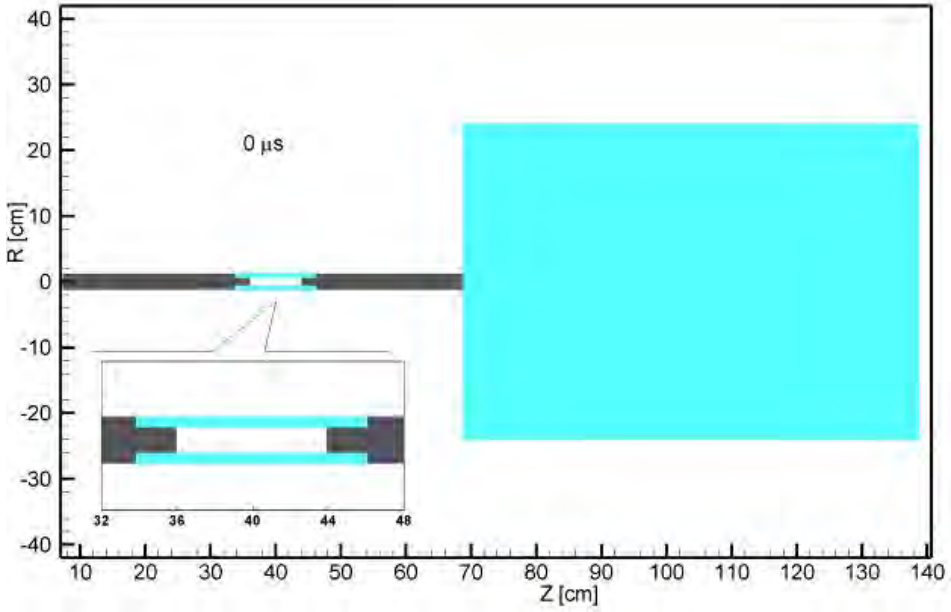

The variants of the segmented penetrators analyzed during optimization.
Distance between tungsten rods: 2, 4, 6, 8 cm.

Configuration of the successive variants

Variants number	Penetrator diameter d [cm]	Penetrator length l [cm]	Hit velocity v(m/s)	Penetrator weight m [g]	Depth of Penetration DOP [cm]	Distance between tungsten rods z [cm]
A	2,3	55,4	1550	3597	46,80	2
B		57,4		3635	44,30	4
C		59,4		3672	45,51	6
D		61,4		3710	39,23	8

Numerical optimization of the distance between tungsten rods

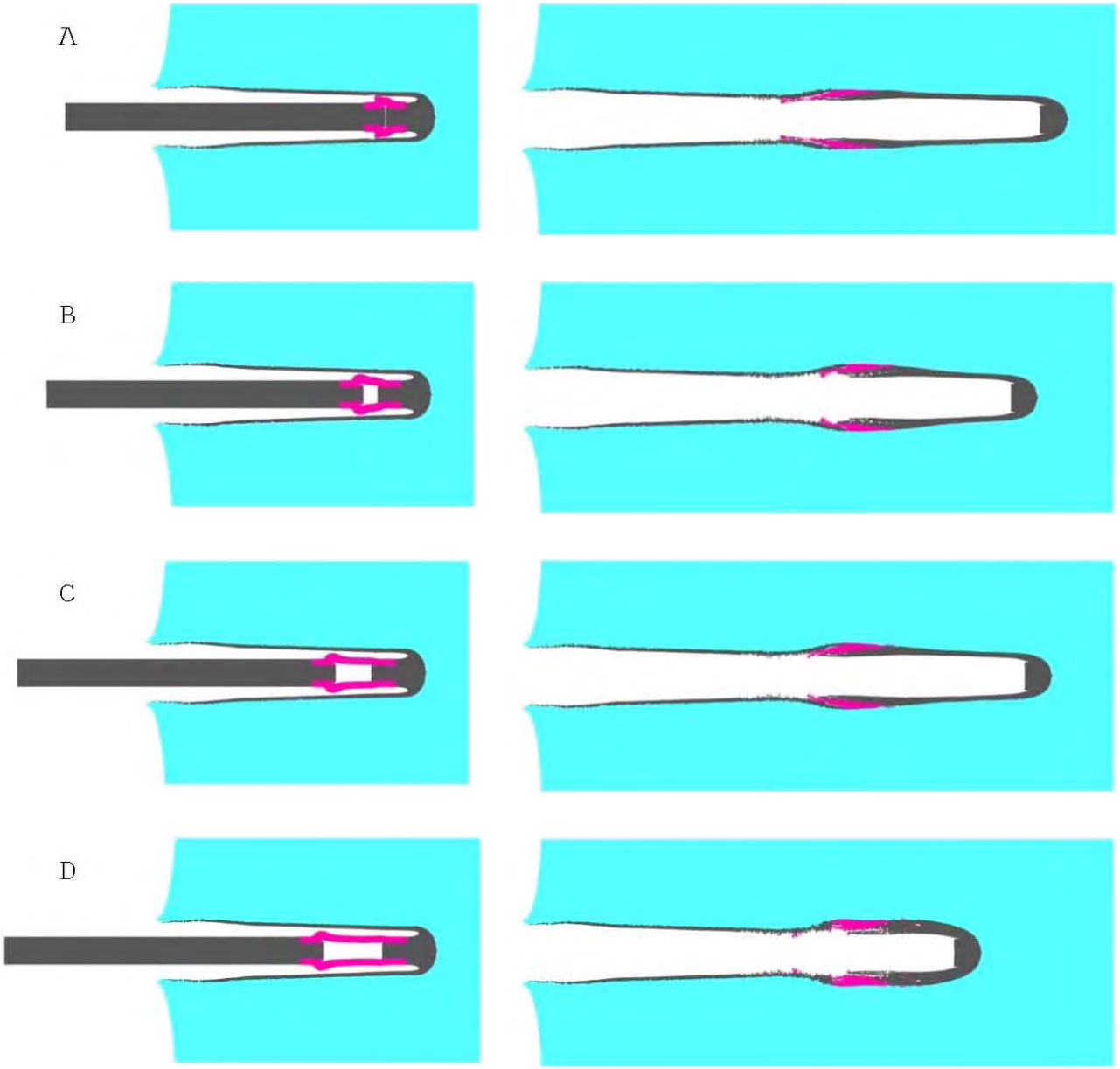

During optimization process it was established that for B variant the penetration depth is similar to the depth for penetrator C. For A variant the penetration depth increases about 5% in comparison with the penetration depth of B and C variants. The penetration depth for variant D decreases about 10% in comparison with the penetration depth of B and C variants. The probable reason is the phenomenon of slowing down of the long connection muff because of getting stuck inside the penetration crater.

Analyses of penetration process with different shapes of the penetrator nose

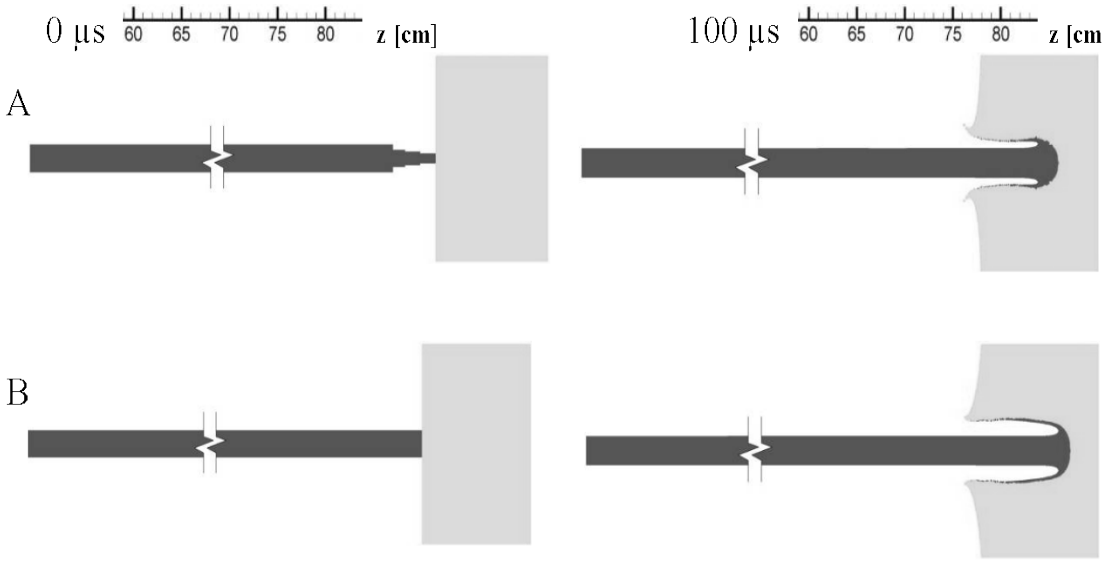

It is visible that the crater is thinner and shallower for the sharp nose penetrator. It is necessary to be told that the weight of the sharp nose penetrator is about 5% lower in comparison with the blunt nose penetrator

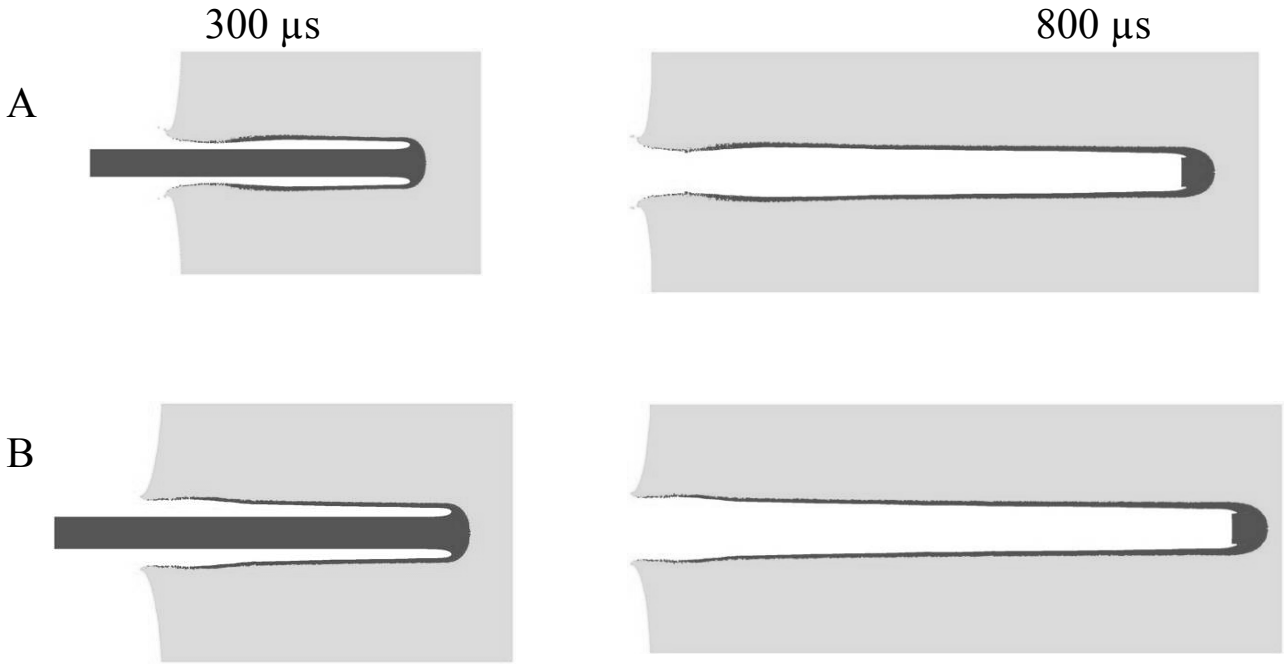

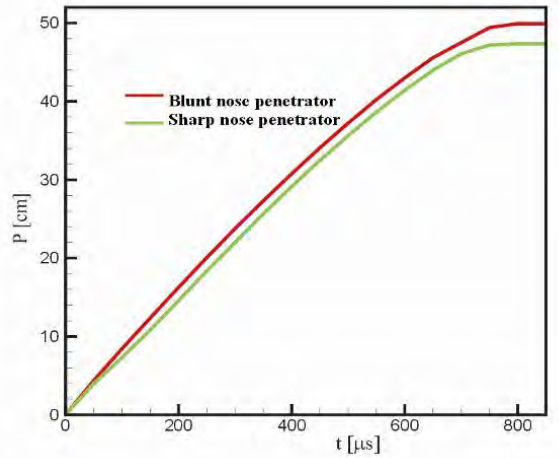

Conclusions

On the base of the numerical results the following conclusions may be drawn:

1. **During optimization process it was established that for B variant the penetration depth is similar to the depth for penetrator C. For A variant the penetration depth increases about 5% in comparison with the penetration depth of B and C variants. The penetration depth for variant D decreases about 10% in comparison with the penetration depth of B and C variants. The probable reason is the phenomenon of slowing down of the long connection muff because of getting stuck inside the penetration crater.**
2. **During analyses of penetration process with different shapes of the penetrator nose it turned out that the crater is thinner and shallower for the sharp nose penetrator in comparison with the blunt nose penetrator.**
3. **According to conclusions 1 and 2 it was decided to develop and produce the subcalibre projectiles with the A and B penetrator variants. For both variants the blunt nose will be applied. The firing test of APFSDS-T rounds with the novel segmented penetrators will be conducted on the Military Institute of Armament Technology (*MIAT*) testing ground. During these tests the projectiles will be fired from ballistic gun to *RHA* plates to compare the penetration depth.**

The results of the firing test will be presented in the next paper.

This R&D is supported by Polish Ministry of Science and High Education - project No R 00 018 02.


MK 2
125 D 81
1 02-361


12
5
8
9
11
7
4
6
10

Inclusion of Rifling and Variable Centerline for Enhanced Modeling of Launch Dynamics

Charles Eichhorst, David A. Hopkins,
William H. Drysdale, Michael Minnicino

TECHNOLOGY DRIVEN. WARFIGHTER FOCUSED.

26th International Symposium on Ballistics
Miami, Florida
September 12-16, 2011

Outline

- Introduction
- Rifled barrel meshing
- Modeling barrel centerlines
- Measuring rigid body dynamics
- Effects/examples

Introduction

- Objective: Improve modeling of gun barrel and projectile interactions and dynamics
  - Streamline the process of adding twisted rifling and barrel centerline data
  - Extract projectile motion data from results
    - Allows rational determination of transverse and spin-up loading
  - Allows for more accurate predictions of projectile motion at muzzle exit
    - Can be used to reduce target impact dispersion

Introduction

- Defining the bore/barrel geometry correctly in FE models can be laborious and prone to user error
  - Automating this process through scripting can greatly reduce these problems
- High-fidelity FE models require a large number of nodes
  - Rigid-body projectile motion found by processing node data from results files

Jump Theory

- Methods described can be used to predict muzzle exit conditions related to jump
- Post-processing can provide projectile angles, angular rates, and velocities
  - Used in jump predictions
- Jump testing can be simulated when combined with exterior ballistics modeling

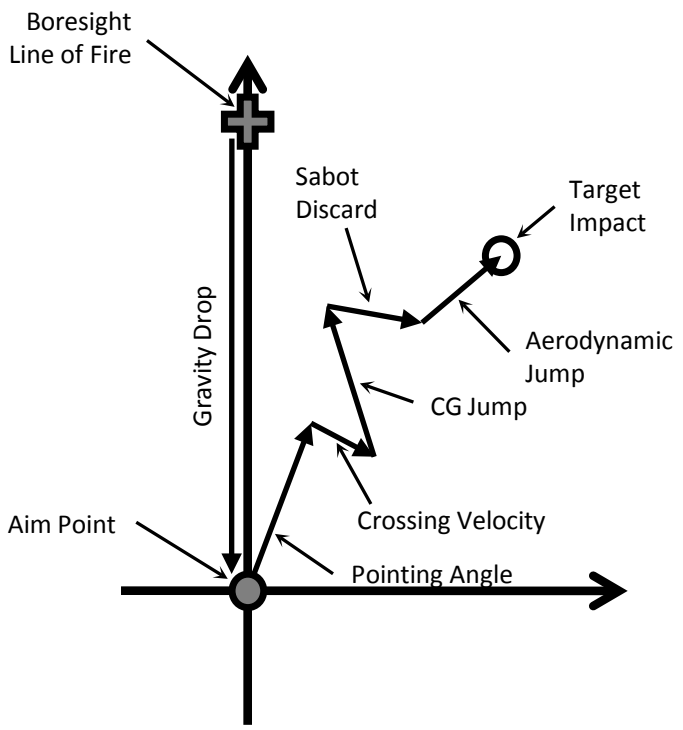

Rifled Barrel Meshing

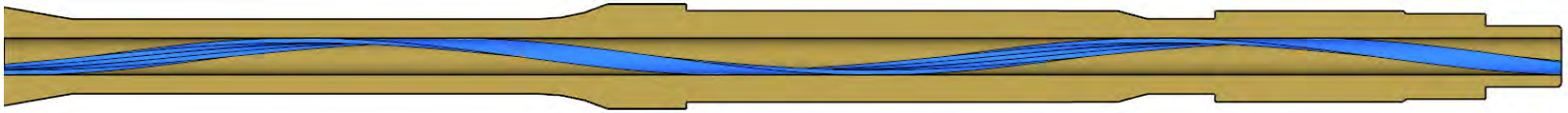

- Rifling is needed for accurate modeling of projectile engraving and spin-up
- CAD geometry often very complex for automated meshing algorithms
  - Many additional steps required to create a high quality hexahedral mesh from a CAD model

Rifled Barrel Meshing

- Base 2D mesh extruded and rotated following a specified twist rate
  - Can be easily automated in pre-processing tools
- Variable twist rates and mesh densities can be specified
- Does not depend on rifled CAD model
  - Allows for easy generation and comparison of different rifling twist rates

Barrel Centerlines

- Barrel centerlines needed for accurate modeling of transverse loads
- Centerline profile controls the CG jump of the projectile

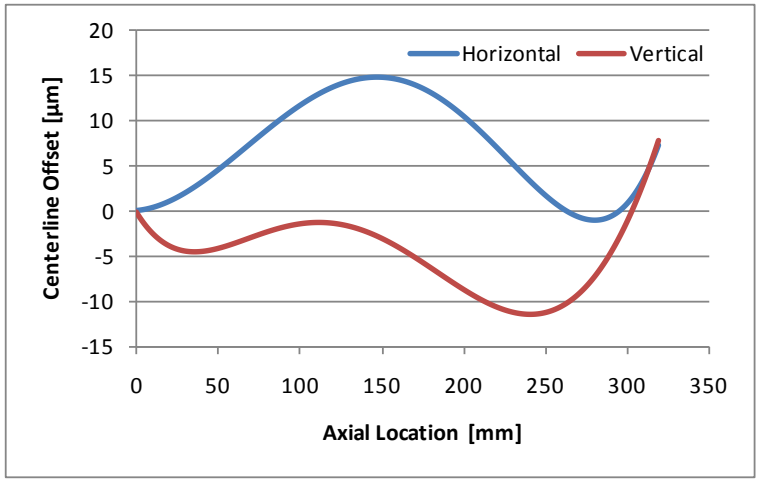

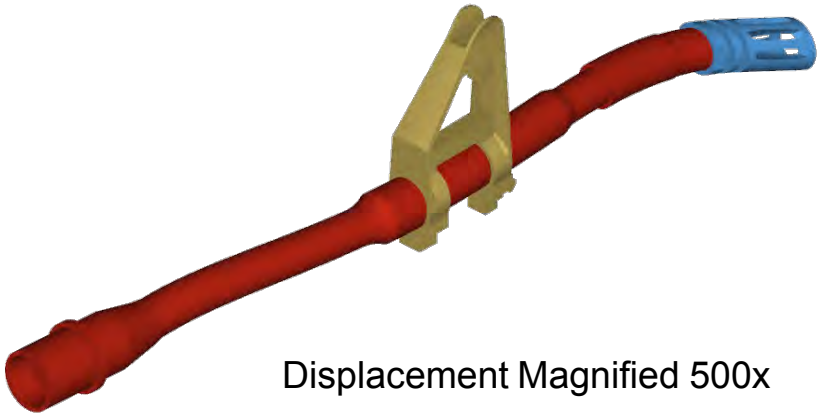

Displacement Magnified 500x

Barrel Centerlines

- Centerline shape can be measured using bore-riding optical sensors
  - This will generate a list of offset coordinates along the barrel's axis
- Pre-processing tools can be scripted to apply these offsets to the barrel's mesh
  - Allows for parametric studies comparing different centerlines

Measuring Projectile Rigid Body Dynamics

- Projectile rigid body motion extracted from results
  - Provides an accurate representation of projectile motion

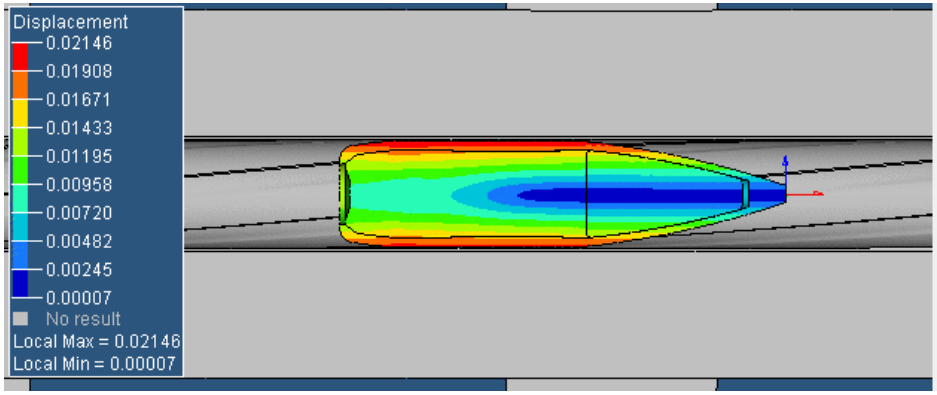

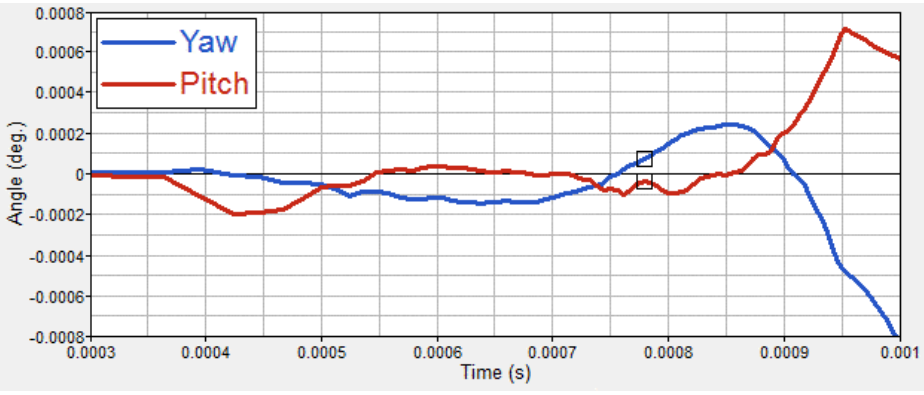

Measuring Projectile Rigid Body Dynamics

$$\mathbf{u}_{CG} = \sum_i \frac{m_i \mathbf{u}_i}{m} \qquad \mathbf{v}_{CG} = \sum_i \frac{m_i \mathbf{v}_i}{m} \qquad \mathbf{a}_{CG} = \sum_i \frac{m_i \mathbf{a}_i}{m}$$

$$\mathbf{u}_i^* = \mathbf{u}_i - \mathbf{u}_{CG} \qquad \mathbf{v}_i^* = \mathbf{v}_i - \mathbf{v}_{CG}$$

$$\mathbf{L} = \sum_i \mathbf{u}_i^* \times m_i \mathbf{v}_i^*$$

$$\mathbf{I} = \sum_i m_i \begin{bmatrix} u_{i,2}^{*\,2} + u_{i,3}^{*\,2} & -u_{i,1}^* u_{i,2}^* & -u_{i,1}^* u_{i,3}^* \\ -u_{i,1}^* u_{i,2}^* & u_{i,1}^{*\,2} + u_{i,3}^{*\,2} & -u_{i,2}^* u_{i,3}^* \\ -u_{i,1}^* u_{i,3}^* & -u_{i,2}^* u_{i,3}^* & u_{i,1}^{*\,2} + u_{i,2}^{*\,2} \end{bmatrix}$$

$$\mathbf{L} = \mathbf{I}\boldsymbol{\omega}$$

- CG motion
  - Mass-weighted average of node motion
- Angular rates
  - Moment of inertia and angular momentum calculated for all nodes
  - Angular momentum of a rigid body solved for angular velocity

Measuring Projectile Rigid Body Dynamics

$$\mathbf{U}^* = \mathbf{A}\mathbf{U}_0^*$$

$$\overline{\mathbf{A}}(\phi,\theta,\psi) = \mathbf{B}_1(\phi)\mathbf{B}_2(\theta)\mathbf{B}_3(\psi)$$

$$\mathbf{R}(\phi,\theta,\psi) = \mathbf{A} - \overline{\mathbf{A}}(\phi,\theta,\psi)$$

$$\mathbf{B}_1(\phi) = \begin{bmatrix} \cos\phi & -\sin\phi & 0 \\ \sin\phi & \cos\phi & 0 \\ 0 & 0 & 1 \end{bmatrix}$$

$$\mathbf{B}_2(\theta) = \begin{bmatrix} \cos\theta & 0 & \sin\theta \\ 0 & 1 & 0 \\ -\sin\theta & 0 & \cos\theta \end{bmatrix}$$

$$\mathbf{B}_3(\psi) = \begin{bmatrix} 1 & 0 & 0 \\ 0 & \cos\psi & -\sin\psi \\ 0 & \sin\psi & \cos\psi \end{bmatrix}$$

- Rotation matrix $\mathbf{A}$ computed from initial ($\mathbf{U}_0^*$) and current ($\mathbf{U}^*$) nodal coordinate matrices
  - Deformation of the material means there is not a direct rotation
  - Iterative method used to find the best fit
- Function $\overline{\mathbf{A}}$ defined as a product of Euler rotations $\mathbf{B}_i$
- Yaw, pitch, and roll found using nonlinear least-squares fitting techniques

Effect of Rifling and Centerline

- Simplified 5.56mm barrel model is used to demonstrate the effects of including rifling and centerlines on the projectile's:
  - Transverse displacements
  - Transverse velocities
  - Yaw and pitch angles
  - Angular rates

Effect of Rifling and Centerline

- Model is of a 5.56mm barrel (with sight and muzzle brake) and projectile
  - Cantilevered support on the barrel
  - Pressure loads determined using IBHVG2 software
  - Simple polynomial centerline

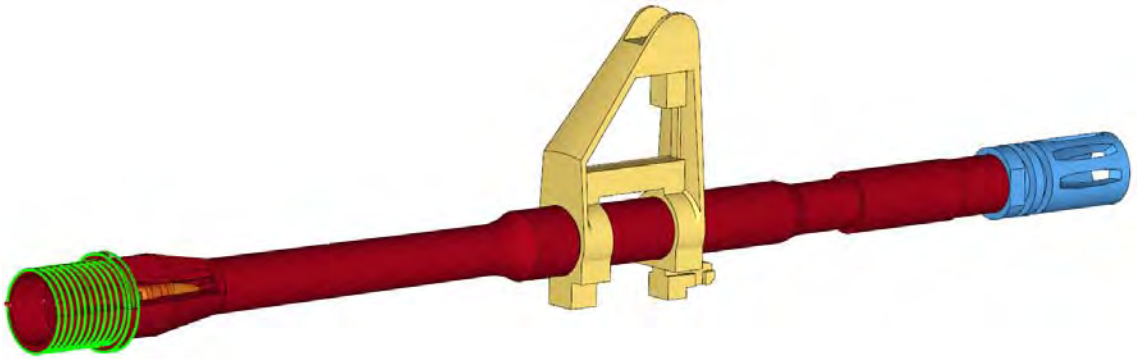

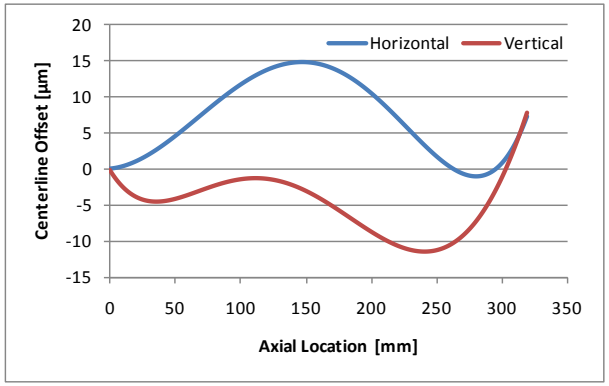

Effect of Rifling and Centerline

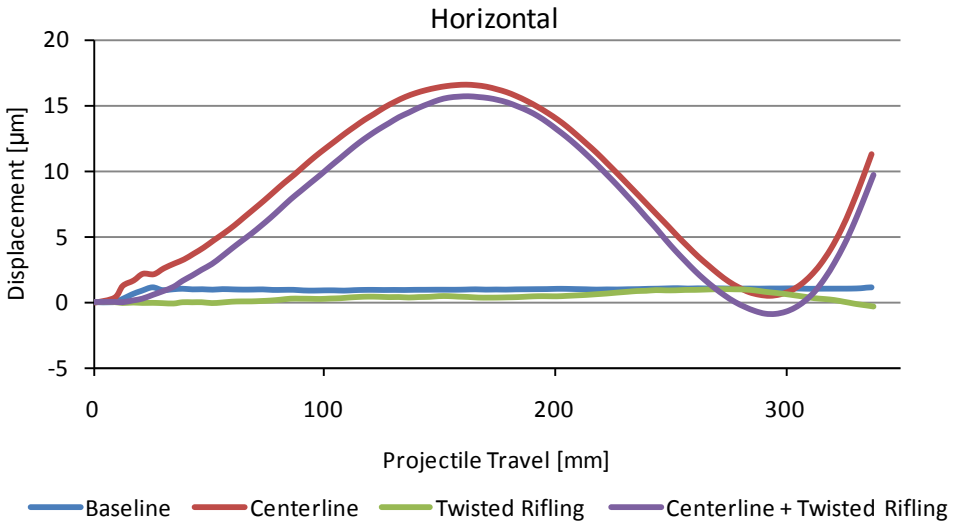

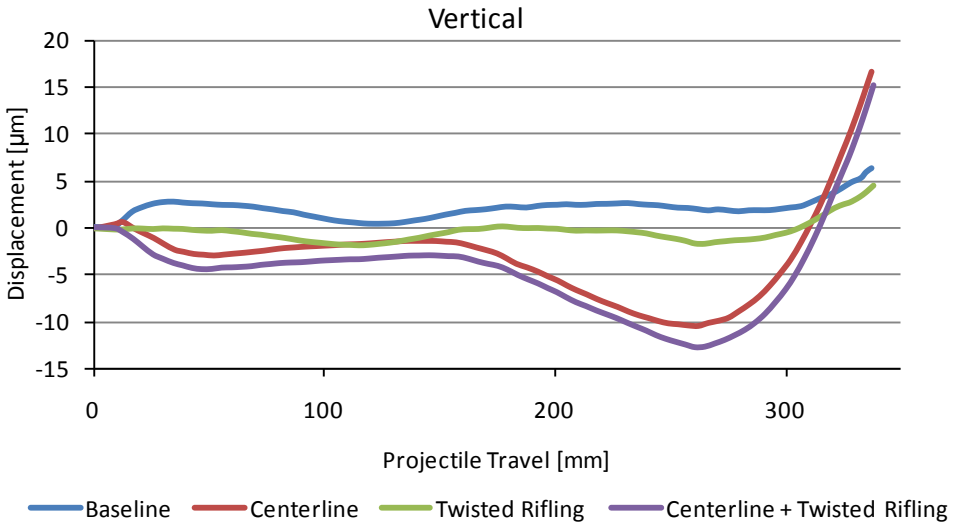

Displacement

- Transverse displacements primarily driven by the centerline profile
  - Only a small difference is created by rifling
  - Sight and muzzle brake also create vertical displacements

Effect of Rifling and Centerline

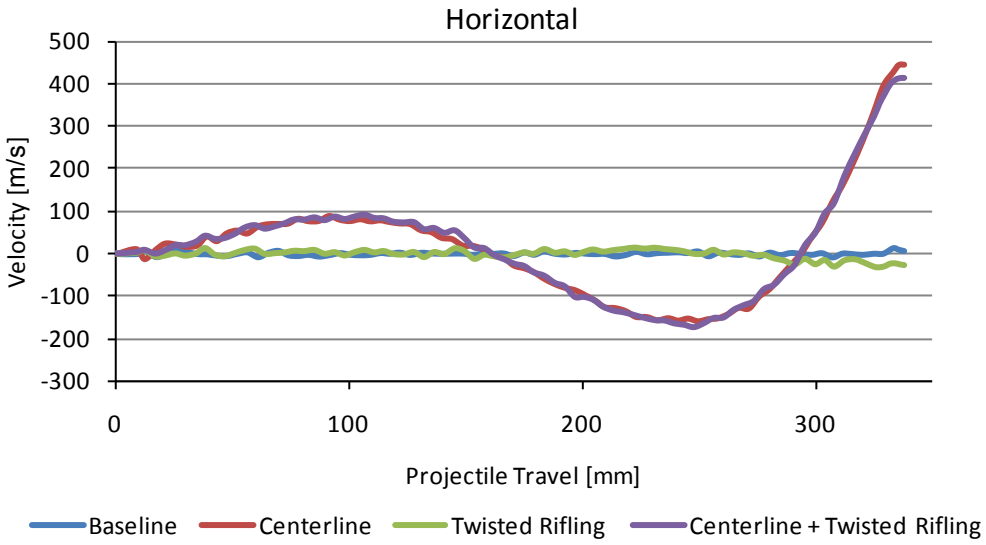

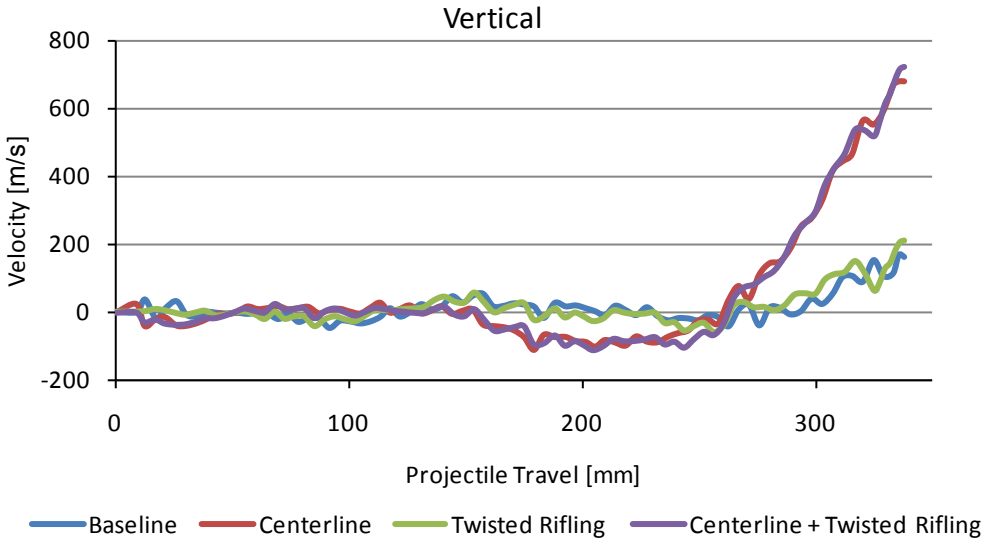

Velocity

- Transverse velocities also show effect of centerline profile

Effect of Rifling and Centerline

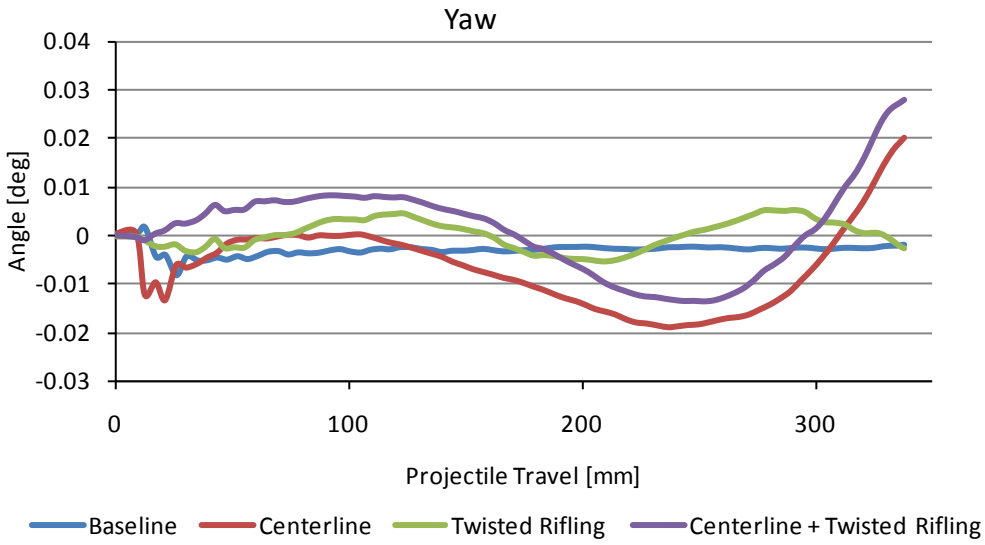

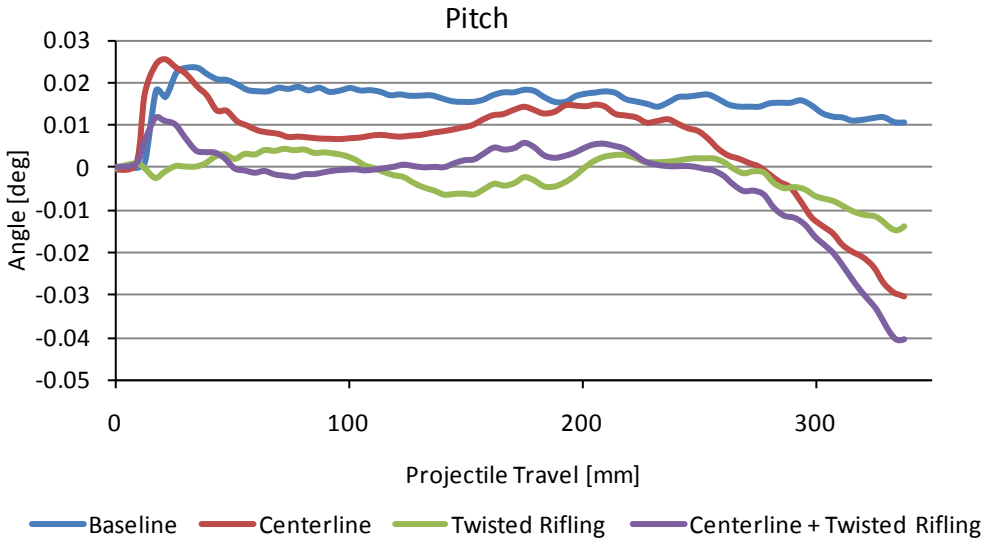

Yaw and Pitch Angle

- Projectile angular results show a clear difference between all test cases

Effect of Rifling and Centerline

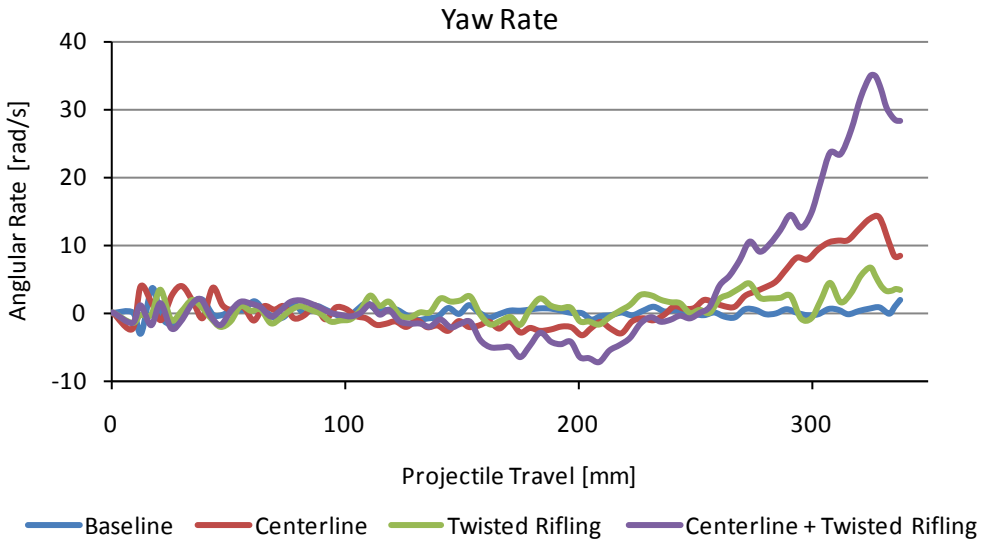

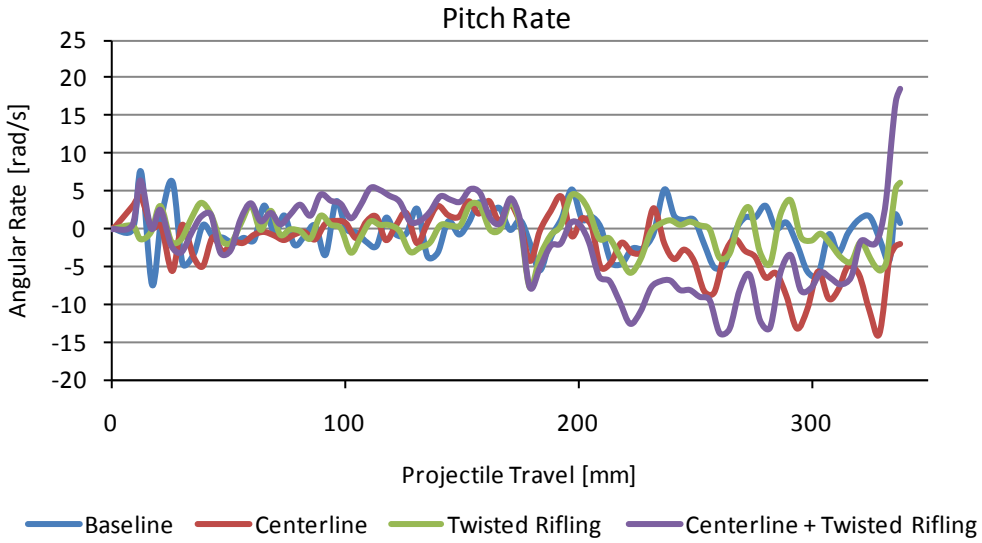

Angular Rate

- Angular rates, although noisy, also show large differences between all test cases, especially at muzzle exit
- Angular rates at muzzle exit have a significant effect on aerodynamic jump

Conclusions

- Rifling and barrel centerlines have a significant effect on in-bore dynamics
- Inclusion of these techniques is important for a high-fidelity finite element analysis
  - Necessary for predicting transverse and spin-up loads
  - Allows for study of muzzle exit conditions and jump
- Scripting and external tools allow these methods to be included in an analysis quickly and reliably

Questions?

Charles Eichhorst
U.S. Army Research Laboratory
Aberdeen Proving Ground, MD 21005
410-306-2233
charles.e.eichhorst.civ@mail.mil

William Drysdale – william.h.drysdale.civ@mail.mil
David Hopkins – david.a.hopkins.civ@mail.mil
Michael Minnicino – michael.a.minnicino.civ@mail.mil

BAE SYSTEMS

26th International Ballistics Symposium

The Trouble with TNT Equivalence

Paper: 11770

Presented by

Paul M. Locking

Energetics Modelling Manager

Technical Specialist (Blast & Ballistics)

Outline

- The big problem with TNT Equivalence
  - Often used to compare explosives performance
  - Many models use TNT as the baseline explosive
  - 1 kg RDX = 1.6 kg TNT, so giving RDX an Equivalence of 1.6
  - 20% to 30% typical error, 50% has been found
- Scaling Laws
  - Scaled Distance, Scaled Impulse
- Trials techniques will not be discussed here -> see paper
- Theoretical Methods for TNT Equivalence
  - Secondary combustion / Aluminised explosives not covered
- Theoretical fit to trials data
  - Error Analysis
- Conclusions

The Problem

Figure 1. Variation in TNT equivalency of three high explosives TATB, HMX & RDX (from a number of different techniques and sources)

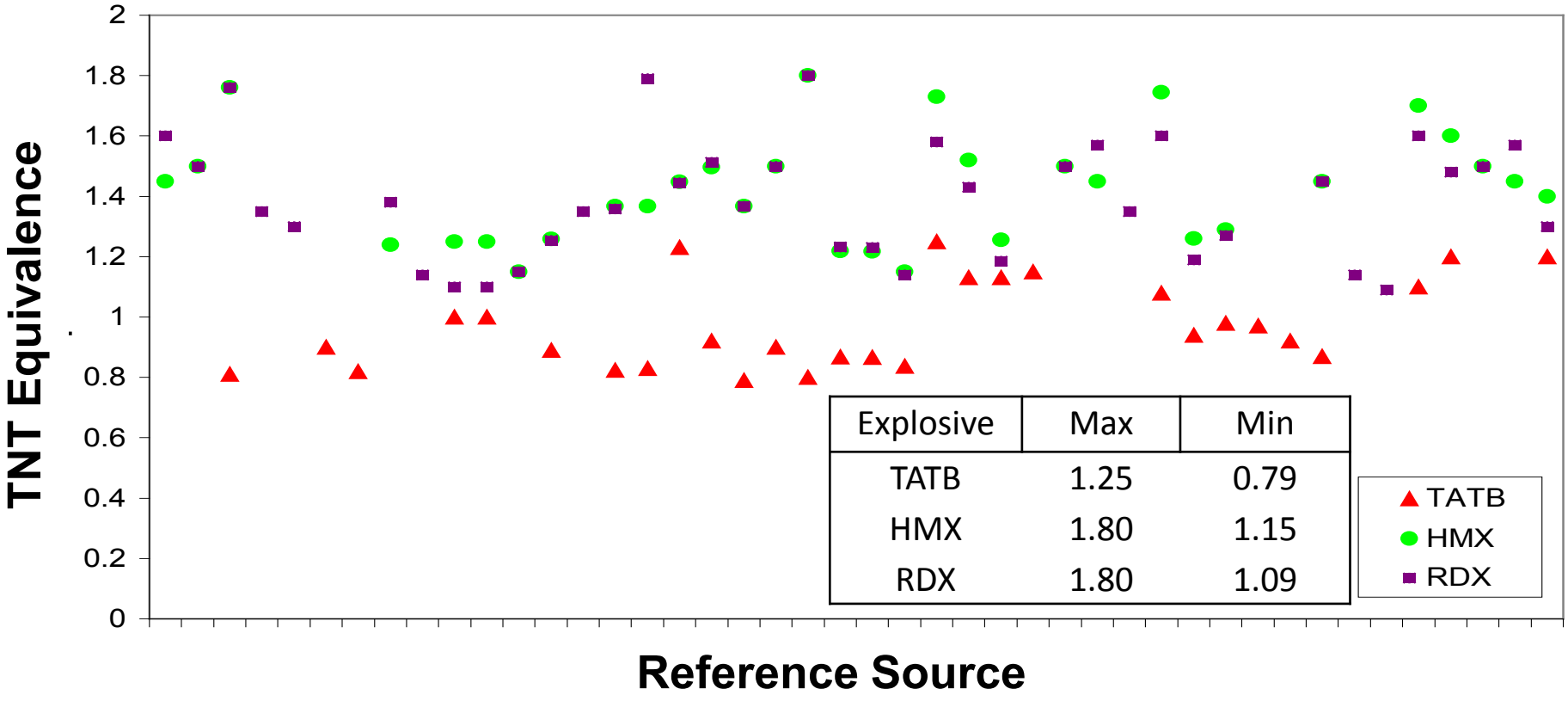

Explosive	Max	Min
TATB	1.25	0.79
HMX	1.80	1.15
RDX	1.80	1.09

(from Cheesman)

Scaling Laws

- Blast wave scaling laws are often called ‘Cube root scaling’
  - Hopkinson (1915) & Cranz (1926)
- Charge performance is a function of Scaled Distance (Z)
- Both peak overpressure & Scaled Impulse are directly related to Scaled Distance

  Scaled Distance (Z) = Range / Charge mass ^ (1/3)

  Scaled Impulse = Impulse / Charge mass ^ (1/3)

Figure 2. Variation of TNT Equivalence with Scaled Distance by Cooper

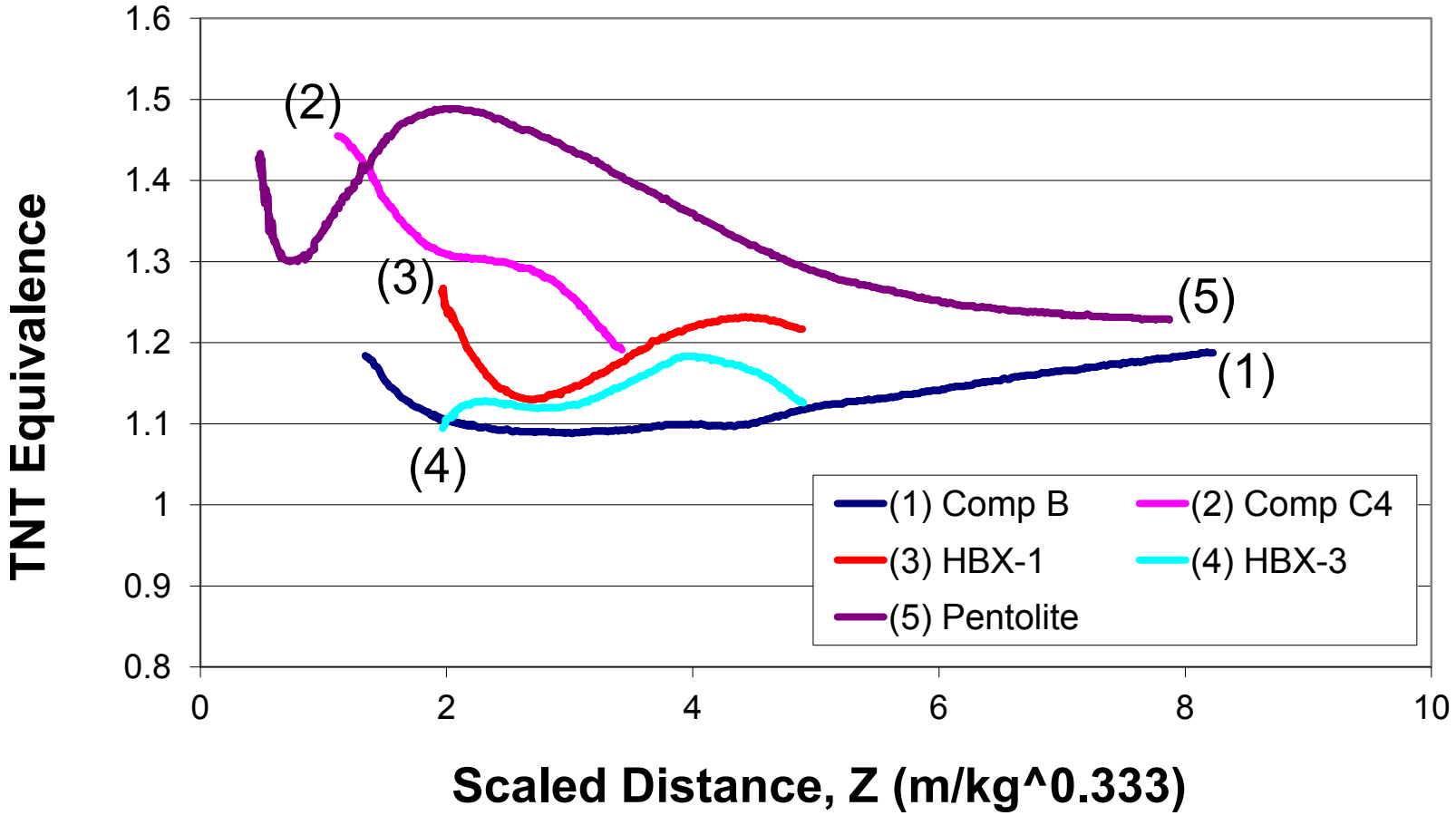

(from Air Blast Calculations and trials by Swisdak)

Figure 3. TNT Equivalence for Peak Positive Incident Pressure

(from UFC 3-340-02 data)

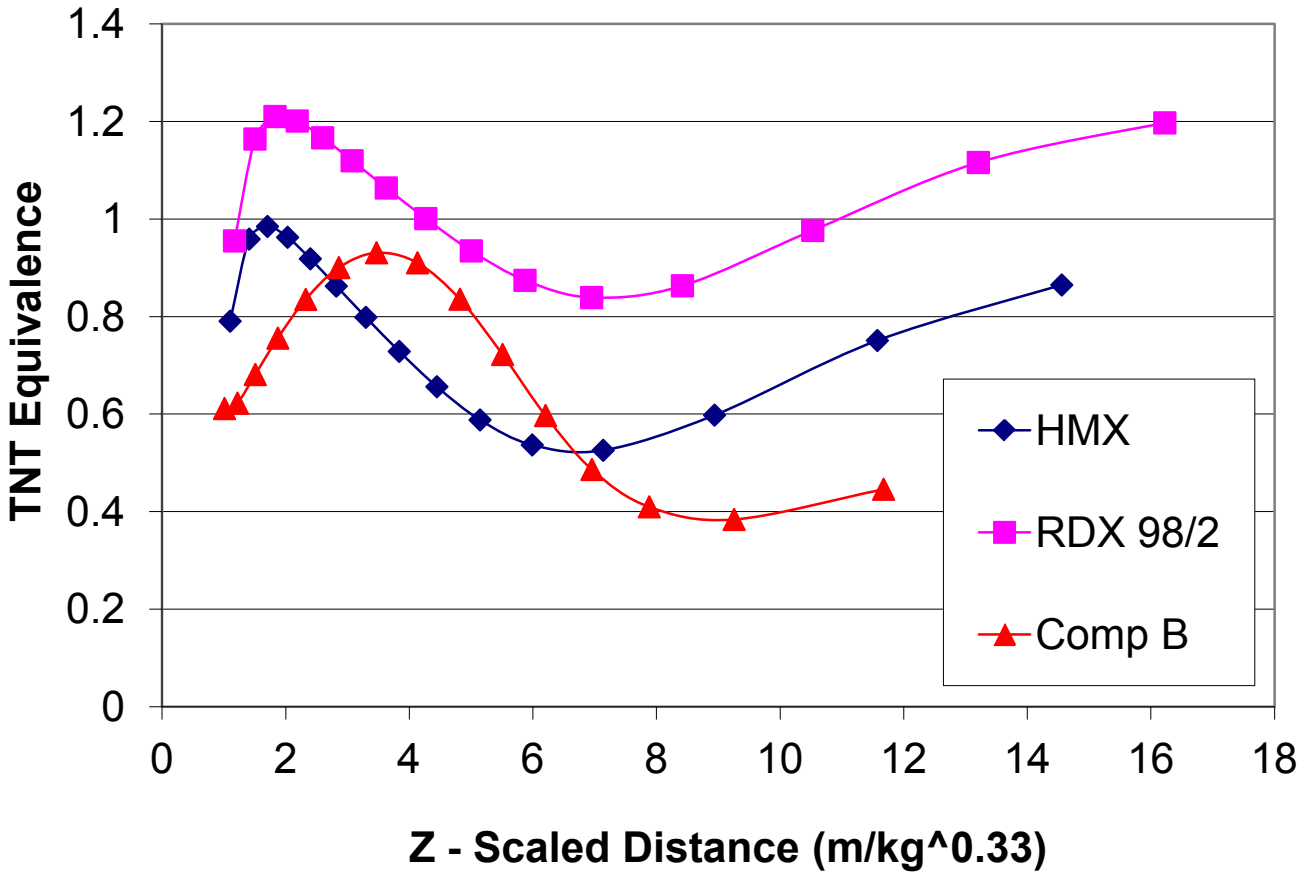

Figure 4. TNT Equivalence for Peak Positive Incident Pressure

(from UFC 3-340-02 data)

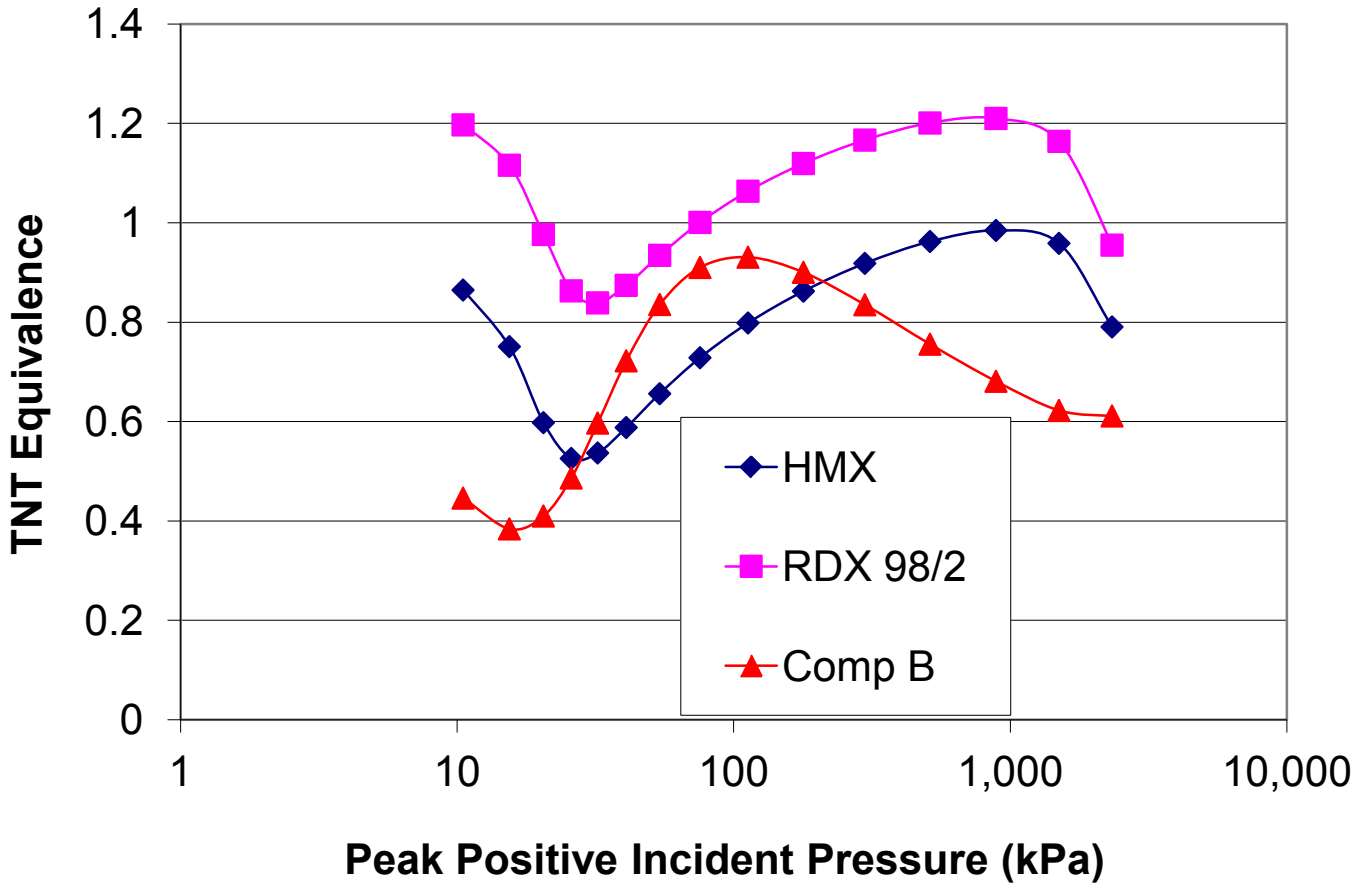

Figure 5. TNT Equivalence for Impulse

(from UFC 3-340-02 data)

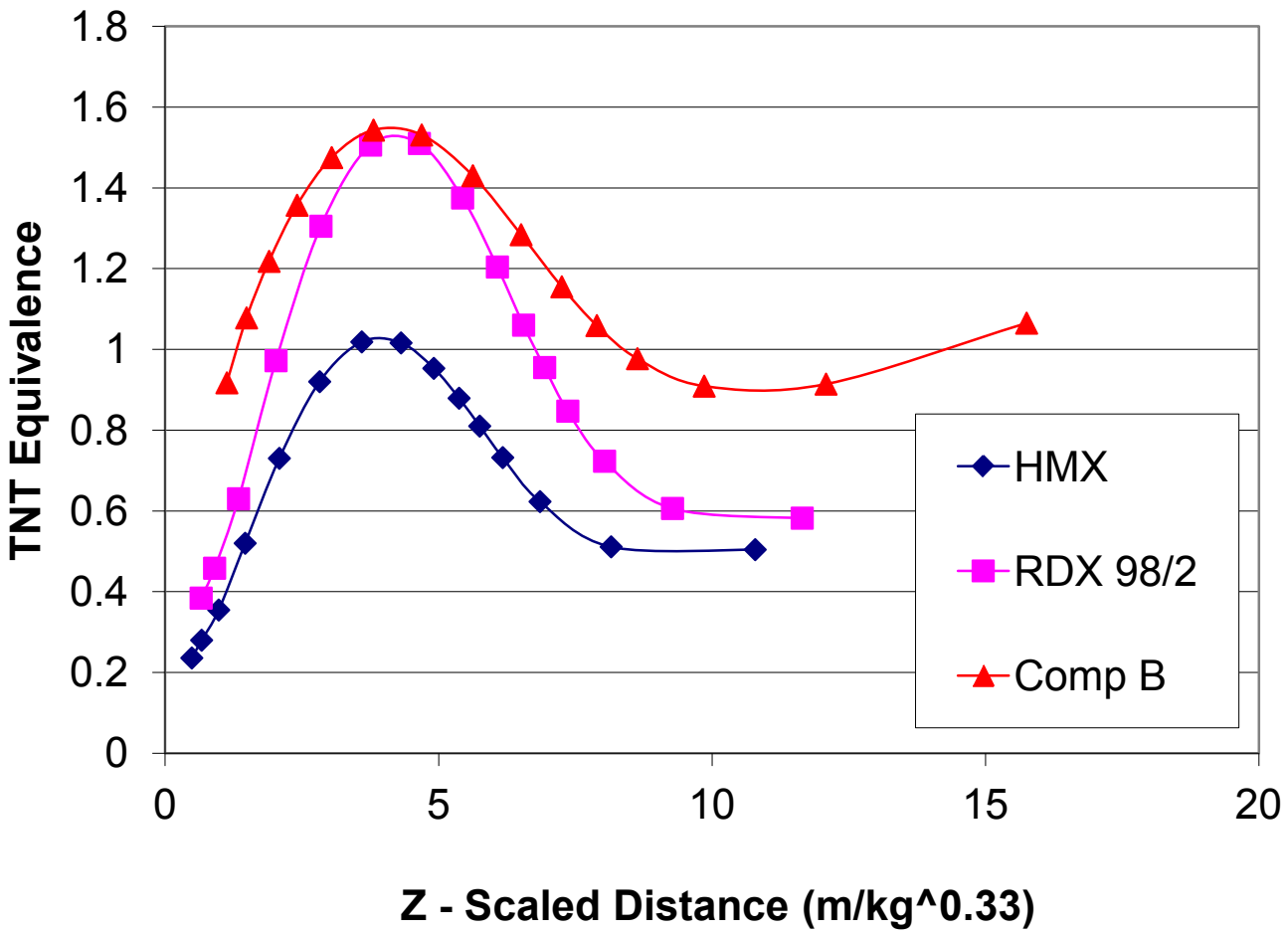

Figure 6. TNT Equivalence for Impulse

(from UFC 3-340-02 data)

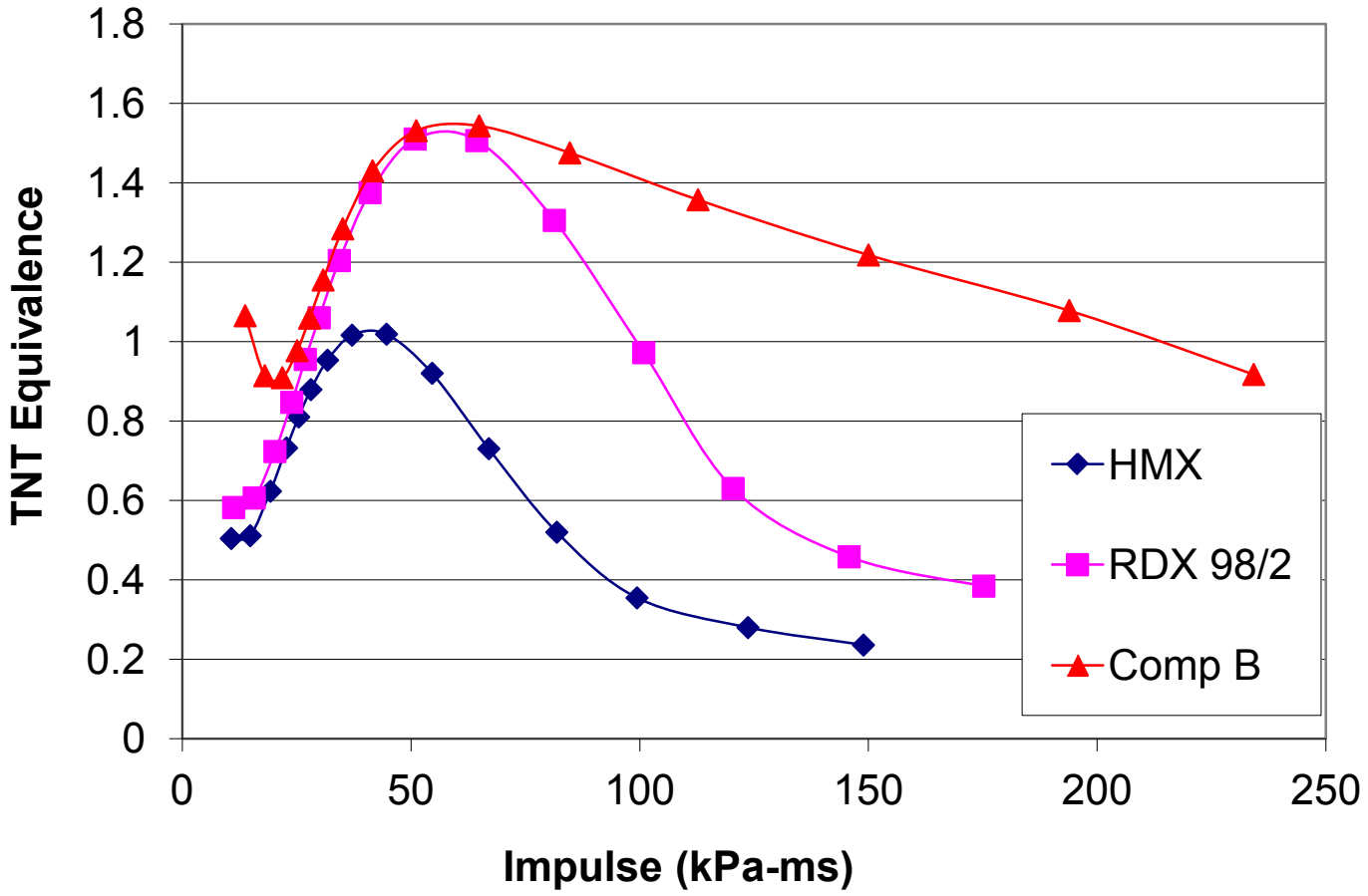

Table II. TNT Equivalence from UFC 3-340-02 Data

(from Figures 3 – 6)

Explosive	TNT Equivalence (%)	
	Peak Incident Pressure	Peak Incident Impulse
HMX	99	102
RDX 98/2	121	151
Comp B	93	154

Theoretical Methods for TNT Equivalence (1 of 3)

- Berthelot Method (1892)
  - TNT Equivalent (%) = 840 . Δn . (- ΔH_R^O) / Molwt $_{EXP}$ ^{2}

    Where:

    Δn – Number of moles of gases / mol of explosive

    ΔH_R^O – Heat of Detonation (kJ/mol)

    Molwt $_{EXP}$ – Molecular weight of the Explosive (g/mol)

- Cooper Method (D^2)
  - TNT Equivalence = D^2_{EXP} / D^2_{TNT}

    Where:

    D – Detonation Velocity (m/s)

BAE SYSTEMS

Theoretical Methods for TNT Equivalence (2 of 3)

- Hydrodynamic Work (E)

  - $E = \int_{P\,CJ}^{P\,AMB} P(V)_S \,.\, dV = 0.36075 \,.\, P_{CJ} / \rho_O \,\hat{}\, 0.96$

    Where:

    P_{CJ} – Chapman-Jouguet (CJ) Detonation Pressure (Pa)

    ρ_O – Density of unreacted explosive (kg/m^3)

- Power Index (PI) – related to Explosive Power (EP) = $Q_{EXP} \,.\, V_{EXP} \,.\, R / (V_{MOL} \,.\, C)$

  - Power Index = $Q_{EXP} \,.\, V_{EXP} / Q_{TNT} \,.\, V_{TNT}$

    Where:

    C – Mean Heat capacity of gases from detonation to stp (J/kg/K)

    Q_{EXP} – Heat of Detonation of explosive for comparison (J/kg)

    Q_{TNT} – Heat of Detonation of TNT (J/kg)

    V_{EXP} – Volume of gases at stp / Mass of explosive for comparison (m^3/kg)

    $V_{MOL} = 22.4$ – Molar volume of gas at stp (m^3/mol)

    V_{TNT} – Volume of gases at stp / Mass of TNT (m^3/kg)

Theoretical Methods for TNT Equivalence (3 of 3)

- Heat of Detonation (Q) – the TM / UFC Standard
  - TNT Equivalence (by Q) = Q_{EXP} / Q_{TNT}

    Where:

    Q_{EXP} – Heat of Detonation of explosive for comparison (J/kg)

    Q_{TNT} – Heat of Detonation of TNT (J/kg)

- Heat of Detonation (Q) – Updated method in paper
  - TNT Equivalence (by Q) = $Q_{EXP} / (Q_{TNT} (1 - d) + m . Q_{EXP})$

    Where:

    d – Line intercept = 0.76862

    m – Line gradient = 0.7341

Figure 7. TNT Equivalence Difference for Heat (Q)

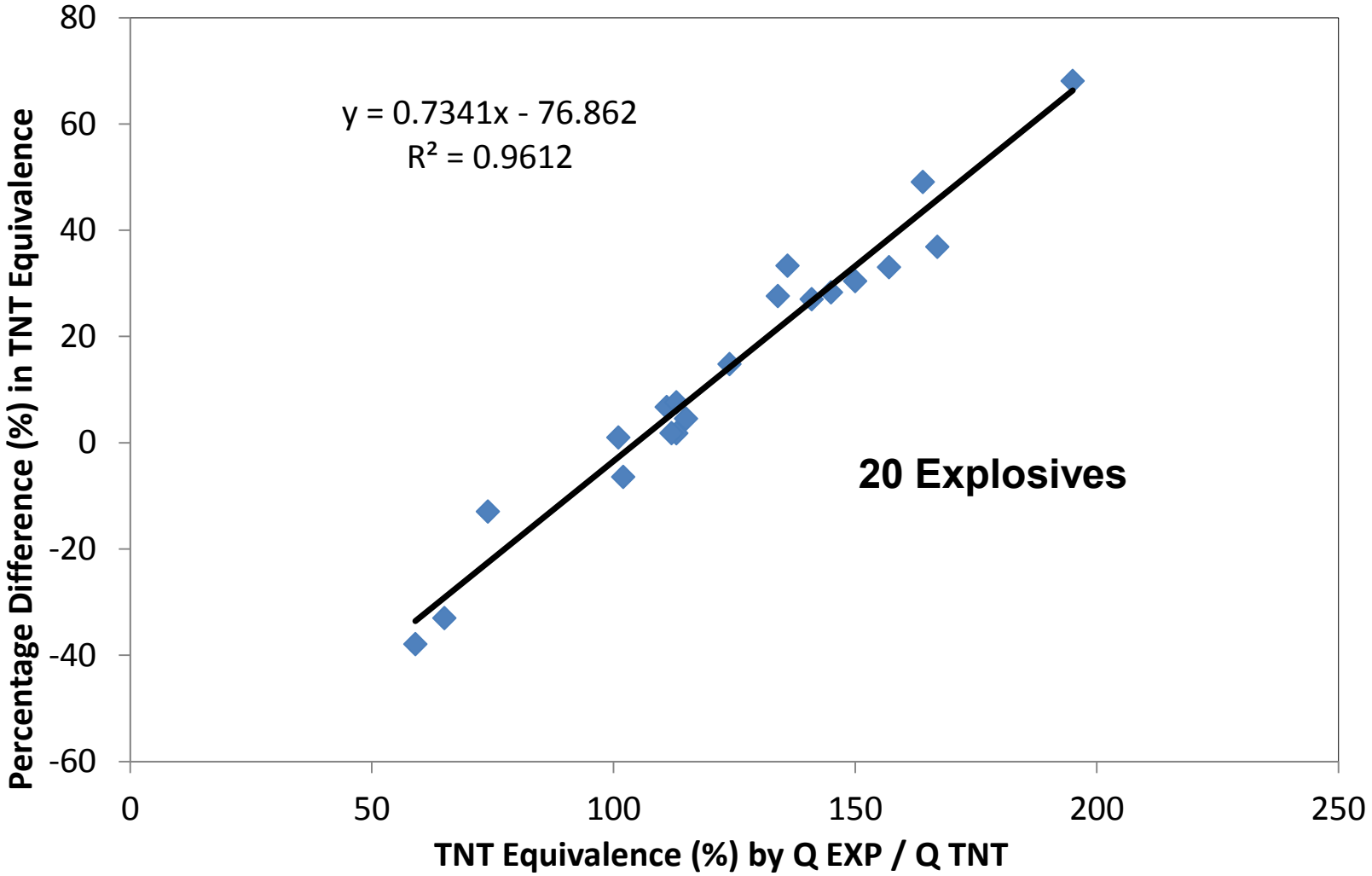

Figure 8. TNT Equivalence Difference for Heat (Q)

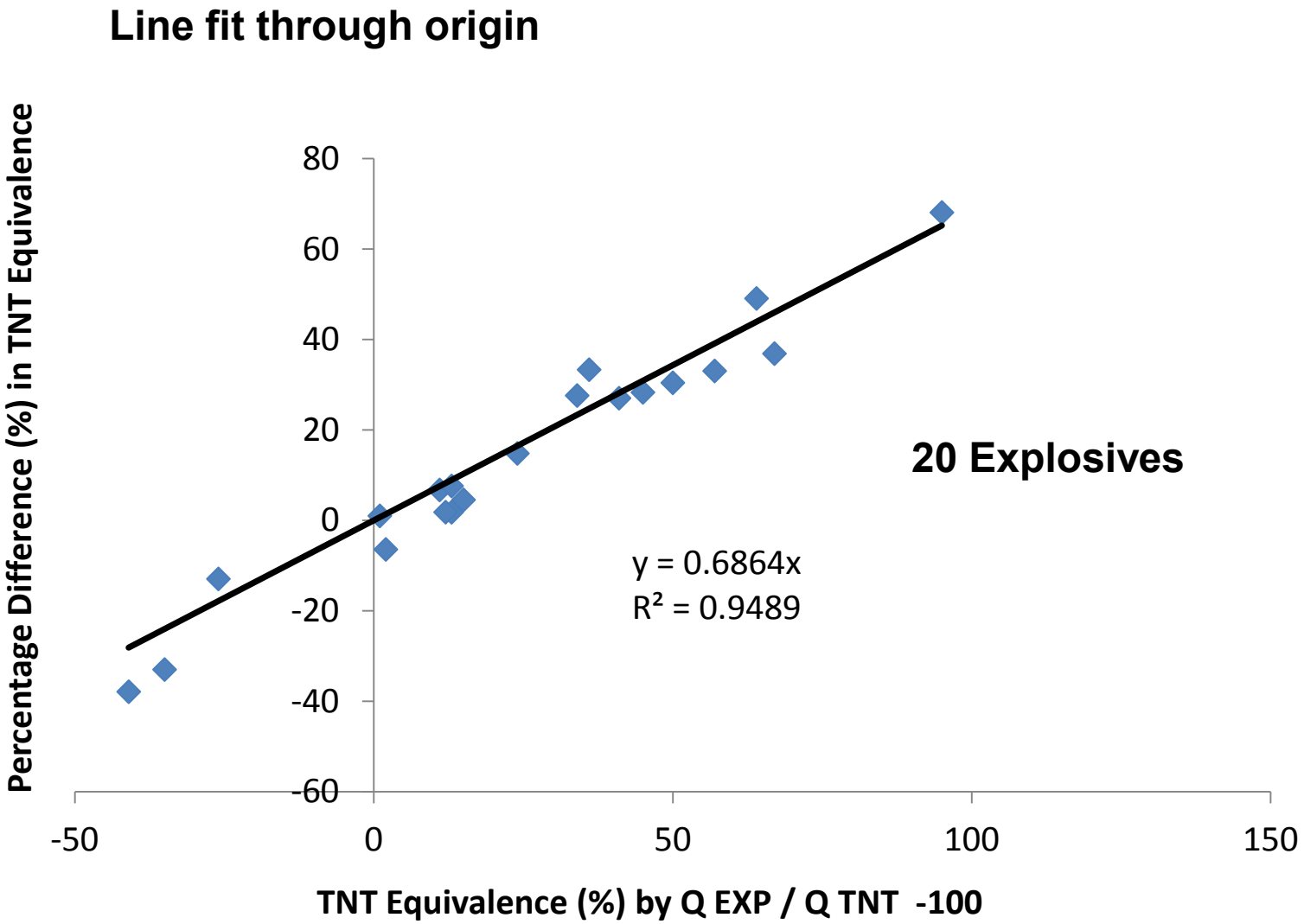

Table III. Some TNT Equivalence Comparisons by Percentage

Table III - has been updated and replaced by Table VI

BAE SYSTEMS

Table IV. Comparison of Work TNT Equivalence Predictions

Explosive	Density (g/cc)	Heat of Detonation (MJ/kg)	CJ Pressure (GPa)	TNT Equivalence (%)				
				Expt	Calc from E	Difference, from E to Expt	Calc from PI	Difference, from PI to Expt
Non-Aluminised								
Ammon. Picrate	1.55	3.349	19.3	85	98	**15.1**	92	**8.4**
Amatol 60/40	1.50	2.638	13.3	95	69	**-26.9**	112	**17.4**
Amatol 50/50	1.55	2.931	16.4	97	84	**-13.9**	114	**17.3**
Comp A-3	1.59	4.605	27.5	109	136	**25.1**	141	**29.5**
Comp B	1.68	5.192	26.9	110	127	**15.3**	131	**18.7**
Comp C-3	1.60	6.071	24.5	105	121	**15.0**	135	**28.7**
Cyclotol 75/25	1.71	5.150	28.3	111	131	**18.4**	137	**23.8**
Cyclotol 70/30	1.73	5.066	29.1	110	134	**21.4**	135	**22.5**
Cyclotol 60/40	1.72	5.024	27.8	104	128	**23.4**	130	**24.5**
Ednatol 55/45	1.63	5.610	23.0	108	112	**3.3**	122	**13.3**
Pentolite 50/50	1.66	5.108	24.2	105	115	**9.7**	122	**16.0**
Picratol 52/48	1.63	4.564	20.8	100	101	**0.6**	103	**3.3**
PTX-1	1.64	6.364	25.2	111	121	**9.3**	123	**10.7**
PTX-2	1.70	6.531	28.8	113	134	**18.6**	133	**17.5**
Aluminised								
DBX	1.65	7.118	18.8	118	90	**-23.7**	143	**21.3**
HBX-3	1.81	8.834	22.3	116	98	**-15.6**	74	**-36.3**
MINOL-2	1.68	6.783	14.8	115	70	**-39.2**	145	**25.7**
MOX-2B	2.00	6.155	11.3	102	45	**-55.8**	49	**-52.3**
Torpex	1.81	7.536	26.1	122	115	**-5.9**	143	**17.5**
Tritonal	1.72	7.411	19.3	110	89	**-18.8**	120	**9.1**
				Mean Absolute Difference		**18.8**		**20.7**

Figure 9. TNT Equivalence Difference comparison for Work

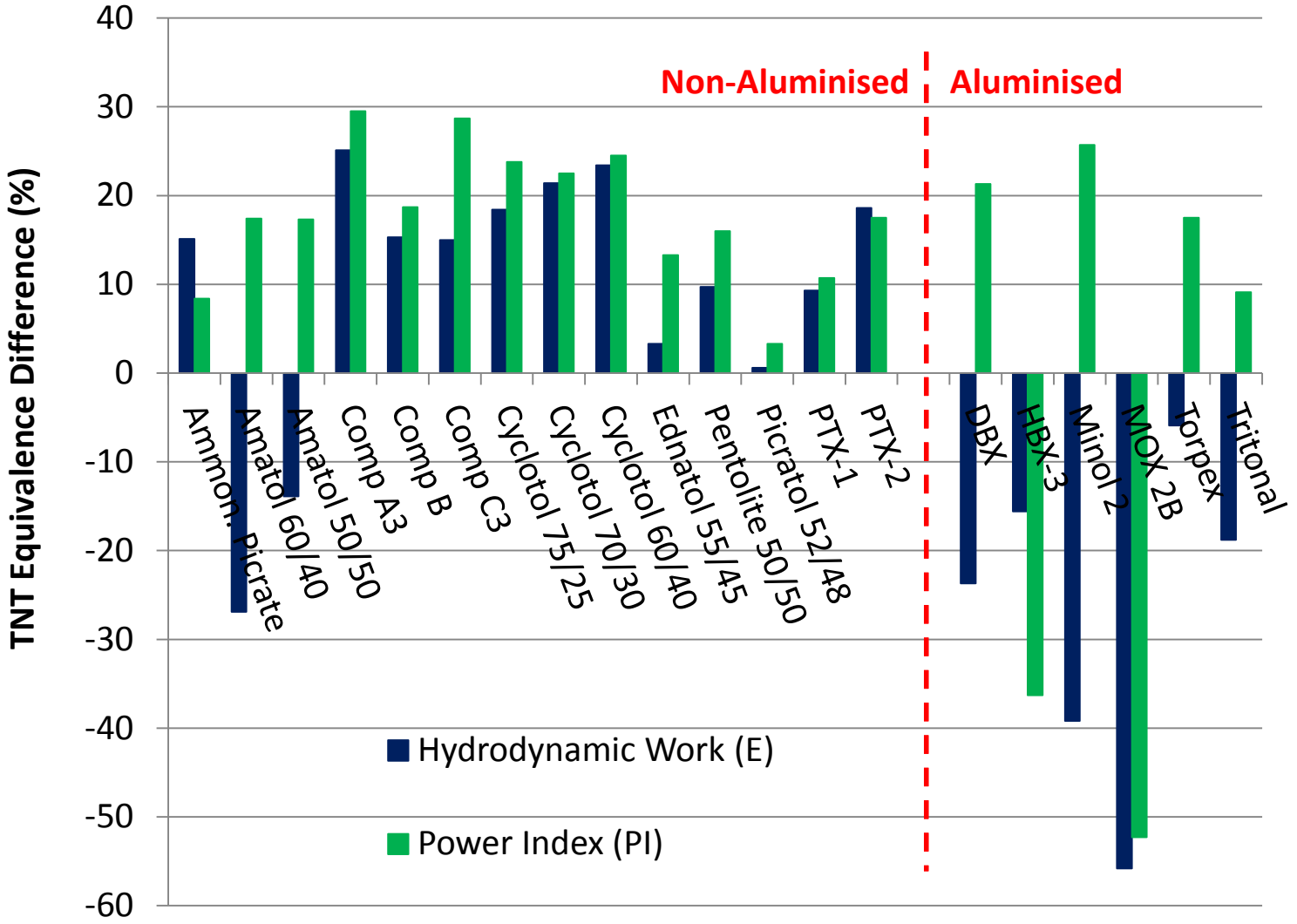

BAE SYSTEMS

Table V. Comparison of Heat TNT Equivalence Predictions

Explosive	TNT Equivalence (%)				
	Expt	Standard Calc from Heat (Q)	Difference, from Standard Q to Expt	Updated Calc from Heat (Q)	Difference, from Updated Q to Expt
Non Aluminised					
Ammon. Picrate	85	74	-12.9	96	12.4
Amatol 60/40	95	59	-37.9	88	-6.9
Amatol 50/50	97	65	-33.0	92	-5.5
Comp A-3	109	102	-6.4	104	-4.6
Comp B	110	115	4.5	107	-2.8
Comp C-3	105	134	27.6	110	5.1
Cyclotol 75/25	111	113	1.8	107	-3.9
Cyclotol 70/30	110	112	1.8	106	-3.4
Cyclotol 60/40	104	111	6.7	106	2.0
Ednatol 55/45	108	124	14.8	109	0.6
Pentolite 50/50	105	113	7.6	107	1.4
Picratol 52/48	100	101	1.0	104	3.8
PTX-1	111	141	27.0	111	0.3
PTX-2	113	145	28.3	112	-1.0
Aluminised					
DBX	118	157	33.1	113	-3.8
HBX-3	116	195	68.1	117	1.1
MINOL-2	115	150	30.4	113	-2.1
MOX-2B	102	136	33.3	111	8.4
Torpex	122	167	36.9	115	-6.1
Tritonal	110	164	49.1	114	3.9
	Mean Absolute Difference		23.1		4.0

Figure 10. TNT Equivalence Difference comparison for Heat

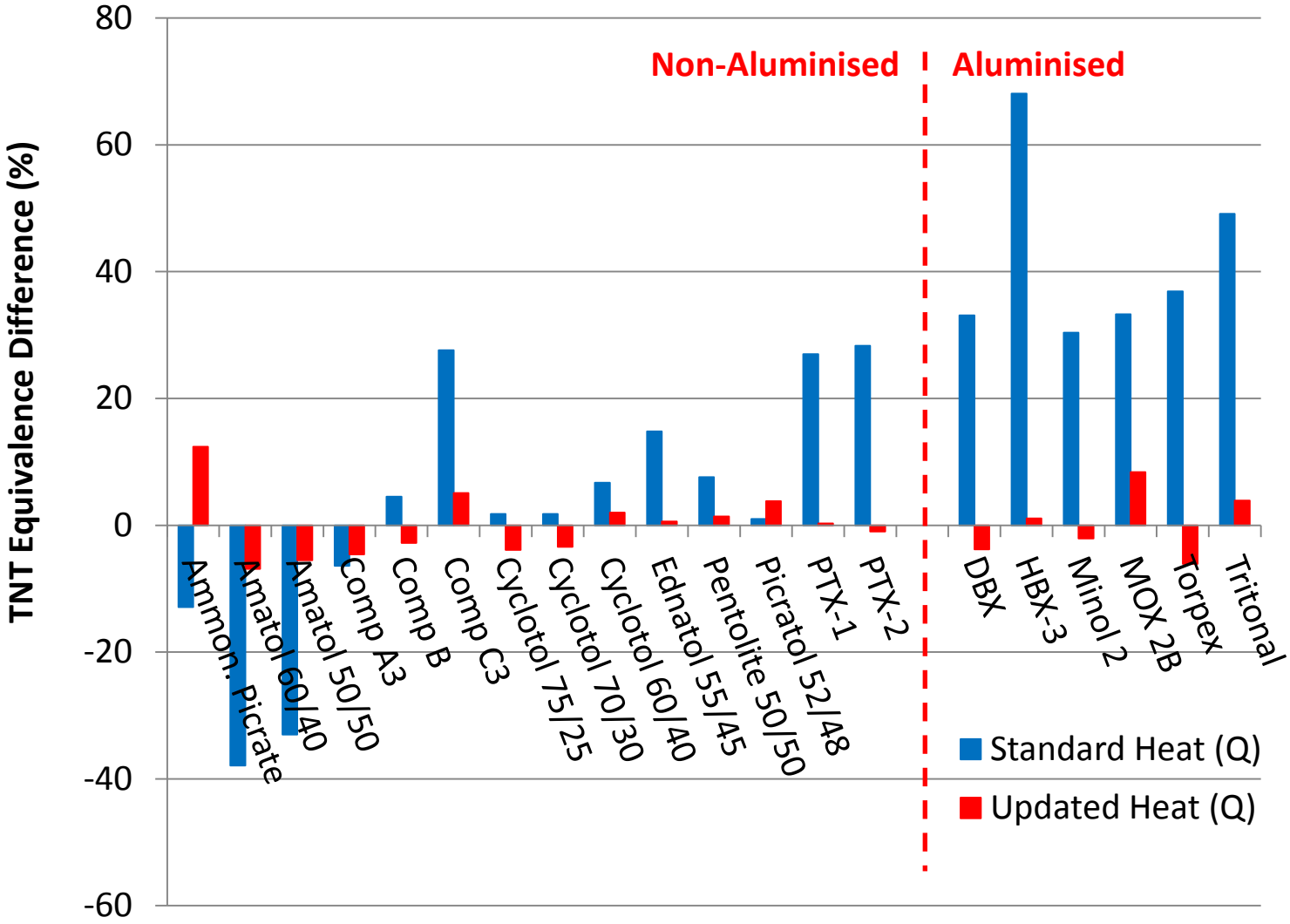

BAE SYSTEMS

Table VI. TNT Equivalence Comparisons by Percentage

Explosive	From Expt	Berthelot Method	Difference Bethelot from Expt (%)	D^2 Method	Difference D^2 from Expt (%)
Non-Aluminised					
Ammon. Picrate	85	110	29.1	109	27.8
Amatol 60/40	95	138	45.6	137	43.8
Amatol 50/50	97	136	39.9	128	31.5
Comp A-3	109	168	54.5	136	24.5
Comp B	110	156	41.5	132	19.8
Comp C-3	105	161	53.5	132	26.1
Cyclotol 75/25	111	164	47.6	139	25.0
Cyclotol 70/30	110	161	46.1	136	23.4
Cyclotol 60/40	104	154	48.5	130	25.1
Ednatol 55/45	108	99	-7.9	67	-38.2
Pentolite 50/50	105	145	38.0	119	13.4
Picratol 52/48	100	115	14.5	105	4.5
PTX-1	111	147	32.0	123	10.8
PTX-2	113	158	40.1	133	17.4
Aluminised					
DBX	118	171	44.6	115	-2.7
HBX-3	116	90	-22.5	86	-26.0
MINOL-2	115	171	48.8	115	0.2
MOX-2B	102	58	-43.0	126	23.8
Torpex	122	171	40.1	110	-9.9
Tritonal	110	143	30.3	85	-22.5
	Mean Absolute Difference		38.4		20.8

Figure 11. TNT Equivalence Difference for Berthelot and Cooper (D^2)

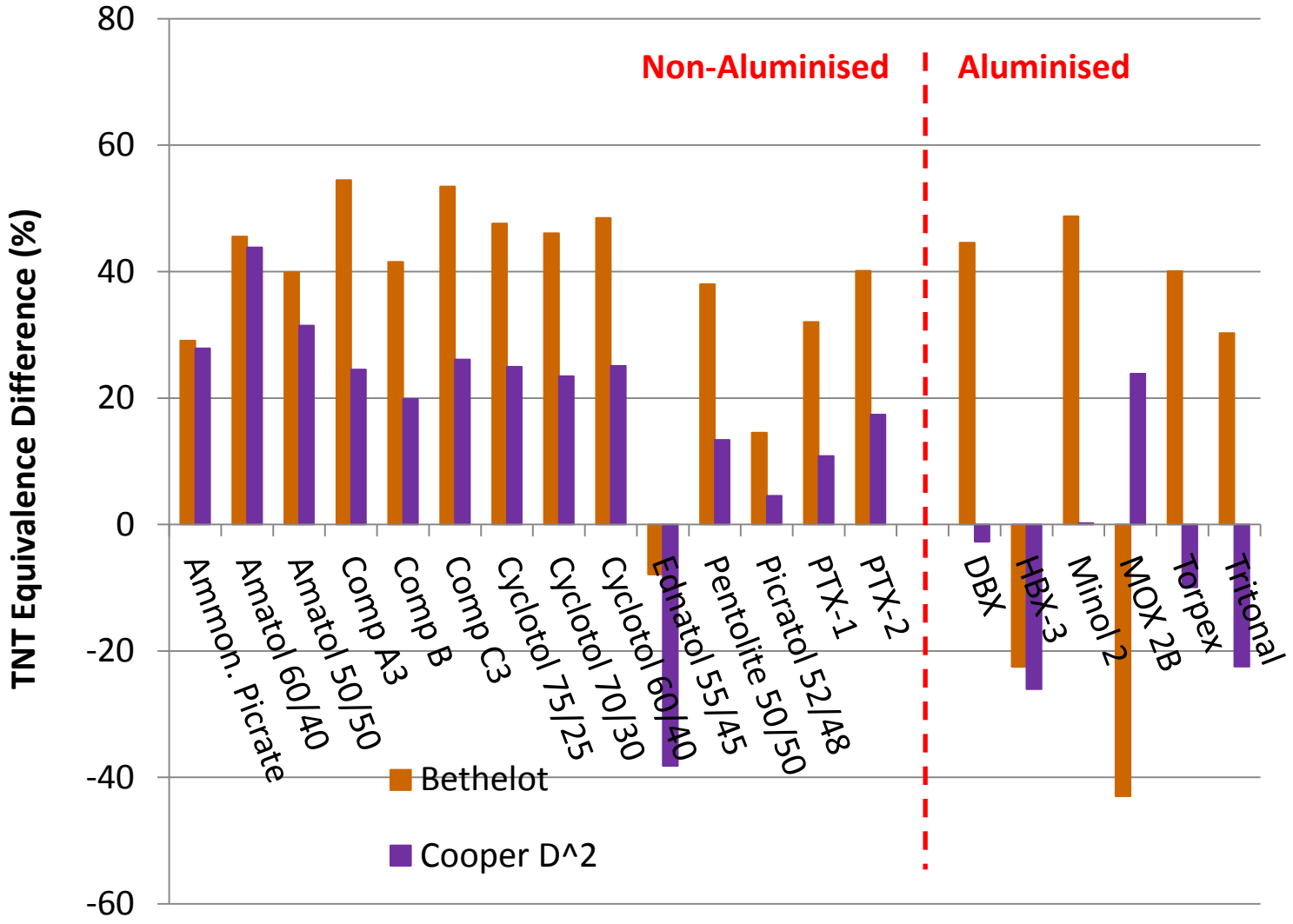

BAE SYSTEMS

Table VII. Error Level Analysis of Methods

TNT Equivalence Difference (%) across the Methods

Method	Mean Absolute Difference	Standard Deviation	Maximum Absolute Difference	Ratio of Absolute Difference to Standard Deviation
Berthelot	**38.4**	**26.3**	**54.5**	**2.1**
D^2 (Cooper)	**20.8**	**21.4**	**43.8**	**2.0**
Hydrodynamic Work Function (E)	**18.8**	**22.9**	**55.9**	**2.4**
Power Index (PI)	**20.7**	**20.5**	**52.3**	**2.6**
Standard Heat (Q)	**23.1**	**26.1**	**68.1**	**2.6**
Updated Heat (Q)	**4.0**	**5.0**	**12.4**	**2.5**
Updated Heat (Q) with fit through point (100,0)	18.4	23.4	55.8	2.4

Ratios of 2 - 3 are typical for a Normal Distribution from a small sample

Conclusion

- A big problem with TNT Equivalence, typically 20% - 30% error
- Scaling Laws – they don't scale for Equivalence
- Five Theories have been detailed
- Theories compared to limited (open) trials data
- Power Index (PI) is the most reliable to date (21%)
  - Accounts for both Heat produced and Work available
- Recommended Standard Heat of Detonation (Q) is poor (26%)
  - But can be adjusted (Q update) to give the best of all fits (5%)

BAE SYSTEMS

Any Questions ?

Paul M. Locking

BAE Systems

+44-(0)1793-78-6427

paul.locking@baesystems.com

ALLEN VANGUARD™

DEFEATING THE THREAT™

Survivability Evaluation of Blast Mitigation Seats for Armored Vehicles

Ming Cheng, Doug Bueley, Jean-Philippe Dionne, Aris Makris

September 15, 2011

OUTLINE

- **Survivability Evaluation Methods for Blast Mitigation Seats**
  - *Field blast-off tests*
  - *Laboratory blast simulation tests (drop-tower and sled)*
- **Seating system analysis**
  - *Analytical modeling*
  - *LS-Dyna FEA analysis*
- **Discussions**

Platform Survivability ≠ Crew Survivability

- **Existing military vehicles retrofitted with add-on ballistic panels**
- **Objective is to defeat emerging threat**
  - IEDs (underbelly, roadside)
  - EFPs, etc.

- **Threat of penetrating vehicle hull has been reduced**
- **Occupant injuries persist**
  - *High-speed impact generates high acceleration on the occupants.*

Vehicle armor

Blast Mitigation Seats for Armored Vehicles

Floor Mounted

Wall Mounted

Ceiling Mounted

Injury Criteria and Tolerance Levels

	Injury Criteria	Tolerance Level	Signification	Specification
Thoraco-Lumbar spine	**Dynamic Response Index (DRIz)**	**17.7**	10% risk of AIS 2+	Based on H3 pelvis vertical acceleration
Lower leg	**Peak lower tibia compression force (-Fz)**	**5.4 kN**	10% risk of AIS 2+	Lower leg position straight upward
Neck	**Compression force (-Fz)**	**4 kN @ 0 ms 1.1 kN @ 30 ms**	Serious (AIS 3) injuries unlikely below tolerance level	Measured at the H3 upper neck
	Peak flexion bending moment (+My)	**190 N-m**	Significant (AIS 2+) injuries unlikely below tolerance level	Measured at the H3 upper neck
	Peak extension bending moment (-My)	**57 N-m**	Significant (AIS 2+) injuries unlikely below tolerance level	Measured at the H3 upper neck
Non-auditory internal organs	**Chest wall velocity predictor (CWVP)**	**3.6 m/s**	No injury	Based on reflection pressure measurement

— AEP-55 Vol. 2 and NATO/RTO HFM-090/TG-25, April 2007

Note: 1) Injury criteria and tolerance levels based on 50th Hybrid III mannequin (occupant) safety
2) Seating can address everything except tibia and chest

Dynamic Response Index (DRI)

$$\zeta = \frac{c}{2m\omega_n} = 0.224$$

$$\omega_n = \sqrt{\frac{k}{m}} = 52.9\ rad/s$$

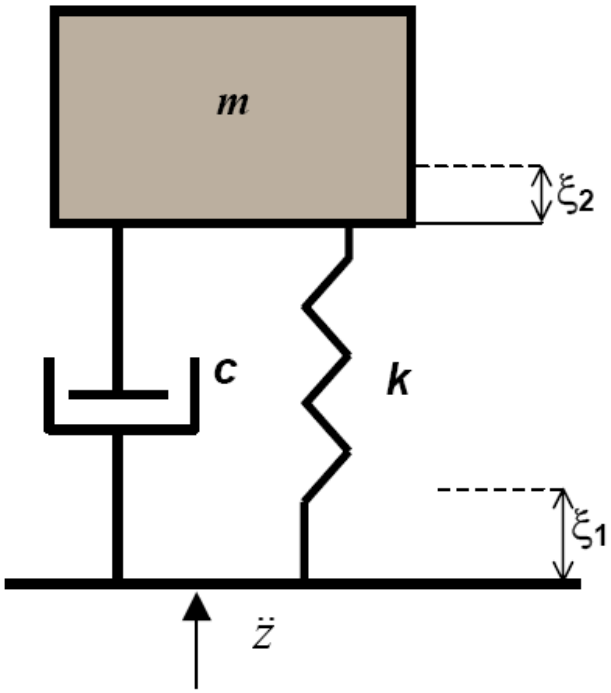

$$\delta(t) = \xi_1 - \xi_2$$

$$\ddot{Z}(t) = \ddot{\delta}(t) + 2\zeta\omega_n\dot{\delta}(t) + \omega_n^2\delta(t)$$

$$DRI_z = \frac{\omega_n^2\,\delta_{\max}}{g} < 17.7 \quad or \quad \delta_{\max} < 62\,\text{mm}$$

Seat Evaluation — Field Blast-Off Tests

Full-Size Vehicle

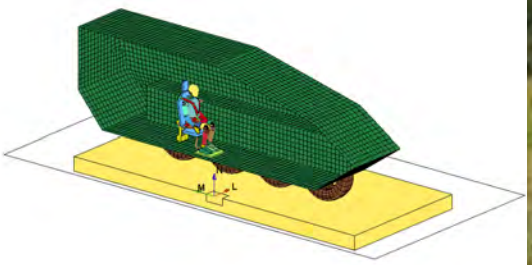

IABG

Surrogate Vehicle Hull

Seat Evaluation — Laboratory Impact Tests

Drop-tower

Various Test Methodologies

	Field Blast Tests		Laboratory Impact Tests	
	Full-size	Surrogate	Drop-Tower	Sled
Objective	Vehicle platform and crew survivability against IEDs of a specific threat level		Seat performance evaluation against a specific acceleration impact pulse	
Closeness to reality	Excellent	Fair	Poor	Poor
Repeatability	Poor	Poor	Good	Good
Seat potential	Poor	Poor	Good	Good
Accel pulse representative	Excellent	Good	(Depending)	Poor
Vehicle Response	Included	Surrogate-dependent	Not included	Not included
Cost	High	Median	Low	Low

Seating System Modeling

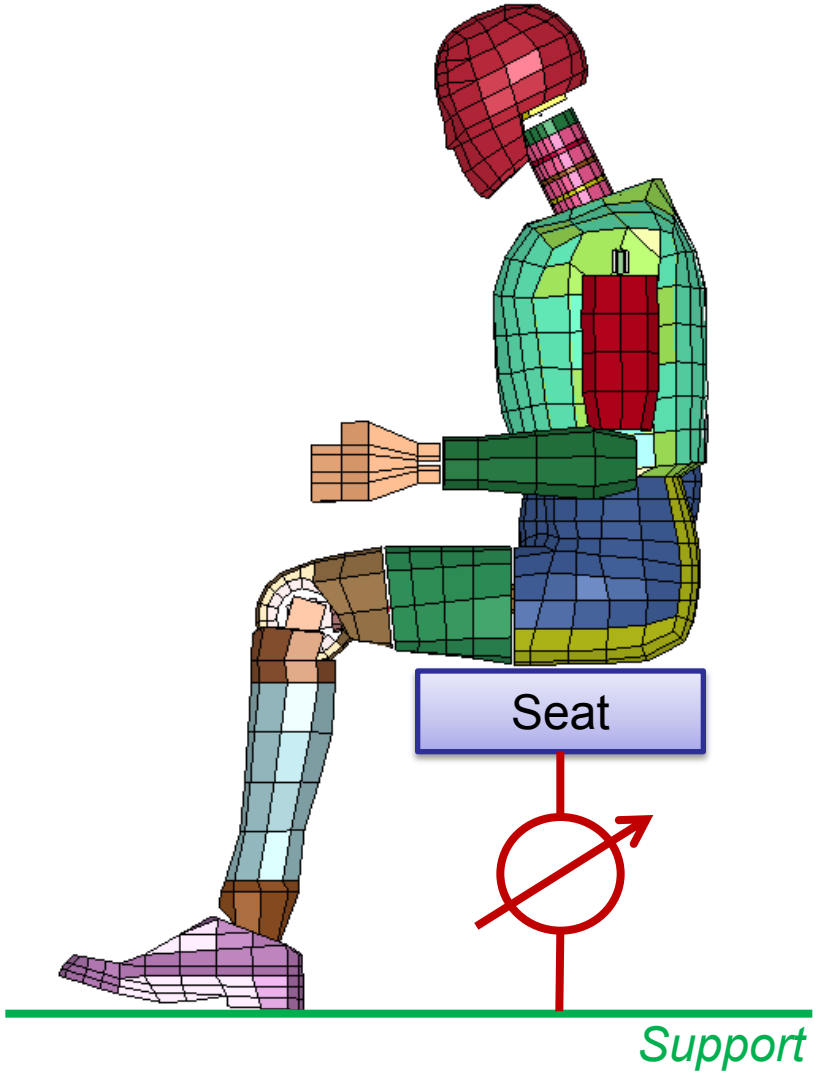

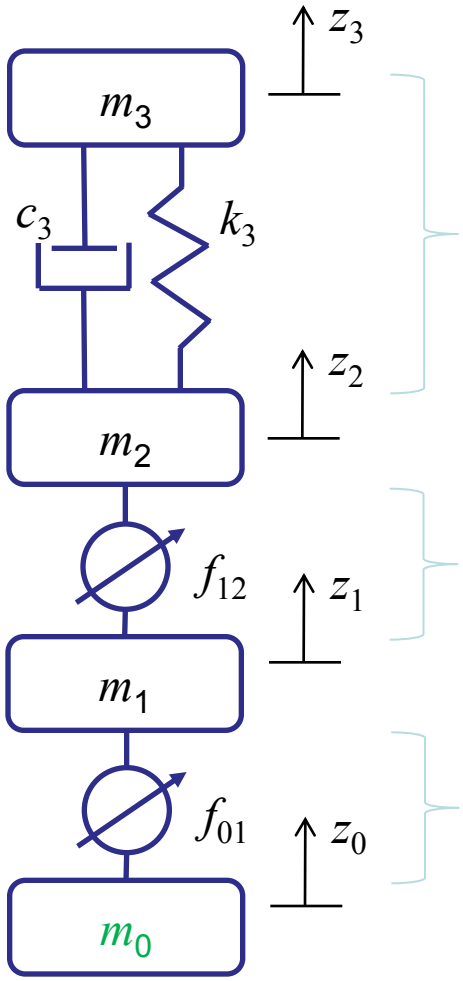

DRI model
(AEP-55 V2, STANAG 4569)

$$\omega_n = \sqrt{\frac{k_3}{m_3}} = 52.9 \text{ rad/s}$$

$$\zeta = \frac{c_3}{2 \cdot m_3 \cdot \omega_n} = 0.224$$

Lower portion
of the mannequin

Cushion contact

Shock Attenuation
Mechanism

Mass of the Support (m_0)

Test Type	Support	Mass (kg)	Direction of Motion
Field blast-off tests	Full-size vehicle	3,000 ~ 50,000	Vertical (Up)
	Surrogate	500 ~ 2,000	Vertical (Up)
Laboratory simulation tests	Sled	200 ~ 2,000	Horizontal
	Tower carriage	100 ~ 300	Vertical (Down & Up)

The mass of the support has a significant influence on the test results

Analytical Modeling of Seating System

Mass above spinal column

Mass under spinal column

Seat

Vehicle platform or drop-tower carriage

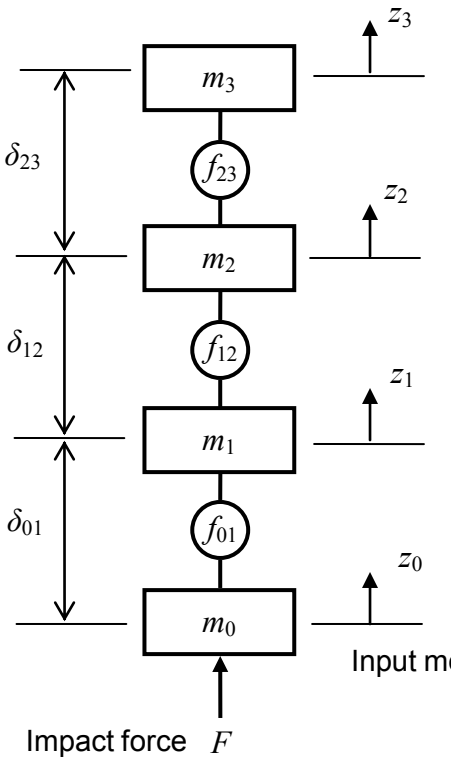

Spinal column

Cushion

Shock absorber

Input motion

Control Forces

$$f_{ij} = f_{ij}\ \ \delta_j, \quad \dot{\delta}_j$$

Equation of Motion

$$\begin{Bmatrix} \ddot{\delta}_{01} \\ \ddot{\delta}_{12} \\ \ddot{\delta}_{23} \end{Bmatrix} + \begin{bmatrix} m_1 & & \\ & m_2 & \\ & & m_3 \end{bmatrix}^{-1} \begin{Bmatrix} f_{01} - f_{12} \\ f_{12} - f_{23} \\ f_{23} \end{Bmatrix} = -\ddot{z}_0 \begin{Bmatrix} 1 \\ 1 \\ 1 \end{Bmatrix}$$

Note:
Same or close enough initial conditions can be achieved for different test methods.

Initial Conditions for Different Test Methods

Variables	Blast-Off	Drop-Tower	Sled
F	Explosion	Ground impact	Piston impact
f_{01}	Compressed	Decompressed	Decompressed
f_{12}	Compressed	Decompressed or decoupled	Decompressed or decoupled
f_{23}	Compressed	Decompressed	Decompressed
f_{34}	Compressed	Decompressed	Decompressed
δ_{01}	0	> 0	> 0
δ_{12}	0	> 0	> 0
δ_{23}	0	> 0	> 0
$d\delta_{01}/dt$	0	0	0
$d\delta_{12}/dt$	0	0	0
$d\delta_{23}/dt$	0	0	0

Can Drop-Tower Test Simulate Blast Test?

- **Drop-tower test can simulate the blast test if**
  - the base acceleration $\ddot{z}_0$ is controlled to be the same
  - the influence of the decompressions is small or compensated

- **However, in practice**
  - base acceleration $\ddot{z}_0$ is only controlled within the impact pulse duration
  - after the pulse duration, it depends on the mass of tower carriage and the characteristics of the shock attenuation mechanism.

Seating System Modeling

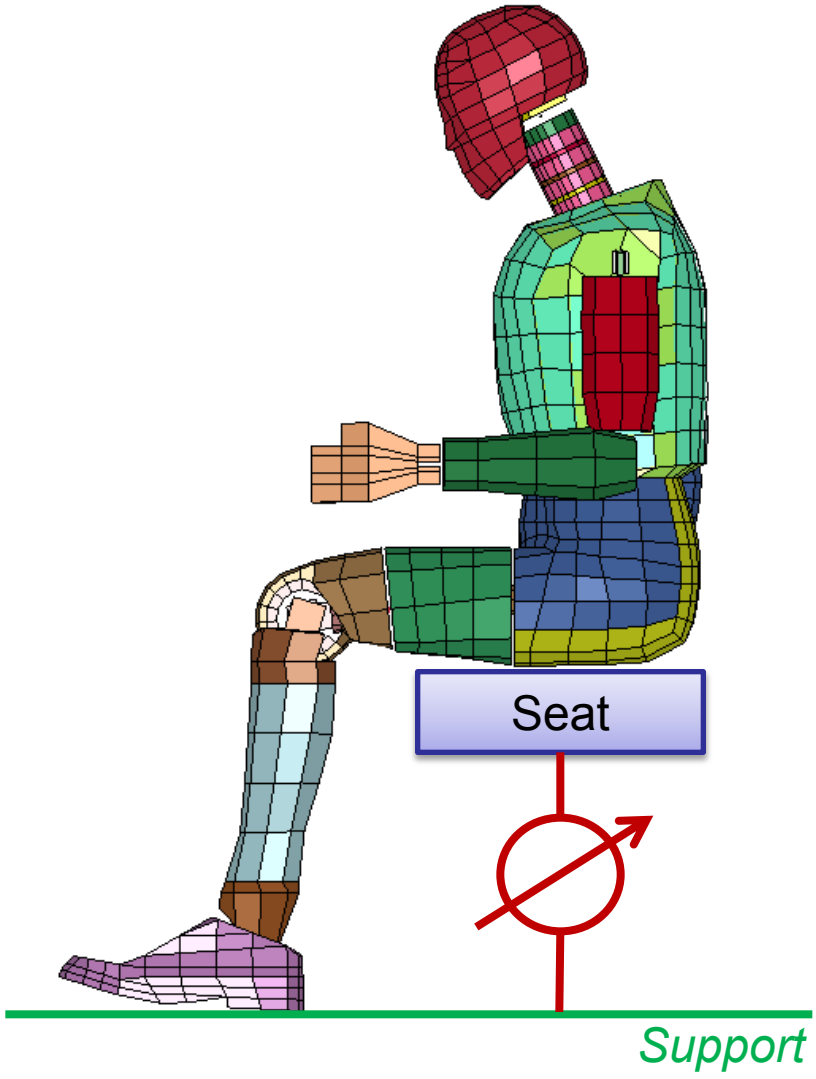

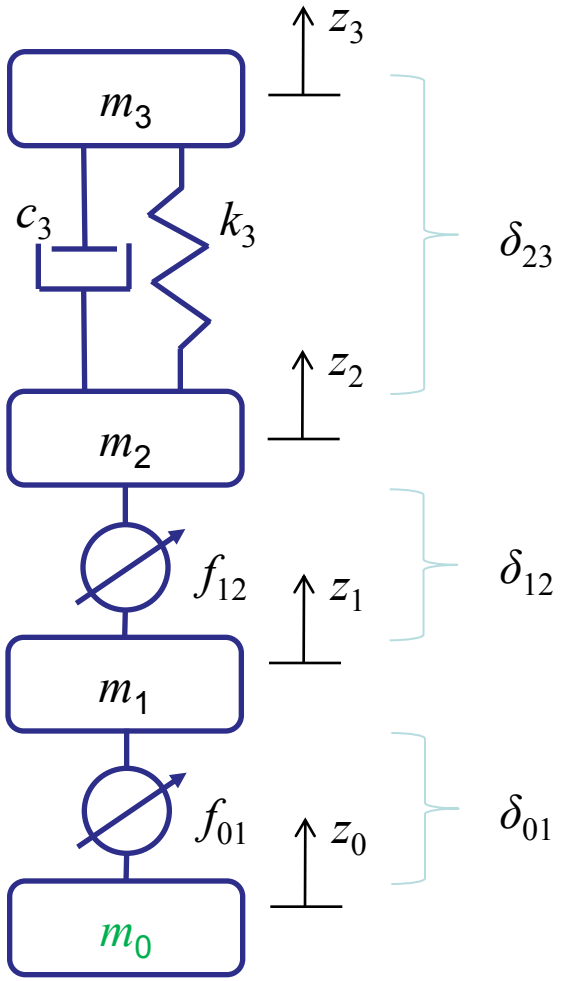

$$\ddot{z}_0(t) = \frac{F}{m_0} + \frac{f_{01}}{m_0}$$

Typical Drop-Tower Carriage Signal

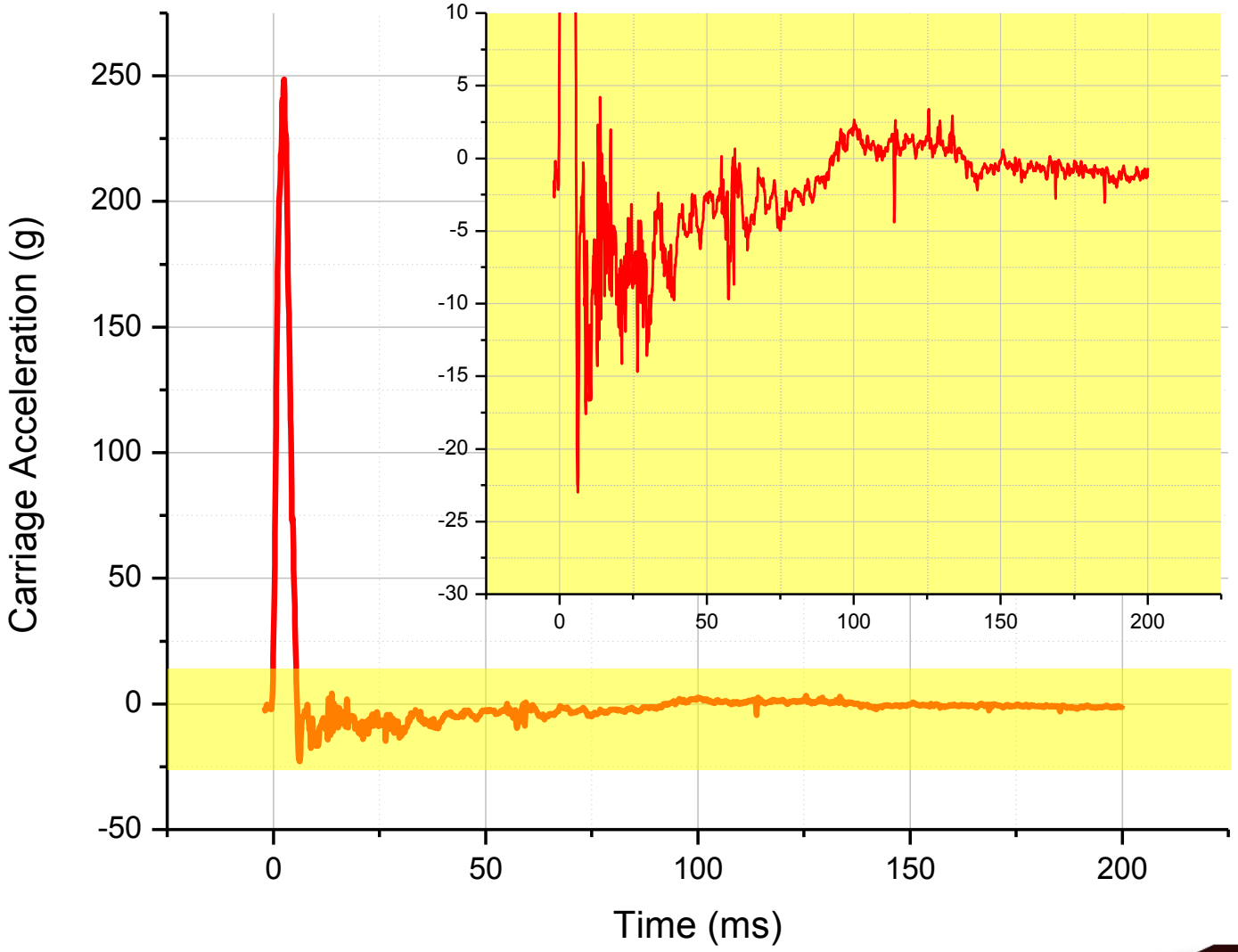

Pelvis Acceleration From Different Test Methods

$$\ddot{Z}_2^{\text{blast-off}} = \ddot{\delta}_{01}^{\text{blast-off}} + \ddot{\delta}_{12}^{\text{blast-off}} + \frac{F^{\text{blast-off}}}{m_0^{\text{blast-off}}} + \frac{f_{01}^{\text{blast-off}}}{m_0^{\text{blast-off}}}$$

$$\ddot{Z}_2^{\text{drop-tower}} = \ddot{\delta}_{01}^{\text{drop-tower}} + \ddot{\delta}_{12}^{\text{drop-tower}} + \frac{F^{\text{drop-tower}}}{m_0^{\text{drop-tower}}} + \frac{f_{01}^{\text{drop-tower}}}{m_0^{\text{drop-tower}}}$$

In the case of using a drop-tower test to simulate the blast-off test:

$$\ddot{Z}_2^{\text{blast-off}} \cong \ddot{Z}_2^{\text{drop-tower}} + \frac{f_{01}^{\text{drop-tower}}}{m_0^{\text{drop-tower}}}\left(1 - \frac{m_0^{\text{drop-tower}}}{m_0^{\text{blast-off}}}\right)$$

Effects of Carriage Mass on DRI

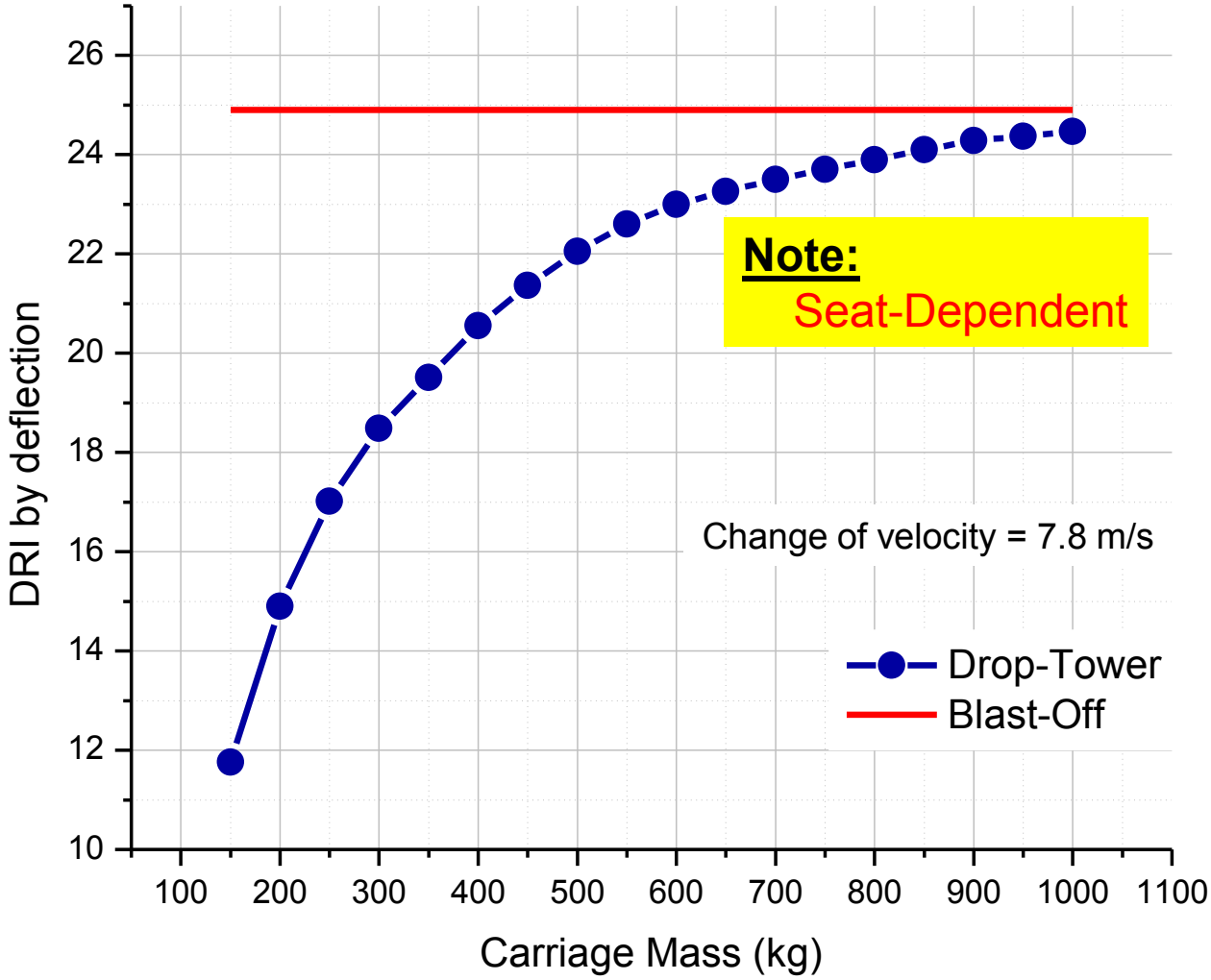

LS-Dyna Model for Simulating Drop-Tower Tests

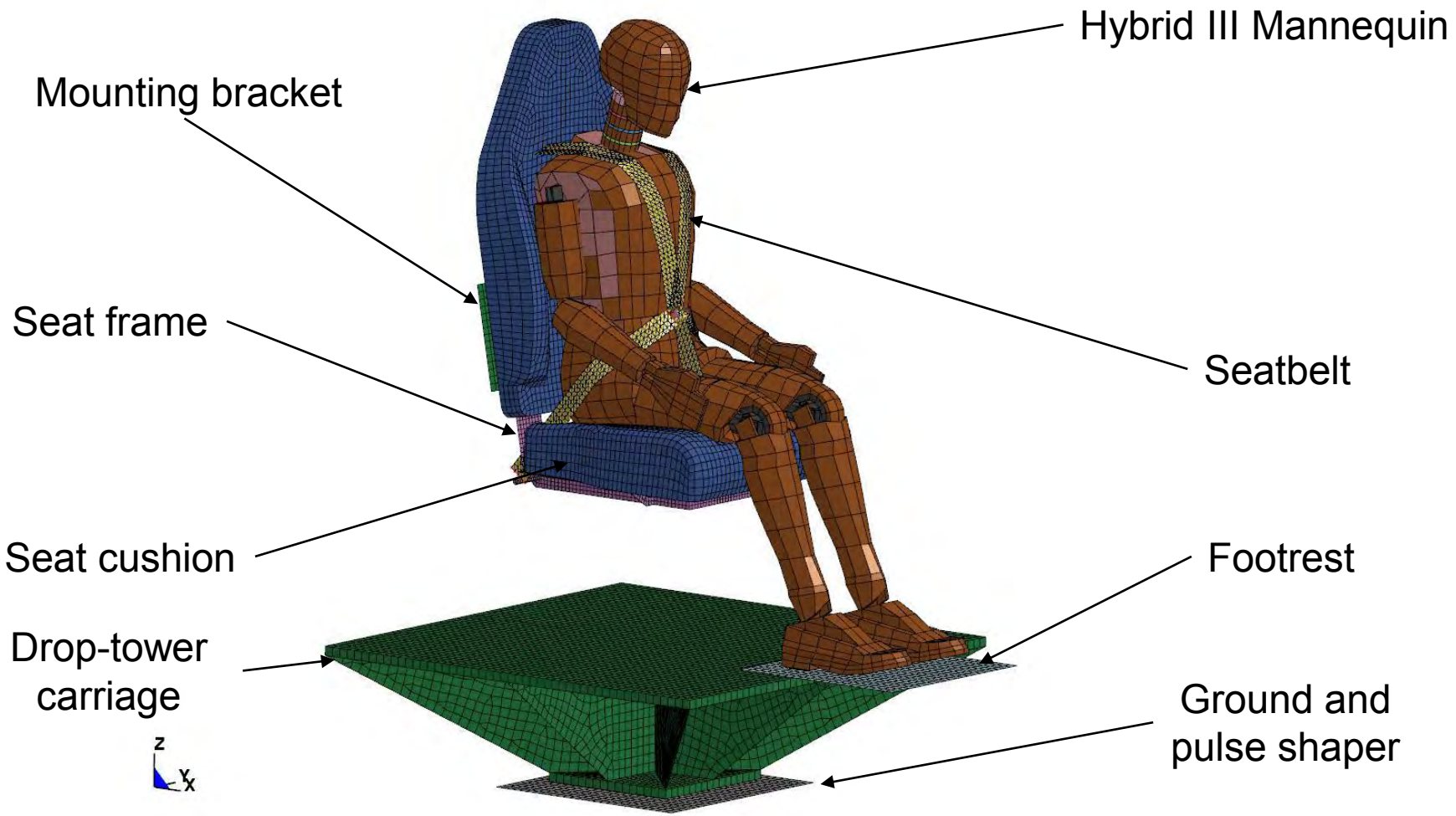

Drop-Tower Tests — Simulation Results

Config.	Impact Type	Pulse Shaper	Carriage Weight (kg)
1	Drop Tower	1/2" EPDM rubber	380
2	Drop Tower	1/2" EPDM rubber	600
3	Drop Tower	Heavy duty damper	380
4	Blast-off	n/a	∞

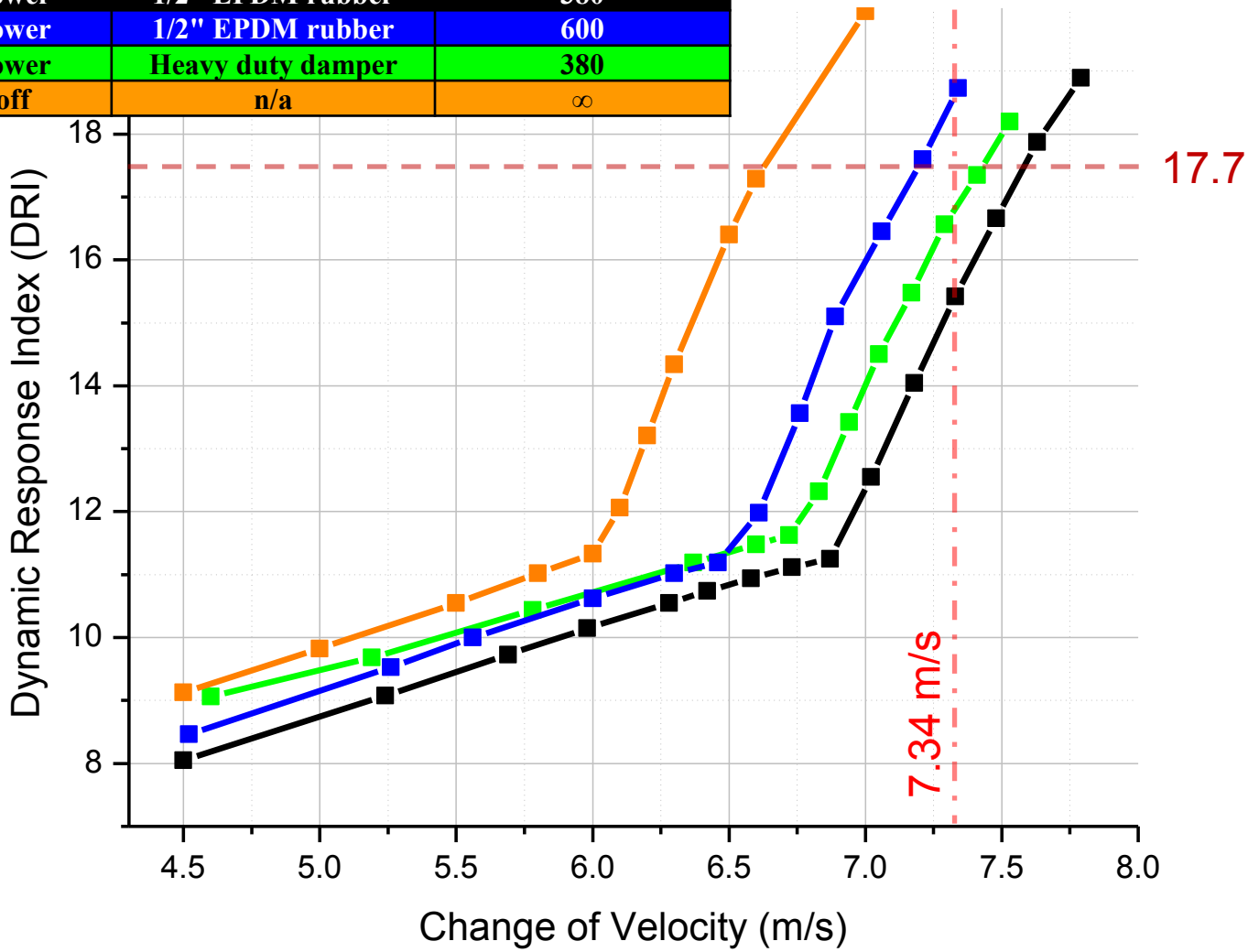

Discussion

- **When using drop-tower test to simulate blast-off test, result interpretation must be careful.**
  - **Differences in the mass and motion of the support (vehicle or carriage)**
  - **Differences in initial conditions**
    - ***Initial distances between masses, especially the one between seat pan and buttocks where there is a recoverable cushion***
    - ***Different contact forces, especially between feet and floor***
    - ***Different mannequin postures***

Discussion

- **When using drop-tower tests for seat performance analysis, a good understanding of the whole system is necessary.**
  - **The motion of the carriage depends not only on the impact force, but also on the force of the shock attenuation mechanism.**

$$\ddot{z}_0(t) = \underbrace{\frac{F}{m_0}}_{0<t<15\text{ ms}} + \underbrace{\frac{f_{01}}{m_0}}_{>50\text{ ms}}$$

  - **It is therefore hard to compare the performance of different seats using drop-tower test results**
  - ***Nevertheless, drop towers remain very useful for the purpose of research and product development***

Discussion

- **The analysis presented so far can be extended to the sled test method with the same analysis procedure**

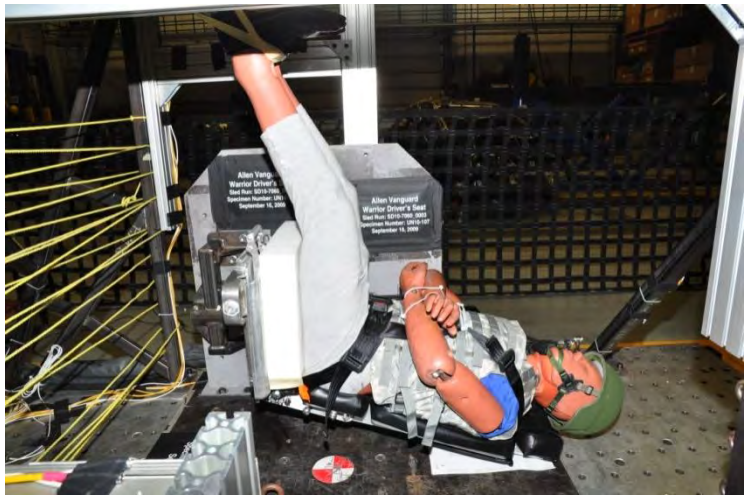

  - *The sled mass is usually much larger than that of the drop-tower carriage, resulting in higher pelvis acceleration and lower seat performance*
  - *Initial conditions are similar to those in drop-tower tests*
  - *Gravity is in transverse direction*

Discussion

- **Even for blast-off tests with a surrogate vehicle hull, the mass of the surrogate is still a problem. However, the deviation of the test results from full-size vehicle blast tests should not be significant,**

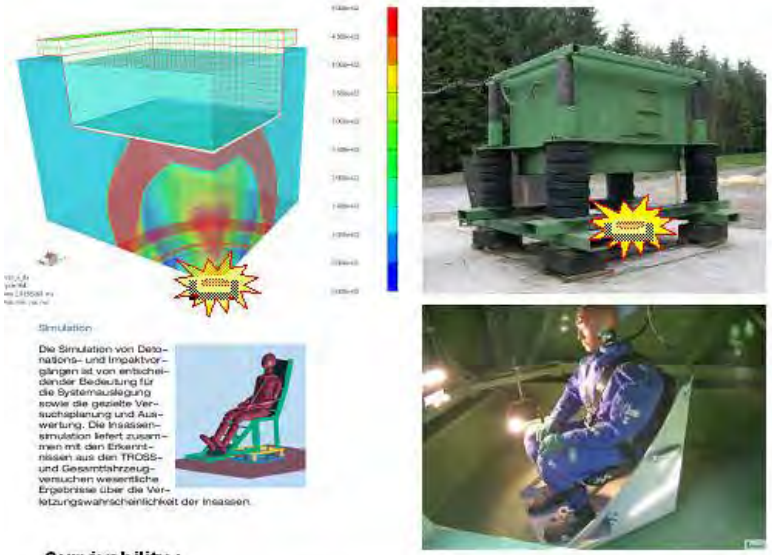

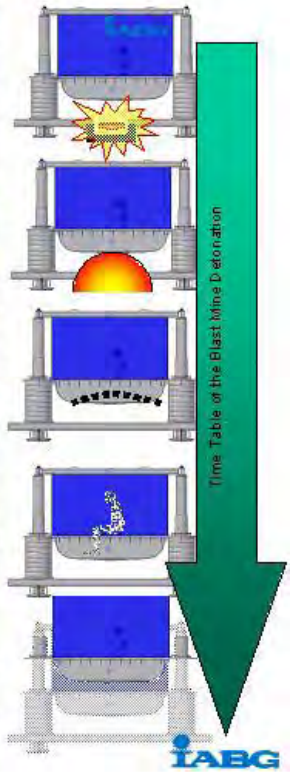

Survivability :

The internal dynamics within a protected vehicle are of essential importance in case of a mine detonation. All aspects of occupant protection in crew compartments can be analyzed in detail within TROSS Test rig configurations.

However, … …

- **The above discussion is based on an idealized acceleration pulse for blast impact on the vehicle**
  - *The actual pulse is the response of the vehicle at the seat mounting location*
  - *The actual pulse depends on the structure of the vehicle*
- **The validity of the above discussion needs further study based on actual signals measured on vehicles in full-size blast-off tests**
  - *Unfortunately, these signals are usually treated classified or confidential by most armor vehicle manufacturers, causing further study difficult.*

Universidad de los Andes
Facultad de Ingeniería

Effect of Set Up Parameters of Landmine Blast over Transferred Energy to a Rigid Body: Experimental and Computational Study

Authors : *J.A. Hoyos-Uribe*
V.H. Bastidas-Poveda
J.P. Casas-Rodriguez

26th International Symposium on Ballistics
Miami, USA,
September 15, 2011

Structural Integrity Group GIE
Mechanical Engineering Department
Carrera 1 este No. 19ª-40 Bogota, Colombia. Tel (57.1) 3394949 Fax. (57.1) 3324323
mecanica.uniandes.edu.co | E-mail: gie@uniandes.edu.co

OUTLINE

1. Introduction
2. Research Objective
3. Experimental Procedure
4. Testing Protocol
5. Computational Simulations
6. Results
7. Conclusions
8. References

Structural Integrity Group GIE
Mechanical Engineering Department
Carrera 1 este No. 19ª-40 Bogota, Colombia. Tel (57.1) 3394949 Fax. (57.1) 3324323
mecanica.uniandes.edu.co | E-mail: gie@uniandes.edu.co

INTRODUCTION

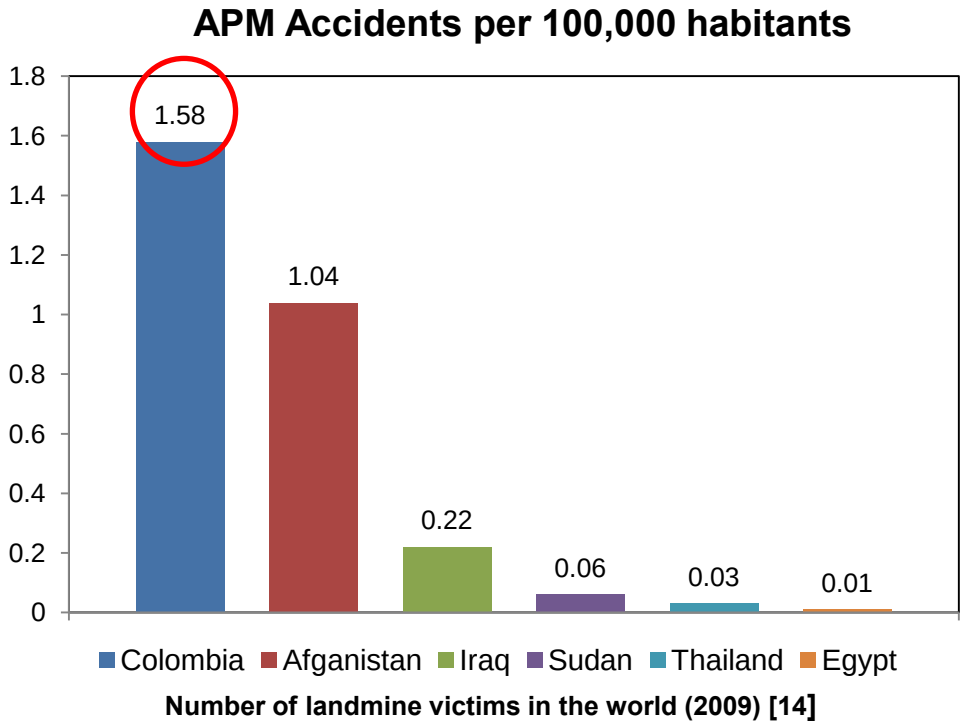

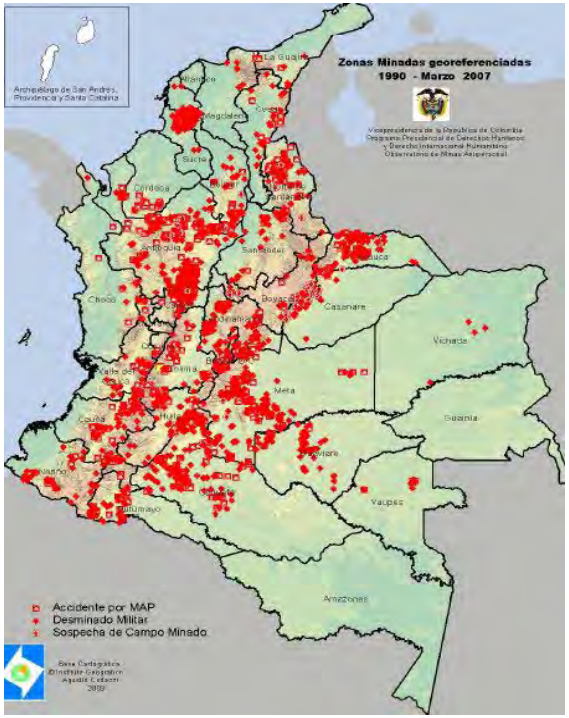

- In Colombia, Antipersonnel mines (APM) are still planted by illegal armed groups
- Colombia presents one of the highest number of landmine victims in the world.

Structural Integrity Group GIE
Mechanical Engineering Department
Carrera 1 este No. 19ª-40 Bogota, Colombia. Tel (57.1) 3394949 Fax. (57.1) 3324323
mecanica.uniandes.edu.co | E-mail: gie@uniandes.edu.co

INTRODUCTION

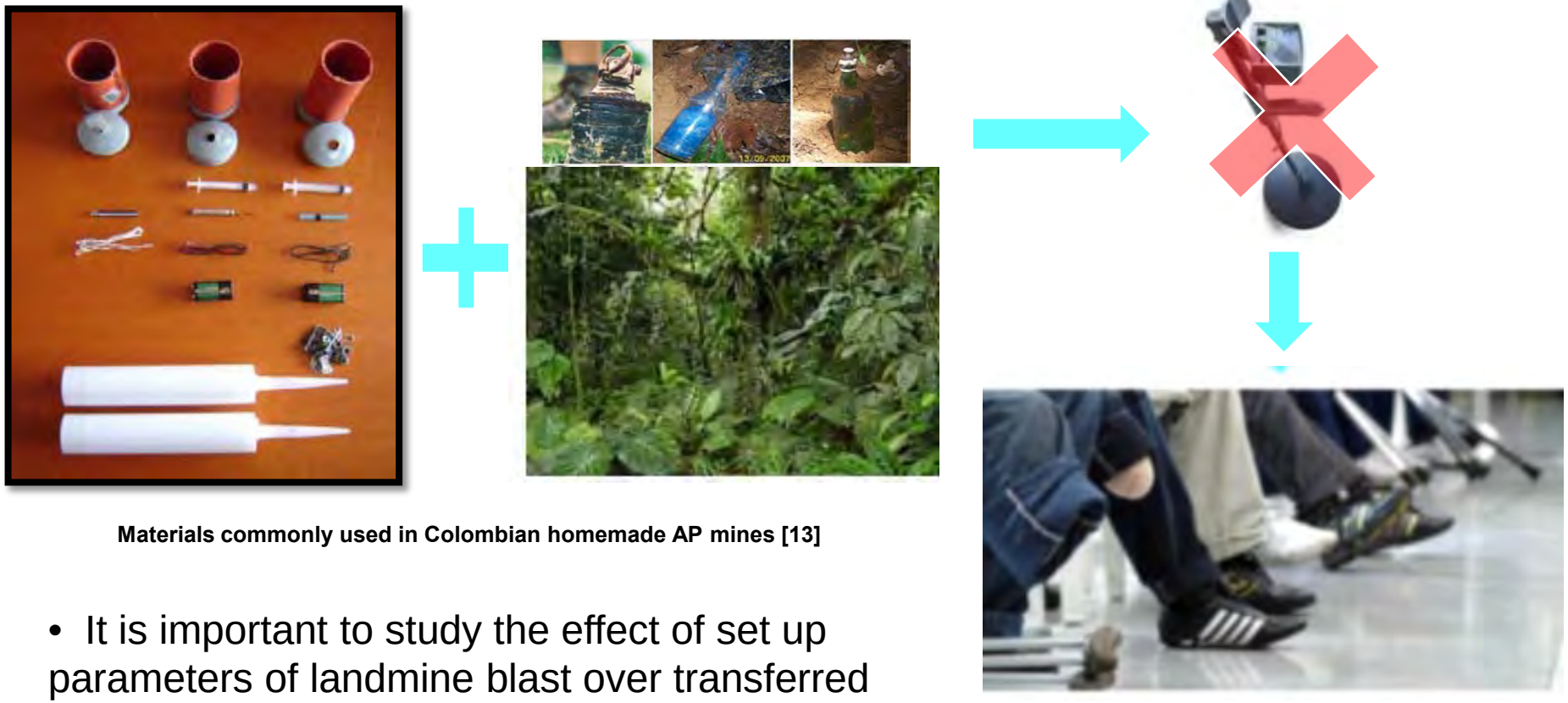

Materials commonly used in Colombian homemade AP mines [13]

- It is important to study the effect of set up parameters of landmine blast over transferred energy to a body.

Structural Integrity Group GIE
Mechanical Engineering Department
Carrera 1 este No. 19ª-40 Bogota, Colombia. Tel (57.1) 3394949 Fax. (57.1) 3324323
mecanica.uniandes.edu.co | E-mail: gie@uniandes.edu.co

INTRODUCTION

Understanding the explosion dynamics: Experimental and Numerical Studies

- Some studies have used
  - **Sand**
  - **Prairie soil**

- Transmitted energy is affected by:

  ✓ **Moisture content**
  ✓ **Compaction level**

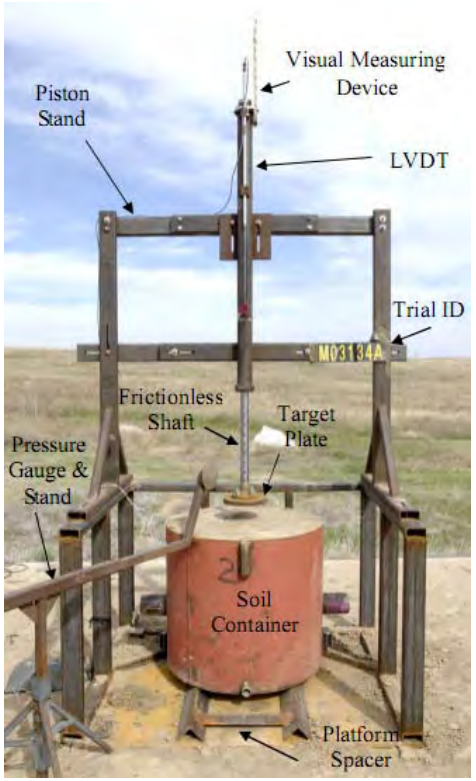

Hlady Setup [10]

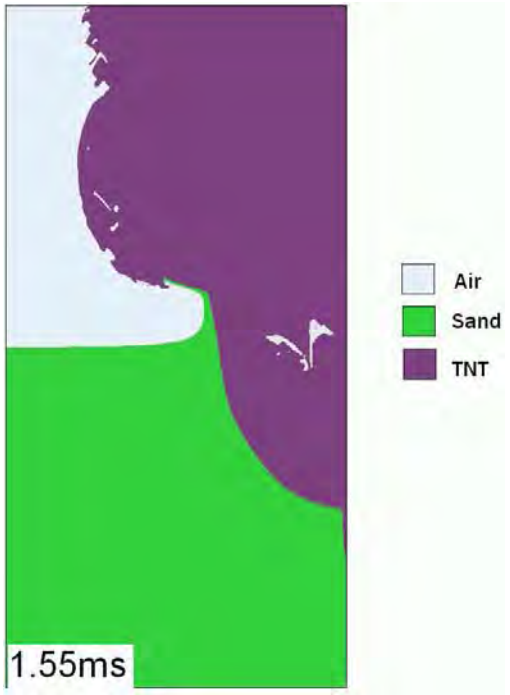

Fiserova-Hameed Simulations [4]

Structural Integrity Group GIE
Mechanical Engineering Department
Carrera 1 este No. 19ª-40 Bogota, Colombia. Tel (57.1) 3394949 Fax. (57.1) 3324323
mecanica.uniandes.edu.co | E-mail: gie@uniandes.edu.co

RESEARCH OBJECTIVE

The aim of this work is to study the dependence of some parameters, such as the mass of the explosive, reaction mass, depth of burial and standoff distance in energy transferred to a rigid objective using a specific soil.

The parametric study involves:

- Development and Calibration of a computational model for a specific soil (using AUTODYN).

- To study the effect of setup parameters during experimental work.

Structural Integrity Group GIE
Mechanical Engineering Department
Carrera 1 este No. 19ª-40 Bogota, Colombia. Tel (57.1) 3394949 Fax. (57.1) 3324323
mecanica.uniandes.edu.co | E-mail: gie@uniandes.edu.co

EXPERIMENTAL PROCEDURE

Equipment used

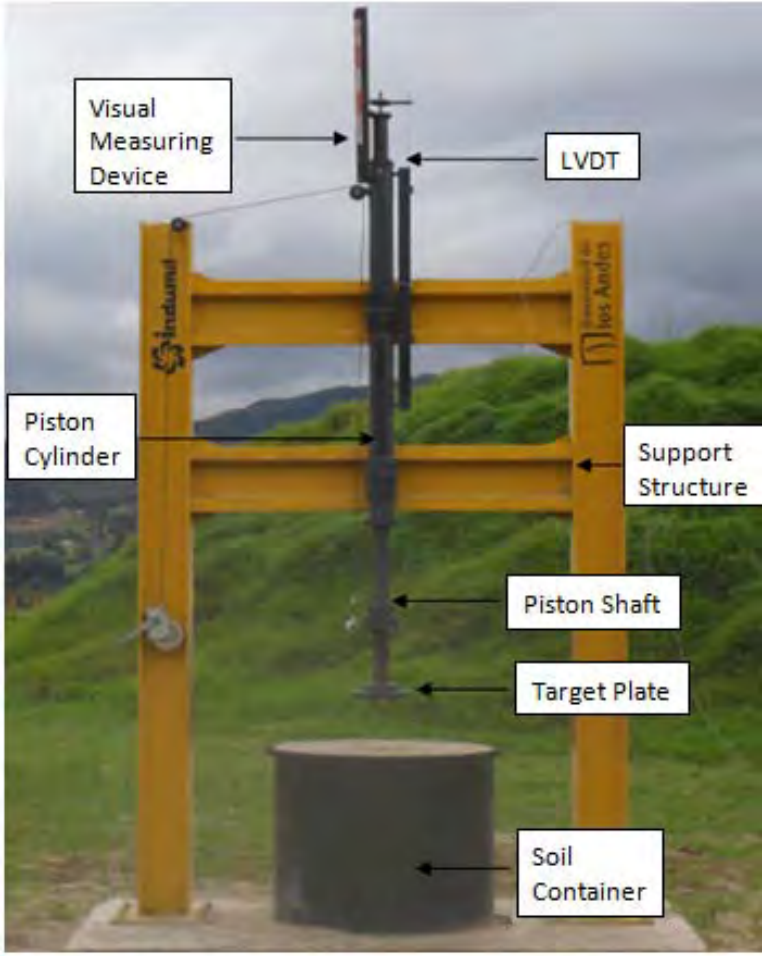

Structural Integrity Group GIE
Mechanical Engineering Department
Carrera 1 este No. 19ª-40 Bogota, Colombia. Tel (57.1) 3394949 Fax. (57.1) 3324323
mecanica.uniandes.edu.co | E-mail: gie@uniandes.edu.co

EXPERIMENTAL PROCEDURE

Soil

- It seems that the behavior of gravel has not been studied experimentally or computationally before.
- Gravel characteristics: Low compaction level and maximum moisture absorption of 1.6%.

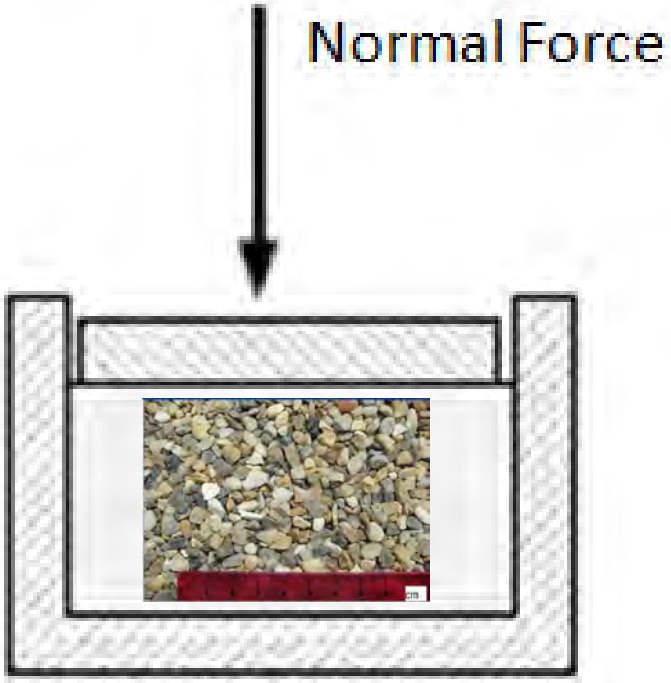

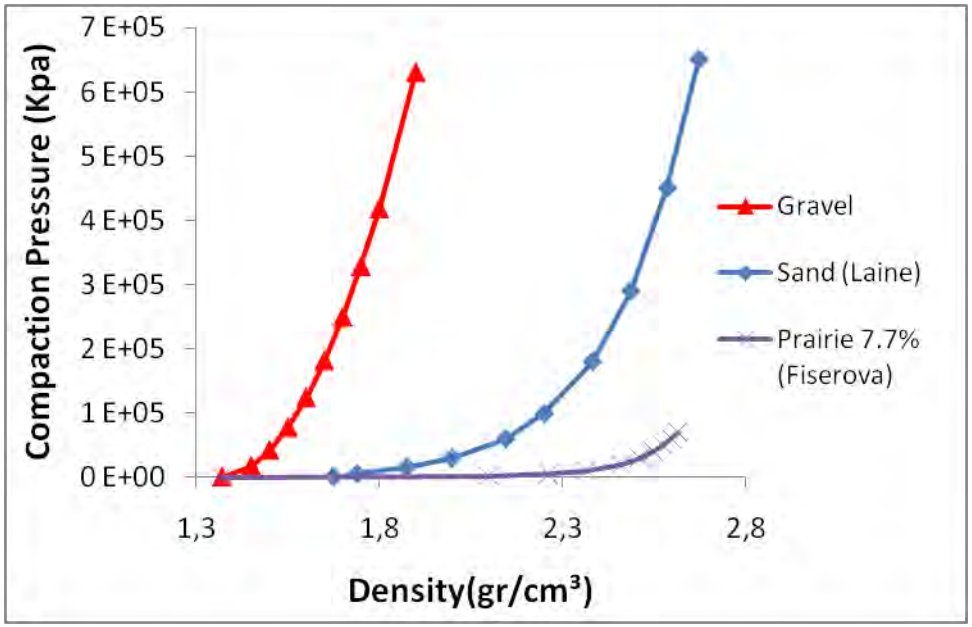

Structural Integrity Group GIE
Mechanical Engineering Department
Carrera 1 este No. 19ª-40 Bogota, Colombia. Tel (57.1) 3394949 Fax. (57.1) 3324323
mecanica.uniandes.edu.co | E-mail: gie@uniandes.edu.co

EXPERIMENTAL PROCEDURE: Experimental Matrix

Evaluated Parameter	Explosive mass	Piston mass	Depth of burial	Standoff distance
Explosive mass	m, 1.4*m & 2*m	M	0	3*SD
Piston mass	1.4*m	M, 1.1*M, 1.2*M & 1.4*M	0	3*SD
Depth of burial	1.4*m	1.4*M	0, OB, 2*OB & 3*OB	3*SD
Standoff distance	1.4*m	1.4*M	0	0, SD & 3*SD

Test Parameters

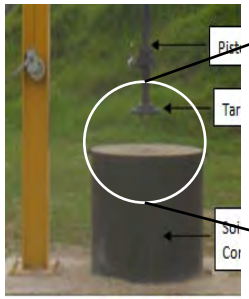

standoff distance

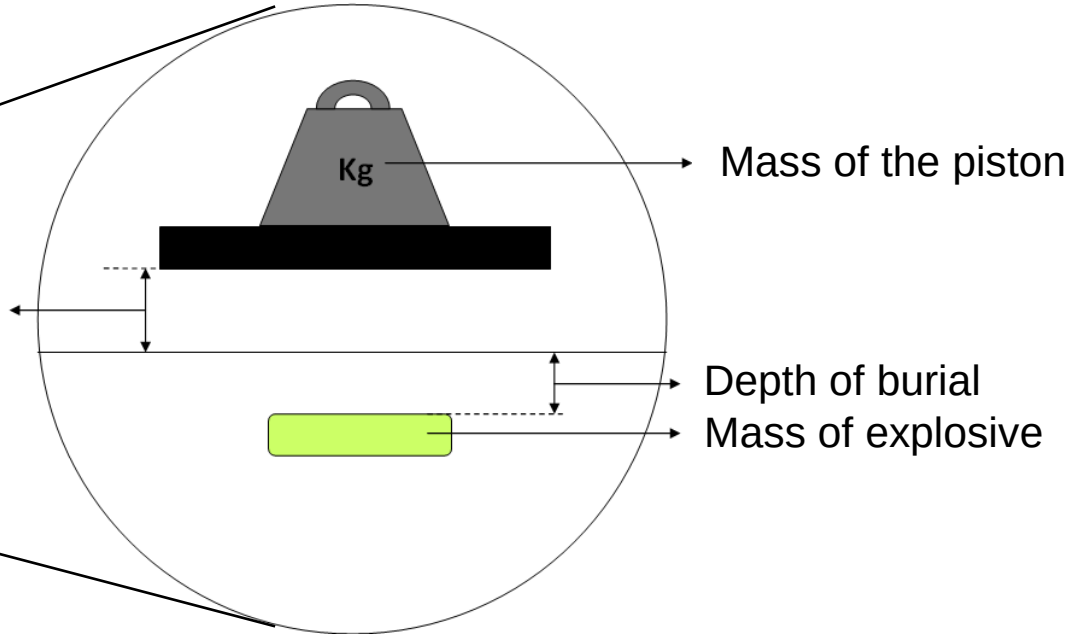

TESTING PROTOCOL

Soil Preparation → Experimental Set up → Measurement Preparation

Detonation

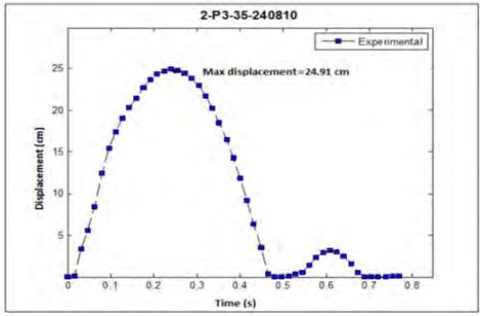

Data acquisition

Structural Integrity Group GIE
Mechanical Engineering Department
Carrera 1 este No. 19ª-40 Bogota, Colombia. Tel (57.1) 3394949 Fax. (57.1) 3324323
mecanica.uniandes.edu.co | E-mail: gie@uniandes.edu.co

COMPUTATIONAL SIMULATIONS IN AUTODYN

Settings

	Value	Observations
Symmetry	2D	Axisymmetric
Materials	Air	Models: Ideal Gas, JWL, Shock, PJC, Compaction, Granular and Hydro Tensile limit.
	TNT	
	Stainless Steel	
	Sand/Gravel	
Initial Conditions	Atmospheric pressure	101.325 KPa
Boundaries Conditions	Flow out	
	Transmit	
Parts	Space	Contains Air, Gravel and TNT (Euler).
	Piston	Contains the steel (Lagrange).
Mesh size	4x4 mm (Euler)	The calibration were based on comparison between previous experimental and computational works
	8x8 mm (Lagrange)	
Simulation time	5 ms (virtual time)	45 min (PC time)

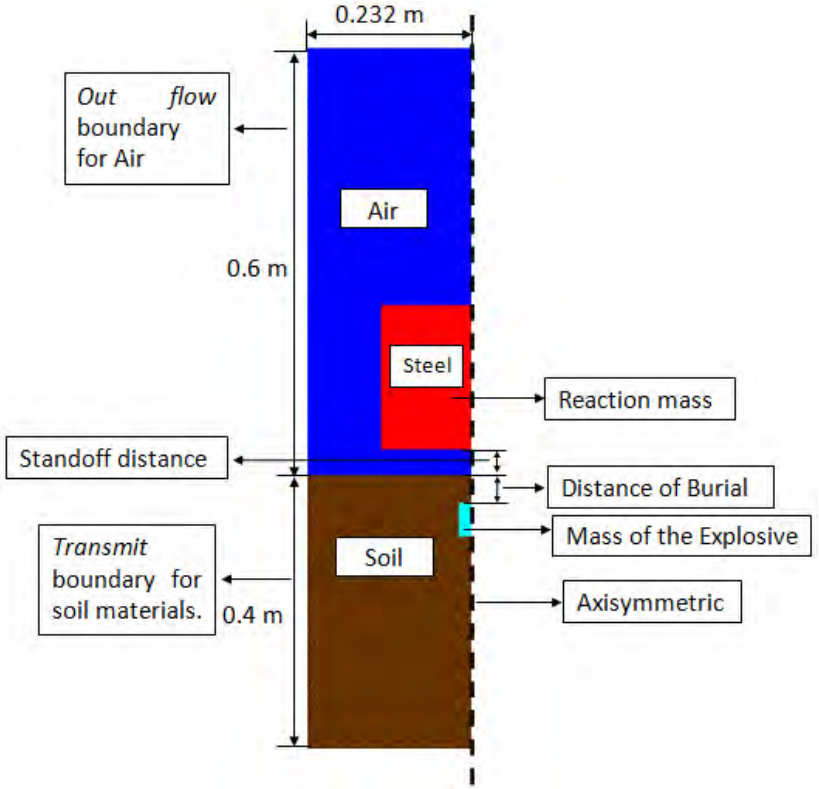

Structural Integrity Group GIE
Mechanical Engineering Department
Carrera 1 este No. 19ª-40 Bogota, Colombia. Tel (57.1) 3394949 Fax. (57.1) 3324323
mecanica.uniandes.edu.co | E-mail: gie@uniandes.edu.co

RESULTS

Gravel soil after detonation

- There was a relatively small dispersion in the experimentation. The reading of the LVDT and the camera agreed.

Structural Integrity Group GIE
Mechanical Engineering Department
Carrera 1 este No. 19ª-40 Bogota, Colombia. Tel (57.1) 3394949 Fax. (57.1) 3324323
mecanica.uniandes.edu.co | E-mail: gie@uniandes.edu.co

RESULTS

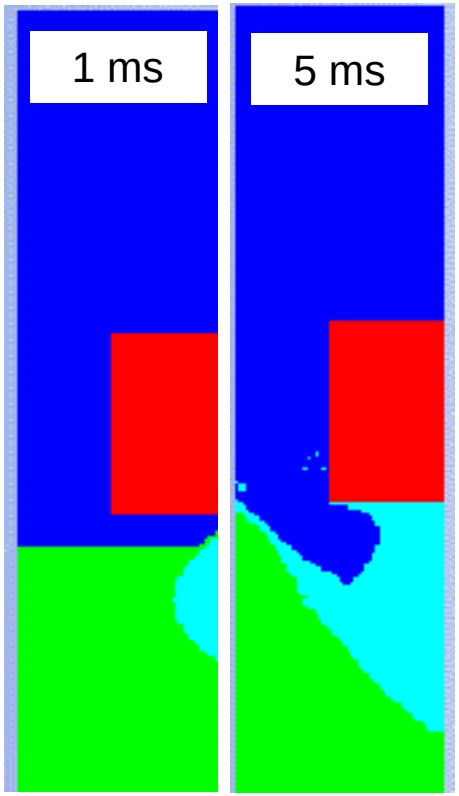

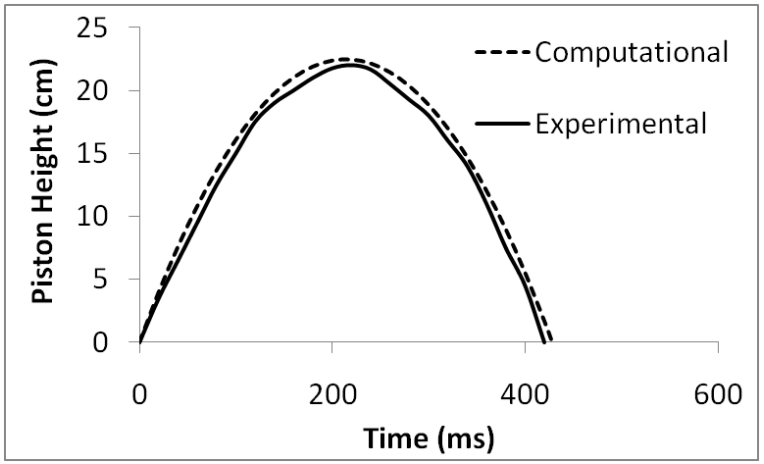

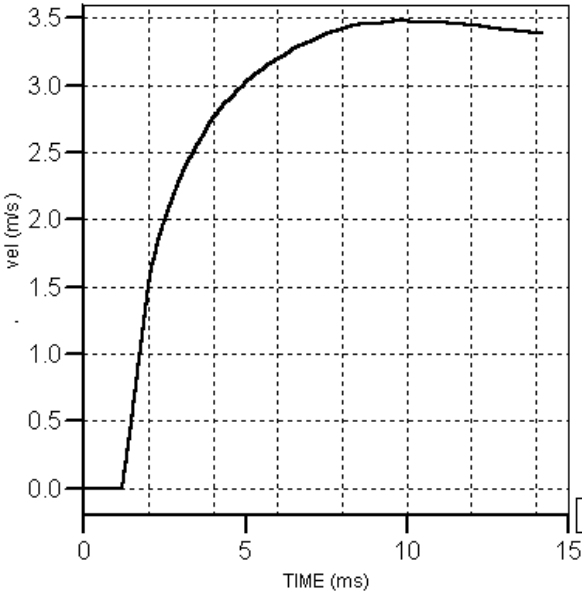

- There was consistency between computational and experimental results.

Structural Integrity Group GIE
Mechanical Engineering Department
Carrera 1 este No. 19ª-40 Bogota, Colombia. Tel (57.1) 3394949 Fax. (57.1) 3324323
mecanica.uniandes.edu.co | E-mail: gie@uniandes.edu.co

RESULTS

Results of effects of some parameters in mine blast

Depth of Burial effect

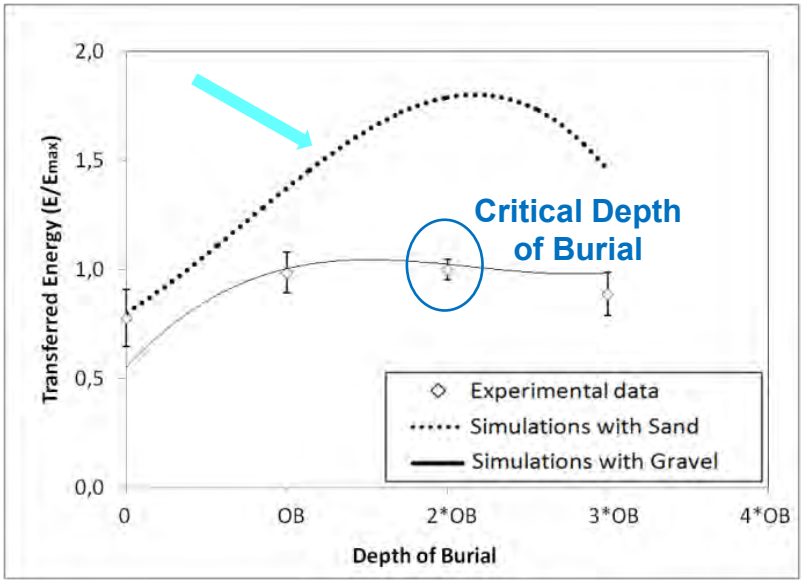

Piston mass effect

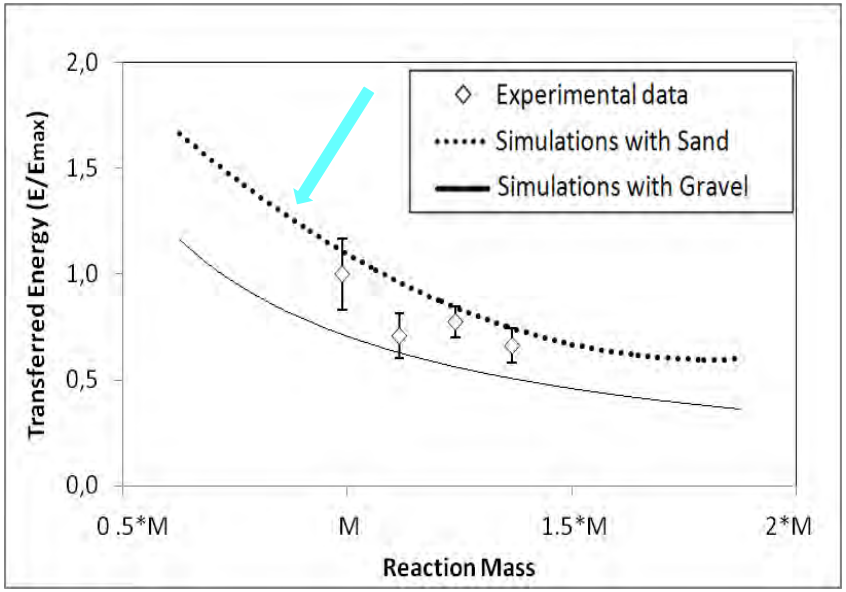

- The critical Depth of Burial that maximizes the transferred energy to the piston is close to 2*OB.
- The less the reaction mass, the more transferred energy is.

Structural Integrity Group GIE
Mechanical Engineering Department
Carrera 1 este No. 19ª-40 Bogota, Colombia. Tel (57.1) 3394949 Fax. (57.1) 3324323
mecanica.uniandes.edu.co | E-mail: gie@uniandes.edu.co

RESULTS

Results of effects of some parameters in mine blast

Mass of Explosive

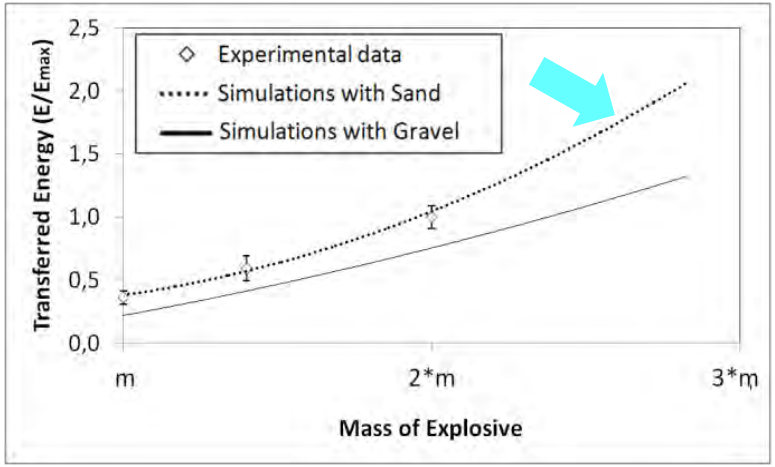

Standoff effect

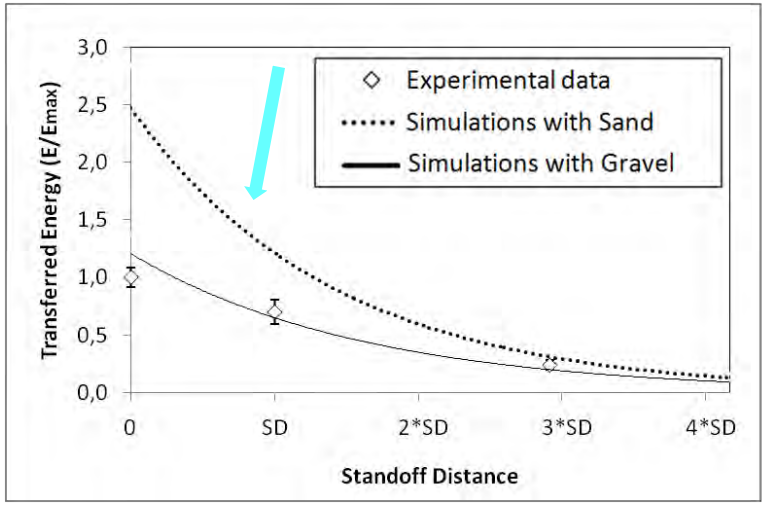

- Energy increases as the explosive mass increases.
- Transferred energy decreases when standoff distance increases. In this particular case, the energy decreases 14 times in average for an increment of standoff distance from 0 to 4*SD.

Structural Integrity Group GIE
Mechanical Engineering Department
Carrera 1 este No. 19ª-40 Bogota, Colombia. Tel (57.1) 3394949 Fax. (57.1) 3324323
mecanica.uniandes.edu.co | E-mail: gie@uniandes.edu.co

CONCLUSIONS

- Gravel soil was successfully used in this work and it is possible to use it for future works due to its relatively easy handling.

- It was concluded that the gravel model (developed in this work) described the experimental data tendency successfully.

- It was observed (computationally) that transferred energy from sand is higher than gravel soil.

- Finally, standoff distance is the most influential parameter over the transferred energy, followed by the amount of explosive mass, reaction mass and depth of burial of mine.

ACKNOWLEDGEMENTS

The authors wish to acknowledge Military Industry (INDUMIL) of Colombia for their economical and human support given for this research.

Structural Integrity Group GIE
Mechanical Engineering Department
Carrera 1 este No. 19ª-40 Bogota, Colombia. Tel (57.1) 3394949 Fax. (57.1) 3324323
mecanica.uniandes.edu.co | E-mail: gie@uniandes.edu.co

REFERENCES

1.Hlady, S. Effect of Soil Parameters on Landmine Blast. in 18th Military Aspects of Blast and Shock (MABS) Conference. 2004. Bad Reichenhall, Germany.
2.Bergeron, D., R. Walker, and C. Coffey, Detonation of 100-gram Anti-Personnel Mine Surrogate Charges in Sand-A Test Case for Computer Code Validation. Report SR, 1998. 668.
3.Wang, J., Simulation of landmine explosion using LS-Dyna3d software: benchmark work of simulation of explosion in soil and air. 2001.
4.Fiserova, D., Numerical analysis of buried mine explosions with emphasis on effect of soil properties on loading, in Defence College of Management and Technology. 2006, Cranfield University.
5.Bues, R., S. Hlady, and D. Bergeron, Pendulum measurement of land mine blast output, Volume 1: Theory and implementation. 2001, Technical report DRES-TR-01-200.
6.Fairlie, G.E. and D. Bergereon, Numerical Simulation of Mine Blast Loading on Structures, in 17 Military Aspects of Blast Symposium. 2002: Las Vegas, Nevada, U.S.A.
7.AUTODYN, Theory Manual. Explicit Software for Nonlinear Dynamics. Revision 4.3. 2005.
8.Rogers, G. and Y. Mayhew, Thermodynamic and transport properties of fluids: SI units. 1995: Blackwell.
9.Lee, E., M. Finger, and W. Collins, JWL equation of state coefficients for high explosives. 1973.
10.Matuska, D.A., HULL users manual. AFATL-TR-84-59, 1984
11. Laine, L. and A. Sandvik. Derivation of mechanical properties for sand. 2001.
12. Landmine Monitor. 20 de Agosto de 2009]; Available from: http://lm.icbl.org
13. Vicepresidencia De La República Programa Presidencial Para La Acción Integral Contra Minas Antipersonal (PAICMA), *Informe Situación De Afectación De Víctimas De Minas Antipersonal (MAP), Artefactos Explosivos Improvisados (AEI) Y Municiones Sin Explotar (MUSE),.* 2008.
14. Las Minas Antipersonal en Colombia: un arma letal contra la población civil. Oficina para la Coordinación de Asuntos Humanitarios de las Naciones Unidas. Bogotá, D.C., Colombia (2009).
15. T. Ngo. Blast Loading and Blast Effects on Structures – An Overview. EJSE Special Issue: Loading on Structures (2007)

U.S. Army Research, Development and Engineering Command

5.56 mm M855 Accuracy and Jump Measurements

TECHNOLOGY DRIVEN. WARFIGHTER FOCUSED.

Ilmars Celmins
U.S. Army Research Laboratory, Flight Sciences Branch

26th International Symposium on Ballistics – September 2011

Outline

- Description of jump components
- M855 reference ammunition test results
- Summary and conclusions
- Backup slides: description of test setup, instrumentation, and measurement techniques

Jump testing measures individual trajectory components

- Three gun motion parameters
  - Static pointing angle
  - Dynamic pointing angle
  - Crossing velocity ratio
- Three projectile motion parameters
  - CG jump
  - Aerodynamic jump
  - Gravity drop (added to impact location)

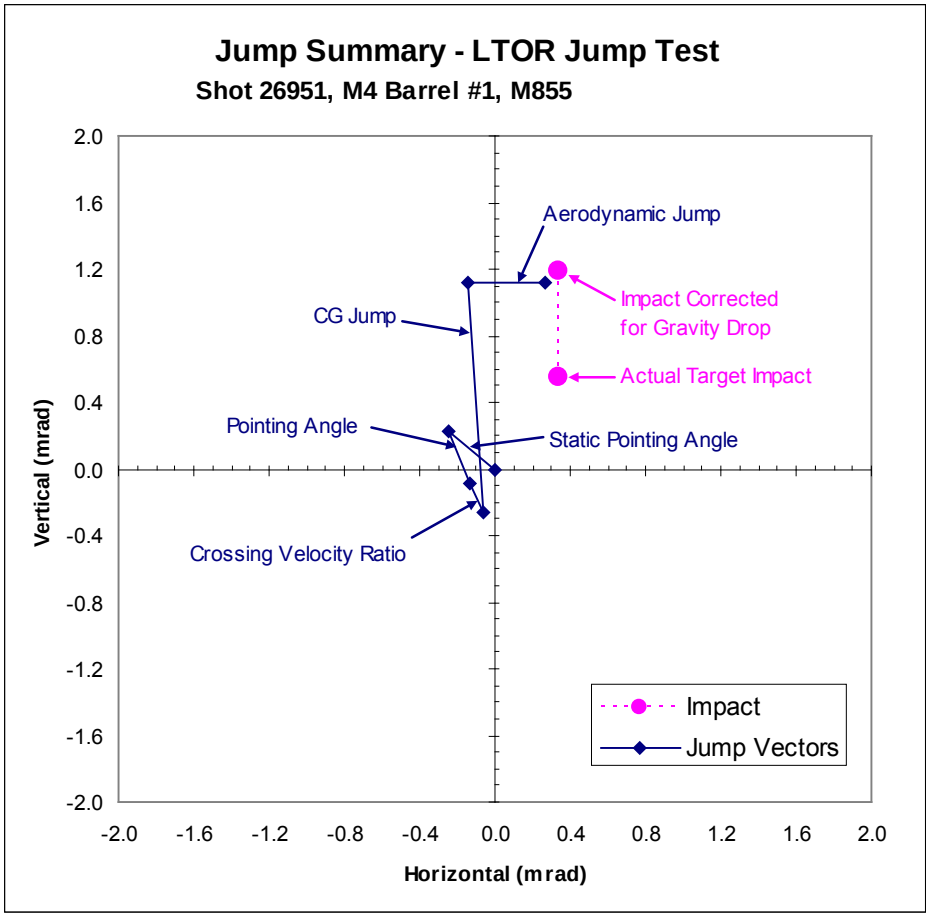

Jump Components, M4 Barrel #2, M855

Jump Summary - LTOR Jump Test
M4 Barrel #2, M855

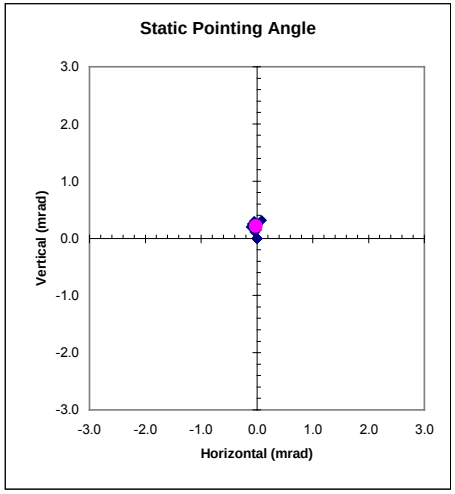

Avg.=(-0.02, 0.21) SD=(0.05, 0.06)

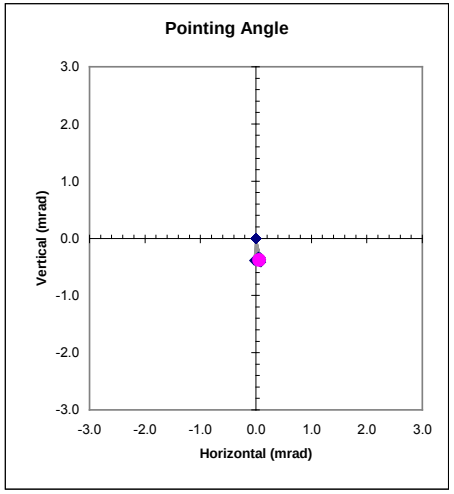

Avg.=(0.06, -0.38) SD=(0.04, 0.03)

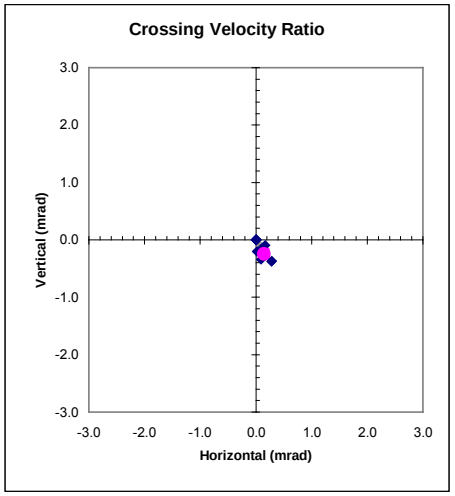

Avg.=(0.15, -0.25) SD=(0.08, 0.09)

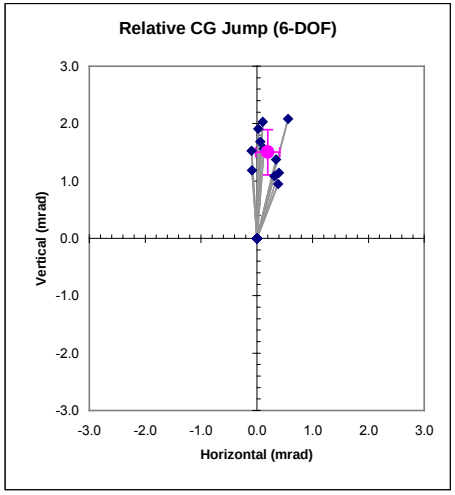

Avg.=(0.20, 1.50) SD=(0.22, 0.39)

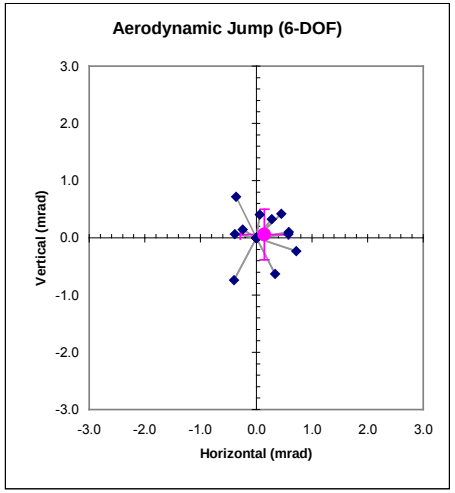

Avg.=(0.15, 0.06) SD=(0.43, 0.44)

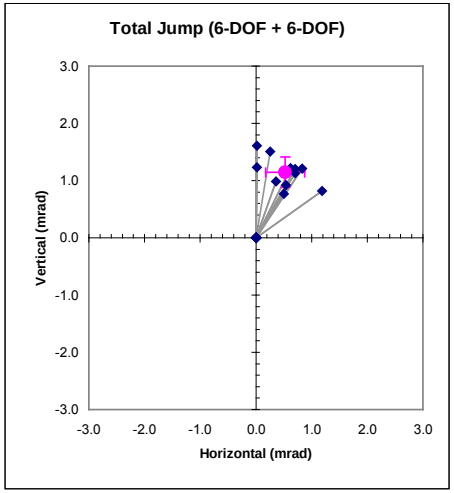

Avg.=(0.52, 1.15) SD=(0.35, 0.26)

M855 reference ammunition tests

Ammunition Lot No. LC-87F000R011

Four different barrel configurations were tested

- M4, Barrel #1
- M4, Barrel #2
- M4, Barrel #2, bare muzzle
- Mann Barrel

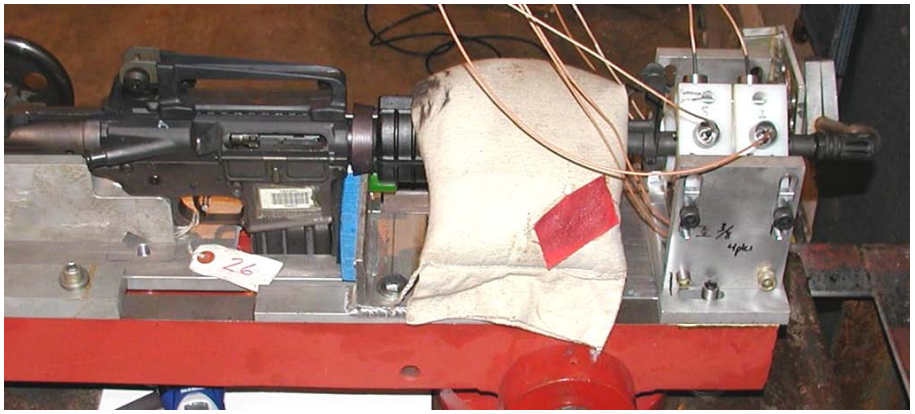

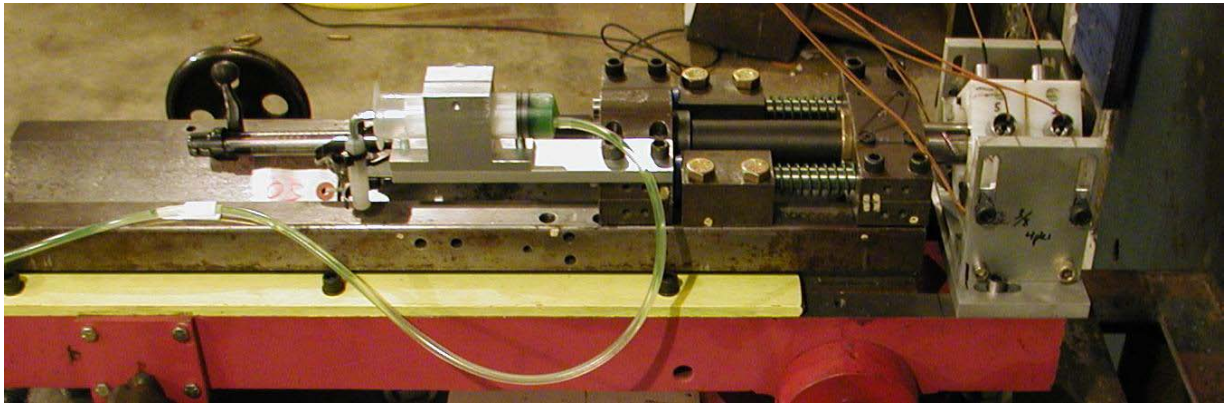

Comparison of Static Pointing Angle Jump Component

Expanded Scale (3X)

M4 Barrel #1, M855

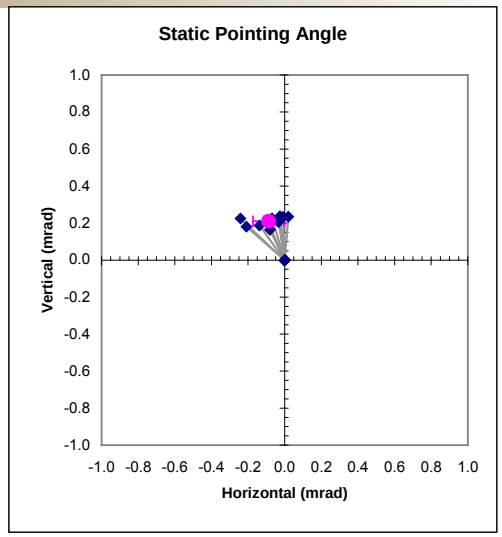

Avg.=(-0.09, 0.21) SD=(0.09, 0.03)

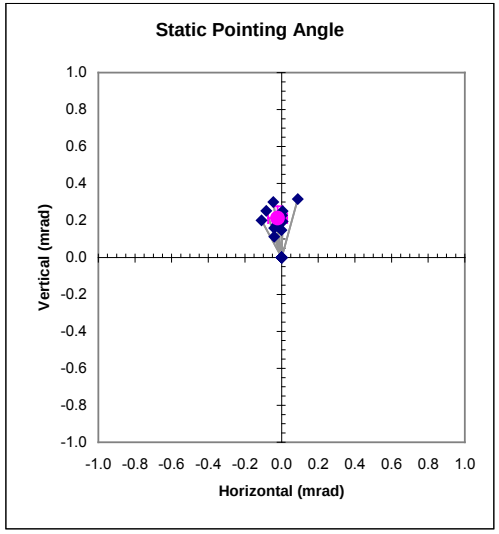

Avg.=(-0.02, 0.21) SD=(0.05, 0.06)

M4 Barrel #2, M855

Mann Barrel, M855

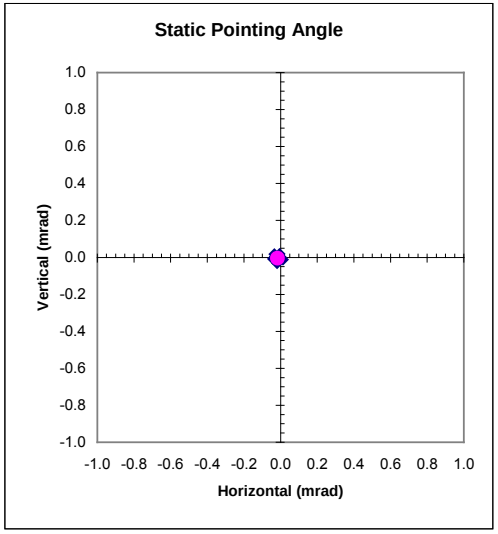

Avg.=(-0.02, 0.00) SD=(0.02, 0.02)

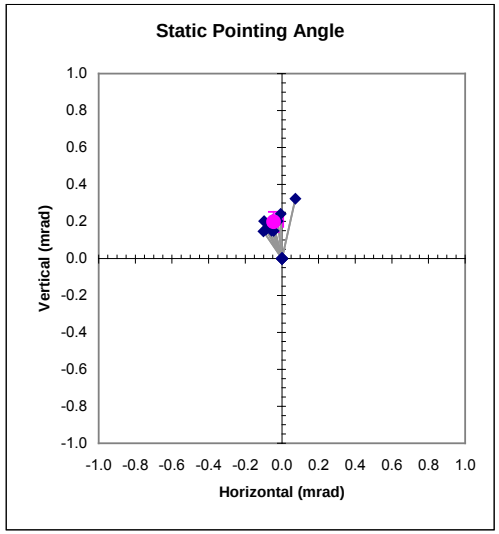

Avg.=(-0.04, 0.20) SD=(0.05, 0.05)

M4 Barrel #2, Bare Muzzle M855

Comparison of Muzzle Pointing Angle Jump Component

Expanded Scale (3X)

M4 Barrel #1, M855

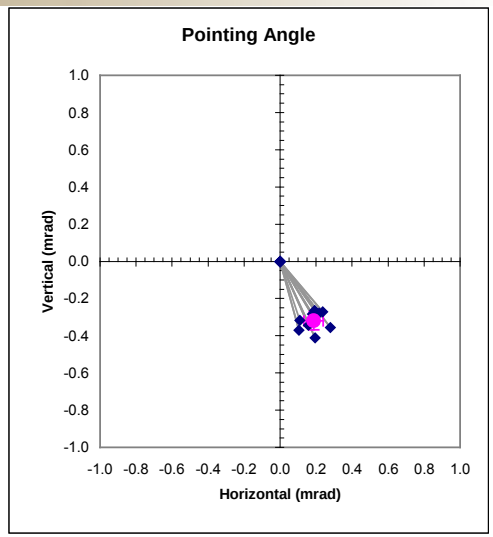

Avg.=(0.19, -0.32) SD=(0.05, 0.05)

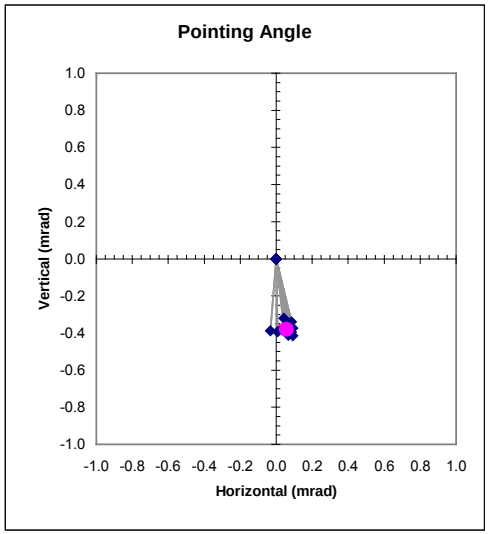

Avg.=(0.06, -0.38) SD=(0.04, 0.03)

M4 Barrel #2, M855

Mann Barrel, M855

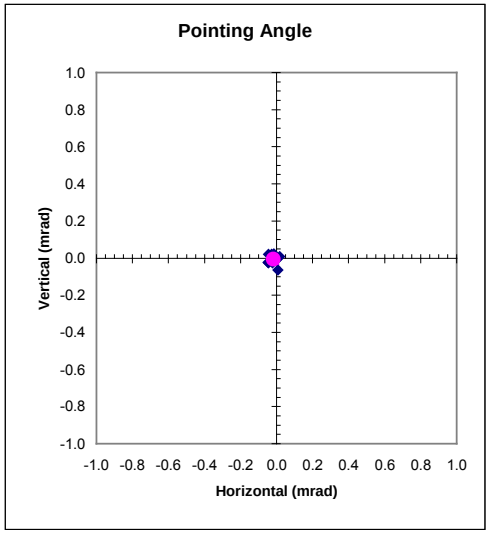

Avg.=(-0.02, -0.01) SD=(0.02, 0.03)

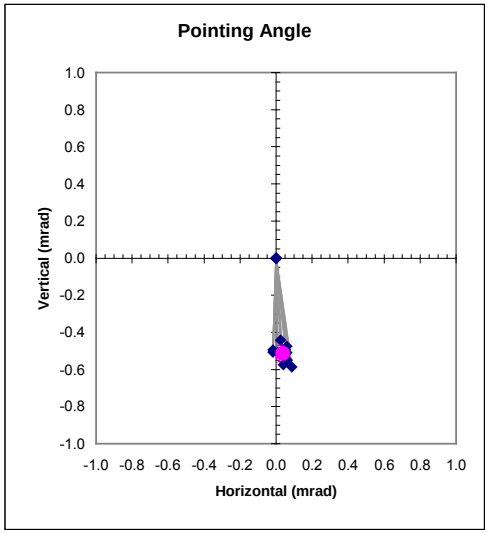

Avg.=(0.04, -0.51) SD=(0.04, 0.04)

M4 Barrel #2, Bare Muzzle M855

Comparison of Muzzle Crossing Velocity Jump Component

Expanded Scale (3X)

M4 Barrel #1, M855

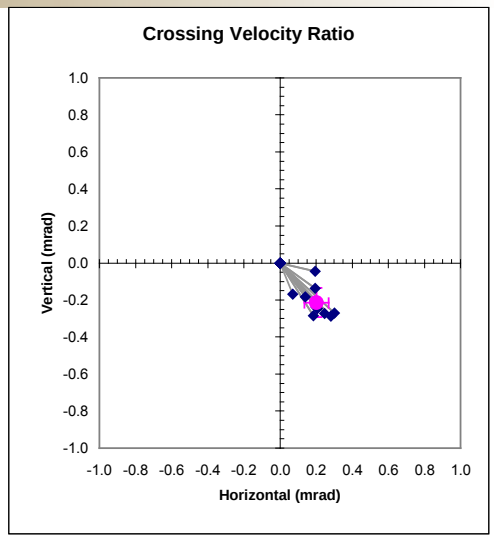

Avg.=(0.20, -0.21) SD=(0.07, 0.08)

M4 Barrel #2, M855

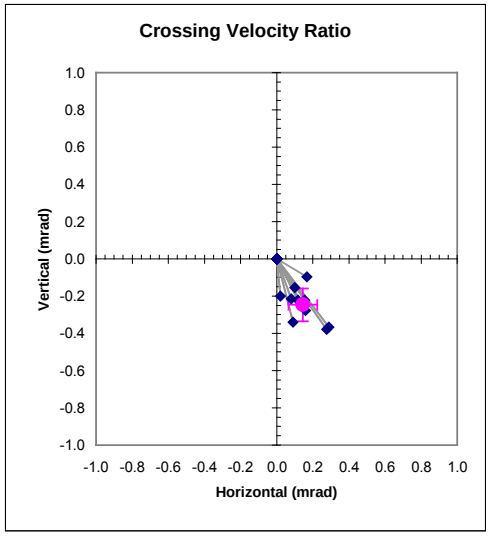

Avg.=(0.15, -0.25) SD=(0.08, 0.09)

Mann Barrel, M855

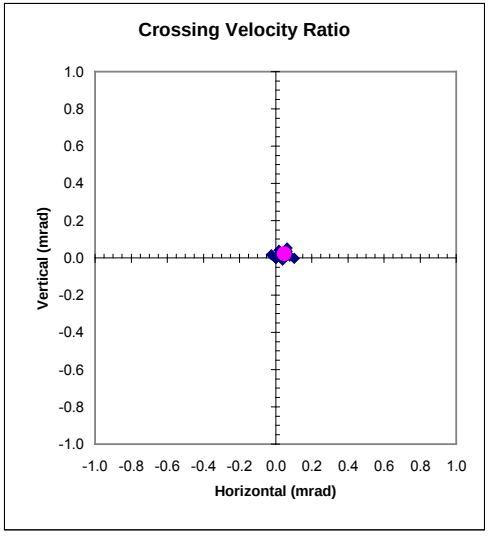

Avg.=(0.05, 0.02) SD=(0.03, 0.02)

M4 Barrel #2, Bare Muzzle M855

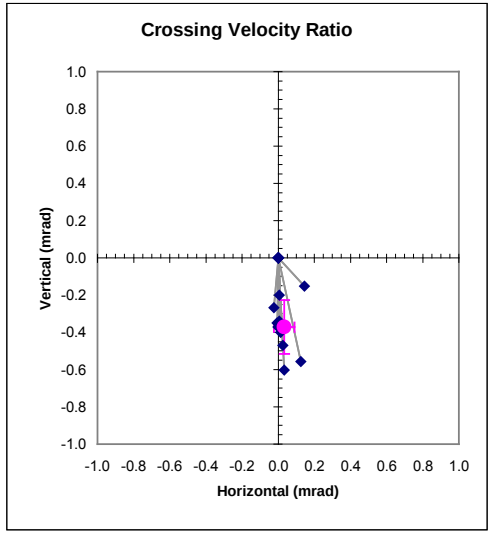

Avg.=(0.03, -0.37) SD=(0.06, 0.14)

Comparison of Relative CG Jump Component

M4 Barrel #1, M855

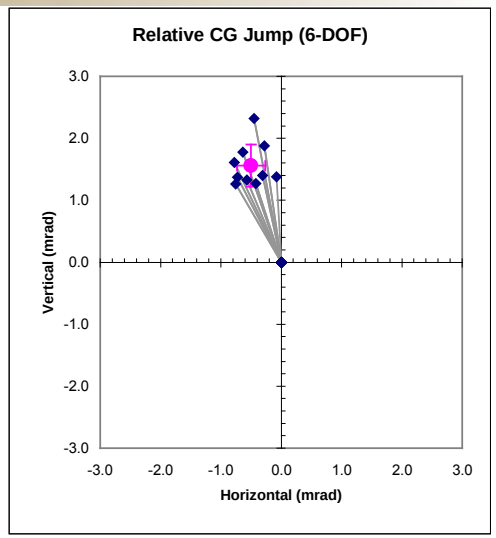

Avg.=(-0.50, 1.56) SD=(0.23, 0.34)

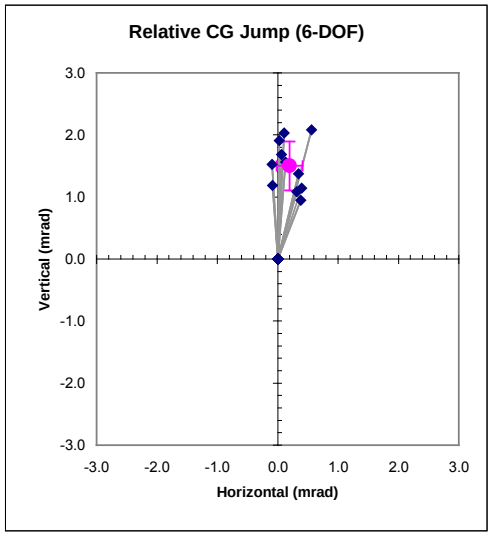

Avg.=(0.20, 1.50) SD=(0.22, 0.39)

M4 Barrel #2, M855

Mann Barrel, M855

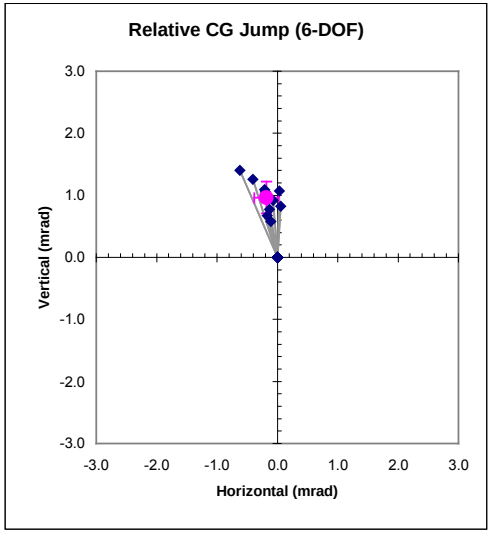

Avg.=(-0.18, 0.96) SD=(0.20, 0.26)

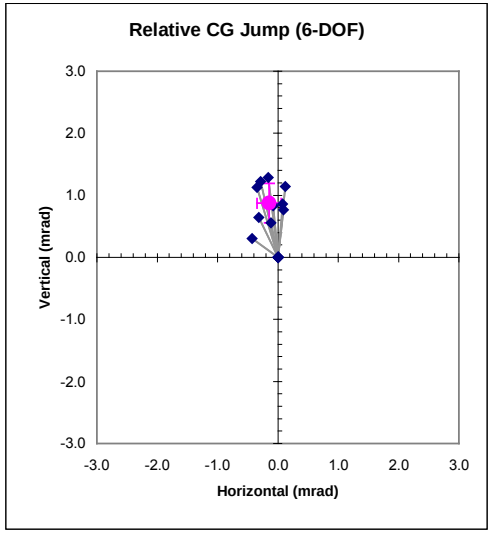

Avg.=(-0.14, 0.87) SD=(0.20, 0.32)

M4 Barrel #2, Bare Muzzle M855

Comparison of Absolute CG Jump Component

M4 Barrel #1, M855

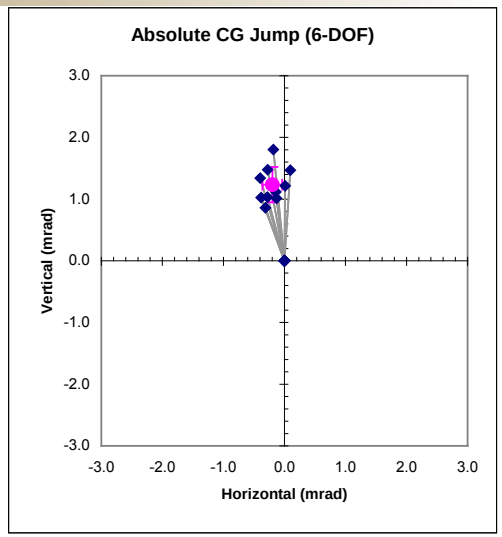

Avg.=(-0.20, 1.23) SD=(0.16, 0.29)

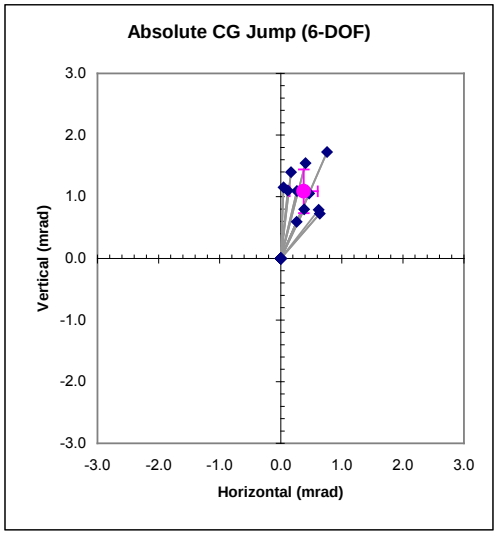

Avg.=(0.38, 1.09) SD=(0.23, 0.36)

M4 Barrel #2, M855

Mann Barrel, M855

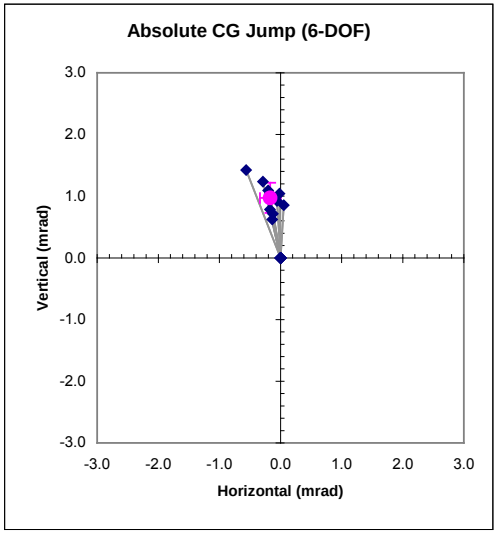

Avg.=(-0.17, 0.97) SD=(0.17, 0.24)

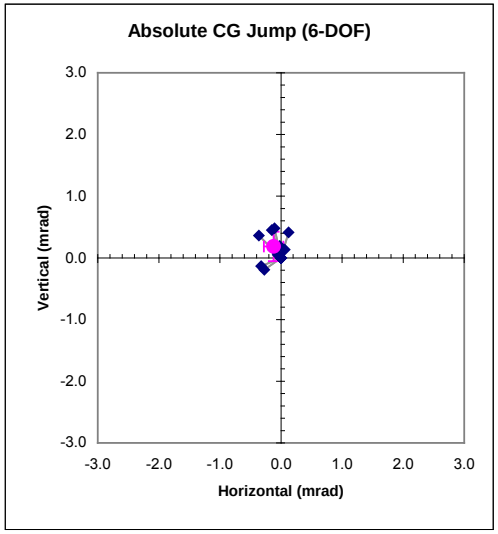

Avg.=(-0.12, 0.19) SD=(0.16, 0.24)

M4 Barrel #2, Bare Muzzle M855

Comparison of Aerodynamic Jump Component

M4 Barrel #1, M855

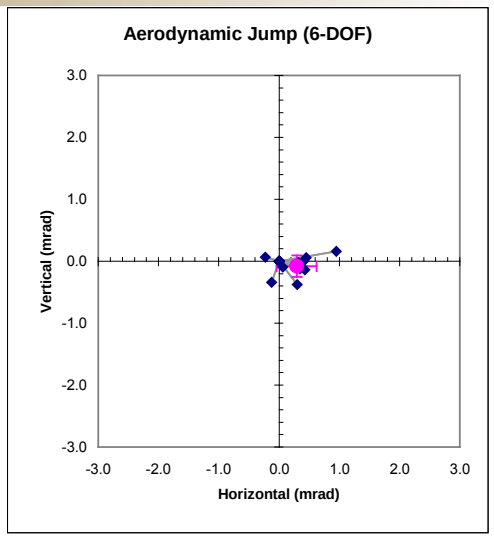

Avg.=(0.29, -0.08) SD=(0.33, 0.17)

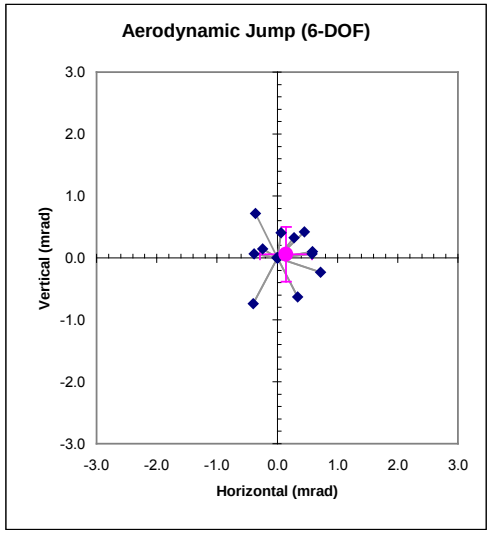

Avg.=(0.15, 0.06) SD=(0.43, 0.44)

M4 Barrel #2, M855

Mann Barrel, M855

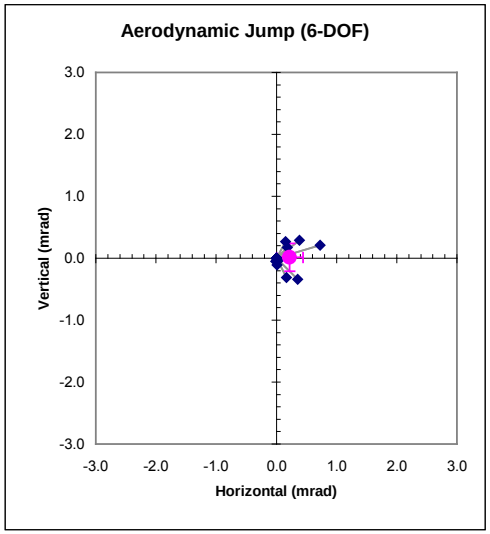

Avg.=(0.22, 0.01) SD=(0.22, 0.23)

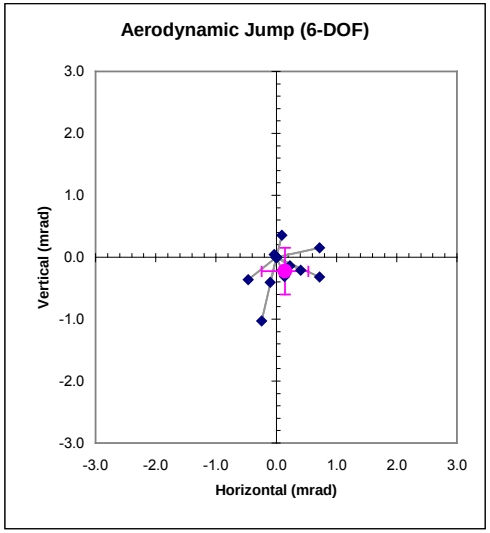

Avg.=(0.15, -0.22) SD=(0.39, 0.38)

M4 Barrel #2, Bare Muzzle M855

Comparison of Total Jump

M4 Barrel #1, M855

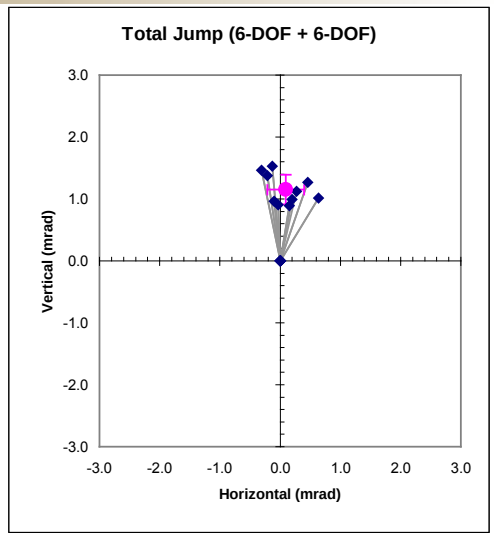

Avg.=(0.09, 1.15) SD=(0.30, 0.24)

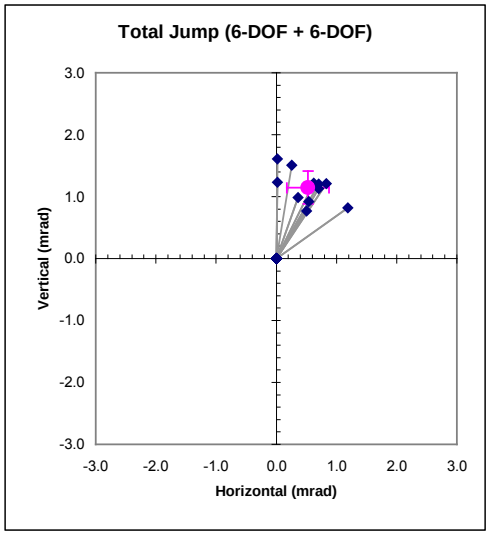

M4 Barrel #2, M855

Mann Barrel, M855

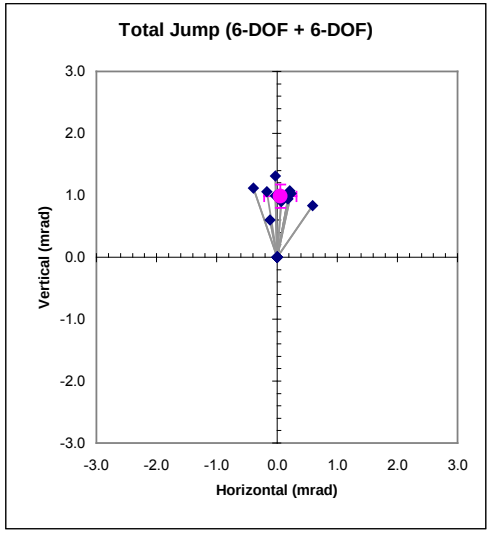

Avg.=(0.06, 0.99) SD=(0.27, 0.19)

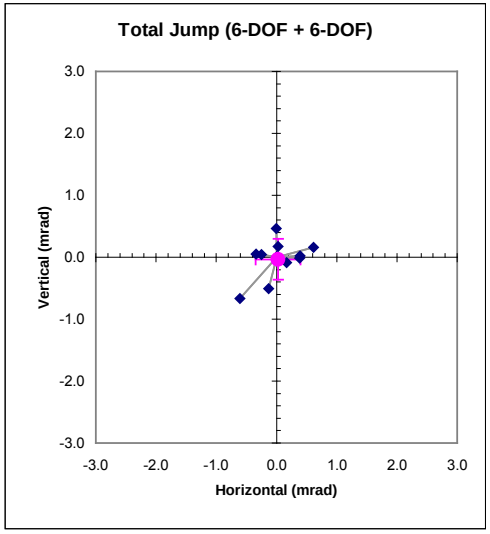

Avg.=(0.03, -0.04) SD=(0.38, 0.33)

M4 Barrel #2, Bare Muzzle M855

Comparison of Dispersion Contributors

M4 Barrel #1, M855

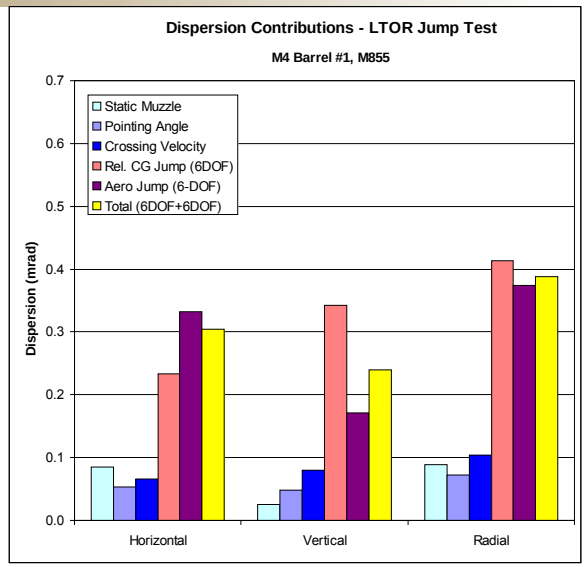

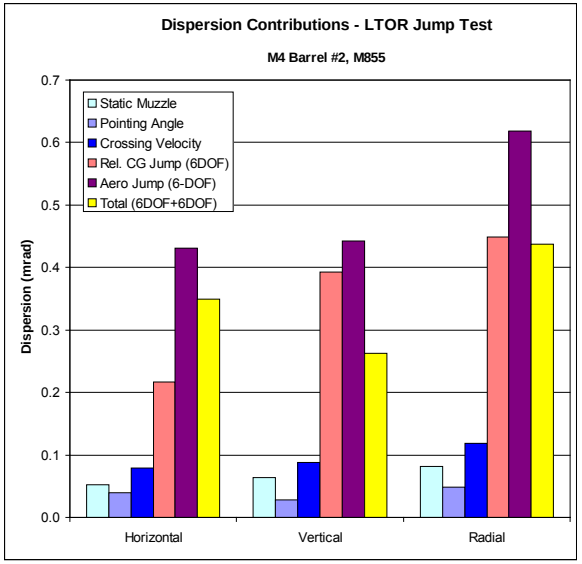

M4 Barrel #2, M855

Mann Barrel, M855

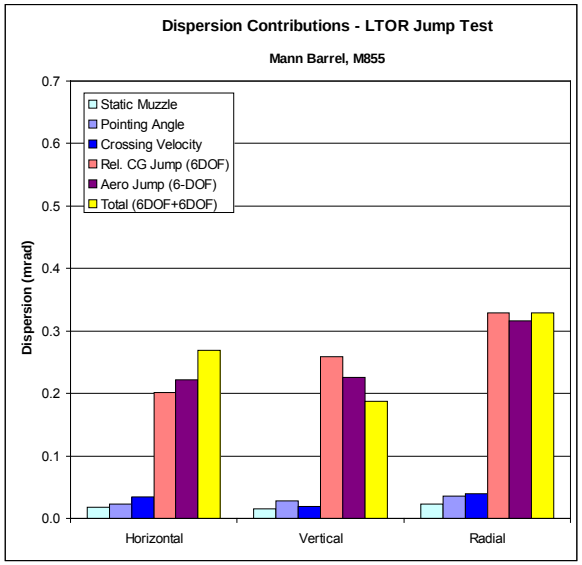

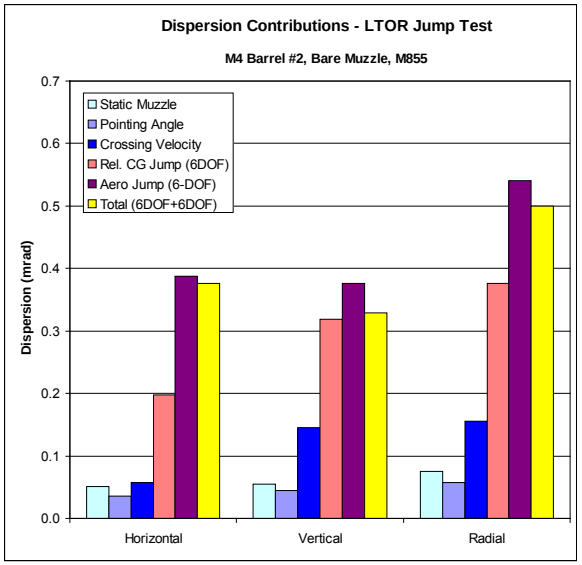

M4 Barrel #2, Bare Muzzle M855

Correlations – Barrel #2, M855

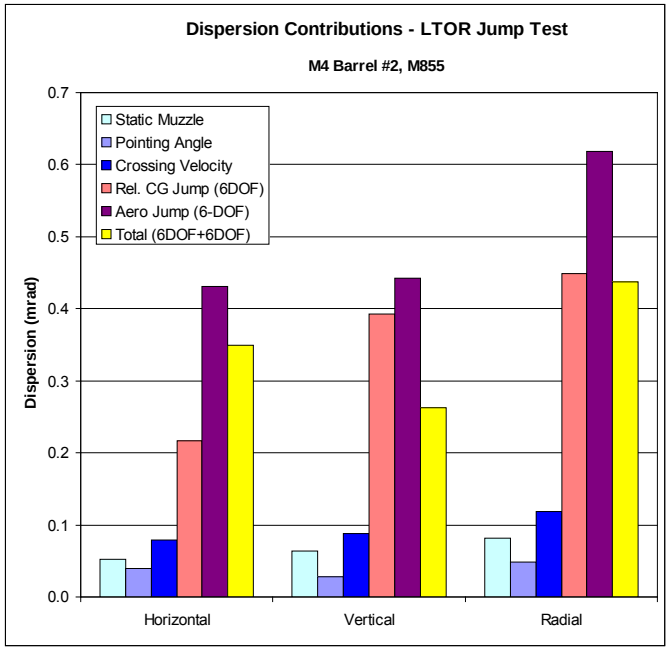

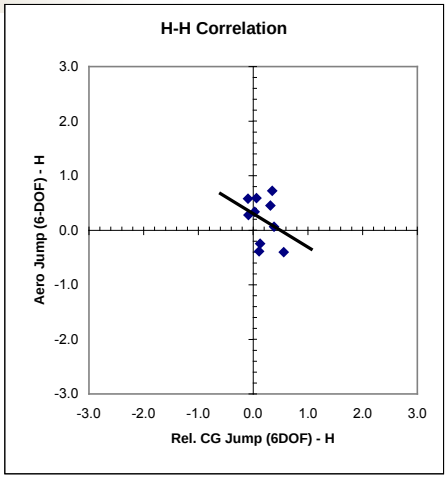

Correlation : -0.319
P value : 0.369
Confidence (%) : 63.1
Slope : -0.615

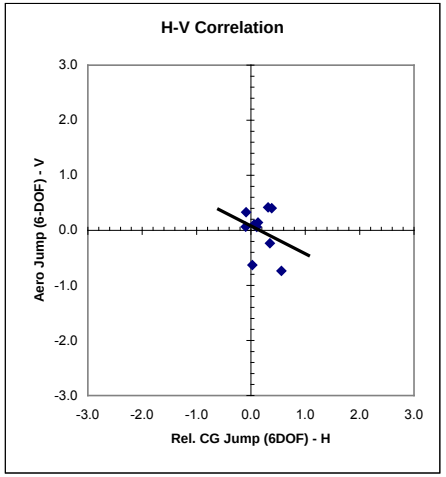

Correlation : -0.271
P value : 0.448
Confidence (%) : 55.2
Slope : -0.506

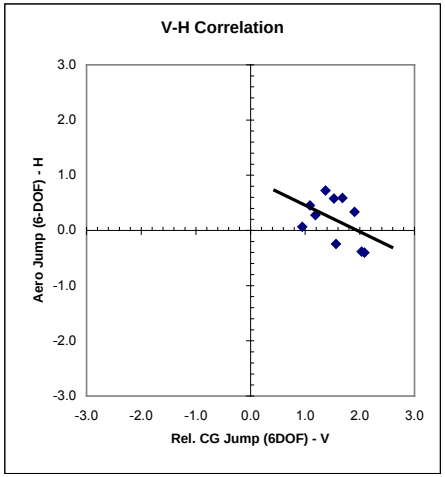

Correlation : -0.455
P value : 0.187
Confidence (%) : 81.3
Slope : -0.481

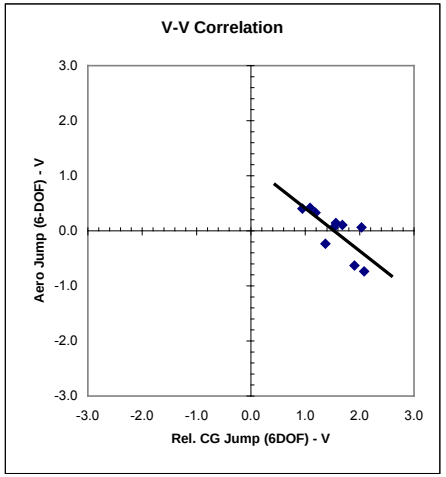

Correlation : -0.754
P value : 0.012
Confidence (%) : 98.8
Slope : -0.774

Muzzle compensator effect

- Muzzle compensator is vertically asymmetrical
- Induces vertical CG jump and negative correlation

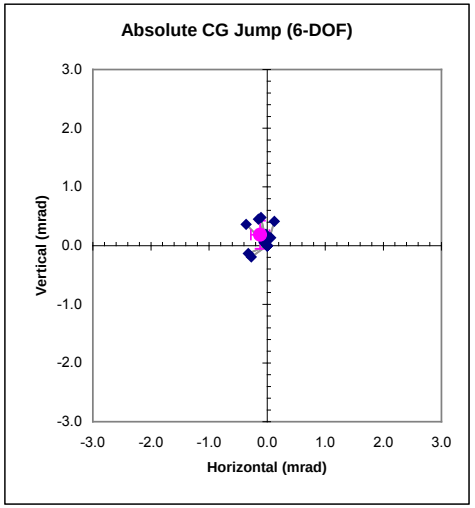

M4, Barrel #2, Bare Muzzle

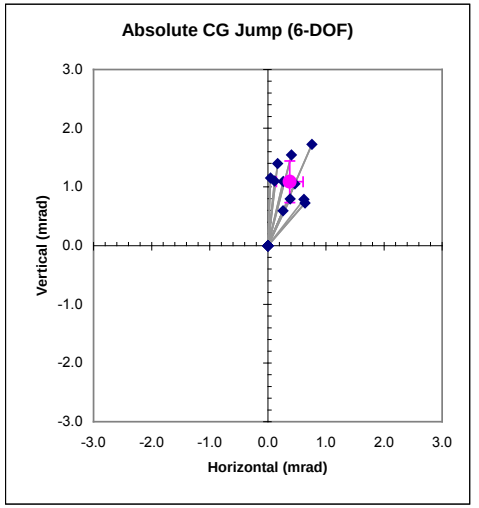

M4, Barrel #2, With Compensator

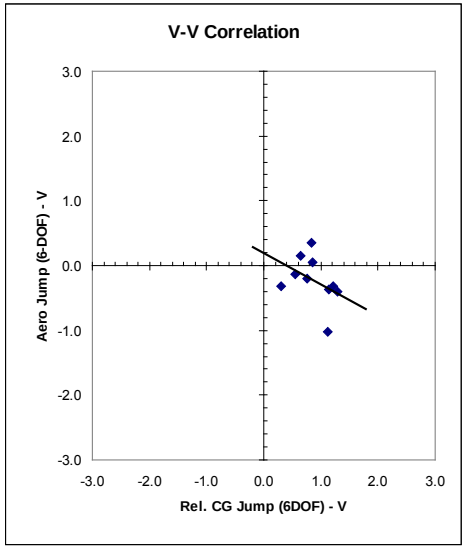

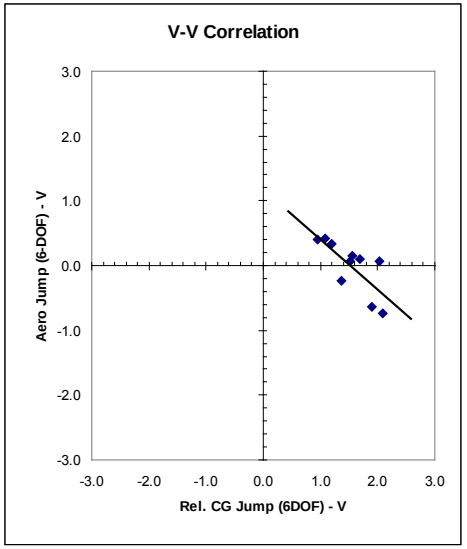

Muzzle compensator effect (continued)

- Magnitude of total jump increases dramatically
  - Total radial jump increase: 0.05 → 1.26 mrad
- Small decrease in dispersion of gun dynamics
  - Pointing angle RSD decrease: 0.06 → 0.05 mrad
  - Crossing velocity RSD decrease: 0.16 → 0.12 mrad
- Slight decrease in total dispersion
  - Total dispersion (RSD) decrease: 0.50 → 0.44 mrad
  - Dispersion decrease is mostly in vertical plane

Net effect of muzzle compensator seems to be positive (total dispersion is reduced).

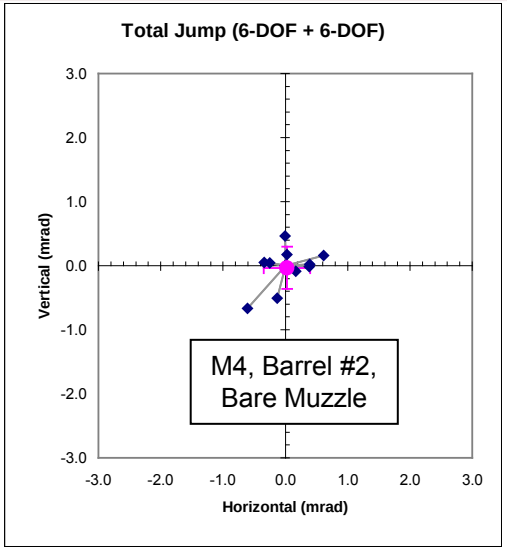

Avg.=(0.03, -0.04) SD=(0.38, 0.33)

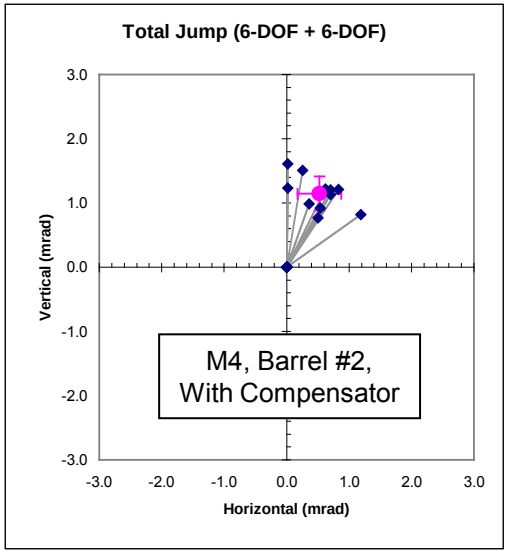

Avg.=(0.52, 1.15) SD=(0.35, 0.26)

Mann Barrel Results

When compared to standard M4 (average of Barrels #1 and #2)

- Magnitude of gun dynamics is reduced dramatically
  - Pointing angle (radial): 0.38 → 0.02 mrad
  - Crossing velocity (radial): 0.29 → 0.05 mrad
- Smaller decrease in dispersion of gun dynamics
  - Pointing angle RSD: 0.06 → 0.04 mrad
  - Crossing velocity RSD: 0.11 → 0.04 mrad
- Slight reduction in total dispersion
  - Total dispersion (RSD): 0.42 → 0.33 mrad

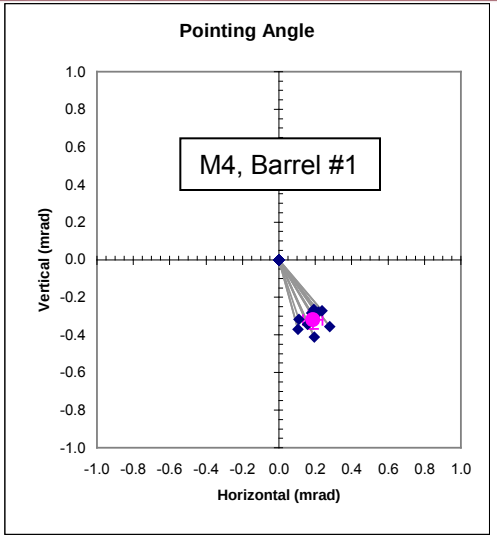

Avg.=(0.19, -0.32) SD=(0.05, 0.05)

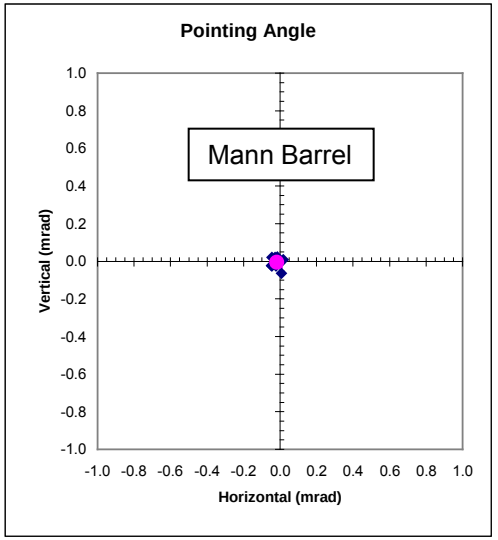

Avg.=(-0.02, -0.01) SD=(0.02, 0.03)

Mann Barrel Results

When compared to bare muzzle M4

- Magnitude of gun dynamics is reduced dramatically
  - Pointing angle (radial): 0.51 → 0.02 mrad
  - Crossing velocity (radial): 0.37 → 0.05 mrad
- Smaller decrease in dispersion of gun dynamics
  - Pointing angle RSD: 0.06 → 0.04 mrad
  - Crossing velocity RSD: 0.16 → 0.04 mrad
- Total dispersion is reduced
  - Total dispersion (RSD): 0.50 → 0.33 mrad

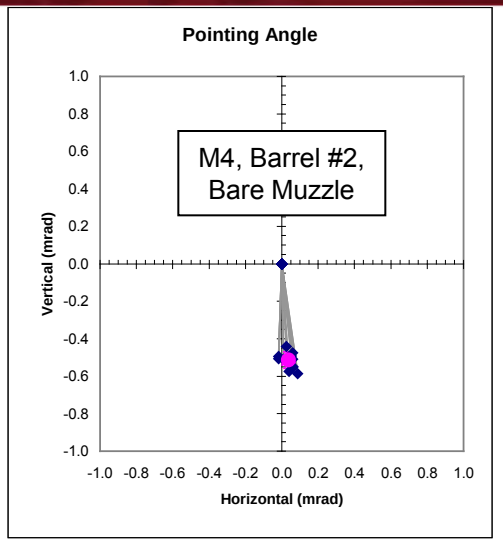

Avg.=(0.04, -0.51) SD=(0.04, 0.04)

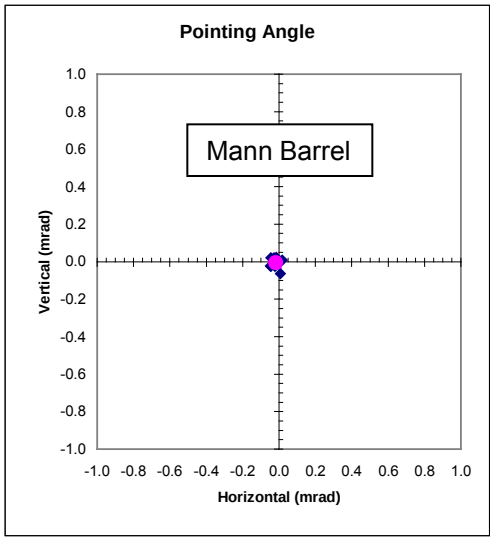

Avg.=(-0.02, -0.01) SD=(0.02, 0.03)

Summary/Conclusions

- Jump test methodology has been developed and validated for small caliber weapon systems
- Gun dynamics account for approx. 25% of dispersion of M4, M855 system
- Negative correlations between CG and Aerodynamic jump reduce total dispersion
- Reducing component dispersions will not always reduce overall target impact dispersion
- Muzzle compensator seems to enhance negative correlations
- Mann barrel launch environment is significantly different from M4
  - Mann barrel testing seems to reduce contribution of gun dynamics to dispersion
  - Some benefit for ammunition comparisons (with caveats)
  - Not valid for assessing system performance

Backup Slides

Description of test setup, instrumentation, and measurement techniques

Jump Test Description

- Description of test setup, instrumentation, and measurement techniques
- Description of jump components

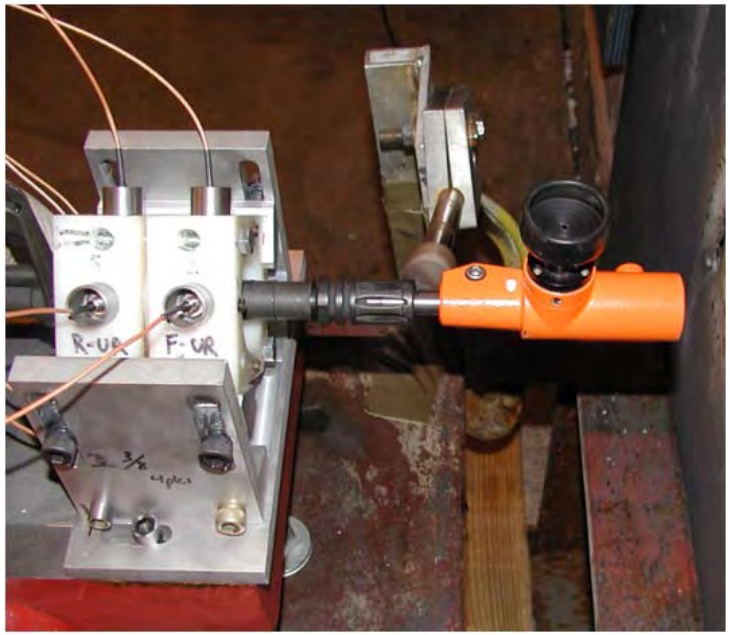

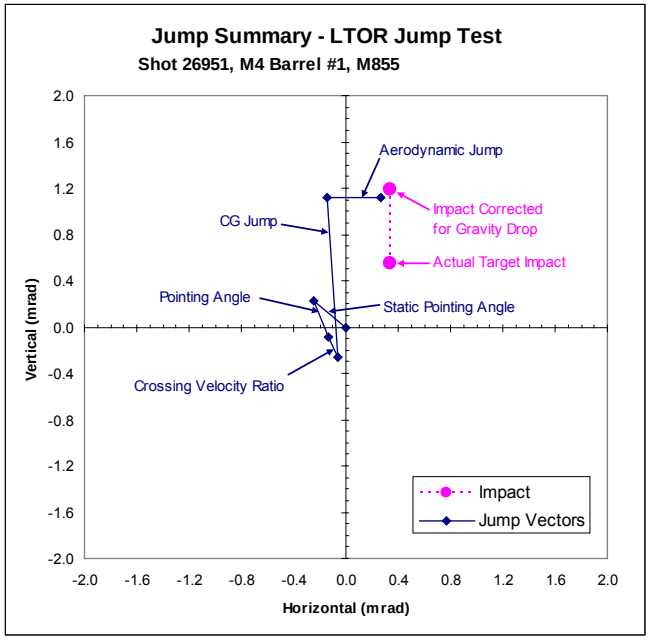

Gun mount

- Efforts were made to simulate a soldier holding the weapon by mounting the gun in a semi-rigid support
- The gun was allowed to recoil, the hand rest was supported underneath, and a shotbag was used to simulate grip

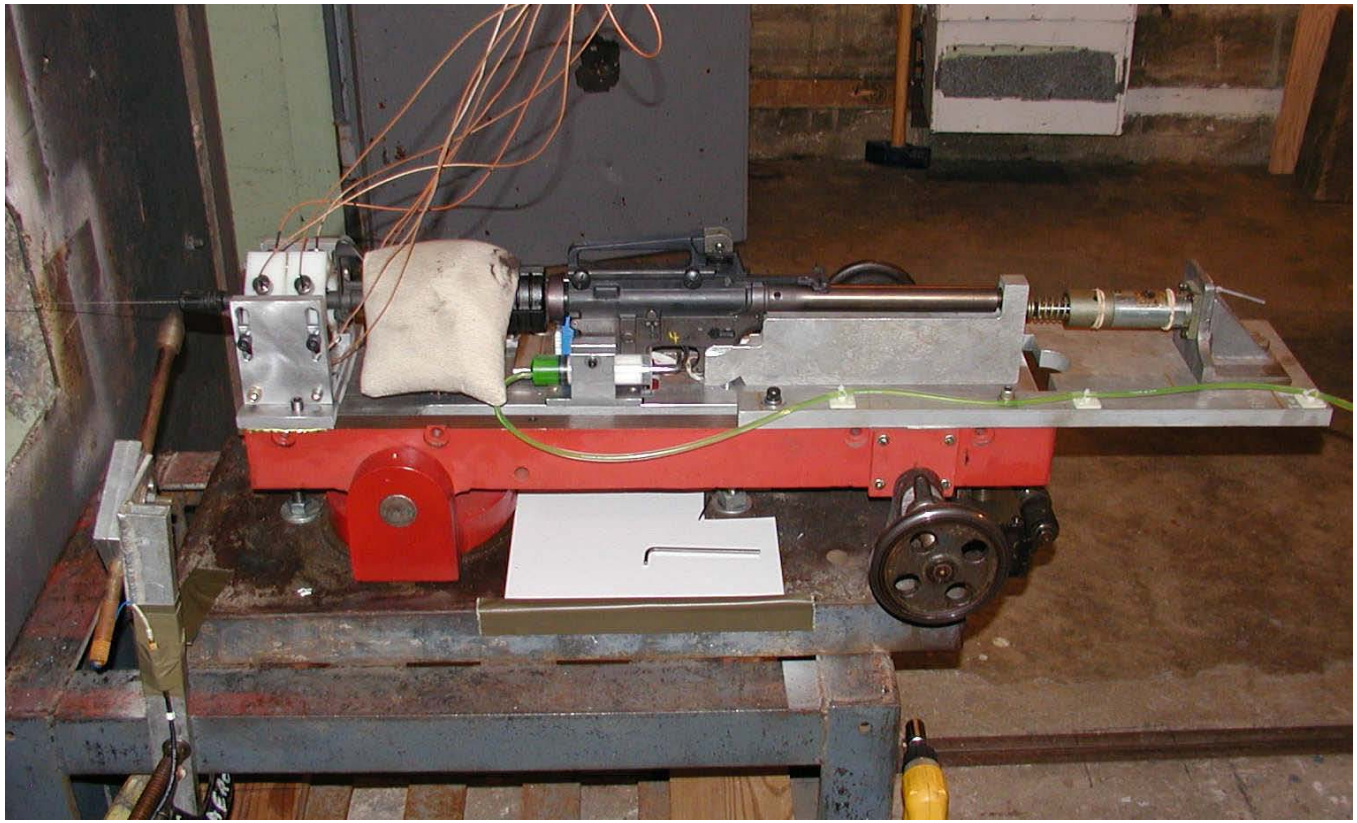

Testing was conducted in the ARL Aerodynamic Experimental Facility

39 direct image orthogonal shadowgraph stations in 5 groups

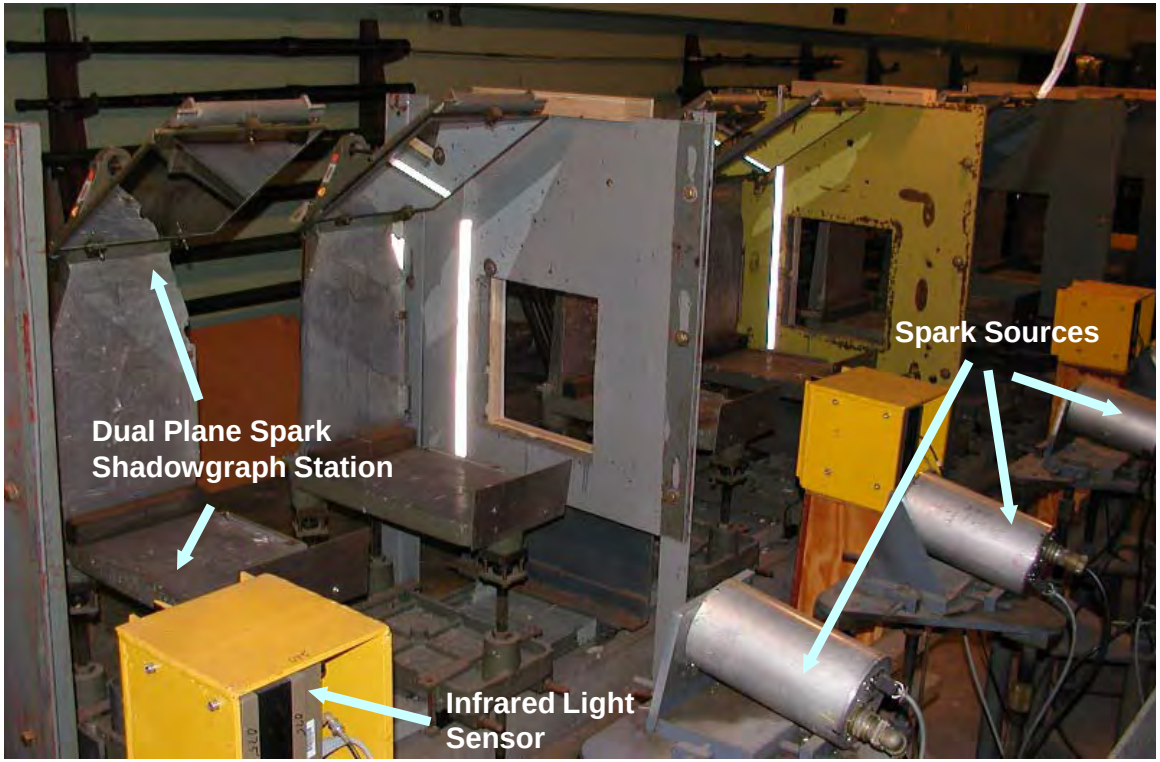

Image window is less than 14 inches across

Spark source triggered at a recorded time after infrared sensor detects passing projectile

Each station surveyed into a fiducial system that is simultaneously imaged on the film with the projectile

The spark shadowgraphs are used to obtain the projectile position and angle

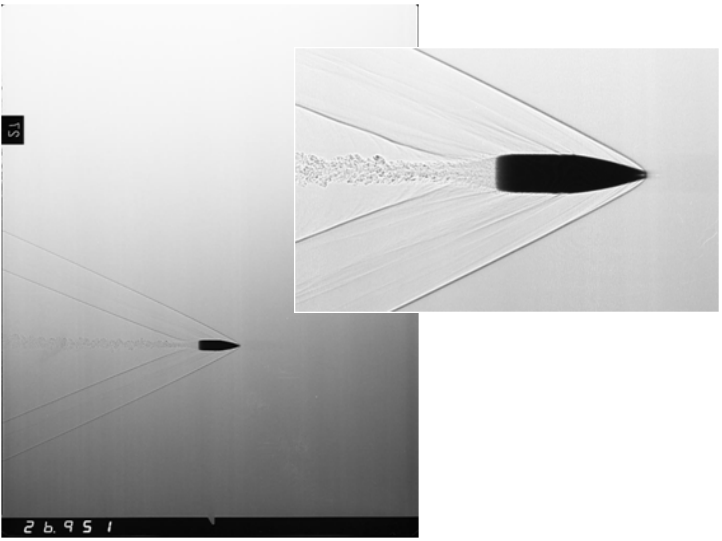

Film is read using a precision light table to determine spatial coordinates and angular orientation of the projectile

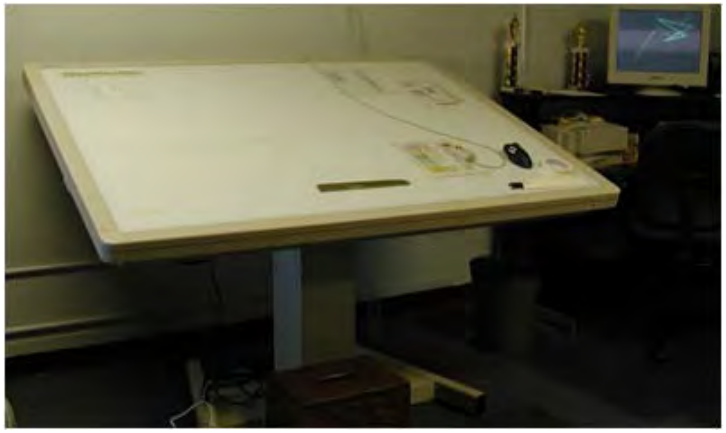

Aero Range Facility Data Analysis Software – ArrowTech Associates

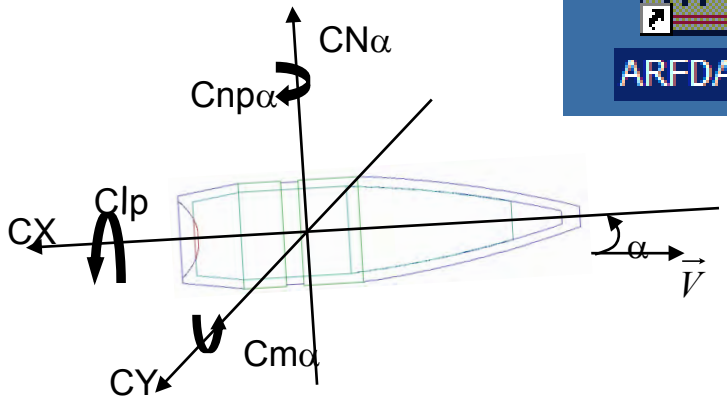

Data is reduced for a 6-DOF fit in order to obtain an aerodynamic model and motion fit

The initial line of fire (LOF) must be established in range coordinates

- LOF is defined by muzzle location and boresighted aimpoint
- Muzzle is located using fiducial cable hung through first group of range stations
- Aimpoint is measured in range coordinates

The muzzle location is determined by hanging a fiducial cable

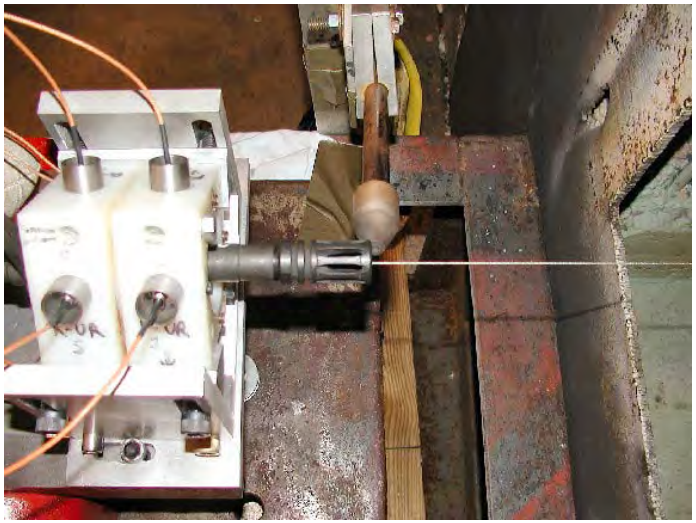

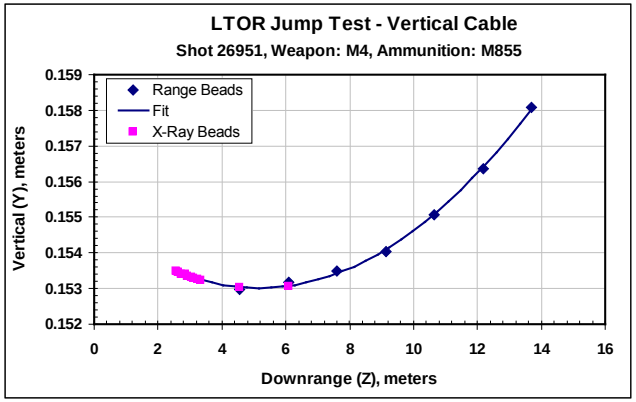

- Cable extends from muzzle through first group of range stations
- Calibrated bead locations are measured in range coordinates
- Extrapolated fit defines muzzle position (and x-ray beads)

Gun motion is measured using proximity (eddy current) probes

- Initial (boresighted) angle
- Dynamic angle and motion at shot exit

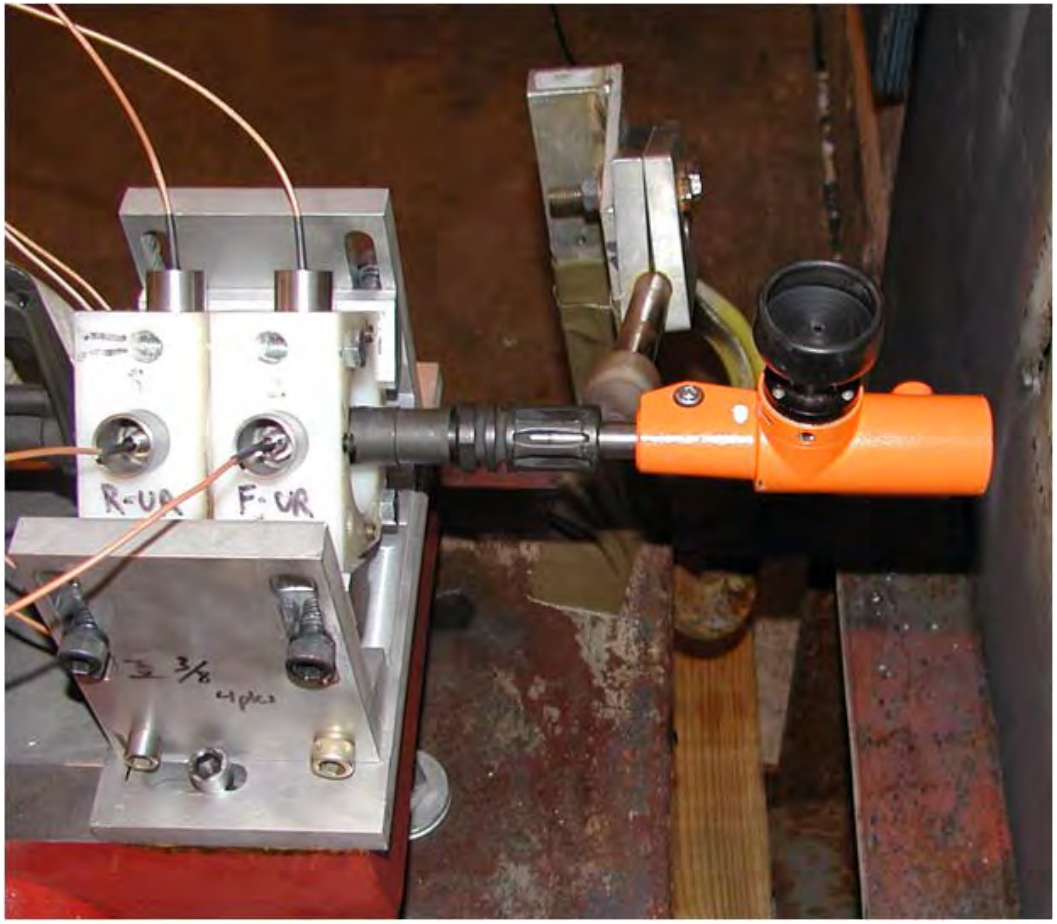

The eddy probe data is processed to determine the muzzle condition at shot exit

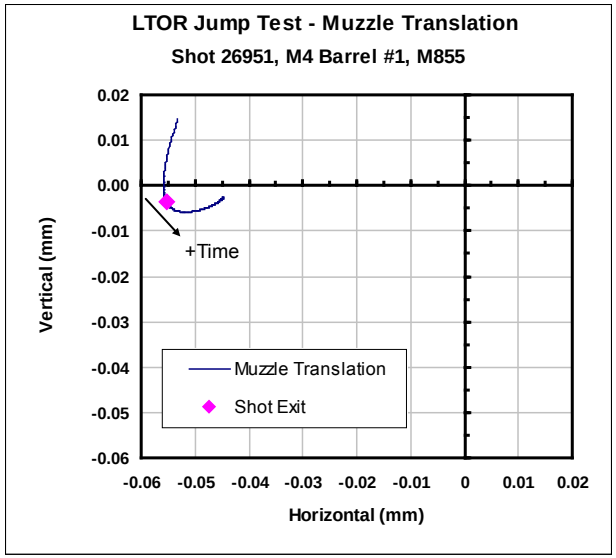

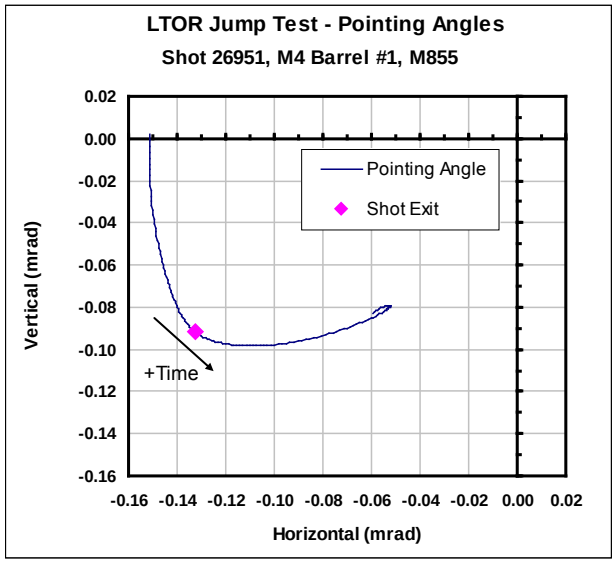

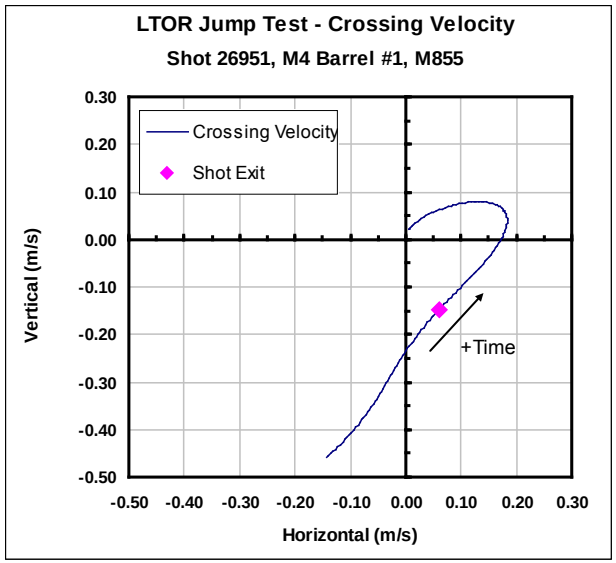

- Muzzle Pointing Angle – where the gun muzzle is pointed at instant of shot exit
- Muzzle Crossing Velocity – which way the gun muzzle is moving at shot exit

Initial CG trajectory is determined from the spark range data

- Initial tests showed x-rays were not needed
- 6-DOF fit to range data is extrapolated back to muzzle to get initial trajectory

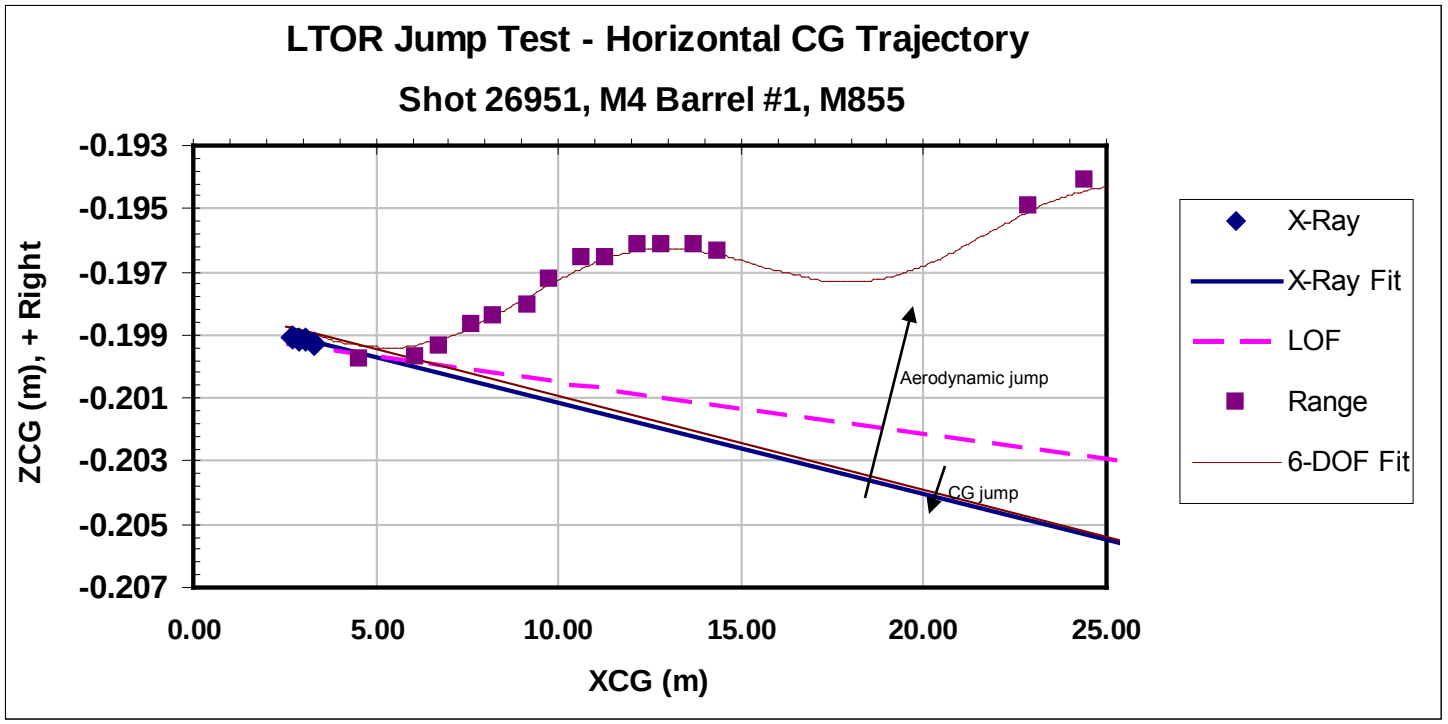

Aerodynamic jump is calculated from initial angles, angular rates, and aerodynamic coefficients

$$A_J = \left(\frac{I_y}{md^2}\right)\left(\frac{C_{L_\alpha}}{C_{M_\alpha}}\right)\left[i\left(\frac{I_x}{I_y}\right)\left(\frac{pd}{V}\right)\xi_0 - \xi_0'\right]$$

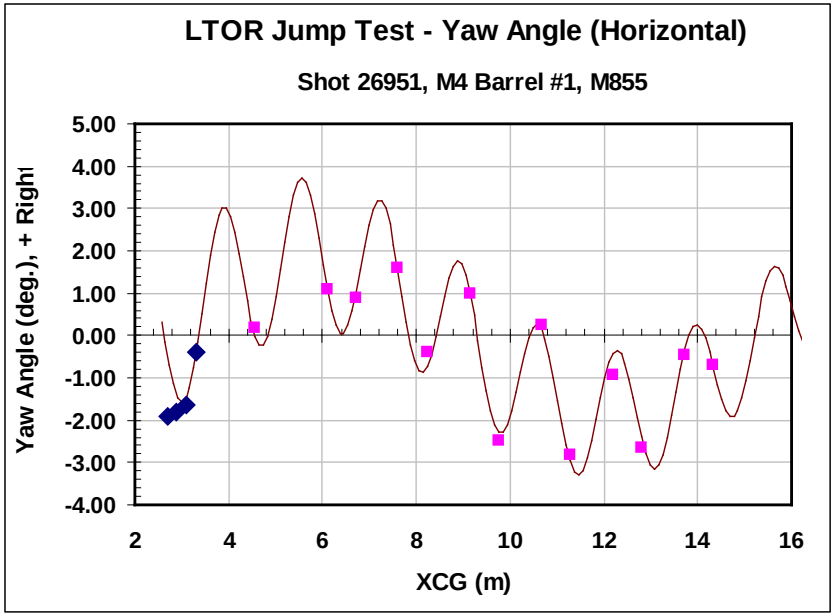

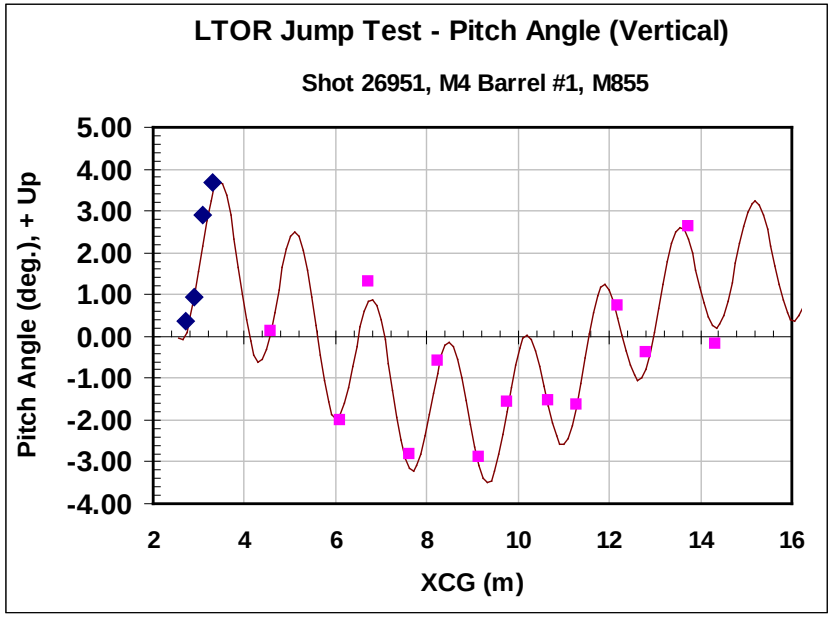

- Initial tests showed x-ray angular measurements were unreliable
- Initial angles and rates are obtained by extrapolating 6-DOF fit of range data back to the gun muzzle
- Aerodynamic coefficients obtained from 6-DOF fit of range data and augmented with results from previous testing

Impact location is measured on the target

- Impact is measured relative to aimpoint
- Impact is adjusted for gravity drop

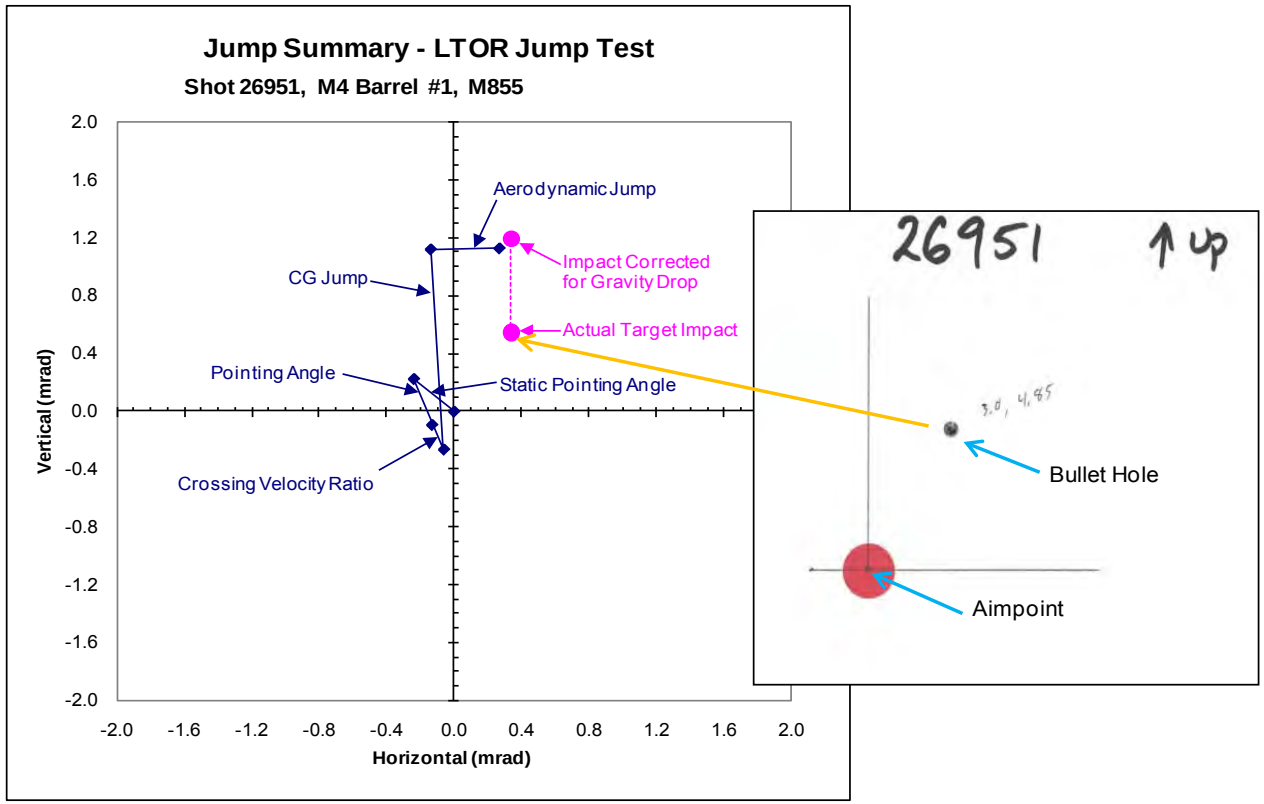

Closure is determined by comparing vector sum of jump components with adjusted impact

Closure diagram for single shot

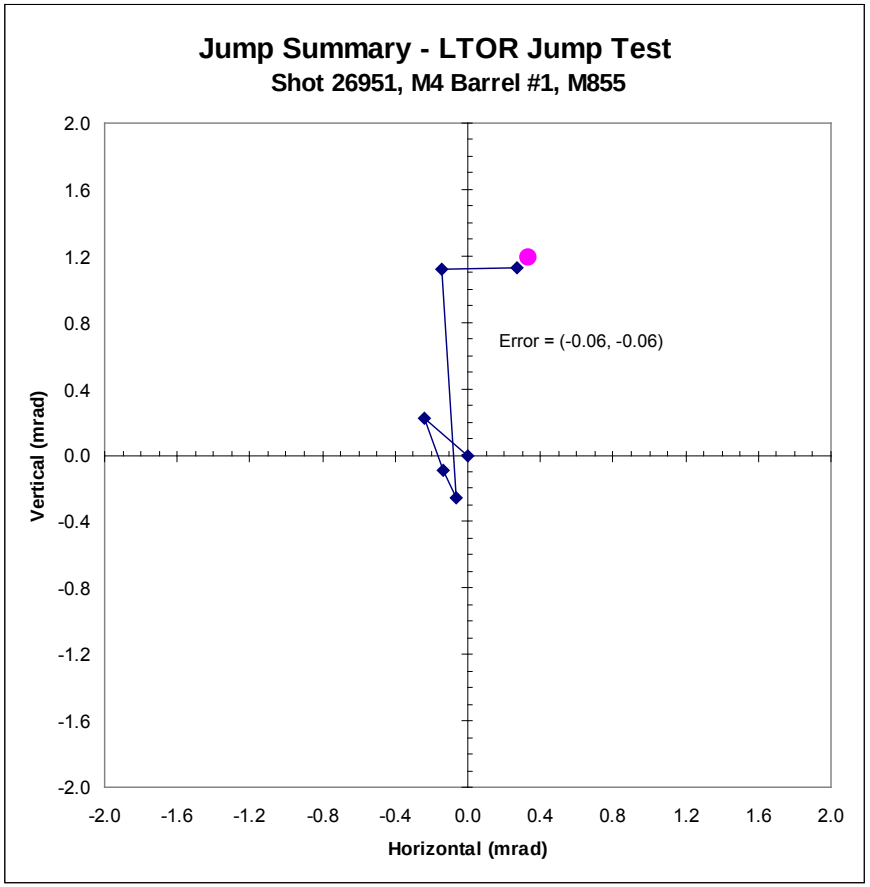

10-shot group, M4 Barrel #1, M855

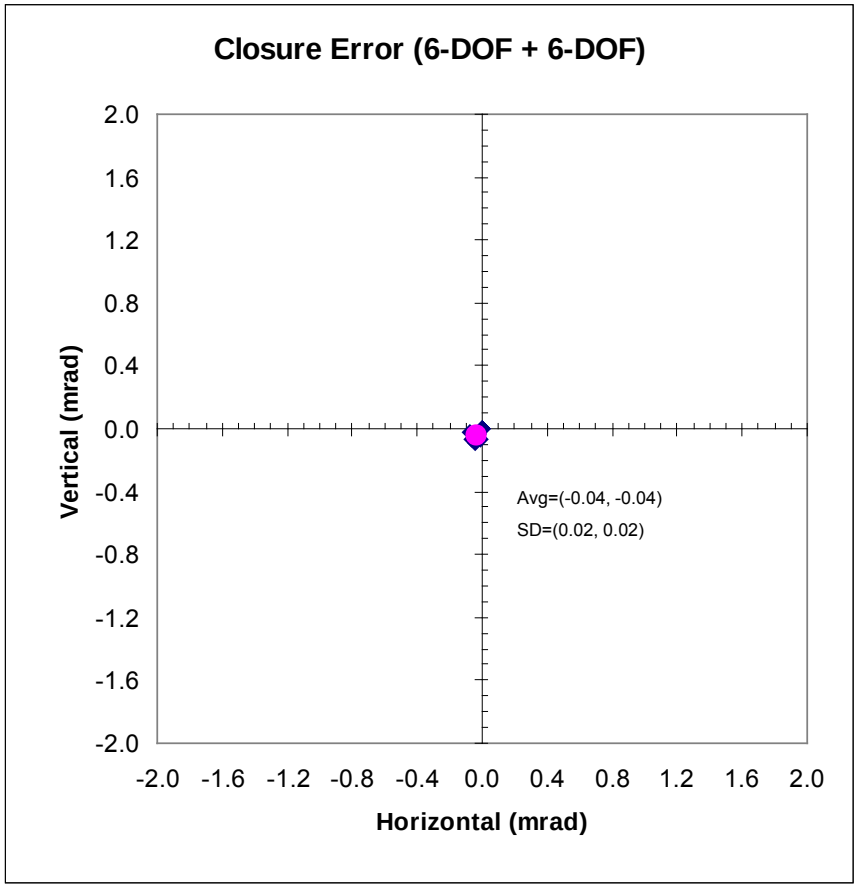

Traditionally, closure is declared when error < 0.2 mrad
For this test setup, 1 bullet diameter = 0.06 mrad.

Contact Info

Ilmars Celmins
U.S. Army Research Laboratory
ATTN: RDRL-WML-E
Aberdeen Proving Ground, MD 21005-5066
410-306-0781 Fax: 410-306-0666
Email: ilmars.celmins.civ@mail.mil

TECHNOLOGY DRIVEN. WARFIGHTER FOCUSED.

Modeling Explosive Cladding of Metallic Liners to Gun Tubes

Jack M. Pincay, Dr. Ernest L. Baker, and David G. Pfau

26th International Symposium on Ballistics

Explosive Cladding Modeling

- Objective: Develop and demonstrate modeling for explosive barrel cladding process design and optimization.
- Approach: Physically model the process of barrel liner cladding.
  - High Explosive Behavior
  - Full scale liner cladding behavior
  - Subscale clad welding dynamics
  - Modeling development , Cladding process design, and optimization.
  - Initial Gun Modeling and Momentum Trap Modeling
- Conclusion

Explosive Cladding

High Explosive Behavior

- **Original Approach (standard)**
  - Thermochemical EOS: JAGUAR
  - Thermodynamic EOS: JWLB
  - Standard method produced poor agreement to detonation velocity of TPL low density low detonation velocity formulations
- **Current Empirical Approach (BondEx-A, D2)**
  - Experimental detonation velocity
  - Empirical gurney velocity relationship
  - Empirically scaled energy output vs. volume expansion
  - Use analytic cylinder and nonlinear optimization to parameterize JWL and JWLB equations of state
- **Desired Empirical Approach**
  - New formulation (reproducible known ingredients)
  - ARDEC cylinder tests (Ta and Cu cylinders)

Cylinder Velocity

ANALYTIC CYLINDER MODEL

JWLB Equation of State:

$$P = \sum_i \mathrm{A}i\left(1 - \frac{\lambda}{\mathrm{R}iV^*}\right)e^{-\mathrm{R}iV^*} + \frac{\lambda E}{V^*} + \mathrm{C}\left(1 - \frac{\lambda}{\omega}\right)V^{*-(\omega+1)}$$

Gruneisen Parameter:

$$\lambda \equiv \sum\left(\mathrm{A}\lambda \mathrm{i}V^* + \mathrm{B}\lambda \mathrm{i}\right)e^{-\mathrm{R}\lambda iV^*} + \omega$$

Analytic Model:

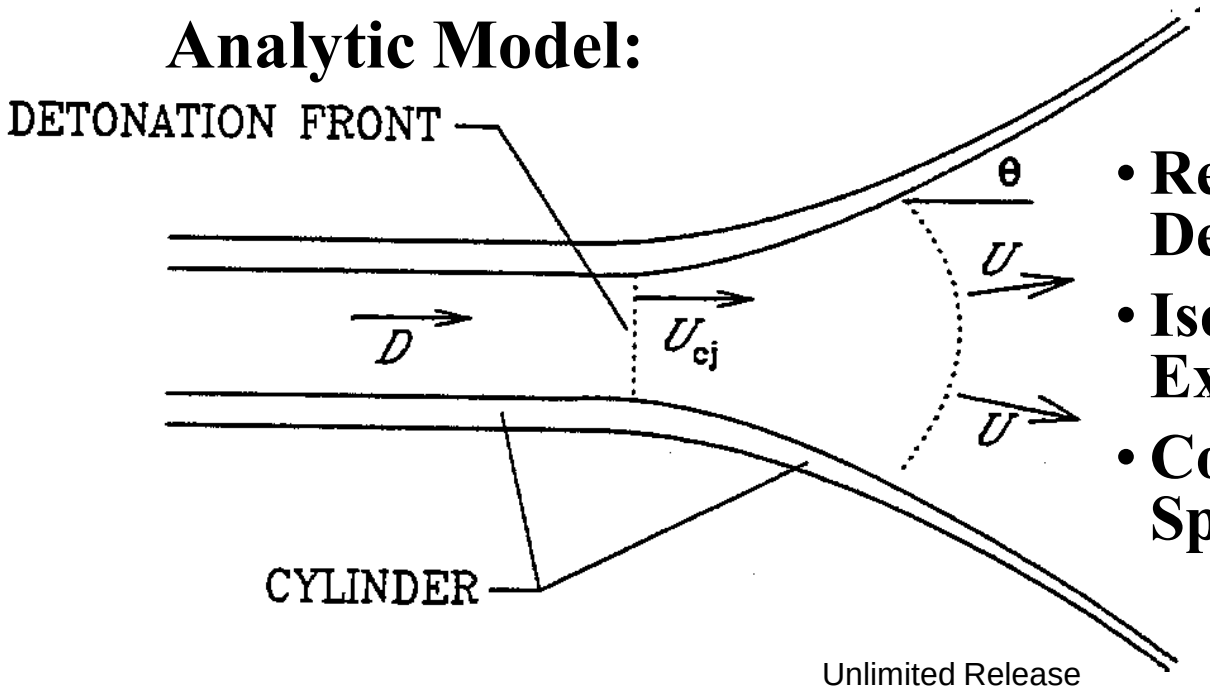

- **Reference Frame at Detonation Velocity**
- **Isentropic Products Expansion**
- **Constant Properties Along Spherical Surfaces**

ARDEC CYLINDER TEST

Experiment Setup

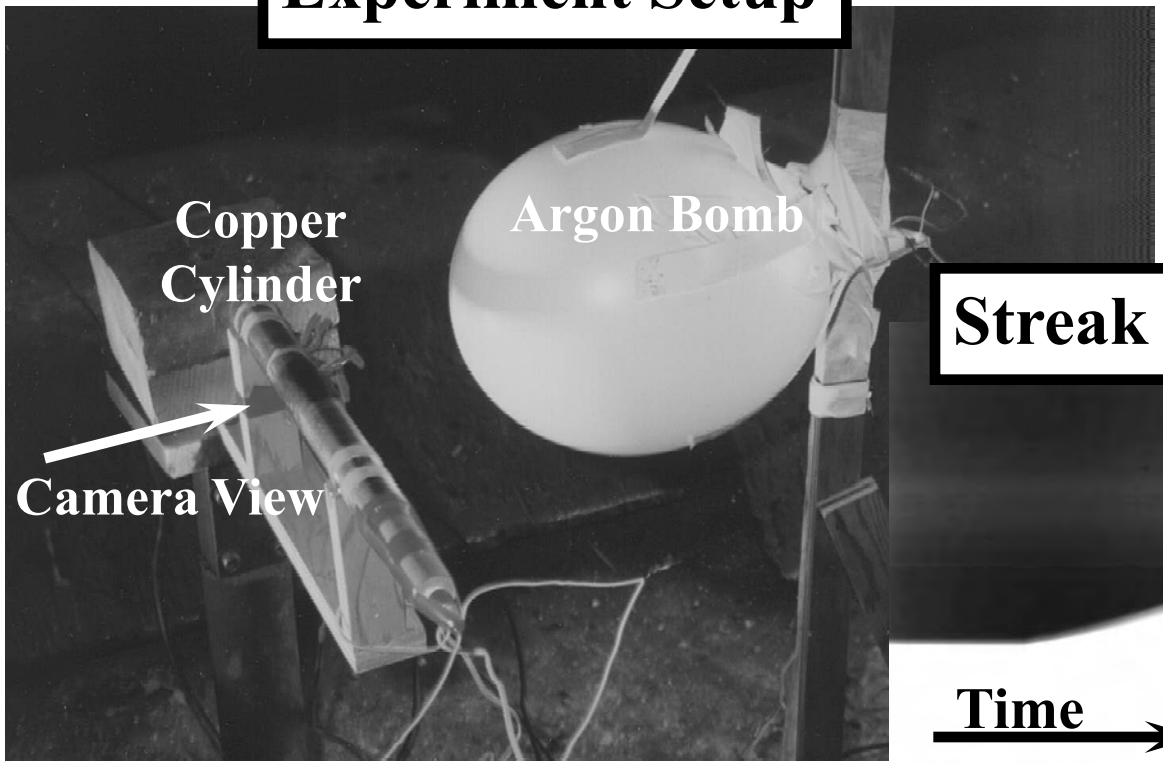

Streak Photograph Result

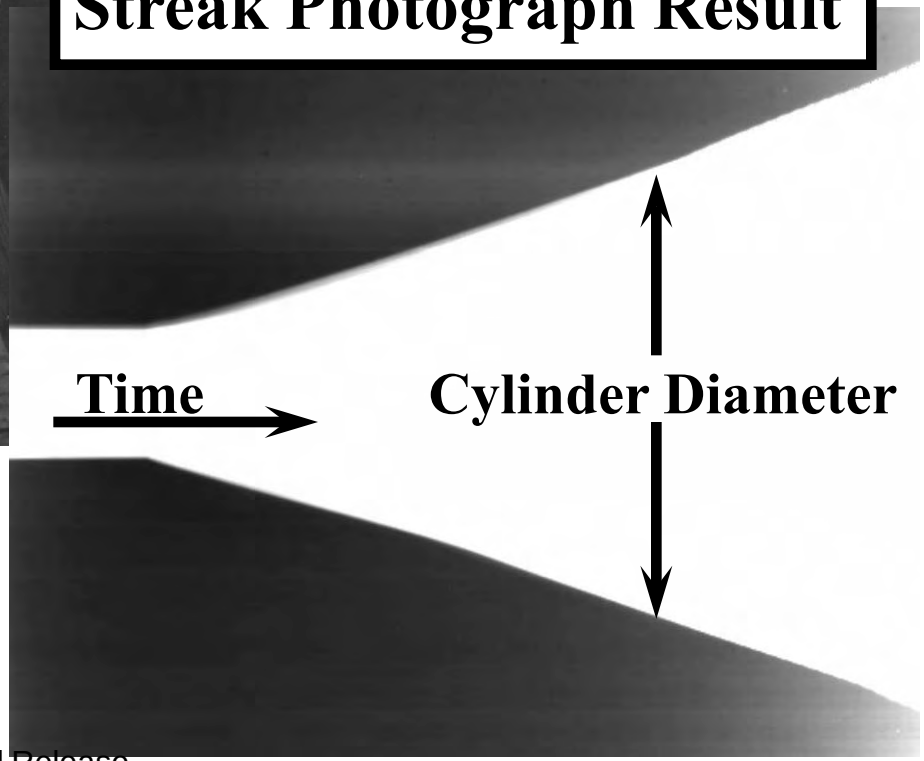

Explosive Cladding

Macro Scale Behavior

Step Test for Development (based on TPL input)

Steel Stepped Cylinder

Cladding Cylinder

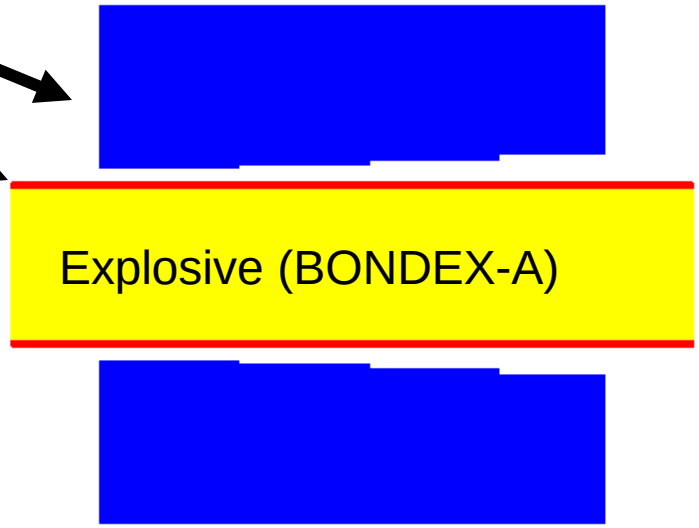

CTH currently being used for modeling due to advanced ZA strength model

Steel Issues: 25mm Bushmaster barrel is D6AC (no current material model)
current modeling using 4340
D6AC samples sent to LANL for Hopkinson bar/material model
Modeling using Zirelli-Armstrong (ZA) strength model

Cladding Cylinder issues: No high rate strength models for Ta-5W-2Mo or Stellite 25
Downselection from step tests will determine if required

High Explosive Clad Setup

- CALE and CTH Trial runs performed
  - CTH downselected due to availability of advanced ZA strength model and parameters
- CTH Modeling
  - Tantalum as the cladding liner material.
  - Ta10W as the cladding liner material.
- Mesh Convergence Study
  - 1 mm mesh, .50 mm mesh, .25 mm mesh
- Macro-Analytic Comparison
  - Analytic Velocity Comparison
- Micro Clad welding Dynamics
  - 0.1 mm mesh

CTH Cladding Model

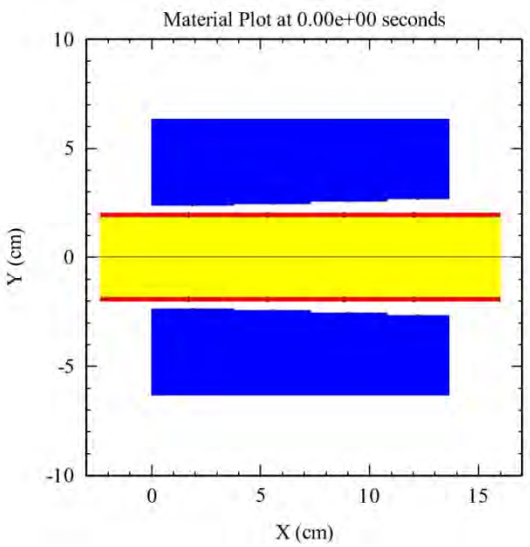

Initial State at Time=0 us

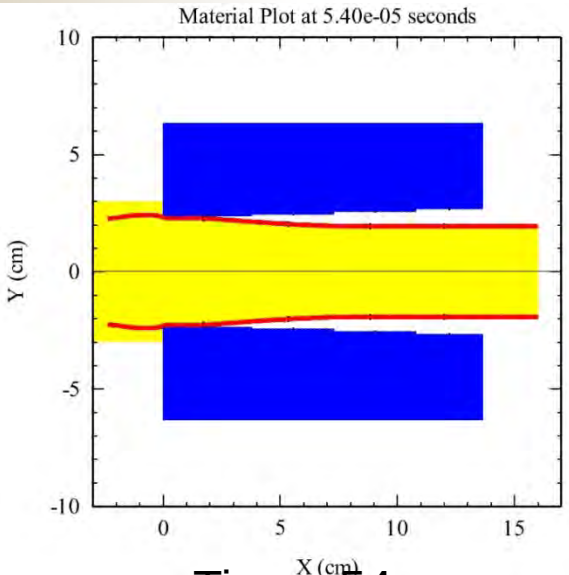

Time= 54 us

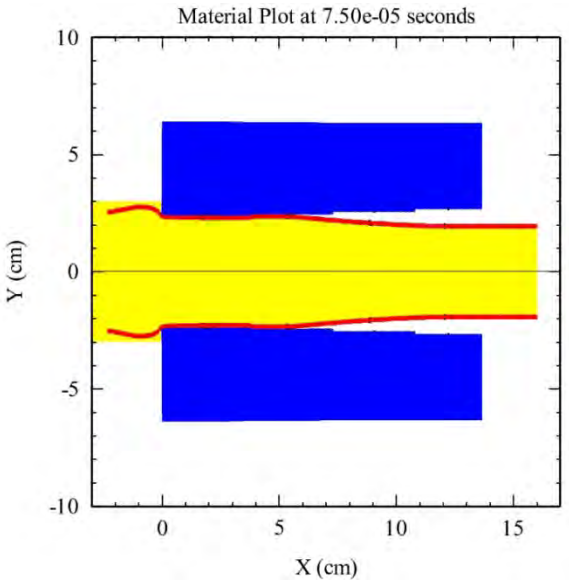

Time= 75 us

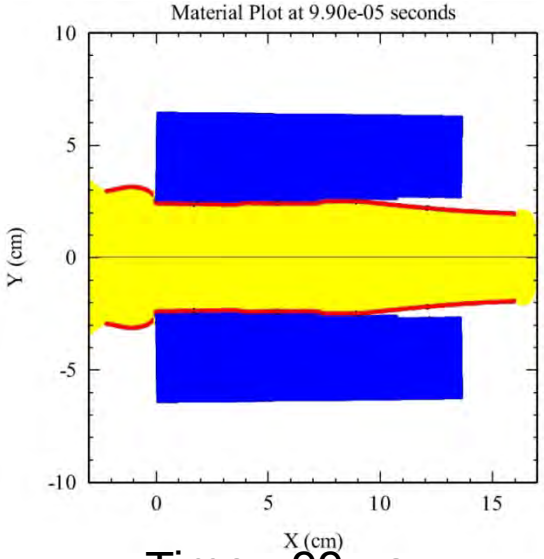

Time= 99 us

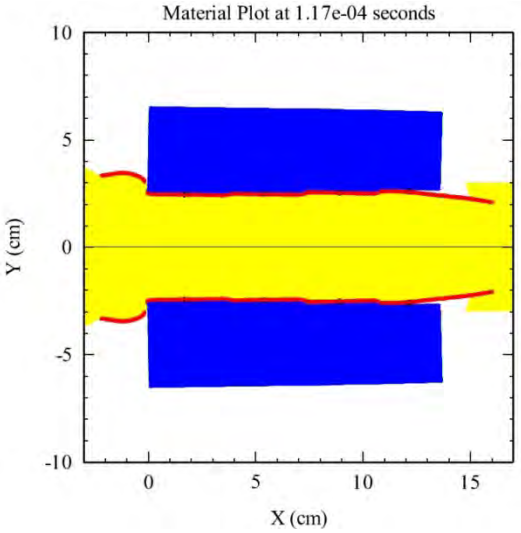

Time= 117 us

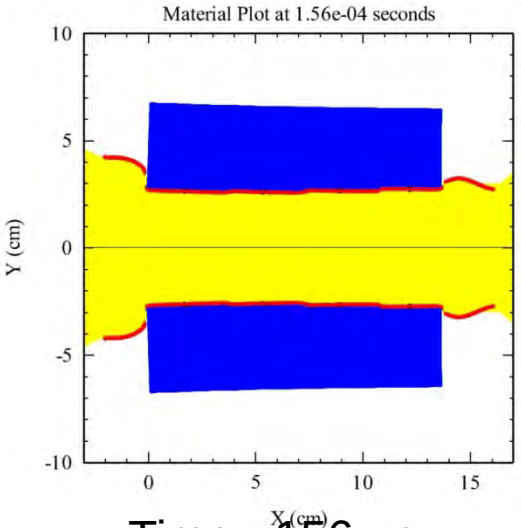

Time= 156 us

Simulation of Step Cladding

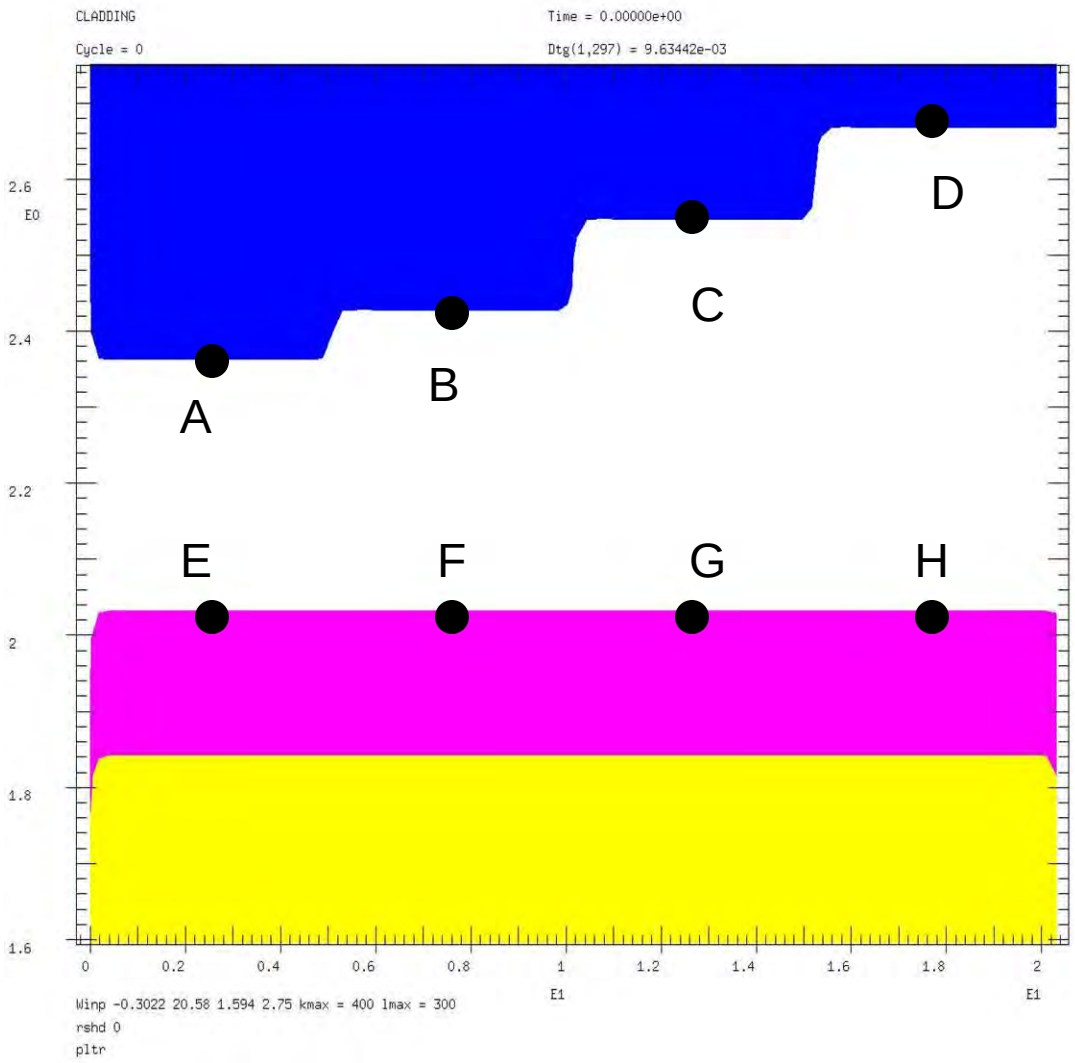

Tracer Particles were added to find velocities and pressures at the middle of each step as the tantalum is hitting the steel.

Particles A,B,C, and D are fixed on the location of the middle of each step.

Particles E,F,G, and H are placed on the tantalum outer surface and move along with the tantalum material.

.50 mm Mesh Plot

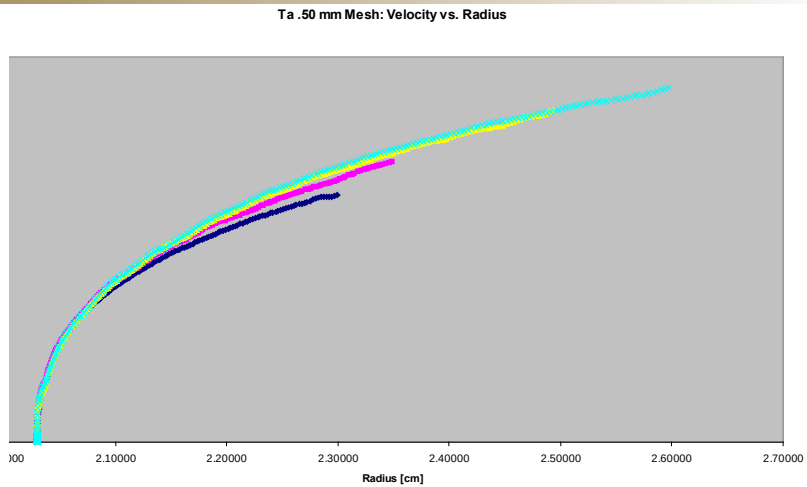

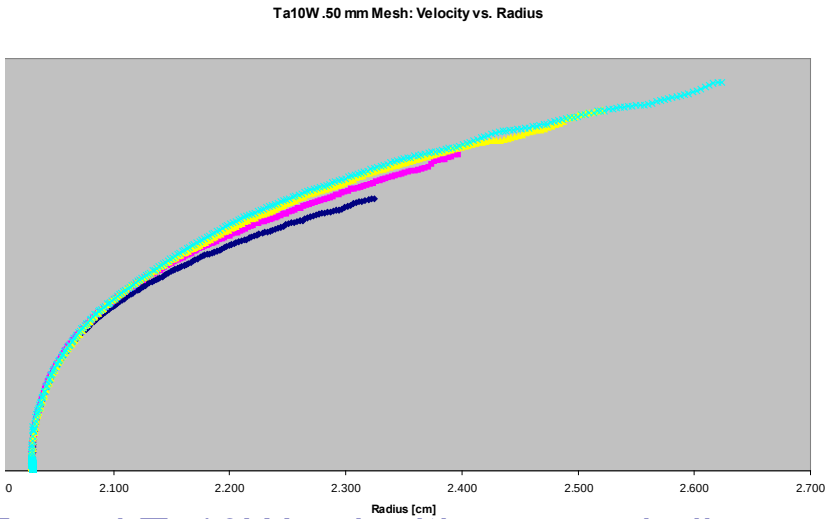

Cladding cylinder accelerates until impact Ta and Ta10W velocities very similar

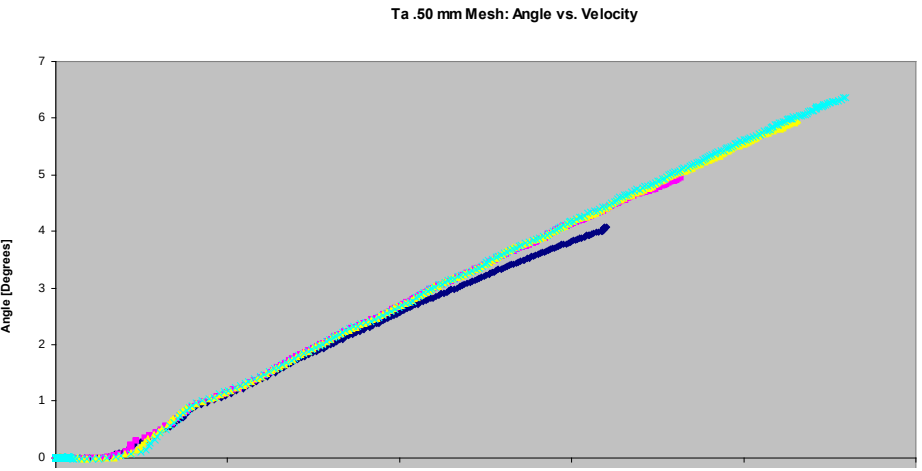

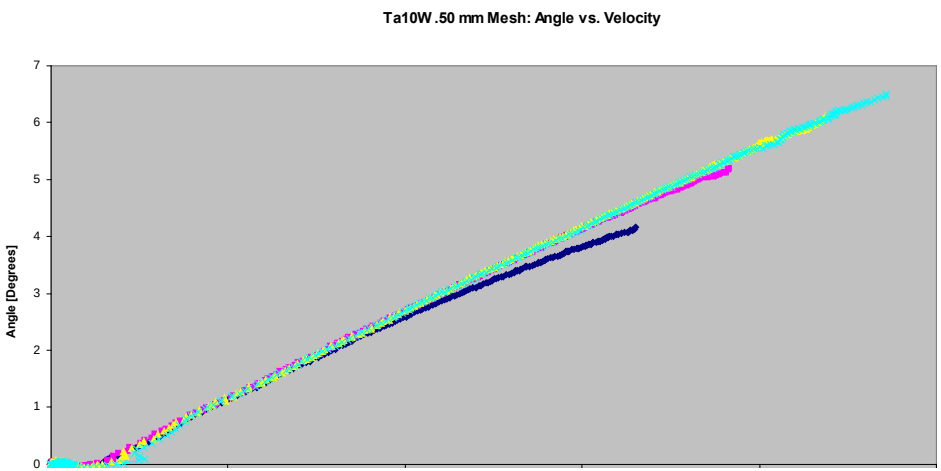

Cylinder angle increases with velocity until impact Linear angle vs. cylinder velocity (Taylor relationship)

Macro Scale Cladding Interface Behavior

.25 mm Mesh Ta Plot Interface

First Step Cladding is close to an arc.

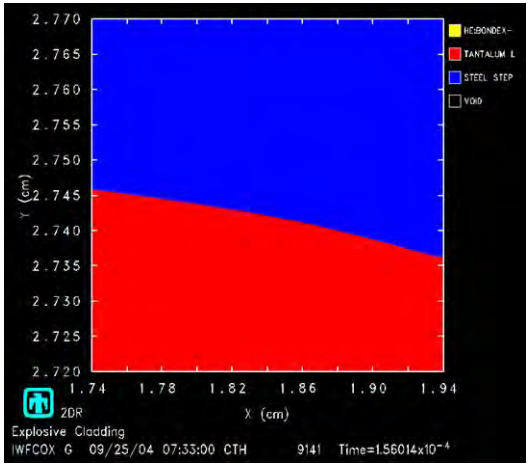

Second Step Cladding is close to a small arc.

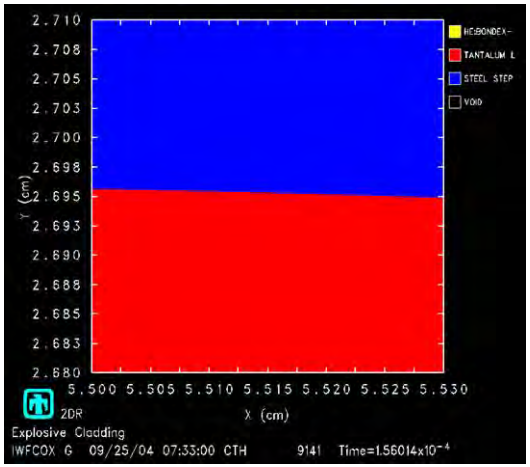

Third Step Cladding is close to a small arc .

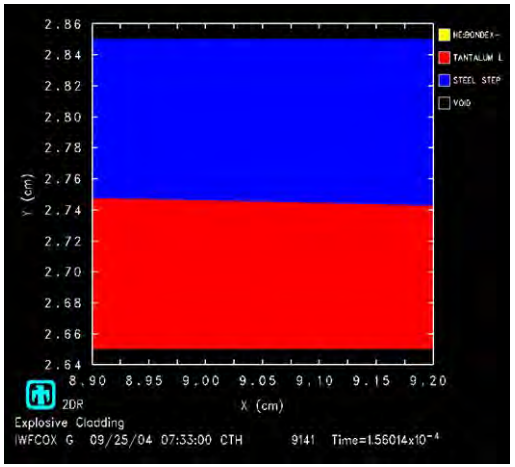

Forth Step Cladding is close to an arc.

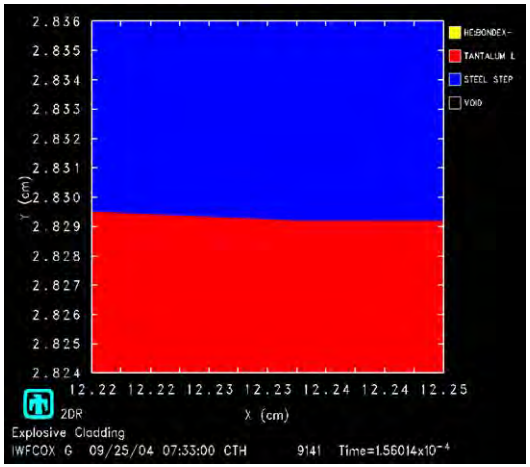

Full macro scale dynamics are fairly well resolved using a .50mm mesh

Explosive Cladding
Micro Scale Behavior

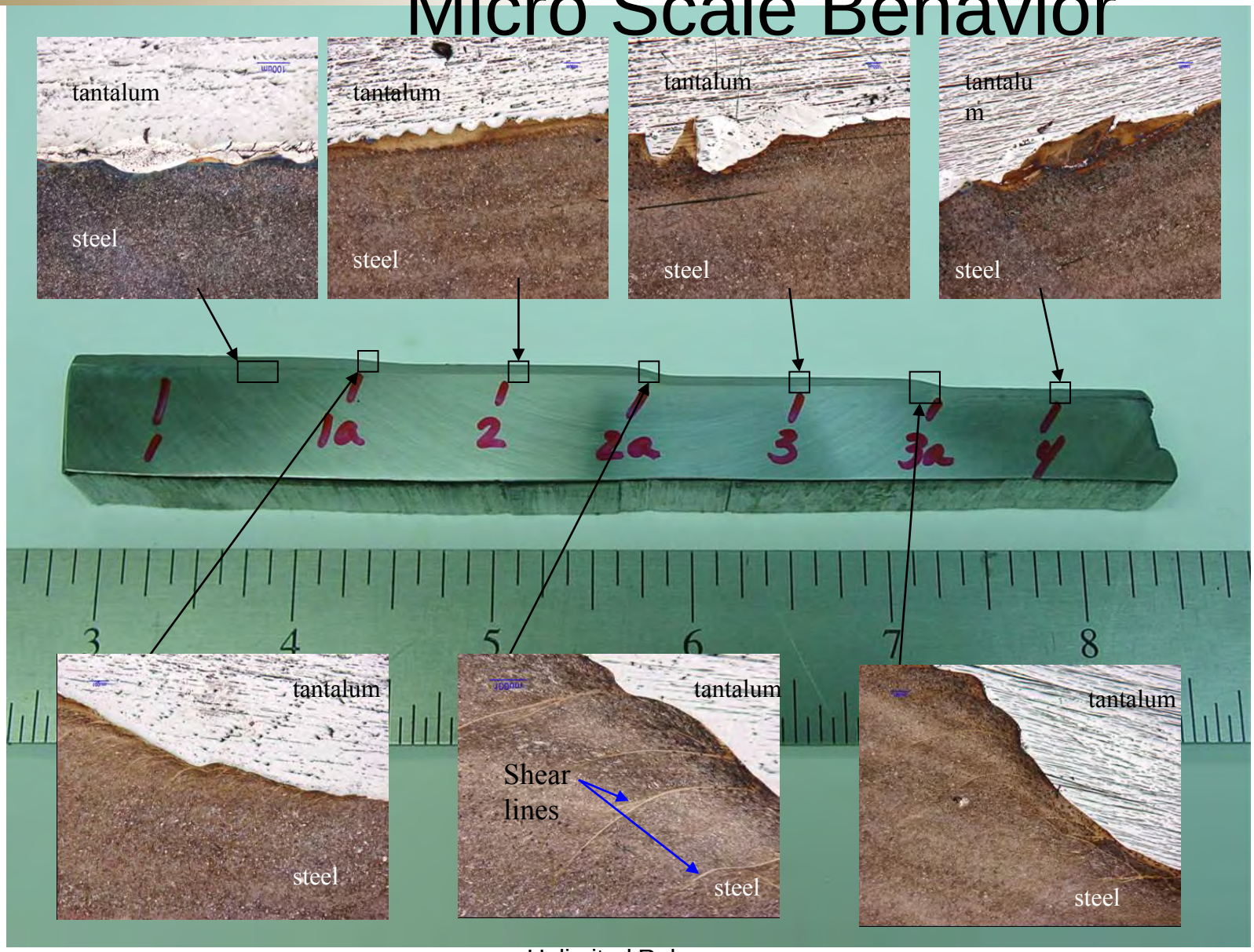

Micro Scale Cladding Interface Behavior

Ta .1 mm Mesh

Step 1

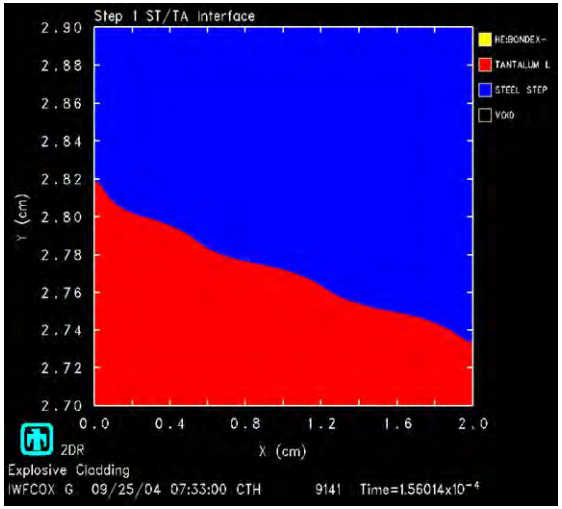

Step 2

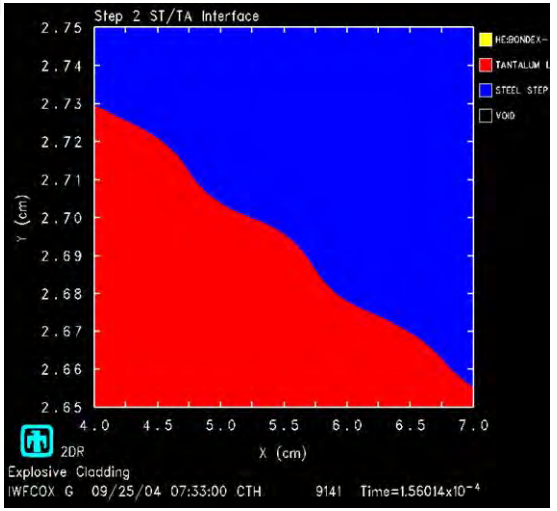

Step 3

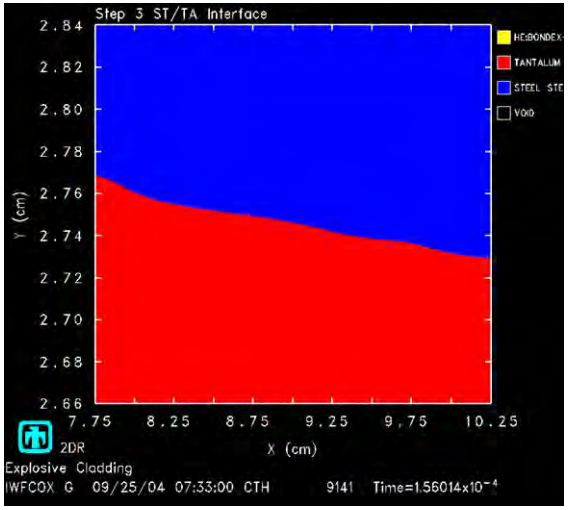

Step 4

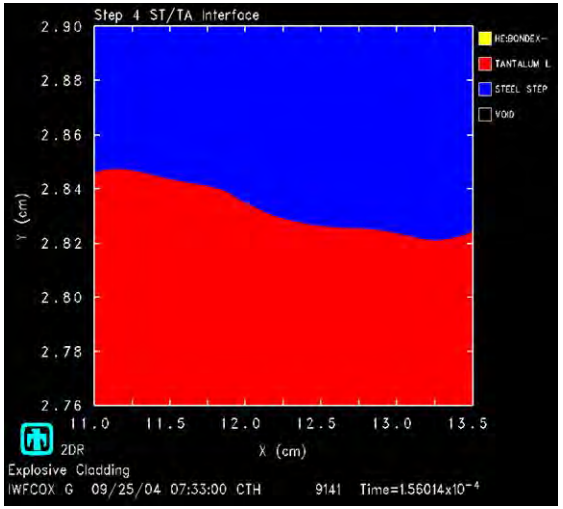

~.30mm interface wavelength identified from fine scale modeling

Hints of undesirable behavior at Step 4?

Micro Scale Cladding Interface Behavior

Ta10W .1 mm Mesh Interface

Step 1

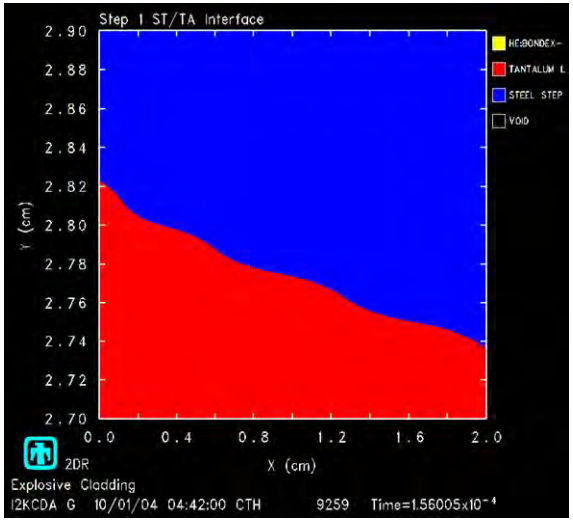

Step 2

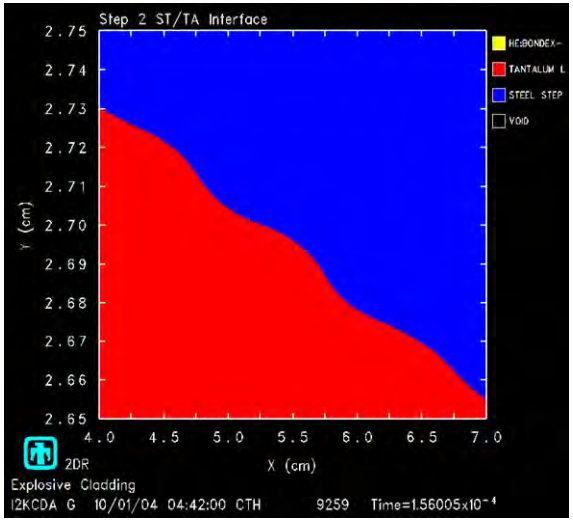

Step 3

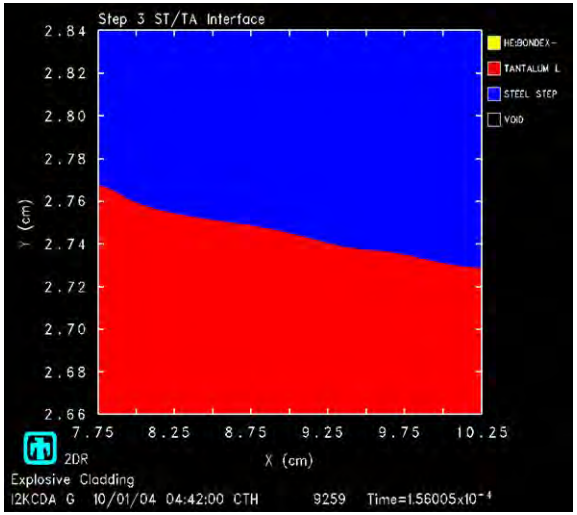

Step 4

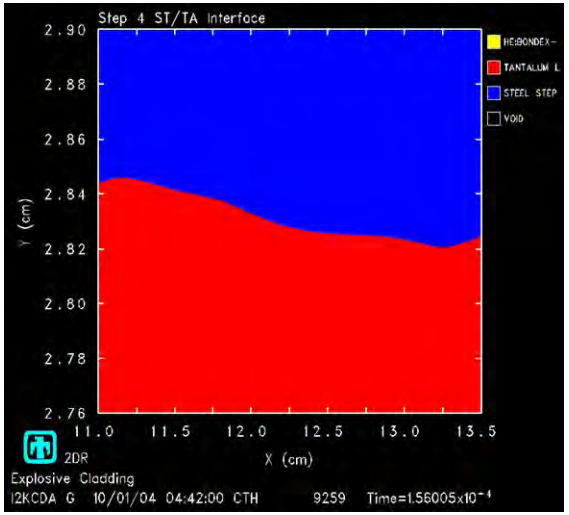

Ta and Ta10W results very similar
Further micro-scale modeling warranted

New Geometry Setup

- BondEx-D2 was used instead of BondEx-A for the explosive
- Five Steps instead of Four Steps
- .95in Geometry has a .95in tantalum outer diameter with .075in thickness
- 1in Geometry has a 1in tantalum outer diameter with .060in thickness

.95 in Tube Geometry

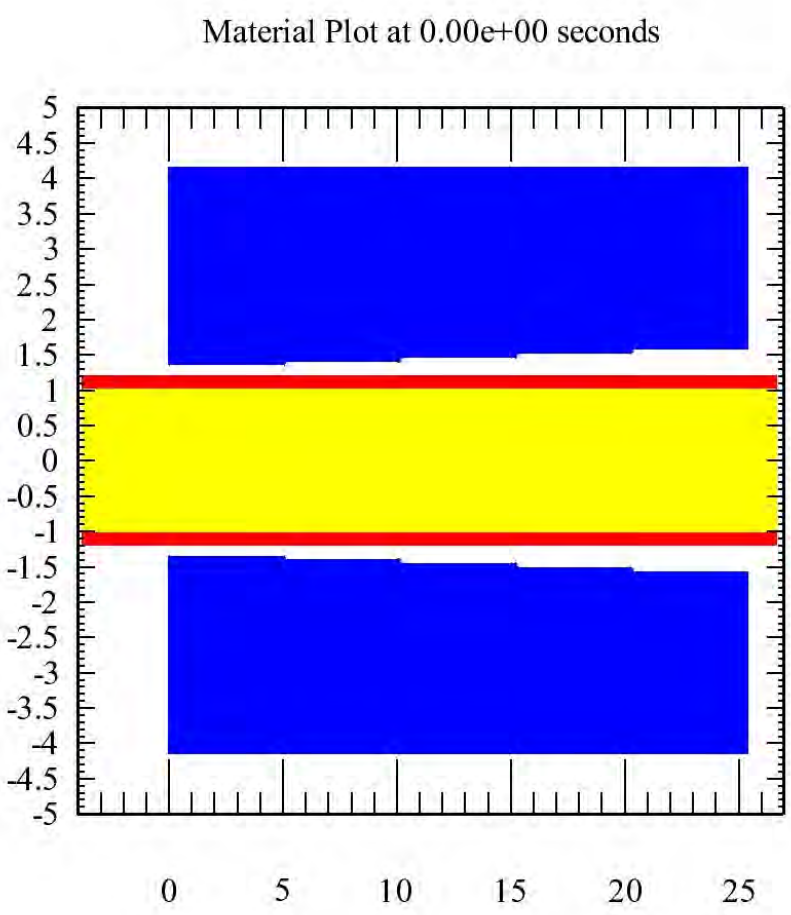

Time 0 us: Initial State

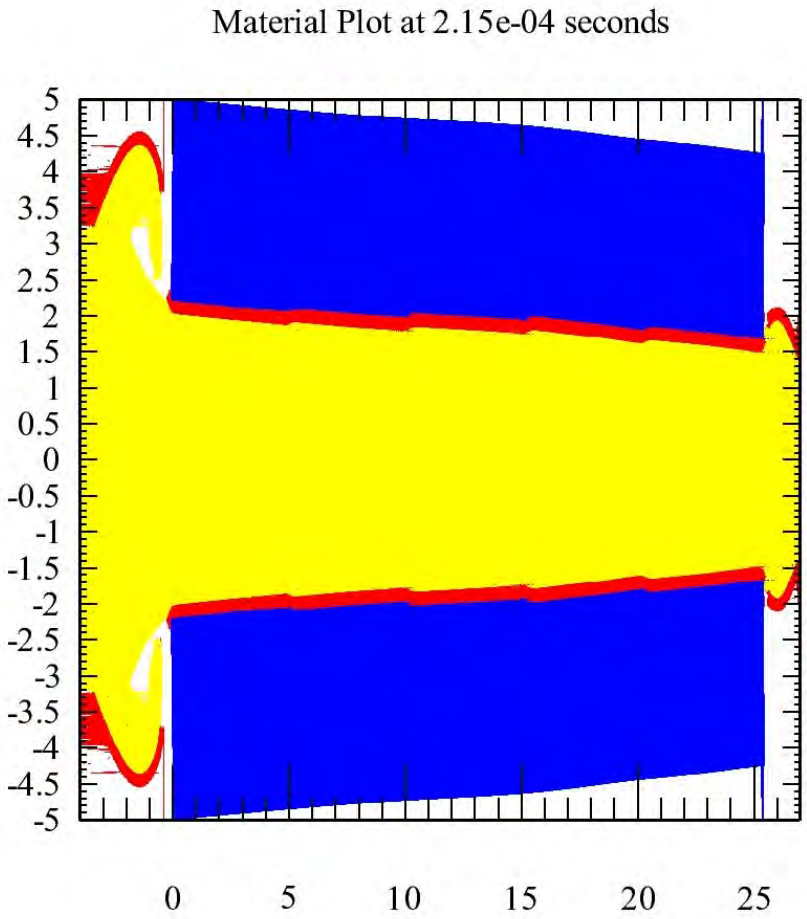

Time 215 us: Cladding Complete

.95in Tube Ta Plot Interface

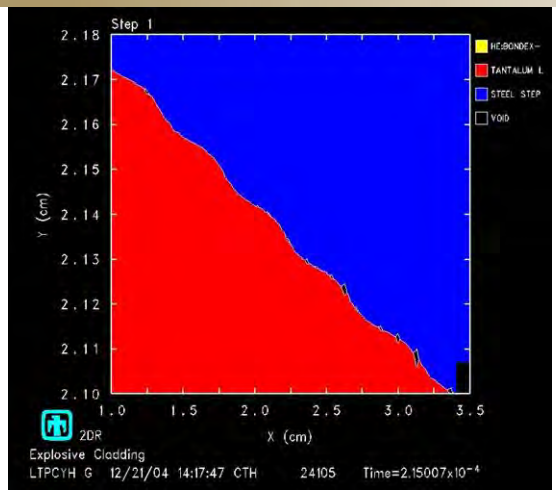

Step 1

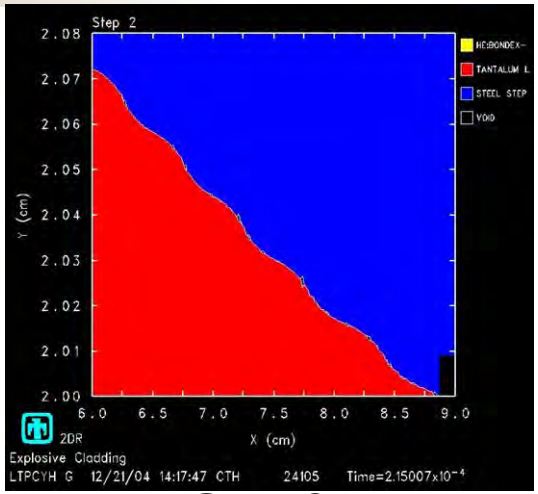

Step 2

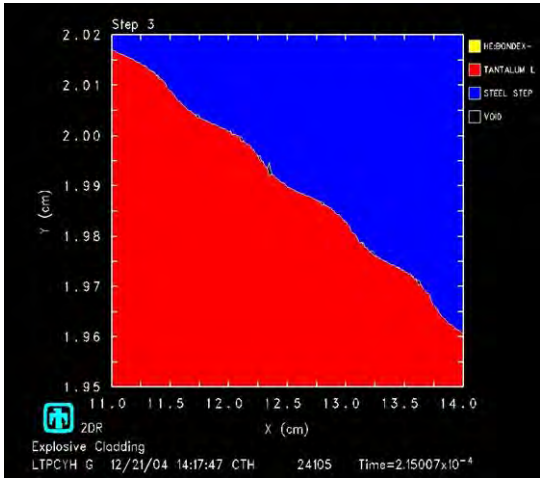

Step 3

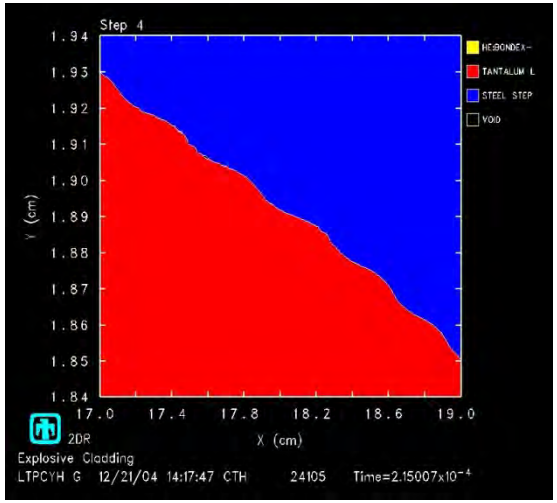

Step 4

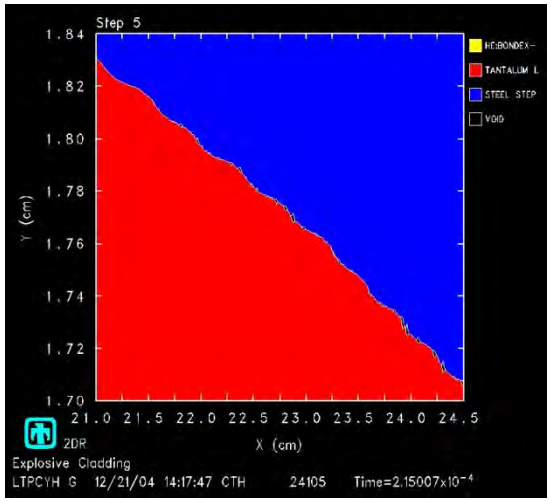

Step 5

.95in Tube Plots

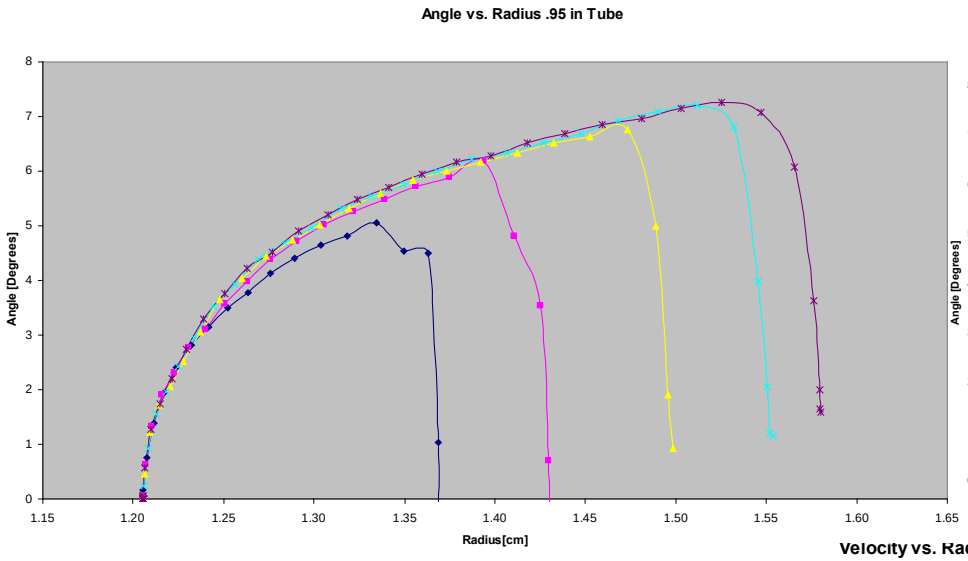

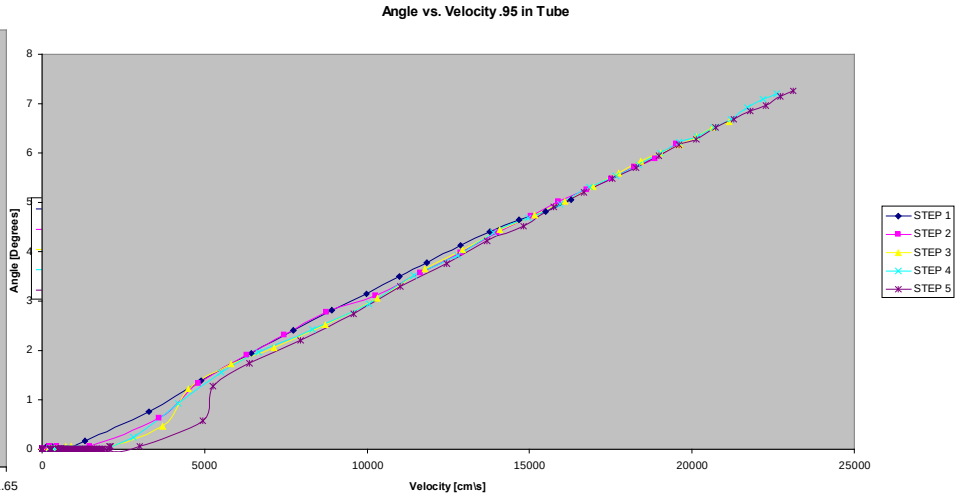

Velocity vs. Radius .95 in Tube

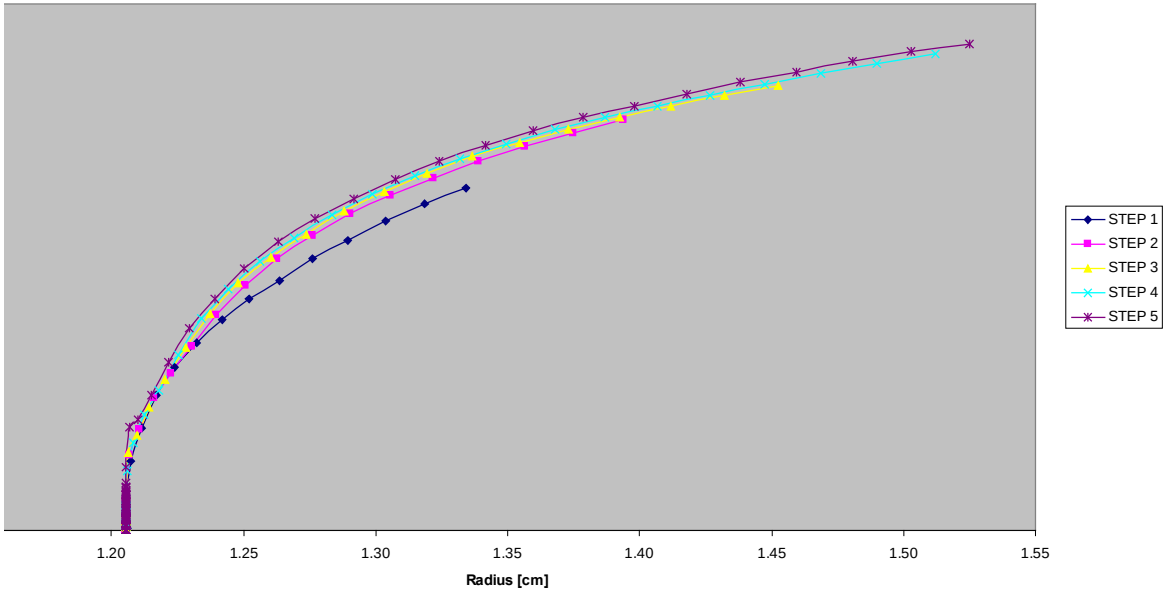

1in Tube Geometry

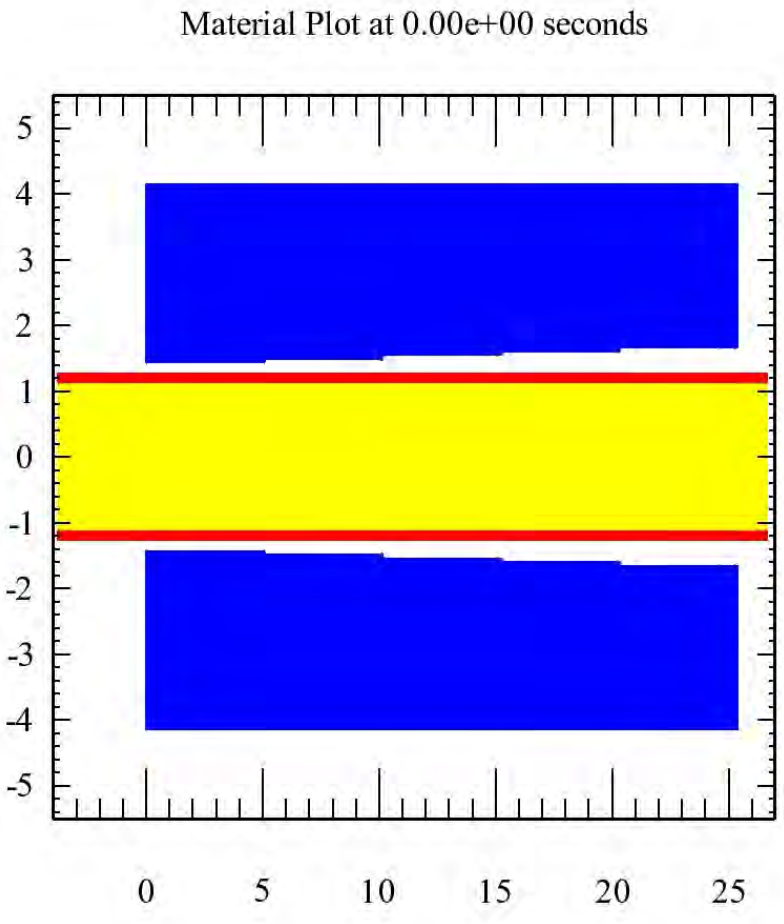

Time 0 us: Initial Setup

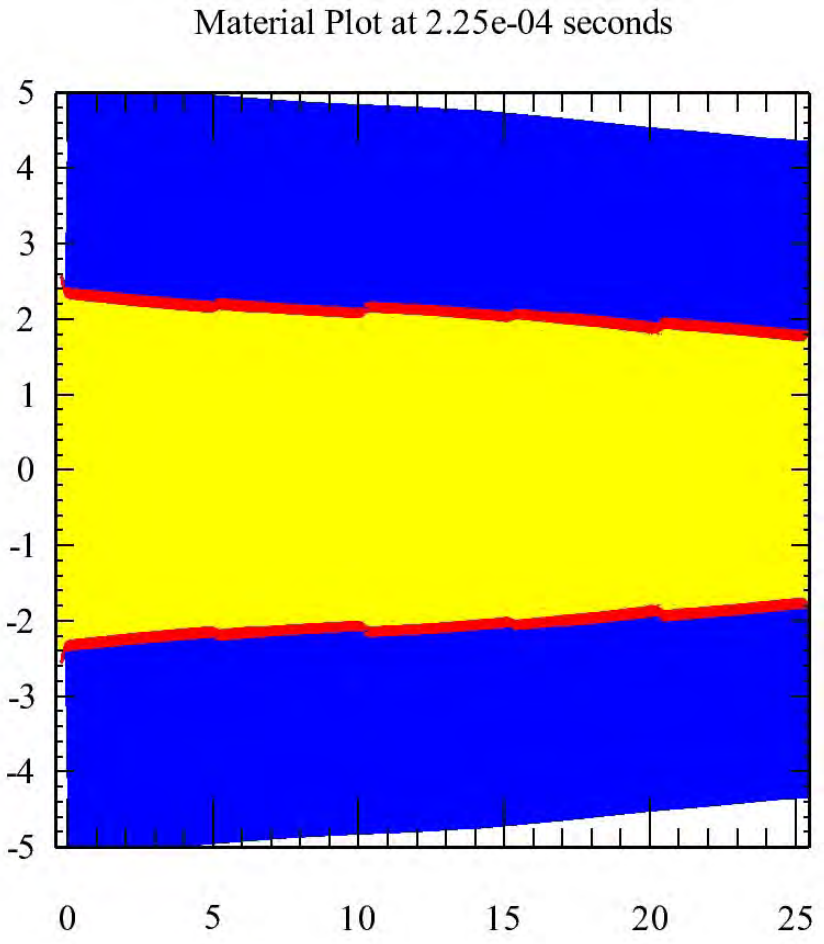

Time 225 us : Cladding Completed

1in Ta Plot Interface

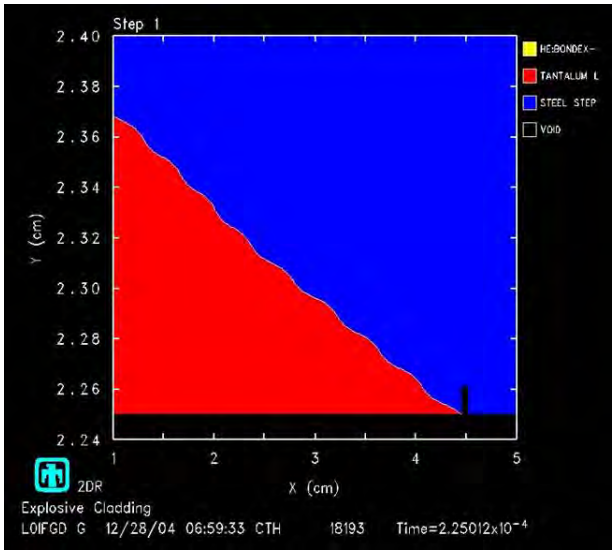

Step 1

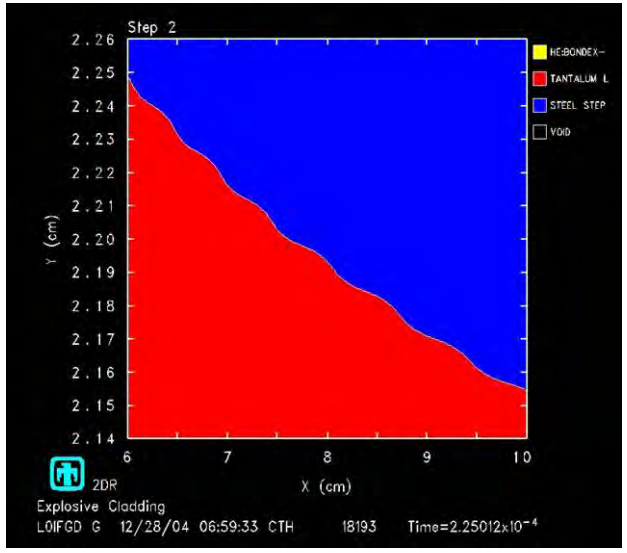

Step 2

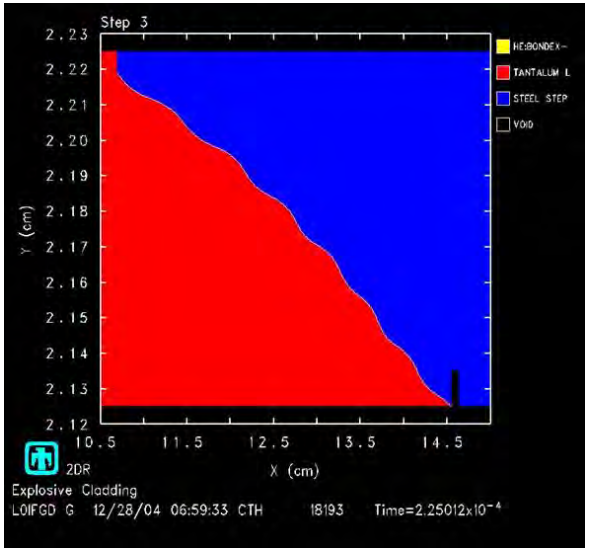

Step 3

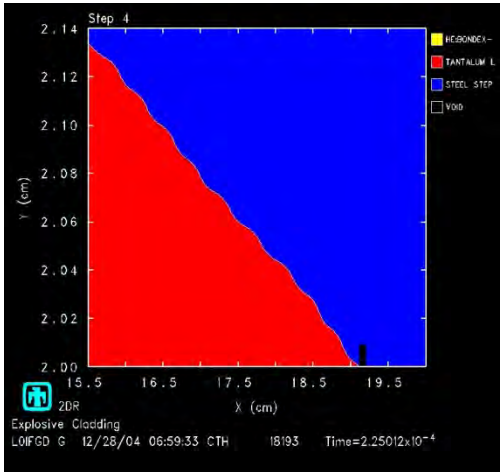

Step 4

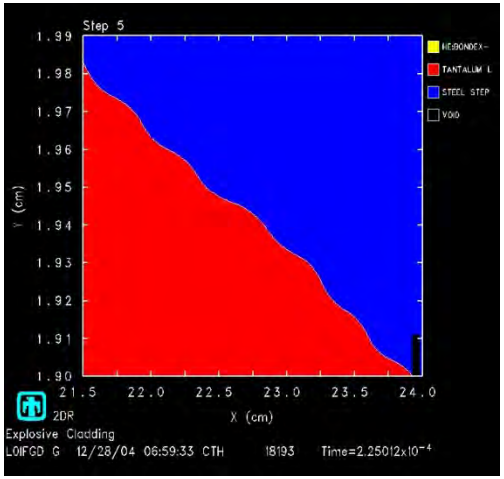

Step 5

1in Tube Plots

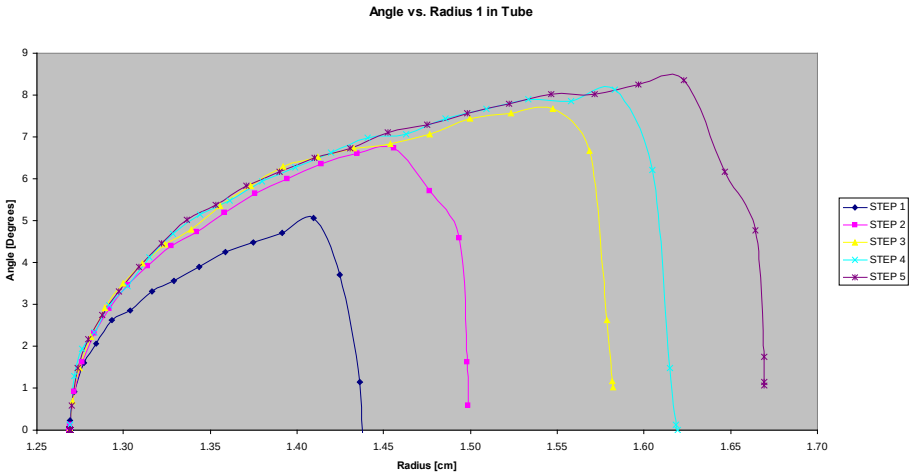

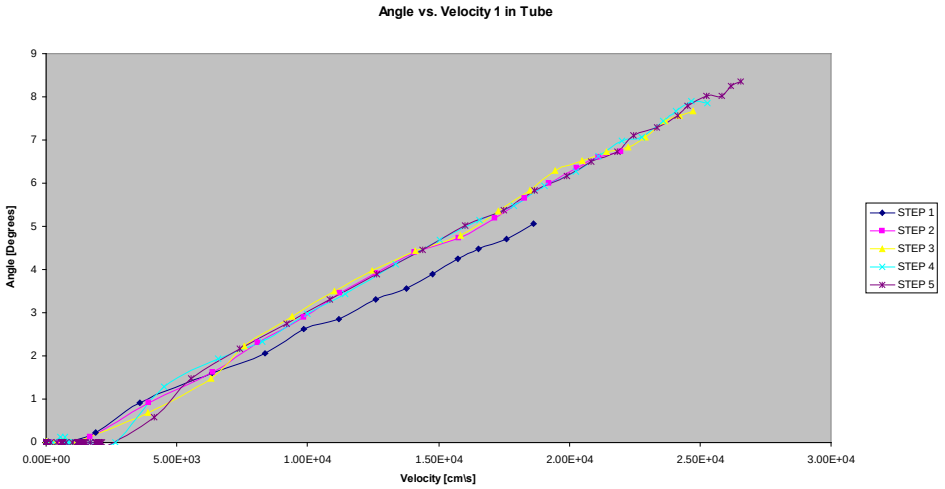

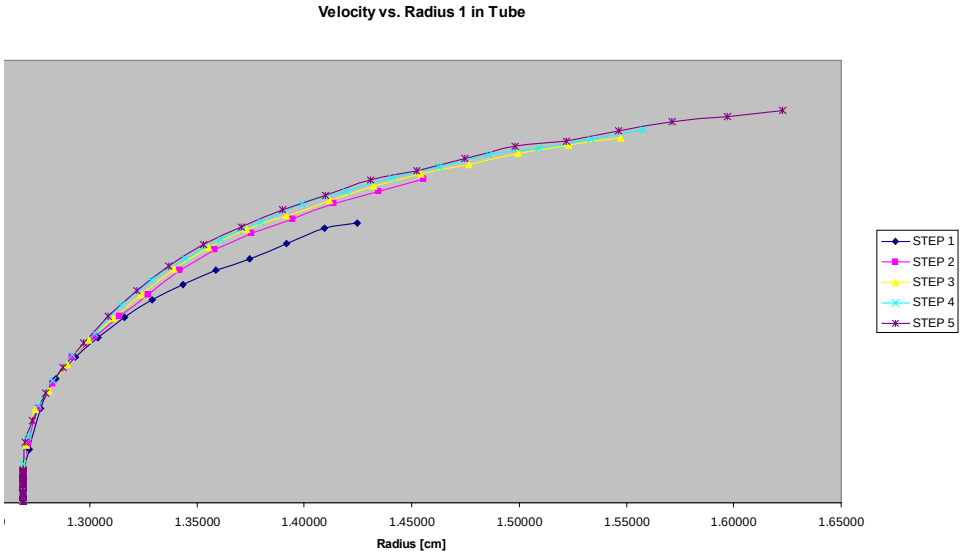

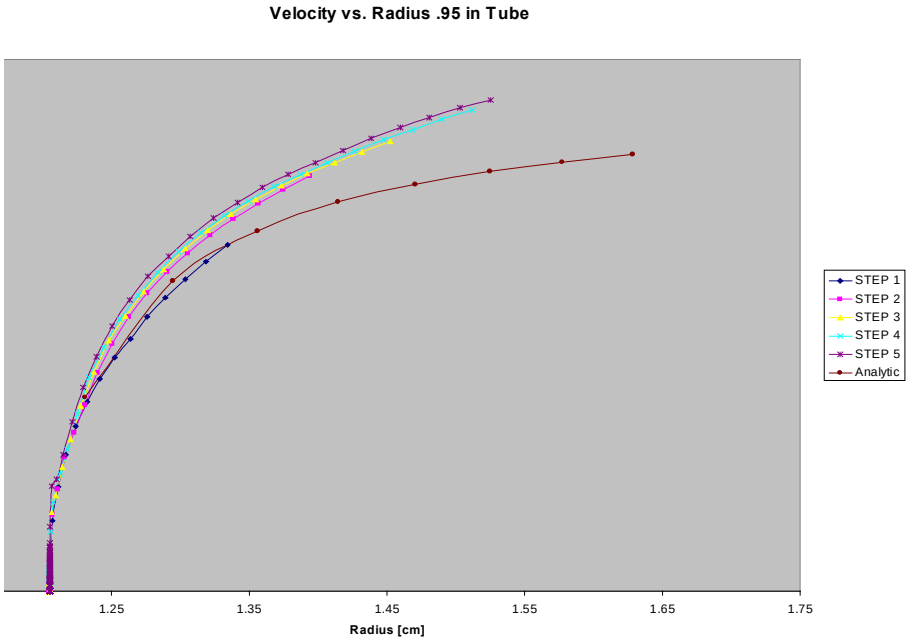

Unlimited Release

Initial Gun Modeling

Planar Model Setup

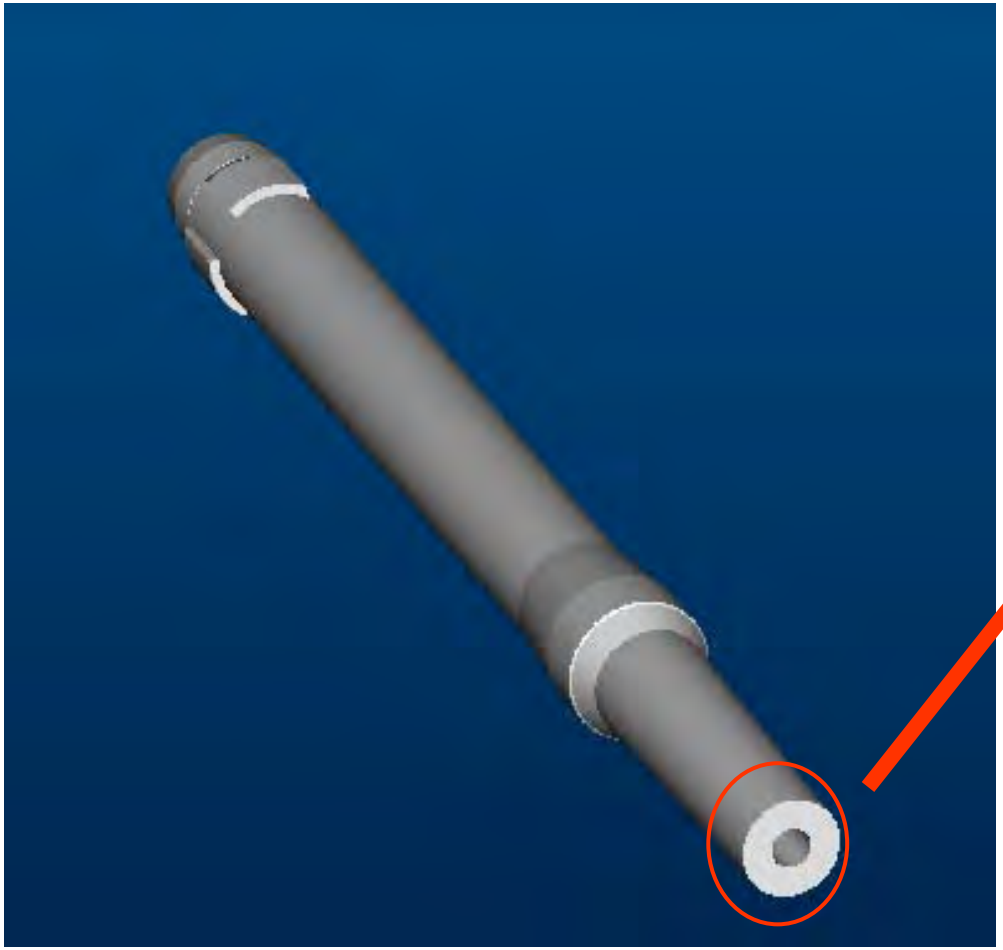

Analysis performed at 1001.5mm
(Middle of Barrel)

CALE Planar symmetry model

Material Legend

- Stainless Steel barrel
- Tantalum Liner
- HNS explosive
- Air

Initial Gun Modeling

Radial Symmetry Analysis

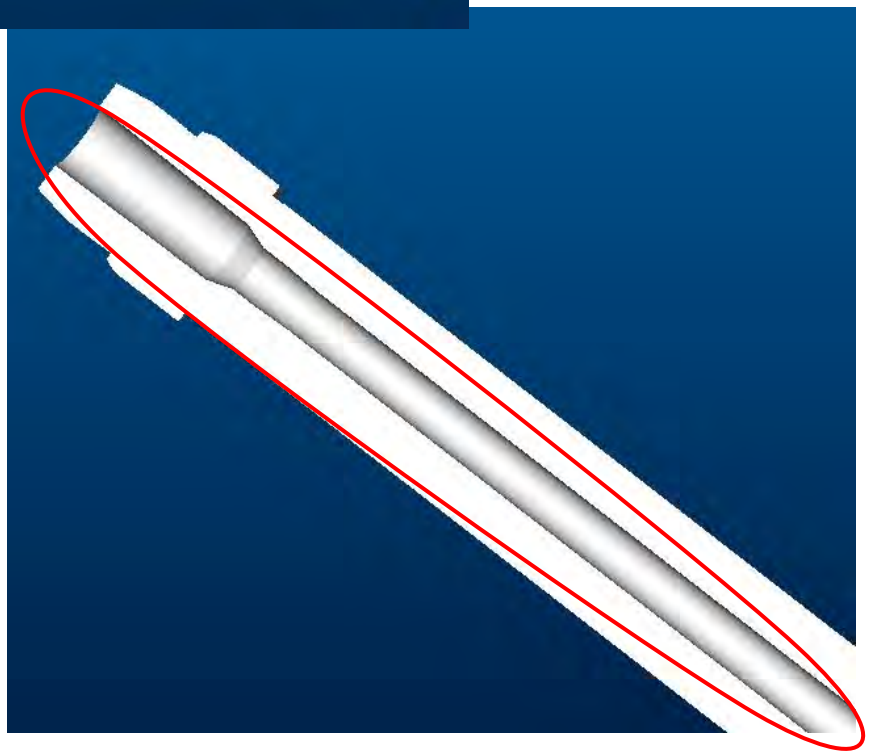

- Analysis performed on entire length of the gun barrel (2003 mm).

Initial Gun Modeling

Radial Symmetry Plots

CALE Time = 0 µs

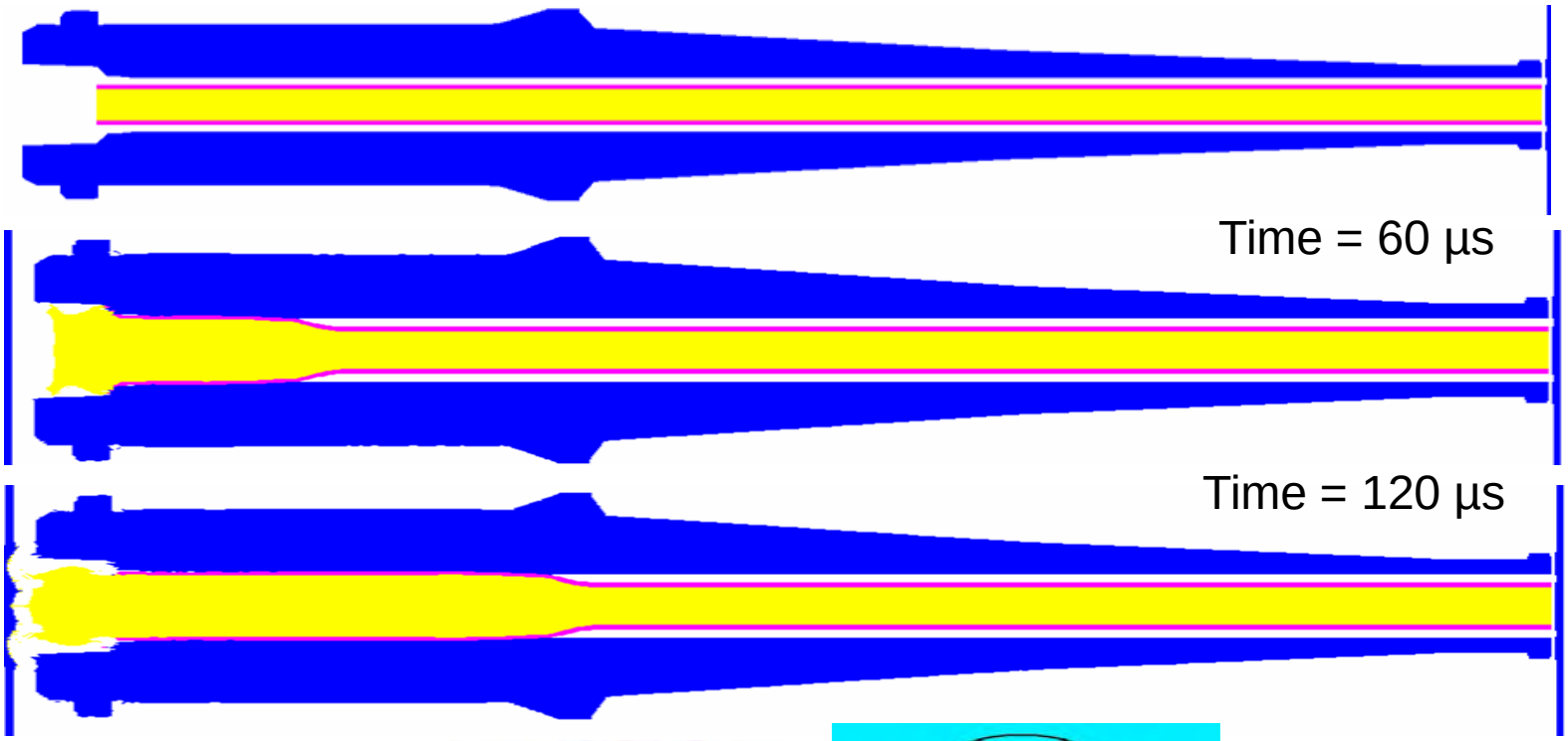

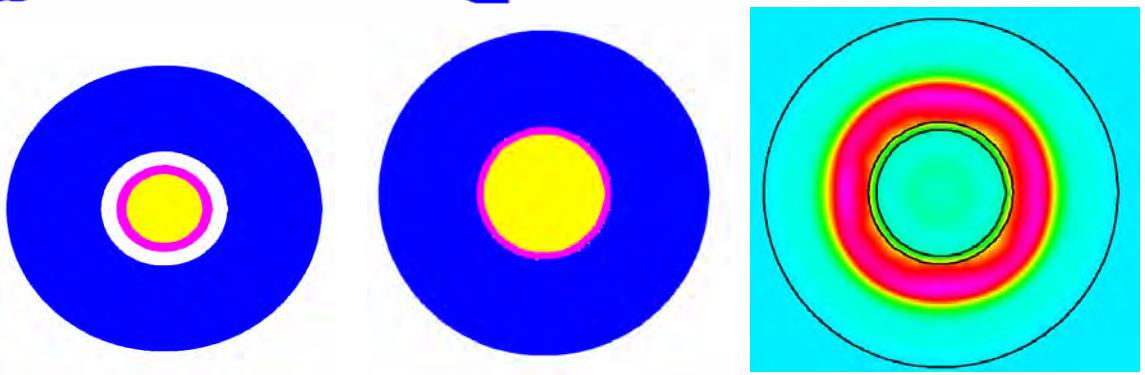

Planar Symmetry Plots

Momentum Trap Setup

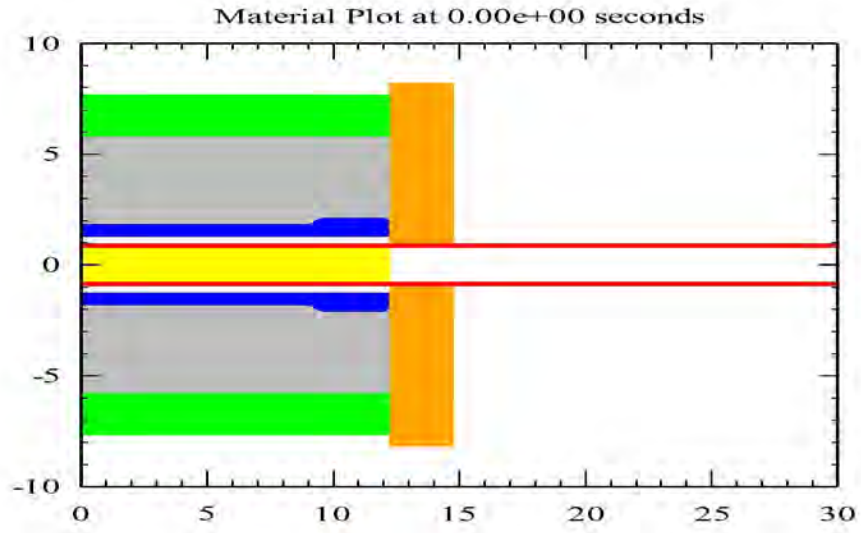

Time 0 us: Initial State

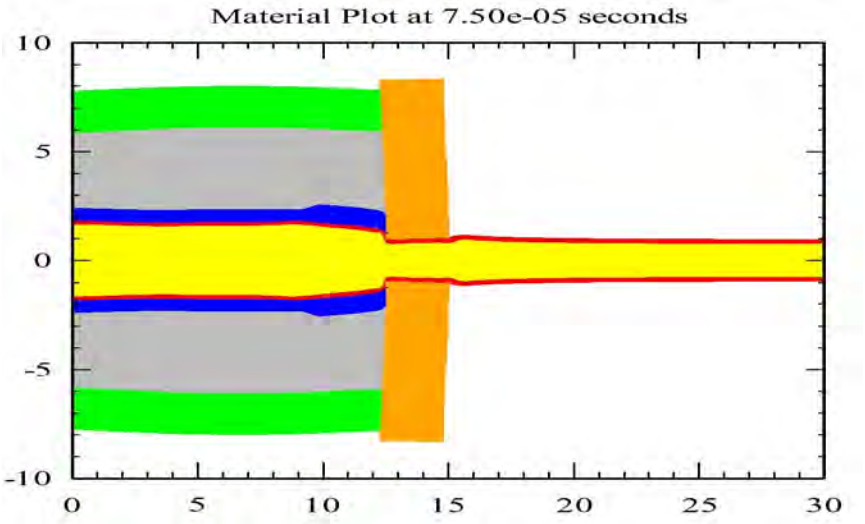

Time 75 us: After HE ignited

- 1 in Steel Plate
- .5 in Steel Plate
- Tantalum Liner
- Steel Gun Barrel
- HE:BondEx-D2
- Alloy 42

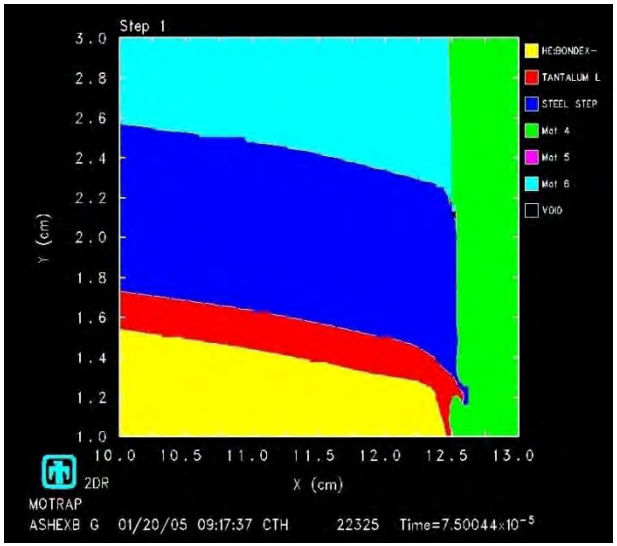

Time 75 us: Close up of Steel Barrel

Conclusions

- Explosive equation of state
  - Empirical BONDEX-A, D2 JWL/JWLB models
  - New formation BONDEX-D2: desire ARDEC cylinder tests (Ta and Cu)
- Full (macro) scale modeling
  - Physics resolved with .50mm mesh
  - Data can be used for analytic/empirical “clad quality model” input
- Sub (micro) scale modeling
  - Further .1mm modeling under investigation
  - Issue with wavelength …calculations predict longer the data …are BONDEX-D2 velocities correct? …Need to do BONDEX-D2 cylinder tests.
- Future Effort: process design and optimization
  - Two approaches: macro-analytic, micro-scale
  - Correlation using macroscale modeled characteristics and explosive experiment results
  - Correlation using further microscale modeling
  - Characterization of new explosive (ie: cylinder tests)
  - High probability for success of macro-analytic approach, micro-scale
  - Momentum trap design investigation initiated.

US ARMY RDECOM

U.S. Army Research, Development and Engineering Command

Results and Analysis from Mine Impulse Experiments Using Stereo-Digital Image Correlation

15 September 2011

TECHNOLOGY DRIVEN. WARFIGHTER FOCUSED.

Craig Barker
Raquel Ciappi
Terry Holdren
Douglas Howle
Jeffrey Koch

Email:
douglas.howle@us.army.mil

Phone:
410-278-5738

Outline

- Issue & Objectives
- Experimental Setup/Target Description
- Test Results & Analysis
- Modeling Approach
- Conclusions
- Recommendations

Context for Army Efforts

Issue

Under-body blast is one of the leading causes of casualties in current operations, but our capability to accurately and efficiently assess its effects on both personnel and vehicles is quite limited.

Modeling & Simulation (M&S) Problem

Finite element modeling has not been validated for supporting Army evaluations in the acquisition community. The under-body blast methodology (UBM) program was developed in part for this purpose.

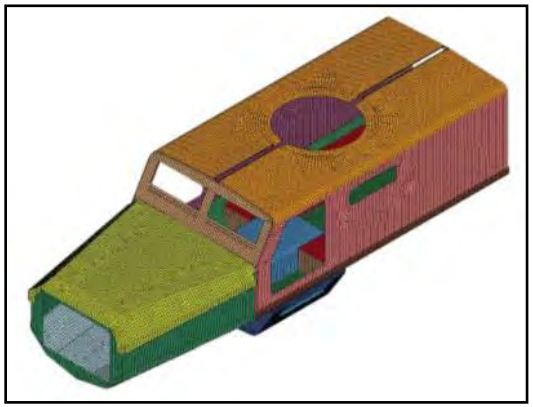

UBM Program Objective

- To provide a robust M&S capability to the U.S. Army Test & Evaluation (T&E) community by:
  - Understanding the fundamentals of the blast effects of buried charges
  - Validating the use of models, including finite element methods, for under-body blast analysis.

- The M&S capability will be used for:
  - Planning Live-Fire Test and Evaluation (LFT&E),
  - Evaluating expanded problem sets (threats, targets, and engagement conditions),
  - Augmenting test data, and
  - Developing survivability/vulnerability data to support broader Army analyses.

Test Series Objective

- Develop and analyze experimental mine impulse data for simple v-shaped structures constructed with a top floor plate.
- Measure, with some degree of confidence, the structural responses of simple targets using stereo-digital image correlation.
- Perform a statistical analysis of the resulting data to identify mathematical trends.
- Use various finite element modeling approaches to replicate test events.

Experimental Setup

- Test Matrix: 24 events were completed including 16 centerline and 8 off-centerline tests.

Target Geometry	**20 Degree Target**			**10 Degree Target**	**30 Degree Target**	
Charge:	600g	800g	1000g	600g	600g	Total Tests
Centerline Shots	4	4	-	4	4	16
Off-Center Shots	1	4	3	-	-	8

- Three target geometries were tested; v-hull angles of 10, 20 and 30 degrees.

Geometry 1 - 10^0

Geometry 2 - 20^0

Geometry 3 - 30^0

Target Description

- Targets constructed from A-36 Mild Steel.
- Target dimensions:
  - H = 50.8 mm
  - L = 700 mm
  - W = 700 mm
- All tests configured with 250mm standoff and 50mm depth of burial.
- Red clay/sand soil was used at the test facility.
- C4 charges weighing 600g, 800g and 1000g were chosen based on facility capabilities and expected target response.

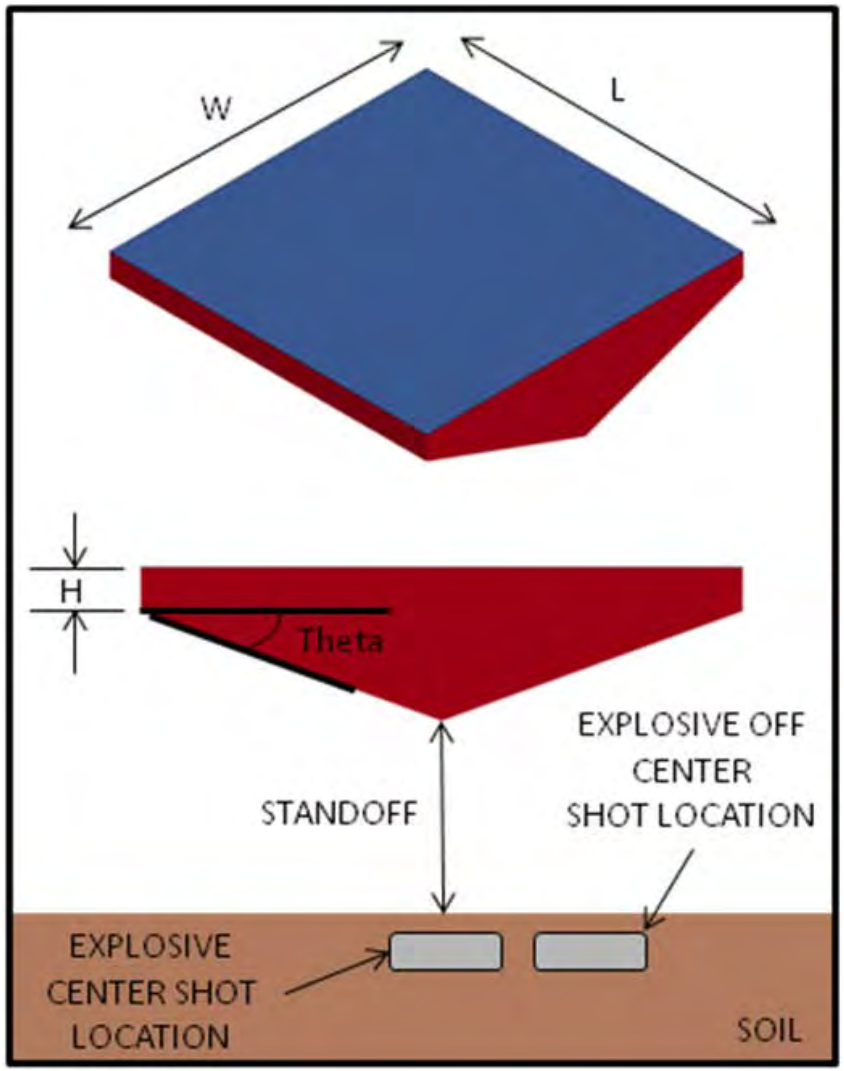

Experimental Data Acquisition

- Target motion data was acquired using two high-speed cameras and processed with stereo-digital imaging correlation software.

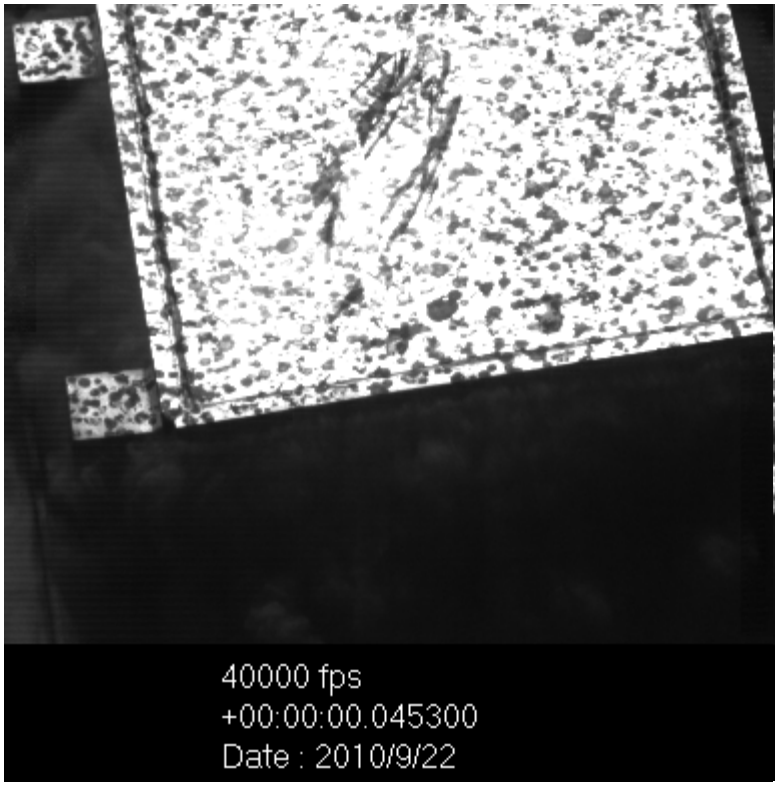

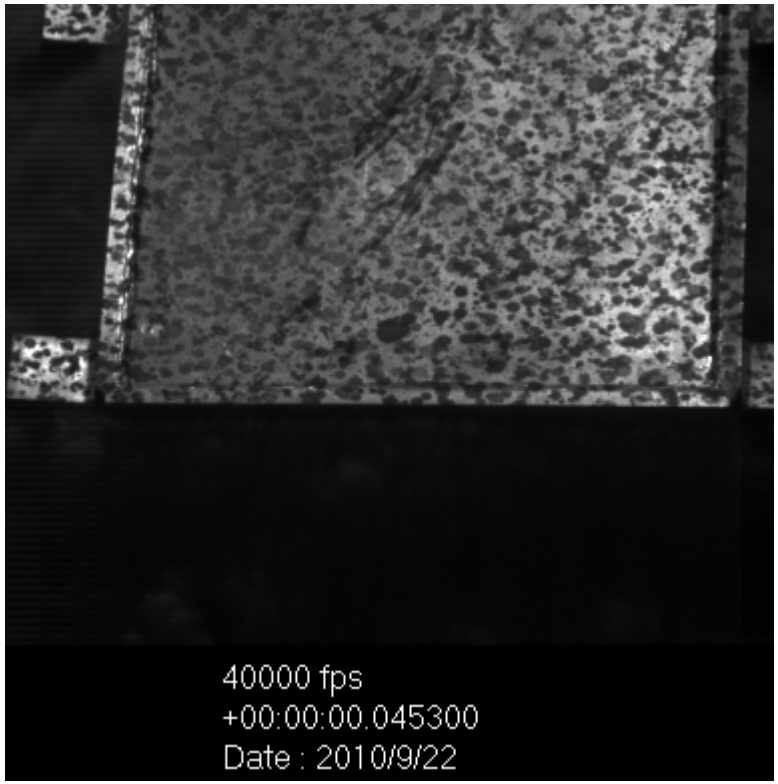

- A speckled pattern on the surface of the target provided the software a way to track oscillatory motion as the speckle marks shifted pixels. The motion also provided a method to estimate impulse.

Experimental Data Acquisition

- Impulse to the target was estimated using the velocity determined by the digital image correlation software and the measured target mass.

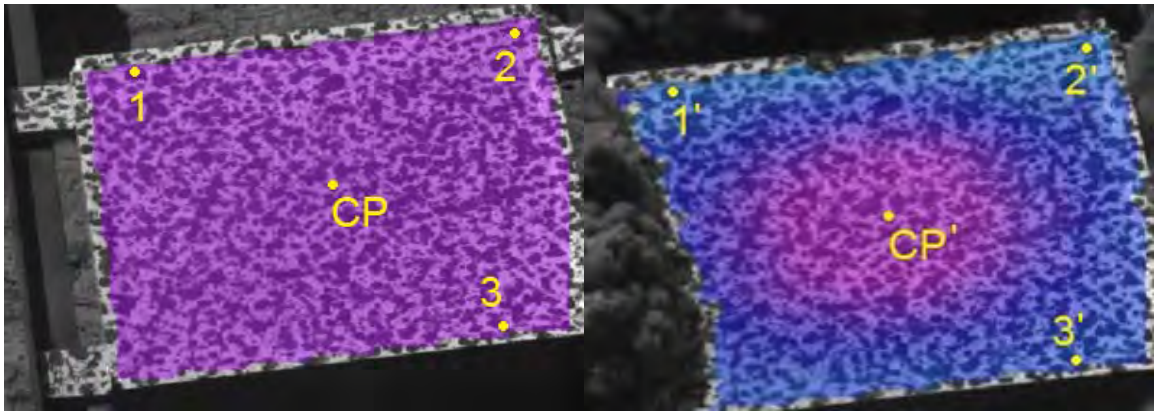

Position vs. Time (CP)

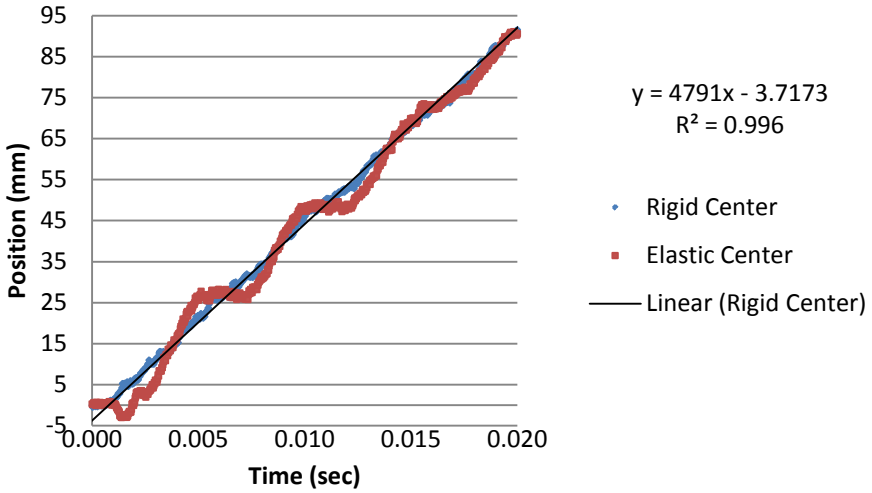

$$a(x_2-x_1, y_2-y_1, z_2-z_1)+b(x_3-x_1, y_3-y_1, z_3-z_1)=(x_{cp}-x_1, y_{cp}-y_1, z_{cp}-z_1)$$

$$I = m \times v$$

Where: I=impulse, m=mass of the target and v=slope of trend line.

Experimental Data Acquisition

- Structural responses were determined by subtracting the calculated rigid body motion of the target from the elastic plate center (CP) position time history obtained from the digital image correlation software.

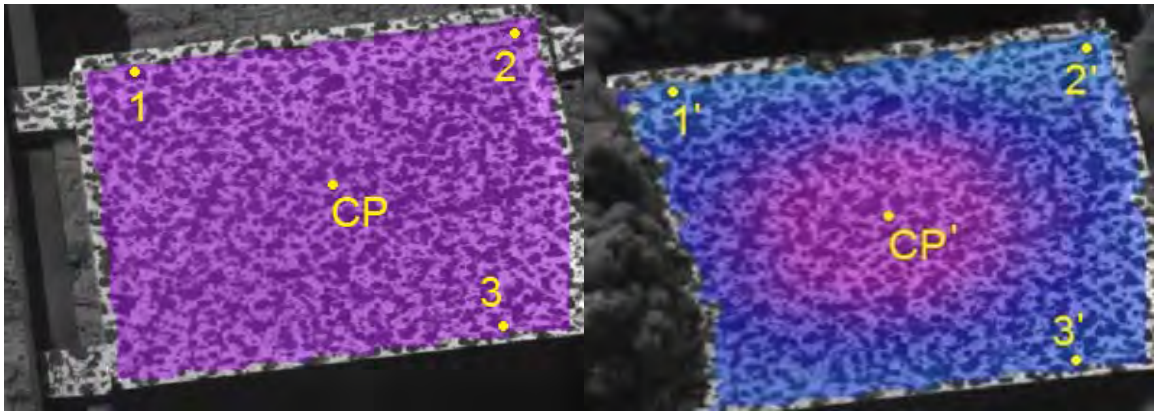

Position vs. Time (CP)

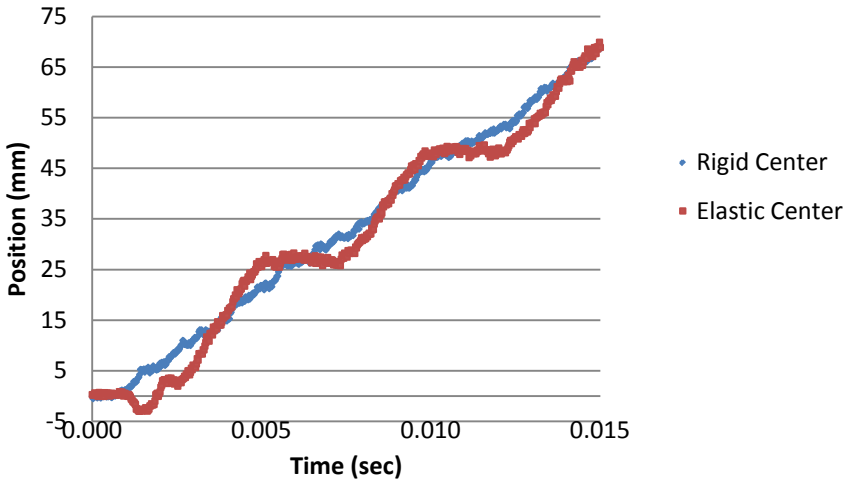

Deflection (CP) vs. Time

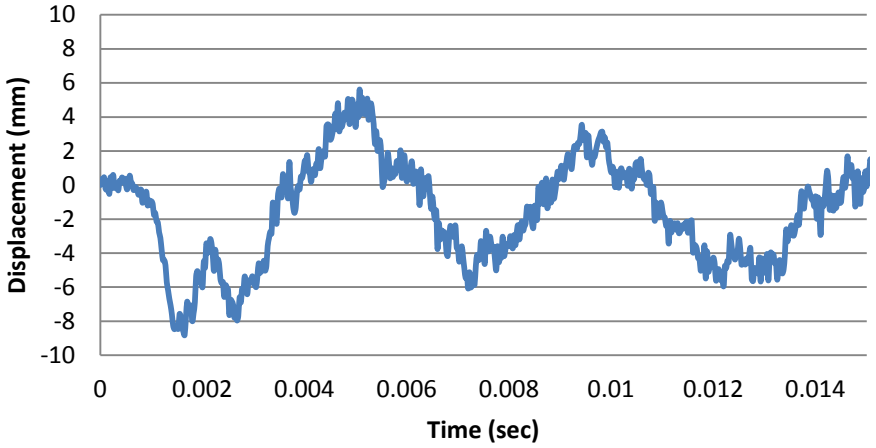

Digital Image Correlation Software

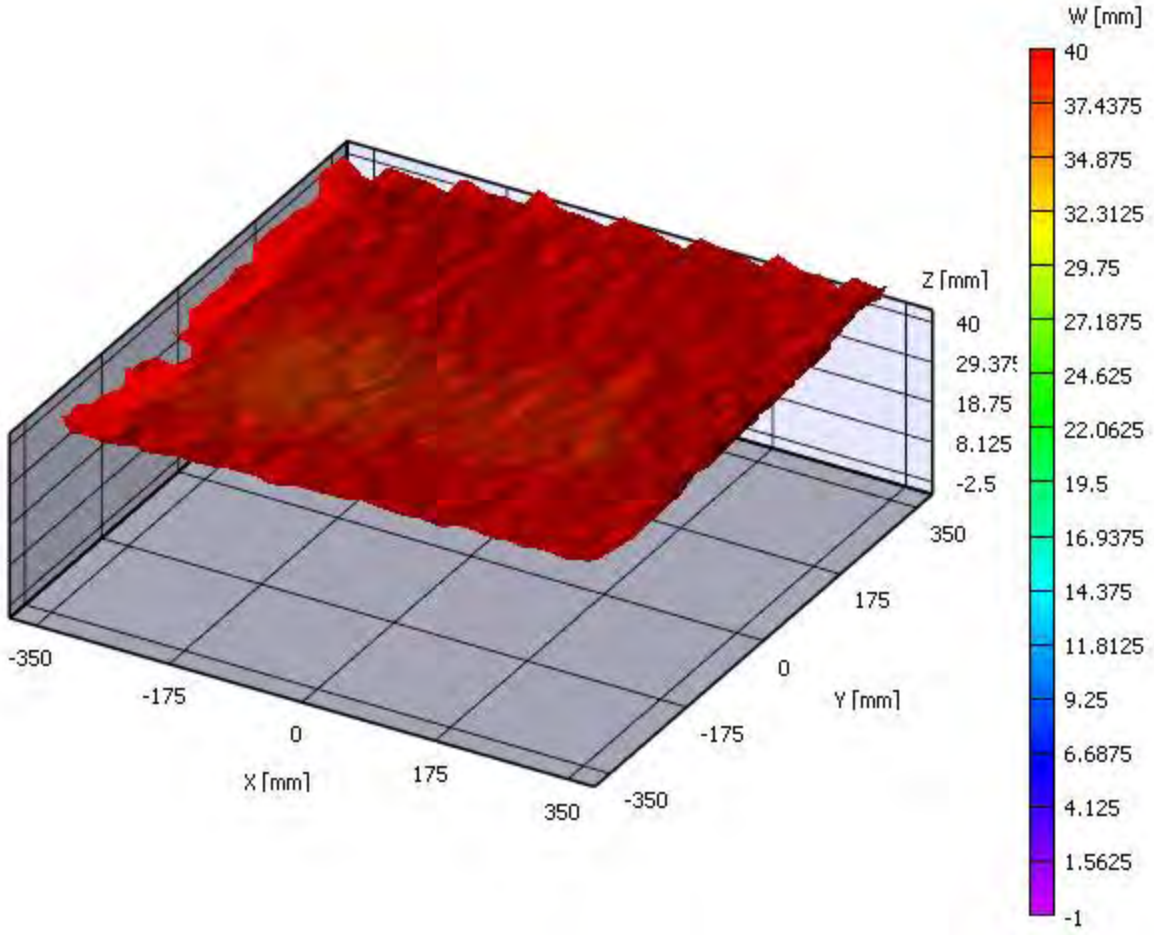

Test Results

- The standard deviation was calculated for various subsets of the overall test data set in order to establish variability from one configuration to another.

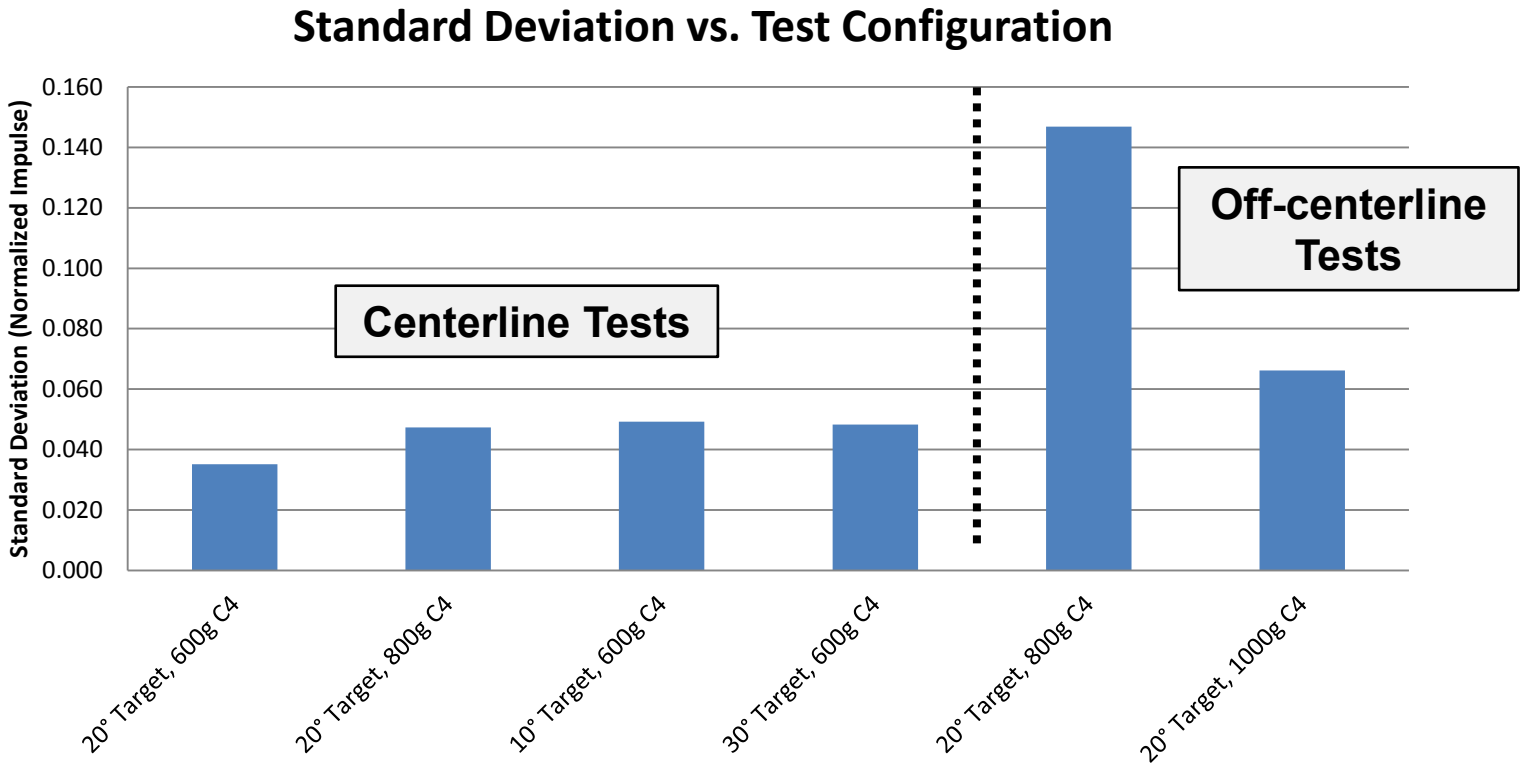

- There appears to be an outlier in the 800g off-centerline data set.

- For the centerline tests, the standard deviation is 6% of the mean, on average.

Test Results (continued)

- Normalized impulse as a function of v-shape angle:

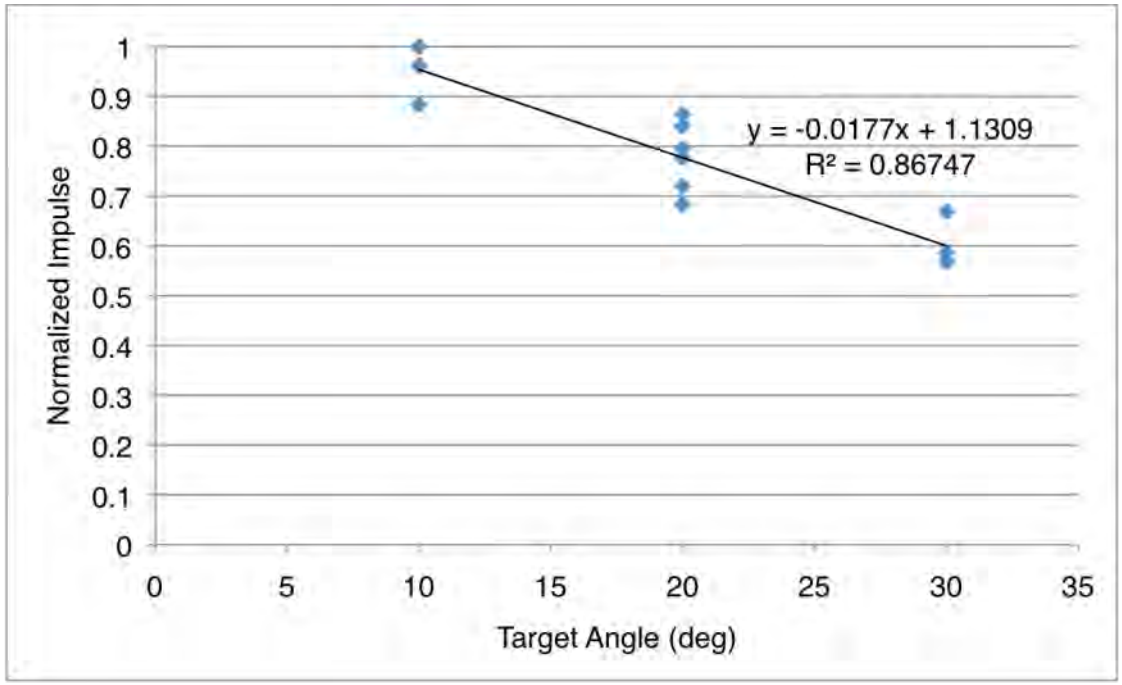

- Trend matches expectations: Impulse decreases with increasing v-hull angle.

- Data plotted only includes the centerline test results.

Statistical Analysis

- Test data was analyzed for correlations:

	Impulse	Charge mass	Target mass	Target angle	Charge offset	Soil moisture
Impulse	1.00					
Charge mass	0.69	1.00				
Target mass	-0.58	-0.07	1.00			
Target angle	-0.52	0.00	0.99	1.00		
Charge offset	0.52	0.69	-0.06	0.00	1.00	
Soil Moisture	0.19	-0.09	-0.13	-0.15	-0.28	1.00

- Statistical analysis of the data determined that the observed impulse difference for the off-centerline and centerline test events were not statistically significant.

- Data collected is insufficient to show that offset shots result in statistically different observed impulse values than the centerline shots.

- Mathematical relations between Impulse and the variables outlined in the correlation matrix were developed with confidence intervals.

FE Modeling Approach

- Events were modeled using the ConWep air-blast loading model in LS-DYNA.
- Targets were modeled using both shell and solid elements.

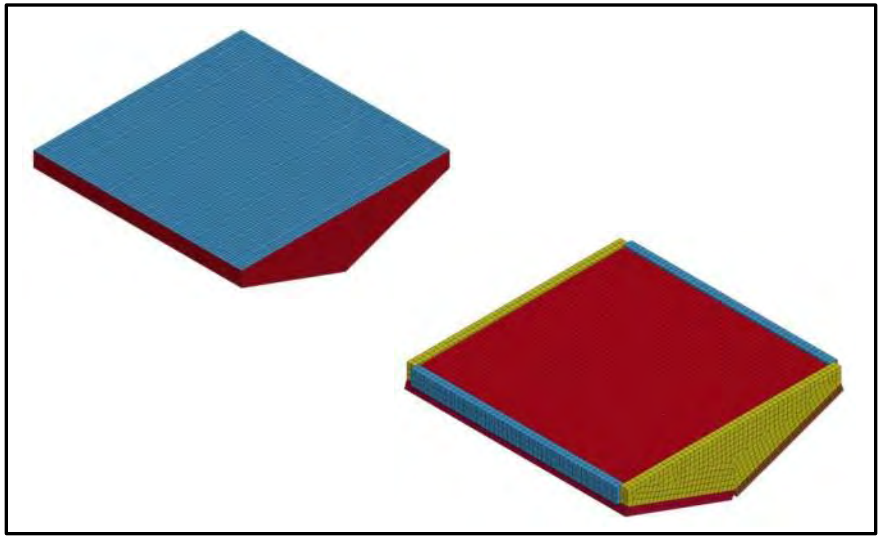

- Mesh size was refined until convergence of structural displacements and velocities was achieved.
- A simplified version of the Johnson Cook material model was used.

Preliminary Structural Modeling Results

- Test event 1, solid model results and comparison:

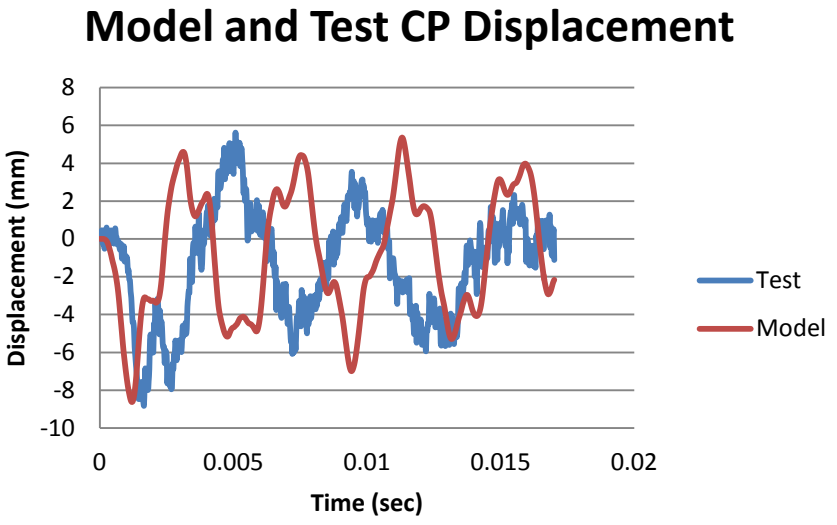

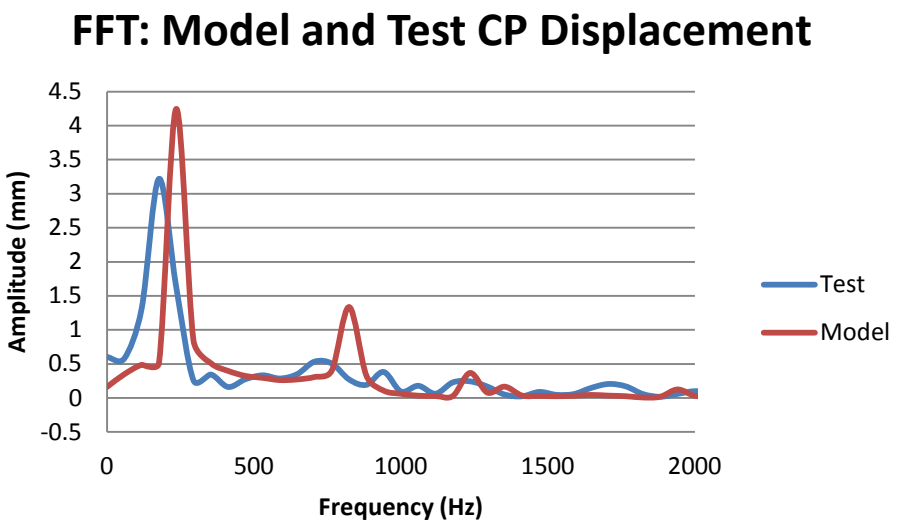

- Results were processed in both the time and frequency domains.

- Determining the basis for acceptability has been a challenge for this project.

Conclusions

- Impulse results obtained from the stereo-digital correlation procedure are consistent with engineering expectations and knowledge from previous tests conducted.
- Structural responses obtained from the stereo-digital correlation process appear reliable. Currently, there is no way to validate the measurement technique.
- The effects of off-center charge locations was not significant, based on the current, limited dataset.

Recommendations

In support of the Army's goal to develop a robust under-body blast modeling capability able to support the acquisition community, we need to:

- Conduct more testing to expand the blast data set for Army model validation exercises.
- Apply stereo-graphic imaging techniques to larger, more complex structures and validate existing structure mounted sensor measurements.
- Model test events with other loading approaches and investigate accuracy and/or applicability of constitutive models.

Detailed Ballistic Performance Characterization of 120-mm Mortar System with Different Flash Tube Configurations

(Paper No. 11956)

Prepared by

Kenneth K. Kuo, Heath Martin, and Eric Boyer

Presented at
26th International Symposium on Ballistics
Miami, Florida

September 15, 2011

PENNSTATE 1855

HPCL

Background and Research Objectives

Background:

- In collaboration with the U.S. Army - ARDEC, a detailed model and code (called Three-dimensional Mortar Interior Ballistic code or 3D-MIB) have been developed for realistic simulation of the interior ballistics of 120-mm mortar system.
- A series of 90 test firings was conducted at the U.S. Army's Aberdeen Test Center (ATC) using a specially designed 120-mm instrumented mortar simulator (IMS).

Objectives:

- To obtain detailed interior ballistic data for use in validation of 3D-MIB code
- To achieve better understanding of the combustion processes inside the mortar tube

Instrumented Mortar System (IMS)

- The IMS, which was designed and fabricated at PSU, contains a total of 38 pressure transducer ports distributed in various longitudinal and circumferential locations.
- Up to 34 channels of pressure data were recorded at a rate of 400 kHz.
- Custom RP120 tourmaline piezo-electric dynamic pressure gauges were used.
- Two Weibel radar systems were used for velocity data:
  - a short-range system for muzzle velocity only
  - a tracking system for both muzzle velocity and trajectory determination
- High-speed video recordings (5000 – 10,000 pictures per second) of the rounds leaving the muzzle were obtained with a Phantom camera.

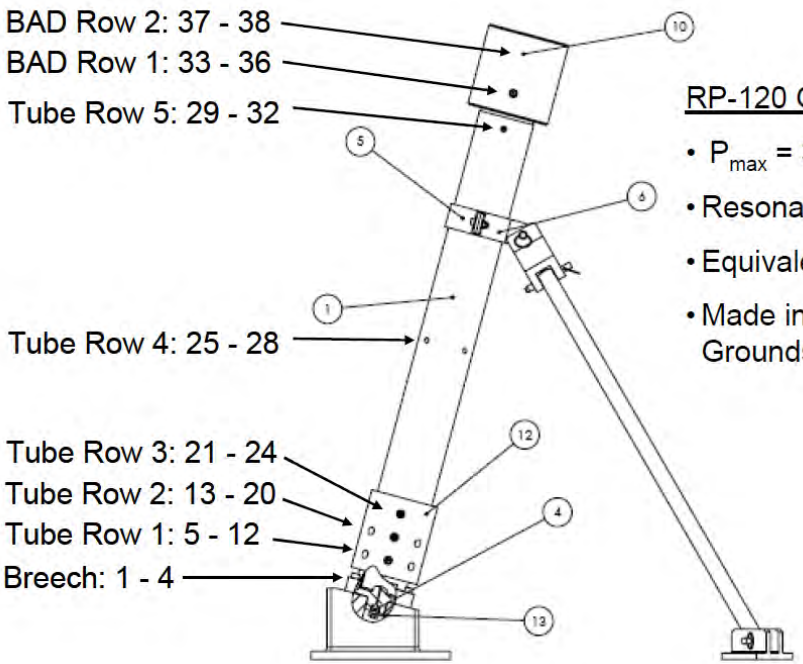

RP-120 Gauge Specifications

- P_{max} = 30,000 psi
- Resonant freq. = 15 -20 kHz
- Equivalent rise time = 5.6 μs
- Made in Yuma Proving Grounds, AZ

Flash Tube Modifications

- Previous investigations of flash tube behavior have indicated that the venting of combustion products from the flash tube is highly non-uniform.
  - To mitigate this non-uniformity, a modification to the flash tubes vent-hole size distribution was made. This case is called Mod 1.
- Moisture Resistant Black Powder Substitute (MRBPS) pellets were found previously to provide greater reproducibility in pressure-time behavior with significantly higher pressure levels in the flash tube than black powder (BP) pellets.
  - Mod 2: replacement of 5 BP pellets with 3 MRBPS pellets and 2 inert pellets

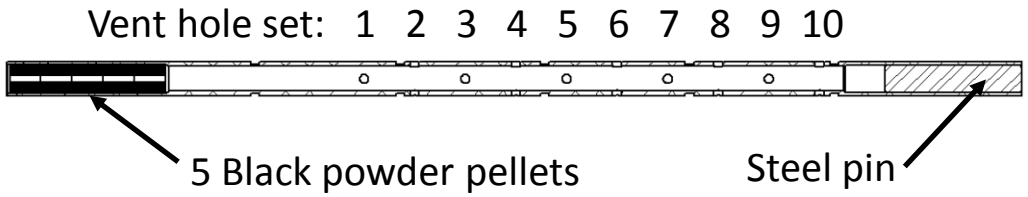

	Vent Hole Diameter (mm)									
Configuration	1	2	3	4	5	6	7	8	9	10
Baseline	1.65	1.65	1.65	1.65	1.65	1.65	1.65	1.65	1.65	1.65
Mod 1	2.18	2.18	2.06	2.06	1.93	1.93	1.40	1.40	1.40	1.40
Drill size	*#44*	*#44*	*#46*	*#46*	*#48*	*#48*	*#54*	*#54*	*#54*	*#54*

Test Matrix (T_i = 21°C)

Flash Tube Configuration	Charge Increments					
	0	*1*	*2*	*3*	*4*	*Total*
Baseline[a]	7	6	7	0	20	40
Mod 1 (different flash tube hole config.)	5	5	5	0	20	35
Mod 2 (3 MRBPS & 2 MXB360 pellets)	5	0	0	0	10	15
						90

- In view of the limited total number of firing tests, the emphasis was placed on the 4 charge increments. Fewer test were conducted for Mod 2 flash tubes.
- Charge 2 and Charge 0 increment cases also have limited test runs.

Charge 4 Baseline Firing

- Ports 1 – 24 are initially below the obturating ring of the projectile, and thus have the earliest and highest pressure rise.
- Once the obturating ring passes a port location, the pressure quickly equilibrates to the pressure levels near the breech.
- The *P-t* traces from ports 25 – 32 exhibit an overshoot and ringing phenomenon that occurs after the sharp pressure rise.
  - Due to recessed mounting of pressure transducers from tube wall.
  - The observed ringing frequency of 6.7 kHz is close to the resonance frequency of the cavity of 1.27 cm.

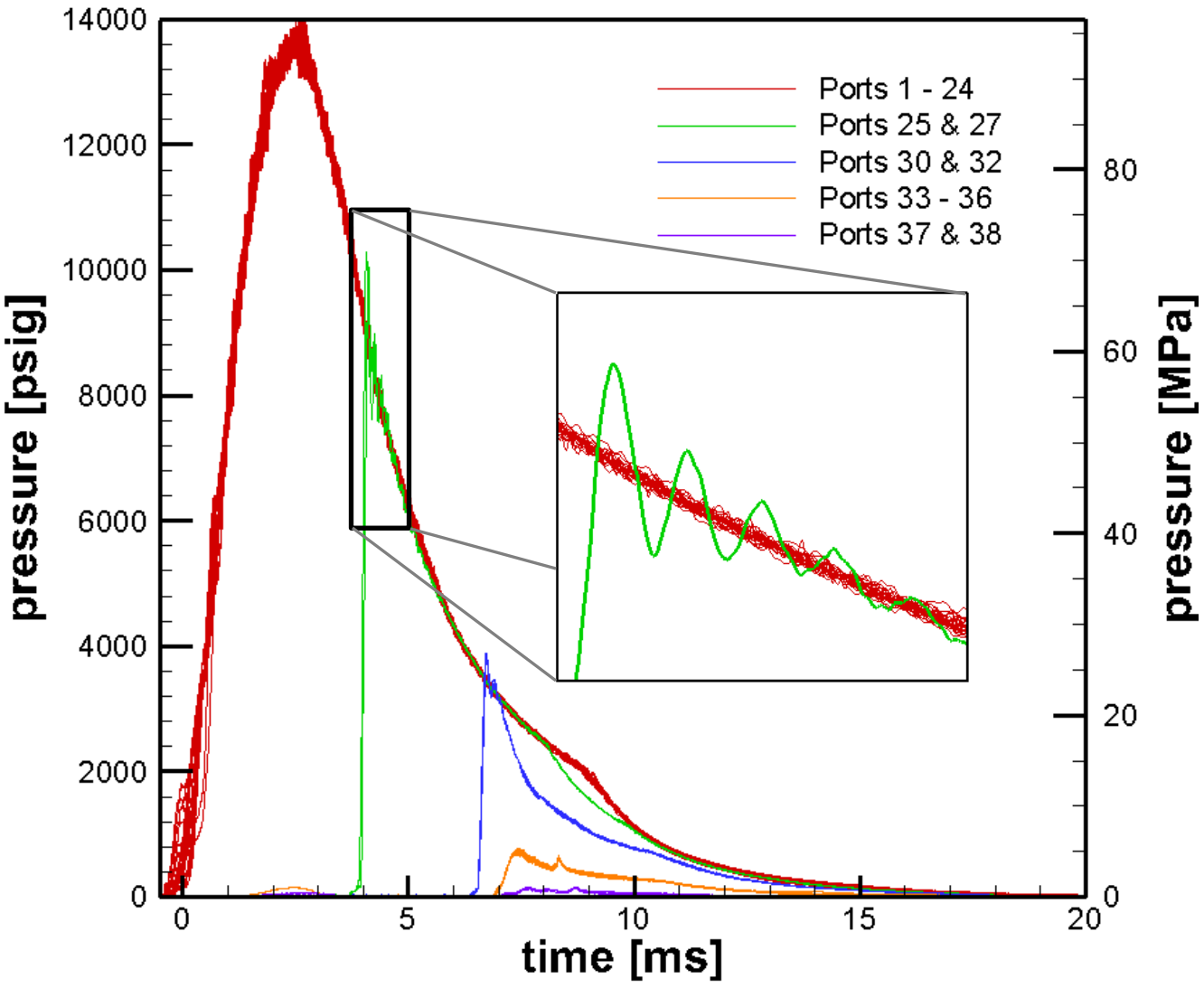

Longitudinal Pressure Waves (Charge 4 Baseline)

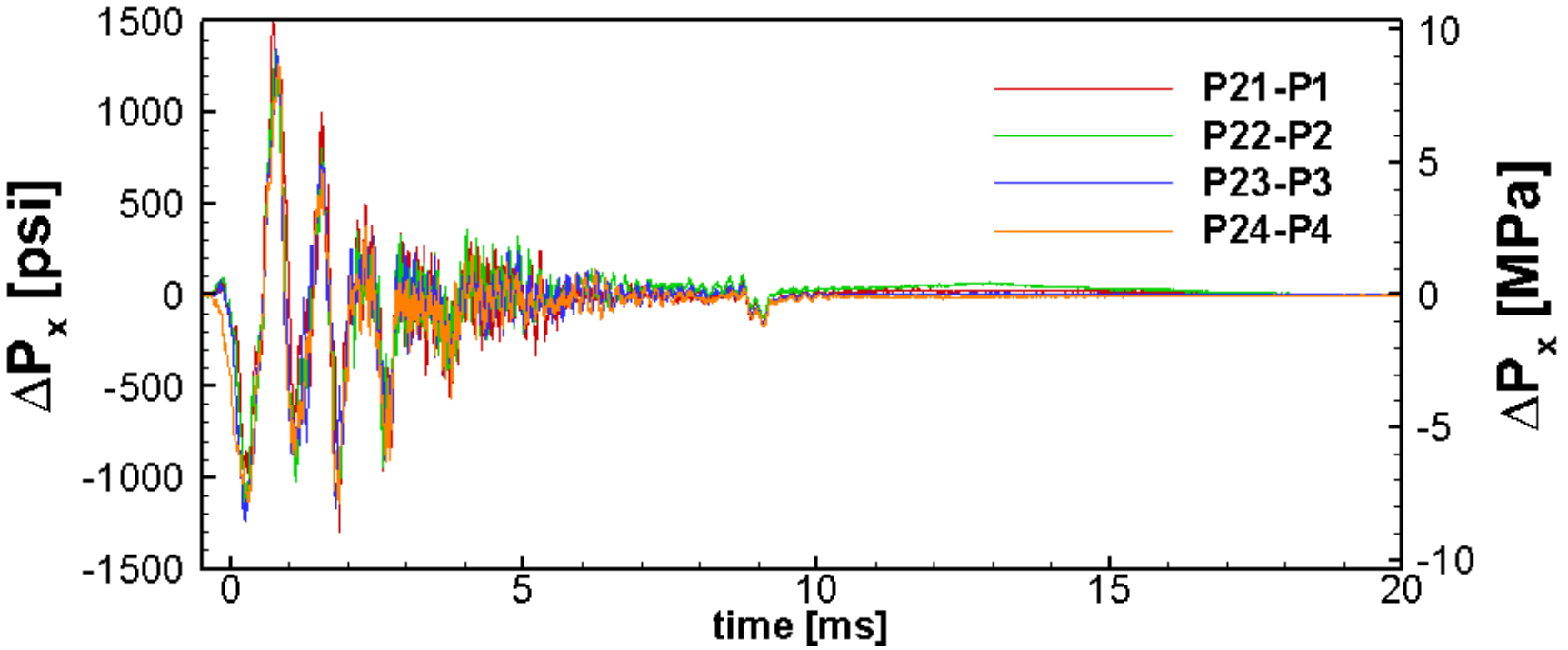

- The 4 charge increment (Charge 4) firings with the baseline flash tube configuration demonstrate significant longitudinal pressure waves.
- These waves are induced by the non-uniform ignition and flame-spreading processes present in the ignition cartridge and mortar tube.
- The existence of strong longitudinal pressure-wave phenomena in the mortar tube is undesirable as it dissipates combustion energy and introduces additional variability into the system.

Circumferential Pressure Gradients (Charge 4 baseline)

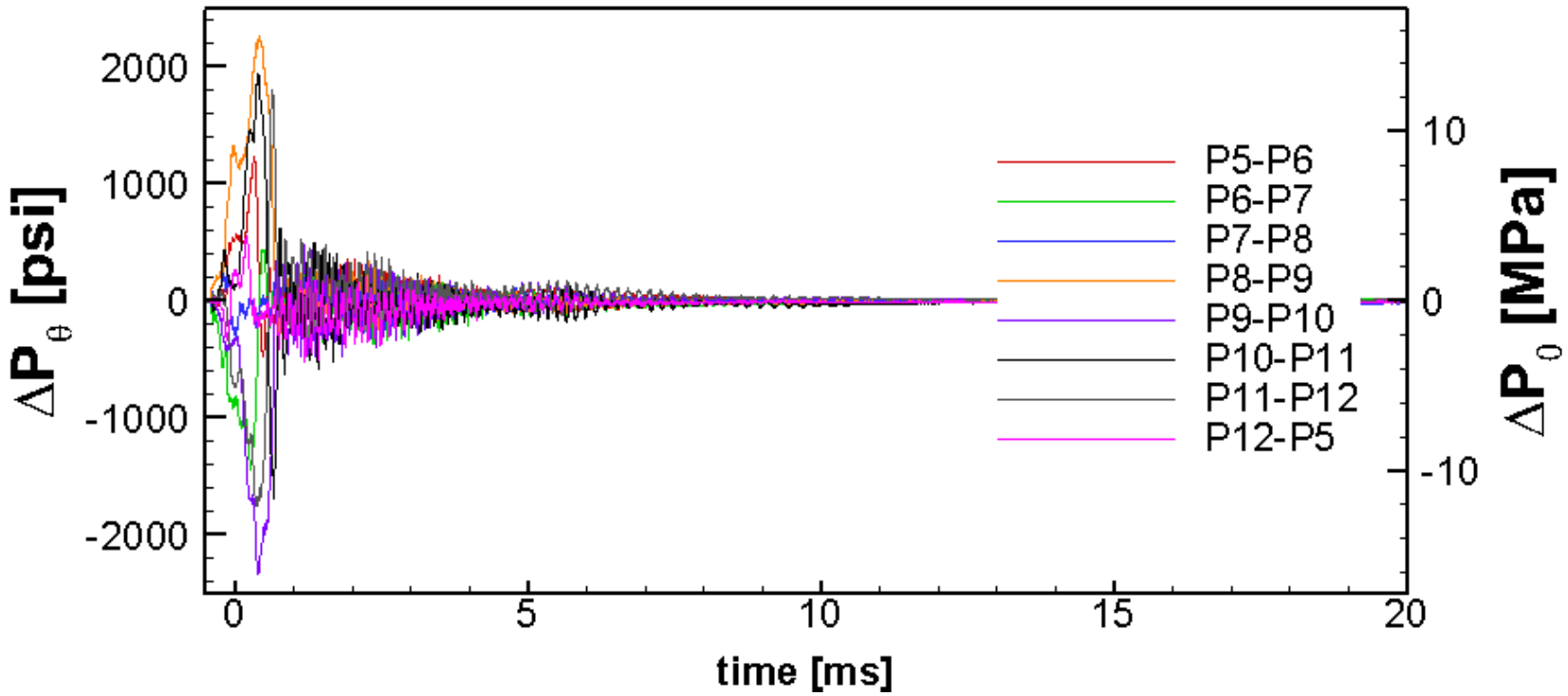

- During the early phase of the ballistic cycle, significant circumferential pressure gradients are present, even when the charge increments were alternated.
- These gradients mainly due to the horseshoe-shaped charge increments, which only supply propellant grains within 270 .
- In some extreme cases, strong circumferential gradients can cause tail boom fins to bend, leading to “short” rounds. The probability for fin-blade damage is very likely if the charge increments are aligned.

Comparison of Averaged *P-t* Traces for Charge 4

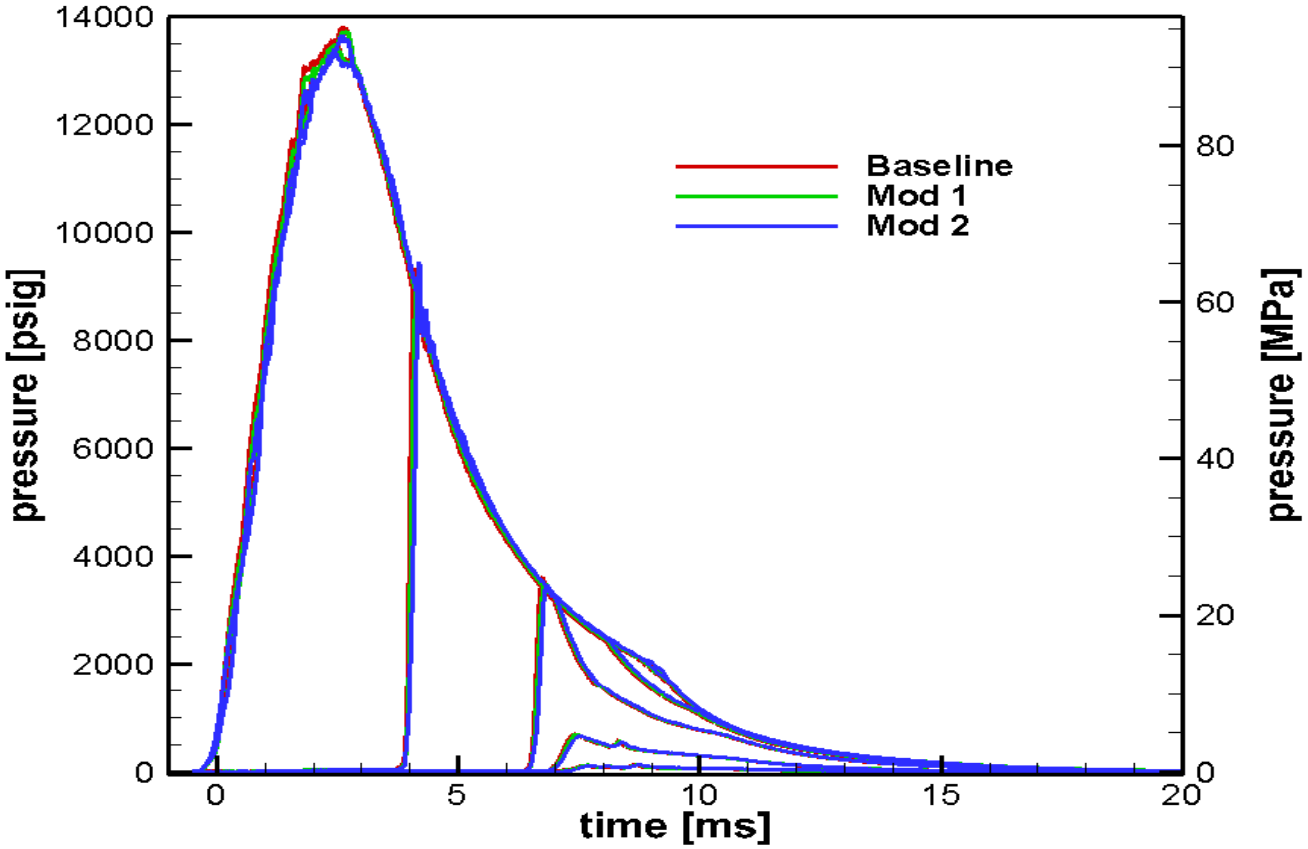

- Average P-t traces for the two modified flash tube configurations showed only minor differences from the baseline case in firings with 4 charge increments

Comparison of Standard Deviation in P-t Traces

- The plot of standard deviation of *P-t* traces are similar for all gauges in the breech region.
- The averaged *P-t* traces at Port 21 were used for comparing the two modified flash tube configurations with the baseline case.
- The standard deviations for both types of modified flash tubes do not demonstrate decreased variability in comparison with the baseline case.
- The higher standard deviation for the Mod 2 firings may be partially due to the smaller number of Mod 2 firings (10 compared to 20 each for Baseline and Mod 1).

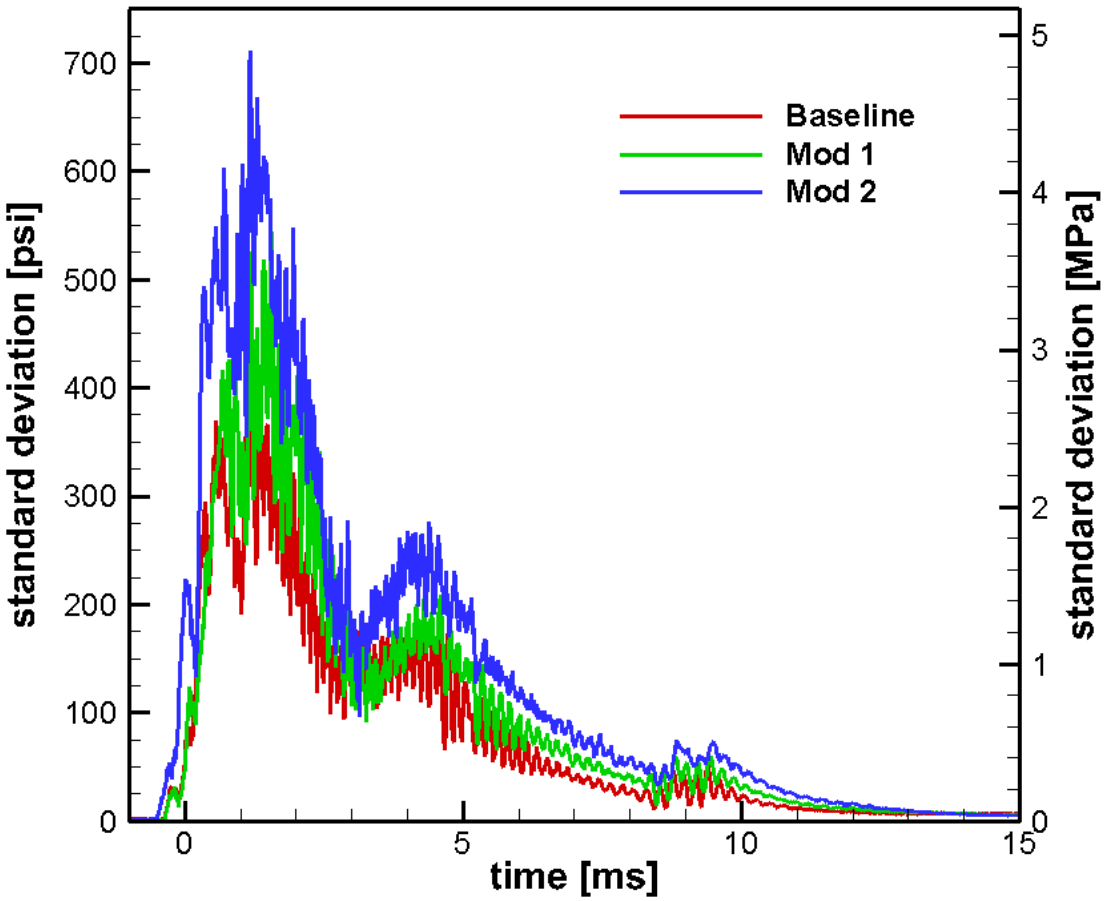

Comparison of Longitudinal Pressure Waves

- This figure displays the pressure difference between ports 21 and 1 ($P_{21} - P_1$) for the averages of the various flash tube configurations.
- These traces display the same general behavior as the single baseline firing.
  - Two distinct types of waves: High-amplitude, low frequency; and low-amplitude, higher-frequency.
- Mod 2 does exhibit lower peak amplitudes than the other configurations.
  - This seems due to destructive interference of the high-frequency waves with the low-frequency waves rather than any alteration in the fundamental cause of the low-frequency waves.
- The flash tube modifications do not show any significant effect on the presence of strong longitudinal pressure waves in the mortar tube.

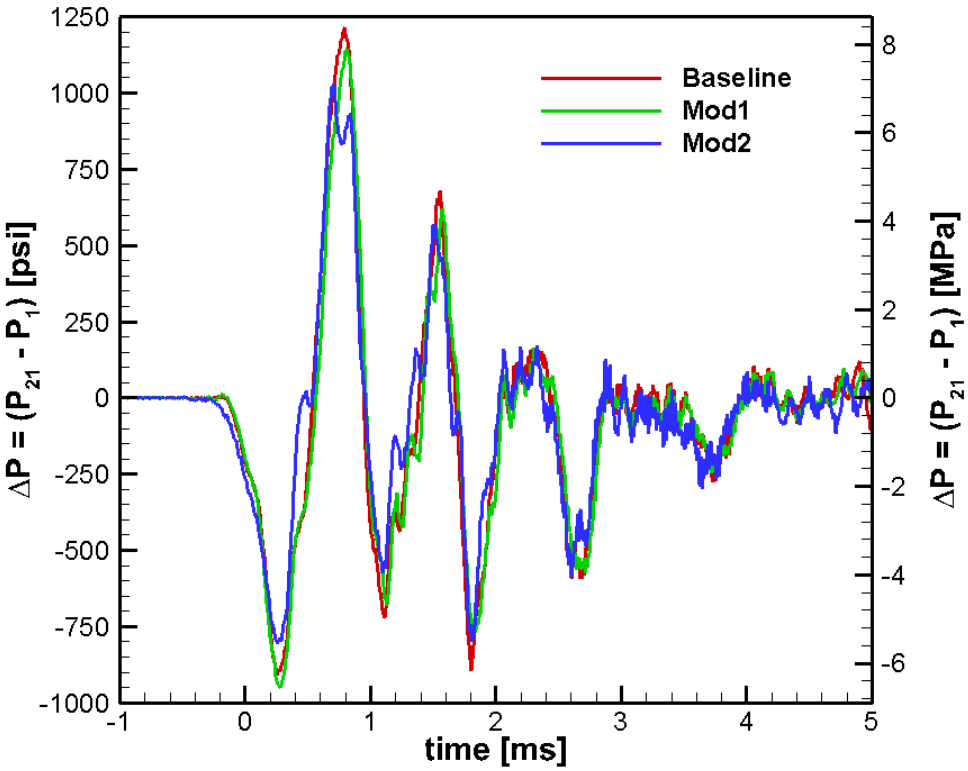

Plot of ($P_{21} - P_1$) vs. time for 4 charge increments

Comparison of Muzzle Velocities

[m/s]	Tests	Mean	Std Dev	95% Conf	Variability (% of mean)
Baseline	20	325.3	0.74	0.35	0.11%
Mod1	20	325.0	0.87	0.41	0.13%
Mod2	10	324.5	1.18	0.84	0.26%

- This data demonstrates that there is no statistically significant difference among the average muzzle velocities for the various ignition cartridge configurations
  - This finding corroborates that from the pressure-time behavior.
- The trend in the standard deviations from the muzzle velocities also mirrors that from the pressure-time behavior, with the baseline configuration having the lowest by a small margin, and the Mod 2 configuration having the highest, due to smaller number of tests.
- The remarkably small value of variability is noted in the table by the ratio of the 95% confidence interval to the mean muzzle velocity . For all configurations, this value is merely a fraction of a percent, which is remarkable given the complexities of the interior ballistics of the mortar system.

Charge 0 and 2 Baseline Firings

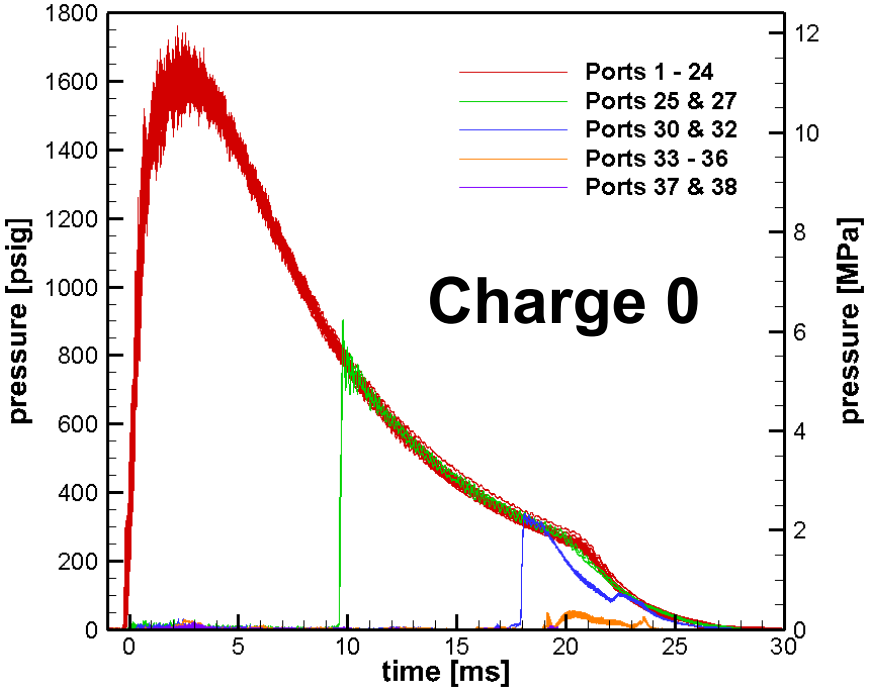

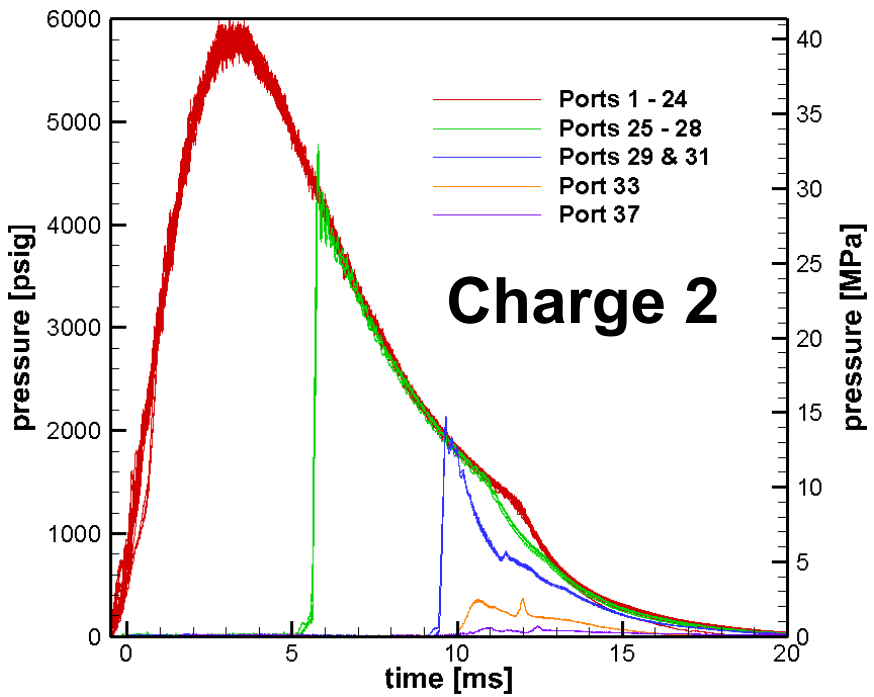

- These are representative firings of the Baseline configuration with 0 and 2 charge increments.
- The pressurization behavior for these charge increment levels is similar to that for the charge 4 firings with predictably reduced pressure magnitudes and projectile velocities resulting in slower depressurization of the mortar tube.

Longitudinal Pressure Waves & Circumferential Pressure Gradients

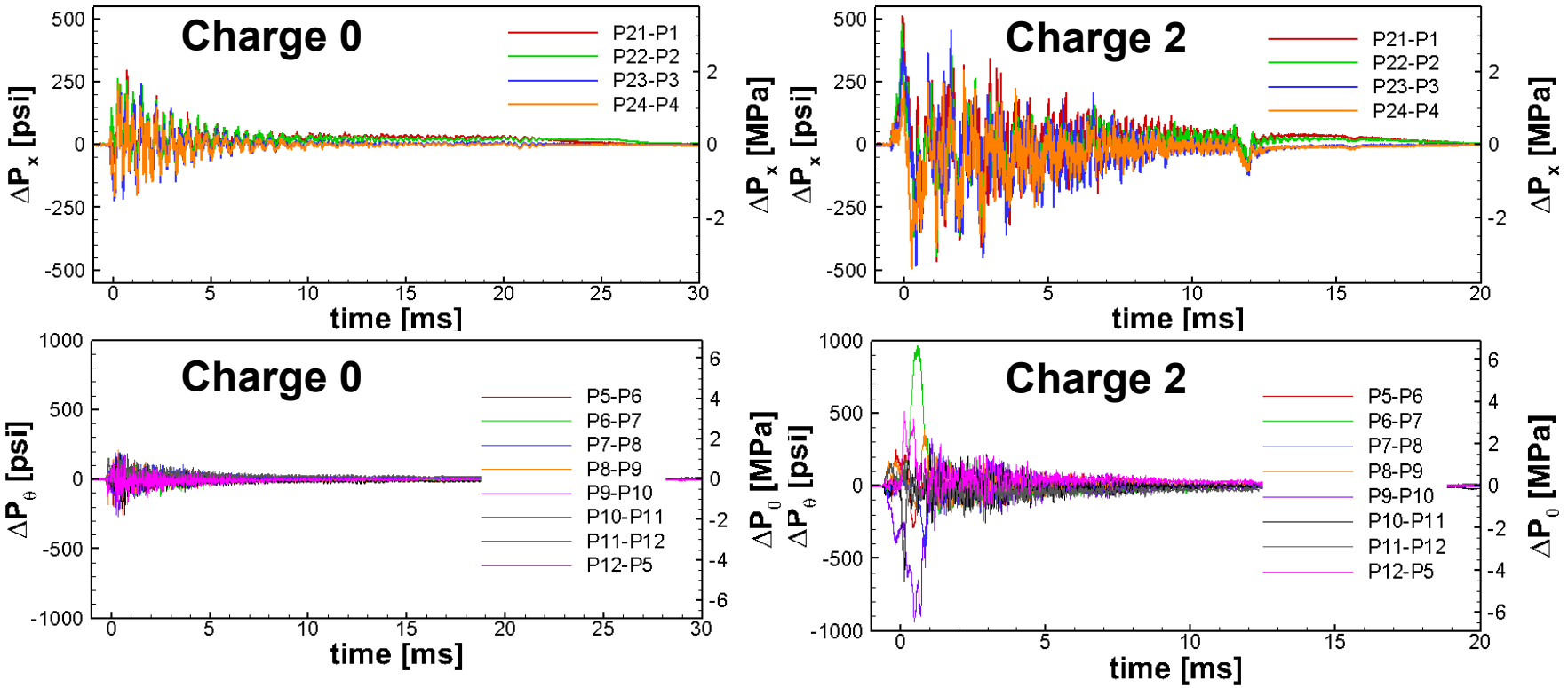

- The maximum absolute amplitude of longitudinal pressure waves for charge 0 and charge 2 firings are much smaller than those of charge 4 firings (~1500psi). ⟹ A nonlinear effect.
- Circumferential pressure gradients are negligibly small for charge 0; as expected due to the lack of charge increments.
- The strongest pressure gradients for charge 2 are approximately half those for charge 4.
  - This indicates almost a linear relationship.

Charge 0 and Charge 2 Average P-t Traces

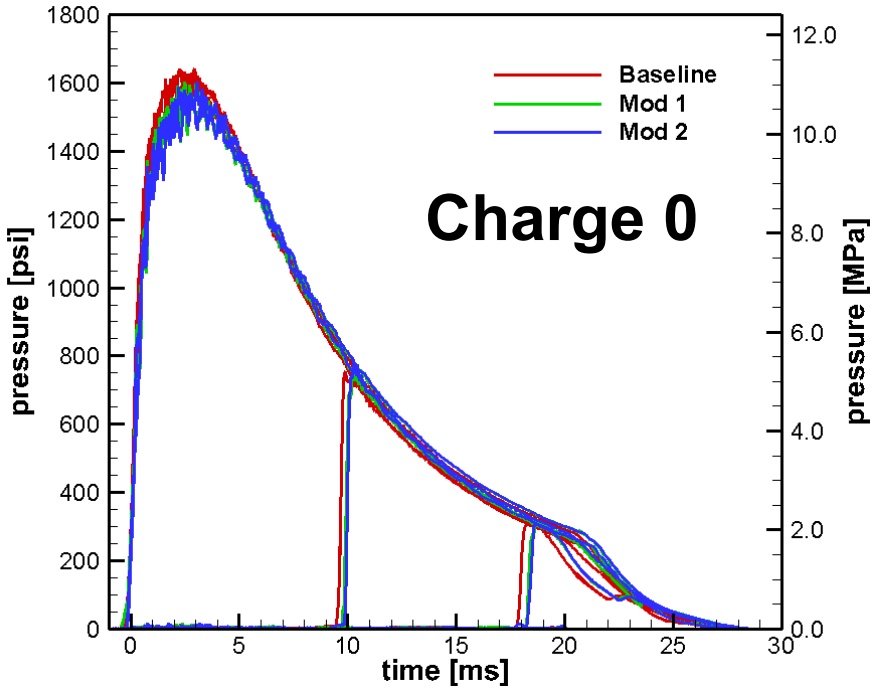

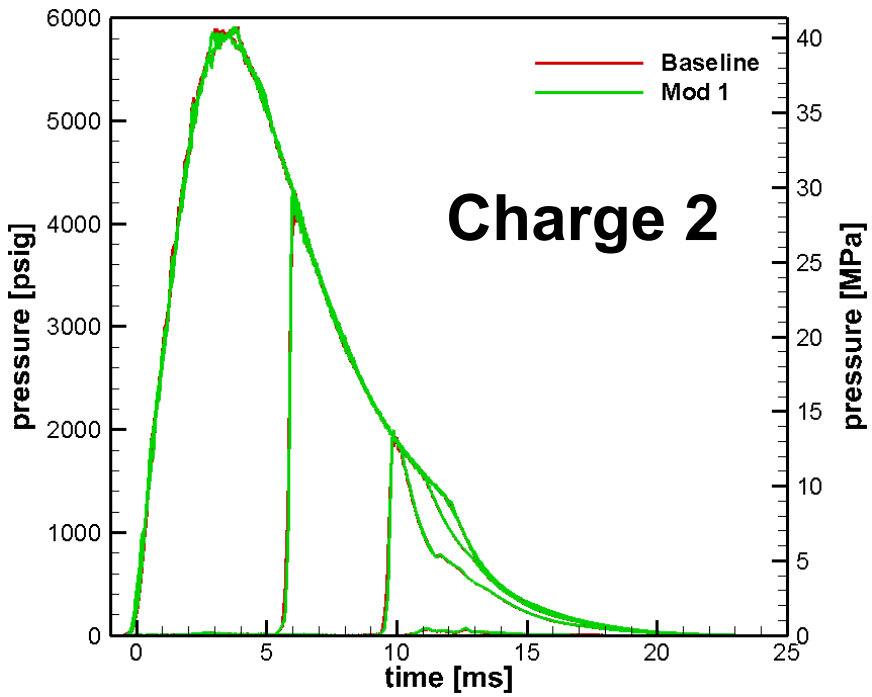

- The flash tube effect is more visible from Charge 0 configuration.
- The baseline configuration for Charge 0 demonstrates slightly higher peak pressures and earlier pressure rises for downstream ports compared to the modified ignition cartridges.
- No discernable difference exists between the average tube pressures for the baseline and Mod 1 configuration with 2 charge increments.

Charge 0 and Charge 2 Standard Deviations

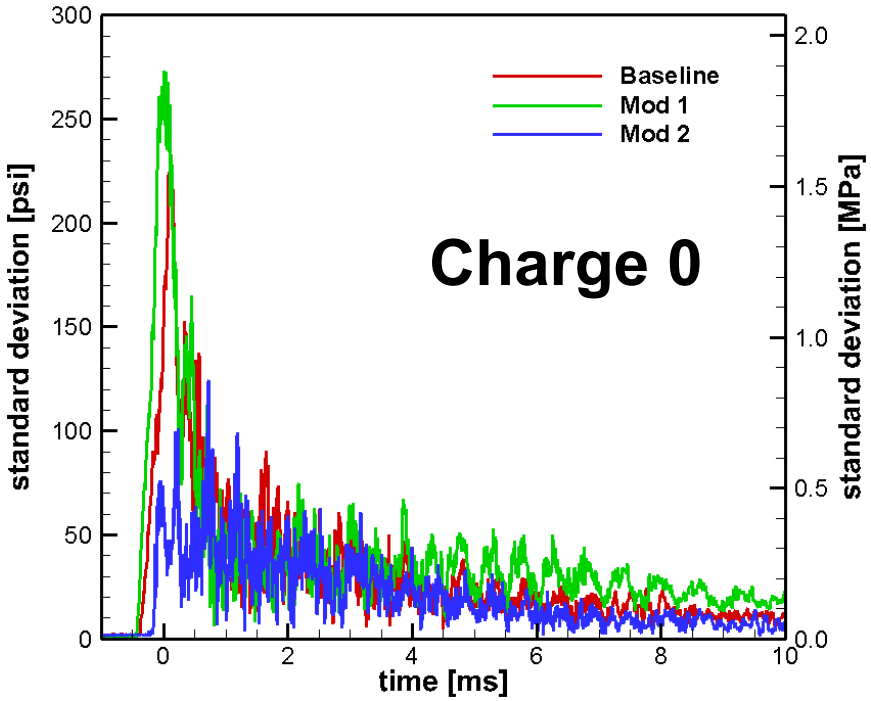

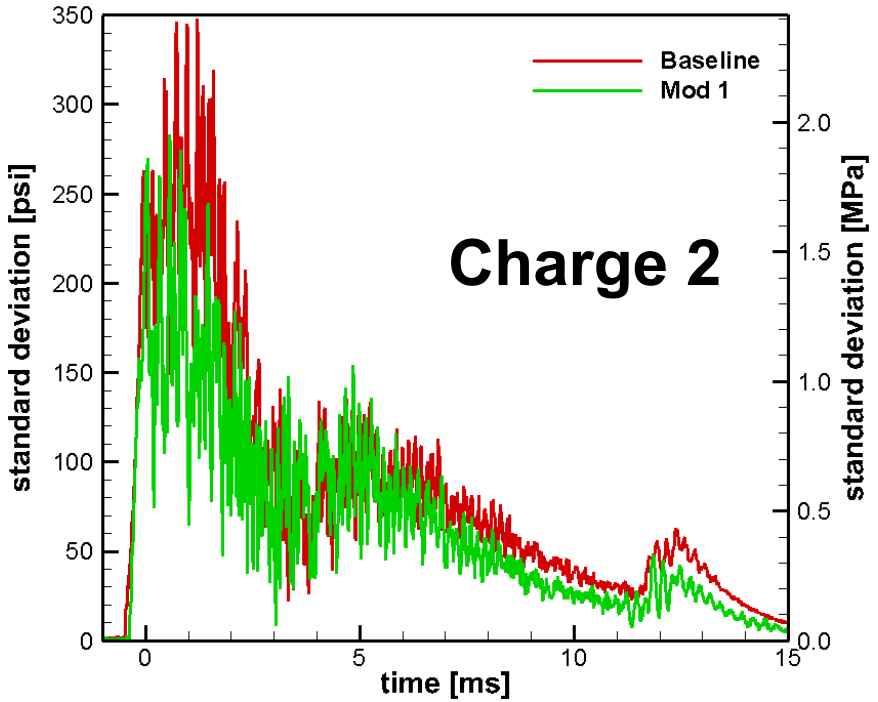

- Standard deviations of the averaged pressure histories at Port 21 for Charges 0 and 2 are shown in the above plots.
- For Charge 0, Mod 2 appears to reduce the variability in the pressure, though Mod 1 does not.
- For Charge 2, Mod 1 demonstrates a slight reduction in pressure variability.

Charge 0 and 2 Longitudinal Pressure Waves

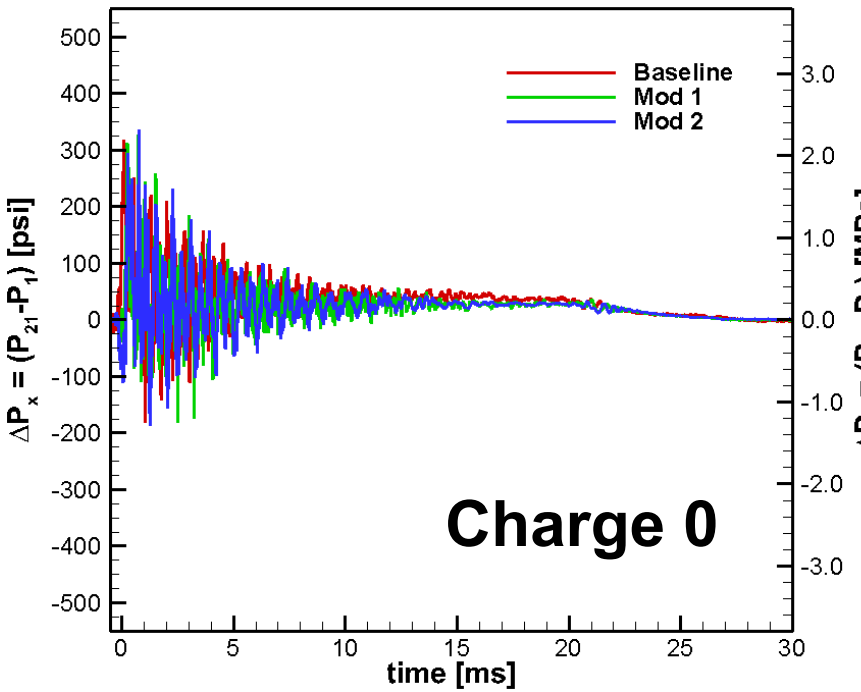

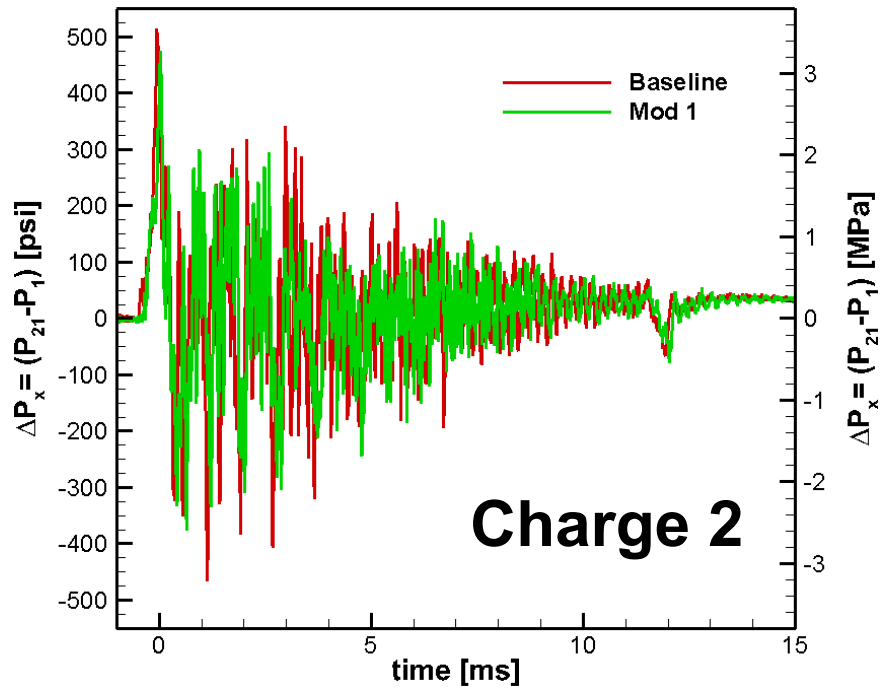

- These figures display the pressure difference between Ports 21 and 1 ($P_{21} - P_1$) for a representative firing from each of the flash tube configurations.
- For Charge 0, there is no significant difference among the Baseline, Mod 1, and Mod 2 configurations.
- For Charge 2, the difference between the Baseline and Mod 1 configurations are insignificant, as well.

Muzzle Velocities (in m/s)

- Fewer Charge 0 and Charge 2 firings were conducted than for Charge 4.
  - Caution is urged in the interpretation of data from such a small sample size.
- For Charge 0:
  - The Baseline ignition cartridge demonstrates a slightly higher average muzzle velocity than the modified configurations.
  - This observation is consistent with the measured pressure-time data.
- For Charge 2:
  - The Baseline and Mod 1 configurations are nearly indistinguishable.
- The ignition cartridge modifications are demonstrated to have a negligible influence on both the magnitude of muzzle velocity and its variability.

Charge 0	No.	Mean	Std Dev	95% Conf	Variability (% of mean)
Baseline	7	99.6	0.32	0.29	0.29%
Mod1	5	98.4	0.78	0.97	0.98%
Mod2	5	98.4	0.56	0.69	0.71%

Charge 2	No.	Mean	Std Dev	95% Conf	Variability (% of mean)
Baseline	7	227.2	0.27	0.25	0.11%
Mod1	5	227.2	0.27	0.34	0.15%

Charge 4	Tests	Mean	Std Dev	95% Conf	Variability (% of mean)
Baseline	20	325.3	0.74	0.35	0.11%
Mod1	20	325.0	0.87	0.41	0.13%
Mod2	10	324.5	1.18	0.84	0.26%

Conclusions

- Through detailed measurements in the instrumented mortar tube, significant longitudinal pressure waves and circumferential pressure gradients were found to exist during the early period of the ballistic cycle.
  - Both phenomena are undesirable to the performance of the mortar system.
  - The circumferential pressure gradients have the potential to cause damage of tail-boom fin blades.
- The two flash-tube modifications have negligible effect on both the magnitude of the muzzle velocity and its variability for different propellant charge increments.
- The flash-tube modifications also have a negligible effect on the magnitude of the longitudinal pressure waves for all charge increment levels.
- For Charge 0, Mod 2 seems to produce a reduction in the variability of the pressure-time behavior.
- For Charge 4, the flash-tube modifications do not reduce the magnitude of P_{max} or the variation in the pressure histories within the mortar tube.
- The results presented in this study have been very useful for model validation.

Acknowledgements

- We would like to thank Mr. Randy Rand and Mr. Marty Moratz of the U.S. Army-ARDEC, and Mr. Jack Sacco of the SAVIT Corporation for their sponsorship of our project under the prime contract DAAE30-03-D-1008.
- Thanks to Mr. Joe Nimphius of the U.S. Army-ARDEC for his effort in arranging the mortar test firing schedules.
- Special thanks are given to Mr. Troy Garcia and his team at the U.S. Army's Aberdeen Test Center for conducting a series of test firings.
- We would also like to thank Dr. Ragini Acharya of our team for her simulation study and the comparison of calculated results with the mortar test data.

Thanks very much for your attention.

Any Questions?

Attenuation of a Blast Wave Through Cranial Bone

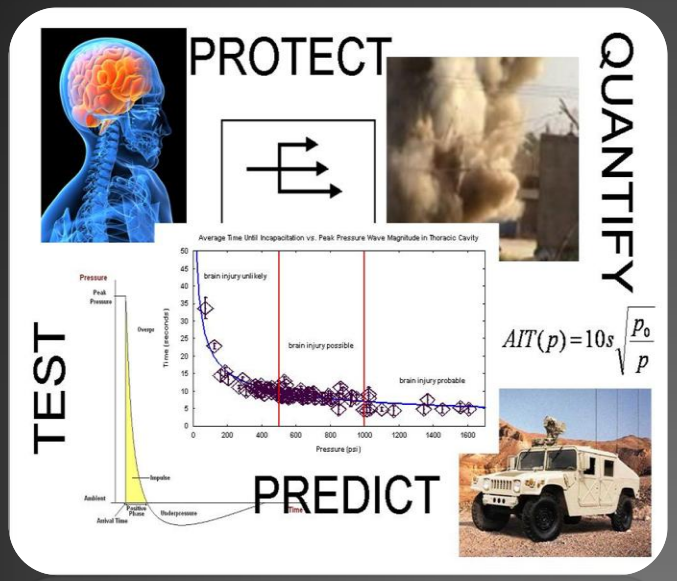

Amy Courtney, Ph.D.
BTG Research
amy_courtney@post.harvard.edu

Michael Courtney, Ph.D.
United States Air Force Academy
Michael.Courtney@usafa.edu

Motivation

- Experimental data on the transmission of blast waves through cranial bone is sparse. (e.g., Romba 1961; Chavko et al., 2007, 2011)
- Methods are needed to apply realistic blast loading to test specimens in the laboratory.
  - Explosive-driven shock tubes are difficult and expensive to install and operate.
  - Compression-driven shock tubes produce suboptimal pressure wave profiles and have an undesirable “jet effect.”

Table-Top Blast-Driven Shock Tube

Courtney, M.W., Courtney, A.C., 2010. A table-top blast driven shock tube. *Rev. Sci. Instrum*., 81:126103.

This is an explosive driven shock tube employing a rifle primer which explodes when impacted by the firing pin. The firearm barrel acts as the shock tube, and the shock wave emerges from the muzzle.

Table-Top Blast-Driven Shock Tube

Courtney, M.W., Courtney, A.C., 2010. A table-top blast driven shock tube. *Rev. Sci. Instrum.*, 81:126103.

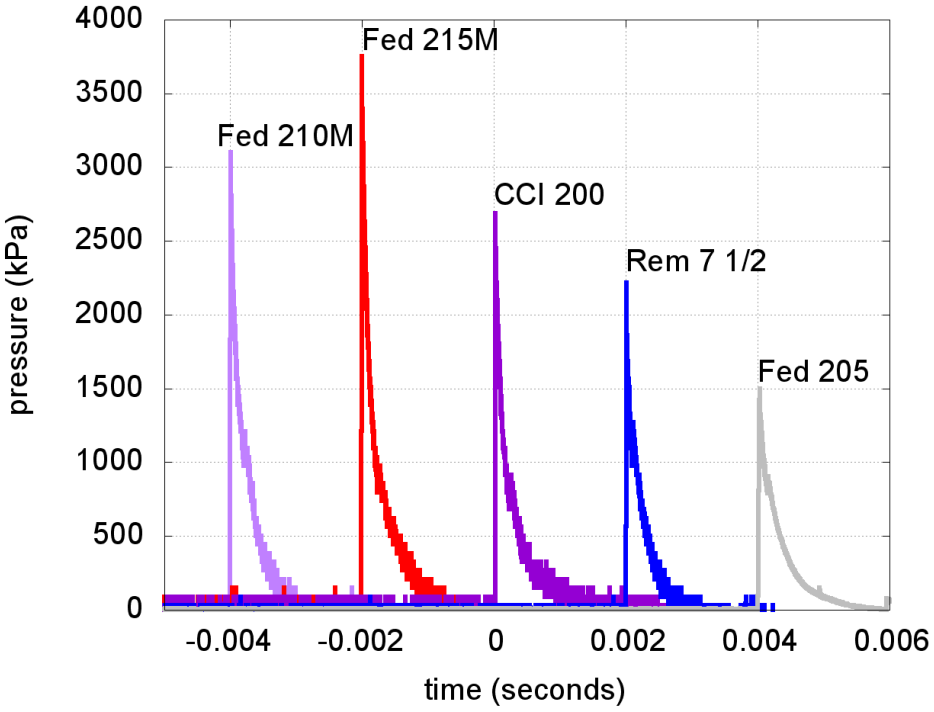

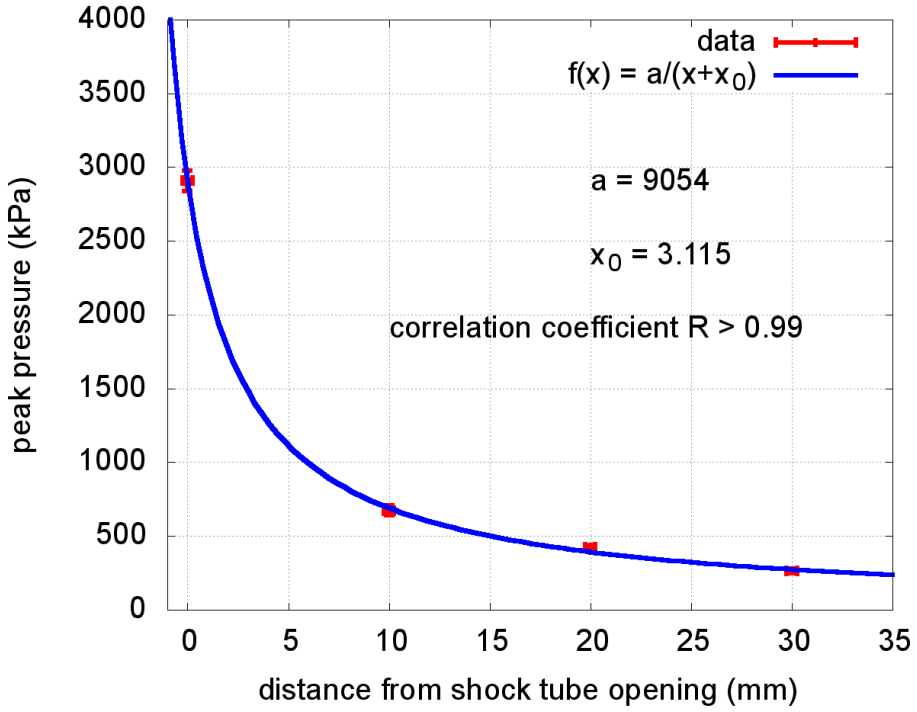

Oxy-Acetylene Driven Laboratory Scale Shock Tubes

- Produce true shock waves with realistic pressure-time profiles and relevant durations.
- Can be employed to study effects of blast waves on materiel or biological samples.
- Modular design facilitates selection of peak pressure and area of application.

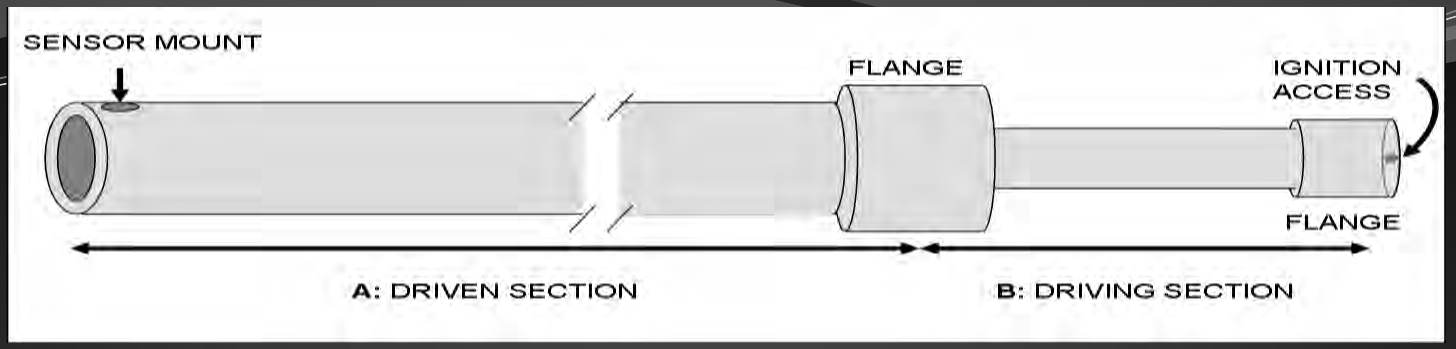

A: DRIVEN SECTION	27 mm	41 mm
Length (cm)	183	305
Inner diameter (cm)	2.65	4.10
Outer diameter (cm)	3.35	4.86
Sensor mount center distance from opening (cm)	1.12	1.22

B: DRIVING SECTION	2	3	4
Length (cm)	26.7	25.4	30.5
Inner diameter (cm)	1.57	2.13	2.71
Outer diameter (cm)	2.17	2.70	3.35

Blast Wave Production

A stoichiometric mixture of oxygen and acetylene was used to produce the blast wave.

$$2\ H_2C_2\ (g) + 5\ O_2\ (g) \Rightarrow 4\ CO_2\ (g) + 2\ H_2O\ (g)$$

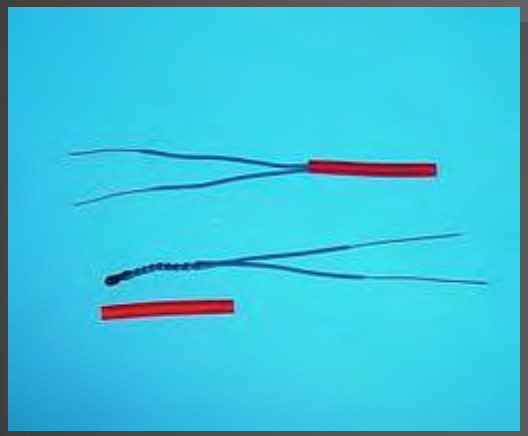

The ignition source consisted of an electric match.

Blast Wave Characterization

Internal Pressure Sensor	PCB 102B15
External Pressure Sensor	PCB 102B18
Sample Rate	1 MHz
Signal Conditioner	PCB 842C
Digitizer	NI PXI-5105 or NI USB-5132

Tests were conducted at 20°C and air pressure of 587 mm Hg

Characterization Results

- Steep shock front
- Exponential decay
- Positive pulse duration of about 2 ms
- Larger driver volume ⇨ higher peak pressure

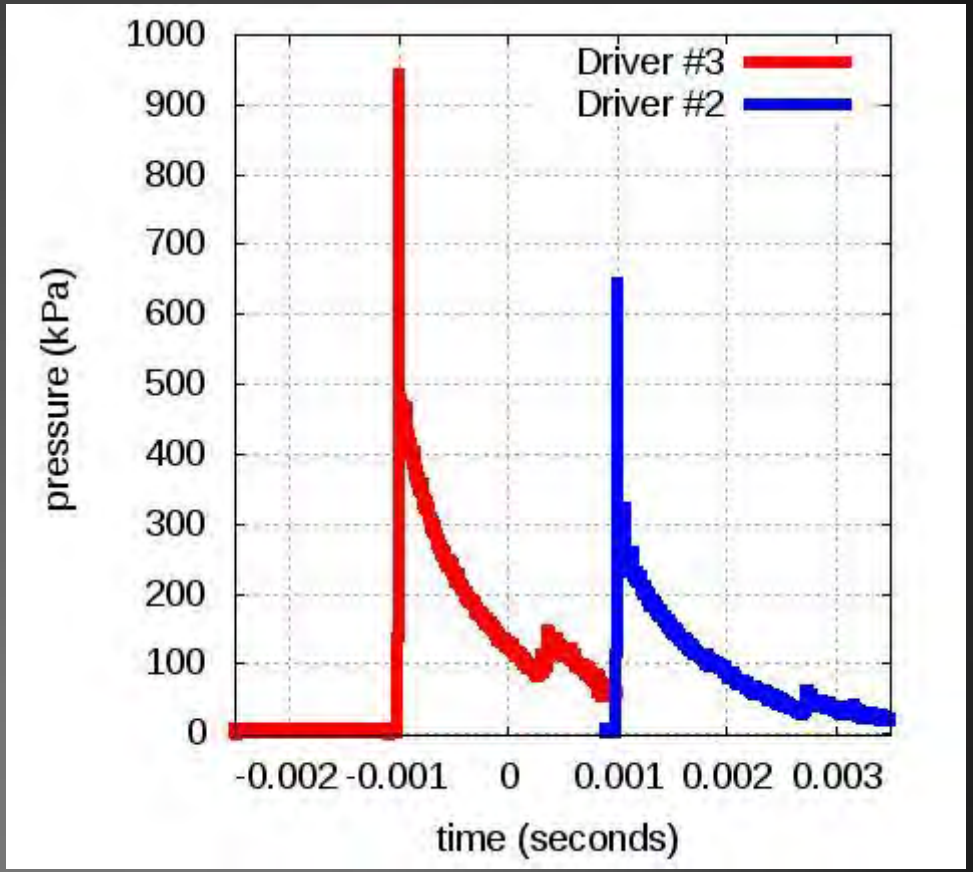

27 mm Diameter Driven Section

Characterization Results

- Same driver, larger shock tube ⇨ lower peak pressure
- Shock wave characteristics consistent across driver/driven section combinations

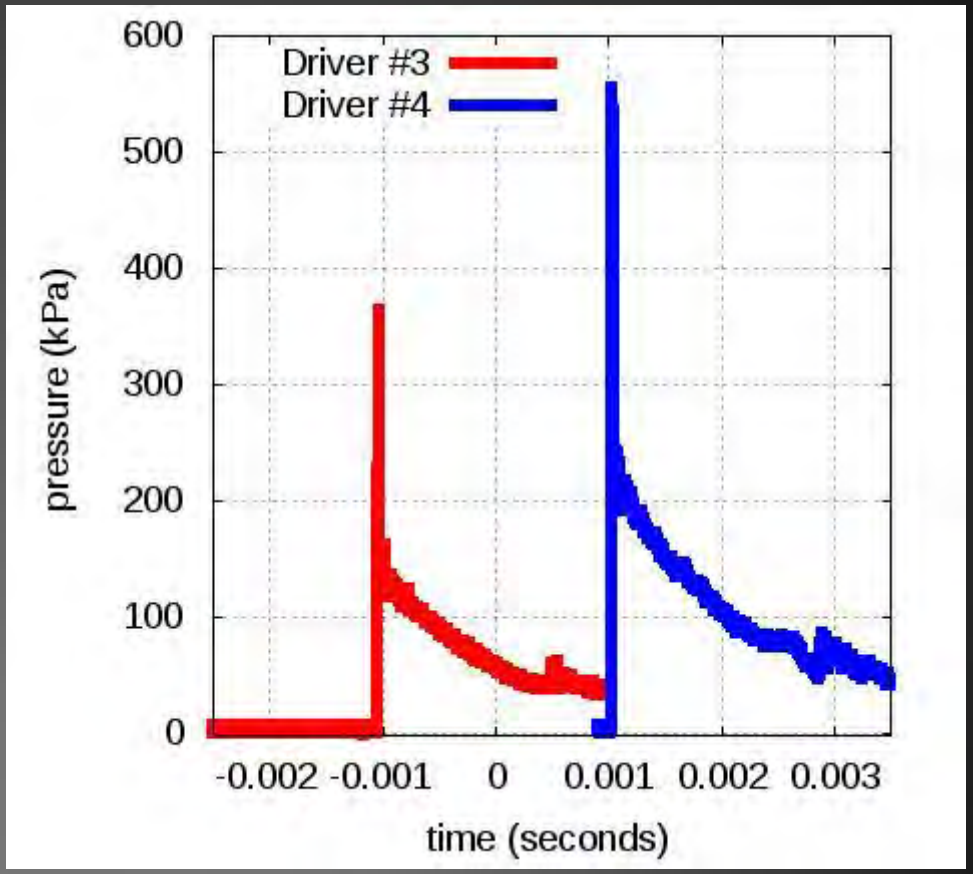

41 mm Diameter Driven Section

Characterization Results

- Peak pressure decreased with distance from opening
- Allows finer control of peak pressure applied to a test sample
- Pattern of decreasing peak pressure is affected by shock tube diameter

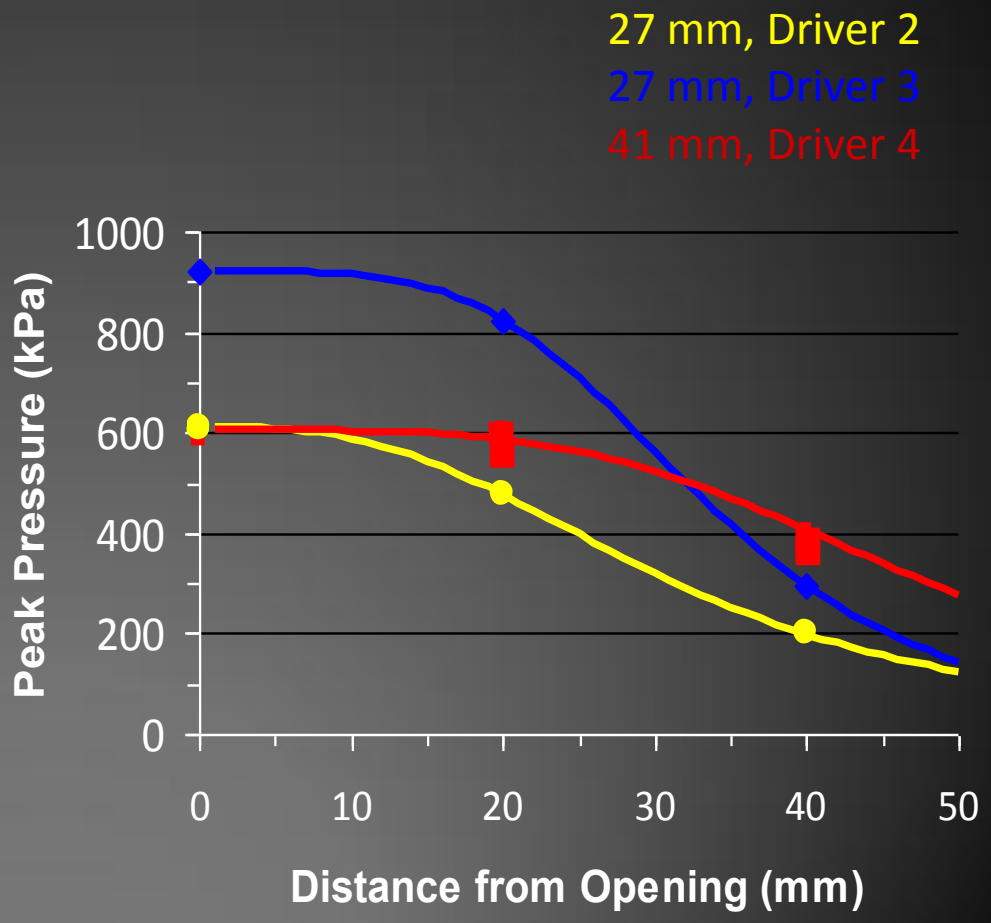

Jet Effect: The volume of additional gas produced by the fuel in a shock tube. The jet follows the shock front and imparts momentum to the test object, possibly confounding primary blast effects.

In calculations for a 632 cm^3 volume driving section*, for example, it can be shown that the oxy-acetylene driven shock tube produces a dramatically smaller jet effect compared to a compressed gas driver.

Source of blast or shock wave	Volume of additional gas produced (cm^3)
Oxy-acetylene	534 – 632 = **-98**
RDX	171 – 0 = **+171**
Compressed Gas	23,177 – 632 = **+22,545**

*5.1 x 30.5 cm cylinder. Comparisons are based on equating the total energy produced. Calculations do not consider temperature effects.

Application: Transmission of a Blast Wave Through Cranial Bone

How does a blast wave reach the brain to cause injury without external wounding?

- **Head acceleration**
- **Thoracic** (pressure surge and/or vaso-vagal response)
- **Direct cranial entry** (transmission, entry through openings, skull flexure?)

These mechanisms are **not mutually exclusive**.

Application: Transmission Through Cranial Bone

Study	Peak (MPa)	Duration (ms)	Magnification*
Hoberecht	0.18	4.0	1.7
Moss et al.	0.20	0.7	1.5
Zhang et al.	0.49 1.50	3.0 0.6	7.0 3.7
Moore et al.	0.51 1.82	0.7 0.6	1.0 2.75
Taylor & Ford	1.30 2.60	1.0 1.0	3.8 3.8

* Approximate factor of predicted magnification of peak intracranial pressure compared to the incident blast wave (at any intracranial location, not including the cranial bone itself).

All studies cited were published in 2009.

Application: Transmission Through Cranial Bone

Application: Transmission Through Cranial Bone

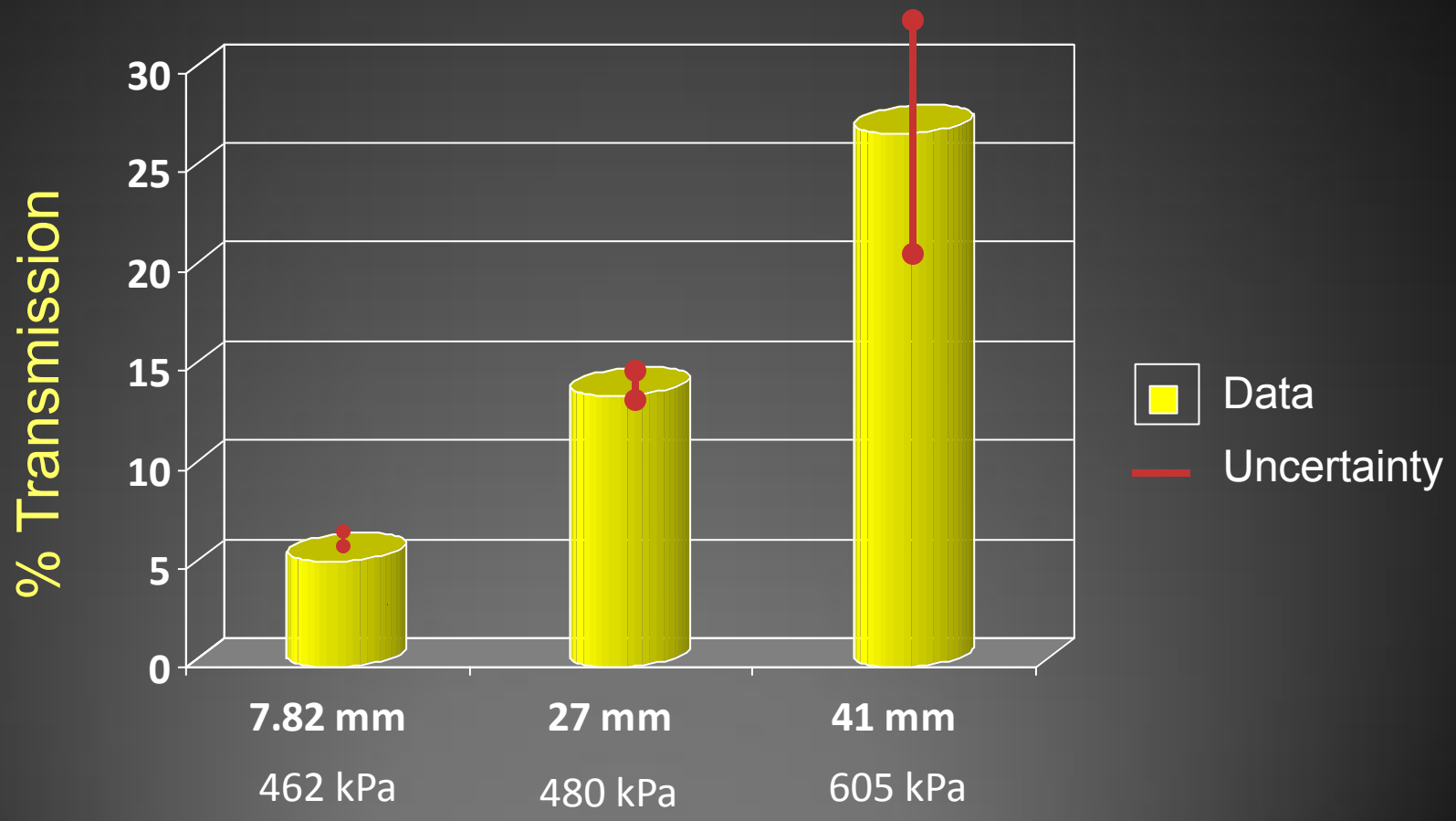

Shock Tube Diameter and Peak Unobstructed Pressure

Application: Transmission Through Cranial Bone

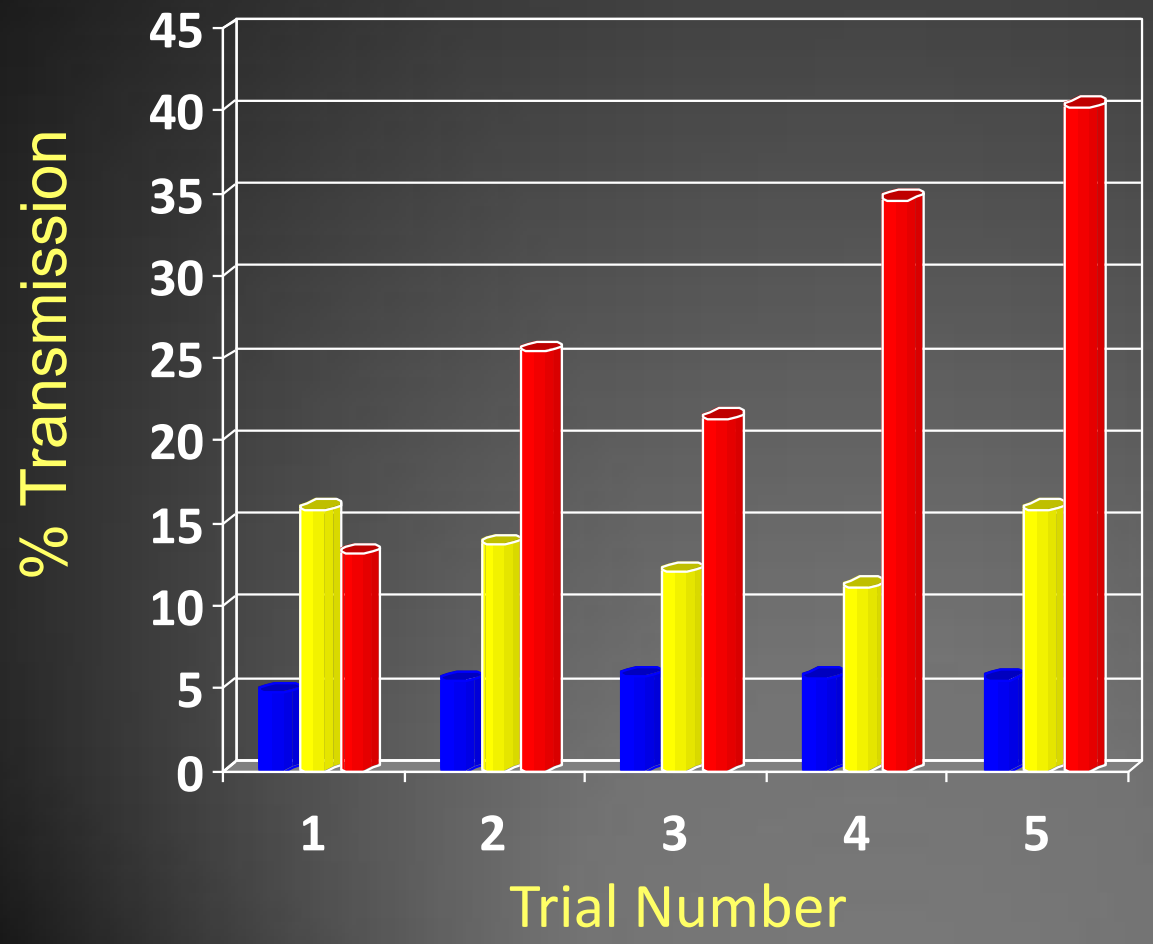

- Transmission increased with successive exposures from the 41 mm shock tube.
- A second specimen showed similar results.

7.82 mm
27 mm
41 mm

- The specimen did not recover after 48 hours but continued to transmit an increasing percentage of the shock wave.

Application: Transmission Through Cranial Bone

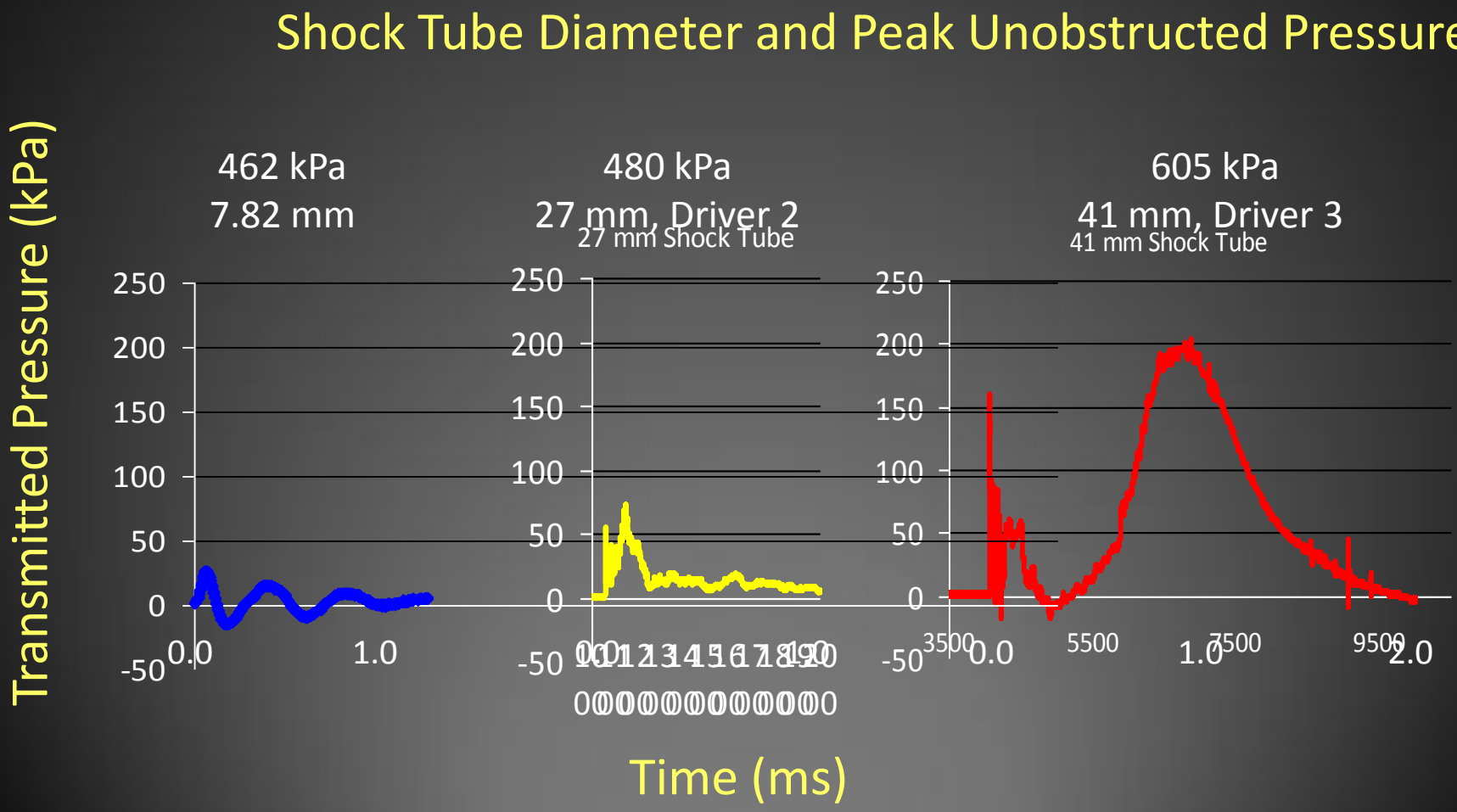

Oxy-Acetylene Driven Laboratory Scale Shock Tubes

- Produce true shock waves with realistic pressure-time profiles and relevant durations.
- Can be used to study effects of blast waves on materiel or biological samples.
- Modular design facilitates selection of peak pressure and area of application. *New 51 mm and 79 mm diameter designs work just as well.*

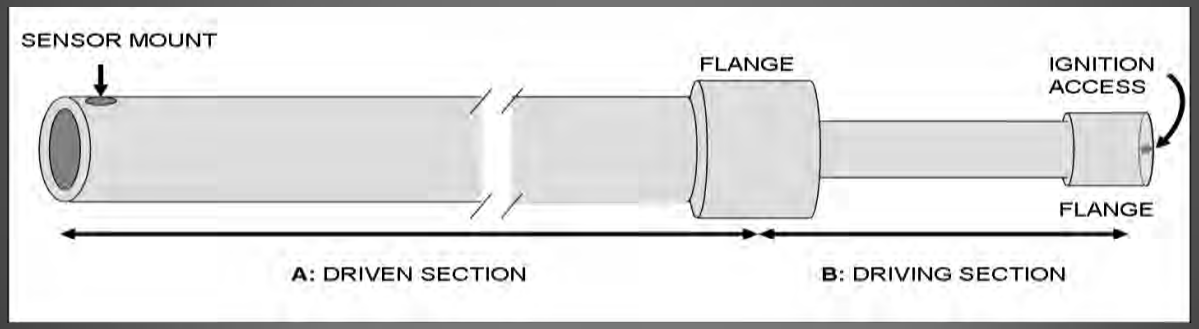

We gratefully acknowledge

financial support from
Force Protection Industries, Inc.

and laboratory assistance
from cadets **Alivia Berg**
and **George Michalke** of the
United States Air Force Academy.

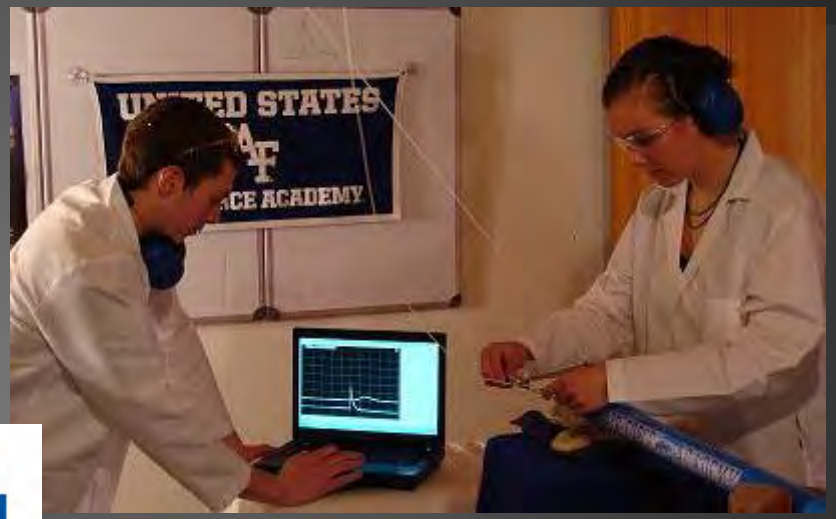

Experimental Studies of Scalable Effects Warhead Technologies

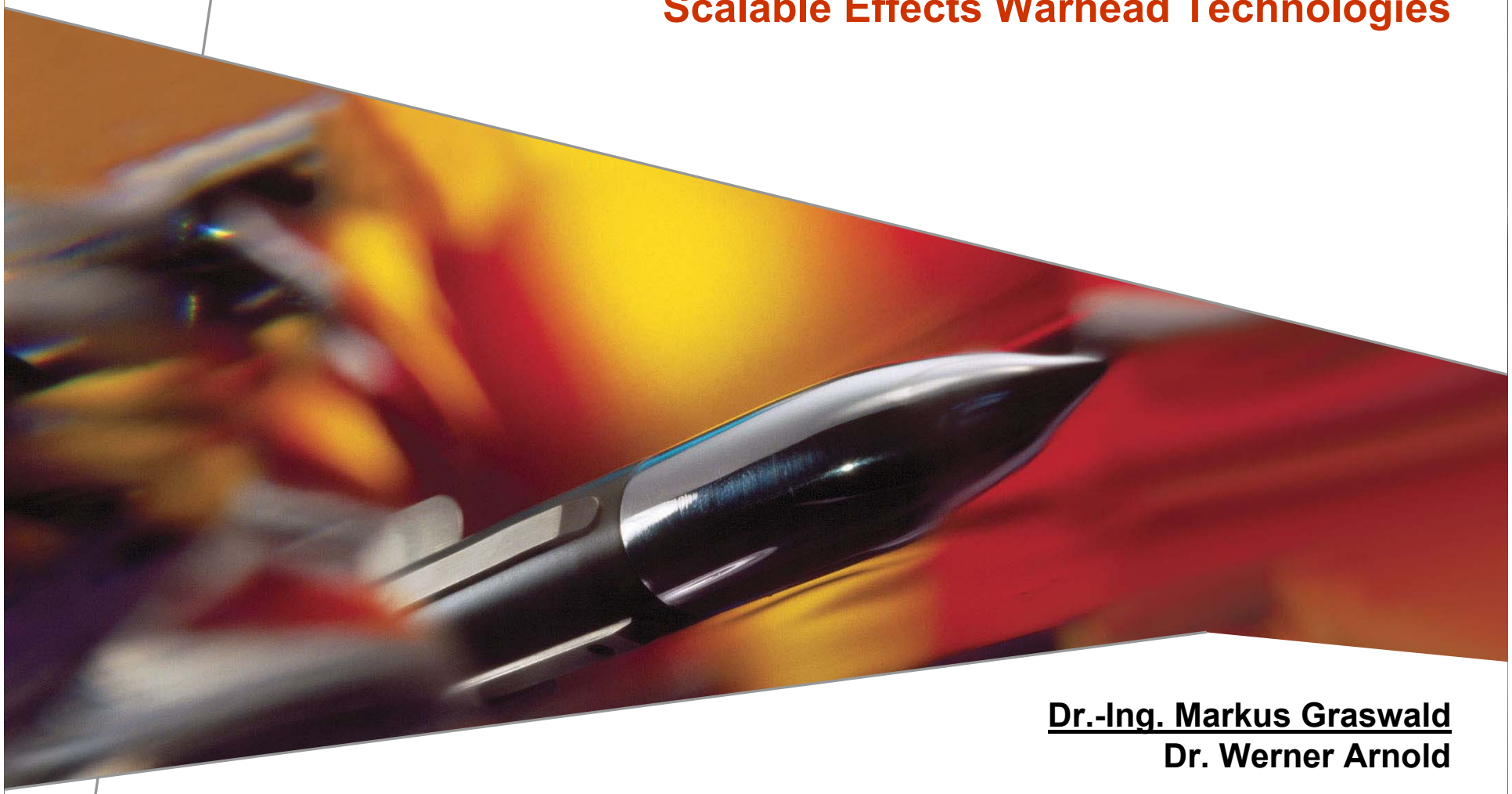

Dr.-Ing. Markus Graswald
Dr. Werner Arnold

TDW Gesellschaft für verteidigungstechnische Wirksysteme mbH
Miami (FL), 15 September 2011

MBDA MISSILE SYSTEMS

Agenda

- Motivation
- Flexible Response Warhead Technologies
- Scalable Effects Warhead
- TDWs Deflagration Cylinder Test
- Variety of Test Charges: Stable Low-output Mode

MBDA MISSILE SYSTEMS

Motivation

- **Current Munitions: Collateral Damages in Urban Terrain**

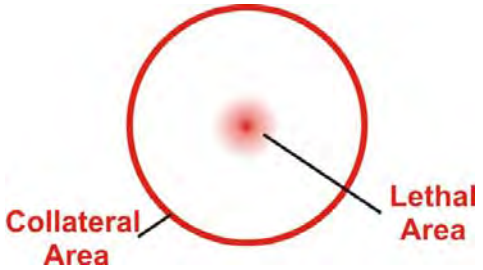

MBDA MISSILE SYSTEMS

Flexible Response Warhead Technologies

Flexible Response Warhead Technologies

- **Scalable Effects Warheads (Dial-a-Yield)**
  - Deflagrator / detonator timing
  - Mechanical measures
  - Densification and Re-densification
- **Switchable Mode Warheads (Dial-a-Mode)**
  - High explosive pellets
  - Multi-point initiation with EFIs
  - Grooved liner
  - Grooved high explosive charge
  - Ejectable cutting grid
- **Aimable Warheads (Dial-a-Direction)**
  - Velocity-enhanced mass-focussed
  - Internal layer
- **Multi-Effects Warheads (Dial-an-Effect)**
  - Shaped charges
  - Penetrator casing
  - Penetrator with enhanced lateral effects (PELE)

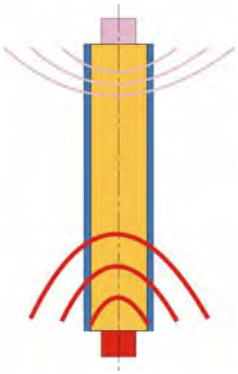

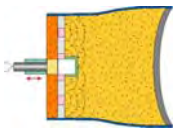

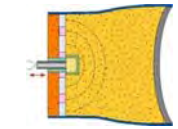

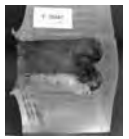

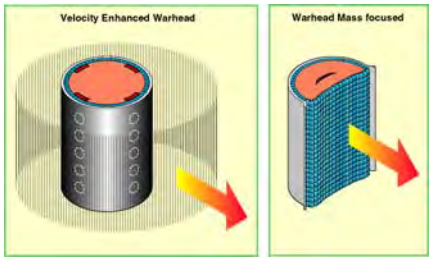

M. Held

MBDA MISSILE SYSTEMS

Scalable Effects Warhead

- **Dial-a-Yield Technology: Lethal and Collateral Radii are Scalable**

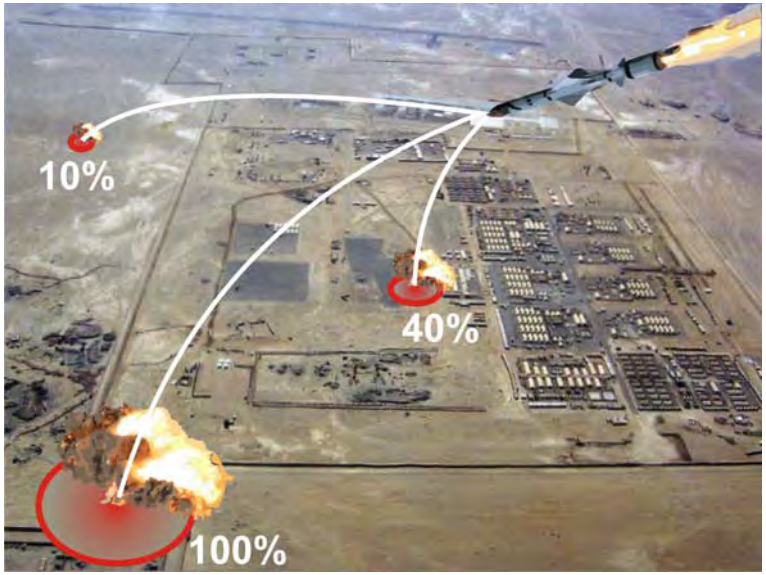

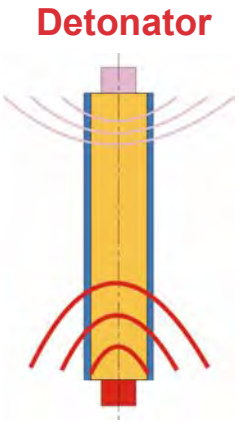

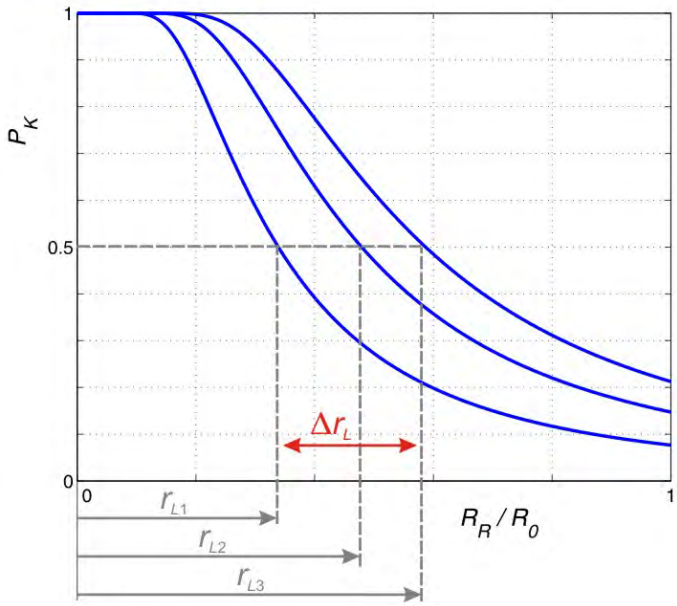

<u>Scalable Effects Warheads</u>

Target-dependent, cockpit-selectable warhead response

MBDA MISSILE SYSTEMS

Scalable Effects Warhead

- **Dial-a-Yield Technology: Variable Fragment Effects**

Low output mode	Scaled output		Full output mode
			
		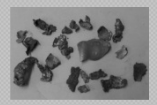	
<10%	40%	80%	100%
Deflagration – ERL IV	ERL III	ERL II	Detonation – ERL I

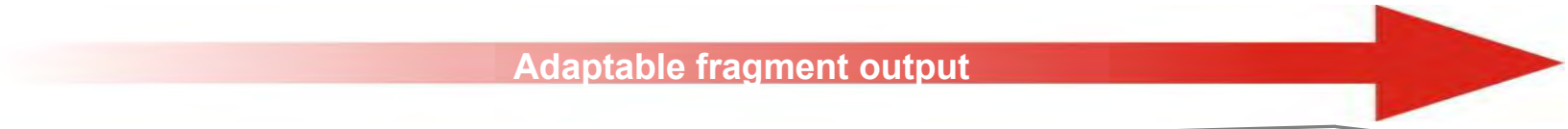

MBDA MISSILE SYSTEMS

Scalable Effects Warhead

- **Dial-a-Yield Technology: Blast Effects are also Scalable**

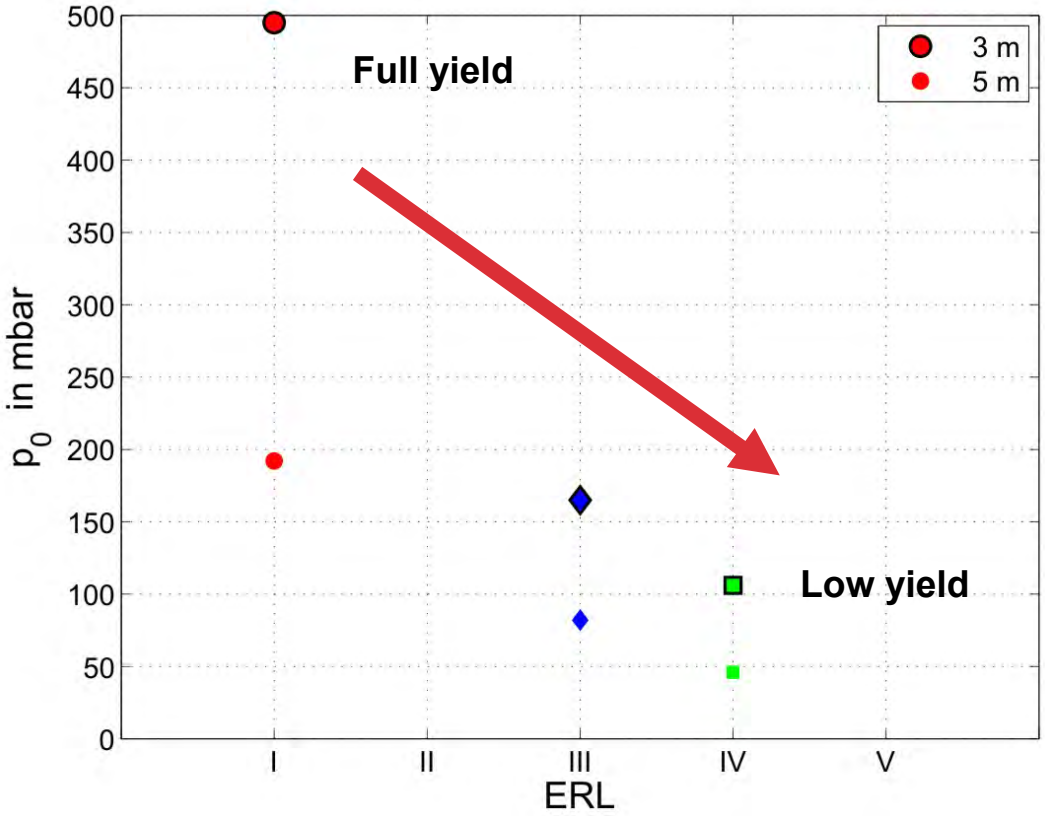

MBDA MISSILE SYSTEMS

Experimental Setup

- **TDWs Deflagration Cylinder Test**

Detonator

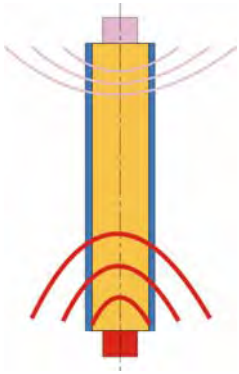

Deflagrator

Protection by concrete barriers and metal plates

Argon bomb

Steel tube with HE charge

Viewing direction of rotating mirror camera

Cordin 200

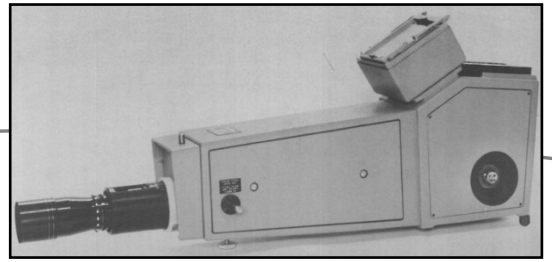

Combined Streak / Framing Records

- **Deflagration Reaction**

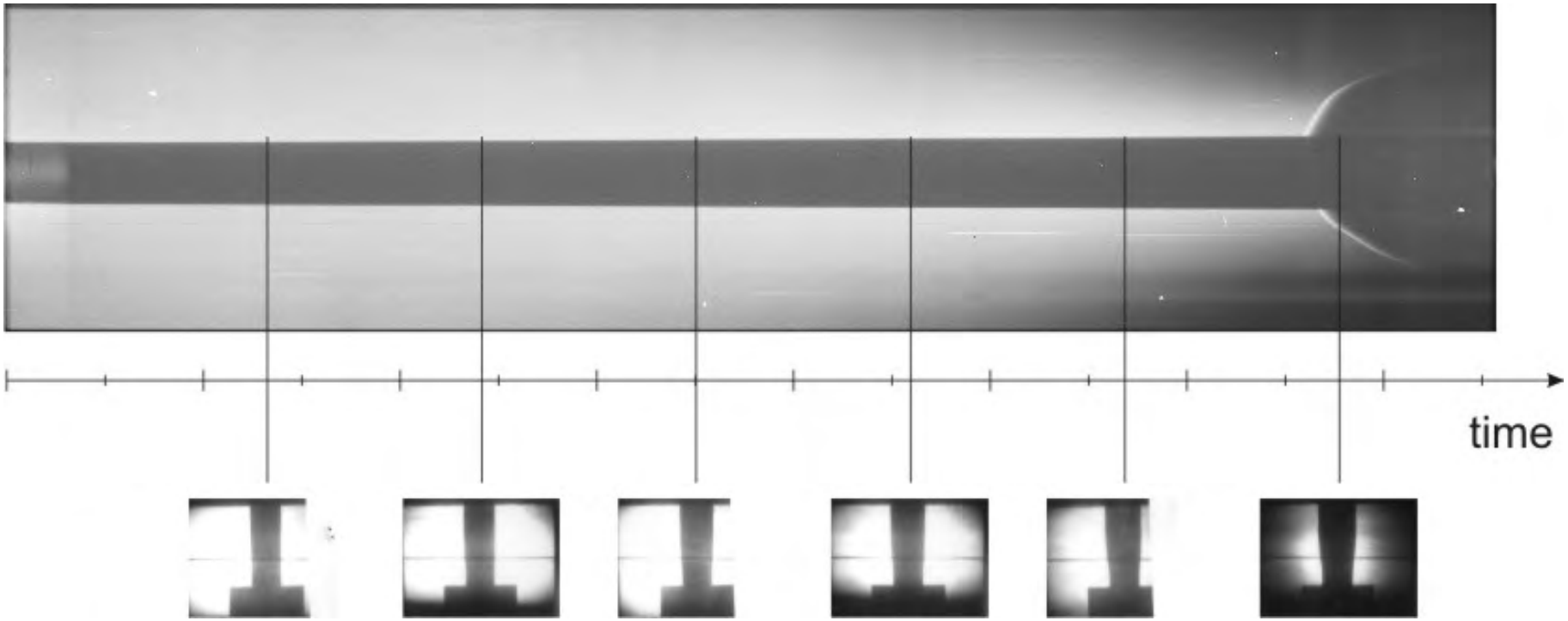

MBDA MISSILE SYSTEMS

Combined Streak / Framing Records

- **Detonation Reaction**

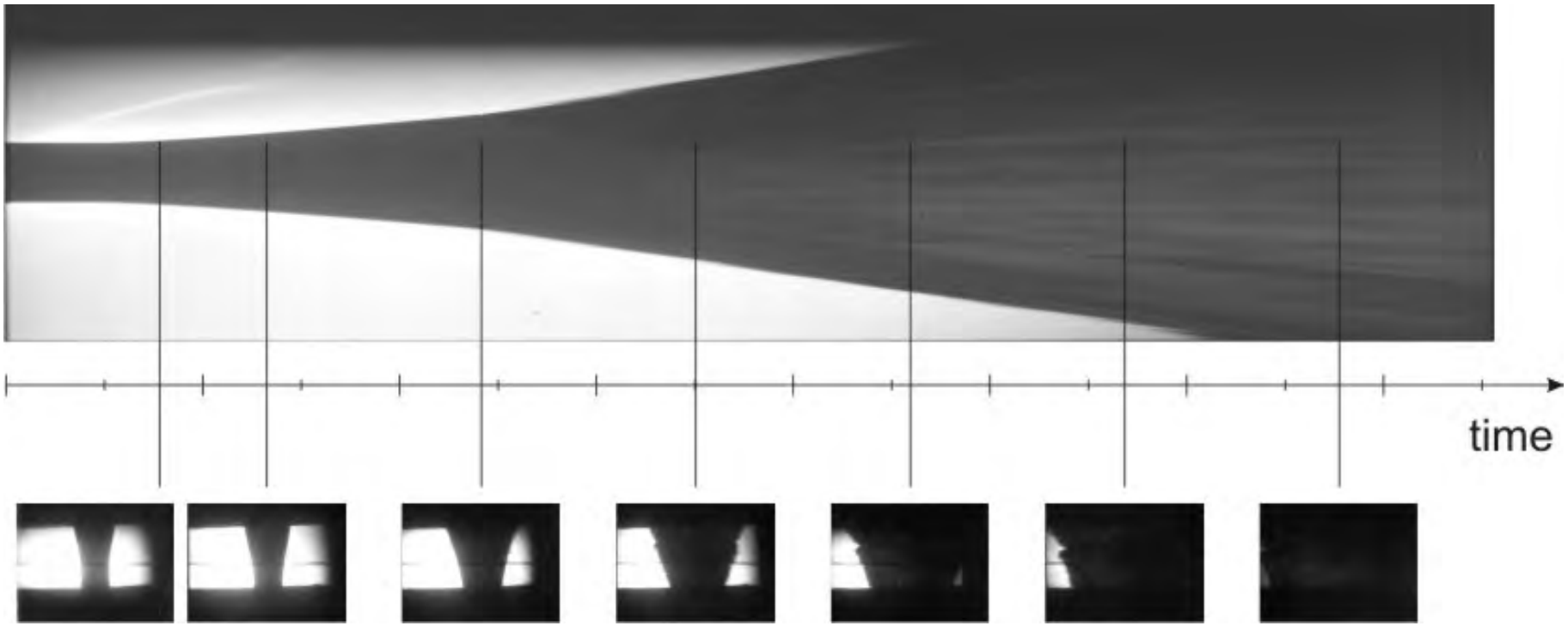

MBDA MISSILE SYSTEMS

Combined Streak / Framing Records

- **Overlayed Reaction**

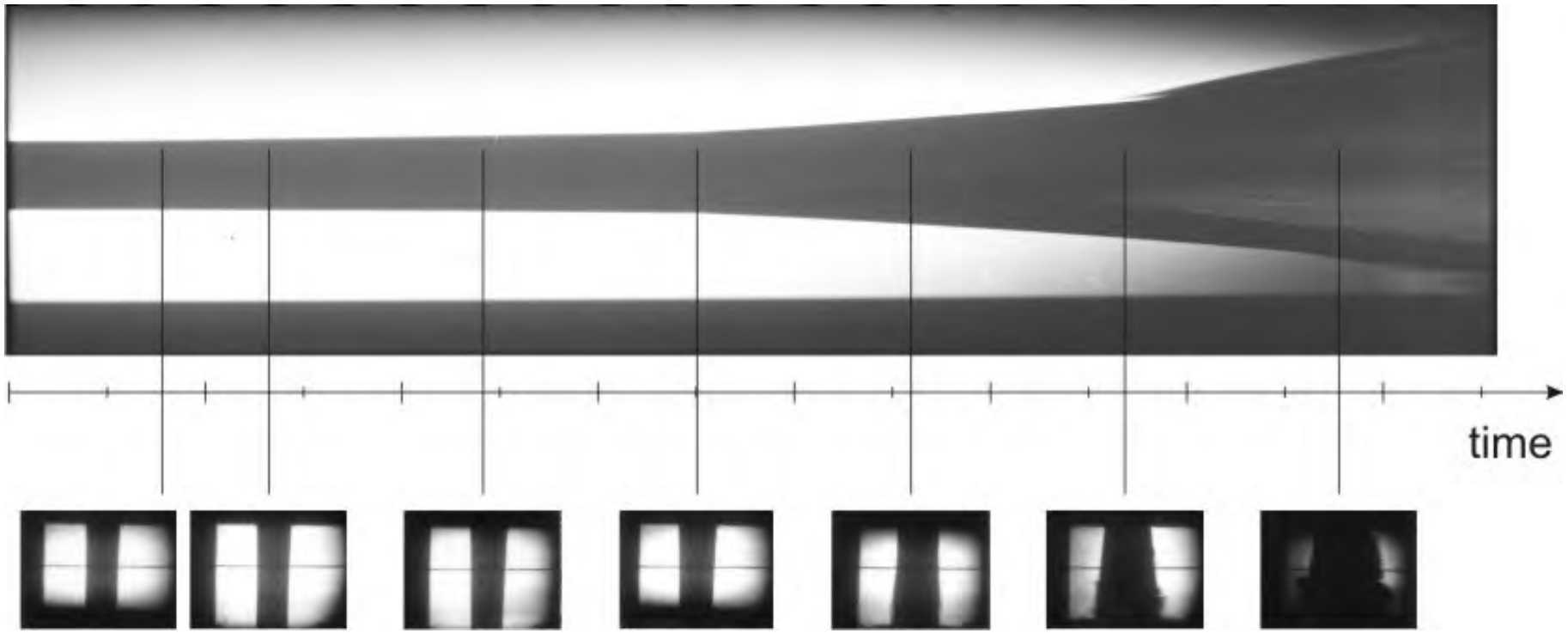

MBDA MISSILE SYSTEMS

Proven Scalability of Fragment Effects of Small-scale Charges

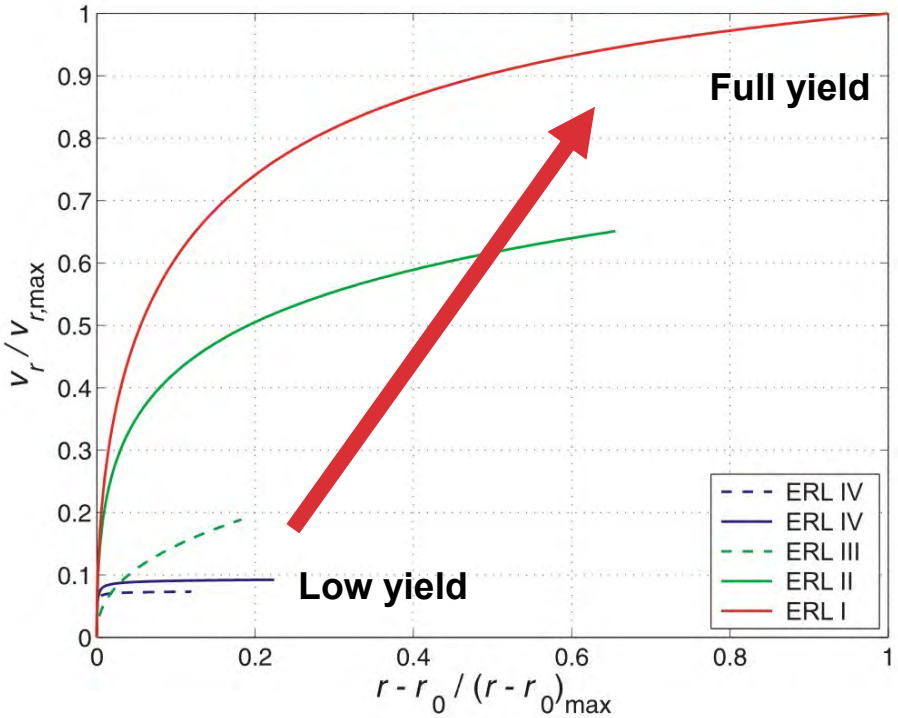

Wall velocities of cylinder expansion

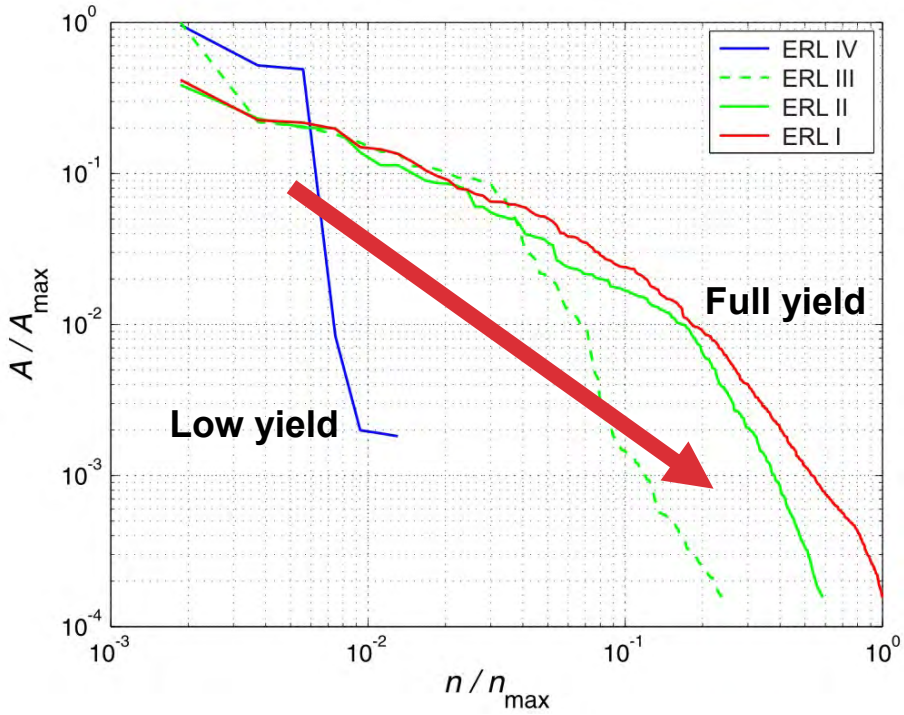

Hole distributions of thin witness panels

Fragment effects are scalable through fragment numbers, sizes, and velocities

MBDA MISSILE SYSTEMS

Thank you very much!

Dr.-Ing. Markus Graswald

TDW Gesellschaft für verteidigungstechnische Wirksysteme mbH
Business Development

+49 8252 99-7264
markus.graswald@mbda-systems.de

MBDA MISSILE SYSTEMS

A NUMERICAL TOOL FOR VALIDATING SOLID PROPELLANTS IGNITION MODELS

C. BOULNOIS[@1], C. STROZZI[2], A. BOUCHAMA[1], P. GILLARD[2]

Presenter *:* **N. ECHES[1]**

[1] NEXTER Munitions,
7 route de Guerry
18000 Bourges France

[2] PRISME Laboratory,
63 av. de Lattre de Tassigny
18000 Bourges France

[@] c.boulnois@nexter-group.fr

Summary

- Introduction
- General presentation of the CFD tool
- Ignition models
  - Temperature threshold ignition criterion
  - Kinetic threshold ignition criterion
  - Low pressure combustion model
- Results
- Conclusion and further work

Summary

Introduction

- Nitrocellulose-based solid propellants
  - Rapid activation of the thermal degradation
  - Homogeneous material, leading to premixed flames
  - Small gap between the solid and the flame zone

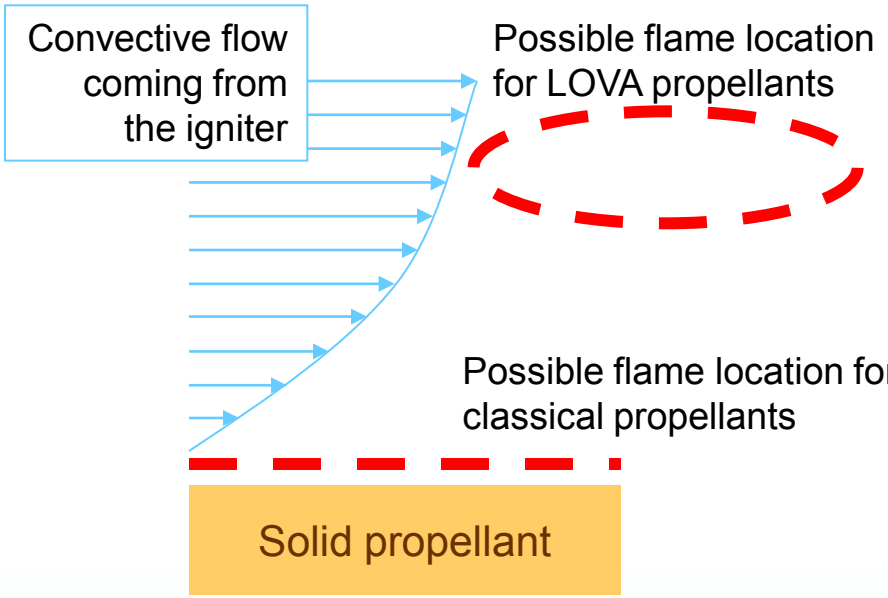

- LOVA solid propellants
  - *Strongly influenced by the chemical composition and pressure of the surrounding gas phase*
  - *Thermal degradation occurs at higher temperatures*
  - *The solid propellant can be heterogeneous, leading to diffusion flames*
  - *The gap between the solid and the flame can be greater*
  - *the reactive species emitted from the propellant can be advected away and react in cooler parts of the chamber*
  - *At high pressures, the reactive system behave like the Vieille's law.*

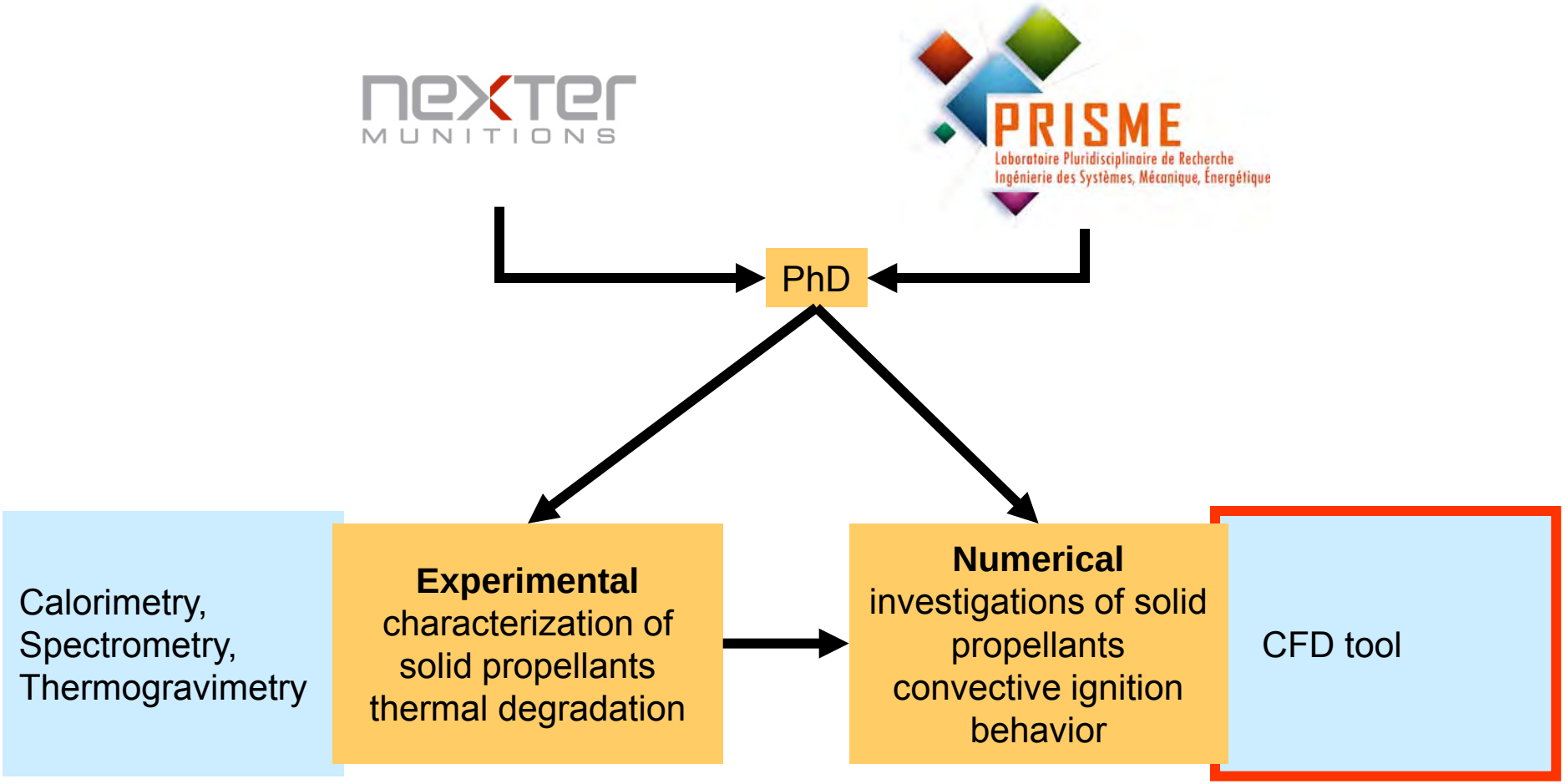
nexter
MUNITIONS
PRISME
Laboratoire Pluridisciplinaire de Recherche
Ingénierie des Systèmes, Mécanique, Énergétique
PhD
Calorimetry,
Spectrometry,
Thermogravimetry
Experimental
characterization of
solid propellants
thermal degradation
Numerical
investigations of solid
propellants
convective ignition
behavior
CFD tool

Summary

General presentation of the CFD tool:

Local submodels
at the grain scale

- Pre-heating of the energetic material
- Decomposition kinetics
- Boundary layer effects
- …

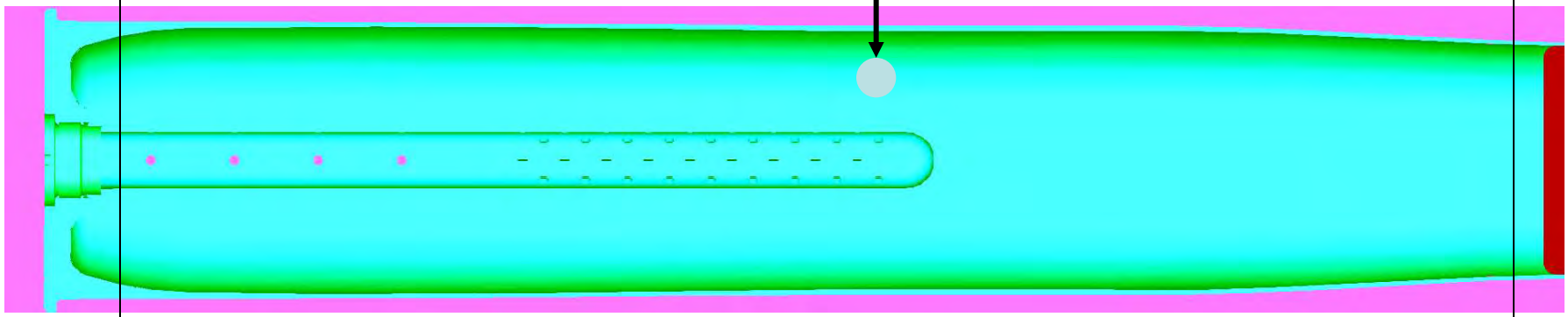

Propellant bed scale

Gaseous mass and heat transport at high velocity.
Mass, heat and momentum transfers with the porous media

General presentation of the CFD tool: the gas phase

- Hypotheses for the fluid flow
  - Eulerian description
  - Chemical equilibrium
  - Constant properties (air)
  - Ideal gas hypothesis

$$\partial_t \vec{\Phi} + \vec{V} \cdot div\left(\vec{\Phi}\right) = \vec{F} \qquad \vec{\Phi} = \left(\rho, \rho\vec{V}, \rho E\right)^T$$

$$\vec{F} = \begin{pmatrix} \dot{\rho} \\ -\overrightarrow{grad}\left(P\right) - \vec{d} \\ -\vec{V} \cdot \left[\overrightarrow{grad}\left(P\right) + \vec{d}\right] + \dot{Q} \end{pmatrix}$$

- Validation of the gas phase behavior: SOD shock tube
  - The propagation of the shock and rarefaction waves agrees with the analytical solution.

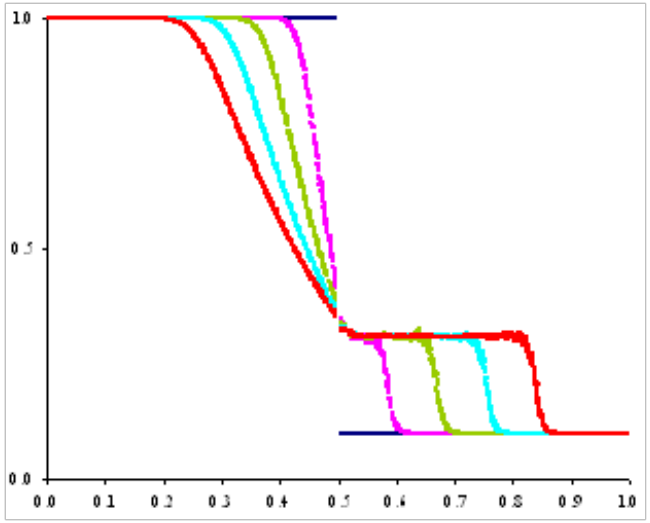

General presentation of the CFD tool: the gas phase

- Validation of the gas phase behavior :
  - Mach 3 wind tunnel with a step : comparison of the pressure fields with a numerical solution at t = 4s

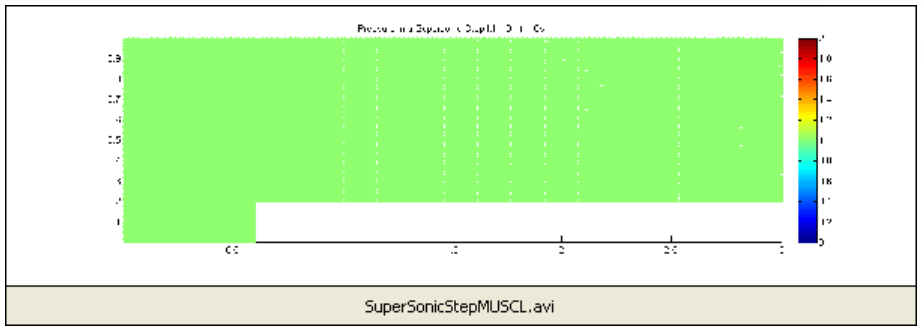

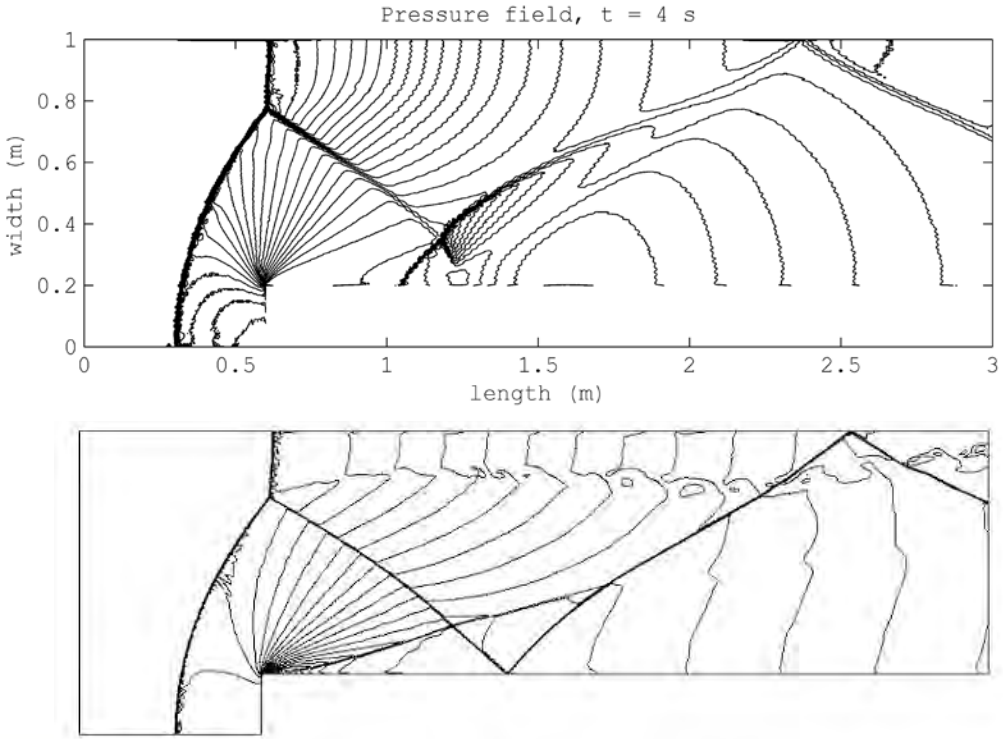

The numerical scheme (AUSM+) based on finite volume method provides relevant results, with moderate numerical diffusion effects.
It is appropriate for describing the flow in the porous medium.

P. Woodward, P. Colella. “The numerical simulation of two-dimensional fluid flow with strong shocks,” in *Journal of Computational Physics*, vol. 54 pp: 115-173, 1984.

General presentation of the CFD tool: the solid phase

$$\rho_s C_s \cdot \left(\partial_t T + r \cdot \partial_x T\right) = \lambda \cdot \partial_x^2 T + Q_s \cdot \Omega_s$$

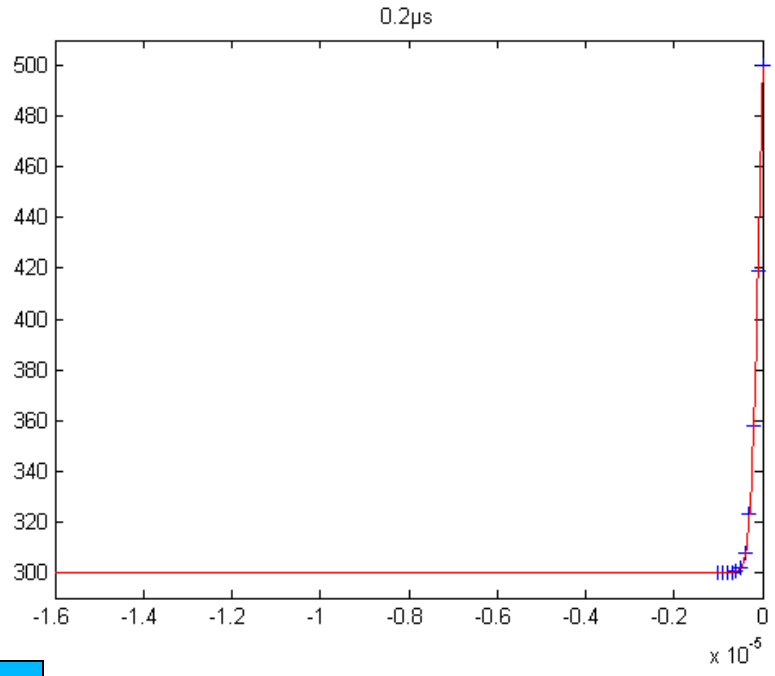

$$\dot{Q} = h \cdot \left(T_{s,x=0} - T_g\right)$$

$$h = \frac{\lambda_g}{D_s}\left(2 + 1.8 \cdot \mathrm{Re}^{1/2} \cdot \mathrm{Pr}^{1/3}\right)$$

- Hypotheses on the solid phase
  - Static
  - Composed of one single chemical specie
  - Thermally conductive
- Description
  - Finite difference method (exponential scheme) on de-refined mesh.
- Validation
  - Kelvin problem (figure)

Summary

- Introduction
- General presentation of the CFD tool
- Ignition models
  - Temperature threshold ignition criterion
  - Kinetic threshold ignition criterion
  - Low pressure combustion model
- Results
- Conclusion and further works

Temperature Ignition Criterion

1. Convective heating of the solid phase
2. At T>400K, the propellant ignites:

   The solid phase is not further described, and the global combustion behavior follows Vieille's law

Typical Internal ballistics ignition criterion

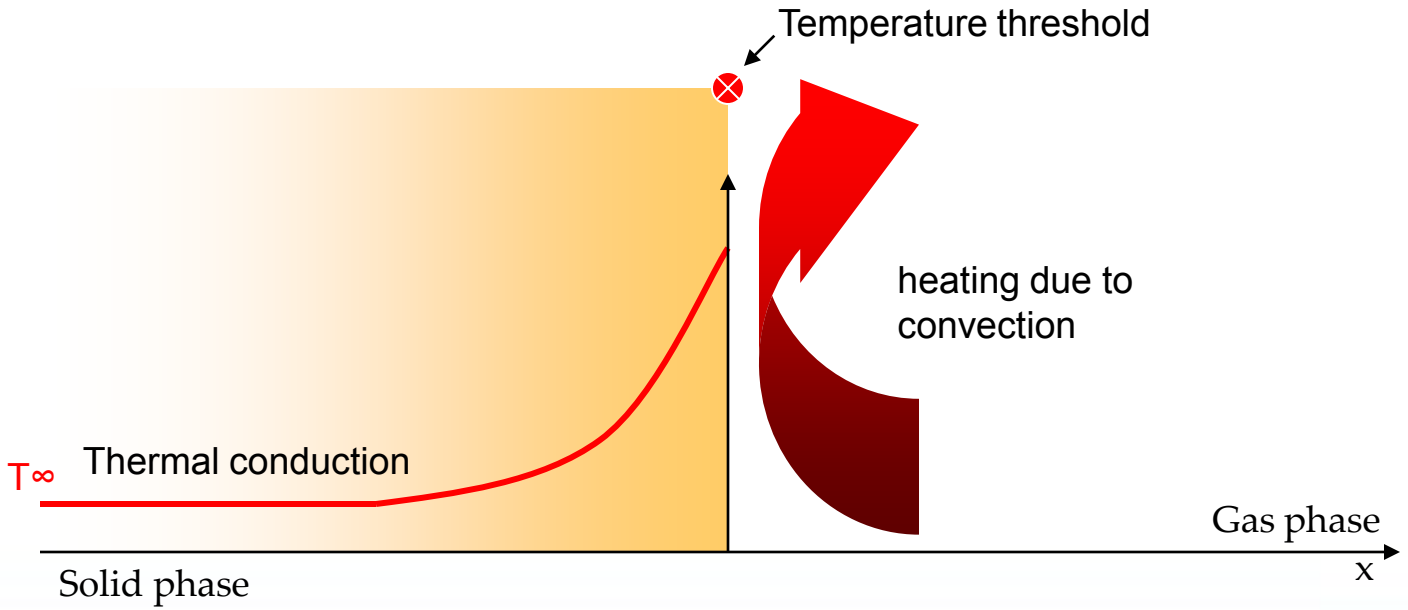

Kinetic ignition criterion G.Lengellé and coll., 1991

1. Convective heating of the solid phase
2. An exothermal reaction is activated in the solid phase (zero order)
3. Ignition occurs once the heat release participates over 15% to the temperature rise:

   The combustion behavior of the solid propellant then follows the Vieille's law.

Evolution of the ignition delay as a function of the incoming heat flux

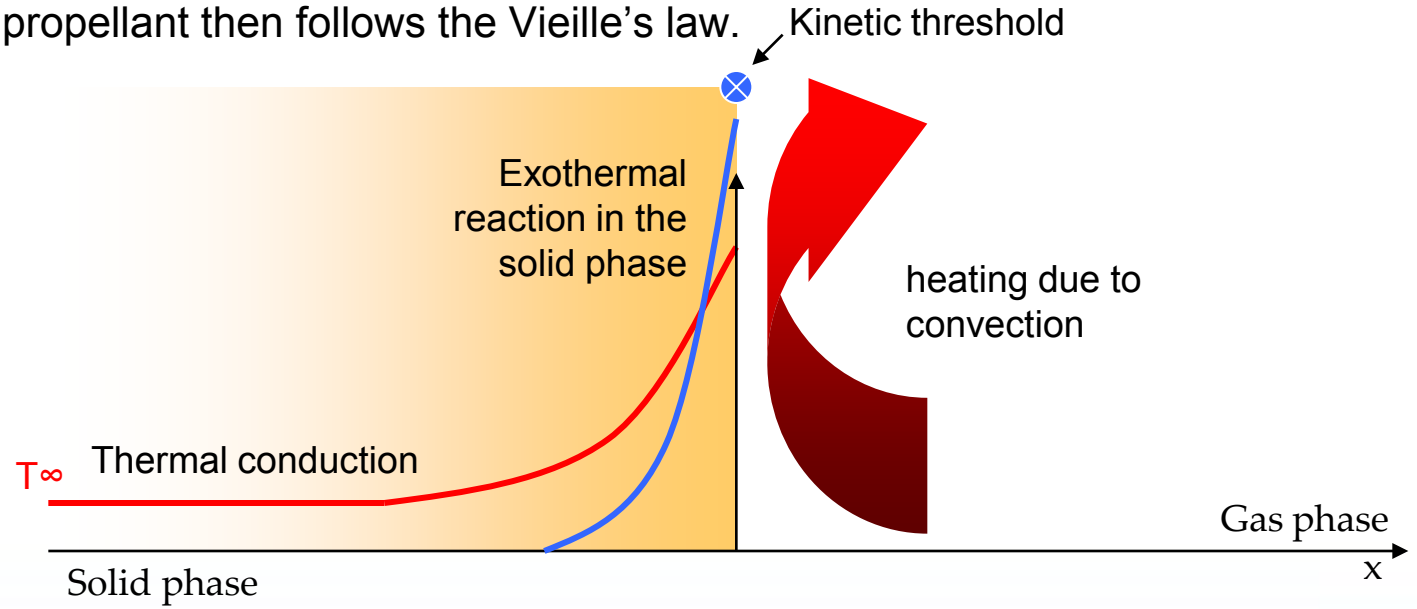

- **Low pressure combustion model** J. Nussbaum, 2007.

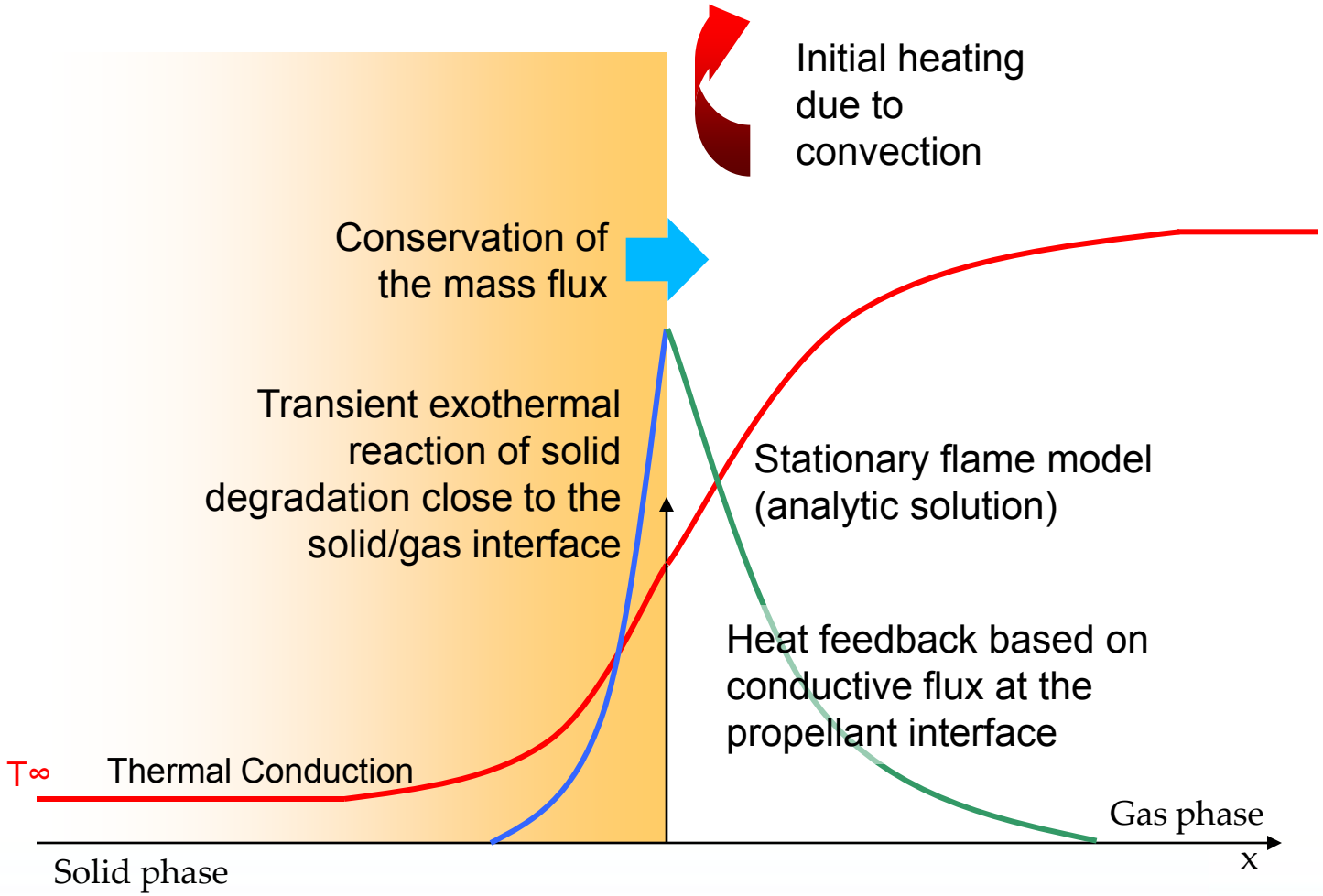

Ignition Models

- **Low pressure combustion model**

1. Constant interaction between solid and gas phase
2. The solid is thermally conductive
3. An exothermal degradation reaction takes place in the solid, while a stationary flame stabilizes in the gas phase.
4. The heat released in the gas phase is transferred to the solid phase by convection. It sustains the thermal degradation.
5. With the increase of temperature, the model converges continuously to Vieille's Law without resorting to an ignition criterion.

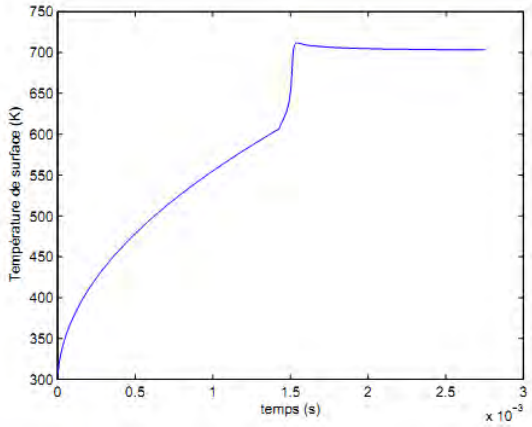

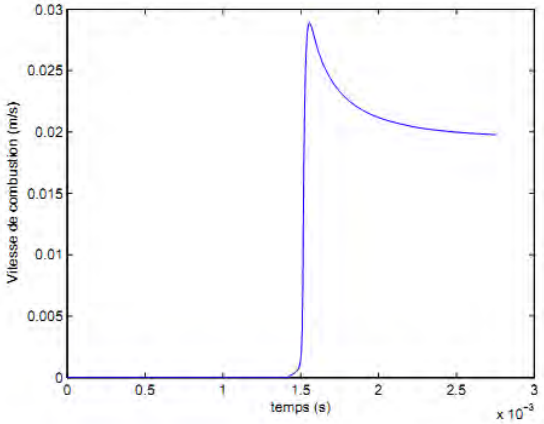

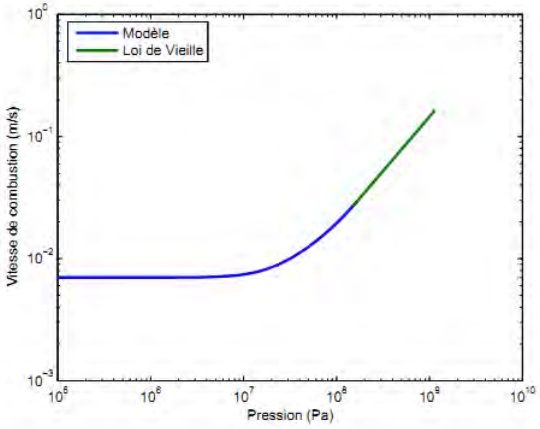

NUSSBAUM, phD thesis, 2007

Summary

- Introduction
- General presentation of the CFD tool
- Ignition models
  - Temperature threshold ignition criterion
  - Kinetic threshold ignition criterion
  - Low pressure combustion model
- Results
- Conclusion and further works

Results

Geometry representative of a 105 mm gun chamber.
Axial symmetry.

The calculation is considered complete when the pressure at the projectile tail reaches 40MPa.

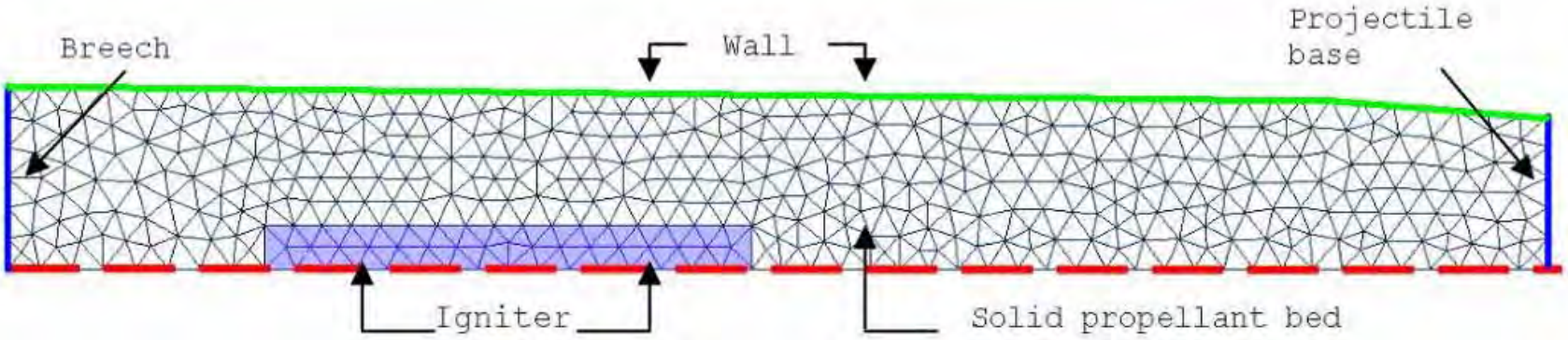

The igniter is modeled as a mass and heat flux released in this part of the computational domain

Results

- Ignition models are compared with an inert shot (non-reacting propellant bed).
- Special care is taken to ensure the energetic consistency between the models.
- Ignition models are compared through the breech and projectile tail pressure evolution.

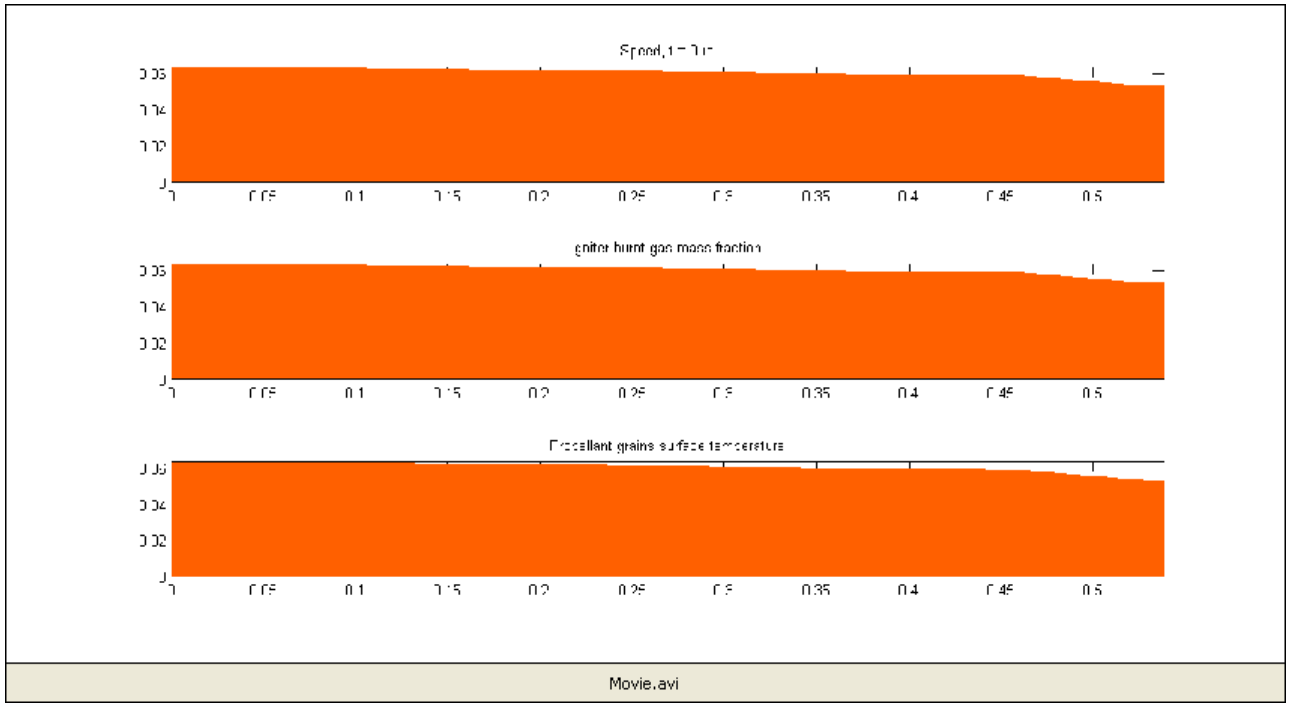

Results

- **Temperature threshold ignition criterion**
  - Temperature threshold set to 400 K
  - The first cell ignites at *t*=150 µs.
  - Ignition starts close to the igniter.
  - The grains ignite ~8 cm after the hot gases wave front.

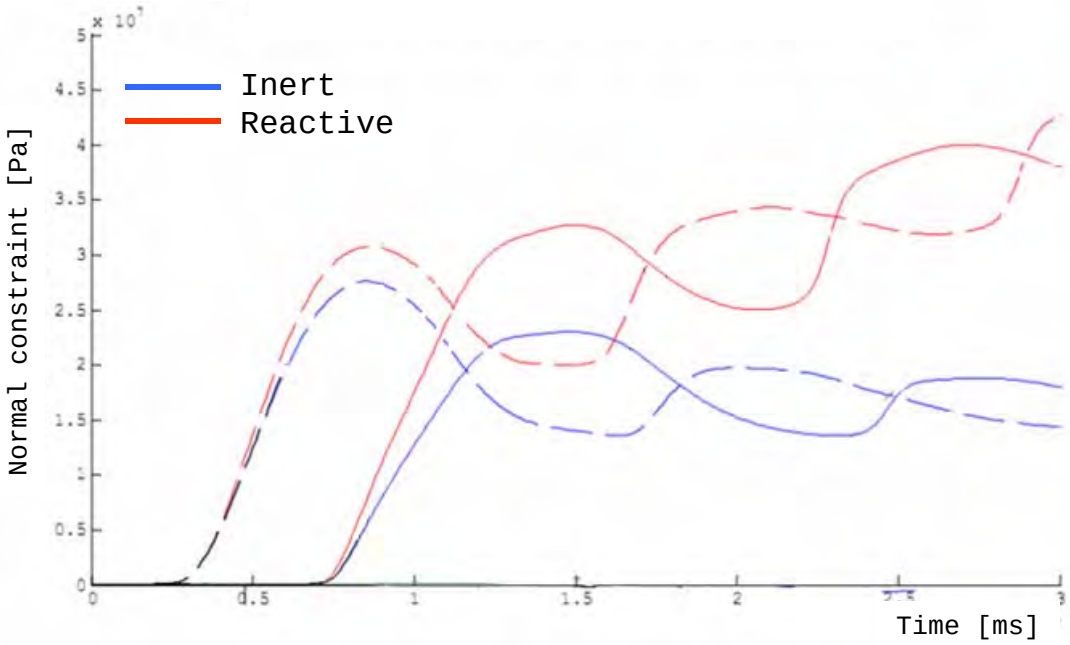

- The ignition wave reaches the projectile base at *t*=680 µs.
- At his instant, the pressure magnitude at the breech is 40 % higher than in the inert case.
- The pressure homogenises in the gun chamber with oscillations as in the inert case.
- The value of 40 MPa at the breech is reached at *t*=2,9 ms.

- **Solid kinetics ignition criterion**
  - Able to predict the ignition delay dependence to the incident heat flux
  - The pressure evolutions at the breech and projectile are similar to the previous ignition criterion (they resort to the same Vieille's Law)
  - The flow structure is not much influenced by the ignition criterion.
  - The intensity of pressure waves is practically the same
  - (It is slightly lower as the ignition delay is increased, resulting in a slower rise of the ignited fraction of propellant).

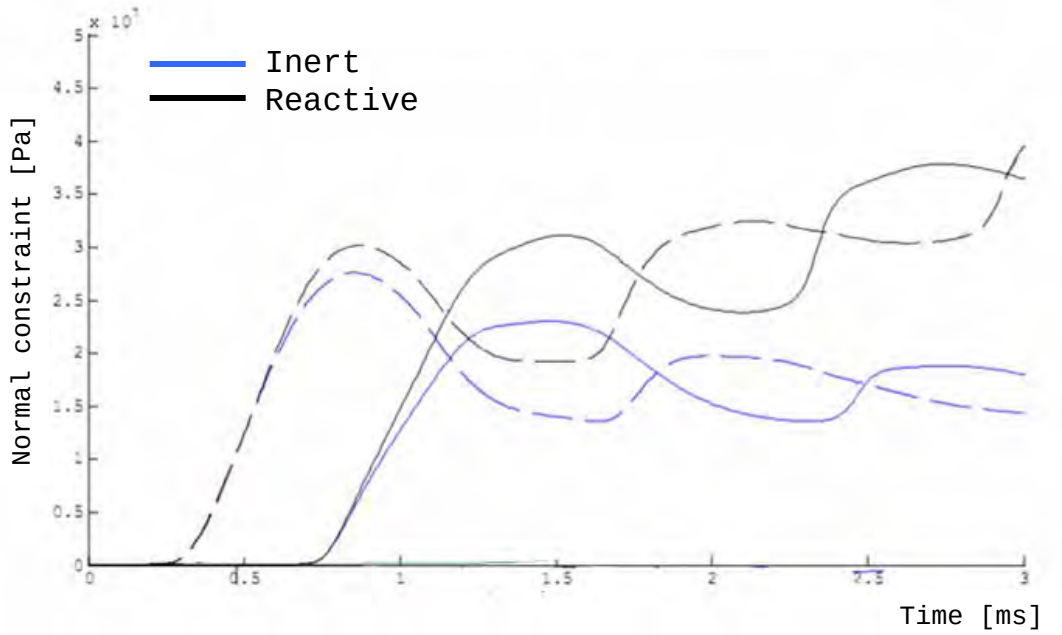

- **Low pressure ignition model**
  - delayed pressure rise
  - smoother pressure evolution than with the other models

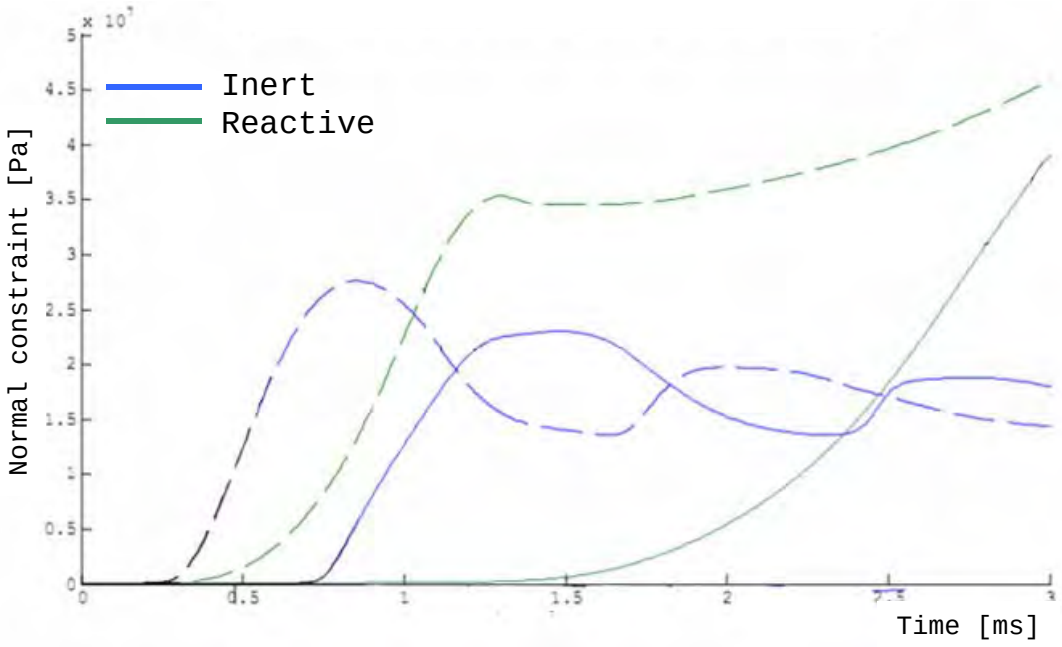

- The burned gases are emitted by the solid propellant at a relatively low velocity
  - This has an effect comparable to a increased drag on the high velocity main flow
  - The pressure evolution at the projectile base is then smoothened by these effect.

Summary

- Introduction
- General presentation of the CFD tool
- Ignition models
  - Temperature threshold ignition criterion
  - Kinetic threshold ignition criterion
  - Low pressure combustion model
- Results
- Conclusion and further works

Conclusion

- A CFD code is developped within the framework of a collaboration between NEXTER Munitions and the PRISME Laboratory.
  - It allows to compare and validate ignition models for LOVA propellants.
    - Three ignition models were tested and compared.

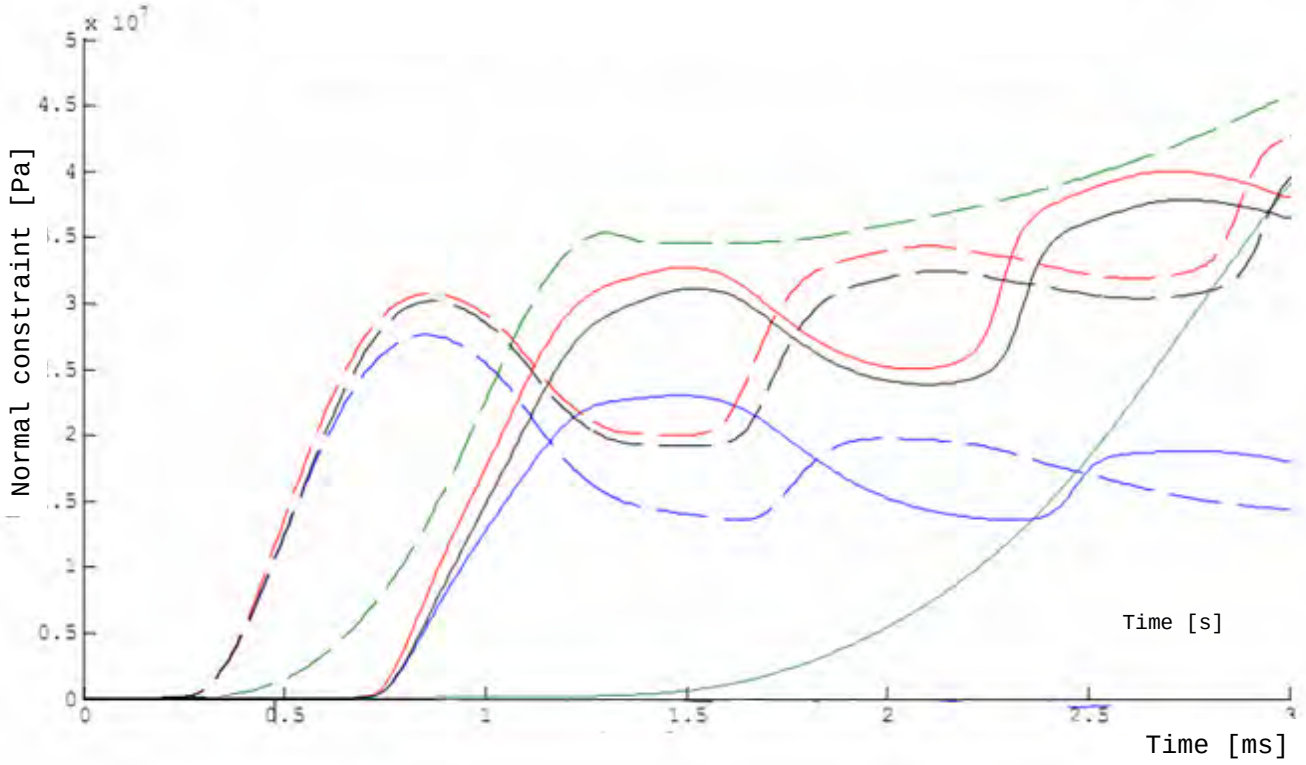

Conclusion

- Similar pressure evolutions obtained for :
  - the temperature ignition criterion
  - the solid kinetics ignition criterion

  Due to :
  - similar ignition temperatures
  - the same Vielle's Law

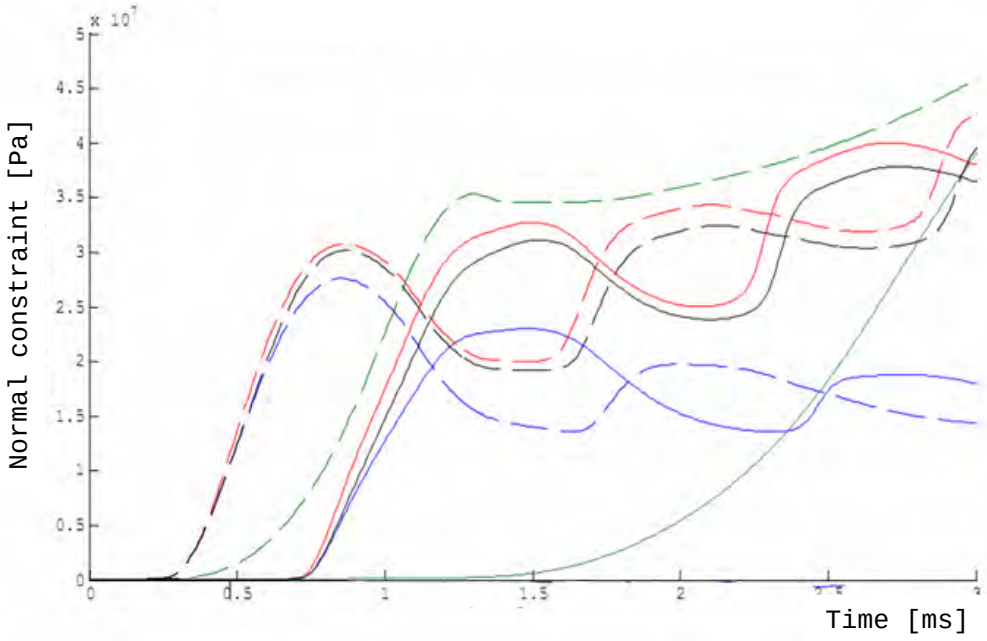

- The third ignition model presents a very different behavior
  - the pressure rise is delayed
  - higher pressures are reached later
  - with a smoother evolution.

  Due to :
  - complex heat and mass transfer interactions between the solid and the gaseous phase.
  - a different description of low pressure combustion of solid propellant
  - This model is therefore better suited to the pressure dependant behavior of LOVA propellants.

Further works

- Further works
  - For the gas phase : future use of CHEMKIN routines for calculating chemical kinetics and equilibriums
  - For the solid phase : Description of a multi-component energetic material and prediction of the emission sequence of the reactive gases.

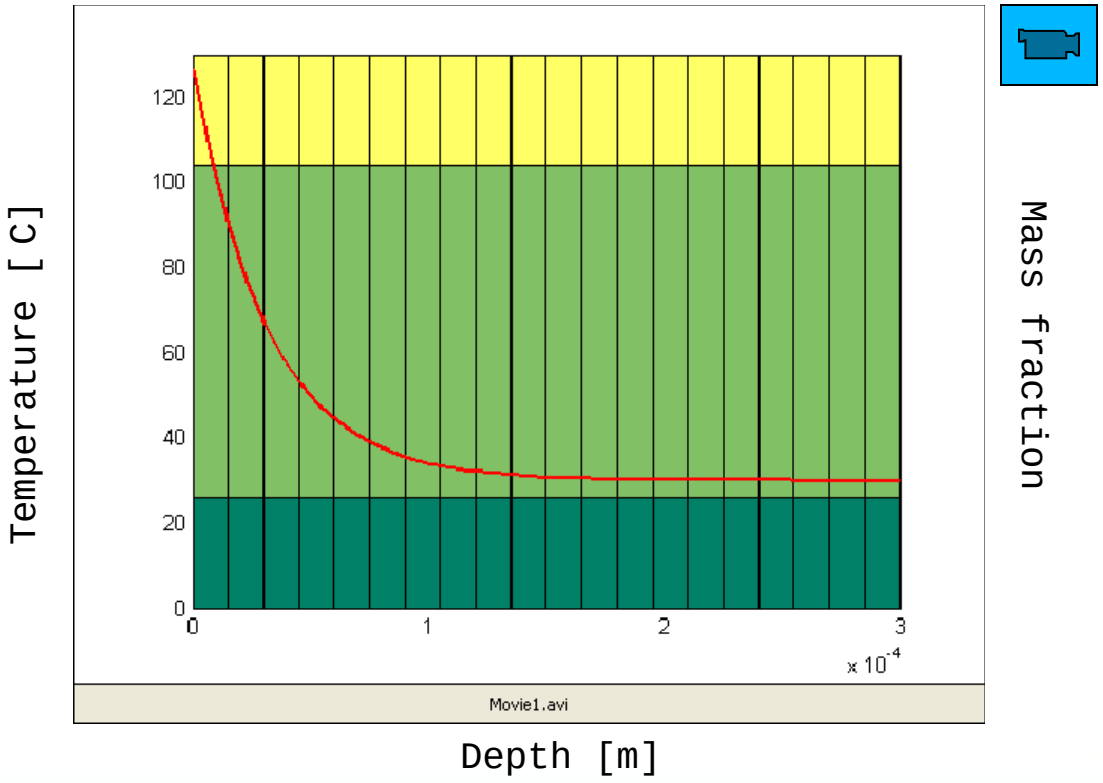

MODELLING OF THE DYNAMICS OF A 40 MM GUN AND AMMUNITION SYSTEM DURING FIRING

N.Eches[1],D.Cosson[1],
Q. Lambert[2,3], A.Langlet[3]

1 Nexter Munitions
2 C.T.A. International
3 Institut PRISME, Université d'Orléans, France

Work sponsored by :

Contents

- Introduction to gun dynamics
- Case Telescoped Ammunition System
- Purpose of the study
- Model description
- Experimental study
- Model calibration
- Conclusions

The problem of accuracy

- For tank ammunition, accuracy is a crucial efficiency factor.

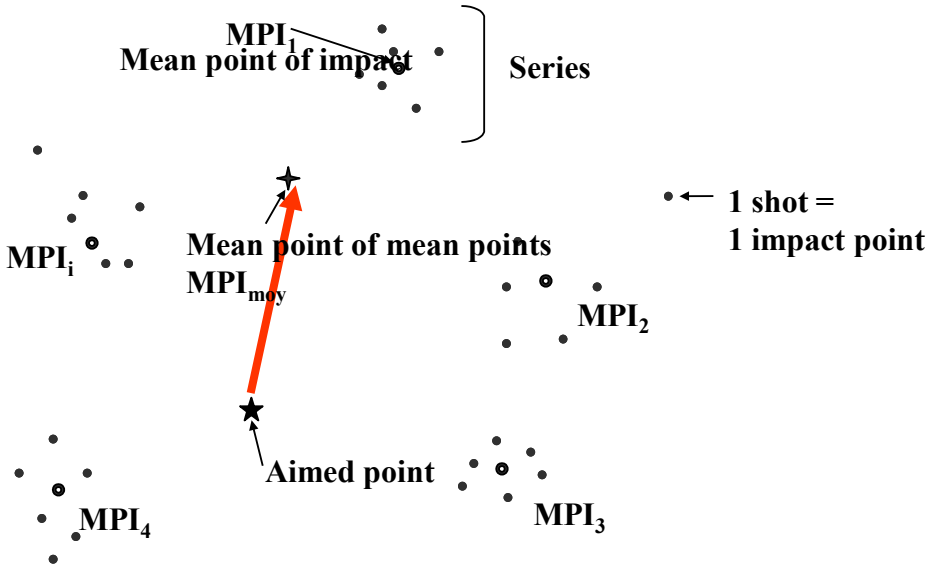

- Accuracy is a function of the perturbations applied on the projectile during :
  - Free-flight : wind, air density, etc
  - In-bore travel : Gun/Ammunition interactions

Gun Dynamics

- Nexter Munitions set up a modelling methodology to study the gun/ammunition interactions in calibre 120 mm (LS-Dyna european conference 2001)
- CTA International, Producer of the 40 mm CTWS weapon system, in cooperation with the Institut PRISME launched a PHD Thesis on the influence of the ammunition design on the consistency.
- As a part of this thesis, work was contracted to Nexter Munitions on a finite element model of the gun/ammunition interaction.
- In parallel, CTA International, in collaboration with Nexter Munitions electronics lab, developped a projectile instrumentation methodology in order to record the ammunition behaviour during its in-bore travel.
- This paper deals with the FE Model set-up, and the comparison of the results obtained with experimental mesurements

What is a Case Telescoped Ammunition

"Traditionnal" Ammunition

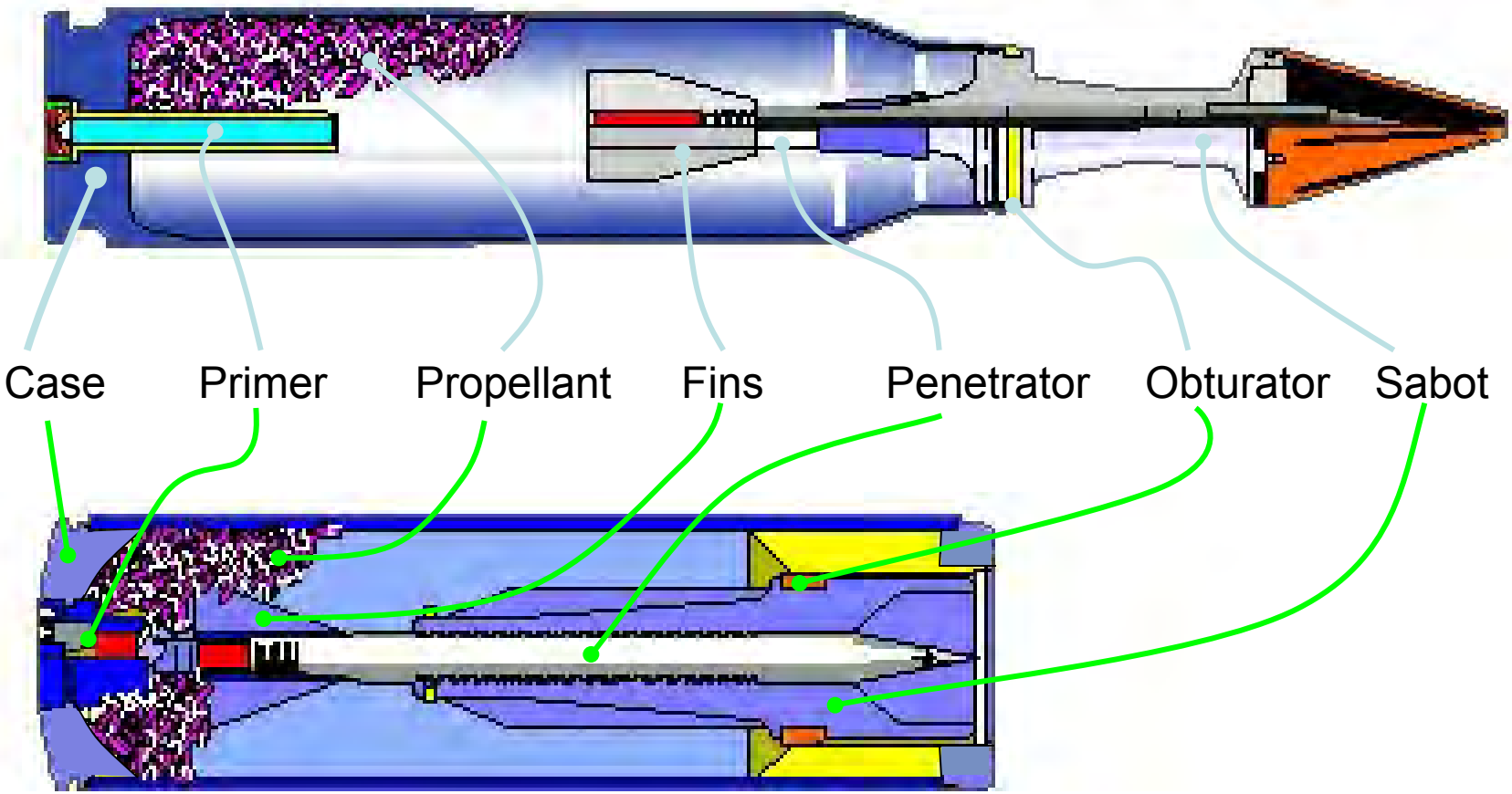

CTA-International Case Telescoped Ammunition

Why a Case Telescoped Ammunition System?

- Larger volume for propellant yields better performances
  - More energy available
- Cylindrical ‘Tin can’ shape makes storage and transportation easier
  - Bulk volume reduction of 30%
- Ammunition feeding & loading in gun chamber is achieved without connectors (links) between two neighbouring rounds, preventing jamming.

40 mm Gun/Ammunition System Model

- Based on the 120 mm model, built in 2001 including a fully functionnal projectile :
  - Realistic interface between rod and sabot
  - Projectile pushed forward by the means of the sabot
  - Sabot discard at muzzle exit
  - Pressure applied on the barrel wall, along with the projectile progression.

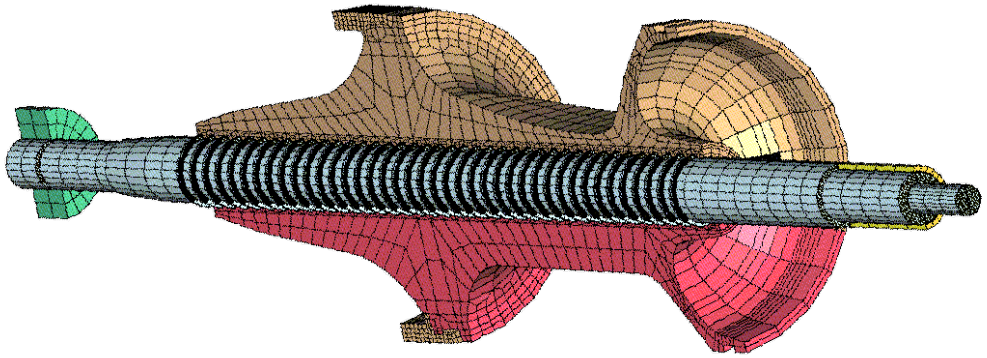

120 mm APFSDS model

40 mm Gun/Ammunition System Model

- Accurate modelling of the experiments configuration
- Faithful geometric description of weapon components including:
  - Rotating chamber
  - Recoil system body and springs
  - Trunnions pins
  - Bearings
- Barrel mapped around actual centreline

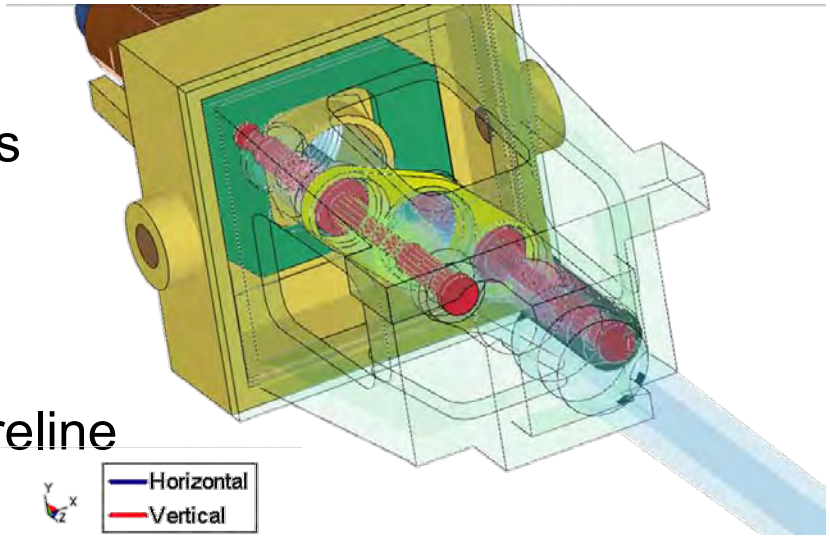

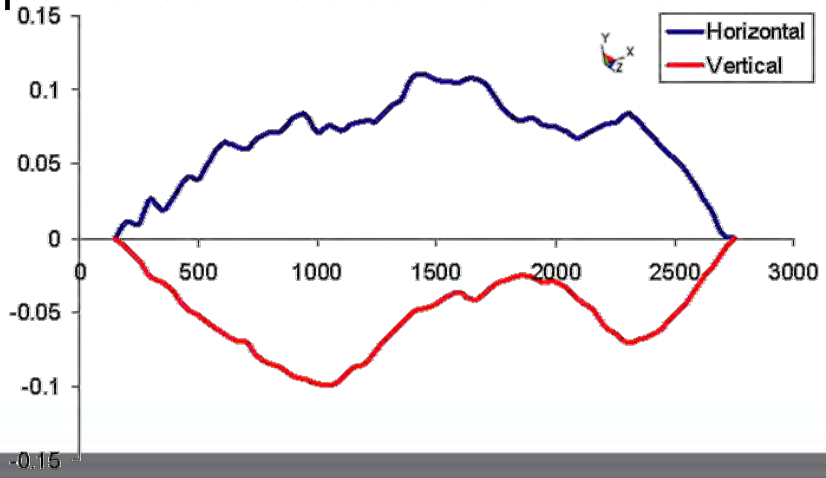

40 mm Gun/Ammunition System Model

- Full 3D model necessary
- Rifling modelled by a mesh twist, according to the rifling law.
- In order to transmit the rifling torque to the projectile, rifling grooves are modelled

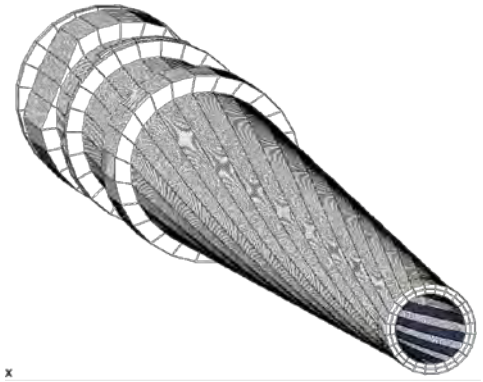

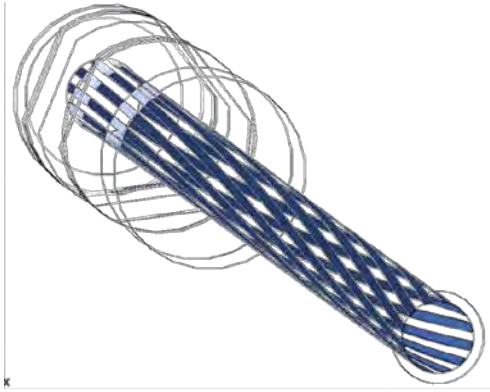

- As the engraving involves too much plastic strain in the obturator, the latter is "pre-rifled" i.e. is meshed with grooves.
- In order to simulate the actual spin rate of the projectile due to the friction of the slipping obturator, the rifling law is modified to give a final projectile spin-rate of around 25% of the full-spin rate, and the obturator is fixed to the sabot

40 mm Gun/Ammunition System Model

High level of details in the projectile model

Sabot petals behave individually

Sabot-Penetrator interface simulated by grooves

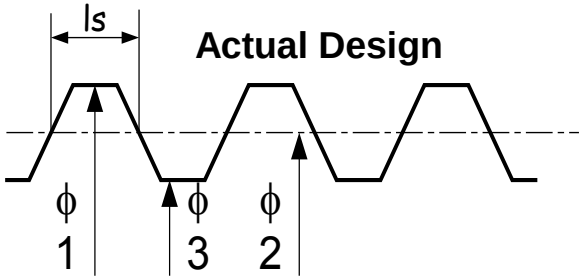

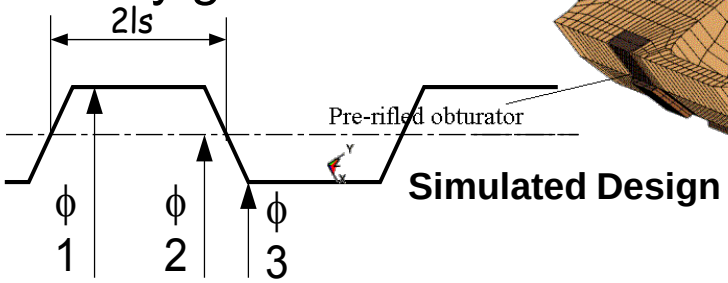

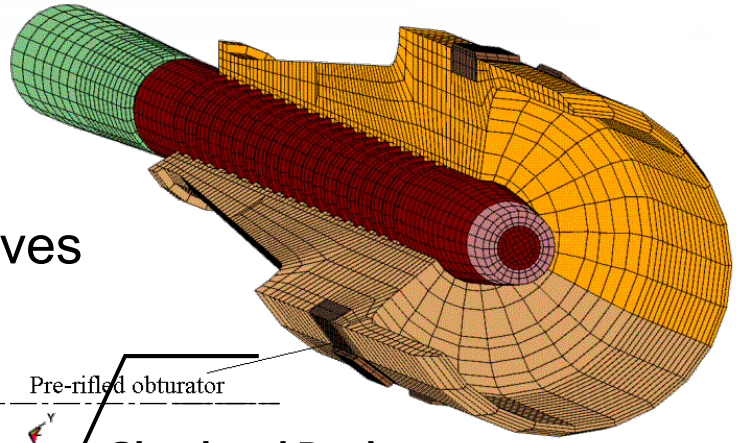

Axial stiffness of the case modelled by an equivalent spring stiffness

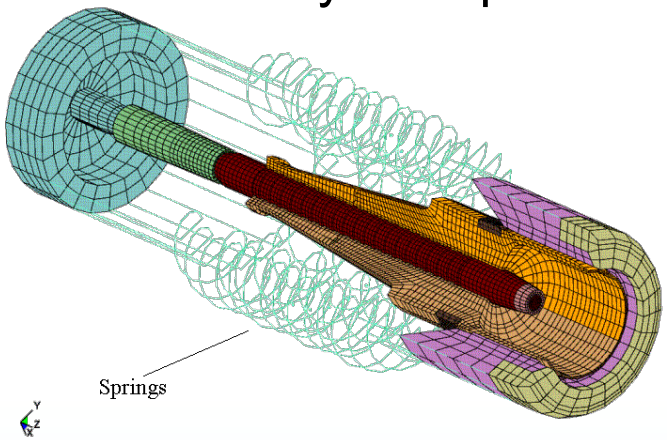

40 mm Gun/Ammunition System Model

- Boundary conditions

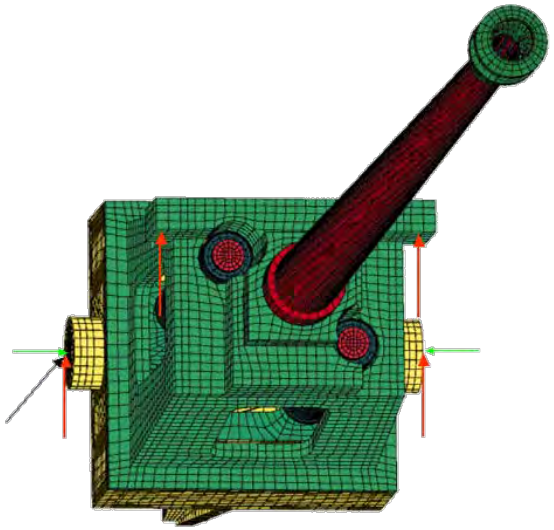

- Loads :
  - Base pressure on the projectile
  - Breech pressure in the chamber
  - One pressure curve per element slice of the barrel, simulating the action of propellant gases on the barrel wall

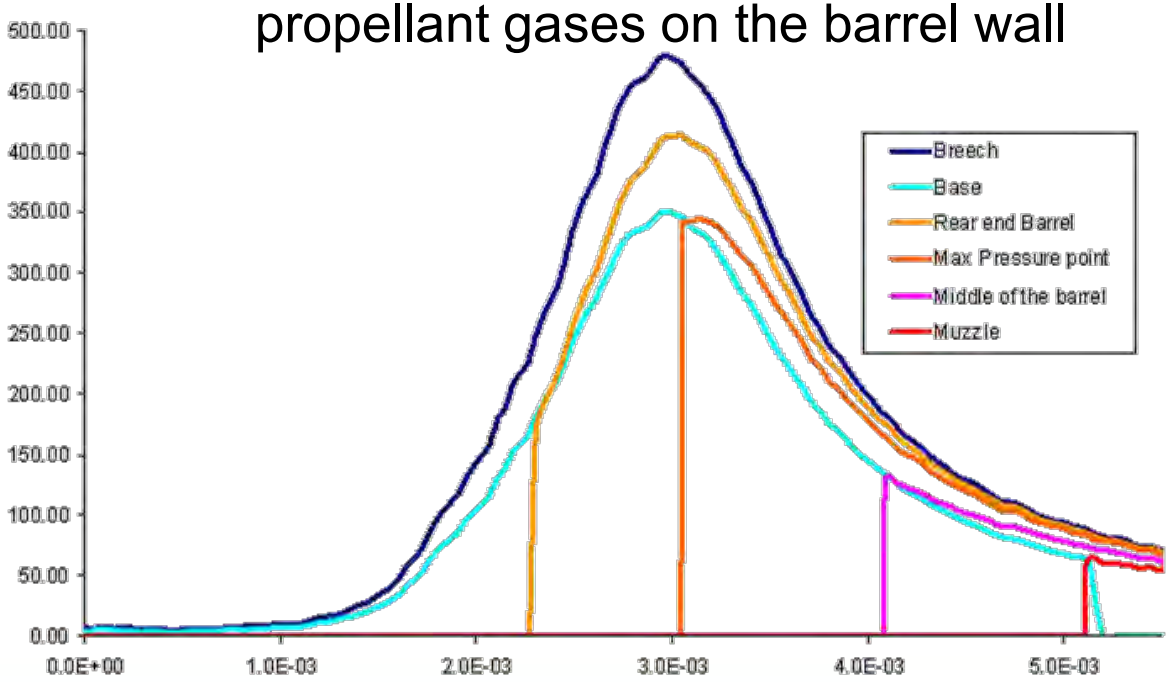

Simulation Sequence

- Modelling with in-house tools plugged to XYZ True-Grid.
  - Pressure curves definition and application
  - Barrel mesh twist and mapping around straightness curve
- Implicit Static Simulation
  - Gravity droop
  - Static contact forces definition
- Explicit dynamic calculation
  - Adjustment of projectile kinematics
  - Synchronisation of barrel loading and projectile axial movement
- Final explicit calculation
- Post-processing, using in-house tools to access all the necessary data from binary history file

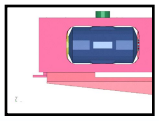
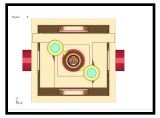
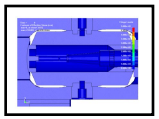

Outputs

- Data delivered by Post-Processing Routine:
  - Muzzle and projectile kinematics
    - Translation
    - Rotations
  - Projectile free-flight initial conditions
  - Projectile deformed geometry
  - Projectile strain on specific points (see experimental study)
  - Barrel expansion on specific locations (see experimental study)

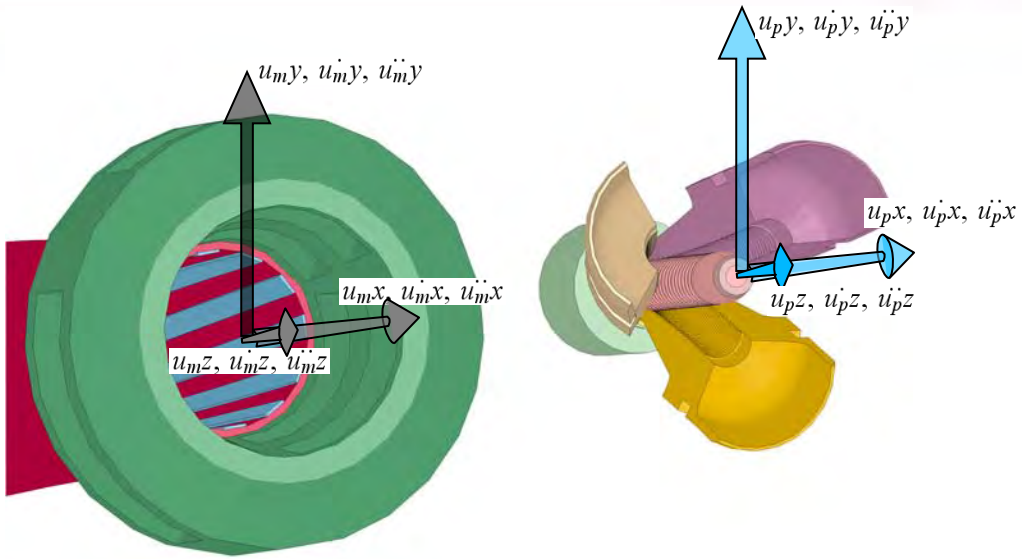

Outputs

- Muzzle kinematics is obtained by averaging inner wall nodes motion
- Barrel expansion is obtained by averaging outer wall diameter variations
- Penetrator free flight initial conditions are obtained by letting the calculation proceed several milli seconds after muzzle exit in order to :
  - Allow sabot separation to occur
  - Establish free motion
  - Then, kinematics quantities are calculated by evaluation of the slope of the different DoF's evolution.

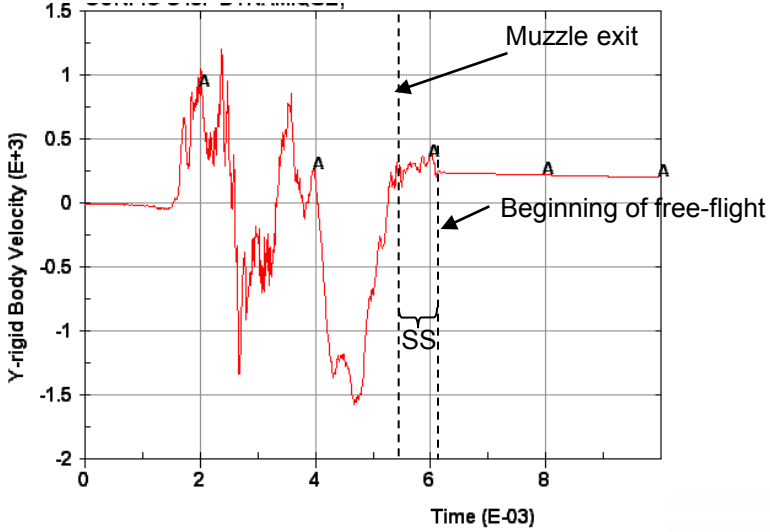

Experimental Study

- Purpose : record bending strains in the projectile rod during the in-bore travel, to obtain data for comparison with the simulation results.
- Methodology : instrumentation of the rod, with pairs of strain gauges

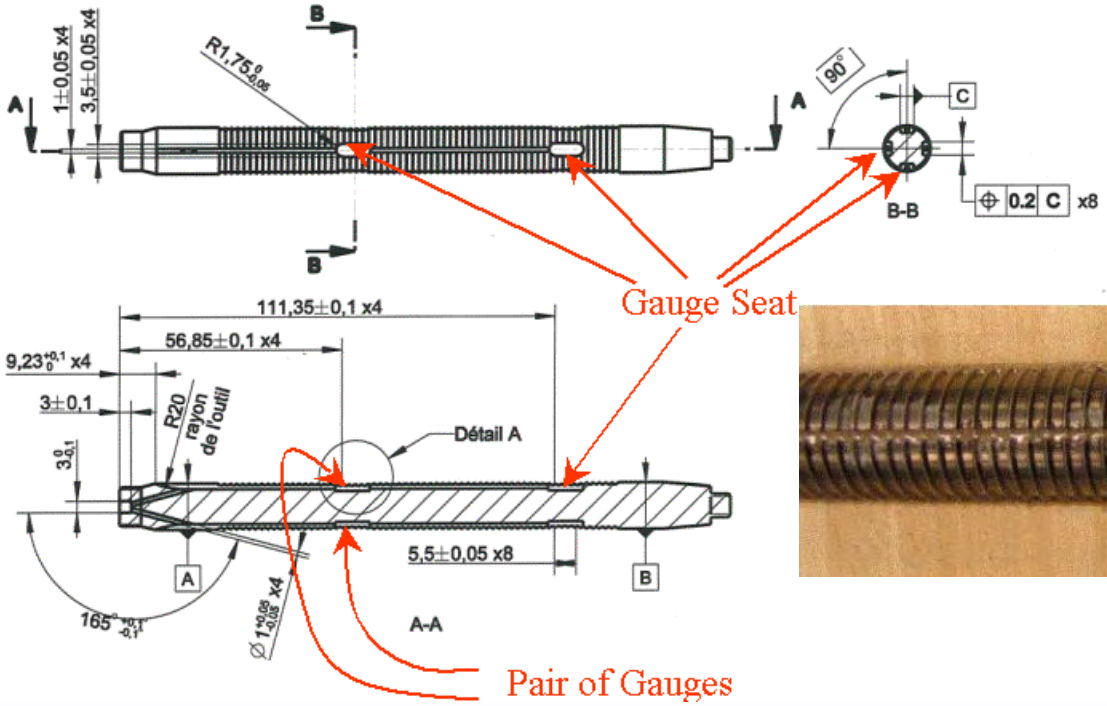

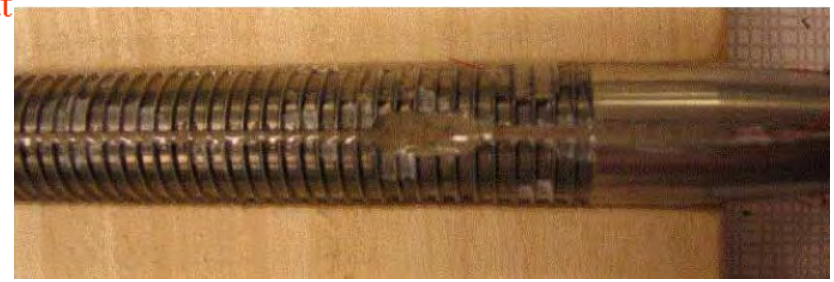

Experimental Study

- Gauges signal recorded with Nexter Munitions data recorder, embedded in projectile flare which replaces the standard fin unit.

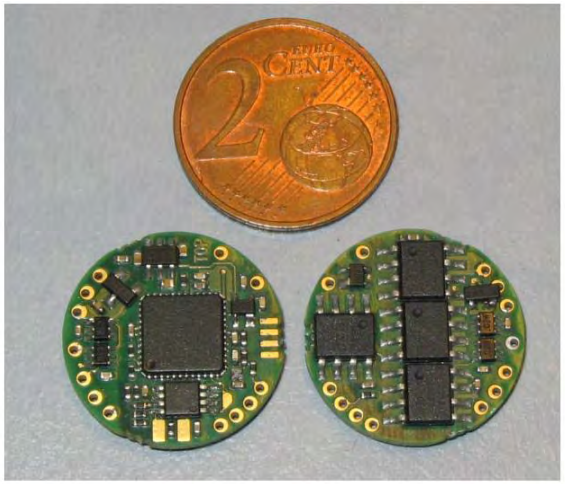

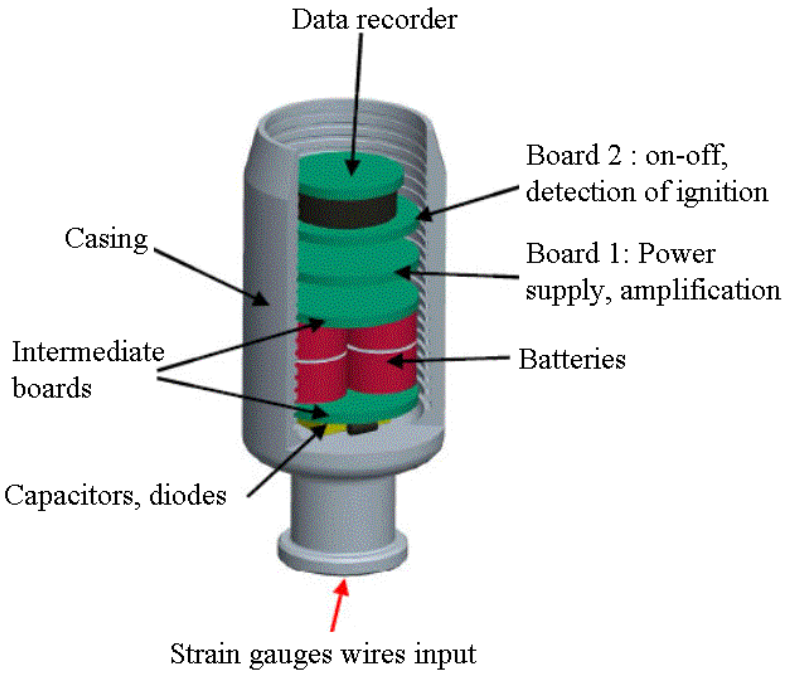

Experimental Study

- Best results obtained with firing #6 : 1320 m/s, 80.000 G'
- Front Gauge pairs, strains=f(t) (m/m,s)

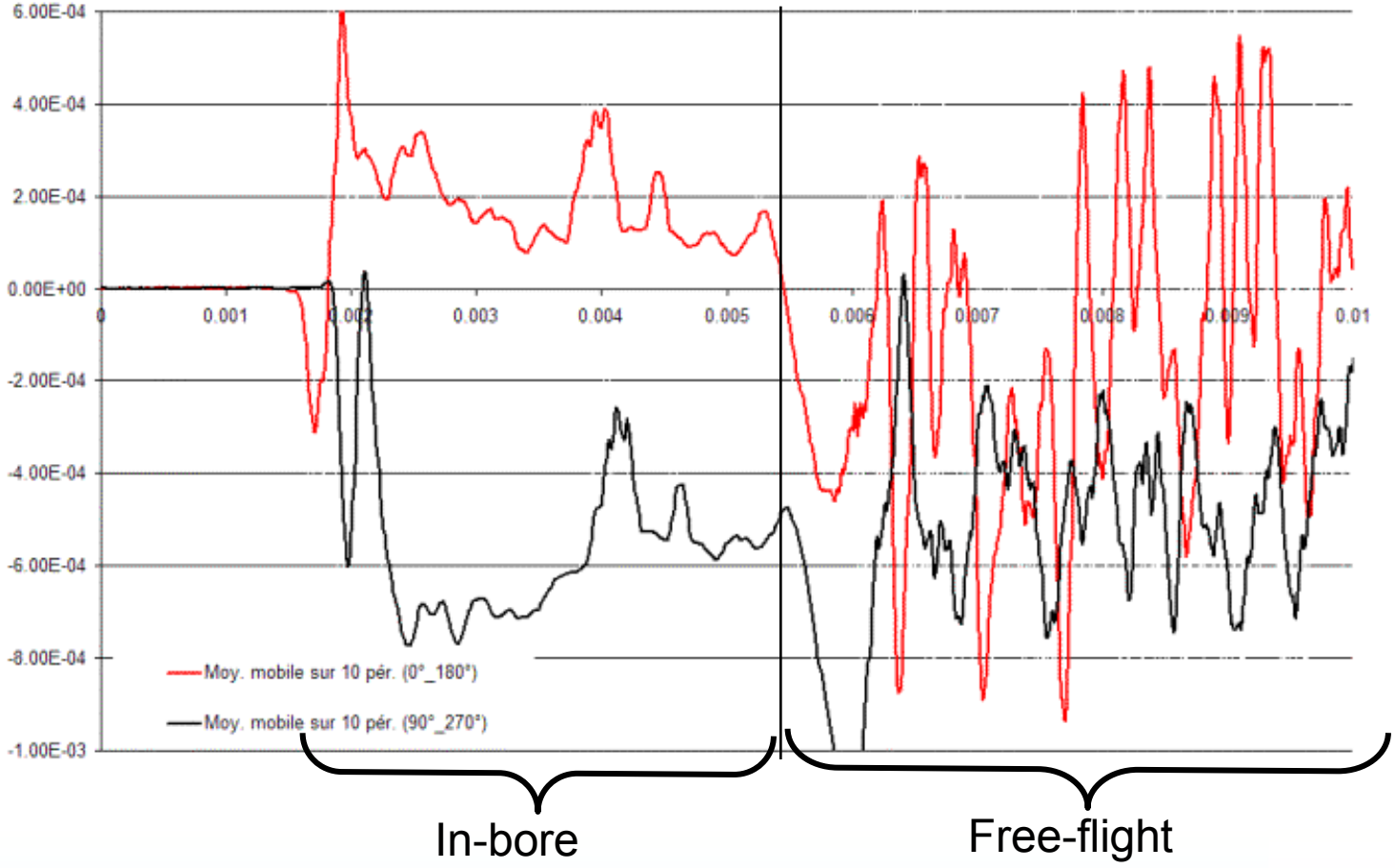

Model Calibration

- Methodology : modelling of firing #6, with same conditions, ie:
  - barrel straightness,
  - Instrumented penetrator
  - flare
  - projectile weight, breech pressure and muzzle velocity

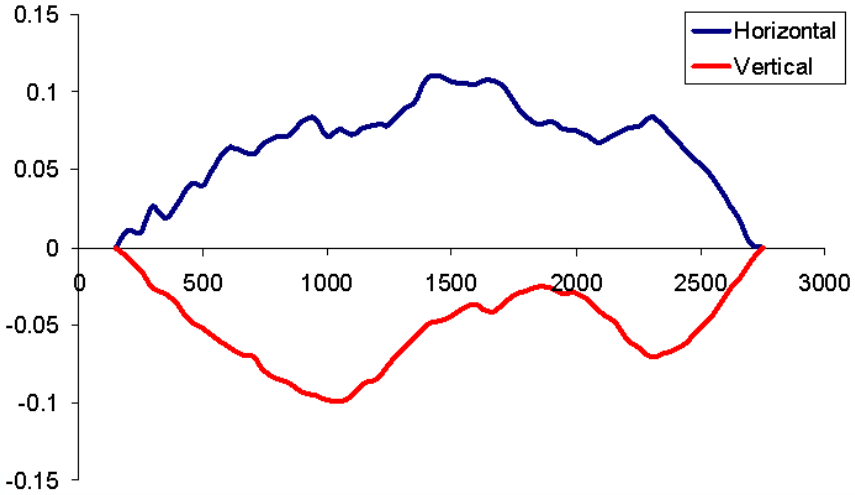

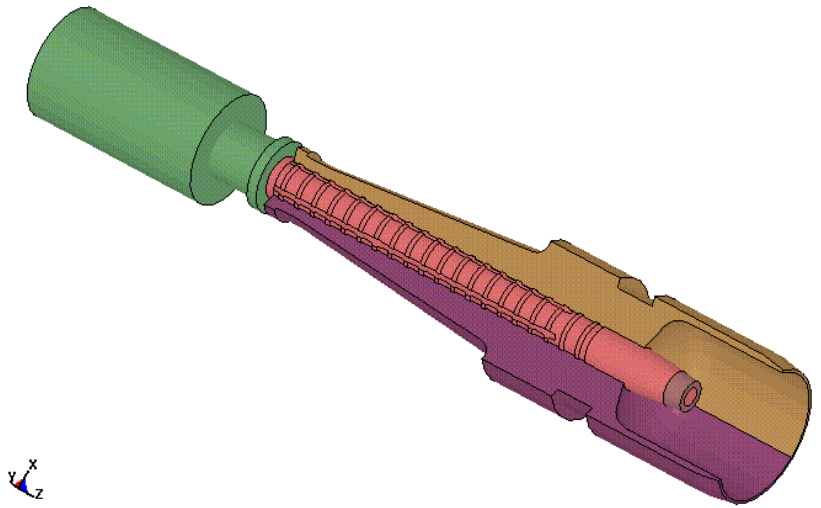

Model Calibration

- Barrel expansion
  - Barrel instrumented with strain gauges pairs on several locations
  - Comparison of experimental and simulation results shows the consistency of moving pressure front modelling

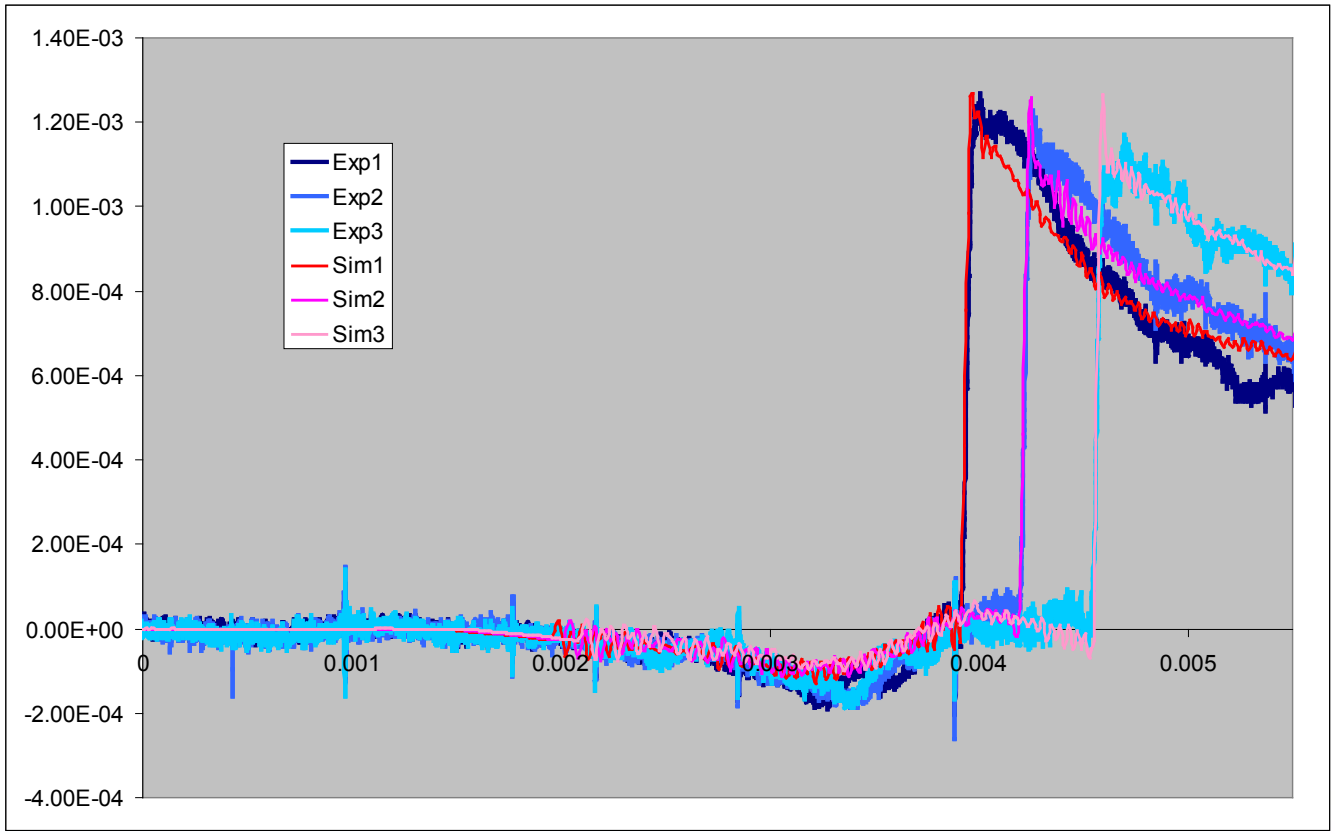

Model Calibration

- Comparison of simulation results with experimental results, with various assumptions contact and friction conditior

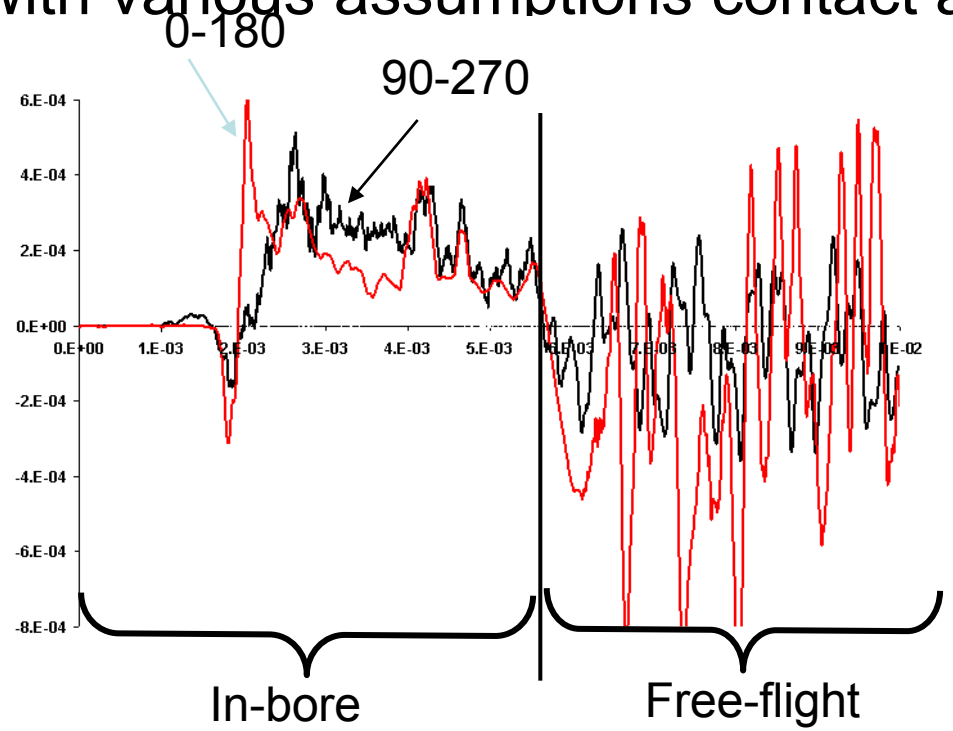

Key :

Config 19

Between sabot petals : surface-to-surface, by parts, no friction

Between penetrator and sabot : surface-to-surface, by segments sets, static friction of 0.1

Experiment

Model Calibration

Key :

Config 30 :

- Between sabot petals : surface-to-surface, by parts, no friction
- Between penetrator and sabot : surface-to-surface, by segments sets, static friction of 0.05

Config 47 :

- Between sabot petals : surface-to-surface, by parts, static friction of 0.1
- Between penetrator and sabot : surface-to-surface, by parts, static friction of 0.05
- Experiments

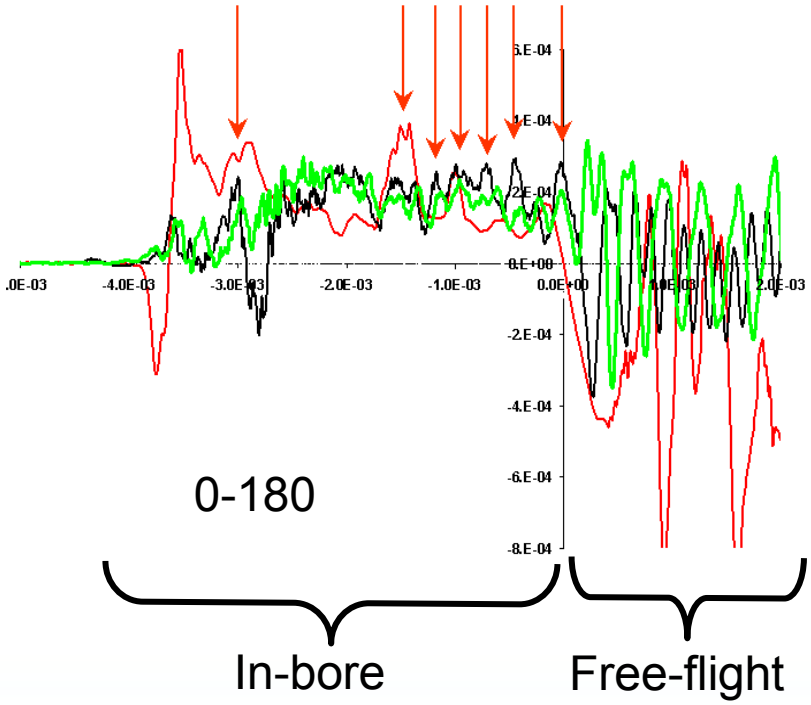

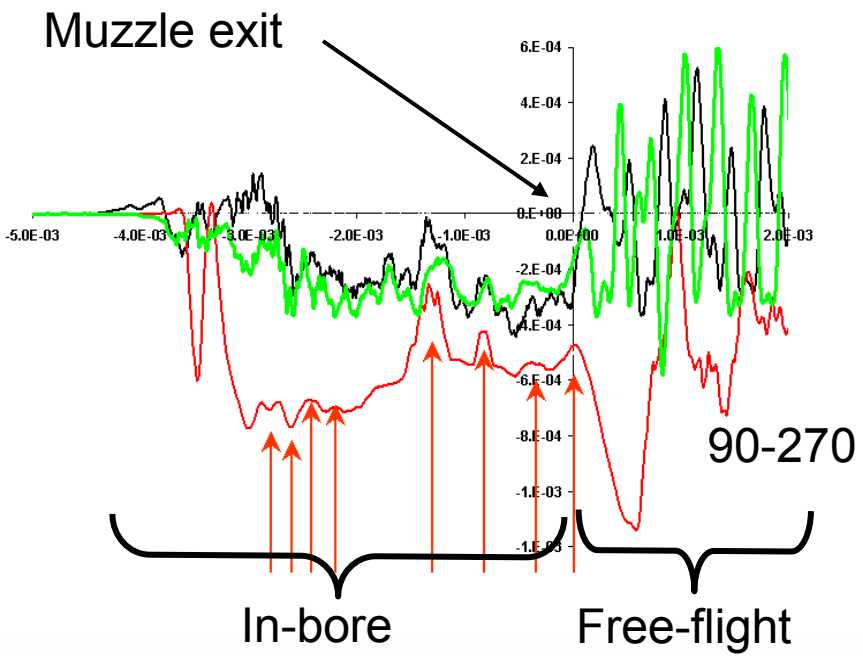

Conclusions

- Parallel progress of numerical and experimental techniques nowadays enables very complex fields of investigation, with very promising results.
- Nevertheless, some work remains to be done in order to
  - Make the experimental techniques more reliable
    - More exploitable firings
    - Reliability of recorded data
  - Improve the match between calculation and firings
    - Investigate the current discrepancies
    - Find out if origin of discrepancies lie in a lack of understanding of the physics, or in a limitation of the numerical techniques

An Investigation of Aerosolization and Associated Phenomena Resulting from the Detonation of Explosives

Luke S. Lebel[1], Patrick Brousseau[2],
Dr. Lorne Erhardt[3], Dr. William Andrews[1]

[1]Department of Chemistry and Chemical Engineering
Royal Military College of Canada

[2]Energetic Material Section
Defence R&D Canada – Valcartier

[3]Radiological Analysis and Defence Group
Defence R&D Canada – Ottawa

26th International Ballistics Symposium

Aerosols

- Common in our environment
  - natural or manmade
- Suspended by atmospheric turbulence
  - can be transported large distances

- Can be used to intentionally disseminate hazardous materials

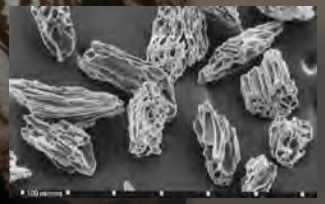

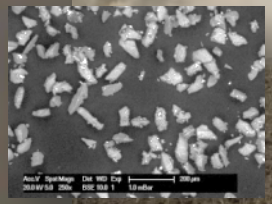

Image Sources: [1] Mila Zinkova, "San Francisco in fog with rays" September 26, 2009 via Wikimedia Commons. [2] Austin Post, USGS, "MSH80 Eruption mount St Helens 05-18-80-dramatic edit" may 18, 1980 via Wikimedia Commons. [3] Dori, "Smokestacks, in Champaign, IL" February 10, 2008 via Wikimedia Commons. [4] Michael Trolove, "September dust" September 25, 2009 via Wikimedia Commons. [5] Federal Highway Administration, "Fly ash" July 14, 2006 via Wikimedia Commons. [6] A.M. Sarna-Wojcicki, "SarnaSem_60-000_large" April 19, 2010 via volcanoes.usgs.org. Creative Commons Attribution. [7] Luke Lebel, "Fine sand SEM" September 24, 2010.

Outline

1. Background
2. Closed Vessel Experiments
3. Experimental Results
4. Conclusions

Outline

Explosive Aerosolization

Time = 0

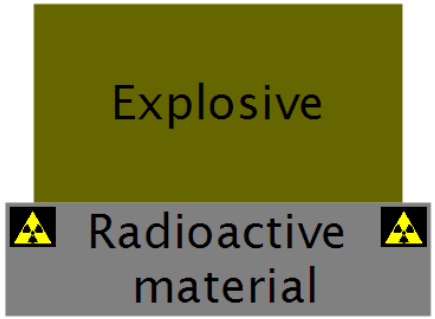

Explosive Aerosolization

Time = ~10 µs

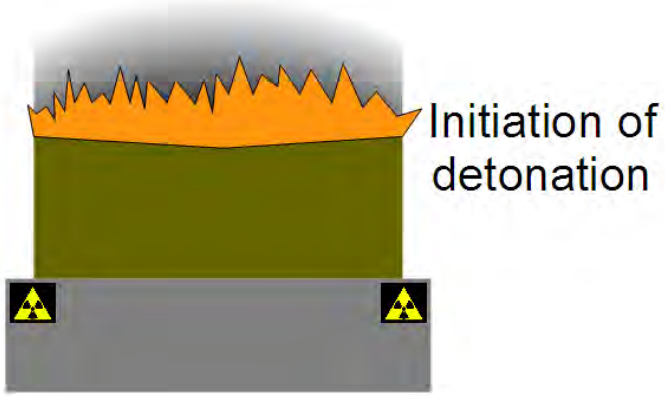

Explosive Aerosolization

Time = ~10 µs

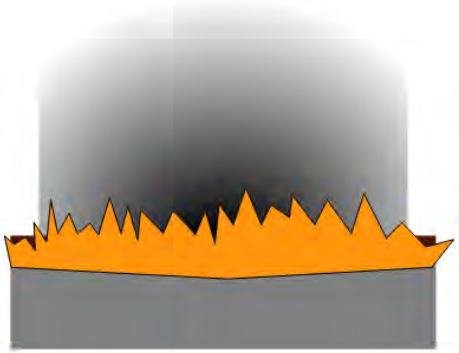

Detonation wave propagates to target material

Explosive Aerosolization

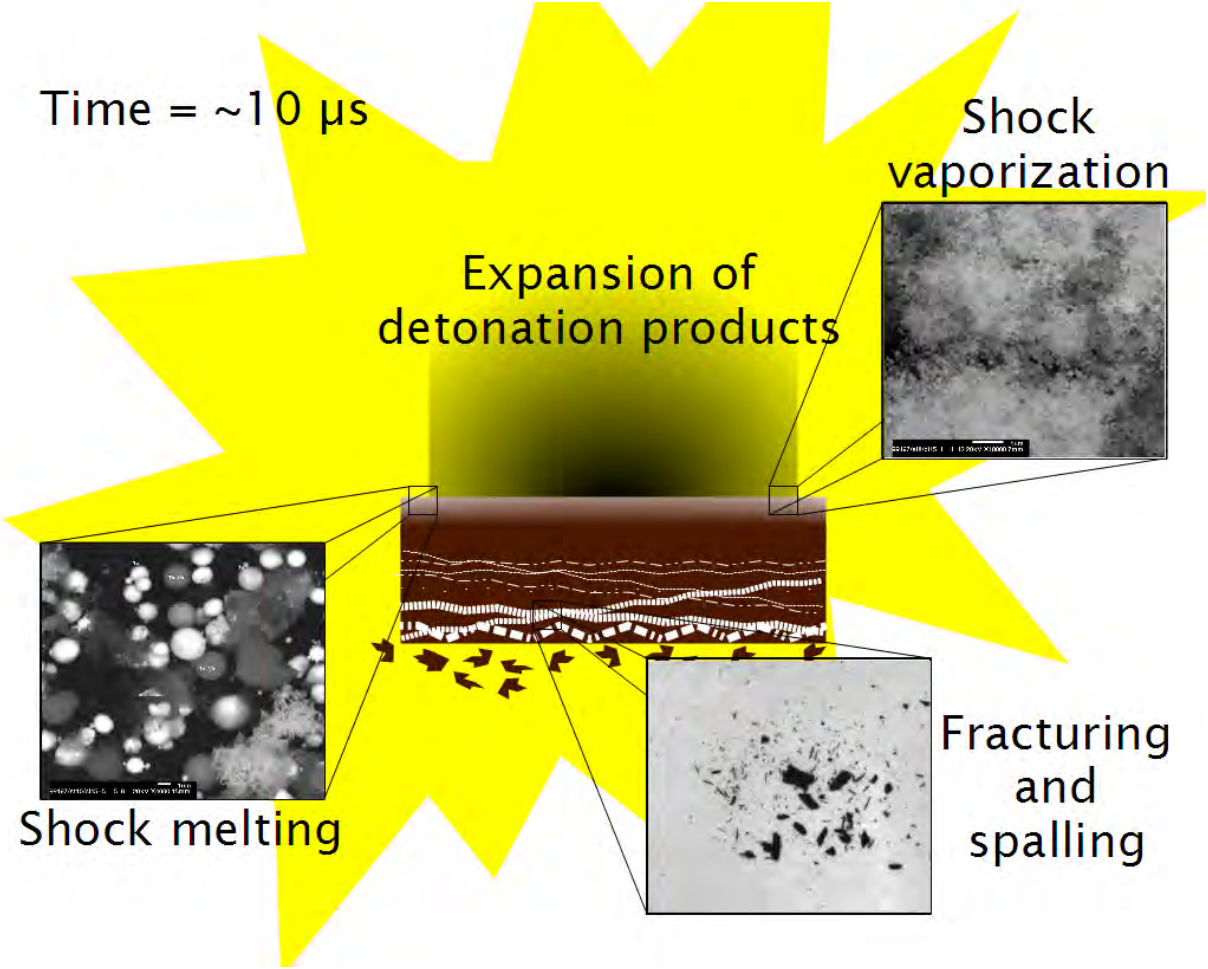

Fireball Mechanics

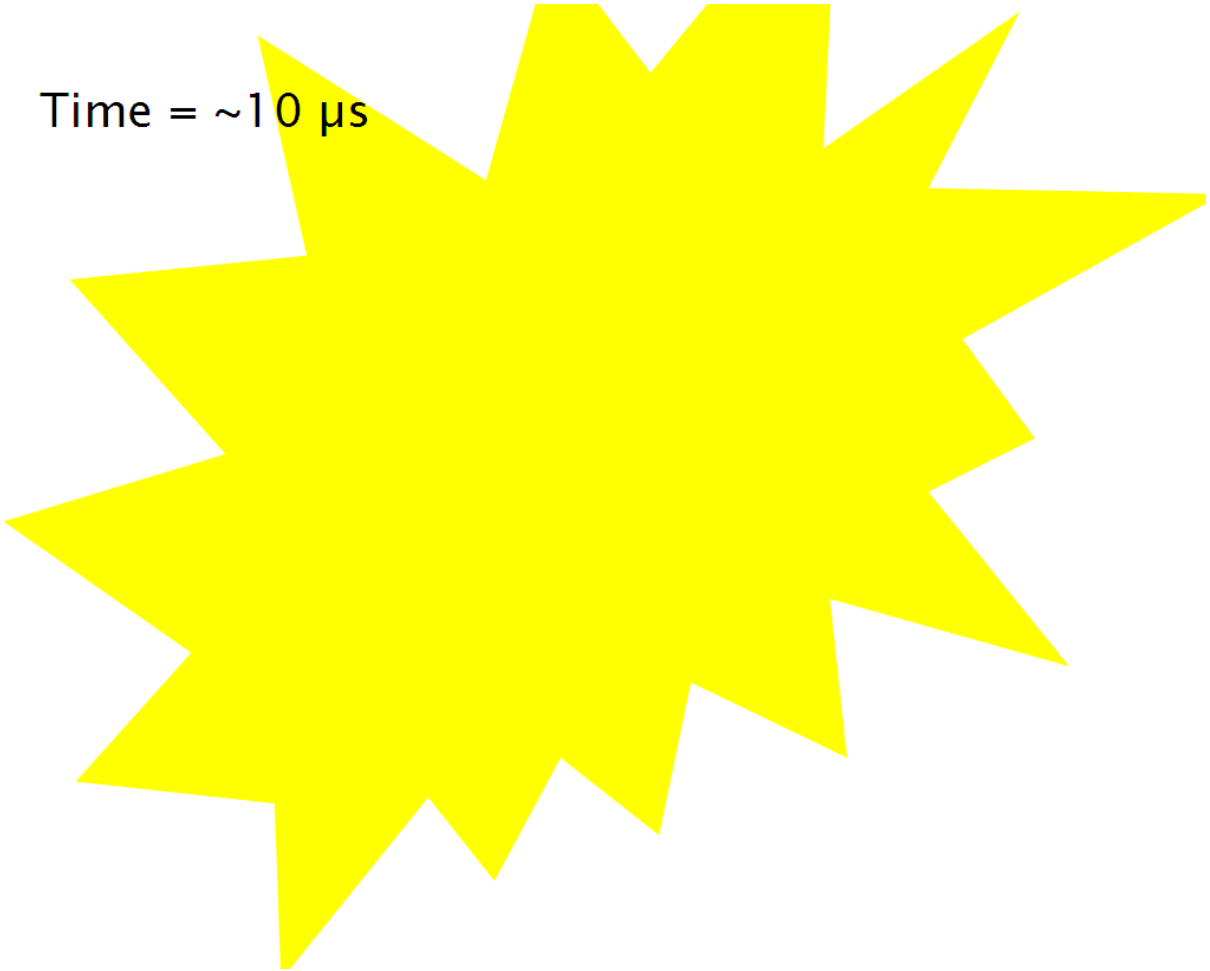

Fireball Mechanics

Time = ~10 ms

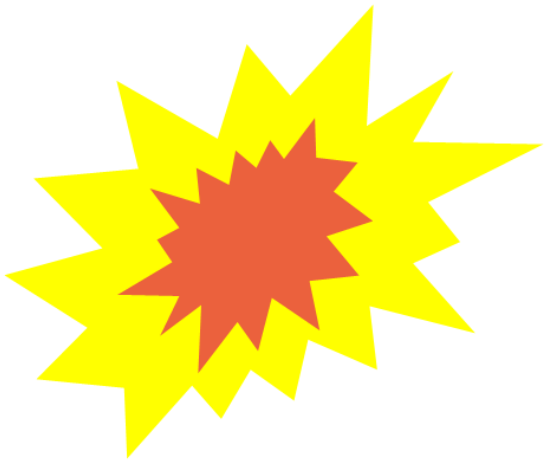

Fireball Mechanics

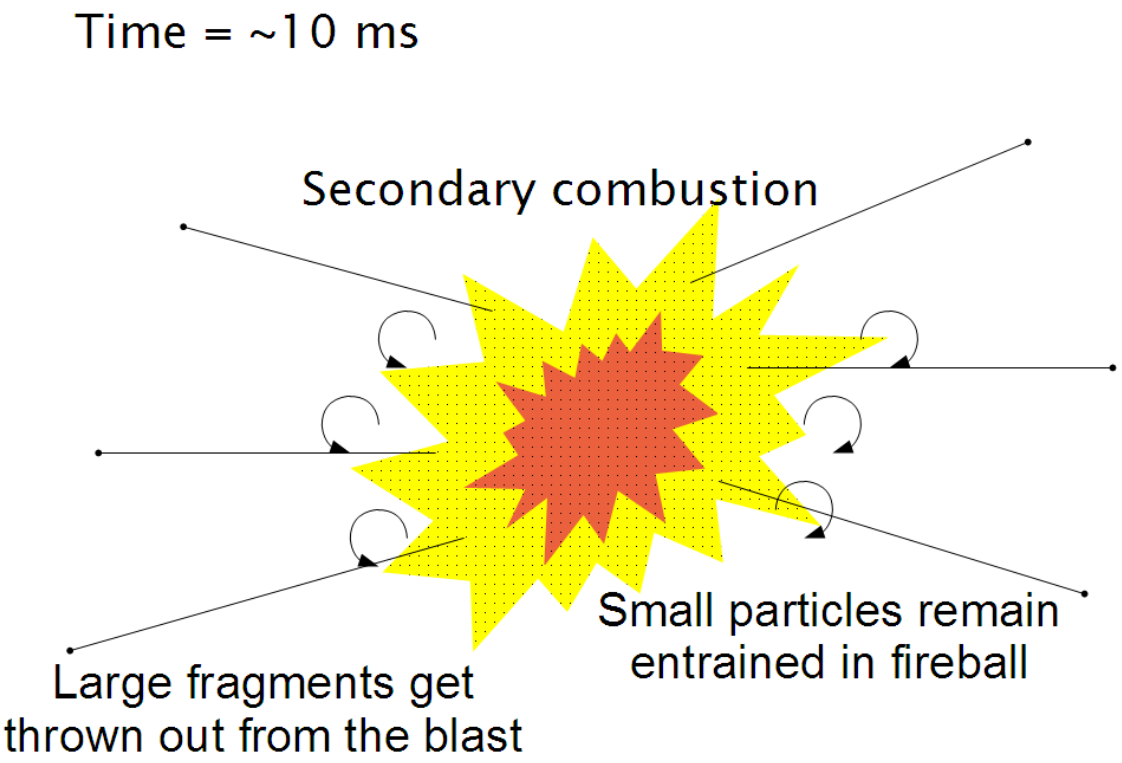

Fireball Mechanics

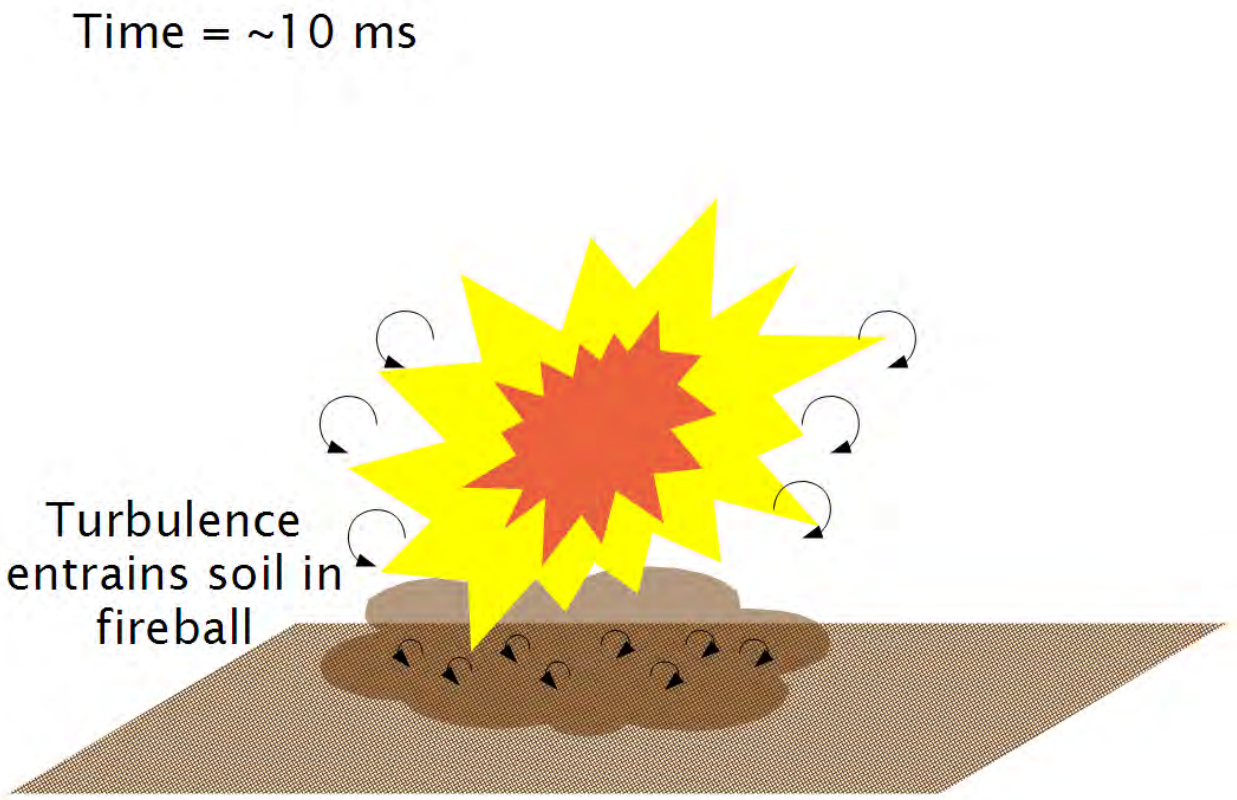

Fireball Mechanics

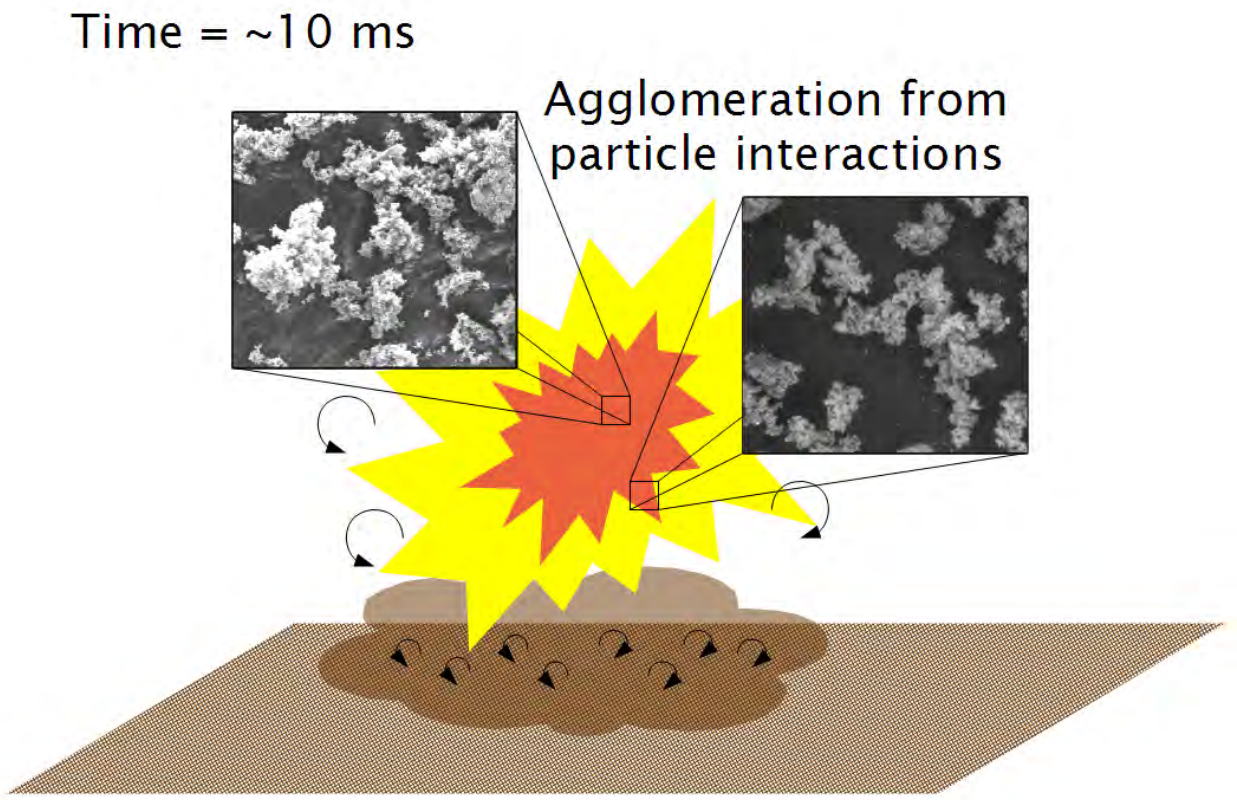

Fireball Mechanics

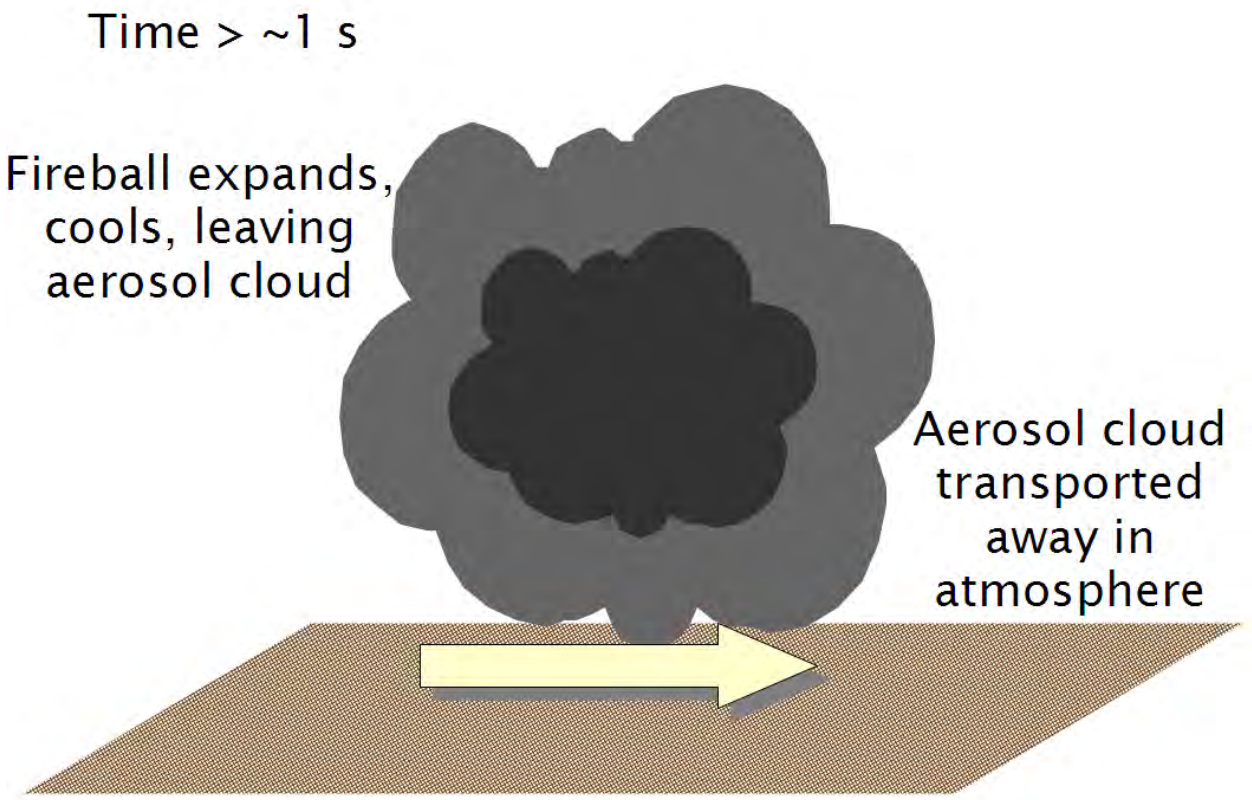

Impetus of Research

- What kind of particles are generated during the initial detonation?
- What role does secondary combustion in the fireball play?
- How do particles interact with entrained material (e.g. soil)?
- What effect does soil entrainment have on explosive aerosolization?

Outline

Detonation Calorimetry

Detonation calorimeter

Detonation Calorimetry

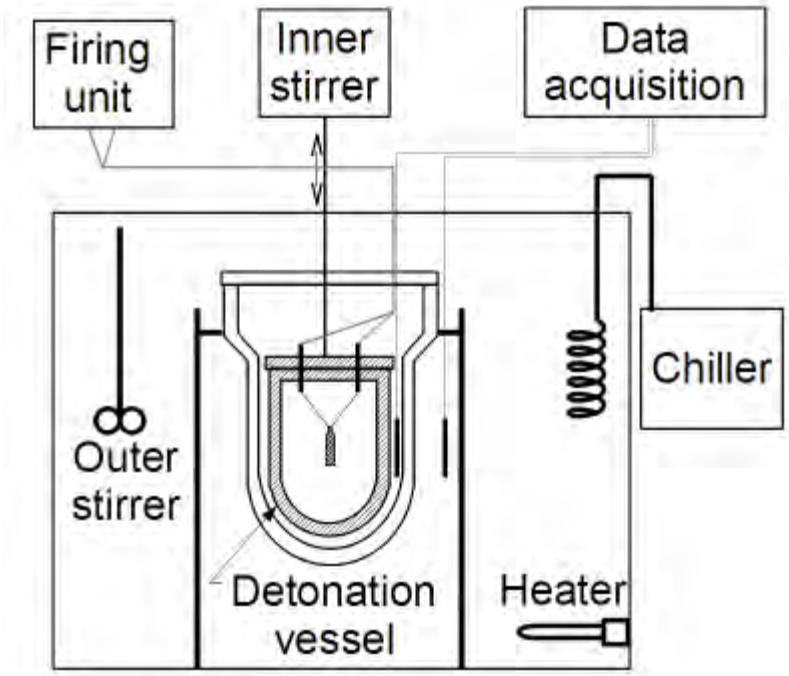

Schematic of detonation calorimeter

- Small charge detonated in closed container
- Characterize energy release from secondary combustion reactions
- Identify particle characteristics
  - with explosives alone
  - with target material
  - with different soils

Experimental Design

Explosive types used for different experimental conditions

Initial Oxygen Partial Pressure (kPa)	Entrained Soil Type				
	None	Coarse Sand	Fine Sand	Black Earth	Clay
0 (pure N_2)	C-4/detasheet	C-4/detasheet	C-4/detasheet	C-4/detasheet	C-4/detasheet
70	-	C-4	C-4	C-4	C-4
100	-	C-4/detasheet	C-4/detasheet	C-4/detasheet	C-4/detasheet
140	C-4/detasheet	C-4/detasheet	C-4/detasheet	C-4/detasheet	C-4/detasheet
200	-	detasheet	detasheet	detasheet	detasheet

- Calorimetry for energy release
- SEM particle morphology analysis
- Particle size analysis → (mechanical sieve + laser diffraction EPCS)

Outline

Calorimetry Results

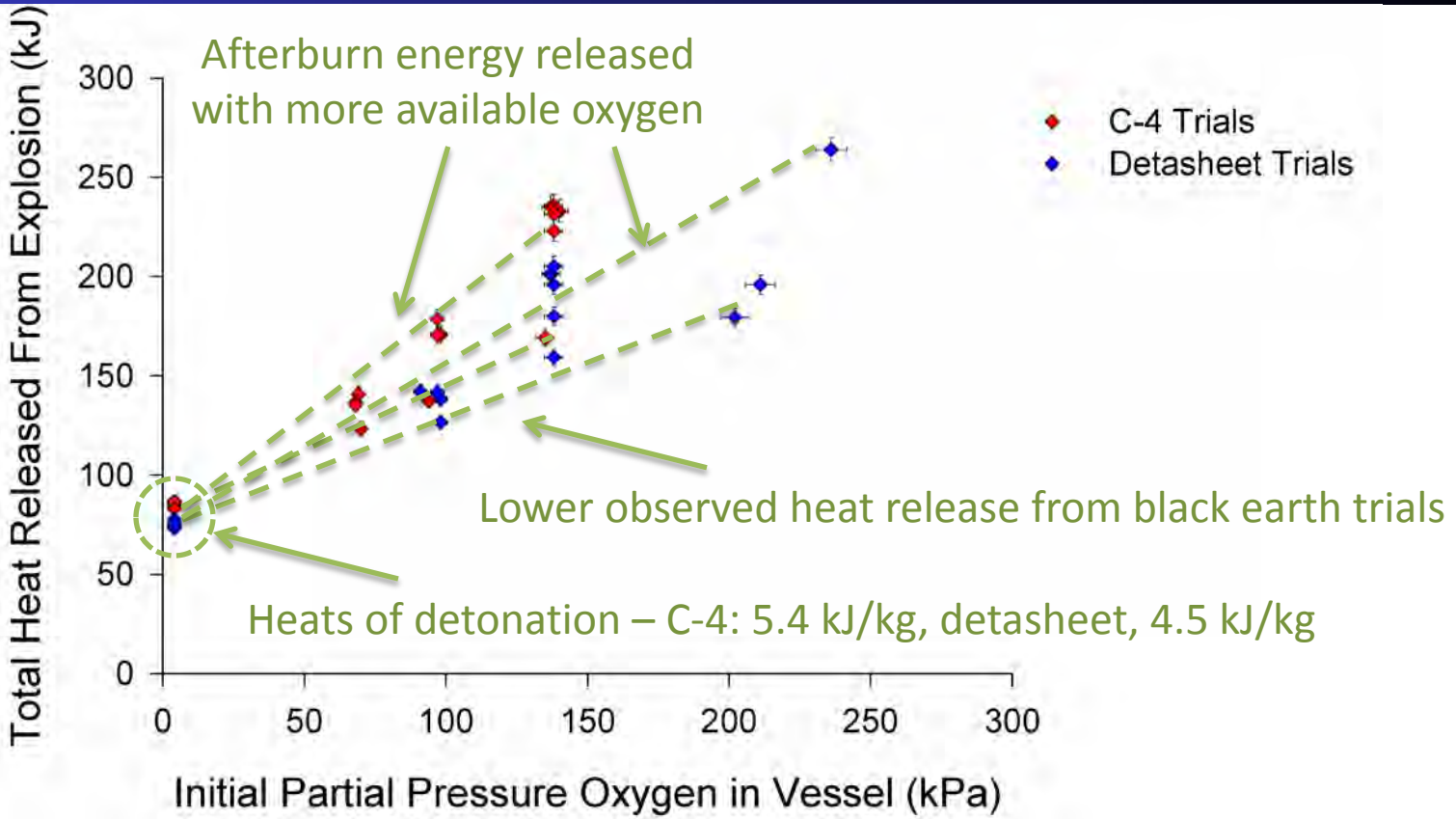

Energy release from explosions as a function of oxygen partial pressure

Outline

Particle Morphology – Fine Quartz Sand

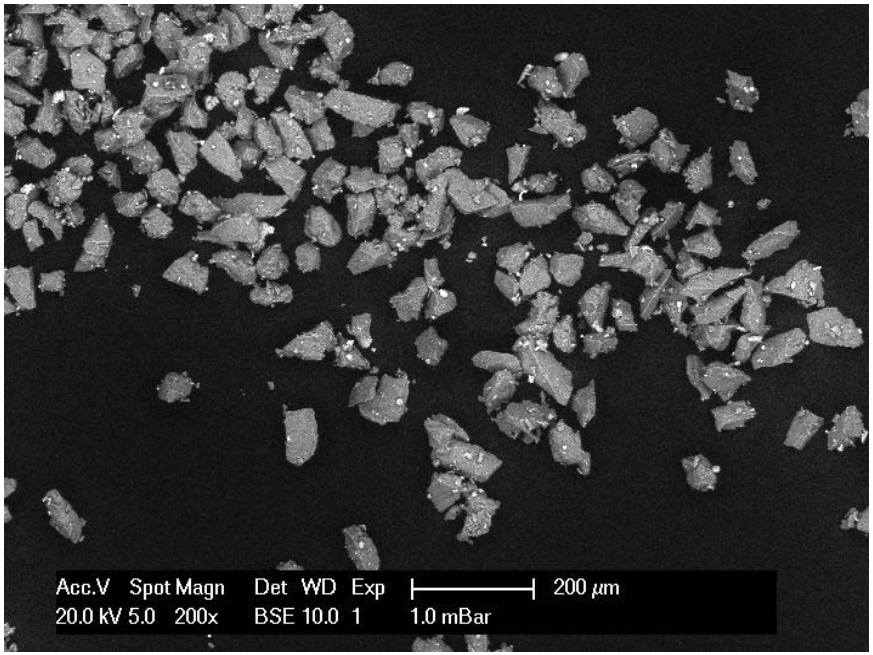

Undetonated – screened to pan

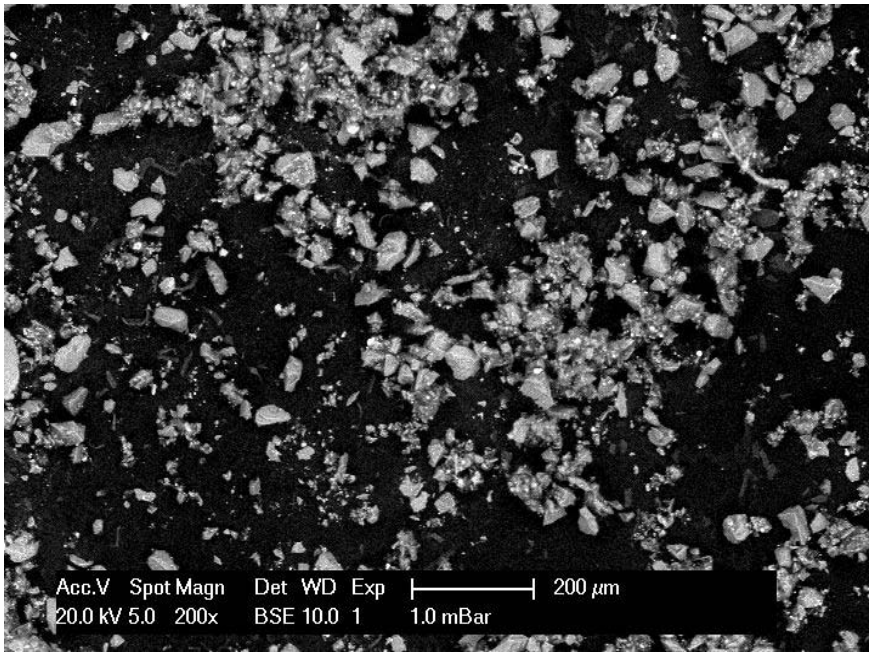

Detonated without O_2 – screened to pan

- Angular grains
- Smooth surface

- Highly angular particles
- Carbonaceous soot

Particle Size Distribution – Fine Quartz Sand

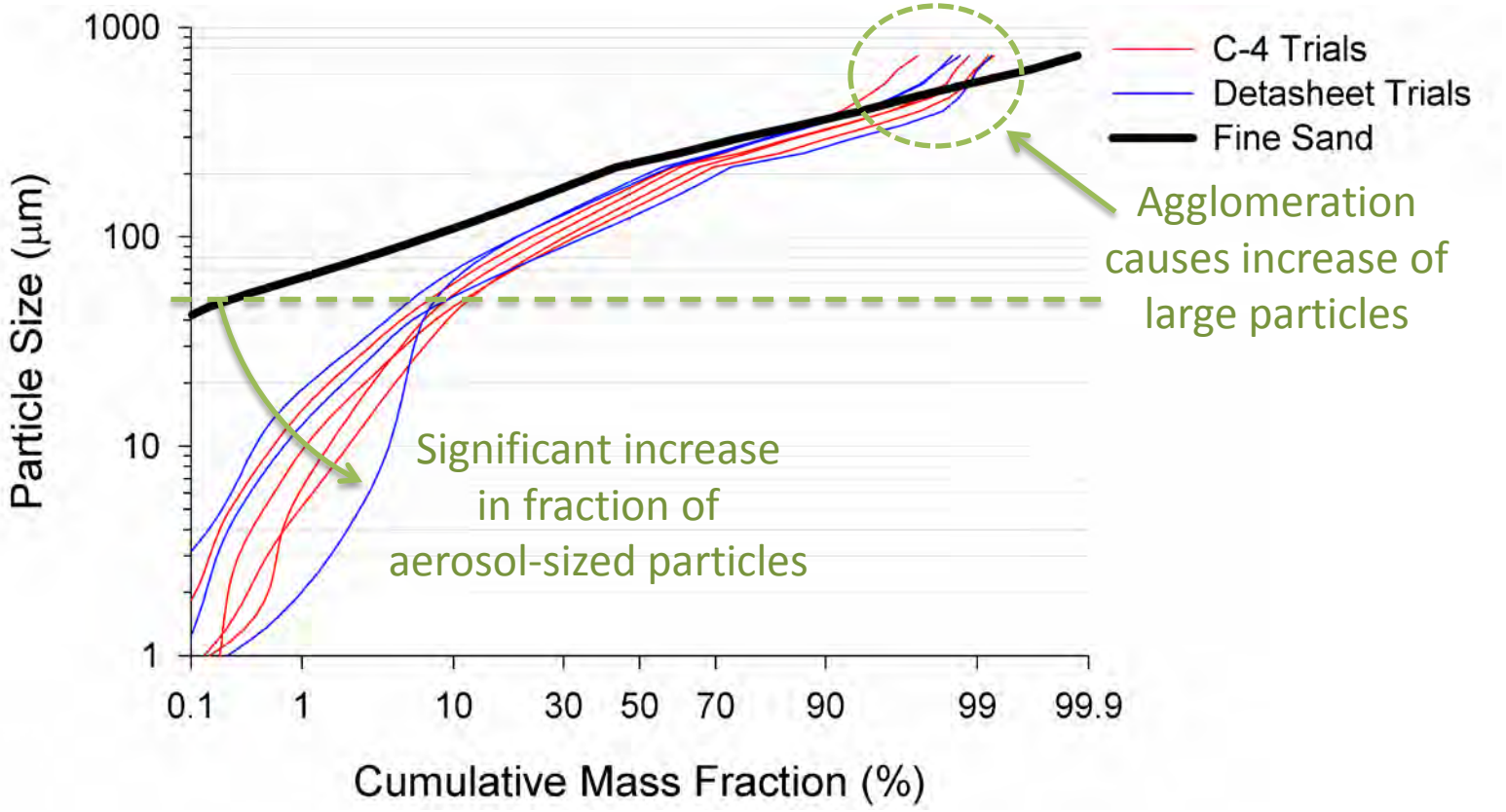

Particle size distribution for fine quartz sand

Particle Morphology – Coarse Quartz Sand

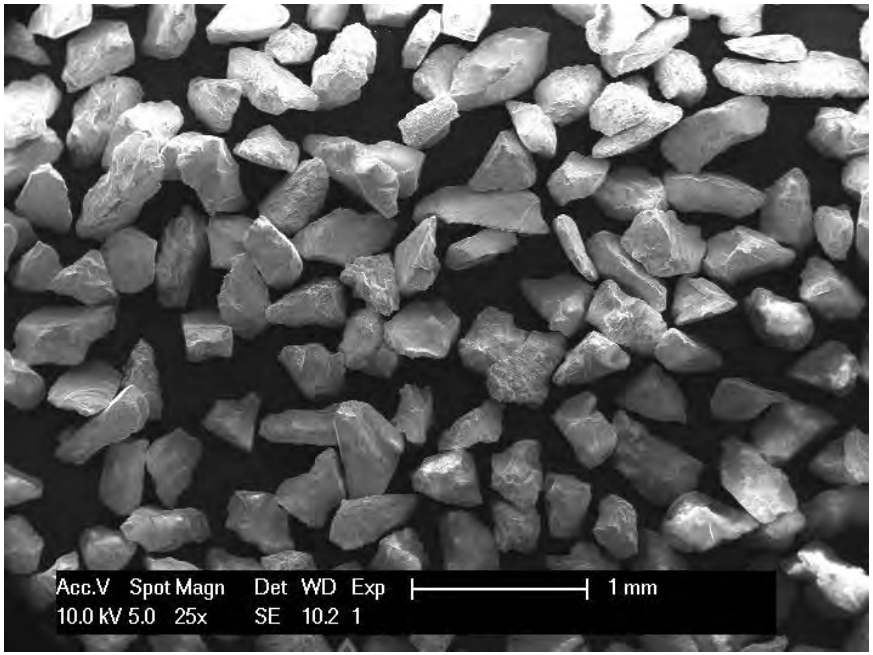

Undetonated – screened to no.60 mesh

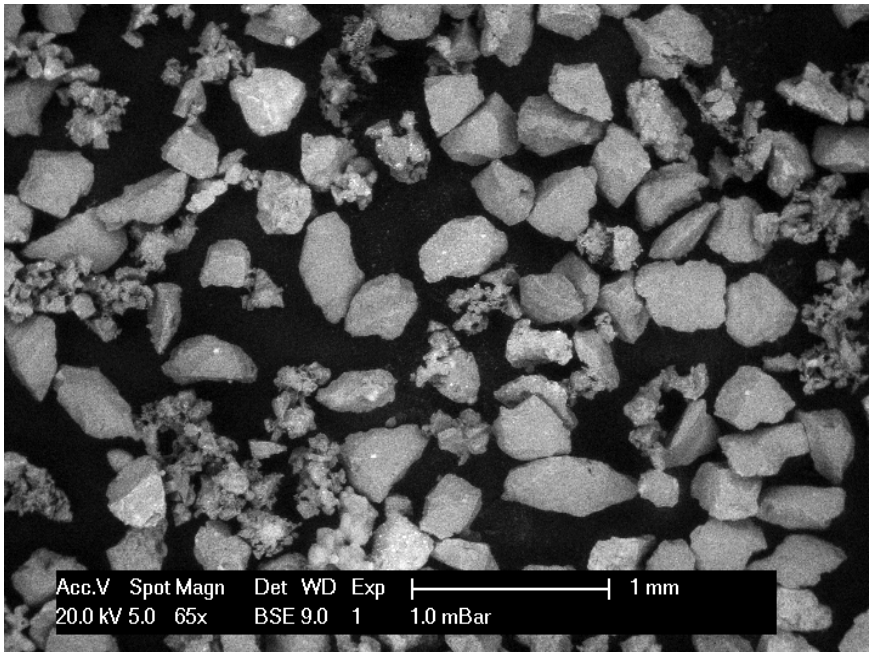

Detonated in presence of O_2 – screened to no.60 mesh

- Similar morphology to undetonated fine sand

- Fused sand grains
- Deposition of explosive residue

Outline

Particle Size Distribution – Black Earth

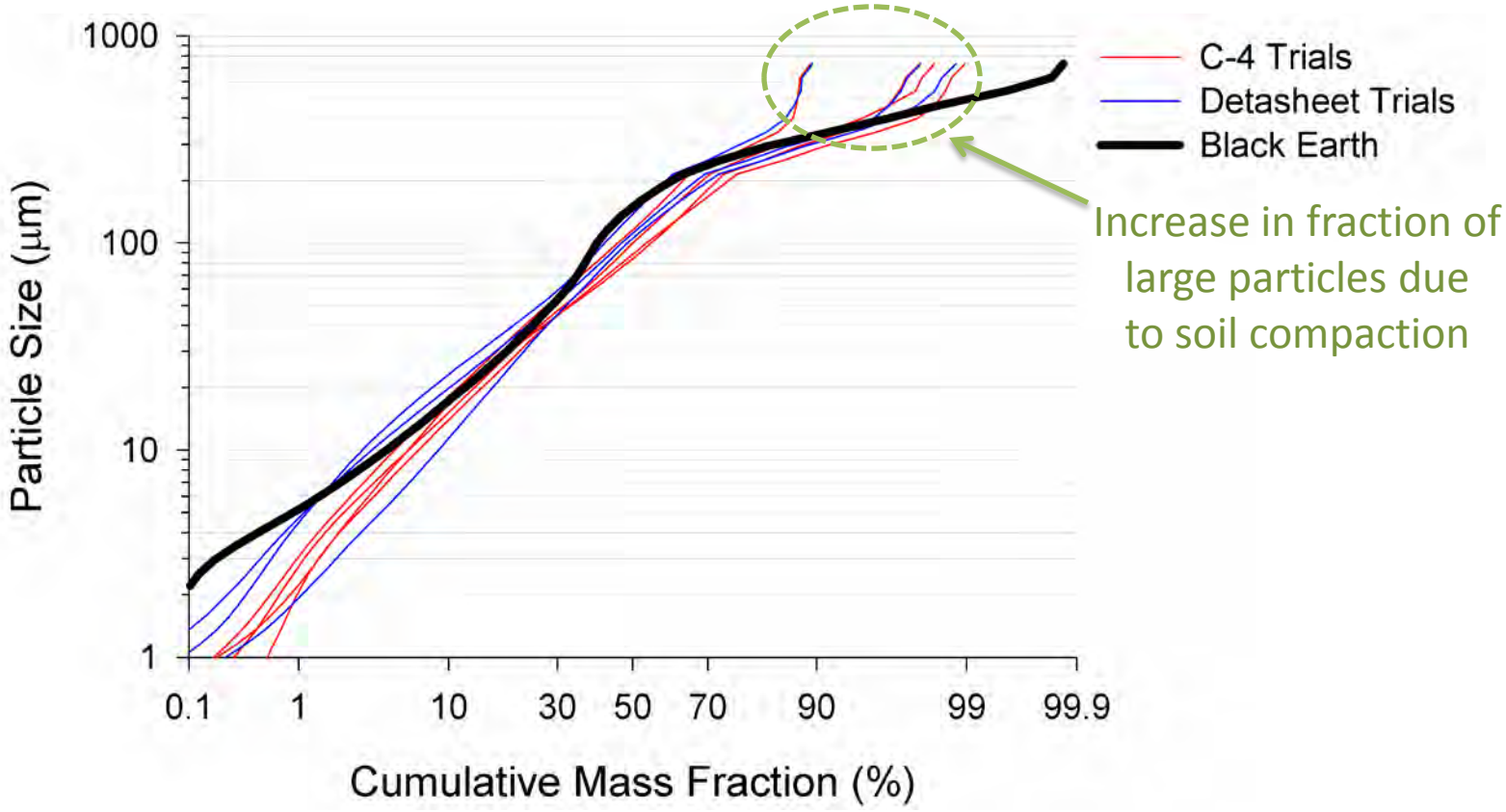

Particle size distribution for black earth

- Little change over most of particle size distribution

Particle Morphology – Black Earth

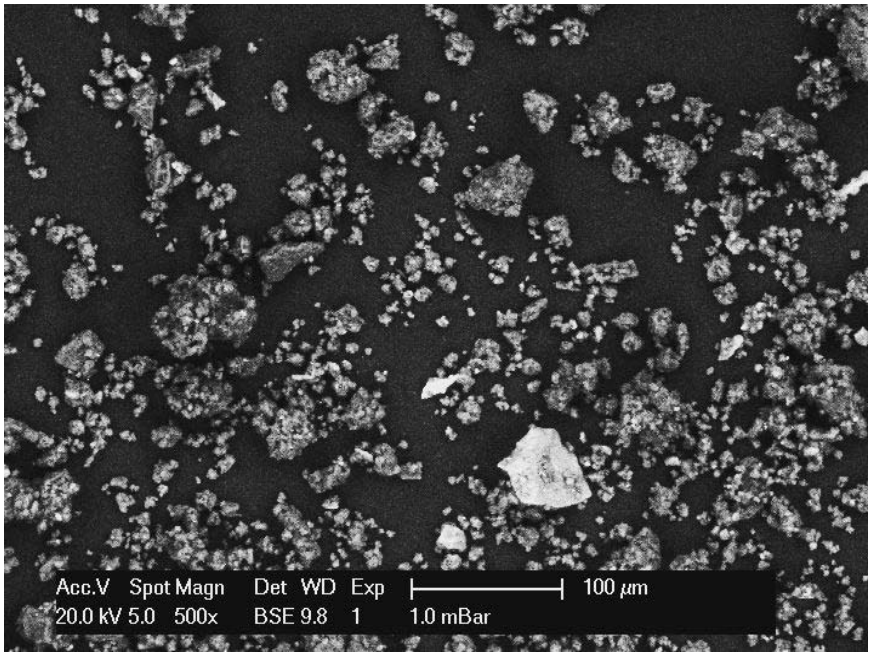

Undetonated – screened to pan

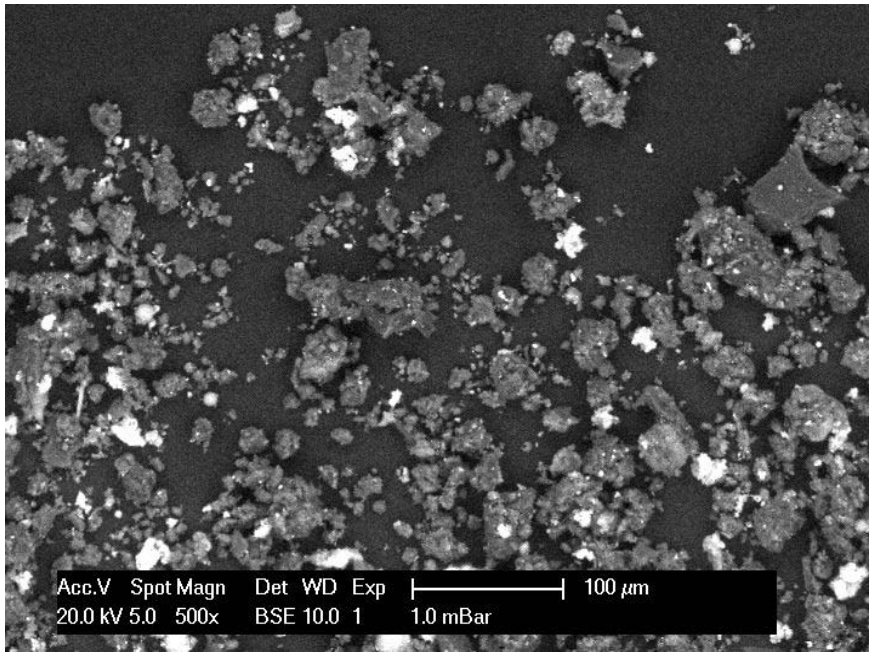

Detonated without O_2 – screened to pan

Essentially no difference in undetonated vs. detonated black earth morphology

Outline

Particle Size Distribution – Clay

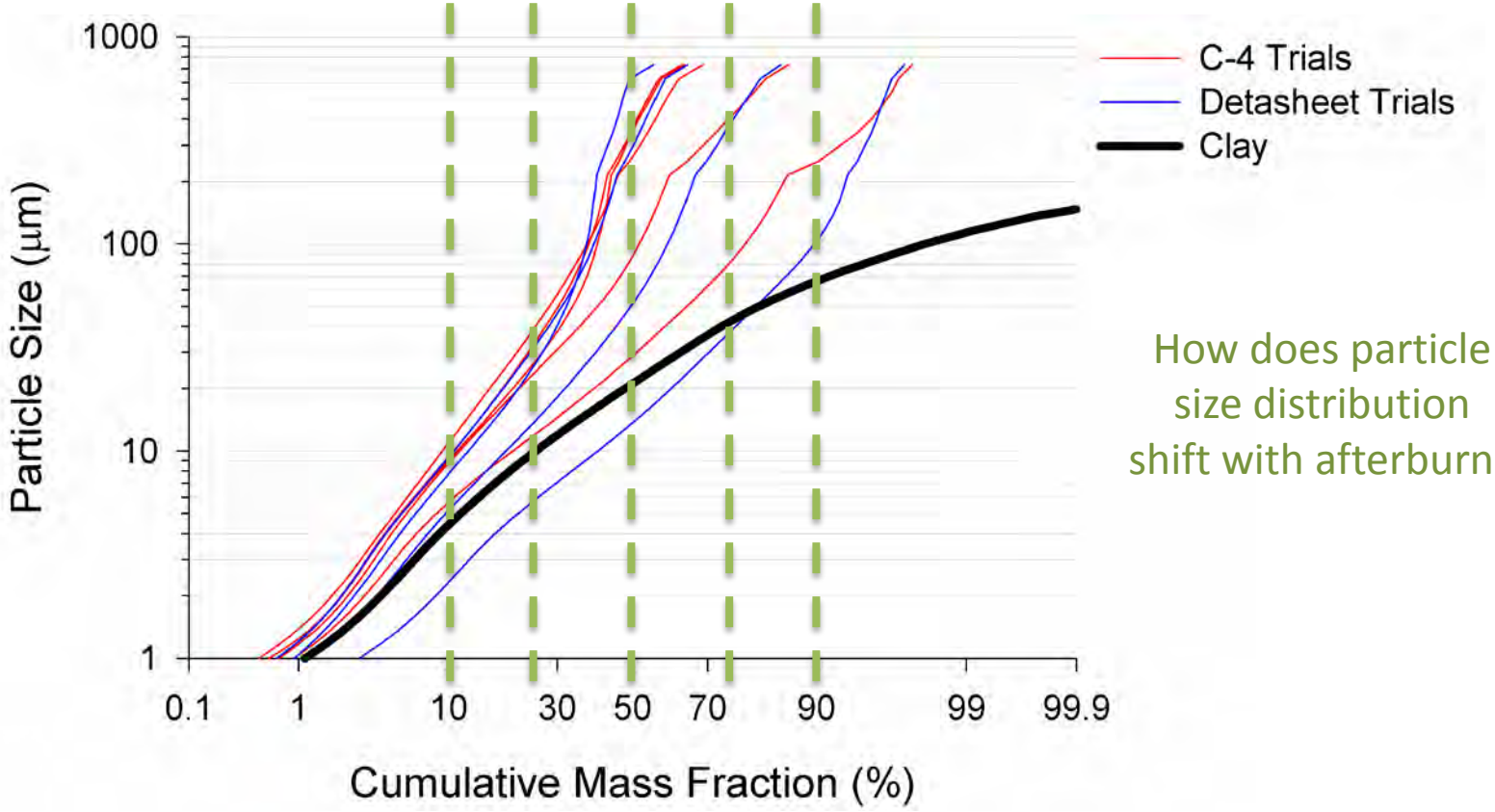

How does particle size distribution shift with afterburn?

Particle size distribution for clay

Particle Agglomeration in Clay

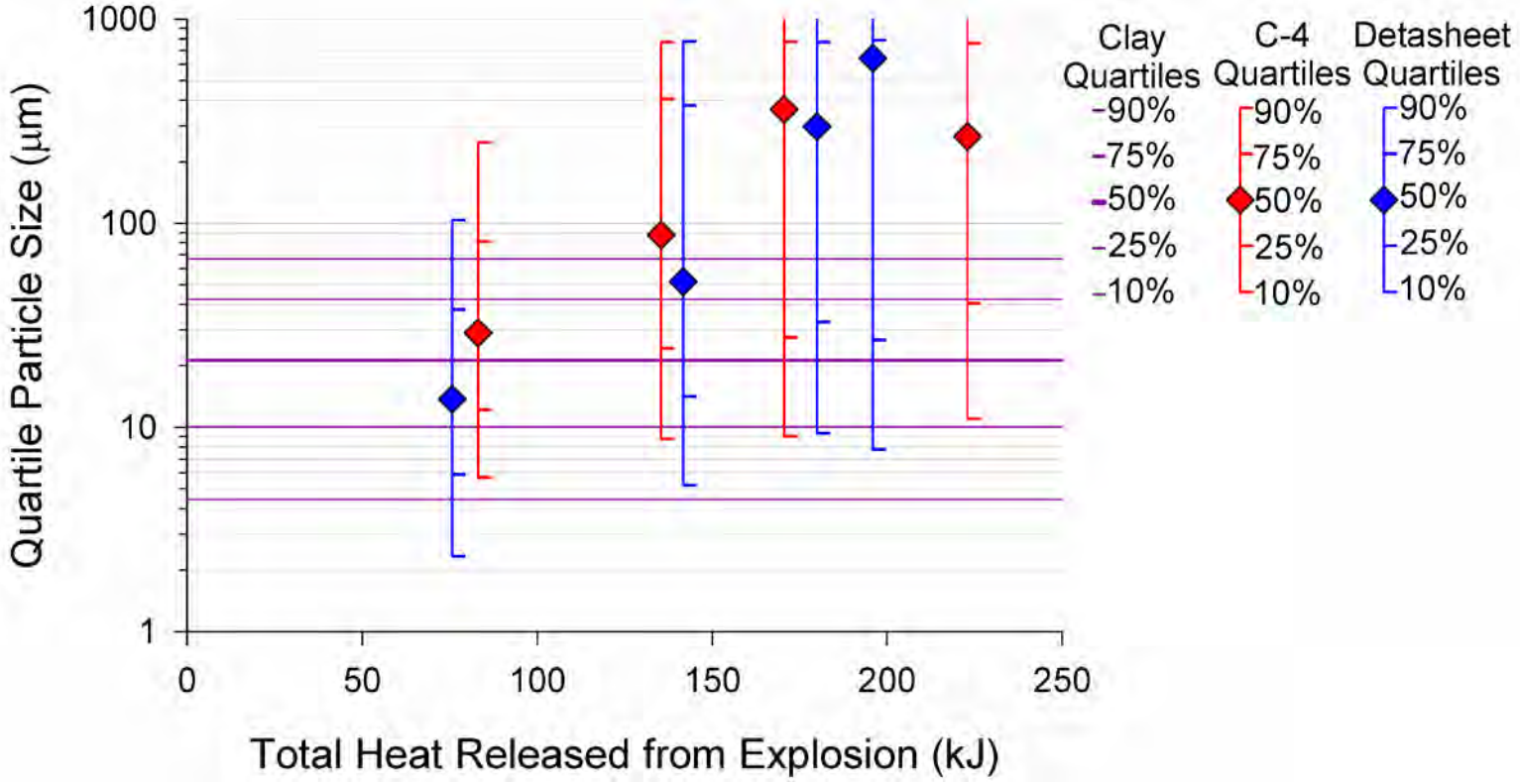

Quartile plot of entrained clay

- With afterburn, particle size increases by orders of magnitude

Particle Morphology – Clay

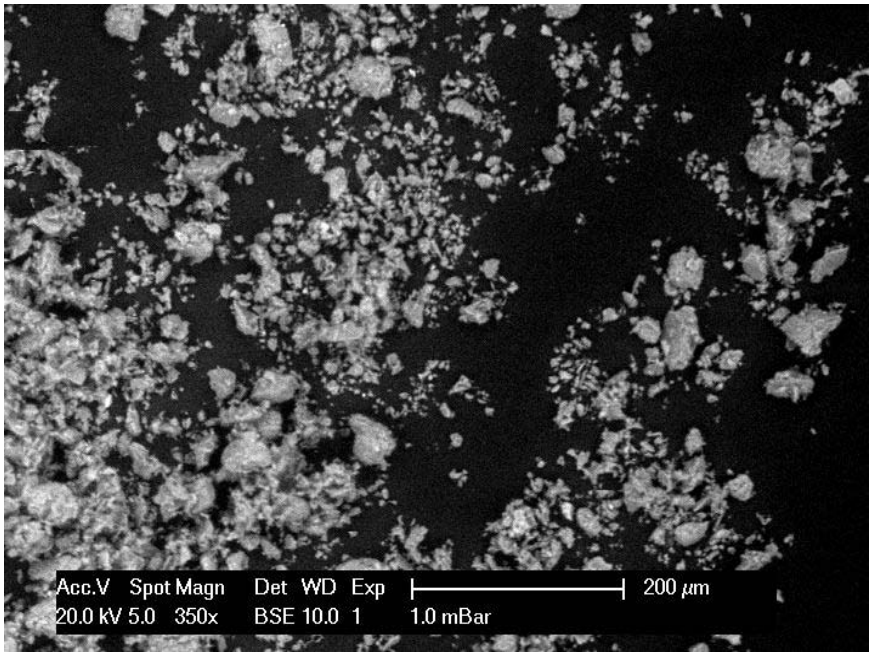

Undetonated clay

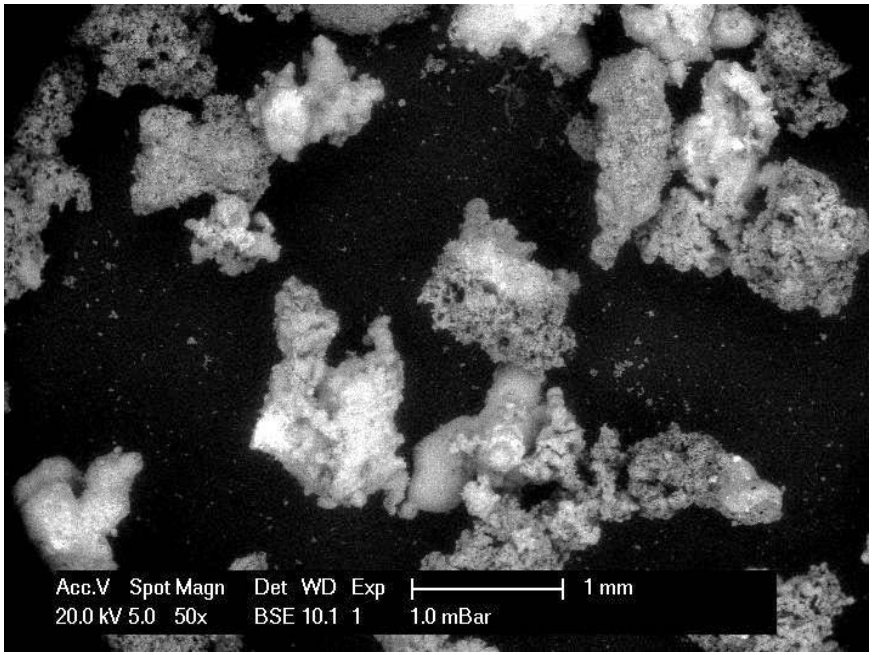

Detonated in presence of O_2 – screened to no.30 mesh

- Small, loose agglomerates
- Huge, porous agglomerates

Outline

Summary

- What kind of particles are generated during the initial detonation?
- What role does secondary combustion in the fireball play?
- How do particles interact with entrained material (e.g. soil)?
- What effect does soil entrainment have on explosive aerosolization?
- How is material that is aerosolized during the detonation distributed throughout entrained soil?
- Can results from closed vessel trials be extrapolated to an open air explosion?

Future Work

- Trials with addition of La_2O_3 powder being carried out
  - analyze elemental composition in different particle size ranges
  - determine how target powder becomes dispersed through entrained soil

- Open air trials planned to supplement closed vessel experiments
  - observe detonations over soil
  - separate real effects from artifacts of closed vessel explosions
  - measure quenching/boosting effects of soil entrainment on fireball

Acknowledgements

- Logistics Support Services, Canadian Forces Base Kingston
- Energetic Materials Section, Defence R&D Canada – Valcartier
- CBRNE Research and Technology Initiative
- Canadian Department of National Defence, Director General Nuclear Safety
- Natural Science and Engineering Research Council of Canada

Thank You!

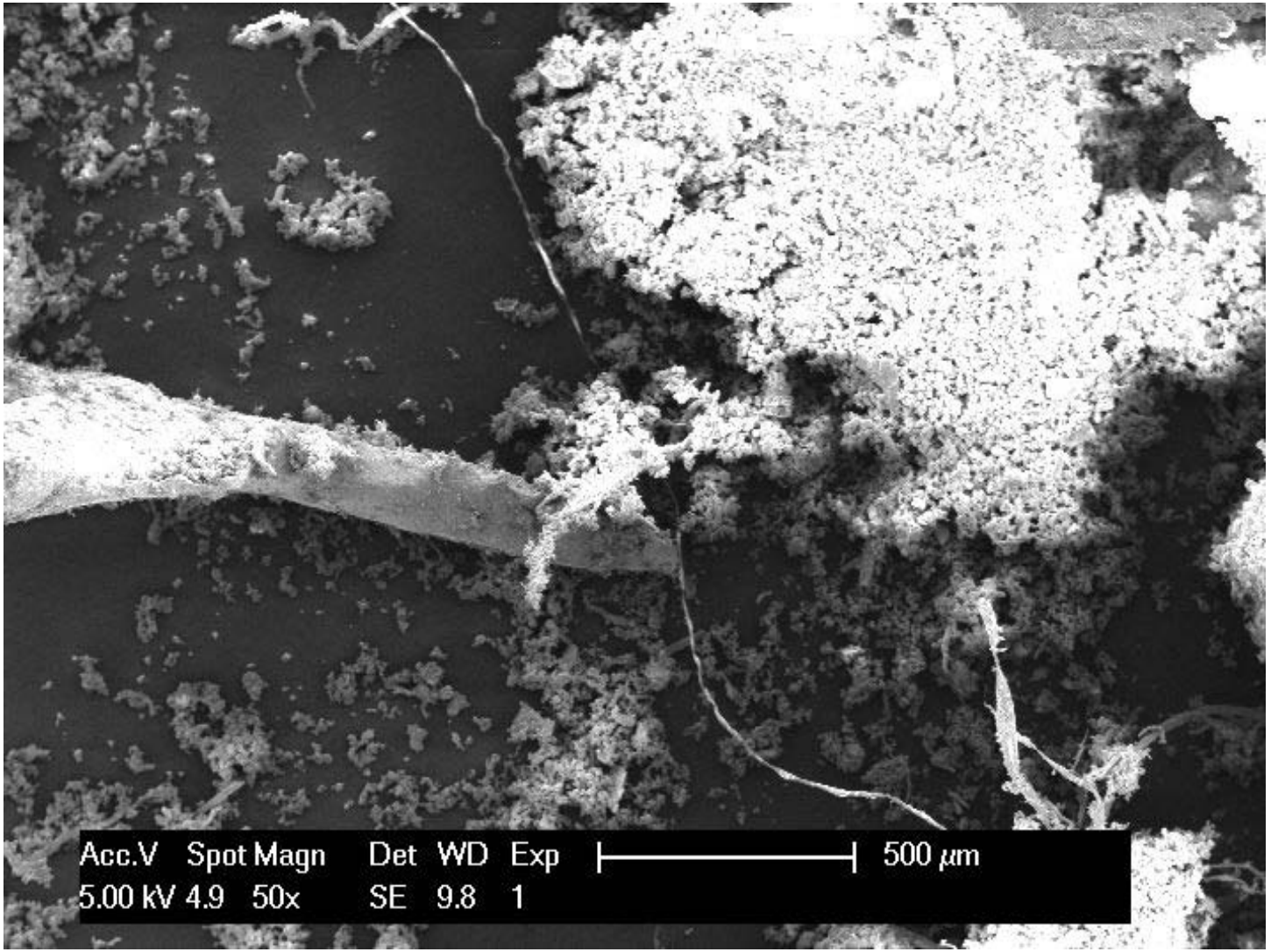

U.S. Army Research, Development and Engineering Command

DESCENT Modeling in Rotorcraft Vulnerability Assessment

TECHNOLOGY DRIVEN. WARFIGHTER FOCUSED.

Andrew Drysdale

Army Research Laboratory

13 Sep 2011

Mission Background

- Army Research Laboratory's Survivability/Lethality Analysis Directorate (ARL/SLAD) performs survivability/ vulnerability analyses on Army vehicles, including rotorcraft

- An important factor in rotorcraft vulnerability analyses is the outcome of a ballistic event that leads to reduced or zero levels of available power

- Modeling of the post-event transition to one-engine-inoperative (OEI) flight or an autorotative impact is used to quantify the rotorcraft outcome

Outcome Definition

- The outcome of a power-loss ballistic event is binned into one of three “kill categories”:
  - Mission Abort (MA)
    - The rotorcraft is able to transition to steady, level flight from its flight conditions at the time of the event
    - It can return to base for repair
  - Forced Landing (FL)
    - The rotorcraft is forced to perform an immediate, but controlled, landing
    - This is the equivalent of a successful autorotation; repairs may be performed on the ground as necessary
  - Attrition (Att)
    - The rotorcraft’s impact velocity exceeds the designated critical velocity for avoiding extensive structural damage
    - Repairs are not feasible, and the vehicle is removed from inventory

Analysis Domains

- Outcomes are modeled in two distinct regions of the rotorcraft's flight envelope
  - High/Fast (H/F):
    - Above 80 kts initial ground speed
    - Between 100-600 ft above ground level
  - Low/Slow (L/S):
    - Below 40 kts initial ground speed
    - Below 100 ft above ground level

- A power-loss event will be modeled at many height/ velocity points throughout each region, and a kill category assigned at each point

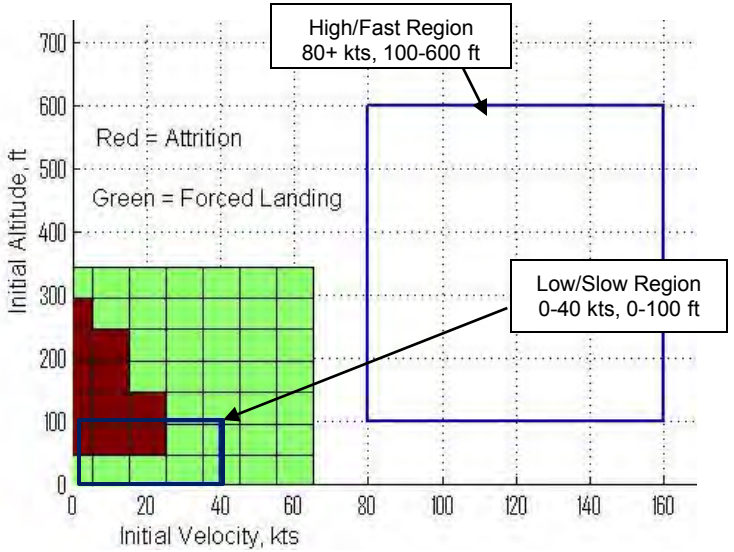

Compiling Results

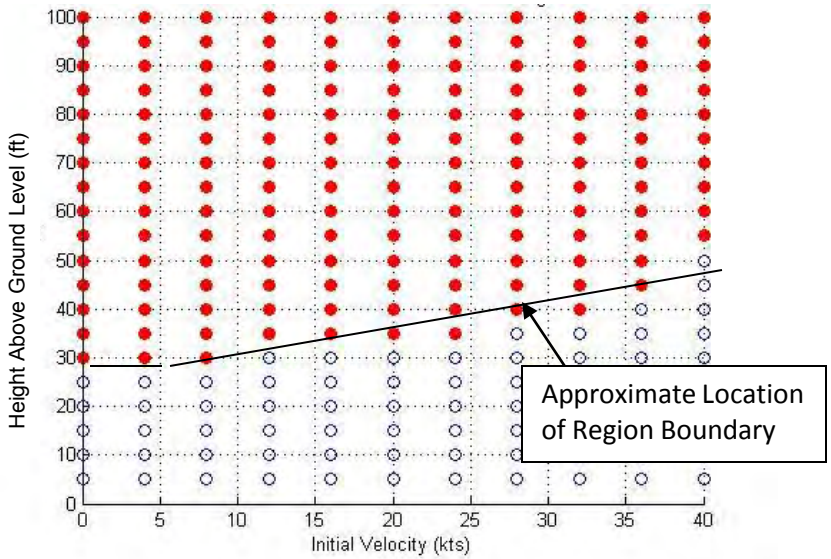

- The percentage of the area of a given region occupied by points binned into each kill category is the kill probability (P_k) for the rotorcraft in that region for that level of power loss

- In the example shown, since about 72% of the Low/Slow region shows an Attrition (red), and 28% shows a Forced Landing (white), the P_k will be:

  - Low/Slow (Zero Power Remaining)
    - MA 0.00
    - FL 0.28
    - Att 0.72

Using the Results

- In this example, the DESCENT model predicts that for total power loss anywhere in the Low/Slow flight region, there is a 72% probability of Attrition and a 28% probability of Forced Landing

- This probabilistic approach allows us to compute P_k inputs before vehicle-level vulnerability modeling occurs and speeds up the processing of the survivability/vulnerability analysis

Model Development

- DESCENT is a rotorcraft flight optimization script developed by ARL/SLAD and ARL's Vehicle Technology Directorate (ARL/VTD)

- The optimization engine is SNOPT, a sparse-matrix non-linear optimization algorithm written at Stanford University

- DESCENT's aerodynamic model is a 2-D actuator disk that allows two degrees of control freedom: lift coefficient, which roughly corresponds to collective pitch, and disk tip-path-plane pitch, which corresponds to longitudinal cyclic

Flight Path Optimization

- DESCENT begins by assuming the controls are set in the trimmed condition for steady, level flight

- SNOPT, running internally, iteratively improves upon that assumption by perturbing the pilot controls (collective and longitudinal cyclic pitch) and "grading" the resulting flight path against an objective function and a set of inviolable constraints
  - Constraints enforce both physical restrictions, such as the rate at which drag slows rotor speed, and characteristics specific to the rotorcraft being modeled
  - The objective function quantifies whether the flight path is an improvement (i.e., exhibits a lower impact velocity) than the previous iteration

- DESCENT finishes when it is established that either 1) a transition to partial-power flight is possible, 2) autorotation to impact at less than a critical velocity is possible, or 3) the flight path is fully optimized without success (Att)

Height-Velocity Diagram

- Comparing DESCENT modeling predictions of rotorcraft autorotation to manufacturer's height-velocity diagram is an accuracy check
- DESCENT-produced diagrams consistently present the same trends as the standard "dead man's curve" with similar no-fly regions
- Differences in the curves are often due to different assumptions about pilot experience and damage tolerance

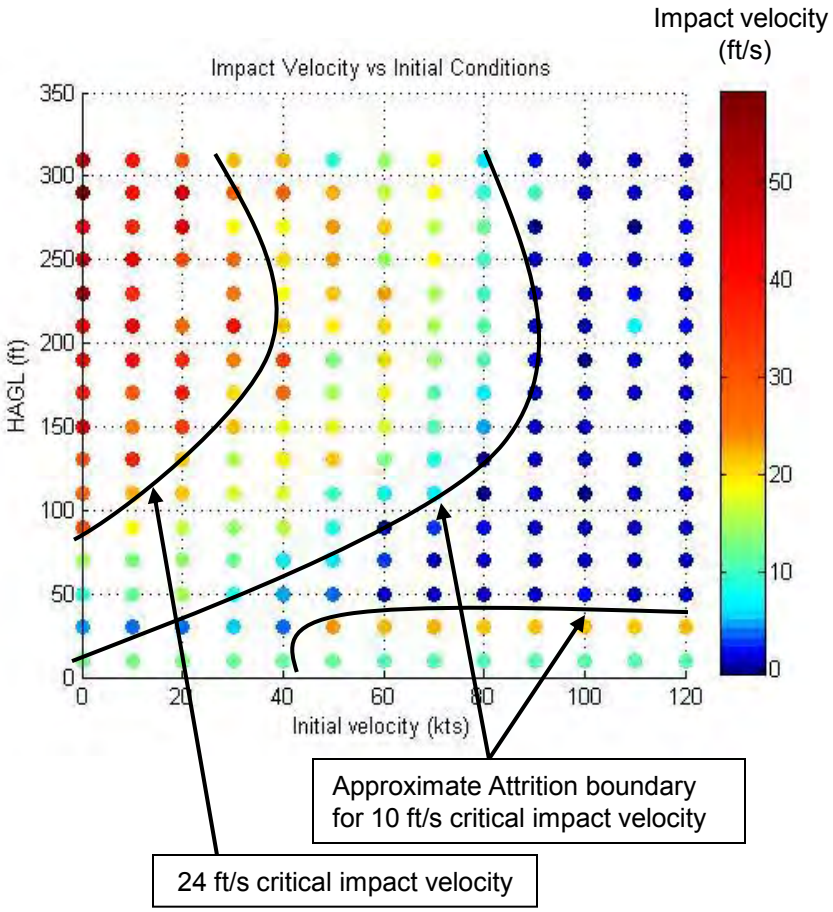

V&V Work (Case Studies)

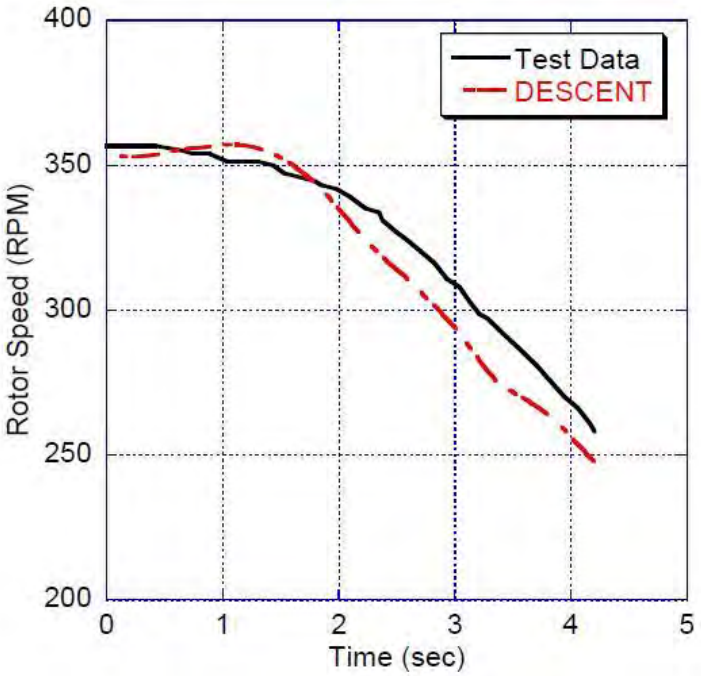

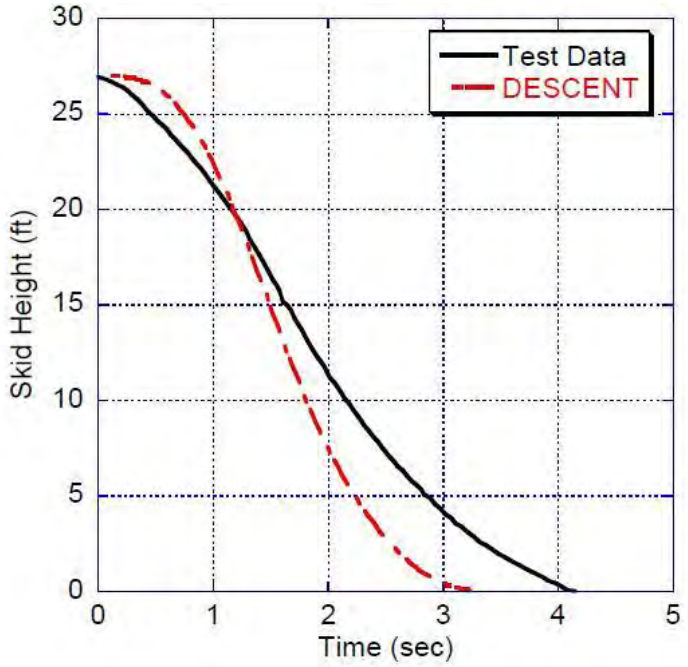

- DESCENT verification and validation work shows good correlation to flight test data state variables in most cases
- A comparison to modified OH-58 autorotation test is shown

Case Studies cont.

- However, other cases demonstrate the need for well-defined constraints and objective (grading) function
- DESCENT identifies a flight path that satisfies the critical velocity requirement and exits (upper graph); nevertheless, the state variables might not match the flight test (lower graph)
- This discrepancy points to differences among a suitable control strategy, an optimal control strategy, and the actual control strategy from test data

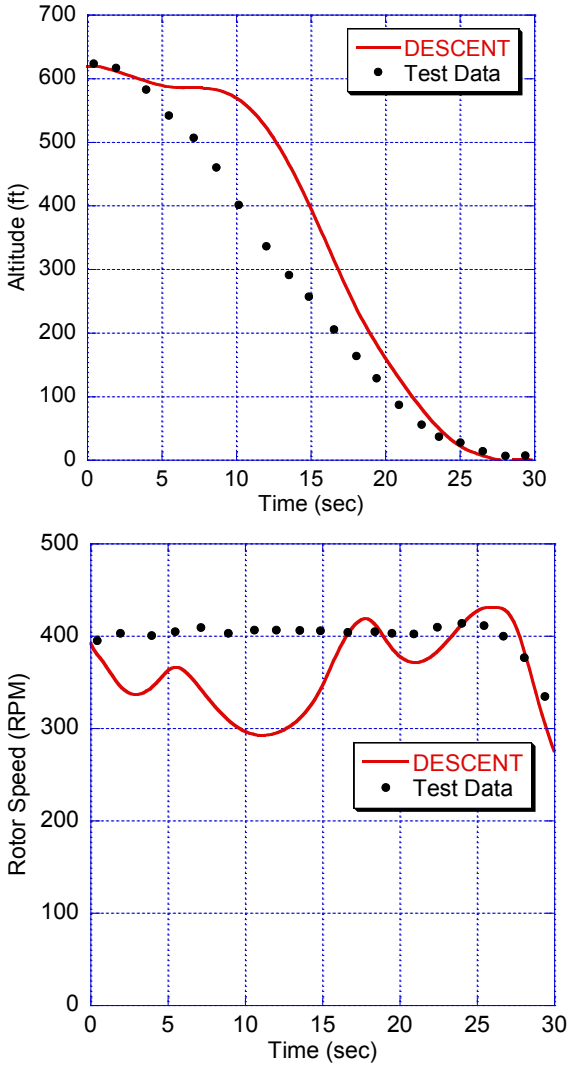

Conclusions

- DESCENT shows good correlation to manufacturer-provided “no fly” curves in identifying Attrition regions
  - Flexibility to assess effect of design changes on vulnerability
- While there is often no single “right” autorotation path, using DESCENT as a predictive tool for flight path details in each particular case is still subject to empirical results
  - Semi-empirical application is possible given enough data to inform constraints and objective function
  - Flight path data often shows considerable variability
- Identifying commonalities between autorotation paths will help transition from aggregate analyses to particular cases

TECHNOLOGY DRIVEN. WARFIGHTER FOCUSED.

Gun Launch Dynamics of Pyrotechnics

Justin K. John, Dr. Aisha Haynes

U.S. Army ARDEC, RDAR-SM, Building 94, 2nd floor, Picatinny, NJ 07806
Phone: (973) 724 – 3815, Fax: (973) 724 – 2417, justin.k.john@us.army.mil

RDECOM

Outline

- Objective of Study
- Mechanical Behavior of Pyrotechnics
- Dynamic FEA of 105 mm Illumination Round
- Behavior of Illumination Candle During Gun Launch
- Summary
- Future Work

Objective

The purpose of this study is to:

- Determine mechanical properties (with thermal and strain dependence) of standard pyrotechnic
  - Perform mechanical testing on standard pyrotechnic (binder, oxidizer, fuel) to determine structural behavior of material
  - Evaluate similarities (if any) between PBX and pyrotechnics
- Determine impact of gun launch on illumination candles in 105mm projectile through modeling and simulation.
  - Explore various design parameters: length, diameter, etc.

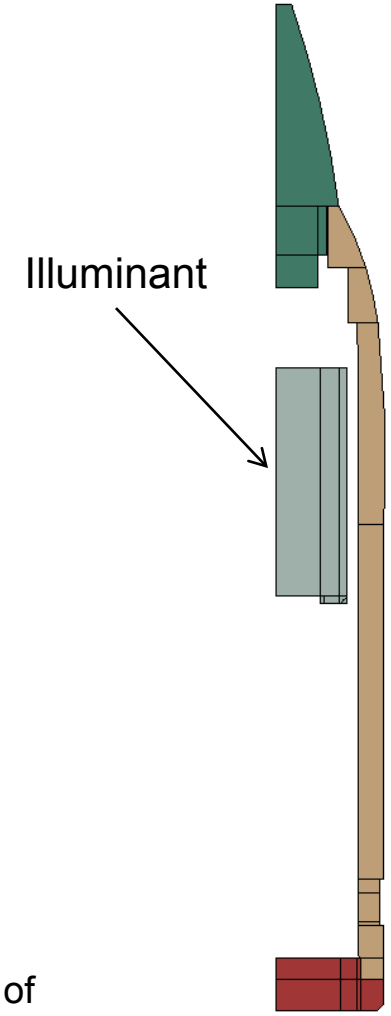

Figure 1. Fuze, projectile body, base and illuminant (gray) of 105mm projectile in half symmetry, axisymmetric model. The voids are locations for other ancillary components(not depicted).

Mechanical Behavior of Pyrotechnic

Mechanical Behavior of Pyrotechnic

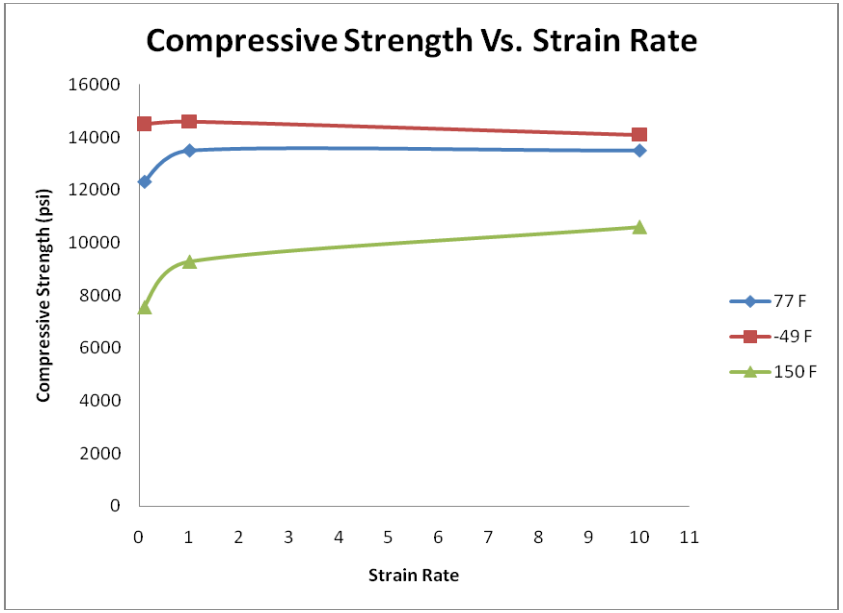

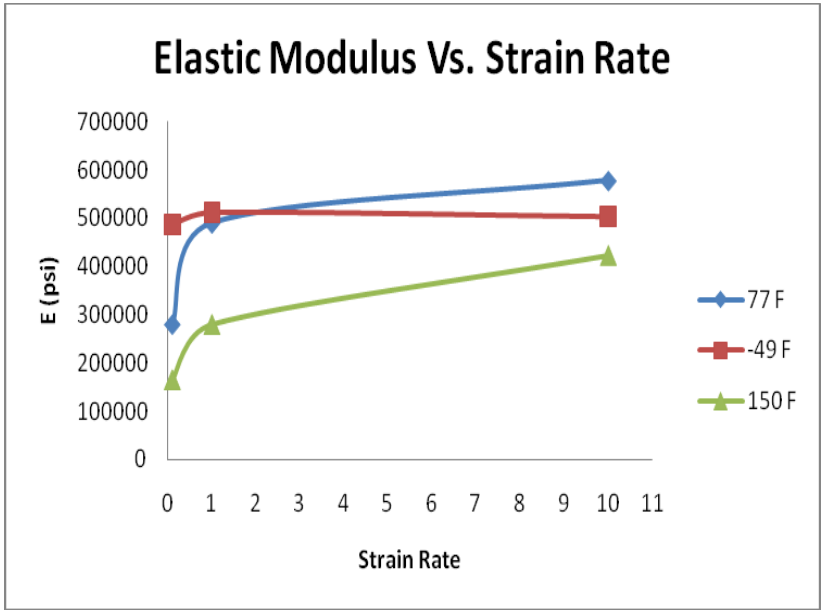

- Uniaxial Compression tests performed at strain rates 0.1/s, 1/s, and 10/s and temperatures -49°F, 77°F, and 150°F.
- Strength and modulus exhibit decreasing sensitivity to strain rate with increasing strain rate and at temperatures below 150°F
  - Sensitivity to strain rate highest at low strain rates. For PBX, the binder dominates mechanical behavior at low strain rates and fuel and oxidize dominate the mechanical behavior of the material at high strain rates*
- Slight increase in elastic modulus with strain rate for hot and ambient samples

*D.A. Wiegand and B. Reddingius, 2005, "Strengthening and Stiffening of Plastic Bonded Explosives Under Pressure and Metal-Like Mechanical Properties", U.S. Army ARDEC Technical Report, AD-E403 069

FEA of Illuminant: 105mm Illumination Round

Analysis Overview

- Analysis simulates a 105mm projectile gun launch to capture stresses experienced in pyrotechnic during setback and setforward
- Structural analysis performed using ABAQUS/Explicit v. 6.9.1
- 2D-axisymmetric model of standard 105mm projectile
  - Model includes all inner components with specific material properties
  - Focus on illuminant behavior (mesh refined)
- Full model: 7172 nodes, 6292 elements

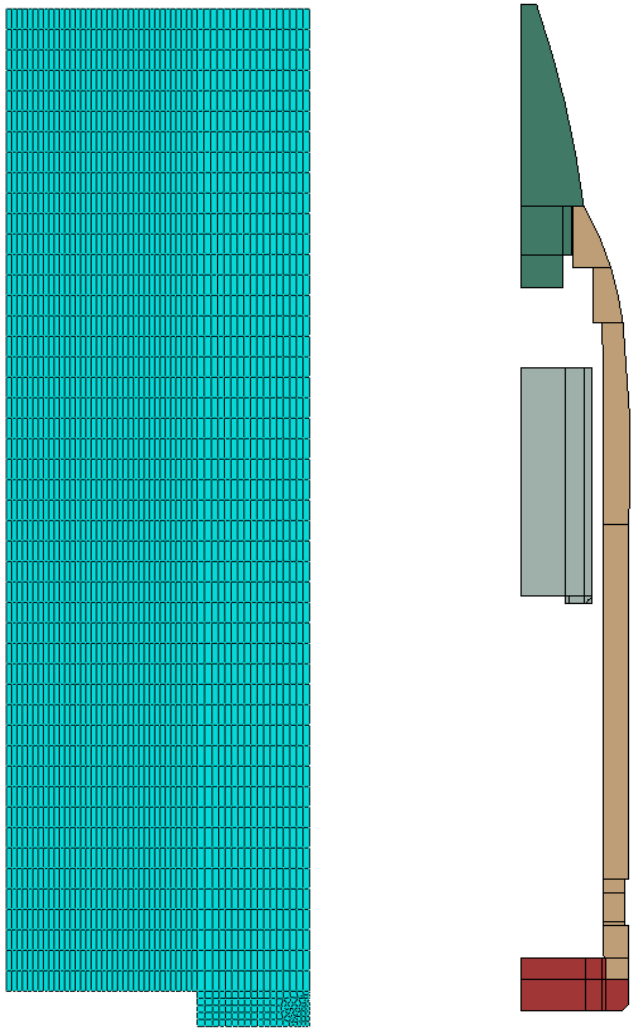

Figure 2. **a)** A depiction of the 2D-axisymmetric pyrotechnic model. The meshed model of the pyrotechnic compound consists of 2761 nodes and 2652 elements. **b)** 105mm projectile and general location of illuminant.

Assumptions

- 2D axisymmetric model:
  - decrease model complexity and analysis run time
  - Unfortunately, projectile spin behavior cannot be performed using this method
- Voids in original model were removed:
  - Projectile components are pressed into body
- Effects of simplifying complex parts negligible:
  - Full 3D baffle gaskets have through holes that are filled to create one continuous 2D part profile
- Pyrotechnic material shape simplified to fill the cylindrical case

Boundary Conditions, Constraints

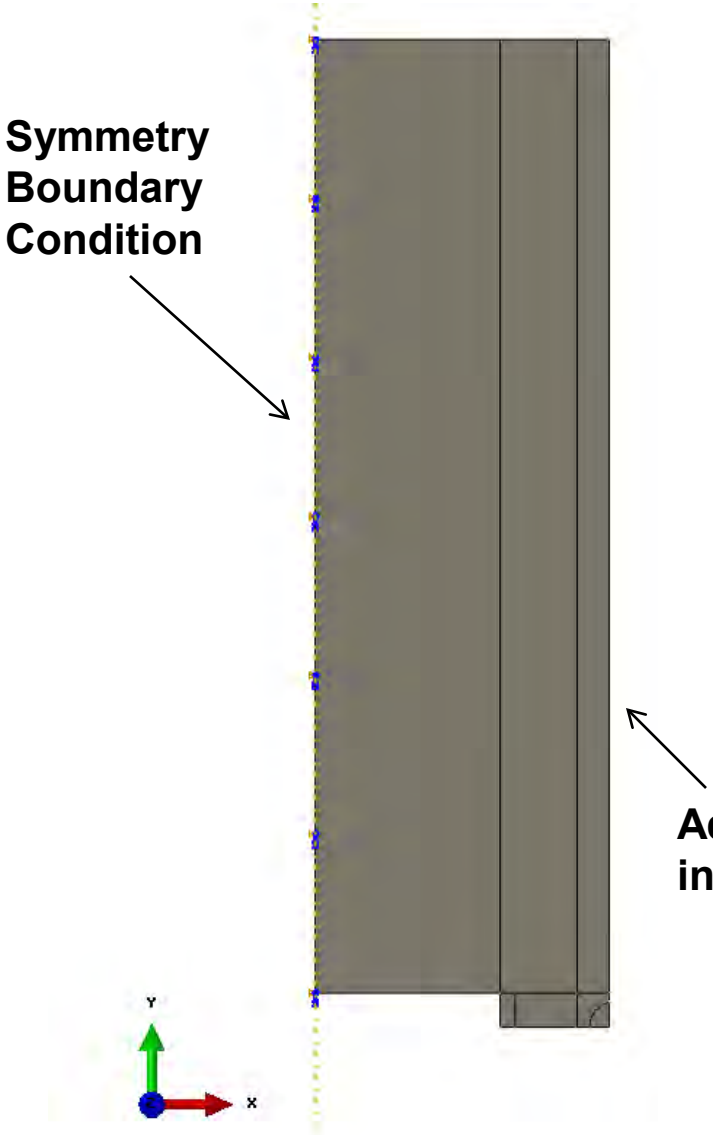

- The pyrotechnic is confined by a fiberboard liner inside a steel cylinder capped at both ends (not depicted).
- A tie constraint simulates the adhesive bond between illuminant surface and fiberboard liner.
  - Nodes aligned along edge of illuminant and cylinder
- Model is oriented in the y axis

Figure 3. Model of the pyrotechnic compound. The axis of symmetry is shown.

Load

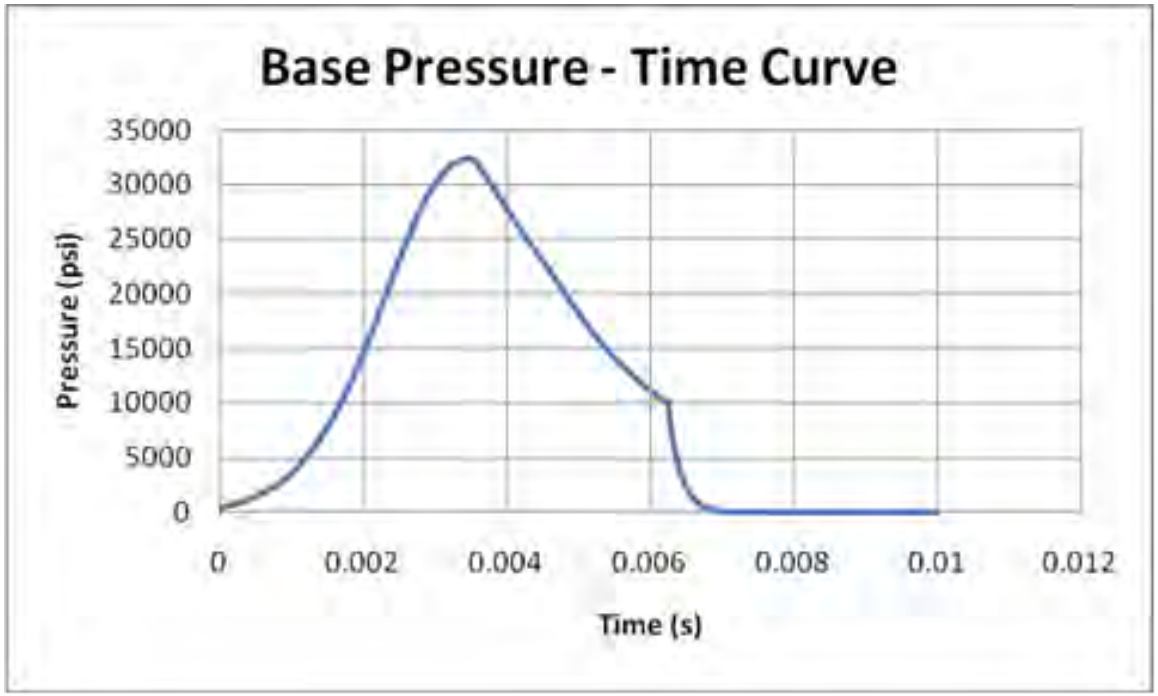

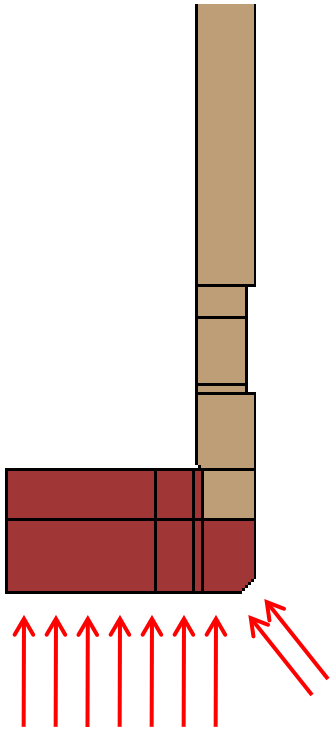

Figure 4. a) A surface force, simulating the Zone 7 propellant charge, is applied to the outer surface of the base of the projectile. The 105mm projectile experiences a maximum pressure of approximately 32000 psi for 6 ms. **b)** Zoom in of projectile base. Arrows depict force placement.

Behavior of Illumination Candle During Gun Launch

Impact of Gun Launch

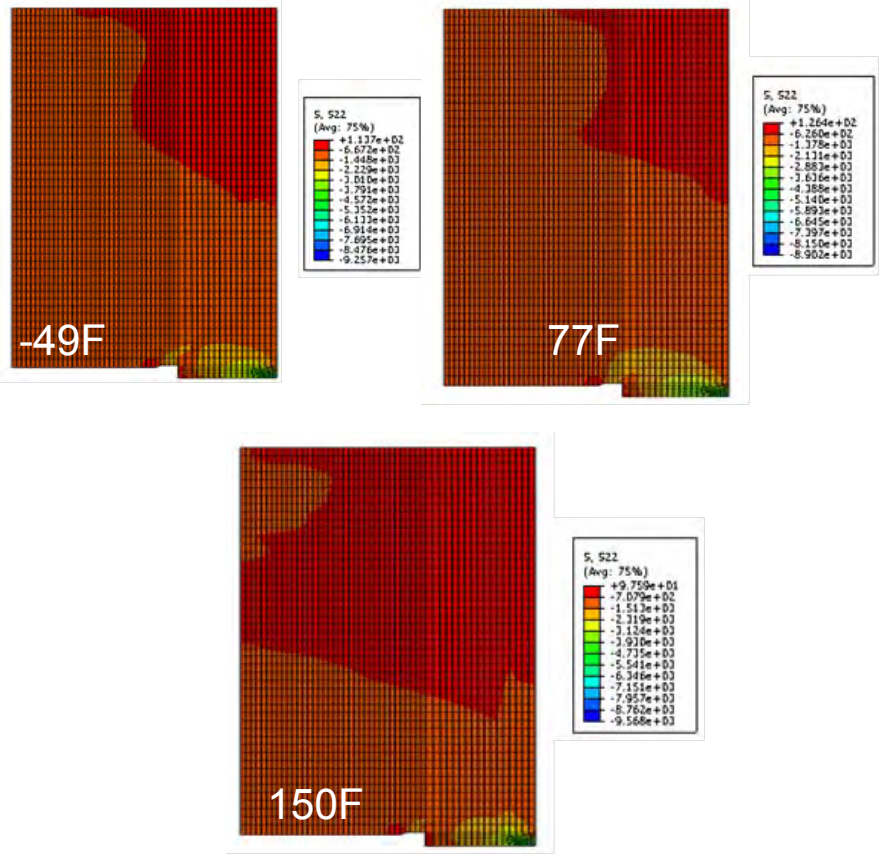

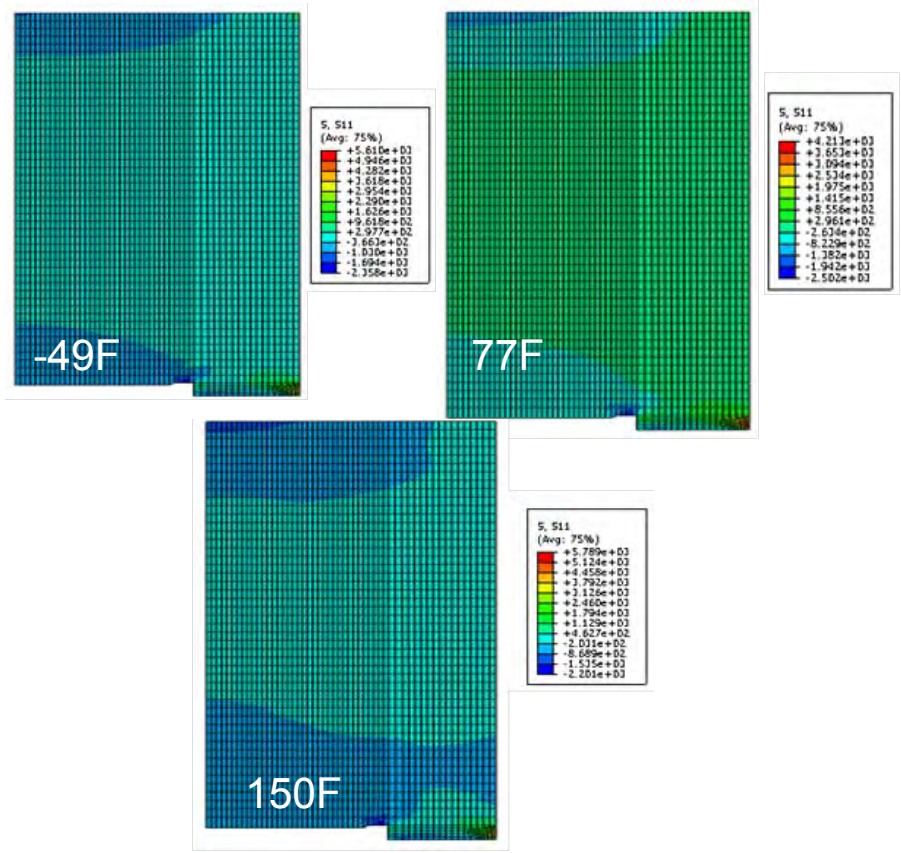

Axial Load Profile (Maximum)

Temperature (°F)	Axial (psi)	Radial (psi)	% Compressive Strength (Axial Stress)
-49	8902	2358	63
77	9257	2502	69
150	9568	2201	90

Radial Load Profile (Maximum)

Design Considerations

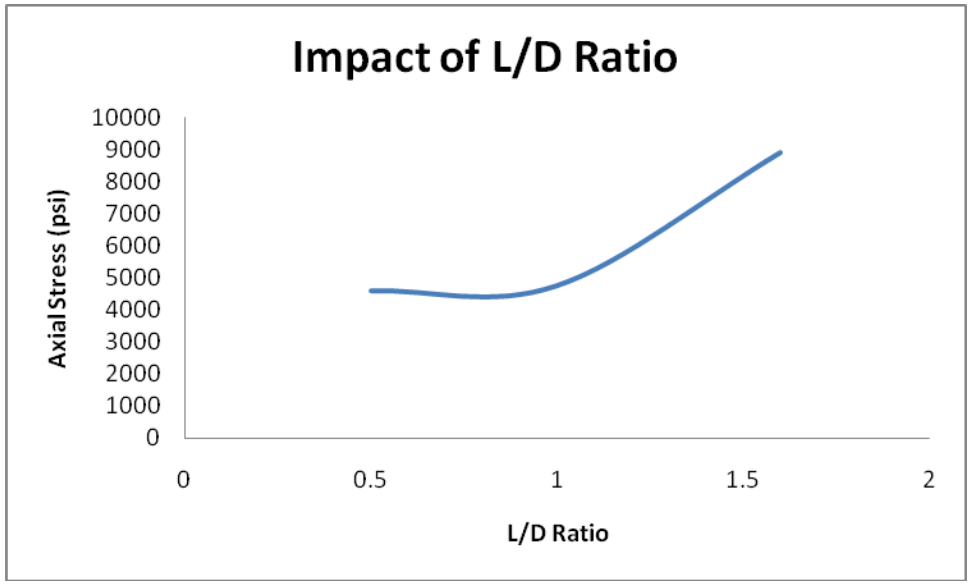

Figure 5. Impact of L/D Ratio of Axial Stress Profile of Pyrotechnic

• The aspect ratio of the pyrotechnic impacts the material's structural integrity during gun launch.

•The higher the length to diameter aspect ratio, the higher the stress on the pyrotechnic under confinement (pressure range in this analysis is 2500 psi – 2700 psi).

Summary

- This study has shown that the structural integrity of the pyrotechnic varies with:
  1. **Strain rate (for high temperatures):** Slight increase in strength and stiffness observed in ambient and hot samples
  2. **Temperature:** At higher temperatures the pyrotechnic is more sensitive to the axial load such that the overall axial stress on the material increases.
  3. **Aspect Ratio:** The length to diameter ratio impacts the structural integrity of the pyrotechnic.

- The behavior observed is similar to that of PBX.
  - One goal of this work is to determine if the mechanical behavior is comparable.
  - Based on what we know about PBXs, we can carry the assumption that the behavior of the pyrotechnic is dominated by the binder at low strain rates and dominated by the fuel and oxidizer at high strain rates.

Future Work

- Evolve material model from Linear Elastic/Plastic to an advanced composite model
  - Triaxial compression testing to determine impact of varying confinement pressure
- Evaluate thermomechanical properties of composite and identify similarities to PBXs
  - Thermal analysis to determine impact of inorganics on binder
  - Curing study of binder
- Develop an intricate material model including damage to evaluate crack propagation in illuminant

Acknowledgements

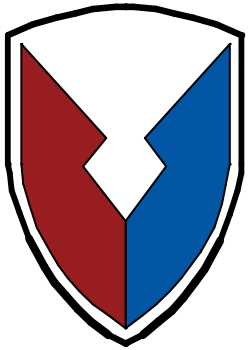

RDECOM

Dr. Don Wiegand, ARDEC for performing mechanical testing on pyrotechnic
Dr. Tom Mason, LANL for providing material input for modeling efforts

Mr. Joseph Donini and Mr. Anthony Sherwood for aiding with their expertise


TNO innovation for life

Ammunition and Weapon Effects in UT

Prepared for 2011 - ISB symposium, Miami, US

Theo Verhagen & Martin van de Voorde
TNO – the Netherlands

Ammunition and Weapon Effects
in
Confined Urban Theatre
in the
vicinity of own troops

- Why
- IST
  - Experimental program
  - Understanding
- Awareness
- Demands
- SOLL

Why
Buildings & Fortications are part of modern operations

Operational units are unfamiliar with:

- **the ‘quality’ of the encountered target;**
- **the ammunition effects;**
- **operational risk and safety in confined space;**
- **(3D) application restraints;**
- **…**

The *<u>available</u>* ammunition types

- **have to be used;**
- **are procured within another mindset.**

Impact:

- **Ammunition consumption**
- **Logistic support**
- **$$$$$$**

<u>Mid-calibre ammunition</u>

- 100 m distance
- Burst of 3 shots (5 times)
- Centre of target
- Penetration found


Transition: *from past to present and beyond…*

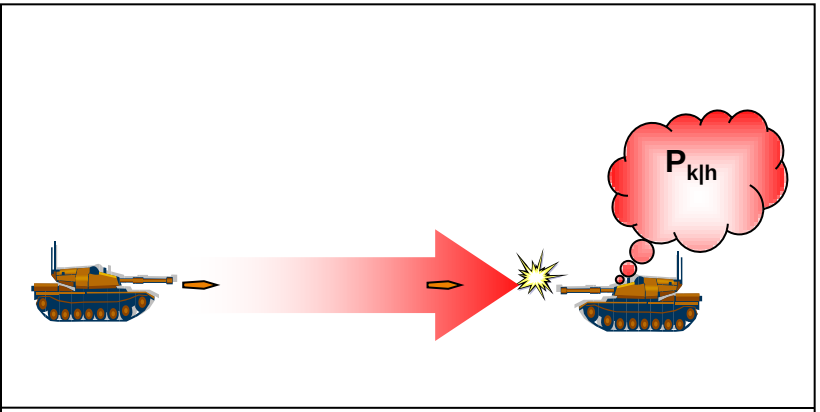

Traditional theatre

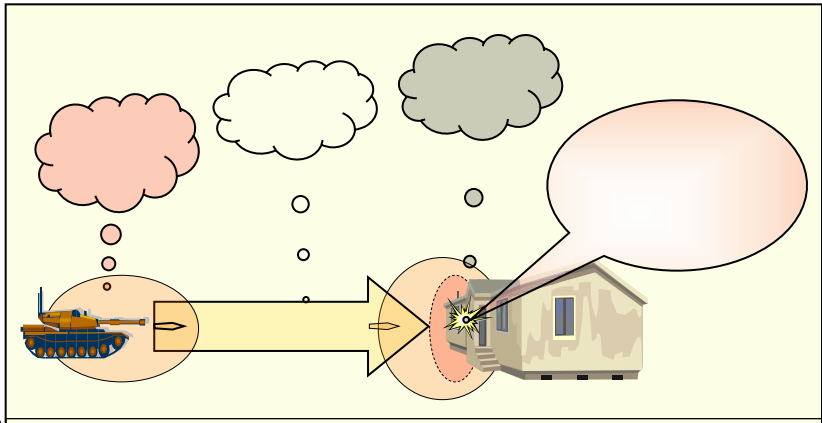

Urban theatre

Measures of Performance
Ammunition Requirements
Ammunition Effects
Fire doctrine
Development

Measures of Performance??
Ammunition Requirements??
Ammunition Effects???
Fire Doctrine??
Development??


IST: Experiments…

ammunition effect on, in front and behind the target

Wall (outer)
(inner wall)

- Ammunition
- Weapon system
- Impact velocity
- Weather conditions
- Photography
- Witness screens
- High Speed Video
- Blast measurements


Targets used

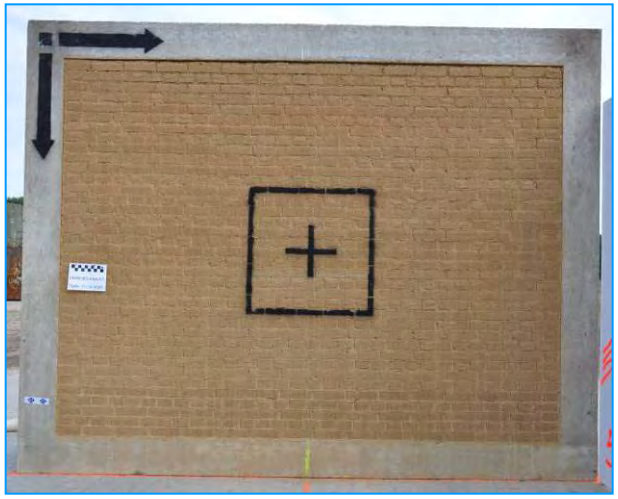

- Thickness:
  - 80cm - 40cm - 20cm
- Build-up
  - Drying time > 14 weeks

Mass (incl. frame) >> 7000 kg

- STANAG4536
  - Thickness: 20 cm
  - Double reinforcement
    - Reinforcement: 9mm bars at width of 10 cm


- Indirect fire (155mm)

- Tank (120mm)

- AT/ASM



- IFV (25 – 30 – 35 mm)


- Air-to-ground (20 – 25 – 30mm)


- Infantry (12.7mm)

TNO innovation for life

‘AMMUNITION’ ’IST+’ considered

AP-HE-MP-ABM-PELE-FAP

12.5mm (…)

20mm

25mm (YPR)

30mm

35mm (CV9035)

120mm (Leo2A6)

155mm (PzH)

60-90-110mm AT

&

TP

Firing distance 20-200 m

0 NATO & 45NATO

ADOBE-CONCRETE-BRICK

RHEINMETALL DEFENCE

DIEHL Defence

GENERAL DYNAMICS Ordnance and Tactical Systems

ATK ALLIANT TECHSYSTEMS

30mm GK
30mm Bushll
127mm

Dynamit Nobel Defence

Nammo

TNO innovation for life

HE (M107) on concrete (zoomed)
… Functioning of ammunition by impact…

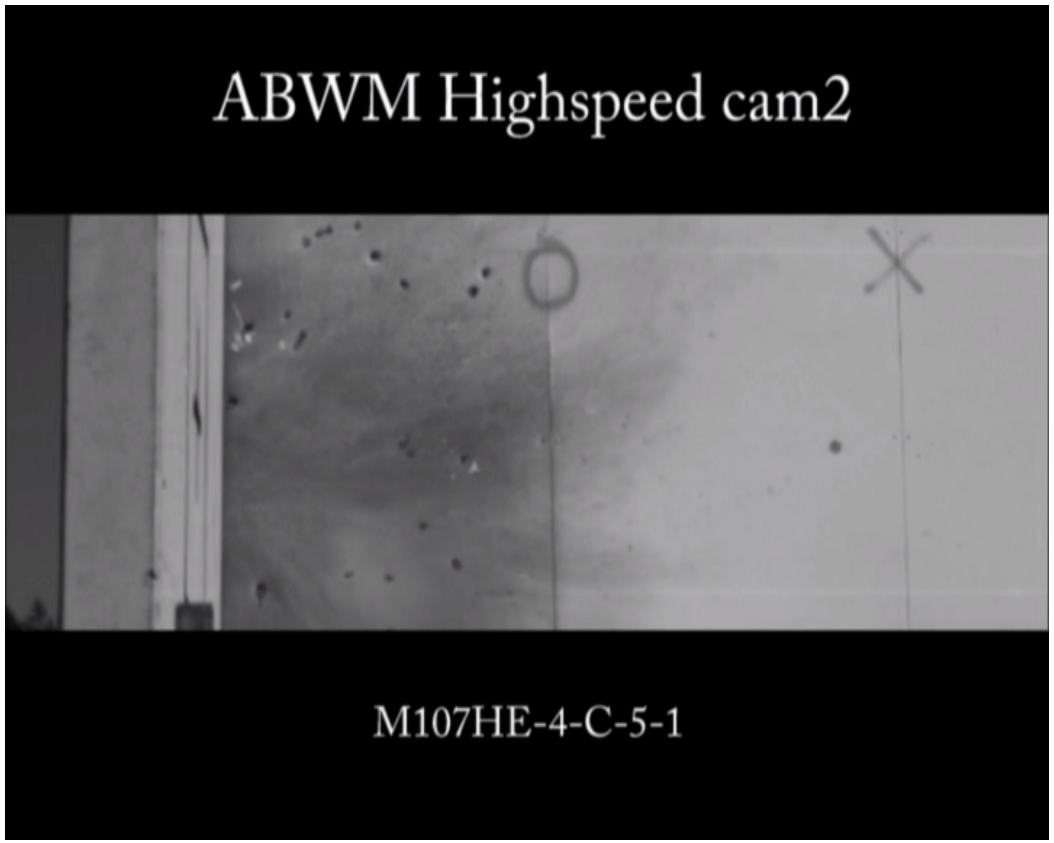

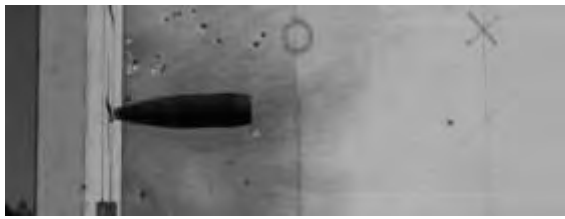

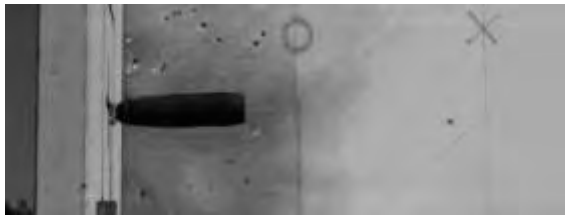

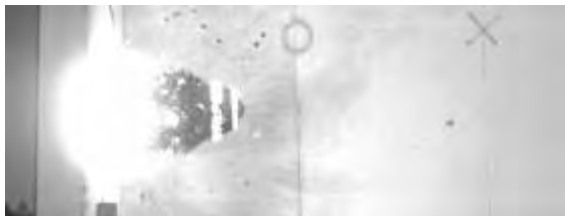

TNO innovation for life

High speed video frames…

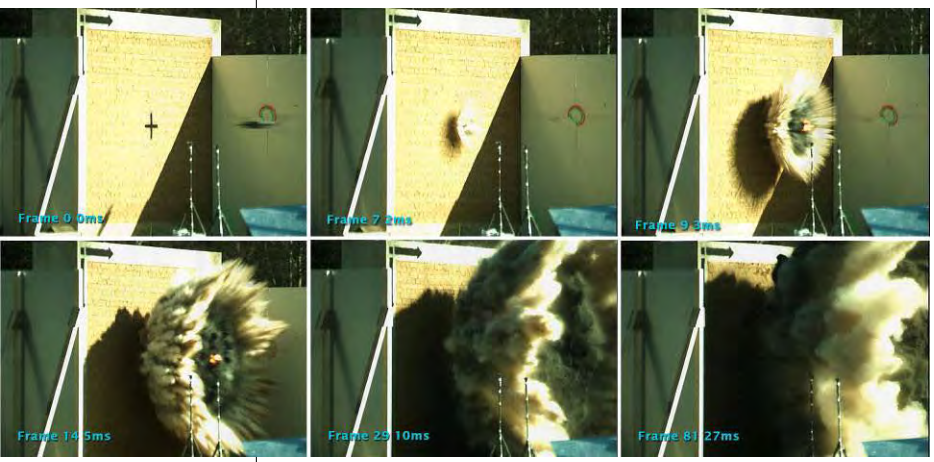

35 mm APFSDS (DM43) on 80 cm // 40 cm Adobe wall


TNO innovation for life

Breach effect

HEAT TP (DM18A4)

HEAT TP (DM18A5)

HEAT TP (M831)

HEAT TP

HEAT

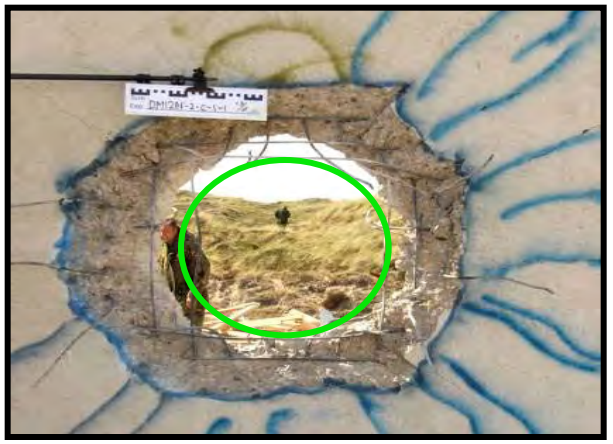

HEAT << **S/A distance**

TNO innovation for life

Multiple impacts

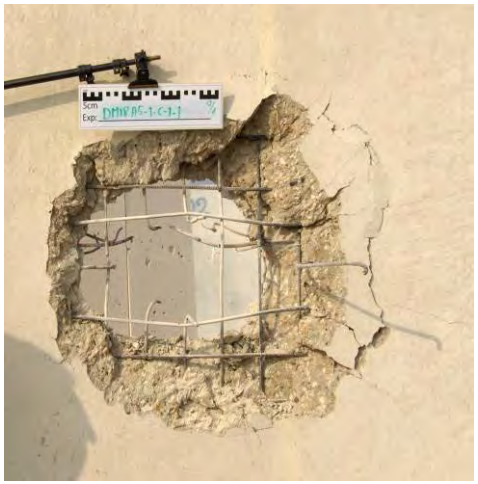	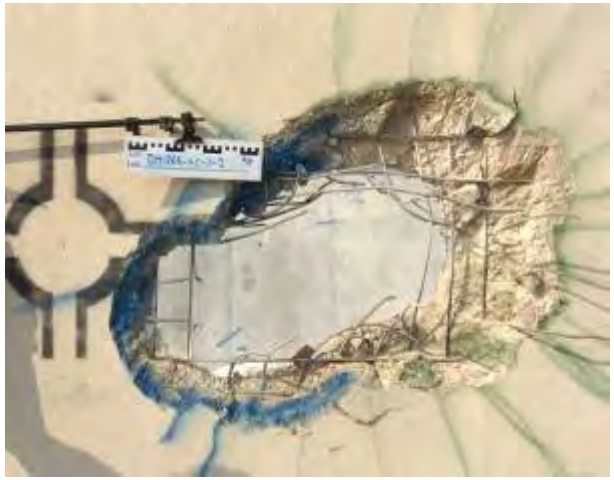	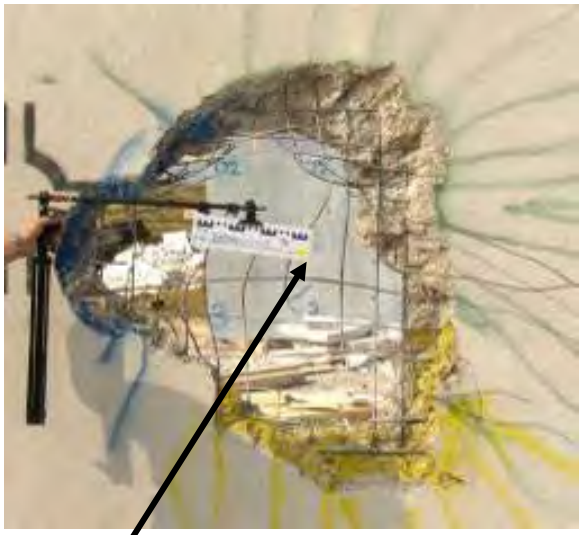
DM18A5 (1st shot)	**DM18A5 (2nd shot)**	**DM18A5 (3rd shot)**

Breaching (crater) effect is limited due to reinforcement

TNO innovation for life

35 mm KETF (nr468) programmed
Airburst: ignition at various distances

Damage at normal initiation distance

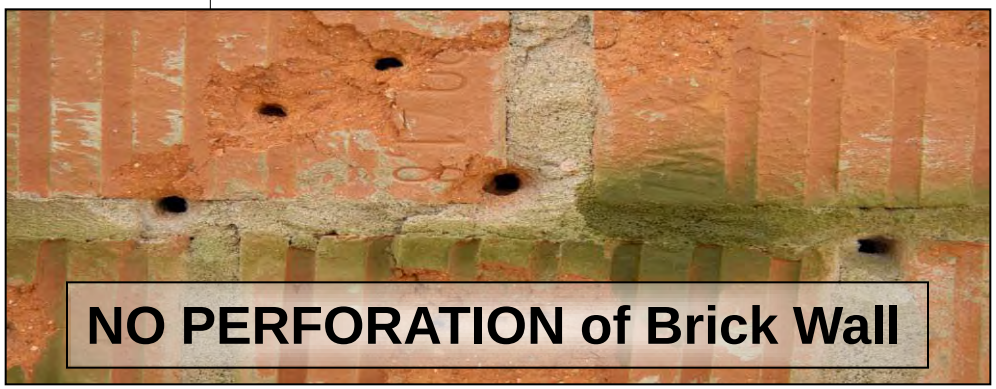
NO PERFORATION of Brick Wall


Ejected pellets


35 mm KETF (nr468) unprogrammed (Brick & Adobe wall)




TNO innovation for life

155mm effect on concrete target


Current ‘IST’ situation…

based on more than 250 firings…

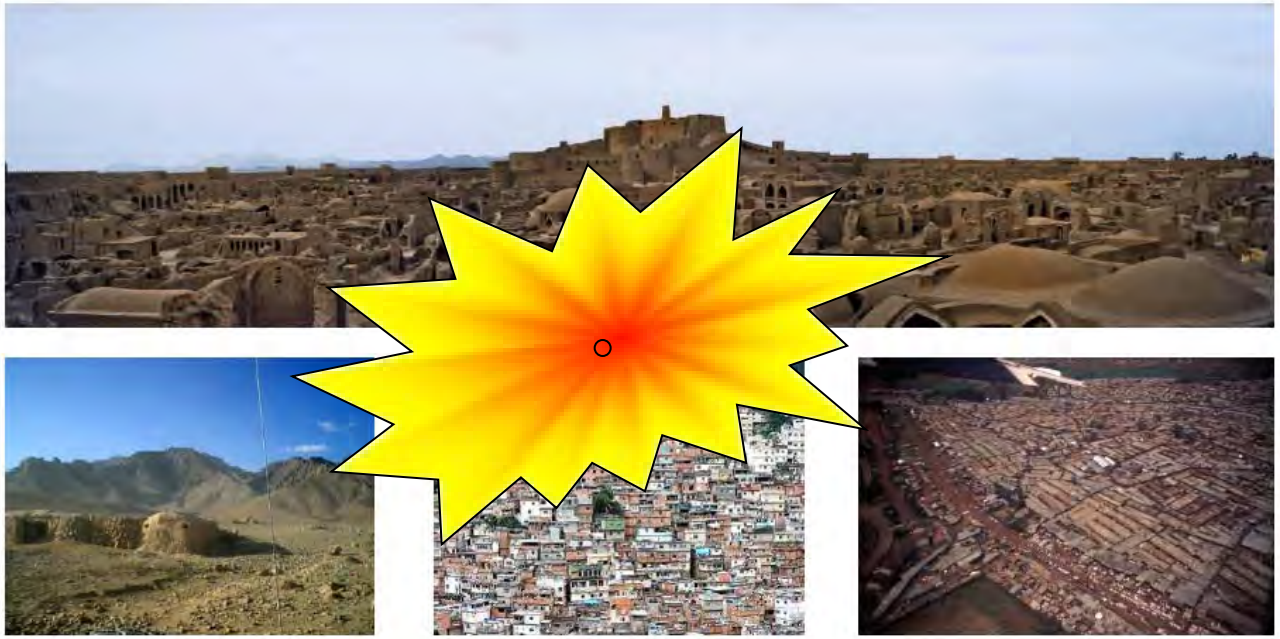

Ammunition procurement

Industry

TNO innovation for life

Qualitative Data Analyses

“Would you tell me, please, which way I ought to go from here?”

“That depends a good deal on where you want to get to”, said the Cat.

“I don’t much care where …” said Alice

“Then it doesn’t matter which way you go”, said the Cat

“… so long as I get somewhere”, Alice added as an explanation.

”Oh, you’re sure to do that”, said the Cat, “if you only walk long enough”

From: Alice’s Adventured in Wonderland, part VI “Pig & Pepper”, Lewis Carroll1865


TNO innovation for life

Qualitative analyses

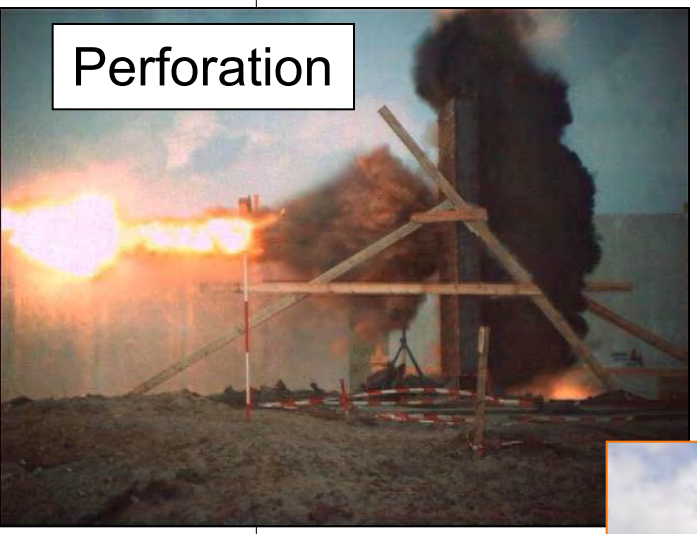

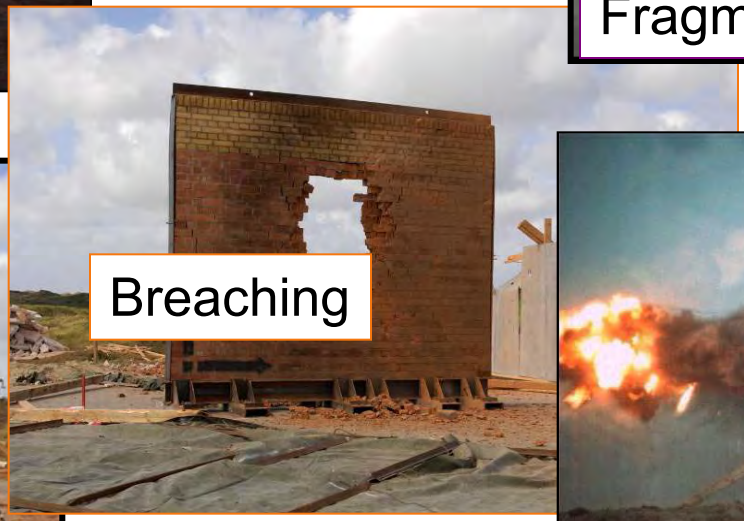

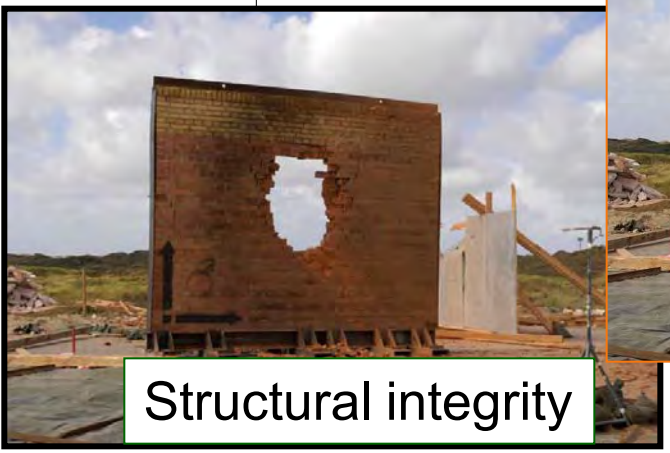


TNO innovation for life

and other effects

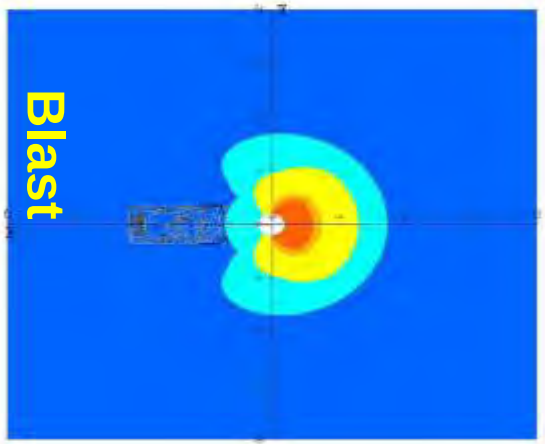

Operations in modern, confined theatre includes operational safety and risk for own and friendly troops, including third parties.

POTENTIAL COMMANDERS OBJECTIVES	Ammunition				
	???	???	???	???	???
Defeat target in front	-	+	+	+	+
Defeat target after wall	-	+	-	+	+
Breach wall	+	-	-	-	+
Defeat infra	-	-	-	-	+

POTENTIAL AREAS OF COMMANDERS CONCERN	Ammunition				
	???	???	???	???	???
Around weapon platform					
Flight zone	-	+	+	-	-
In front Wall	-	-	+	-	+
“Integrity” Wall/infra	-	-	-	-	+
Behind Wall	-	+	-	+	+

Some thoughts…
Ammunition and threat mechanisms generated

		Threat Mechanism					
		Blunt	Rod	Fragment	Jet	Charge	???
Ammunition type	TP	X					?
	AP		X				?
	AT				X	X	?
	HE			X		X	?
	HEAT			X	X	X	?
	??	?	?	?	?	?	?

Some damage observations …
in front / behind the wall …

	Threat Mechanism					
	Blunt	**Rod**	**Fragment**	**Jet**	**Charge**	**??**
Front debris	Minimal	Minimal	Minimal	Minimal	Much	
Behind deb.	yes	minimal	minimal	minimal	much	
Res threat	no	yes	no	yes	possible	

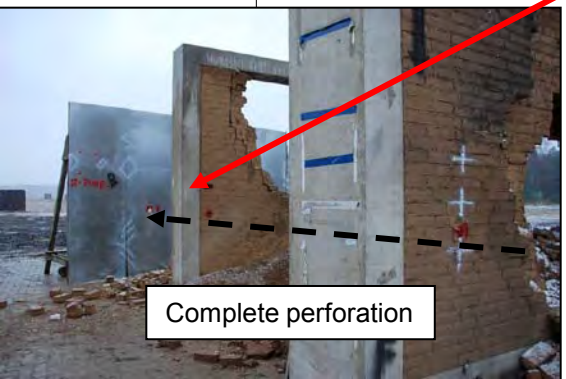


TNO innovation for life

Some damage observations… on the wall

	Threat Mechanism					
	Blunt	Rod	Fragment	Jet	Charge	??
Cracks front	Minimal	Minimal	No	No	Yes	
Crater front	Minimal	Minimal	no	Minimal	Yes	
Perforation ø	~ ø	~ ø rod	no	~ ø jet	Large	
Crater rear	relative	Minimal	No	Minimal	Yes	
Cracks rear	relative	Minimal	No	No	Yes	
Reinforcement	Local	Local	Intact	Local	Intact	
Deflection	minimal	No	No	No	Yes	
Integrity	Intact	Intact	Intact	Intact	Damage	


VL TARVAC assessment

- VL simulation environment: physical interaction → Military terms

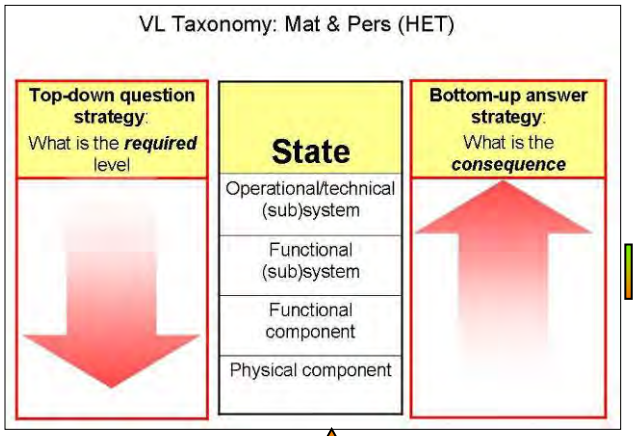

VL based simulations

Our VL modelling focus

- To assess ammunition – target interaction effect in terms of:
  - Measures of Succes ("Pk – Bonus") in combination with
  - Measures of Concern ("Pk - Malus").

	Metrics					
	Success	Integrity	Collateral	Risk	Safety	Tempo
Def. target before wall						
Def. target behind wall						
Breach						
Def. infra						

TNO innovation for life

SNEAK PREVIEW

SOLL - Application of gained knowldege

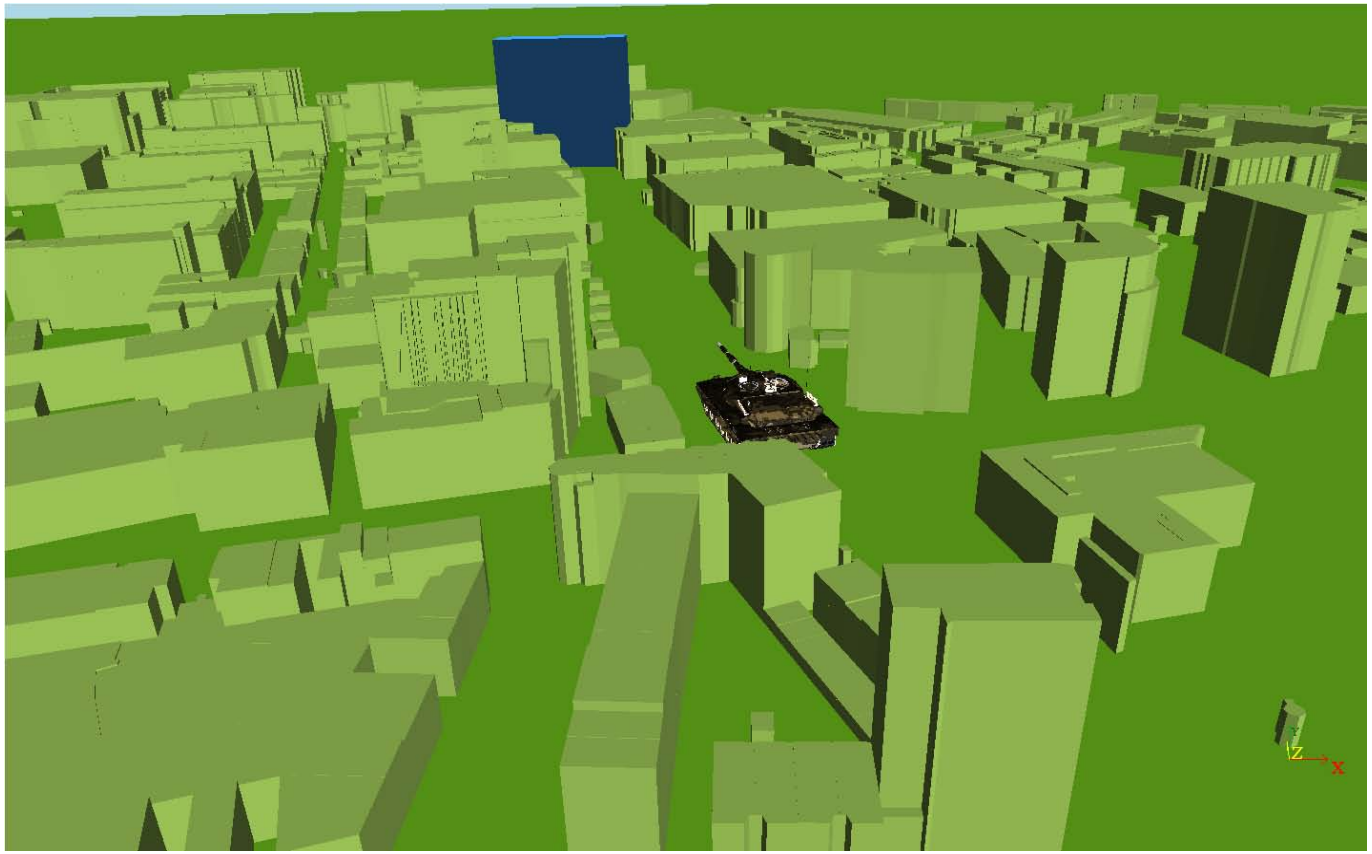

TNO innovation for life

SNEAK PREVIEW

Selection of ammunition

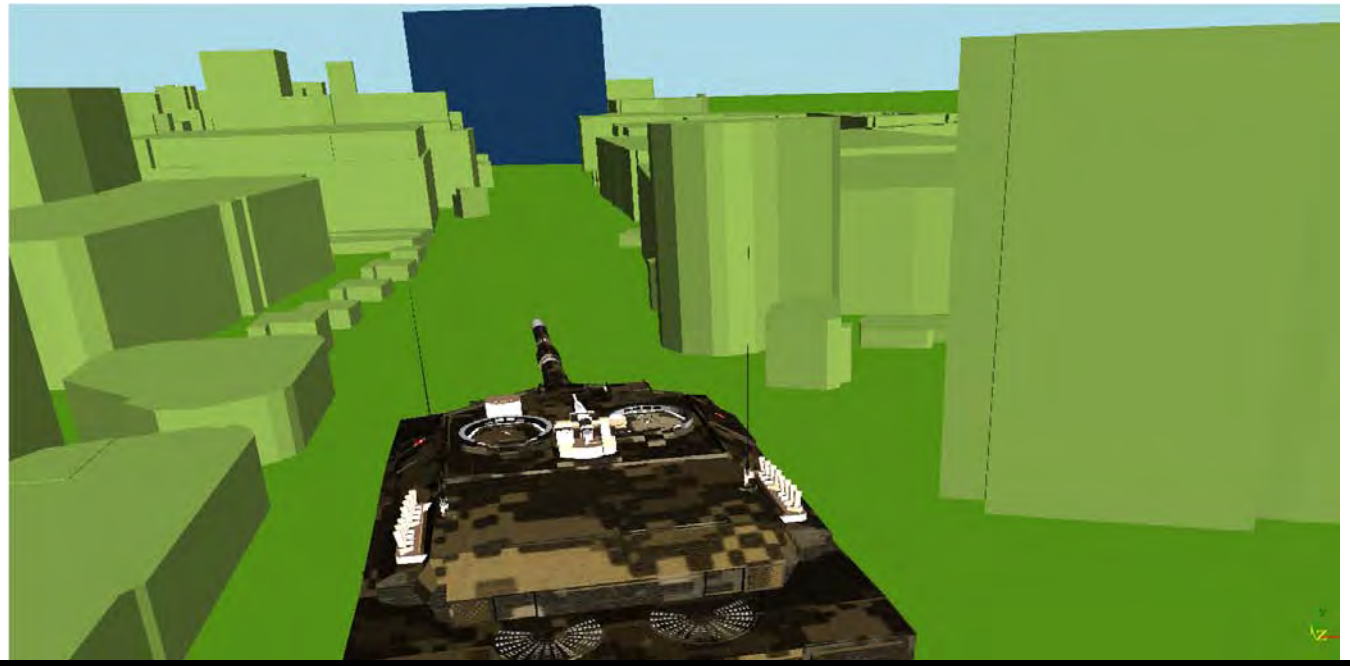

- Mun-1
- Mun-2 ←
- Mun-3
- Mun-4

TNO innovation for life

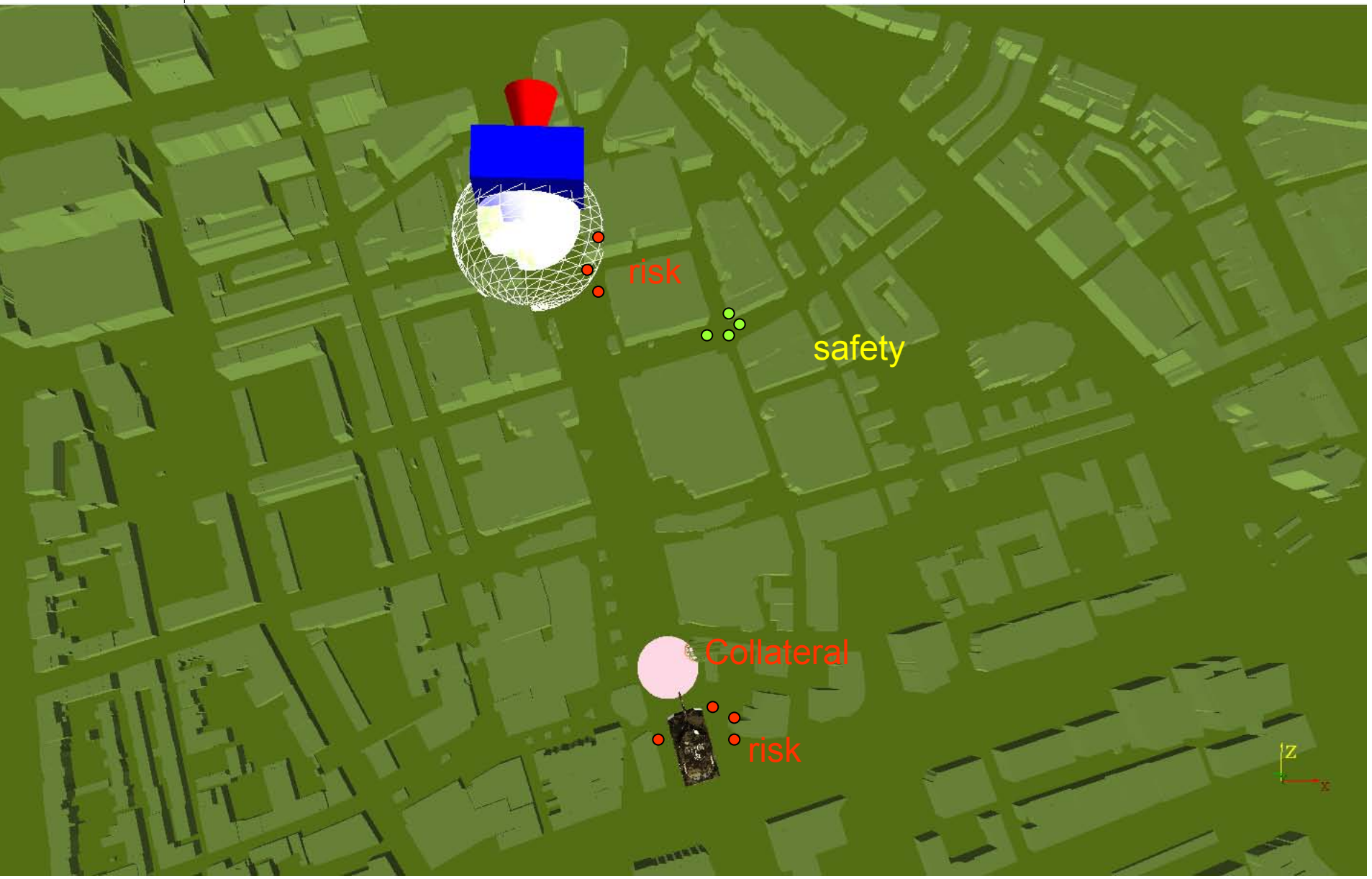

UO

Combined / joint <-> opposing weapon systems

Munition deployment

Doctrine | O&T | Preparation | Operation

Strategic Munition storage

Mission Munition storage

Munition Logistics

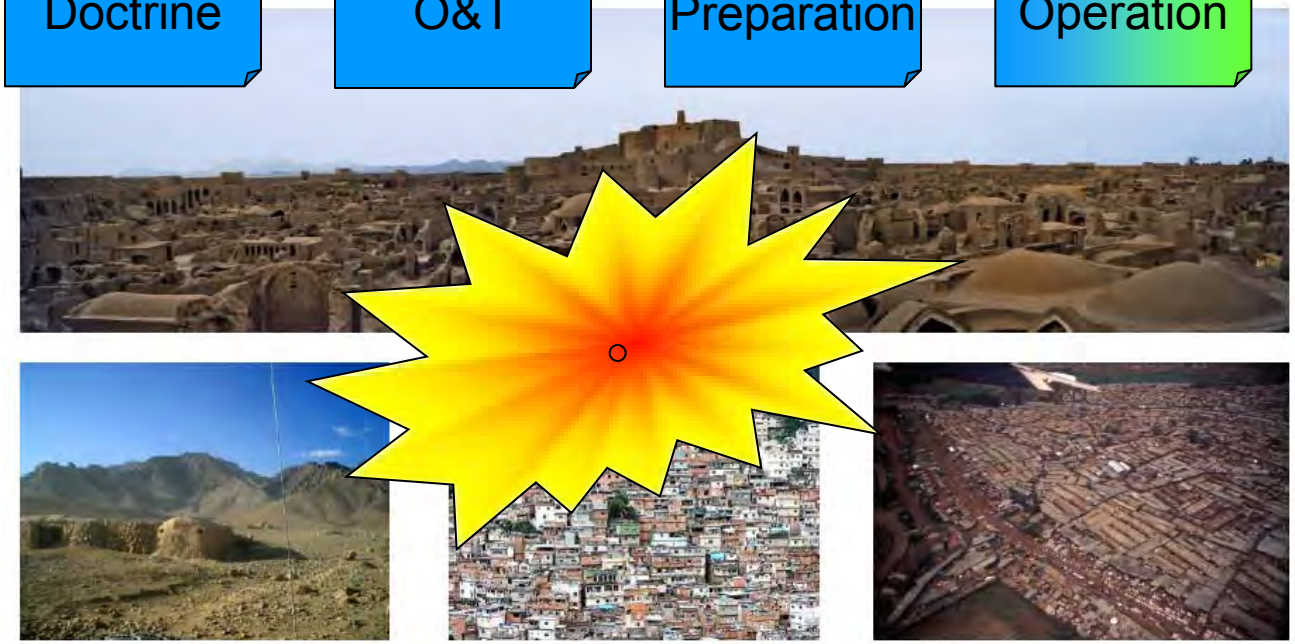

Materiel

Personal

Infra

Ammunition procurement

Industry


Conclusion….summary

- IST
  - Large scale experimental program & analyses
- SOLL
  - Discussion between Defence – Research – Industry
  - International Standardisation
- VL TARVAC 7 modelling in progress, including
  - MOUT targets
  - Single target -> scenario
  - Multi-metrics assessment
  - Time included

PoC Hans Hoeneveld
NL - DMO / Ammunition Department
JC.Hoeneveld@mindef.nl

Theo Verhagen
TNO Defence, Security and Safety
Theo.Verhagen@tno.nl

TNO innovation for life

Finite Element Modeling of Primer Impact to Understand the Dynamics of Misfires

Mark Lee, P.E.
Finite Element Analysis Engineer
ATK Small Caliber Systems
(816) 796-5155
MarkD.Lee@atk.com

September 15, 2011

OSR #11-S-1835

Goals for Primers

Reliable and Consistent Performance

- **No Misfires**
- **No Inadvertent Firing**
- **No Leaky Primers**
- **No Pierced Primers**
- **No Dropped Primers**

Goal for this Analysis

Quantify the effects of Geometry and Material Strength on Primer Sensitivity

- **Geometry—Base Thickness—Thin or Thick**
- **Material Strength—Cup Hardness—Soft or Hard**
- **Combination determine Primer Strength**
- **Both controllable in manufacturing**
- **FEA eliminates other variables for focus**
- **FEA can differentiate results with finer resolution than bang or no bang**

Finite Element Model—Primer

Axisymmetric Finite Element Analysis using ABAQUS Explicit

Two Primer Cup Geometries—Thin and Thick = 4/3 Thin

Two Primer Cup Materials—Soft and Hard

Mix material model designed to approximate events leading to detonation

All else the same

Thin

Thick

Material Models—Primer Cup

Soft Implies Low Elastic Limit

Hard Implies High Elastic Limit

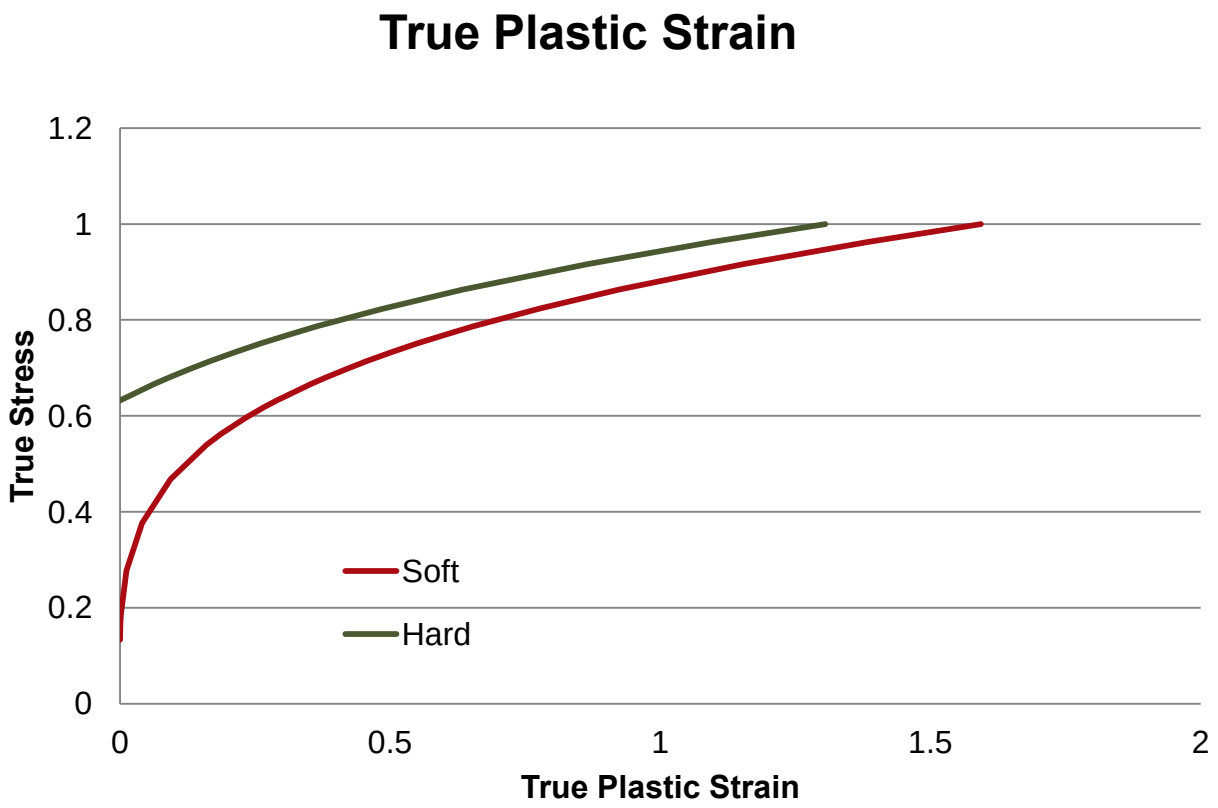

The Finite Element Model—Assembly

Identical for every simulation—not possible in physical testing

- **Energy input to firing pin—low for a weapon**
- **Firing Pin**
- **Bolt Face**
- **Primer Anvil**
- **Primer Depth**
- **Case**
- **Chamber**

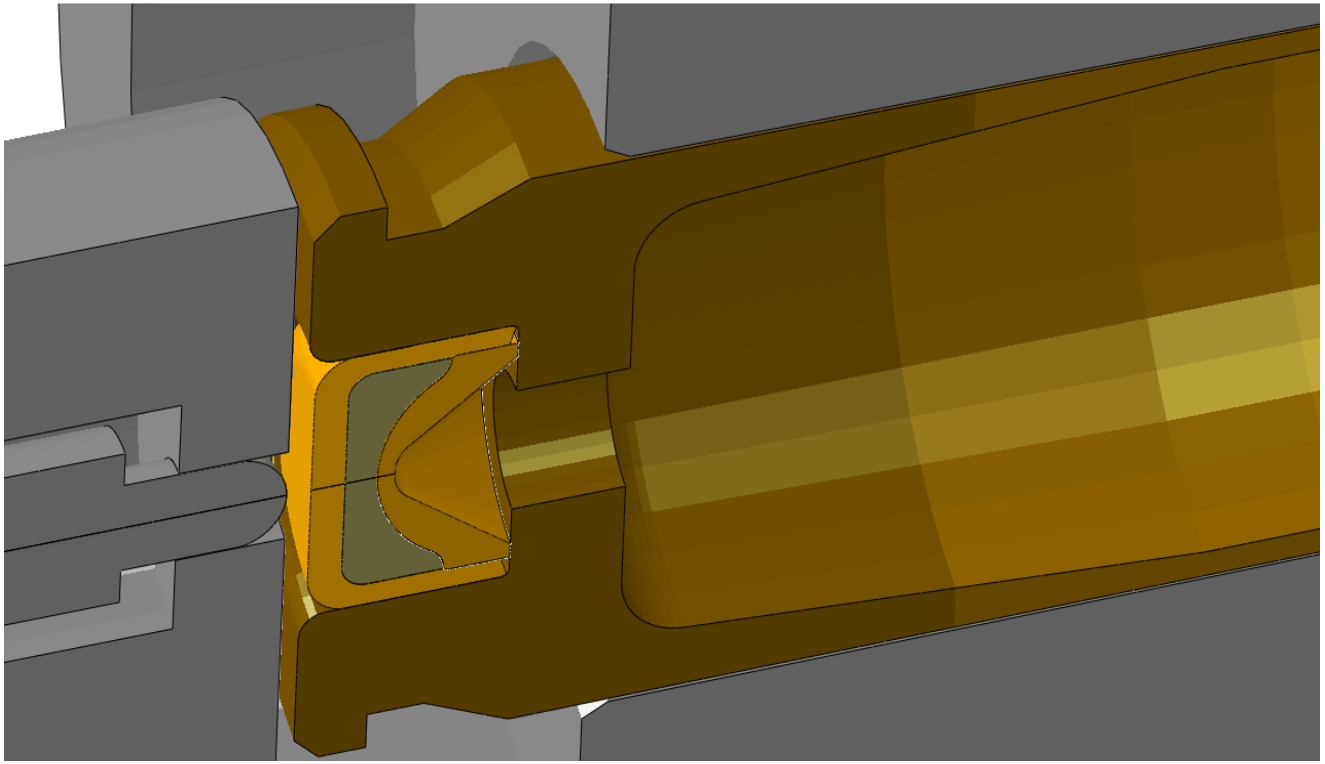

Primer Impact Sequence Shows Pressure Development

A premier aerospace and defense company

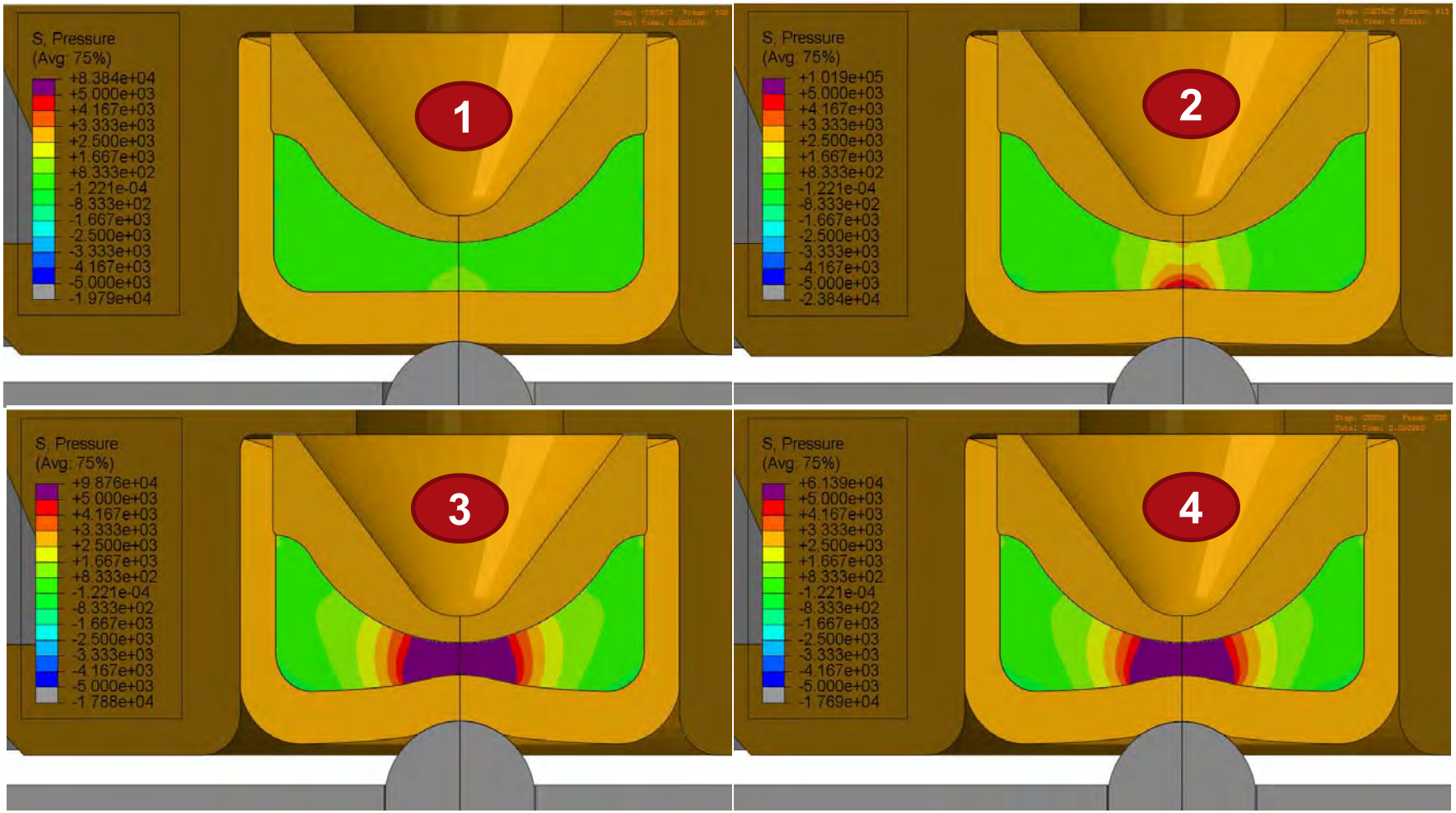

Extent of “threshold” pressure

A premier aerospace and defense company

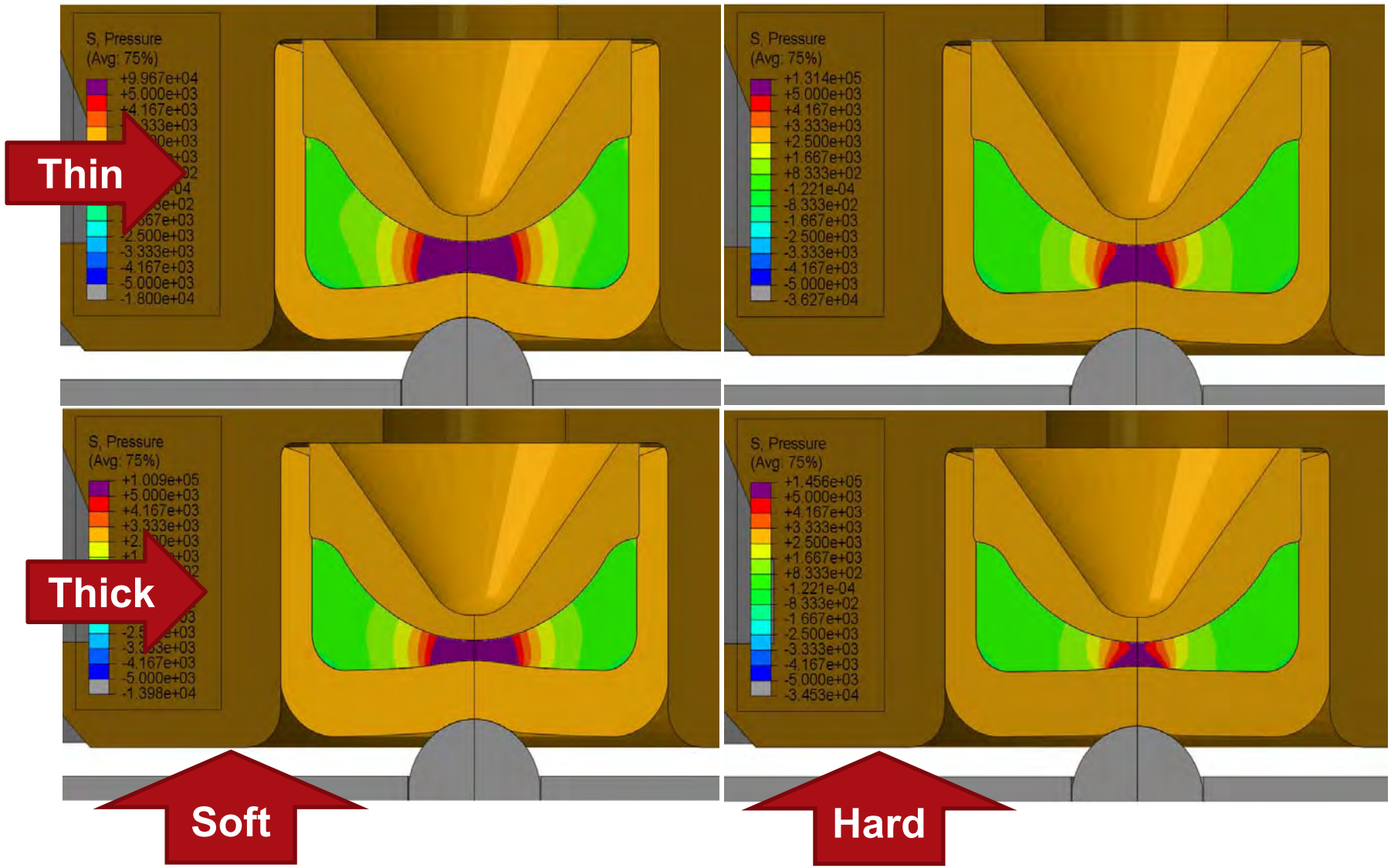

Displacement and Pressure

The green curves show displacement at the top and bottom center of the mix

The red curves show pressure

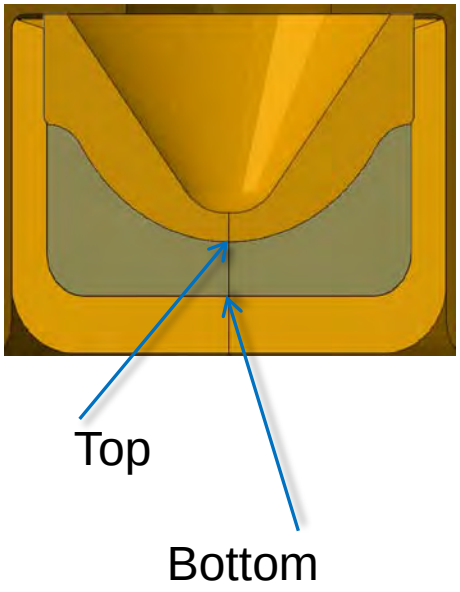

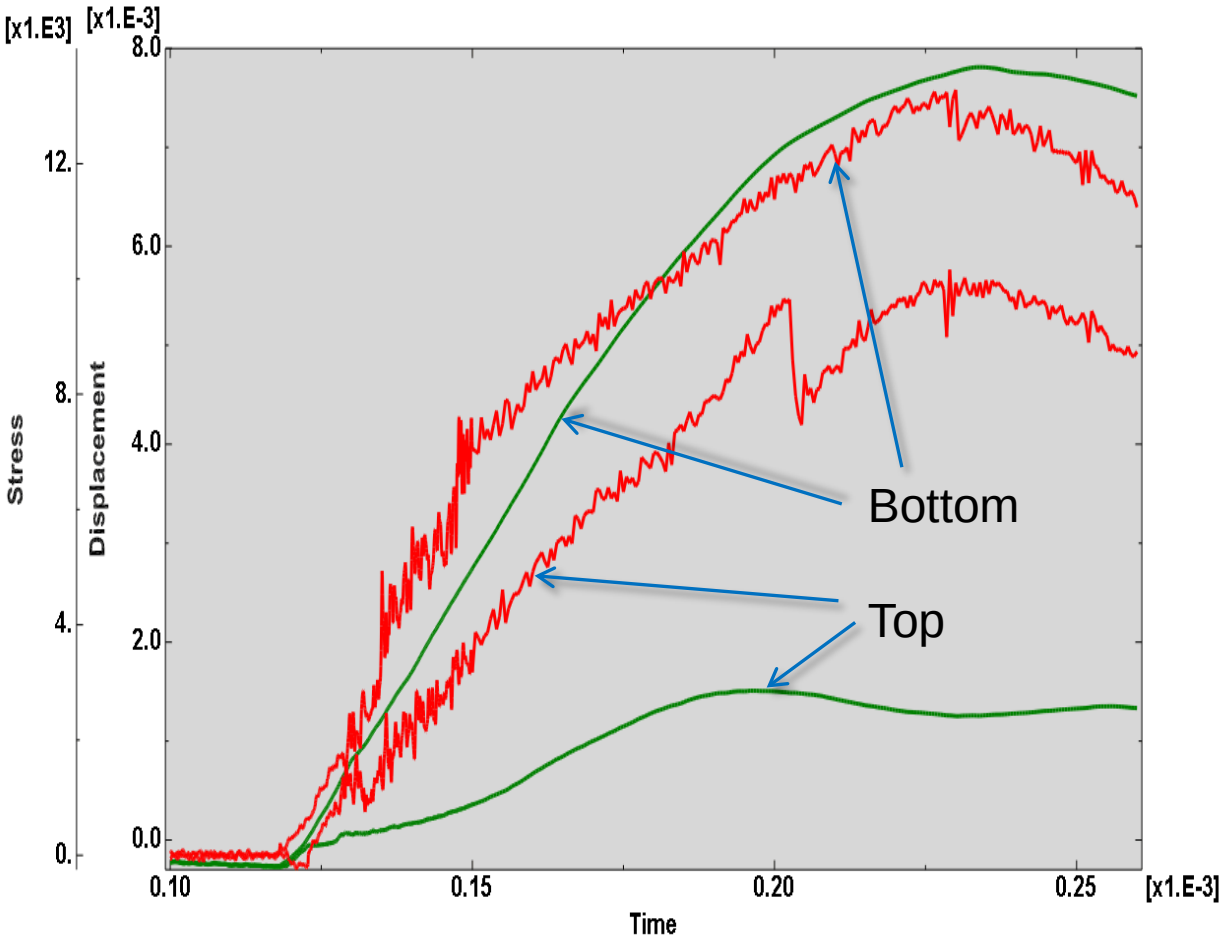

Pressure and Displacement History

A premier aerospace and defense company

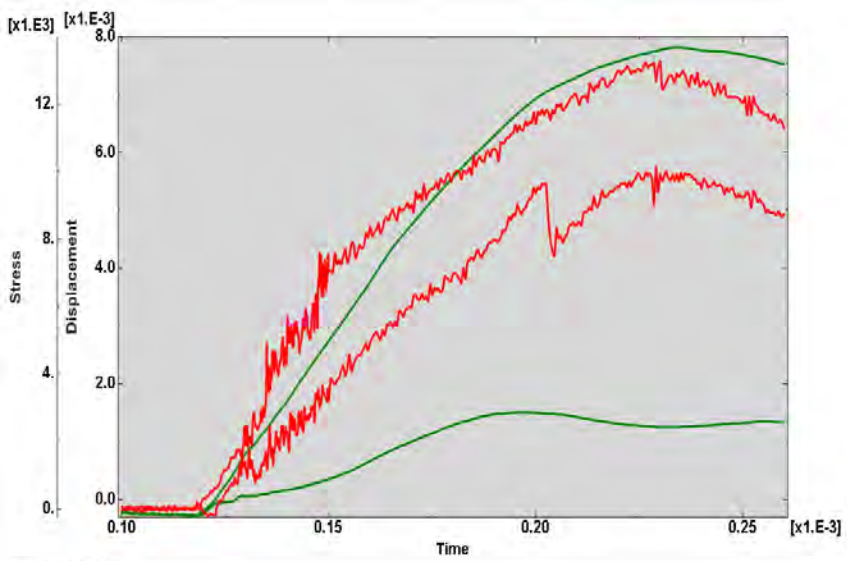

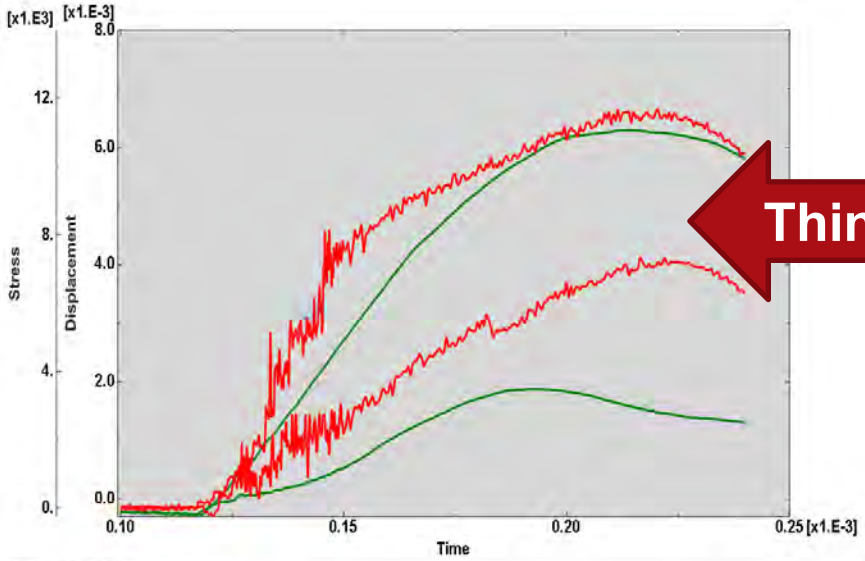

Thin

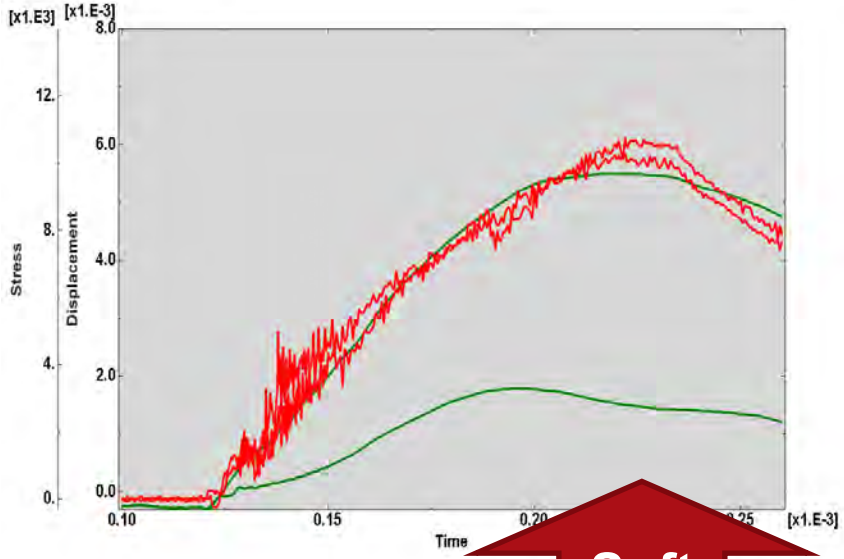

Soft

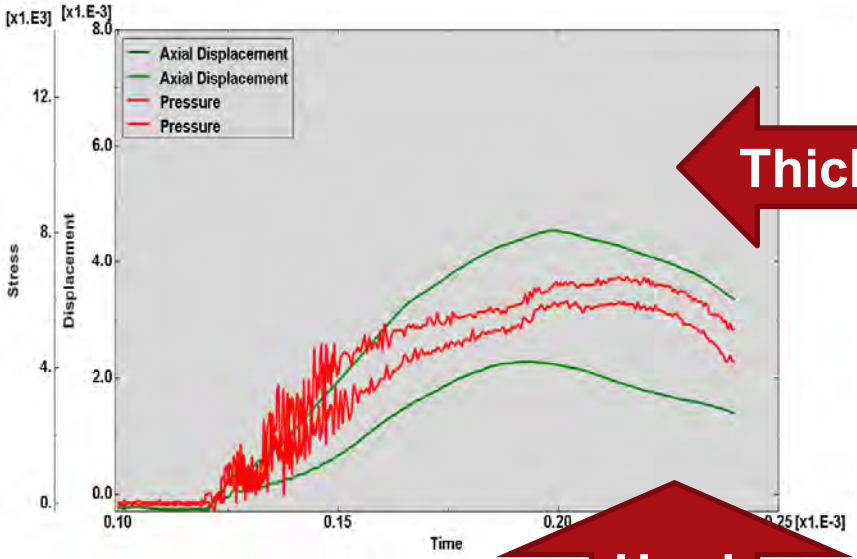

Thick

Hard

Conclusions

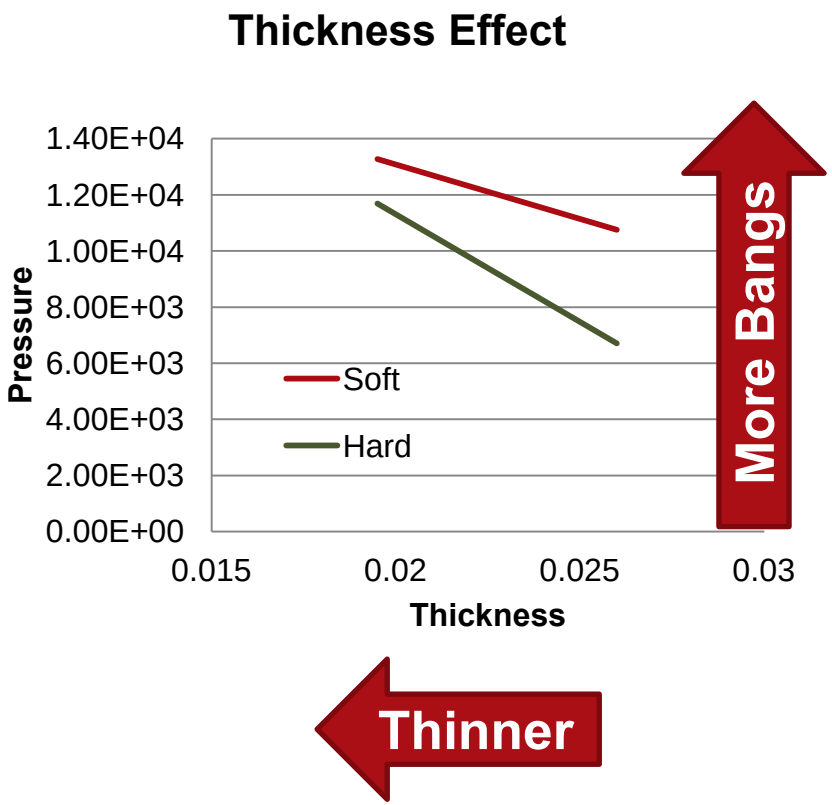

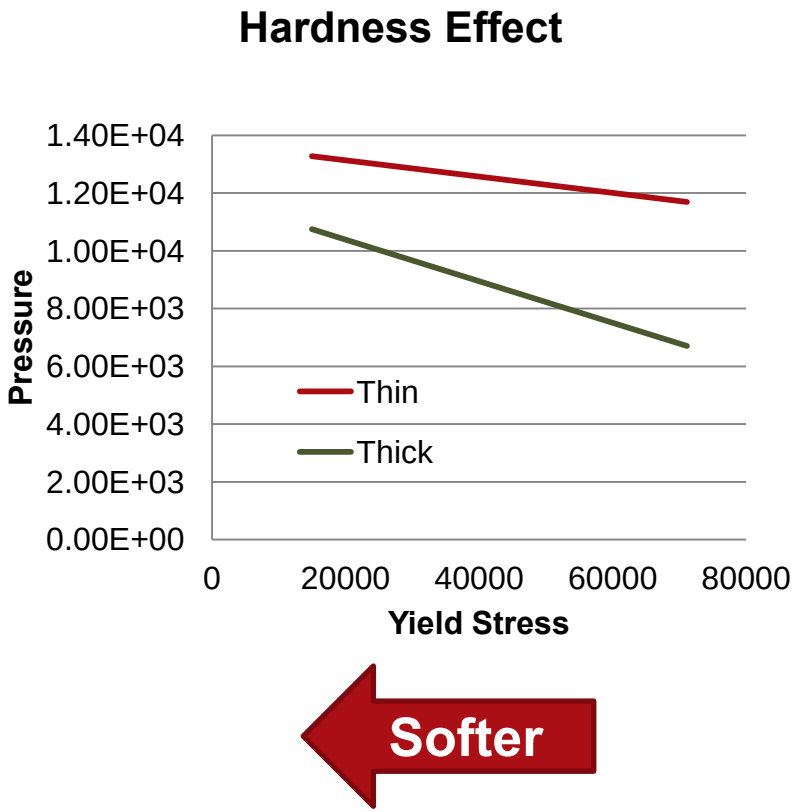

Penetration of Rigid Projectiles in Sand

presented by

Stephan Bless
Institute for Advanced Technology
sbless@iat.utexas.edu

Co-authors: William Cooper, Keiko Watanabi.
Collaborators: Bobby Peden, Garet Itz, Magued Iskander

Three shape projectiles and two sands

Investigator	Projectile	Sand	Notes
IAT	Steel and W L/D=10 hemi nose	Ottawa	Stablized Horizontal
OU	Steel L/D=2 flat	Eglin	Vertical
AFRL	Steel L/D=5 hemi	Eglin	Horizontal
IAT	Steel .50 bullet	Ottawa	Horizontal

Sand density was “as poured”.
Projectile diameters: OU-26, AFRL-20, IAT-5 or 7.5 mm

IAT projectiles were stabilized rods

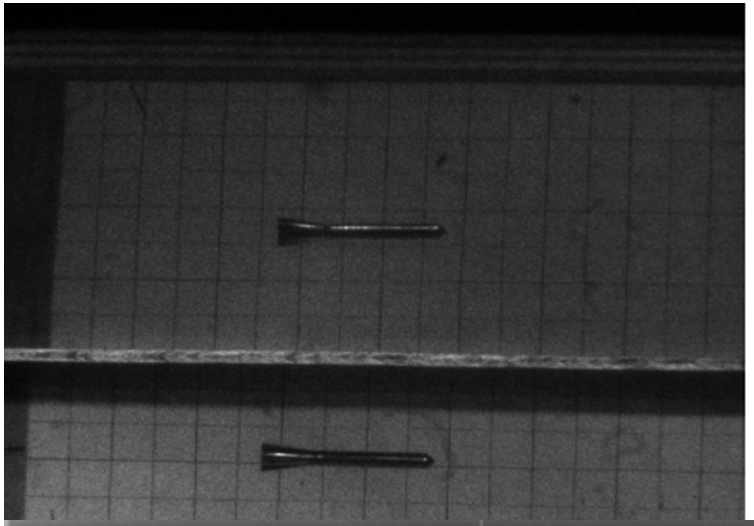

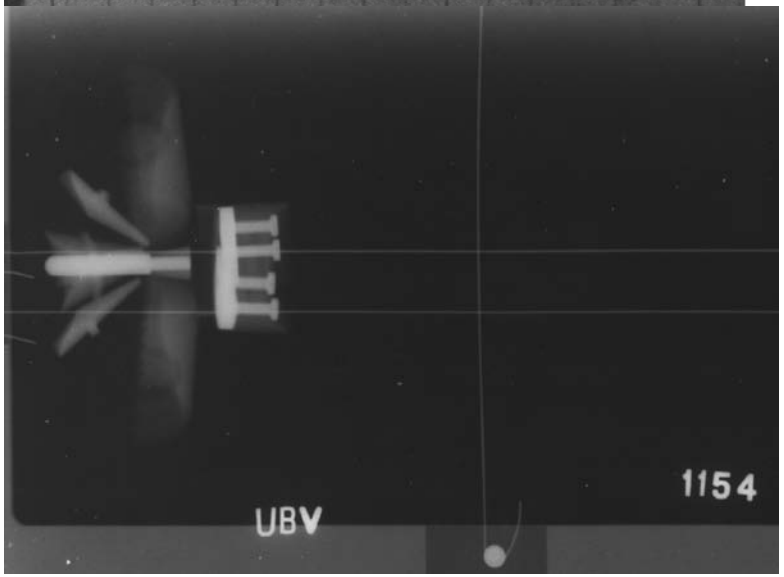

50 mm long, 15 g mass
These projectiles stayed rigid up to about 700 m/s.

Penetration in stand leaves trail of fractured grains

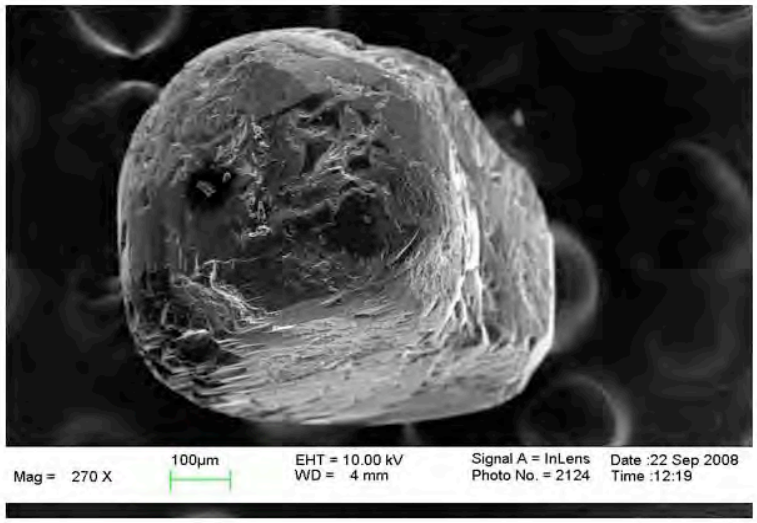

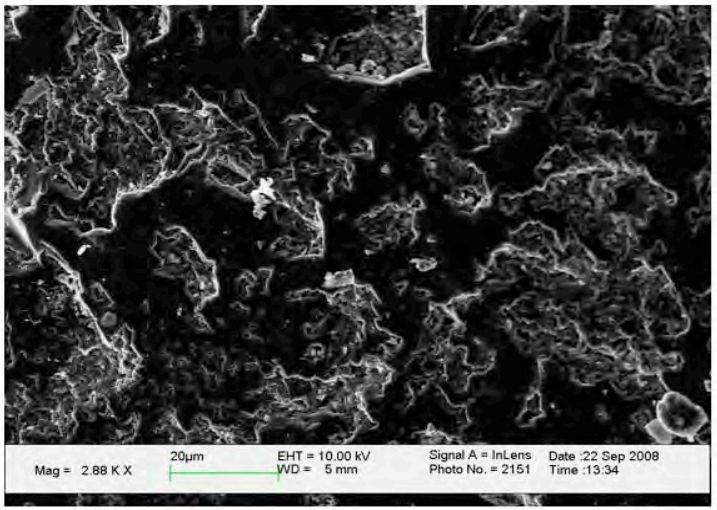

Some trends seen in data

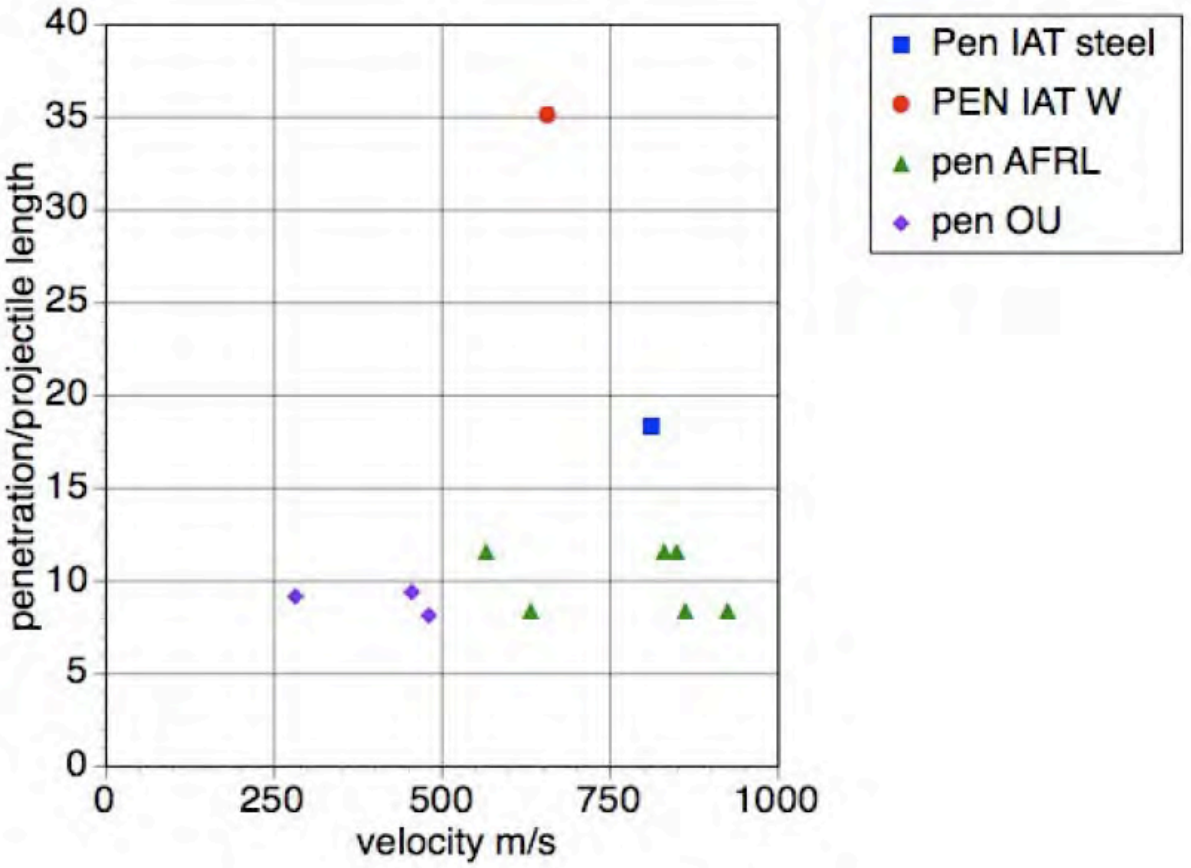

Penetration scales as sectional density.

The angular Eglin sand is harder to penetrate than Ottowa sand.

Penetration is only weakly dependent on velocity.

Final stage of penetration takes place at relatively low velocities.

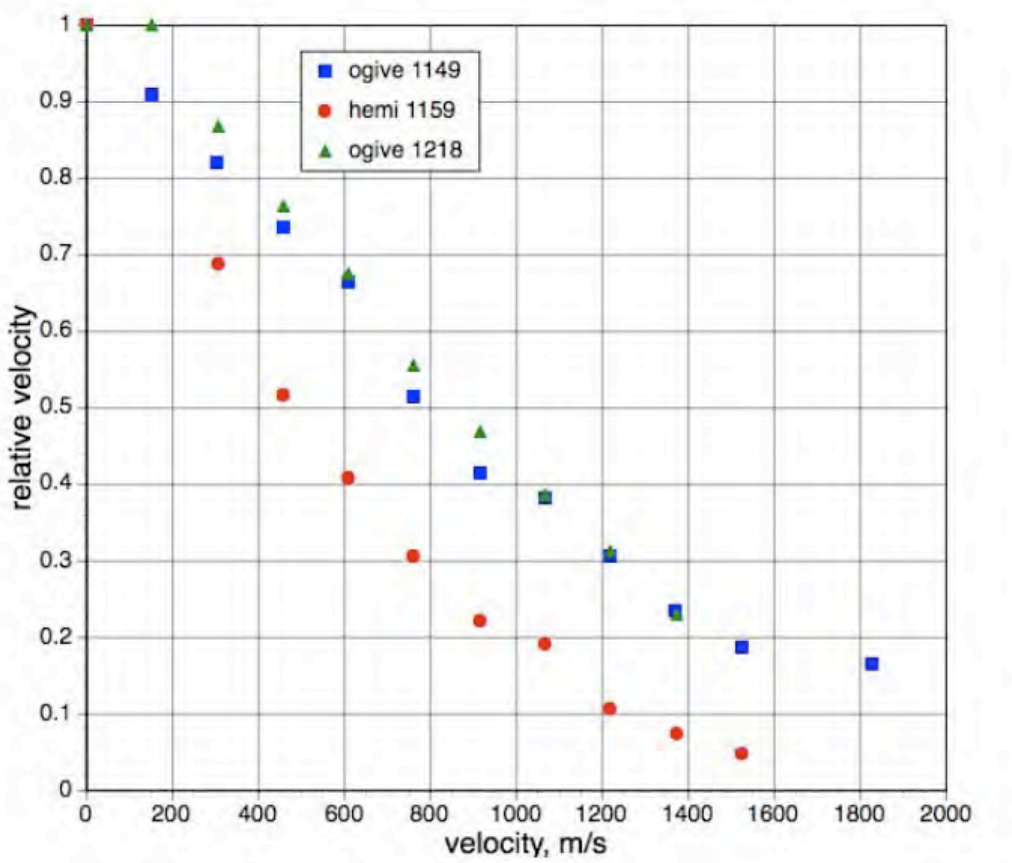

This implies that there is a lot of penetration at very low speed. Measuring penetration depth is probably not a very good way to characterize projectile performance.

Projectile motion described by Poncelet Equation

$$M\frac{dV}{dt} = -(\rho_s C_p A V^2 + R)$$ Poncelet

$$x = \frac{M}{\rho C A}\left[\ell n\left(1 + \frac{V_0 \rho C_p A}{M}\right)t\right].$$

R=0 is purely drag. Then penetration is infinite.

$$x = \frac{1}{k} ln\left[\frac{V_0^2 + \frac{R}{\rho C_p}}{u^2 + \frac{R}{\rho C_p}}\right],$$ $K=2\rho C_p/\rho_p L$

Penetration prediction

Effect of static strength

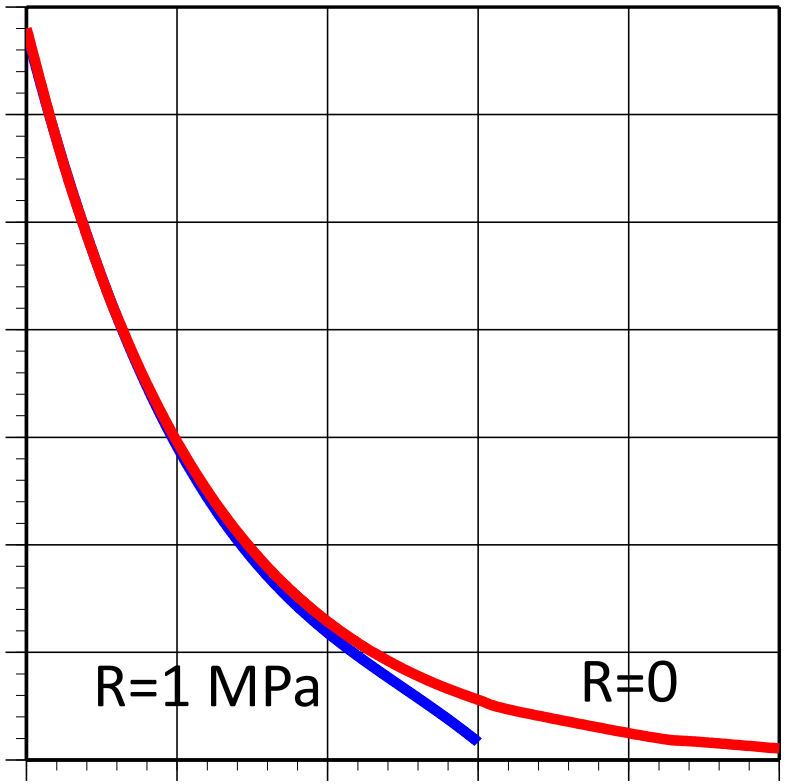

Final depth of penetration very sensitive to ill-defined static strength of sand.

More precise measurements of C

A PDV was used to observe the back of .50 bullets as the embedded into sand targets.

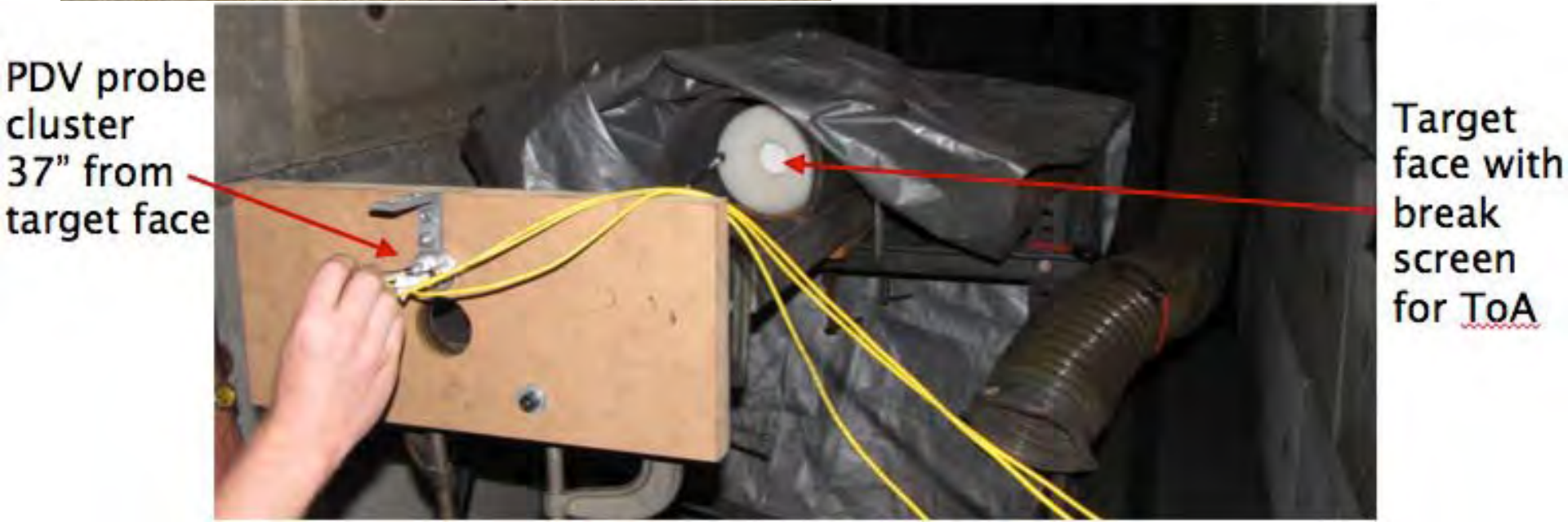

This was inspired by experiments from OU group.

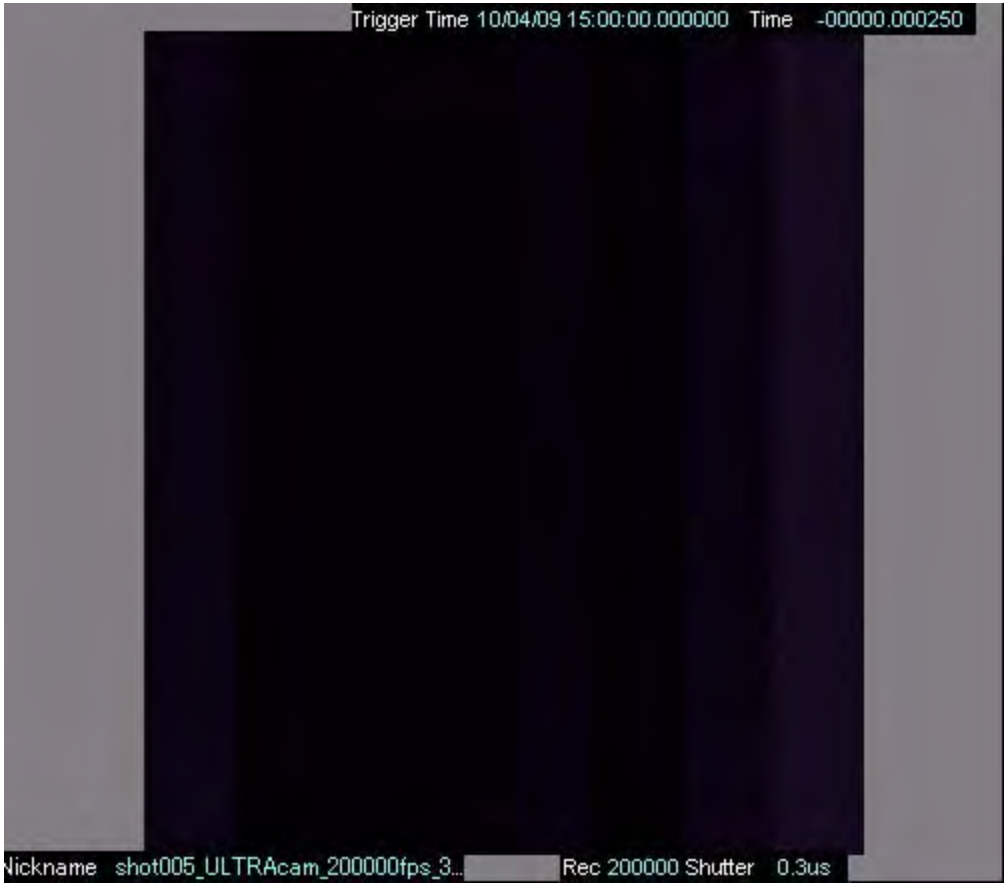

Deceleration of .50 ogive

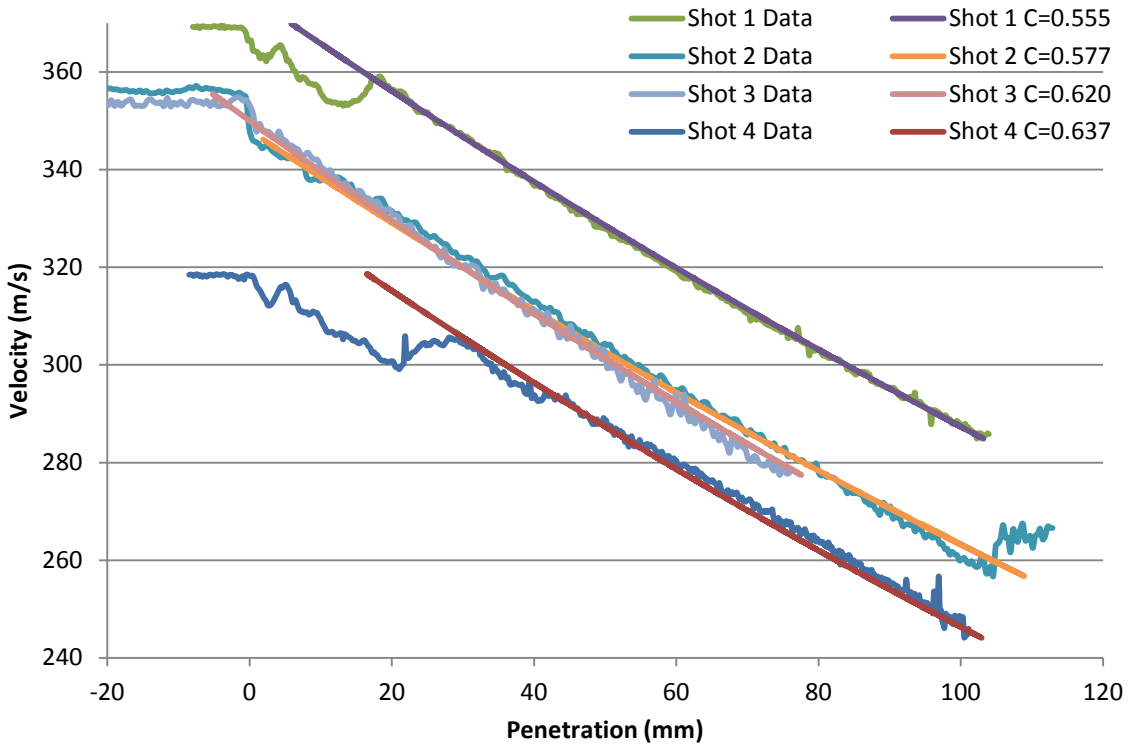

Four shots. Projectile could be followed for 100mm! Deceleration nearly constant. Data are fit to V^2 force law. This defines the "effective drag", C'. We find C' is about 0.6 and decreases slightly with velocity.

The initial transient is due to jacket setback

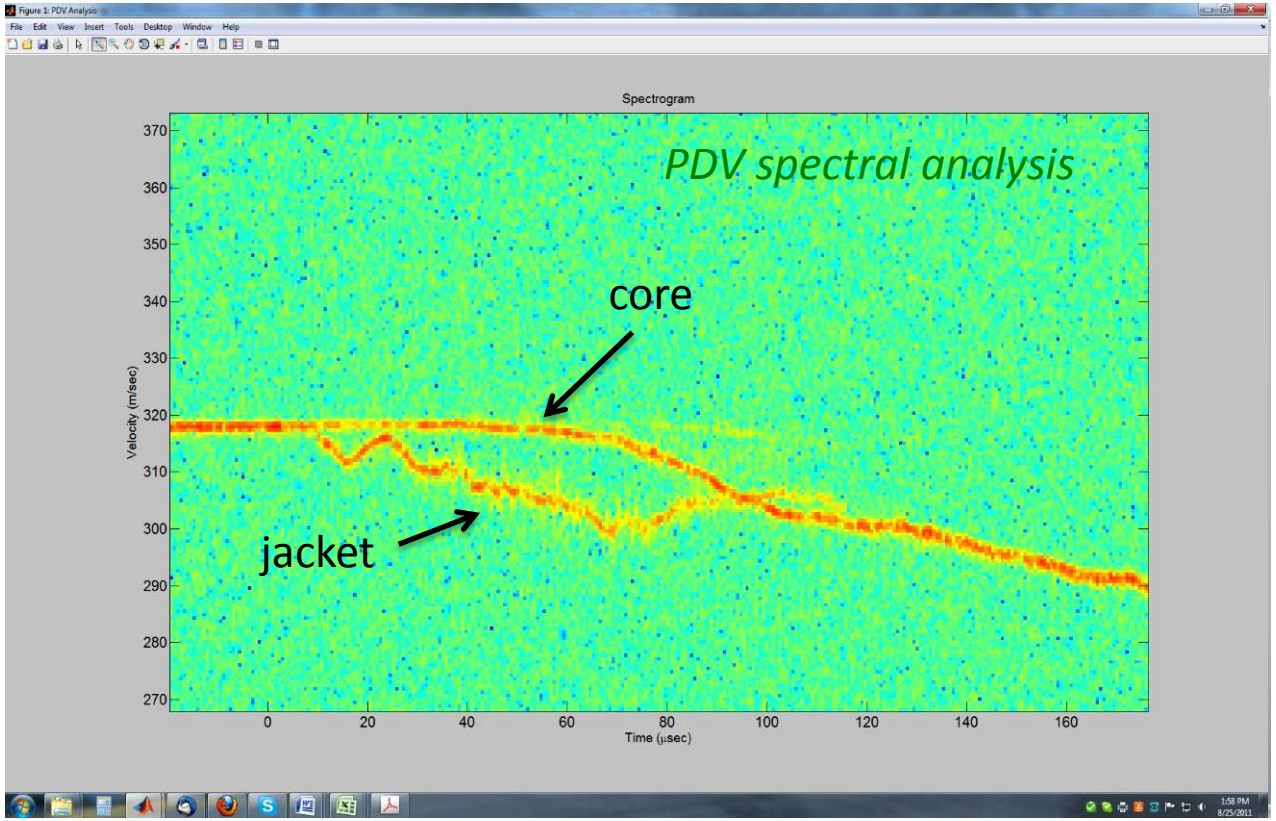

The PDV separately tracks distinct velocities. This slippage integrates to exactly the observed value of about 1 mm. (The data processing algorithm picks the brighter branch.)

Role of strength of sand

- Sand is usually modeled with strength proportional to pressure. E.g. Laine and Sandvik:

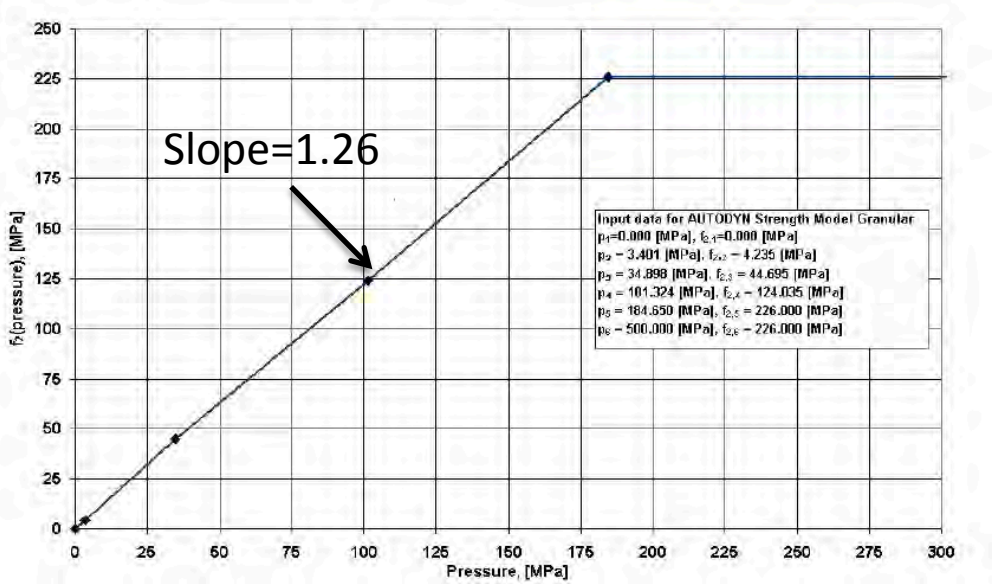

- If we take R ≈Y = αP, and P = ½$\rho_s V^{2,}$ then the effective value of C, C', is given by

$$C' = C_P + \alpha/2$$

since the peak stress at our velocity is below the 177 MPa cap.

Effective drag C' has two sources

- C_p is assumed due soley to KE delivered to sand. Our projectile is similar to a 1:3 cone. If V = velocity of projectile, the sand moves laterally with velocity u = V/3.

- In time Δt, the loss of energy of the projectile is $\rho_p LV(dV/dt)\Delta t$. The gain of energy of the sand is $\frac{1}{2}\rho_s V\Delta t u^2 = (1/18)\rho_s V^3\Delta t$. This implies

$$dV/dt = -(1/18)(\rho_s/\rho_p)V^2/L$$

The Poncelet solution (for R=0) is $dV/dt = -C_p(\rho_s/\rho_p)V^2/L$

Hence C_p=1/18 for a 1:3 nose.

Caveats in the analysis on this and previous slide:

We do not know the "wetted area"

We do not know alpha for dynamic compression of Ottawa sand

The impacts are transonic in thesdand.

Importance of strength

- From Laine and Sandvick, $\alpha = 1.26$.
- Thus, the dynamic strength alone gives C'=0.63.
- Combined C' should be about 0.68.
- Indeed this is very close to the observed value.
- The implication is that most of the penetration resistance of sand is due to Mohr-Coulomb strength, e.g. friction.

Conclusions

- Penetration depends on sand type, sand density, and projectile density.
- The more angular Eglin sand is harder to penetrate.
- The penetration resistance of sand is to a good approximation proportion to velocity squared.
- Most of the resistance of sand is due to friction.
- For a given type of sand, total penetration depends little on velocity.

sbless@iat.utexas.edu

Measurement of Blast Reflected Overpressure at Small Charge Standoff with Tourmaline Piezoelectric Transducers

Roger L. Veldman, Ph.D.
Hope College

Mark W. Nansteel, Ph.D.
Battelle Memorial Institute

Charles Chih-Tsai Chen, Ph.D.
Transportation Security Laboratory
Science and Technology Directorate
U.S. Department of Homeland Security

September 16, 2011

Homeland Security
Science and Technology

Presentation Outline

- TSL and EEL Overview
- Objective
- Literature Survey
- Test System and Setup
- Test Results
- Conclusions

Homeland Security
Science and Technology

Explosive Effects Laboratory (EEL)

Mission: The Explosive Effects Lab performs fundamental research to characterize improvised explosive devices and their effects on structures.

Focus:

- Research Area 1: Blast response testing and measurement
- Research Area 2: Explosive characterization & equivalency testing
- Research Area 3: Blast response modeling & simulation
- Research Area 4: Blast effects mitigation

Homeland Security
Science and Technology

Objective of the Study

Conduct explosive tests to measure blast reflected overpressure and impulse at small charge standoff using tourmaline piezoelectric transducers.

Overpressure and Impulse are important and useful parameters for quantifying:

- blast intensity
- characterizing the blast loading of structures
- assigning explosive equivalence.

Homeland Security
Science and Technology

Literature Survey

Previous Small-Standoff Measurement Studies

Authors	**Year**	**Test Method**	**Charges** (Pentolite spheres)	**Standoff (inches)**	**z (ft/lb$^{1/3}$)**
Johnson et al. [3]	1957	Impulse Plug	1/2 – 2 lb	5 - 38	0.5 - 2.5
Huffington and Ewing [4]	1985	Impulse Plug	1/2 – 2 lb	1.4 - 7.5	0.15 – 0.5
Hoffman and Mills [6]	1956	Tourmaline Gages	1/2 – 8 lb	23-161	1.48 - 14.81
Jack [7]	1963	Tourmaline Gages	1/8 lb	3 - 39	0.5 - 6.5

Literature Survey (contd.)

Impulse Plug Measurement

- Utilize the final velocity of an unrestrained cylindrical plug, ejected from a hole in a large rigid steel plate, to measure reflected blast impulse
- Previous efforts provide a comprehensive set of reflected impulse data for standoff distances from near contact out to several feet
- Method yields impulse only – not blast pressure history

Literature Survey (contd.)

Reflected Blast Pressure Measurements

- Numerous attempts to use piezoelectric transducers at close range
- Transducer response is increasingly dominated by oscillatory noise as the charge standoff is reduced
- At small distances the recorded pressure histories of nominally identical tests showed large variability and none of the histories exhibited the sharp pressure rise followed by exponential decay that is typically observed at larger scaled distances.

Literature Survey (contd.)

Reflected Blast Pressure Measurements (contd.)

- Jack (1963) measured normally reflected pressures up to nearly 30,000 psi for 1/8 pound Pentolite spheres over a scaled distance range of 0.5 to 6.5 ft/lb$^{1/3}$ using tourmaline-based piezoelectric pressure gages
- Morozov et al. (1992), using shadowgraph techniques, determined that the cloud of detonation products can extend out to between 20 and 30 charge radii

Literature Survey (contd.)

Key Challenges to Blast Pressure Measurement at Small Standoff

- Severe ringing of the response at close range, probably related to resonant excitation of the transducer
- Transducer operation within the cloud of detonation product gases
- Gage-to-gage and shot-to-shot response non-uniformity

Test System and Setup

Selected transducers selected for these tests are PCB model 134A02 due to their high resonant frequency (1.5 MHz).

Measure reflected blast pressure at near normal incidence and standoff distances from 5 to 25 inches from the center of detonating half-pound spherical C-4 charges.

Photo from http://www.pcb.com/spec_sheet.asp?model=134A27&item_id=10839

Homeland Security
Science and Technology

Test System and Setup (contd.)

An array of four pressure transducers installed in a concentric pattern with sensing faces mounted flush to the upward-facing horizontal surface of a rectangular steel transducer block.

Two of the transducers were threaded directly into the steel transducer block. The two remaining transducers were mounted with vibration isolation.

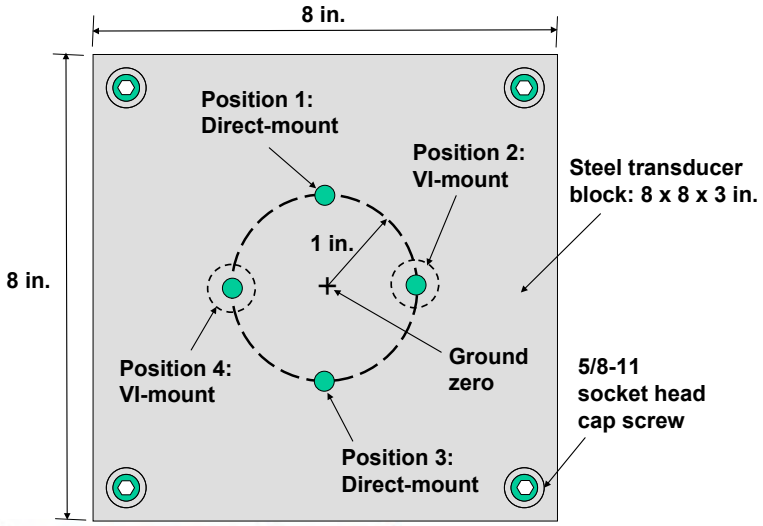

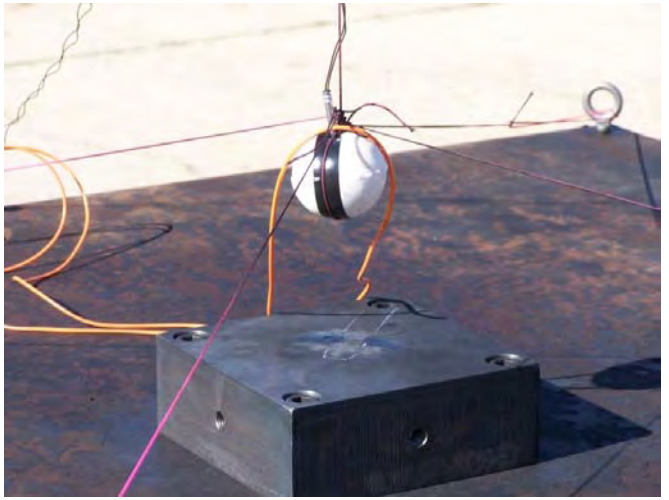

Homeland Security
Science and Technology

Test System and Setup (contd.)

Transducer block was rigidly mounted at the center of a massive steel support table

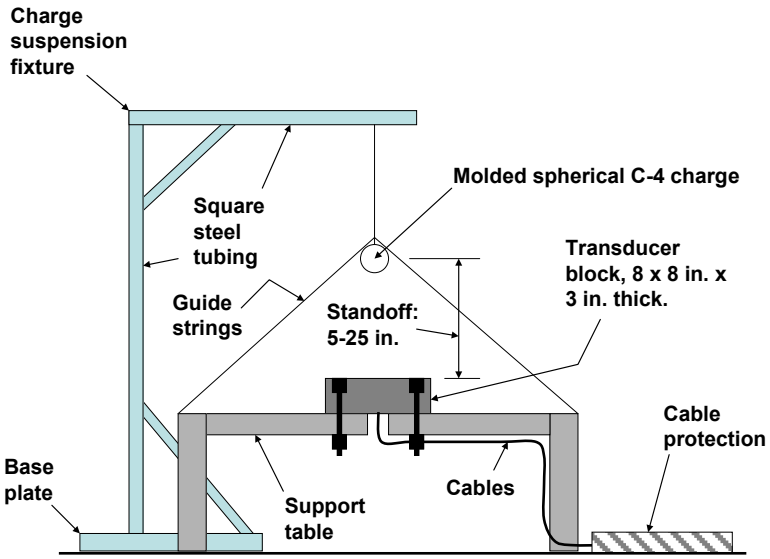

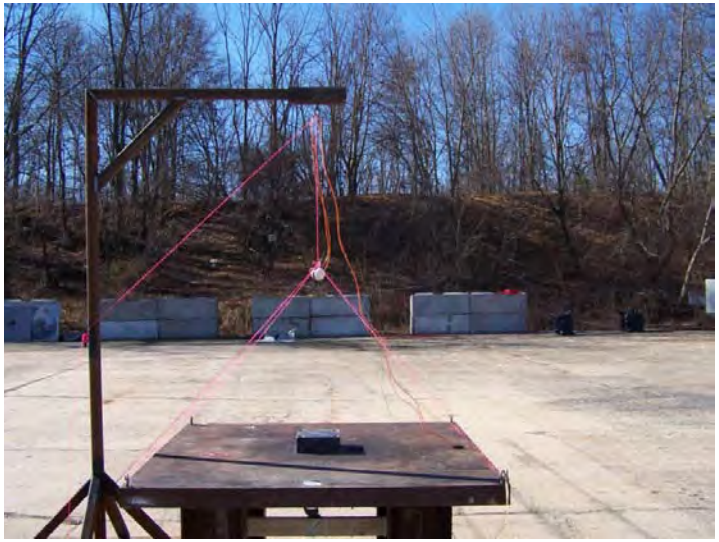

Homeland Security
Science and Technology

Test System and Setup (contd.)

The sensing face of each of the four transducers was recessed about 0.5 mm below the surface of the transducer block and coated with either Dow Corning 340 heat sink compound or silicone grease heavily doped with graphite powder in order to reduce transducer thermal response.

In some tests a piezo-pin was installed vertically in a narrow drilling in the block at the ground zero position to sense blast wave arrival time. In some of the tests a second piezo-pin was installed in the charge to sense detonation, independent of the fiber optic break-wire for triggering data acquisition.

Each pressure transducer was coupled to a PCB 402A03 charge converter and connected to the Data Acquisition System (DAS). A 10 MHz data sampling rate was used. Data collection continued for 2 ms after the DAS was triggered.

Homeland Security

Science and Technology

Charge Radii and Scaled Distance

	Near-Field Limits for 0.5 lb C-4		Standoff	
	R_{min} = 1.83 in.	R_{max} = 4.66 in.	5 in.	25 in.
Charge radii*	1.44	3.68	3.95	19.7
z [ft/lb$^{1/3}$]	0.192	0.489	0.525	2.62
z_{TNT} [ft/lb-TNT$^{1/3}$]	0.176	0.451	0.484	2.42

*1.267 in. charge radius for 0.5 lb C-4

Homeland Security
Science and Technology

Test Results

A total of 32 tests were carried out with charge standoffs of 5, 7.5, 12.5, 17.5, and 25 inches to ground zero on the transducer block.

Present pressure transducer arrival times and ground zero (piezo-pin) arrival times

Present raw peak pressure and raw impulse and fitted peak pressure and fitted impulse (Friedlander curve).

Homeland Security
Science and Technology

Test Data Summary

		Responses		
Standoff	Tests	Pressure	Pin on Block	Pin on Charge
25	9	35/36	5	1
17.5	6	21/24	3	1
12.5	6	20/24	5	1
7.5	6	17/24	5	1
5	5	20/20	2	1

Homeland Security
Science and Technology

Blast Wave Mean Arrival times

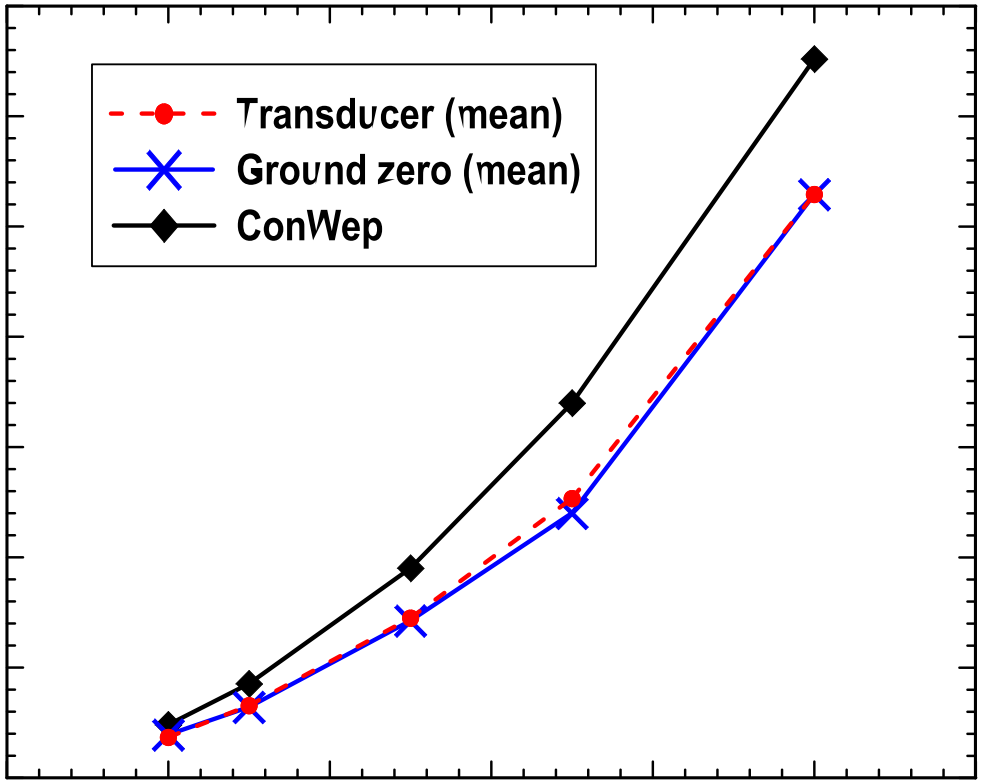

Homeland Security
Science and Technology

Raw and Fitted Overpressure Curves

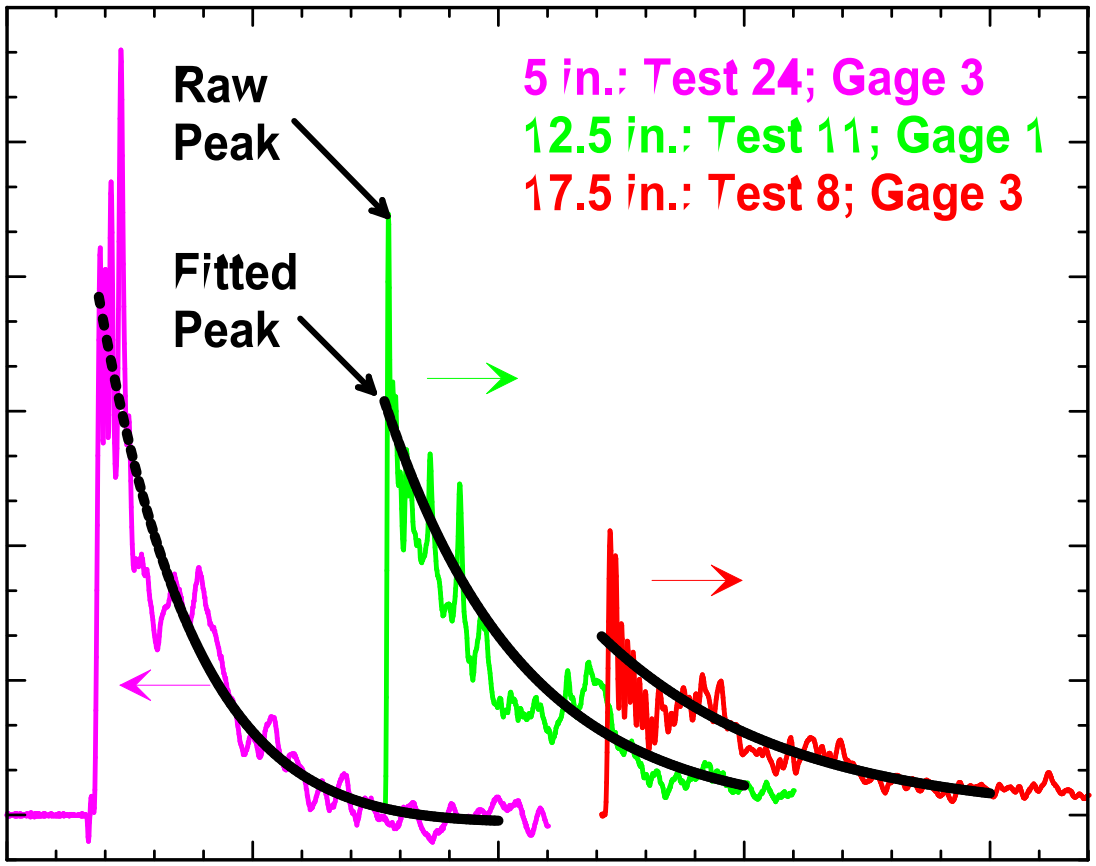

Homeland Security
Science and Technology

Peak Reflected Overpressure

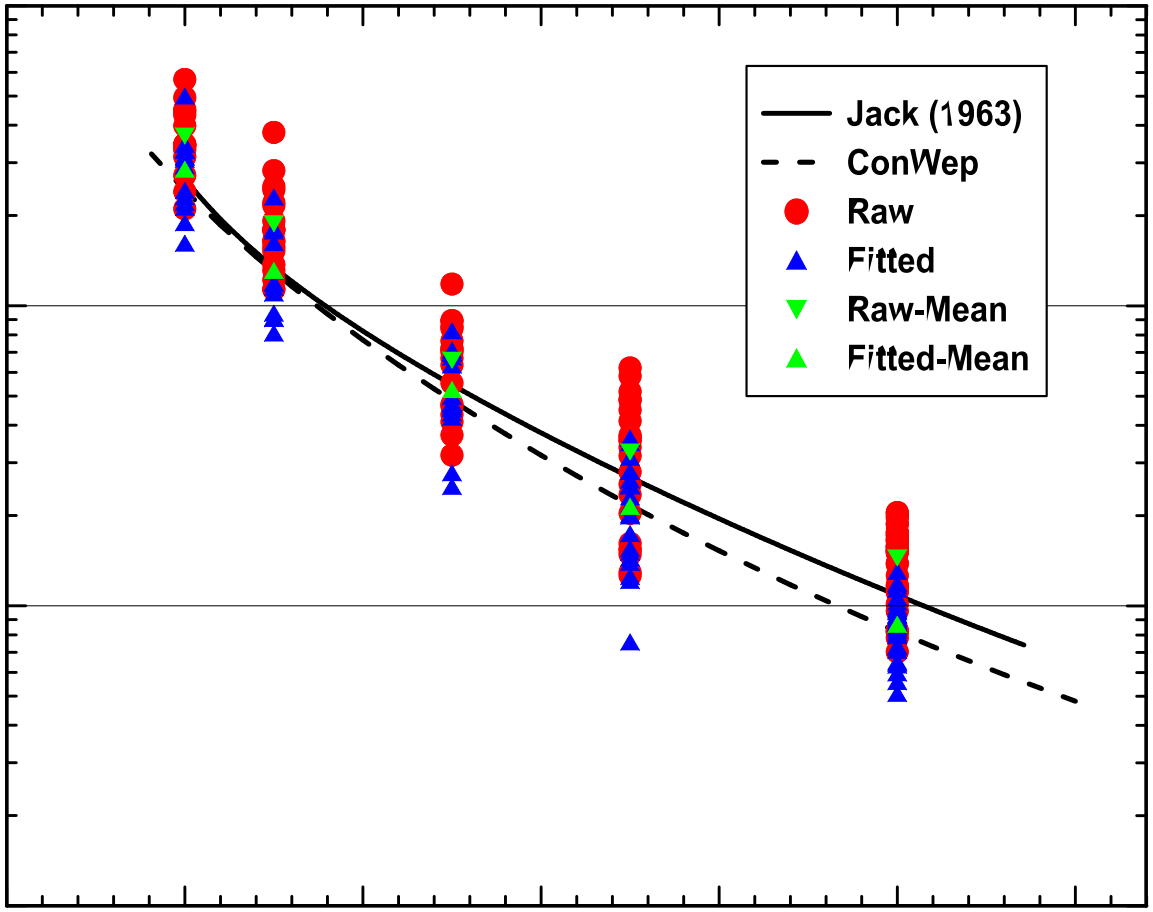

Homeland Security
Science and Technology

Reflected Impulse

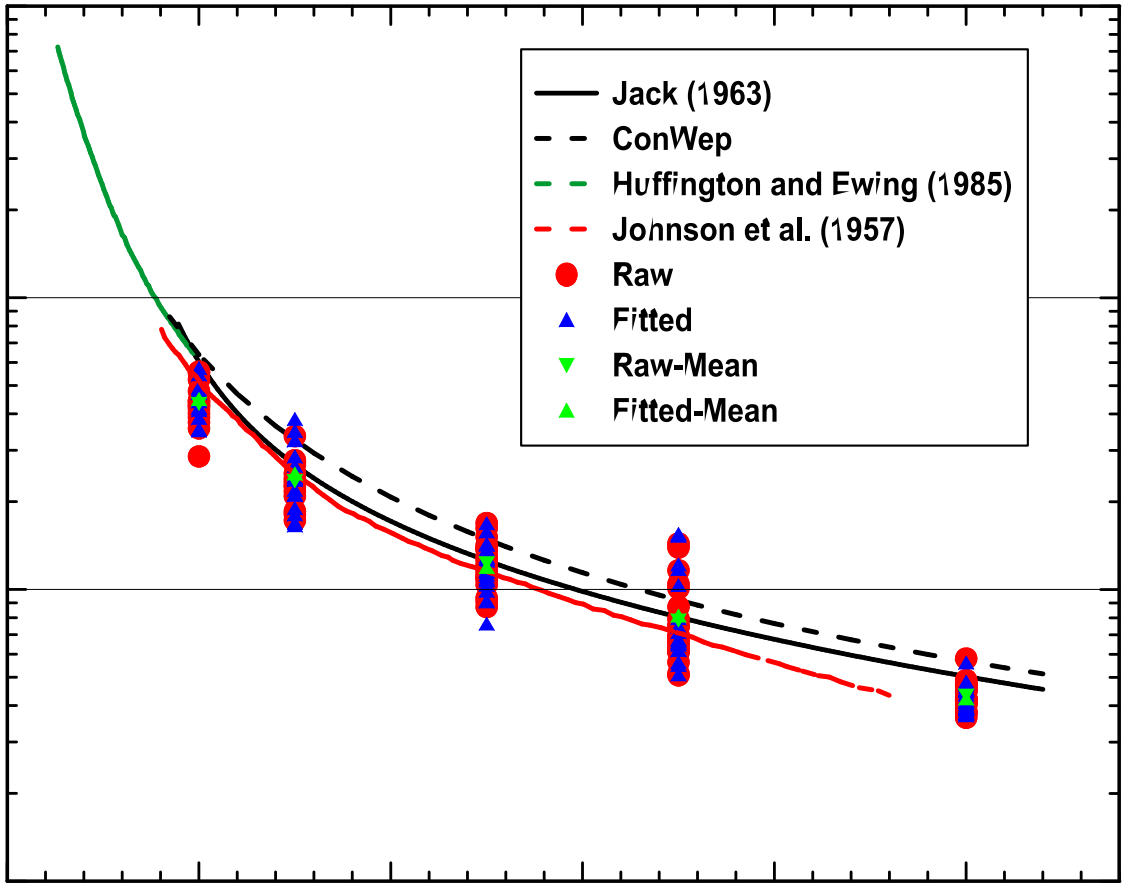

Homeland Security
Science and Technology

Mean Raw and Fitted Data

Standoff [in.]	Tests	Gages	Pressure* [psi]		Impulse* [psi-ms]	
			Raw	Fitted	Raw	Fitted
25	9	35	1451 (387)	867 (81.7)	43.5 (4.3)	42.3 (4.2)
17.5	6	21	3270 (1506)	2143 (794)	78.6 (25.8)	81.3 (30.4)
12.5	6	20	6616 (2268)	5257 (1567)	124 (22.7)	119 (23.1)
7.5	6	17	18,854 (6634)	13,099 (4431)	236 (44.0)	249 (62.6)
5	5	20	36,954 (9699)	28,523 (8525)	435 (73.3)	449 (62.9)

Data Comparison

Standoff [in.]	Peak Pressure [psi]			Impulse [psi-ms]		
	Present (Fitted)	Jack	ConWep	Present (Fitted)	Jack	ConWep
25	867	1132	819	42.3	52.7	56.7
17.5	2143	2640	2166	81.3	80.8	91.8
12.5	5257	5472	4834	119	121	149
7.5	13,099	13,641	12,990	249	274	325
5	28,523	26,404	24,270	449	620	637

Conclusions

For standoff less than 25 inches, measured pressure histories exhibited considerable variability in the gage-to-gage sense for a given test and in the shot-to-shot sense for a particular gage.

This non-uniformity was observed undiminished in the peak pressure data, but to a lesser degree in the impulse data due to averaging of the response oscillations by the integration process.

Peak reflected pressure ranged from about 900 psi at 25 inches to more than 28,000 psi at 5 inch standoff.

Homeland Security
Science and Technology

Conclusions (contd.)

The present peak pressure measurements agree with:

- ConWep predictions within 15%
- Early BRL/Aberdeen measurements to within 5-30%

Impulse measurements deviate from:

- ConWep and early BRL data by 15-40%.

It is believed that the tourmaline transducers used here may be useful for pressure testing at small charge standoff provided that a sufficiently large number of tests are performed to reduce the measurement uncertainty to an acceptable level.

Homeland Security
Science and Technology

Homeland Security

Science and Technology

E.T.S.I. Caminos. U.P.M.
DEPARTAMENTO DE CIENCIA DE MATERIALES

CISDEM
CENTRO DE INVESTIGACIÓN EN SEGURIDAD
Y DURABILIDAD ESTRUCTURAL Y DE MATERIALES

Blast response analysis of reinforced concrete slabs. Experimental procedure and numerical simulation.

Gustavo Morales – Alonso
gustavo.morales@mater.upm.es

David A. Cendón
Francisco Gálvez
Borja Erice
Vicente Sánchez - Gálvez

Materials Science Department, U.P.M. Madrid, Spain

Blast response analysis of reinforced concrete slabs.

- Introduction
- Experimental Program
- Numerical Simulation
- Conclusions

Experimental procedure and numerical simulation.

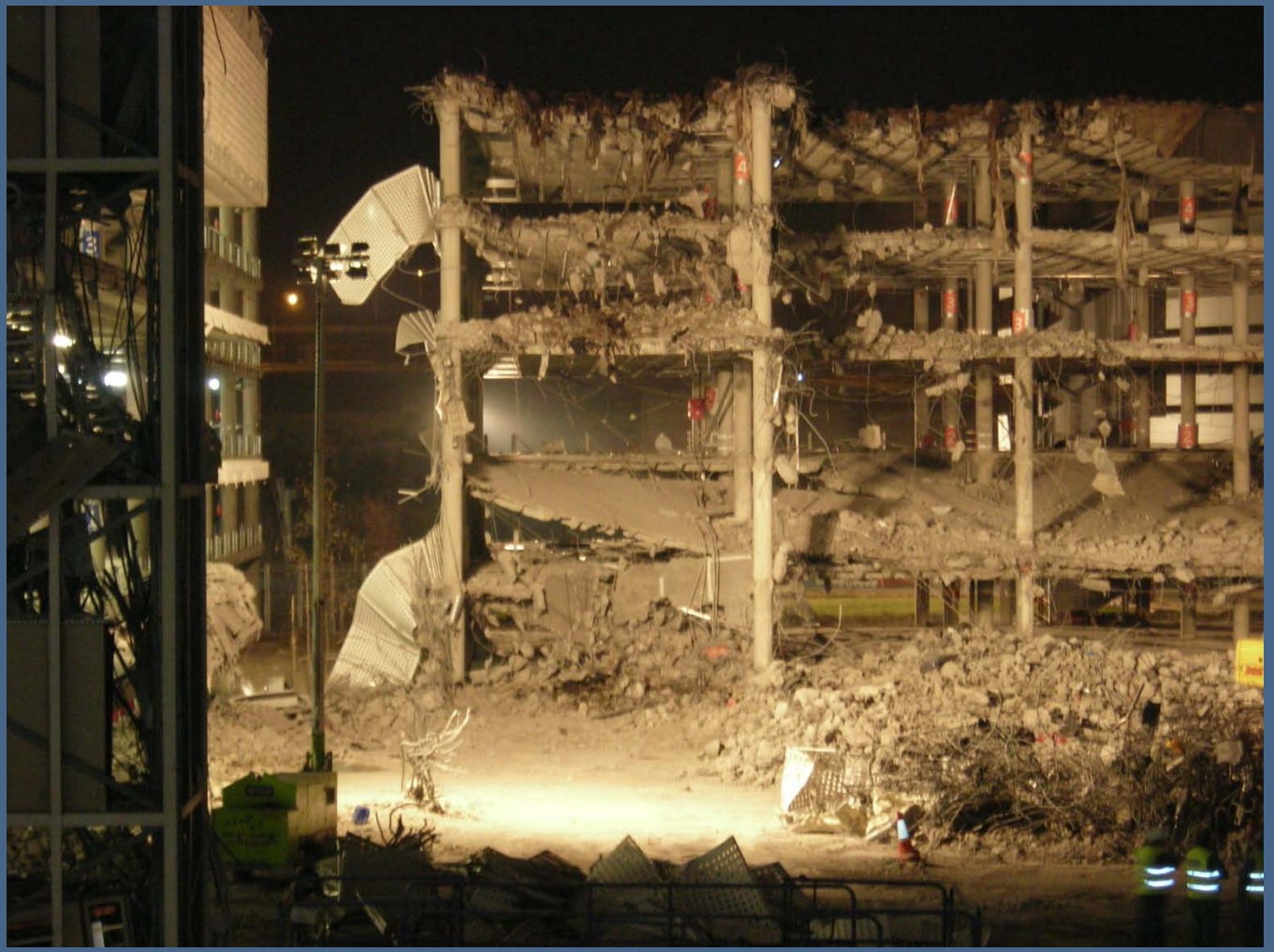

December 30th, 2006. Madrid-Barajas Airport, Spain

April 19th, 1995. Oklahoma, USA




July 22nd, 2011. Oslo, Norway

Scope: Numerical Simulation ⇨ Constitutive Models for RC

Most of currently used models: Plasticity – based, complex in compression, simple in tension

Validation of existing models requires experimental results

Blast tests results are not easy to find in scientific literature

New experimental set – up for blast tests & numerical simulations with existing models are presented

CISDEM
CENTRO DE INVESTIGACIÓN EN SEGURIDAD Y DURABILIDAD ESTRUCTURAL Y DE MATERIALES

Blast response analysis of reinforced concrete slabs.

Experimental procedure and numerical simulation.

- Introduction
- Experimental Program
- Numerical Simulation
- Conclusions

Threefold goal:

- Generate open results of blast tests on RC elements
- Identify main parameters governing material & structural response
- Validation, adjustment and development of numerical tools

New set – up for testing up to four RC samples subjected to blast

Design criteria of experimental set – up:

1. Up to four slabs are to be tested with each detonation

Design criteria of experimental set – up:

1. Up to four slabs are to be tested with each detonation

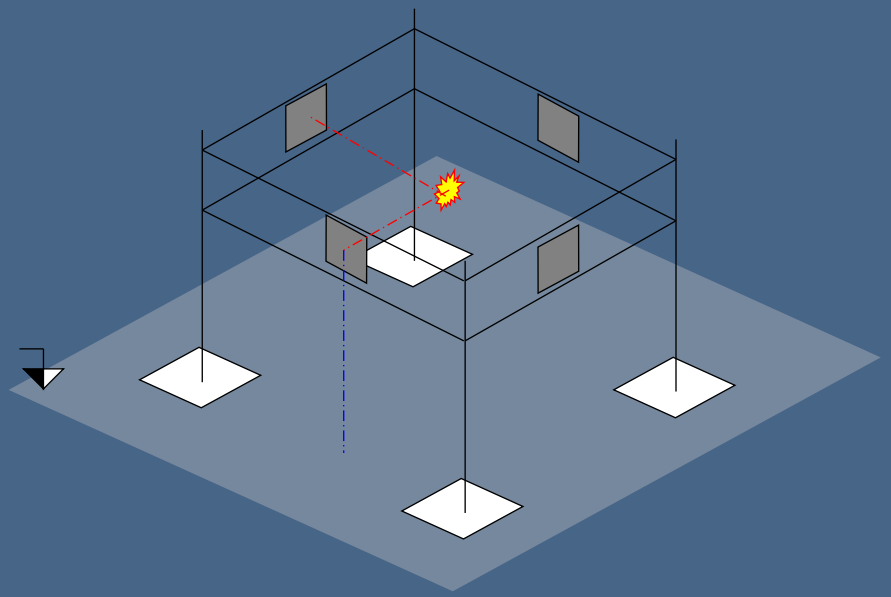

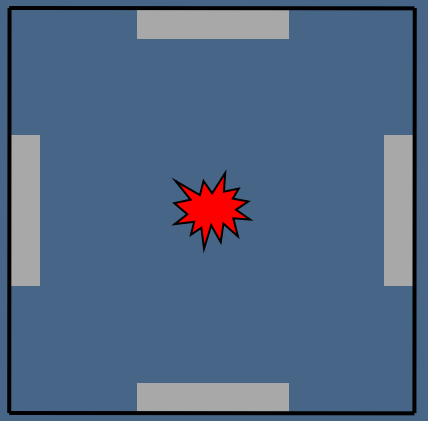

Design criteria of experimental set – up:

1. Up to four slabs are to be tested with each detonation
2. Shock wave reflections with the ground avoided

Design criteria of experimental set – up:

1. Up to four slabs are to be tested with each detonation
2. Shock wave reflections with the ground avoided

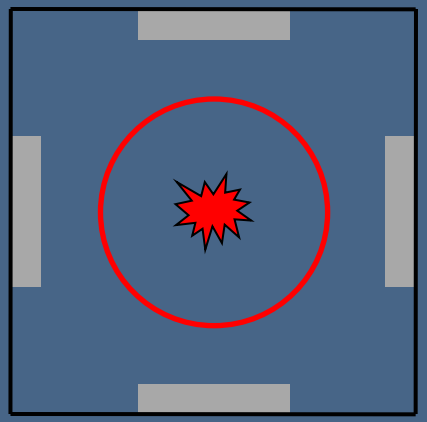

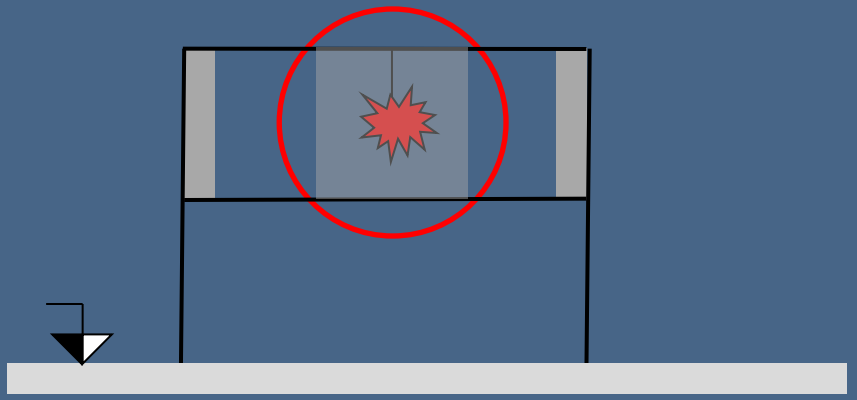

Design criteria of experimental set – up:

1. Up to four slabs are to be tested with each detonation
2. Shock wave reflections with the ground avoided

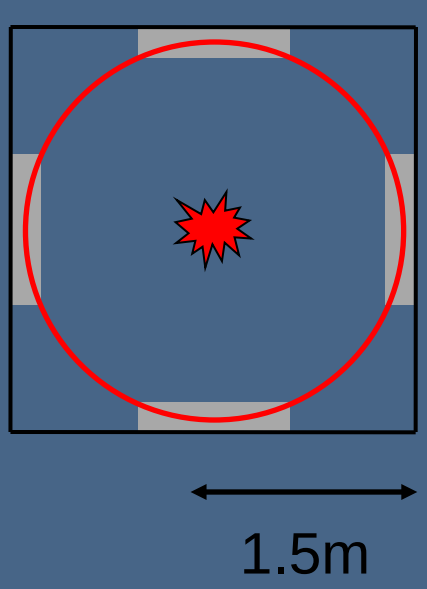

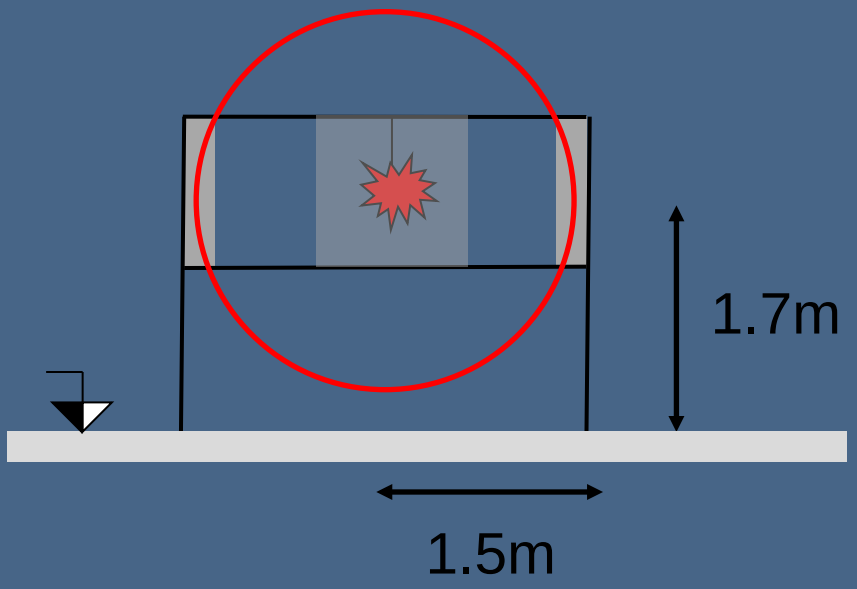

Design criteria of experimental set – up:

1. Up to four slabs are to be tested with each detonation
2. Shock wave reflections with the ground avoided
3. Plane wave shock

Design criteria of experimental set – up:

1. Up to four slabs are to be tested with each detonation
2. Shock wave reflections with the ground avoided
3. Plane wave shock

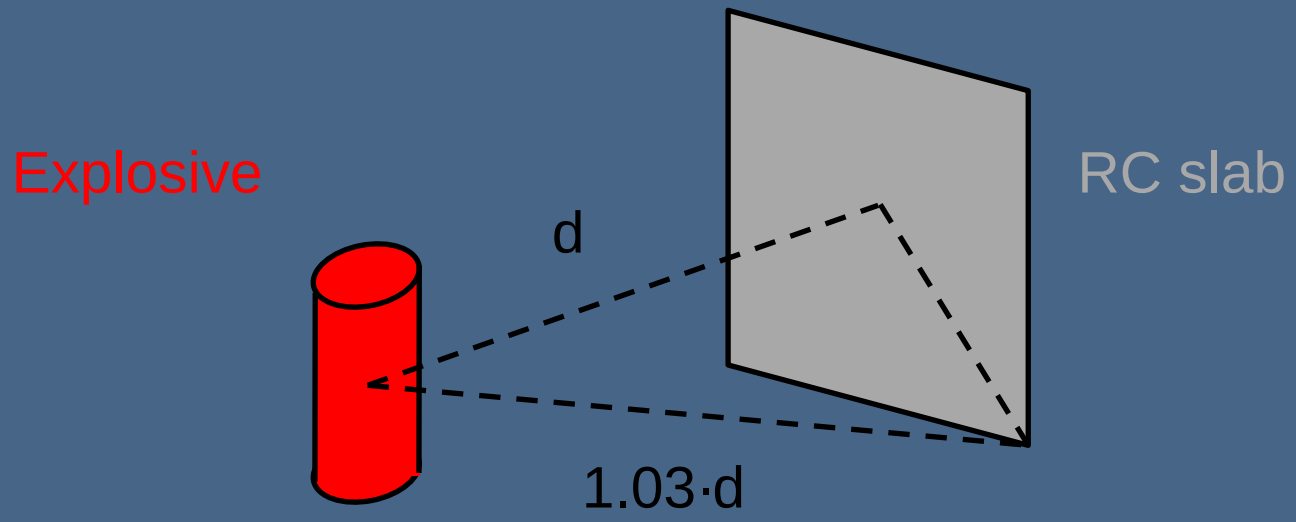

Experimental set – up :

Major assets of the of experimental set – up:

1. Control of experimental scattering
2. Cost effectiveness: reduction of complexity and time expenses

Materials:

Reinforced concrete slabs:

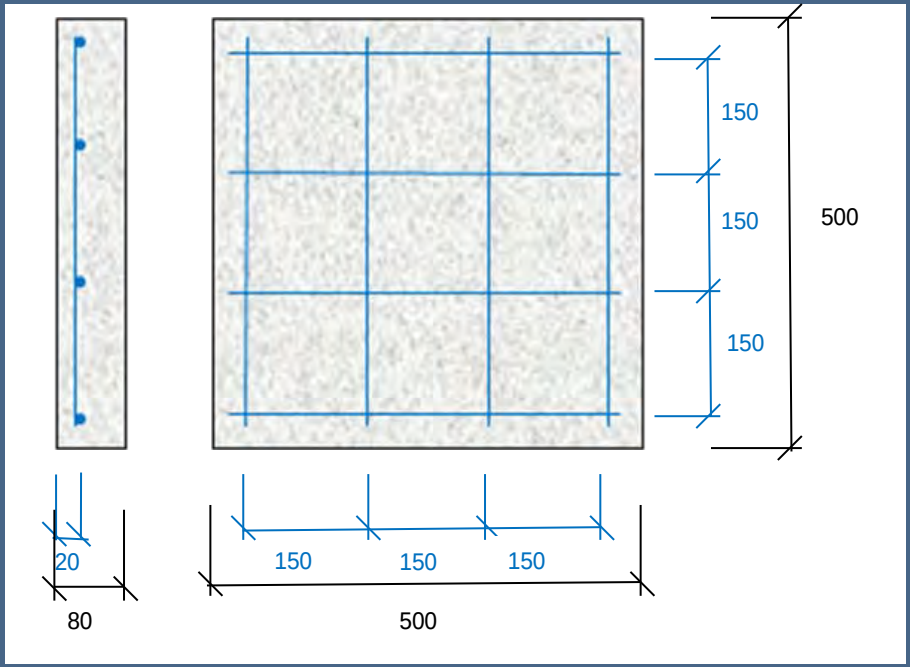

Six slabs of Normal Strength Concrete (NSC) σ_c = 50 MPa
Six slabs of High Strength Concrete (HSC) σ_c = 91 MPa

Experimental procedure:

- The amount of explosive was the same in every detonation, and equivalent to 5 kg TNT
- The explosive was hung with its axis vertical and detonated from its center

Experimental procedure:

- The amount of explosive was the same in every detonation, and equivalent to 5 kg TNT
- The explosive was hung with its axis vertical and detonated from its center
- Three out of the four positions were used for reinforced concrete slabs of the same type
- On the fourth position, a control Aluminum (5083 H112) plate was placed

Instrumentation:

1. Pressure sensor for the measurement of reflected pressure

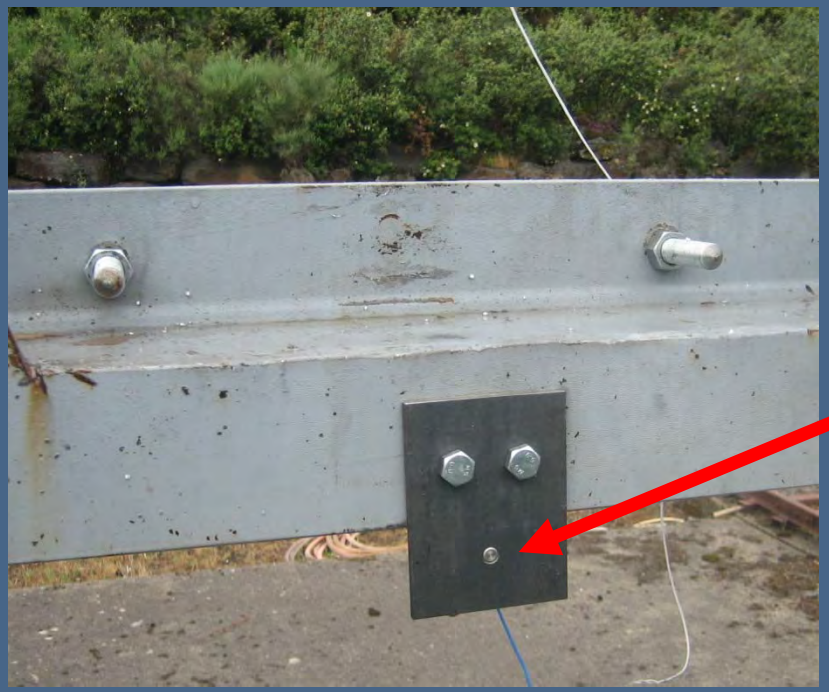

Instrumentation:

1. Pressure sensor for the measurement of reflected pressure
2. Filming of crack pattern development on tensioned side of slab

Instrumentation:

1. Pressure sensor for the measurement of reflected pressure
2. Filming of crack pattern development on tensioned side of slab
3. Control Aluminum plates with strain gauges

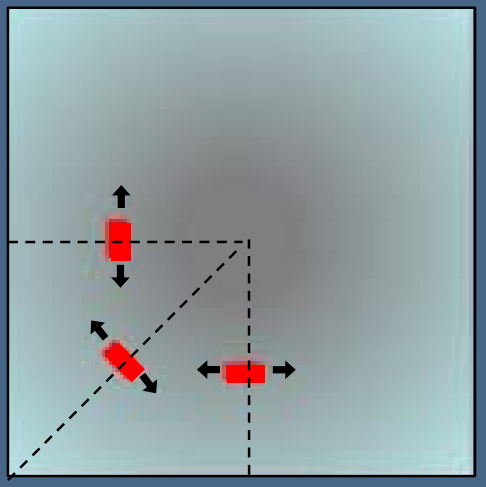

Instrumentation:

1. Pressure sensor for the measurement of reflected pressure
2. Filming of crack pattern development on tensioned side of slab
3. Control Aluminum plates with strain gauges
4. Control of rear spalling projections

Results on Normal Strength Concrete (tests #6 & #7):

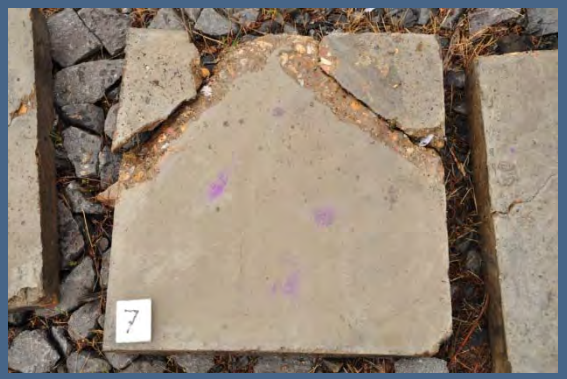

Results on Normal Strength Concrete (tests #6 & #7):

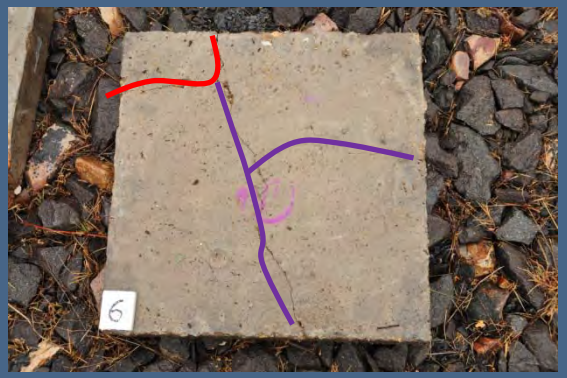




Bending failure mode Shear failure mode

Results on High Strength Concrete (tests #8 & #9):

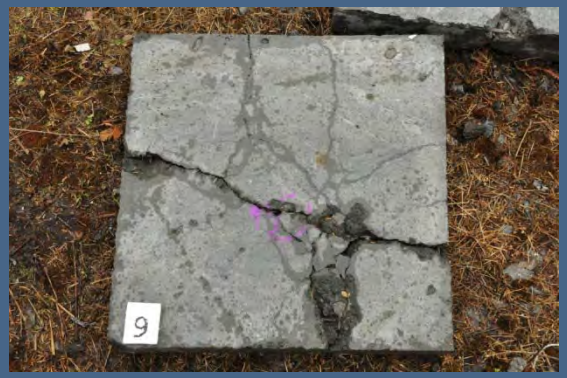

Results on High Strength Concrete (tests #8 & #9):

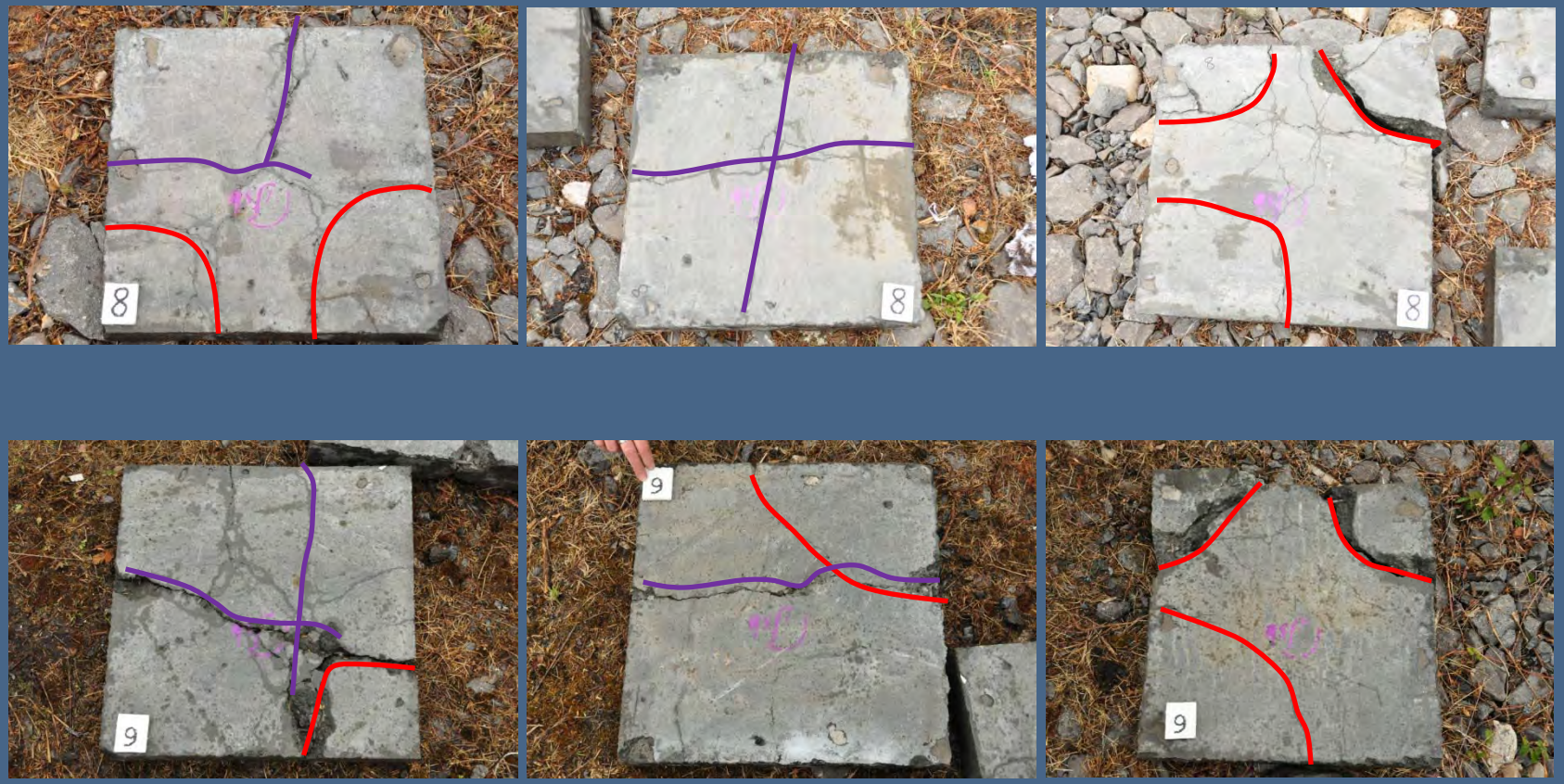

Bending failure mode Shear failure mode

Results:

Concrete type	Failure mode (number of specimens)		
	Bending	Shear	Mixed mode
Normal Strength Concrete	1	5	0
High Strength Concrete	2	2	2

The ability of both concrete types to withstand the same explosive load is similar.
This is blamed on the tension strength of concrete, which is thought to be governing the failure of the slabs.

Results:

Results:

CISDEM
CENTRO DE INVESTIGACIÓN EN SEGURIDAD Y DURABILIDAD ESTRUCTURAL Y DE MATERIALES

Blast response analysis of reinforced concrete slabs.

Experimental procedure and numerical simulation.

- Introduction
- Experimental Program
- Numerical Simulation
- Conclusions

Finite Element Analysis with LS-DYNA

Twofold goal:

- Analyze the experimental results obtained
- Verify the adjustment of existing constitutive models:
    - Model #1: Winfrith Concrete Model
      Plasticity - based
      Compressive behavior: Ottosen surface failure
    - Model #2: Brittle Damage Model
      Compressive behavior: Linear elastic (no failure)

CISDEM
CENTRO DE INVESTIGACIÓN EN SEGURIDAD Y DURABILIDAD ESTRUCTURAL Y DE MATERIALES

Concrete slabs simulation:

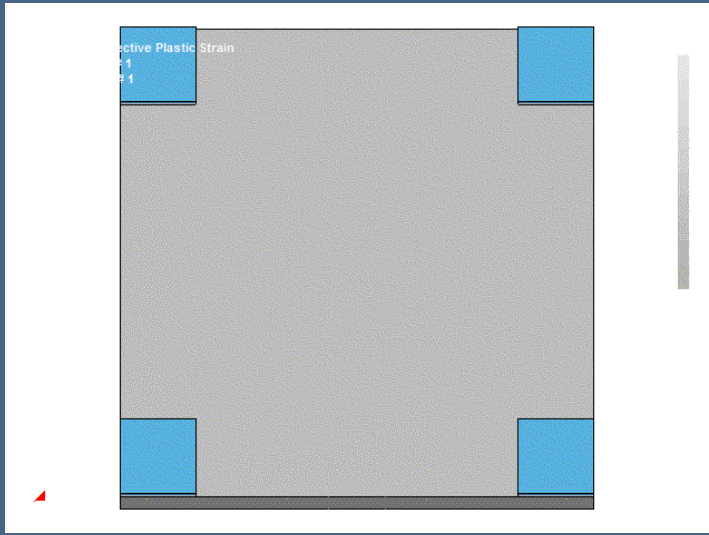

Winfrith Concrete Model

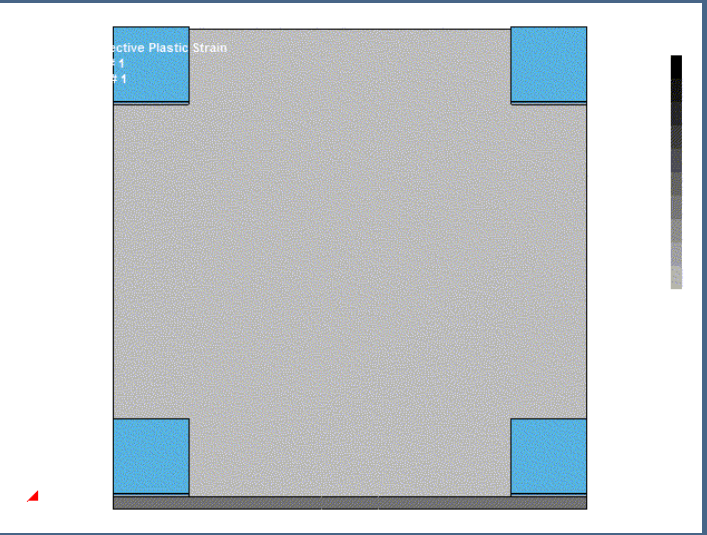

Brittle Damage Model

Concrete slabs simulation:

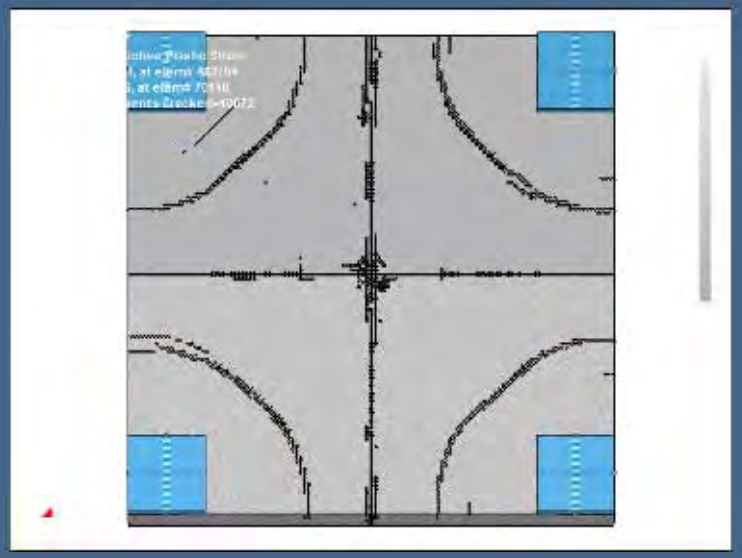

Winfrith Concrete Model

Brittle Damage Model

Concrete slabs simulation. Results on Normal Strength Concrete:

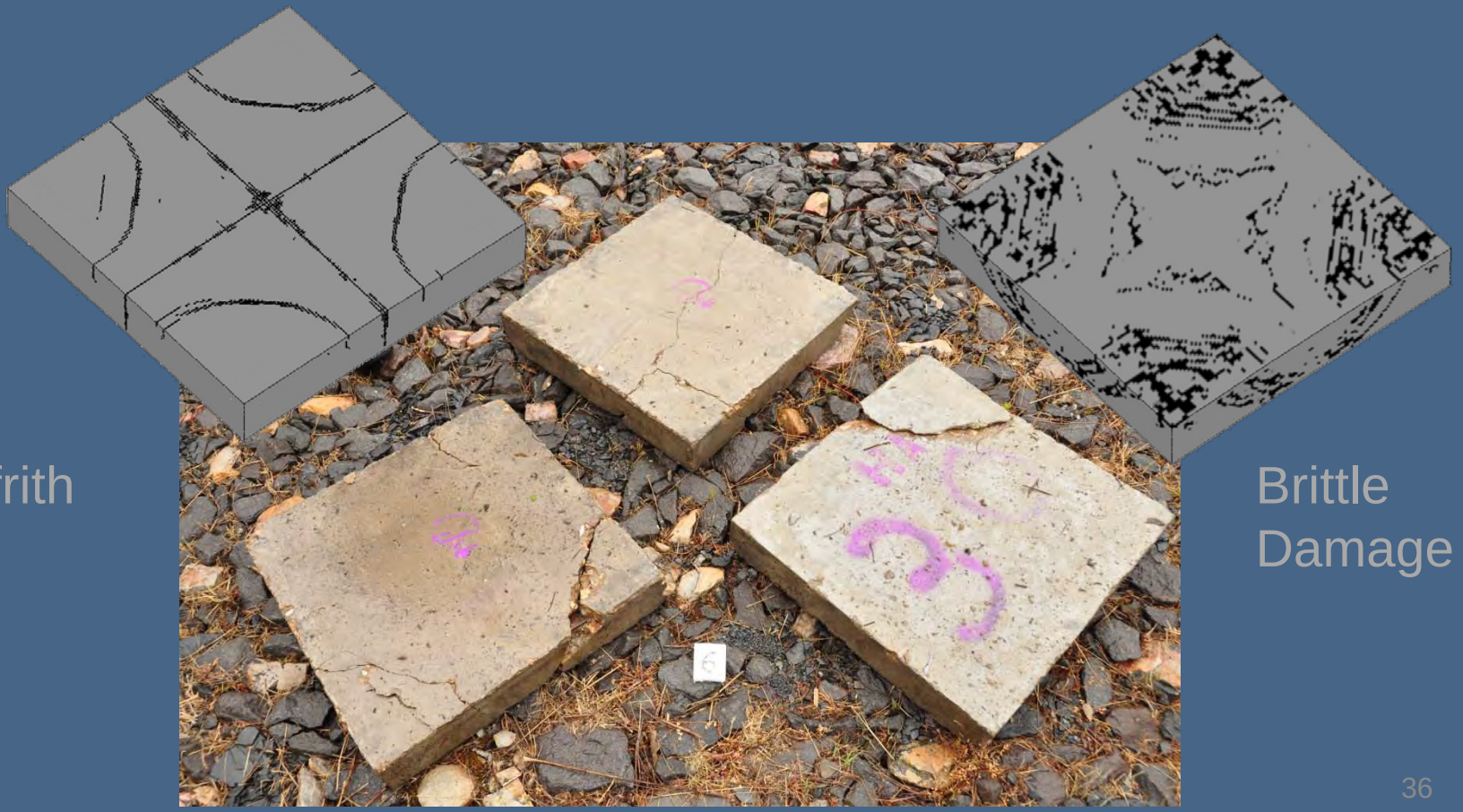

Winfrith

Brittle Damage

Concrete slabs simulation. Results on High Strength Concrete:

Winfrith

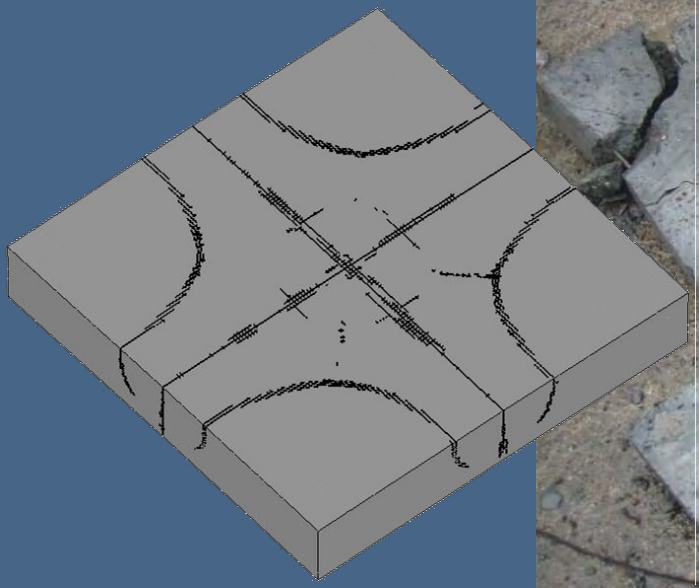

Brittle Damage

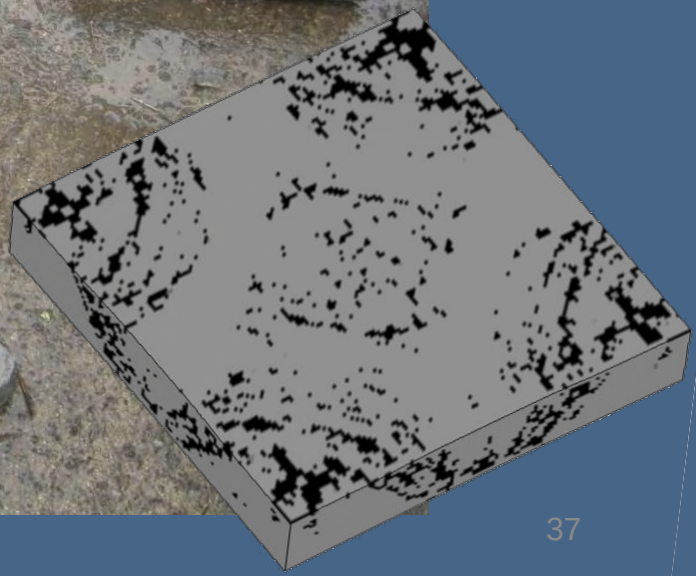

Blast response analysis of reinforced concrete slabs.

Experimental procedure and numerical simulation.

- Introduction
- Experimental Program
- Numerical Simulation
- Conclusions

An experimental set – up that allows testing up to four RC elements under the same blast load is presented

The results from the experimental program suggest that the ability of RC structures to withstand blast loads is primarily governed by its tensile strength

Numerical simulations on LS-DYNA show that good results can be achieved using simplified material models with suitable cracking and tensile failure criteria

E.T.S.I. Caminos. U.P.M.
DEPARTAMENTO DE CIENCIA DE MATERIALES

CISDEM
CENTRO DE INVESTIGACIÓN EN SEGURIDAD
Y DURABILIDAD ESTRUCTURAL Y DE MATERIALES

Blast response analysis of reinforced concrete slabs. Experimental procedure and numerical simulation.

Gustavo Morales – Alonso
gustavo.morales@mater.upm.es

David A. Cendón
Francisco Gálvez
Borja Erice
Vicente Sánchez - Gálvez

Materials Science Department, U.P.M. Madrid, Spain

IBS – 2011 26th International Symposium on Ballistics
9/12/2011 - 9/16/2011, Miami, USA

Effect of frictions on ballistic performance of a 3D warp interlock fabric: Numerical analysis

Presented by François BOUSSU

Authors:

Cuong HA MINH (*ENSAIT, Polytech'Lille*)

François BOUSSU *(ENSAIT)*

Toufik KANIT *(Polytech'Lille)*

David CREPIN *(ENSAIT)*

Abdellatif IMAD *(Polytech'Lille)*

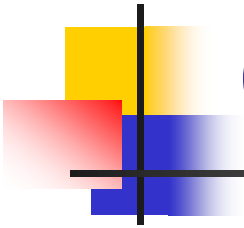

Outline

1. 3D woven fabrics

2. Overview onto geometrical modeling of 3D woven fabrics

3. New numerical tool and application in studying friction effects during ballistic impact onto a 3D fabric

4. Works in progress

5. Conclusions and Perspectives

North of France

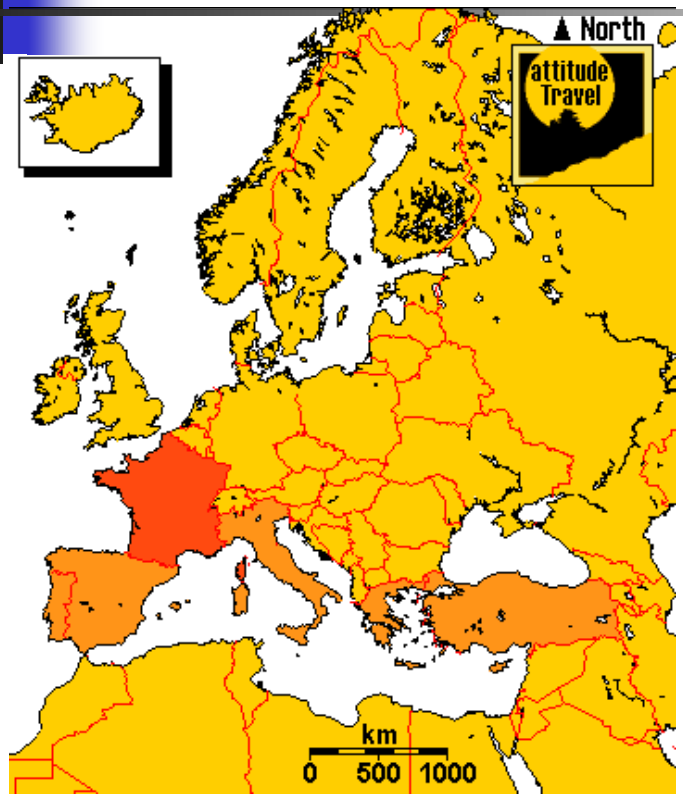

ENSAIT (www.ensait.fr)

since 1881

National Textile Institute

GEMTEX Laboratory Equipment

Side view of the automatic multi-layer weaving machine and its specific warp beams creel

Adaptation of a 24 frames dobby weaving machine for aramid yarns.

3D Warp Interlock Fabric

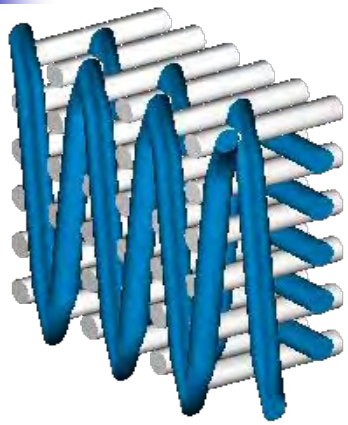

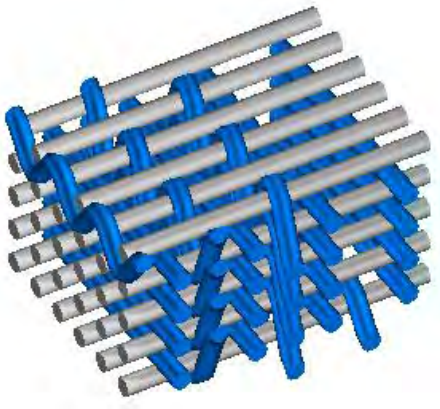

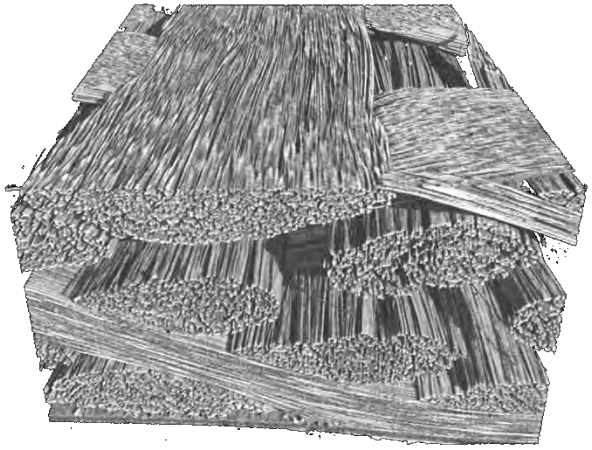

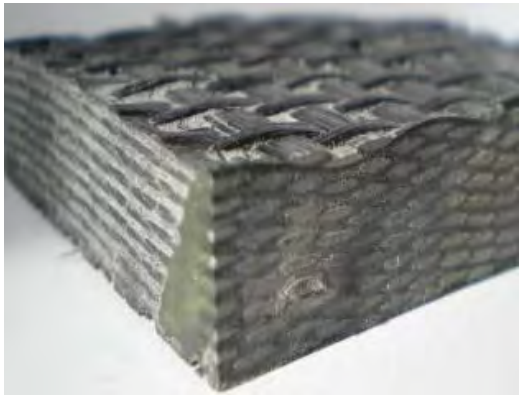

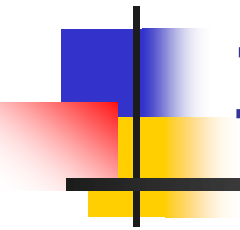

1. 3D woven fabrics

1. 3D woven fabrics

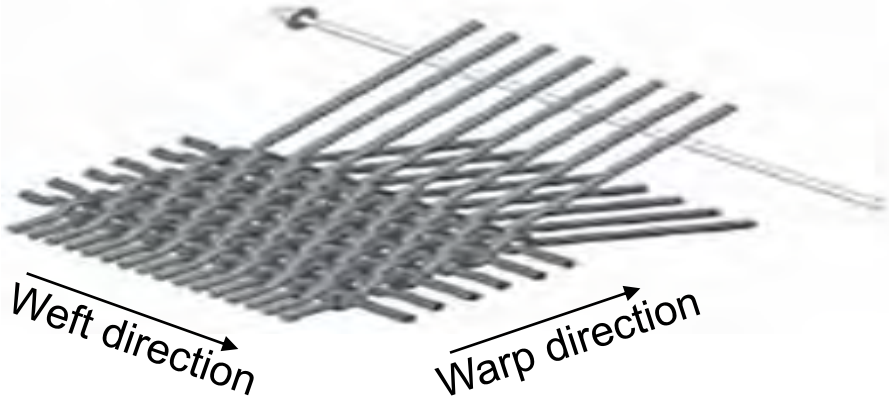

2D Weave

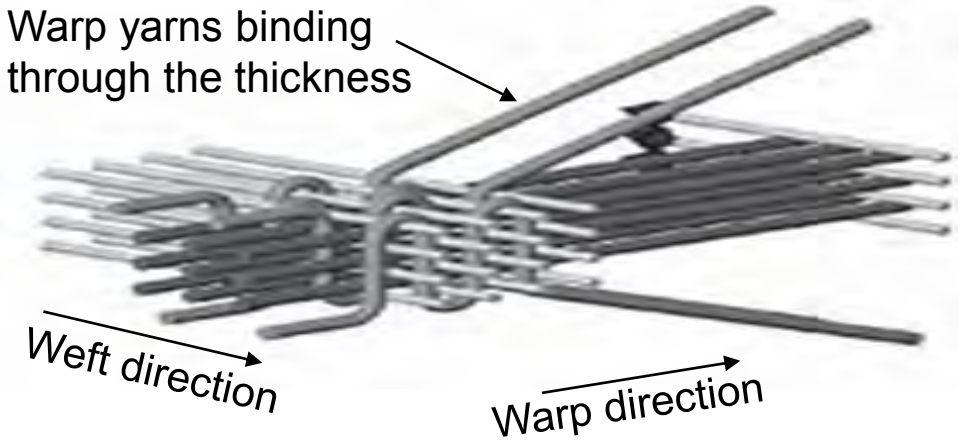

3D Weave

Main advantages of 3D woven fabrics regarding to 2D woven ones:

1. Facility in creating complex structures by the near-net-shape technology
2. Better mechanical interlaminar and through-the-thickness properties
3. Higher ballistic multi-impact damage resistance

1. 3D woven fabrics

A 2D fabric

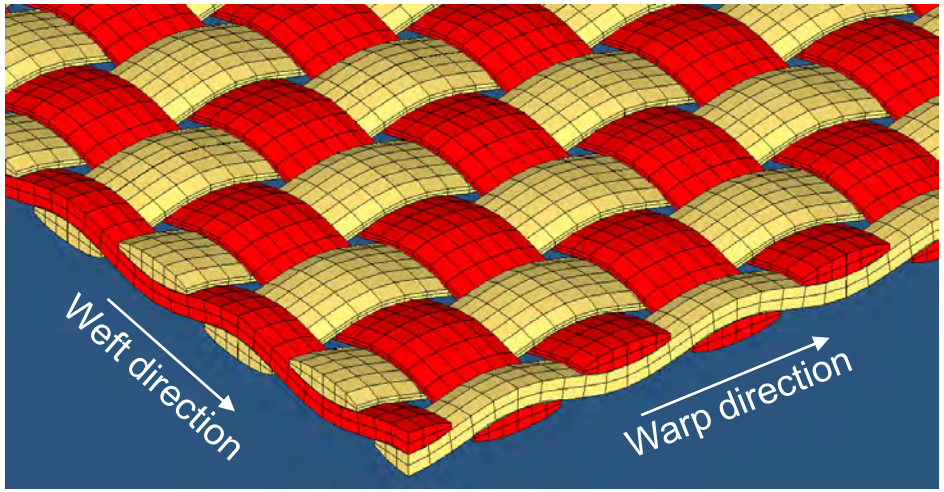

A 3D fabric

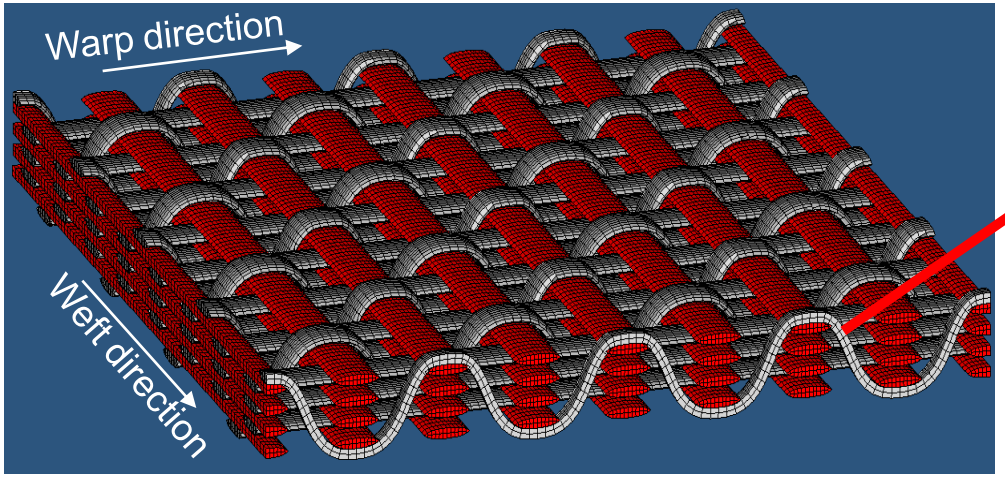

Warp yarn binding through the thickness

1. 3D woven fabrics

Depth through the thickness

Path of binding warp yarns

Crimp angle

1. AT: Angle – Through the thickness
2. AL: Angle – Layer to layer
3. OT: Orthogonal – Through the thickness
4. OL: Orthogonal – Layer to layer

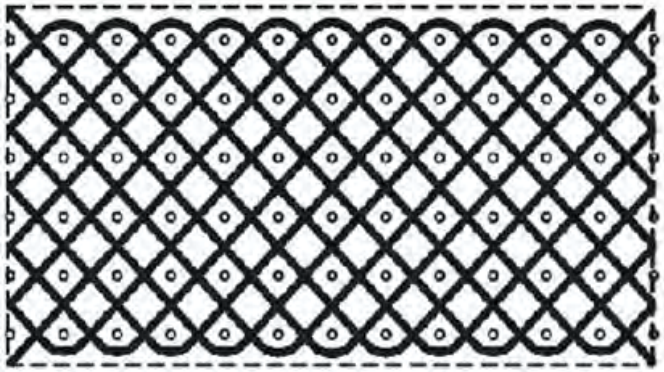

AT Fabric

AL Fabric

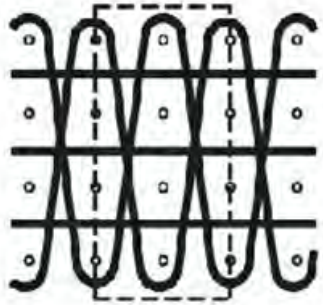

OT Fabric

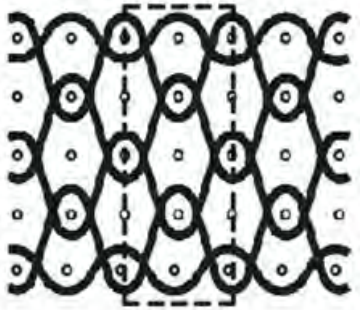

OL Fabric

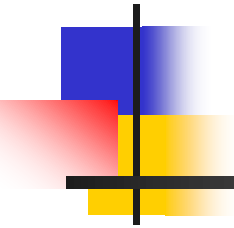

2. Overview onto geometrical modeling of 3D woven fabrics

Overview onto geometrical modeling of 3D woven fabric

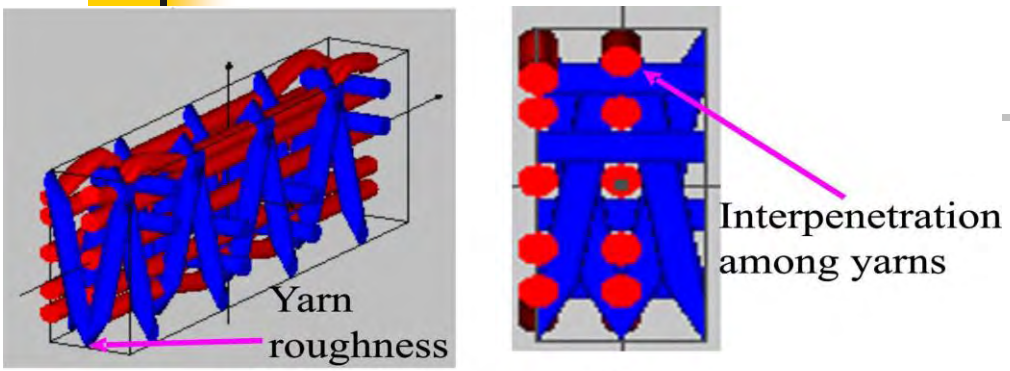

A geometrical model of the 3D orthogonal 5-layer fabric in WiseTex: (a) 3D view; (b) Side view

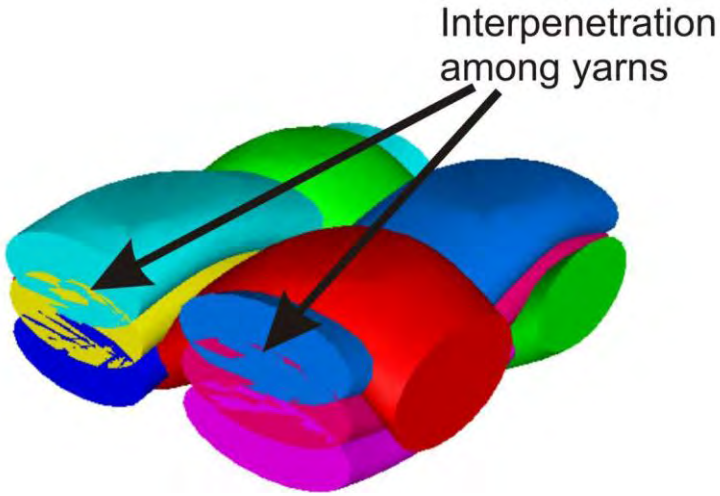

A geometrical model of the 3D orthogonal 3-layer fabric in TexGen

Disadvantages of current softwares:

1. Limited application only for a few fabric types
2. Difficulty in use because users cannot correct errors in a graphic interface of these softwares
3. Interpenetration between yarns
4. Roughness of yarn path in fabric
5. Incompatibility between these softwares and popular finite element codes

3. New numerical tool and in studying friction effects during ballistic impact onto a 3D fabric

New numerical tool

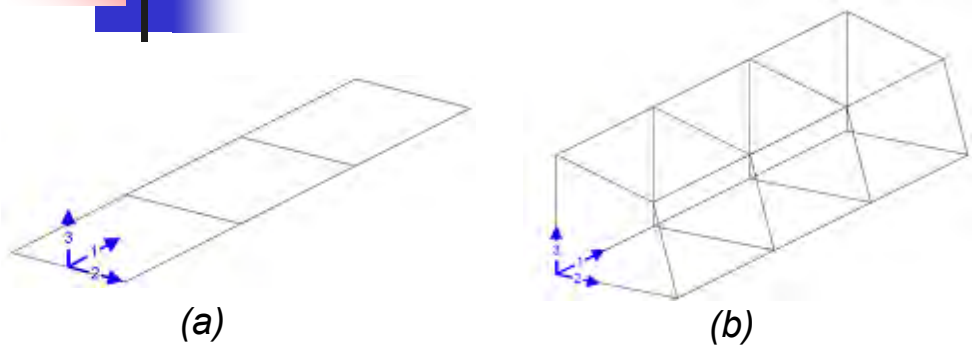

(a) (b)

Orientation of the local axes of a solid element in a yarn: (a) Shell elements; (b) Solid elements

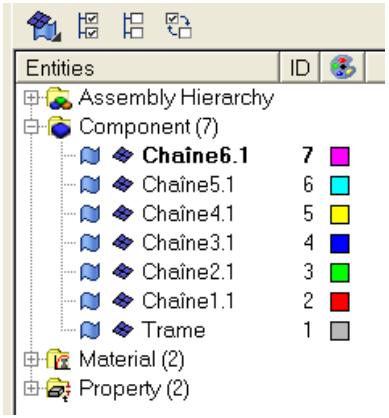

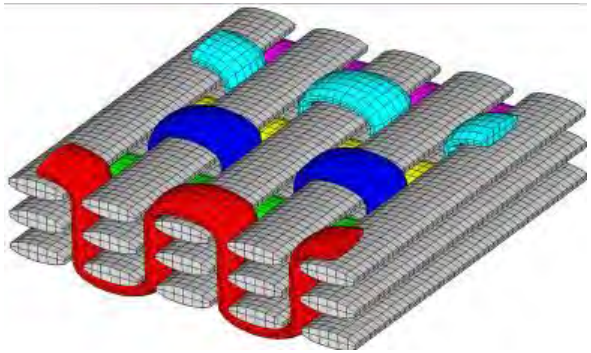

Organization of yarns and elements in groups on a friendly graphic interface

Advantages of new numerical tool:

1. Large application for all types of woven fabrics
2. Regular smoothness of yarn paths & Exclusion of interpenetrations between yarns
3. Orientation of local axes of elements along yarn direction
4. Automatic contact between yarns
5. Compatibility with popular finite element codes: Abaqus, Ansys, Radioss …

Results of new numerical tool

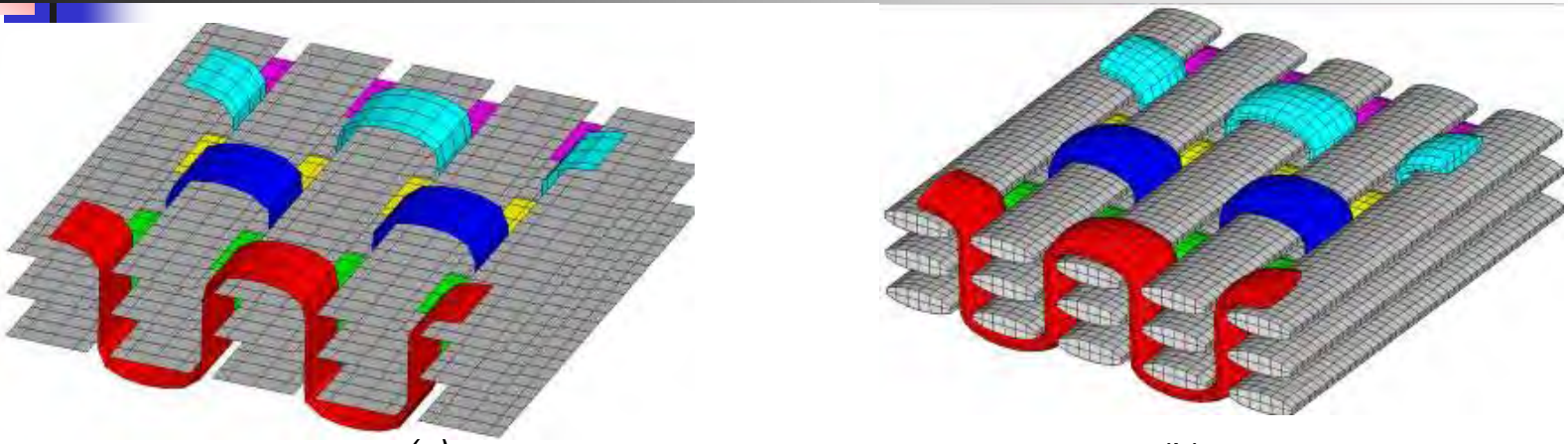

(a) (b)

A geometrical model of the 3D orthogonal 3-layer fabric created by new tool: (a) Shell elements; (b) Solid elements

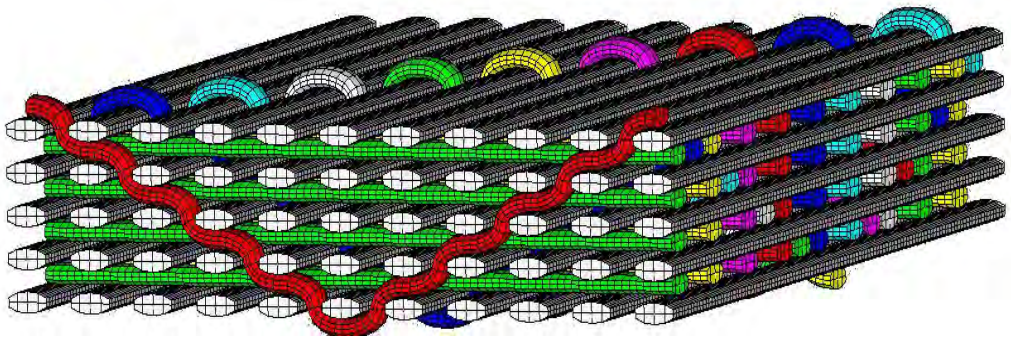

A geometrical model of the 3D orthogonal 5-layer fabric created by new tool: (a) Shell elements; (b) Solid elements

Configuration of the impact onto 3D fabric

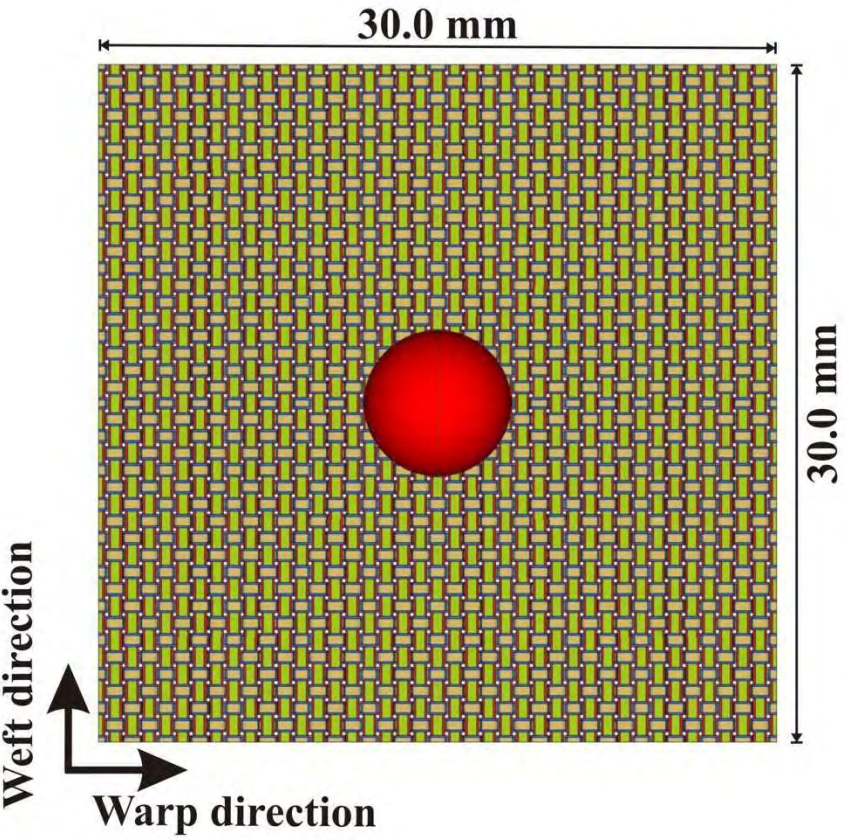

Configuration of a 900 m/s impact on the 3D orthogonal 5-layer woven fabric

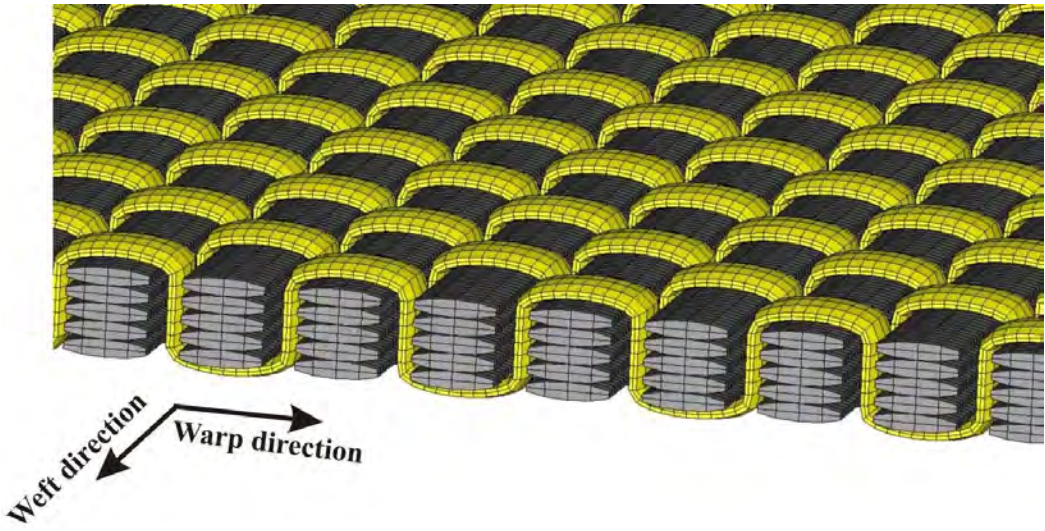

Geometry of the 3D orthogonal 5-layer woven fabric

Results of numerical simulation

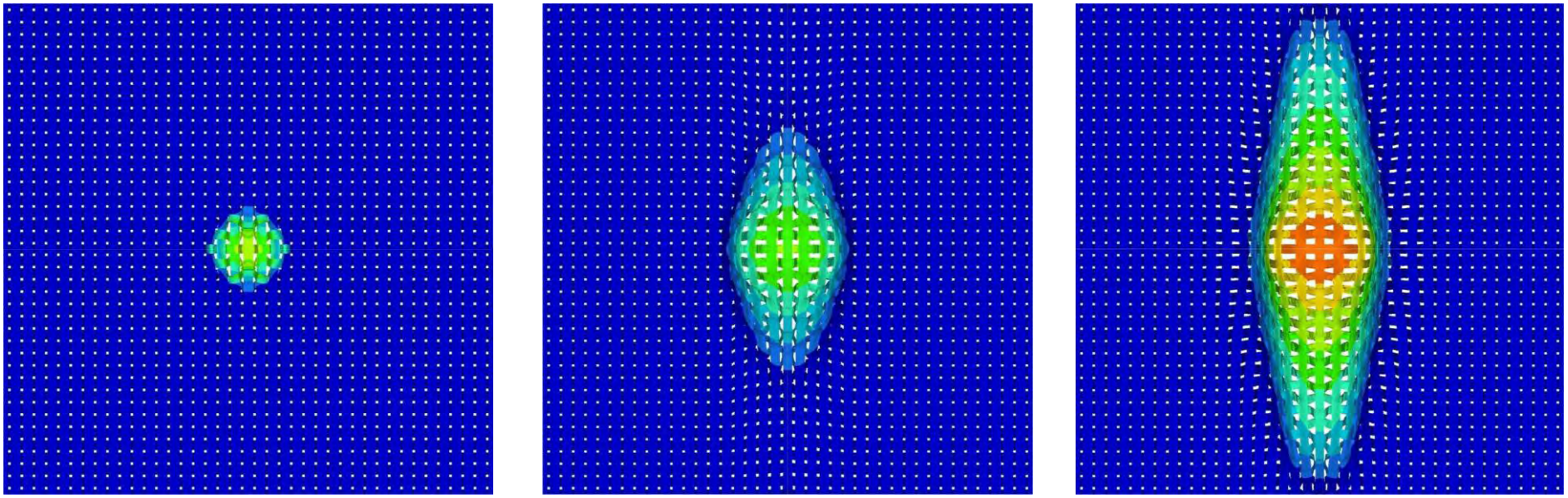

(a) (b) (c)

Behavior of the 3D orthogonal 5-layer woven fabric subjected to a 900 m/s ballistic impact :
(a) at 1.5 µs; (b) at 6 µs ; (c) at 10 µs

Results of numerical simulation

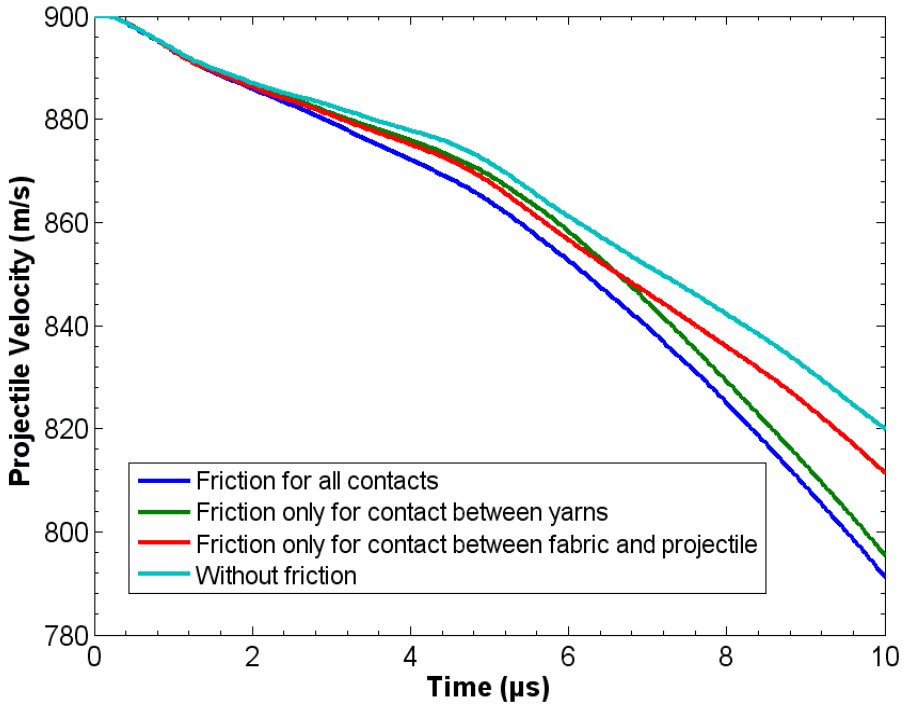

Projectile velocity versus time during a 900 m/s impact on the 3D orthogonal 5-layer woven fabric

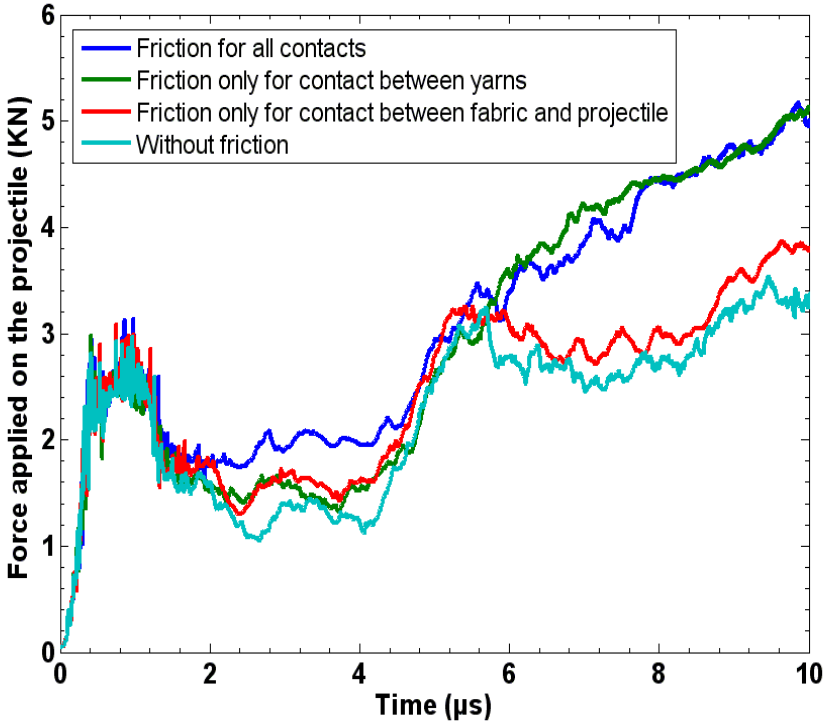

Force applied on the projectile during a 900 m/s impact on the 3D orthogonal 5-layer woven fabric

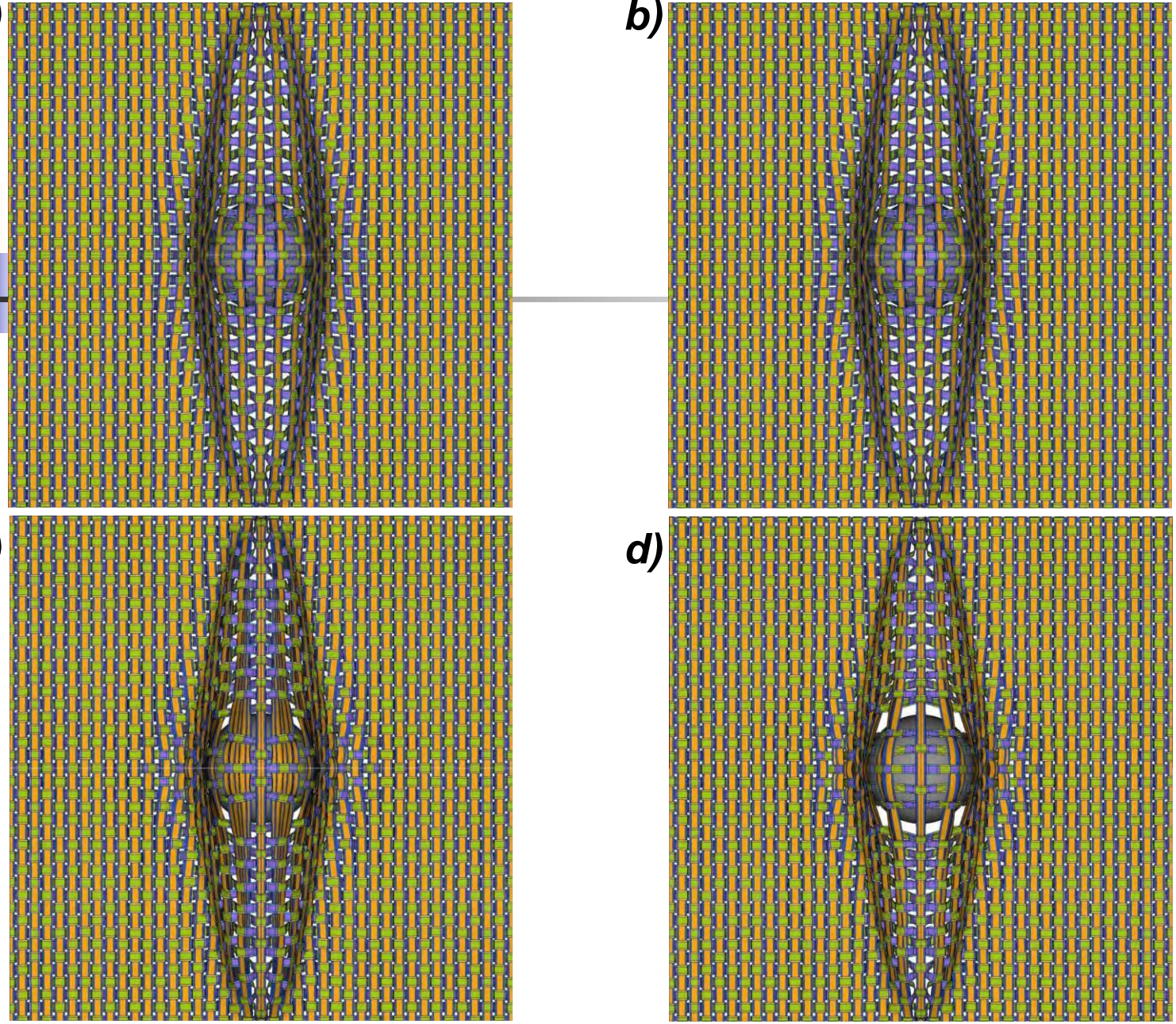

Configurations of the 3D orthogonal 5-layer fabric subjected to 900 m/s impact at 10 µs :
a) Friction at all contacts; b) Friction only at the contact between yarns;
c) Friction only at the contact between fabric and projectile; d) Without friction

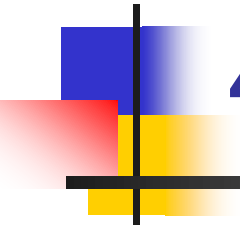

4. Works in progress

Works in progress

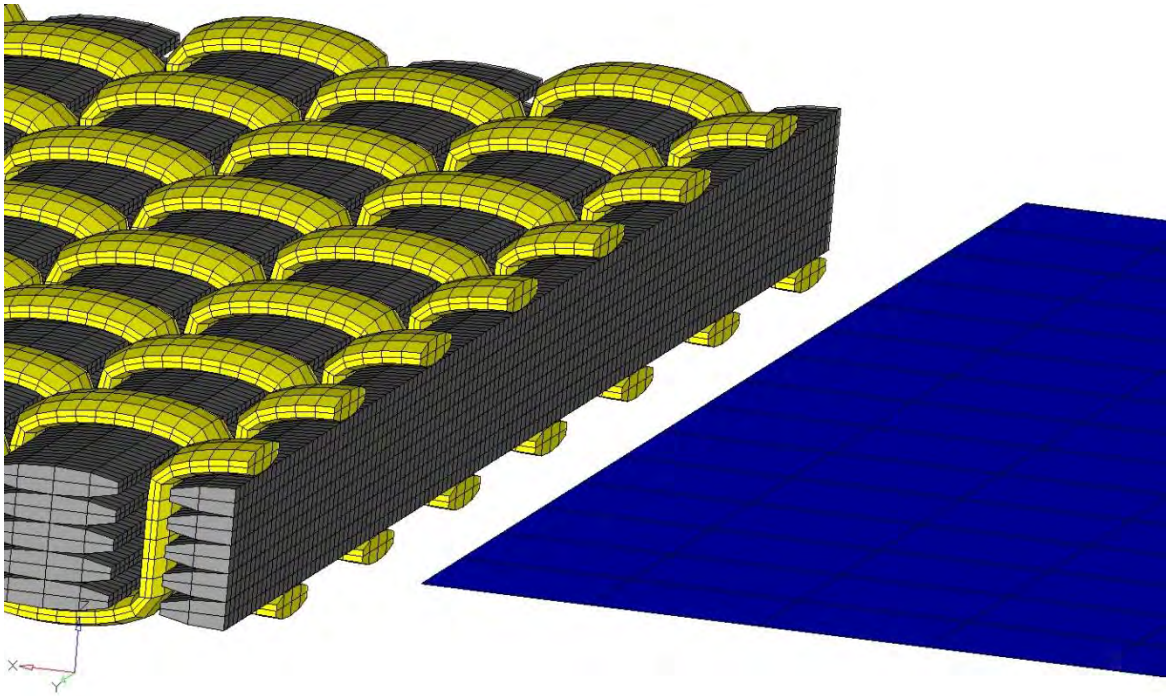

Connection between macroscopic and mesoscopic zones in 3D woven fabrics

Works in progress

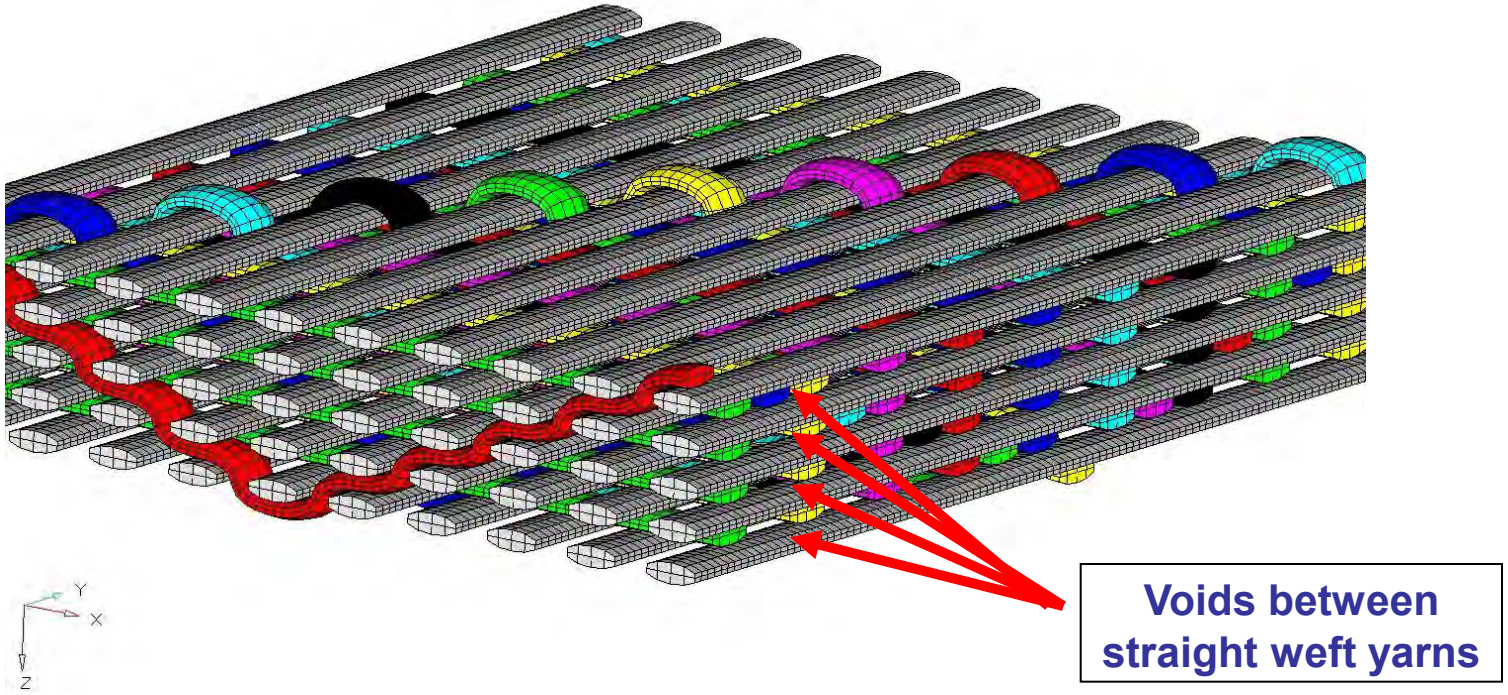

Voids in the interlock-warp woven fabric due to straight weft yarns

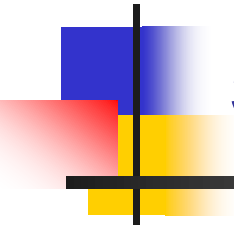

5. Conclusions and perspectives

Conclusions

An effective numerical tool – Ktex_pattern is successfully created for geometrical representation and finite element modeling of textile woven fabrics

With Ktex_pattern, the ballistic impact behavior of a 3D interlock warp woven fabric and friction effects are studied numerically

Perspectives

Improvement of the algorithm of the numerical geometric tool Ktex_pattern for creating automatically more realistic models

New numerical technique for the connection between two macroscopic and mesoscopic zones the 3D woven fabrics

Perspectives

Create a more realistic geometric model and then, an impact finite element model of the 3D fabrics from tomographic images

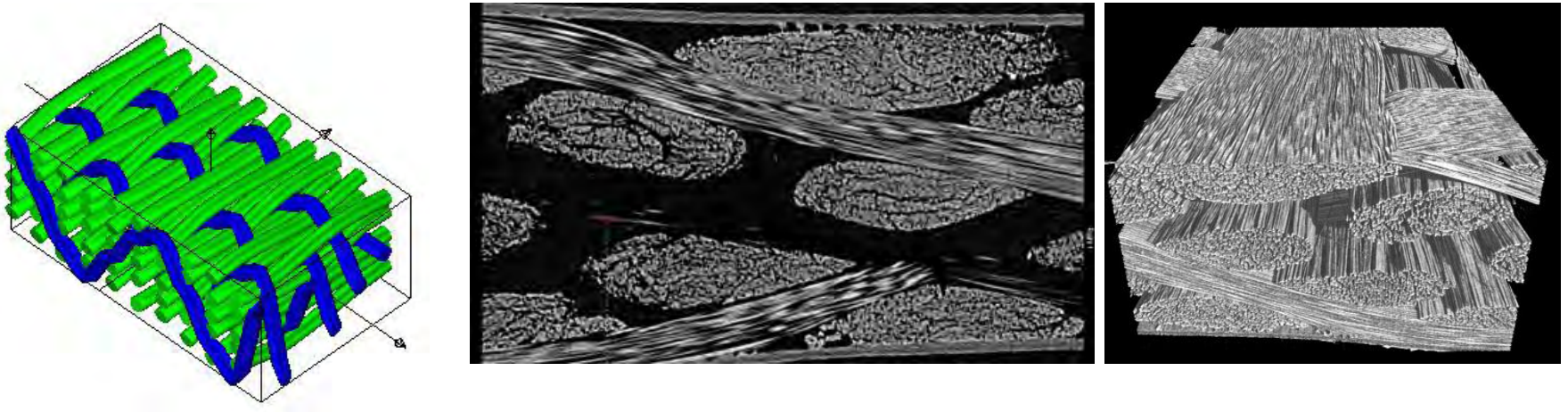

Description of warp interlock fabric
(left) Wisetex modelling geometric view
(middle) photomicrographs of longitudinal sections
(right) 3D tomography view in weft direction

Thank you for your attention

Acknowledgment: We would like to thank the EDA for the financial support to conduct this study

Why Impacted Yarns Break at Lower Speed Than Classical Theory Predicts

James D. Walker and Sidney Chocron

Southwest Research Institute

San Antonio, Texas 78228

j:\engdyn\jdw\aps2001i.ppt

j:\engdyn\jdw\aps2001i.ppt

Genesis of the Talk

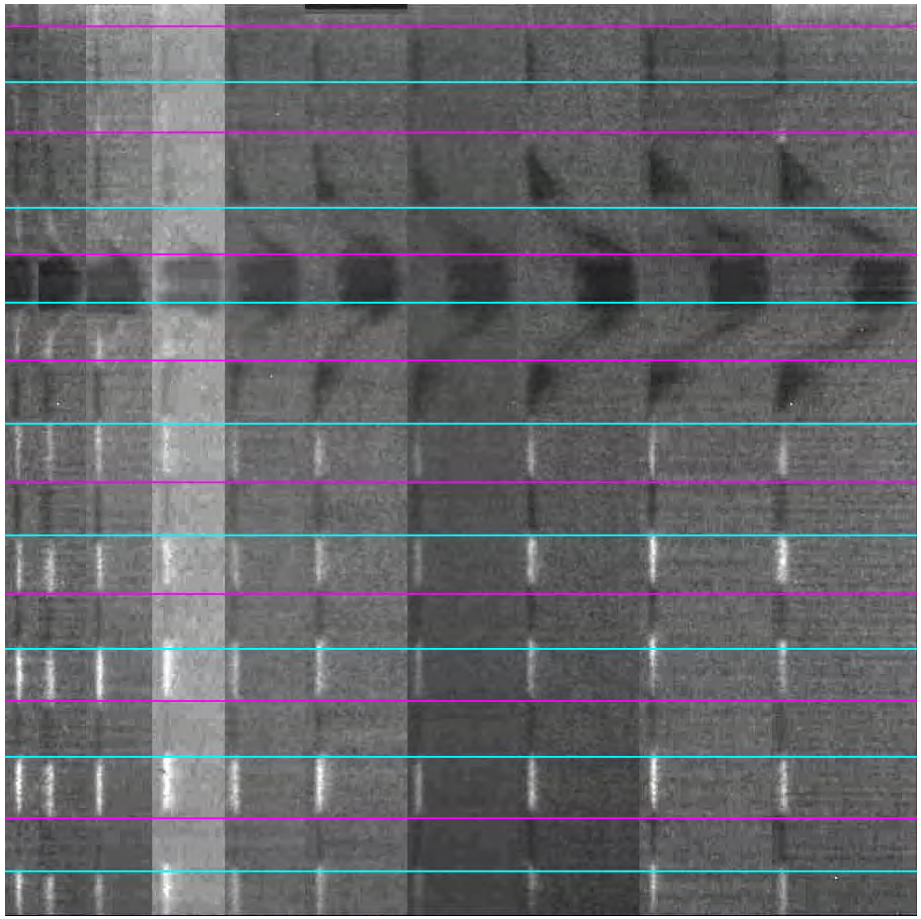

- In September 2010 in Quebec City at PASS, Harm van der Werff of DSM pointed out to Sidney Chocron the fact in the title.
- Sidney returned to Southwest Research Institute and confirmed with already existing SwRI data that it was indeed the case.
- Sidney told James about it – James felt we had the analytic tools to understand the effect.
- In particular, the authors had included the dynamic deformation of yarns in their Advanced Solid Mechanics course they were teaching at the University of Texas at San Antonio that semester.

Yarn 12 – Dyneema – 517m/s
4 μs per frame

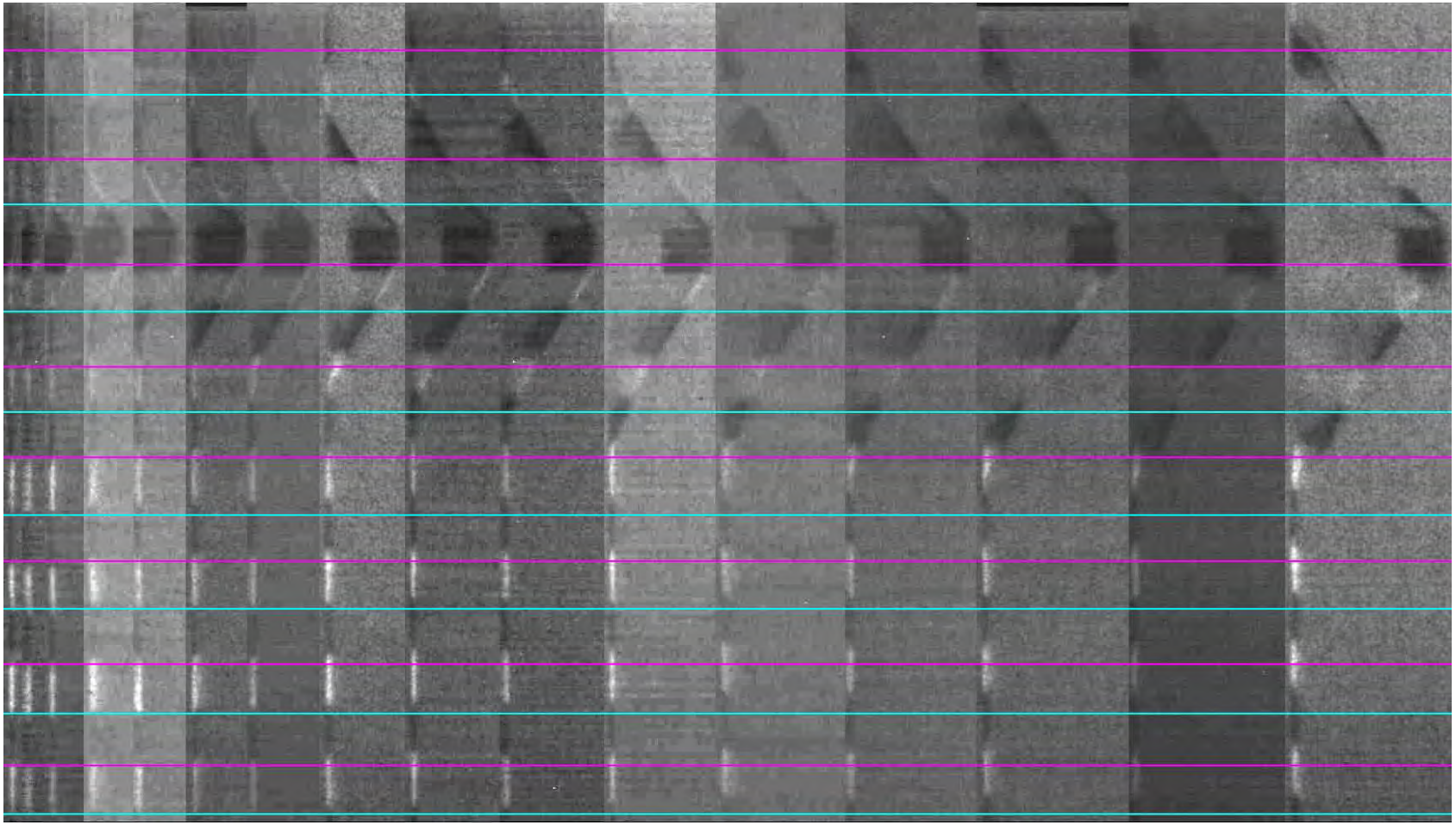

No failure

3

Yarn 11 – Dyneema – 583m/s
4 μs per frame

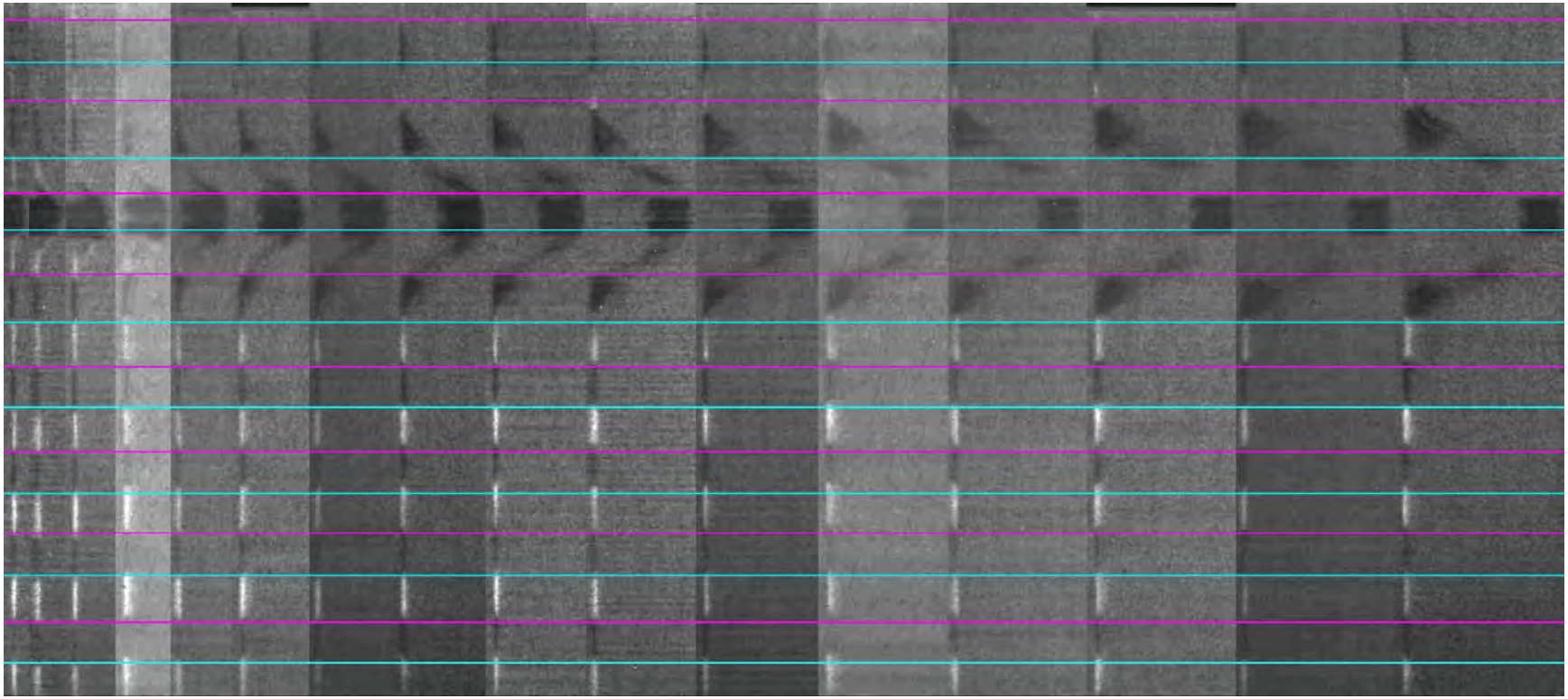

Immediate failure

4

Fact Observed by Other Researchers

1970: **Wilde, Ricca, Cole and Rogers**. Dynamic response of a constrained fibrous system subjected to transverse impact Part 1 – Transient responses and breaking energies of nylon yarns. Technical Report, Army Materials and Mechanics Research Center, Watertown, Massachusetts, 02172. Report no. AMMRC TR 70-32.

1982: **Carr**. Failure mechanisms of yarns subjected to ballistic impact. *Journal of Material Science Letters*, 18(7):585-588.

1990: **Field and Sun**. A high speed photographic study of impact on fibres and woven fabrics. In SPIE Vol. 1358, 19th International Congress on High-Speed Photography and Photonics.

1992: **Wang, Field and Sun**. Dynamic behaviour of pre-stressed high strength polymeric yarns transversely impacted by a blade. In Proceedings of the Int. Symp on Intense Dynamic Loading and Its Effects, pages 354-359. Chinese Society of Theoretical and Applied Mechanics, Sichuan Univ. Press, Chengdu, China.

2001: **Bazhenov, Dukhovskii, Kovalev and Rozhkov**. The fracture of SVM aramide fibers upon a high-velocity transverse impact. *Polymer Science*, Ser. A, 1:61-71. [Had an explanation, which did not seem to work.]

2010: **van der Werff and Heisserer**. Personal communication.

Classical Theory of Smith

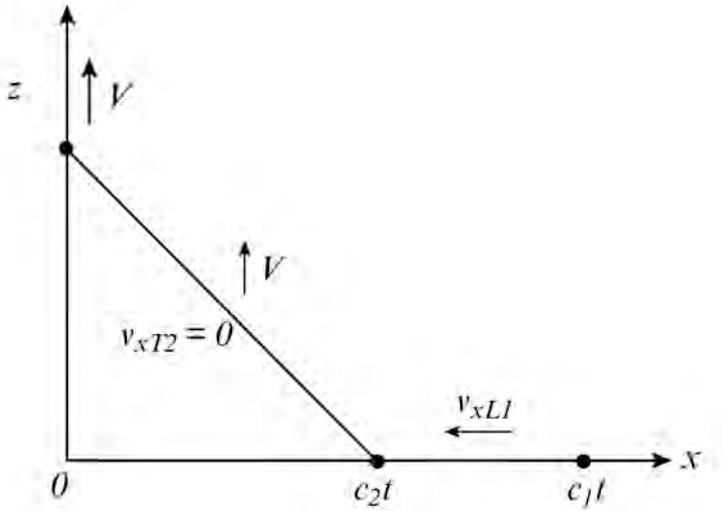

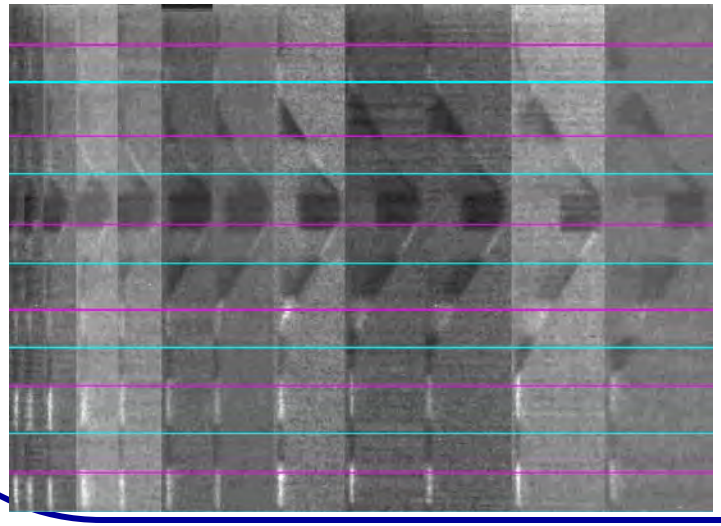

- The classical theory of yarn deformation developed by Smith and published in 1958 dealt with a yarn that was deformed by a perpendicular motion at one end.
- Two waves develop:
  - A tensile longitudinal wave in the yarn, and
  - A transverse wave in the yarn.
- It is possible to explicitly solve for these waves.

New Approach to Classical Theory

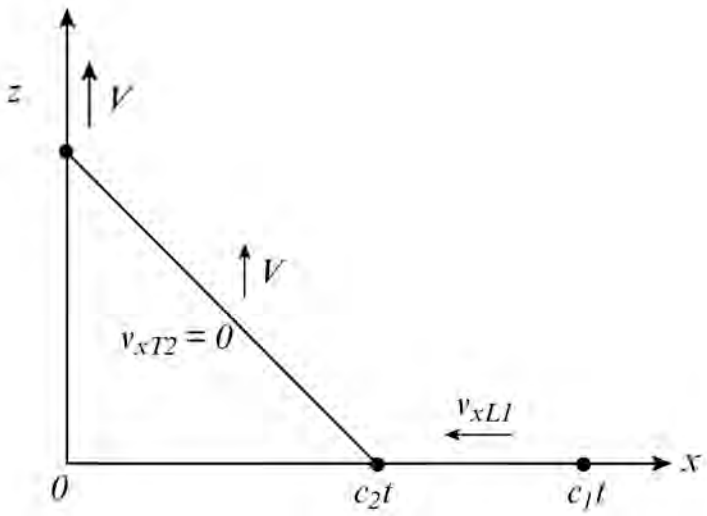

$$\sum_{j=1}^{3} \frac{\partial S_{ji}}{\partial x_j} + \rho_0 b_i = \rho_0 \frac{\partial v_i}{\partial t} = \frac{\partial}{\partial t}(\rho_0 v_i)$$

$$[-S_{ji}] = c[\rho_0 v_i]$$

$$S = \frac{\rho_0}{\rho} F^{-1} \sigma \quad \text{where} \quad F = \delta_{ij} + \frac{\partial u_i}{\partial x_j}$$

- A new approach to solving the equations for the deformation of the yarn is to do it in the original, undeformed frame of reference of the yarn.
  - Yields an exact solution, even for large strains.
  - Framework for solving the harder problem.
- The stress when written in this reference frame is referred to as the Piola-Kirchhoff stress.
- In particular, we use what is referred to as the first Piola-Kirchhoff stress tensor, which is not symmetric.
- The stress is the force with respect to the undeformed area.
- The wave motion can be solved by the Hugoniot jump conditions at the two wave fronts (the longitudinal and the transverse).

The Yarn is Assumed Linear Elastic

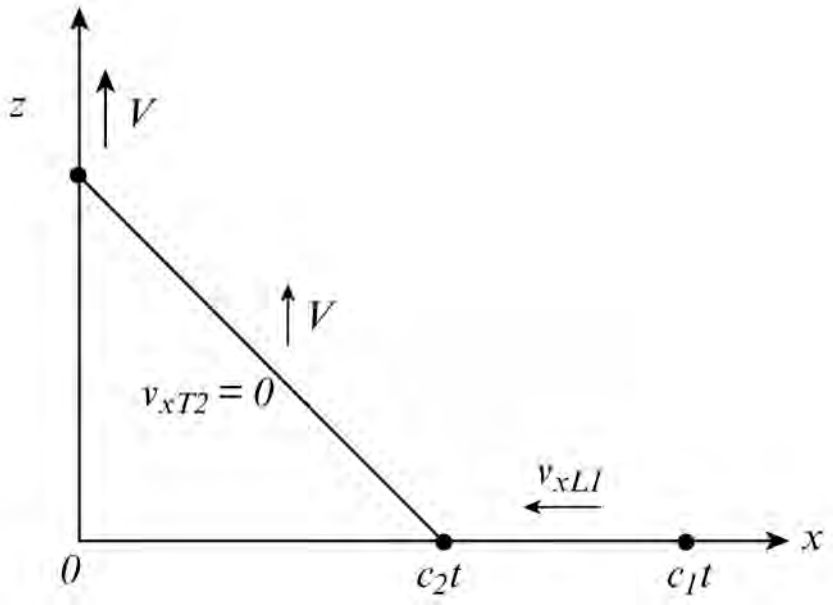

- The yarn deformation is assumed to be linear elastic, based on energy, with a constant modulus E and a strain to failure ε_f. The conjugate variable to the first Piola-Kirchhoff stress is the transpose of the deformation gradient, F^T.

$$e = \frac{1}{2} E (E_{11})^2$$

$$(E_{ij}) = \frac{1}{2}(F^T F - I)$$

$$S_{ij} = \frac{\partial e}{\partial F_{ij}^T} = \frac{\partial e}{\partial F_{ji}}$$

$$S_{11} = \frac{\partial e}{\partial F_{11}} = E E_{11} F_{11}, \quad S_{13} = \frac{\partial e}{\partial F_{31}} = E E_{11} F_{31}$$

- In these expressions, the first Piola-Kirchhoff stress has been written in terms of the deformation gradient F and the Lagrangian (Green) strain E_{ij}.

The Exact Solution

- Solving with the linear stress-strain relation, assuming a boundary condition of an applied tangential velocity at one end of the yarn, yields an exact solution (this applies even to large strain), most easily expressed in terms of strain in the deformed section of yarn E_{11}:

$$\left(\frac{c_1}{c_E}\right)^2 = \frac{1}{2} + \frac{1}{2}\sqrt{1+2E_{11}} + E_{11},$$

$$\left(\frac{c_2}{c_E}\right)^2 = E_{11},$$

$$\frac{v_{xL1}}{c_1} = 1 - \sqrt{1+2E_{11}},$$

$$\left(\frac{V}{c_E}\right)^2 = \sqrt{E_{11}}\left(\sqrt{1+2E_{11}} - 1\right)\sqrt{\frac{1}{2} + \frac{1}{2}\sqrt{1+2E_{11}} + E_{11}}$$

$$\times\left\{2\sqrt{1+2E_{11}} + \left(1-\sqrt{1+2E_{11}}\right)\sqrt{\frac{1}{2E_{11}} + \frac{\sqrt{1+2E_{11}}}{2E_{11}} + 1}\right\}.$$

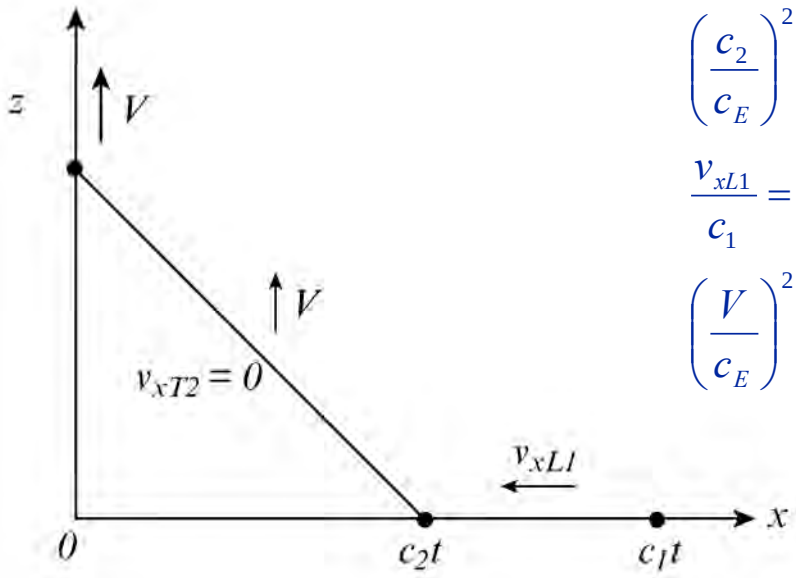

For Small Strain, the Exact Solution Reduces to Smith's Solution

$$\frac{c_1}{c_E} = 1, \quad \frac{c_2}{c_E} = \sqrt{E_{11}}, \quad \frac{v_{xL1}}{c_1} = -E_{11}, \quad \frac{V}{c_E} = (E_{11})^{3/4}\sqrt{2-\sqrt{E_{11}}}\,.$$

$$V / c_E = \sqrt{\varepsilon(2\sqrt{\varepsilon(1+\varepsilon)} - \varepsilon)}$$

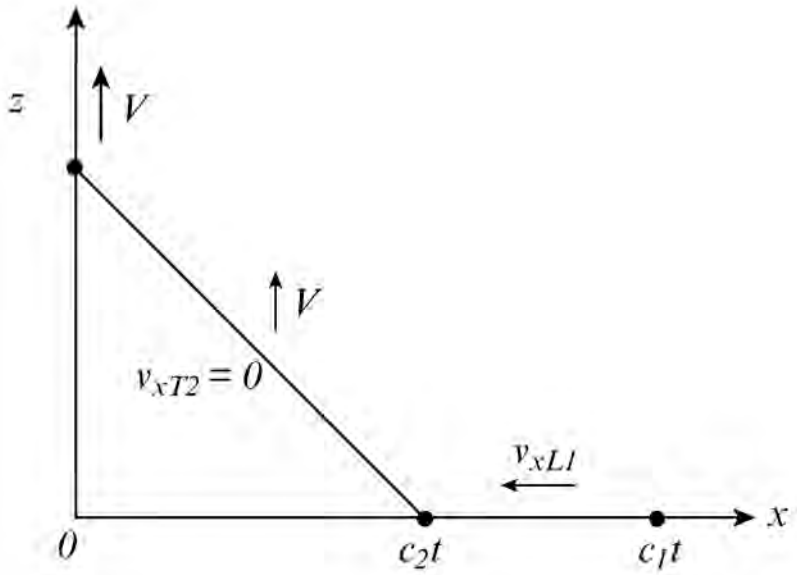

- The experimental transverse wave speed, which is a function of impact velocity and the longitudinal wave speed in the yarn, has been shown to agree with this result for various yarns.
- The natural idea is to assume that during impact the projectile speed that will break a yarn is given by setting $E_{11} = \varepsilon_f$.
- However, that doesn't agree with experiment.

Experimental Impact Speeds that Break Yarn do not Agree with Classical Theory

- These are experiments performed at SwRI by Chocron, et al. (reported Tuesday in the first general session).
- Clearly there is a large discrepancy.

Yarn	Longitudinal sound speed in the yarn	Yarn breaking strain ε_f	Breaking speed from experiment [Chocron, et al.]	Breaking speed from classical theory
	(km/s)	(%)	(m/s)	(m/s)
KM2 S5705	7.45	4.25	Between 621 and 634	934
Dyneema SK-65	9.89	3.60	Between 517 and 583	1100
PBO	10.7	3.25	Between 523 and 610	1105

Why is there a Discrepancy?

- If the classical theory agrees for transverse wave speed, why does it not agree for the impact speed that breaks the yarn?
- The reason is that for a the boundary condition that occurs during impact of a flat-faced projectile is not the same as the applied boundary condition from the classical (Smith) theory.
- However, for a small projectile and when the yarn does not break, a few microseconds after impact the boundary condition approaches the Smith boundary condition.

The Initial Boundary Condition is Not the Same (impact speed 555 m/s)

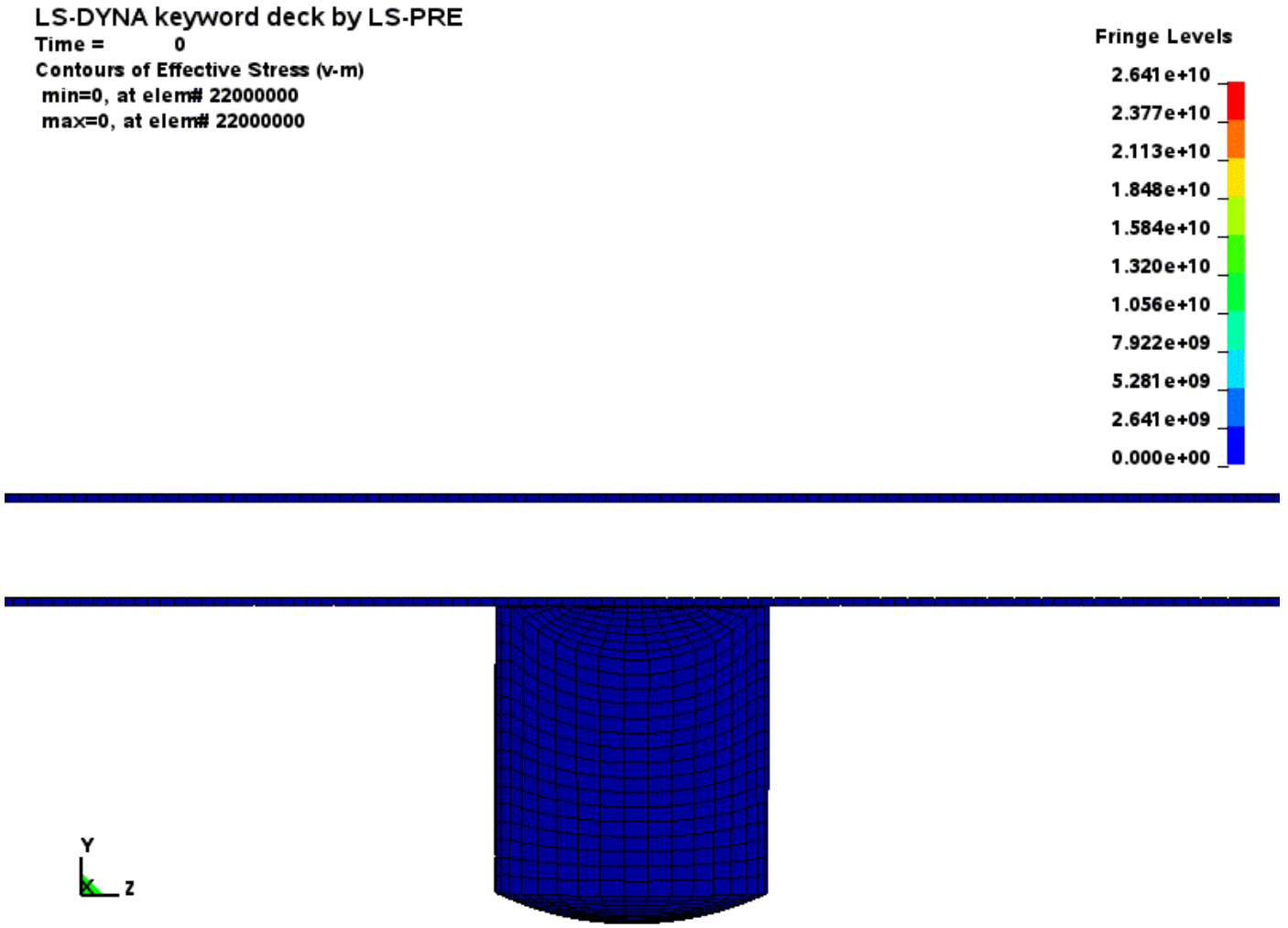

For A Higher Impact Speed, the Yarn Breaks ALMOST Immediately

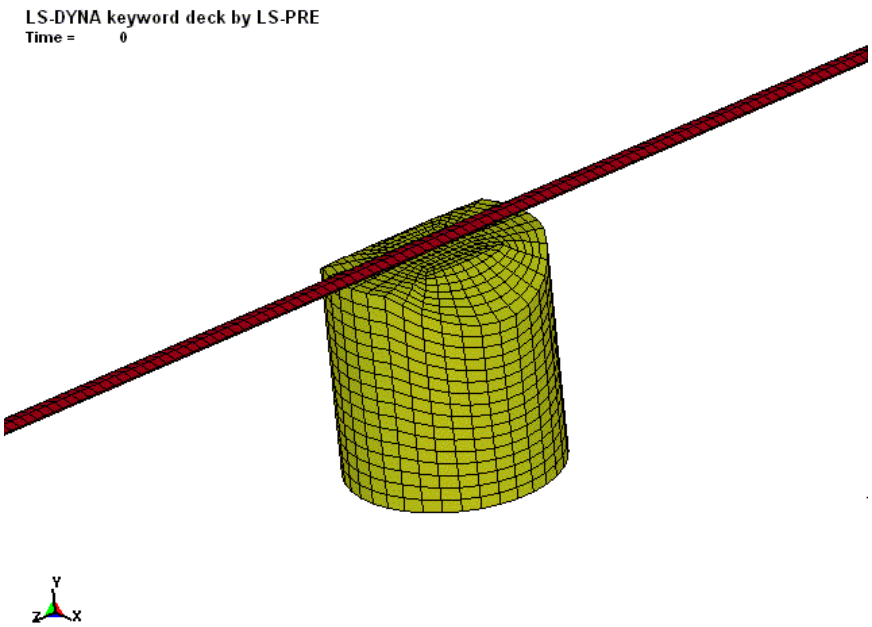

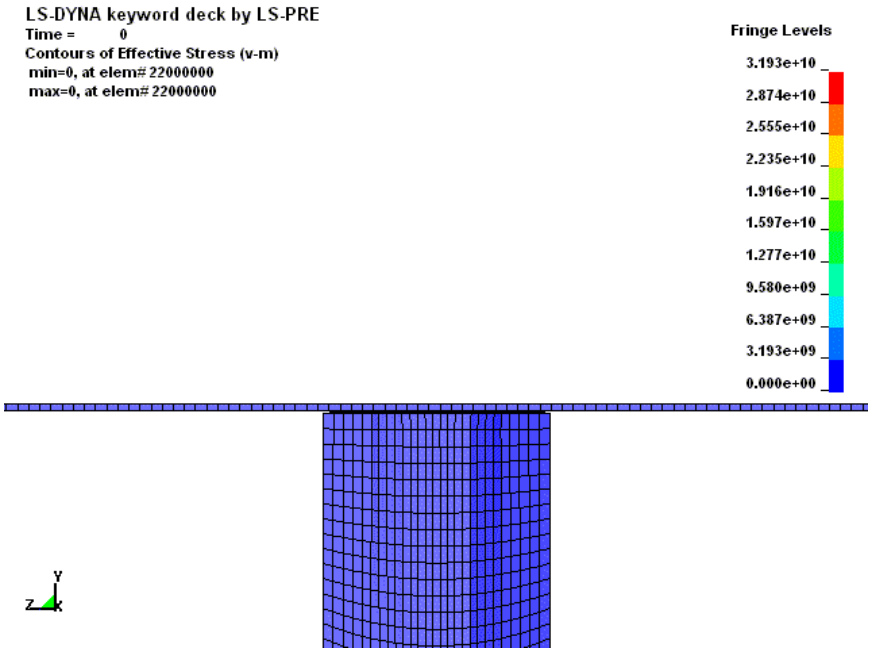

Flat-face Projectile Impact on Yarn

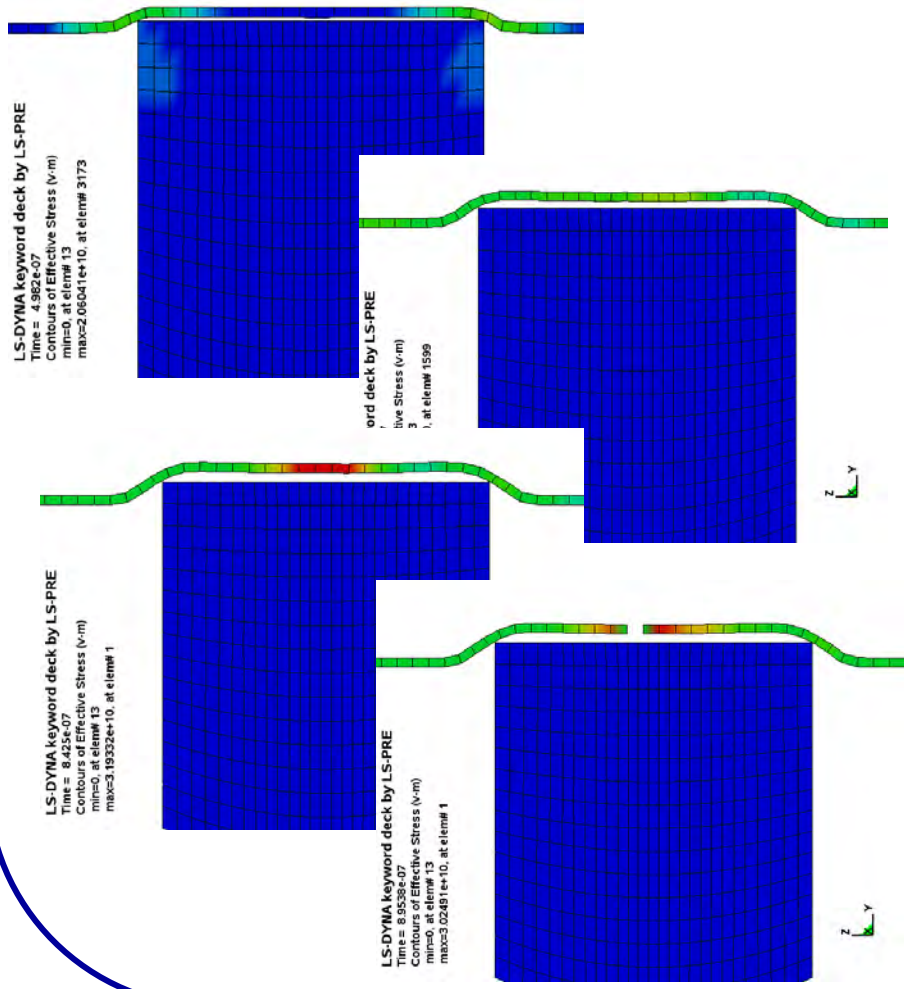

- The flat projectile face strikes the yarn.
- The yarn bounces off the surface in the direction of impact, at twice the impact speed for an elastic impact.
- From both sides where the yarn touches the projectile, longitudinal and transverse waves emanate along the yarn in both directions.
- Two longitudinal waves meet above the center of the projectile, doubling the stress and strain.
- If the stress and strain are high enough, the yarn breaks.

Solving for the More Complicated Condition

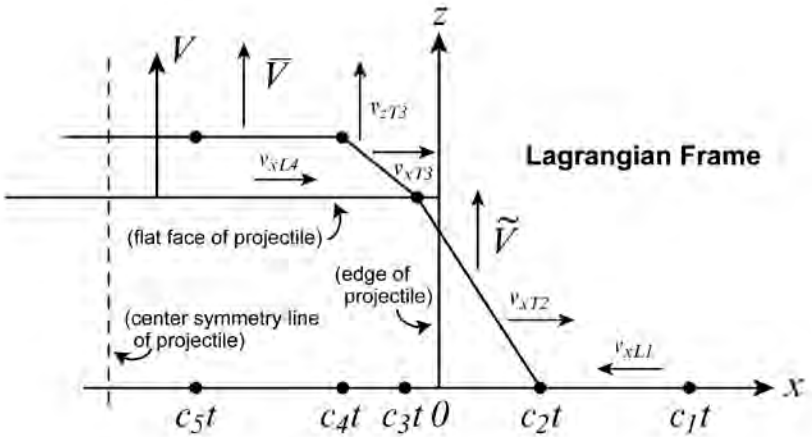

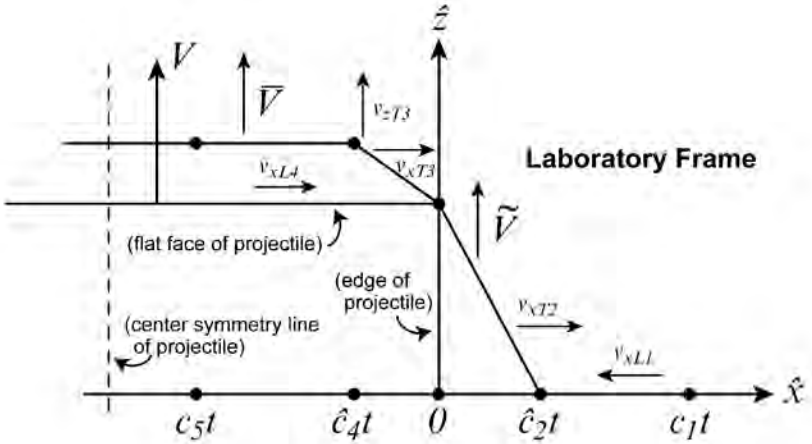

- We focus on just one side of the projectile.
- Four waves emanate along the yarn from that point, two longitudinal waves and two transverse waves.
- The particle velocity and wave speed of these fronts can be explicitly determined by solving the Hugoniot jump condition at each wave front.

The Assumptions

- We include the fact that the yarn “bounces” off the face of the projectile in varying amounts, from no bounce (stays on surface) to elastic bounce (twice the impact speed). Yarn bounce plays a significant role in the yarn breaking speed.
- We assume that the strain in the yarn does not change where it touches the edges of the projectile, thus yielding the result that strain is uniform in the deformed region of yarn.
- The previous assumption allows us to use a geometric approximation to determine the strain in the yarn.
- The strain in the yarn due to the initial impact doubles when the waves in the yarn meet from the opposite edges of the projectile.

The Solution

$$E_{11}^{5/2}(2-\sqrt{E_{11}}) = \frac{E_{11}}{2}\left\{\left(\frac{V}{c_E}\right)^2 + \left(\frac{\overline{V}-V}{c_E}\right)^2\right\} - \frac{1}{16}\left\{\left(\frac{V}{c_E}\right)^2 - \left(\frac{\overline{V}-V}{c_E}\right)^2\right\}^2$$

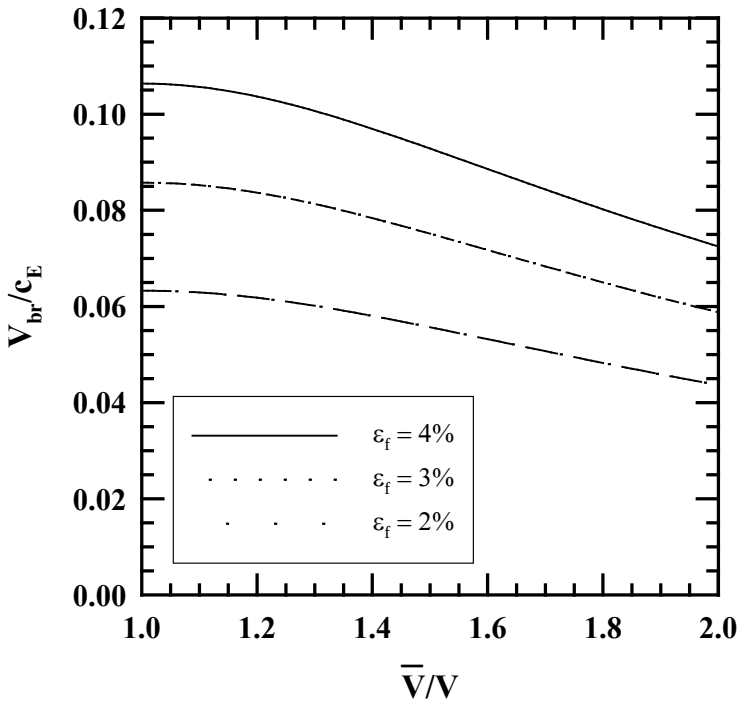

- This equation relates the yarn bounce, the impact speed, and the strain in the yarn.
- If we set $E_{11} = \varepsilon_f$ in this equation, then the resulting $V = V_{br}$ is the impact speed that breaks the yarn.

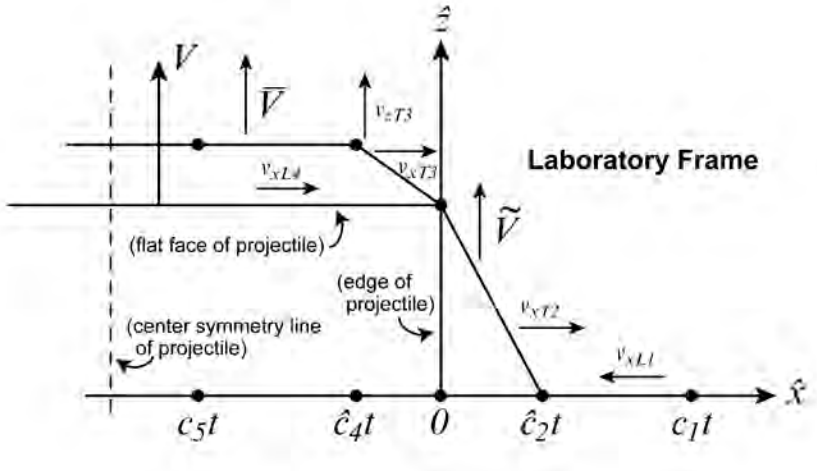

The Solution

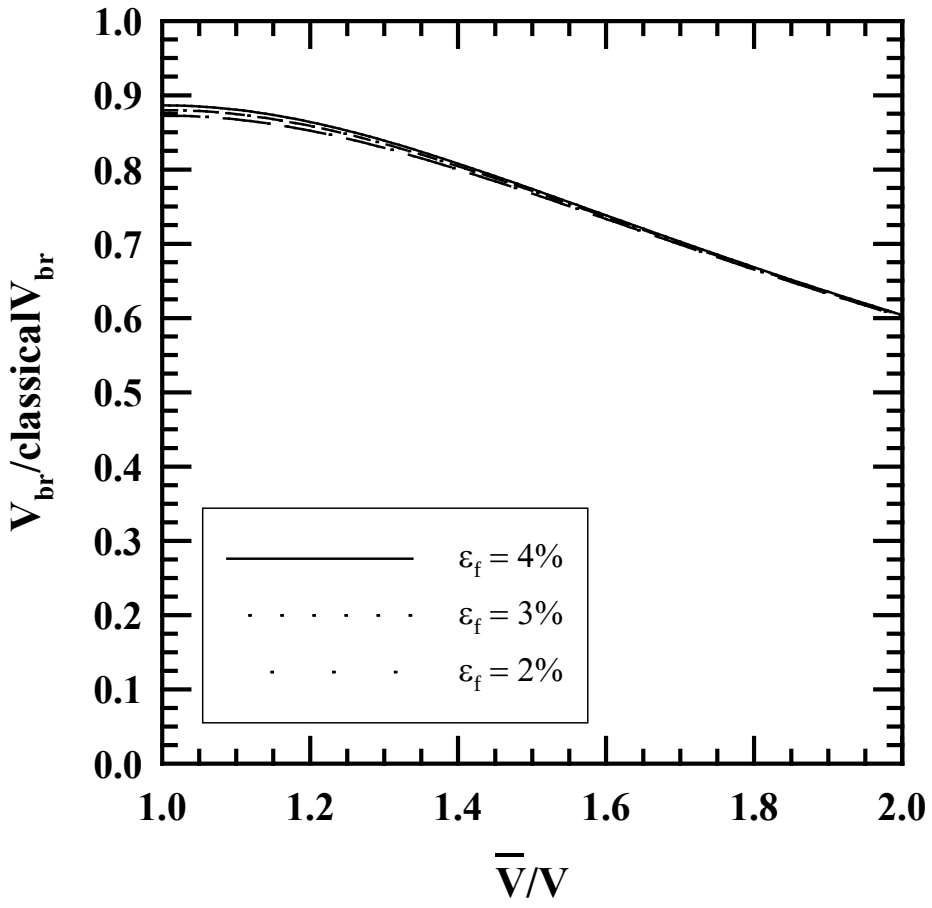

- This plot shows that the decrease in velocity for no bounce is 11% - thus, this is the largest possible breaking speed due to impact with a flat-faced projectile.
- If the bounce is at twice the impact velocity (an elastic bounce) then the decrease in impact speed that breaks the yarn is 40%.

Comparison with Data

Yarn	Breaking speed from experiment [Chocron, et al.]	Breaking speed from classical theory	Breaking speed with no bounce	Breaking speed with elastic bounce
	(m/s)	(m/s)	(m/s)	(m/s)
KM2 S5705	Between 621 and 634	934	829	565
Dyneema SK-65	Between 517 and 583	1100	972	664
PBO	Between 523 and 610	1105	973	666

- Thus, we are have reasonable agreement for an elastic bounce.
- As an aside, computations with LS-DYNA give the yarn breaking speeds as 557±3 m/s, 672±3 m/s, and 692±3 m/s, showing that the analytical model and DYNA agree.

Conclusions

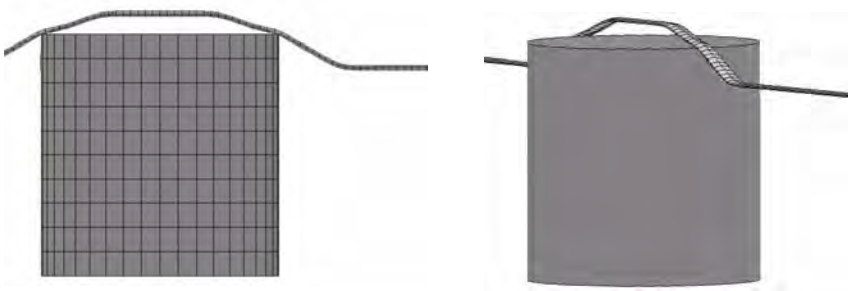

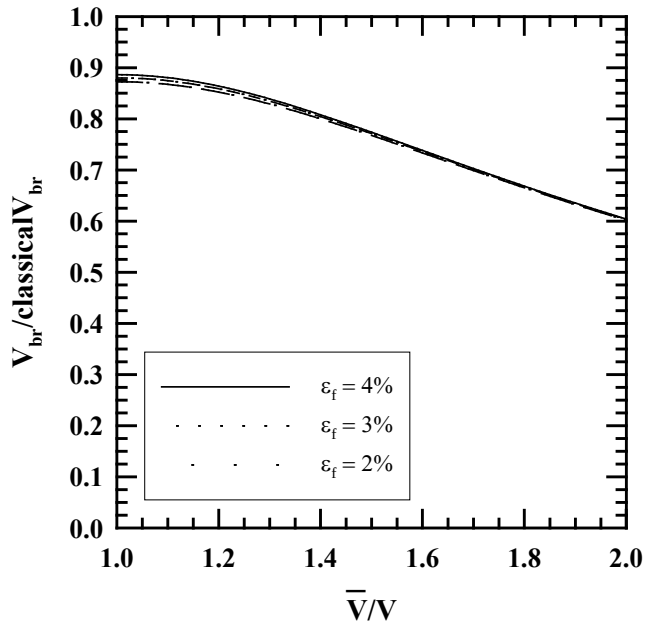

- The boundary condition when a flat-faced projectile strikes a yarn is not the same as applying a velocity to the end of the yarn.
- Working through the details yields a reduction in yarn breaking impact speed of 11% to 40%.
- These new predicted yarn breaking speeds values have reasonable agreement with experiment.

Acknowledgements

- The discrepancy in yarn breaking impact speeds between classical theory and experiment was originally pointed out to the authors at the PASS conference by
  - Harm van der Werff of DSM Dynemma (Geleen, The Netherlands) and
  - C. Leigh Phoenix of Cornell University (Ithaca, New York, USA).
- There was some discussion of this effect with van der Werff, Phoenix, and Uli Heisserer, also of DSM Dyneema.
- The LS-DYNA computations were performed by Trenton T. Kirchdoerfer (SwRI).

Extra Slides

Yarn 03 – Dyneema – 477m/s
5 us per frame

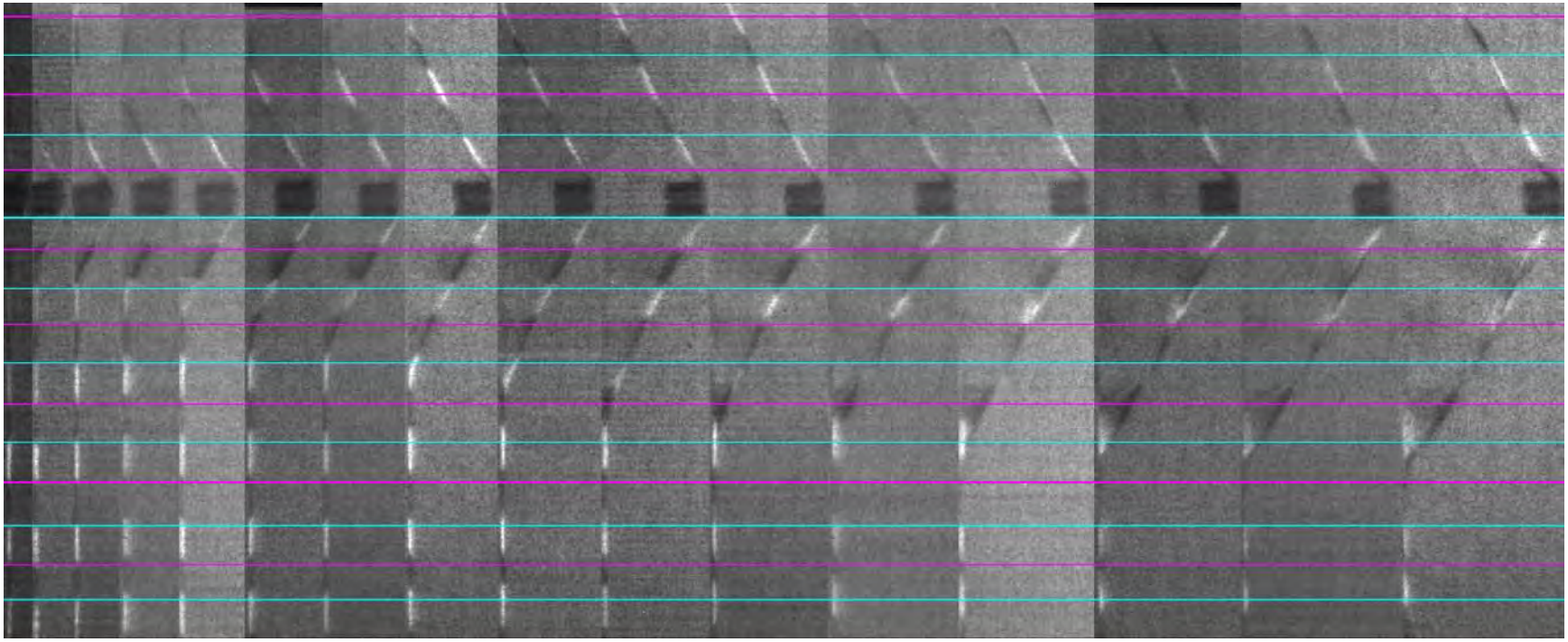

No failure

24

Yarn 06 – Dyneema – 474m/s
4 us per frame

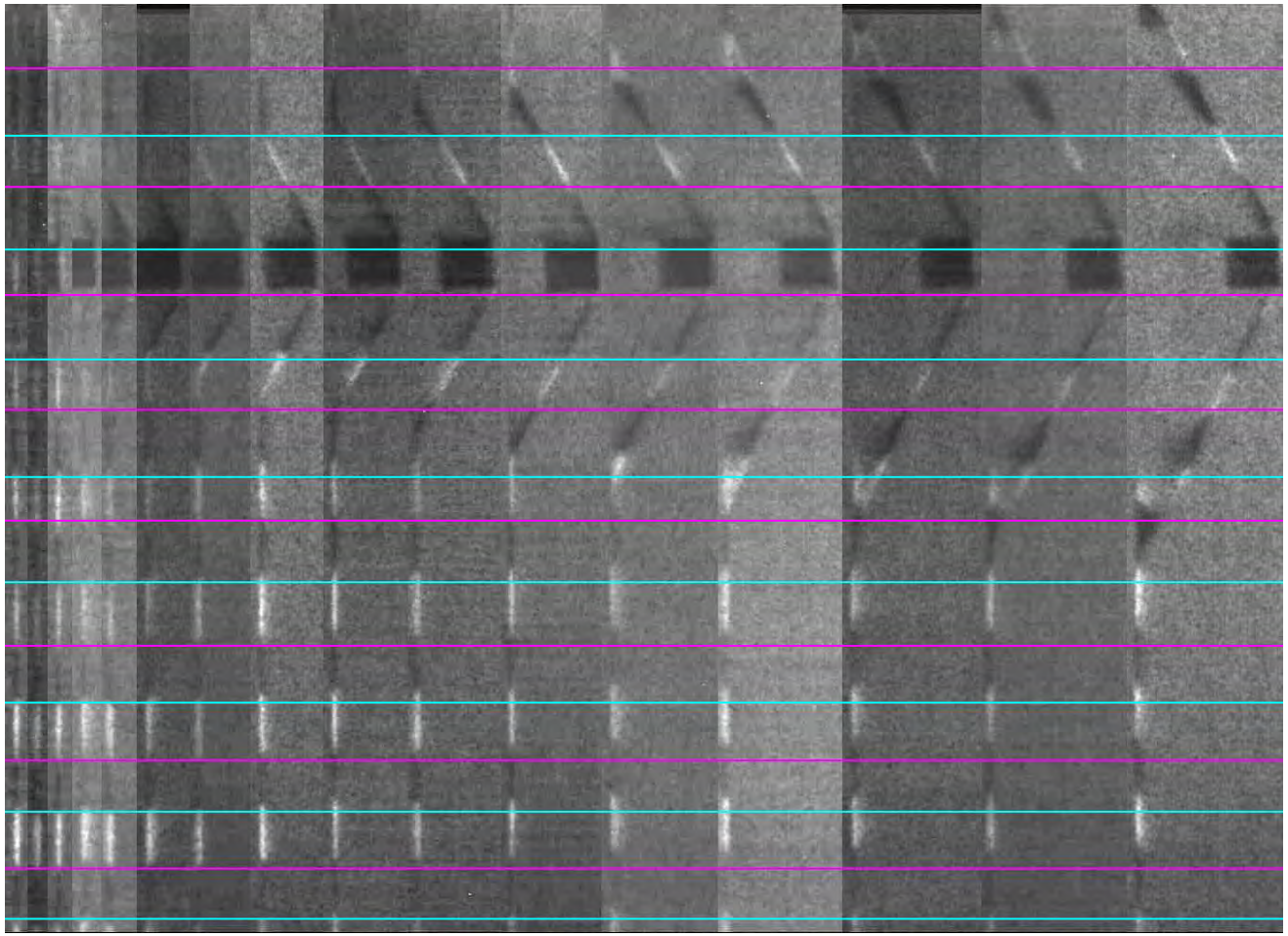

No failure

25

Yarn 09 – Dyneema – 672m/s
4 us per frame

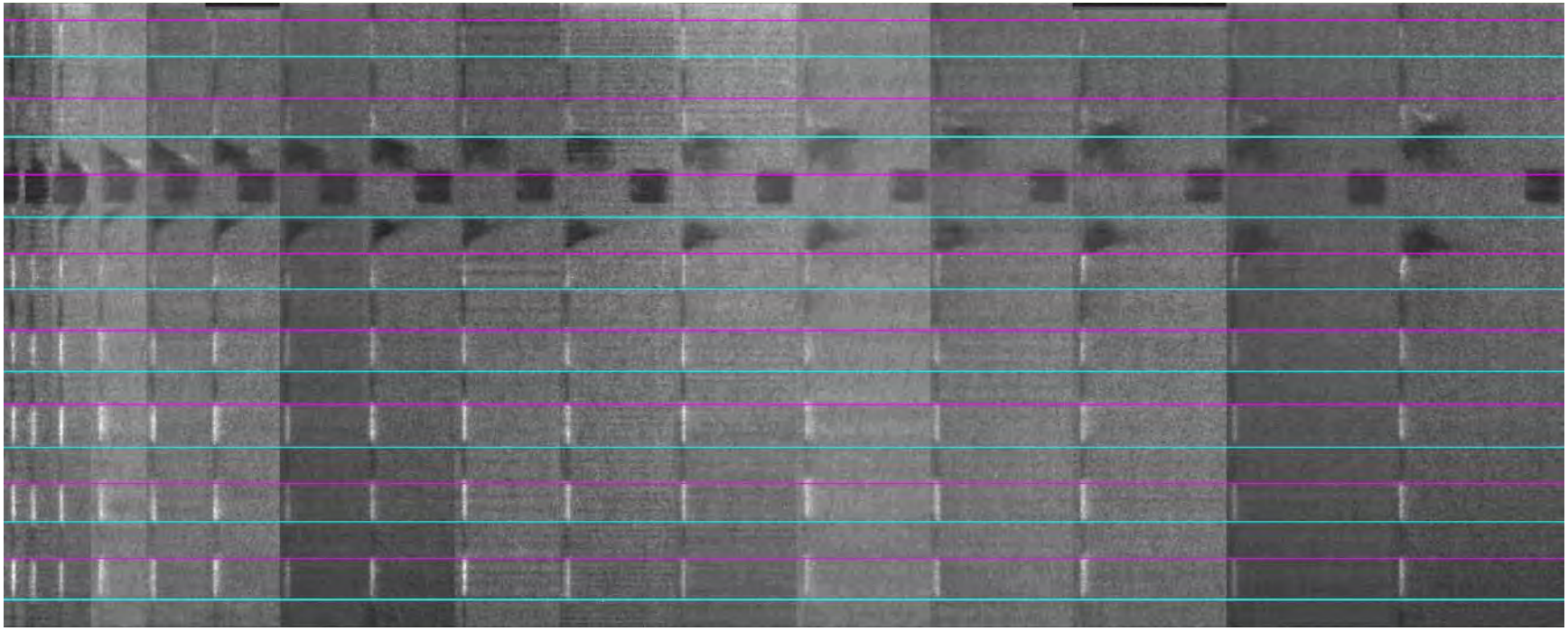

Immediate failure

26

Yarn 13 – PBO – 523m/s
4 us per frame

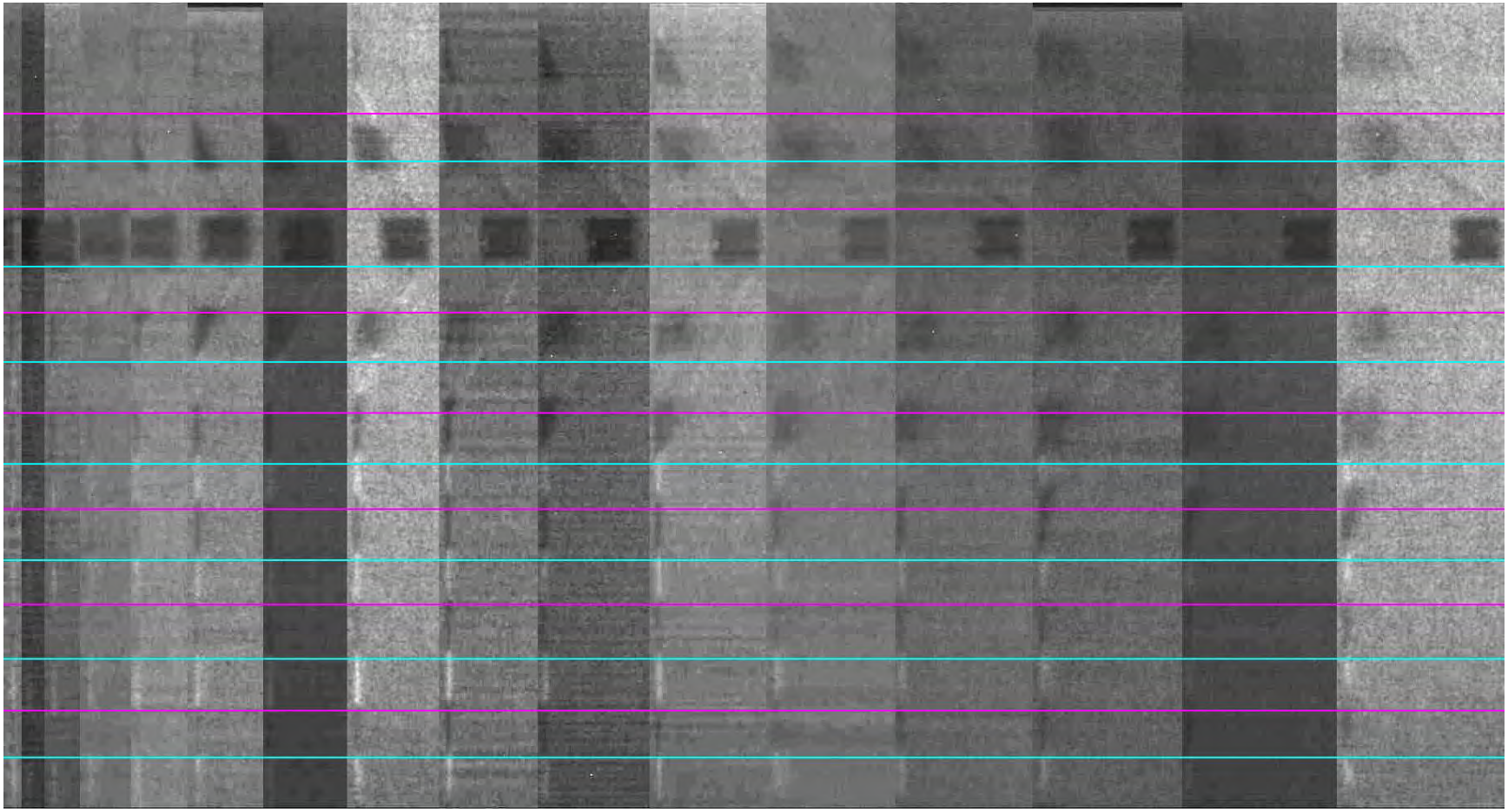

No failure

27

Yarn 18 – PBO – 610m/s
4 us per frame

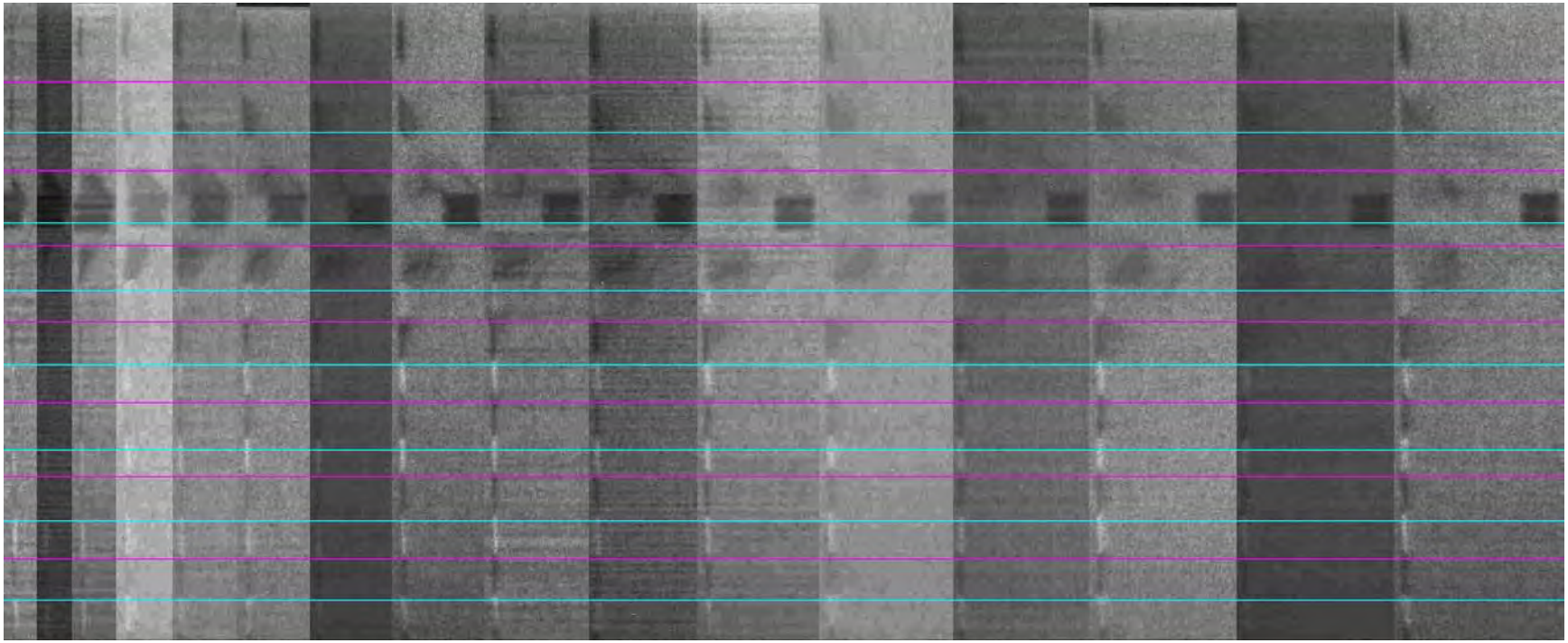

Immediate failure

28

End of Slides

U.S. ARMY ARMAMENT RESEARCH, DEVELOPMENT, & ENGINEERING CENTER (ARDEC)

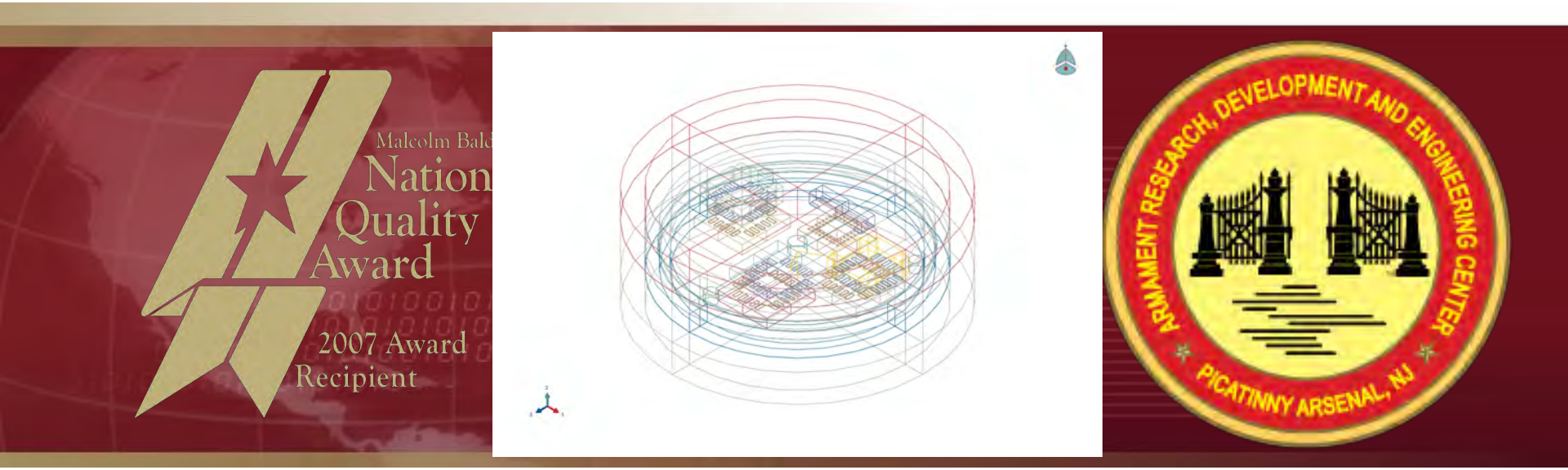

TECHNOLOGY DRIVEN. WARFIGHTER FOCUSED.

Characterization of a Potting Material for Gun Launch

Dr. Aisha Haynes, USA & Dr. Jennifer A. Cordes (Speaker)

26th International Symposium on BALLISTICS, Miami, FL, September 12-16 2011
Talk: 12062, Session: Launch Dynamics

Picatinny Arsenal, Dover NJ, USA, jennifer.cordes@us.army.mil; 973-724-6147

Outline

- Introduction
- Experimental Test Results, Example Potting
- Method: Modeling and Simulation Of Electronics With Potting
- Results: Simple Study
- Conclusions

Introduction: Goals

- Goals – compare displacements and stresses for a simple electronics module potted and unpotted under gun launch.
- Finite Element Models:
  - Board with chips, supported by potting ring
  - Board with chips, supported by full potting
- Temperatures: ambient, (-40C, 60C)
- Material Model: Linear Elastic, (Hyper-elastic), visco-elastic
- Load – 'OBR2' PMP+5% accelerations from Excalibur (actual recorded accelerations)

Introduction: Potting Issues for Gun Fired Electronics

Potting Electronic Components

Pros

- Good dynamic support of components
- Damping of shock and vibratory loads on electronics during gun launch and vibration

Cons

- Modeling and simulation with potting is more difficult than without potting
- Changes in property over temperature range
- Manufacture/process control is more difficult
- Residual stresses from curing
- Thermal stresses result from mismatch of coefficient of thermal expansion

Introduction: Statement of Problem, Model 1

Goal: Determine the impact of potting on a simple electronics system under gun launch.

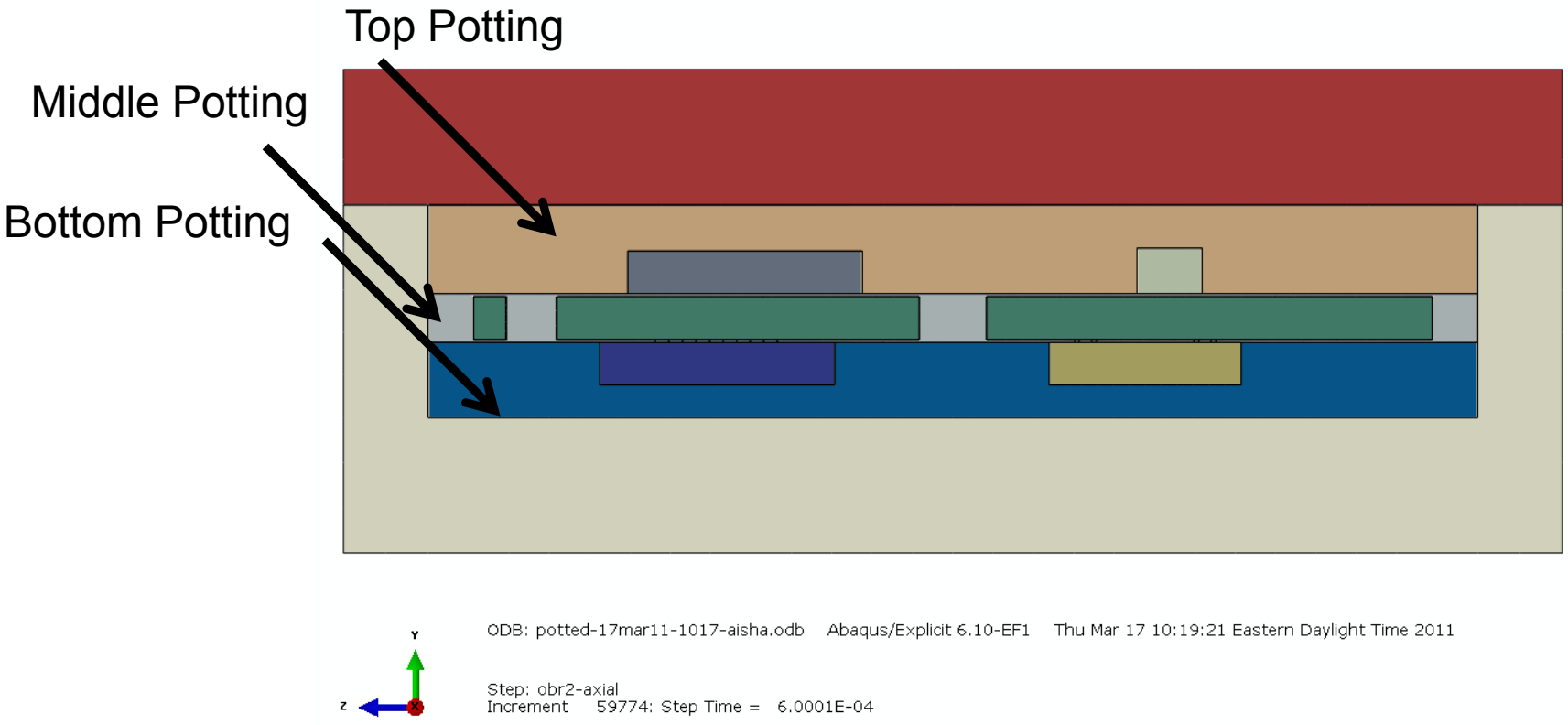

Statement of Problem, Model 2

Note: this is a representative electronics package.
It is not an actual electronics package

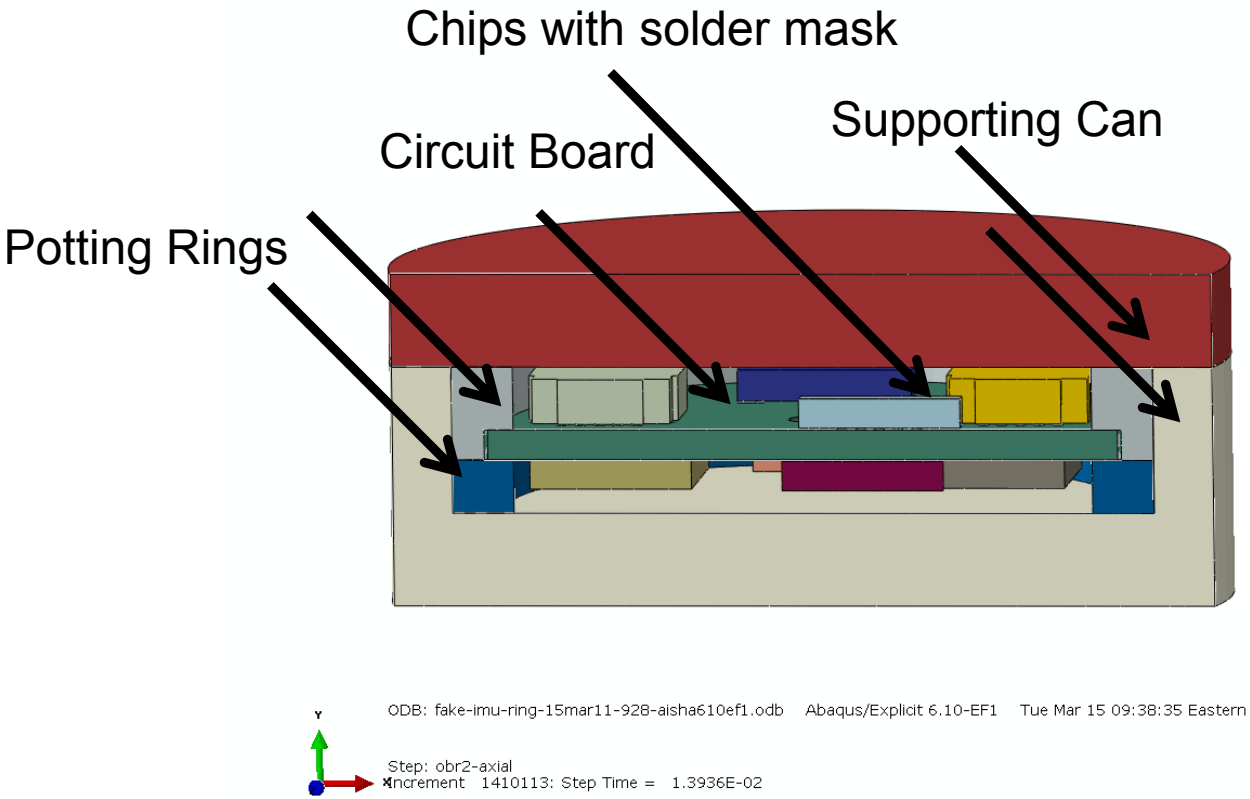

Introduction: Statement of Problem, Loads

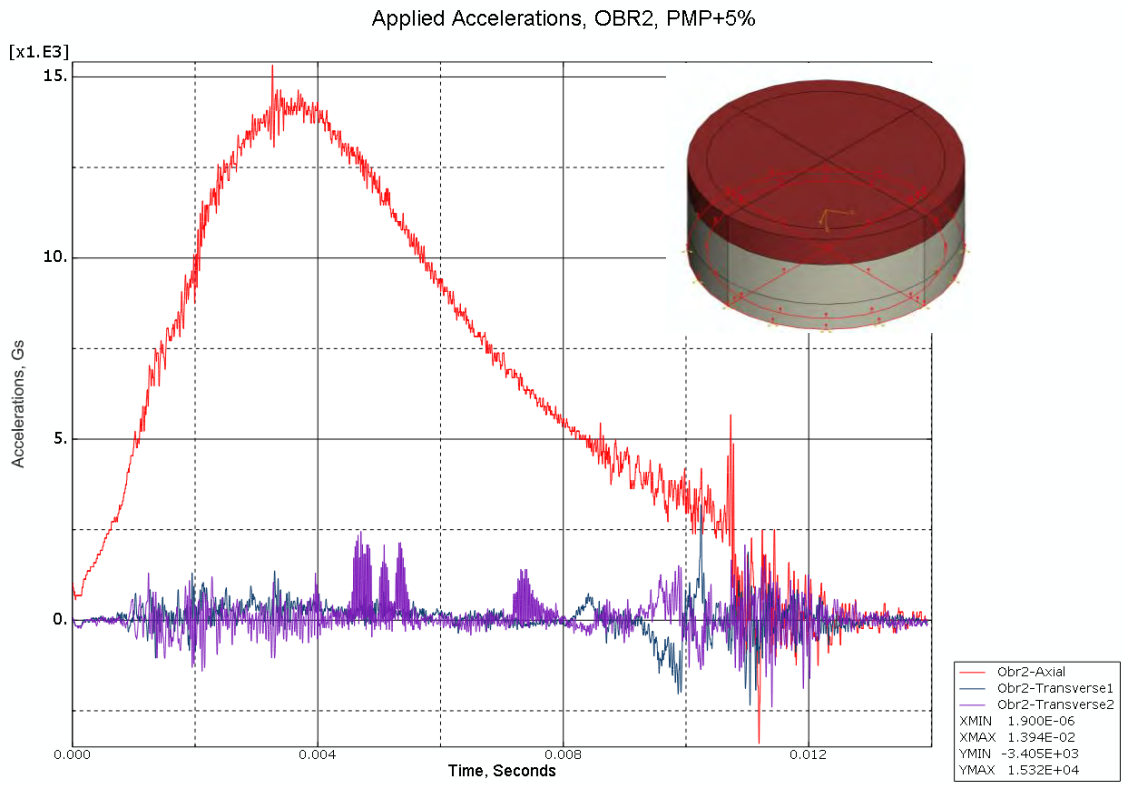

- Dynamic Loads:
- Applied through the projectile and mating structure
- Loads are 3-dimensional
- Loads are highly dynamic

- ==========

- Thermal Loads from Storage
- Repeated temperature cycles

Experimental Results: What tests do you need?

For modeling and Simulation, we need accurate material properties and material models at different temperatures

- Dynamic Mechanical Analysis (for example: ASTM standard 7028)
- Poisson's ratio & density
- Tensile/compressive stress strain data (to failure) for modeling hyper-elasticity
  - Limitation: Plasticity/Damage cannot be modeled with visco-elastic material definition in ABAQUS
-
- **High strain rate/high frequency data (optional)
- Coefficient of Thermal Expansion
- Specific Heat
-
- Thermal Conductivity

Material Model Potting: Assumptions

Potting Material: filled polyurethane system

From the DMA data, the glass transition temperature is in the range between -10C and 20C depending on the criteria used

Constitutive Material models:

Elastic or Hyper-elastic

Visco-elastic

DMA data was 3-point bend data providing E' and E" values. These were converted to shear modulii, $G=E/2*(1+\mu)$

The calculated shear modulus at 1Hz was assumed to be the long term shear modulus, G_∞

The material is incompressible. Poisson's ratio is around 0.5. For dynamic/explicit analysis, ABAQUS recommends 0.475 .

The sample was subjected to multiple frequency oscillations under varying temperatures from -101 C to 71 C (-150 F to 160 F). 11 Frequencies.

Experimental: Storage and Loss Modulus (dynamic tests)

Dynamic Mechanical Analysis (DMA)

- Provides modulus data
- Can provide damping data
- Can be used to model material visco-elasticity

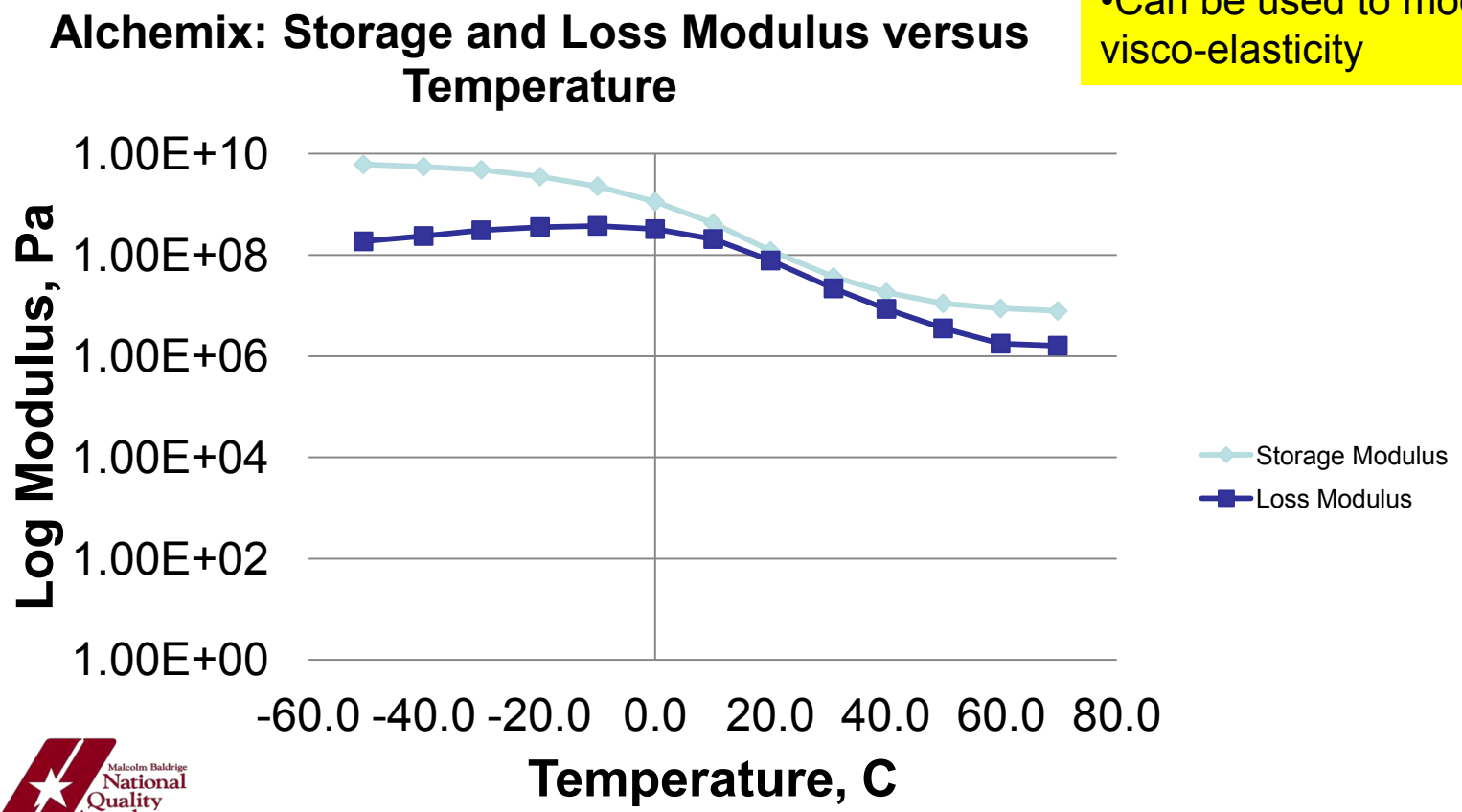

Table 2. Material Assumptions

Materials

Parts	Material	Material	Young's Modulus	Poisson's	Mass Density
		Type	MPa	Ratio	kg-m3
Ceramic Chips	CERAMIC_X7R	Elastic	104954	0.3	5.92E+03
can-1	Aluminum	Elastic	69049	0.3	2.72E+03
board-gyro	FR4	Elastic	25548	0.15	1.93E+03
solder	solder-sn60-pb40	Elastic/plastic	30044	0.4	8.61E+03
potting	ALCHEMIX_DMA-	Visco-Elastic	120.	0.49	1.60E+03
Plastic Connector	Plastic	Elastic	36043	0.3	5.12E+03

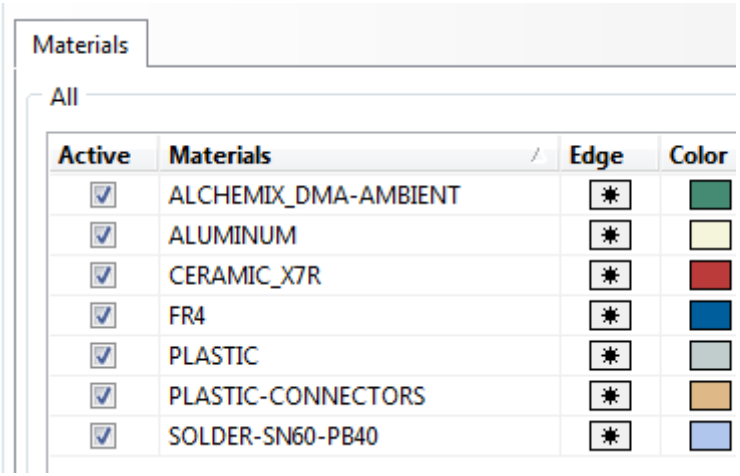

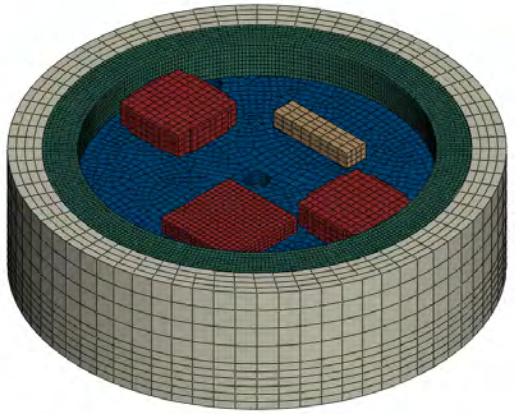

Material Model: Potting Assumptions

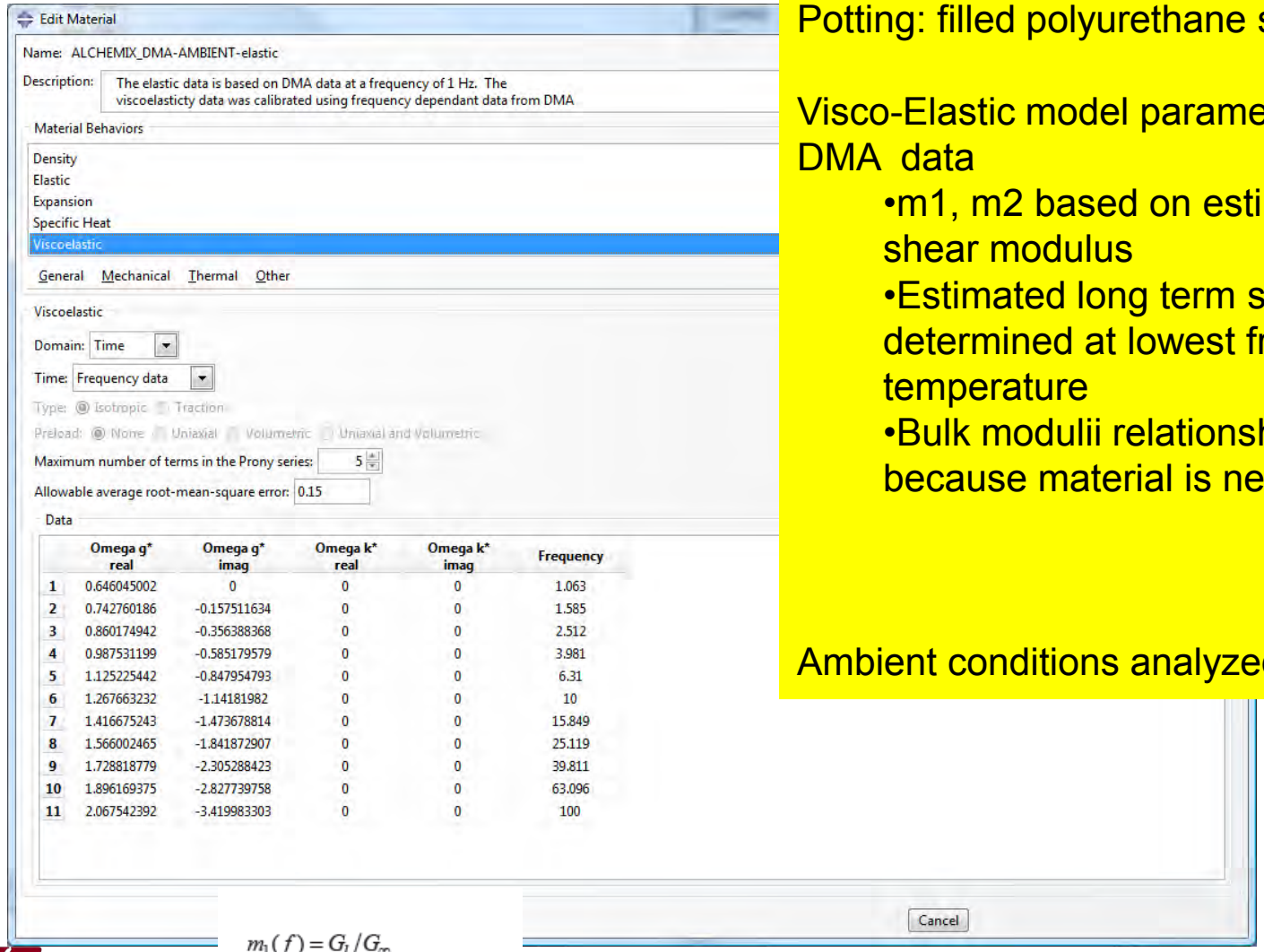

	Omega g* real	Omega g* imag	Omega k* real	Omega k* imag	Frequency
1	0.646045002	0	0	0	1.063
2	0.742760186	-0.157511634	0	0	1.585
3	0.860174942	-0.356388368	0	0	2.512
4	0.987531199	-0.585179579	0	0	3.981
5	1.125225442	-0.847954793	0	0	6.31
6	1.267663232	-1.14181982	0	0	10
7	1.416675243	-1.473678814	0	0	15.849
8	1.566002465	-1.841872907	0	0	25.119
9	1.728818779	-2.305288423	0	0	39.811
10	1.896169375	-2.827739758	0	0	63.096
11	2.067542392	-3.419983303	0	0	100

Potting: filled polyurethane system, Alchemix

Visco-Elastic model parameters defined using DMA data

- m1, m2 based on estimated long term shear modulus
- Estimated long term shear modulus is determined at lowest frequency for each temperature
- Bulk modulii relationships negligible because material is near incompressible

Ambient conditions analyzed

$$m_1(f) = G_l / G_\infty$$
$$m_2(f) = 1 - G_s / G_\infty$$
$$m_3(f) = K_l / K_\infty$$
$$m_4(f) = 1 - K_s / K_\infty$$

Internal Constraints

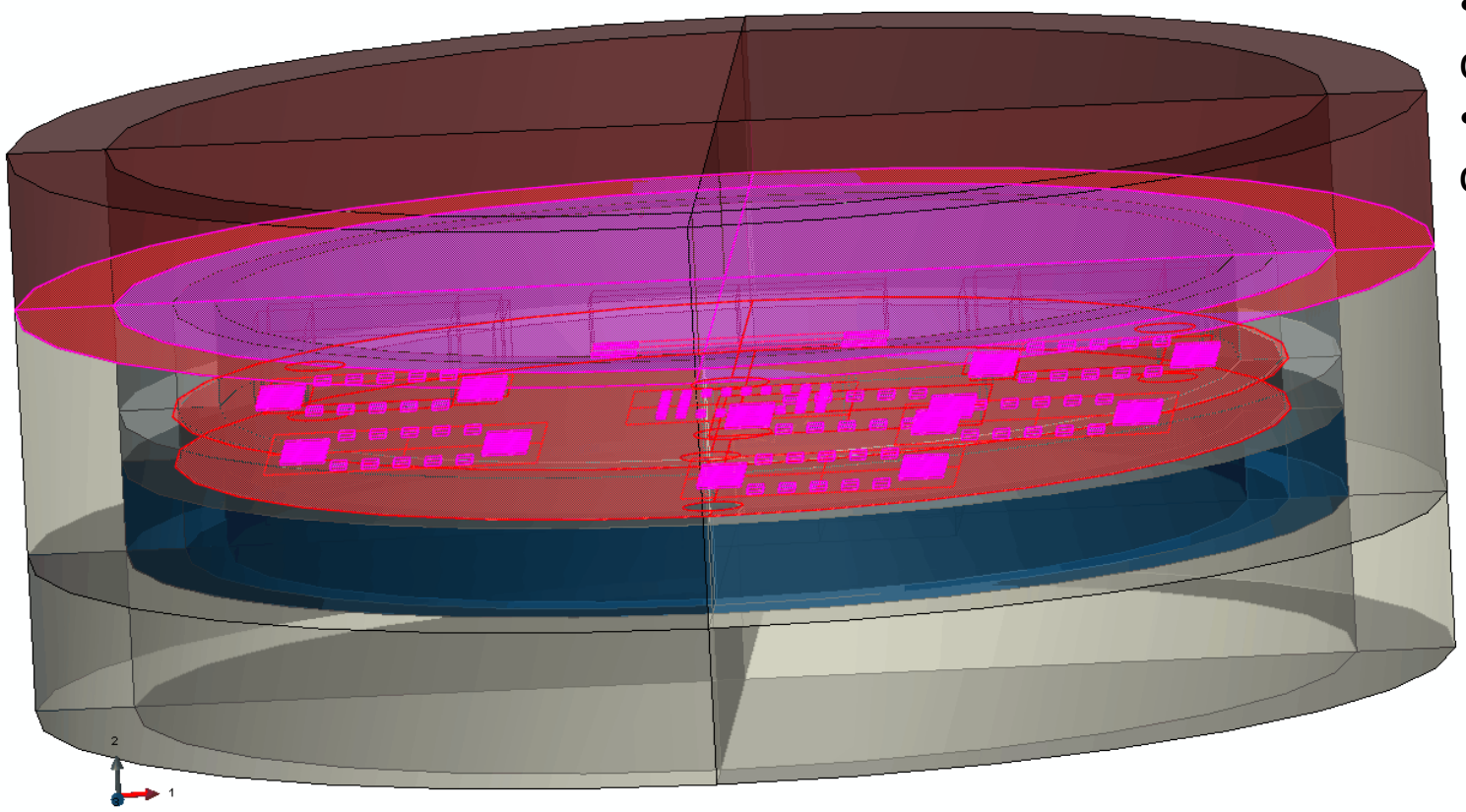

Ties
- Solder to board
- Solder to chips
- Lid to bottom of can

Method – Modeling and Simulation
General method, assumptions, errors

- General Purpose Finite Element Software: ABAQUS Explicit 6.111.
- Analysis: nonlinear geometry, nonlinear materials
- Loads: obr2 measured acceleration data PMP+5, 3-D accelerations
- Elements: 8-node brick elements
- Tied: Potting glued together. Potting not glued to boards, can, or chips.
- Solder is included under chips. Potting does not extend under chips
- Materials: elastic/plastic, (hyper-elastic), visco-elastic
- Materials properties: Tested properties for potting (Dynamic Mechanical Analysis)
- Errors and omissions – room temperature results only, material models are approximate
- Friction: 0.00001, penalty method
- Damping: None other than visco-elastic model for potting
- Initial Conditions: no pre-stress, no initial velocity, ambient temperature
- Location: old files hpcc2 ‘fakeimu’; new corona fakeimu; imu/cae *foraisha*cae; potting-jul11

Results, comparisons

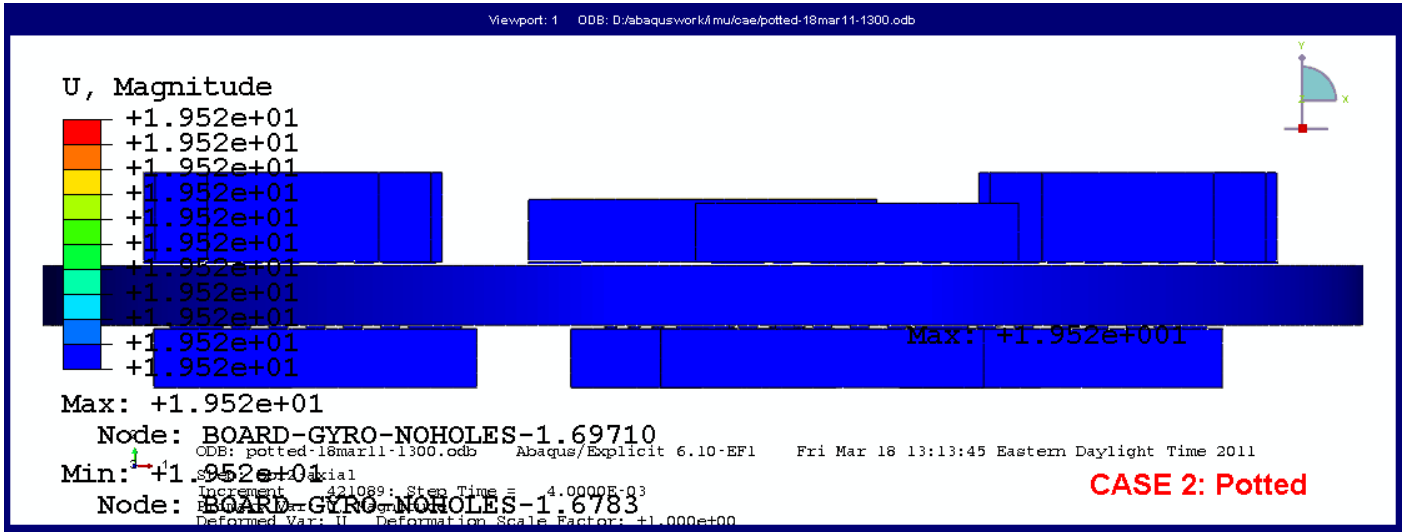

> 10x the deflection in the ringed
Relative deflection
In the chips okay

Results, comparisons

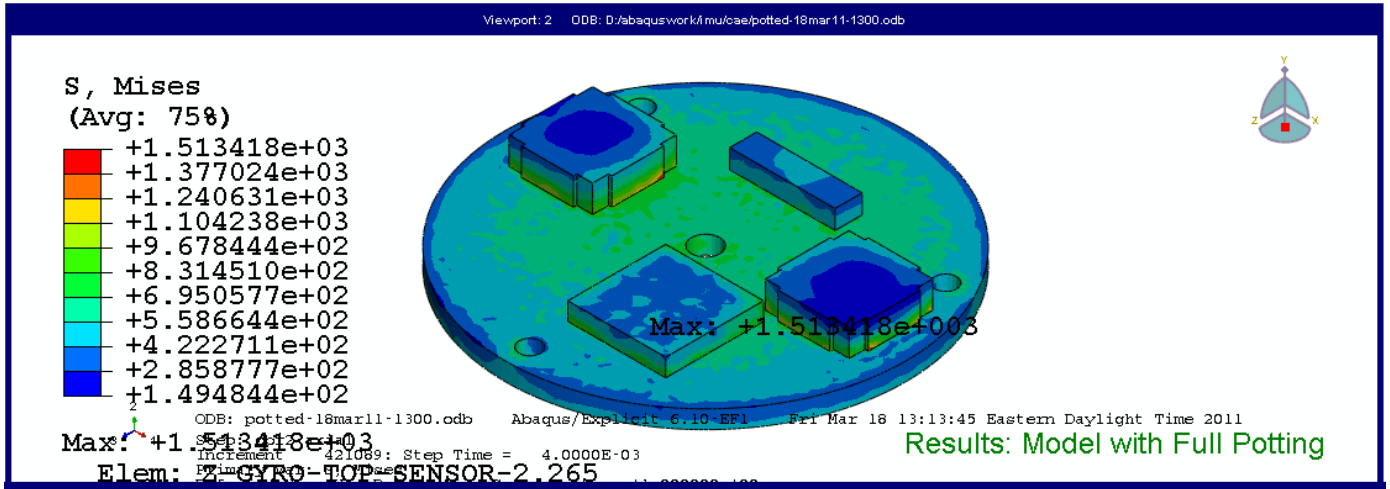

Results: Model with Full Potting

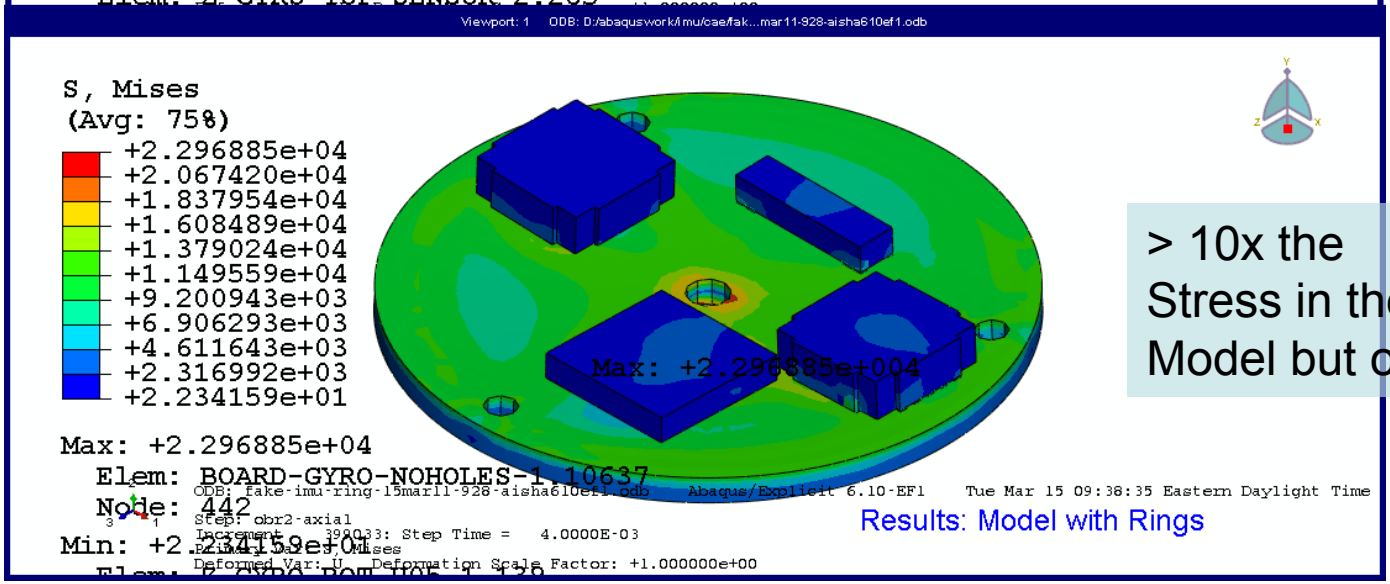

Results: Model with Rings

> 10x the Stress in the ringed Model but okay

Results, comparisons

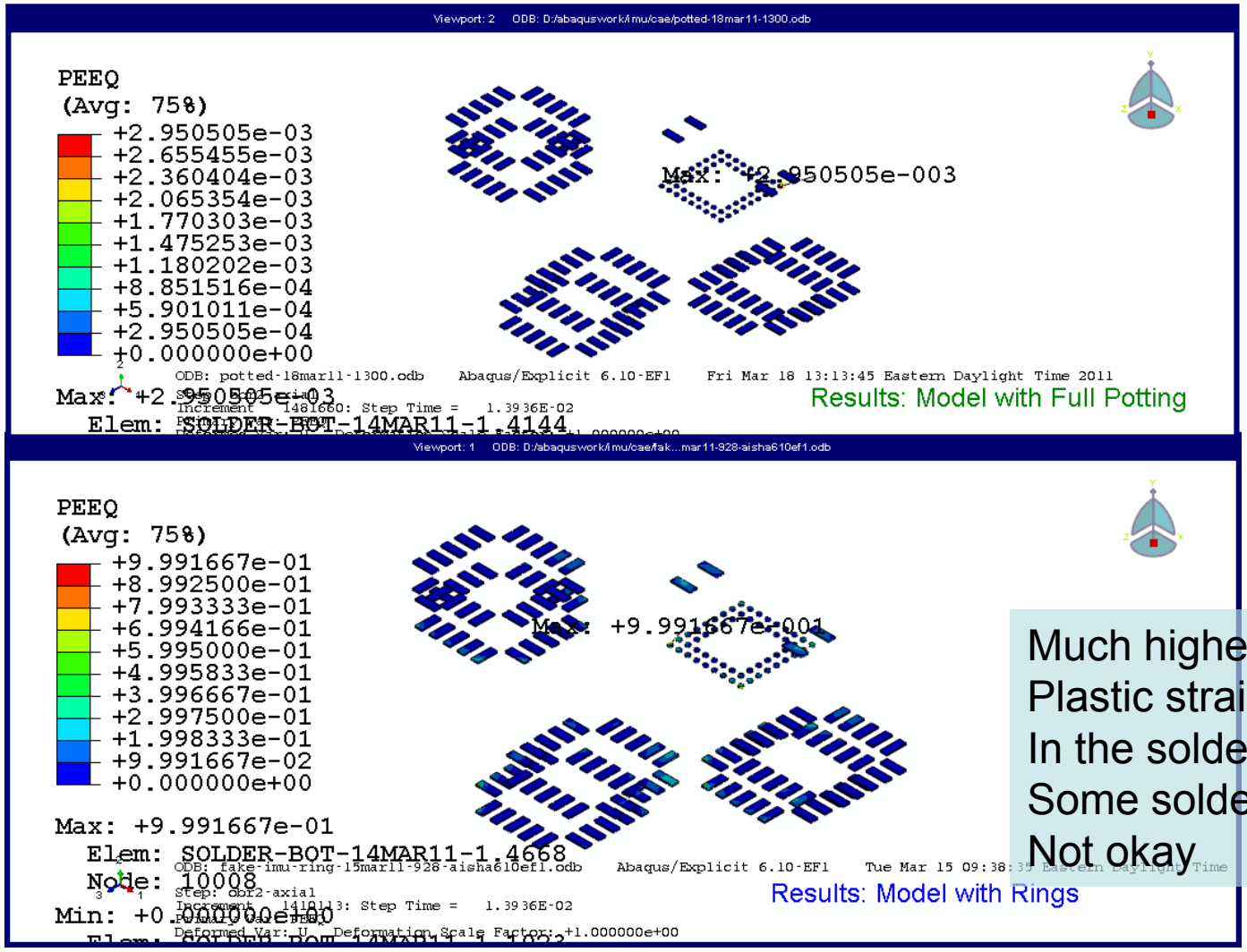

Much higher
Plastic strains
In the solder;
Some solder pads
Not okay

Conclusion

- For the brief case presented:
  - Experimental comments –
    - The glass transition temperature is in operating range
    - The potting does provide some damping of the motion
  - Modeling and Simulation, ambient
    - Relative chip deflection was within 7.6E-5m (3/1000 inch) ringed model
    - Hyper-elastic material model would be better for the ringed model
    - The stresses in the potted electronics result in about 10% of the non-potted stresses
    - Thermal issues not addressed in this study
    - Repeat for temperature extremes

Future/current work

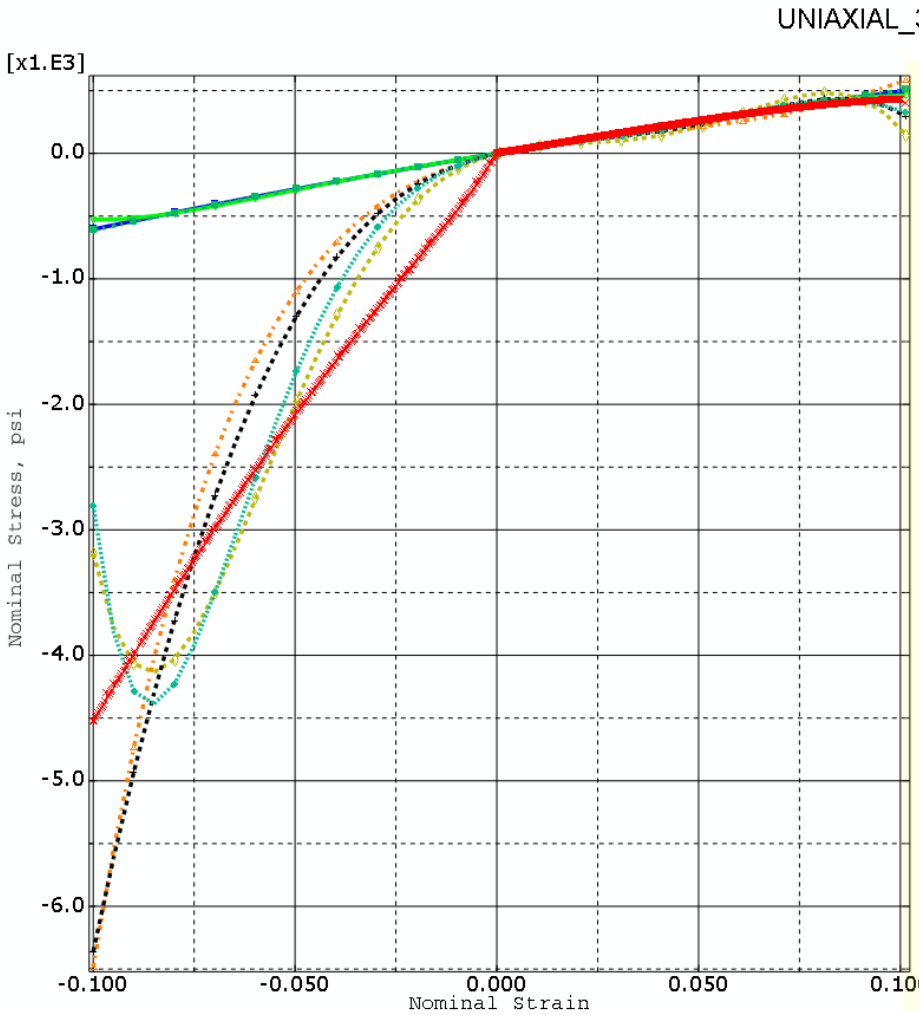

Shown; comparison of stress strain Data using different hyper-elastic models.

Best matches: Ogden N4 larger

Range of stable strain:

-0.038 < strain < .09

Aruda Boyce unconditionally stable

Poly N3 similar to Aruda Boyce, Slightly better in tension

Comparison of temperature extremes

Questions?

- Questions
- Thank you

UNUSUAL TRANSVERSE COMPRESSION RESPONSE OF NON-WOVEN BALLISTIC LAMINATES

Brian Scott PhD, PE
Major, Ordnance, USAR (ret)
US Army Research Laboratory
APG, Md 21005

TECHNOLOGY DRIVEN. WARFIGHTER FOCUSED.

26th International Symposium on Ballistics
Miami, Florida
12 September 2011

Outline

- Reasons for compression testing
- Transverse constrained compression testing
- Unusual response of unidirectional laminates “unis”
- Implications on the mechanics of penetration

Penetration Cavities Measured by Woodward, et al.

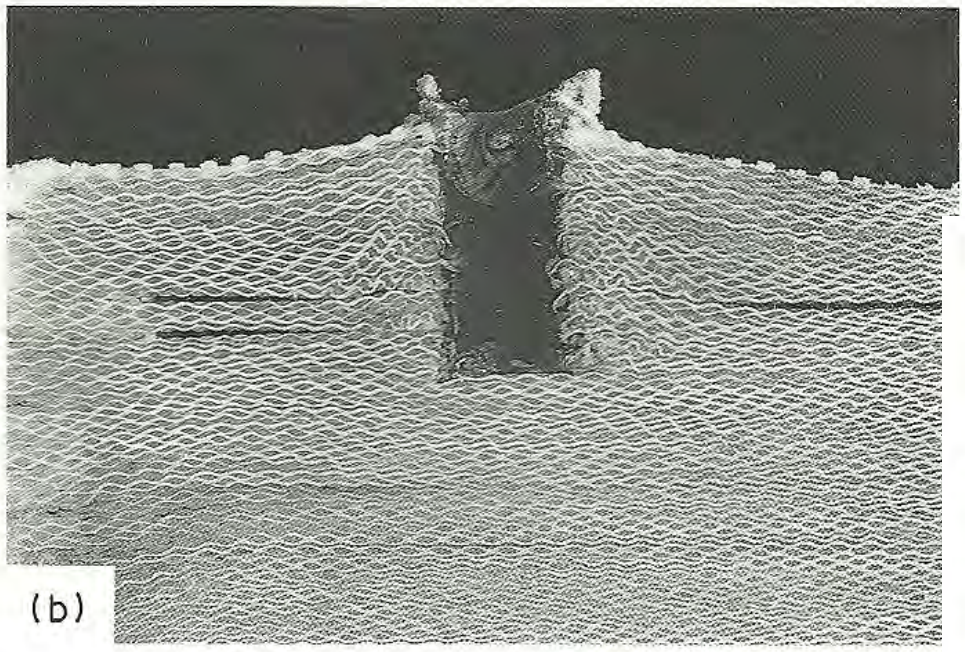

Woven Kevlar @ 336 m/s

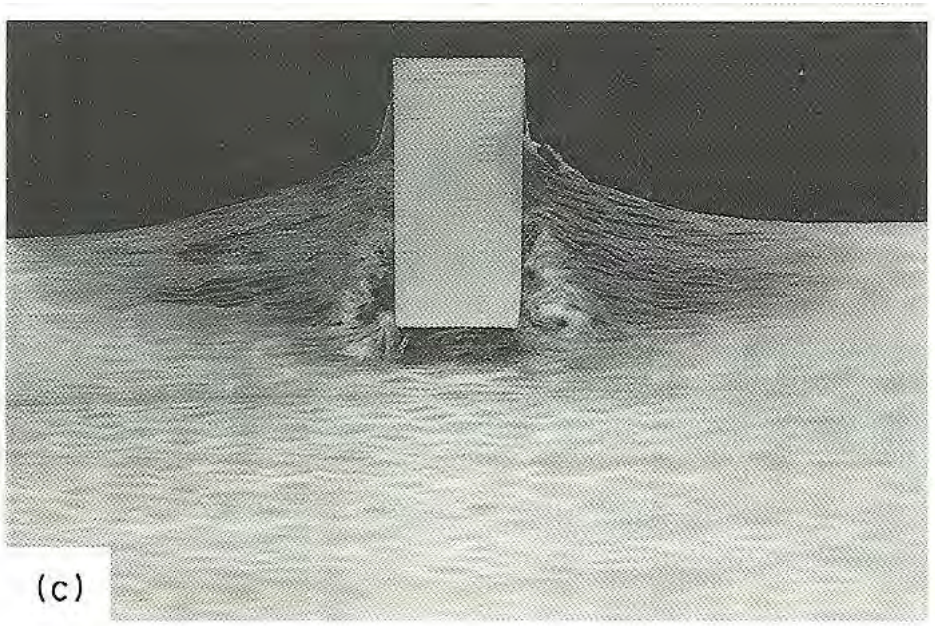

Woven GRP @ 330 m/s

Woodward, R.L, Egglestone, G.T, Baxter, B.J, and Challis, K, "Resistance to Penetration of Fibre-Reinforced Composite Materials", Composites Engineering, Vol 4, No.3, pp 329, 1994.

Assumed Simplified Behavior

CROSS PLIED UNIDIRECTIONAL LAMINATES

WOVEN OR STRUCTURAL LAMINATES

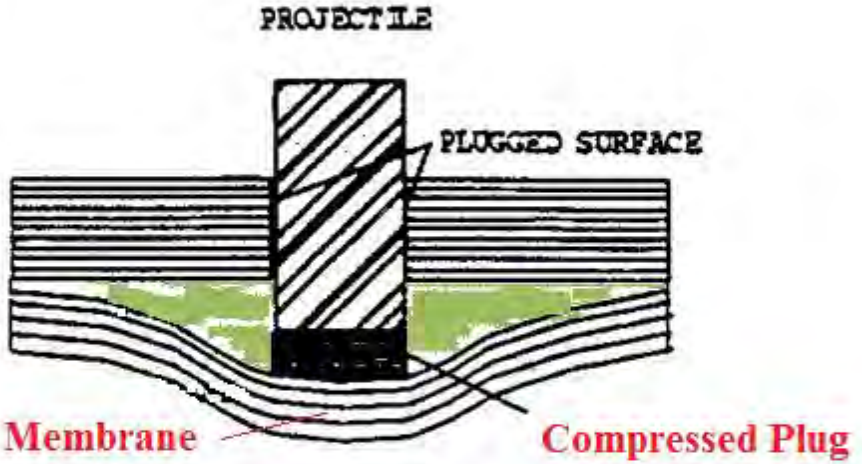

Classic Plug and Membrane

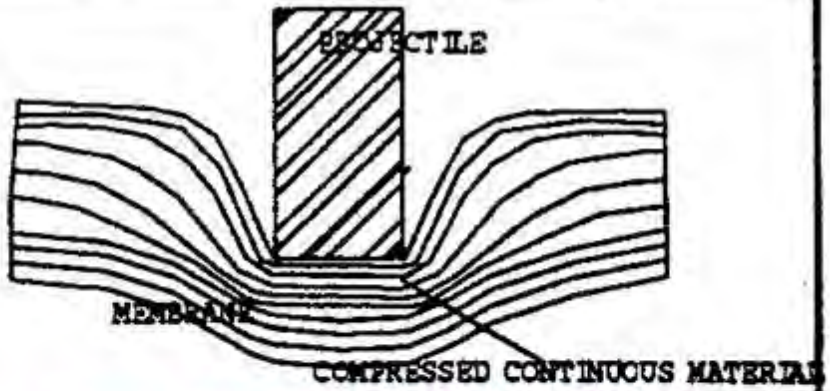

Stage I Prior to front layer rupture

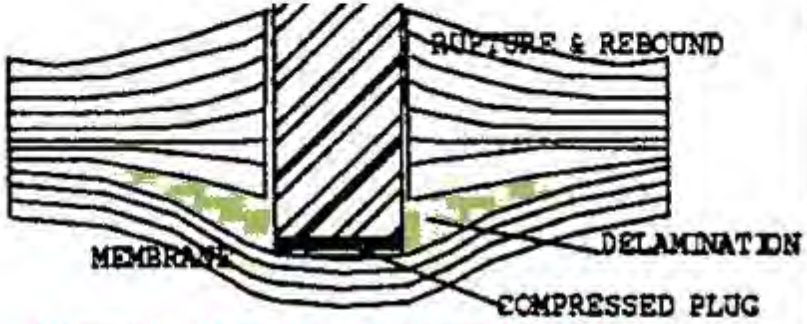

Stage II Post front layers rupture

Predominant Deceleration Forces

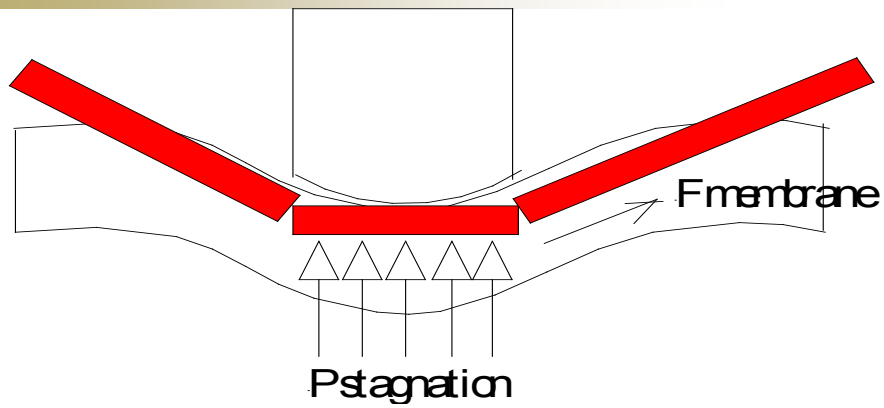

Assume : the absence of localized shear

Post phase I deceleration

Total axial retardation force

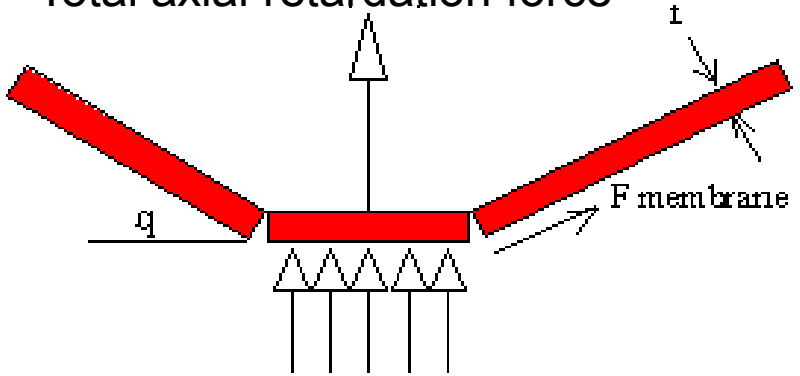

Z compression stress + stagnation P

Woodward's analytic model in two stages: phase I : momentum transfer with plug compression and static resistance

phase II: membrane energy capacity

NEED THE STATIC AXIAL RESISTANCE FORCE

Woodward, R. L. and I. G. Crouch, "A Computational Model of the Perforation of Multi-Layer Metallic Laminates," MRL-RR-9-89, Materials Research Lab, DSTO, Australia, 1989.

Measurement of Static Axial Resistance Force

Constrained Compression Test

Composites Engineering, Vol 4, No. 3, Woodward, et al, 1994

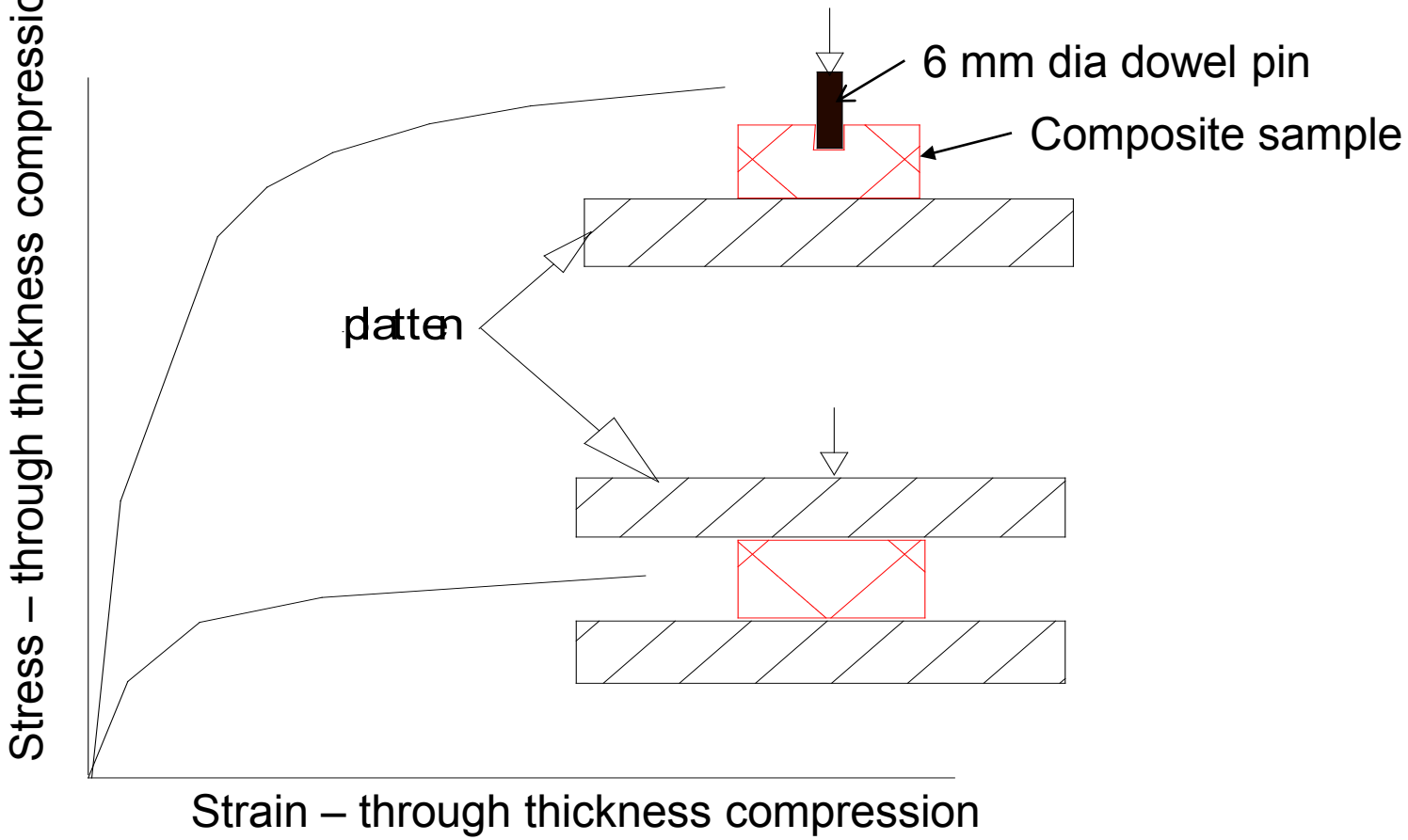

Woodward's Observations

Woodward, R.L, Egglestone, G.T, Baxter, B.J, and Challis, K, "Resistance to Penetration of Fibre-Reinforced Composite Materials", Composites Engineering, Vol 4, No.3, pp 329, 1994.

WOVEN REINFORCEMENT

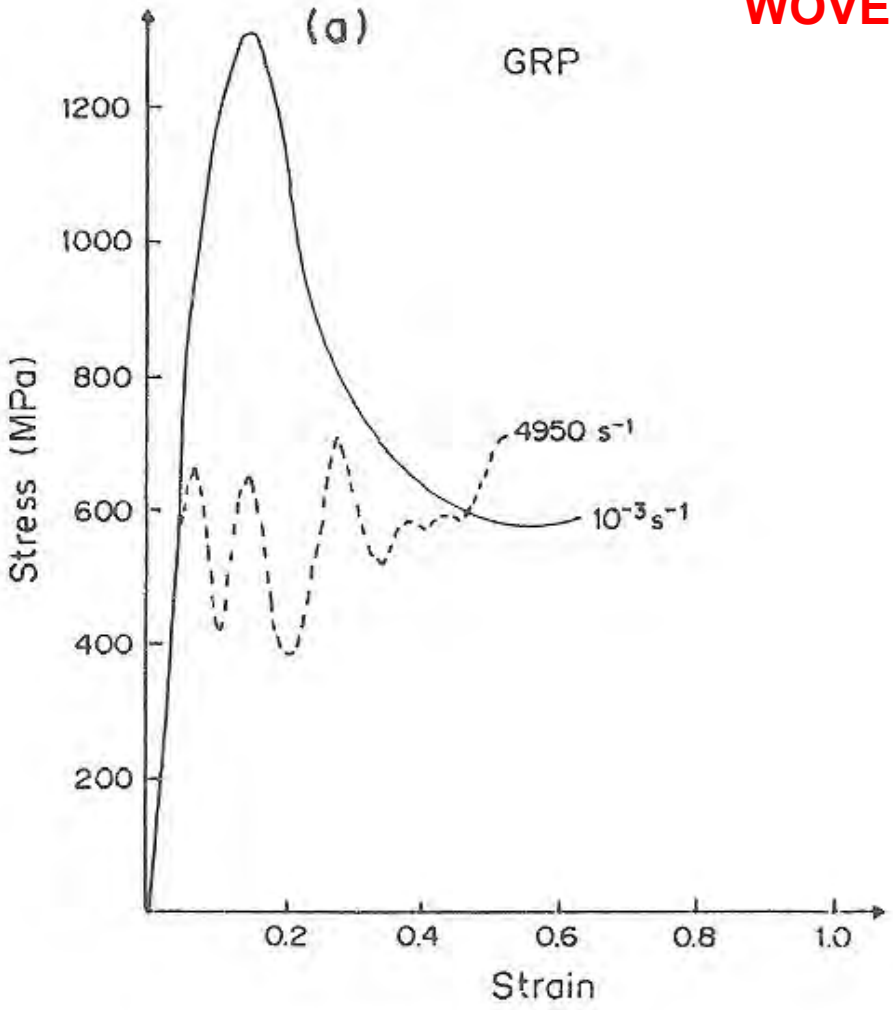

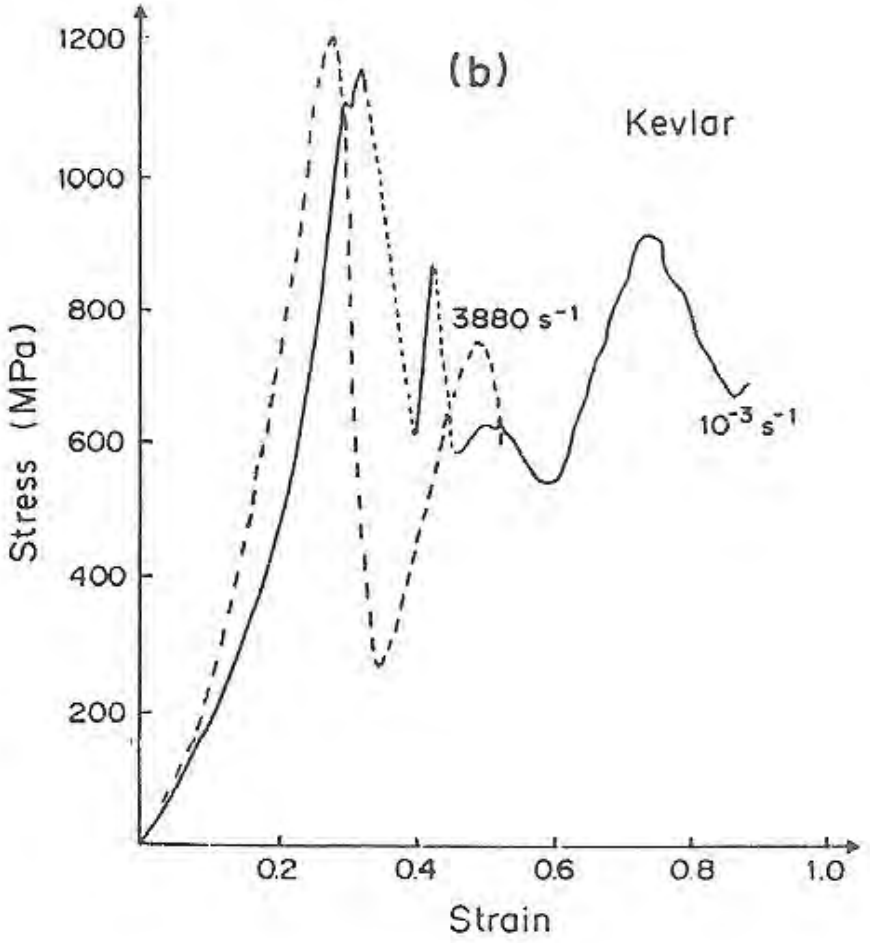

OBSERVED RESPONSE WITH UNIDIRECTIONAL LAMINATES

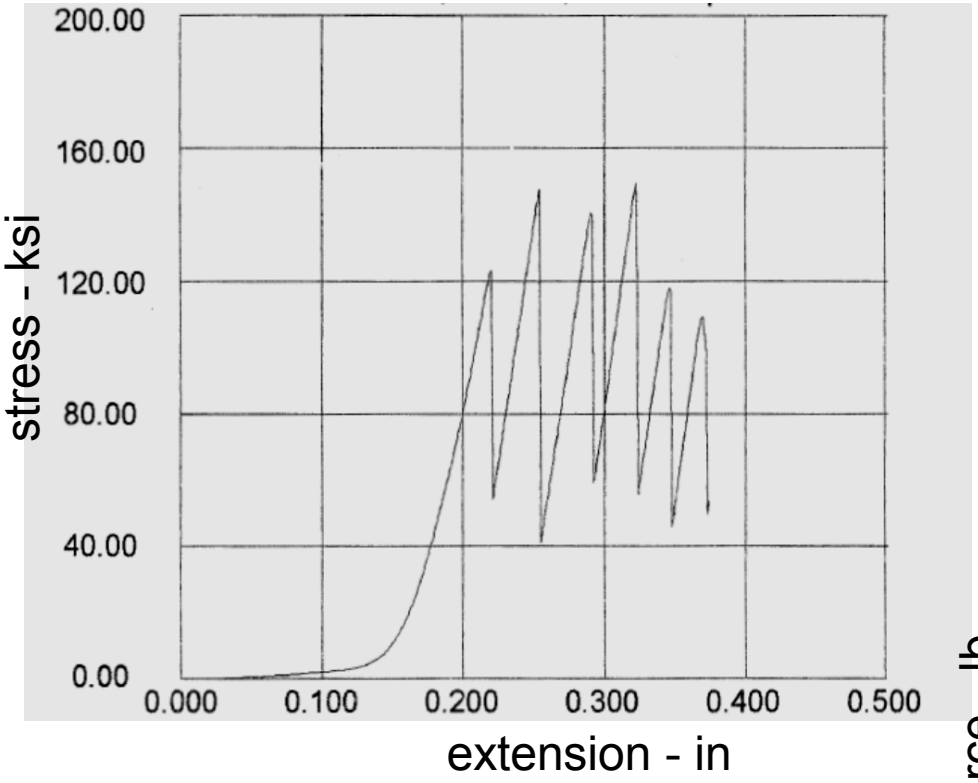

Quasi-static, constrained compression, Aramid fiber, polyolefin unidirectional laminate

Quasi-static, constrained compression, UHMWPE fiber, polyolefin unidirectional laminate

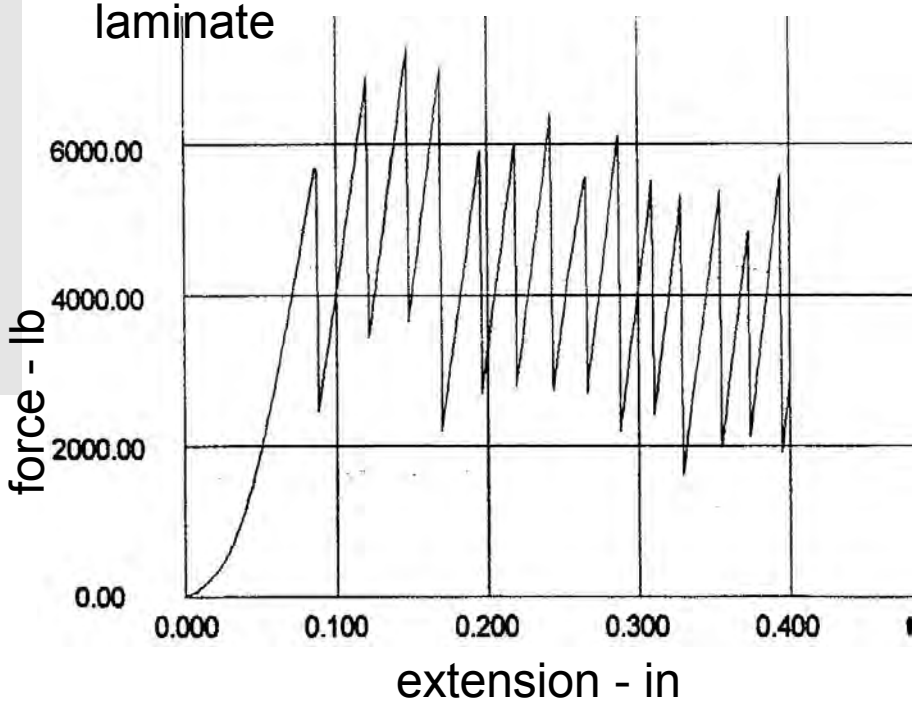

CYCLIC RESPONSE !
(both aramid and uhmwpe)

Material Matrix For Repeat Constrained Compression Testing

Material	Dimensions (Length, Width, Thickness)	Mold Pressure (psi)	Process Temp (°F)	Areal Density (lb/ft^2)	
S2-HJ1 (MIL-DTL-64154, Class A)	6.00,6.00,~1.0			10.0	
KRP (MIL-DTL-62474, Class D)	6.00,6.00,~1.0	250	291	7.3	Woven and uni
Honeywell Spectra Shield II SR-3124	6.00,6.00,~1.0	819	257	5.04	High & low pressure
Honeywell Spectra Shield II SR-3124	6.00,6.00,1.0	2833	258	5.04	
Dyneema HB-26	6.00,6.00,1.0	805	258	5.08	
Dyneema HB-26	6.00,6.00,1.0	712	258	5.09	High & low peak temperature
Honeywell Spectra Shield II SR-3124	6.00,6.00,1.0	2708	275	5.0	
Dyneema HB-26	6.00,6.00,1.0	2708	277.6	5.0	
TBA (Thermo Ballistic A)	6.00,6.00,-.--				

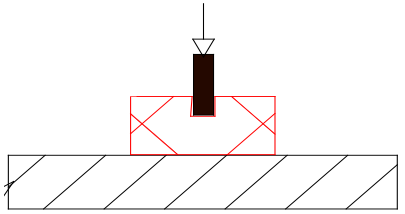

Woven Laminates

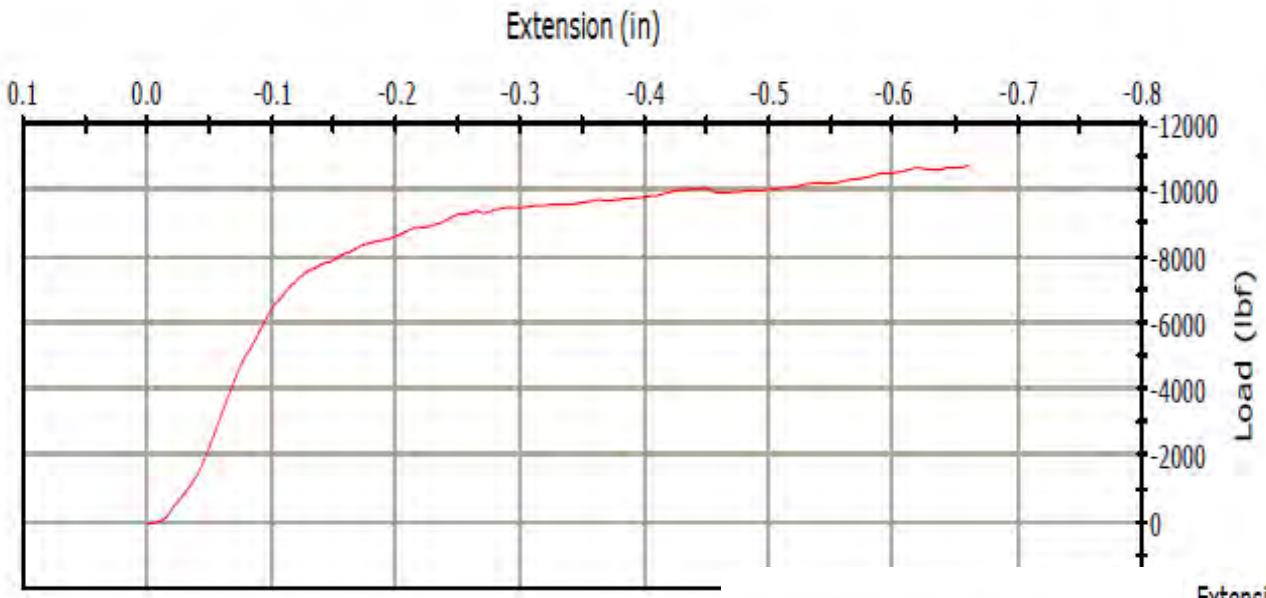

S2/phenolic, woven
MIL DTL 64154B class A

Monotonic response
(large static strength)

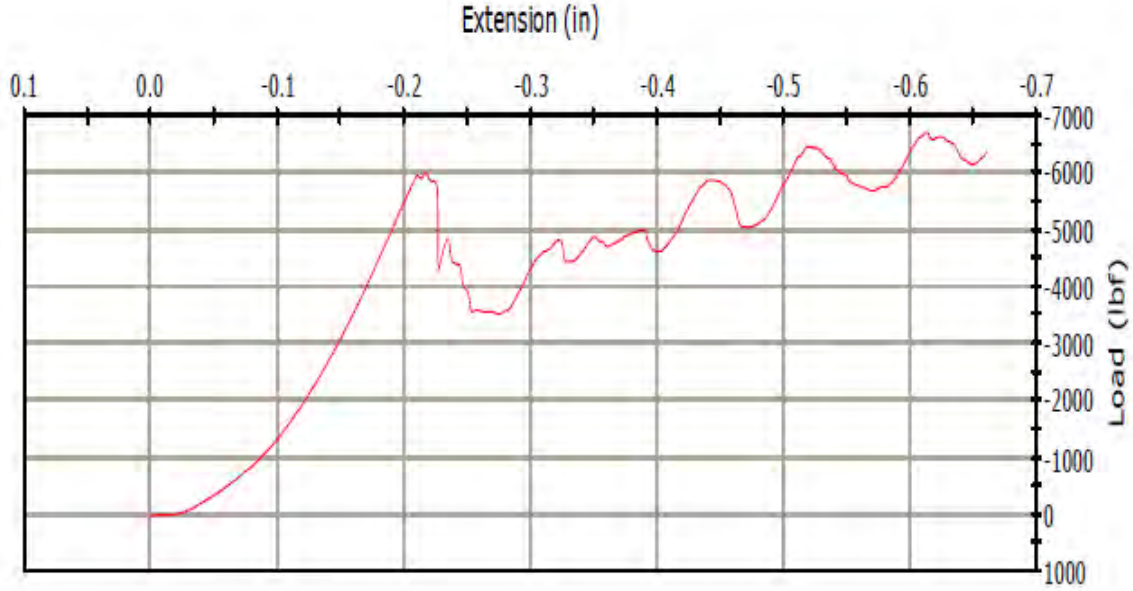

Kevlar/phenolic, woven
MIL DTL 62474F class D

Moderate cycling + increasing average

Constrained Compression SSII at Two Consolidation Pressures

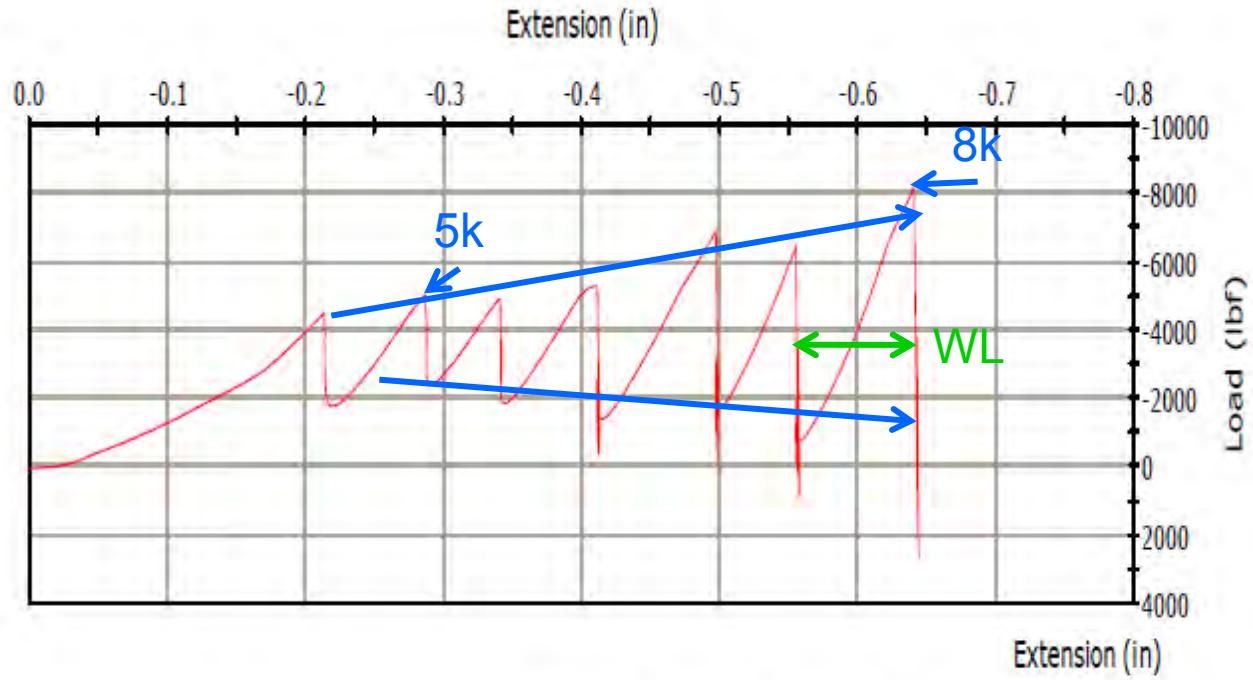

Spectrashield II, uni
Pressed @ 800 psi

WL= number of plies ruptured per cycle

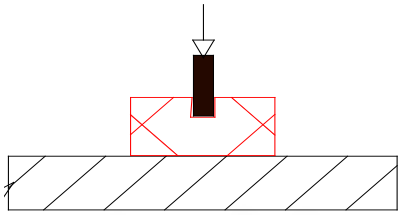

Spectrashield II, uni
Pressed @ 2800 psi

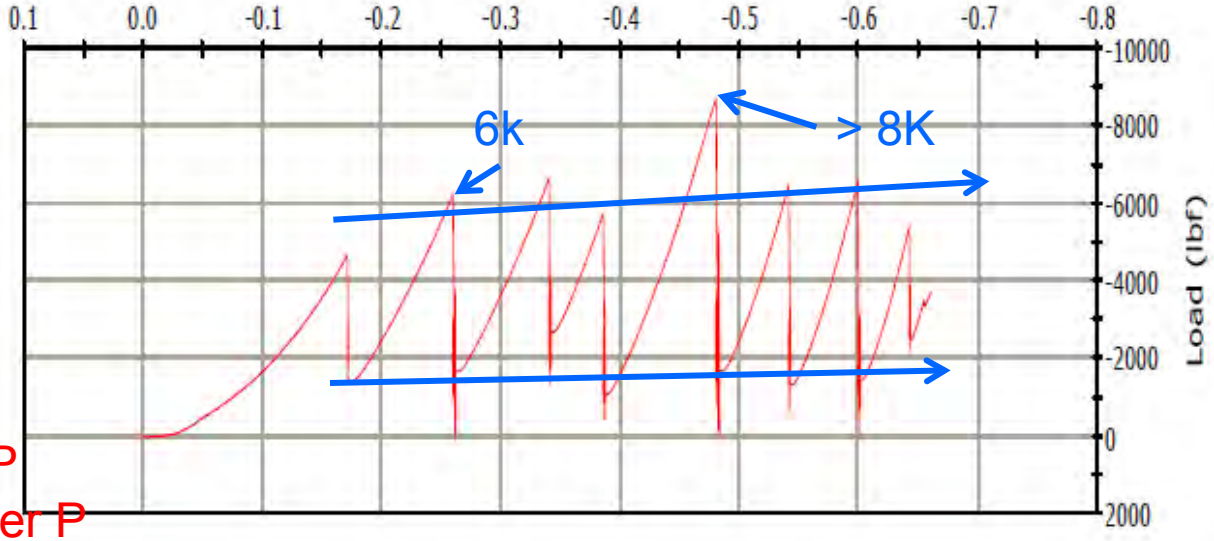

Flatter response at high P
Strength higher with higher P

Constrained Compression HB26 at Two Consolidation Pressures

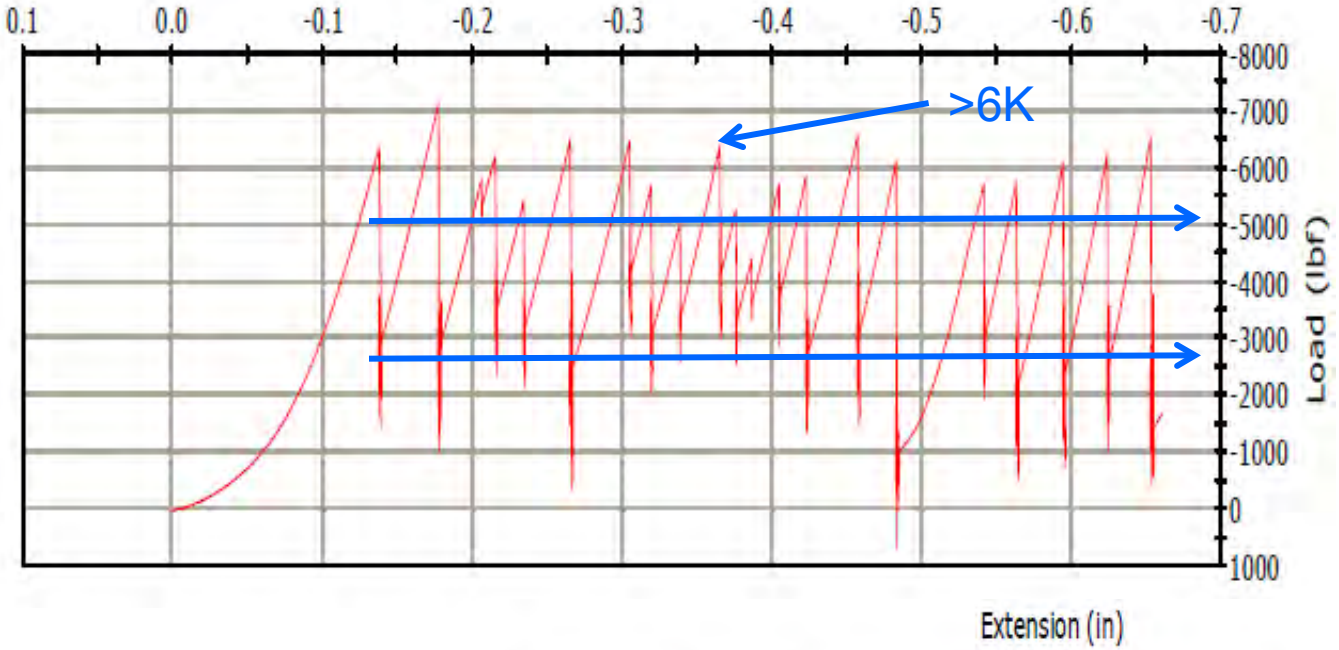

Dyneema HB26, uni
Pressed @ 800 psi

HB26 flat at both P
HB26 peak < SSII peak

WL (HB26)< WL(SSII)

transverse compression strength HB26 > SSII`

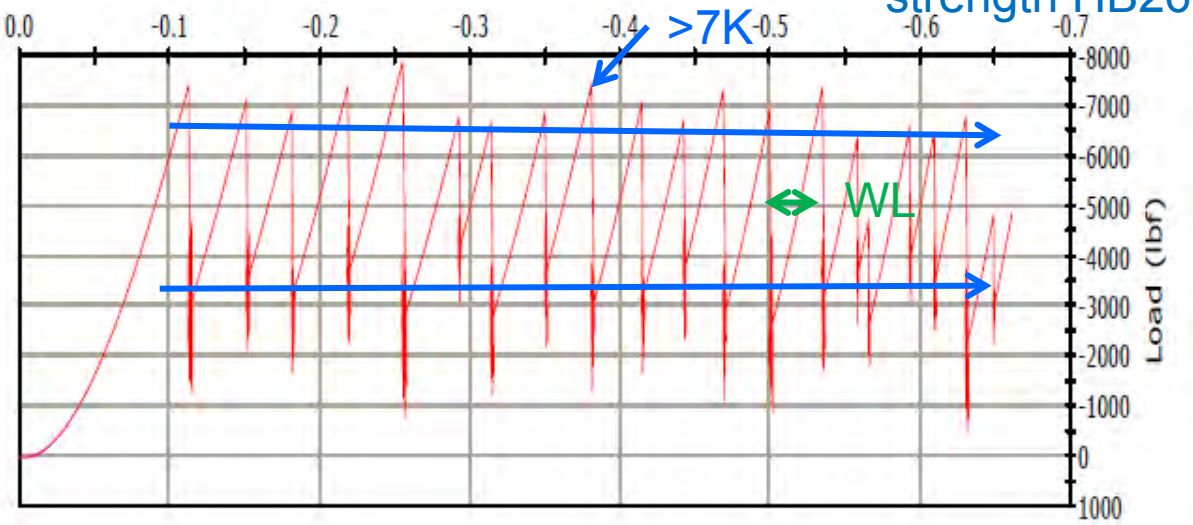

Dyneema HB26, uni
Pressed @ 2700 psi

Impulse vs time (quasi-static)

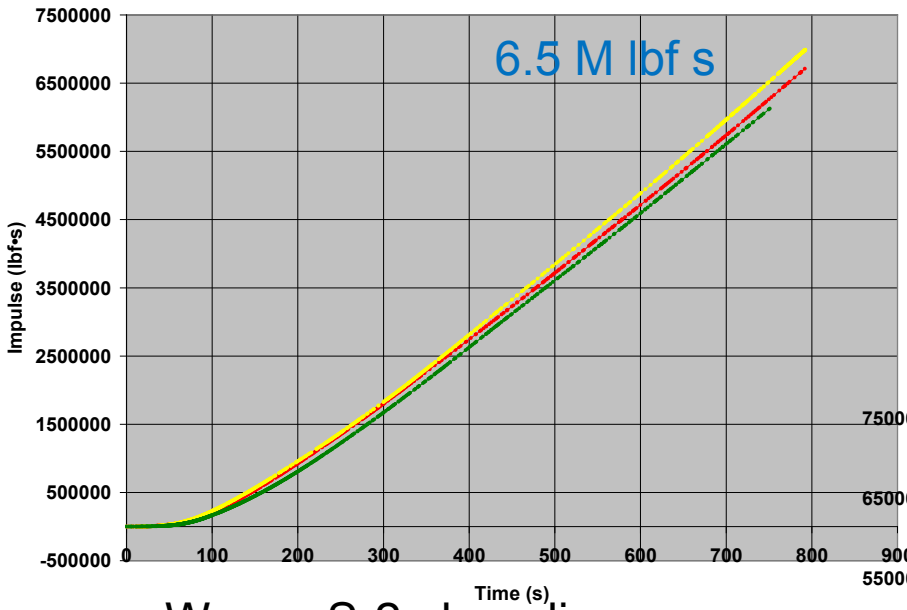

Woven S-2 phenolic

Impulse is the integrated resistance force over time (in this case all at constant cross-head rate of .0008 in/s

Note: quasi static impulse capacity of GRP greater than SSII at same time increment?

Spectrashield II uni

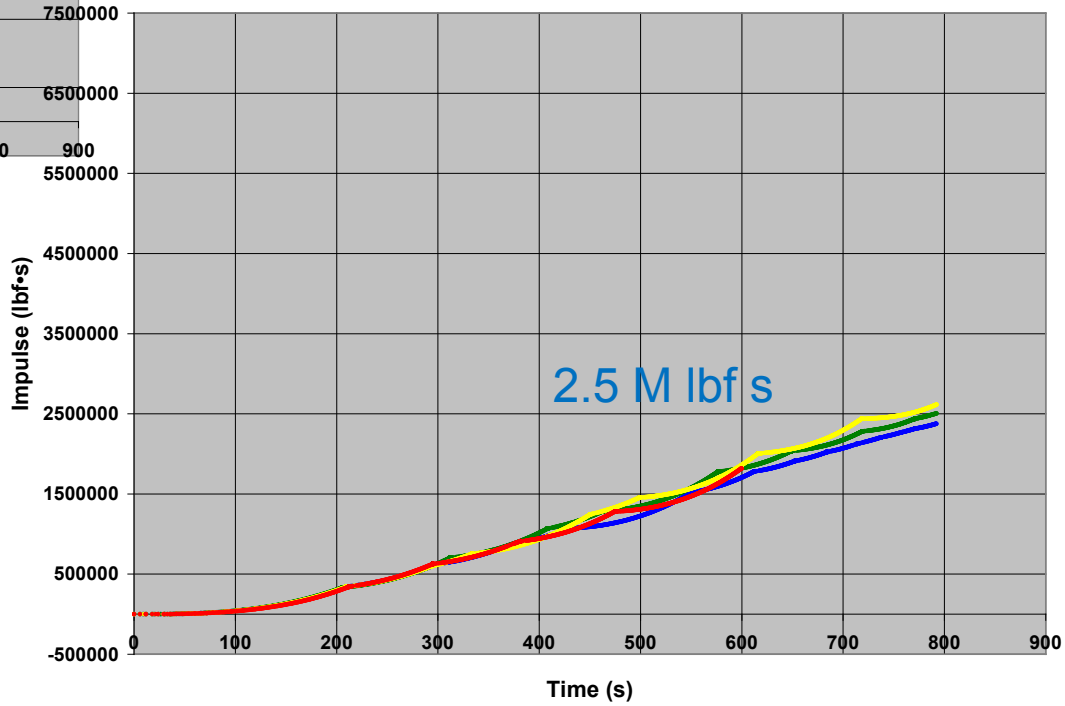

4 specimens each suggest reasonable reproducibility of each material test

Linear response suggests uniform load resistance cycle since time interval is constant

Summary of Observations

- Cyclic response more prevalent in uni constructions
- Aramids and UHMWPE exhibit similar behavior, glass laminate is unique (quasi-static)
- Cyclic response likely superposition of normal compression plus membrane
- Wavelength is consistent grouping of plies SSII > HB26
- Constant slope of impulse suggests uniform response per cycle
- Lamina thickness or matrix properties may influence wavelength (since HB26/SSII are different in resin system)
- With quasi-static loading, membrane contribution > compression
- Peak stress may correlate with ballistic efficiency since SSII has highest peak values
- High impulse capacity of GRP can be rationalized by normalizing response by density
- SSII may have apparent Szz lower than HB26, but perhaps higher membrane capacity

Implications on Penetration Resistance

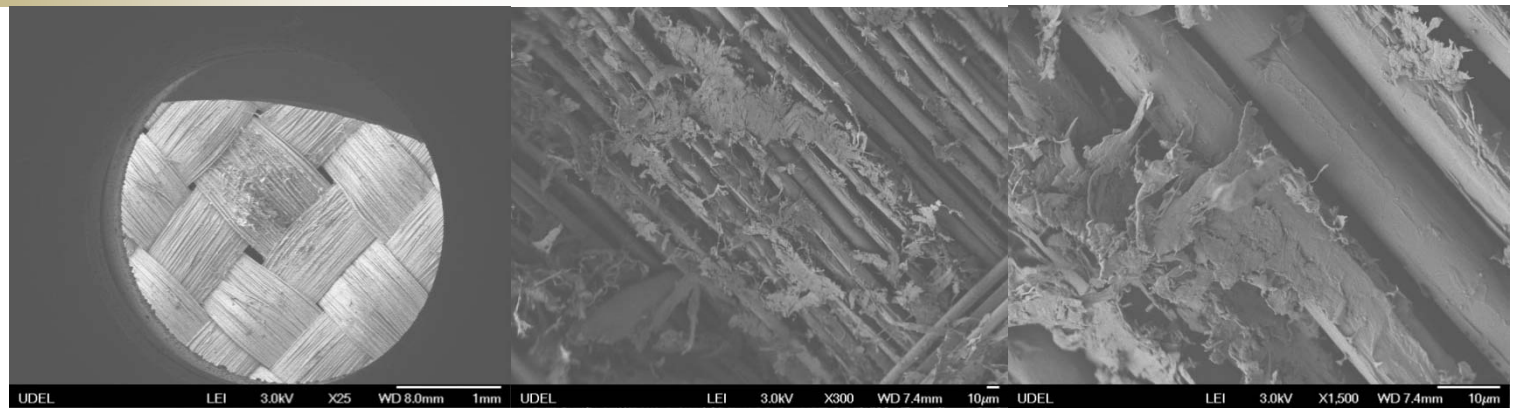

Images of Kevlar filaments subject to low speed impact at increasing magnification levels (Courtesy of E Wetzel/ D. Kalman, ARL/Univ of Delaware)[13]

Previous studies have detailed even better examples of flattening and fibrillation of transversly compressed fibers: Phoenix, Textiles Research Journal 65:934-940, 1974 and Singletary, J, Jour. of Materials Sci., 35, (2000)

Soft response in transverse compression may not effect tensile strength (10,11)

Fibrillation or plastic flattening may allow for extended membrane stretching prior to rupture

Cunniff[14] suggests increased Ts with hydrostatic pressure

Hydrodynamic pressures may increase axial resistance (8)

Self confined compression may explain observations (8)(Scott/Cheeseman -2008 IBS)

Conclusions

- During confined compression testing, uni-directionals exhibited cyclic loading response
- High penetration resistance may correlate with high hydrostatic pressures or increased membrane stretching and rupture
- The cyclic behavior is constant thru thickness
- The failure modes involving fiber axial tensile strength and transverse compressive strength appear to be uncoupled (10,11)
- Increases in rupture strength were observed with higher consolidation pressures

Presented to:

International Ballistics Symposium

September 2011

AMRDEC Lethality Modeling and Simulation Methodologies for Aerial Targets

TECHNOLOGY DRIVEN. WARFIGHTER FOCUSED.

Presented by:

Dustin Clark

SSDD

dustin.h.clark@us.army.mil

256.842.9523

Co-Authors: Dedra Moore

Brent Deerman

U.S. Army Aviation and Missile Research, Development, and Engineering Center

System Assessment Process

Acronyms:

ARL:	Army Research Laboratory	SLAD:	Survivability/Lethality Analysis Directorate
NGIC:	National Ground Intelligence Center	AMSAA:	Army Materiel Systems Analysis Activity
WMRD:	Weapon Materials Research Directorate	AOA:	Analysis of Alternatives
KTR:	Contractor	JTCG:	Joint Technical Coordinating Group
RTTC:	Redstone Technical Test Center	AEC:	Army Evaluation Center
		M/S:	Milestone

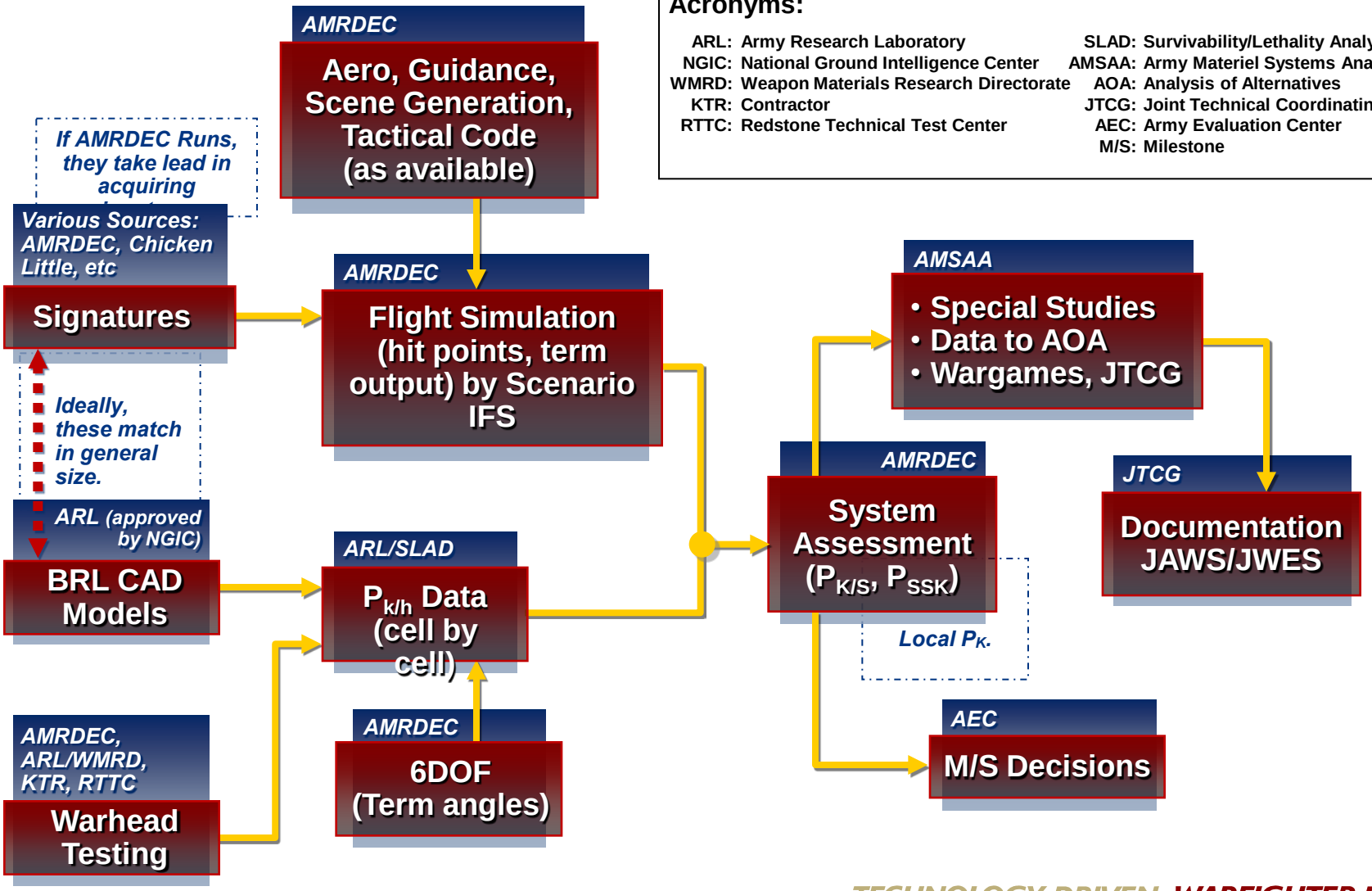

Types of Aerial Targets – AD/AP

AIR DEFENSE

Large Number of Fragments to Increase Probability of Hit on Target

AREA PROTECTION (RAM)

Kinetic Energy with Multiple Hits on Target

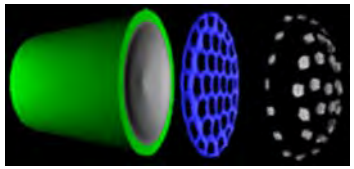

Multiple EFP

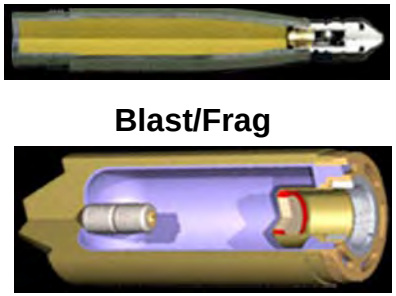

Blast/Frag

Target Modeling

- **BRL-CAD™ was developed by what is now the US Army Research Laboratory's Survivability/Lethality Analysis Directorate (ARL/SLAD) in the 1980s**
- **The ARL resolution standard for target geometric modeling is down to the wiring and hydraulic lines level**

Sample Shotline with Material

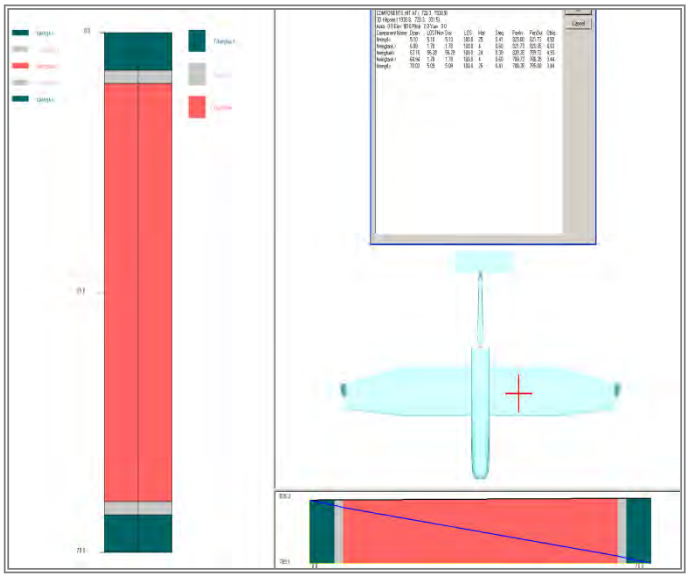

Sample Model Ghosted to Show Components

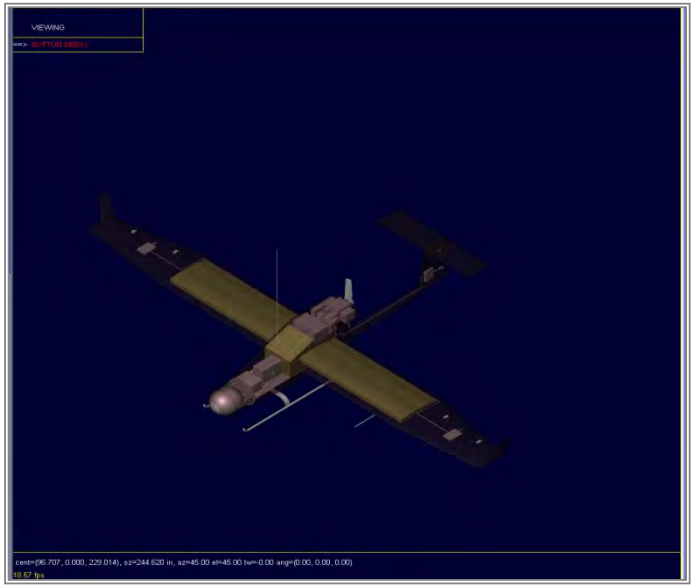

Fragmentation Technology

Natural Fragmentation	Embossed Fragmentation	Preformed Fragmentation
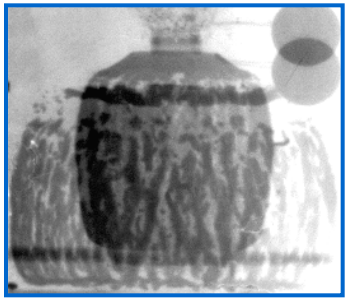	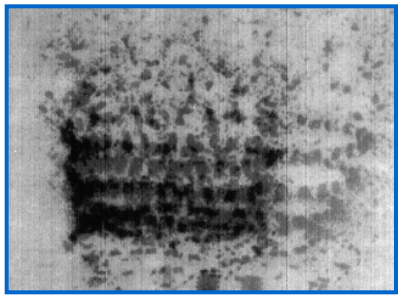	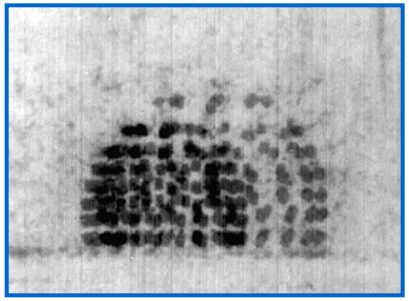
Wasted Mass/Energy	Less Wasted Mass/Energy Improved Lethality, Low Cost	Efficient Mass/Energy Optimized Lethality, More Cost
Least Cost		*Most Cost*
Least Mass Efficient		*Most Mass Efficient*
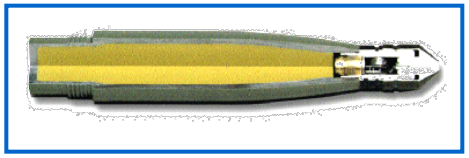	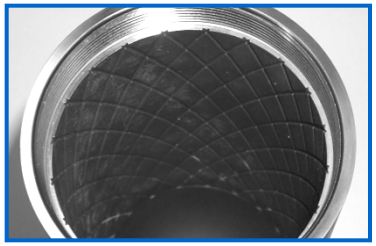	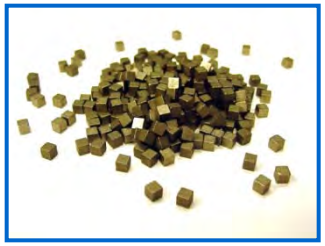
M151 Warhead	Pearson or V-Notch Scoring	Tungsten Fragments

Optimization Balances Cost and Performance

Courtesy of Dr. Ernest Baker, ARDEC

Arena Test Setup

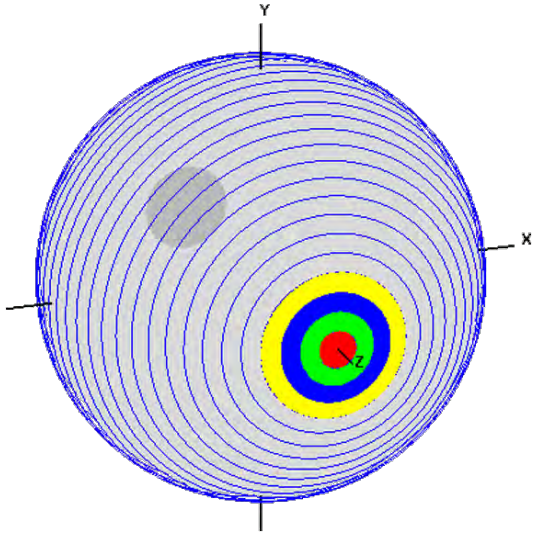

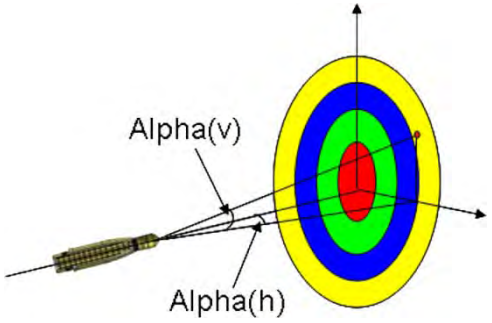

- **Fragments are collected in bins that represent polar angles around the rocket/missile**

Warhead Fragmentation Modeling

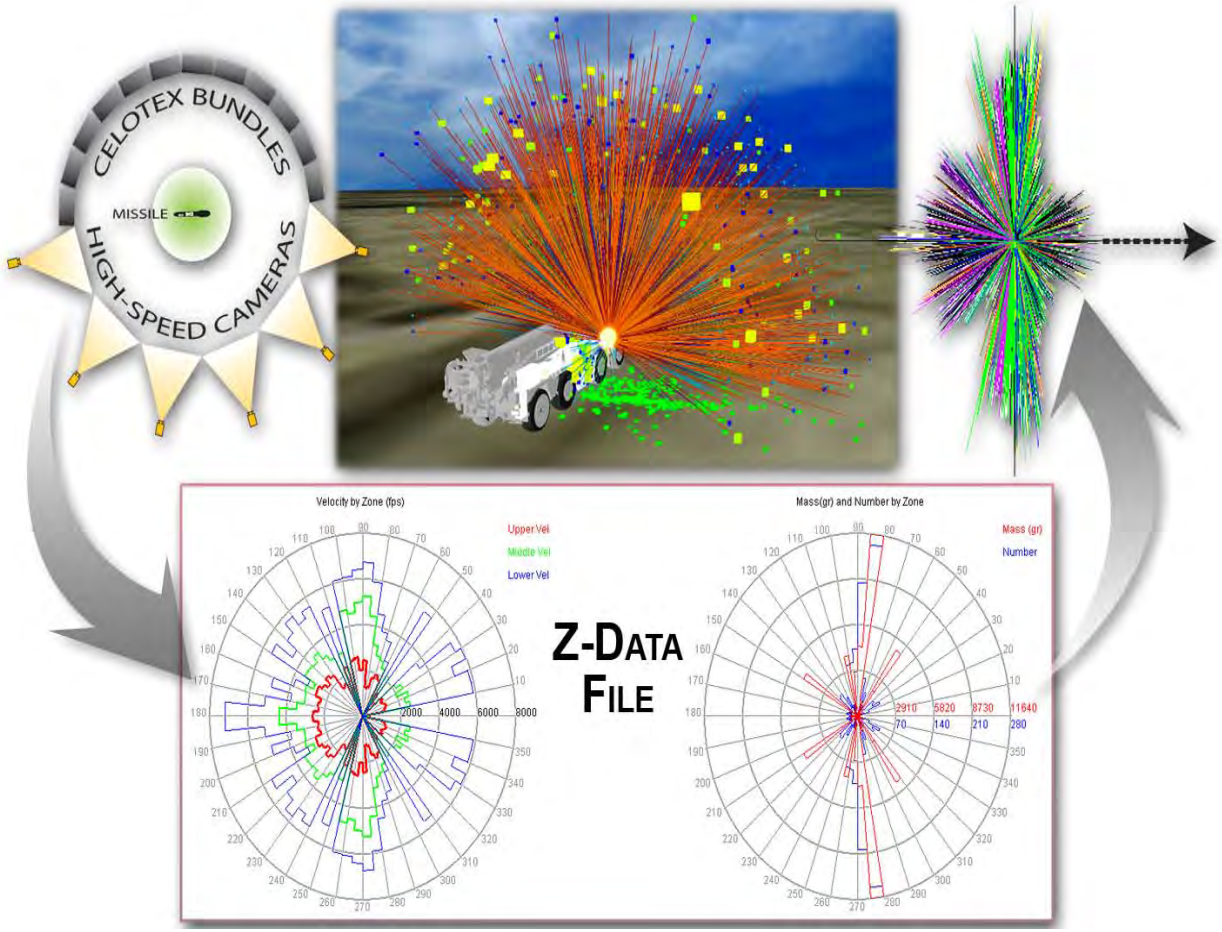

- **Fragments are modeled to represent size, mass and material type**

System Lethality Assessment Process

Lethal Mechanism Model Development

- Pre-Release/Detonation Characteristics
- Detonation Characteristics with Statistical Variation Estimate

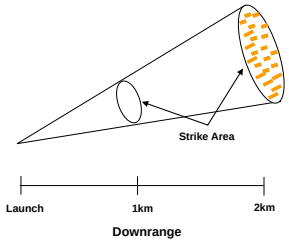

System Error Characterization

- Sensor / Aiming Errors
- Fuzing Errors
- Mechanical Errors

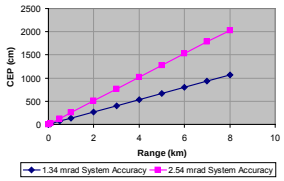

System Kinematic / Scenario Analysis

- Velocity / Range Estimates
- Engagement Scenario Development
- Miss Distance Characterization

Analysis Development

Revisions Based Upon New Data or Observations

Downrange (km)	Flechettes on Fuze*	Flechettes on Target*	PK – Objective Criteria
Target 1			
1	5.8	23.34	0.15
2	1.95	7.76	0.0
Target 2			
1	3.83	37.5	0.0
2	2.73	20.19	0.0
Target 3			
1	4.25	68.02	0.27
2	2.59	32.37	0.0
Target 4			
1	5.69	74.23	0.0
2	3.14	35.04	0.0

*Flechette Hits: Detail near missed burst

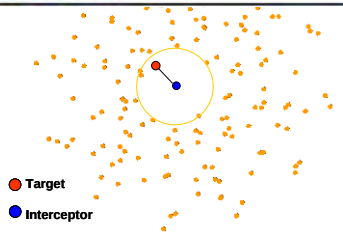

Data Reduction and Analysis

- Visual Inspection
- Lethality Extraction
- Comparison to Expectations
- Comparison Between Systems

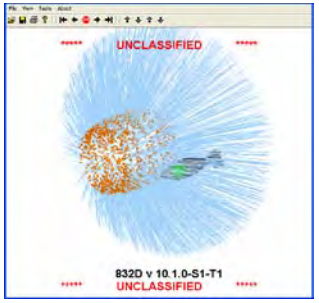

End Game Lethality Simulation Analyses

- Monte-Carlo Scenario Variation
- Threat Suite
- Lethal Mechanism-Specific Effects

Analysis Performance

RAM Targets

- **Mortars are Quite Difficult to Kill Due To Their Simplicity:**
  - **Generally Small Targets Flying For Short Periods of Time**
  - **No Guidance & Control or Electronics to Disable**
  - **Thick Casing Surrounding Payload**
  - **Threats Have Low Velocity Reducing Contribution to Overall Energy Available at End Game**
- **A Recognizable Detonation of the Mortar is the Desired Kill Mechanism as the Defeat is Immediately Recognized by the Warfighter. This is Driven by:**
  - **Explosive**
  - **Impacting Projectile**
  - **Case Surrounding the Explosive**
- **Dudding the Mortar is Not a Perferred Option as the Warfighter Cannot Distinguish Mission Success Until the Mortar Strikes the Ground.**

Mortar Arena Test – Fragment Penetration with No Mortar Response

Fast-Running Models Require Accurate Modeling of the Defensive System Performance and the Conditions at the Point of Engagement

Safe Separation Inputs

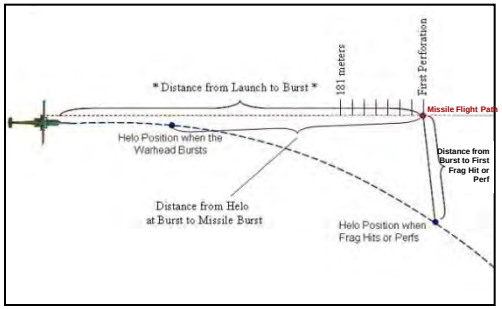

INPUT

- Z Data File
- Missile Flight Trajectories
- Helicopter Geometries

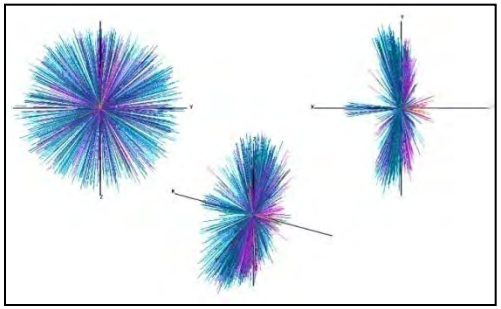

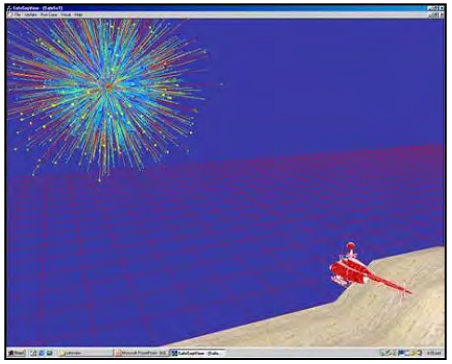

SIMULATION

- Random Draw on Fragment Pattern & Missile Trajectory
- Motion of Helicopter (Hover, Running, Diving)
- Fragment Impact (Trajectory Computation Including Drag/Gravity)
- Fragment Penetration Project (THOR Equations & BRL-CAD™ Ray-Tracing)

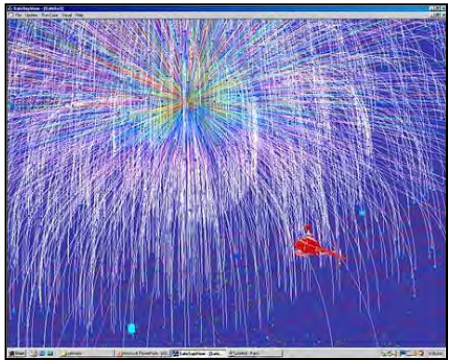

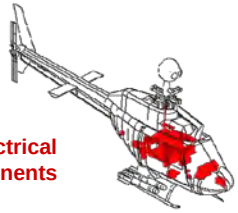

Critical Electrical Components

POST PROCESSING

- Determination of Critical Components (SME Opinion)
- Computation of Statistics on Performance of Critical Components

Critical Flight Control Components

Safe Separation Methodology and Analysis

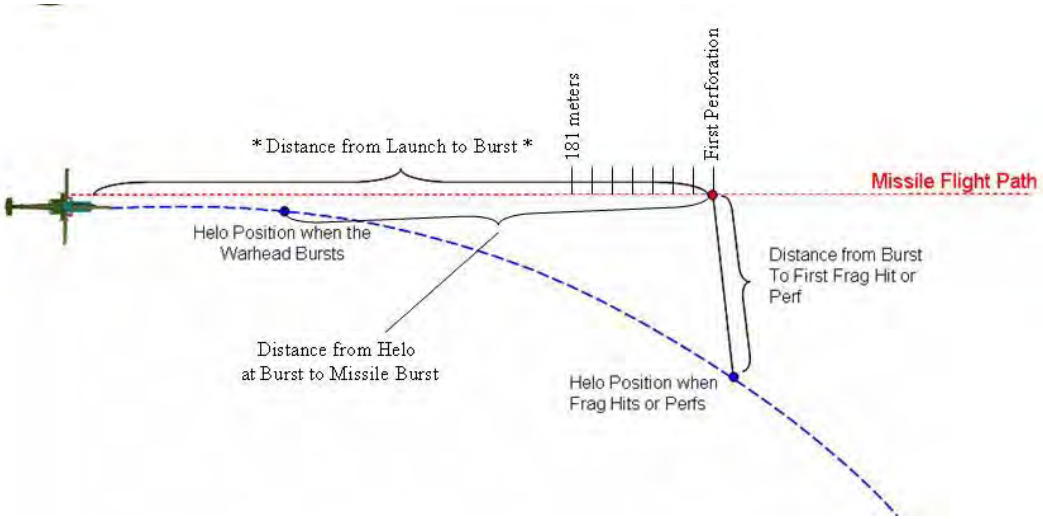

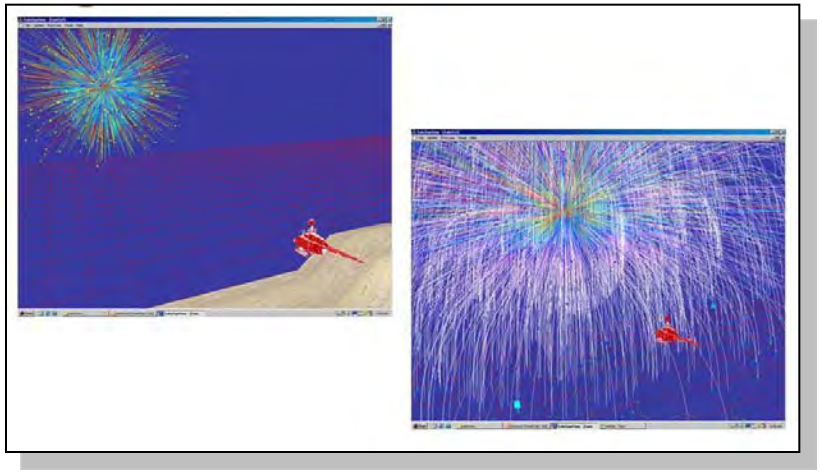

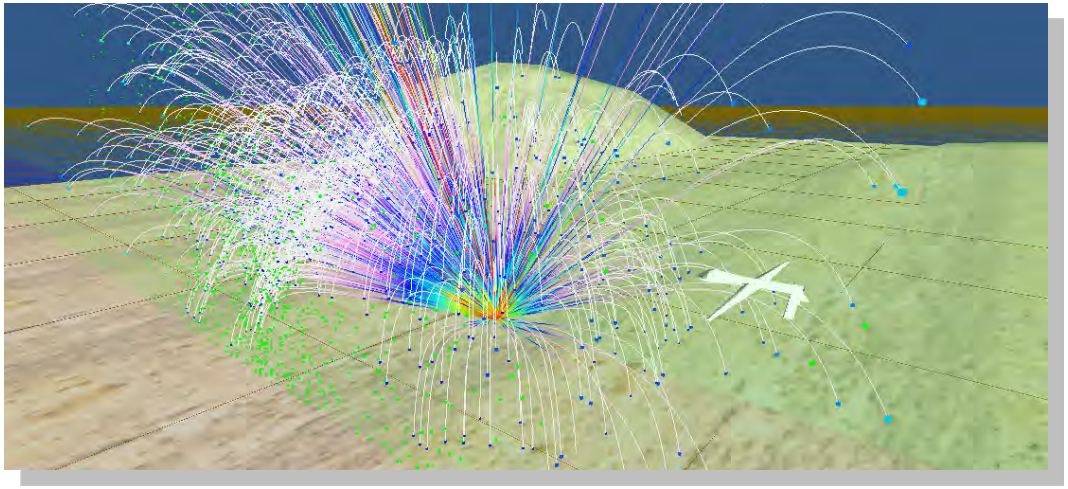

- **High Fidelity Simulation Run in Monte Carlo Mode**
- **Scenario Repeated From Specified Trajectory Location Back to Minimum Arming Distance**
- **Fragment Hits on ALL Critical Components Analyzed**

U.S. ARMY RDECOM

UAV Vulnerability Characterization

AMRDEC

Purpose:

- Determine the vulnerability of UAVs to fragment impact and blast effects

Payoff:

- Determine effectiveness of air defense warheads against UAVs (both lethality and survivability)
- Determine safe separation distance of armed U.S. UAVs

Protection of Light Armors Against Shaped Charge Projectiles

Prof. Ph.D. D.Sc. Adam Wisniewski

Military Institute of Armament Technology

Ul. Wyszynskiego 7

05-220 Zielonka, Poland

Phone/fax: 48 22 761 46 06

Fax: 48 22 761 44 45

E-mail: adam.wisniewski@witu.mil.pl

http://www.witu.mil.pl

KE (Kinetic Energy)

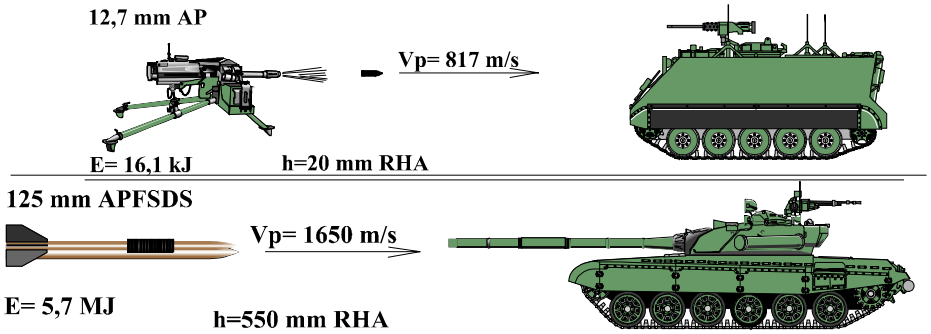

CE (Chemical Energy)

HEAT (HIGH EXPLOSIVE ANTI TANK)

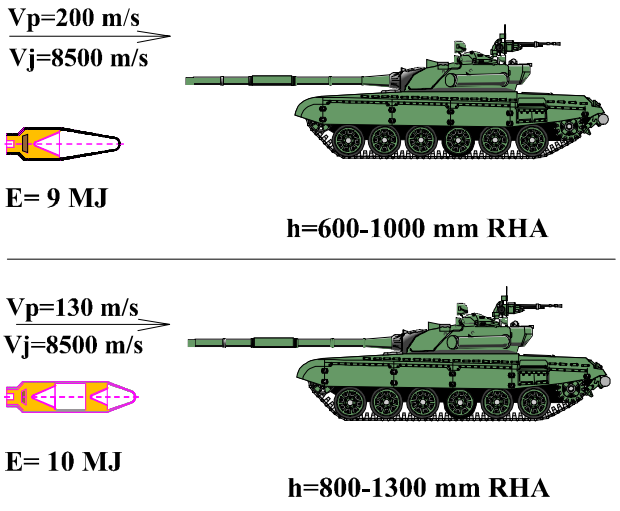

EFP (EXPLOSIVELY FORMED PROJECTILE)

ACTIVITIES

1. **Passive** protection

Protection of helikopters against 7.62 mm and 12.7 mm AP

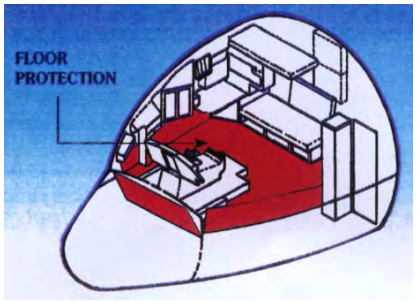

Protection against blast of terrorist bomb with fragments

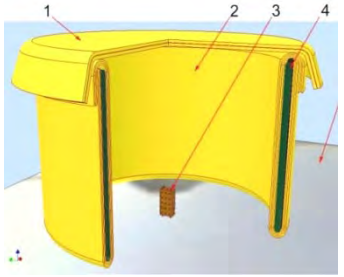

2. **Reactive** protection
3. **Passive-reactive** protection
4. **Active** protection
5. **Passive-active** protection

STOPFIRE
Optoelectronic Fire Extinguishing System for armored vehicles and helicopters

Protection enhancement of electrical installations against the effect of „graphite bomb”

Research scheme of composite armor

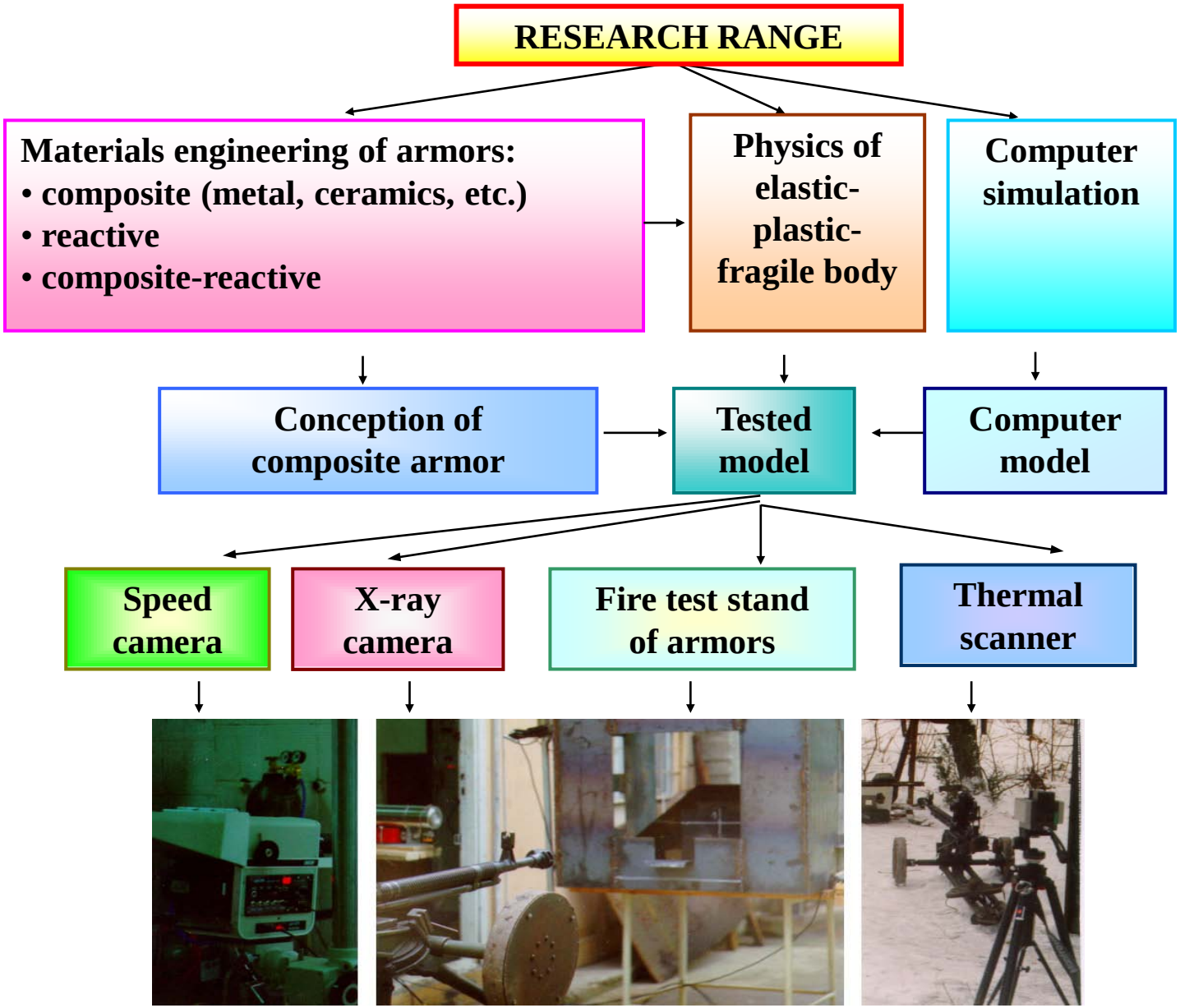

Tested materials:

1. Light metals
2. RHA (rolled homegeneous steel)
3. HHS (high hardness steel)
4. Nanostructural steel:
   - nanostructural maraging steel - new generation,
   - high carbon bainitic steel,
   - amorphous-nanocrystalline steel
5. Ceramics CA (ceramic armor): Al_2O_3, SiC, B_4C, Ti_3SiC_2, AlN
6. Plastic (laminate, polyethylene, etc.)
7. Woven fabric (aramid, textile laminate, etc.)
8. Rheological fluids (STH - Shear Thickening Fluid) - for smart armor
9. Magnetorheological fluid (MRF) - for smart armor
10. Explosives

NSNanoSteel - Development Project - POIG.01.03.01-00-042/08

"Technology of production of superhard nanostructural Fe-based alloys and their application in passive and passive-reactive armours"

1. Beneficjent: Institute for Ferrous Metallurgy, Gliwice, Poland
Beneficiary: Leader: Ph.D., D.Sc Bogdan Garbarz, tel: +48 32 2345249, bgarbarz@imz.pl

2. Partner: Military Institute of Armament Technology, Zielonka, Poland
Partner: Coordinator: Prof. Ph.D., D.Sc Adam Wiśniewski, adam.wisniewski@witu.mil.pl

1. Elaboration of chemical compositions and production parameters of new nanostructural steels grades

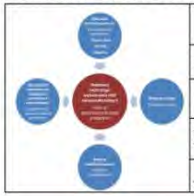

Assumed parameters of nanostructural steels			
Steel grade	R_e	HV	A_5
Maraging steel new generation	>2,5 GPa	> 750	min. 5%
Bainitic nanostructural steel	> 1,7 GPa	> 650	min. 5%
Amorphous - nanostructural steel	> 2,0 GPa	> 700	min. 4%

2. Elaboration of computer simulation of striking at nanostructural steel armour

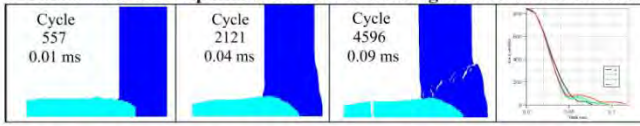

Penetration of 12.7 mm projectile into armour in the function of time - AUTODYN 5 programme

3. Elaboration of production technology of new generation of nanostructural maraging and high carbon bainitic steels

Vacuum VSG 100S furnace (a) for steel and alloys melting (100 kg), copper mould (b)

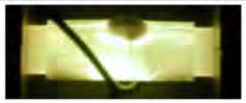

Multi-purpose system for simulations of metallurgical processes Gleeble

4. Elaboration technology of production of amorphous-nanocrystalline steels and Fe-based alloys

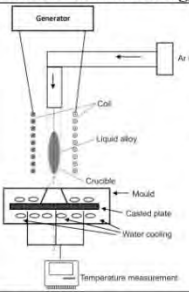

Scheme of the experimental apparatus for manufacturing of amorphous-nanocrystalline steel or Fe-based alloy plates using pressure casting method

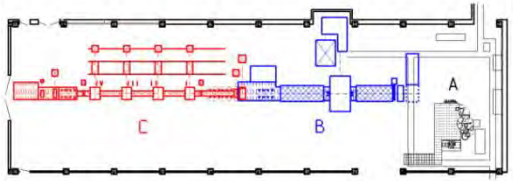

Line for simulation of production processes of metals and alloys products **LPS**

5. Elaboration technology of production of armour models with the nanostructures and firing them

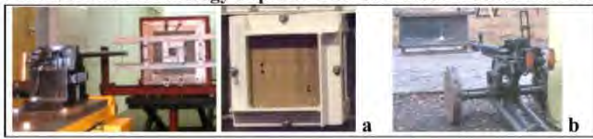

The tests of armour firing: a - standard fragments, b - AP projectiles of the different caliber

INNOVATIVE ECONOMY
NATIONAL COHESION STRATEGY

European Union
European Regional Development Fund

1. Institute for Ferrous Metallurgy, Karola Miarki st. 12, 44-100 Gliwice, Poland
2. Military Institute of Armament Technology, Pr. St. Wyszyńskiego st. 7, 05-220 Zielonka, Poland

INNOVATIVE ECONOMY
NATIONAL COHESION STRATEGY

SMARTARMOUR

European Union
European Regional
Development Fund

SMARTARMOUR - SMART PASSIVE BODY ARMOURS WITH THE USE OF RHEOLOGICAL FLUIDS WITH NANOSTRUCTURES

DEVELOPMENT PROJECT NO. POIG.01.03.01-00-060/08

1. Beneficiary: Leader: Warsaw University of Technology, Warszawa, Poland
Prof. Ph.D., D.Sc Marcin Leonowicz, tel: +48 22 234 8450, *mkl@inmat.pw.edu.pl*
2. Partner: Coordinator: Military Institute of Armament Technology, Zielonka, Poland
Prof. Ph.D., D.Sc Adam Wiśniewski, *adam.wisniewski@witu.mil.pl*
3. Partner: Coordinator: Institute of Security Technology "MORATEX", Łódź, Poland
PhD. Eng. Jadwiga Polak, *poigs@moratex.eu*
PhD. Eng. Marcin H. Struszczyk, *poigs@moratex.eu*

1. Warsaw University of Technology,
Pl. Politechniki 1, 00-661 Warszawa, Poland

2. Military Institute of Armament Technology,
Pr. St. Wyszyńskiego str. 7, 05-220 Zielonka, Poland

3. Institute of Security Technology "MORATEX",
Marii Skłodowskiej - Curie str. 3, 90-965 Łódź, Poland

1. ELABORATION OF RHEOLOGICAL FLUIDS FOR SMART ARMOUR

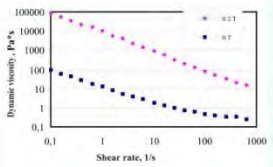

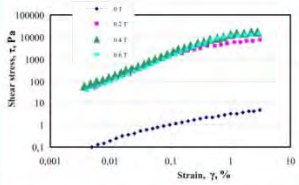

LORD 132 DG fluid under magnetic field

2. ELABORATION AND BUILDING THE MAGNETIZING SYSTEM FOR THE MAGNETORHEOLOGICAL FLUID

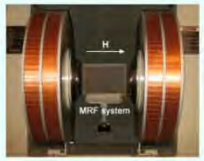

Magnetorheological fluid - MRF between magnetic poles

3. ELABORATION AND CARRYING OUT COMPUTER SIMULATION OF PROJECTILE STRIKING INTO SMART ARMOUR

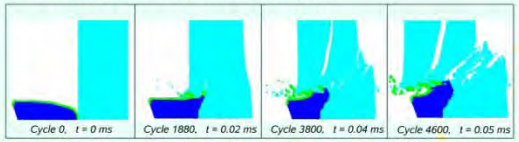

Penetration of 9 mm Parabellum bullet into Kevlar armour in the function of time - AUTODYN 5 software

4. ELABORATION OF TECHNOLOGY, BUILDING TEXTILE SMART ARMOURS AND TESTING THEM

Smart armours protection ability tests against white weapon striking

5. ELABORATION OF TECHNOLOGY, BUILDING SMART ARMOURS MODELS AND FIRING THEM

a - balistic tests: fragment- and bulletproofness tests;

b - armour's model.

DEVELOPMENT PROJECT REALIZED
IN NATIONAL COHESION STRATEGY 2007 - 2013
IS FINANCIALLY SUPPORTED BY
EUROPEAN REGIONAL DEVELOPMENT FUND

Nowadays tendency

Constructors gave up the previous tendency that FV armor thickness should be similar to tank armor thickness.

Light armors of FV should be protected:

1. by armor lighter than RHA,
2. against penetration RPG-7 grenade launcher (*DP* = 300 mm RHA)
3. against AP bullets *d* = 25÷40 mm.
4. against radar detecting and recognizing**.**

Light fighting vehicles with ERA cassettes

ERA cassettes (1) protecting from shaped charge projectiles of the PG-7 type;

Bradley with different non modular cassettes

FV432 Mk3 BULLDOG with modular cassettes

BRADLEY with ERA

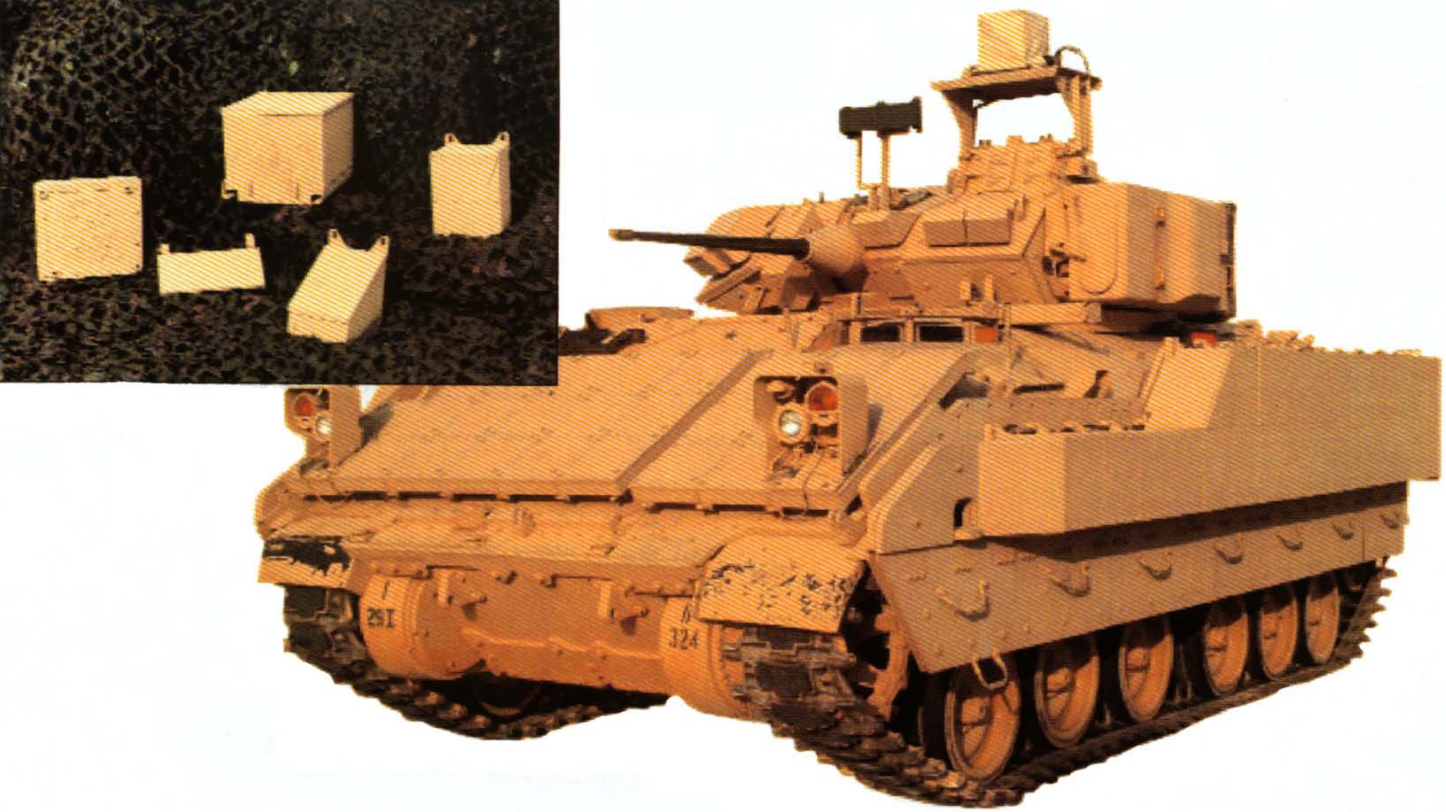

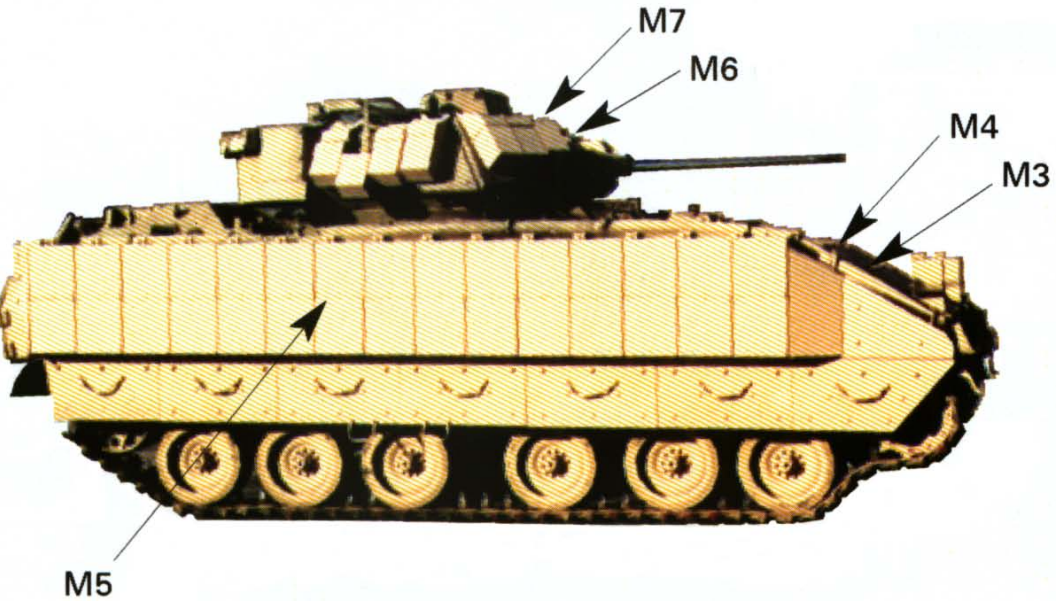

BFVS armor tiles

M3 - wedge	-	26 pcs
M4 - frontal	-	9 pcs
M5 - side	-	55 pcs
M6 - turret	-	7 pcs
M7 - turret wedge	-	8 pcs
Total tiles per vehicle set	-	105 pcs

ERA + AFV

ERA for IFV

M113, VCC-1, AA7A1 - Israeli EAAK cassettes of Rafael firm with inertial layers and TOGA armor with metal sheets, which contain holes.

Protecting against HEAT projectiles of RPG-7 type and 14.5 mm AP bullets:

M113A fighting vehicle with Israeli reactive armor

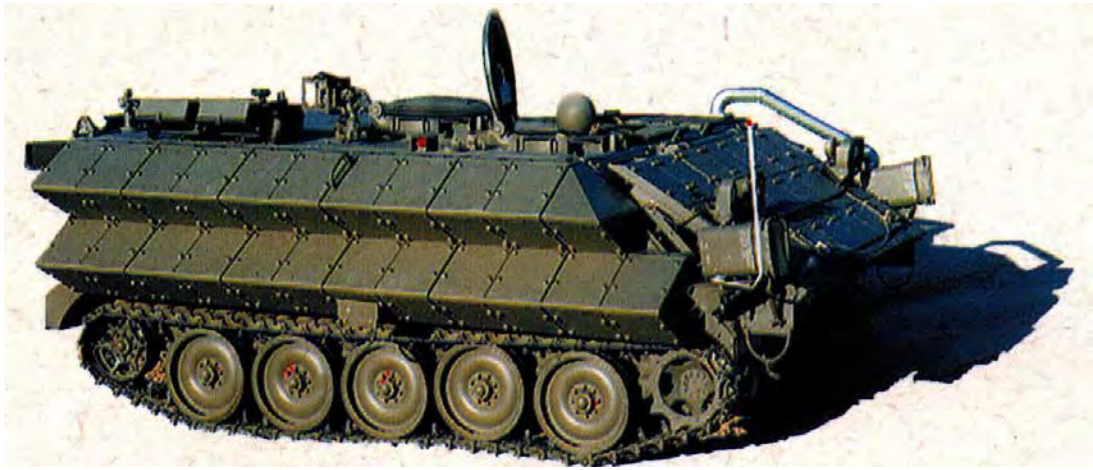

M113 fighting vehicle with Israeli reactive armor

French M113 with ERA

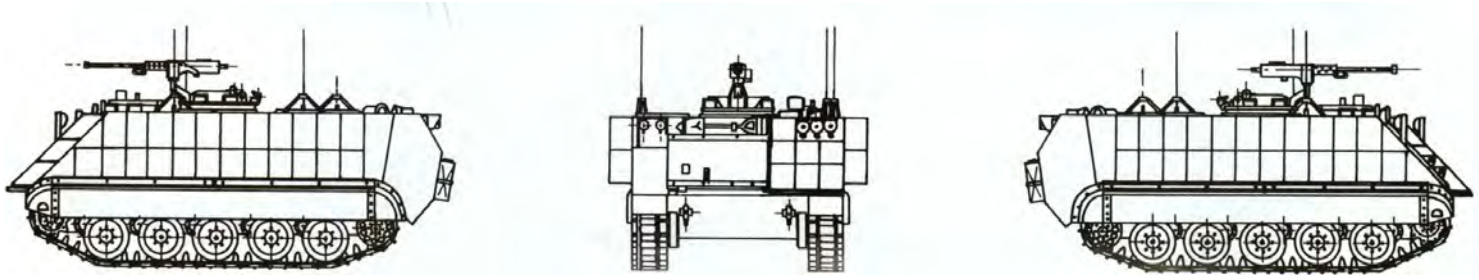

Kind of vehicle	M113 i A2	M113 A3
Total mass	980 kg	1900 kg
Protection area	3,6 m^2	6,6 m^2
Angle of hit for all types of threat	160^o	160^o
Protection against perforation for the following projectiles	12,7 mm AP z 100 m 14.5 mm AP z 100 m 20 i 23 mm AP z 300 m **RPG-7**	12,7 mm AP z 100 m 14.5 mm AP z 100 m 20 i 23 mm AP z 300 m **RPG-7**
Number of cassettes for 3 different types	30	56

There is no information whether reactive cassettes are resistant to fire from small-calibre ammunition as a result of using in them so-called composite-reactive armor.

The BWP-1 with the CERAWA-1 composite-reactive armor

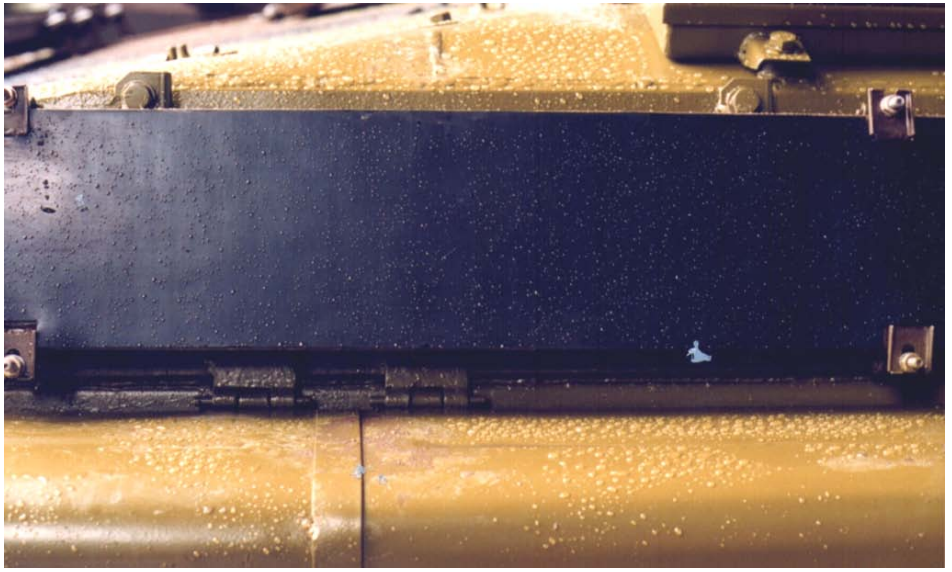

The CERAWA-1 composite-reactive armor

The CERAWA-1 composite-reactive armor consists of:

1. Unified, mutually replaceable hermetic cassettes (72 pieces of modules - **306x156x44 mm**, area - **3.5 m^2**), which apart from ceramics contain, among other things, explosive material. The cassettes are located on:
   - the plates of the front turret - 9 pieces,
   - the front of all plates of the left and right side of the turret - 2 x 7 = 14 pieces,
   - the front upper plate of the hull and the breakwater - 23 pieces,
   - the front bottom plate of the hull - 12 pieces,
   - the side part of the hull - 2 x 7 = 14 pieces.
2. Frame holding the CERAWA-1 armor.
3. RAM (radar absorber material)

72 pieces of the CERAWA-1 cassettes is a basic equipment of the IFV but it is possible to use greater quantity of the cassettes depending on the requirements.

The CERAWA-1 composite-reactive armor

Protecting features

The CERAWA-1 protects main surfaces the BWP-1 (10 mm thickness) in sector of **frontal horizontal fire and observation 70°** (on the right and left from axis of vehicle) against:

1. penetration with HEAT with penetration capacityof h = 300 mm RHA,
2. penetration with armor-piercing bullets with AP calibre d = 14.5 mm,
3. detection and recognizing by radar.

Result of firing of the CERAWA-1 cassettes with 12.7 mm AP bullets

a

reactive cassette which was not perforated after perforation of passive layer

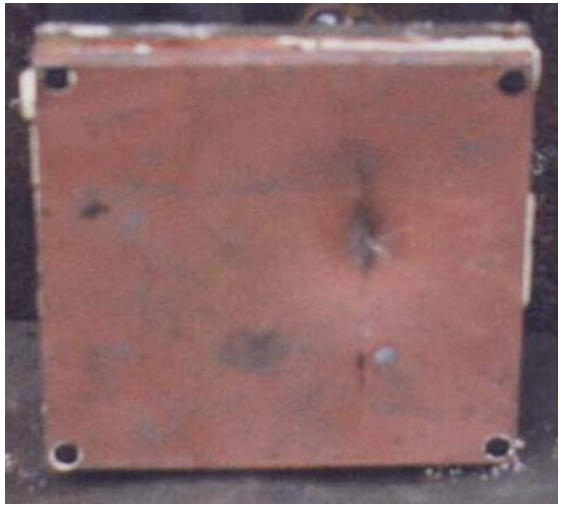

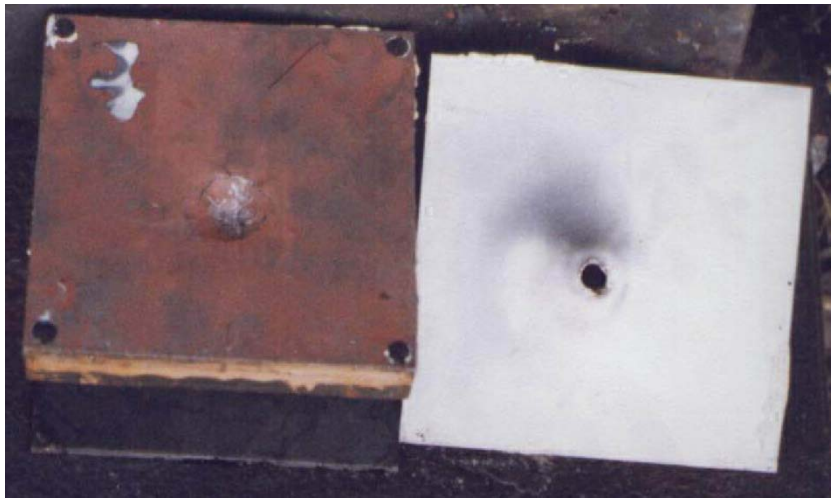

b

reactive cassette which was not perforated and perforated passive layer

Result of firing of the CERAWA-1 cassettes with 14.5 mm AP bullets

a

reactive layer which was not perforated

b

perforated reactive layer

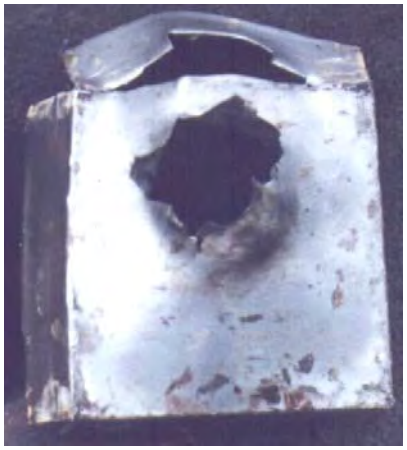

c

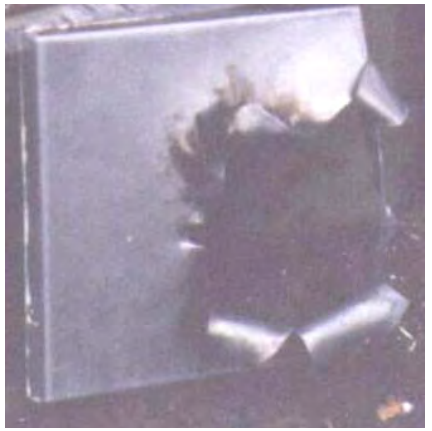

d

perforated and torn passive layer

Impact test of the CERAWA-1 cassettes with the fragments of 122 mm projectile

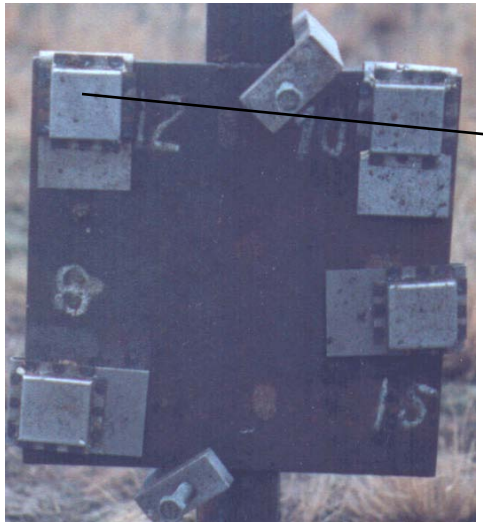

before initiation

steel plate
with cassettes
No: 6, 10, 12, 15

before initiation

projectile arrangement
in relation to cassettes

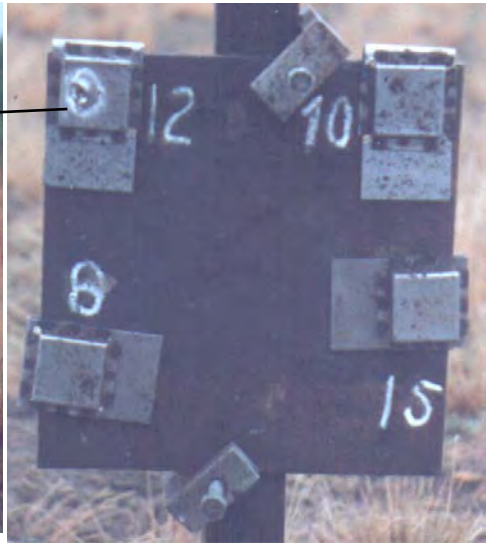

after explosion

hit result
of the CERAWA-1
cassette No 12
with the fragment
of 122 mm
projectile

The results of static test of the PG-7M + CERAWA-1 composite-reactive armor on the RHA plate with the thickness *b* = 10 mm

penetrated of the RHA plate

only deep deformation
without penetration

PG-7M with capacityof the RHA penetration *h* = 300 mm

ERAWA-1 and ERAWA-2 cassettes

Marking:

ERAWA-1 - TX01 - 24-02 – WITU

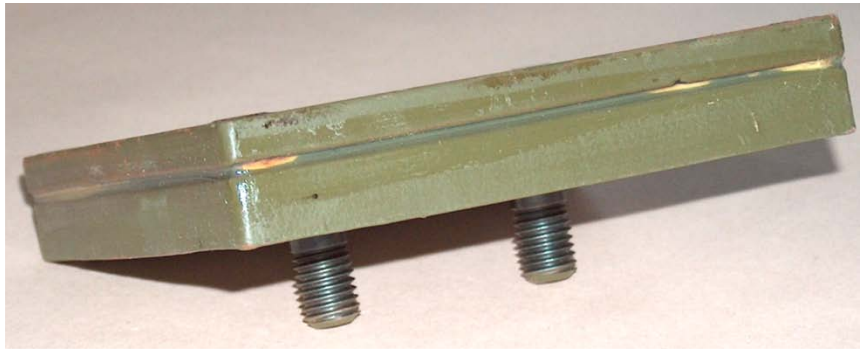

ERAWA-2 - TX02 - 24-02 - WITU

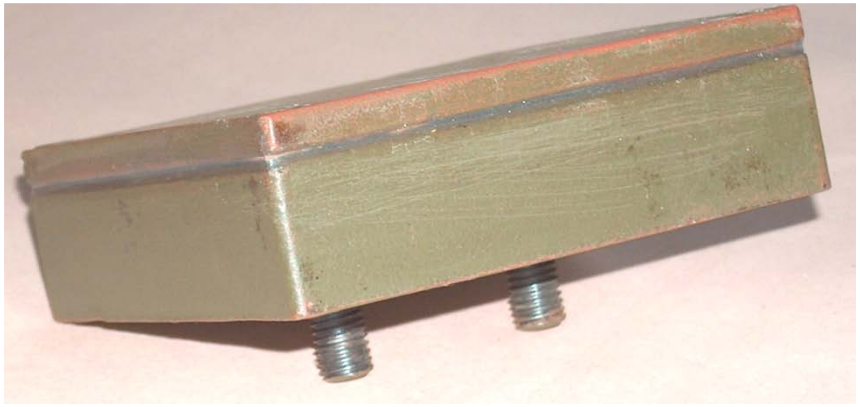

Easy and very fast to install
ERAWA-1 and ERAWA-2

Explosive reactive armor -
III generation

I. Parameters

1. **Size of the ERAWA-1 cassette - 150x150x26 mm**
2. **Size of the ERAWA-2 cassette - 150x150x46 mm**
3. **Mass of the ERAWA-1 cassette - 2.9 kg**
4. **Mass of the ERAWA-2 cassette - 4.7 kg**
5. **Number of the ERAWA-1 cassettes - 164 pieces**
6. **Number of the ERAWA-2 cassettes - 95 pieces**
7. **Protected area (glacis plate, hull, skirts) - 5.9 m^2**

Scheme of test of protection capacity of the ERAWA-1 cassette

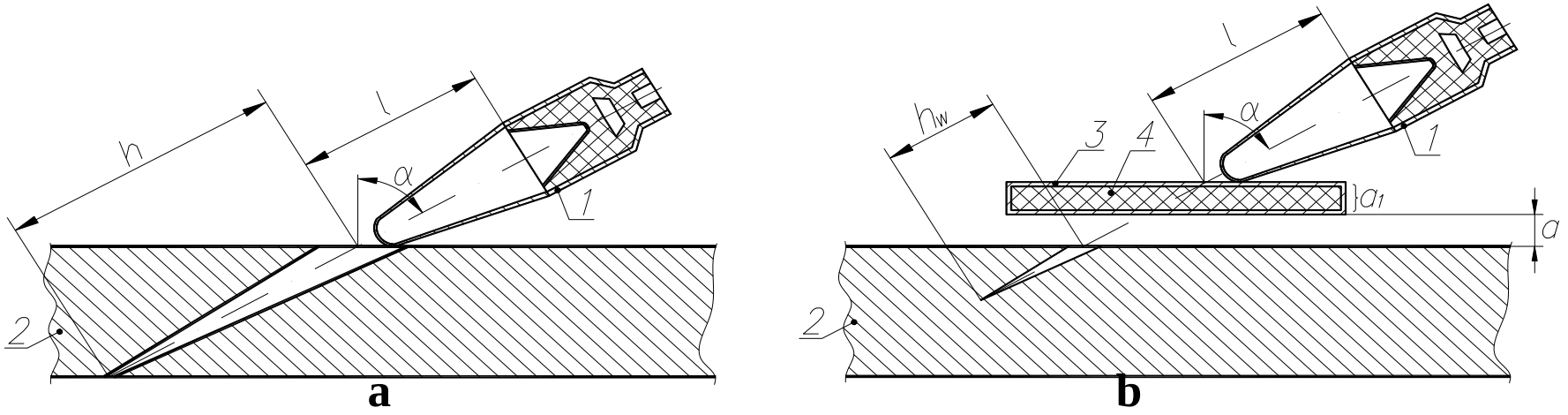

a - warranted capacity of penetration of the RHA with thickness *h*

b - depth of penetration *hw* in witness plate, protected with the ERAWA-1 cassette

1 - shaped charge before detonation

a_1 - the ERAWA-1 cassette before detonation

2 - the RHA

3 - casing of the ERAWA-1 cassette

4 - explosive

h - warranted depth of the RHA penetration

hw - depth of penetration of the RHA protected with cassette

α - angle of shaped charge jet penetration of the ERAWA-1 cassette and the RHA

HEAT: PG-7, FAGOT + ERAWA

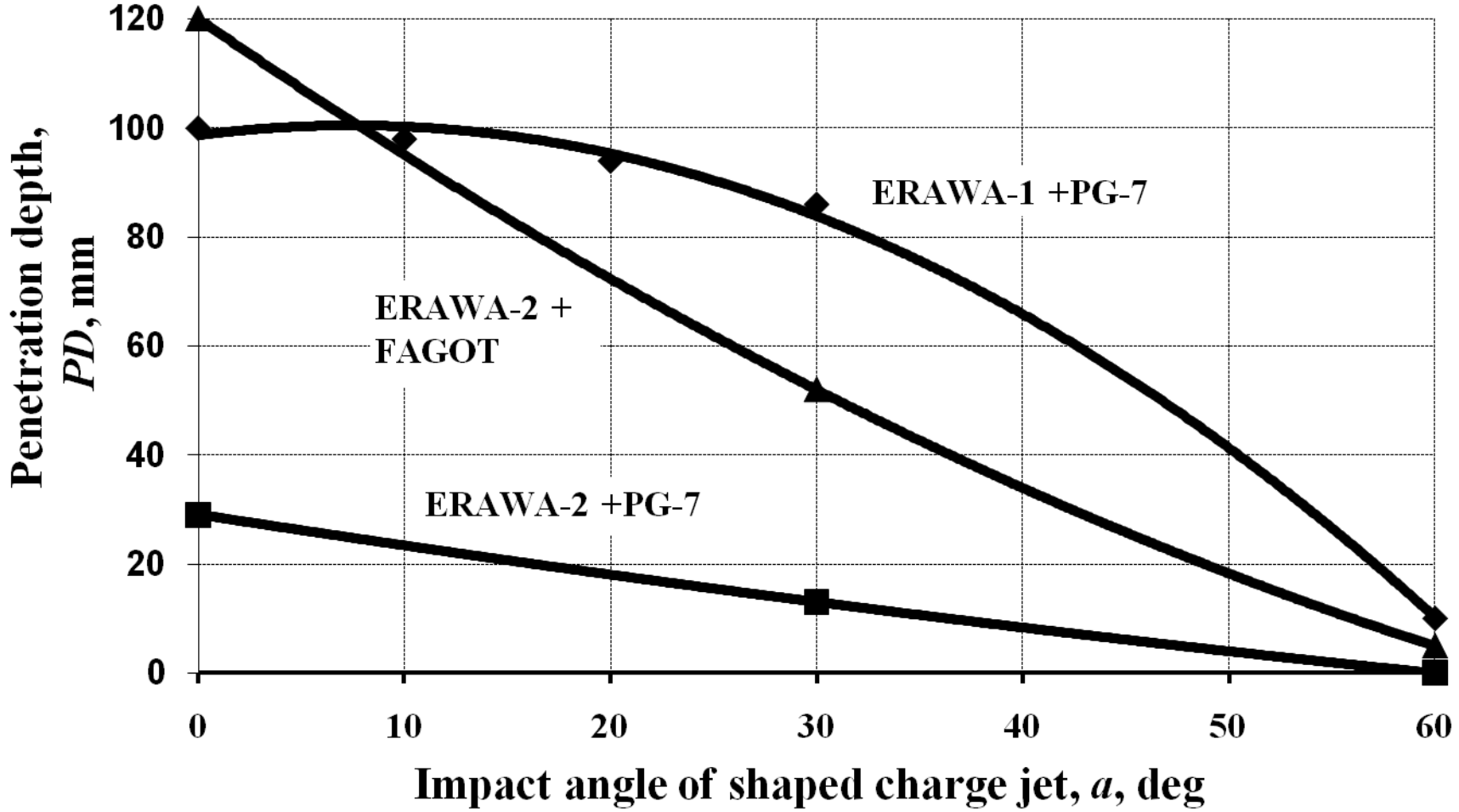

Penetration depth (*hw*) of the RHA protected with the ERAWA cassettes in the function of the impact angle (∝- in relation to normal to surface of cassette) of different jets of shaped charge projectiles

Reactive-passive panels supported in: two (a - version 1 and 2) and three (b - version 3) places

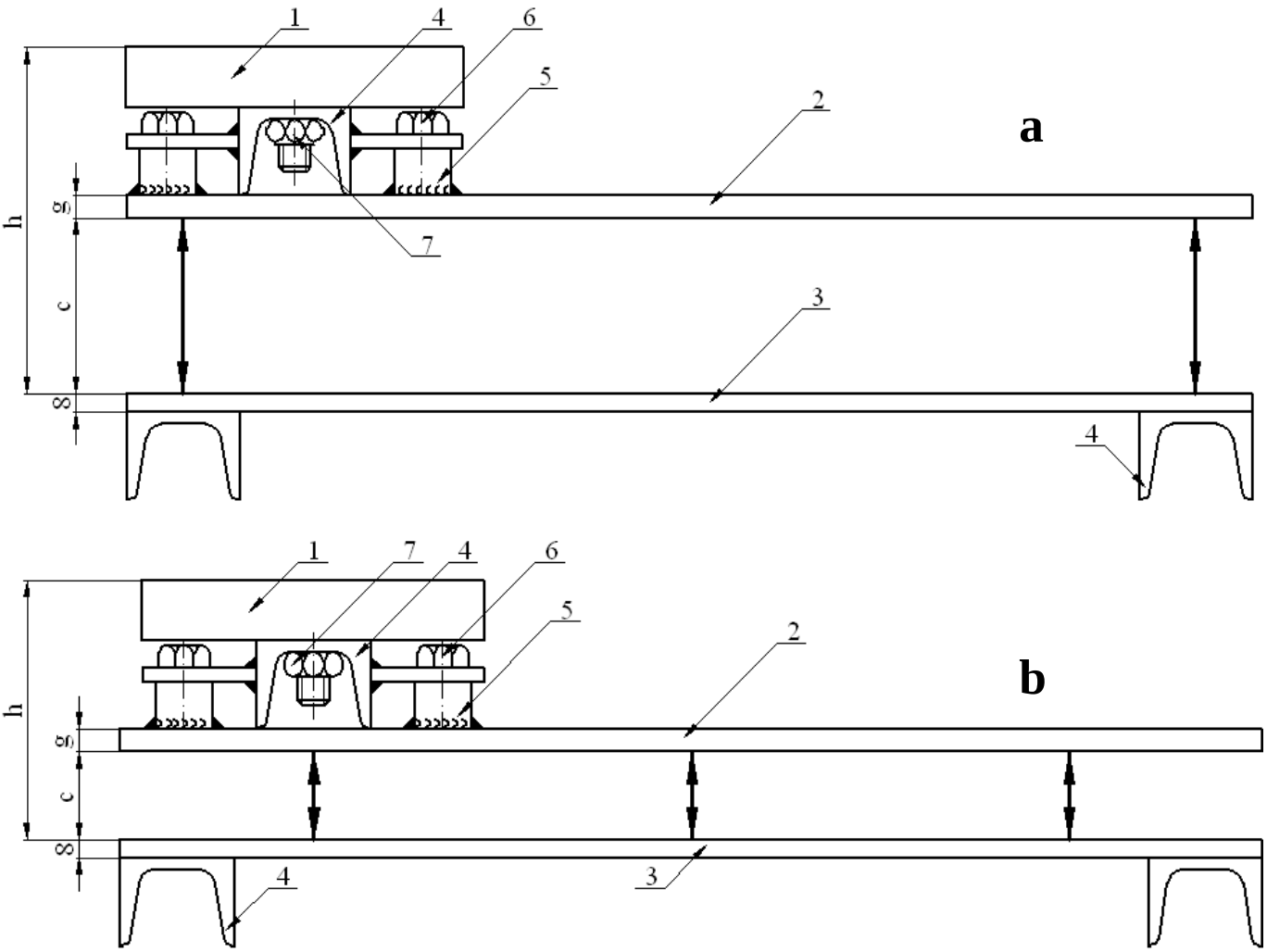

1 - ERAWA-1 cassette,
2 - steel plate 1,
3 - RHA witness plate 2,
4 - steel channel section,
5 - sleeve,
6 - screw,
7 - nut

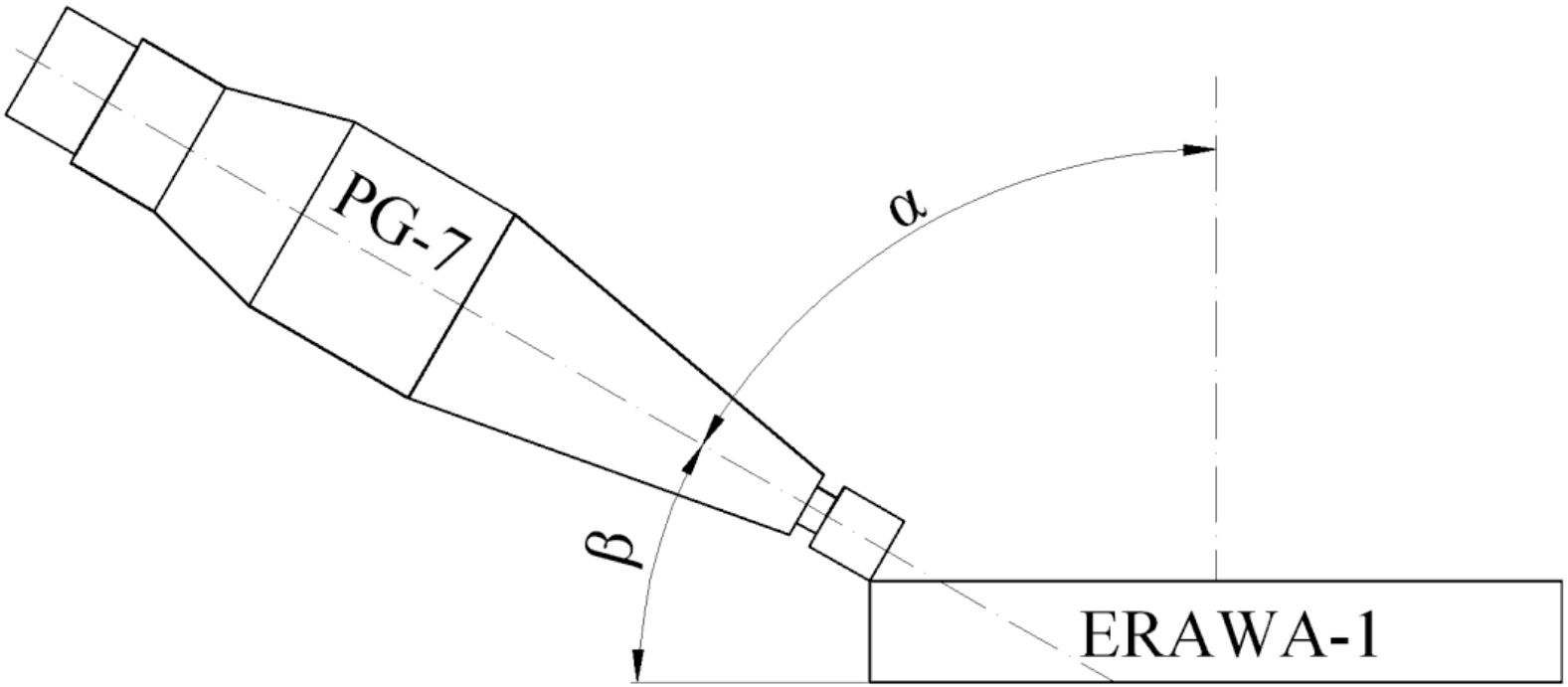

The arrangement of the PG-7 shaped charge projectile in relation to the ERAWA-1 reactive cassette

Testing of the reaction of the ERAWA cassettes to the shaped charge jet of the PG-7WM projectile

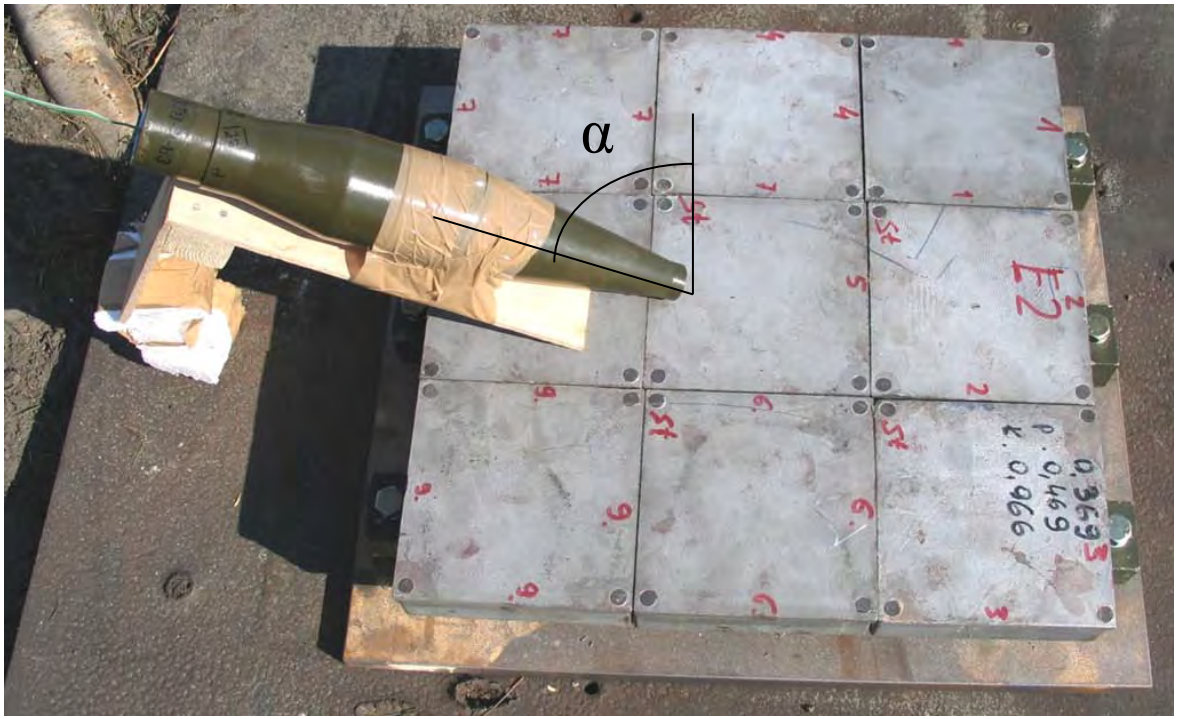

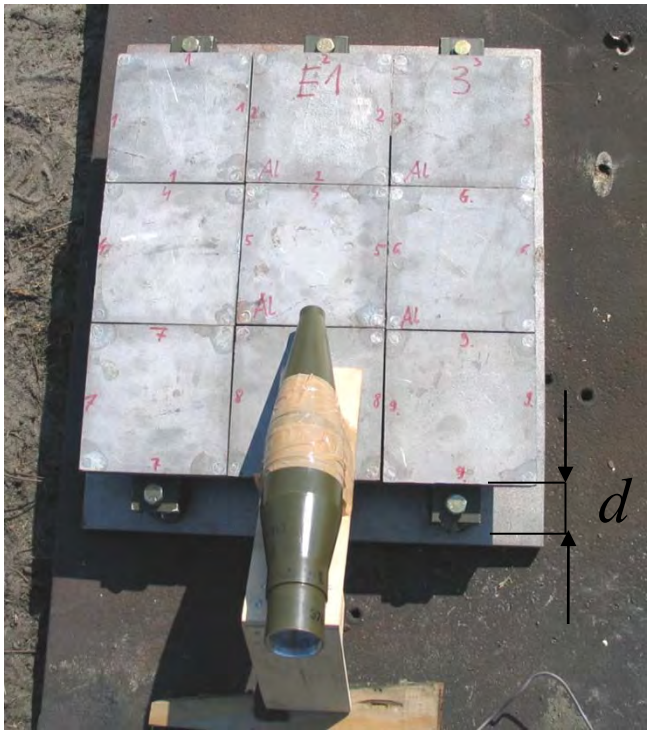

Nine-element aluminium panel ERAWA-1 cassettes before initiation with the PG-7WM shaped charge projectile

Reactive-passive panel - version 1

Parameters of panels of passive-reactive armors

No of panel / No of variant	Setting angle of PG-7 projectile in relation to normal to the surface of ERAWA-1 cassette, deg	Material of plate 1	Surface mass of panel, m, kg/m^2
1/1	72	RHA	227
2/1	60	RHA	227
3/2	72	St3	211
4/2	60	St3	211
5/3	72	RHA	221
6/3	60	RHA	221

Panels with the ERAWA-1 cassettes from aluminium alloy before and after the initiation of the PG-7 projectile

The PG-7 projectile at angles of α from normal to the cassettes:

a

a - panel 1, α=72

b

lack of copper trace on witness plate 2 (panel 1)

c

panel 2, α=60

d

DP=1 and copper trace on witness plate 2 (panel 2)

Panels with the ERAWA-1 cassettes from aluminium alloy before and after the initiation of the PG-7 projectile

The PG-7 projectile at angles of α from normal to the cassette:

a

panel 3,
α=72
DP =4.5 mm
copper trace on
witness plate 2

b

panel 4,
α=60
DP=8 mm
perforation
of witness plate 2

c

panel 5,
α=72
copper trace
on witness plate 2

d

panel 6,
α=60
DP=2 mm and
copper trace on
witness plate 2

Results of firing of panels of passive-reactive armors with the use of the PG-7 projectiles

No of panel / No of variant / setting angle of PG-7, α, º	Material of steel plate 1 / penetration depth of RHA plate 2 (witness), *DP*, mm	Sizes of holes in RHA plate 2 (witness), *a* x *b*, mm		Deflection of RHA plate 2 (witness), *d*, mm
		inlet	outlet	
1 / 1 / 72	RHA / -	-	-	-
2 / 1 / 60	RHA / 1	~3x3	-	-
3 / 2 / 72	St3 / 4,5	51x13	-	8
4 / 2 / 60	St3 / 8	34x17	10x6	27
5 / 3 / 72	RHA / -	-	-	11
6 / 3 / 60	RHA / 2	~3x3	-	13

The depth of penetration

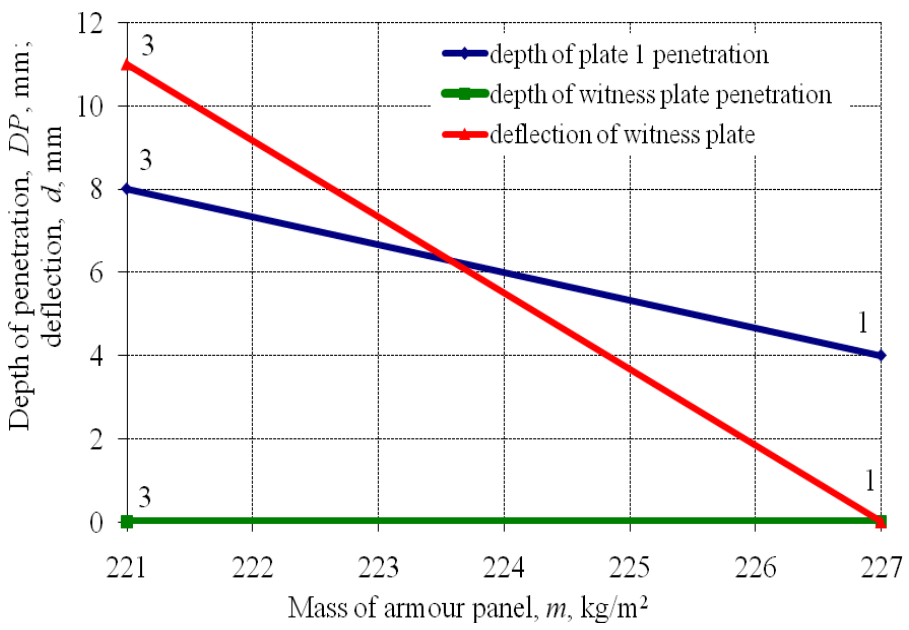

α=72

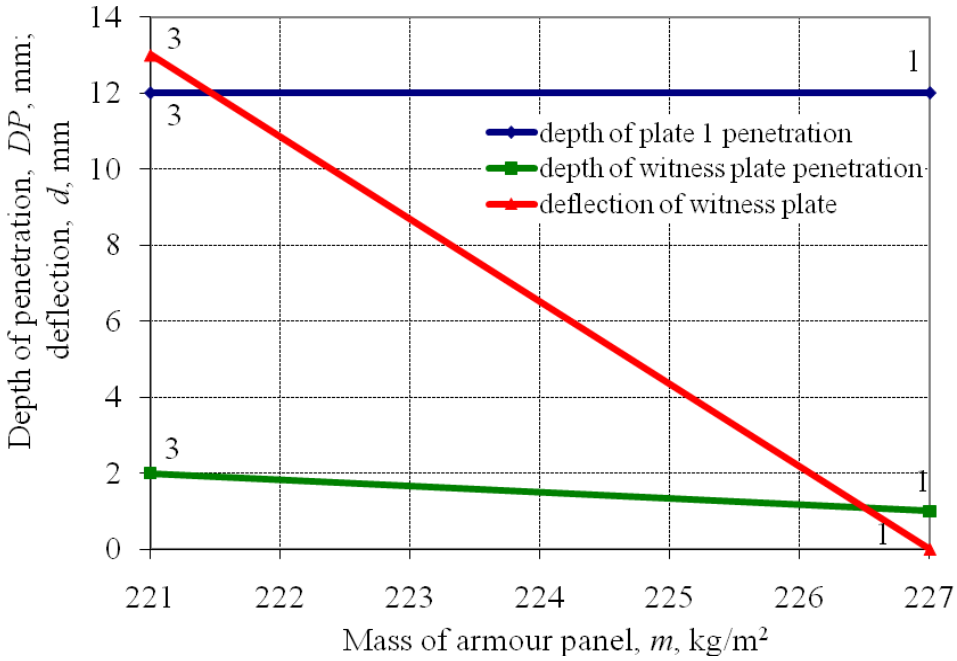

α=60

The depth of penetration of the steel plate 1, the RHA plate 2 (witness) and the deflection of the RHA plate 2 (witness): in the function of the mass of the armor panel for the angles of α=72 and α=60

The depth of penetration

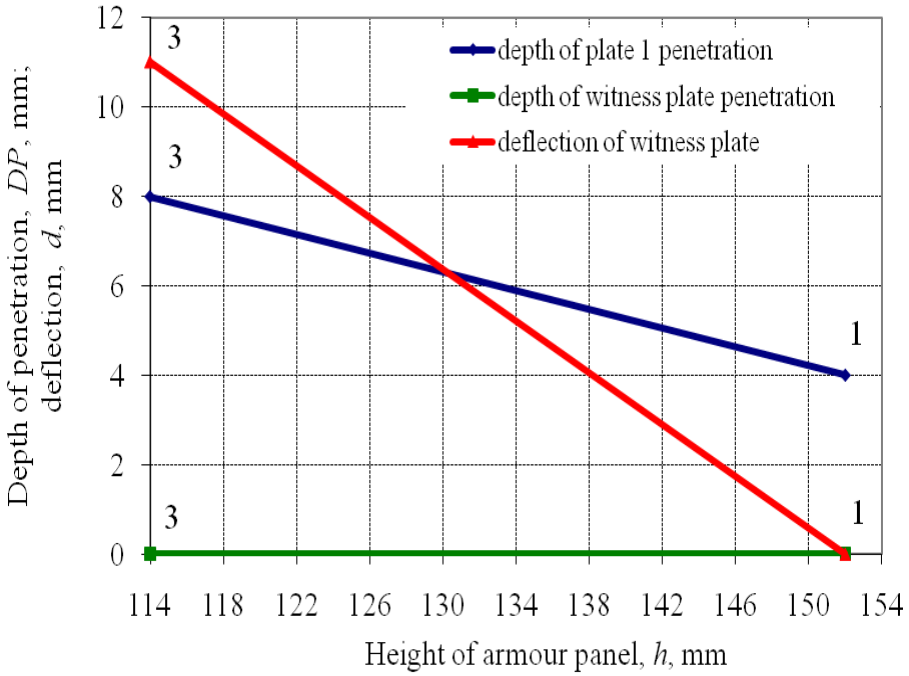

α=72

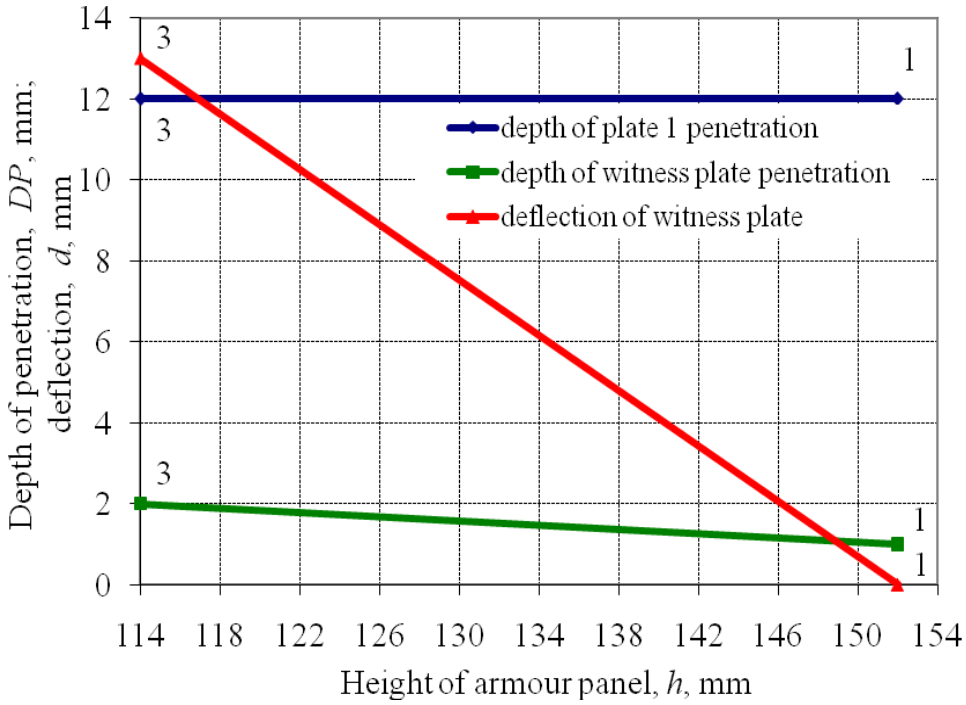

α=60

The depth of penetration of the steel plate 1, the RHA plate 2 (witness) and the deflection of the RHA plate 2 (witness): in the function of the height of the armor panel for the angles of α=72 and α=60

Conclusions

The CERAWA-1 composite-reactive armor

1. The CERAWA-1 composite-reactive armor cassettes are the first solution of this type in the world. These cassettes are characterized by little thickness in relation to similar foreign cassettes and can be used on infantry fighting vehicle BWP-1 or on other light armored vehicles. As a result of firing tests of CERAWA-1 cassettes it can be stated that:

- Passive layer with ceramics in cassette of CERAWA-1 composite-reactive armor does not diminish the protection capacity of explosive of this cassette.
- CERAWA-1 cassettes protect RHA with thickness of b = 10 mm against perforation with 12.7 mm bullets of B-32 type with penetration capacity of RHA h = 20 mm and against PG-7 shaped charge projectiles with penetration capacity of RHA h = 300 mm.
- After the perforation of the reactive-passive armor on the surface of the hull of protected vehicle small craters with the depth of several millimeters and traces of dispersed copper of shaped charge jet of PG-7 can occur.

Conclusions

Reactive-passive armor with ERAWA-1 cassettes from aluminium alloy

2. The panel of the reactive-passive armor with ERAWA-1 cassettes from aluminium alloy can protect light armored fighting vehicles against the perforation of PG-7 projectiles hitting this armor at the angle of $60^{o} \leq \alpha \leq 72^{o}$ from normal to this armor.
3. After the perforation of the reactive-passive armor on the surface of the hull of the protected vehicle, some small craters with a depth of several millimeters and some traces of dispersed copper from the shaped charge jet of the PG-7WM can occur.
4. The best protection was provided by the reactive-passive armor in the version 1. The shaped charge jet did not pierce the plate 1 with the size of 500×500 mm, both for the angle of $\alpha = 72°$ and $\alpha = 60°$. There was also no deflection of the steel armor witness plate with the size of 600×500×8 mm as a result of the initiation of the explosive of the shaped charge jet projectile and the ERAWA-1 cassette.

Conclusions

Reactive-passive armor with ERAWA-1 cassettes from aluminium alloy

5. The protection against the perforation of the shaped charge jet was also provided by the reactive-passive armor in the variant 3. The deflections of the RHA witness plates (of 11 mm for the panel 5 and 13 mm for the panel 6) occurred for the $\alpha = 60$ and $\alpha = 72$ setting angles of the shaped charge jet PG-7WM projectile in relation to the normal external surface of the cassette. They were caused by:
   - smaller distances between the plates 1 and 2,
   - greater stiffness of the plate 1 due to its support in three places on the plate 2 (the witness one),
   - distances between the plates 1 and 2 in the variant 3 smaller than in the variants 1 and the variants 1 and 2.

	H	Q	R
1	**Registrant Full Name**	**Organization**	**Title**
2	Dr. Elena Abadjieva	TNO Applied Scientific Research	
3	Mr. Louk Absil	TNO Defence, Security, and Safety	Dr. Ir.
4	Mr. Carlton Adam	U.S. Army ARDEC	
5	Mr. Yusuf Fatih Akdas	STM AS	Quality Assurance Representative
6	Dr. Zbynek Akstein	Explosia a.s.	
7	Mr. Kari Ala-Mikkula	FDF Army Materiel Command HQ	
8	Mr. Robert Allen	Alliant Small Caliber Ammunition Co.	Program Manager
9	Dr. Richard G. Ames	Raytheon Company	Engineer
10	Dr. Charles E. Anderson Jr.	Southwest Research Institute	Director
11	Mr. Olof Andersson	FOI Swedish Defence Research Agency	Research Engineer
12	Mr. Walter Andrefsky	Aberdeen Test Center	Test Officer
13	Dr. William S. Andrews	Royal Military College	Professor
14	Dr. Werner Arnold	MBDA-TDW	
15	Dr. Zvi Asaf	Plasan Sasa Ltd.	Senior Analysis Engineer
16	Mr. John Auten	US Army Research Laboratory	Operations Research Analyst
17	Mr. Lior Avital		
18	Mr. Ilan Azulay	Israel Military Industries, Central Laboratory Division	
19	Mr. Mike P Baca	Los Alamos National Laboratory	Explosives Tech
20	Mr. Joseph E. Backofen Jr.	BRIGS Company	President
21	Dr. Ernest L. Baker	U.S. Army ARDEC	Research Physicist
22	Mrs. Lisa Jayne Baker	Defence Science and Technology Laboratory	
23	Doug Barna	SKYDEX Technologies, Inc.	
24	Mr. Darrel R. Barnette	Institute for Advanced Technology at UT	Research Associate
25	Mr. Christopher S Bartley	NAWCWD China Lake	Aero Engr. Tech
26	Mr. Victor H. Bastidas	Universidad de los Andes	Mechnical Engineer
27	Ivan Bastin	FN Herstal S.A	
28	Mr. Laurens Baudoin	Defense Materiel Organisation	
29	Dr. Dennis W. Baum	Lawrence Livermore National Laboratory	Associate Program Director/Weapon Complex Integration
30	Dr. Joseph D. Baum	Science Applications Int'l Corporation	AVP Technical Lead
31	Dr. Rafal Bazela	Military Institute of Armament Technology	Expert of Fuse Systems
32	Mr. Thilo Behner	Fraunhofer EMI	
33	Mr. Luca Benassi	EADS Deutschland GmbH	
34	Mr. Brian Benesch	SURVICE Engineering Company	Engineer
35	Mr. Juvenal Benitez Palmeth	AGP Group	
36	Mr. Richard A. Benjamin	U.S. Army Research Lab	Physical Science Technician
37	Mr. Arie Ben-Tal	Israel Military Industries, Ltd. (IMI)	Program Manager
38	Dr. Magnus Bergh	Swedish Defence Research Agency (FOI)	Scientist
39	Mr. Albert D. Bermudez	NAWCWD China Lake	Lead
40	Dr. Claude Berner		
41	Mr. Todd Bessey	BAE Systems Global Tactical Systems	
42	Mr. Jaime Jose Bestard	46th Test Group - Aerospace Survivability and Safety Operating Location	Mechanical Engineer
43	Mr. David Betancourt	Baker Atlas	
44	Dr. Richard A. Beyer	U.S. Army Research Laboratory	Research Physicist
45	Mr. Stefano Bianchi		
46	Mr. Roy B. Bilkert	Ministry of Defence, The Netherlands	
47	Mr. Cagin Gorkem Bingol	Tubitak-Sage	
48	Dr. Stephan J. Bless	Institute for Advanced Technology at UT	Associate Director
49	Mr. John H. Bockbrader	Leading Technology Composites Inc.	Manufactring Engineer
50	Mr. Michael Boczek	BAE Systems Mobility & Protection Systems	
51	Mr. Roger D. Boeka	General Dynamics Corporation	Senior Scientist
52	J. Buford Boone III	Federal Bureau of Investigation	Supervisory Special Agent
53	Mrs. Asaf Menahem Borenstein	Plasan Sasa	
54	Mr. Francois Boussu	ENSAIT	
55	Mr. Robert L. Bowen	U.S. Army Research Laboratory	Division Chief
56	Ms. Alexandra Britt	Alternate Business Consultants	
57	Ms. Nicole Brockhoff	OSD/DOT&E	Biologist
58	Ms. Jeanne C. Brooks	U.S. Army ARDEC	Mechanical Engineer
59	Dr. Ronald Brown	Naval Postgraduate School	Professor
60	Mr. William James Bruchey III	Survice Engineering	Project Engineer
61	Dr. Jaroslav Buchar	SVS FEM s.r.o.	Professor
62	Mr. TANER BUDAK	ASELSAN, Inc.	
63	Mr. Mark Burdeshaw	U.S. Army Research Laboratory	Team Leader of the MUVES 3 Development Team
64	Dr. Wojciech Burian	Institute for Ferrous Metallurgy	

	H	Q	R
65	Mr. Cornelis Buysrogge	TNO	Research Manager
66	Mr. HeQuan Cao	China Academy of Ordnance Science	
67	Mr. Elbert Caravaca	ARDEC	Propulsion Engineering Supervisor
68	Dr. Leopoldo A. Carbajal	DuPont	Sr Engineer
69	David W. Carlson	Teijin Aramid USA, Inc.	Sales Manager - Ballistics
70	Dr. Donald E. Carlucci	U.S. Army ARDEC	Mechanical Engineer
71	Mr. James Carter	QinetiQ North America	
72	Dr. Erik Carton	TNO Defence, Security, and Safety	
73	Dr. Juan P. Casas	Universidad de los Andes	
74	Dr. Enrico Cavallini	University of Rome - Sapienza	Research Fellow
75	Dr. Roxan Cayzac	Nexter Munitions	
76	Mr. Ilmars Celmins	U.S. Army Research Laboratory	Mechanical Engineer
77	Dr. Jeffrey A. Chambers	DuPont Company	Research Fellow
78	Dr. Karl K. Chang	DuPont	Research Associate
79	Dr. Lang M Chang	Dynamic Science Inc.	Senior Engineer/Project Manager
80	Mr. Cho Changyeon	Poongsan	
81	Mr. Pierre Y. Chanteret	ISL French-German Research Institute Saint Louis	
82	Mr. Larry Chao	Horus Vision, LLC	Product Development Manager
83	Mr. Raymond Chaplin	US ARMY ARDEC	Mechanical Engineer
84	Chih Tsai Chen	Department of Homeland Security	General Engineer
85	Dr. Weinong W. Chen	Purdue University	Professor
86	Dr. Ming Cheng	Allen Vanguard Corporation	Research Scientist
87	David B. Chi	Aerojet	
88	Mr. Theodore Joseph Chiesa	SURVICE Engineering Company	Senior Engineer
89	Mr. Hee Sik Chin	Poongsan	
90	Dr. Taehwan Cho	Gyeong Sang National University	Professor
91	Dr. Sidney Chocron	Southwest Research Institute	Senior Research Engineer
92	Mr. Pawat Chusilp	Defence Technology Institute (Thailand)	Researcher
93	Mr. Dustin Clark	RDECOM - AMRDEC	
94	Dr. Carl F. Cline	Advanced Materials Technology Int.	President
95	Mr. Robert Cole	Force Protection Industries, Inc.	Research & Development Engineer
96	Mr. John A. Condon	U.S. Army Research Laboratory	Mechanical Engineer
97	Mrs. Katy Conner		
98	Dr. Steven J. Coppella	N P Aerospace	Director Product Engineering
99	Dr. Jennifer Cordes	US ARMY ARDEC	Mechanical Engineer
100	Dr. Daniel Corriveau	Defence Research and Development Canada	
101	Mr. Luis Costa	U.S. Army ARDEC	
102	Dr. Amy C Courtney	Force Protection Industries, Inc.	Research Scientist
103	Dr. Ian G. Cullis	QINETIQ	Technical Consultant
104	Mr. Philip M. Cunniff	US Army NATICK Soldier Center	Mechanical Engineer
105	Mr. Dave Cunningham	DSM Dyneema	Technical Director
106	Mr. Arthur S. Daniels	US Army RDECOM-ARDEC	
107	Mr. Michael J. Daniti	U.S. Government	Mechanical Engineer
108	Mr. Evan Davies	DFTA	
109	Mr. David K. Davison	Shock Transients, Inc.	President
110	Ms. Tammy Dean	American Ordnance LLC	Business Development
111	Mr. Stanley E. DeFisher	U.S. Army RDECOM-ARDEC	
112	Mr. William E. DeGenaro	DAI	President
113	Ms. Hélène Demailly	Nexter Munitions	
114	Mr. Patrick den Engelsman		
115	Dr. James DeSpirito	U.S. Army Research Laboratory	Aerospace Engineer
116	1LT Suresh Devu	BAE Systems Security	Sr. Engineer
117	Mr. Anthony R. Di Stasio	U.S. Army ARDEC	ARDEC Project Officer
118	Dr. Andre A. Diederen	TNO Defence, Security, and Safety	Senior Research Scientist
119	Dr. Jie Ding	Defence Science Technology Organisation	
120	Yiun Ning Diwu		
121	Mr. Anthony M. Dolan	U.S. Army Tank Automotive Research, Development, and Engineering Center	Mechanical Engineer
122	Mr. Michael J. Donadio	U.S. Army Research, Development and Engineering Command	Senior Systems Engineer
123	Mr. Heinrich G. Dorsch	IABG CC51	
124	Jaurette Dozier		
125	Mr. Andrew Drysdale	U.S. Army Research Laboratory	Aerospace Engineer
126	Mr. Roelof Lodewikus Du Plessis	Denel Dynamics	
127	Nicolas Eches	Nexter Munitions	
128	Dr. Michael Edwards	Cranfield University	Senior Lecturer
129	Mr. Terje Egge		

	H	Q	R
130	Dr. Ronald G. Egres	DuPont Company	Senior Research Engineer
131	Mr. Charles Eichhorst	U.S. Army Research Laboratory	Mechanical Engineer
132	Mr. Sandor I. Einstein	U.S. Army RDECOM - ARDEC	Senior Propulsion Technologist
133	Mr. Gregory Engleman	Force Protection Industries, Inc.	
134	Mr. M. Nejad Ensan	National Research Council of Cananda-IAR	
135	Mr. Juan C. Espinosa	AGP Group	Engineer
136	Dr. Alexandre Fallet	Constellium	R & D Engineer
137	Dr. Thomas Falter	Diehl BGT Defence	Head of Conceptional Design
138	Mr. Salvatore A. Fanelli	Marine Corps Systems Command	Senior Lead Systems Engineer
139	Mr. Vadim Favorsky	Plasan SaSa Ltd.	Analysis Engineer
140	Mr. Jan Ferreira	Armscor	
141	Dr. William J. Flis	DE Technologies Inc.	Director of Research
142	Mr. Richard Fong	US ARMY ARDEC	Senior Research Scientist/Warhead Technology
143	Dr. Costas G. Fountzoulas	U.S. Army Research Laboratory	Materials Research Engineer
144	Mr. Darin M Franzoni	NASA JSC White Sands Test Facility	Hypervelocity Engineer
145	Ms. Patricia Frounfelker	U.S. Army Research Laboratory	General Engineer
146	Dr. Mark A. Fry	Department of Homeland Security, Science & Techonology	Chief, Conveyance Protection
147	Mr. Alon Gal	Embassy of Israel	
148	Mr. Patrick John Gallagher		
149	Mr. Denver Gallardy	U.S. Army Research Laboratory	General Engineer
150	Dr. Francisco Galvez	Polytechnic University of Madrid	Professor, Aeronautical Engineer
151	Mr. Kevin W. Genson	Naval Surface Warfare Center-Indian Head	Engineer
152	Mr. Guy L. Gettle	Sierra Protective Technologies	President
153	Mr. Grady H. Gilbert	Department of Defense	Engineer
154	MARC GIRAUD		Dr
155	Dr. Dimitrios N Gkritzapis	Hellenic Police & Hellenic Army Academy	Captain of Hellenic Police and Lecturer in Hellenic Army Academy
156	Dr. Vladimir Gold	US ARMY TACOM-ARDEC	Mechanical Engineer
157	Mr. William August Gooch Jr.	WA Gooch Consulting Inc	Engineer
158	Dr. Fred I. Grace	Enig Associates, Inc.	
159	Dr. Markus Graswald	TDW / MBDA Germany	
160	Mr. Andrew J. Gray	ONT	Mechanical Engineer
161	Mr. Matthew C. Grillo	MSA Corp	Development Engineer
162	Mr. Michael Gringauz		
163	Mr. Brenden Grove	Schlumberger Technology Corp	
164	Mr. Maurice E. Grudza	DE Technologies Inc.	
165	Mr. Daniel R. Gubernat	U.S. Army RDECOM - ARDEC	Chemical Engineer
166	Dr. Yulin Gui	China Academy of Engineering Physics	Senior Research Fellow
167	Ms. Jamie Gumina	Naval Surface Warfare Center-Indian Head	Ballistician
168	Mr. Ozdemir Gumusay	ASELSAN, Inc.	
169	Mei Fang Guo		
170	Mr. James C. Gurganus III	U.S. Army Research Laboratory	Mechanical Engineer
171	Mr. Amer Hameed	Cranfield University	Head of Centre for defence Engineering, Director of Weapon & Vechicle Systems
172	Dan Hammond	Department of National Defence	DND
173	Dr. Thomas Hartmann	Numerics GmbH	
174	Mr. Bill Harvey	Baker Atlas	
175	Mr. Thomas J. Hatch-Aguilar	Naval Weapons Center	Mechanical Engineer
176	Mr. Shimon Hayoun		
177	Mr. Lawrence Head	ATK Security & Sporting	Manager, Ammunition Systems
178	Dr. Norbert Heider	Ernst-Mach-Institute	
179	Dr. Andreas Heine	Fraunhofer EMI	Research Fellow
180	Mr. Jyrki Helander	SAAB DYNAMICS AB	
181	Dr. Andreas Helte	FOI Swedish Defence Research Agency	Senior Scientist
182	Mr. Tommy J Herrera	Los Alamos National Laboratory	
183	Mrs. Anne K. Herron	AIM	Vice President
184	Linda Kay Heuer	ATK	Design and Analysis Engineer
185	Mr. Yoav Hirschberg	Plasan Sasa	R & D Ballistics Engineer
186	Mr. Daniel Hladio	Materials Research & Design, Inc.	Research Engineer
187	Mr. Timothy John Holmquist	Southwest Research Institute	Staff Engineer
188	Zhu Hong-Zhi	China Academy of Engineering Physics	Intern Researcher
189	Mr. Scott H. Hornung	U.S. Army Research Laboratory	Team leader
190	Mr. Albert W. Horst	Dynamic Science, Inc.	Propulsion Physicist
191	Mr. Kevin J. Hovden	American Ordnance LLC	Director, Warheads & Special Projects
192	Mr. Douglas Howle	U.S. Army Research Laboratory	Mechanical Engineer
193	Mr. Zhengxiang Huang	Nanjing Univ. of Science & Tech.	Professor
194	Dr. Elaine Humiston	U.S. Army ARDEC	Mechanical Engineer

	H	Q	R
195	Dr. David L. Hunn	Lockheed Martin Missiles and Fire Control	Chief Scientist
196	Mrs. Elaine M. Hunt	U.S. Army Research Laboratory	Operations Research Analyst
197	Mr. Timothy S. Hutchison	NAVAIR	Survivability Engineer
198	Mr. Heihachiro Iida		
199	Mr. Mark D. Ilg	US Army Research Laboratory	Mechanical Engineer
200	Dr. Victoria Ingamells	QinetiQ	
201	Mr. Brian James Isle	BAE Armament Systems Division	Sr. Staff Engineer
202	Ariffin Ismail	National Defence University of Malaysia	
203	Mr. Garet L. Itz	Institute for Advanced Technology at UT	Engineering Scientist Associate
204	Jonathan Jablonski	US ARMY ARDEC	Mechanical Engineer
205	Mr. Thomas P. Jacobson	Nammo Talley Inc.	Project Engineer
206	Mr. Jin-Sung Jang	INHA University	
207	Dr. Bo S.G. Janzon	SECRAB Security Research	Chief Executive Officer
208	Dr. SangEon Je	Hanwha Corporation	
209	Trevor Jerdee	NAVAIR	Mechanical Engineer
210	Mr. Daniel John	COTESA	
211	Mr. Justin John	US ARMY ARDEC	Mechanical Engineer
212	Dr. Gordon R. Johnson	Southwest Research Institute	Program Director
213	Mr. Lowell D. Johnson	U.S. Government	Supervisory Engineer
214	Pat Johnson	NGen Solutions	Research Engineer
215	Mr. Timothy Johnson	South Dakota School of Mines & Technology	Research Assistant
216	Dr. Ian Johnston	Defence Science Technology Organisation	Senior Scientist
217	Mr. Charles A. Jones	Aerojet	Director, Business Development, Warheads
218	Mr. Chris Jones	Rogers Research Group	Research Engineer
219	Mr. Stuart Jones	BAE Systems Global Combat Systems - Munitions	
220	Mr. Tyrone L. Jones	U.S. Army Research Laboratory	Mechanical Engineer
221	Mr. Wendell Jones	BAE Systems Ordnance Systems	Marketing
222	Mr. Florian Kaiser	Diehl BGT Defence	
223	Dr. Valeriy V. Kartuzov	Frantsevich Institute for Problems in Materials Science	
224	Dr. Hanspeter Kaufmann	RUAG Defence	Survivability technology
225	Dr. Roy Kelly	Transatlantic Group	Partner
226	Dr. Paul V. Kelsey	BAE Systems	Sr. Scientist
227	Mr. Evgeny Khmelnikov	Ural Federal University	Head of Department
228	Mr. Ho Soo Kim	Agency for Defense Development	Senior Researcher
229	Jung Ha KIM		
230	Dr. Seokbong Kim	ADD	
231	Mr. Jo Hagness Kiran	Norwegian Defence Research Establishment (FFI)	Scientist
232	Mr. Junichi Kitagawa	IHI Corporation	
233	Mr. David S. Kleponis	U.S. Army Research Lab	Mechanical Engineer
234	Mr. J. Michael Kochman	Navistar Defense Engineering	Chief Designer - Navistar Defense Engineering
235	Dr. L. Bart Koene	Netherlands Defence Academy	Assistant Professor
236	Robert Koontz	NAVAIR Weapons Dept China Lake, Ca	Engineer
237	Dr. John P. Korbin	Sandia National Laboratories	Member of Technical Staff
238	Mr. Jeffrey Koshko	TARDEC	
239	Dr. Klaus-Achim Kratzsch	Rheinmetall Waffe Munition GmbH	
240	Ben Kruse	Tencate	R&D Project Engineer
241	Dr. Nils Kubberud	Nammo Raufoss AS	Section Manager
242	Ms. Helga Kuhlmann	DuPont	Engineer
243	Dr. Kenneth K. Kuo	Penn State University/Applied Research Lab	Distinguished Professor of Mechanical Engineering
244	Dr. Przemyslaw Arnold Kupidura	Military University of Technology	
245	Dr. Sergey Ladov	Bauman Moscow State Technical University	Associate Professor
246	Dr. David E. Lambert	Air Force Research Laboratory	Principal Mechanical Engr.
247	Dr. Samuel Lambrakos	U.S. Naval Research Laboratory	
248	Mr. uriel landman	Israel Military Industries Ltd.	
249	Mr. Larseric Larsson	BAE Systems Bofors	Mr
250	Dr. Jerry C. LaSalvia	U.S. Army Research Labortatory	
251	Mr. Eric Chin Seng Lau		
252	Mr. John R. Leach	Battelle	Reseach Scientist
253	Mr. Luke S. Lebel	Royal Military College of Canada	
254	Dr. Zbigniew Leciejewski	Military University of Technology	
255	Dr. Jeong Ho Lee	Embassy of Korea	Defense Science Attache
256	Mr. Mark Lee	ATK	Finite Element Analysis Engineer
257	Dr. Sang J. Lee	Lockheed Martin Missiles and Fire Control	Principal Engineer
258	Mr. Wei Yao Lee	Advanced Technology Research Centre	
259	Katherine Leighton	SCHOTT Diamondview Armor Products, LLC	

	H	Q	R
260	Dr. Lara Leininger	Lawrence Livermore National Laboratory	
261	Dr. Vitaly Leus	Rafael/Manor	Researcher
262	Mr. Asher Levy	Rafael Armament Development Authority	Engineer
263	Mr. BING LI		
264	Mr. Dongguang Li	Bejing Institute of Technology	Professor
265	Jicheng Li	Institute of Setuctural Mechanics, China Academy of Engineering Physics	Engineer
266	Dr. Weibing Li	Nanjing University of Science and Technology	
267	Dr. Ewa Lidén	FOI Swedish Defence Research Agency	Senior Scientist
268	Dr. Seokbin (Bin) Lim	New Mexico Tech	Assistant Professor
269	Mr. Hendrik Lips	Dynamit Nobel Defence GmbH	Engineer
270	Dr. Ning Liu	Nanjing University of Science & Technology	
271	Mr. Paul M. Locking	BAE Systems Land Systems UK	Energetics Modelling Manager
272	Dr. Xin Lu	Nanjing University of Science & Technology	
273	Mr. Martin Lueck	Fraunhofer EMI	
274	Van Thuan Luu	ENSMA	Research Scientist
275	Dr. Nicholas J. Lynch	QinetiQ	
276	Xiao Fei Ma		
277	Mr. Roderick K. Mackenzie	Canadian Special Operations Forces Command	EMT AMMO
278	Mr. Brian Maeng	National Ground Intelligence Center	
279	Mr. Andrea Maggi	OTO MELARA	
280	Dr. Mariusz Magier	Military Institute of Armament Technology	Head of Artiliery Department
281	Mr. Warren R. Maines	Air Force Research Laboratory	Mechanical Engineer
282	Mr. Tim Mallory	SKYDEX Technologies, Inc.	
283	Dr. Thelma G. Manning	U.S. Army RDECOM - ARDEC	Chemical Engineer
284	Peter Manternach		Engineer
285	Dr. Edgar A. Maranon	Univeridad de los Andes	
286	Dr. Jaroslaw Marcisz	Institute for Ferrous Metallurgy	
287	Mr. Alan H. Marshall	FBI Academy	Engineering Tech Ballistics
288	Mr. Heath T. Martin	Penn State University/Applied Research Lab	
289	Dr. Thomas A. Mason	Los Alamos National Laboratory	Research Engineer
290	Dr. Arne Mattsson	Scandiflash AB	
291	Dr. Meir Mayseless	Rafael Armament Development Authority	Scientist
292	Mr. Walter G. McDonough	National Institute of Standards & Technology	Materials Engineer
293	Ms. Kendra Danielle Meggett-Carr	U.S. Army Evaluation Center	Survivability/Lethality Evaluator
294	Mr. Christopher S. Meyer	U.S. Army Research Laboratory	Mechanical Engineer
295	Mr. Ron Michaelis	Rafael Armament Development Authority	
296	Mr. Mark Minisi	U.S. Army ARDEC	Mechanical Engineer
297	Sarah Minkoff	Lawrence Livermore National Laboratory	
298	Mr. Michael A. Minnicino	U.S. Army Research Laboratory	Mechanical Engineer
299	Mr. Alex Mitchell	Applied Research Technology	Researcher
300	Dr. Hiroaki Miura	Keio University	Research Associate
301	Ms. Dedra Moore	AMRDEC	General Engineer
302	Mr. Gustavo Morales Alonso	Universidad Politécnica Madrid	Civil Engineer
303	CAPT (Ret) Charles Michael Moss	Institute for Defense Analyses	
304	Dr. Frederik J. Mostert	DPSS, CSIR	
305	Mr. John F. Moxnes	Norwegian Defence Research Establishment (FFI)	Principal Scientist
306	Mr. Thomas J. Moynihan	MSA Corp	Princpal Engineer
307	Mr. Anthony B. Muccio	AFRL/RW	Chief, Damage Mechanisms Branch
308	Mr. Scott A. Mullin	Southwest Research Institute	Manager, Ballistics and Explosives Engineering
309	Dr. Narcizo Munoz	Instituto Politecnico Nacional	
310	Dr. Michael J. Murphy	Lawrence Livermore National Laboratory	Engineer
311	Dr. Yellapu Murty	Cellular Materials International, Inc.	
312	Mr. Saif J. Musalli	U.S. Army ARDEC	Mechanical Engineer
313	Dr. Mark W. Nansteel	Battelle Memorial Institute	Senior Research Scientist
314	Dr. Pieter B. Nel	Armscor	Senior Manager: Artillery
315	Dr. Avi Neuberger	A. N. Protection Solutions, Ltd.	
316	Mr. Chris Newton	Force Protection Industries, Inc.	
317	George Newton	Henkel	Business Manager- Defense
318	Mr. William D. Ng	US Army RDECOM-ARDEC	Mechanical Engineer
319	Mr. Dat A. Nguyen	U.S. Army Aberdeen Test Center	Electronic Engineer
320	Catherine T. Nolan	Naveodtech Div	Mechanical Engineer
321	Mr. RamaKrishna Nookala	Nolax, Inc.	Manager
322	Dr. Michael J. Normandia	Ceradyne, Inc.	Chief Scientist - Armor Development
323	Mr. Nestor Ndompetelo Nsiampa	Royal Military Academy	Researcher
324	Dr. Michael J. Nusca	U.S. Army Research Laboratory	Aerospace Engineer

	H	Q	R
325	Dr. Julien Nussbaum	ISL French-German Research Institute Saint Louis	
326	Mr. Alexander Nygård		
327	Mr. Leslie Nyogeri	Defence Ordnance Safety Group	
328	Mr. Gard Odegardstuen	Nammo Raufoss AS	Manager R&D
329	Mr. Hans G. Ohlsson	Saab Bofors Dynamics AB	
330	MSgt (Ret) Leonardo Ojeda		Ammunition technician
331	Mr. Paul Osbun	Force Protection Industries, Inc.	Engineer 1
332	Mr. Amar OUKARA		
333	Dr. Ivar Øye	Computational Industry Technologies AS	
334	Dr. Motoyoshi Ozaki	Ministry of Defense Japan	
335	Mr. Gilles Pageau	Defence R/D Canada	Project Manager
336	Mr. Richard J. Palicka	BAE Systems Global Tactical Systems	
337	Dr. Alexandre Papy	Royal Military Academy	Professor
338	Mr. Hwun Park	Purdue University	Research Assistant
339	Dr. LeeJu Park	ADD	
340	Mr. Scott Patterson	Federal Bureau of Investigation, Defensive Systems Unit	Supervisory Special Agent
341	Mr. Julien Pavier	Nexter Munitions	
342	Mr. John J. Pavon	Pavon Mfg. Group, Inc.	President
343	Mr. Nathaniel Paykel	Force Protection Industries, Inc.	
344	Mr. Nicholas Payne	U.S. Army ARDEC	Mechanical Engineer
345	Mr. Jaroslav Pechacek	SWORDFISH	Col.ret.
346	Miss Inger Marie Pedersen	National Police Computing and Material Service	Chief Engineer Body Armour
347	Mr. Bradley A Pederson	Plasan North America	
348	Dr. Ake K. Persson	Dynaholding AB	
349	Dr. Jonas C Persson	Dynamec Research AB	
350	Mr. Bryan Peterson	ATK Security & Sporting	Product Development Engineer
351	Mr. Thomas Pettersson	BAE Systems Bofors AB	Engineer
352	Mr. Aron W. Pila	IMI	Simulation Engineer
353	Mr. Jack Mark Pincay	U.S. Army RDECOM - ARDEC	Mechanical Engineer
354	Ms. Karen M. Pizzolato	U.S. Army Research Laboratory, Survivability/Lethality Analysis Directorate	Forensic Chemist
355	Dr. Bartlomiej Plonka	Institute of Non Ferrous Metals, Light Metals Division	Ph.D.
356	Michael G Pontin	Ceradyne, Inc.	
357	Mr. Tobias Pontius	WTD 52	
358	Mr. Subodh Prasad	PM AAA	Survivability Engineer
359	Mr. Daniel W. Pratt	Owen Oil Tools LP	VP - Engineering & Explosives Technology
360	Ms. Anne Kathrine Prytz	Nammo Raufoss AS	Project Manager
361	Linfang Qian	Nanjing University of Science & Technology	Professor
362	Dr. Francisco Javier Ramirez Fernandez	Expal Systems, Spain	
363	Dr. Moshe Ravid	RIMAT Advanced Technologies, Ltd.	General Manager
364	Dr. Stephen Ray	BAE Systems	Senior Staff Engineer
365	Mr. Muhammad Aamir Raza	Northwestern Polytechnical University	Research Scholar
366	Mr. Stephen Recchia	U.S. Army ARDEC	Mechanical Engineer
367	Mr. Lyonel Reinhardt	US ARMY ARDEC	Mechanical Engineer
368	Mr. Andres German Restrepo		
369	Mr. Michael D. Reynolds	BAE Systems Security & Survivability	Engineering
370	Mr. Vincent Ricard	Defence Research and Development Canada	
371	Frederick Rickert	U.S. Army Tank Automotive Research, Development, and Engineering Center	
372	Mr. John P. Riegel III	R3 Technology, Inc.	President
373	Mr. Rolf Rittel	Dynamit Nobel Defence GmbH	Graduate Engineer
374	Mrs. Lisa K. Roach	U.S. Army Research Laboratory	Chief, Warfighter Survivability Branch
375	Mr. Cyril Robbe	Royal Military Academy	Researcher
376	Dr. Geert Roebroeks	TNO Defence, Security, and Safety	
377	Mr. Stanislav Rolc		
378	Mr. Glenn E. Romanczuk	U.S. Army RDECOM	Aerospace Engineer
379	Mr. Raymond C. Roncase	Naval Air Warfare Center	Vulnerability Engineer
380	Mr. Fabien Rondot	ISL French-German Research Institute Saint Louis	
381	Mr. John Rowe	Program Executive Office, Ground Combat Systems	Survivability Engineer
382	Dr. Eugene Rozumov	U.S. Army ARDEC	Research Chemist
383	Mr. Zhao Yang Ruan	China Academy of Engineering Physics	Research Associate
384	Mr. Dan Rubashkin	Rafael Armament Development Authority	
385	Dr. Tony Russell		
386	Mr. John Ryan	Concurrent Technologies Corporation	Principal Mechanical Engineer
387	Dr. Shannon Ryan	Defence Science Technology Organisation	
388	Mr. Tom Birger Saghei	National Police Computing and Material service	Senior Engineer
389	Mr. Timo Sailaranta	Aalto University	Researcher

	H	Q	R
390	Mr. Michael Saleh	ANSTO Australian Nuclear Science and Technology Organisation	
391	Dr. Manfred E Salk	Fraunhofer Institute for High Speed Dynamics	Head of Department Experimental Ballistics
392	Mr. Juan M Sandoval	Instituto Politechnico Nacional	Teacher
393	Dr. Ajit Y Sane	General Dynamics ATP	Sr. Principal Project Engineer
394	Mr. Richard G. Sayre	OSD / DOT & E	SES
395	Mr. Carlo Scarinci	PPG Aerospace	Development Engineer
396	Dr. Kurt Schaupert	Schott AG	Senior Scientist
397	Dr. Edward M. Schmidt	Dynamic Science, Inc.	Army Civilian - Retired
398	Mr. Stephen J. Schraml	U.S. Army Research Laboratory	Mechanical Engineer
399	Dr. Brian R. Scott	U.S. Army Research Laboratory	Mechanical/Materials Engineer
400	Shai Sela	Israel Defense Forces	Project Manager
401	Mr. Sonny Sergerie	Department of National Defence	Master-Warrant Officer
402	Mr. Trent Shackelford	QinetiQ North America	Director, Survivability R&D
403	Xiaojun Shao	Northwest Institute of Mechanical and Electrical Engineering	Engineer
404	Mr. Nimrod Shapira	RIMAT Advanced Technologies Ltd.	Manager
405	Dr. Ashok K. Sharma	Terminal Ballistics Research Laboratory	
406	Mr. Eldad Shemer	Oran Safety Glass	R&D Researcher
407	Mr. Moran Shpitzer	Rafael Armament Development Authority	
408	Ms. April Siano	U.S. Army Research Laboratory	Mathematician
409	Dr. Sidra I Silton	U.S. Army Research Laboratory	Aerospace Engineer
410	Ms. Erin G. Silva	Air Force Research Laboratory	Associate Research Mechanical Engineer
411	Mr. Usiel Sandino Silva Rivera	Instituto Politecnico Nacional	Research Assistant
412	Mr. Avner Sinay	Rafael Armament Development Authority	
413	Mr. Sanjeev K. Singh	US Army RDECOM-ARDEC	Engineer
414	Dr. James Neal Singletary	DuPont	Senior Research Associate
415	Miss Alexandra Sirois	Defence Research and Development Canada	
416	Dr. Francois Smit	University of Stellenbosch	
417	Ms. Stephanie L. Snead	U.S. Army Research Laboratory	Chief Systems Analysis Branch
418	Dr. Izak M. Snyman	CSIR	
419	Dr. Bo Song	Sandia National Laboratories	Senior Member of Technical Staff
420	Mr. Jag Sookhdeo	Dayton T. Brown, Inc.	Ballistics Engineer
421	Dr. Mikhail Sotskiy	Bauman Moscow State Technical University	Assocate Professor
422	Mr. Robert Spink	U.S. Army Research Laboratory	Biomedical Engineer
423	Steven Stawarz	Concurrent Technologies Corporation	
424	Mr. Adriaan JT Steenkamp	Armscor Defence Institutes	Consulting Engineer
425	Dr. Martin O Steinhauser	Fraunhofer Institute for High-Speed Dynamics, EMI	Senior Scientist
426	Mr. Elmar Strassburger	Fraunhofer-EMI	
427	Mr. Ish-Mael Stroobant	OTO MELARA	Engineer
428	Mr. David W Stubler	ATK	Lead Manufacturing Engineer
429	Mr. Vasen Subroyen	Armscor	Manager, Technical Armour Systems
430	Dr. Zbigniew Surma	Military University of Technology	
431	Mr. Vidar Svindal	National Police Computing and Material service	
432	Steven Swenson		
433	Mr. Patrick M. Swoboda	U.S. Army Research Laboratory	
434	Mr. Robert C. Sykes	QinetiQ North America	Senior Engineering Manager
435	Ms. Teresa Szydlowska		
436	Mr. Wonseok Tae	Korea Military Academy	Instructor
437	Mr. Timothy Talladay	U.S. Army Tank Automotive Research, Development, and Engineering Center	Test Engineer
438	Mr. Keng Kiang Tan		
439	Kian Chong Tan	Singapore Armed Forces	Army Officer
440	Dr. Ganchai Tanapornraweekit	Defence Technology Institute	
441	Mr. Jingwei Tang	DSO National Laboratories	Engineer
442	Dr. Rabih Tannous		
443	Mr. John James Tartis	Aerojet	Manager, Business Development
444	Mr. Marco Tatta	General Dynamics Land Systems	
445	Mr. Jan Arild Teland	Norwegian Defence Research Establishment (FFI)	
446	Dr. Douglas Templeton	U.S. Army Tank Automotive Research, Development, and Engineering Center	Senior Technical Expert - Survivability
447	Mr. Wilson Teo	Defence Science & Technology Agency	Senior Engineer
448	Dr. Cornelis Jean Terblanche	Rheinmetall Denel Munition	Chief Scientist
449	Dr. Klaus Thoma	Fraunhofer Institute for High Speed Dynamics	Professor
450	Mr. LaMar J. Thompson	U.S. Army RDECOM-ARDEC	Mechanical Engineer
451	Mr. Christer Thuman	BAE Systems Bofors AB	
452	Mr. Jukka S. Tiainen	Patria Land Systems Oy	Technical Manager, Weapon Systems
453	Dr. David Touati	Israel Military Industries Ltd.	
454	Mr. William Turner	PKA Solutions	Program Manager

	H	Q	R
455	Dr. Jerome T. Tzeng	U.S. Army Research Lab	Mechanical Engineer
456	Mr. Muhammet E. Uguz	STM Savunma Teknolojileri Muhendislik A.S.	Quality Engineer
457	Mr. Daniel Vallee	Nexter Systems	
458	Dr. Chris van Driel	TNO Defence, Security, and Safety	
459	Mr. Cornelius Van Niekerk	Denel Land Systems	
460	Mrs. Rebecca VanAmburg	U.S. Army Research Laboratory	Electrical Engineer
461	Mr. David Vanek	Leading Technology Composites Inc.	Vehicle Protection Market Manager
462	Dr. Lionel R. Vargas-Gonzalez	U.S. Army Research Laboratory	Materials Engineer
463	Dr. Vladislav A. Veldanov	Bouman Moscow State Technical University	Associate Professor
464	Dr. Roger L Veldman	Hope College	Professor
465	Mr. Theo Verhagen	TNO Defence Safety & Security	
466	Mr. Amit Viesel	Plasan Sasa	
467	Dr. James D. Walker	Southwest Research Institute	Institute Scientist
468	Dr. William P. Walters	U.S. Army Research Laboratory	Research Engineer
469	Mr. Bao-yuan Wang	Nortwest Institute of Mechanical and Electrical Engineering	Measurement Principle of Moment of Inertia for Turret
470	Mr. Zhongyuan Wang	Ballistic Research Lab of China	
471	Ms. Caitlin M. Weaver	US ARMY ARDEC	Mechanical Engineer
472	Mr. Christopher J. Weiland	Naval Surface Warfare Center-Dahlgren	Engineer
473	Dr. Paul Weinacht	US Army Research Laboratory	
474	Carsten Weinhold	SCHOTT North America Inc.	Scientist
475	Corey Weis	AMTEC Corporation	40mm Systems Engineer
476	Mr. Pierre Wey	ISL French-German Research Institute Saint Louis	Defense Scientist
477	Mr. James White	Force Protection Industries, Inc.	Researcher III
478	Mr. Aaron D. Whitley	BAE Systems Ordnance Systems	Marketing Repr.
479	Dr. Matthias Wickert	Fraunhofer Institut	Head of Impact Physics Divisions
480	Mr. Thomas Widlund	Saab Bofors Dynamics AB	
481	Mr. Paul Willis-Patel	Atomic Weapons Establishment	
482	Adam Wisniewski	Military Institute of Armament Technology	Head of Material Engineering Department
483	Mr. Clive R. Woodley	QinetiQ Ltd.	Principal Scientist
484	Hui Min Wu		Measurement Principle of Moment of Inertia for Turnet
485	Mr. Yida Xu	China Ordnance	
486	Mr. Ridwan Yahaya	Stride, Ministry of Defence Malaysia	
487	Mr. Yonghui Yang	China Academy of Engineering Physics	Research Fellow
488	Dr. Yufeng Yao	Kingston University	Reader in Aerospace Engineering
489	Mr. Mehmet Sarper Yavuz	Tubitak-Sage	Research Engineer
490	Dr. Dan Yaziv	RAFAEL	Armor Systems Directorate
491	SGT (Ret) Daniel HS Yoon		121 General Hospital 18th Medcom
492	Dr. Yonggang Yu	Nanjing University of Science & Technology	Professor
493	Mr. Xiaobing Zhang	Nanjing University of Science & Technology	Professor
494	Mr. Ji bo Zhao	Institute of Fluid Physics, China Academy of Engineering Physics	Associate Researcher
495	Mr. Ji bo Zhao	Institute of Fluid Physics, China Academy of Engineering Physics	Associate Researcher
496	Dr. wang zheng	Institue of Applied Physical and Computational Mathematics	
497	Mr. Hong-zhi Zhu	China Academy of Engineering Physics	Intern Researcher
498	Mr. Charles B. Zisette	ATK	Technical Director
499	Mr. Alexander Zlatkis	IDF	
500	Mr. Michael Zoltoski	US Army Research Laboratory	Acting Director - WMPD

The Rosalind and Pei Chi Chou Award for Young Authors

NATIONAL DEFENSE INDUSTRIAL ASSOCIATION

NDIA

ISB

Purpose

- To enrich the program of the ISB by encouraging young authors in all fields of ballistics to submit papers and to attend the symposium.
- The Award consists of a plaque and a stipend, presented jointly by the IBS and NDIA.

Eligibility

- Not older than 35 years.
- All fields of ballistics.
- Oral and poster presentations.
- If multiple authors, the Young Author must have made a significant contribution to the paper.
- The Young Author must attend the symposium and present the paper.

Previous Awardees

- David Littlefield, SwRI, USA, 16th ISB
- H. Arisawa, Propellants & Explosives Laboratory, Japan, 17th ISB
- Saed Mausavi, FOA, Sweden, 18th ISB
- I. Sidney Chocron, Polytechnic Univ. of Madrid, Spain, 19th ISB
- Stany Gallier, SNPE, France, 20th ISB
- Irina Järnebark, FOA, Sweden, 21st ISB
- Eluned Lewis, DCRPS, UK, 22nd ISB
- Amal Bouamoul, DRDC, Canada, 23rd ISB
- Markus Graswald, HSU, Germany, 24th ISB
- Chen Xin-hong, Nanjing U., China, 25th ISB

Dr. Manfred Held
Memorial Presentation

A Celebration

Scientist
Innovator
Educator
& Friend

1933 to 2011

Determination

Strength

Generosity

The same qualities that the German Flag symbolizes
were embodied in our colleague;
who was also an ambassador of ballistics to the world.

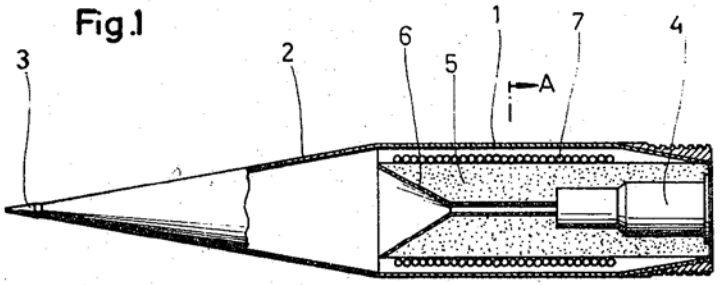

US Patent 3,474,731 Warhead Containing a Hollow Charge and Fragmenting Section

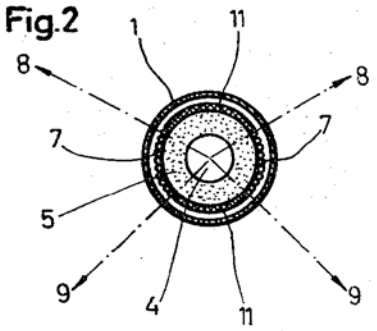

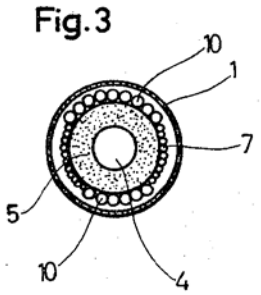

(Walter Trinks)

Thomanek → Held

A LEGACY INHERITED TO A LEGACY GAINED

Manfred’s First Challenge

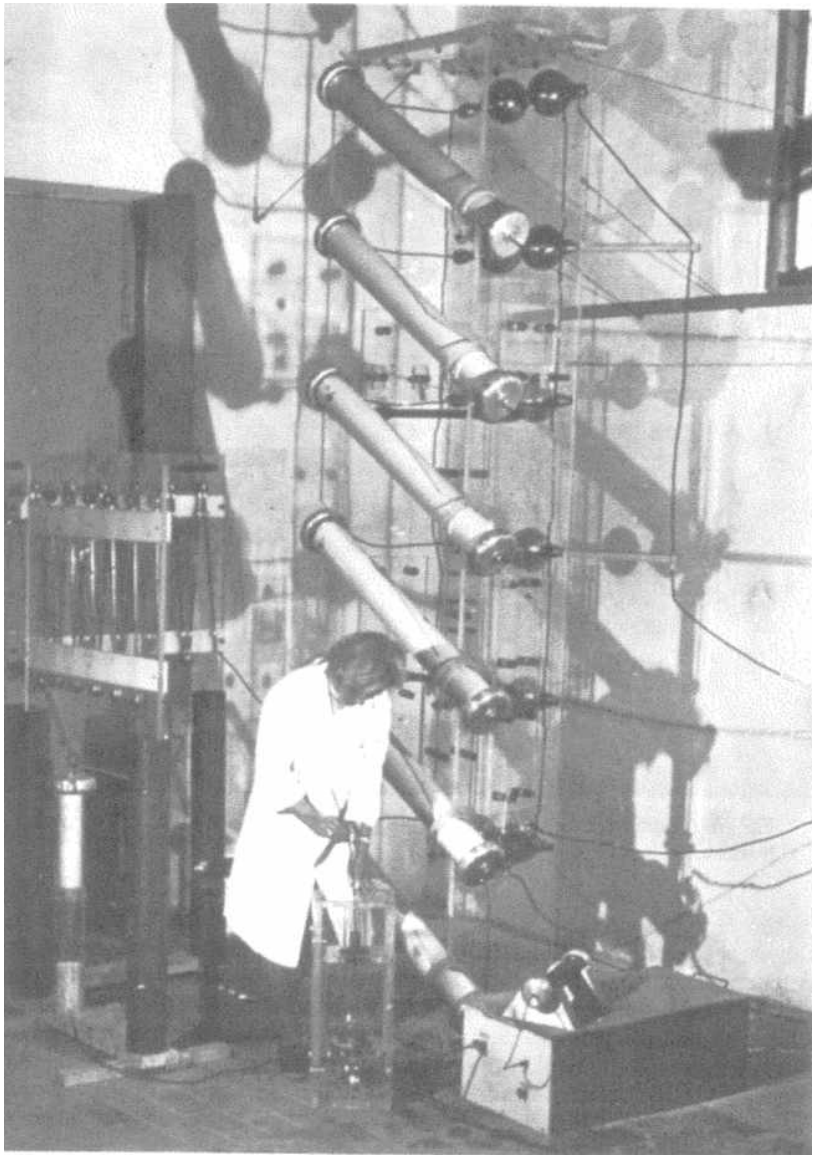

The Essential Tool of Held's Work

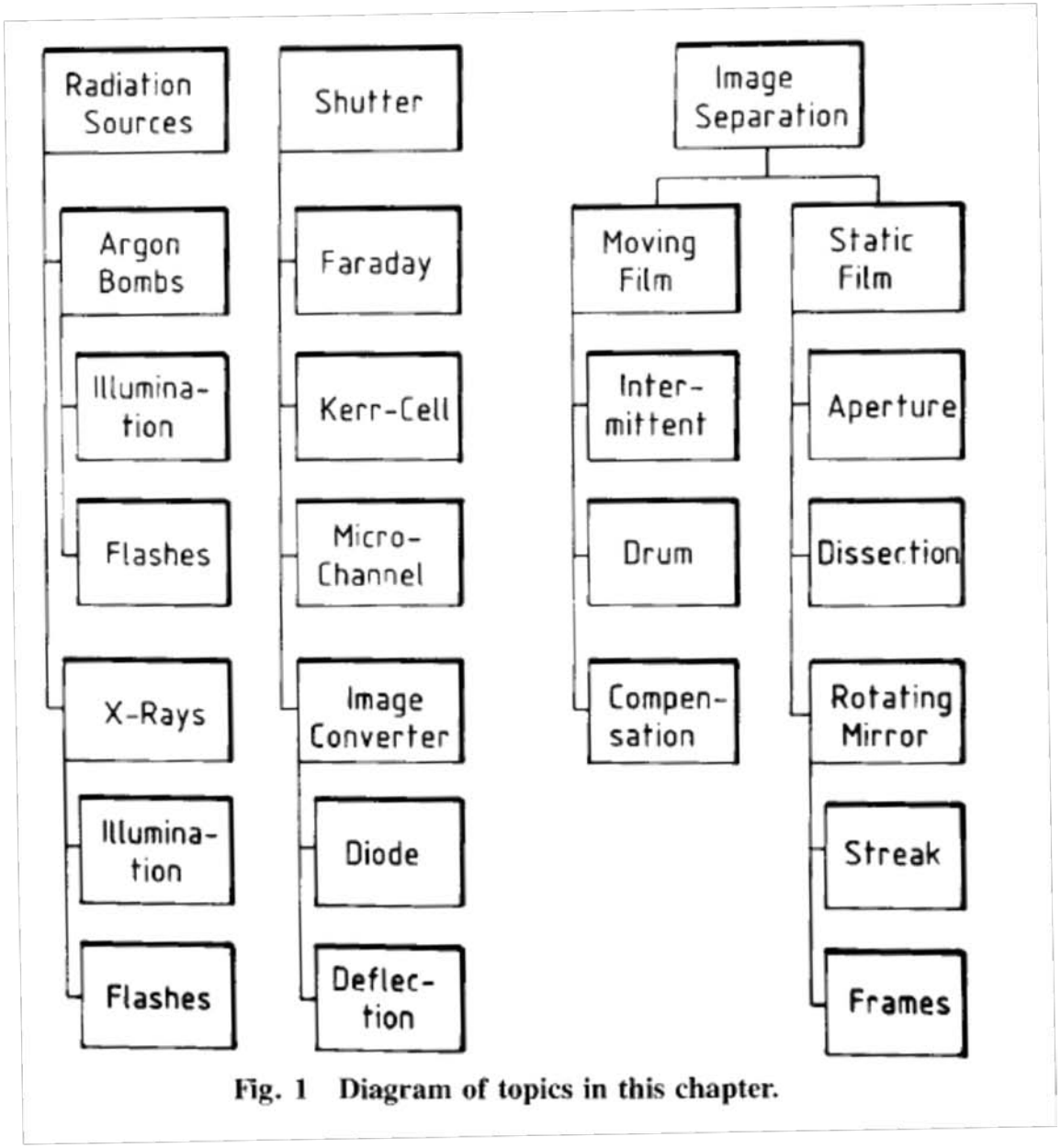

Fig. 1 Diagram of topics in this chapter.

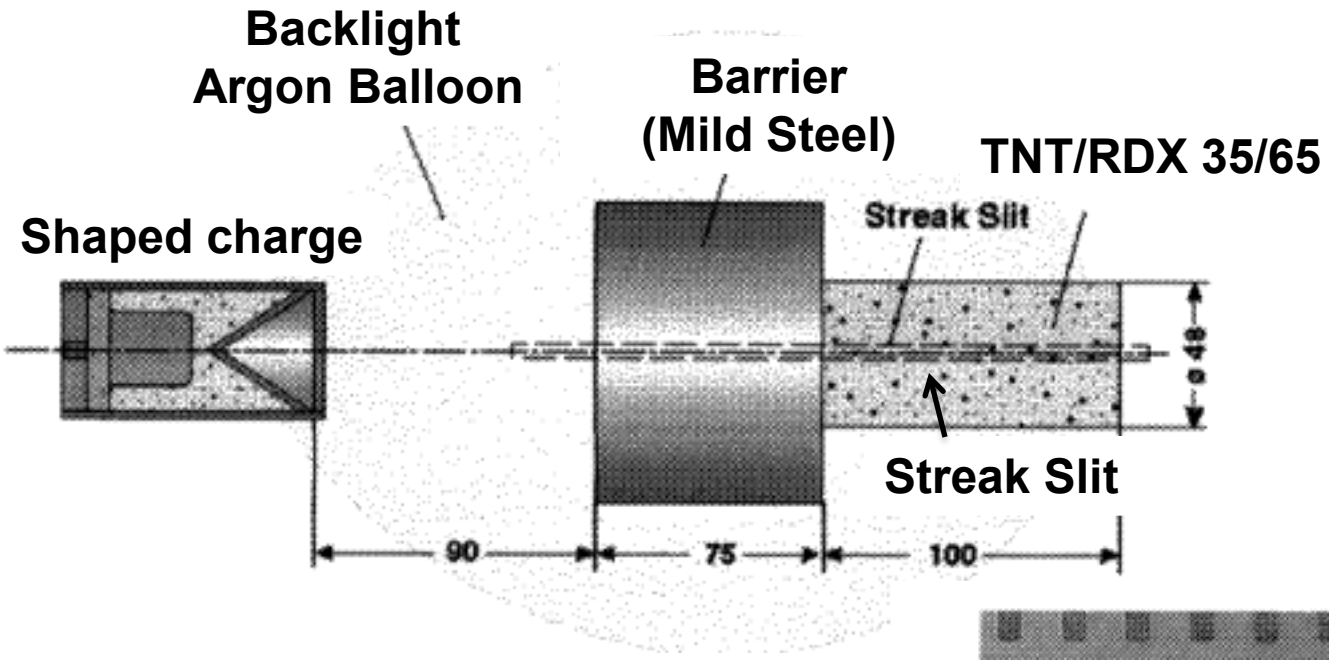

Application for

- ✓ Explosive Trains & Fuzing
- ✓ Gap Testing
- ✓ Protection & Safety
- ✓ Initiation

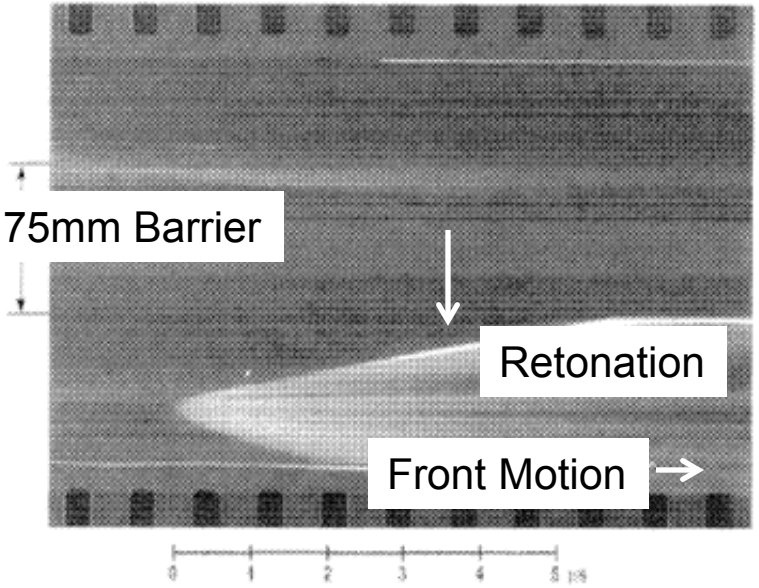

~5.5 mm/usec Streak Velocity

"Diagnostic of Jet Initiation Phenomena", 25th SPIE, 4948 (2003)

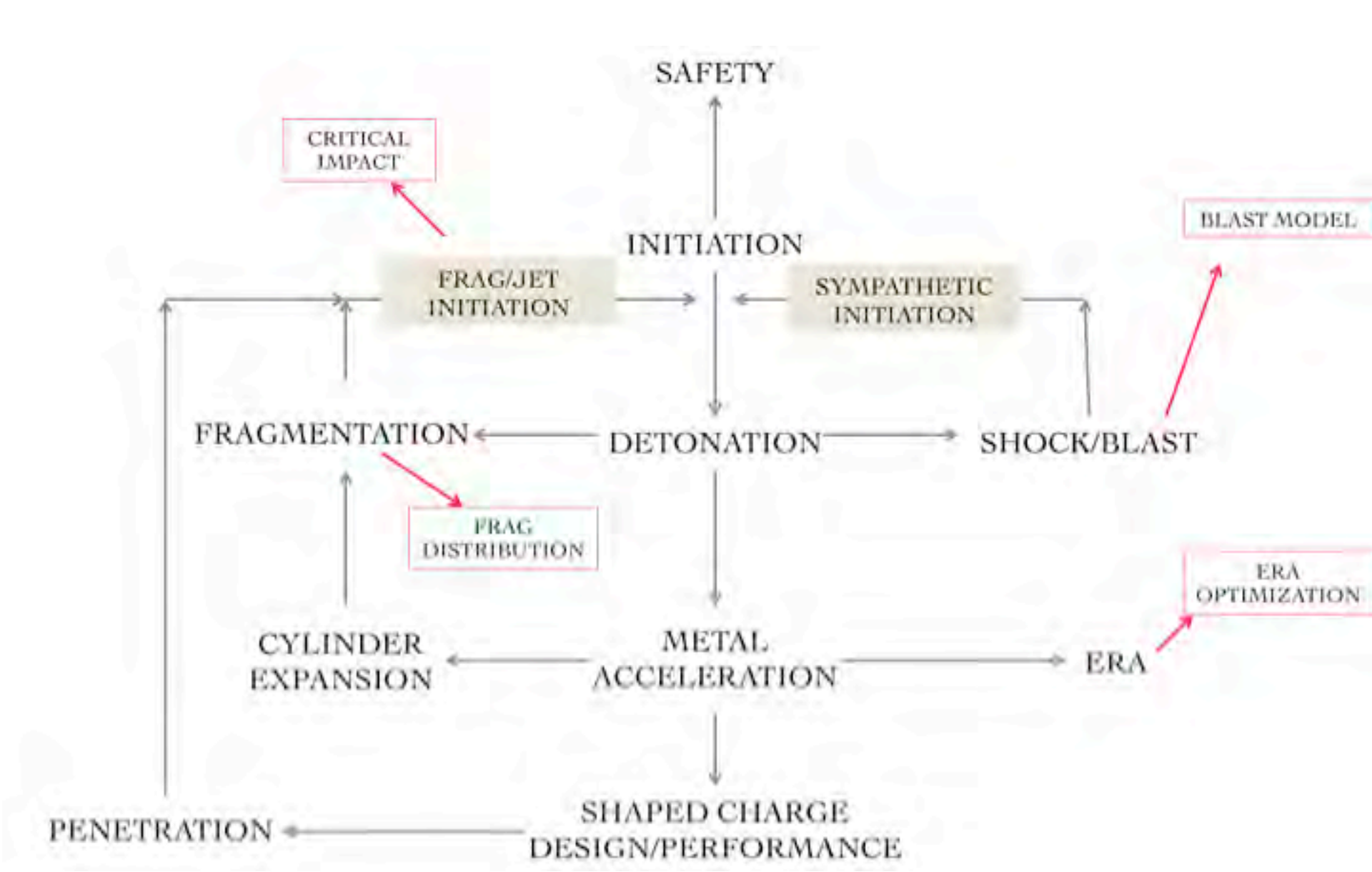

Chronology of ISB Papers

ISB	Year	Title
1	1974	Streak Technique as a Diagnostic Method in Detonics
2	1976	The Performance of the Different Types of Conventional High Explosive Charges
3	1977	Explosive Formed Projectiles **
4		
5	1980	Cutting Charge
6	1981	Evaluation of Shaped Charge Penetration Efficiency by Advanced Diagnostic Techniques
7	1983	Characterizing Shaped Charge Performance by Standoff Behavior
8	1984	Transverse Shaped Charges
9		
10	1987	Refined Shaped Charge Jet Penetration Measurement in Various Materials Versus Hydrodynamic Prediction
11	1989	Particulation of Shaped Charge Jets
12		
13	1992	Aimable Fragmenting Warheads ***
14	1993	Armour
15	1995	Truncated Shaped Charges (**Defeat Mechanism for ERA)
16	1996	Design and Tests of Shaped Charges with L/D About 1
17	1998	Jet Observations in Synchro-Streak or Profile Streak Technique **
17	1998	Survivability of Fragments (with Kleinschnitger, Schmolinske, Stilp)
18	1999	Anti-ERA Shaped Charge Warhead System
18	2001	Special Shaped Charges for Off-Shore Application
19		Active Protection Against KE-Rounds and Shaped Charges at Short Distances*
19	2002	Defeating Active Defense Systems by Double-Firing of Missiles
19		Steerable Hitiles Against TBM Warheads
20	2004	Improvements of the Probability to Kill Chemical and Biological Submunitions in TBM Warheads
20	2005	Warhead Mechanisms (Review Article)
21	2007	Steerable Fragment Masses (shared session chair)
22		The Future of Warheads, Armour and Ballistics (Keynote, shared authorship)
23	2008	Fuze Sensor Requirements of the Different Aimable Anti Air Warhead Layouts
23	2010	Behind Armour Effects at Shaped Charge Attacks
24		IED Mine Threats
		RECOGNITION & TRIBUTES

ISB	Year	Title
1	1974	Streak Technique as a Diagnostic Method in Detonics
2	1976	The Performance of the Different Types of Conventional High Explosive Charges
3	1977	Explosive Formed Projectiles **
4		
5	1980	Cutting Charge
6	1981	Evaluation of Shaped Charge Penetration Efficiency by Advanced Diagnostic Techniques
7	1983	Characterizing Shaped Charge Performance by Standoff Behavior
8	1984	Transverse Shaped Charges
9		
10	1987	Refined Shaped Charge Jet Penetration Measurement in Various Materials Versus Hydrodynamic Prediction
11	1989	Particulation of Shaped Charge Jets
12		
13	1992	Aimable Fragmenting Warheads ***
14	1993	Armour
15	1995	Truncated Shaped Charges (**Defeat Mechanism for ERA)
16	1996	Design and Tests of Shaped Charges with L/D About 1
17	1998	Jet Observations in Synchro-Streak or Profile Streak Technique **
17	1998	Survivability of Fragments (with Kleinschnitger, Schmolinske, Stilp)
18	1999	Anti-ERA Shaped Charge Warhead System
18		Special Shaped Charges for Off-Shore Application
19	2001	Active Protection Against KE-Rounds and Shaped Charges at Short Distances*
19		Defeating Active Defense Systems by Double-Firing of Missiles
19	2002	Steerable Hitiles Against TBM Warheads
20		Improvements of the Probability to Kill Chemical and Biological Submunitions in TBM Warheads
20	2004	Warhead Mechanisms (Review Article)
21	2005	Steerable Fragment Masses (shared session chair)
22	2007	The Future of Warheads, Armour and Ballistics (Keynote, shared authorship)
23		Fuze Sensor Requirements of the Different Aimable Anti Air Warhead Layouts
23	2008	Behind Armour Effects at Shaped Charge Attacks
24	2010	IED Mine Threats
		RECOGNITION & TRIBUTES

Chronology of ISB Papers

& the only person who has participated in each symposium.

Including the Paper Selection Meeting for the 26th ISB

With Bo Janzon (7 Dec 2010)

Manfred Held, our first Ballistics Fellow resting on the Great Wall of China at a break during the 25th Symposium.
(May 2010)

Author of major book chapters

•"*Shaped Charge Jet*", in: T. L. Boggs, R. L. Derr (Eds.), Hazard Studies for Solid Propellant Rocket Motors, NATO Advisory Group for Aerospace Research and Development, AGARD Monograph No. 316, 1990, pp. 117–36.

• "*Blast Effects of Detonating Small Charges*", Vol. 1–2, (to be published).

•"*Fragmentation Warheads*", in: J. Carleone (Ed.), Tactical Missile Warheads, American Inst. of Aeronautics and Astronautics, Washington, DC, 1993, pp. 387–464 (1993)

•"*High-Speed Photography*", ibid. pp. 609–673.

•"*Flash Radiography*", in J. Carleone (Ed.), ibid., pp. 555–608.

Other Seminal Papers covering

- Overviews of Detonation Theory
- Effects of aluminum on detonation & metal acceleration
- Fragmentation
- Energy Coupling
- Aimable Warhead
- Chemical/Biological Defeat

Publications per topics

Cross-Referenced Publications

- Initiation
- Detonation
- Fragmentation
- Blast/Shock
- Penetration
- Shaped charges
- ERA
- Safety
- Diagnostics
- Terminal ballistics
- Explosives
- Other

Cross-Referenced Publications

Publications per topics

- Initiation
- Detonation
- Fragmentation
- Blast/Shock
- Penetration
- Shaped charges
- ERA
- Safety
- Diagnostics
- Terminal ballistics
- Explosives
- Other

Cross-referenced catalog of papers and patents incorporated in

EV2 Florian Bouvenot (French Navy)
"The Legacy of Manfred Held and Critique"
Master's Degree Thesis (Physics)
Naval Postgraduate School, Sept 2011

One CLICK AWAY!

INITIATION

[005] Held, M. (1968). **Initiation of explosives, a multiple problem of the physics of detonation** [Initiierung von Sprengstoffen, ein vielschichtiges Problem der Detonationsphysik]. *Explosivstoffe* , *5*, 2-17.

The following will treat the induction or the excitation of a more or less continuous process, a process about which not much is known. By the process we mean here the detonation of solid (especially military) high-energy explosives such as TNT hexogen and octogen and their mixtures. The induction of detonation, or the excitation of explosive charges to undergo detonation-type decomposition is called "initiation." The first part discusses the general theory of initiation, and the second part reports on results and peculiarities in the initiation of explosive charges, as found at Schrobenhausen during the handling of various kinds of projects.

[006] Held, M. (1969). **Protecting and transport container for high explosive charges** [Schutz- und Transportbehalter fur Sprengladungen]. *Wehrtechnik, 8*, 266-268. No abstract available in English

[010] Held, M. (1974). **A structure for protection against projectiles** [Dispositif de protection contre projectiles ou corps analogues]. Patent, Messerschmitt-Bçlkow-Blohm GmbH, Munchen, Germany.

A protective arrangement against projectiles is a wall structure formed from a wall layer of explosive material, and at least one additional wail layer covering at least one face of the wall layer of explosive material. The additional wall layer is made of a non- explosive, inert high-density material such as metal. In one embodiment both faces of the explosive wall layer are covered with a layer of inert, non-explosive high-density material such as metal. The protective arrangement is particularly suitable for protection against the destructive force of hollow explosive charge projectiles.

SOME RESEARCH & DEVELOPMENT HIGHLIGHTS

Photographic challenges

9.9 km/sec jet tip

25 km/sec

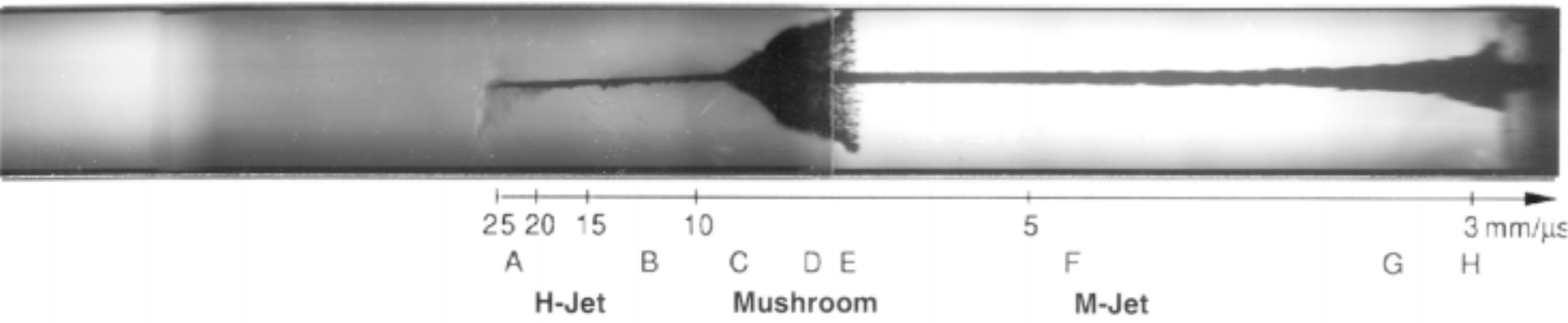

"Diagnostic of Super-fast Jets with 25 km/s Tip Velocities", Propellants, Explosives, Pyrotechnics, 23, 229 (1998)

1967-69 ERA
Israeli 1st application

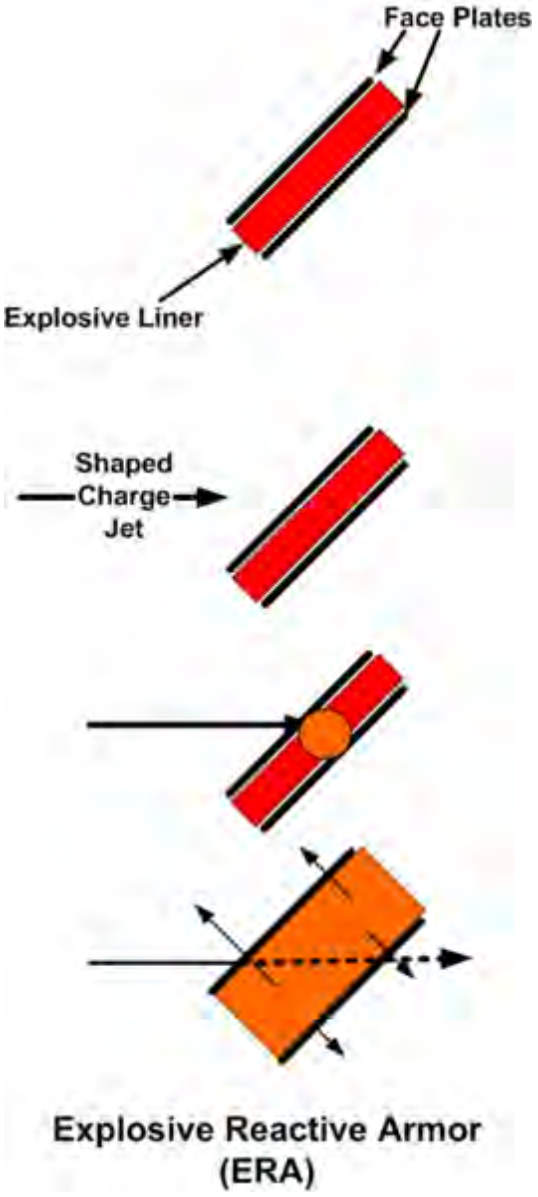

Explosive Reactive Armor
(ERA)

http://en.wikipedia.org/wiki/File:Image_Explosive_Reactive_Armor.png

Fig.1

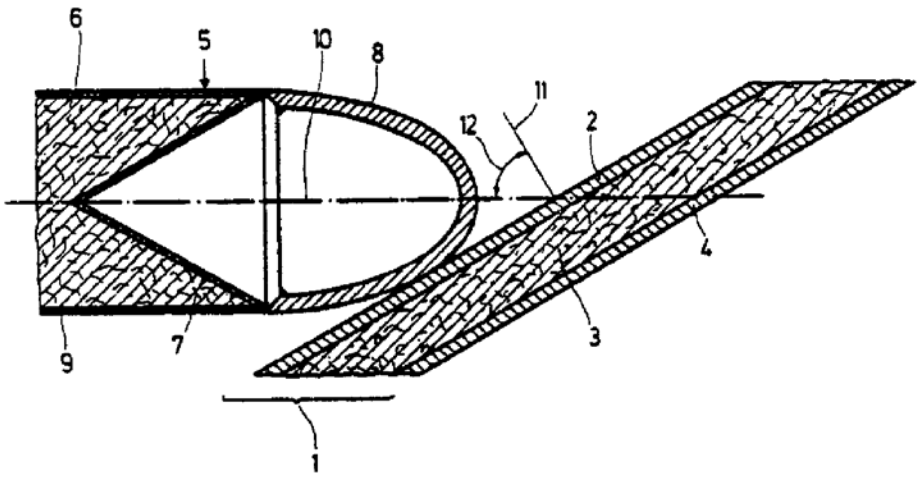

Year	
1980	US 4,368,660
	Applications
1978	951,085
1977	842,177
1976	706,067
1074	495,834

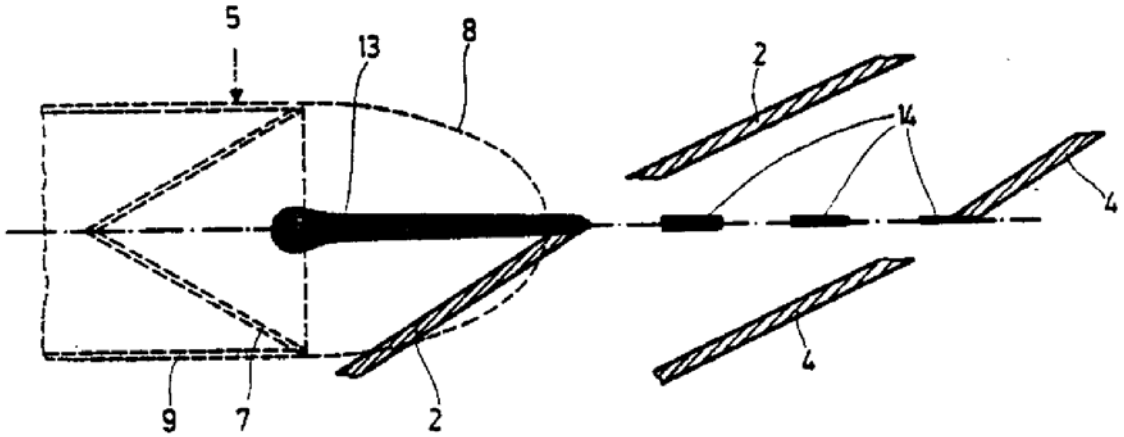

Protective Arrangement Against Projectiles, Particular Hollow Explosive Charge Projectiles

Stratgey for defeating ERA increase jet velocity

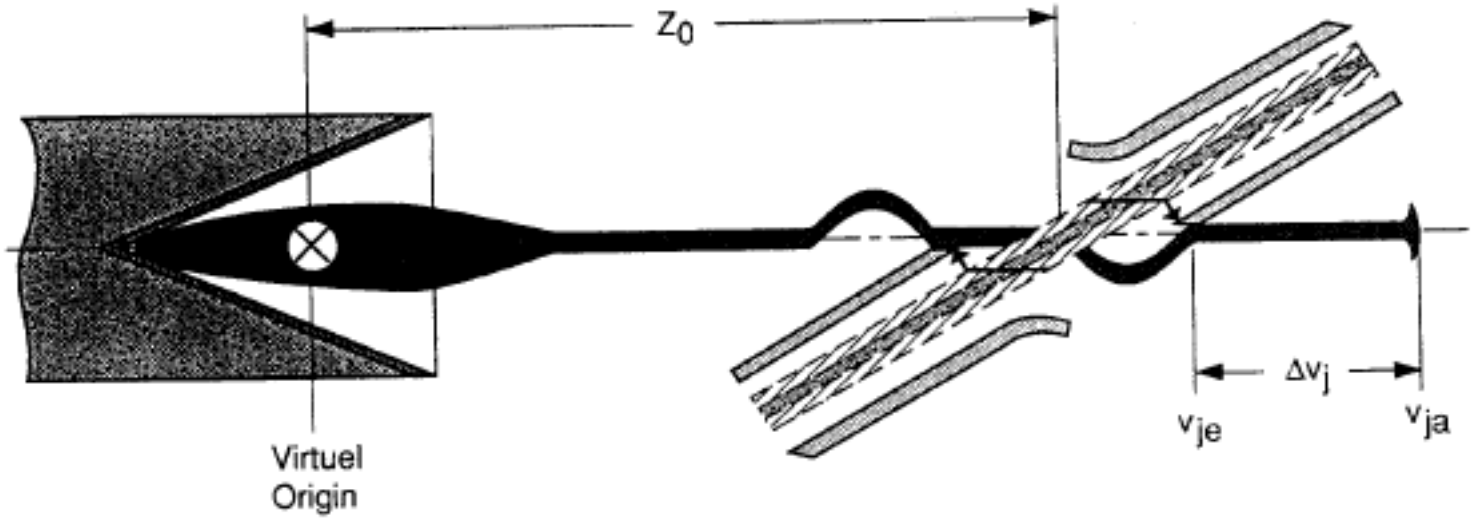

Can anyone dispute the observation that active protection was motivated by finding means for extending the basic effectiveness of ERA!

Continuation of Work Thomanek's Work: Effects of Asymmetry on Shaped Charge Jetting Confinement

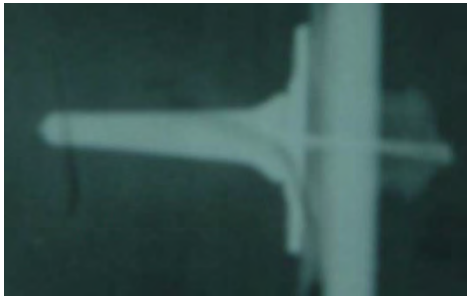

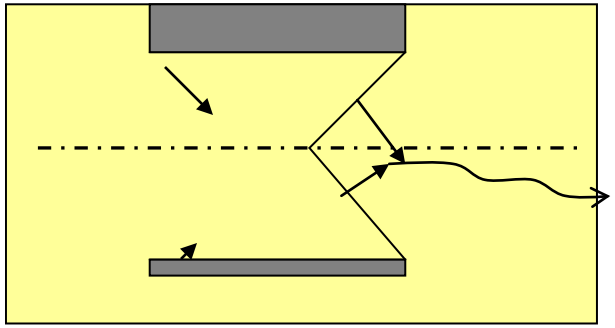

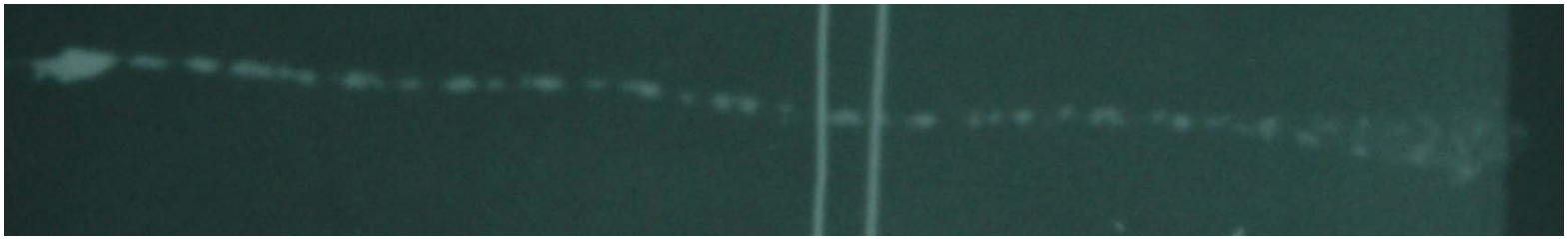

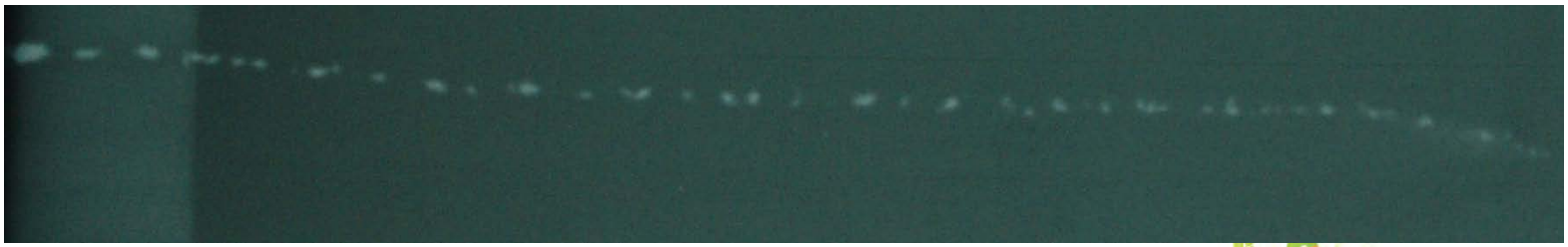

Australia, 2004

Tarragona, 2007

Beijing, 2010

Prof Held during a tour for the 25th ISB Paper Selection Committee

A toast between

- Mr. Ma, Chairman of the China Ordnance Society,
- Prof Dr. Manfred Held, First Ballistics Science Fellow of the society, and
- Mr. Riegel, President of the International Ballistics Society at the 25th ISB Banquet

Propellants, Explosives, Pyrotechnics *21*, 235–237 (1996)

Initiation Criteria of High Explosives at Different Projectile or Jet Densities

Manfred Held

TDW Gesellschaft für verteidigungstechnische Wirksysteme mbH, D-86523 Schrobenhausen (Germany)

Impact Initiation Investigation

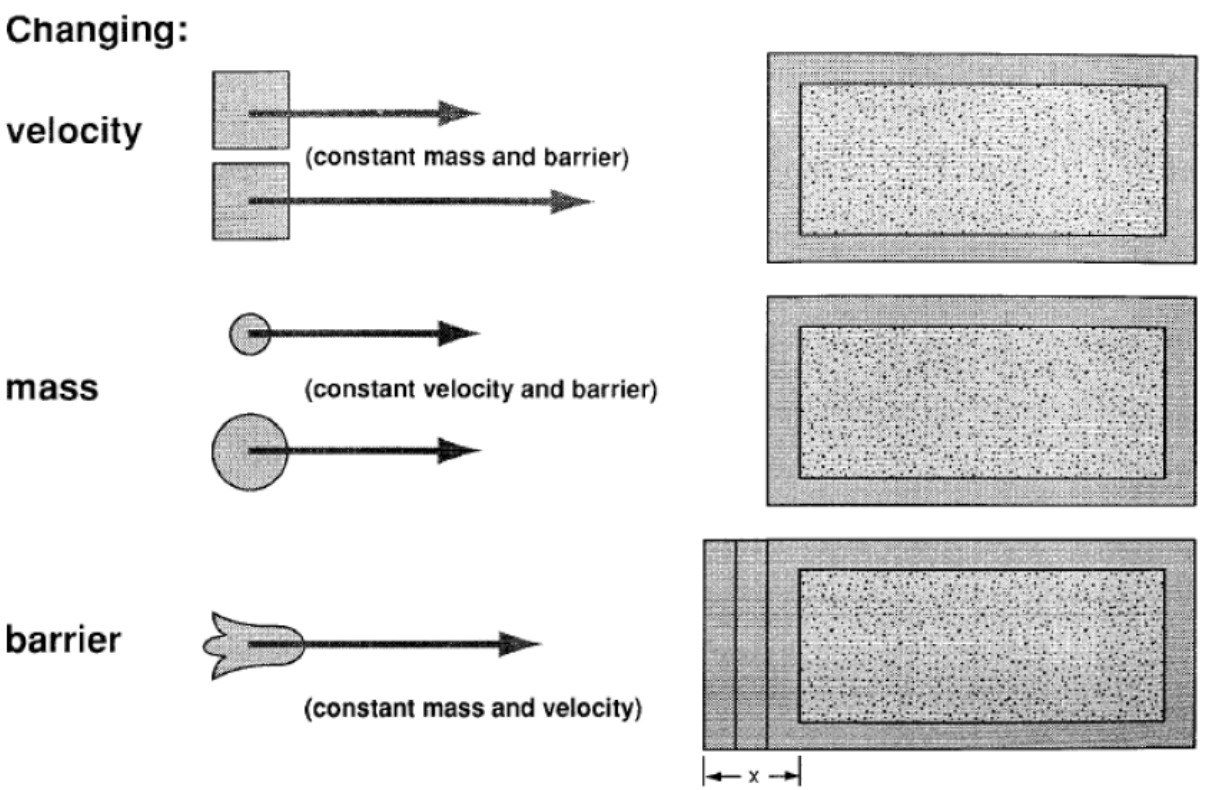

Postulated Sensitivities

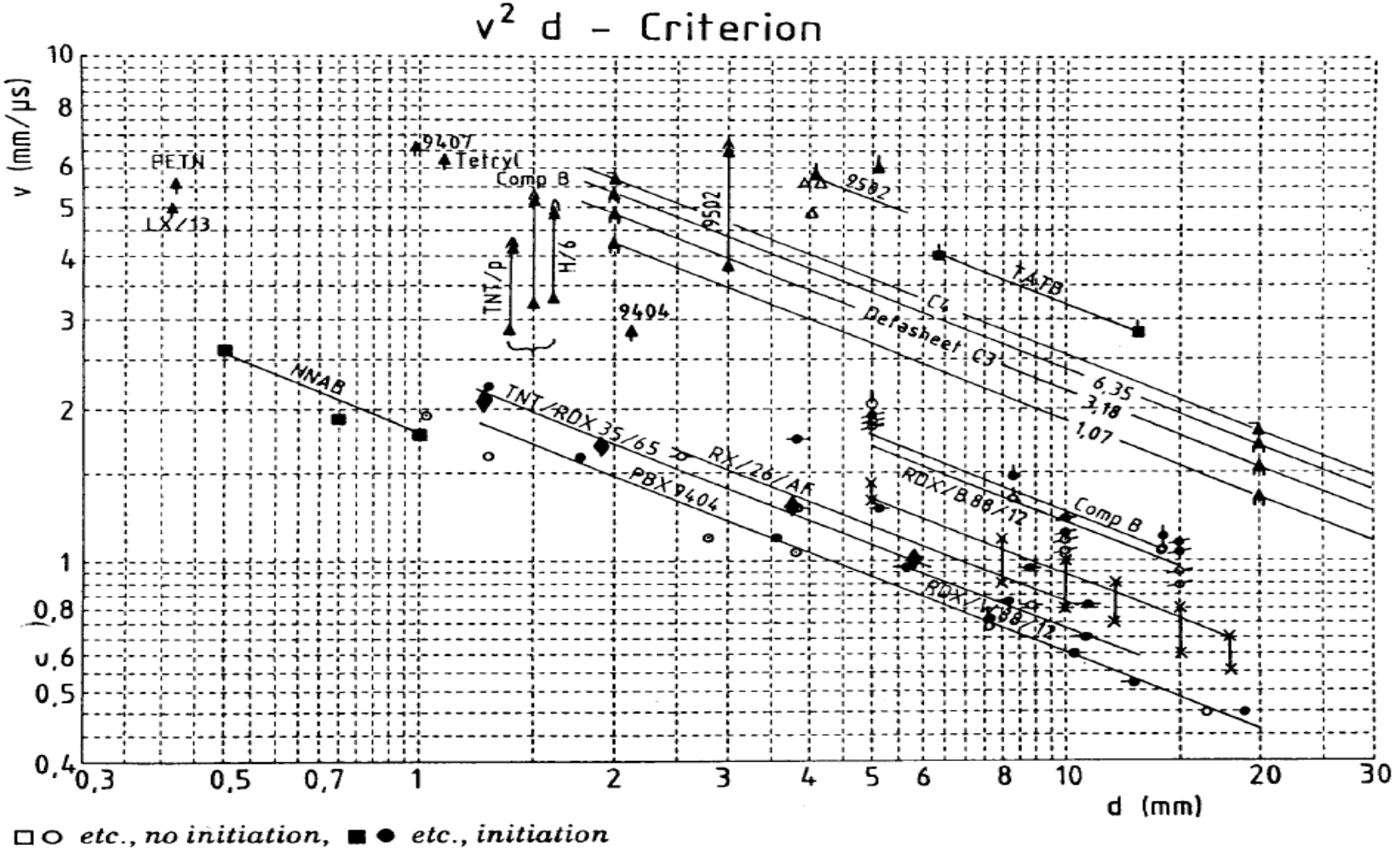

Nature of the Problem

Explosive	Scientists	Experimental conditions (steel projectile)	Projectile diameters tested (mm)	Held values of v^2d ($mm^3/\mu s^2$)	Our Estimate ($mm^3/\mu s^2$)
PBX9404 (1.84 g/cm^3)	Weingart, [026]	Flat nosed projectiles	2 - 12		3.9 - 4.5
	Moulard [027]	Small cylindrical projectiles	2 - 8	4	4 - 5.5
	LeRoy Green [028]	Long cylindrical tool projectile	2 - 12		4.5 - 8.5
	James [029]	Flat nosed projectiles	2 - 12		3 - 4.5
Comp. B (35/65) (1.73 g/cm^3)	Moulard [027]	Small cylindrical projectiles	6 - 12	16	13 - 19.5
Comp. B-3 (60/40) (1.70 g/cm^3)	LeRoy Green [028]	Flat nosed projectiles	4 - 12		14.5 - 16
TNT (cast) (1.59 g/cm^3)	Zoellner [030]	0.25 mm thick flyer	13 - 17		325 - 425
Octol7030 (1.81 g/cm^3)	Zoellner [030]	0.25 mm thick flyer	3 - 8		44 - 83
TATB (1.80 g/cm^3)	Weingart [026]	0.25 mm thick flyer	6 - 12	108	87 - 96

New criteria “Pd” takes takes into account Hugoniot characteristics.

A Legacy to be continued!

12 April 2010 was the 50th anniversary of Manfred Held's association with the ordnance establishment in Schrobenhausen (formerly MBB). He was duly honored for his accomplishments, which extended from his contributions to the sciences of detonation to airbag development, and for his numerous publications and patents.

Prof. Dr. Manfred Held – 50 Jahre im Dienste des Unternehmens und der Wissenschaft

Anlässlich der 50-jährigen Firmenzugehörigkeit von Prof. Dr. Manfred Held würdigte Dr. Helmut Muthig am 12. April 2010 in Schrobenhausen das Lebenswerk von Prof. Dr. Held.

„Der Standort Schrobenhausen ist, unabhängig davon, wie die jeweils hier aktiven Firmen geheißen haben, untrennbar mit dem Namen Prof. Dr. Manfred Held verbunden", sagte Dr. Muthig bevor er einige Stationen der langen Karriere von Prof. Dr. Held aufzählte. Diese reichten von der Kurzzeit-Messtechnik über neuartige Gefechtsköpfe bis hin zum Airbag-Auslösesensor.

Prof. Dr. Held meldete in seinem Berufsleben mehr als 140 Patente an. 1986 erhielt er die Diesel-Medaille für seine zahlreichen Erfindungen und Patente in der Detonik und seine Leistungen in der Forschung und Entwicklung, die zur Einführung vielfältiger Innovationen in der industriellen Fertigung führten. Bis Ende letzten Jahres hatte Prof. Held 445 wissenschaftliche Beiträge veröffentlicht.

Werner Kaltenegger und Dr. Muthig bedankten sich bei Prof. Dr. Held für das, was er in 50 Jahren für das Unternehmen geleistet hat, und eröffneten eine Ausstellung über sein Lebenswerk. Die Ausstellung kann noch bis einschließlich 16. April 2010 im Foyer des Gebäudes 201 besichtigt werden.

Ballistics Science Fellow of the International Ballistics Society (IBS)
The first person in this society, receiving an Honorary Lifetime Membership with membership number 001.

Mr. Jack Riegel, President of the International Ballistics Society presents Professor Held with a plaque to commemorate his being the first IBS Ballistics Science Fellow

SOME OF THE MANY MEMORIES & CONTINUING CHALLENGES

STOP

Photographic challenges

9.9 km/sec jet tip

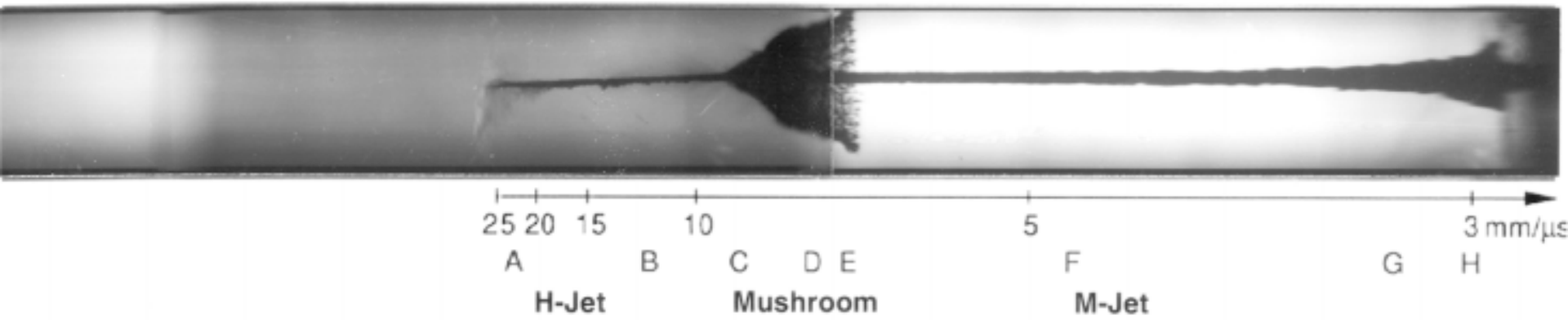

"Diagnostic of Super-fast Jets with 25 km/s Tip Velocities", Propellants, Explosives, Pyrotechnics, 23, 229 (1998)

Continuation of Work Thomanek's Work: Effects of Asymmetry on Shaped Charge Jetting Confinement

Higher pressures and
faster rebounding particle velocities

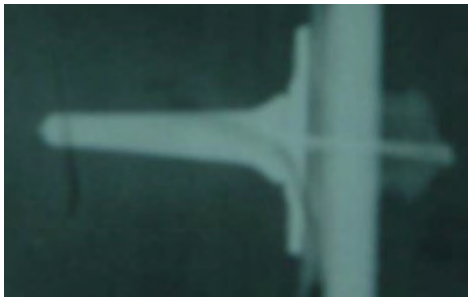

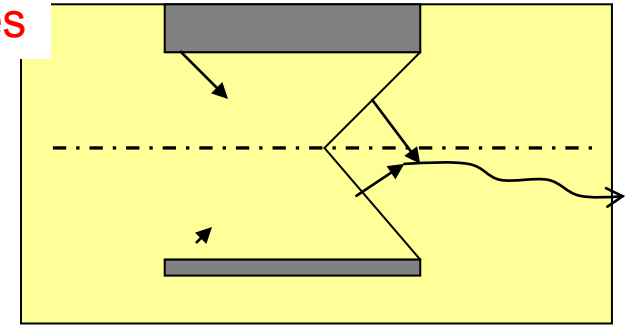

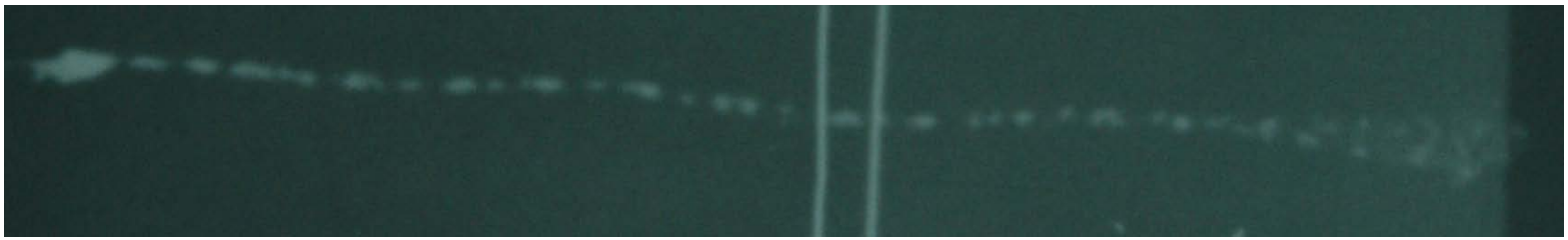

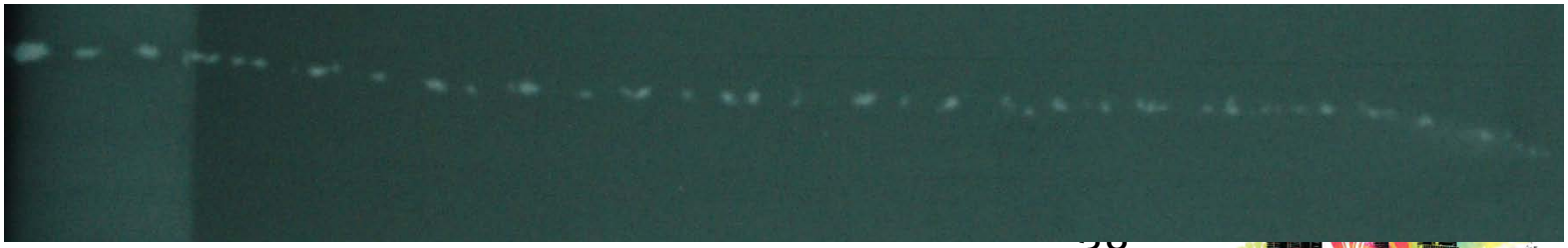

Manfred Held

1933–2011

On February 8th 2011, Professor Manfred Held passed away from a sudden heart attack.

Professor Bo Janzon Professor Manfred Held

26th International Symposium on Ballistics Paper Selection Meeting
7 December 2010, Miami, Florida

Franz Rudol Thomanek
Founder of MBB-Schrobenhausen

Walter Trinks, Prominent scientist and

•Manfred Held was born in Regensburg on the 28th of September 1933.

•Physics Diploma (Physics) and Doctorate (Physical Chemistry), Technical University of Munich (1959)
•Joined MBB-Schrobenhausen (1960)

- •The founder of this establishment, Franz Rudolf Thomanek (1913–1990) worked closely together with Manfred Held and made him his successor.
- •Thomanek was connected with Dr. Walter Trinks (1910–1996), German MoD, by their common endeavour of shaped charge weapons.
- •Dr. Trinks supported the Schrobenhausen plant, enabling the acquisition of the latest and best technical equipment for high speed diagnostics research.
- •Dr. Held and his colleagues further developed the associated electronic equipment, giving rise to a unique research facility.
- •The product of this facility is documented in around 500 publications and 150 patents.

The nature of Held the ballistician & scientist

“Flash radiography is an important technique in all fields of ballistic experimentation, with the main emphasis undoubtedly on terminal ballistics . In what follows, we shall not dwell in scientific thoroughness on the fundamentals of flash radiography with all the related theories and details . For such details the reader is referred to an excellent book by Francis Jamet and Gustav Thomer and an article by Francis Charbonnier. 2 Both contain extensive lists of references .

To complement these references, the present contribution will demonstrate, by means of examples, why x-ray flash radiography holds such a preeminent position in the entire field of ballistics and particularly, in high-explosive warheads.”

- Dr. Held undertook many kinds of investigations investigations
  - Detonation and retonation
  - Corner turning effects
  - Initiation, initiators and related sensors including those for air-bag applications.
  - Shaped charge warhead systems (Milan, Hot, Kormoran, Roland)
  - Dispenser munitions
  - Explosively Formed Projectiles (EFPs)
  - Fragmenting warheads (including directional effects)
  - Invented reactive armour in 1970, which was later used by Israel and Russia.
  - Blast: developed the “momentum method” for determining and characterizing blast effects. Strongly involved with with this subject during his latter years.

Initiation Sensitivities

Type of HE	v^2d in $mm^3/\mu s^2$	Reference
HNAB	3	Hasman
PBX 9404	4	Bahl
RDX/Wax 88/12	5	Griffiths
TNT/RDX 35/65	6	Held
PETN 1.77	13	Vigil
Comp B	16	Chick, Moulard
H6	16.5	Chick
Detasheet	36-53	Weickert
C3 9407	40	Vigil
Tetryl	44	Vigil
C4	64	Weickert
TATB	108	Weingart
9502	128	Campell

3 - 8.5

13 - 19.5

Material Location

STEEL 1006

PBX9404JJ3

1 Projectile diameter from 2 mm to 12 mm

2 Projectile length of 10 mm

3 Air Gap width of 1 mm

4 Explosive length of 50 mm

5 Explosive width of 15 mm

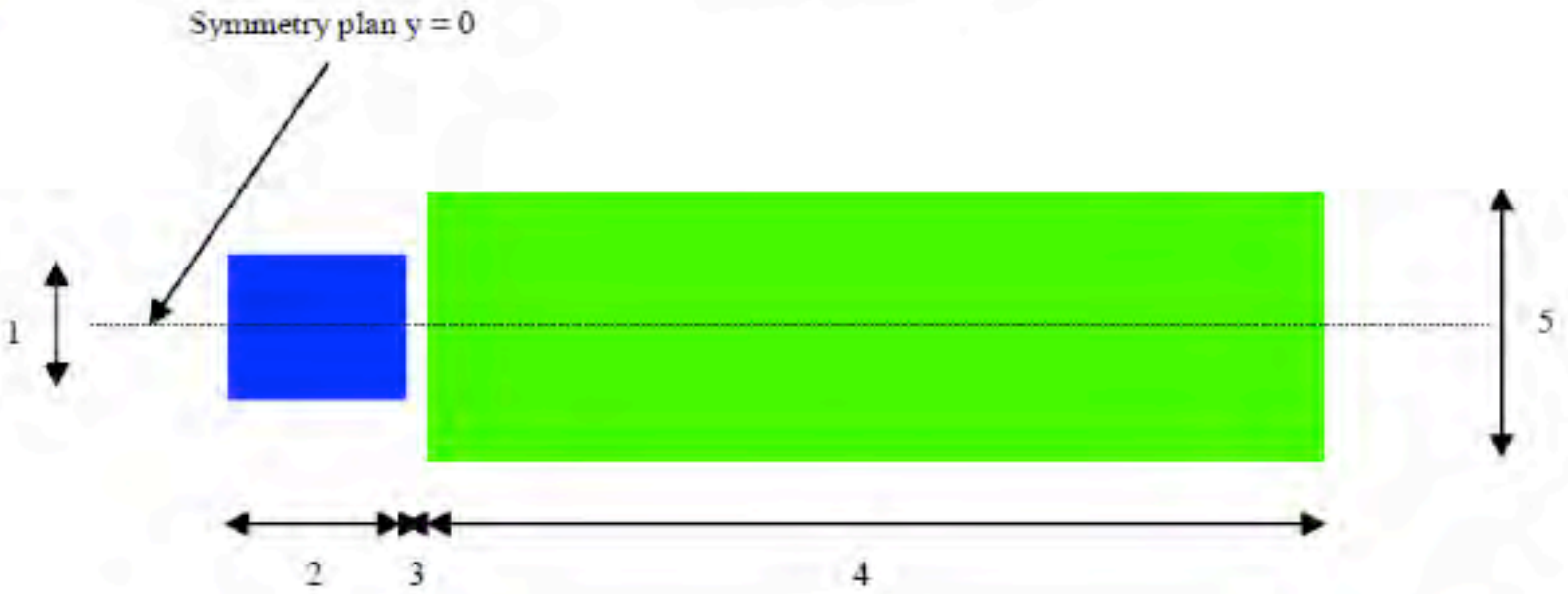

Wave Impingement against a Plate

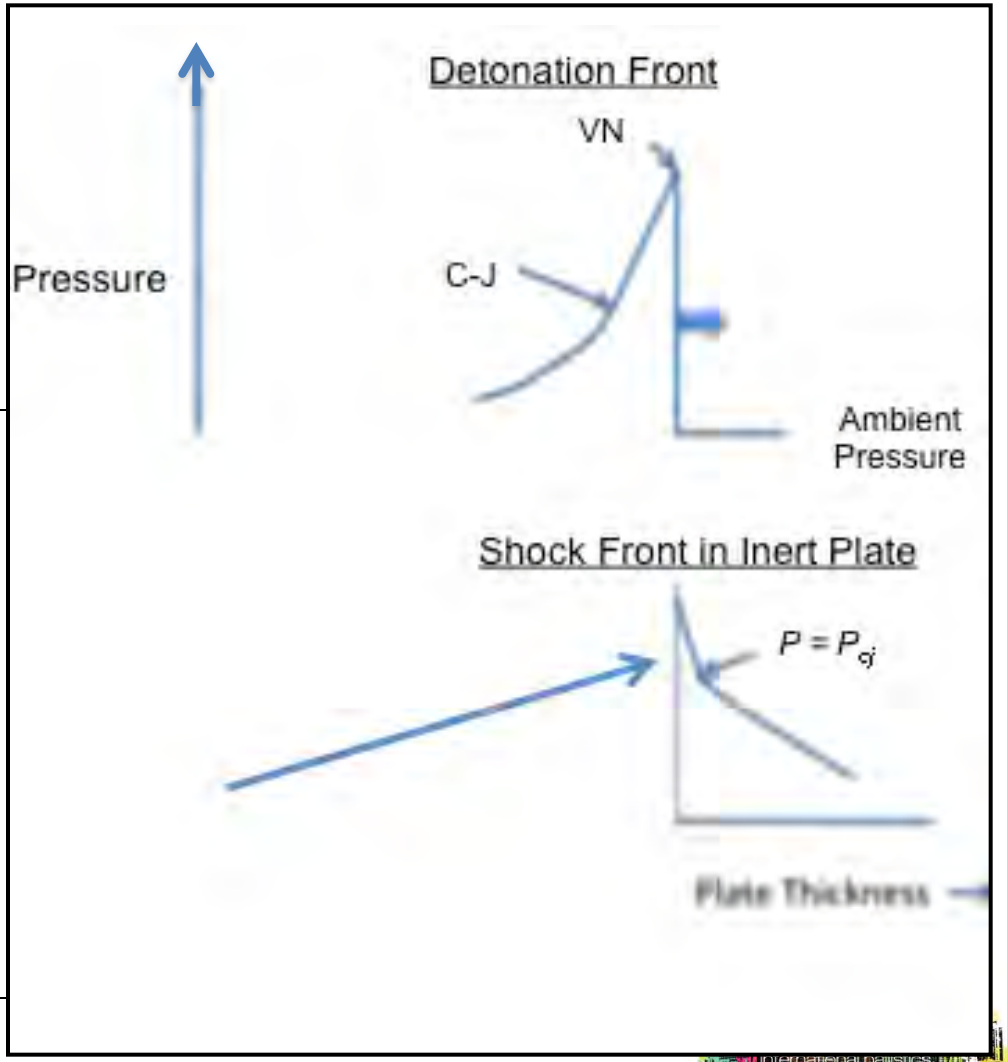

When a wave impinges upon an inert material in contact with the explosive, the wave transmitted is a shock followed closely by a steep rarefaction which is in turn followed by a more gradual rarefaction.
As this wave travels thru the material, the steep rarefaction overtakes and destroys that portion of the wave corresponding to the von

Review

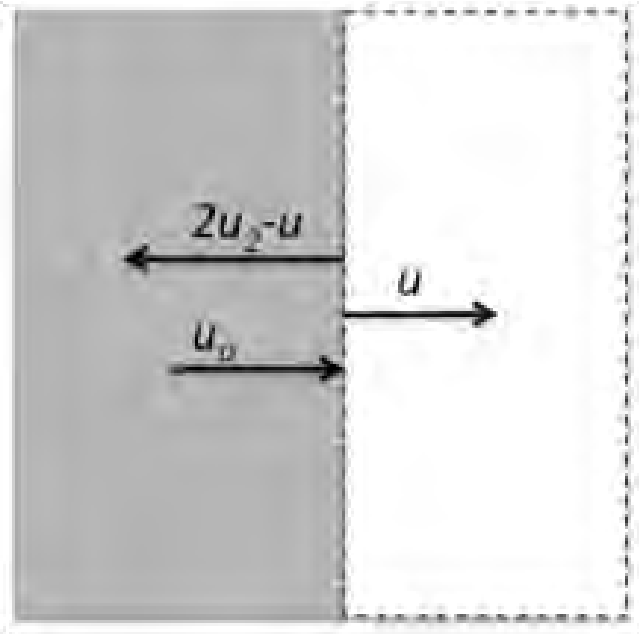

Zero

$$\rho_m \left[c_{m0} (u - 2u_0) + s_m (u - 2u_0)^2 \right] = \rho_{air} \left[c_{air,0} u + s_{air} u^2 \right] \equiv 0$$

$$u = 2u_0$$

Effect of the Free-Surface Material Shock Response

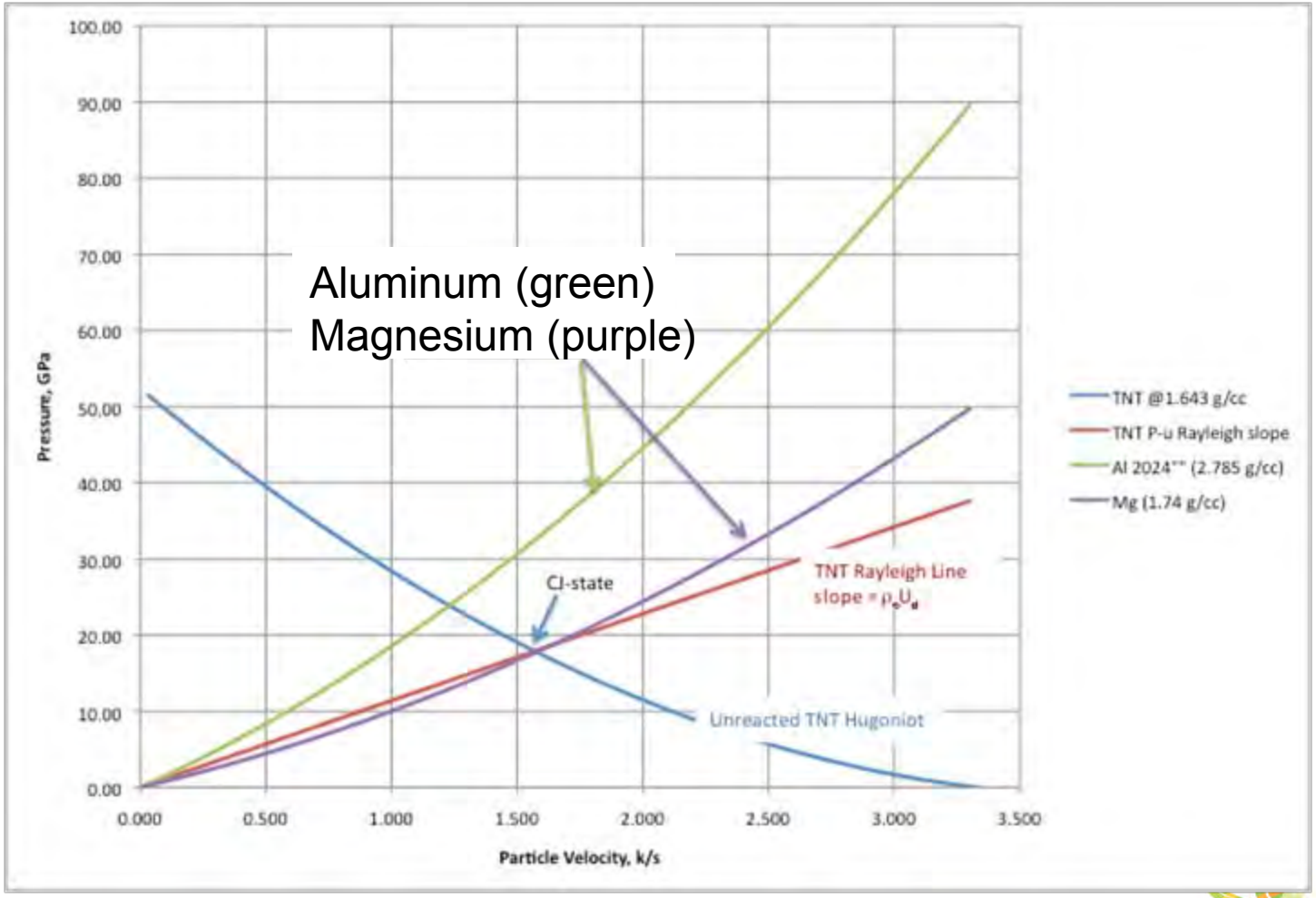

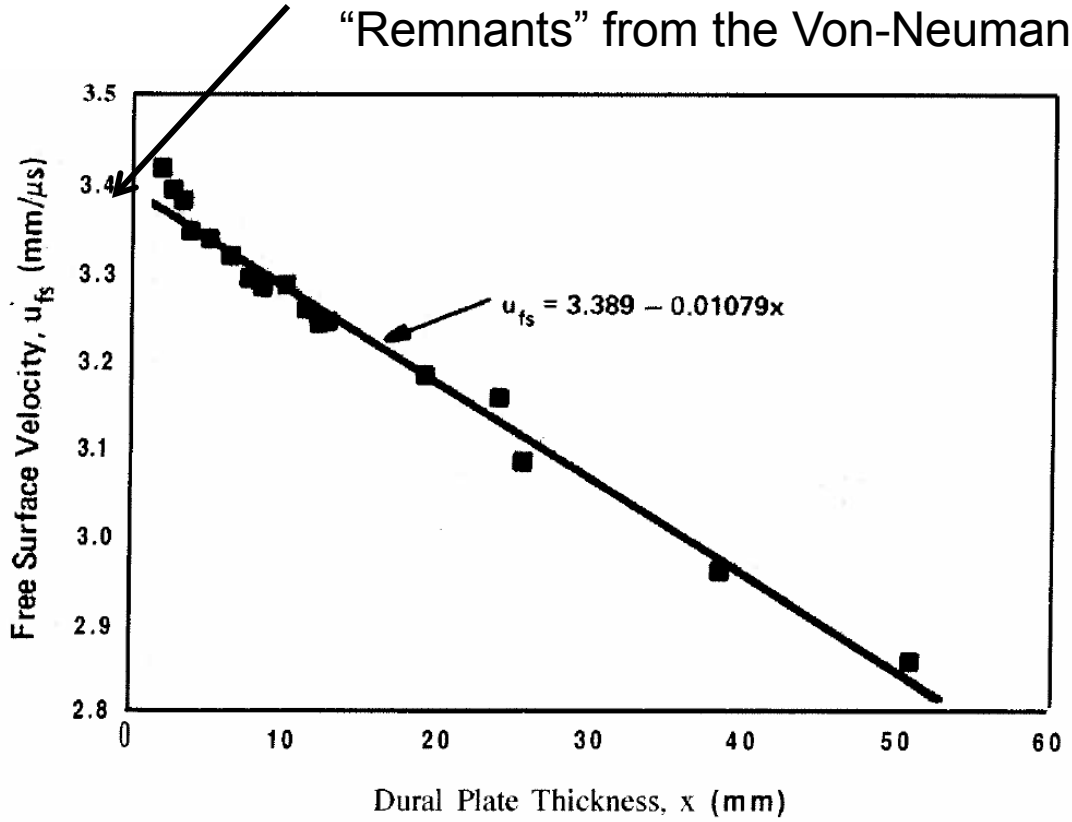

Estimated free-surface velocity imparted to 24ST aluminum plates by Composition B detonation. The line is the linear least square fit to the data. The intercept with the ordinate corresponds to the free-surface velocity of a zero-thickness plate.

From Deal, W.E., "The Measurement of Chapman-Jouguet Pressure for Explosives" , 1st International Symposium on Detonation, 327-342 (1955)

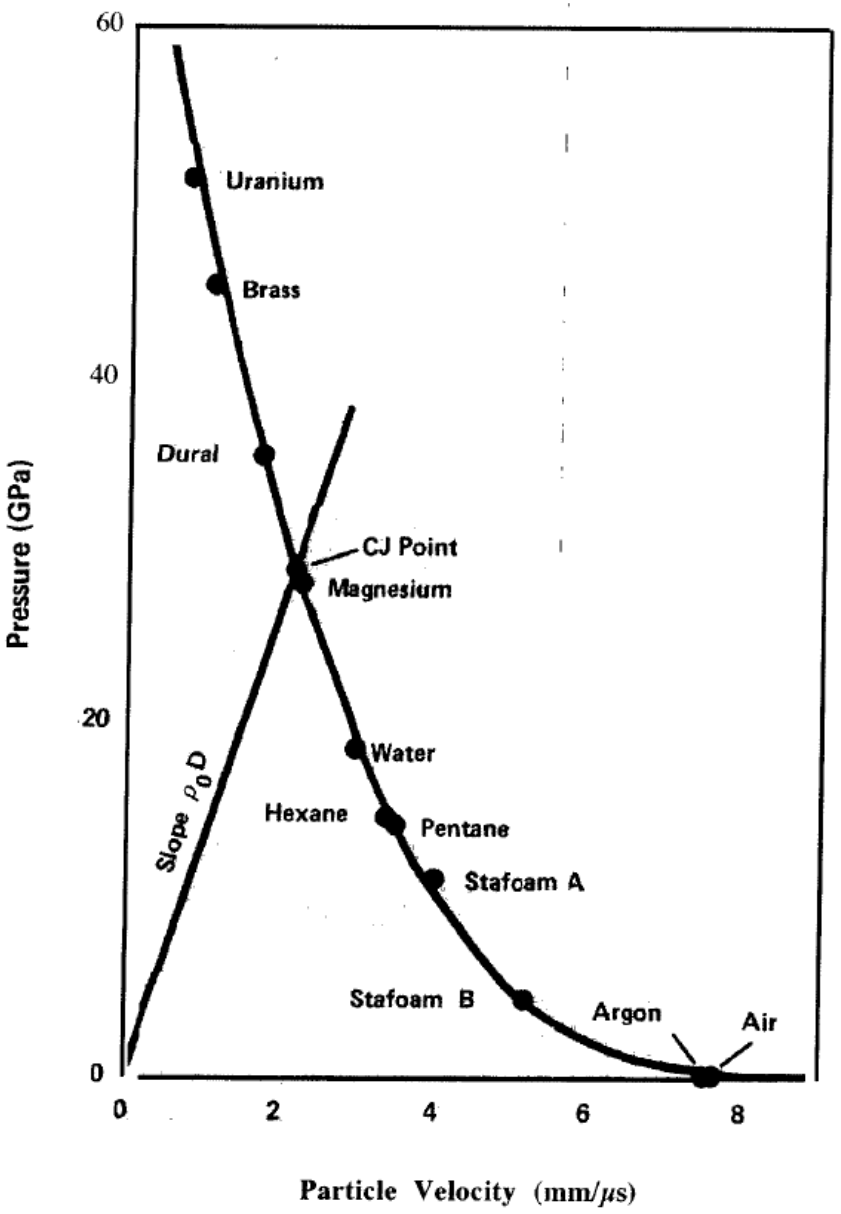

Pressure and particle velocity obtained from zero-thickness free-surface velocity measurements from various materials at the surface of Composition B detonation.

The CJ point must lie on the Rayleigh lined from the measured detonation velocity

Held's Use of Polymethacrylate Reduces Number of Tests

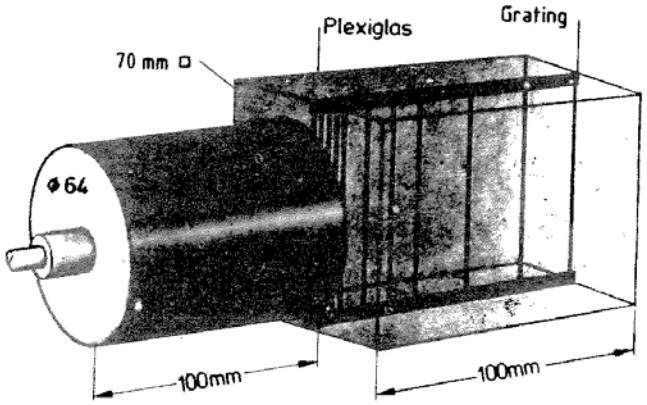

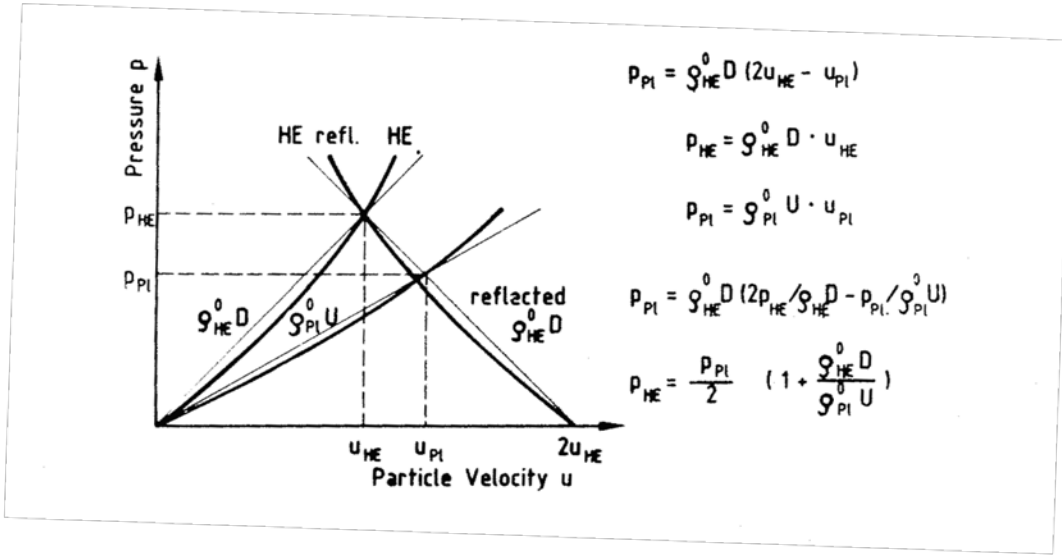

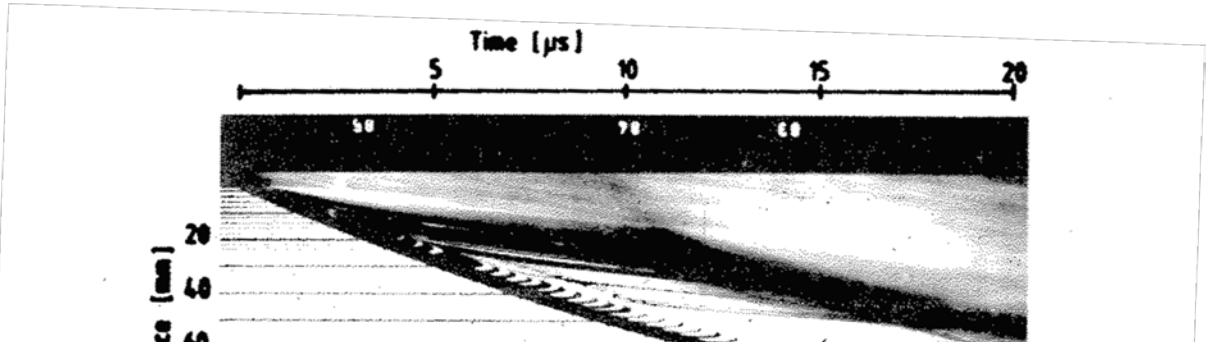

Contributor : Bettina Pinegger
Last changed : 18/02/2011

Professor Dr. Manfred Held passed away

18/02/2011

On 8 February, Professor Dr. Manfred Held passed away at the age of 77. For over 50 years, he worked for MBDA Germany and its predecessors. His name and his work are indelibly linked with the history of our Schrobenhausen site.

The physicist worked on warheads for the Milan, HOT, Kormoran and Roland missile systems and on many other projects.

He invented the so-called "reactive" armour in 1969. Another of his successes was the tandem shaped-charge warhead in 1974.

Professor Held was internationally renowned for his research in the field of high-speed diagnostics, explosive reactive armour and tandem shaped-charge warheads.

He also taught at numerous institutes of higher learning, such as the Bundeswehr University at Neubiberg near Munich and the Cranfield University in Shrivenham.

During his career, Professor Held registered over 140 patents and published more than 500 scientific articles.

He was also named an honorary member of the well-known International Ballistics Society (IBS). China's Nanchang University awarded him the title of Honorary Professor in recognition of his achievements. In 1986, he received the Diesel Medal from the German Institute for Invention (DIE).

Jacquet

Current Headlines

Professor Dr. Manfred Held passed away

Defence analysis - February

MBDA Employee Opinion Survey

A Look at Held's Initiation Criteria

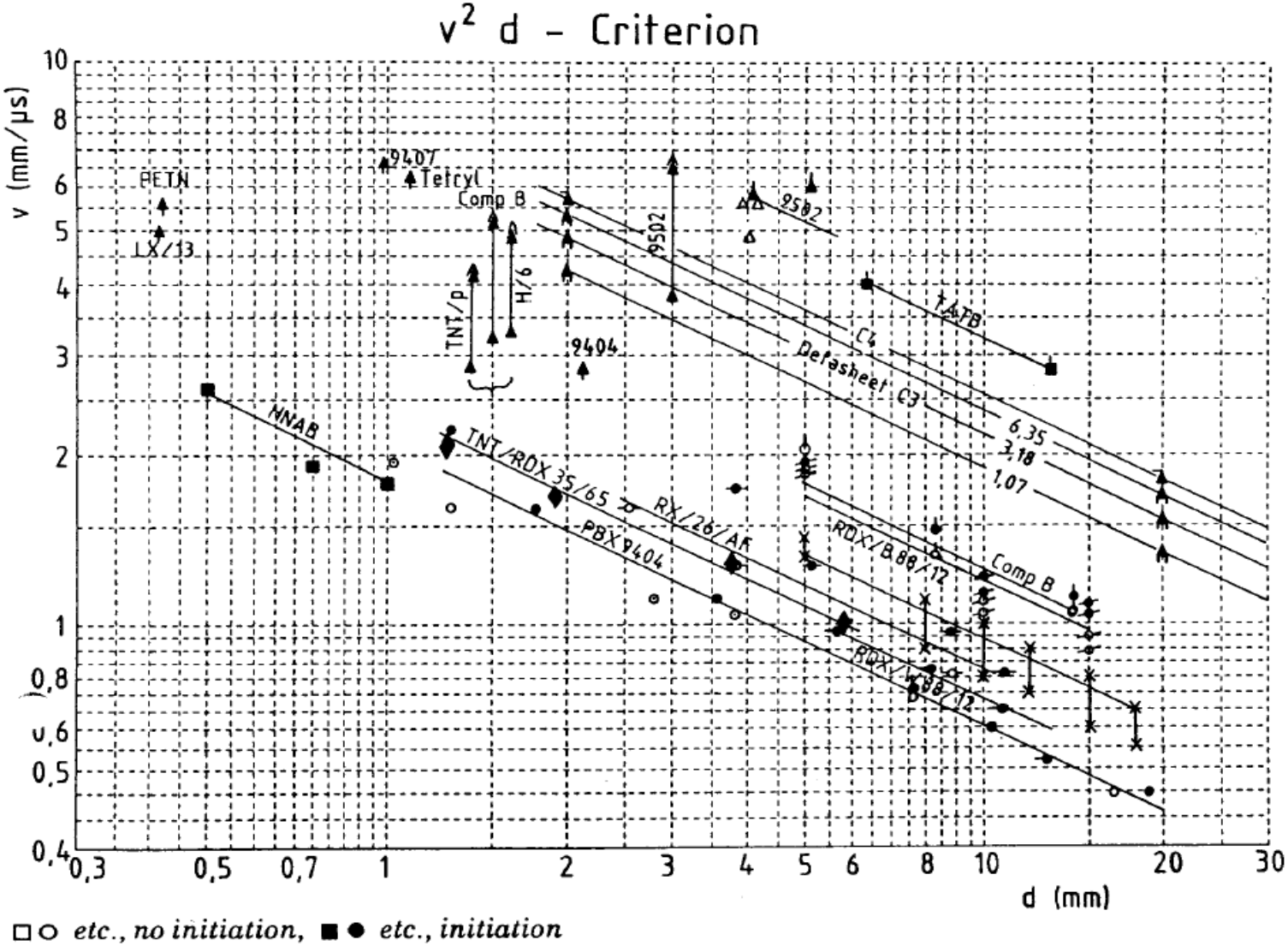

Guidance and expertise for National and International Authorities and Bodies.

•Editorial Board of this journal, the Chinese Journal of Energetic Materials (Henning Cailiao)
•Scientific Committee of the International Seminars NTREM at the Faculty of
•Chemical Technology, University of Pardubice, Czechia,
•Board of Trustees of the Fraunhofer Institute for Chemical Technology (ICT), Germany.

Lecturer
•University of the Federal Armed Forces, Munich
•Carl-Cranz educational seminars and courses
•Institute of Chemical Materials, CAEP., Beijing
•German Physical Society
•Presented at every International Annual Conference of the Fraunhofer ICT since 1970

Outstanding honours
•Diesel-Medal in Silver for his significant number of patents
•Professor h.c. by the University Nanking, China

Hypervelocity Impact Symposium 2012

Baltimore, Maryland USA

September 16-20, 2012

Hyatt Regency Baltimore on the Inner Harbor

www.HVIS2012.org (active 1Oct)

Symposium Co-Chairs: David Lambert (AFRL) and Todd Bjerke (ARL)
Technical Program Co-Chairs: Brett Sorensen (ARL) and Lalit Chhabildas (AFRL)